TABLE OF CONTENTS

Contents

I. JOINT DISCUSSIONS

1. NON-ELECTROMAGNETIC WINDOWS FOR ASTROPHYSICS

Chairperson: *M. Salvati*
Editors: *P. Blasi and M. Salvati*

2. MERCURY

Chairpersons: *R. Schulz and N. Thomas*
Editors: *R. Schulz, N. Thomas, and A. Sprague*

3. MAGNETIC FIELD AND HELICITY IN THE SUN AND HELIOSPHERE

Chairpersons: *B. Schmieder and D. Rust*
Editors: *B. Schmieder and D. Rust*

6. EXTRAGALACTIC GLOBULAR CLUSTERS AND THEIR HOST GALAXIES

Chairpersons: *T. Bridges and D. Forbes*
Editors: *T. Bridges and D. Forbes*

7. THE SUN AND THE HELIOSPHERE AS AN INTEGRATED SYSTEM

Chairpersons: *G. Poletto and S. T. Suess*
Editors: *G. Poletto and S. T. Suess*

8. LARGE TELESCOPES AND VIRTUAL OBSERVATORY: VISIONS FOR THE FUTURE

Chairpersons: *F. Genova and Ding-qiang Su*
Editors: *F. Genova and Xiangqun Cui*

9. ASTSROTOMOGRAPHY

Chairpersons: *M. Richards and L. Morales Rueda*
Editors: *A. Collier Cameron, A. Schwope, and S. Vrielmann*

10. EVOLUTION IN GALAXY CLUSTERS: A MULTIWAVELENGTH APPROACH

Chairpersons: *L. Feretti and R.W. Hunstead*
Editors: *R. W. Hunstead, L. Feretti, B. Gibson, and P. Nulsen*

11. DYNAMICS AND EVOLUTION OF DENSE STELLAR SYSTEMS

Chairpersons: *F. Combes and D. Richstone*
Editors: *F. Combes, P. Hut, and D. Richstone*

12. SOLAR AND SOLAR-LIKE OSCILLATIONS: INSIGHTS AND CHALLENGES FOR THE SUN AND STARS

Chairpersons: *T. R. Bedding and J. Leibacher*
Editors: *T. R. Bedding and J. Leibacher*

13. EXTRAGALACTIC BINARIES

Chairperson: *A. Giménez and I. Ribas*
Editor: *A. Gimenez and I. Ribas*

14. FORMATION OF COMETARY MATERIAL

Chairperson: *W. F. Huebner*
Editor: *W. F. Huebner, P. Ehrenfreund, and H.-U. Keller*

16. THE INTERNATIONAL CELESTIAL REFERENCE SYSTEM: MAINTENANCE AND FUTURE REALIZATION

Chairpersons: *D. McCarthy and F. Mignard*
Editors: *D. McCarthy, R. Gauma, and J. Souchay*

17. DATA FOR X-RAY ASTRONOMY

Chairperson: *A. K. Pradhan*
Editor: *P. L. Smith, A. K. Pradhan, and Sultana Nahar*

18. QUASAR CORES AND JETS

Chairperson: *D.L. Jauncey*
Editors: *D. L. Jauncey, K. I. Kellermann, and J. V. Wall*

19. PHYSICAL PROPERTIES AND MORPHOLOGY OF SMALL SOLAR SYSTEM BODIES

Chairpersons: *H. U. Keller and E. F. Tedesco*
Editors: *E. F. Tedesco, W. F. Huebner, and H. U. Keller*

20. FRONTIERS OF HIGH RESOLUTION SPECTROSCOPY

Chairperson: *J. Linsky*
Editor: *J. Linsky*

II. SPECIAL SCIENTIFIC SESSIONS

SPS 1. RECENT PROGRESS IN PLANETARY EXPLORATION

Chairpersons: *C. de Bergh and D. Cruikshank*
Editors: *D. Cruikshank and C. de Bergh*

SPS 2. ASTRONOMY IN ANTARCTICA

Chairperson: *M. Burton*
Editor: *M. Burton*

SPS 3. A NEW CLASSIFICATION SCHEME FOR DOUBLE STARS

Chairpersons: *W. I. Hartkopf and B. D. Mason*
Editors: *B. D. Mason and W. I. Hartkopf*

SPS 4. EFFECTIVE TEACHING AND LEARNING OF ASTRONOMY

Chairperson: *J. R. Percy*
Editor: *J. R. Percy*

Preface

The XXVth IAU General Assembly took place in Sydney, Australia, 13-26 July 2003 and it featured an impressively rich and varied scientific program of 6 Symposia, 21 Joint Discussions and 4 Special Scientific Sessions. In addition were held a large number of meetings of the IAU Divisions, Commissions and Working Groups.

This IAU Highlights of Astronomy contains the Proceedings from 20 out of the 21 Joint Discussions and the 4 Special Scientific Sessions. A fair and meaningful allocation of page space for these 24 different meeting made it necessary to print this volume of the Highlights of Astronomy in two books. The organizers of four Joint Discussions (JD04, JD09, JD13 and JD16) informed us that they wished to publish full Proceedings of their meetings which would consume a lot more space that available to them in this joint Proceedings. These organizers therefore submitted summaries and abstracts for the Highlights of Astronomy arranged for separate, full Proceedings from their meetings with other publishers. In addition, the Proceedings of the six Symposia (nos. 216 - 221) are being published in regular IAU Symposium Series.

I am deeply grateful to all authors and Editors of the individual events for their kind cooperation by following the instructions given by submitting their manuscripts on time. Only a very few manuscripts were late incoming and manuscripts from only one meeting were never received.

A special thank goes to Dr. Terry Mahoney who, as a consultant to the ASP, prepared the LaTeX style file for this volume, and most importantly, with gracious permission from the ASP, also helped prepare the Table of Content and the Authors Index.

Oslo and Paris, August 2004
Oddbjørn Engvold
General Secretary

I. JOINT DISCUSSIONS

JD1

Non Electromagnetic Windows
For Astrophysics

Chairperson: M. Salvati

Editors: P. Blasi and M. Salvati (Chief-Editor)

Highlights of Astronomy, Vol. 13
International Astronomical Union, 2003
O. Engvold, ed.

Neutrino Properties from Measurements using Astrophysical and Terrestrial Sources

A.B. McDonald

Physics Department, Queen's University, Kingston, Ontario, Canada, K7L3N6

Abstract. The current knowledge of neutrino properties has been derived from measurements performed with both astrophysical and terrestrial sources. Observations of neutrino flavor change have been made with neutrinos generated in the solar core, through cosmic ray interactions in the atmosphere and in nuclear reactors. A summary is presented of the current knowledge of neutrino properties and a description is provided for future measurements that could provide more complete information on neutrino properties.

2. Introduction

The neutrino has been very elusive in revealing its basic properties to experimenters. However, it provides a very attractive means for the study of many astrophysical objects such as the Sun, supernovae and other astrophysical sources producing high energy particles. The study of neutrinos from these sources can provide information on both the sources and on basic properties of neutrinos themselves. This paper will discuss the current state of information on neutrino properties, in several cases obtained from measurements with astrophysical sources. Future neutrino measurements will be described for astrophysical or terrestrial sources. Other papers in this session will discuss measurements of astrophysical sources using this basic information on neutrino properties.

3. Neutrino Properties

3.1. Number of neutrino types

The number of active neutrino types has been restricted for many years by studies of Big Bang Nucleosynthesis (for a summary see Hagiwara et al, 2002) to be less than about 4, but considerably more accuracy has been obtained through measurements of the width of the Z^0 resonance that set a number of 2.994 ± 0.012. Neutrino flavor change measurements show no evidence for sterile neutrinos.

3.2. Neutrino Flavor Change

Several measurements have indicated that neutrino flavor change occurs; the most favored explanation for the mechanism is neutrino oscillations among finite mass eigenstates. The neutrino flavor fields ν_ℓ can be expressed as superpositions of the components ν_k of the fields of neutrinos with definite masses m_k via U, the 3 x 3 unitary Maki-Nakagawa-Sakata-Pontecorvo (MNSP) mixing matrix (Maki et al, 1962, Gribov and Pontecorvo, 1969).

The MNSP matrix can be parameterized in terms of 3 Euler angle rotations and a CP-violating phase δ_{CP},

$$\mathbf{U} = \begin{pmatrix} c_{12}c_{13} & s_{12}c_{13} & s_{13}e^{-i\delta_{CP}} \\ -s_{12}c_{23} - c_{12}s_{23}s_{13}e^{i\delta_{CP}} & c_{12}c_{23} - s_{12}s_{23}s_{13}e^{i\delta_{CP}} & s_{23}c_{13} \\ s_{12}s_{23} - c_{12}c_{23}s_{13}e^{i\delta_{CP}} & -c_{12}s_{23} - s_{12}c_{23}s_{13}e^{i\delta_{CP}} & c_{23}c_{13} \end{pmatrix}$$

where $c_{ij} = \cos\theta_{ij}$ and $s_{ij} = \sin\theta_{ij}$.

When the neutrinos travel in a vacuum or low density region and two mass eigenstates dominate the process, the following probability is predicted for subsequent detection of a given neutrino type after it has traveled for a distance L in vacuum: $P = 1 - 1/2sin^2(2\theta_{ij})(1 - cos(2.54\Delta m^2 L/E)$, where Δm^2 is the difference between the two relevant mass eigenstates in eV^2, L is the source-detector distance in meters, E is the neutrino energy in MeV and θ_{ij} is defined above. When the neutrinos pass through regions of high electron density, the difference in the interaction of electron neutrinos and other neutrinos due to the charged current interaction can add extra terms to the MNSP matrix, resulting in a change to the effective masses and coupling constants. This is referred to as the MSW effect (Mikeyev and Smirnov, 1985, Wolfenstein, 1978) and can be used to determine the sign of the mass difference of the two dominant neutrinos involved in the oscillation.

Atmospheric Neutrinos Super-Kamiokande has observed a zenith angle dependence that is consistent with flavor change of atmospheric muon neutrinos through oscillations with a baseline of the Earth's diameter. The zenith angle dependence for electron neutrinos is consistent with Monte Carlo calculations for no flavor change, implying that the muon flavor change is predominantly to tau neutrinos. The hypothesis of neutrino oscillations is consistent with measurements made by a number of other detectors of an anomalous ratio of muon to electron atmospheric neutrinos.

Solar Neutrinos Since Davis' experiments starting in the 1960's, a discrepancy was identified between the experimental measurements and the theoretical calculations for solar neutrino fluxes. The fluxes are factors of two or three lower than predictions in each case, leading to the conclusion that either solar models are incomplete or there are processes occurring such as flavor change to other neutrino types for which the experiments have little or no sensitivity. This 30-year old discrepancy had come to be known as the "Solar Neutrino Problem".

Many attempts have been made to understand these discrepancies in terms of modifications to the solar model, without significant success. The results may be understood in terms of neutrino flavor change with matter enhancement in the sun. However, because the various experiments have different thresholds and are sensitive to different combinations of the nuclear reactions in the sun, this explanation is solar model-dependent. Solar model-independent approaches, including searches for spectral distortion, day-night and seasonal flux differences provided no clear indication of flavor change.

Measurements by the Sudbury Neutrino Observatory (SNO) of interactions of ^8B solar neutrinos in a heavy water detector have provided a solar-model-independent "appearance" measurement of neutrino flavor change by comparing charged current (CC) interactions on deuterium sensitive only to electron neutrinos and neutral current (NC) interactions sensitive to all neutrino types. A null hypothesis test for flavor change was performed, assuming no spectral change for the CC reaction. The flux of active neutrinos or anti-neutrinos other than electron neutrinos inferred from the NC measurements yielded a 5.3σ difference from the CC flux, providing clear evidence for flavor change. The result for the total active neutrino flux obtained with the NC reaction, $5.09^{+0.44}_{-0.43}(stat.)^{+0.46}_{-0.43}(syst.)$, is in very good agreement with the value calculated (Bahcall et al, 2001) by solar models: $5.05 \pm 1.0 \times 10^6$ cm^{-2}s^{-1}.

The solar neutrino measurements to date are best fit by neutrino oscillation parameters (see Table 1) including the MSW effect in the sun, referred to as the Large Mixing Angle (LMA) region. Note that the matter interaction defines m_2 to be greater than m_1 and that the mixing angle is somewhat smaller than maximal mixing.

Terrestrial Measurements Measurements of the survival of ν_μ neutrinos produced at the KEK accelerator have been made with the Super-Kamiokande detector, (K2K experiment). The preliminary data (Nishikawa, 2002) show agreement with the m_2 to m_3 oscillation parameters observed for atmospheric neutrinos. The KamLAND experiment (Eguchi et al, 2003) has studied the flux of electron anti-neutrinos observed at a 1000 ton liquid scintillator detector (converted from the original water-based Kamiokande detector). They find a flux suppression consistent only with the LMA region for m_1 - m_2 oscillation as defined by solar neutrinos and restricting the region obtained with solar neutrino measurements alone. Results from the LSND experiment have indicated the appearance of a small flux of anti-ν_e from an anti-ν_μ accelerator beam. The majority of the allowed oscillation region for this experiment has been restricted by the Karmen experiment. The MINIBOONE experiment has just begun operation with neutrino beams from Fermilab and should approach the LSND measurements with substantially higher sensitivity.

Summary of flavor change information to date Atmospheric, solar, and reactor neutrino oscillation data currently fix or limit the 3 angles. They also provide values for the differences between the squares of the masses. They provide no information yet on the phase(s). The data to date is summarized in Table 1.

3.3. Neutrino Mass

The most sensitive direct measurements of electron neutrino mass have been made by searching for curvature induced near the end point of the spectrum of electrons emitted during the beta decay of tritium. The current limit obtained from these measurements is 2.8 eV (90 % CL.). Measurements of neutrinoless double beta decay are also sensitive to neutrino mass if the neutrino is a Majorana particle. Measurements to date set limits less than 0.4 eV for the effective mass associated with this process. There is also a controversial claim of a greater than 2 σ effect for a mass of 0.35 eV in a neutrinoless double beta decay measurement in Ge reported by a subset of the Heidelberg-Moscow experimental group.

Table 1. Current knowledge of active neutrino mass and mixing from neutrino oscillations. One-σ errors are shown, except for θ_{13}, which is at the 90% CL.

Quantity	Value
θ_{12}	$32.6(32)^o$
θ_{13}	$< 10^o$
θ_{23}	$45(8)^o$
δ_{CP}	?
$m_2^2 - m_1^2$	$+7.3(11) \times 10^{-5}$ eV^2
$m_3^2 - m_2^2$	$\pm 2.5(6) \times 10^{-3}$ eV^2

Model-dependent limits with sensitivity of about 1 eV can also be obtained from combined fits to the cosmic microwave and large scale structure data.

4. Future measurements

All of the types of measurements discussed above are being pursued very actively for the future. The next generation measurements for tritium beta decay and neutrinoless double beta decay should extend the mass sensitivity by a factor of about 10. This sensitivity is approaching the mass differences identified by the oscillation measurements. Flavor change measurements will be extended for solar and terrestrial neutrinos with improved accuracy. The definition of these parameters has also led to plans for a next generation of long-baseline experiments to quantify θ_{13} through accelerator and reactor experiments and seek the mass hierarchy through matter interactions and CP violating phase through experiments with accelerator and detector properties scaled up by factors of 10.

Our knowledge of neutrino properties has expanded greatly during the past 10 years. The next generations of experiments have the potential to prove as comprehensive information for the lepton sector as has been obtained for quarks, thereby making it possible to use neutrinos as a unique astrophysical probe.

References

Please note that, in the interests of space, all experimental references contained in the 2002 summary by the Particle Data Group are not repeated here.

Hagiwara, K. et al (Particle Data Group) 2002, Phys.Rev.D66, 010001.

Maki, Z., Nakagawa, N. and Sakata, S. 1962, Prog. Theor. Phys., 28, 870.

Gribov, V. and Pontecorvo, B. 1969, Phys. Lett. B,28, 493.

Mikheyev, S.P. and Smirnov, A.Y. 1985, Sov. Jour. Nucl. Phys., 42, 913.

Wolfenstein, L. 1978, Phys.Rev.D, 17, 2369.

Bahcall, J.N., Pinsonneault, M.H and Basu, S. 2001 ApJ, 555, 990.

Eguchi, K. et al 2003 Phys.Rev.Lett, 90, 021802.

Highlights of Astronomy, Vol. 13
International Astronomical Union, 2003
O. Engvold, ed.

MeV Neutrino Sources: The Sun and the Supernovae

Sylvaine Turck-Chize

SAp/DAPNIA/DSM/CEA CE Saclay, 91191 Gif sur Yvette, France

Abstract. The two sources of MeV neutrinos, the Sun and the Supernovae are very interesting to study nowadays. Seismology aboard SoHO has properly constrained the solar emitted neutrino fluxes and consequently contributes to an unambiguous evidence of the solar neutrino oscillations. The main role of seismology stays nevertheless the description of the magneto-hydrodynamic processes and this progress provokes a renewal of the stellar discipline. Important results are noticed these three years, for the Sun. Future will be richer implying a large number of stars with an evident impact on supernovae and solar neutrino properties.

1. The Two Sources of Neutrinos

The two natural Neutrino MeV Sources, the Sun and the Supernovae, are studied with more and more interest as the richness of their plasma properties is inaccessible in laboratories. Nevertheless, the level of knowledge of these sources is extremely different. The solar internal structure is scrutinized for twenty years with two independent probes: neutrinos and acoustic modes. In the case of supernovae, the emitted neutrinos have been detected once only, for the Supernova 1987A. It is evident that these two sources are extremely different. If the Sun has a continuous emission of neutrinos, the emission coming from a supernova explosion is quasi instantaneous, with a peak of 0.025 s. Only 6.4 % of the produced solar energy is emitted by the neutrinos, though the main part of the released energy in a supernova explosion is contained in the neutrino emission. If the Sun emits neutrinos up to 14 MeV and has a well determined energy spectrum, the range of emission for the supernovae is large from 5 MeV to about 100 MeV. The impact of the different neutrino oscillation solutions on the supernova energy spectrum is high, mainly for the SNO detector, even the waiting statistics in Superkamiokande is higher, so there is extremely large interest to detect supernova neutrinos in the present observatories to put more constraints on the neutrino properties or on the explosion mechanism. The diversity of the supernovae (Heger et al. 2003) and consequently of the supernova explosions encourages also the study of the different supernova precursors. Supernovae Ia have initial mass below 8 $M_\odot$, and final mass probably below 1.5 $M_\odot$, Supernovae II have initial mass between 8 to 30 $M_\odot$, final mass below 10 $M_\odot$, Supernovae Ib and c have initial mass above 30 $M_\odot$ and final mass always below 10 $M_\odot$. With such a range in mass, questions on geometry, asphericity, rotation, metallicity have not a clear answer today.

The geometry of stars and the mass loss processes are more under control at different stages of evolution, so there is a renewal in stellar structure, which will benefit by seismic observations, capabilities of parallel computers and the introduction of macroscopic motions. The direct and indirect role of the rotation is now proven for the determination of the oblateness of massive stars. The impact on the geometry of the explosion is waiting. The role of the stellar metallicity is also a determinant factor, with cosmological consequences, it must be studied to interpret correctly the incoming large dataset supernova light curves.

We are convinced that a clear hydrostatic and hydrodynamic vision of stars will emerged within the next decade, thank to the spatial COROT and EDDINGTON projects with consequences for supernovae progenitors. Let summarize here the highlights of the last 3 years for the Sun which is the first star for which this effort is already well advanced.

2. The Sun as a laboratory for emitted neutrino fluxes

The Sun is a unique case for which we have today 40 years of observations: five neutrino experiments using different techniques, 3 helioseismic ground networks and 3 spatial helioseismic experiments aboard SoHO running since 7 years.

Since 1988, we have controlled the emitted solar neutrino fluxes, in confronting the solar theoretical structure to the seismic one. Using this probe as a reference, constant progress has been noticed on the determination of these fluxes (Turck-Chize et al. 1988, Turck-Chize and Lopes 1993, Dzitko et al. 1995, Brun, T-C & Morel, 1998, Brun, T-C & Zahn, 1999, Turck-Chize et al. 2001a, Turck-Chize et al. 2001b, Couvidat, Turck-Chize & Kosovichev 2003).

Helioseismology has contributed to stabilize the structure of the Sun thanks to the sound speed profile, helping to answer to questions on:

- 1) a proper determination of the metal opacity coefficients
- 2) a proper description of the microscopic diffusion
- 3) a proper description of the role of the plasma in nuclear reaction rates
- 4) the existence or not of a potential mixing in the very central core
- 5) the adequation of a Maxwellian distribution for particle velocities
- 6) the proper description of the pp reaction rate
- 7) the existence of mixing in the radiation-convection region partly inhibiting the microscopic diffusion.

It is because we have found answers to these questions that neutrino predictions coming from different groups have converged. If the two first questions have been solved with ground observations, the other ones, largely important for determining properly the neutrino fluxes, have needed the SoHO satellite. This is due to the nature of acoustic modes.

Excited by the superficial granulation, these modes are mainly sensitive to the convection zone more than the nuclear core. But the high energy neutrinos, those produced by the ppIII chain, the ^8B neutrinos detected in Superkamiokande and SNO, are produced below 0.1 $R_\odot$, it is also the case for the ^{17}F and ^{15}O neutrinos. All these neutrinos are extremely dependent on the central temperature. But the extraction of the very internal structure from acoustic frequencies needs a great accuracy on the frequency determination. Unfortunately, for the easily detected global modes, the precision is degraded by stochastic excitation and variability with the solar cycle. The only way to escape this difficulty is to integrate the signal for a very long time, in order to reach acoustic modes of low frequency, less perturbed by these kind of processes.

Figure 1 of Couvidat, Turck-Chièze & Kosovichev 2003, hereafter CTCK-2003, shows the improvement obtained on the quality of the data with the GOLF (Global Oscillations at Low Frequency, Gabriel et al. 1995) instrument aboard SoHO. This quality can be translated in an accuracy of 10^{-4} on the sound speed in the solar core (Turck-Chize et al. 2001b). Such results put strong constraints and partial answers to questions 3 to 7 (Turck-Chize et al. 2001a). Including progress on theoretical, instrumental and observational sides, we have finally produced seismic theoretical models. Nowadays, the number of emitted neutrino fluxes, and in particular the ^8B neutrinos, is constrained by the helioseismic probe. A flux of 4.95 0.72 $10^6 cm^{-2}s^{-1}$ for the ^8B neutrinos has been determined by Turck-Chize et al. 2001b, with an error bar of only 14%, including physics beyond standard hypotheses. The perfect agreement of this number with the results of the SNO detections is determinant to solve the neutrino puzzle, to demonstrate the solar oscillations and to put strong constraints on energy production including CNO cycle.

3. Is the Sun standard or not?

Helioseismology reveals that the Sun is not standard. The main objectives of this probe is to go beyond this simple representation which neglects the effects of the macroscopic motions. During these last 3 years, variabilities connected to the evolution during the solar cycle have been extracted and internal migrating flows have been observed. The history of the angular momentum evolution is crucial to understand the dynamo process and the range of internal magnetic field which is an essential property of the solar plasma.

Due to solar rotation and magnetic field, the frequencies of two modes of the same degree ℓ and order n are splitted in m components varying between $\pm\ell$. The corresponding splitting contains information on the internal rotation and presently one can extract this rotation profile down to the limit of the nuclear core, typically 0.2 R$\odot$, for the first time without ambiguity thanks to the longevity, the stability and the position of the SoHO satellite (Couvidat et al. 2003). It appears that the radiative zone rotates as a solid body with a constant rate but in examining gravity mode candidates, one cannot exclude a small core with a different axis and a quicker rotation, a release of the early rotation? (Turck-Chièze et al. 2003).

The problem could be to see the impact of such phenomenon on the neutrino productions. We have concluded in CTCK2003 that it must be small (no more than 12% on the previous neutrino flux) with a limit on the magnetic field of 30 MG in the radiative zone. Of course such assumptions must be confirmed by further works and probably a new generation of instruments that we are preparing. From the rotation profile, one begins to develop hydrodynamical calculations which have for objectives to reproduce the differential rotation in the convective zone (Brun & Toomre, 2002). These hydrodynamic simulations may be useful to try to estimate some order of magnitude of the internal magnetic field to reproduce the solar magnetic cycle. Several works attack these problems.

4. The search for neutrino properties and Perspectives

It is interesting now to study if some properties of the solar plasma may play a role on the neutrino propagation or transformation. It is why we (CTCK2003) have delivered the radial electron and neutron density profiles for our seismic model, together with some limits on the magnetic field and the magnetic neutrino moment: $\mu_\nu > 5\,10^{-15}\mu_B$ in the radiative zone and $\mu_\nu > 3\,10^{-12}\mu_B$ in the transition region between radiation and convection. We also give some probabilities on the RSFP transition for estimated magnetic field. We are also looking for effective variation of the magnetic field along the solar cycle in the external layers (Turck-Chièze, Nghiem and Piau 2003).

We are also trying to extract some effect in the neutrino data. Consequently, we have analyzed the Superkamiokande 10 days released data. In the research of periodicies, we note significant peaks around half the rotation of the Sun, and some others with a period around the rotation, but the spectrum is not unambiguous as it is the case of acoustic modes. We have also studied the correlation between the neutrino dataset and magnetic indicators. We note some correlation with a delay of several hundred days, which may translate some internal interaction. The same analysis has been repeated with SAGE data. But all the effects are not sufficiently significant.

I strongly recommend to deliver datasets of 5 days for Superkamiokande and SNO and to try to extract data in the low energy experiments at the same time, effectively, the magnetic activity evolves strongly at the scale of days.

References

Brun, A. S., Turck-Chize, S., & Morel, P. 1998, ApJ, 506, 913

Brun, A. S., Turck-Chize, S., & Zahn, J.P. 1999, ApJ, 525, 1032

Brun, A. S., Toomre, J. 2002, ApJ, 570, 865

Couvidat , S., Turck-Chize, S, & Kosovichev, A. 2003, ApJ, in press

Couvidat, S., Garcia, R. A., Turck-Chize, S., Corbard, T. Henney, C. J., & Jimenez-Reyes, S. 2003, ApJ Lett., vol 597

Dzitko, H., Turck-Chize, S., Delbourgo Salvador, P. & Lagrange, C. 1995, ApJ, 447, 428

Gabriel, A., Grec, G., Charra, J., Robillot, JM., Roca Cortes, T., Turck-Chize, S., et al. 1995, Sol. Phys., 162, 39

Heger, A., Fryer, C. L., Woosley, S. E., Langer, N., & Hartmann, D. H. 2003, ApJ, 591, 288

Turck-Chize, S., Cahen, S., Cass, M. & Doom, C. 1988, ApJ, 335, 415

Turck-Chize, S. & Lopes, I. 1993, ApJ, 408, 347

Turck-Chize, S., Nghiem, P. , Couvidat, S., and Turcotte, S. 2001a, Sol. Phys, 323

Turck-Chize, S., et al. 2001b, ApJ 555, L69

Turck-Chize, S., Garcia, R.A., Couvidat, S. et al. 2003, ApJ, accepted

Turck-Chize, S., Nghiem, P., & Piau, L. 2003, Highlights of Astronomy, **13**, JD12

Highlights of Astronomy, Vol. 13
International Astronomical Union, 2003
O. Engvold, ed.

High-energy Neutrino Astronomy: From AMANDA to IceCube

Francis Halzen

Department of Physics, University of Wisconsin, Madison, WI 53706

Abstract. Kilometer-scale neutrino detectors such as IceCube are discovery instruments covering nuclear and particle physics, cosmology and astronomy. Examples of their multidisciplinary missions include the search for the particle nature of dark matter and for additional small dimensions of space. In the end, their conceptual design is very much anchored to the observational fact that Nature accelerates protons and photons to energies in excess of 10^{20} and 10^{13} eV, respectively. The cosmic ray connection sets the scale of cosmic neutrino fluxes. In this context, we discuss the first results of the completed AMANDA detector and the reach of its extension, IceCube.

1. Neutrinos Associated with the Highest Energy Cosmic Rays

The flux of cosmic rays is summarized in Fig. 1a,b (Gaisser 2002). The energy spectrum follows a broken power law. The two power laws are separated by a feature referred to as the "knee"; see Fig. 1a. There is evidence that cosmic rays, up to several EeV, originate in galactic sources. This correlation disappears in the vicinity of a second feature in the spectrum dubbed the "ankle". Above the ankle, the gyroradius of a proton exceeds the size of the galaxy and it is generally assumed that we are witnessing the onset of an extragalactic component in the spectrum that extends to energies beyond 100 EeV. Experiments indicate that the highest energy cosmic rays are predominantly protons. Above a threshold of 50 EeV these protons interact with CMBR photons and therefore lose their energy to pions before reaching our detectors. This limits their sources to tens of Mpc, the so-called Greissen-Zatsepin-Kuzmin cutoff.

Models for the origin of the highest energy cosmic rays fall into two categories, top-down and bottom-up. In top-down models it is assumed that the cosmic rays are the decay products of cosmological remnants with Grand Unified energy scale $M_{GUT} \sim 10^{24}$ eV. These models predict neutrino fluxes most likely within reach of AMANDA, and certainly IceCube.

In bottom-up scenarios it is assumed that cosmic rays originate in cosmic accelerators. Accelerating particles to TeV energy and above requires massive bulk flows of relativistic charged particles. These are likely to originate from the exceptional gravitational forces in the vicinity of black holes. Examples include the dense cores of exploding stars, inflows onto super-massive black holes at the centers of active galaxies and annihilating black holes or neutron stars. Before leaving the source, accelerated particles pass through intense radiation fields or dense clouds of gas surrounding the black hole. This results in interactions

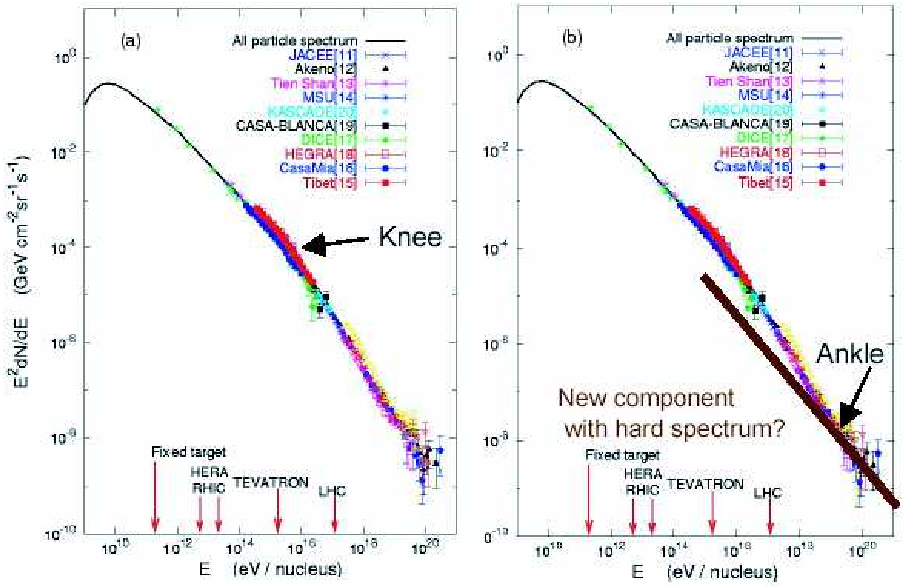

Figure 1. At the energies of interest here, the cosmic ray spectrum consists of a sequence of 3 power laws. The first two are separated by the "knee" (left panel), the second and third by the "ankle". There is evidence that the cosmic rays beyond the ankle are a new population of particles produced in extragalactic sources; see right panel.

producing pions decaying into secondary photons and neutrinos that accompany the primary cosmic ray beam as illustrated in Fig. 2.

How many neutrinos are produced in association with the cosmic ray beam? The answer to this question, among many others (Gaisser, Halzen & Stanev 1995), provides the rationale for building kilometer-scale neutrino detectors. We first consider a neutrino beam produced at an accelerator laboratory; see Fig. 2. Here the target absorbs all parent protons as well as the muons, electrons and gamma rays produced. A pure neutrino beam exits the dump. If nature constructed such a "hidden source" in the heavens, conventional astronomy will not reveal it. It cannot be the source of the cosmic rays, however, because the dump would have to be partially transparent to protons. The extreme opposite case is a "transparent source" where the accelerated proton interacts once and escapes the dump after producing photons as well as neutrinos. Elementary particle physics is now sufficient to relate all particle fluxes because a fraction (1/6 to 1/2 depending on the energy) of the interacting proton goes into pion production. This energy is equally shared between gamma rays and neutrinos, of which one half are muon-neutrinos. Therefore, at most one quarter of the energy ends up in muon-neutrinos compared to cosmic rays. The flux of a transparent cosmic ray source is often referred to as the Waxman-Bahcall flux (Bahcall & Waxman 2001). It is easy to derive and the derivation is revealing.

Fig. 1b shows a fit to the observed cosmic ray spectrum assuming an extragalactic component fitted above the "ankle". The energy content of this component is $\sim 3 \times 10^{-19}$ erg cm^{-3}, assuming an E^{-2} energy spectrum with a

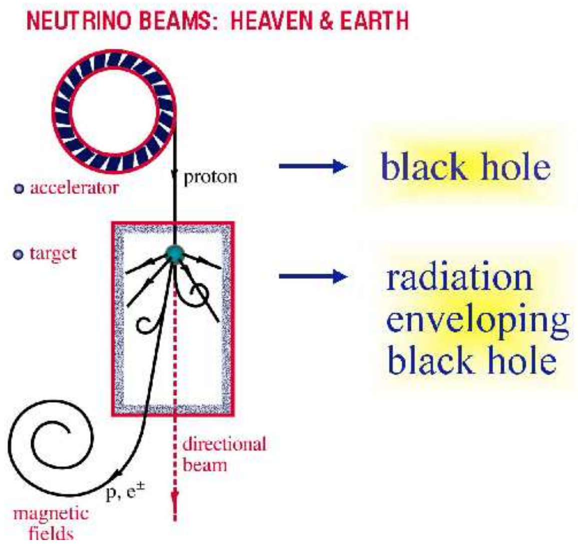

Figure 2. Diagram of cosmic ray accelerator producing photons and neutrinos.

GZK cutoff. The power required to generate this energy density in the Hubble time of 10^{10} years is $\sim 3\times10^{37}\,\mathrm{erg\ s^{-1}}$ per $(\mathrm{Mpc})^3$. This works out to (Gaisser 1997)

- $\sim 3\times10^{39}\,\mathrm{erg\ s^{-1}}$ per galaxy,
- $\sim 3\times10^{42}\,\mathrm{erg\ s^{-1}}$ per cluster of galaxies,
- $\sim 2\times10^{44}\,\mathrm{erg\ s^{-1}}$ per active galaxy, or
- $\sim 2\times10^{52}$ erg per cosmological gamma ray burst.

The coincidence between these numbers and the observed electromagnetic energy output of these sources explains why they have emerged as the leading candidates for the cosmic ray accelerators. The coincidence is consistent with the relationship between cosmic rays and photons built into the "transparent" source previously introduced. The relationship can be extended to neutrinos.

Assuming the same energy density of $\rho_E \sim 3\times10^{-19}\,\mathrm{erg\ cm^{-3}}$ in neutrinos with a spectrum $E_\nu dN/dE_\nu \sim E^{-\gamma}\,\mathrm{cm^{-2}\,s^{-1}\,sr^{-1}}$ that continues up to a maximum energy E_{max}, the neutrino flux follows from $\int E_\nu dN/dE_\nu = c\rho_E/4\pi$. For $\gamma = 1$ and $E_{max} = 10^8$ GeV, the generic source of the highest energy cosmic rays produces 50 detected muon neutrinos per km^2 per year (Gaisser 1997). [Here we have folded the predicted flux with the probability that the neutrino is actually detected given by (Gaisser et al. 1995) the ratio of the muon and neutrino interaction lengths in ice, λ_μ/λ_ν.] The number depends weakly on E_{max} and γ. A similar analysis can be performed for galactic sources (Gaisser et al. 1995).

As previously stated, for one interaction and only one, the neutrino flux should be reduced by a factor ~ 4. On the other hand, there are more cosmic rays in the universe producing neutrinos than observed at earth because of the

GZK-effect. The diffuse muon neutrino flux associated with the highest energy cosmic rays is estimated to be ${E_\nu}^2 dN/dE_\nu \sim 5 \times 10^{-8}\,\mathrm{GeV\,cm^{-2}\,s^{-1}\,sr^{-1}}$, to be compared to the sensitivity achieved with the first 3 years of the completed AMANDA detector of $10^{-7}\,\mathrm{GeV\ cm^{-2}\,s^{-1}\,sr^{-1}}$. The analysis has not been completed but a limit has been published that is 5 times larger obtained with data taken with the partially deployed detector in 1997 (Ahrens et al. 2003). On the other hand, after three years of operation IceCube will reach a diffuse flux limit of $E_\nu^2 dN/dE_\nu = 8.1 \times 10^{-9}\,\mathrm{GeV\,cm^{-2}\,s^{-1}\,sr^{-1}}$.

2. Neutrino Telescopes: the First Generation

While it has been realized for many decades that the case for neutrino astronomy is compelling, the challenge has been to develop a reliable, expandable and affordable detector technology to build the kilometer-scale telescopes required to do the science. Conceptually, the technique is simple. In the case of a high-energy muon neutrino, for instance, the neutrino interacts with a hydrogen or oxygen nucleus in deep ocean water and produces a muon traveling in nearly the same direction as the neutrino. The blue Cerenkov light emitted along the muon's kilometer-long trajectory is detected by strings of photomultiplier tubes deployed at depth shielded from radiation. The orientation of the Cerenkov cone reveals the neutrino direction.

The AMANDA detector, using natural 1 mile deep Antarctic ice as a Cerenkov detector, has operated for more than 3 years in its final configuration of 680 optical modules on 19 strings. The detector is in steady operation collecting roughly four neutrinos per day using fast on-line analysis software. Its performance has been calibrated by reconstructing muons produced by atmospheric muon neutrinos (Andres et al. 2001).

Using the first of 3 years of AMANDA II data, the AMANDA collaboration is performing a (blind) search for the emission of muon neutrinos from spatially localized directions in the northern sky (Karle et al. 2002). Only the year 2000 data have been unblinded. The sky-plot is shown in Fig. 3. 90% upper limits on the fluency of point sources is at the level of $2 \times 10^{-7}\,\mathrm{GeV\,cm^{-2}\,s^{-1}}$ or $3 \times 10^{-10}\,\mathrm{erg\ cm^{-2}\,s^{-1}}$, averaged over declination . This corresponds to a flux of $2 \times 10^{-8}\,\mathrm{cm^{-2}\,s^{-1}}$ integrated above 10 GeV. The most significant excess is 8 events observed on an expected background of 2.1, occurring at approximately 68 deg N dec, 21.1 hr R.A; for details see Hauschildt & Steele (2003). Unblinding the data collected in 2001, 2002 may reveal sources or confirm the consistency of the year 2000 sky-plot with statistical fluctuations on the atmospheric neutrino background.

With this search the AMANDA II detector has reached a high-energy effective telescope area of 25,000∼40,000 m^2, depending on declination. This represents an interesting milestone: sources with an E^{-2} spectrum should be observed provided the number of gamma rays and neutrinos are roughly equal as expected from cosmic ray accelerators producing pions (Alvarez-Muniz & Halzen 2002).

Overall, AMANDA represents a proof of concept for the kilometer-scale neutrino observatory, IceCube (Wissing 2003), now under construction. The detector is described elsewhere in this volume (Halzen 2003).

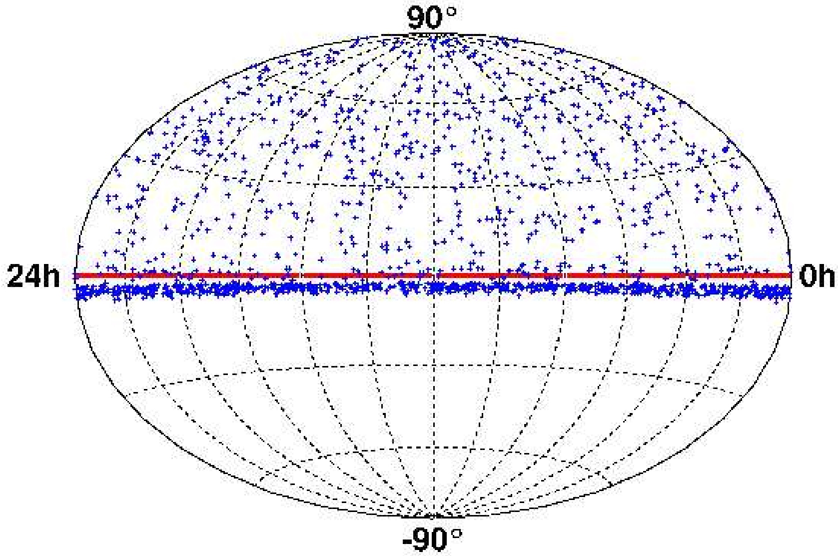

Figure 3. Skymap showing declination and right ascension of neutrinos detected by the completed AMANDA II detector during its first Antarctic winter of operation in 2000.

References

Ahrens, J. et al. (AMANDA Collaboration) 2003, Phys. Rev. Lett. 90, 251101, astro-ph/0303218

Alvarez-Muniz, J. & Halzen, F. 2002, Ap. J. 576, L33; Crocker, R. M. 2002, PhD thesis (University of Melbourne)

Andres, E. et al. (AMANDA Collaboration) 2001, Nature 410, 441; 2000, Astroparticle Physics 13, 1

Bahcall, J. N. & Waxman, E. 2001, Phys. Rev. D64, 023002

Gaisser, T. K. 2002, in Proceedings of the 31st International Conference on High Energy Physics, Amsterdam, The Netherlands, July 2002

Gaisser, T. K. 1997, astro-ph/9707283, talk presented at the OECD Megascience Forum, Taormina, Italy, 1997

Gaisser, T. K., Halzen, F. & Stanev, T. 1995, Phys. Rept. 258, 173 [Erratum 271, 355 (1995)], hep-ph/9410384

Halzen, F. 2003, these proceedings

Hauschildt, T. & Steele, D. 2003, in Proc. of the 28th International Cosmic Ray Conference, Tsukuba, Japan, August 2003

Karle, A. et al. (IceCube Collaboration) 2002, in Proc. of the XXth International Conference on Neutrino Physics and Astrophysics, Munich, Germany, May 2002, astro-ph/020955

Wissing, H. 2003, PhD thesis (Humbold University, Berlin); Particle Astrophysics (in press) and http://icecube.wisc.edu/science/sci-tech-docs/

Highlights of Astronomy, Vol. 13
International Astronomical Union, 2003
O. Engvold, ed.

Neutrinos from Pulsar Environments

A. Melatos

School of Physics, University of Melbourne, Parkville VIC 3010, Australia

Abstract. Recent calculations of the neutrino fluxes and spectra from pulsar magnetospheres and wind nebulae are reviewed. The neutrinos, produced in pp and $p\gamma$ collisions via pion decays, are a signature of TeV ions accelerated electrostatically in the magnetosphere, in the wind termination shock (Fermi), or in the wind neutral sheet (wave surfing and/or reconnection). The fluxes and spectra are related to the energy and density of the accelerated ion beam and the densities of the target species, thereby constraining ion-loaded pulsar wind models originally developed to explain the variable wisps in pulsar-driven supernova remnants. The neutrino signal may be detectable by km^2 telescopes (e.g. IceCube) and is correlated with TeV γ-ray emission. Related sources are also reviewed, such as early-phase post-supernova pulsar winds, pulsar-driven γ-ray-burst afterglows, and accreting neutron stars. The possibility of long baseline oscillation experiments, to search for fine splitting of neutrino mass eigenstates and non-radiative neutrino decays, is noted.

1. Relativistic Ions

Rotation-powered pulsars emit thermal neutrinos, via the modified URCA reaction, and non-thermal neutrinos, via the hadronic decay of relativistic protons (or heavier ions) accelerated electrically by the star. The thermal neutrino luminosity, $L_\nu \approx 10^{39}(T_c/10^9\,\mathrm{K})^8\,\mathrm{erg\,s^{-1}}$, where T_c denotes the core temperature (Shapiro & Teukolsky 1983), is emitted mainly at energies $E_\nu \approx k_B T_c \lesssim 1\,\mathrm{MeV}$, below the operating band of next generation (km^2) neutrino telescopes. It is not discussed further here. The non-thermal L_ν depends on the ion acceleration efficiency and density of the environment. The ion source is the pulsar itself, which acts as a unipolar inductor, developing a voltage $\Phi = B\Omega^2 R^3/c^2 \approx 3\times 10^{15}(B/10^{12}\,\mathrm{G})(\Omega/10^2\,\mathrm{rad\,s^{-1}})^2\,\mathrm{V}$ across its polar cap, where B is the polar magnetic field and Ω is the angular frequency of the star. As Φ exceeds the work function at the surface, ions are emitted freely at the Goldreich-Julian rate $\dot{N}_i = \dot{N}_{GJ} = c\Phi/Ze$, so that the magnetospheric charge density shorts out $\mathbf{E}$ parallel to $\mathbf{B}$ (e.g. Arons 2003). In addition, an electron-positron ($e^\pm$) outflow is generated in pair cascades in charge-starved regions near the polar cap and light cylinder (outer gap), with $\dot{N}_\pm = \kappa_\pm \dot{N}_{GJ}$ and $10 \lesssim \kappa_\pm \lesssim 10^3$.

Four pulsar-driven supernova remnants (plerions) have now been detected as unpulsed TeV γ-ray sources by atmospheric Cerenkov imaging telescopes: the Crab (Weekes et al. 1989; Aharonian et al. 2000), PSR B1706−44 (Kifune et al. 1995), Vela (Yoshikoshi et al. 1997), and PSR B1509−58 (Sako et al. 2000). The differential energy spectrum of each object is fitted by $dN/dE \propto E^{-2.5\pm 0.2}$ (units: $\mathrm{cm^{-2}\,s^{-1}}$), with luminosity $\lesssim 10^{-2} I\Omega\dot{\Omega}$ above 1 TeV. The γ rays are unlikely to originate from the magnetosphere, as they are unpulsed. Instead, they have been attributed to hadronic processes involving accelerated ions in the pulsar wind nebula (PWN; Amato, Guetta & Blasi 2003; Bednarek 2003), or to inverse Compton scattering if the magnetic field is below equipartition (Bednarek & Protheroe 1997; Bednarek 2003; Guetta & Amato 2003).

Independent evidence for ion acceleration in pulsars is provided by the arc-like, sub-arsecond features (wisps) observed in the optical and X-rays in several PWNe (Hester et al. 1995, 2002; Gaensler et al. 2002). The wisps are observed to expand as circular ripples (pattern speed $\approx 0.5c$), whose spacing is comparable to the Larmor radius $r_{\rm L}$ of protons with Lorentz factor $\gamma_p \gtrsim 10^5$ in the magnetic field $B_s \approx 0.3\,{\rm mG}$ downstream from the termination shock in the equatorial plane of the pulsar wind. At the magnetic step of the shock, cold upstream ions gyrate forward in an $\mathbf{E}\times\mathbf{B}$ drift, compressing the frozen-in magnetic field into spikes which react back to marshal the ions quasiperiodically into bunches. The bunches (wisps) propagate downstream for several $r_{\rm L}$ before thermalizing by absorbing self-emitted magnetosonic waves (Gallant & Arons 1994; Spitkovsky & Arons 2004). The theory correctly predicts the wisp luminosity (including Doppler boosting), spacing, variability, and pattern speed for $\dot{N}_p = \dot{N}_{\rm GJ}$, $\gamma_p = 4\times 10^5$, $\kappa_\pm = 10^3$, and $\dot{N}_p\gamma_p m_p c^2 \approx 0.2 I\Omega\dot{\Omega}$ for the Crab. An alternative (steady-state) model explains the wisps as intersecting internal shocks in the backflow from a mono-polar wind (Komissarov & Lyubarsky 2003).

2. Neutrino and Gamma-Ray Fluxes and Spectra

Relativistic protons yield neutrinos in two ways (Alvarez-Muñiz & Halzen 2002): (i) inelastic collisions with an ambient cold proton, e.g. in the supernova remnant ($pp \to \pi^0\pi^\pm$, cross-section $\sigma_{pp} \approx 0.1\sigma_{\rm T}$), where the pions share the initial energy equally; and (ii) photo-meson production via a delta resonance ($p\gamma \to \Delta \to \pi^0 p$ or $\pi^0 n$, cross-section $\sigma_{p\gamma} \approx 0.01\sigma_{\rm T}$), where $E_p E_\gamma \approx m_\Delta^2 \approx 0.3\,{\rm GeV}^2$. The neutral pions decay into TeV γ rays ($\pi^0 \to \gamma\gamma$), which are observable, whereas the charged pions decay into muons then neutrinos (e.g. $\pi^+ \to \mu^+\nu_\mu \to e^+\nu_e\overline{\nu}_\mu\nu_\mu$). This suggests a clean observational test: if neutrinos from pulsars are produced by hadronic processes, the observed γ-ray and μ-neutrino fluxes ought to be related by $\int dE_\gamma\, E_\gamma(dN_\gamma/dE_\gamma) = k\int dE_\nu\, E_\nu(dN_\nu/dE_\nu)$, with $k=1$ for pp interactions and $k=4$ for $p\gamma$ interactions in the Δ-resonance approximation (Alvarez-Muñiz & Halzen 2002). The lower and upper bounds of dN_γ/dE_γ and dN_ν/dE_ν are set in terms of E_p by the collision kinematics.

The neutrino luminosity for pp collisions is given by $L_\nu = \frac{1}{3}\dot{N}_p E_p {\rm min}(1,\tau_{pp})$, where the optical depth satisfies $\tau_{pp} \gtrsim 10^{-5}$ for $3M_\odot$ of ejecta in the filaments of the supernova remnant (Amato et al. 2003) and one has $\dot{N}_p E_p \approx 0.2 I\Omega\dot{\Omega}$. The luminosity is reduced for $p\gamma$ collisions ($E_\nu < 0.05 E_p$), when the synchrotron or inverse Compton lifetime of μ^+ or π^+ is shorter than the decay lifetime (Amato et al. 2003), and by flavor oscillations. The predicted neutrino event rate at Earth is given by the neutrino flux multiplied by E_ν^{-1} times the probability $P_{\nu\mu}$ that a neutrino converts to a muon in the detector, integrated over E_ν and detector area (Alvarez-Muñiz & Halzen 2002). In the regime $1 \le E_\nu/{\rm TeV} \le 10^2$, where planned km^2 detectors will be most sensitive, one finds $P_{\nu\mu} \propto E_\nu$.

3. Pulsar Magnetospheres

Neutrino and γ-ray emission from charged heavy nuclei N accelerated by magnetospheric potentials in an outer gap was analyzed by Bednarek & Protheroe (1997). The heavy nuclei photodisintegrate via $N\gamma \to Nn$ in the local MeV photon bath ($n_\gamma \approx 10^{15}\,\mathrm{cm}^{-3}$; Chiang & Romani 1994), yielding $e^\pm$ which quench the gap potential; Fe nuclei disintegrate for $\gamma_\mathrm{i} \gtrsim 10^3$ and He nuclei for $\gamma_\mathrm{i} \gtrsim 10^{6.5}$ (Fig. 1 of Bednarek & Protheroe 1997). The neutrons then decay to relativistic protons which collide with photons or cold protons in the supernova remnant (§2). Protons are either trapped inside the nebula and cool adiabatically, or escape as neutrons (just after the supernova) and re-enter later as protons by diffusing through the tangled magnetic field ($\sim 5\,\mu$G) of the remnant. From Monte-Carlo simulations with initial spin periods 5–10 ms, nebula radii 1–2 pc, $\dot{N}_p = \dot{N}_\mathrm{GJ}$, and $\dot{N}_p E_p = 0.1 I\Omega\dot{\Omega}$, Bednarek & Protheroe (1997) predicted a ν_μ flux up to ~ 10 times above the background for a $1^\circ \times 1^\circ$ field of view.

4. Pulsar-Driven Supernova Remnants

Neutrino emission from hadronic processes in Crab-like PWNe was first proposed by Berezinskii & Prilutskii (1977) and has recently enjoyed a renaissance (Amato et al. 2003; Bednarek 2003). Guetta & Amato (2003) estimate the proton deceleration time as $t_{pp} \approx 10^7 (\rho_\mathrm{N}/M_\odot\,\mathrm{pc}^{-3})^{-1}\,\mathrm{yr}$ for pp collisions and $t_{p\gamma} \approx 10^{16}\,\mathrm{yr}$ for $p\gamma$ collisions; clearly, pp collisions dominate in PWNe. However, the density and location of the target protons (and hence t_{pp}) is uncertain; they reside in a cage of Rayleigh-Taylor filaments around the PWN, whose filling factor and magnetic field structure are poorly known (Hester et al. 1996).

As a PWN ages, the p and $e^\pm$ spectra evolve due to adiabatic and synchrotron cooling, $\nabla\mathbf{B}$ escape, and inverse Compton scattering (Amato et al. 2003; Bednarek 2003). Moreover, $I\Omega\dot{\Omega}$ decreases as the pulsar spins down, and the magnetic field evolves in concert. It is found that synchrotron losses always dominate inverse Compton, if the thermal radiation field is weak (Beall & Bednarek 2002), reducing the $p\gamma$ (but not pp) efficiency for $t_\mathrm{N} \gtrsim 10^{-2}\gamma_p\,\mathrm{yr}$ to less than ≈ 0.3 (Fig. 4 of Amato et al. 2003), where t_N is the nebula age. Hence the theoretical Crab neutrino spectrum exceeds the detection threshold for IceCube and the $2^\circ \times 2^\circ$ sky background for $E_\nu \le 10^2\,\mathrm{TeV}$ provided one has $\gamma_p/t_\mathrm{N} \gtrsim 10^4\,\mathrm{yr}^{-1}$ (depending on the filling factor of the filaments; Amato et al. 2003), and the theoretical γ-ray flux for $E_\gamma \le 10^2\,\mathrm{TeV}$ (where inverse Compton is appreciable; Aharonian et al. 2000) slightly exceeds existing measurements in the regime $10^5 \le \gamma_p \le 10^6$ implied by wisp models (Arons & Spitkovsky 2004). That is, the Crab should yield ~ 10 events per yr in a km^2 detector for $10^4 \le \gamma_p \le 10^7$ (Amato et al. 2003), as should Vela and PSR B1509−58 (Guetta & Amato 2003). However, Bednarek (2003) cautions against scaling the neutrino flux in proportion to the observed γ-ray flux without correcting for inverse Compton, and claims that Vela, PSR B1509−58, PSR J0205+6449 and PSR B1951+32 are not detectable by km^2 detectors; Vela's event rate is comparable to the Crab but peaks at $< 10\,\mathrm{TeV}$ where the background is high.

Relativistic protons scatter off Alfvén waves in the PWN. How important is this? Scattering requires gyroresonance, i.e. $\omega \pm \Omega_{\rm ci} - k_{\|}c = 0$, with $\omega = k_{\|}V_{\rm A}$, where $\Omega_{\rm ci}$ is the ion gyrofrequency and $V_{\rm A}$ is the Alfvén speed. In the Crab ($B = 0.3\,{\rm mG}$, $V_{\rm A} = 10^7\,{\rm cm\,s^{-1}}$, $\gamma_p = 10^6$), one obtains $2\pi/k_{\|} = 0.02\,{\rm pc} \ll R_{\rm N}$ and $\omega < \Omega_{\rm ci}$ (Alfvénic regime). The pitch-angle-averaged scattering time is then $t_{p{\rm A}} = cP^2/2\pi^2(Ze)^2 W_{\rm a}(k_{\rm r})$, where P is the proton's momentum and $W_{\rm a}(k_{\rm r})$ is the energy per unit wavenumber per unit volume at the resonant wavenumber $k_{\rm r}$; that is, $t_{p{\rm A}} \approx 2 \times 10^1\,{\rm s} \times$ (fraction of $I\Omega\dot{\Omega}$ converted to Alfven waves).

5. Wave-Like Pulsar Winds

The wind of a rotation-powered pulsar is wave-like, not steady-state: the conduction current ($nec \propto r^{-2}$) cannot shield the displacement current ($\Omega E/4\pi \propto r^{-1}$) induced by the rotating magnetic dipole (Coroniti 1990; Melatos & Melrose 1996). The wave can be an entropy mode, where alternating stripes of magnetic field separated by neutral sheets are convected with the flow (Coroniti 1990; Lyubarksy & Kirk 2001), or a super/subluminal mode with a corrugated, equatorial current sheet (cf. transverse, electromagnetic oscillations in an unmagnetized plasma; Melatos 1998; Arons 2003). Like the vacuum rotator, the wind is circularly polarized along the rotation axis, where the optical/X-ray jets and knots lie in PWNe, and linearly polarized in the equatorial plane, where the wisps and torus lie (Hester et al. 2002; Gaensler et al. 2002).

Protons can be accelerated in three ways in the wind. First, they feel the ponderomotive force from the oscillating $\mathbf{E}$ in the relativistic plasma wave, attaining $\gamma_p \approx (1 + e^2E^2/m_p^2c^2\Omega^2)^{1/2} \gtrsim 10^5$ in one wave period and implying a kinetic-dominated flow ($\sigma_{\rm s} \approx 10^{-3}$) at the termination shock (radius $r_{\rm s}$), in accord with observations (Melatos & Melrose 1996; Melatos 1998; Arons 2003). Second, in the entropy mode, protons are heated by tearing-mode reconnection in the neutral sheets (internal gas pressure $\propto r^{-8/3}$, external magnetic pressure $\propto r^{-2}$; Coroniti 1990) at radii $r \gtrsim 2\kappa_{\pm}c/\Omega \ll r_{\rm s}$. Heating reaccelerates the flow and dilates the reconnection rate, so that it is incomplete at $r_{\rm s}$ (Lyubarksy & Kirk 2001). A detailed analysis of the tearing mode dynamics is needed to determine the relative efficiency of p and $e^{\pm}$ acceleration. Third, if the wind of the oblique rotator approaches the split-monopole geometry of the force-free, aligned rotator ($\rho\mathbf{E}+\mathbf{J}\times\mathbf{B} = 0$), it can be shown that the wind accelerates due to $\mathbf{E}\times\mathbf{B}$ drift, with $v_E/c = \mathbf{E}\times\mathbf{B}/B^2$, $\gamma_E = (1+x^2)^{1/2}$, and $x = (r\Omega/c)\sin\theta$, where θ denotes the colatitude (Contopoulos & Kazanas 2002). Ions surf the field lines because their (small) inertia induces a polarization drift velocity $\perp \mathbf{B}$, given by $mc\mathbf{B} \times d(\gamma\mathbf{v}_E)/dt/eB^2$. Beyond $r \sim 10^6 c/\Omega \ll r_{\rm s}$, where $\sigma \leq 1$, the force-free condition breaks down and ponderomotive acceleration in the wave takes over, yielding a maximum proton energy $e\Phi/(1 + 2\kappa_{\pm}m_e/m_p)$ (Arons 2003).

An appealing application of wind acceleration is to magnetars, ultramagnetized objects ($B \sim 10^{14}\,{\rm G}$) born spinning near centrifugal break-up ($\Omega \sim 10^3\,{\rm rad\,s^{-1}}$), with $\Phi \sim 10^{22}\,{\rm V}$. Arons (2003) predicts a broken proton injection spectrum (E^{-1}/E^{-2} below/above the voltage $\sim 3\times10^{20}\,{\rm V}$ when electromagnetic and gravitational wave losses balance) that escapes due to Rayleigh-Taylor disruption of the supernova remnant, with a GZK cutoff (flattening) at $10^{20}\,{\rm eV}$ at Earth if gravitational wave losses do (do not) dominate.

6. Alternative Sources and Applications

Several other pulsar-driven neutrino sources have been postulated. Beall & Bednarek (2002) argued that an early-phase supernova driven by a 10^{12} G pulsar can accelerate Fe nuclei which then photodisintegrate due to collisions with thermal photons from the hot ejecta, giving a signal detectable by a km^2 telescope above 1 TeV within ~ 1 hr of birth. Similarly, Guetta & Granot (2003) proposed a pulsar-driven γ-ray burst where protons are Fermi accelerated in mildly relativistic internal shocks ($dN_p/dE_p \propto E_p^{-2}$) and $p\gamma$ collisions dominate. Anchordoqui et al. (2003) argued that accreting neutron stars (e.g. A0535+26) develop potentials $\Phi_{\rm a} \sim 10^{14}$ V in the layer between the Alfvén and inner disk radii, with target protons and keV photons in the disk, although they note that an improved calculation of the electrodynamics is required.

Nonthermal pulsar neutrinos may also enable new tests of the Standard Model. Pulsars offer lengthy ($\sim$ kpc) baselines for oscillation experiments that are sensitive to nonstandard physics, e.g. splitting of mass eigenstates, majoron processes. Moreover, by measuring the relative fluxes of ν_e, ν_μ, and ν_τ arriving at Earth, it is possible to constrain the flavor mix at the source and test for simple neutrino decay scenarios (e.g. $\nu \rightarrow$ light gauge boson) that violate CPT symmetry (Barenboim & Quigg 2003).

Acknowledgments. I am indebted to Dafne Guetta for a lucid and comprehensive tutorial on hadronic physics in pulsar environments.

7. References

Aharonian, F. A., et al. 2000, ApJ, 539, 317
Alvarez-Muñiz, J., & Halzen, F. 2002, ApJ, 576, L33
Amato, E., Guetta, D., & Blasi, P. 2003, A&A, 402, 827
Anchordoqui, L. A., et al. 2003, ApJ, 589, 481
Arons, J. 2003, ApJ, 589, 871
Barenboim, G., & Quigg, C. 2003, Phys.Rev.D, 67, 073024
Beall, J. H., & Bednarek, W. 2002, ApJ, 569, 343
Bednarek, W. 2003, A&A, 407, 1
Bednarek, W., & Protheroe, R. J. 1997, Phys.Rev.Lett, 79, 2616
Berezinskii, V. S., & Prilutskii, O. F. 1977, Soviet Ast., 3, L79
Chiang, J., & Romani, R. W. 1994, ApJ, 436, 754
Contopoulos, I., & Kazanas, D. 2002, ApJ, 566, 336
Coroniti, F. V. 1990, ApJ, 349, 538
Gaensler, B. M., et al. 2002, ApJ, 569, 878
Gallant, Y. A., & Arons, J. 1994, ApJ, 435, 230
Guetta, D., & Amato, E. 2003, Astropart. Phys., 19, 403
Guetta, D., & Granot, J. 2003, Phys.Rev.Lett, 90, 201103
Hester, J. J., et al. 1995, ApJ, 448, 240
Hester, J. J., et al. 1996, ApJ, 456, 225
Hester, J. J., et al. 2002, ApJ, 577, L49
Kifune, T., et al. 1995, ApJ, 438, 91
Komissarov, S. S., & Lyubarsky, Y. E. 2003, MNRAS, submitted
Lyubarsky, Y., & Kirk, J. 2001, ApJ, 547, 437

Melatos, A. 1998, Mem. Soc. Ast. It., 69, 1009
Melatos, A., & Melrose, D. B. 1996, MNRAS, 279, 1168
Sako, T., et al. 2000, ApJ, 537, 422
Shapiro, S. L., & Teukolsky, S. A. 1983, Black Holes, White Dwarfs, and Neutron Stars (New York: Wiley)
Spitkovksy, A., & Arons, J. 2004, ApJ, in press
Weekes, T. C., et al. 1989, ApJ, 342, 379
Yoshikoshi, T., et al. 1997, ApJ, 487, L65

Highlights of Astronomy, Vol. 13
International Astronomical Union, 2003
O. Engvold, ed.

Some Aspects of Galactic Cosmic Ray Acceleration

Yousaf Mahmood Butt
Harvard-Smithsonian Center for Astrophysics, 60 Garden St., Cambridge, MA, USA

Abstract. I give a synopsis of two aspects of the Galactic Cosmic Ray (GCR) acceleration problem: the importance of the medium energy gamma-ray window, and several specific astrophysical sources which merit further investigation. NOTE: figures may be found in the on-line version only: astro-ph/0309758.

1. INTRODUCTION

Cosmic rays continually rain down on our heads, but we have virtually no better idea where they come from than did investigators fifty years ago (eg. Shklovskii, 1953). Gamma-ray astronomy has been the tool of choice to investigate their origin(s) since a local overdensity of freshly accelerated GCRs are expected to produce co-spatial high energy (gamma-ray) photons. Of course, the proper interpretation of such gamma-ray data (specifically, whether electrons or nuclei are generating the detected radiation) requires as broad a multi-wavelength coverage as practical: gamma-ray data is necessary but not sufficient to prove the existence of a GCR acceleration site. Unfortunately, sufficient multi-wavelength coverage of requisite fidelity is often simply unavailable. As outlined by Francis Halzen in this session, now neutrino astronomy also appears poised to contribute to GCR research in the 'non-wavelength' window.

Despite almost 40 years of concerted effort in gamma-ray astronomy, not a single source of nucleonic GCRs has yet been firmly identified. The main reason for this is the rather marginal spatial resolution of virtually all gamma-ray instrumentation flown, which results in severe source confusion - eg. are the gamma-rays coming from a Supernova Remnant (SNR) shock or a related, or unrelated, pulsar? The latest ground-based stereo Cherenkov telescopes and the next-generation orbiting GeV detectors promise to finally overcome this limitation.

Currently, there are two favored theoretical mechanisms for accelerating GCRs, and both invoke shocks: either the shocks of isolated SNRs in the $\sim 10^4 - 10^5$ yrs after explosion (eg. Drury et al., 2001; see Torres et al., 2003 for a recent review and Plaga, 2002 for an alternative hypothesis); or, the cumulative shocks of massive stars and/or multiple SNRs in massive stellar associations (or after evolution, 'superbubbles') which last $\sim 10^7$ yrs (eg. Cesarsky & Montmerle, 1983; Bykov 2001). It is certainly also possible that both mechanisms could be operating simultaneously in the Galaxy. Although as a class only SN appear to have the required power input to the ISM to explain the local energy density of GCRs, it is unclear whether the physical mechanism for accelerating nucleonic GCRs requires that multiple SNRs be embedded in a superbubble or stellar cluster. Interestingly, although the bulk of SN are expected to occur in superbubbles, many more individual, isolated, SNRs have been identified and cataloged than superbubbles.

2. THE IMPORTANCE OF THE MeV WINDOW

Although the acceleration of high energy CRs in a given source cannot be proven without the detection of similarly high energy (GeV–TeV, and even higher energies) radiation localized with the source, the lower-energy MeV window is still very important in discriminating the nature of the particles generating the detected gamma-rays: electrons vs. nuclei. This is because in the case of a hadronic origin there is a plateau expected in the gamma-ray spectrum in the approx. 1–100 MeV range. Such a discontinuous 'plateau-ing' of the photon spectrum is not expected from purely leptonic bremsstrahlung or inverse-Compton emissions. The inability to distinguish the nature of the particles generating the detected gamma-rays has been a major stumbling block in nucleonic GCR origin studies (eg. see Reimer & Pohl, 2002 and Butt et al., 2002). High signal-to-noise data in the soft-gamma window greatly simplifies our ability to assign a hadronic vs. leptonic origin to the detected gamma-rays (Fig. 1). This is a direct consequence of characteristic shape of the hadronic pion-decay spectrum: in fact, were it not for the existence of, and emission from, hadronically-generated secondary electrons, we would expect a highly distinctive, symmetrical pion 'hump' centered at 67.5 MeV (=half the pion rest mass) in the case that hadrons were producing the gamma-rays (eg. Schlickeiser 1982). Note that in Schlickeiser's paper a steady-state leptonic population was assumed so that the expected plateau in SNRs/stellar associations' hadronic emission will be even more distinctive than shown in that study as steady-state has not been reached in the typical lifetimes of those objects, and thus less secondaries are present. Though the INTEGRAL satellite covers the 1-10 MeV bandpass with relatively good spatial resolution, there is unfortunately a gap in the important approx. 10-100 MeV range. (The > 50 MeV bandpass will be covered by AGILE and GLAST instruments in the near future.) Orbiting detectors, such as the proposed MEGA instrument (Kanbach et al., 2003) would thus be very useful for GCR studies by filling-in this bandpass gap.

3. SPECIFIC SOURCES

Below I provide an incomplete list of sources which would be useful to observe in gamma-rays as well as other wavelengths. I have divided the sources into three categories: isolated SNRs, stellar clusters/superbubbles, and extragalactic starburst galaxies. There are many other sources worth investigating: the list is not exhaustive.

I. Isolated Galactic Supernova Remnants (SNRs)

a. G347.3-0.5 (RX J1713.7-3946)

The SNR G347.3-0.5 (RX J1713.7-3946) and its environs are amongst the best laboratories for investigating shock-driven particle acceleration processes in our Galaxy. Photons spanning 17 orders of magnitude in frequency, from radio through TeV range, have been reported as being plausibly associated with this

SNR, or with its putative shock-molecular cloud interactions (Fig 2). Deeper radio observations of this source would help pin down the contributions of electrons vs. nucleons to the gamma-ray emission. High resolution mm observations of $1 \rightarrow 0$, $2 \rightarrow 1$, and higher rotational level transitions of CO would help better determine the cloud excitation, and possibly, also whether the cloud shape 'meshes' with the SNR shock front. Similarly, high spatial resolution (CHANDRA) X-ray observations are needed towards the N of the remnant to image whether indeed the shock front and clouds are interacting. This is important in settling whether the clouds and the SNR are interacting, which is the key in determining the distance to the SNR. (The distance to the SNR is currently assumed be the same as the clouds with which it is thought to be interacting). Gamma-ray observations would also help narrowing down the rather large EGRET error box associated with this source. Specifically, one would like to know whether gamma-ray emission is consistent with the location of the molecular clouds, and whether it's spectrum agrees with a hadronic origin. The recent report of a hard ASCA source (AX J1714.1-3912) seen immediately adjacent to the SNR rim (Uchiyama et al., 2002) and superposed with 'cloud A' lends particular urgency and significance to multi-wavelength observations of this highly non-thermal SNR.

b. The SNRs W28 (G6.4-0.1); W44 (G34.7-0.4); and W66 (gamma-Cygni, G78.2+2.1) All three of these SNR-EGRET gamma-ray source coincidences have been discussed extensively in the literature, and are reviewed in detail by Torres et al. (2003). These SNRs all appear to be in interaction with neighboring massive molecular clouds which may explain the detected gamma-ray emissions; however, all three gamma-ray sources are also in coincidence with energetic pulsars/compact objects which could, alternatively - or, in addition - be generating the gamma-rays. Similar figures as Fig. 2 above for all three cases are available in Torres et al. (2003) [see Fig.'s 21, 22, 25, 28 therein], and are not reproduced here in the interest of brevity. Even before AGILE and GLAST are launched, INTEGRAL observations of these SNRs are needed to better localize the gamma-ray emission region(s). Such data will simultaneously greatly aid in clarifying the nature (hadronic vs. leptonic) of the emissions in these 3 important SNRs by providing a MeV spectrum (eg. see Fig. 1). Although not detected in the TeV range with the previous generation of Cherenkov telescopes (eg. Buckley et al., 1997), deeper observations with the updated arrays would be of great use.

c. RCW 86 (MSH 14-63, G315.4-2.3)

RCW 86 is a bright shell-like SNR with non-thermal X-ray and radio emission which is especially strong towards the SW, where there is also evidence of interaction with a molecular cloud (eg. Borkowski et al., 2001; Rosado et al., 1996). In fact, the intensity of the the non-thermal X-ray emission from the SW shell is even brighter than that of SN 1006. RCW 86 also appears to be associated with a neighboring OB association (Westerlund, 1969). Very recently the CANGAROO collaboration has reported the detection (at the approx. 4 sigma level) of TeV range gamma-rays from the non-thermal X-ray bright southwest shell at a level of $\sim (3 \pm 0.7)10^{-12}$ photons cm^{-2}sec^{-1} (Watanabe et al., 2003). Vink et al. (2000) and Gvaramadze & Vikhlinin (2003) also report the presence of point-like X-ray sources towards the same SW shell. Data in the INTEGRAL wave band, and at higher energies, of this SNR will be useful to test whether there is associated MeV-range gamma-ray emission from the SW shell; again, the spectrum of such putative emission will greatly aid in discriminating the origin of the high-energy flux. Due to their high spatial resolution, JEM-X (and IBIS) data will be especially useful in examining whether it is the point-like sources in the SW or rather the extended shock there that is generating the gamma-rays.

d. Monogem Ring SNR/PSR B0656+14

The Monogem Ring is a very large (20 degree diameter), bright SNR with a young radio pulsar PSR B0656+14 projected virtually at its geometric center (see Fig. 1 in Thorsett et al., 2003 for an X-ray mosaic image). Very recently, Thorsett et al. (2003) have convincingly argued that the pulsar and the SNR are indeed related (contrary to some previous studies), and that this SNR - by itself - may be responsible for the existence of the 'knee' in the GCR spectrum at $\sim 3PeV$(310^{15}eV). Indeed, Erlykin & Wolfendale (1997, 2003) already theorized that a single SNR of age 100kyr and 325pc from earth could by itself explain the knee feature - these parameters agree surprisingly well with those of the Monogem Ring SNR. In contrast to the previously mentioned SNRs in this presentation there is no high-energy EGRET source or reports of TeV emission associated with this SNR. However, this may not be surprising given its large size which would tend to 'wash-out' the signal due to the integrated background over the large SNR region.

II. Galactic OB Associations/Superbubbles

a. Cygnus OB2

Cyg OB2 is the most massive OB association known in the Galaxy, thought to contain in excess of 2500 OB type stars (Knoldseder 2002). Indeed, Hanson (2003) mentions several new massive star members in this association which were previously unknown due to the heavy extinction in the Cygnus direction. Recently, the HEGRA Chrenkov array group has reported a steady and extended TeV-range gamma-ray source within this association (TeV J2032+4032; Aharonian et al., 2002). An EGRET source, 3EG 2033+4118, and a GeV source are coincident with, and nearby, the TeV source, respectively. We have carried out preliminary CHANDRA and VLA observations of this intriguing TeV source and have argued that the most likely explanation is that nuclei (rather than electrons) accelerated to high energies are responsible for the gamma-ray emissions (Butt et al., 2003). If confirmed by future observations, such a scenario would strongly support a stellar association/superbubble origin of GCRs, as has been theoretically argued for some time (eg. Cesarsky & Montmerle, 1983; Bykov, 2001; and Parizot, 2002).

b. RCW 38 & NGC3603

I group these two stellar clusters together since recent CHANDRA observations have found evidence for hard, diffuse X-ray emission associated with both. Diffuse non-thermal X-ray emission from the southern stellar cluster RCW 38 was found in a recent 100 ksec CHANDRA observation (Wolk et al., 2002). This is one of the brightest HII regions at radio wavelengths (eg. Wilson et al., 1970), and is a natural candidate for deeper multi-frequency observations. The X-ray emission fills the center of a radio ring, reminiscent of some shell-type SNRs (Fig 3) and is very intriguing in the context of a young cluster/HII region.

If hard X-ray/gamma-ray emission is discovered superposed to the non-thermal X-rays, this would be a very significant result and would argue strongly in favor of collective shocks from the young stars accelerating GCRs to very high energies as proposed by, eg., Cesarsky & Montmerle (1983). (The age of the cluster is too young for there to be any 'contaminating' contributions from SNRs).

NGC 3603 is among the most massive and luminous visible starburst regions in the Galaxy. A recent 50 ksec CHANDRA observation has similarly found hard diffuse X-ray emission spatially coincident with the cluster core (Moffat et al., 2002). Those authors attribute this emission to the collective effects induced by the multiple, colliding stellar winds from the large population of massive stars in the region. As in the case of RCW38, if future observations find significant hard X-ray/gamma-ray emission then this would be a major result since it would again favor the collective stellar wind hypothesis of the origin of (at least some fraction of) GCRs. CHANDRA has also detected diffuse X-ray emission from the Omega (M17/W38) & Rosette Nebulae (NGC2237-2246) but since the emission is soft (Townsley et al., 2003 & Dunne et al., 2003), we do not anticipate that these objects are significant GCR accelerators.

III. The Starbursts NGC 253 & M82 (NGC 3034)

NGC 253 and M82 are amongst the brightest IR galaxies and are considered the prototypical starbursts. At 2.6 Mpc NGC 253 is also one of the closest. The OSSE spectrometer aboard CGRO has already positively detected continuum emission from NGC 253 up to 165 keV (Bhattacharya et al., 1994) and very recently the CANGAROO Cherenkov telescope collaboration has also reported a detection of this source in TeV-range gamma-rays (Itoh et al., 2003a). Although those authors have favored an explanation in terms of electronic IC emission (Itoh et al., 2003b), others have provided an alternative theory: that the high energy emission may be due to nucleonic cosmic rays accelerated to high energies via the collective effects engendered by the starburst activity (Romero & Torres, 2003; see also Vlk, 2003; and Sugai et al., 2003). In effect, these starbursts can be considered simply scaled-up versions of Galactic HII regions mentioned in the previous section. The goal of further multi-wavelength (in particular, gamma-ray) observations would be to confirm the soft gamma-ray emission from these starbursts and, in combination with future AGILE and GLAST datasets, to resolve the question over the type of particles producing the emission.

At 3.2 Mpc M82 is only slightly further away than NGC 253, and this alone may have been the cause of its non-detection in the OSSE datasets until 1994 (Battacharya et al., 1994). Note that M82 was detected by the HEAO A4 detector (Gruber & MacDonald, 1993), and future multi-wavelength studies are suggested.

This brief review benefited from discussions with A. Bykov, P. Benaglia, J. Combi, T. Dame, J. Drake, Ph. Durouchoux, M. Kaufman Bernad, P. Milne, F. Miniati, M. Pohl, O. Reimer, J. Rodriguez, G. Romero, M. Rupen, D. Torres, and S. Wolk. The support of the CHANDRA project, NASA Contract NAS8-39073, is gratefully acknowledged.

References

Aharonian, F., et al., 2001, A&A, 370, 112

Aharonian, F., et al., 2002, A&A, 393L, 37
Bhattacharya, D., et al., 1994, ApJ, 437, 173
Butt, Y., et al., 2001, ApJ, 562L, 167
Butt, Y., et al., 2002, Nature 418, 499
Butt, Y., et al., 2003, ApJ, accepted, astro-ph/0302342
Bykov, A., 2001, SSRv, 99, 317
Borkowski, A., et al., 2001 ApJ, 550, 334
Cesarsky, C., & Montmerle, T., 1983, SSRv, 36, 173
Drury, L., et al., 2001, SSRv, 99, 329
Dunne, B., et al., 2003, ApJ, 590, 306
Enomoto, R., et al., 2002, Nature 416, 823
Erlykin, A., & Wolfendale, A., 1997, J. Phys. G, 23, 979
Erlykin, A., & Wolfendale, A., 2003, J. Phys. G, 29, 709
Gruber, D., & MacDonald, 1993, priv. comm. as plotted in Figure 2 of Bhattacharya et al., 1994
Gvaramadze, V. V., & Vikhlinin, A. A., 2003, A&A, 401, 625
Hanson, M., 2003, ApJ in press, astro-ph/0307540
Hartman, R. C., et al., 1999, ApJS, 123, 79
Itoh, C., et al., 2003a A&A, 402, 443I
Itoh, C., et al., 2003b, ApJ Lett, submitted, astro-ph/0301147
Kanbach, G., et al., 2003 (SPIE) X-Ray and Gamma-Ray Telescopes and Instruments for Astronomy. Edited by Joachim E. Truemper, Harvey D. Tananbaum. Proceedings of the SPIE, Volume 4851, pp. 1209-1220
Knodlseder, J., 2003 proceedings of the IAU Symp 212, A Massive Star Odessey from Main Sequence to Supernova, in press
Moffat, A., et al., 2002, ApJ, 573, 191
Plaga, R., 2002, New Astronomy, 7, 317
Parizot, E., 2002, in the Proceedings of the XXXVIIth RENCONTRES DE MORIOND meeting, Les Arcs, March 9-16, 2002.
Pfeffermann, E. & Aschenbach, B., 1996, Proc. 'Rntgenstrahlung from the Universe', eds. Zimmermann, H.U.; Trmper, J.; and Yorke, H.; MPE Report 263, p. 267-268
Plaga, R., 2002, New Astronomy, Volume 7, Issue 6, p. 317
Reimer, O., & Pohl, M., 2002, A&A, 390L, 43
Romero, G. & Torres, D., 2003, ApJ, 586L, 33
Rosado, M., et al., 1996, A&A, 315, 243
Schlickeiser, R., et al., 1982, A&A, 106L, 5
Shklovskii, I. S., 1953, Dokl. Akad. Nauk SSSR, 91, No 3, 475-478 (1953) [Library of Congress Translation n. RT-1495]
Slane, P., et al., 1999, ApJ, 525, 357S
Sugai et al., 2003, ApJ, 584L, 9
The, L. S., et al., 1997, In proc. of the 4th COMPTON symposium, April 27-30, 1997; astro-ph/9707086
Thorsett, S. E., et al., 2003, ApJ, 592L, 71
Torres, D., et al., 2003, Physics Reports, Vol. 382, No. 6, August 2003
Townsley, L., et al.,2003, ApJ in press, astro-ph/0305133
Uchiyama, Y., et al., 2002, PASJ, 54L, 73

Vink, J., et al., 2000, A&A, 362, 711

Volk, H., 2003 Invited paper presented at "The Universe Viewed in Gamma-Rays" held on 25-28 Sept. 2002 in Kashiwa Japan , astro-ph/0303078

Watanabe, J., et al., 2003, Proceedings of the 28th ICRC, pp. 2397-2400, in press

Westerlund, B. E., 1969, AJ, 74, 879

Wilson, T. L., et al., 1970, A&A, 6, 364

Wolk, S. et al., 2002, ApJ, 580L, 161

Highlights of Astronomy, Vol. 13
International Astronomical Union, 2003
O. Engvold, ed.

Overview of Interferometer Type Gravitational Wave Detectors

David E McClelland

Department of Physics, Faculty of Science, The Australian Naiotnal University, Canberra, 0200, Australia

Abstract. Within the next decade giant laser interferometers should detect gravitational waves. Here we present an overview of these instruments including both ground and spaced based antennae.

1. Introduction to Gravitational Waves

Gravitational waves, or ripples in the curvature of space-time, are predicted by Einstein's General Theory of Relativity. They are quadrupolar in nature and propagate at the speed of light. Their existence has been confirmed by observing the energy loss of the binary pulsar PSR1913+16 due to gravitational wave emission. Figure 1a shows measurements of the shift of periastron time as a function of time (Taylor & Weinberg 2000). The points are the measurements with error bars too small to show up on this plot. The curve is the prediction based on gravitational wave emission. Hulse & Taylor won a Nobel Prize for this work in 1993. Today, the direct detection of gravitational radiation remains a major goal of fundamental physics.

Gravitational waves (GW) are emitted by the most violent events in the universe, provided they exhibit some non spherical geometry. As summarized by Schutz in this volume, these include compact binary in spirals and mergers, supernovae, pulsars, stochastic sources such as the relic spectrum left over from the Big Bang and undiscovered events which have no electromagnetic signature. As depicted in Figure 1b, the GW spectrum covers many orders of magnitude. Ground based detectors such as LIGO (LIGO 2003) and VIRGO (VIRGO 2003) explore the audio spectrum from 10 Hz, whilst antennae in space such as LISA (LISA 2003), will be sensitive in the frequency range from 0.1 mHz to 1Hz.

2. Detection using Laser Interferometry

The most promising technology for gravitational wave detection is long baseline laser interferometry. A passing gravitational wave will alternately stretch then contract one arm of a Michelson interferometer whilst contracting then stretching the other arm. The problem is that the effect is extremely small: expressed as a relative length change, $\delta L/L$, it is of the order of 10^{-22}. Whilst for the ground based detectors, the interferometer arms contain mirrors to reflect light, LISA uses a transponder based system in which the incoming beam from a distant spacecraft is detected, the signal then used to phase lock a second laser, which sends light back to the first spacecraft.

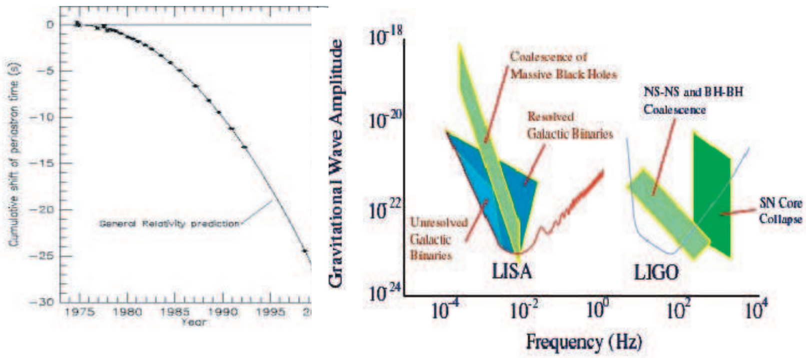

Figure 1. (a) Comparison between observations of the binary pulsar PSR1913+16 and the predictions of general relativity (b) Gravity wave frequency band.

Figure 2. (a) LIGO site Hanford Washington (b) VIRGO site Cascina.

2.1. Ground Based Detectors

Current Currently there are 4 funded mid to long baseline interferometer projects: the US LIGO Project (Figure 2a); the French/Italian VIRGO Project (Figure 2b); the German/British collaboration GEO600 (GEO 2003), and the Japanese Project TAMA300 (TAMA 2003). Based in the main part on technology developed early last decade, the first generation of large instruments (LIGO/VIRGO) are predicted to reach a spectral sensitivity of $10^{-22}/\sqrt{Hz}$ between 50 Hz and 1000 Hz by the year 2004. The optical layout for the long baseline first generation detectors is shown in Figure 3a. It consists of a standard Michelson interferometer with arm cavities to increase the sensitivity to phase change, and a power recycling mirror to build up the laser power thereby decreasing shot noise. As shown in Figure 3b, LIGO has already achieved a sensitivity on the order of $2.5\text{x}10^{-22}/\sqrt{Hz}$ at 200 Hz (LIGO 2003).

Typically such interferometers are limited at low frequency (below 40 Hz) by seismic noise (ultimately, below 4 Hz, noise from direct Newtonian coupling of the interferometers mirrors to the environment). Midband noise is thermal

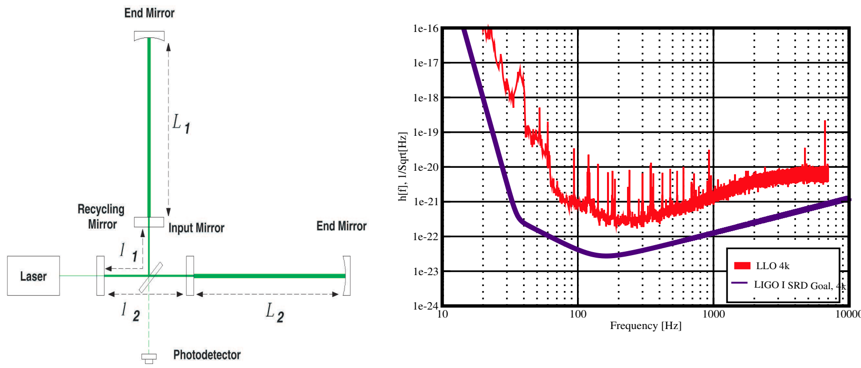

Figure 3. (a) Optical layout of first generation interferometers (b) Measured LIGO sensitivity curve 2003.

noise due to Brownian motion in the test masses and their suspension; above 200 Hz or so, photon shot noise combines with the averaging of the signal in the arm cavities to produce the roll up in response shown in Figure 1b.

The Future To ensure detection and the birth of gravitational wave astronomy the sensitivity of ground based interferometers must be improved by at least a factor of order 10, increasing the accessible volume of the universe by 1000 times. Toward this end, an international R&D effort on the four main detector subsystems (Laser and Optics; Configurations; Isolation, Suspension and Thermal Noise; Data Analysis) is underway. The key elements of an upgrade are (LSC 2003): an increase in laser power to greater than 100W; the adoption of a low thermal noise suspension system; the use of new materials such as sapphire for the test masses; the implementation of a signal recycling optical configuration; and possibly, cooling of the test masses (LCGT 2003).

3. Space based Detectors

The Laser interferometer Space Antenna (LISA) consists of 3 spacecraft (see Figure 4a) separated by 5 million km, in solar orbit trailing the earth by 20 degrees. The spacecraft roll on a cone of half angle 60 degrees with each moving in a slightly elliptic and inclined orbit around the sun. This configuration ensures that: the spacecraft face the sun at a constant angle giving a stable thermal environment; the orbits of the 3 spacecraft form a stable configuration; the center of the spacecraft triangle trails the earth by 20 degrees (or 50 million km) ensuring that the distance to the earth is quite stable for radio communication.

The LISA sensitivity curve (see Figure 1b) is low frequency limited by acceleration noise such as noise, not shielded by the drag free system, from gravitating masses on the craft when temperature changes their distances; charging of the test masses due to cosmic radiation; and residual gas in test mass housing. Shot noise limits the sensitivity between 1 mHz and 10 mHz with only a few nanowatts of light collected by the telescope on the distant space craft. The sensitivity rolls off at high higher frequencies (above 10 mHz) due to averaging out of the signal.

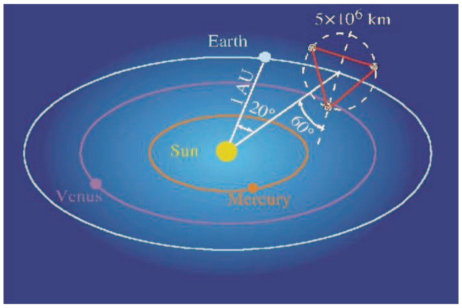

Figure 4. (a) orbit of the LISA spacecraft (b) ACIGA Facility, Gingin

LISA is planned for launch in 2011. Due to the enormous cost of the LISA mission (estimated at greater than A$2 billion in total), it is a combined ESA-NASA project. The development of space based trials of key LISA hardware is well advanced with the SMART-2 mission planned for launch in 2006.

4. Australia's role to date

The Australian Consortium for Interferometric Gravitational Astronomy (ACIGA) (ACIGA 2003) carries out research on all detectors subsystems. Its facility in Gingin in Western Australia (Figure 4b), at 80 m in length, is an ideal instrument for integrating next generation technologies associated with high power interferometry.

Acknowledgments. I would like to thank LIGO, VIRGO, GEO600, TAMA300 and LISA for making available picture and information for this overview.

References

Taylor, J.H. and Weinberg, J.M. 2000, unpublished
LIGO 2003, http://www.ligo.caltech.edu
VIRGO 2003, http://www.virgo.infn.it
LISA 2003, http://sci.esa.int/science-e/www/area/index.cfm?fareaid=27,
LISA 2003, http://lisa.jpl.nasa.gov
GEO 2003, http://www.geo600.uni-hannover.de
TAMA 2003, http://tamago.mtk.nao.ac.jp
LSC 1999, LSC White Paper on Detector R & D, http://www.ligo.org
LCGT 2003, http://www.icrr.u-tokyo.ac.jp/gr/gre.html
ACIGA 2003, http://www.anu.edu.au/Physics/ACIGA

Highlights of Astronomy, Vol. 13
International Astronomical Union, 2003
O. Engvold, ed.

A Window on the Ultra High Energy Universe

Pasquale Blasi

INAF/Osservatorio Astrofisico di Arcetri
Largo E. Fermi, 5 - I50125 Firenze, Italy

Abstract. Cosmic rays with energy around and in excess of 10^{20} eV have been detected. Despite the uncertainties associated with the difficult measurements of extremely low fluxes (about a particle per square kilometer per century) the same existence of such high energy cosmic rays raises important questions that deserve an appropriate answer. I briefly summarize here what are these questions and how to look for the answers.

1. The highest energy particles

In the eighty years of history of cosmic rays, there has been a constant search for the end of the cosmic ray spectrum. It has long been thought that this end of the spectrum would be determined by the highest energy that cosmic accelerators might be able to achieve. Despite this continuous search, no end was found. In 1966, right after the discovery of the cosmic microwave background (CMB), it was understood (Greisen 1966, Zatsepin and Kuzmin 1966) that high energy protons would inelastically scatter the photons of the CMB and produce pions. The concept of GZK cutoff was introduced and for the first time the end of the cosmic ray spectrum was associated with a physical process rather than with speculations on the nature of the accelerators. For the first time, the end of the cosmic ray spectrum was predicted to be at a well defined energy, around 10^{20} eV, where the so-called photopion production starts to be kinematically allowed. Forty years later, we are still seeking a confirmation that the cosmic ray spectrum has in fact such a flux suppression, although we understood that it is not a sharp cutoff. The two largest experiments currently operating in the energy range of interest, namely AGASA and HiRes, appear to have discrepant results in the highest energy end of the spectrum. While the data collected by the former appear to be consistent with the extension of the lower energy spectrum, the latter experiment suggests that the GZK feature is present in the data. In fact, it has been shown by De Marco, Blasi & Olinto (2003) that this discrepancy is only at the level of $\sim 2.6\sigma$ and even less significant (about 2σ) if a systematic error in the energy determination is introduced, something which in fact would also explain an offset between the fluxes as measured by the two experiments (. The required systematic error is of 30%, which can be shared between the two experiments, being compatible with the published estimates of such errors. More and better data are required to say the final word about the detection of the GZK suppression.

2. A short summary of the observations

The GZK feature should not be considered as the whole of the problem of UHECRs. Many questions remain open, whether the GZK feature is discovered or not. In this section I briefly summarize the main pieces of the puzzle of UHECRs:

Isotropy: The directions of arrival of the events at energies above $\sim 4\times10^{19}$ eV appear isotropically distributed in the sky. No immediate association with local structures (galactic disc, supergalactic plane) arises from the data.

Missing identification: No association of the observed events with known powerful nearby sources has been found. It is important to realize that this may be a problem only for the highest energy events, with energy higher than 10^{20} eV, for which the loss length is small and the sources are forced to be closeby. Even at 4×10^{19} eV the loss length is comparable with the size of the universe and it is therefore difficult to find a counterpart, in particular because of the poor angular resolution of current experiments.

Small Scale Anisotropies: The AGASA data show several doublets and triplets of events on angular scales comparable with the resolution of the instrument. The statistical significance of these multiplets is still the subject of some debate [see for instance (Finley and Westerhoff, 2003)], but if confirmed as not just the result of statistical fluctuations they could in fact represent the first evidence that UHECRs are accelerated in astrophysical point sources. This evidence would point against most so-called top-down models, in which the emission is truly diffuse.

The composition: At the highest energies the information about the chemical composition is so far very poor. A reanalysis of the Haverah Park inclined showers allowed to constrain the fraction of gamma rays at energy larger than 4×10^{19} eV to about 50% (Ave, et al. 2002). This is unfortunately still too weak a limit to disprove most top-down models.

3. What are the sources of UHECRs?

This is a clear example of a question that will long survive the detection or the lack of detection of the GZK feature. Many possibilities have been put forward in the literature but at present there is no clear indication in favor of one specific model. Rather than briefly listing a bunch of models that may in principle be responsible for the acceleration of UHECRs, I prefer here to discuss some lines of thought that might in fact bring us toward the identification of one or more classes of sources. Two problems have made this step very difficult: first, the lack of any identification of counterparts for the highest Fly's Eye event at energy 3×10^{20} eV (Bird, et al. 1993); second, the fact that from the energy budget in the form of UHECRs per unit volume it is not easy to know whether many sources with low luminosity or a few powerful sources are responsible for the acceleration of UHECRs. I will call this the *degeneracy problem*.

For the first obstacle, the situation has not changed in the last decades: on the other hand one should think of this situation as similar to what happened for gamma ray bursts (GRBs). Until a few years ago, GRBs were defined as gamma ray flashes with no counterpart at any wavelengths. After the identification of the afterglows, the situation has completely changed and much has been understood on the nature of the sources, although a complete picture is still lacking.

The *degeneracy problem* on the contrary has changed appreciably during the last few years, after the discovery of the small scale anisotropies in the directions of arrival of UHECRs. Although the statistical significance of these anisotropies is still matter of debate, their appearance forced us to think of them as a powerful tool to probe a distribution of point sources of UHECRs. Several authors pointed out that the number density of sources is related to the number of doublets and triplets of events, or in other words, to the two-point correlation function. Blasi & De marco (2003) showed that current observations favor sources with space density around $10^{-6} - 10^{-5}$ Mpc^{-3}, corresponding to an integrated luminosity above 10^{19} eV of $10^{42} - 10^{43}$ erg s^{-1}. This is the first time that the degeneracy between source density and luminosity of the single sources gets broken. It does not imply that the sources of UHECRs have been identified, but certainly selects some classes of sources. In (Blasi & De marco, 2003) it was shown that future experiments such as Auger and EUSO have the potential to accumulate enough statistics to improve on this front significantly. In fact, for the range of source densities mentioned above, it should be possible even to measure the spectrum of single nearby sources of UHECRs and infer their distance (Blasi & De Marco 2003).

The unambiguous detection of small scale anisotropies in the distribution of arrival directions would represent a strong argument in favor of astrophysical point sources and therefore against the alternative top-down scenarios.

4. What is the chemical composition of UHECRs?

The measurement of the chemical composition of UHECRs is difficult because of the low statistics of events and because of the large fluctuations in the shower development. Upcoming experiments such as Auger and EUSO represent clear improvements on the present situation, although the measurement of the composition will remain challenging.

The chemical composition represents a discriminant factor among different models for the generation of UHECRs. In some acceleration scenarios (e.g. Blasi, Epstein, & Olinto 2000) the composition is expected to be dominated by iron nuclei. On the other hand, in the context of top-down models, an appreciable fraction of the cosmic rays is expected to be in the form of gamma rays. More specifically, the spectrum generated in the case of decay of supermassive relic particles clustered in the galactic halo is expected to contain predominantly gamma rays. More dependent upon the details of the propagation is the composition in the case of topological defects, where absorption of gamma rays upon the diffuse extragalactic radio background becomes important. This background is unfortunately poorly known, because of the impossibility to measure this background from within the Galaxy, due to free-free absorption. The detection of gamma rays at the highest energies would be a smoking gun in favor of top-down scenarios and an unprecedented discovery of new physics in the early universe.

References

Abu-Zayyad, T., et al., preprint astro-ph/0208243

Ave, M., Hinton, J.A., Vazquez, R.A., Watson, A.A., Zas, E. 2002, Phys. Rev., D65, 063007

Bird, D.J., et al 1993, Phys. Rev. Lett., 71, 3401

Blasi, P. & De Marco, Astropart. Phys., in press (preprint astro-ph/0307067)

Blasi, P., Epstein, R.I., & Olinto, A.V. 2000, ApJ Lett., 533, 123

De Marco, D., Blasi, P., & Olinto, A.V. 2003, Astropart. Phys., 20, 53

Finley, C.B., & S. Westerhoff, preprint astro-ph/0309159

Greisen, K. 1966, Phys. Rev. Lett., 16, 748

Zatsepin, G.T., & and Kuzmin, V.A. 1966, Sov. Phys. JETP Lett., 4, 78

Takeda, M., et al., preprint astro-ph/0209422

Highlights of Astronomy, Vol. 13
International Astronomical Union, 2003
O. Engvold, ed.

Experimental Progress in the Direct Detection of Dark Matter

Nigel J.T. Smith

Particle Physics Department, CCLRC Rutherford Appleton Laboratory, Chilton, Didcot, Oxon, OX11 0QX, U.K.

Abstract. Several experimental approaches are being utilised for the direct detection of the hypothetical weakly interacting massive particle which may constitute the majority of the non-luminous component of the Galaxy. These experimental techniques exploit the coherent recoil of target nuclei during an interaction and include thermal, ionisation, scintillation and tracking detectors. The challenges associated with this detection, the techniques employed and the current status of these searches are reviewed.

1. Introduction

A standard cosmological model of the Universe has been evolving over the last few years from observational data collected at multiple wavelengths, incorporating different epochs of the Universe and different physics principles. One of the consequences of this emergent 'convergence' model is that up to 90% of the matter in the Universe is in the form of non-relativistic, non-baryonic, non-luminous material (Spergel, 2003). One possible solution to this cold dark matter problem, supported by theoretically favoured supersymmetric extensions to the standard model of particle physics, is that this material comprises Weakly Interacting Massive Particles (WIMPs). Examples of such particles are the neutralino of the CMSSM (Ellis et al, 2003), the lightest stable admixture of the neutral supersymmetric particles, with expected masses in the 100GeV range.

The direct observation of a neutralino population within the Galaxy would impart information to the fields of cosmology and astrophysics allowing refinement and confirmation of the current standard paradigm. Within particle physics, such an observation would also provide complementary information to accelerator of supersymmetric models through investigation of spin dependence, target mass dependence and, uniquely, testing R-parity conservation a multiplicative quantum number prohibiting the decay of supersymmetric particles.

The Galactic component of this cold dark matter may be directly observed through the coherent elastic scattering off target nuclei. This is a near-maximal energy transfer process due to the comparable masses of the dark matter WIMP and the target nuclei in many detector systems (Smith & Lewin, 1990).

2. Dark Matter detector requirements

The expected scalar interaction cross section for neutralino dark matter elastic scattering is in the range 10^{-8} pb to 10^{-10} pb (Ellis et al, 2003). This translates to an expected event rate in a target material of between 0.01 and 0.0001 events/kg/day, i.e. of order events/tonne/week for the lower bound. The expected recoil energy deposition for a WIMP interaction is below 50 keV, with an exponential energy spectrum. The low interaction rate and small energy deposition require detectors with high signal to noise capability (better than 10^5), low energy threshold (keV), ultimately high mass (tonne scale), and low intrinsic background levels (event/kg/day of target). A low energy threshold also reduces the effect of the form factor introduced in the coherent scattering process.

The key requirement for direct dark matter detectors, following maximal background reduction, is the ability to differentiate the nuclear recoils initiated by WIMP collisions and the more frequent electron recoils due to gamma and beta backgrounds. In addition nuclear recoils due to neutrons must be clearly quantified and sufficient shielding or active veto be in place to reduce these events well below the expected WIMP rate. These neutrons arise from (α, n) reactions from uranium and thorium impurities in the experimental cavern walls, detector shielding and detector components, as well as muon spallation neutrons from these regions generated by the high energy cosmic ray muons that penetrate to the detector cavern. Position sensitivity is a characteristic of the new generation of dark matter detectors, which will allow the rejection of internal background through the definition of a fiducial volume, and the rejection of neutrons through segmentation and multiple scattering.

Ultimately the use of targets with different mass and spin components, or different targets and techniques, will be required to provide information about the characteristics of the WIMP nucleon interaction. The use of multiple targets also provides cross checks on systematics and backgrounds due to the A^2 dependence of the scalar interaction rate of the WIMPs as opposed to the A dependence on neutron scattering.

An alternative approach to the nuclear recoil discrimination is the use of directional information to correlate the motion of the Earth through the Galactic dark matter halo, or the modulation of the signal due to the annual or diurnal variations due to the Earth's rotation. This technique provides the ability to perform dark matter halo studies within the local environment and will be complementary to indirect searches where integration of the WIMP flux occurs in the Galactic centre or Sun.

3. Dark Matter detectors

Many experiments are currently being undertaken to search for WIMP interactions, using many different detector technologies (Morales, 2003). All detector systems achieve low background levels through the use of radio-pure materials in construction, radio-pure gamma shielding of the detector from the surroundings and operation of the detector at depth to reduce the effect of cosmic rays. Detector technologies currently affording the best limits on the scalar WIMP cross sections, at about 10^{-6}pb, are based on two technologies cryogenic semiconductor devices and scintillation based detectors.

The EDELWEISS (Benoit et al, 2002) and CDMS (Schnee et al, 1998) collaborations use detectors based on cryogenic semiconductor devices where the ionisation and phonons created in the target during a particle interaction

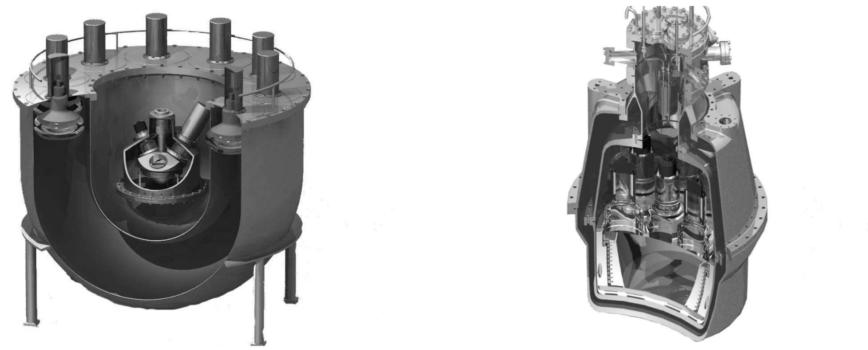

Figure 1. Cut-away diagrams showing examples of direct dark matter detection targets using liquid xenon in scintillation and scintillation/ionisation mode.. The ZEPLIN I and ZEPLIN II liquid xenon targets are operated at the Boulby mine to reduce muon initiated backgrounds. Left, ZEPLIN I - a 5kg chamber of liquid xenon is viewed by three photomultipliers through 3cm liquid xenon turrets. The target is surrounded by a 1 tonne liquid scintillator veto to reject Compton scattered high energy gamma from the PMTs, and a lead castle, not shown. Right, ZEPLIN II - a two phase chamber where the ionisation from the interaction is extracted into the gas phase and observed through electroluminescence in a high field region.

are observed. The ratio of these two signal channels provides a powerful method of discrimination between the WIMP induced nuclear recoils and background induced electron recoils.

The ZEPLIN collaboration (Smith et al, 2003) is developing a series of detector based on liquid xenon (shown in Fig. 1). ZEPLIN I (Barton et al, 2003) is a single phase detector and utilises the scintillation light produced in particle interactions. The time constant of emission of this light is used as a statistical discriminant between nuclear and electron recoils. Future generations of these detectors will utilise two phase operation where the ionisation created in the interaction is also measured, through extraction into the gas phase and observation through electroluminescence, providing improved discrimination.

The DAMA collaboration (Bernabei et al , 2000) utilise a 100kg array of nine NaI detectors, again measuring the scintillation light produced during an interaction. Although photomultiplier noise pulses are rejected based on the time constant of the light observed, the WIMP identification strategy utilised in this experiment is to search for the expected annual modulation as the Earth rotates around the sun within the WIMP halo. Such an annual modulation has been observed over four years and has been interpreted as a WIMP signature in the absence of other variable backgrounds (Bernabei et al, 2000).

4. Current status

The current status of direct dark matter searches is shown in Fig. 2 produced from the web based limit plotter provided by Gaitskel & Mandic (2003). For spin dependent interactions only 90% c.l. upper limits are shown for various experiments, with references summarised by Gaitskel & Mandic. For spin independent

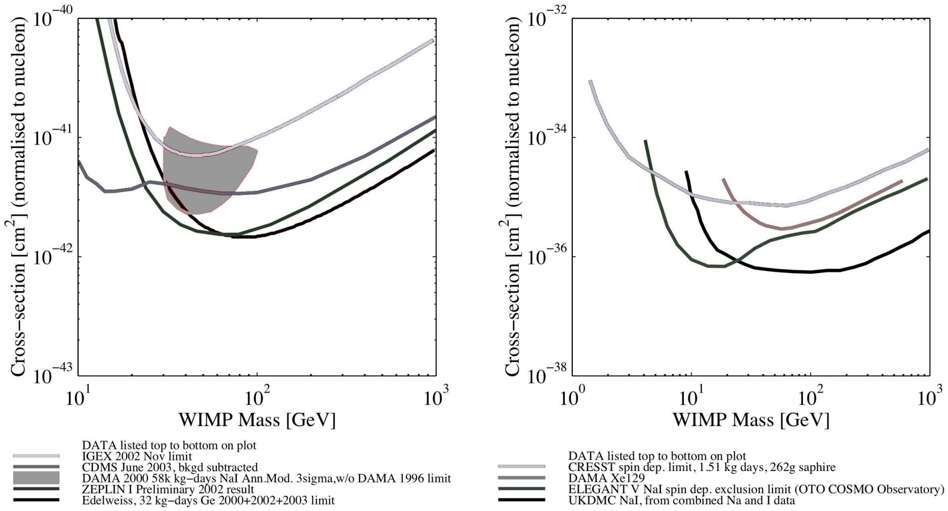

Figure 2. Current status of dark matter searches, shown as WIMP-nucleon cross section vs. WIMP mass. Left diagram shows spin independent, i.e. scalar, interactions, whilst right diagram shows spin dependent cross section, both normalised to one nucleon.

interactions the solid region is the interpretation of the DAMA annual modulation as a WIMP signature based on a fully spin independent interaction. The curves are 90% c.l. upper limits set by the experiments discussed above, where no signal is detected. For comparison, current supersymmetric models predict a range of interactions between 10^{-8} pb to 10^{-10}pb in the spin independent case.

References

Barton J. C. et al, 2003, Workshop on Identification of Dark Matter (York) 302

Benoit, A. et al, 2002, Phys. Lett B, 545, 43

Bernabei R. et al, 2000, Phys. Lett. B, 480, 23

Ellis, J. R. et al, 2003, Phys. Lett B, 565, 176

Gaitskel R., Mandic V., 2003 http://dendera.Berkeley.EDU/plotter/entryform.html

Morales, A., 2003, Nucl. Phys. Proc. Suppl. 114, 39

Schnee, R. et al, 1998, Phys. Rep. 307, 283

Smith, P. F., Lewin J.D. 1990, Phys. Rep. 187, 203

Smith, N. J. T. et al, 2002, Heidelberg Conference (Cape Town) 499

Spergel D. N. et al, 2003, ApJS, 148, 175

Highlights of Astronomy, Vol. 13
International Astronomical Union, 2003
O. Engvold, ed.

DARK MATTER: Astronomical Aspects

Virginia Trimble

Department of Physics and Astronomy, University of California, Irvine CA 92697 USA, and Astronomy Department, University of Maryland, College Park MD 20742 USA

Abstract. The chief evidence for appreciable dark matter in the universe comes from the monotonic increase in mass to light ratios measured for various astronomical systems as one looks on larger and larger length scales. Though the evidence comes from photons, most of the dark matter is non-photonic, and, for that matter, non-baryonic. There remain several questions about the nature and behavior of dark matter to which conventional astronomical observations are (probably) relevant. The most germain to this JD is whether astronomers have seen decay or annihilation products from dark matter particles, to which the current answer seems to be no. We look at a few of the others.

Single stars and clusters have mass-to-light ratios of order unity, in solar units, while the largest scale structures and global values reach about 300, corresponding to a matter density of about 30% of closure density. If you think of this as a graph with a nearly straight line sloping from lower left to upper right, then the standard points on it pertain to the solar neighborhood (and inner bright parts of other galaxies), the outskirts of galaxies (rotation curves, globular cluster velocities, etc), binary galaxies and small groups, rich clusters, superclusters, and the universe as a whole. Curiously, by giving a little thought to the assorted distances scales in use at various times, you could have drawn this line before World War II, using the solar neighborhood numbers of Kapteyn (1922) and Jeans (1922), the Babcock (1939) rotation curve for M31, the binary galaxies of Holmberg (1937), and the work on the Coma and Virgo clusters by, respectively, Zwicky (1933) and Smith (1936). Holmberg drew attention to this qualitatively, by saying he thought it reasonable that his typical mass for a galaxy should come somewhere between those found by Hubble (for visible parts) and those found by Zwicky and Smith if you divide the mass of the whole clusters by the number of galaxies you see.

Most astronomers working in extragalactic astronomy would endorse the previous paragraph. There remain, however, three sorts of alternatives. The first is that gravity might not behave as described by the equations of Newton and Einstein. Two examples are the MOdified Newtonian Dynamics (MOND) of Milgrom (2002) and the conformal gravity of Mannheim (2001). The second goes further, with non-standard contributions to the velocities we observe as well as to the forces exerted by matter. The quasi-steady state theory (Narlikar et al. 2003) is the best-known example in this class. Third is something that none of us has thought of yet, for which there are necessarily no references except to the speaker who was originally scheduled to give this talk.

In the absence of direct laboratory detection of dark matter particles, most of the evidence we have for their properties comes from astronomical observations. Many of the results have been around for long enough to be well known: the universe is not closed by primordial black holes (or Hawking radiation does not exist, or both); the universe is not closed by billion solar mass black holes (or many more QSOs and GRBs would be lensed); the universe is not closed by gravitational radiation in a subset of possible wavelength bands (or pulsar timings would be much more erratic); the Milky Way is not dominated by MAssive Compact Halo Objects (or there would be more microlensing of LMC stars); the universe is not closed by hot (neutrino-ish) dark matter (or galaxies would not have formed in time). My own earlier views on these and related topics can be found in Trimble (1987, 2003) and annual updates (Trimble and Aschwanden 2003, plus earlier, and probably later, papers in the same series)

An assortment of other astronomical questions are still open, and may turn out to have answers that bear on the nature of dark matter. Here is a subset:

Where are the missing satellite galaxies? The three classes of answers floating around are not mutually exclusive. (A) They were unable to accrete gas because of re-ionization, but show up as lumps in lensing studies of halos, (B) They accreted gas but made no stars and are the high velocity HI clouds, and (C) They accreted gas and made stars, but were later damaged, with the dwarf spheroidal galaxies being the tip of the mass distribution and globular clusters being the stripped cores of the others.

Do halos (galaxies or clusters) have cusps or cores at their center? The observers' answers look much more like isothermal cores than like singular cusps, so the question goes back to the theory team to see if they can modify the CDM prediction by adding other sorts of DM, including baryons.

Are most halos fairly round? Yes, probably, with the structure of polar ring galaxies the traditional supporting evidence, Iodice et al. (2003) and mild triaxiality implied by disk flaring (Bekki and Freeman 2002).

Could the Milky Way have a significant disk dark matter component? If each paper in the past two years gets one vote, than it is about 7:1 against, but take a look at the minority view (Kalberla 2003) before the refutation (Drake and Cook 2003)

Have we seen decay, annihilation, or collision products from dark matter candidates? A fascinating (but apparently wrong) suggestion was the Sciama neutrino, whose mass was just a bit more than twice the Lyman limit energy, so that the decaying particles made a large contribution to intergalactic and galactic fringe ionization. Recent ultraviolet observations have not found the predicted photons. Still open is whether the highest energy "cosmic rays" might actually be produced in the galactic halo by something (presumably very high energy neutrinos) coming from very far away but not subject to the ZKG limit hitting something that has been here all along (presumably the dark matter particles in the halo).

Is there a real, significant discrepancy between global values of the total density of dark matter, which tend to fall around or above 0.3 of closure and the values derived from clusters of galaxies, which tend to fall around or below 0.2? This turns out to be an enormously over-simplified version of a broader question about whether the various determinations of all the cosmological parameters (the good ones anyhow) are mutually consistent. The answer is clearly no (Bridle et al. 2003). As always, "further observations are needed" to decide whether it will eventually all come together, or the situations will become serious but not desperate (as the German general said to the Austrian general) or desperate but not serious (as the Austrian general said to the German general).

Acknowledgments. I am grateful to the Harry Messel International Science School and the Peter Gruber Foundation for contributions to travel expenses to the IAU GA and distinctly ungrateful to Sir Martin Rees for deciding not to come. One version of his own views on the subject should appear next year (Rees 2004).

References

Babcock, H.W. 1939 Lick Observator Bulletin 19, 41

Bekki, K. & Freeman, K.C. 2002. ApJ 566, 245

Bridle, W.L. et al. 2003. Science 299, 1532

Drake, A.J. & Cook, K.H. 2003. ApJ 589, 281

Holmberg, E. 1937. Lund Annals 6, 1

Iodice, E. et al. 2003. ApJ 585, 730

Jeans, J.H. 1922. MNRAS 82, 122

Kalberla, P.M.W. 2003. ApJ 588, 805

Kapteyn, J.C. 1922 ApJ 55, 302

Mannheim, P. D. 2001. ApJ 561, 1

Milgrom, M. 2002. ApJ 571, L81

Narlikar, J. et al. 2002. ApJ 585, 1

Rees, M.J. 2004. Discover Magazine, to appear

Smith, S. 1936. ApJ 83, 23

Trimble, V. 1987. ARA&A 25, 425

.....2003 in W. Freedman ed. Measuring and Modeling the Universe. Cambridge University Press, in press

Trimble , V. & Aschwanden, M. 2003. PASP 115, 514

Zwicky, F. 1933. Helv. Phys. Acta 6, 110

Highlights of Astronomy, Vol. 13
International Astronomical Union, 2003
O. Engvold, ed.

Concluding Remarks: Non Electromagnetic Windows in Astrophysics

Catherine J. Cesarsky

European Southern Observatory, Karl-Schwarzschild-Str. 2, D-85748 Garching, Germany

It is a pleasure, once again, to take part in a meeting dedicated to a host of exciting topics in high energy and particle astrophysics at an IAU General Assembly; my last time was at a meeting I had myself organized at the GA in Baltimore 15 years ago. In the mean time these subjects have attracted much interest among particle physicists, but had been receiving less attention from the general astrophysicists attending IAU GAs.

In those fifteen years, there has been an explosion of knowledge in astrophysics, due to simultaneous advances at virtually all the wavelengths of the electromagnetic spectrum. This led to breakthroughs in numerous fields such as cosmology, galaxy evolution and star formation. At the same time, extra solar planets have at long last been unambiguously discovered. In comparison, excluding neutrino discoveries, which led to a Nobel Prize in 2002, astrophysics from non electromagnetic windows appears to have progressed at a slower pace and to have attracted less attention. When so many important discoveries are at hand, or easy to get, why struggle and attempt more difficult searches?

At this Joint Discussion, we heard from the adventurous at heart, pioneers who are prepared to risk considerable parts of their career building experiments that aim at ambitious, but unassured objectives. And we also heard that the first or next generation of experiments is getting ready to go, so that the forthcoming years promise to be exciting in these exploratory fields too.

We heard first about the huge success of the solar neutrino experiments, which make it possible now to truly understand the source of the solar energy, and at the same time have extremely interesting implications on neutrino oscillations. This has naturally become also a hot topic for particle physicists. The study of solar oscillations brings additional, crucial information enhancing the understanding of neutrino properties and of important stellar processes, convection and rotation.

Gamma ray astrophysics was not discussed here, but the results obtained in this particular electromagnetic window are well connected to topics covered, such as cosmic ray acceleration and high-energy neutrinos, and give impressions of what can be obtained. We now have a reasonable understanding of the emission of the galaxy from the tens of MeV to the few GeV region, and even point source and diffuse emission in gamma ray lines has been reported; the Integral satellite will bring new and possibly decisive information on these topics. Ground Cerenkov experiments continue to monitor sources at higher energies, up to the several TeV range, detecting continuous sources and occasional outbursts, but not supernova remnants. The space mission GLAST, which will reach 300 GeV, will soon complement them. Bold ground experiments aiming at the detection of gamma rays at even higher energies have only been able to establish upper limits. It is the study of gamma ray bursts that has advanced most in the last few years, as it is now proven that their sources are at cosmological distances and that one class at least is due to hypernova explosions. In the future, gamma ray bursts may become an excellent tool to study the universe at high redshifts, surpassing absorption studies in quasars if the optical or infrared afterglows can be caught sufficiently early.

The studies and measurements made until now have not permitted to identify with certainty the sources of cosmic ray nuclei, even if inferences can be made about supernovae and/or OB associations, as we were reminded at this meeting. The direct detection of high-energy neutrinos would of course radically change the panorama. Predictions of the emissions expected according to various models of galactic sources of cosmic rays and of pulsars have been established, and the experiments are forthcoming. With AMANDA, at least interesting limits on the putative galactic sources will be obtained in the near future, and eventually Ice Cube and ANTARES will explore also extragalactic space.

The new generation of gravitational wave detectors will have an equally adventurous task. While there is little doubt in the community that gravitational waves pervade the universe, there is a wide range of predictions, and, in my opinion, a high chance of surprises. The measurements are extremely delicate, and I wish much luck to LIGO, and to VIRGO, inaugurated in Italy during the Sydney IAU GA. After these exploratory ground experiments, which probably need enhancements such as that planned for LIGO to be sensitive enough to discover cosmic sources, the space mission LISA will open a whole new parameter space, with superior chances of success.

Even more adventurous and brave are the attempts at direct detection of dark matter. The density of dark matter in the universe as a whole, or in clusters of galaxies, is today better constrained than that of dark matter in the solar neighborhood. In any case, the various experiments available today do not appear yet to exhibit sensitivities that could be conducive to detection. But the progress is steady, and the stakes are very high. In the mean time, more about dark matter distribution and properties will be learned using classical astrophysical tools, optical and X ray telescopes, combined with models of weak shear and of the thermal behavior of intergalactic gas.

I left for the end the Ultra High Energy Cosmic Ray experiments. Having worked myself on cosmic rays for many years in the first part of my career, I am particularly excited by the opportunities offered by the forthcoming experiments in this field. Here again, generations of experiments have shown that cosmic rays of energies as high as 10^{20} eV exist, even if the upper limit in energy is under dispute, and if the statistics have never allowed to reach credible conclusions on the distribution or distance of the sources, a situation quite similar to that of gamma ray bursts before the Compton Gamma Ray Observatory. The Auger collaboration, especially if it succeeds in building the northern as well as the southern part of the experiment, should for the first time obtain results with sufficient statistical weight (see also, later, the Space Station mission EUSO for real UHE Cosmic Ray astronomy!). It is intriguing to think that we may have a better chance of discovering the sources of UHECR than those of the bulk of the particles in the GeV range!

In conclusion: this was a very interesting Joint Discussion, and I hope to hear more about these topics and about the results of the new experiments, at the next IAU GA in Prague.

JD2

Mercury

Chairpersons: R. Schulz and N. Thomas

Editors: R. Schulz, N. Thomas (Chief-Editor) and A. Sprague

Highlights of Astronomy, Vol. 13
International Astronomical Union, 2003
O. Engvold, ed.

Recent Advances in Ground-based Observation of Mercury

Warell, J.

Lunar and Planetary Laboratory, The University of Arizona, Tucson, AZ 85721, USA

Abstract. The last decade has seen an efficient use of ground-based telescopes for remote-sensing studies of Mercury's surface at optical, infrared and microwave wavelengths. This has resulted in a substantially improved knowledge of its regolith composition, material and light scattering properties and structures on the poorly known hemisphere. This paper summarizes recent observations and results on the regolith properties of Mercury.

1. Important observational studies

We may identify three main types of observational methods that have been contributed significantly, and in which efforts in the near future will probably be concentrated. Radar has been used to investigate topographical units and for probing fundamental material properties; spectroscopy and imaging spectrophotometry to identify the surface composition, particularly in the thermal infrared; and high-resolution imaging in the optical and near-infrared to map the albedo distribution of the surface with the ultimate goal of identifying geologic provinces on the poorly known hemisphere (i.e., the longitudes 180–360° which were not imaged by Mariner 10).

Remarkable km-scale spatial resolution images of the surface have been obtained at microwave and radar wavelengths through delay-Doppler and full-disk imaging with the Goldstone/Very Large Array and Arecibo radio telescopes (Harmon et al. 2001, Harmon & Campbell 2002), and are our best source of information regarding topographic features on the poorly known hemisphere. Small areas of very high radar backscatter intensity within high latitude craters have been interpreted as due to either buried water ice or sulfur deposits (Slade et al. 1992; Sprague, Hunten, & Lodders 1995). Microwave radar studies (Mitchell & de Pater 1994; Jeanloz et al. 1995) and related laboratory studies have shown that the material properties are consistent with those of alkaline silicates, with a greater transparency and smaller dielectric loss tangent than that of the Moon, signifying a lower abundance of opaque minerals such as iron and titanium in a predominantly feldspathic crust.

The infrared regime have provided us with the best opportunities to extract information about the mineralogical composition of Mercury's regolith. Instrumentation on the Infrared Telescope Facility (IRTF), the McMath-Pierce and Steward telescopes at Kitt Peak, and the Kuiper Airborne Observatory have been used to obtain spectra and images at thermal infrared wavelengths (Emery et al. 1998; Cooper et al. 2001; Sprague et al. 2002). Such spectra are often complex and emission features vary in terms of location and intensity between

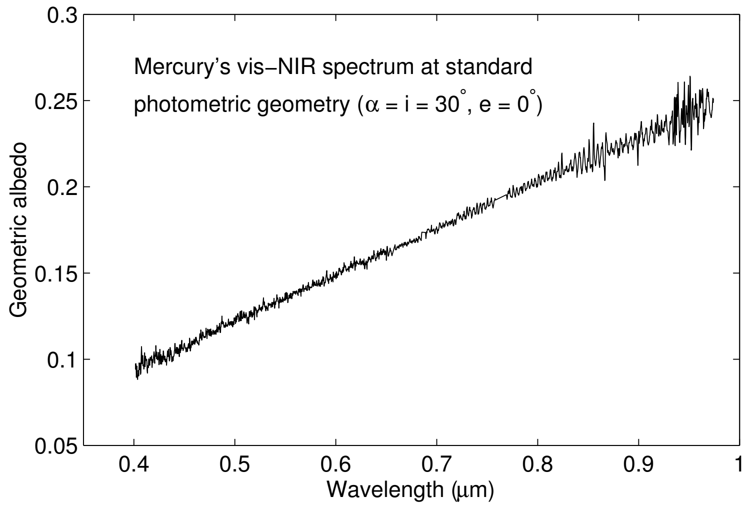

Figure 1. An average Mercury spectrum for the wavelength range 0.4–1.0 μm obtained with the Nordic Optical Telescope (Warell and Blewett 2003), scaled with a geometric albedo of 0.136 at 0.55 μm from Warell (2003b). The vis-NIR spectrum of Mercury is linear and lacks any detectable mineralogical absorption features.

different longitudes on the surface. This is taken as evidence of a compositionally heterogeneous surface composed of intermediate and basic soils, pyroxenes and anorthosite, possibly with geologic units of highly different thermal properties.

The situation is superficially different for spectra obtained in the optical and near-infrared range, which are similar for all longitudes (Blewett et al. 1997). The 0.9 μm absorption band due to Fe^{2+} crystal field transitions in ferrous silicates and a characteristic of lunar spectra is absent on Mercury, indicating a very low abundance of iron (Sprague et al. 2003; Warell 2003a; Warell & Blewett 2003). Albedo features around 200 km in size have been detected on the non-Mariner 10 hemisphere with the Mt. Wilson 1.5-m reflector (Baumgardner et al. 2000) and the Swedish Vacuum Solar Telescope (Warell & Limaye 2001), showing that there is no statistical difference between the morphology and distribution features on a global scale. This provides evidence for a similar post-heavy bombardment geologic evolution of both hemispheres.

A new V-band phase curve from photometric observations from the ground and with the Solar and Heliospheric Observatory was published by Mallama et al. (2002), and signifies the first good data set for very low and very high phase angles. That work and Warell (2003b) indicate a microscopically smoother surface than determined previously (Veverka et al. 1988).

2. Mercury's regolith: summary of best knowledge

In terms of composition, recent observations indicate that Mercury's surface is primarily feldspathic with intermediate plagioclase as the dominant phase. Minor low-iron hypersthene and mafic basalts may be present locally. Volatile minerals, possibly water ice or sulfur, are mixed in the subsurface at permanently shaded locations at the poles.

Hapke (1993, 2002) modeling indicates a chemical composition of FeO ∼1–2 wt%, TiO_2 ∼0 wt%, and Fe^0 ∼0.2 wt% (Warell and Blewett 2003). This supports the observed small microwave dielectric loss tangent characteristic of a surface low in opaques. The original unweathered rock types of the present crust may thus have been iron-free, with iron (oxidized and native) and volatiles delivered by infall during and following the late bombardment era.

The average optically active grain size appears to be about 30 μm or half the dimension of lunar highland grains, which is consistent with the stronger maturation at Mercury (Cintala 1992). The physical porosity of the optically active top soil is similar to the Moon's and is consistent with a small radar cross section (Pettengil, Dyce, & Campbell 1967) and negative branch of polarization (Dollfus & Auriere 1974). Though the maturation induced metallic iron abundance appears to be at most half of the Moon's, the maturation appears more evolved in terms of a probably higher abundance of semi transparent and strongly backscattering complex agglutinates.

The optical scattering properties are lunar-like, but Mercury appears to have a stronger backscattering efficiency and dependence of color on geometry. The backscattering anisotropy increases with wavelength, which supports microwave opacity data. The average particle angular scattering function corresponds more closely to that of lunar maria than highlands. At least some surfaces, consistent in location with smooth plains imaged by Mariner 10, have a small photometric roughness of $\bar{\theta}$ ∼10°, though the typical regionally averaged surface appears consistent with a roughness twice as high.

In terms of Mercurys evolution, the available evidence indicate that it either sampled only a limited feeding zone during the protoplanetary accretion phase, and/or experienced subsequent post accretion volatilization or impact ejection of the bulk silicate component. This would account for a very low abundance of iron, facilitated by the gravitational sinking of high density minerals in a magma ocean. Such an event would also allow thorough mixing of the present crustal material to effectively average out strong compositional variations.

Acknowledgments. This work was made possible in part by a grant from the Wenner-Gren Foundations.

References

Baumgardner, J., Mendillo, M., Wilson, J.K. 2000, AJ 119, 2458

Blewett, D.T., Lucey, P.G., Hawke, B.R., Ling, G.G., & Robinson, M.S. 1997, Icarus, 129, 217

Cintala, M.J. 1992, J. Geophys. Res., 97, 947

Cooper, B., Potter, A., Killen, R., & Morgan, T. 2001, JGR 106, 32803

Dollfus, A., & Auriere, M. 1974, Icarus, 23, 465

Emery, J.P., Sprague, A.L., Witteborn, F.C., Colwell, J.E., Kozlowski, R.W.H., & Wooden, D.H. 1998, Icarus, 136, 104

Hapke, B. 1993, Theory of reflectance and emittance spectroscopy (Cambridge: Cambridge University Press)

Hapke, B. 2002, Icarus, 157, 523

Harmon, J.K., Perillat, P.J., & Slade, M.A. 2001, Icarus, 149, 1

Harmon, J.K. & Campbell, D.B. 2002, Lunar and Planetary Sci. Conf. 33, 1858

Jeanloz, R., Mitchell, D.L., Sprague, A.L., & de Pater, I. 1995, Science, 268, 1455

Mitchell, D., & de Pater, I. 1994, Icarus, 110, 2

Pettengil, G.H., Dyce, R.B., & Campbell, D.B. 1967, AJ, 72, 330

Sprague, A.L., Hunten, D.M., & Lodders, K. 1995, Icarus, 118, 211

Sprague, A.L., Emery, J.P., Donaldson, K.L., Russell, R.W., Lunch, D.K., & Mazuk, A.L. 2002, Meteoritics & Planetary Science, 37, 1255

Sprague, A.L., Emery, J., Warell, J., Long, A., Rayner, J., & Cushing, M. 2003, this volume

Veverka, J., Helfenstein, P., Hapke, B., & Goguen, J. 1988, in Mercury, ed. F. Vilas, C.R. Chapman & M.S. Matthews (Tucson: University of Arizona Press), 37

Warell, J. 2002, Icarus, 156, 303

Warell, J. 2003a, Icarus, 161, 199

Warell, J. 2003b, Icarus, in press

Warell, J. & Limaye, S.S. 2001, Planetary & Space Science, 49, 1531

Warell, J. & Blewett, D. 2003, Icarus, in press

Highlights of Astronomy, Vol. 13
International Astronomical Union, 2003
O. Engvold, ed.

SpeX Spectroscopy of Mercury: 0.8 – 5.2 μ m

Ann L. Sprague, Johan Warell

LPL, The University of Arizona, Tucson, AZ

Joshua Emery

NASA Ames Research Center, Moffet Field, CA

Angela Long

Susquehanna University, Selinsgrove, PA

John Rayner, Mike Cushing

Institute for Astronomy, Honolulu, HI

Abstract. Spectra of Mercury were obtained at the Infrared Telescope Facility on Mauna Kea, HI using SpeX. There is no indication of any absorption feature associated with FeO in Mercury's regolith. There is a 5 μ m excess in thermal flux similar to that observed from the Kuiper Airborne Observatory (KAO) using HIFOGS. Spectra from varying locations do exhibit different slopes and flux indicating different surface temperatures at different locations.

1. Introduction

In order to continue the search for any evidence of oxidized iron on Mercury's surface we have obtained very high signal-to-noise (S/N) ratio spectra between 0.8 and 5.2 μ m using SpeX at the Infrared Telescope Facility (IRTF) on Mauna Kea, HI. This is of interest because we wish to know the surface composition of Mercury to get clues to its formation and cooling history. Every other terrestrial planet in our solar system has at least several percent oxidized iron on its surface. So far, no search for FeO by any observational group has discovered its unambiguous presence by observing the reflectance absorption centered near 0.9 or 2.2 μ m.

2. Observations

Observations were obtained in clear daytime on three consecutive days in June, 2002. We show spectra from 23 June 2002 in this paper. The spectrograph slit was placed across the illuminated disk of the planet at several different locations.

3. Near Infrared Spectral Mapping With SpeX

SpeX operates in several modes with slightly different resolving power (R = 1000 - 2000). For these observations we use SXD from 0.8 – 2.4 μ m and LXD from 2.2 – 5.4 μ m. Because there are some telluric H_2O, CO_2, and N_2O bands in this spectral region that cause spurious features if proper correction is not obtained, we have in some cases removed sections of the data from the spectra displayed. Fig. 1 (left) shows the entire spectral range for about 250 degrees longitude on Mercury's surface.

Because the S/N is very high in these data, it is possible to divide the data along the slit into several sectors. This has the advantage of providing increased spatial resolution in the data to search for variations in composition with respect to latitude. At the IRTF using SpeX the spatial resolution is seeing limited in the 0.8 – 5.5 μ m spectral region. Our seeing for the days observations was about 1 arcsecond. We thus chose to divide the slit into 4 sectors, each covering slightly less than 2 arcseconds across Mercury's surface. It is advantageous to divide the spectra by a thermal model of Mercury for the location of the slit to remove the steep slope caused by Mercury's thermal emission. We use the thermal model developed specifically for Mercury spectral data analysis (Emery et al. 1998). It includes the effects of slow rotation, a rough cratered surface, and the orbital and geometric parameters of the observations. After data are divided by the thermal model, any spectral features become more apparent.

Previous observations made from the KAO with HIFOGS (Emery et al. 1998) found an excess of emission in the 5 μ m spectral region. These data corroborate that discovery. The excess is clearly seen relative to the thermal model but the lack of space in this brief article precludes the inclusion of an illustration.

A different set of previous observations of Mercury around the 5 μ m region were made with BASS (Sprague et al. 2002) at a resolving power of about 150. In those spectra there were some spectral features in the 5 μ m region that were interpreted as indicative of pyroxene in the surface material. We do not see similar unambiguous features in this data set.

The wavelength region of the SXD mode has also been observed previously by McCord and Clark (1979). Other observers have also obtained spectra from about 0.4 – 1.2 μ m but we do not discuss those here. The scatter in the McCord and Clark spectra near the 2.2 μ m absorption (indicative of oxidized iron in pyroxene and olivine) permitted calculating an upper limit of at most 6% FeO. Their spectrum shows no indication of absorption owing to oxidized iron centered at 0.9 μ m. At the Moon this absorption band is ubiquitous at varying depths. Our SpeX data show no evidence for FeO at either absorption band. Serendipitously the region observed by McCord and Clark was centered on the same side of Mercury and near 250° longitude. While our spectra are longitudinally resolved to about 1 arcsecond, that of McCord and Clark is a disk integration within a circular aperture encompassing the entire Earth-facing disk of Mercury. The comparisons are shown in Fig. 1 (right).

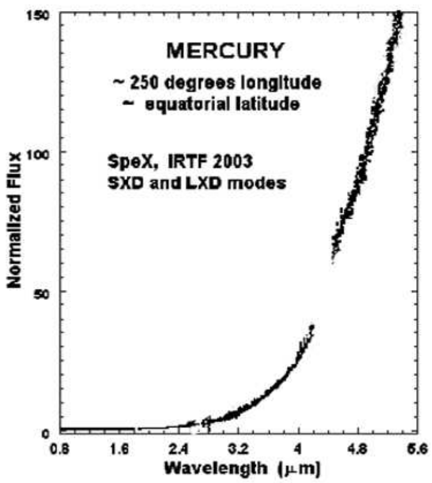

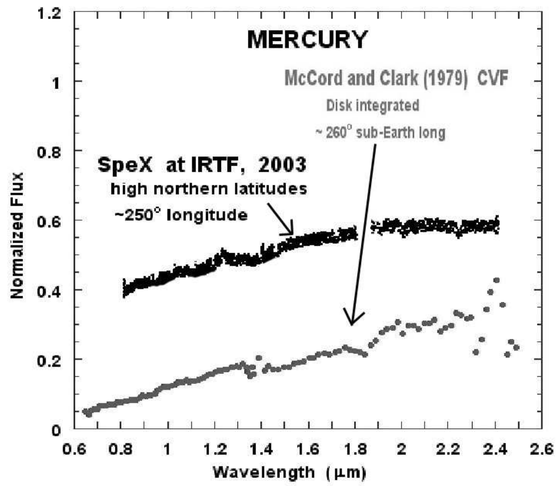

Figure 1. (left) Full range of SpeX data from Mercury before division by a thermal model. (right) SpeX data plotted along with data of McCord and Clark (1979). See text for explanation.

4. Conclusions

The 5 μ m excess is an outstanding spectral feature in this data set. It appears in every spectrum at all locations examined so far. The fact that the emission is enhanced above the theoretical prediction made by our rough surface thermal model indicates something of very high emissivity in Mercury's regolith. This high emissivity is likely a clue to the composition of the material responsible but we do not have enough information to identify it at this time.

The data show no evidence whatsoever for the absorption bands of FeO at 0.9 and 2.2 μ m. The reason for this must be the absence of oxidized iron. This does not preclude iron blebs in the surface regolith caused by aeons of meteoritic bombardment and other space weathering.

Acknowledgments. Sprague, Emery and Warell were visiting Astronomers at the Infrared Telescope Facility, which is operated by the University of Hawaii under Cooperative Agreement no. NCC 5-538 with the National Aeronautics and Space Administration, Office of Space Science, Planetary Astronomy Program. In addition we thank Dave Griep for his operation of the telescope and assistance with observations.

References

Emery, J. P., Sprague, A. L., Witteborn, F. C., Colwell, J. E., Kozlowski, R. W. H., & Wooden, D. H. 1998, Icarus, 136, 104-123.

Sprague A. L., Emery J. P., Donaldson K. L., Russell R. W., Lynch D. K., and Mazuk A. L. 2002, Meteoritics & Planetary Sci., 37, 1255-1268.

McCord T. B. and Clark R. N. 1979, J. Geophys. Res., 84, 7664 - 7668.

Highlights of Astronomy, Vol. 13
International Astronomical Union, 2003
O. Engvold, ed.

The Surface-Bounded Exosphere of Mercury

Andrew Potter

National Solar Observatory, 950 N. Cherry Avenue, Tucson, Arizona 85726, U.S.A.

1. Background

Almost thirty years ago, the instruments on the Mariner 10 spacecraft detected traces of hydrogen, helium, and possibly oxygen in the atmosphere of Mercury. There the matter rested until the mid-80's, when emission lines of sodium (Potter & Morgan 1985) and potassium (Potter & Morgan 1986) were found in the spectrum of Mercury, resulting from resonance scattering of sunlight by metal atoms in the atmosphere. Searches for other metals in the Mercury atmosphere were fruitless until recently, when an emission line attributed to calcium has been observed (Bida, Killen & Morgan 2000). The densities of all these species are so low that gas phase collisions are negligible, so that the Mercury atmosphere is an exosphere bounded at its base by the surface of the planet. The fact that the exosphere is bounded by the Mercury surface means that interactions with the surface must occur. Energy exchange, surface absorption and desorption, and ion neutralization can take place, and these must be accounted for in models of the exosphere. None of these atmospheric species can survive long on Mercury, being lost mainly by photoionization followed by trapping in the solar wind and partly by solar radiation acceleration. Consequently, the species that we observe must be in a steady state, being generated as fast as they are lost to space. The metals must originate from the surface of the regolith, with the supply of fresh surface material maintained by gardening of the surface by meteoroid impact. The metals are released from the surface into the exosphere by photon-stimulated desorption (Madey et al. 1998), particle sputtering (McGrath, Johnson & Lanzerotti 1986), and meteoroid impact vaporization (Morgan, Zook & Potter 1988). Thermal evaporation of species condensed on the cold side may be important for determining their distribution over the planet (Hunten & Sprague 2002). The interaction and relative importance of all these processes has been discussed by Killen & Morgan (1993). Much can be said about these processes, but this review is focused primarily on the current status of observations of sodium, potassium, and calcium.

2. Sodium

Since the sodium resonance emissions were discovered, hundreds of observations have been made (for example, Sprague, et al. 1997). The average column density of sodium is of the order of 10^{11}atoms/cm^2, varying in an apparently random fashion by a factor of two or three throughout the Mercury year, with a tendency to be largest at perihelion and aphelion, and smallest in the parts of the orbit where heliocentric velocity and the corresponding radiation pressure on sodium are the largest. The density of sodium is usually not uniform over the planet, displaying "spots" or peaks of sodium emission in north or south hemispheres, or sometimes in both (Potter & Morgan 1990). These features could result from local concentrations of sodium in the surface rocks (Sprague, Schmitt & Fink 1998), or evaporation of sodium resulting from implantation of magnetospheric sodium ions in the surface (Sprague 1992, Ip 1993), or directly from sputtering of sodium from the surface rocks (Potter & Morgan 1990). Another characteristic of the sodium distribution is that it is variable, sometimes changing from day to day (Potter & Morgan 1990; Potter, Killen & Morgan 1999). Again, this could be the result of geographic factors or the result of changes in local solar weather, causing either changes in the magnetospheric particle deposition, or variations in the amount of solar particle sputtering. The temperature of the sodium atoms is approximately 1000°K (Killen et al. 1999), in reasonable agreement with the temperature expected for sodium released from the surface by photo-stimulated desorption, suggesting that this is the dominant process for sodium production. Sodium column density near the dawn terminator is often greater than at the dusk terminator, suggesting the evaporation of condensed sodium from the cold dark side as it rotates into sunlight (Hunten & Sprague 2002). Further advances in understanding the processes at work in the sodium exosphere of Mercury await observations at improved spatial resolution. These could be achieved with modern adaptive optics technology.

One of the more intriguing predictions of the models of the sodium exosphere was the prediction that there might be a sodium tail, not unlike a comet tail. If sodium atoms are released from the surface with velocities greater than about 2 km/s when Mercury is at greatest heliocentric velocity and maximum radiation pressure, the atoms will escape the planet to form a tail. Ip (1985) and Smyth & Marconi (1995) both predicted the formation of a tail, and generated models of what the tail might look like. The tail is faint, but can be detected when Mercury is visible against a dark sky just before sunrise or just after sunset (Potter, Killen & Morgan 2002). Sodium atoms in the tail display velocities up to 4 km/s normal to the tail direction, suggesting that an energetic process such as sputtering produces the sodium in the tail. Somewhere between 1 and 10 percent of the sodium generated can be lost to space from the tail. But this happens only when radiation acceleration is high. When it is not, the tail must vanish, or rather turn into an extended cloud around Mercury (Smyth & Marconi 1995).

Recent modeling studies have improved our understanding of the sodium exosphere. The magnetosphere opens in response to a southward IMF, allowing solar wind particles to impact the surface, leading to sputtering of sodium from the surface (Sarantos et al. 2001). This effect was used to explain changes observed in the sodium exosphere (Killen et al. 2001). The effects of a Solar Energetic Particle event on Mercury have been modeled, and the results show that sodium ions would be precipitated to the surface in patterns similar to those observed (Leblanc et al. 2003). A 3-D Monte Carlo model with all known sources and sinks for sodium has been developed, that reproduces most of the observed features of the sodium exosphere; dawn-dusk asymmetries, high latitude spots, and the sodium tail (Leblanc & Johnson 2003).

3. Potassium

Potassium is much more difficult to observe than sodium. The D_2 line at 7664 A (the strongest emission of the D_1 - D_2 pair) is usually hidden under an atmospheric oxygen absorption line, and can be seen only when the Doppler shift is large enough blue-wards to bring it out from under the line. The weaker D_1 line at 7699 A can only be clearly seen when the Doppler shift is large enough to bring it entirely up and out of the potassium Fraunhofer absorption line. So observations of the potassium emission are few. Same-day observations of sodium and potassium show their distributions to be similar, both showing high latitude emission peaks (Potter & Morgan 1997). Considering the chemical similarity of sodium and potassium, this is not surprising. However, there is a puzzle, in that the ratio of sodium to potassium emission is variable from one observation to the next, with values ranging from about 20 to 140 (Potter et al. 2002). This is in contrast to the Moon, where the Na/K ratio stays at about 7, not far from the ratio of the elements in the surface rocks. One possibility suggested was that potassium levels in the surface rocks vary from place to place (Sprague, Kozlowski & Hunten 1990) But it appears more likely that some process, as yet not understood, removes potassium faster than sodium from the exosphere, at varying rates (Potter et al. 2002). The magnetosphere may play a role, since it is present on Mercury, but absent on the Moon, where the ratio is closer to the expected value.

4. Calcium

Calcium is the most recently discovered element in the Mercury exosphere (Bida, Killen & Morgan 2000). An emission corresponding to the calcium Ca I line at 4226.7 A was found in spectra taken at evening twilight with the Keck telescope. The line is Doppler-shifted to the blue, corresponding to velocities up to 4 km/s. The emission line is not seen on the planet itself, but appears at distances up to a planetary diameter away from the planet. The emission is faint, and perhaps that is why no observations are reported close to the planet. On the planet, the weak line would be overwhelmed by stronger reflections from the planetary surface. The source process for the calcium is not understood. It must either be particle sputtering or meteoroid impact since these are the only processes that could generate the observed velocities.

5. Summary

Sodium is easy to observe, and so we have many sodium observations. These have stimulated serious theoretical modeling, and we now understand in principle the sodium exosphere. For further refinements, we need measurements with much better spatial resolution, and we need accurate information about the magnetosphere and how it responds to solar influences. Potassium and calcium are less well understood. The measurements are difficult and as a consequence, there is much less information available for these species than for sodium. We realize that there must be still other exospheric species that cannot be detected by ground-based observations. The currently planned missions to Mercury will detect these species, and map the magnetosphere, leading to a major improvement in our understanding of the Mercury exosphere, as well as the interaction of the space environment with planetary surfaces.

Acknowledgments. This work was supported by the NASA Planetary Astronomy Program and by the National Solar Observatory.

References

Bida, T.A., Killen, R.M. & Morgan, T.H. 2000, Nature, **404**, 159

Hunten, D.M. & Sprague, A.L. 2002, Meteoritics and Planetary Science, **37**, 1191

Ip, W. -H. 1986, Geophys. Res. Lett., **13**, 423

Ip, W. -H. 1993, Ap. J., **418**, 451

Killen, R.M. and Morgan, T.H. 1993, Icarus, **101**, 293

Killen, R.M., Potter, A.E., Fitzsimmons, A. & Morgan, T.H. 1999, Planetary & Space Science, **47**, 1449

Killen, R.M., Potter, A.E., Reiff, P., Sarantos, M., Jackson, B.V., Hick, P. & Giles, B. 2001, Jour. Geophys. Res., **106**, 20509

Leblanc, F., Luhmann, J.G., Johnson, R.E. & Liu, M. 2003, Planetary & Space Science, **51**, 339

Leblanc, F. & Johnson, R.E. 2003, Icarus, **164**, 261

McGrath, M.A., Johnson, R.E., & Lanzerotti, L.J. 1986, Nature, **323**, 694

Madey, T.E., Yakshinskiy, B.V., Ageev, V.N. & Johnson, R.E. 1998, Jour. Geophys. Res., **103**, 58773

Morgan, T.H., Zook, H.A., & Potter, A.E. 1988, Icarus, **75**, 156

Potter, A.E. & Morgan, T.H. 1985, Science, **229**, 651

Potter, A.E. & Morgan, T.H. 1986, Icarus, **67**, 336

Potter, A.E. & Morgan, T.H. 1990, Science, **248**, 835

Potter, A.E. & Morgan, T.H. 1997, Planetary & Space Science, **45**, 95

Potter, A.E., Killen, R.M. & Morgan, T.H. 1999, Planetary & Space Science, **47**, 1441

Potter, A.E., Killen, R.M., & Morgan, T.H. 2002, Meteoritics & Planetary Science, **37**, 1165

Potter, A.E., Anderson, C.M., Killen, R.M., & Morgan, T.H. 2002, Jour. Geophys. Res., **107**, 10.1029/2000Je001493

Sarantos, M., Reiff, P.H., Hill, T.W., Killen, R.M., & Urquhart, A.L. 2001, PASP, **49**, 1629

Smyth, W.H. & Marconi, M.L. 1995, Ap. J., **441**, 839

Sprague, A.L., Kozlowski, R.W.H., & Hunten, D.M. 1990, Science, **249**, 1140

Sprague, A.L. 1992, Jour. Geophys. Res., **97**, 18257

Sprague, A.L., Kozlowski, R.W.H., Hunten, D.M., Schneider, N.M., Domingue, D.L., Wells, W.K., Schmitt, W. & Fink, U. 1997, Icarus, **129**, 506

Sprague, A.L., Schmitt, W.J. & Hill, R.E. 1998, Icarus, **136**, 104

Highlights of Astronomy, Vol. 13
International Astronomical Union, 2003
O. Engvold, ed.

Recycling of Ions in Mercury's Magnetosphere

Rosemary Killen

The University of Maryland, Dept. of Astronomy, College Park, MD 20742-2425, U.S.A.

Andrew Potter

National Solar Observatory, 950 N. Cherry, Tucson, AZ 85726, U.S.A.

Menelaos Sarantos

Rice University, Dept. of Physics and Astronomy, 6100 S. Main, Houston, TX 77005-1892, U.S.A.

Patricia Reiff

Rice University, Dept. of Physics and Astronomy, 6100 S. Main, Houston, TX 77005-1892, U.S.A.

Abstract. To determine the relative rates of ion recycling to the surface and loss of ions to the solar wind, we followed 3,500 Na ions in a tight grid of magnetic and electric fields at Mercury. We conclude that up to 60% of the photoions launched on the dayside near the surface will re-impact the dayside. For a dawn - dusk electric field, we find that most of the returning ions impact the dayside. This will be the case for a southward IMF. Photoions do not impact the dayside with sufficient energy to cause secondary sputtering, but on the nightside they will be accelerated to keV energies, and may cause secondary sputtering there.

1. Introduction

Photoionization is believed to be the predominant loss process for exospheric neutral sodium atoms in Mercury's exosphere. The efficiency of ion recycling to the surface has implications for the long-term volatile budget, for possible sequestration of volatiles in cold traps or high latitude bands, and for relative enrichment of one volatile over another. It has been suggested that the relative loss rates of Na^+ and K^+ may affect the Na/K ratio in the Hermean exosphere. Generally, it has been assumed that about 50% of these photoions escape by entrainment in the solar wind, and the remaining 50% re-impact the surface, as first suggested by Goldstein et al. (1981). Heretofore, this assumption has never been tested by sampling sodium ion trajectories in a magnetosphere model specifically tuned to Hermean conditions. Therefore, we have developed a full-particle tracing code to map the trajectories of charged particles under gravitational, magnetic and electric forces.

2. Ion Trajectories

Our code is based on the Toffoletto & Hill (1993) model, scaled to the Hermean dipole field, and with the ring current removed. Specifics of the model are given in Sarantos (2000) and Sarantos et al. (2001). We followed 3,500 Na ions in a tight grid of magnetic and electric fields at Mercury. The ions were launched at the surface, with an isotropic angular distribution with respect to the vertical at each launching site. Particles were set in motion at sites sampled every 15 degrees of latitude and 30 degrees of longitude to cover the entire dayside. The initial energy was taken to be ~1 eV. Since we only sampled neutrals produced via photon-sputtering, we let the initial ion spatial distribution vary as $\cos f \cos q$, where f and q are the launching latitude and longitude measured from the sub-solar point. We also ran cases in which ions were launched with an isotropic spatial distribution from the dayside surface. The ions were followed until either they hit the surface of the planet, crossed the magnetopause, or reached 7 Mercury radii (Rm) down the tail. It takes less than 10 seconds for an emitted ion to hit the surface of the planet, 30 seconds to a minute to escape to the solar wind, or up to a few minutes to re-impact the nightside by traveling down the tail and turning around.

In order to determine how the ion and accompanying neutral distributions respond to changes in the IMF, we show two runs using nominal magnetic field values. The coordinate system is Cartesian with +x toward the sun, +z normal to the ecliptic in the direction of north as defined at Earth, and y completes a right-handed coordinate system. We first chose a strong negative Bx: B(x,y,z)= (-30,+15,-10) nT. We then tried a second configuration with B(x,y,z) = (20,-10,-10) nT. These values are consistent with the dominance of the Bx component at the orbit of Mercury. In both cases the IMF was southward, which results in the maximum reconnection between Hermean fields and the IMF.

We chart the net change (ions recovered minus ions launched) per dayside surface element and unit local flux under the two aforementioned IMF configurations in Figure 1. Fifty ions were launched isotropically at every other grid point. Areas color-coded in red retained all ions launched. In both figures, dawn is to the left and dusk is to the right. No ions were launched from areas shown in white. A dawn-dusk asymmetry is evident in the spatial pattern in which ions are retained. Ions launched from dawn-side areas are more likely to be retained, whereas ions launched from the dusk-side have a tendency to escape to the solar wind. This is due to the assumption of a predominantly dawn-dusk electric field and may change for different assumed values of By (i.e. a northward IMF case).

Recycling is found to be very important. In either case roughly 60% of ions launched neutralize by impacting the surface. This result is in good agreement with earlier estimates (Ip, 1987). The IMF configuration and magnitude regulates how much sodium is returned to the surface after each sputtering ionization cycle. That has significant implications for the containment of heavy volatiles over geological times.

Because ions that hit the dayside surface have computed energies of 10 - 100 eV upon impact, no significant Na^+ sputtering occurs on the dayside as a result of returning photo-ions. In contrast, about 5 - 10% of ions launched follow Speiser-type orbits and accelerate up to 10 keV before they impact the surface on the nightside. An example of such trajectories is seen in Figure 2 for Na and Figure 3 for K ions. For both figures the IMF was B(x,y,z)=(-30, 15,-10) nT, and ions are launched with identical energies. The K^+ ions travel farther down the tail, and end up in the evening sector. The Na^+ ions have a tighter trajectory and impact on the dawn-side near 6 AM. These ions, which account for up to a tenth of photoionization losses, are mostly implanted into the regolith, but some cause secondary neutral production.

3. Conclusions and Directions for Future Work

We conclude that up to 60% of the photoions launched on the dayside near the surface will re-impact the dayside. For a dawn-dusk electric field, we find that most of the returning ions impact the dayside. This will be the case for a southward IMF. These photoions do not impact the dayside with sufficient energy to cause secondary sputtering, but on the nightside they will be accelerated to keV energies, and may cause secondary sputtering there. We plan to extend these results by 1) considering northward IMF, and 2) using a more realistic distribution of neutrals, both vertically and distributed around the planet. Our rate of ion retention is expected to decrease as we include ions created at progressively higher altitude, and as we increase the relative number of atoms closer to the terminator.

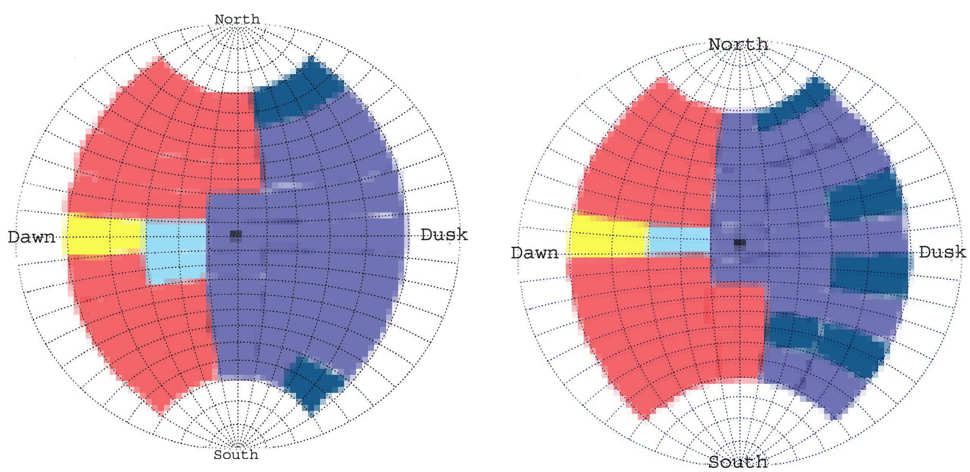

Figure 1. Ion retention pattern for ions launched isotropically from the surface with IMF B(x,y,z)=(-30, 15, -10) nT and B(x,y,z)=(20, -10, -10) nT, on the LHS and RHS, respectively. Red areas retain all ions launched within their boundaries, while dark blue areas lose all ions. Dawn is to the left.

Acknowledgments. This work was supported by the NASA Planetary Atmospheres program under Grants NAG5-11047 and NAG5-12566.

References

Goldstein, B.E., Suess, S.T. & Walker,R.J. 1981, J. Geophys. Res.,**86**, 5485

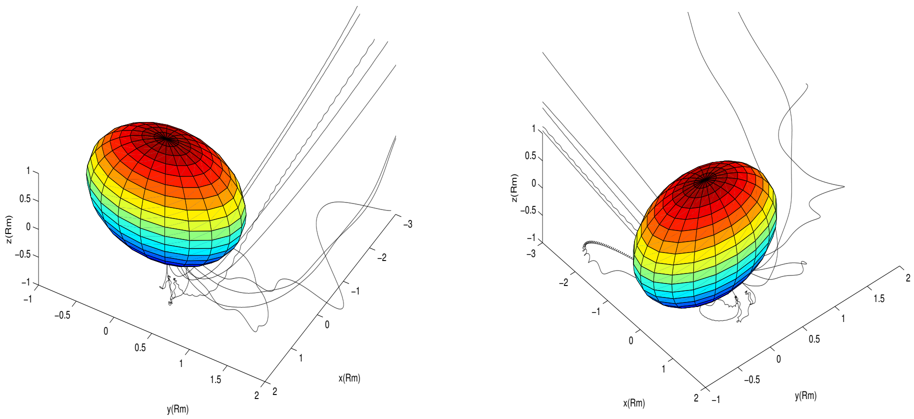

Figure 2. Comparison of the trajectories of K ions (left) and Na ions (right) launched from the same spots with identical IMF configurations B(x,y,z)=(-30,15,-10) nT. Ions have the same initial energy. The K ion ends up on the evening sector, while the Na ion impacts the dawn sector near 6 AM.

Sarantos, M. 2000, Masters Thesis (Houston: Rice Univ.)

Sarantos, M., Reiff, P.H., Hill, T.W., Killen, R.M. & Urquhart, A.L. 2001, Planet. Space Sci.,**49**, 1629

Toffoletto, F. R.& Hill, T.W. 1993, J. Geophys. Res., **98**, 1339

Highlights of Astronomy, Vol. 13
International Astronomical Union, 2003
O. Engvold, ed.

An Accurate Model of Mercury's Spin-Orbit Motion

Nicolas Rambaux & Eric Bois

Observatoire Aquitain des Sciences de l'Univers, UMR L3AB CNRS/INSU 5804, B.P. 89, F-33270 Floirac France

Abstract. Our work deals with the physical and dynamical causes that induce librations of Mercury around an equilibrium state defined by the 3:2 spin-orbit resonance. In order to integrate the spin-orbit motion of Mercury, we have used our gravitational model of the solar system including the Moon's spin-orbit motion. This model, called SONYR (acronym of Spin-Orbit N-bodY Relativistic model), was previously built by Bois, Journet and Vokrouhlickỳ in accordance with the requirements of the Lunar Laser Ranging observational accuracy.

Using the model, we have identified the main perturbations acting on the spin-orbit motion of Mercury such as the planetary interactions or the dynamical figure of the planet. Moreover, the complete rotation of Mercury exhibits two proper frequencies, namely 15.847 and 1 066 years, and in addition one spin-orbit secular resonance (298 898 years). A new determination of the mean obliquity of Mercury has been proposed. Besides, we have identified in the Hermean librations the impact of the uncertainty of the greatest principal moment of inertia (C/MR^2) on the obliquity as well as on the libration in longitude (2.3 mas and 0.45 as respectively for an increase of 1% on the C/MR^2 value). These accurate relations have to be taken into account in the context of the two upcoming missions BepiColombo and MESSENGER.

1. Introduction

The 3:2 spin-orbit resonance between the rotational and orbital motions of Mercury results from a functional dependence of the tidal friction adding to a non-zero eccentricity and a permanent asymmetry in the equatorial plane of the planet (Balogh and Giamperi, 2002). The upcoming space missions, MESSENGER (Solomon et al., 2001) and BepiColombo (Milani et al., 2001) with on-board instrumentation capable of measuring the Hermean rotational parameters stimulate the objective to reach an accurate theory of the rotational motion of Mercury. We use our BJV relativistic model of solar system integration (first post-Newtonian approximation level) including the spin-orbit coupled motion of the Moon (Bois and Vokrouhlickỳ, 1995; Bois, 2000). We extended this model to the spin-orbit couplings of the terrestrial planets Mercury, Venus, the Earth, the Moon and Mars; this updated model is at present called SONYR (acronym of Spin-Orbit N-BodY Relativistic model). The SONYR model permits to identify the different families of rotational librations in the spin-orbit motion of Mercury by clearly analyzing their causes (Rambaux and Bois, 2003).

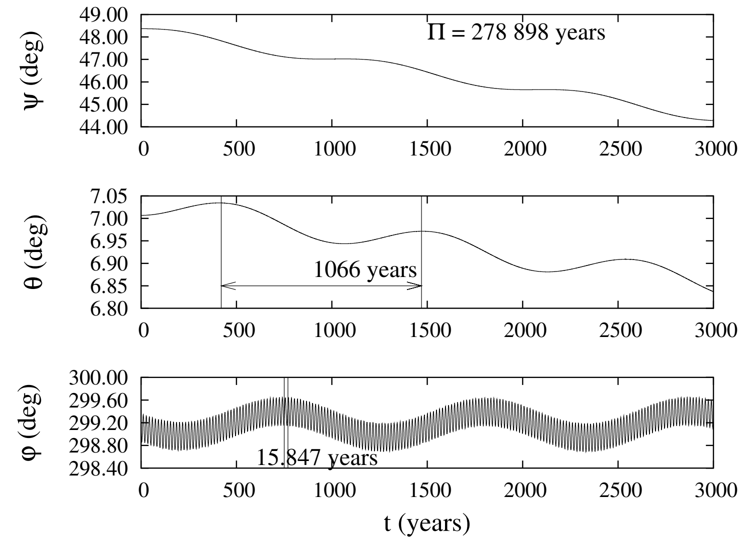

Figure 1. The rotational motion of Mercury in the 3-1-3 Eulerian sequence (ψ, θ, φ). The reference frame is given by the ecliptic J2000.

2. The Mercury's spin-orbit motion and its instantaneous obliquity

The figure 1 presents the rotational motion of Mercury in the usual 3-1-3 Eulerian sequence (ψ, θ, φ). The spin-orbit resonance of Mercury is characterized by two proper frequencies, namely 15.847 years and 1066 years. Moreover, the dynamical behavior of Mercury presents a secular variation of 278 898 years, which is due to the nodal precession of the equatorial plane of Mercury relative to the ecliptic plane. This secular variation can be understood as a spin-orbit secular resonance playing the role of a second synchronism.

In integrating the SONYR model, we also obtain the dynamical behavior of the η Hermean instantaneous obliquity. The dynamical evolution of η is presented in Figure 2. The dynamical behavior of η makes in evidence a sine function according to a long period of 1 066 years with an amplitude of 0.5 amin. The resulting mean obliquity η_{mean} of Mercury is 1.665 arc-minutes. Let us emphasize that the large amplitude of η could seriously make ambiguous the determination of η_{mean} by space missions.

3. The librations of Mercury

We have identified in the Hermean librations the impact of the variations of the greatest principal moment of inertia (C/MR^2) on the obliquity as well as on the libration in longitude φ, as follows :

$$\Delta\ (C/MR^2) \;=\; 1\,\% \;\Longrightarrow\; \begin{array}{ll} 2.3 \text{ mas} & \text{on } \eta \\ 0.45 \text{ as} & \text{on } \varphi \end{array} \qquad (1)$$

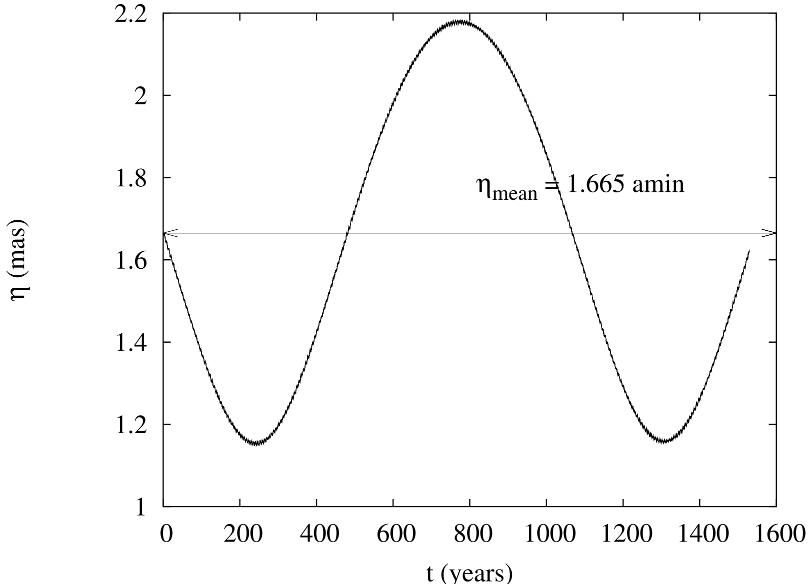

Figure 2. The η obliquity of Mercury plotted over 1 600 years. The resulting mean obliquity of Mercury is 1.665 arc-minutes.

Such librations belong to the family of potential librations according to the general terminology given in Bois (1995). One of the main objectives of the BepiColombo and MESSENGER missions is to measure the rotation parameters of Mercury up to an accuracy allowing to constrain size and physical state of the Hermean core (Solomon et al., 2001; Milani et al., 2001). In order to reach such an objective, the BepiColombo mission has to obtain a value of the C/MR^2 coefficient with an accuracy of 0.003, i.e. 1%. As a consequence, this mission foresees measuring the libration angle and the obliquity with an accuracy of 3.2 and 3.7 arcsec respectively (Milani et al., 2001). According to (1) coming from SONYR, these two signatures are very faint and probably too much with respect to the accuracy expected by the space missions.

References

Balogh, A., & Giamperi, G., 2002, Rep.Prog.Phys., 65, 529

Bois, E., & Vokrouhlicky, D., 1995, A & A, 300, 559

Bois, E., 1995, A & A 296, 850

Bois, E., 2000, C. R. Acad. Sci. Paris, T. 1, Serie IV, p. 809-823

Milani, A., Vokrouhlicky, D., & Bonanno, C., 2001, Planetary and Space Science, 49, 1579

Rambaux, N., & Bois, E., A & A, in press

Solomon, S.C., et al., 2001, Planetary and Space Science, 49, 1445

Highlights of Astronomy, Vol. 13
International Astronomical Union, 2003
O. Engvold, ed.

Plasma Dynamics in Mercury's Magnetosphere

Wing-Huen Ip

Institutes of Astronomy and Space Science, National Central University
Chung-Li, Taiwan 32054

Abstract. Mercury is in all sense of the words still Terra Incognito, its magnetosphere is hence little known. The only source of knowledge came from the in-situ measurements by the Mariner 10 close encounters in 1974. This has been complemented since by ground-based observations of the atomic sodium and potassium emissions in the vicinity of the planetary disk. This series of optical observations has produced intriguing evidence of magnetospheric and/or solar wind effects on the surface-plasma interaction processes. In this review we will describe the current theories of the corresponding space weather effects.

Most of our knowledge on Mercury's magnetosphere came from the Mariner 10 encounters in 1974 and 1975 (Ness et al. 1974; Simpson et al. 1974). The plasma and magnetic field measurements during the nightside crossing on March 29, 1974, have been analyzed and reviewed in many places (Connerney & Ness 1988; Russell et al. 1988; Christon 1989) we will not repeat this feat here. What we want to do is to give an update of the recent development in connection to the preparation for the new space missions to Mercury, namely, the MESSENGER Project of NASA and the BepiColombo Project of ESA and ISAS. There are several noteworthy results. On the observational side, the most important result which has generated a lot of discussions has to do with the discovery of a long lasting (week-long) event in the sodium brightness enhancement (Potter & Morgan 1997). A number of theoretical models have been proposed to expound the physical cause of such dramatic time variability in the surface brightness of atomic sodium emission. These include (1) the work by Luhmann et al. (1998) who applied the Tsyganenko model of the terrestrial magnetosphere to explore the driven mechanism of the solar wind at Mercury; (2) Kabin et al. (2000) who used the Michigan MHD code to study the response of Mercury's magnetosphere to different solar wind parameters; (3) Killen et al. (2001) who adapted the "Rice model" to study the changes of the configuration and position of Mercury's magnetospheric polar cusp because of the variabilities in the interplanetary magnetic field direction and dynamic pressure of the solar wind; (4) Ip & Kopp (2002) who produced resistive MHD models of Mercury's magnetosphere for the "open" and "closed" cases; (5) Kallio & Janhunen (2003) who used a 3D quasi-neutral hybrid model (to deal with the finite gyro radius effect) to explore the impact geometry of solar wind protons and "trapped" magnetospheric ions on the planetary surface; and (6) Leblanc et al. (2003) who simulated the recycling process of magnetospheric ions via surface sputtering and near-planet ionization.

Another issue of emerging interest has to do with the possible existence of field-aligned current (FAC). Slavin et al. (1997) reported the finding of strong FAC in the magneto-tail region by reanalysis of the Mariner 10 data. In the numerical simulation by Ip & Kopp (2002), FAC systems can be generated with different configurations under different solar wind conditions. But how could they be supported since there is no ionosphere to speak of at Mercury? They argued that the closure of such FAC can be maintained by the pickup ion current from ionization of the neutral exosphere (Ip & Kopp, 2003). The initial displacements of the new ions and electrons lead to the establishment of a current flow transverse to the magnetic field. According to Cheng et al. (1987), the equivalent integrated conductivity could be as much as 0.1-0.3 Mho. This value may be compared to a value of 1-10 Mho of the dayside integrated Pedersen conductivity of the terrestrial ionosphere. In this case, the path of FAC being organized by localized ionization process could be very patchy. Janhunen & Kallio (2003) proposed instead that partially closure could still be achieved at the planetary surface since the electrical conductivities of some minerals are not negligible (Glassmeier 1997). Another important topic, seldom addressed, concerns the magnetosphere-surface coupling effect via surface charging and photoemission (Grard et al. 1997) which could introduce strong day-night asymmetry in the magnetic and electric field structures of Mercury's magnetosphere. Without in-situ measurements it is difficult to assess the electric fields and plasma wave activity at Mercury (Blomberg 1997). However, it is interesting to note that Potter et al. (2002) reported that the radio of sodium to potassium in the Mercury exosphere is highly variable and that it's average value of about 100 is much higher than that for the moon. Furthermore, the potassium column density was observed to decrease with increasing level of solar activity. We might draw the inference that Mercury's polar caps are infected with ion cyclotron waves because of solar wind interaction. As a result, the potassium ions would be preferentially accelerated because of its lower gyrofrequency in comparison with that of the sodium ions (Ip & Kopp 2002). From this point of view, there are a great number of interesting phenomena to be explored by the new Mercury missions, to be supplemented by ground-based observations and spacecraft remote-sensing measurements.

Acknowledgments. This work was partially supported by National Science Council, Taiwan, under grant NSC 92-2111-M-008-001 and NSC 92-2112-M-008-023.

References

Blomberg, L.G. 1997, Mercury's magnetosphere, exosphere and surface: low-frequency field and wave measurements as a diagnostic tool, Planet. Space Sci., 45, 143

Cheng, A.F., Johnson, R.E., Krimigis, S.M. & Lanzerotti, L.J. 1987, Magnetosphere, exosphere, and surface of Mercury, Icarus, 71, 430

Christon, S.P., 1989, A comparison of the Mercury and Earth magnetospheres: Electron measurements and substorm time scales, Icarus, 71, 448

Connerney, J.E.P. & Ness, N.F. 1988, Mercury's magnetic field and interior, in Mercury, Eds. F. Vilas, C.R. Chapman & M. S. Matthews, pp. 494-513, Univ. Arizona, Press

Glassmeier, K.-H. 2000, Currents in Mercury's magnetosphere, in Magnetospheric Current Systems, AGU Geophysical Monograph 118, pp. 371-380

Grard, R. 1997, Photoemission on the surface of Mercury and related electrical phenomena, Planet. Space Sci., 45, 67

Ip, W.-H. & Kopp, A. 2002, MHD simulations of the solar wind interaction with Mercury, J. Geophys. Res., 107, 1348, doi:10.1029/2001JA009171

Ip, W.-H. & Kopp, A. 2003, Mercury's Birkeland current system, Adv. Space Res., in press

Janhunen, P. & Kallio, E. 2003, Surface conductivity of Mercury provides current closure and may affect magnetospheric symmetry, Ann. Geophys. In press

Kabin, K., Gobmosi, T.I., DeZeeuw, D.L. & Powell, K.G. 2000, Interaction of Mercury with the solar wind, Icarus, 143, 397

Kallio, E. & Janhunen, P. 2003, Modelling the solar wind interaction with Mercury by a quasineutral hybrid model, Ann. Geophys. in press

Killen, R.M., Potter, A.E., Reiff, P., Sarantos, M., Jackson, B.V., Hick, P. & Giles, B, 2001, Evidence for space weather at Mercury, J. Geophys. Res., 106, 20509

Leblanc, F., Delcourt, D., & Johnson, R.E. 2003, Medrcury's sodium exosphere: magnetospheric ion recycling, Icanus, in press.

Luhmann, J.G., Russell, C.T., & Tsyganenko, N.A. 1998, Disturbances in Merucyr's magnetosphere: Are the Mariner 10 "substorms" simply driven? J. Geophys. Res., 103, 9113

Ness, N.F., Behannon, K.W., Lepping, R.P., Whang, Y.C., & Schatten, K.H. 1974, Magnetic field observations near Mercury: Preliminary results from Mariner 10, Science, 185,151

Potter, A.E. & Morgan, T.H. 1997, Evidence for suprathermal sodium on Mercury, Adv. Space Rees., 19(10), 1571

Potter, A.E., Anderson, C.M., Killen, R.M. & Morgan, T.H., Ratio of sodium to potassium in the Mercury exosphere, J. Geophys. Res., 107, 5050, doi:10.1029/2000JE001493

Russell, C.T., Baker, D.N. & J.A. Slavin, The magnetosphere of Mercury, Eds. F. Vilas, C.R. Chapman, & M.S. Matthews, pp.514-561, Univ. Arizona Press

Simpson, J.A., Eraker, J.H., Lamport, J.E., & Walpole, P.H. 1974, Electrons and protons accelerated in Mercury's magnetic field, Science, 185, 160

Slavin, J.A., Owen, J.C.J., Connerney, J.E.P. & Christon, S.P. 1997, Mariner 10 observations of field-aligned currents at Mercury, Planet. Space Sci., 45, 133

Highlights of Astronomy, Vol. 13
International Astronomical Union, 2003
O. Engvold, ed.

Space Studies of the Black-Drop Effect at a Mercury Transit

Glenn Schneider

Steward Observatory, 933 N. Cherry Ave., University of Arizona, Tucson, Arizona 85721

Jay M. Pasachoff

Williams College-Hopkins Observatory, 33 Lab Campus Dr., Williamstown, MA 01267

Leon Golub

Smithsonian Astrophysical Observatory, Mail Stop 58, 60 Garden St., Cambridge, MA 02138

Abstract. Transits of Mercury and Venus across the face of the Sun are rare. The 20th century had 15 transits of Mercury and the 21st century will have 14, the two most recent occurring on 15 November 1999 and 7 May 2003. We report on our observations and analysis of a black-drop effect at the 1999 and 2003 transits of Mercury seen in high spatial resolution optical imaging with NASA's Transition Region and Coronal Explorer (TRACE) spacecraft. We have separated the primary contributors to this effect, solar limb darkening and broadening due to the instrumental point spread function, for the 1999 event. The observations are important for understanding historical observations of transits of Venus, which in the 18th and 19th centuries were basic for the determination of the scale of the solar system. Our observations are in preparation for the 8 June 2004 transit of Venus, the first to occur since 1882. Only five transits of Venus have ever been seen – in 1639, 1761, 1769, 1874, and 1882. These events occur in pairs, whose members are separated by 8 years, with an interval between pairs of 105 or 122 years. Nobody alive has ever seen a transit of Venus.

1. Motivation

Historically, transits of Venus were the major method for hundreds of years of determining the Astronomical Unit and thus the scale of the solar system, given that Kepler's laws of 1609/1618 are mere proportions. Edmond Halley presented a method of determining the A.U. by observing the durations of the chords across the Sun from a number of different locations on Earth. Accordingly, dozens of expeditions from many countries traveled around the world for the 18th and 19th-century transits, most famously including the voyage of Captain James Cook, who was sent to Tahiti to observe the 1769 event.

The accuracy of the measurements was severely impaired, however, by the "black-drop effect," in which the silhouette of Venus did not separate cleanly from the limb of the Sun during its inner contact. The timing accuracy was thus closer to a minute than to the expected second or two. As Schaefer (2001) has shown, many people have mistakenly attributed, and continue to mistakenly attribute, the black-drop effect to the atmosphere of Venus.

Our space observations of the transit of Mercury have shown the presence of a black-drop effect (Figure 1). Since Mercury has no substantial atmosphere and since the observations were taken from outside the Earth's atmosphere, clearly the effect – at least for Mercury – has causes other than due to a planetary atmosphere. By implication, Venus's black-drop effect would arise, at least in part, from similar causes.

2. Observations

The Transition Region and Explorer spacecraft can observe the Sun in a variety of ultraviolet wavelengths. For our studies of the 1999 transit of Mercury, we used only data from its broad band white-light channel. TRACE's 0.5 arc sec pixels, and temporally stable point-spread function unaffected by the Earth's atmosphere, give it spatial high resolution. A black-drop effect was observed in all frames near the point of internal tangency of the Mercurian and solar disks.

We discuss our calibrations, methods of analysis and extensive modeling in Schneider, Pasachoff & Golub (2001, 2004). We found major contributors giving rise to the black-drop effect come from two causes, that of the point-spread function of the telescope and that of the solar limb darkening. Removing those two contributions left us with images of the limb of Mercury unaffected by the solar limb.

The data for the 1999 event were sent to Earth in lossless uncompressed image format. Though we had worked with the TRACE planning team for the 2003 event to obtain a white-light data set at higher temporal cadence, those observations were downlinked in a compressed format normally used for solar observations. A irrecoverable loss of image fidelity at the bottom end of the dynamic sampling range resulted, and we were unable to recover sufficient accuracy to repeat our earlier analysis. We will make sure that the data for the upcoming Venus transit are returned to Earth in uncompressed format.

3. Future Work

Our immediate intention is to observe the 8 June 2004 transit of Venus from TRACE in orbit and from telescopes on the ground. Massive world-wide efforts will take place to observe this Venus transit. The European Southern Observatory, for example, is coordinating a public observation campaign. The International Astronomical Union's Commission on Education and Development has a Web site at http://www.transitofvenus.info that lists past and future observations, shows images, and provides links. We also intend to observe the transit of Mercury of 8 November 2006. After that, the following transits of Mercury aren't until 9 May 2016 and 11 November 2019.

Acknowledgments. This work was partially supported by NSF grant ATM-000545; Pasachoff's work on eclipses has also been supported in part by NGS/CRE. TRACE is supported by a NASA/GSFC contract to the Lockheed Martin Corp. NICMOS IDT S/W (NASA grant NAG 5-3042) was used extensively.

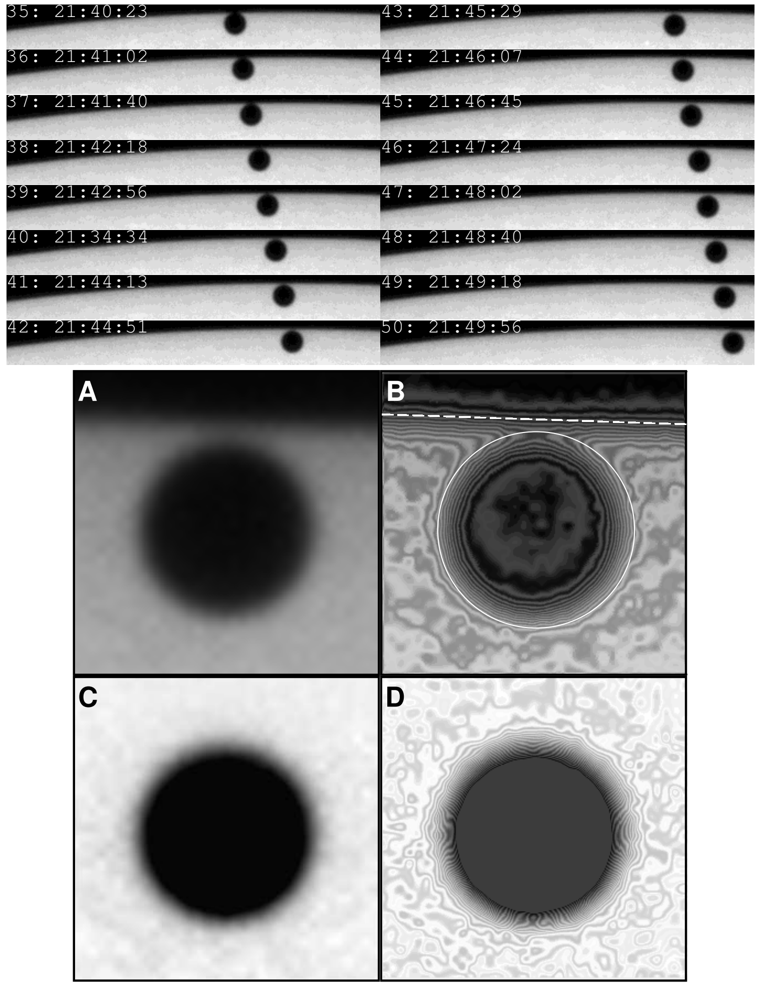

Figure 1. TRACE images. A-D from frame 50. A (image) & B (5% intensity contours; dashed line = solar limb, white circle = Mercury disk). Post-processed: C & D (1/2% contours) show no black-drop.

References

Schaefer, B. E., 2001, JHA, xxxii, 325

Schneider, G., Pasachoff, J. M., & Golub, L., 2001, BAAS, 33, 1037.

Schneider, G., Pasachoff, J. M., & Golub, L., 2004, Icarus, in press.

Highlights of Astronomy, Vol. 13
International Astronomical Union, 2003
O. Engvold, ed.

Origin and Bulk Chemical Composition of Mercury

Andrew J. R. Prentice and Daniel Jontof-Hutter

Mathematical Sciences, Monash University, Victoria 3800, Australia

Abstract. The origin of Mercury's high metal content is examined within a gas ring model for the condensation of the planetary system. Mercury's axial moment-of-inertia factor is predicted to be 0.325 ± 0.002.

The planet Mercury is remarkable because its mean uncompressed density ~ 5.3 g/cm^3 implies a Fe-Ni mass percent content of $\sim 67\%$. This is more than twice that of its neighbor Venus. This factor, coupled with other marked chemical differences between the four terrestrial planets, points to the conclusion that each planet 'received the overwhelming majority of its mass from narrow, compositionally-distinct annuli of material around the Sun' (Drake & Righter 2002). This situation finds a natural explanation within the Modern Laplacian theory of Solar system origin [hereafter MLT] (Prentice 1978, 2001a, 2001b).

According to the MLT, the planetary system condensed from a concentric family of gas rings. Discrete ring shedding takes place through the action of a radial turbulent stress $\langle \rho_t v_t^2 \rangle$ arising from powerful convective motions of speed v_t within the proto-solar cloud [PSC] cloud. If $\langle \rho_t v_t^2 \rangle$ equals $F_t \sim 35$ times the gas pressure $\rho v_s^2/\gamma$ at the PSC surface, where ρ is the density, v_s is the adiabatic sound speed and $\gamma = 1.4$, then a steep density rise by a factor $(1 + F_t)$ occurs and the orbital radii R_n $(n = 0, 1, 2, \ldots)$ of the rings match the mean planetary distances. Such large values of F_t, however, imply $v_t \geq 5v_s$, which is unlikely. To resolve this difficulty, Prentice & Dyt (2003) conducted a numerical simulation of supersonic turbulent convection in a model atmosphere to mimic the upper layer of the PSC. They discovered that the introduction of a velocity-dependent thermal diffusivity κ_t to model subgrid-scale motions induces a sharp negative temperature gradient at the top boundary. A modest density upturn factor of 3.5 ensues for peak vertical speeds $\langle v_t \rangle_p \simeq 1.1v_s$. This implies that the MLT may be validated with values $\langle v_t \rangle_p \simeq 3v_s$ and $F_t \simeq 10-15$, which are reasonable.

Consider now the results of a representative numerical simulation of the PSC's gravitational contraction which (i) accounts for the mean planetary distances, (ii) produces a Sun of the observed mass $M_\odot$, (iii) accounts for Mercury's high metal content and (iv) accounts for the 0.50 : 0.50 sub-solar ice-to-rock mass fractions of Ganymede and Callisto. In this simulation, the Mercurian gas ring is shed at orbital radius $R_n = 76.9R_\odot$, the residual cloud mass there is $M_n = 1.082M_\odot$, $T_n = 1643$ K and $p_n = 0.1566$ bar.

A schematic view of the gas ring cast off at Mercury's initial orbit R_n is given below. The ring is assumed to have a uniform temperature T_n and orbital angular momentum per unit mass $\sqrt{GM_nR_n}$, where G is the gravitation constant. The gas pressure at distance ξ from the mean circular orbit is $p_{\rm gas}(\xi) = p_n \exp(-\frac{1}{2}\alpha_n \xi^2/R_n^2)$, where $\alpha_n = \mu GM_n/\Re T_nR_n \simeq 467$ is a constant and $\mu = 2.379$ is the mean molecular weight. Consider next the condensation of a chemical species i whose vapor pressure is $p_{i,\rm vap} = \exp(B_i - A_i/T_n)$. Here A_i, B_i are thermodynamic constants – given below for reference temperature 1600 K. Let $p_{i,n}(\xi) = (\mu/\mu_i)X_i p_{\rm gas}$ denote the initial partial pressure, where μ_i and X_i are the molecular weight and total mass fraction of the species. Condensation is then restricted to minor radii $\xi < \xi_i$ where $p_{i,n}(\xi) > p_{i,n}(\xi_i) = p_{i,\rm vap}(T_n)$. The condensed mass fraction is $X_{i,\rm cond} = X_i[1 - (1 + f_i)\exp(-f_i)]$, where $f_i = A_i(1/T_n - 1/T_{i,n})$ and $T_{i,n} = A_i/(B_i - \log(p_{i,n}(0))$ is the condensation temperature on the mean orbit $\xi = 0$. For Fe ($i = 1$), we have $X_1/\mu_1 = 2.223 \times 10^{-5}$, $A_1 = 47670$, $B_1 = 16.089$, $T_{1,n} = 1715$ K and $X_{1,\rm cond}/X_1 = 0.346$. For species 2 we choose $MgSiO_3$. Here $X_2 = (X_{\rm H_2O}/X_{\rm H_2})\sqrt{X_{\rm Mg}X_{\rm SiO}} = 8.89 \times 10^{-6}$, $\mu_2 = 292.5$, $A_2 = 63773$, $B_2 = 20.759$, and hence $T_{2,n} = 1633$ K. Since $T_{2,n} < T_n$, $X_{2,\rm cond} = 0$. Mercury thus condensed at such a high temperature that $MgSiO_3$ (and also Mg_2SiO_4) was excluded from its bulk chemical makeup. Such an explanation for Mercury's low silicate content was first considered by Lewis (1972).

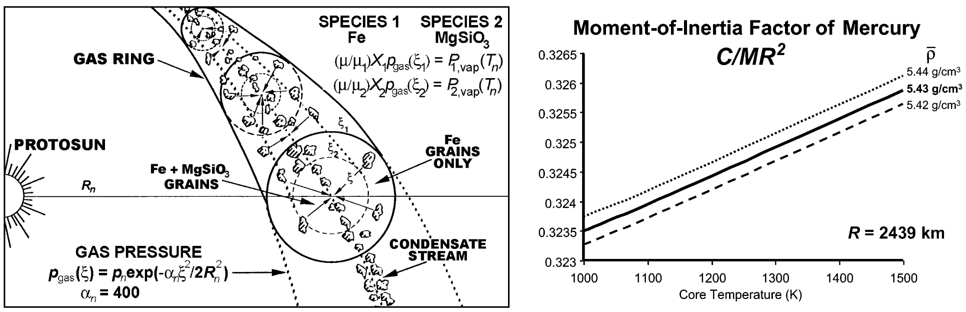

Figure 1. Left: A schematic view of the gas ring cast off at Mercury's initial orbit. Right: A plot of the moment-of-inertia factor vs T_c

The bulk composition (& mass percents) of the Mercurian condensate are Fe-Ni-Cr-Co-V (67.00), $Ca_2Al_2SiO_7$ (26.12), $MgAl_2O_4$ (4.07), Al_2O_3 (1.73) and $CaTiO_3$ (1.08). A suite of simplified two-zone structural models based on this mix has been constructed. Each model has a Fe-Ni core of mass 67% and uniform temperature T_c, and a gehlenite-spinel mantle of temperature T_m. Self-compression is modeled with the properties of Fe and spinel. T_m is chosen so that $\overline{\rho}$ matches the observed value 5.43 ± 0.01 g/cm^3, subject to 700 K $\leq T_m \leq T_c \leq$ 1500 K. A plot of the moment-of-inertia factor vs T_c is shown. We predict that $C/MR^2 = 0.325 \pm 0.002$. This coincides with Siegfried & Solomon (1974). We thank Charles Morgan and Steven Morton for technical assistance.

References

Drake, M.J.,& Righter, K. 2002, Nature, 416, 39
Lewis, J.S. 1972, Earth Planet. Sci. Lett., 15, 286
Prentice, A. J. R. 1978, Moon & Planets, 19, 341
Prentice, A. J. R. 2001a, Earth Moon & Planets, 87, 11
Prentice, A. J. R. 2001b, http://www.lpi.usra.edu/meetings/mercury01/pdf/8061.pdf
Prentice, A. J. R., & Dyt, C.P. 2003, MNRAS, 341, 644
Siegfried, R.W., & Solomon, S.C. 1974, Icarus, 23, 192

Highlights of Astronomy, Vol. 13
International Astronomical Union, 2003
O. Engvold, ed.

The BepiColombo Mission

Rita Schulz

Research and Scientific Support Department of ESA, ESTEC, Postbus 299, 2200 AG Noordwijk, The Netherlands

Peter Falkner, Anthony Peacock, Christian Erd, Nicola Rando

Science Payloads and Advanced Concepts Office of ESA, ESTEC, Postbus 299, 2200 AG Noordwijk, The Netherlands

Stefan Kraft

cosine Research B.V., Niels Bohrweg 11, 2333 CA Leiden, The Netherlands

Abstract.

BepiColombo is an interdisciplinary mission to the planet Mercury which will provide the detailed information necessary to understand Mercury and its magnetospheric environment. The mission is envisaged to consist of three spacecrafts, the Mercury Planetary Orbiter (MPO), the Mercury Magnetospheric Orbiter (MMO) and the Mercury Surface Element (MSE). The mission went through a re-assessment with the aim of optimizing resources and and advancing the scientific return. Various mission scenarios were investigated and new payload concepts were adopted. The newly defined mission will be presented focusing on the launch scenario and the MPO reference payload.

1. Introduction

Mercury bears information, which unraveled might be the key to understanding the origin and early evolution of our solar system. The necessary details of its properties can, however, only be provided by a space mission. Nevertheless, only one spacecraft ever visited Mercury almost 30 years ago, when Mariner 10 performed three fly-byes in 1974-1975. Hence, precise characterization is still imminent. Drawing conclusions on the formation and evolution of Mercury requires a complete description of the planet and its environment. BepiColombo therefore is an interdisciplinary mission dedicated to a comprehensive investigation of the four basic components of the Mercury system: the planet's interior, surface, exosphere and magnetosphere. As such it will open a new frontier in the study of our solar system. The mission went through a re-assessment process to optimize resources and advance the scientific return. The new mission scenario is presented in a concise overview.

2. Mission Overview

BepiColombo has been defined as a collaboration between ESA and ISAS/JAXA. It shall consist of three scientific elements, the Mercury Planetary Orbiter (MPO), the Mercury Magnetospheric Orbiter (MMO) and the Mercury Surface Element (MSE). The MMO, provided by ISAS/JAXA, focuses on investigating the wave and particle environment of the planet from an eccentric orbit. The spinning spacecraft accommodates mostly field, wave and particle instruments (ESA, 2000). The MPO and MSE are dedicated to the characterization of Mercury itself. The MPO is three-axis-stabilized and nadir pointing. Its low-eccentricity polar orbit will provide excellent spatial resolution over the entire planet surface. The MSE shall perform in-situ investigations of Mercury's surface and subsurface. For more details on the MSE see Thomas et al. (this volume).

During the re-assessment various mission profiles as well as new payload concepts and technologies were investigated in parallel. In the newly defined BepiColombo mission the MPO and MMO will no longer be launched separately on two Soyuz Fregats, but together on a single stack whereby the MPO will carry the MMO. This new scenario leaves the second Soyuz Fregat free for the launch of the MSE. The launch of the MPO/MMO complement is planned for 2012. Solar electric propulsion will be used for the journey to Mercury and chemical propulsion for the insertion of the spacecrafts into their dedicated orbits.

Accommodating both orbiters on a single Soyuz Fregat required to decrease the mass of the cruise composite, hence to optimize the mission in terms of hardware (scientific elements, propulsion modules) and mission analysis for cruise and orbit insertion (to save propellant mass). This has been achieved without compromising on the overall scientific return of the mission.

2.1. The MPO Reference Payload

A new payload concept was adopted which is based on a high level of integration. The MPO reference payload does no longer consist of individual instruments, but of the front ends of these instruments which share common subsystems such as DPU, electronics and power. In addition advantage was taken of the fact that new technologies and miniaturization techniques have been developed in recent years which allow alternative approaches in instrument design and increased instrument performances. The new concept led to a reduction of the payload mass by about 20 kg while at the same time more instruments could be accommodated. The MPO reference payload now also contains a thermal IR mapping spectrometer and radiometer, a neutral and ion particle analyzer, a limb pointing camera and a magnetometer. Figure 1 outlines the MPO reference payload and the topics addressed by the measurements.

Major effort was also put into optimizing the scientific return by defining the payload complement such that individual measurements can be interrelated and complement each other. The spatial resolution of the instruments measuring the elemental and mineralogical surface composition has for instance been adjusted to that of the camera, mapping the global surface morphology. This not only allows the morphological characterization of individual surface features (craters, basins, etc.) but also identification of compositional variations between features. The neutron spectrometer and the radiometer will take complemen-

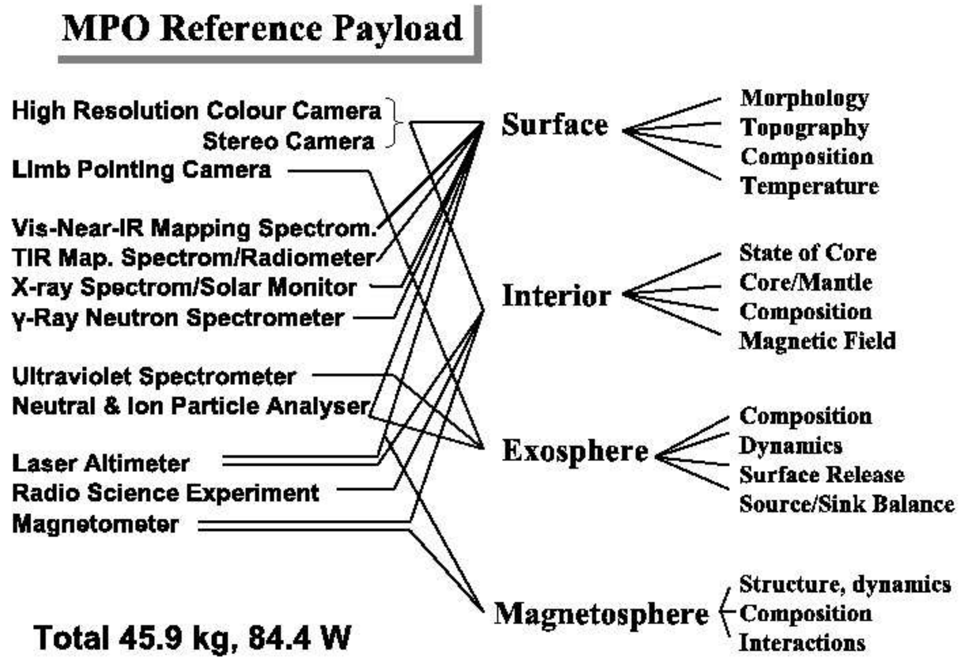

Figure 1. The MPO Reference Payload

tary measurements of the radar-bright spots in the polar regions to identify their composition. The measurements of the radio science experiment in combination with the high resolution camera and the laser altimeter will provide insight into the interior of the planet. Simultaneous measurements from MPO and MMO will resolve spatial and temporal ambiguities in the exosphere and magnetosphere that would arise from single point observations. For instance, having magnetometers on board both orbiters will allow to disentangle the contribution of the planetary magnetic field from that of the magnetosphere.

3. Summary

The MPO and MMO are on dedicated orbits optimized for the study of Mercury and its magnetosphere. Together they will provide the information needed to understand the planet and its environment, such as high accuracy measurements of the planet's interior structure, a full coverage of the planet surface at a resolution of 500 m, the detailed structure of the planetary magnetic field and a complete characterization of Mercury's exosphere. Surface morphology will be correlated to surface composition. The MPO orbit provides optimal coverage of the polar regions. Hence the material of the radar-bright spots observed from ground and suspected to be either water ice or sulfur will be identified. A detection of sulfur would strongly support the presence of an at least partially molten core.

4. Reference List

References

ESA (2000) BepiColombo: An interdisciplinary cornerstone mission to the planet Mercury, System Technology Study Report, April 2000, ESA-SCI(2000)1.

Thomas, N., Schulz, R., & Falkner, P., The BepiColombo Lander - MSE, this volume

Highlights of Astronomy, Vol. 13
International Astronomical Union, 2003
O. Engvold, ed.

The BepiColombo Lander – MSE

Nicolas Thomas

Physikalisches Institut, University of Bern, Sidlerstr. 5, CH-3012 Bern, Switzerland.

Rita Schulz

Research and Scientific Support Department, European Space Research and Technology Centre (ESTEC), Keplerlaan 1, 2200 AG Noordwijk, The Netherlands.

Peter Falkner

Science Payload and Advanced Concepts Office, European Space Research and Technology Centre (ESTEC), Keplerlaan 1, 2200 AG Noordwijk, The Netherlands.

Abstract. The European Space Agency's BepiColombo mission to the planet, Mercury, is planned for launch in 2012. A lander called the MSE (Mercury Surface Element) has been proposed for the mission. To be compatible with all the constraints for a soft-landing on Mercury, the payload must be highly miniaturized. Although the requirements are challenging, significant study, design, and bread-board work has been performed which suggests that excellent science can be accomplished within a total payload mass of around 7 kg. The MSE would provide a substantial increase in our knowledge of the Hermean surface after that which can be obtained from orbital remote sensing.

1. Introduction

BepiColombo (BpC) is one of the main missions of the European Space Agency's Cosmic Vision programme. The mission is to provide a detailed investigation of the planet, Mercury (see Schulz, this volume). It was recognized early in the study phase that a complete investigation requires measurements which could only be acquired by landing on the surface. Hence, as a complement to the Mercury Planetary Orbiter (MPO) and the Mercury Magnetospheric Orbiter (MMO), a lander package known as the Mercury Surface Element (MSE) was studied. Two concepts were originally investigated (ESA, 2000). A hard landing system (penetrator) was one option. However, such systems have to be designed to withstand enormous shock levels. Perhaps more importantly, experiments can be compromised because the landing site is physically affected by the impact itself. In order to sample unaffected material, the experiments must somehow get to it. Hence, a soft landing was also studied. It was clear immediately that a soft landing would require a lot of fuel to decelerate the lander because of the absence of a Hermean atmosphere. The primary concern was mass. How massive would the lander have to be in order to provide a significant payload mass together with the accompanying infrastructure (landing system, communications sub-system, power supply and distribution unit, etc.) needed to conduct the experiments. Indications are that payload masses of the order of 5 to 7 kg could be available. Given the advantages of soft landing and the degree of payload miniaturization possible, it was decided, following mission selection in May 2000, to pursue this option exclusively. Here, we describe briefly the landing system, the scientific objectives, and the payload.

2. Scientific Objectives

The objectives of the MSE are
- to determine the elemental and mineralogical composition of the surface,
- to determine the mechanical and optical properties of the regolith,
- to search for small scale inhomogeneity,
- to determine the local magnetic field strength,
- to study the properties of the local exosphere,
- to determine the surface heat flow.
- to provide "ground-truth" for the measurements made from orbit.

3. The Landing System

The MSE will be launched separately from the MPO and MMO. It will enter orbit around Mercury and descent will begin by firing the main engine. A radar altimeter will be used to determine its altitude until it is approximately 2 km above the surface. The lander's horizontal velocity will then be reduced to allow direct descent to the surface. At 100 m above the surface thrusters will be fired again to slow the vertical descent. The main tanks will then be jettisoned to reduce impact mass. Airbags will then inflate and the lander will bounce onto the surface. Once the lander has stop rolling, the airbags will be released and the small lander will drop to the surface ready for deployment.

4. Landing Site Constraints

The solar flux at Mercury can be as high as 10 times that at Earth. With no atmosphere, any surface normal to the solar flux will heat to an equilibrium temperature determined by the surface albedo. Because of the proposed landing system and the large-scale surface roughness, it is hard to control the lander's orientation with respect to the Sun and thereby provide protection from the heat. Although not yet selected, it seems probable that the landing site should be on the night-side of the planet but close to the morning terminator. This would allow the lander to make an initial series of measurements and determine its own orientation before sunrise. Solar panels would then be oriented by the lander autonomously to provide both power and protection from the Sun.

5. The Strawman Payload

The payload has yet to be selected but, for engineering purposes, a payload which could fulfill the objectives within the available mass has been compiled.

5.1. Panoramic Camera

A stereo camera on a mast with an set of filters is, since the Imager for Mars Pathfinder (Smith et al., 1997), standard equipment on landers. Lighter versions are now possible through the development of integrated read-out electronics carried out by ESA within the technical research programme. The night-side landing makes provision of a "flash light" based on light-emitting diodes, an attractive addition.

5.2. Invasive Device

A lander allows penetration of the surface which gives access to material which has not been affected by recent space weathering. A penetration device (the "Mole") has been developed for the Beagle 2 lander and a modified version of this system is foreseen for the MSE. This version will incorporate temperature sensors and permittivity probes to make in situ measurements.

5.3. Mobility - Microrover

It has been recognized that mobility in a lander is a critical item. It can be used to limit bias because of local inhomogeneity. Mobility also allows experiments to get away from areas "damaged" by the landing itself. A 2.2 kg microrover (the "nanokhod") has been developed as part of an ESA study. The device runs on tracks and is powered by the lander itself through cables. This limits the total distance the rover can travel (up to 100 m traverses are nevertheless possible) but it greatly reduces the mass needed and is, for this reason, ideal for the MSE. The rover has a payload bay in which several experiments can be housed. The payload bay can be rotated and moved to bring the analytical experiment to the sample. Each experiment bay is small but 1.1 kg can be carried. Development of several experiments to fit in this mass and volume has been performed.

Micro-imager A proto-type stereo optical imaging system has been built to provide data on the regolith of the Hermean surface. Resolutions of about 100 microns are expected.

Mössbauer Spectrometer Mössbauer spectrometers are currently flying on Beagle 2 and the Mars Exploration Rovers in order to determine the iron mineralogy of the Martian surface. Similar goals could be envisaged for Mercury. The mass of the current devices are around 500 g but could be reduced for the MSE.

Alpha, X-ray Spectrometer The elemental composition of the surface can be addressed by alpha and X-ray spectroscopy. Similar systems have flown on, for example, Mars Pathfinder. Again, around 500 g would allow a fairly sophisticated instrument.

Laser Mass Spectrometer Laser-induced ablation followed by investigation of the mass spectrum via time of flight analysis is a relatively new technique in planetary exploration. However, new technological developments have been made which suggest that resolutions of 300 are achievable within a mass of roughly 250 g. This would allow isotopic composition analysis. A proto-type with a resolution of at least 60 has already been built.

5.4. Magnetometer

A magnetometer on the MSE would provide a lightweight estimate of the field strength at the surface. The MPO and the MMO both carry magnetometers but the influence of the solar wind on the magnetic field configuration of the planet is not likely to be simple. A magnetometer on the surface will constrain models by providing the largest "signal to noise" from the planet itself.

5.5. Other experiments

The payload is by no means fixed and other lightweight experiments might still be accommodated. There are several interesting possibilities. Seismometry would be desirable although with only one station on the surface, the interpretation of the data would not be straightforward. Investigation of the regolith structure might be achieved by an IR spectrometer and microscope combination. A corner reflector for a laser altimeter in orbit would be a further lightweight addition to the payload which could potentially enhance the science return.

The densities of the exosphere are highest at the surface, of course, and hence an investigation of the exospheric composition and its variation in composition and density with time is also an interesting experiment. One potential problem here is the influence of the landing system because the mass of propellant being used to slow the lander down before impact is a significant fraction of the local exosphere mass. This remains the subject of further research.

6. Concluding Remarks

The MSE is itself a challenging experiment. However, further progress in the field of planetology requires in situ investigation of planetary surfaces. The MSE is an example of how this might be achieved.

Further details on the MSE and the whole BepiColombo mission are given in ESA (2000). Updated reports on the mission will appear in due course.

7. References

ESA (2000) BepiColombo: An interdisciplinary cornerstone mission to the planet Mercury, System Technology Study Report, April 2000, ESA-SCI(2000)1.

Schulz, R. (2003) The BepiColombo mission, this volume.

Smith, P.H. et al. (1997) The Imager for Mars Pathfinder experiment, J. Geophys. Res., 102, 4003.

JD3

Magnetic Field & Helicity in the Sun & Heliosphere

Chairpersons: B. Schmieder and D. Rust

Editors: B. Schmieder (Chief-Editor) and D. Rust

Highlights of Astronomy, Vol. 13
International Astronomical Union, 2003
O. Engvold, ed.

Magnetic Helicity Conservation

Mitchell A. Berger

Mathematics, University College London, Gower Street London WC1E 6BT U.K.

Abstract. Magnetic Helicity measures basic structural properties of magnetic fields such as twist, shear, linking, writhe, and handedness. It is conserved in ideal MHD and approximately conserved during reconnection. The minimum energy state of a field with a given magnetic helicity is a linear force free field. Helicity plays an important role in MHD turbulence and dynamo theory, and provides a valuable observational tool in solar and space physics. Helicity conservation can be tracked from the solar dynamo to active regions to coronal mass ejections to magnetic clouds in interplanetary space.

1. Magnetic Helicity: Basic Properties

We can define the magnetic helicity of all space as a double integral over the magnetic field:

$$H = \frac{1}{4\pi} \int \int \mathbf{B}(\mathbf{x}) \cdot \frac{\mathbf{r}}{r^3} \times \mathbf{B}(\mathbf{y})\ \mathrm{d}^3y\ \mathrm{d}^3x \qquad (\mathbf{r} = \mathbf{y} - \mathbf{x}). \tag{1}$$

This formula also works inside a volume bounded by a magnetic surface S, where $\mathbf{B} \cdot \hat{n}|_S = 0$ (Moffatt 1969). Nobody computes with this formula, but it has the advantage of being independent of gauge, and it has a similar form to the Gauss linking integral. For ease of use, we remove one of the integrals via the Coulomb gauge (Biot–Savart) vector potential (Cantarella et al. 2001)

$$\mathbf{A}(\mathbf{x}) = \frac{1}{4\pi} \int \frac{\mathbf{r}}{r^3} \times \mathbf{B}(\mathbf{y})\ \mathrm{d}^3y, \tag{2}$$

which gives the more familiar form $H = \int \mathbf{A} \cdot \mathbf{B}\ \mathrm{d}^3x$.

For volumes $\mathcal{V}$ not bounded by a magnetic surface the helicity is measured relative to that of the potential field P, where $\nabla \times \mathbf{P} = 0$ and $\mathbf{P} \cdot \hat{n}|_S = \mathbf{B} \cdot \hat{n}|_S$:

$$H_{\mathcal{V}} = \int_{corona} (\mathbf{A} + \mathbf{A}_P) \cdot (\mathbf{B} - \mathbf{B}_P)\ \mathrm{d}^3x \tag{3}$$

(Berger & Field 1984; Finn & Antonsen 1985). This formula gives the same result for any choice of gauge; however a particularly convenient choice satisfies

$$\nabla \times \mathbf{A}_P = \mathbf{P}, \qquad \hat{\mathbf{n}} \cdot \nabla \times \mathbf{A}_P = B_n, \tag{4}$$

$$\nabla \cdot \mathbf{A}_P = 0, \qquad \mathbf{A}_P \cdot \hat{\mathbf{n}} = 0. \tag{5}$$

With the above expressions, we can compute time derivatives due to internal dissipation and to flow through boundaries. For example, the time derivative of the magnetic helicity H_{corona} of the solar corona is

$$\frac{\mathrm{d}H_{corona}}{\mathrm{d}t} = -2\int_{corona} \mathbf{E}\cdot\mathbf{B}\ \mathrm{d}^3x - 2\oint_{photosphere} \mathbf{A}_P \times \mathbf{E}\cdot\hat{\mathbf{n}}\ \mathrm{d}^2x. \qquad (6)$$

The volume integral of $\mathbf{E}\cdot\mathbf{B}$ gives helicity dissipation. In ideal MHD the parallel electric field vanishes, so magnetic helicity is conserved, and only changes due to flow through the boundary. For finite resistivity, an inequality relates helicity dissipation to energy dissipation (Berger 1984). If we let the magnetic energy $W = \frac{1}{2}\int B^2\ \mathrm{d}^3x$, then we can define a length scale $L \equiv |H|/2W$. The corresponding dissipation time is $\tau_d = L^2/\eta$. Consider a reconnection occurring over a time Δt. Then the inequality gives

$$\left|\frac{\Delta H}{H}\right| \leq \sqrt{\frac{\Delta t}{\tau_d}}. \qquad (7)$$

For solar flares, if we choose $\Delta t \sim 10^3 s$, $L \sim 10^6$ m, $\eta \sim 1\,\mathrm{m}^2 s^{-1}$, then $\tau_d \sim 10^{12} s$ and $|\Delta H/H| < 3\times 10^{-5}$.

These results can be generalized to situations where a simple Ohm's law is not appropriate (Berger 1984). Also we should note that helicity is not conserved (and not even well defined) in a periodic box with net flux (Berger 1997). The approximate conservation of magnetic helicity during reconnection can generate twist in coronal loops by changing mutual helicity into self helicity (Berger 1982; Song & Lysak 1989; Wright & Berger 1989).

The minimum energy state for a given helicity is a linear force free field (Woltjer 1958; Dixon et al. 1989). Taylor (1974) pointed out that reconnection would be necessary to achieve this minimum energy state. Heyvaerts & Priest (1984) applied the theory of relaxation to force-free fields to coronal heating theory.

2. Helicity Observations

Northern coronal structures tend to have negative helicity; Southern structures tend to have positive helicity (Hale 1927; Seehafer 1990; Rust & Kumar 1994; Martin et al. 1994; Pevtsov et al. 1995; Canfield et al. 1999). This tells us the *sign* of helicity, and already gives us important clues to the nature of solar magnetism. However, new work emphasizes *quantitative* measurements of helicity. Can we detail the total magnetic helicity balance of the sun and heliosphere? (Rust & Kumar 1994; Rust & Kumar 1996).

On the largest scale, rotation of the solar dipole injects positive helicity into the Southern Parker spiral (Bieber et al. 1987). On the scale of the entire sun, differential rotation of the solar field injects positive helicity into the Southern interior, with consequences for the solar dynamo (Berger & Ruzmaikin 2000).

The helicity of coronal fields has been measured in several different ways. Vector magnetogram studies give part of the current helicity (j_z/B_z) (Abremenko et al. 1997; Bao & Zhang 1998; Leka & Skumanich 1999; Pevtsov et al. 2002). Differential rotation can inject helicity into active regions (van Ballegooijen et al. 1998; DeVore 2000, Demoulin et al. 2002). Magnetograms can be

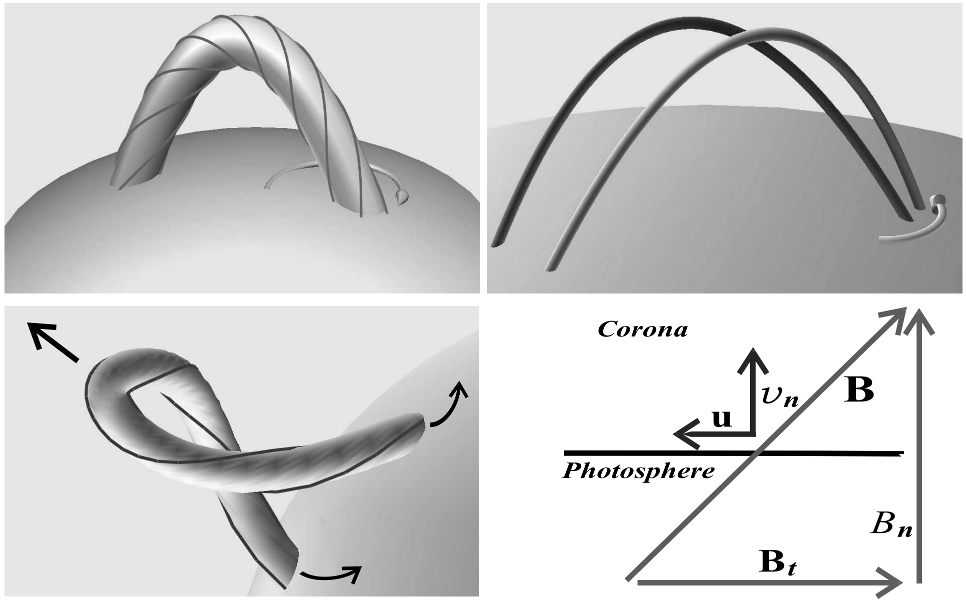

Figure 1. Top: photospheric motions can twist, shear, or braid corona fields. Bottom: The footpoints of a rising flux tube display an apparent transverse motion $\mathbf{u}$. Geometrically, $\mathbf{u}/v_n = -\mathbf{B}_t/B_n$.

combined with best fit force-free extrapolations to estimate the helicity (Green et al. 2002).

Let the photospheric plasma velocity be $\mathbf{v} = \mathbf{v}_t + v_n\hat{r}$ in terms of its tangential and normal (radial) components. Then the flow of helicity through the photosphere (6) is

$$\frac{\mathrm{d}H_{corona}}{\mathrm{d}t} = 2\oint_{photosphere}((\mathbf{A}_P\cdot\mathbf{B}_t)\mathbf{v}_n - (\mathbf{A}_P\cdot\mathbf{v}_t)B_n)\ \mathrm{d}^2x \tag{8}$$

(Kusano et al. 2002). We can infer the components of $\mathbf{v}$ from Döppler measurements. Alternatively, local correlation tracking velocity techniques give the motion $\mathbf{u}$ of a magnetic element across the photosphere (Chae 2001; Nindos et al. 2003). A rising field line has an *apparent* transverse motion $-(v_n/B_n)\mathbf{B}_t$. Adding the plasma transverse motion, we obtain $\mathbf{u} = \mathbf{u}_t - (v_n/B_n)\mathbf{B}_t$. This makes the helicity flow equation especially simple (Démoulin & Berger 2003):

$$\frac{\mathrm{d}H_{corona}}{\mathrm{d}t} = -2\oint_{photosphere}(\mathbf{A}_P\cdot\mathbf{u})B_n\ \mathrm{d}^2x. \tag{9}$$

Energy flow also can be expressed in terms of the tracking velocity:

$$\frac{\mathrm{d}E_{corona}}{\mathrm{d}t} = -\frac{1}{\mu_0}\oint_{photosphere}(\mathbf{B}\cdot\mathbf{u})B_n\ \mathrm{d}^2x. \tag{10}$$

References

Abramenko, V. I. Wang, T., & Yurchishin, V. B. 1997, Solar Phys., 174, 291

Bao, S. & Zhang, H. 1998, ApJ, 496, L43

Berger, M. A. 1982, Bull. Am. Astron. Soc., 14, 978

Berger, M. A. 1984, Geophys. Astrophys. Fluid Dyn., 30, 79

Berger, M. A. & Field, G. B. 1984, J. Fluid Mech., 147, 133

Berger, M. A. 1997, JGR, 102, 2637

Berger, M. A. & Ruzmaikin, A. 2000, JGR, 105, 10481

Bieber, J. W., Evenson, P., & Matthaeus, W. H. 1987, ApJ, 315, 700

Canfield, R. C., Hudson, H. S., & McKenzie, D. E. 1999, JGR Lett., 26, 627

Cantarella, J., DeTurck, D., & Gluck, H. 2001, J Math Phys 42, 876

Chae, J. 2001, ApJ, 560, L95

Démoulin, P., Mandrini, C. H., Van Driel-Gesztelyi, L., Lopez Fuentes, M. C., & G. Aulanier 2002, Solar Phys., 207, 87

Démoulin, P. & Berger, M. A. 2003 Solar Phys., 215, 203

DeVore, C. R. 2000, ApJ, 539, 944

Dixon, A., Berger, M. A., Browning, P., & Priest, E. R. 1989, å, 225, 156

Finn, J. M. & Antonsen, T. M. Jr. 1985, Com.Plas.Phys. Cont.Fus., 9, 11

Green, L. G. et al. 2002 Solar Phys., 208, 43

Hale, G. E. 1927 *Nature*, 119, 708

Heyvaerts, J. & Priest, E.R. 1984, A&A, 137, 63

Kusano, K., Maeshiro, T., Yokoyama, T. & Sakurai, T. 2002, ApJ, 577, 501

Leka, K. D., & Skumanich, A. 1999, Solar Phys., 188, 3

Martin, S. F., Billamoria, R. & Tracadas, P. W. 1994, Solar surface magnetism, R. J. Rutten and C. J. Schrijver eds., Kluwer, page 303.

Moffatt, H. K. 1969 J Fluid Mech., 35, 117

Nindos, A., Zhang, J., & Zhang, H. 2003, ApJ, 594, 1033

Pevtsov, A. A., Canfield, R. C., & Metcalf, T. R. 1995, ApJ, 440, L109

Rust, D. M. & Kumar, A. 1994, Solar Phys., 155, 69

Rust, D. M. & Kumar, A. 1996, ApJ, 464, L199

Seehafer, N. 1990, Solar Phys., 125, 219

Song, Y. & Lysak, R. L. 1989, JGR, 94, 5273

Taylor, J. B. 1986, Rev. Mod. Phys., 58, 741

van Ballegooijen, A. A., Cartledge, N., & Priest,E. R. 1998,

Woltjer, L. 1958, Proc. Nat Acad. Sci, 44, 489

Wright, A. & Berger, M. A. 1989, J. Geophys. Research, 94, 1295

Highlights of Astronomy, Vol. 13
International Astronomical Union, 2003
O. Engvold, ed.

Helicity Generation and Signature in Solar Atmosphere

A. A. Pevtsov

National Solar Observatory, Sunspot, NM 88349, U.S.A.

Abstract. To fully understand the origin, evolution and topology of solar magnetic fields, one should comprehend their magnetic helicity. Observationally, non-zero helicity reveals itself in the patterns of electric currents inside active regions, superpenumbral sunspot whirls, the shape of coronal loops and the fine structure of chromospheric filaments. Some patterns may bear information about deep sub-photospheric processes (e.g., dynamo, turbulent convection). Others may originate at or near the photosphere. This presentation reviews the observations of magnetic and current helicity on the Sun, discusses the possible mechanisms of helicity generation, and compares them with the observations.

1. Observations of Magnetic and Current Helicity

Magnetic helicity (H_m) plays a fundamental role in understanding the origin, evolution and topology of solar magnetic fields on different spatial and temporal scales (for review, see individual papers in Brown, Canfield, & Pevtsov 1999). H_m is a product of magnetic induction **B** and the vector potential **A** integrated over a closed volume ($\mathbf{n} \cdot \mathbf{B} = 0$ on the volume boundary). Typically, the magnetic fields are observed in a single level in solar atmosphere (photosphere or chromosphere), and hence, **A** cannot be computed in a general case. However, the sign of helicity can be determined from existing observations. For example, one can use the α coefficient of linear force free field $\nabla \times B = \alpha B$ (Seehafer 1990; Pevtsov, Canfield, & Metcalf 1995) or the vertical component of current helicity density $h_c = B_z \cdot (\nabla \times B)_z$ (Abramenko, Wang, & Yurchishin 1997; Bao & Zhang 1998). In addition, the sign of helicity can be inferred from the curvature of superpenumbral filaments (Hale 1927), the shape of coronal sigmoids (Rust & Kumar 1996), the skew of coronal arcades (Martin & McAllister 1996), or the orientation of the barbs in the chromospheric filaments (Martin, Bilimoria, & Tracadas 1994). One can also determine the helicity of photospheric field relative to the potential field (Berger & Field 1984; Chae 2001; Démoulin et al. 2002; Kusano et al. 2002).

The independent studies established following properties of helicity:

- Solar magnetic fields exhibit a tendency for negative (positive) helicity in the northern (southern) hemisphere. However, the latitudinal dependence shows significant scatter (Figure 1).
- The hemispheric rule is independent of solar cycle (Hale 1927; Martin et al. 1994; Pevtsov, Canfield, & Latushko 2001). However, there were reports that the rule may not hold in some phases of solar cycle (Sakurai & Hagino 2003).

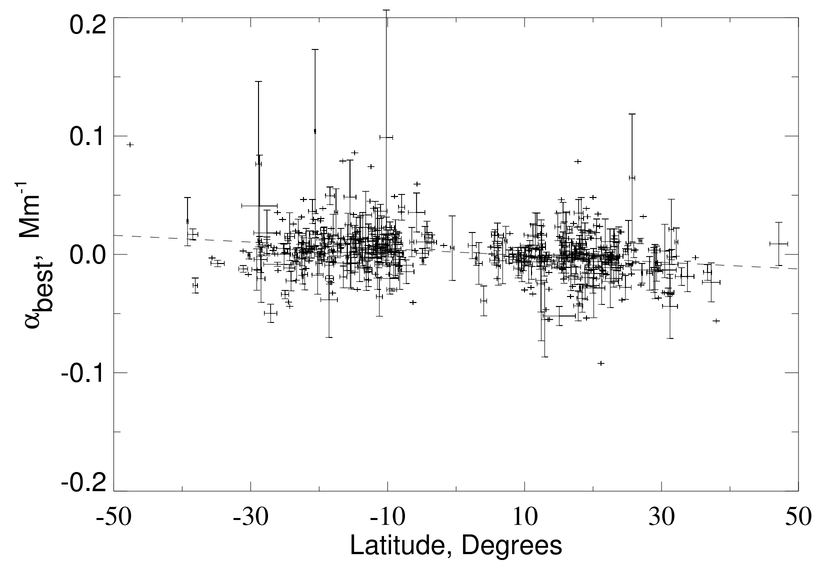

Figure 1. Latitudinal dependence of α for 466 active regions observed from 1998-2000 by the Haleakala Stokes Polarimeter (HSP, Mickey 1985). The dashed line is a least-square linear best fit.

- Magnetic flux emerges with non-zero twist (Leka et al. 1996; Portier-Fozzani et al. 2001; Grigoryev & Ermakova 2002).
- Relative helicity of a typical active region is about 10^{43} Mx^2 (Updike & Pevtsov 2003). In a large, CME-productive region coronal mass ejections may remove as much as 3.6×10^{43} Mx^2 over a lifetime of the region (Démoulin et al. 2002).

2. Origin of Helicity

The hemispheric helicity rule may result from the differential rotation, action of the Coriolis force on a flux tube rising through the convection zone, subsurface dynamo, and turbulence-magnetic field interaction in the convection zone.

DeVore (2000) showed that the surface differential rotation may generate sufficient amount of helicity over a lifetime of a small active region. On the other hand, Chae (2001) and Moon et al. (2002) found that the contribution of the photospheric local horizontal motions may significantly exceed the contribution of the differential rotation. Démoulin et al. (2002) concluded that the differential rotation cannot account for helicity lost due to CMEs.

The Coriolis force acting on plasma flowing in the rising and expanding magnetic flux tube distorts the shape of the tube. Above the photosphere, the tube appears as a bipolar region tilted relative to the equator (Joy's law). In addition to tilt, the same action will twist the magnetic field inside the tube. If the magnetic helicity of active regions was created by this mechanism, the twist and tilt should be in negative correlation (the sign of correlation depends on the definition of sign of tilt). Indeed, Tian et al. (2001) found a negative correlation between the active regions' tilt and twist. On the other hand, Canfield & Pevtsov (1998), and Sakurai & Hagino (2003) concluded that a correlation between tilt and twist cannot be explained by the action of the Coriolis force.

Longcope, Fisher, & Pevtsov (1998) suggested that the interaction between magnetic flux tubes and turbulent convection in the convection zone (Σ-effect) may explain the weak hemispheric preference and significant scatter of the helicity rule. Longcope et al. (1999) showed that a contribution of the Σ-effect is comparable with the observed helicity of active regions. The estimated contribution of the overshoot-region and and mean-field dynamos (Longcope et al. 1999; Seehafer et al. 2003) is at least on the order of a magnitude smaller.

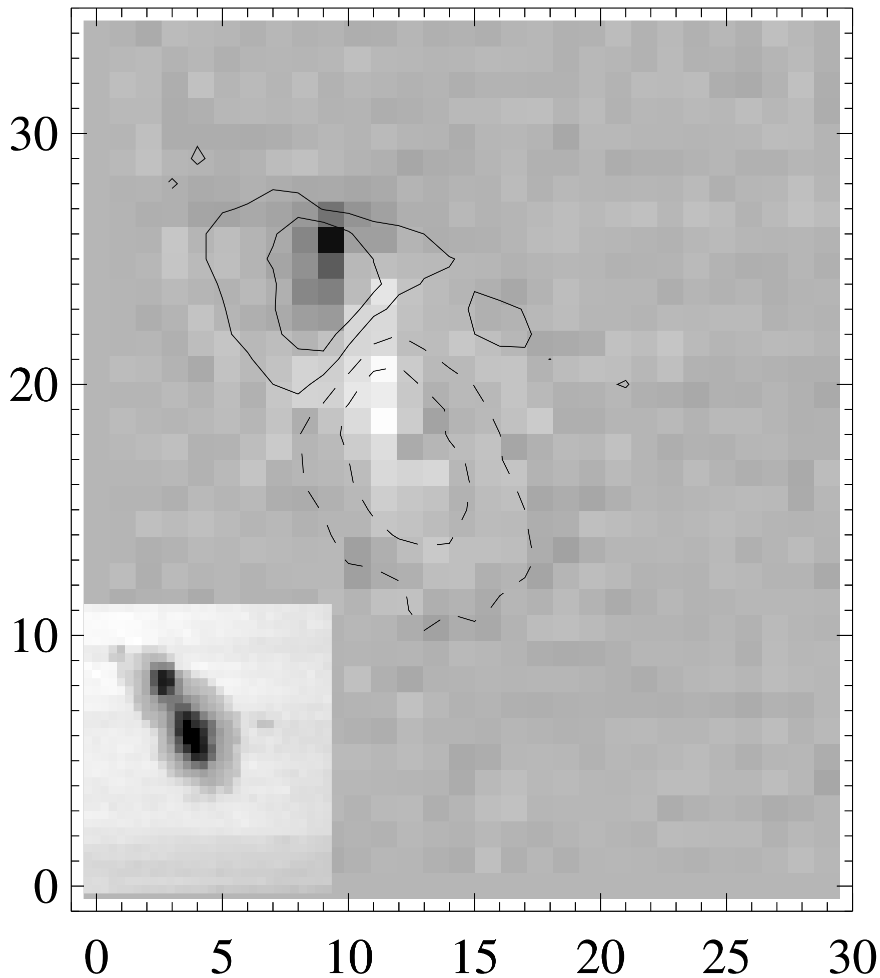

Figure 2. Electric currents (background) and vertical field (contours) of δ-spots NOAA 6619. Insert shows the white-light image.

The δ-spots provide an additional support for the sub-photospheric origin of helicity. Upon emergence, these regions exhibit significant shear and strong electric currents. In a typical (not δ-) sunspot both positive and negative currents are usually present inside a single polarity field (e.g., umbra). In the δ-spots, however, the currents show strong polarity dependence. For example, in δ-spot shown on Figure 2, the currents flow up in the negative polarity field, and they flow down in the positive polarity. This topology supports the model of a δ-spot as significantly distorted (and perhaps kinked) flux tube (Linton et al. 1998). Using HSP vector magnetograms of three large δ-spots, we computed the correlation between the vertical magnetic flux B_z and the vertical component of electric current density J_z. In all three cases, the J_z and B_z are strongly correlated: τ = –0.66 ± 0.07 (NOAA AR 5747), –0.58 ± 0.17 (NOAA AR 6619), and –0.60 ± 0.05 (NOAA AR 6659). This significant correlation indicates that in δ-spots electric currents are confined to the corresponding polarities (similar to Figure 2). The NOAA 6659 was the second rotation of NOAA 6619. However, the magnetic field was more twisted in NOAA 6619, i.e., $\alpha = (-3.20 \pm 0.36) \times 10^{-8}$ m^{-1} (NOAA 6619), $\alpha = (-1.87 \pm 0.75) \times 10^{-8}$ m^{-1} (NOAA 6659). Thus, the evolution of the twist in this δ-spot (NOAA 6619-6659) does not support the differential rotation as the source of helicity.

References

Abramenko, V. I., Wang, T. & Yurchishin, V. B. 1997, Solar Phys., 174, 291

Bao S. & Zhang, H. 1998, ApJ, 496, L43

Berger, M. A. & Field, G. B. 1984, J. Fluid Mech., 147, 133

Brown, M. R., Canfield, R. C., & Pevtsov, A. A., Editors, 1999, Magnetic Helicity in Space and Laboratory Plasmas, (Washington, D.C.: AGU)

Chae, J. 2001, ApJ, 560, L95

Démoulin, P., Mandrini, C. H., van Driel-Gesztelyi, L., Thompson, B., Plunkett, S., Kővári, Z., Aulanier, G., & Young, A. 2002, A&A, 382, 650

DeVore, C. R. 2000, ApJ, 539, 944

Grigoryev, V. M. & Ermakova, L. V. 2002, Solar Phys., 207, 309

Hale, G. E. 1927, Nature, 119, 708

Kusano, K., Maeshiro, T., Yokoyama, T. & Sakurai, T. 2002, ApJ, 577, 501

Linton, M. G., Dahlburg, R. B., Fisher, G. H., & Longcope, D. W. 1998, ApJ, 507, 404

Longcope, D. W., Fisher, G. H., & Pevtsov, A. A. 1998, ApJ, 507, 417

Longcope, D. W., Linton, M. G., Pevtsov, A. A., Fisher, G. H., & Klapper, I. 1999, in Magnetic Helicity in Space and Laboratory Plasmas, ed. M. R. Brown, R. C. Canfield & A. A. Pevtsov (Washington, D.C.: AGU), 93

Martin, S. F., Bilimoria, R., & Tracadas, P. W. 1994, in Solar Surface Magnetism, ed. R. J. Rutten & C. J. Schrijver, (Dordrecht: Kluwer), 303

Martin, S. F. & McAllister, A. H. 1996, in Magnetodynamic Phenomena in the Solar Atmosphere – Prototypes of Stellar Magnetic Activity, ed. Y. Uchida, T.Kosugi & H. S. Hudson, (Dordrecht: Kluwer), 497

Mickey, D. L. 1985, Solar Phys., 97, 223

Moon, Y.-J., Chae, J., Choe, G. S., Wang, H., Park, Y. D., Yun, H. S., Yurchyshyn, V., & Goode, P. R. 2002, ApJ, 574, 1066

Pevtsov, A. A., Canfield, R. C., & Latushko, S. M. 2001, ApJ, 549, L261

Pevtsov, A. A., Canfield, R. C., & Metcalf, T. R. 1995, ApJ, 440, L109

Rust, D. M. & Kumar, A. 1996, ApJ, 464, L199

Sakurai, T. & Hagino, M. 2003, J. Korean Astron. Soc., 36, S7

Seehafer, N. 1990, Solar Phys., 125, 219

Seehafer, N., Gellert, M. Kuzanyan, K. M., & Pipin, V. V. 2003, Adv. Space Research, in press

Tian, L., Bao, S., Zhang, H., & Wang, H. 2001, A&A, 374, 294

Updike, A. & Pevtsov, A. A. 2003, ApJ, in preparation

Highlights of Astronomy, Vol. 13
International Astronomical Union, 2003
O. Engvold, ed.

Magnetohydrodynamic 3–D Models of the Solar Convection Zone

Allan Sacha Brun

DSM/DAPNIA/SAp, CEA-Saclay, 91191 Gif-sur-Yvette, France

We have conducted 3–D simulations of the complex magnetohydrodynamics of the solar convective envelope in spherical shells using our anelastic spherical harmonics (ASH) code (Brun & Toomre 2002). We here briefly discuss the properties of the kinetic and current helicities established in such systems.

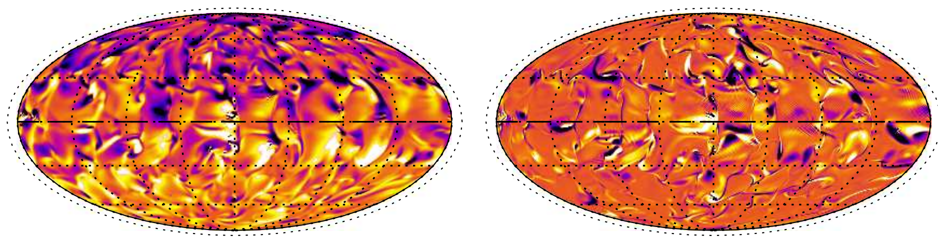

Figure 1. Snapshots of the kinetic (left) and current (right) helicities achieved in case $M3$ near the top of the domain ($r = 0.96R_{\odot}$). Positive values appear bright. Clearly the kinetic helicity possesses a sign preference in a given hemisphere (negative in the northern hemisphere for the displayed depth) whereas the current helicity does not.

In Figure 1, we represent at a given time the kinetic and current helicities achieved in one of our simulations of turbulent convection under the influence of rotation and magnetic fields (namely case $M3$ of Brun, Miesch & Toomre 2004). This solution possesses both a realistic solar-like differential rotation and sustained dynamo generated magnetic fields (the magnetic energy being about 10% of the kinetic energy contained in the shell). The kinetic helicity is mostly negative in the northern hemisphere, possessing its highest value near the strongest downflow lanes where cyclonic vortical structures are present. In contrast the current helicity does not show such a sign preference, having both negative and positive values distributed over the whole surface; it also delineates the downflow lanes, into which the magnetic fields have been swept and concentrated. This indicates that turbulent convection does not favor a particular sign for current helicity. In order to explain the dominant S-shape seen in active regions of the southern hemisphere (Pevtsov, Canfield & Latushko 2001), such topological 'twist' is more likely arising from the region where the flux tubes are formed, namely the tachocline at the base of the solar convective zone ($r \sim 0.7R_{\odot}$).

Brun, A.S. & Toomre, J. 2002, ApJ, 570, 865.
Brun, A.S., Miesch, M.S. & Toomre, J. 2004, ApJ submitted.
Pevtsov, A.A, Canfield, R.C. & Latushko, S.M. 2001, ApJ, 549, L261.

Highlights of Astronomy, Vol. 13
International Astronomical Union, 2003
O. Engvold, ed.

Helicity and The Alpha-Effect: Dynamo Theory and Observations

Kirill Kuzanyan

IZMIRAN, Troitsk, Moscow Region 142190, Russia

Abstract. Spatial and temporal distributions of tracers of the alpha-effect in the solar convection zone, such as current helicity and twist factor averaged over solar active regions are available by vector magnetographic observations. We discuss the data obtained at Huairou Solar Observing Station of Chinese Academy of Sciences and confront them with predictions of dynamo theory. At the present time, though the observations are rough, we still have a statistically representative sampling to conclude that the observations do not contradict the theory.

The α-effect plays an important role in mean field dynamo theory as a measure of regeneration of the poloidal fields from toroidal ones and *vice versa*. Furthermore, the magnetic helicity being an integral of motion is crucial for dynamo models. It is challenging to probe these quantities in real astrophysical dynamos, though they have no direct observational counterparts. However, the quantities like current helicity $H_c = \langle b_z(\nabla\times\mathbf{b})_\mathbf{z}\rangle$ and twist $a_{\rm ff} = j_z/b_z$, where $\mathbf{j} = a_{\rm ff}\mathbf{B}$ can be deduced from vector magnetographic observations. Under certain conditions, the latter can be considered as observational tracers of the alpha-effect and magnetic helicity. The problem of calculation of these quantities requires extraction of information on both line-of-sight and transversal magnetic field components, and further, calculation of currents seriously suffers from limited observational accuracy. Nevertheless, consideration of a large number of observations may reveal regularities of spatial and temporal distribution of the averaged quantities useful for confronting the theory. The summarized observational data follow in Table 1.

We develop a one-dimensional Parker dynamo model in an inhomogeneous layer for generation of magnetic fields and evolution of helicity with nonlinear quenching of the α-effect in a form of two additives: one hydrodynamic part is explicitly quenched by magnetic field (e.g., Rogachevkii & Kleeorin 2000), and the other magnetic part depends on current helicity. Our model depends on a number of phenomenological parameters (see Kleeorin et al. 2003 for details). We can estimate their range *a-priori* but some of them (namely, the diffusion and non-advective helicity flux coefficients) must be adjusted by our model calculations in order to reproduce a cyclic dynamo with the profile of helicity similar to its observational counterpart, provided the sign of helicity changes from one hemisphere to another. Thus, we use observational constrains on outputs of our model, and so select the range of our phenomenological parameters.

Then we study evolution of current helicity with solar magnetic cycle. We adjust the phase of the solar cycle using calculated magnetic field energy versus an observational tracer of solar activity (group sunspot number). Thus, we confront our model calculations with observational data on helicity evolution.

Table 1. Upper panel: Latitude Θ, with the averaging interval in brackets, the twist $\langle a_{\rm ff}\rangle$ in units of $10^{-8}\,{\rm m}^{-1}$, the current helicity $\langle H_c\rangle$ in units of $10^{-3}{\rm G}^2{\rm m}^{-1}$, and N is the number of active regions available. The errors correspond to the 95% confidence level. Lower panel: The same data binned by hemisphere and year of observation.

Θ	$\langle a_{\rm ff}\rangle$	$\langle H_c\rangle$	N
28 (24 - 32)	-0.4 ± 1.2	-1.6 ± 1.7	18
20 (16 - 24)	-0.9 ± 0.8	-0.9 ± 0.4	51
14 (12 - 16)	-1.7 ± 1.3	-0.6 ± 0.4	34
10 (8 - 12)	-2.2 ± 0.6	-0.4 ± 0.2	49
4 (0 - 8)	-1.9 ± 0.8	-0.6 ± 0.2	44
-4 (-8 -0)	0.3 ± 0.7	0.7 ± 0.5	31
-10 (-12 - -8)	1.2 ± 0.7	0.7 ± 0.4	59
-14 (-16 - -12)	0.9 ± 0.7	0.9 ± 0.7	46
-20 (-24 - -16)	1.0 ± 0.8	0.4 ± 0.2	68
-28 (-32 - -24)	1.6 ± 1.7	0.5 ± 0.9	14

T	$\langle a_{\rm ff}\rangle$	$\langle H_c\rangle$	N
North			
1988-89	-1.1 ± 0.8	-1.0 ± 0.5	50
1990-91	-1.0 ± 0.7	-1.0 ± 0.5	61
1992-93	-2.1 ± 0.7	-0.7 ± 0.3	45
1994-95	-2.6 ± 0.9	-0.3 ± 0.1	34
1996-97	-1.2 ± 1.0	-0.2 ± 0.2	9
South			
1988-89	1.0 ± 1.2	0.2 ± 0.3	38
1990-91	0.9 ± 0.7	0.8 ± 0.6	65
1992-93	1.2 ± 0.5	0.9 ± 0.3	77
1994-95	0.7 ± 0.9	0.1 ± 0.1	35
1996-97	0.3 ± 2.0	0.2 ± 0.3	8

Our observations cover one sunspot cycle. The results show, that the trends in evolution of observable current helicity can be seen in some general sense in our model calculations (Kleeorin et al. 2003, in particular their Fig 3).

Though our dynamo model is simple, we may, nevertheless, conclude, that the observations (noisy though they are) are sufficient to enable us to constrain phenomenological parameters of the model. At the same time, the evolution of current helicity calculated in our model is in accord with observations.

Acknowledgments. The author's thanks go to the IAU for travel grant which enabled him to attend the 25th IAU.

References

Kleeorin, N., Kuzanyan, K., Moss, D., Rogachevskii, I., Sokoloff, D., & Zhang, H. 2003 A&A, 409, 1097

Rogachevskii, I., & Kleeorin, N. 2000, Phys. Rev. E., 61, 5202

Highlights of Astronomy, Vol. 13
International Astronomical Union, 2003
O. Engvold, ed.

Magnetic Helicity Propagation from Inside the Sun

Dana Longcope

Department of Physics, Montana State University, Bozeman, MT 59717

Abstract. Models of twisted flux tube evolution provide a picture of how magnetic helicity is propagated through the solar convection zone into the corona. According to the models, helicity tends toward an approximately *uniform* length-density along a tube, rather than concentrating at wider portions. Coronal fields lengthen rapidly during active region emergence, requiring additional helicity to propagate from the submerged flux tube. Recent observations of emerging active regions show an evolution consistent with this prediction, and no evidence of helicity concentrating in wider sections.

1. Twisted Flux Tubes

The solar magnetic field has been modeled as *flux tubes*, ever since Parker introduced the concept and elucidated many of their properties. His comprehensive monograph, *Cosmical Magnetic Fields; Their Origin and Their Activity* (Parker 1979), devotes three chapters exclusively to flux tubes. Shortly after its publication, Spruit (1981) introduced a particularly useful non-linear model for the dynamical evolution of *thin* flux tubes (cross-sectional radius $a \ll H_p$ the pressure scale height), by expanding the magnetohydrodynamic equations about the tube's axis. Solutions of these equations for rising active region tubes agree with many observed characteristics of bipolar active regions (see Fisher et al. 2000, and references therein).

Recent interest in the chirality of the solar magnetic field motivated Longcope and Klapper (1997) to extend the standard thin flux tube model to include degrees of freedom they called twist $q(s,t)$ and spin $\omega(s,t)$. These define the azimuthal magnetic field $B_\phi = qr\bar{B}$ and plasma velocity $v_\phi = \omega r$ small distances r from the axis ($\bar{B} = \Phi/\pi a^2$ is the mean axial magnetic field in a tube of flux Φ). The twisted tube carries an axial current $I = 2q\Phi$ along its field lines and an opposite return current along its outer surface.

Expanding both the ideal induction equation and the first moment of the momentum equation (i.e. the equation of axial angular momentum) yields dynamical equations coupling twist and spin (Longcope and Klapper 1997)

$$\frac{dq}{dt} = \frac{\partial \omega}{\partial s} - q\,\hat{\mathbf{s}}\cdot\frac{\partial \mathbf{v}_a}{\partial s} + (\hat{\mathbf{s}}\times\frac{\partial \hat{\mathbf{s}}}{\partial s})\cdot\frac{\partial \mathbf{v}_a}{\partial s} \quad , \quad \frac{d\omega}{dt} = v_{\rm A}^2\frac{\partial q}{\partial s} - \omega\frac{d\ln a^2}{dt} \quad , \qquad (1)$$

where $\mathbf{v}_a(s,t)$ is the velocity of the axis at length coordinate s, and $\hat{\mathbf{s}}$ is the axis normal. The spin and twist are clearly affected by the dynamics of the tube's axis through $\mathbf{v}_a$ and $\dot{a}$ in equations (1). For a *slightly twisted* tube, one for which $qa \ll 1$, the axis dynamics are *not affected* by twist or spin.

In the case of a stationary axis, $\mathbf{v}_a = \dot{a} = 0$, the spin and twist satisfy a pair of telegrapher's equations

$$\frac{dq}{dt} = \frac{\partial \omega}{\partial s} \quad , \quad \frac{d\omega}{dt} = v_{\rm A}^2 \frac{\partial q}{\partial s} \quad , \tag{2}$$

whose solutions are torsional Alfvén waves. Evidently, to be in equilibrium the tube's twist must be uniformly distributed along its axis, $\partial q/\partial s = 0$, *regardless* of any variation in its radius $a(s)$. This tendency for uniform twist can be viewed as a consequence of either continuity of axial current $I = 2q\Phi$, or a balance of axial torque. A violation, i.e. an interruption of current or a torque imbalance, will lead to a torsional Alfvén pulse, whose propagation will move the variation toward the ends of the tube, thereby "seeking" to restore uniformity.

The tendency for twist uniformity exhibited by the Longcope and Klapper thin twisted flux tube model contradicts a common assertion that twist will concentrate in the widest portions of a flux tube. Such assertions are typically justified by referring to *Cosmical Magnetic Fields* (Parker 1979), particularly to results from the chapter devoted to the internal structure of axisymmetric flux tubes, not restricted to thin tubes. We return shortly to show that when applied to thin tubes Parker's result actually *corroborates* the tendency toward twist uniformity, rather than predicting a concentration at wider regions.

2. Coupling to the Corona

The thin flux tube model generally fails within the several megameters below the photosphere. Higher still, in the corona, the field is believed to approximate a force-free equilibrium. Torque balance across the intervening layer shows that, except during brief transients, the tube's internal axial current must pass completely into the corona (Longcope and Welsch 2000). The flux tube's surface current, including the axial return current, joins the horizontal surface current of the merging layer. Thus we expect that twist observed in photospheric and coronal magnetic fields, generally of order $|q| \sim 10^{-8}\,\mathrm{m}^{-1}$ (Pevstov et al. 1995), reflects a twist in the convection zone flux tubes to which they connect.

Let us assume that the coronal field directly connected to the active region, and thus to the flux tube, consists of closed loops which together fill a finite volume of characteristic scale $\sim d$, the separation between the photospheric poles. In equilibrium these loops will compose a force-free field carrying a net current I_c between footpoints. The detailed structure of this field will be complex depending as it does on the distribution of photospheric flux and current. Nevertheless, it will have a relative helicity H, which we assume to be finite and, on dimensional grounds, to be $H \simeq CI_c\Phi d$, for some constant C.

During the process of emergence, the flux tube evidently injects the helicity H into the corona. It must do this while injecting little mass since the ratio of helicity per mass is greater in the corona than in the convection zone by $\sim \rho_{\rm cz}a^2/\rho_{\rm cor}d^2 \gg 1$. Thus the emerging flux tube cannot "carry" its helicity into the corona by vertical flow, but must instead "wind" it into to coronal field by horizontal rotational motion. Evidently there is spin, ω_+ and ω_-, in the positive and negative legs of the emerging flux tube which map to photospheric rotations. This spin, which can be decomposed into upward and downward propagating torsional Alfvén waves within the sub-photospheric legs, produces a coronal helicity flux (Pevtsov et al. 2003)

$$dH/dt = 2C\Phi^2(q_c\dot{d} + \dot{q}_c d) = -\Phi^2(\omega_+ + \omega_-)/2\pi \quad , \tag{3}$$

where $q_c = I_c/2\Phi$ is the value of twist where the thin flux tubes meet the corona.

Pevtsov et al. (2003) used combined MDI and EIT observations of six emerging active regions to test this model of helicity injection. With the exception of one apparently untwisted case, the coronal twist increased from zero to a final value over about 1.5 days. In all five cases with twist, the time history of $d(t)$ and $q_c(t)$ were fit by solutions of (2) and (3), with similar values of sub-photospheric Alfvén speed and asymptotic twist $q \sim 10^{-8}\,\mathrm{m}^{-1}$. According to this interpretation, the separating poles ($\dot{d} > 0$), lengthened the coronal field lines, causing helicity to be drawn from the submerged tubes over a time d/v_{A}.

3. Internal Twist Distribution

It is worth comparing this to Parker's model for the internal distribution of twist in an axisymmetric, vertical, equilibrium flux tube. A general axisymmetric field can be written in terms of a flux function[1] $\psi(r,z)$ as $\mathbf{B} = \nabla\psi \times \nabla\phi + B_\phi(r,z)\hat{\boldsymbol{\phi}}$. The flux function rises monotonically from zero on axis to $\psi(a,z) = \Phi/2\pi$ at the outer surface, $r = a(z)$.

Since the azimuthal Lorentz force (i.e. magnetic torque) cannot be compensated by pressure, it must vanish in equilibrium, requiring $rB_\phi = F(\psi)$ a general function of the flux function. Following Parker we argue that the internal plasma pressure is hydrostatic, and thereby obtain the zero-β Grad-Shafranov equation for the flux function

$$r^2\nabla\cdot\Big(r^{-2}\nabla\psi\Big) \;=\; -\,F'(\psi)\,F(\psi) \quad . \tag{4}$$

The function $F(\psi)$ determines the azimuthal field even where $a(z)$ varies significantly. Parker argues that in any section which can be considered *thin*, so $\psi \simeq \bar{B}r^2/2$, $F(\psi)$ can be approximated by the leading term from its series, $F(\psi) \simeq 2q\psi$. Here q has the same meaning as in the thin-tube dynamical theory of Longcope and Klapper (1997). Since $F(\psi)$ must be the same in every portion of the tube, Parker's theory confirms that q is uniform throughout the equilibrium, *regardless of radius.*

In a non-thin tube section equation (4) demands a linear force-free field with $\alpha = 2q$. In a thin or approximately straight section $\partial^2\psi/\partial s^2$ may be dropped yieliding the Lundquist solution found by Parker

$$\psi = \frac{\Phi}{2\pi}\frac{rJ_1(2qr)}{aJ_1(2qa)} \quad , \quad B_z = \frac{1}{r}\frac{d\psi}{dr} = \frac{q\Phi}{\pi a J_1(2qa)}J_0(2qr) \tag{5}$$

where $J_n(x)$ is the Bessel function of order n. The common assertion about twist concentration follows from the observation that when the tube is wide

[1]Parker casts his analysis in terms of a generating function, f, related to ψ and B_ϕ.

enough that $2qa = j_{0,1} = 2.405$, the axial field vanishes and the *local* twist, B_ϕ/rB_z, diverges at the tube surface. This large twist is achieved, it is argued, by concentrating all of the tube's twist in this one wider section.

The previous section showed that the dynamically significant quantity is not the local twist, but rather the helicity per unit length,

$$\mathcal{H} = 4\pi \int_0^a \psi F(\psi) \frac{dr}{r} = \frac{q\Phi^2}{\pi} \left\{ \frac{J_0^2(2qa)}{J_1^2(2qa)} - \frac{J_0(2qa)}{qaJ_1(2qa)} + 1 \right\} \quad , \tag{6}$$

for the Lundquist field (5). In the weakly twisted limit, $qa \ll 1$, the factor in braces approaches one-half, recovering the Longcope and Klapper limit, $\mathcal{H} \simeq q\Phi^2/2\pi$, *independent of tube radius* a. Even the pathologically "fat" tube, $2qa = j_{0,1}$ has helicity only two times greater (in spite of an *infinite* twist density). Cross-section alone, it seems, can only double the helicity requirement of the tube apex, while its net *extension* requires far more.

Solar flux tubes have such small values of twist, $q \simeq 10^{-8}\,\mathrm{m}^{-1}$, that even their widest sections, while not thin, are still weakly twisted, $qa \ll 1$, and will seek uniform helicity density. Only the coronal field, $d \sim 10^8$ m, might depart from this regime, however, this is also the section most poorly approximated as axisymmetric. The helicity density in a maximum width 1d (Lundquist) field (Parker 1979) is double that of a thin tube, however, 2d axisymmetric fields show slightly different enhancements (Longcope and Welsch 2000).

In conclusion, there is no strong tendency for twist or helicity to move preferentially toward wider portions of flux tubes, or even into the zero-β coronal field. It will instead seek *uniform* density per length, and thus flow to *lengthening* portions. Observations show evidence of this tendency as emerging active regions fill with helicity through horizontal photospheric motions. This same reasoning predicts that removal of coronal helicity, by cornal mass ejections for instance, should be followed by replenishing photospheric motions driven by the twisted flux tube below. In this way the corona and heliosphere together may function as a sink of helicity produced in the solar interior.

References

Fisher, G. H., Fan, Y., Longcope, D. W., Linton, M. G., and Abbett, W. P. 2000, Phys. Plasmas 7(5), 2173.

Longcope, D. W. and Klapper, I. 1997, ApJ 488, 443.

Longcope, D. W. and Welsch, B. T. 2000, ApJ 545, 1089.

Parker, E. N. 1979, *Cosmical Magnetic Fields, Their Origin and Their Activity*, Clarendon Press, Oxford.

Pevtsov, A. A., Canfield, R. C., and Metcalf, T. R. 1995, ApJ 440, L109.

Pevtsov, A. A., Maleev, V., and Longcope, D. W. 2003, ApJ 593, 1217.

Spruit, H. C. 1981, A&A 98, 155.

Highlights of Astronomy, Vol. 13
International Astronomical Union, 2003
O. Engvold, ed.

Ejection of Bi-Helical Fields from the Sun

Axel Brandenburg

Nordita, Blegdamsvej 17, DK-2100 Copenhagen Ø, Denmark

Eric G. Blackman

Department of Physics & Astronomy, University of Rochester, Rochester NY 14627, USA

Abstract. It is argued that much of the observed magnetic helicity losses at the solar surface may represent a reduction of an otherwise more dominant nonlinearity of solar and stellar dynamos. This nonlinearity is proportional to the internal twist (as opposed to writhe) of helical and sigmoidal surface structures.

1. Introduction

Dynamo action is possible both for helical and non-helical turbulence [see, e.g., Meneguzzi et al. (1980) for early numerical work]. However, the reason one is particularly interested in helical dynamos is that there is a well-known mechanism (the $\alpha\Omega$ mechanism) driving cyclic behavior together with latitudinal migration of a large scale field. Both cyclic behavior and latitudinal migration are important features of dynamos in the sun and many late-type stars.

The α-effect is formally introduced via the longitudinally averaged induction equation. This effect characterizes the conversion of toroidal mean field into poloidal via a sequence of events, all of which produce similarly oriented loops that are tilted in a clockwise sense against the toroidal direction in the northern hemisphere, and anti-clockwise in the southern. This effect is the result of the combined action of Coriolis force and non-uniformity of the turbulence, as embodied by the formula (e.g. Rüdiger & Kitchatinov 1993)

$$\alpha_0 \approx -\tau^2 \overline{\mathbf{u}^2}\, \boldsymbol{\Omega} \cdot \boldsymbol{\nabla} \ln(\rho \overline{\mathbf{u}^2}). \tag{1}$$

This equation, which has been obtained using different approaches (see Moffatt 1980), reflects the fact that the turbulent velocity field has attained *kinetic* helicity. The subscript 0 indicates that the nonlinear feedback is not included.

2. Connection with magnetic helicity

It is first of all important to realize that practically no net magnetic helicity can be generated in the sun. What is possible, however, is a *segregation* of the magnetic field into its positively and negatively helical constituents. Such a segregation can occur either in wavenumber space or in real space. The latter can be accomplished by differential rotation acting on field lines crossing the

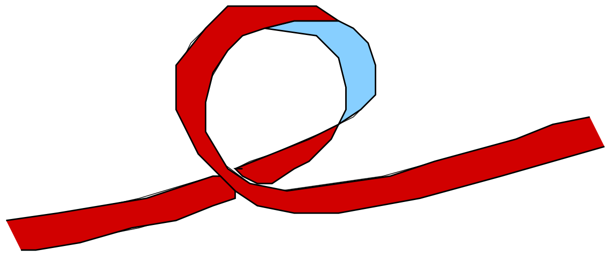

Figure 1. Tilting of the rising tube due to the Coriolis force. Note that the tilting of the rising loop causes also internal twist.

equator, while the former can be the result of the α-effect. This will now be discussed in more detail.

Consider the rise of a toroidal flux tube lifted upward either by thermal or magnetic buoyancy. As it rises, it gets tilted by the Coriolis force and, as a consequence, it must develop some internal twist. This is already quite clear from a simple sketch (Fig. 1), where the flux tube is depicted as a ribbon, so one can trace the induced twist.

Mathematically, magnetic helicity is the sum of writhe and twist helicities, and their sum must stay nearly unchanged (magnetic helicity conservation). In the example shown in Fig. 1, the overall structure of the tube follows the right hand rule, corresponding to positive writhe helicity. At the same time, the interval twist of the tube follows the left hand rule, corresponding to negative twist helicity. On the southern hemisphere both signs would be reversed.

3. Writhe and twist as driver and killer in dynamo theory

We have already eluded to the fact that the tilted magnetic field from the α-effect contributes directly (via many systematic and similar events) to the large scale poloidal field, $\overline{\mathbf{B}}_{\rm pol}$. Since α is positive, it should give a positive contribution to the current helicity of the mean field, i.e. $\overline{\mathbf{J}}\cdot\overline{\mathbf{B}}>0$. We also know from helicity spectra of magnetic flux tube experiments that the magnetic helicity from the negative internal twist contributes at scales smaller than from the positive writhe (Blackman & Brandenburg 2003). To put this into numbers, we expect the scales of the large scale poloidal field to be on the order of around 300 Mm, which corresponds to the latitudinal extent of the toroidal flux belts of around 20-30°. The typical scale associated with the twist is expected to be smaller, perhaps 30-300 Mm, but the dividing line between small and large scales may not be very clear. (Obviously, what is small scale to a dynamo theorist may be large scale to a solar observer!)

The internal twist is of tremendous importance in dynamo theory. As explained in the previous section, if the writhe helicity is composed of large scale field, the twist helicity must be composed of small scale field (where ‘small’ could be anywhere between 30-300 Mm!). We may therefore identify the helicity from the internal twist with the current helicity of the small scale field, $\overline{\mathbf{j}\cdot\mathbf{b}}$. Here, lower characters denote the small scale field, i.e. we have decomposed the field as $\mathbf{B} = \overline{\mathbf{B}} + \mathbf{b}$ and likewise the current as $\mathbf{J} = \overline{\mathbf{J}} + \mathbf{j}$.

The significance of the $\overline{\mathbf{j} \cdot \mathbf{b}}$ term is that it gives an extra contribution to the α-effect (Pouquet et al. 1976),

$$\alpha = \alpha_0 + \tfrac{1}{3}\tau\overline{\mathbf{j} \cdot \mathbf{b}}/\rho, \tag{2}$$

but it acts such as to suppress or quench the dynamo (α_0 and $\overline{\mathbf{j} \cdot \mathbf{b}}$ tend to have opposite signs). Indeed, the $\overline{\mathbf{j} \cdot \mathbf{b}}$ term constitutes the main nonlinearity of α-effect dynamos. There are other nonlinearities, such as a direct suppression of terms in equation (1), but such nonlinearities are never catastrophic in the sense that they do not depend on the magnetic Reynolds number[2].

4. Why coronal mass ejections might be good for the dynamo

Active regions and coronal mass ejections are the main contributors of magnetic helicity flux from the solar surface (e.g. Démoulin et al. 2002). It might not be appropriate to associate them with small scale losses only. Instead, in view of the combined presence of large and small scale fields in a single field structure (Fig. 1), such losses occur probably simultaneously at large and small scale fields. In this section we argue that this leads to an optimal scenario for dynamos.

Phenomenologically, surface losses of large and small scale helical fields may be described by diffusion terms. This concept has been tested against simulations in the case where losses occur almost entirely at large scales (Brandenburg & Dobler 2001). The results are twofold: the saturation time is formally decreased, but only at the expense of lowering the saturation field strength.

The rest of a possible success story is still speculation, but is based on physical reasoning and a numerical experiment: if losses occur preferentially on small scales, then the saturation amplitude of the large scale field is increased. This is because $\overline{\mathbf{j} \cdot \mathbf{b}}$, the 'quencher' in dynamo theory, is constantly being removed. This is confirmed by simulation where small scale magnetic field is artificially removed (Fig. 2). Even in the absence of such losses, the saturation value of the large scale field may be sufficient for the sun, but the cycle period may be too long. The primary importance of small scale losses may actually be to maintain the observed cycle period. This needs further investigation.

5. Conclusions

An important missing link in the story outlined above is, in our view, a simulation of a coronal mass ejection and an analysis in terms of the magnetic helicity budget. At the same time, it will be necessary to improve mean field theory to take helicity fluxes properly into account. For attempts in that direction we refer to recent work by Kleeorin and collaborators (2003).

---

[2]By contrast, equation (2) can lead to a catastrophic quenching formula: use Keinigs' (1983) formula for the *saturated* state, $\alpha = -\eta\overline{\mathbf{j} \cdot \mathbf{b}}/\overline{\mathbf{B}}^2$ (which follows from the magnetic helicity equation), eliminate $\overline{\mathbf{j} \cdot \mathbf{b}}$ from (2), to get catastrophic quenching: $\alpha = \alpha_0/(1 + R_\mathrm{m}\overline{\mathbf{B}}^2/B_\mathrm{eq}^2)$. Here we have used $R_\mathrm{m} = \eta_\mathrm{t}/\eta$, with $\eta_\mathrm{t} = \frac{1}{3}\tau\overline{\mathbf{u}^2}$ and defined $B_\mathrm{eq} = (\mu_0\rho\overline{\mathbf{u}^2})^{1/2}$ to eliminate τ; see Eqs (18) and (40) of Blackman & Brandenburg (2002) for a more general formulation.

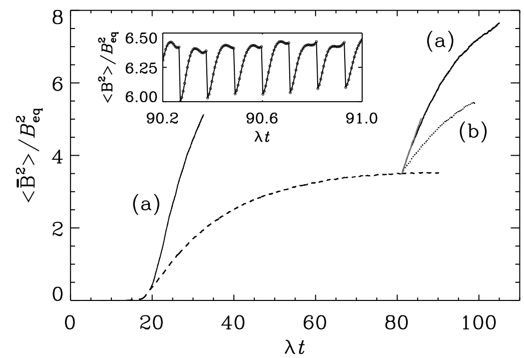

Figure 2. The effect of removing small scale magnetic energy in regular time intervals Δt on the evolution of the large scale field (solid lines). The dashed line gives the evolution of $\langle\overline{\mathbf{B}}^2\rangle$ for Run 3 of Brandenburg (2001), where no such energy removal was included. The two solid lines show the evolution after restarting at $\lambda t = 20$ and $\lambda t = 80$. Time is scaled with the kinematic growth rate λ. The curves labeled (a) give the result for $\Delta t = 0.12\lambda^{-1}$ and those labeled (b) for $\Delta t = 0.4\lambda^{-1}$. The inset shows, for a short time interval, the sudden drop and subsequent recovery of the total (small and large scale) magnetic energy in regular time intervals (adapted from Brandenburg et al. 2002).

References

Blackman, E. G., & Brandenburg, A. 2002, ApJ, 579, 359

Blackman, E. G., & Brandenburg, A. 2003, ApJ, 584, L99

Brandenburg, A. 2001, ApJ, 550, 824

Brandenburg, A., & Dobler, W. 2001, A&A, 369, 329

Brandenburg, A., Dobler, W., & Subramanian, K. 2002, AN, 323, 99

Démoulin, P., Mandrini, C. H., van Driel-Gesztelyi, L. 2002, ApJ, 382, 650

Keinigs, R. K. 1983, Phys. Fluids, 26, 2558

Kleeorin, N. I, Kuzanyan, K., Moss, D., et al. 2003, A&A, 409, 1097

Meneguzzi, M., Frisch, U., & Pouquet, A. 1981, PRL, 47, 1060

Moffatt, H. K. 1978, Magnetic Field Generation in Electrically Conducting Fluids (Cambridge University Press, Cambridge)

Pouquet, A., Frisch, U., & Léorat, J. 1976, JFM, 77, 321

Rüdiger, G., & Kitchatinov, L. L. 1993, A&A, 269, 581

Highlights of Astronomy, Vol. 13
International Astronomical Union, 2003
O. Engvold, ed.

Magnetic Helicity in Sigmoids, Coronal Mass Ejections and Magnetic Clouds

D. M. Rust

The Johns Hopkins University Applied Physics Laboratory, 11100 Johns Hopkins Road, Laurel, MD 20723, USA

Abstract. Sigmoids, coronal mass ejections (CMEs) and magnetic clouds (MCs) all show signatures of twisted and writhing magnetic fields. CMEs are often associated with MCs, whose fields are regularly mapped with sensitive magnetometers. These measurements reveal that MC fields are helical, and each MC carries magnetic helicity away from the sun. It is more difficult to determine the magnetic helicity of the corresponding features on the sun. This presentation surveys recent work on helicity in solar features, focusing especially on the interpretation of sigmoids, which are S-shaped, bright features seen in images from the Yohkoh soft X-ray telescope. Several lines of evidence indicate that sigmoids are twisted and writhing flux ropes that erupt as components of CMEs. CMEs may be initiated by MHD-instable flux ropes. The fact that the ejected flux ropes carry off a large amount of positive helicity from the south and negative helicity from the north each solar cycle implies an equal, compensating flow of helicity through the sun's equatorial plane.

1. Introduction

Since it was suggested that interplanetary MCs (Burlaga et al. 1982) systematically carry magnetic helicity away from the sun (Rust 1994; Bieber & Rust 1995), many authors have studied solar phenomena in search of the origins of this helicity flow. The role of magnetic helicity in producing CMEs, from which the MCs evolve, is one of the most intriguing new challenges in solar physics. An appealing picture would have the magnetic helicity generated in or at the base of the convection zone, from which it buoys upward and bursts through the photosphere into the corona. There, it accumulates and forms 'sigmoids' (Rust & Kumar 1996). Sigmoids are S-shaped, bright features that are best seen in images from the Yohkoh soft X-ray telescope. These features presage CMEs (Canfield, Hudson, & McKenzie 1999), and the eruption of a sigmoid often signals the onset of a CME. CMEs from the northern hemisphere predominantly carry off negative helicity while those from the southern hemisphere carry off positive helicity. Equal amounts, $\sim 10^{46}$ Mx^2 of helicity are carried off from each hemisphere in the course of each solar cycle. This escape of helicity may be necessary to the successful functioning of the solar dynamo (Brandenburg, Bigazzi, & Subramanian 2001). Studies of the flow of helicity through the photosphere and corona and into interplanetary space may thus provide important clues to understanding how the solar dynamo works.

The picture just described is not universally accepted, and there are many disputed and unresolved issues. The build-up of helicity in CMEs has been attributed alternatively to (1) the effects of surface differential rotation on the footpoints of coronal loops (DeVore 2000); (2) a systematic effect of the Coriolis force on rising flux tubes (the alpha effect), producing CMEs that simultaneously liberate small-scale twist and large-scale writhe of opposite sign (Blackman & Brandenburg 2003); and (3) a statistical effect on flux tubes due to turbulence and Coriolis forces (the sigma effect) (Longcope, Fisher, & Pevtsov 1998). In addition, there are numerous interpretations of sigmoids: the X-ray emitting plasma of sigmoids may outline writhing flux rope axes, current sheets, or force-free fieldlines. Similarly, the role of helicity escape in the dynamo is not clear: (1) the helicity seen at the sun's surface may be associated with the small-scale or large-scale component of the classical alpha-omega dynamo (Brandenburg & Dobler 2001); helicity may flow globally as described above and by Berger & Ruzmaikin (2000); or (3) no net helicity is released in either hemisphere, the writhe helicity of the flux ropes being equal and opposite to the twist helicity in each flux rope. See Berger (1999) for a tutorial on magnetic helicity.

In this paper, I discuss various interpretations of the origin of helicity, the helicity budget of CME-producing active regions (ARs), and the interpretation of sigmoids, which is an area of much current research; sigmoids are indeed a crucial element in understanding the link between helicity generation in the sun and CMEs .

2. Generation of Magnetic Helicity

Differential rotation at the sun's surface can transfer helicity to coronal magnetic loops. DeVore (2000) found that the effect of differential rotation on 1000 idealized ARs would produce the amount of helicity ejected from the sun each solar cycle by an estimated 5000 CMEs. However, several recent studies (e.g., Démoulin et al. 2002; Pevtsov, Maleev, & Longcope 2003) of helicity generation in ARs whose CME production rate is known from LASCO observations showed that differential rotation could not impart enough helicity to account for the CMEs, assuming that each CME carries off a net helicity of $\sim 2 \times 10^{42}$ Mx^2. The helicity loss rate depends on two important assumptions: that most CMEs include a flux rope-like structure that evolves into the well-documented flux rope structure of a MC, and that magnetic helicity is conserved as the event propagates from sun to Earth. No one has ever directly measured the magnetic helicity of a CME, but recently, Bleybel et al. (2002) used non-linear force-free field reconstructions based on a series of vector magnetograms to show that the magnetic helicity in an AR decreased by 0.7×10^{42} Mx^2 after a CME. This quantity is consistent with CME helicity estimates.

Longcope, Fisher & Pevtsov (1998) proposed that solar AR helicity is produced by the combined effects of the Coriolis force and convective turbulence on rising flux tubes. Their mechanism would seem to produce no net helicity in the corona because the writhe helicity imparted in the flux tube is equal and opposite to the induced twist helicity, under the assumption of helicity conservation. Their so-called sigma mechanism accounts very nicely for the statistical spread of AR twist helicities. If they can keep the writhe helicity from canceling out the twist helicity as the fields emerge into the corona, then the mechanism may be the correct one. According to Berger & Ruzmaikin (2000), however, an emerging flux rope should quickly untwist and unkink if its net helicity is zero.

Like the sigma effect, the classical alpha effect of dynamo theory produces no net helicity in the fields reaching the corona, as pointed out by Blackman & Brandenburg (2003), who proposed that sigmoids in the southern hemisphere, for example, are writhed in the left-handed sense and twisted equally in the right-handed sense. However, relaxation in the corona should proceed at the Alfvén speed, which is generally 300 - 1000 km/s.

3. Interpretation of Sigmoids

Rust and Kumar (1996) interpreted sigmoids as writhing flux ropes, that is, as twisted magnetic fields in which at least one turn of twist helicity has been converted in an $m = 1$ kink instability into writhe of the axis. In their picture, the twist and writhe have the same sign, and twist can accumulate either by transfer from beneath the photosphere or by reconnections with similarly twisted flux ropes. $H\alpha$ filaments sometimes also take on a sigmoidal shape, and their fields might be explained by the same mechanism (Sakurai 1976). On the other hand, Pevtsov, Canfield, & McClymont (1997) showed that linear force-free fields computed from photospheric magnetograms in 140 ARs can nicely fit the corresponding sigmoids. More recently, Low and Berger (2003) proposed that sigmoids trace-out a family of field lines that is in contact with the photosphere near a polarity inversion line in the photospheric fields. Their model is in general agreement with the empirical description of sigmoids offered by Moore et al. (2001). From the observations and the model one gains the impression that a sigmoid is illuminated in soft X-rays because of heating by currents near a so-called bald patch (Titov, Priest, & Demoulin 1993) and that this patch corresponds to the bright waist sometimes seen in sigmoids. The waist is where the field lines writhe downward, so that a sigmoid with positive writhe looks from above like an S. This interpretation is consistent with the findings of Pevtsov, Canfield, & McClymont and others, that positive helical fields associate with S-shaped sigmoids and negative fields associate with Z-shaped sigmoids. Low and Berger also conclude that sigmoids' twist and writhe have the same sign. This implies that the helicity in sigmoids is predominantly positive in the southern hemisphere, because S-sigmoids predominate there, and negative in the north. Hα filaments have the same hemispheric distribution, that is, those which positive helical fields fit best predominate in the south, etc. Ruzmaikin, Martin, & Hu (2003) found three MCs with remnants of solar filaments, as revealed by higher density plasma at 1 AU. They showed in each case that the flux rope threading the filament remnants had the same chirality as the flux rope of the surrounding MCs.

4. Conclusions

Recent work tends to confirm that there is an accumulation of magnetic helicity in sigmoids and that this helicity is carried into interplanetary space by CMEs and filament eruptions. This has an important implication for understanding CME onset, suggesting that it could be due to an MHD instability caused by an excess of helicity in the fields. The MHD kink instability might become non-linear in certain instances (Baty et al. 1998) and start a CME. This idea can be tested in part by measurements of the flow of helicity into the corona. New techniques (e.g. Chae 2001; Kusano et al. 2002; Bleybel et al. 2002) should enable better comparisons of helicity flow with CME rates. A second implication is that since helicity (mostly right-handed in the southern hemisphere and left-handed in the northern hemisphere) is carried off by CMEs, there must be a compensating flow of helicity through the solar equatorial plane, as pointed out by Berger and Ruzmaikin (2000). Positive helicity must flow from north to south, and taking this into account may lead to an explanation of how the activity cycle in the south keeps in phase with that in the north.

References

Baty, H., Einaudi, G., Lionello, R., & Velli, M. 1998, A&A, 333, 313

Berger, M. 1999, in Magnetic Helicity in Space and Laboratory Plasmas, eds. M. Brown, R. Canfield, & A. Pevtsov, AGU Geophys. Monog.111, 1

Berger, M. A., & Ruzmaikin, A. 2000, JGR, 105, 10481

Bieber, J. W., & Rust, D. M. 1995, ApJ, 453, 911

Blackman, E. G., & Brandenburg, A. 2003, ApJ, 584, L99

Bleybel, A., Amari, T., van Driel, L., & Leka, K. D. 2002, A&A, 395, 685

Brandenburg, A., Bigazzi, A., & Subramanian, K. 2001, MNRAS, 325, 685

Brandenburg, A., & Dobler, W. 2001, A&A, 369, 329

Burlaga, L. F., et al. 1982, GRL, 9, 1317

Canfield, R. C., Hudson, H. S., & McKenzie, D. E. 1999, GRL, 26, 627

Chae, J. 2001, ApJ, 560, L95

Démoulin, P., et al. 2002, A&A, 382, 650

DeVore, C. R. 2000, ApJ, 539, 944

Kusano, K., Maeshiro, T., Yokoyama, T., & Sakurai, T. 2002, ApJ, 577, 501

Longcope, D. W., Fisher, G. H., & Pevtsov, A. A. 1998, ApJ, 507, 417

Low, B. C., & Berger, M. A. 2003, ApJ, 589, 644

Moore, R., Sterling, A., Hudson, H., & Lemen, J. 2001, ApJ, 552, 833

Pevtsov, A. A., Canfield, R. C., & McClymont, A. N. 1997, ApJ, 481, 973

Rust, D. M. 1994, GRL, 21, 241

Rust, D. M., & Kumar, A. 1996, ApJ, 464, L199

Ruzmaikin, A., Martin, S., & Hu, Q. 2003, JGR, 108b

Sakurai, T. 1976, PASJ, 28, 177

Titov, V. S., Priest, E. R., & Demoulin, P. 1993, A&A, 276, 564

Highlights of Astronomy, Vol. 13
International Astronomical Union, 2003
O. Engvold, ed.

Technique for Inferring Magnetic Helicity of Active Regions

Jongchul Chae

Astronomy Program, SEES, Seoul National University, Seoul 151-742, Korea

Yong-Jae Moon

Korea Astronomy Observatory, Whaamdong, Yooseong-ku, Daejeon 305-348, Korea

Abstract. We provide the rationale for the wide applicability of the LCT method for inferring the magnetic helicity of an active region, with an illustrative application made to NOAA 10365. We also report that the determined rate of helicity change is not much sensitive to the free parameters of the LCT method. The application of the method to active regions by several investigators has produced results suggesting that the magnetic helicity of a major active region with flux 10^{22} Mx may be usually of the order of 10^{43} Mx^2 or less, being twisted at most 0.1 turns as a whole.

1. Introduction

It is now well known that the change rate of the magnetic helicity of a coronal volume H is given by the equation (Berger & Field 1984)

$$dH/dt = \oint 2(\mathbf{B}_t \cdot \mathbf{A}_p)v_n \, dS - \oint 2(\mathbf{v}_t \cdot \mathbf{A}_p)B_n \, dS \qquad (1)$$

where the subscripts t and n refer to the components of magnetic field $\mathbf{B}$ and plasma velocity $\mathbf{v}$ that are tangential and normal to the surface, respectively. $\mathbf{A}_p$ is the vector potential of potential field. The method of local correlation tracking (LCT) was proposed by Chae (2001) as a way of tracing the horizontal motion of footpoints of predominantly vertical field lines and of determining the latter term in Eq. (1)— the so-called shearing term. Being successfully applied to the line-of-sight magnetograms taken by SOHO/MDI, this method has produced the meaningful estimates of magnetic helicity change in different active regions in relation to the prominence formation (Chae et al. 2001), flares (Moon et al. 2002a, b) and coronal mass ejections (Nindos et al. 2002, 2003). Subsequently generalizing the LCT method, Kusano et al. (2002) proposed a way of determining the other term in Eq. (1)— the advection term. They calculated the normal component of velocity from the induction equation and the LCT velocities. Very recently Demoulin & Berger (2003) found that the amount of helicity change determined by Chae's LCT method, when applied to inclined magnetic fields, in fact includes the contribution of vertical motion, too, not to speak of that of horizontal motion, negating the need to add the extra advection term due to the vertical motion. This finding opens a possibility of the wider applicability of the LCT method than was originally proposed by Chae (2001).

2. Rationale for the LCT Method

The LCT technique determines the horizontal velocity from the lateral displacement of flux density pattern across the solar surface. It basically assumes that the velocity field is uniform locally in space and time so that it follows

$$B_n(\mathbf{r}+\Delta\mathbf{r}/2, t+\Delta t/2) \approx B_n(\mathbf{r}-\Delta\mathbf{r}/2, t-\Delta t/2) \tag{2}$$

for $|\mathbf{r}-\mathbf{r}_0| < \delta r$ and $|t-t_0| < \delta t$. The LCT velocity is defined as $\mathbf{v}_{\rm LCT}(\mathbf{r}_0, t_0) = \Delta\mathbf{r}/\Delta t$. Note that for the LCT technique to work best the magnetic flux density should vary sharply in space with a length scale shorter than that of the velocity variation. Under this condition Eq (2) can be recast into

$$\partial B_n/\partial t + \nabla_t \cdot [\mathbf{v}_{\rm LCT} B_n] \approx 0 \tag{3}$$

where the operator ∇_t refers to the tangential component of the gradient operator, which is defined on the photospheric surface.

On the other hand, one can start with the well-known magnetic induction equation and derive the equation

$$\partial B_n/\partial t + \nabla_t \cdot [\mathbf{v}_t B_n - v_n \mathbf{B}_t] = \partial B_n/\partial t + \nabla_t \cdot [\mathbf{u} B_n] = 0 \tag{4}$$

which looks very similar to Eq (3) with the newly introduced velocity $\mathbf{u}$ defined by $\mathbf{u}B_n \equiv \mathbf{v}_t B_n - v_n \mathbf{B}_t$. Note that $\mathbf{u}$ stands for the apparent motion of footpoints of field lines across the photospheric surface. The two kinds of velocity $\mathbf{u}$ and $\mathbf{v}_{\rm LCT}$ are related to each other via $\nabla_t \cdot (\mathbf{v}_{\rm LCT} B_n - \mathbf{u} B_n) \approx 0$ or $\mathbf{u}B_n \approx \mathbf{v}_{\rm LCT} B_n + \nabla_t \times (\Psi \mathbf{n})$ where Ψ is an arbitrary function of $\mathbf{r}$. Therefore, but for the Ψ ambiguity, it follows $\mathbf{v}_{\rm LCT} \approx \mathbf{u}$ at regions with $B_n \neq 0$. This means that at the presence of non-zero horizonal fields the velocity $\mathbf{v}_{\rm LCT}$ determined using the LCT method is contributed not only by the horizonal component of plasma motion, but also its vertical component. An important consequence is that the two terms in Eq (1) may be combined into one

$$dH/dt = -2 \oint (\mathbf{u} \cdot \mathbf{A}_p) B_n \, dS \approx -2 \oint (\mathbf{v}_{\rm LCT} \cdot \mathbf{A}_p) B_n \, dS \, . \tag{5}$$

This indicates that the LCT method gives a measure of the total amount of helicity change, namely the sum of both the shearing term and the advection term. This is the important finding of Demoulin & Berger (2003).

3. Results and Conclusion

It is now obvious that the LCT method can be applied to active regions in the phase of flux emergence in which the advection term may be significant. As an illustration, we apply the LCT method to the active region NOAA 10365 that

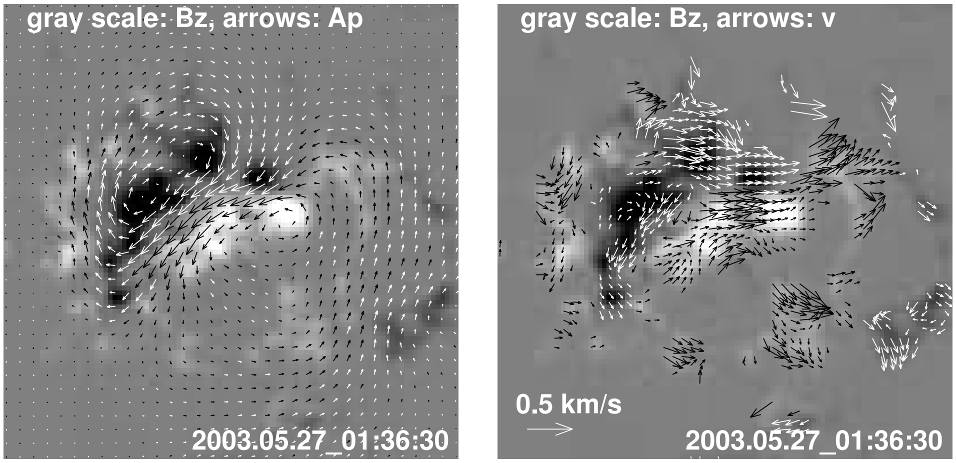

Figure 1. *left:* $\mathbf{A}_\mathrm{p}$ field (arrow) superposed on B_n field (gray-sclae) in NOAA 10365. *right:* $\mathbf{v}_\mathrm{LCT}$ field (arrow) superposed on B_n field (gray-scale).

was under emergence while it stayed near the disk center in 2003 May. It was the only dominant, flare-productive active region on the disk during the days of our interest. Here we present the results obtained from the 96-min cadence full-disk magnetograms taken by SOHO/MDI.

Figure 1 shows the spatial distributions of B_n, $\mathbf{A}_\mathrm{p}$ and $\mathbf{v}_\mathrm{LCT}$ at an instant as determined using the method described by Chae (2001). It can be seen from the figure that the vector potential $\mathbf{A}_\mathrm{p}$ is the strongest on the polarity inversion line, and strong shearing motion occurs near the polarity inversion line, which should be important in the transfer of magnetic helicity.

Figure 2 shows that the magnetic fluxes of the active region steadily increased for several days from its birth. The total fluxes that newly emerged are found to be about 1.4×10^{22} Mx (positive flux) and 1.1×10^{22} Mx (negative flux). The right panel of the figure shows that magnetic helicity was transferred through the photosphere at a rate of up to 2.5×10^{41} Mx^2 h^{-1}. Figure 2 also shows the accumulated amount of helicity as a function of time. It is obvious from the figure that the helicity steadily increased as the fluxes did, but not in proportion to the fluxes. The final amount of magnetic helicity that was transferred during this emergence period is found to be 8×10^{42} Mx^2, which yields $n \equiv H/\Phi^2 \approx 0.05$ for an estimate of number of twist of the active region as a whole.

We have examined the dependence of the LCT method on the two free LCT parameters — apodizing window size and time interval — by comparing results from high cadence, high resolution magnetograms with those from 96-minute cadence, full-disk magnetograms. As a result we have found that smaller values of these parameters usually result in larger-amplitude temporal fluctuations of the rate of helicity. Its average taken over the time interval of about an hour or longer, however, is found to be very insensitive to the two parameters. This may be because short-lived, small-scale flows is insignificant in transferring magnetic helicity. This result supports that the LCT method may be safely applied to

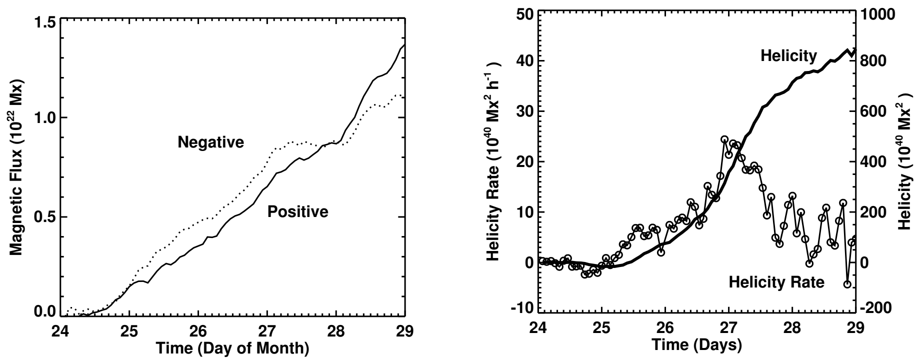

Figure 2. The temporal variations of positive and negative fluxes (left), and the rate and accumulated amount of magnetic helicity change (right) in NOAA 10365 observed in May 2003.

96-minute cadence full-disk MDI magnetograms as far as the magnetic helicity budget of active regions is concerned.

It is concluded that the LCT method is a practical and effective tool to infer the rate of helicity change in active regions. Its application to different active regions of comparable size by different authors (Chae et al. 2001; Nindos & Zhang 2002; Nindos et al. 2003; the present study) has revealed that significant injection of magnetic helicity may occur both during and after flux emergence with a time scale of a few days, suggesting that typical helicity budget of major active regions with flux 10^{22} Mx may be equal to or less than $\sim 10^{43}$ Mx^2 or twisted at most 0.1 turns as a whole.

Acknowledgments. This work was supported by the BK21 Project, and the KOSEF grant R14-2002-043-0100-0, and the National Research Laboratory M10104000059-01J00002500 of the Korean government.

References

Berger, M. A., & Field, G. B. 1984, J. Fluid Mech., 147, 133

Chae, J. 2001, ApJ, 560, L95

Chae, J., Wang, H., Qiu, J., Goode, P. R., Strous, L., & Yun, H. S. 2001, ApJ, 560, 476

Demoulin, P. & Berger, M. A. 2003, Solar Physics, 215, 203

Kusano, K., Maeshiro, T., Yokoyama, T., & Sakurai, T. 2002, ApJ, 577, 501

Moon, Y.-J., Chae, J., Choe, G. S., Wang, H., Park, Y. D., Yun, H. S., Yurchyshyn, V., & Goode, P. R. 2002a, ApJ, 574, 1066

Moon, Y.-J., Chae, J., Wang, H., Choe, G. S., & Park, Y. D. 2002b, ApJ, 580, 528

Nindos, A. & Zhang, H. 2002, ApJ, 573, L133

Nindos, A., Zhang, J., & Zhang, H. 2003, ApJ, 594, 1033

Highlights of Astronomy, Vol. 13
International Astronomical Union, 2003
O. Engvold, ed.

Generation and Annihilation of Magnetic Helicity in Active Regions

K.Kusano

Graduate School of Advanced Sciences of Matter, Hiroshima University, Higashi-Hiroshima, Hiroshima 739-8530, Japan

Abstract. Generation and annihilation processes of magnetic helicity in solar coronal active regions are investigated based on the observations and the simulations. We first examined the reliability of the numerical techniques, which enable to measure the magnetic helicity flux through the photosphere based on the magnetogram data. Secondly, in terms of the new technique, we found that magnetic helicities of the both signs are simultaneously injected into active regions. Motivated by this result, finally, we investigated the nonlinear process of the magnetic helicity annihilation, using the three-dimensional numerical simulations. The simulations clearly indicated that the helicity reversal can cause the eruption of large-scale plasmoid through the nonlinear process of the resistive instability growing on the helicity inversion layer. From these studies, we point out that the annihilation of magnetic helicity is a key process for the onset mechanism of solar flares.

1. Introduction

Magnetic helicity is believed to be an important quantity to understand the solar coronal activities, such as flares and the coronal mass ejections (CMEs). However, the previous studies of magnetic helicity in the solar corona were restricted mainly to the theoretical and conceptual models. One reason of that is attributed to the fact that the measurable magnetic field in the solar corona is limited only to the photospheric and coromospheric levels, while the helicity is defined as the spatial integration over the whole domain.

Recently, new methodologies to evaluate the helicity flux out of the sun have been proposed (Kusano et al. 2002, Démoulin and Berger 2003). In this paper, first we will review the principle of the helicity measurement and examine the reliability using the benchmark model. Secondly, we will discuss about the possibility that the annihilation of magnetic helicity works as the trigger mechanism of solar flares, based on the measurement of the helicity flux and the three-dimensional numerical simulations.

2. Measurement of Helicity Flux

According to Berger and Field (1984), the helicity flux across a plane S is described by

$$\dot{H} = 2 \int_S \boldsymbol{A}_P \times \boldsymbol{E} \cdot \boldsymbol{n} dS, \tag{1}$$

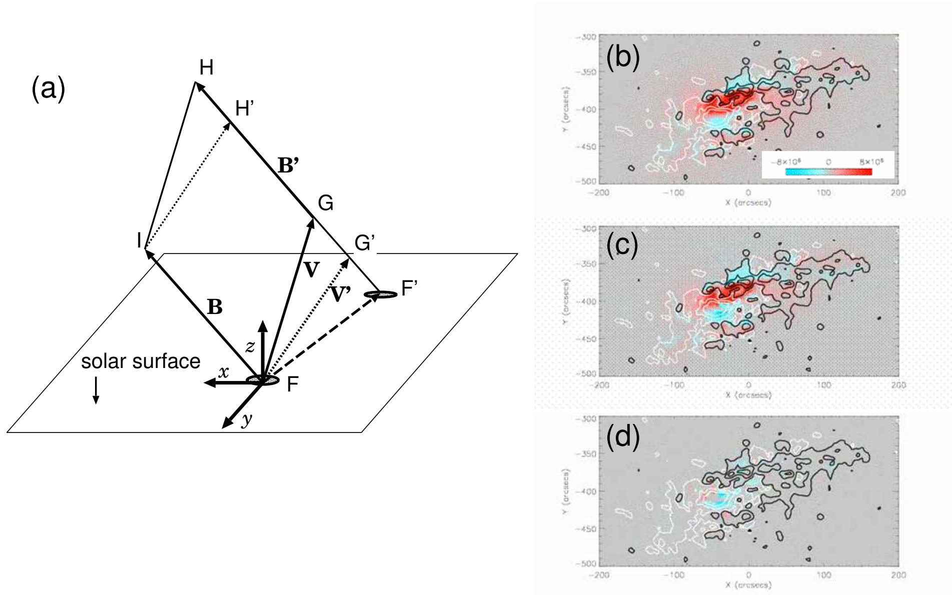

Figure 1. (a) The illustration of field line variation on the solar surface. (b) to (d) The benchmark test of the helicity flux measurement. The color shading and the contours indicate the helicity flow and the magnetic field, respectively. (b) is the correct answer. (c) is the result by the combination method of the induction equation and the LCT. (d) is the result by the LCT method.

where $\boldsymbol{A}_P$ is the vector potential of the current free field, which is derived from the magnetic field normal to the boundary. It indicates that the electric field $\boldsymbol{E}$ is a key quantity for the helicity measurement. In the ideal magnetohydrodynamic (MHD) regime, the electric field is related with the plasma velocity $\boldsymbol{V}$ through the generalized Ohm's law $\boldsymbol{E} = -\boldsymbol{V} \times \boldsymbol{B}$.

In Fig.1a, let us consider the situation that the magnetic field line $\boldsymbol{B}$ is transfered by the velocity $\boldsymbol{V}$ for a unit time into $\boldsymbol{B}'$. In the case, the electric field vector $\boldsymbol{E}$ corresponds to the parallelogram FGHI, in which the amplitude and the direction are indicated by the area and the normal vector, respectively. Here, we should note also that the parallelogram made by any vector connecting the two field lines, for instance FG'H'I, has the same area and the same normal direction as FGHI. It means that any vector connecting the two field lines forms a consistent virtual velocity $\boldsymbol{V}'$, which satisfies $\boldsymbol{E} = -\boldsymbol{V}' \times \boldsymbol{B}$. Thus, the helicity flux is able to be derived without the measurement of the real velocity $\boldsymbol{V}$, if we can detect the virtual velocity $\boldsymbol{V}'$.

Recently, two different ways were proposed for the derivation of the virtual velocity. Démoulin & Berger (2003) pointed out that, since the vector along the foot point motion FF' forms the virtual velocity, the apparent velocity derived by the local correlation tracking (LCT) of the magnetograms could be used for the helicity measurement. This proposition is valid, if and only if each foot point of field line is identified. However, there is no guarantee that the apparent motion derived by the LCT technique satisfies the definition of the virtual velocity, because we can observe only the magnetic pattern on the photospheric surface rather than each foot point of the field lines. Furthermore, when the field line is tangential to the solar surface, the measurement of the foot point motion could be much difficult, because the apparent velocity must diverges into infinity,

On the other hand, Kusano et al. (2002) demonstrated that the virtual velocity can be derived by inversely solving the induction equation of the normal component on the solar surface,

$$\partial \boldsymbol{B}_n/\partial t = [\nabla \times (\boldsymbol{V}' \times \boldsymbol{B})]_n, \tag{2}$$

in which the magnetic field vector $\boldsymbol{B}$ and the variation of the normal component $\partial \boldsymbol{B}_n/\partial t$ are given by the magnetograph observation, and only $\boldsymbol{V}'$ remains as an unknown. This method has an advantage that the solution automatically satisfies the definition of the virtual velocity.

However, the induction equation cannot determine the velocity component orthogonal both to the vertical vector $\boldsymbol{B}_n$ and the tangential vector $\boldsymbol{B}_t$ of the magnetic field (*i.e.* the y component in Fig.1a). Therefore, we need the help of the LCT technique in order to determine V_y'. Here, notice that the y component of the foot point motion does not diverge even if the field line is tangent to the solar surface. It is another advantageous point of this method.

Figures 1(b) to 1(d) represent the result of a benchmark test of the two methods. Here, we first calculated the three-dimensional linear force-free field, which satisfies $\nabla \times \boldsymbol{B}_{lff} = \alpha \boldsymbol{B}_{lff}$, from the SOHO/MDI data. Then, the helicity flow in the case that the whole active region is uniformly elevated was derived by the two different methods only from the fields on the two horizontal cross sections at different levels, *i.e.* $\boldsymbol{B}_{lff}(z = z_0)$ and $\boldsymbol{B}_{lff}(z = z_0 + \Delta z)$. The result clearly indicates that the combination of the induction equation and the LCT technique can derive the better answer than the result only by the LCT.

Our measurement with this combination technique revealed that positive and negative magnetic helicities are simultaneously injected in flare productive active regions (Kusano et al. 2002). As a result, the structure of magnetic helicity in the active regions were much complicated both in time and space, so that even the sign of the magnetic helicity often changes (Kusano et al. 2003)

This new finding suggested another possibility of the mechanism of energy liberation. If positive and negative helicities coexist within an active region, magnetic reconnection could cancel the helicity by merging the counter helicity fluxes. If it does, the magnetic field may relax to the helicity-free field, and the free energy should be released. This process can be understood as the annihilation of magnetic helicity.

3. Simulation of Helicity Annihilation

In order to examine the hypothesis of the helicity annihilation, the nonlinear MHD process, in which the foot-point shear motion reverses the pre-loaded magnetic helicity, was investigated using the numerical simulations. As a result, it was clearly demonstrated that the reversal of magnetic helicity can cause a large scale eruption of the magnetic arcade through the following processes. First, the resistive tearing mode instability grows on the helicity inversion layer. Secondly, magnetic reconnection driven by the tearing mode annihilates the

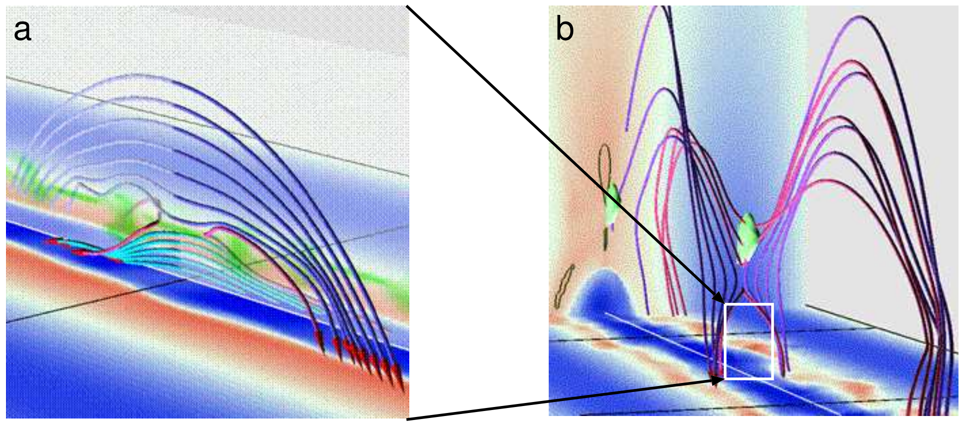

Figure 2. Magnetic field line structure in the numerical simulation of the helicity annihilation process.

positive and negative magnetic fluxes parallel to the magnetic neutral line, as indicated by red lines in Fig.2(a). Thirdly, the flux annihilation is followed by collapse of the magnetic arcade, so that the vertical current sheet is generated. Fourthly, the new current sheet drives the second reconnection, which causes the plasmoid ejection, as seen in Fig.2(b). Finally, the total system reaches a loss-of-equilibrium state, and the whole magnetic arcade is erupted upward.

This model can well explain the explosive property of flare onset, even though the growth rate of the original instability is much slower than the MHD time-scale. Although the reality of our model in the coronal plasma is still unclear, the annihilation of magnetic helicity is a promising concept for the onset mechanism of solar flares and the further investigation is required.

References

Berger, M.A., Field, G.B. 1984, J. Fluid Mech., 147, 133

Démoulin, P. & Berger,M.A. 2003, Solar Phys.215 203

Kusano, K., Maeshiro, T., Yokoyama, T., & Sakukrai T. 2002, ApJ, 577, 501

Kusano, K., Maeshiro, T., Yokoyama, T., & Sakukrai T. 2003, Advances in Space Research (in press)

Highlights of Astronomy, Vol. 13
International Astronomical Union, 2003
O. Engvold, ed.

Transport of Magnetic Helicity and Dynamics of Solar Active Regions

M. K. Georgoulis, B. J. LaBonte, & D. M. Rust

The Johns Hopkins University Applied Physics Laboratory, 11100 Johns Hopkins Rd., Laurel, MD 20723, USA

Abstract. We introduce a method to calculate the magnetic helicity density in a given active-region vector magnetogram, and a lower limit of it, based on a linear force-free (lff) approximation. Moreover, we provide a lower limit of the total magnetic helicity in the active region (AR). A time series of magnetograms can be used to calculate the rate of helicity transport. The results can be then correlated with manifestations of the dynamical activity in ARs, such as flares and filament eruptions.

1. Introduction and Method Description

Magnetic helicity in ARs is given by $H_m = \int_V \mathbf{A} \cdot \mathbf{B} dV$, where $\mathbf{B}$ is the magnetic field vector, $\mathbf{A}$ is the vector potential and the integration refers to the volume V of the magnetic structure. Therefore, the integrand $\mathbf{A} \cdot \mathbf{B}$ is a *magnetic helicity density* h_m at a given volume element. Following a lff approximation ($\alpha = const$), h_m is thought to be given by (e.g. Pevtsov et al. 1995)

$$h_m = \frac{B^2}{\alpha} \quad ; \quad \alpha = const. \tag{1}$$

Eq. (1) is incorrect. Indeed, for potential fields ($\alpha = 0$) we find $h_m \to \infty$, where we should find $h_m = 0$. In the lff approximation h_m is, in fact, given by

$$h_m = \frac{1}{\alpha}|B^2 - \mathbf{B} \cdot \mathbf{B_p}| \quad ; \quad \alpha = const, \tag{2}$$

where $\mathbf{B_p}$ is the potential field. From eq. (2) we now find $h_m \to 0$ for $\mathbf{B} \to \mathbf{B_p}$. The overall α can be calculated by a variety of methods (Leka 1999). From the resulting force-free field $\mathbf{B_{ff}}$, one may also calculate $h'_m = (1/\alpha)|B^2_{ff} - \mathbf{B_{ff}} \cdot \mathbf{B_p}|$. It turns out that $|h'_m|$ is a *lower limit* of $|h_m|$, since $\mathbf{B_{ff}}$ is the closest field to $\mathbf{B_p}$, for which $h_m \to 0$ (eq. (2)). Comparing $\mathbf{B_{ff}}$ and $\mathbf{B_p}$, one can now calculate h'_m anywhere in the AR. A helicity budget can then be found, i.e. $H'_m = \int_V h'_m dV$. H'_m is a *lower limit* of the actual H_m in the AR. From a time series of vector magnetograms, one may find both $H'_m(t)$ and (dH'_m/dt), i.e. the *rate of helicity transport* in the AR and compare it with dynamical activity in the AR.

Our method is applied to NOAA AR 9114 (Fig. 1). Notice the match between $\mathbf{B}$ (Fig. 1a) and $\mathbf{B_{ff}}$ (Fig. 1b). A change in the sign of α forces $h_m(t)$ to change sign (Fig. 1c). $|h'_m(t)|$ is indeed a lower limit for $|h_m(t)|$ (Fig. 1d). Notice the correspondence between the peaks of $h_m(t)$ and $H'_m(t)$ (Figs. 1a and 1e). This suggests that our method may be reasonable, although approximate.

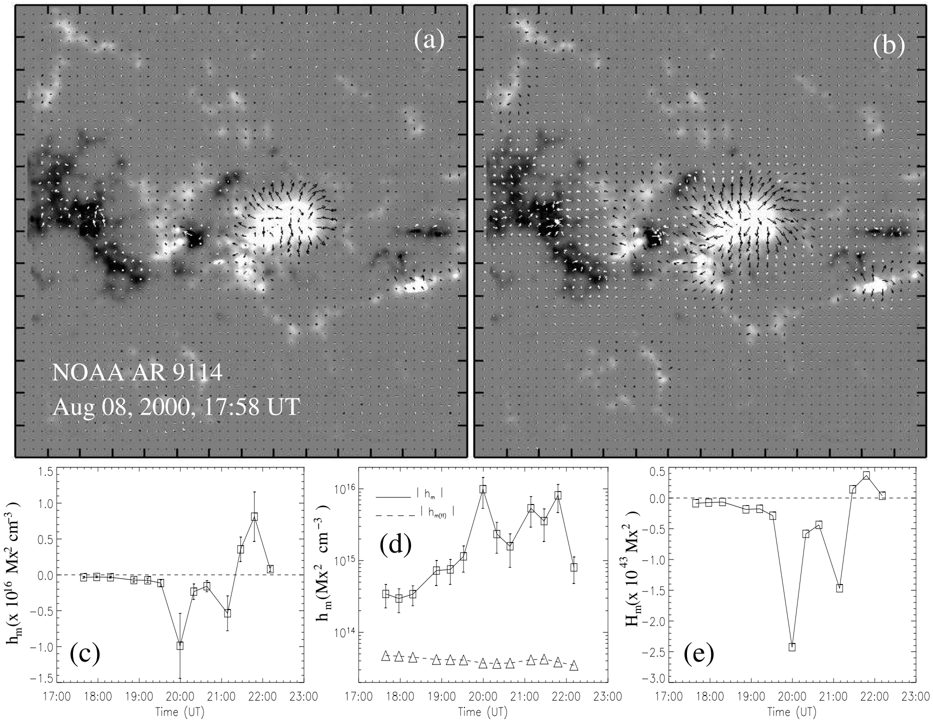

Figure 1. Helicity calculation in NOAA AR 9114, observed by IVM. **(a)** The actual **B** at a given time. **(b)** The best $\mathbf{B_{ff}}$ at this time. Tic mark separation in **a** and **b** is $20''$. **(c)** Average $h_m(t)$. **(d)** Average $|h_m(t)|$ (squares, solid line) and $|h'_m(t)|$ (triangles, dashed line). **(e)** Minimum total magnetic helicity $H'_m(t)$.

2. Conclusion

Using only vector magnetograms, we estimate a lower limit of the total magnetic helicity budget and the rate of helicity transport in solar ARs for the first time. Helicity variations can be calculated only partially, with the formulation of Berger & Field (1984), for ARs close to disk center and by means of the highly uncertain velocity field (Chae 2001). Our method may prove quite useful, provided that the lff approximation manages to capture the dynamical evolution in the active-region solar atmosphere.

References

Berger, M. E., & Field, G. B., 1984, J. Fluid Mech., **147**, 133

Chae, J., 2001, ApJ, **560**, L95

Leka, K. D., 1999, Sol. Phys., **188**, 21

Pevtsov, A. A., Canfield, R. C., & Leka, K. D., 1995, ApJ, **440**, 109

Highlights of Astronomy, Vol. 13
International Astronomical Union, 2003
O. Engvold, ed.

Magnetic Field and Helicity in Solar Active Regions

Hongqi Zhang

National Astronomical Observatories, Chinese Academy of Sciences, Beijing 100012, China, E-mail: hzhang@bao.ac.cn

The measurements of photospheric vector magnetograms provide an important chance to understand the basic properties of the solar magnetic field and the relationship with magnetic helicity in the solar atmosphere. Some questions on the analysis of photospheric vector magnetograms obtained at Huairou solar Observing Station have been discussed:

(1) The slight deviations for the data sets of vector magnetograms obtained at different observatories normally can be fond, which probably caused by the observing methods, magneto-optical effects and data reducing process etc. The analysis of magneto-optical effects on the measurements of vector magnetic field with FeIλ5324.19Å line by Huairou vector magnetograph (and the comparison with some observing results obtained other magnetographs) provides an estimation on the measurement accuracy of magnetic field.

(2) Several methods (such as, $\overline{\alpha}$, α_{best} or $\mathbf{B} \cdot (\bigtriangledown \times \mathbf{B})_{\|}$) can be used to analyze the chirality of magnetic field inferred from photospheric vector magnetograms. Due to the incompleteness of the observational magnetic field data for the calculation of current helicity density etc in the solar atmosphere, some priori assumptions probably have been remained, which also cause some non-determinacy on the analysis of helicity.

(3) Due to the opacity of solar photosphere, the generation of helical magnetic field in the solar sub-atmosphere is an interesting topic. The relationship between the newly emerging magnetic flux and evolution of the helicity in the solar atmosphere provides an important massage on the transfer of magnetic helicity from the sub-atmosphere into the solar atmosphere, which is also necessary for us to understand the possible geometry of magnetic field in the sub-atmosphere and the topology of helical magnetic field in the corona. A relevant result is that as the emergence of kinked magnetic ropes formed in the sub-atmosphere, one probably can detect the possible trace from a series of photospheric vector magnetograms.

Highlights of Astronomy, Vol. 13
International Astronomical Union, 2003
O. Engvold, ed.

Twist and writhe of δ active region magnetic fields

Lirong Tian[1] & Jing Yang[2]

[1]*National Astronomical Observatories, Chinese Academy of Sciences, Beijing 100012, China (tlr@ns.bao.ac.cn);* [2]*Astronomical Department, Beijing Normal University, Beijing 100875, China*

Twist is a parameter to measure turning of the field lines around axis of the flux tube. Observations show that each active region (AR) has a pronounced overall twist, following hemispheric helicity rule (Pevtsov et al. 1995; Bao & Zhang 1998). α_{best}, best-fit single value for a whole AR, is used to characterize the overall twist. Writhe is a measure of the spatial turning of the axis of the flux tube. It is described by systematic tilt angle of an AR, an angle of joined line of opposite main polarities with respect to the equator. Observations show that most ARs follow Joy's Law (Zirin 1988). The relationship between the twist and writhe is important to studying origin of the twist and solar activities. Canfield & Pevtsov (1998) found the same handedness of the twist as that of writhe, using 99 ARs observed at MSO. However, Tian et al. (2001) found opposite handedness of them for 286 ARs taken at HSOS, among which only 19% have δ magnetic configuration. López Fuentes et al. (2003) also obtained opposite handedness for 22 ARs measured again at MSO, among which 41% have δ magnetic class. Most recently, Tian & Liu (2003) found that the twist and the writhe have same handedness for major flare-producing ARs.

A kink hypothesis predict that sign of the twist and writhe should be same where a kink instability has developed and for δ ARs (Linton et al. 1999; Fisher et al. 2000). Therefore, the motivation of this work is to investigate if kink instability prefers to occur in δ ARs. We select 104 ARs with δ magnetic configuration from 1996 to 2002. SOHO/MDI 96m full disk magnetograms are used to calculate the tilt angle and vector magnetograms from HSOS are used to calculate the α_{best}. In our sample, most ARs have two main polarities and a dominant sign of the α_{best} unchanged in several days. Three sets of magnetograms near the central meridian are used to obtain a mean value and error for the tilt and α_{best}. The signs of the mean values denote the handedness of the writhe and twist: the positive/negative values corresponding to the right/left writhe(twist). The results show that (1) only 54% of the ARs follow Joy's law and 50% obey the hemispheric helicity rule; (2) 67% (35.9% with positive tilts and α_{best} and 31.1% with negative tilts and α_{best}) of the ARs have the same handedness of the twist and writhe. A least-square fit for all 104 ARs demonstrates a positive correlation (correlation coefficient, 0.322) between them with more than 99% confidence level. Thus, we further believe that the different relationship between the twist and writhe, obtained in above papers, is due to difference of sample selection: opposite handedness for ARs with simple magnetic configuration and producing less flares and same handedness for ARs with complex magnetic configuration and producing more major flares.

Highlights of Astronomy, Vol. 13
International Astronomical Union, 2003
O. Engvold, ed.

Solar and Interplanetary Magnetic Helicity Balance of Active Regions

Cristina H. Mandrini

Instituto de Astronomía y Física del Espacio, CC.67, Suc.28, 1428, Buenos Aires, Argentina

Pascal Démoulin

1. Observatoire de Paris, LESIA, F-92195, Meudon, France

Lidia van Driel-Gesztelyi[1,2,3]

2. Konkoly Observatory, H-1525 Budapest, P.O. Box 67, Hungary

3. Mullard Space Science Laboratory, UCL, Holmbury St. Mary, Dorking, Surrey, RH5 6NT, UK

Sergio Dasso

Instituto de Astronomía y Física del Espacio, CC.67, Suc.28, 1428, Buenos Aires, Argentina

Lucinda M. Green

Mullard Space Science Laboratory, UCL, Holmbury St. Mary, Dorking, Surrey, RH5 6NT, UK

Marcelo López Fuentes

Naval Research Laboratory, Code 7675, Washington,DC 20375-5352

Abstract. We analyzed the long-term evolution of two active regions (ARs), NOAA 7978 and 8100, from their emergence through their decay using observations from several instruments on board SoHO (MDI, EIT and LASCO) and Yohkoh/SXT. We computed the evolution of the relative coronal magnetic helicity from one central meridian passage to the next, combining data from MDI and SXT with linear force-free models of the coronal magnetic field. Next, we calculated the injection of helicity by photospheric differential rotation using MDI magnetic maps and a mean differential rotation profile. To estimate the depletion of magnetic helicity we counted all the CMEs of which these ARs were the source, and we evaluated their helicity assuming a one to one correspondence with magnetic clouds (MCs) with an average helicity content; this value was computed for a sample of 18 clouds using a cylindrical linear force-free model. Out of our three helicity estimates (variation of coronal magnetic helicity, injection by differential rotation and ejection via CMEs) the one with the largest uncertainty is the amount of helicity ejected via CMEs. However, we determined, by modeling a particular MC using three different approaches in cylindrical geometry (two force-free models and a non force-free model with constant current), that its magnetic helicity content was nearly independent of the model used to fit in situ field observations (Dasso et al. 2003, in preparation). This result justi-

fies our use of the average magnetic helicity value considering only a single MC model. Comparing the three components in the helicity balance (see Table 1), we find that photospheric differential rotation is a minor contributor to the AR magnetic helicity budget. CMEs carry away at least 10 times more helicity than the one differential rotation can provide. Therefore, the magnetic helicity flux needed in the global balance should come from localized photospheric motions that, at least partially, reflect the emergence of twisted flux tubes. Taking into account the magnetic flux in the ARs and the number of turns that a uniformly twisted flux tube should have to survive its rise through the convection zone, we have found that the total helicity carried away in CMEs is approximately equal to the end-to-end helicity of the flux tubes that formed these two ARs. Therefore, we conclude that most of the helicity ejected in CMEs is generated below the photosphere and emerges with the magnetic flux. Extended versions of this work were published in Démoulin et al. (2002, Astronomy & Astrophys. 382, 650) and in Green et al. (2002, Solar Phys. 208, 43), while in Mandrini et al. (2003, Astrophys. & Space Sci., in press) and van Driel-Gesytelyi et al. (2003, Adv. Space Res., in press) the helicity computations were revised to include the underestimation of magnetic flux density found in MDI data. After this revision, we confirmed our former results.

Table 1. The total magnetic helicity balance of AR 7978 and AR 8100 along five and four solar rotations, respectively. $\Delta H_{\mathrm{cor.}}$ and $\Delta H_{\mathrm{d.r.}}$ are the coronal helicity variation and the helicity injected by differential rotation, respectively. The helicity in MCs ($\Delta H_{\mathrm{m.cl.}}$) is given taking two extreme lengths (0.5 and 2 AU) and using the observed and corrected CME numbers (corrections done for gaps and far-side locations). All values are in units of 10^{42} Mx^2.

Active Region	$\Delta H_{\mathrm{cor.}}$	$\Delta H_{\mathrm{d.r.}}$	$\Delta H_{\mathrm{m.cl.}}$ (CME obs.)	$\Delta H_{\mathrm{m.cl.}}$ (CME cor.)
NOAA 7978	-11.0	16.2	[36.,144.]	[40.,160.]
NOAA 8100	-38.8	-14.6	[38.,152.]	[82.,328.]

Acknowledgments. The authors thank the SOHO/MDI consortium for SOHO data and the MSSL/UCL Solar UK Research Facility for Yohkoh data. SOHO is a joint project by ESA and NASA. L.v.D.G. acknowledges the Hungarian government grant OTKA T-038013. C.H.M. and L.v.D.G. acknowledge financial support from TET (Hungary) and SECyT (Argentina) through their cooperative science program (AR03/02-HU/A01/UIII/01). P.D. and C.H.M. acknowledge support from ECOS (France) and SECyT through their cooperation agreement (A01U04).

Highlights of Astronomy, Vol. 13
International Astronomical Union, 2003
O. Engvold, ed.

Heating the Solar Corona

L. C. Woods

Mathematical Institute, 24-29 St Giles, Oxford, England

A typical temperature for the quiet solar corona is $\sim 1.5 \times 10^6$K, whereas the photosphere – the likely source of the thermal energy – has a temperature less than 6×10^3 K. Although many theories have been advanced to explain why the corona is so much hotter than the photosphere, this old problem remains unsolved. However, there is a mechanism based on second-order transport that may provide the answer, or at least part of the answer. This process, described by the author in *Thermodynamic inequalities in gases and magnetoplasmas*, John Wiley & Sons Ltd, 1996, causes heat to be transported across strong magnetic fields *up* temperature gradients.

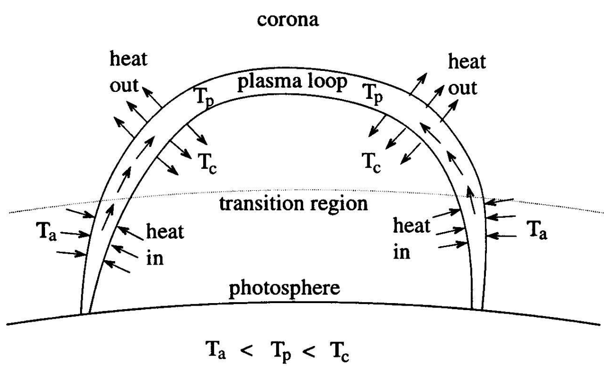

Fig. 1. Transporting heat to the corona via plasma loops

Plasma loops in the solar atmosphere (see Fig. 1) exist with a wide range of temperatures and in particular there are loops that are hotter than ambient in the chromosphere/transition region (10^4 K $< T < 5 \times 10^5$ K) and cooler than ambient in the corona (10^6 K $< T < 2 \times 10^6$ K). The theory of second-order transport suggests the mechanism illustrated in Fig. 1; heat is transported *upwards* from the upper chromosphere and transition regions, using appropriate flux tubes as conduits. In the region below the transition region, the loop temperature is greater than that in the ambient plasma and by second-order transport, heat flows up the temperature gradient, across the magnetic field into the loop. This causes a local increase in temperature, and a relatively small temperature gradient is established around the loop that conducts the thermal energy up to that part of the loop high in the corona. This stage is 'normal' heat flux, i.e. along the magnetic fields lines and down the temperature gradient. High in the loop the situation is the reverse of that in the chromospheric region, that is the temperature in the loop is less than that in the ambient corona and heat therefore flows out of the loop into the hotter corona. This mechanism can easily supply the power of about 3×10^2 Wm^{-2} required for the quiet corona and also the $\sim 10^4$Wm^{-2} required for the active corona.

Highlights of Astronomy, Vol. 13
International Astronomical Union, 2003
O. Engvold, ed.

Helicity Pattern of CME Source Active Regions

Jingxiu Wang, Guiping Zhou, and Jun Zhang

National Astronomical Observatories, Chinese Academy of Sciences
Beijing 100012, China

Coronal mass ejections are thought to originate from the over accumulation of magnetic helicity (Rust & Kumar, 1994). While recent studies revealed the incompetence of CME associated active regions in creating enough helicity for CMEs (Nindos, Zhang, & Zhang, 2003 and references therein), we have tried to seek, on the other hand, if particular helicity patterns are retained by CME-associated active regions.

We select 14 CME-associated ARs. The selection is based on the correlation study of CMEs and surface magnetic activity by Zhou, Wang and Cao (2003). All the CMEs are Earth-directed halo CMEs whose source regions and associated surface activity were well identified. The very CME-prolific ARs took priority in the selection.

Two proxies are used in this work to quantify the helical nature of the AR fields. The first proxy is the force-free coefficient, α_{best}, by which the extrapolated force-free fields fit best the observed transverse fields in the photosphere. It is related the magnetic helicity under the force-free assumption (Wang, 1996; Georgoulis, 2003). The second proxy is the fractional current helicity (Abramenko, Wang, & Yurchishin, 1996), $h_{\|}$. Under the assumption of force-free field, the h_c and α are of the same sign.

Contrary to the helicity charging picture, the newly emerging flux often brings up the helicity of the sign opposite to that of the dominant helicity of the active regions. Moreover the flare/CME initiation site was always characterized by the close contacting of opposite sign helicity. This revelation suggests that the interaction of different flux systems with opposite sign helicity is a key factor in the magnetism of CME initiation.

Acknowledgments The work is supported by National Key Basic Research Science Foundation (G2000078404) and National Science Foundation of China (10233050).

References

Abramenko, V.I., Wang, T., Yurchishin, V. B., 1996, Solar Phys., 168, 75.

Georgoulis, M.K. 2003, this volume

Nindos, A., Zhang, J., Zhang, H. 2003, ApJ, 594, 1033

Rust, D.W. & Kumar, A. 1994, solar Phys. 155, 69.

Wang, J. 1996, Solar Phys., 163, 319.

Zhou, G.P., Wang, J.X., & Cao, Z.L. 2003, A&A, 397, 1057.

Zirin, H. 1985, 1985, Aust. J. Phys. 38, 961.

Highlights of Astronomy, Vol. 13
International Astronomical Union, 2003
O. Engvold, ed.

Helicity and the SOLIS Vector-Spectromagnetograph

Christoph U. Keller, John W. Harvey, Carl J. Henney

National Solar Observatory, 950 N. Cherry Ave., Tucson, AZ 85719, USA

Harrison P. Jones

NASA/Goddard Space Flight Center, 950 N. Cherry Ave., Tucson, AZ 85719, USA

Abstract. The SOLIS Vector-Spectromagnetograph (VSM) is a compact, highly efficient vector-polarimeter that measures the magnetic field vector over the full solar disk within 12 minutes. Helicity-related quantities will be derived from the observed vector field.

1. Overview

SOLIS (Synoptic Optical Long-term Investigations of the Sun) is a suite of three innovative instruments that greatly improve ground-based synoptic solar observations. The VSM is a 50-cm effective aperture telescope with a tip-tilt secondary mirror and filled with helium to reduce internal seeing. The spectrograph has a Littrow design that is insensitive to temperature changes. The entrance slit is scanned in declination to provide 2048 by 2048 pixel scans of the full solar disk at three wavelengths. The polarization modulation is performed by ferroelectric liquid crystal retarders. Two 1024 by 256 CMOS-Hybrid cameras acquire 92 frames per second, which are then analyzed to obtain all Stokes parameters. The VSM is capable of recording vector magnetograms in two FeI lines around 630.2 nm, deep longitudinal magnetograms in the same lines, longitudinal magnetograms in CaII 854.2 nm, and intensity in HeI 1083.0 nm. Regular full-disk scans will be recorded within 12 minutes, while active regions can be scanned in as little as 30 seconds. The Stokes spectra are reduced to physical quantities including field strength, azimuth, inclination, and filling factor with a Milne-Eddington inversion code. The VSM will be the prime instrument for synoptic studies of helicity in the solar photosphere. In addition, the SOLIS Full-Disk Patrol (FDP) will provide the velocity vector to measure the flux of magnetic helicity through the photosphere. More information on SOLIS is available at `solis.nso.edu`.

Acknowledgments

The National Solar Observatory is operated by AURA Inc. under cooperative agreement with the National Science Foundation.

Highlights of Astronomy, Vol. 13
International Astronomical Union, 2003
O. Engvold, ed.

Prominence Formation Processes

B.T. Welsch

Space Sciences Lab, University of California, 7 Gauss Way, Berkeley, CA 94720-7450

C. R. DeVore

Laboratory for Computational Physics and Fluid Dynamics, Code 6440, Naval Research Laboratory, Washington DC 20375-5344

S. K. Antiochos

E. O. Hulburt Center for Space Research, Code 7675, Naval Research Laboratory, Washington DC 20375-5352

Abstract. We summarize our attempts simulate the prominence formation model proposed by Martens & Zwaan (2001, ApJ, 558, 872) in which differential rotation drives reconnection between two initially unconnected bipolar active regions to form helical field lines along the polarity inversion line (PIL) between the flux systems.

In Cartesian coronal simulations, we used the ARMS code, an MHD solver with adaptive refinement, to model field evolution resulting from an imposed shear flow on the bottom boundary (to mimic photospheric differential rotation), which contained two bipolar flux concentrations. The boundary fluxes were chosen such that, by symmetry, no coronal lines initially joined the bipolar flux systems. In some runs, the pre-shearing fields were potential, but in others we "spun up" the flux systems prior to shearing (by flows tangent to normal flux contours) to model flux systems possessing helicity at emergence. Work to understand how pre-shearing helicity affects reconnection after shearing onset continues, but we summarize three related conclusions below. In general, prominence-like field topologies did not form by reconnection in "double bipole" configurations, but dipped or helical field lines did form in cases with initial fields with an unphysical bald patch along the PIL. We are currently studying how background fields and/or converging flows modify the field evolution. Reconnection does not readily occur without sufficient topological complexity. Small footpoint displacements induced reconnection in fields with nulls and/or bald patches, but even large footpoint displacements led to little or no reconnection in fields without such topological features. Twisting drives reconnection more strongly than shearing. In contrast to our expectations, we essentially found that shear only weakly drove reconnection, while spin-up readily drove reconnection.

This work was supported by ONR, NASA, and by a grant of computer time from the DOD High Performance Computing Modernization Program at the ERDC MSRC.

Highlights of Astronomy, Vol. 13
International Astronomical Union, 2003
O. Engvold, ed.

The Role of Magnetic Helicity in Solar Flares

Mark G. Linton

Naval Research Laboratory, 4555 Overlook Ave. SW, Washington, DC 20375-5352

Abstract. Helicity in coronal magnetic fields, often occurring in the form of twisted or sheared fields, can provide surplus energy which is available for release in solar flares. In this paper, several models of how this extra, non-potential, energy can be released will be reviewed. For example, twisted flux tubes can release excess energy via the kink instability. Or energy can be released via a transfer of helicity between different magnetic tubes. For untwisted field, the mutual helicity between flux tubes provides a measure of the shear in the fields, and therefore how much energy is available for release in a flare. For twisted flux tubes, the twist helicity of each tube in combination with the mutual helicity between the tubes dictate what type of reconnection the tubes can undergo and how much energy is available for release. Measuring the helicity of coronal active regions, and studying how this helicity affects magnetic energy release is therefore vital for our understanding of and our ability to predict solar flares.

1. Introduction

This paper will review several mechanisms which can release magnetic energy via the conversion of one type of magnetic helicity to another. A full review of the topic cannot be accomplished in this short space, so the focus here will be on scenarios involving magnetic flux tubes, the basic building blocks of the coronal magnetic field. Several energy release mechanisms relying on helicity transfer will be discussed and, for each, one or more numerical simulations which exemplifies the mechanism will be briefly reviewed.

Berger & Field (1984) showed that the helicity of a single flux tube can be split into two parts: the twist helicity and the writhe helicity. The twist helicity describes the amount by which field lines in a flux tube wrap around the flux tube axis. The writhe helicity measures the amount by which the axis wraps around itself. Thus a helical flux tube axis has a writhe helicity, just as a helical field line has a twist helicity. The third type of helicity relevant to our discussion of flux tubes is the crossing helicity. This measures the amount by which a pair of flux tubes wrap around each other, or the sense in which flux tubes cross over each other (see Wright & Berger 1989). In the following discussion, we will illustrate how the conversion of helicity from one of these types to another can be effected, and how this can lead to a reduction in the total magnetic energy of the configuration.

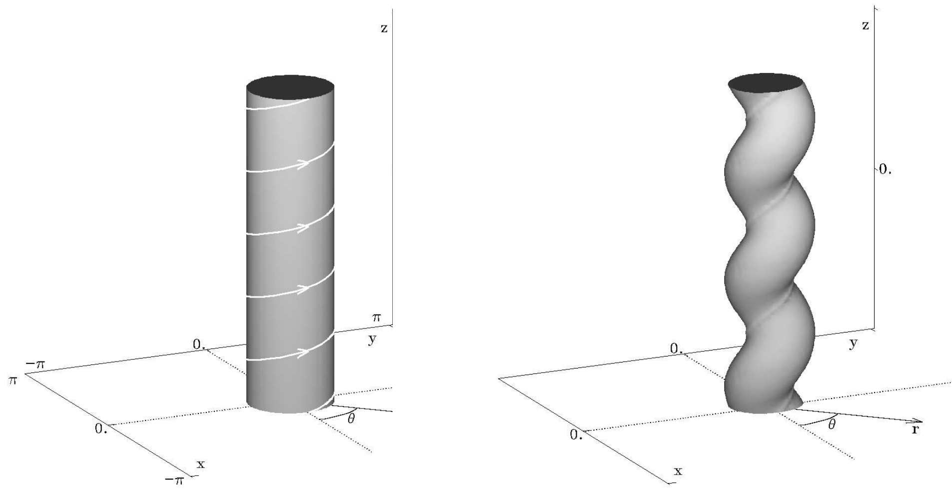

Figure 1. Kink instability: an unkinked, twisted flux tube (left side) kinks with the same handedness as its twist (right side).

2. Transfer of Twist, Writhe, and Crossing Helicity

Tanaka (1991), Leka et al. (1996) and others studied δ-spots, the solar active regions which generate about 80% of large flares (Sammis & Zirin, 2000), and found support for the theory that these regions are created by kinked magnetic flux tubes. These active regions exhibit an unusually high amount of magnetic stress or helicity: their fields are highly twisted, and the spots themselves exhibit rotational motion as they emerge, suggesting both twist and writhe helicity are important. This could be produced by the kink instability, which reduces the energy of a highly twisted flux tube, such as that on the left side of Figure 1, by distorting the tube axis into a helical shape, as on the right side of Figure 1. This converts twist helicity, T, into writhe helicity, W, while conserving the total helicity: $T + W = const.$ (Berger & Field 1984). This reduces the tube's twist magnetic energy, but, at the same time, makes the tube longer and therefore increases its axial magnetic energy. Thus if the twist energy is large enough relative to the axial energy, the total energy is reduced (Linton et al 1996). Fan et al. (1999) and Linton et al. (1998) simulated this kink instability in the context of flux tube emergence, and found that the behavior of the kinked flux tubes was consistent with δ-spot behavior, thus arguing that one could look to the kink instability to explain the high flare activity of these regions. Lionello (1998), Gerrard et al. (2001), and others have simulated the kink instability of twisted coronal loops, and found these are also good candidates for solar flare energy release.

A second way to reduce the twist of flux tubes, and thereby release non-potential magnetic energy, is to reconnect two tubes of different twist. The new connections between the tubes allows twist to be transferred between them and can therefore lead to a more even, lower energy, distribution of twist. In this case, helicity conservation dictates that the sum of the twist in both tubes is fixed: $T_1 + T_2 = const.$ For example, if an untwisted tube reconnects completely with a twisted tube of twist N the result will be two tubes each with twist

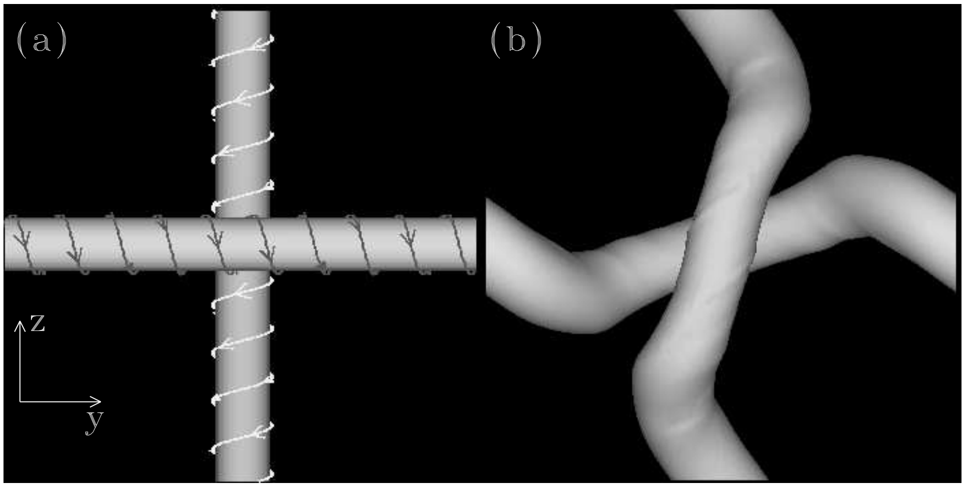

Figure 2. The tunnel reconnection of a pair of flux tubes. The right hand twist is reduced to conserve helicity when the flux tubes tunnel from a left handed crossing (a) to a right handed crossing (b).

$N/2$. This was seen in a simulation by Amari & Luciani (2000). They twisted the footpoints of a flux tube until it kinked and reconnected with overlying, untwisted field to create a pair of twisted tubes at lower total energy. Such reconnection can even lead to a destruction of twist: two regions of *opposite* twist helicity can combine in such a way that their twist cancels. Linton et al. (2001) have shown that this works for the reconnection of oppositely twisted flux tubes. Reconnection connects the twisted field of one flux tube directly to the twisted field of the second flux tube, and the canceling twists simply annihilate each other as torsional Alfvén waves propagate along the reconnected flux tubes. Due to this cancellation of twist, the energy release from such opposite helicity reconnection is quite large compared to other types of flux tube energy release. This has also been shown in a simulation by Ozaki and Sato (1997) where they twisted the footpoints of two coronal loops in opposite directions until they were kink unstable. They found that the kink causes the loops to arch and distort until they collide with each other. They then reconnect, cancel each others' twist and release the stored twist energy.

A third mechanism for energy release via helicity conversion is where the crossing helicity, C, of a pair of tubes is transferred into the twist helicity of both tubes. Here helicity conservation dictates that the sum of crossing plus twist helicities is fixed: $C + T_1 + T_2 = const.$ The two tubes shown in Figure 2(a) cross each other in a left handed sense and therefore have a negative crossing helicity. For a pair of right hand twisted tubes of $T_1 = T_2 = N$, the total helicity is therefore $C + 2N < 2N$. Dahlburg et al. (1997) found that when these two flux tubes collide, they reconnect twice and pass through each other to form the flux tube pair of Figure 2(b). When these flux tubes pass through each other, their crossing helicity changes from from C to $C + 2$. As this occurs, the twist per flux tube must reduce from N to $N-1$ so that $C+2N \rightarrow (C+2)+2(N-1)$, and helicity is conserved (Linton & Antiochos 2002). As there is no magnetic energy in the crossing of the flux tubes, this reduction in twist means that the magnetic energy is reduced, and flare energy has been released.

3. Summary

We have presented a selective discussion of the role of helicity in solar flares, in particular of the role of flux tube helicity in magnetic energy release. We have discussed how one can transfer helicity between the twist of field lines in flux tubes, the writhe of flux tubes' axes, and the crossing of flux tubes over each other. While we have discussed only flux tubes rather than general configurations, one can argue that most magnetic fields can be reduced to a set of individual flux tubes, and so the helicity and energy of a complex region can be described in terms of the flux tube helicity discussed here. Flux tube helicity can therefore provide an intuitive yet powerful way to analyze magnetic energy release, and to develop models for understanding and predicting solar flares.

References

Amari, T. & Luciani, J. 2000, PRL, 84, 1196
Berger, M. & Field, G. 1984, JFM, 147, 133
Dahlburg, R., Antiochos, S. & Norton, D. 1997, Phys. Rev. E, 56, 2094
Fan, Y., Zweibel, E., Linton, M., & Fisher, G. 1999, ApJ, 521, 460
Gerrard, C., Arber, T., Hood, A., & Van der Linden, R. 2001, A&A, 373, 1089
Leka, K., Canfield, R., McClymont, A., & van Driel Gesztelyi, L. 1996, ApJ, 462, 547
Linton, M. & Antiochos, S. 2002, ApJ, 581, 703
Linton, M., Dahlburg, R., Antiochos, S. 2001, ApJ, 553, 905
Linton, M., Dahlburg, R., Longcope, D., & Fisher, G. 1998, ApJ, 507, 404
Linton, M., Longcope, D., & Fisher, G. 1996, ApJ, 469, 954
Lionello, R., Velli, M., Einaudi, G., & Mikic, Z. 1998, ApJ, 494, 840
Longcope, D. & Klapper, I. 1997, ApJ, 488, 443
Ozaki, M. & Sato, T. 1997, ApJ, 481, 524
Sammis, I. R. & Zirin, H. 2000, ApJ, 540, 583
Tanaka, K. 1991, Sol. Phys., 136, 133
Wright, A. N. & Berger, M. A. 1989, JGR, 94, 1295

Highlights of Astronomy, Vol. 13
International Astronomical Union, 2003
O. Engvold, ed.

Helicity of Magnetic Clouds and Their Associated Active Regions

Robert J. Leamon and Richard C. Canfield

Department of Physics, Montana State University, Bozeman, MT 59717-3840 USA.

Sarah L. Jones

Department of Physics and Astronomy, Dartmouth College, Hanover, NH 03755 USA.

Keith Lambkin

Experimental Physics Department, University College Dublin, Dublin 4, Republic of Ireland.

Brian J. Lundberg

Department of Physics, The University of Arizona, Tucson, AZ 85721 USA

Alexei A. Pevtsov

National Solar Observatory, Sunspot, NM 88349 USA.

Abstract. Magnetic clouds are associated with many Coronal Mass Ejections. Many CMEs involve active regions. In this work we focus on the relationship between twelve magnetic clouds and their associated active regions. We use a cylindrically symmetric constant-α force-free model to derive field line twist, total current, and total magnetic flux from in situ observations of magnetic clouds. We compare these properties with those of the associated solar active regions, which we infer from solar vector magnetograms.

Our comparison of fluxes and currents reveals: (1) the total (unsigned) flux ratios Φ_{MC}/Φ_{AR} tend to be of order unity; (2) the total flux ratios tend to be orders of magnitude larger than the total (unsigned) current ratios I_{MC}/I_{AR}; and (3) there is a statistically significant proportionality between them. Our key findings in comparing total twists αL, where L is the axial dimension of the system, are: (1) the values of $(\alpha L)_{MC}$ are typically an order of magnitude greater than those of $(\alpha L)_{AR}$; and (2) there is no systematic sign or amplitude relationship between them. These findings compel us to believe that magnetic clouds associated with active region eruptions are formed by magnetic reconnection between these regions and their larger-scale surroundings, rather than pre-existing structures in the corona or chromosphere.

Highlights of Astronomy, Vol. 13
International Astronomical Union, 2003
O. Engvold, ed.

New Force-Free Models of Magnetic Clouds

M. Vandas

Astronomical Institute, Academy of Sciences, Boční II 1401, 141 31 Praha 4, Czech Republic

E. P. Romashets

Institute of Terrestrial Magnetism, Ionosphere, and Radio Wave Propagation, Russian Academy of Sciences, Troitsk, Moscow Region, 142190, Russia

S. Watari

Communications Research Laboratory, 4-2-1 Nukui-Kita, Koganei, Tokyo 184-8795, Japan

Abstract. Magnetic clouds are thought to be large flux ropes propagating through the heliosphere. Their twisted magnetic fields are mostly modeled by a constant-alpha force-free field in a circular cylindrical flux rope (the Lundquist solution). However, the interplanetary flux ropes are three dimensional objects. In reality they possibly have a curved shape and an oblate cross section. Recently we have found two force-free models of flux ropes which takes into account the mentioned features. These are (i) a constant-alpha force-free configuration in an elliptic flux rope (Vandas & Romashets 2003), and (ii) a non-constant-alpha force-free field in a toroid with arbitrary aspect ratio (Romashets & Vandas 2003). Two magnetic cloud observations were analyzed. The magnetic cloud of October 18–19, 1995 has been fitted by Lepping et al. (1997) with use of the Lundquist solution. The cloud has a very flat magnetic field magnitude profile. We fitted it by the elliptic solution (i). The magnetic cloud of November 17–18, 1975 has been fitted by Marubashi (1997) with use of a toroidally adjusted Lundquist solution. The cloud has a large magnetic field vector rotation and a large magnetic field magnitude increase over the background level. We fitted it by the toroidal solution (ii). The both fits match the rotation of the magnetic field vector in a comparable quality to the former fits, but the description of the magnetic field magnitude profiles is remarkable better. It is possible to incorporate temporal effects (expansion) of magnetic clouds into the new solutions through a time-dependent alpha parameter as in Shimazu & Vandas (2002).

This work was supported by grant 205/03/0953 from the Grant Agency of the Czech Republic, by project ME501 from MŠMT ČR, by project S1003006 from AV ČR, by EU/INTAS/ESA grant 99-00727, by CRDF grant TGP-944, and by the Japan Society for Promotion of Science.

Highlights of Astronomy, Vol. 13
International Astronomical Union, 2003
O. Engvold, ed.

Magnetic helicity generated together with evolution of the large-scale magnetic field

Pavel Ambrož

Astronomical Institute of the Acad. Sci. of the Czech Rep., CZ-25165 Ondřejov , Czech Republic

Abstract. Text below is an extended abstract of the poster, presented on JD03 session during 25th GA IAU in Sydney.

Large-scale magnetic regions evolve their structure in the photosphere relatively slowly during their many months long lifetime. Their evolution is partly influenced by turbulent diffusion, but also by large-scale velocity fields with both axially symmetric and non-axially symmetric components. In the latter case, horizontal velocities vary in both longitude and latitude. The horizontal transport velocities responsible for the evolution of the magnetic flux were inferred for each Carrington rotation (CR) for each of the last three activity cycles Nos. 21, 22 and 23. The measurements of magnetic field from WSO of Stanford University were used. Zonal transport velocities averaged over longitude during each CR give a very good approximation of the latitude-dependent differential rotation. The velocity distribution, however, demonstrates that non-axially symmetric horizontal flows create large-scale eddies and helical structures. They are persistent, and the structures persist for up to 4 CRs. The detected flow systems create discrete giant flow patterns that are from 40 to 60 heliographic degrees wide in the equatorial zone. From the surface distribution of horizontal velocities we computed for each CR more than 2500 values of relative "shear" velocities $\Delta\mathbf{v}$ and we determined regions where due to shear the maximal helical turbulence can occur. Such regions are necessary for generation of magnetic helicity, but another necessary condition is the value of the total magnetic field $\mathbf{B}$. Total values were summed from measured $\mathbf{B_{m,r}}$ (radial) and current-free extrapolated $\mathbf{B_{p,t}}$(transversal) components. Product of $\mathbf{B^2}$ and $\Delta\mathbf{v}$ can be expressed in the form relating with the "available" magnetic energy. This is considered to be a part of the magnetic energy, which can be released when is above the threshold of instability of the coronal magnetic configuration. Regions with high rate of available energy were tested with about 95 thousand specific values of flare index derived from observed H_α flares. The occurrence of flares was strictly concentrated in regions with a high rate of available energy. The "shear" regions are frequently distributed in the solar photosphere and usually don't coincide with the "shear zone" expected due to axially symmetric differential rotation. Such a zone is nearly absent in our results. The "shear" regions frequently coincide with the strong magnetic fields of the active or bipolar magnetic regions, and therefore, during each CR, only a very limited number of regions are able to produce and transport a concentrated amount of magnetic helicity to the corona.

Study was supported by GAČR 205/10/0657 and GA AVČR S1003006.

Highlights of Astronomy, Vol. 13
International Astronomical Union, 2003
O. Engvold, ed.

Of Tilt and Twist

Zachary A. Holder, Richard C. Canfield, Rebecca A. McMullen

Department of Physics, Montana State University, Bozeman, MT 59717-3840, U.S.A.

Robert F. Howard

National Solar Observatory/Kitt Peak[1], Tucson, AZ 85726, U.S.A.

Alexei A. Pevtsov

National Solar Observatory/Sacramento Peak[1], PO Box 62, Sunspot, NM 88349, U.S.A.

Abstract. Using Mees Solar Observatory active-region vector magnetograms and Mt. Wilson Observatory full-disk longitudinal magnetograms, we measure both the twist and tilt of the magnetic fields of 368 active regions. This dataset clearly shows two well-known phenomena, Joy's law and the hemispheric helicity rule, as well as a lesser-known twist-tilt relationship, which is the point of this work. Those regions that closely follow Joy's law show no twist-tilt relationship, which is a predicted consequence of convective buffeting of initially untwisted and unwrithed flux tubes through the Σ effect. Those regions that strongly depart from Joy's law show significantly larger than average twist and a very strong twist-tilt relationship. These properties suggest that the twist-tilt relationship in these regions is due to kinking of flux tubes that are highly twisted but not strongly writhed.

Highlights of Astronomy, Vol. 13
International Astronomical Union, 2003
O. Engvold, ed.

A Non-helical Dynamo — MHD Simulations of Dynamo Action by a Non-helical Flow

V. Archontis

Instituto de Astrofisica de Canarias, Via Lactea, E-38200 La Laguna

S.B.F. Dorch

The Niels Bohr Institute, Juliane Maries Vej 30, DK-2100 Copenhagen

Abstract. We illustrate that helicity is not a necessary ingredient for fast dynamo action; we use the stagger-grid method of Galsgaard, Nordlund and others (e.g. Galsgaard & Nordlund 1997, and applied to dynamos by e.g. Dorch 2000): we solve the full MHD equations including a forcing term that keeps the kinetic energy at an approximately constant level. A 3-d flow with no mean helicity (an ABC-like flow without cosines, cf. Galloway & Proctor 1992) is implemented and it turns out that apart from the high growth rate in the linear regime (compared to kinematic dynamo action, cf. Archontis & Dorch 2003a), the dynamo saturates at a level significantly higher that the intermittent turbulent dynamos (cf. Archontis & Dorch 2003b); namely at exact energy equipartition. During the linear regime, several kinematic modes are present, e.g. a sheet/vortex-mode and a mode that resembles the ABC "double cigar" mode (e.g. Dorch 2000). In the non-linear regime, the magnetic topology is not symmetric, but the initial structure of the velocity field is retained. The presence of helicity is not a requirement for dynamo action but it is rather the stretching ability of the flow that amplifies the magnetic energy in an exponential manner (Archontis & Dorch, in preparation).

A miniature copy (A4) of the poster may be downloaded (MS PowerPoint) from the following URL:

`http://www.astro.ku.dk/~dorch/posters/JD03.ppt`

Acknowledgments. VA thanks the EU-TMR for support through a Marie Curie Fellowship. SBFD was supported by the Danish Natural Science Research Foundation, through a Steno research grant.

References

Archontis, V., Dorch, S.B.F. & Nordlund, Å. 2003a, A&A, 397, 393
Archontis, V., Dorch, S.B.F. & Nordlund, Å. 2003b, A&A, in press
Dorch, S.B.F. 2000, Physica Scripta, 61, 717
Galloway, D. & Proctor, M. 1992, Nature, 356, 691
Galsgaard, K. & Nordlund, Å. 1997, J. Geophys. Rev., 102, 219

Highlights of Astronomy, Vol. 13
International Astronomical Union, 2003
O. Engvold, ed.

RATAN-600 Observations of Unusual Inversion of Polarization in Sunspot associated Microwave Sources

Gizani, N.

Institute of Astronomy & Astrophysics, National Observatory of Athens, I. Metaxa & B. Paulou, Lofos Koufou, Penteli, Athens

Alissandrakis, C.

University of Ioannina, Section of Astrogeophysics, GR-45110 Ioannina, Greece

Bogod, V. & Garaimov, V.

Special Astrophysical Observatory, 357147, Karachaevo-Cherkessia, Russia

Zheleznyakov, V.

Pulkovo Astronomical Observatory, 196140, Pulkovo, Russia

Zlotnik, E.

Institute of Applied Physics, 603600 Nizhnij Novgorod, Russia

1. Summary

We have discovered unusual inversion of circular polarization in *both components* of an active region. We have observed the region for six consecutive days in May 96 using the RATAN-600 radio telescope with high polarization accuracy up to 0.5 %. The observations were taken in the range of 1.7 to 30 cm. At short wavelengths the circular polarization scans revealed a bipolar structure, expected since the magnetic field is bipolar. However, for all six days and while the region was moving from the center of the disk to the west limb, the circular polarization dropped practically to zero at 14.5 cm and at longer wavelengths the sense of the polarization was reversed.

We show that this unusual polarization inversion cannot be interpreted in terms of the known propagation effects under conditions of weak and strong coupling. Linear coupling could explain the observed polarization only if the magnetic field was parallel to a solar meridian (i.e. perpendicular to the magnetic dipole axis of the active region). Then the polarization would be independent of the solar rotation and the reversal would occur for both group components at the same frequency. This field could be the very large scale, global solar magnetic field, but its existence is not confirmed observationally (EUV and soft X-ray). The most likely interpretation is the change of the predominant emission mechanism near the wavelength of polarization reversal. The change from thermal at shorter wavelengths to non-thermal at longer ones could cause the predominance of o-mode emission at lower frequencies.

Highlights of Astronomy, Vol. 13
International Astronomical Union, 2003
O. Engvold, ed.

Magnetic Neutral Line Rotations in Flare-productive Regions

Takako T. Ishii, Ayumi Asai, Hiroki Kurokawa

Kwasan and Hida Observatories, Kyoto-U., Yamashina-ku, Kyoto, JAPAN 607-8471

Tsutomu T. Takeuchi

NAOJ, Mitaka, Tokyo, JAPAN 181-8588

Abstract. We examined the evolution of active regions and found that rotational motions of the neutral line in the δ-type magnetic configuration are common in the flare-productive active regions.

1. Introduction

What is the common magnetic field configuration among flare-productive active regions? In our previous studies, we have found that the magnetic neutral line shows a rotational motion in a δ-type active region NOAA 9026, where three X-class flares successively occurred (Kurokawa et al. 2002). In this paper, we show other examples of magnetic neutral line rotations in flare-productive regions.

2. Results

During the current solar maximum (cycle 23), we studied the evolution of all the active regions that have produced at least one X-class flare and have been observed by the Solar and Heliospheric Observatory (*SOHO*) / Michelson Doppler Imager (MDI). We examined 35 active regions from 1996 through 2003 June, and found clear rotational motions of the neutral line in the δ-type magnetic configuration in the following active regions; NOAA 9026, 9393, 9415, 9591, 9661, 9672, 0039, and 0314. The angular velocity is about 20 degree par day in each active region and the motion continues about four days. The clock-wise motion dominates in the north-hemisphere regions (three in three), and the counter-clock-wise in the south-hemisphere (three in five, one region shows both rotations). These motions suggest the existence of magnetic flux knots and its relation to magnetic helicity. Such a magnetic knot should be the energy storage for major flares.

References

Kurokawa, H., Wang, T.J., & Ishii, T.T. 2002, ApJ, 572, 598

Highlights of Astronomy, Vol. 13
International Astronomical Union, 2003
O. Engvold, ed.

Diagnosis of Faraday rotation with Video Vector Magnetograph at Huairou

Jiangtao Su and Hongqi Zhang

National Astronomical Observatories, Chinese Academy of Sciences, Beijing 100012, China

Over the wavelength interval of 150 mÅ redward of line center of the FeI λ5324.19 Å to 150 mÅ to the blue, in steps of 10 mÅ, observations of a simple sunspot were obtained with the Video Vector Magnetograph at Huairou Solar Observing Station (HSOS) of National Astronomical Observatories. In this paper, we present results of the inversion of stokes polarization profiles of this sunspot to recover the vector magnetic field parameters of the spectral line forming region using the FeI λ5324.19 Å using a nonlinear least-squares fitting. At the same time, curves of the observed variation of azimuth with wavelength were compared with model calculations for the azimuth at each wavelength as derived the inverse Zeeman effect modified by Faraday rotation. Hagyard, et al. (2000, Solar Phys. 191, 309) find it is difficult to separate two effects of Faraday rotation and $\pi-\sigma$ rotation. However, $\pi-\sigma$ rotation relates to the Landé factor of a spectral line. For the spectral line FeI 5324.19 Å, its Landé factor g = 1.5. In the solar magnetic field atmosphere, its Zeeman split is less than that of line FeI 5250.22 Å which has larger Landé factor g = 3. The correlations in Figure 1 show that the azimuth rotation increases as the field strength increases and inclination angle decreases. The results show that rotation of the azimuth is less significant in observation taken near the center of the FeI λ5324.19 Å than that of FeI λ5252.22 Å line.

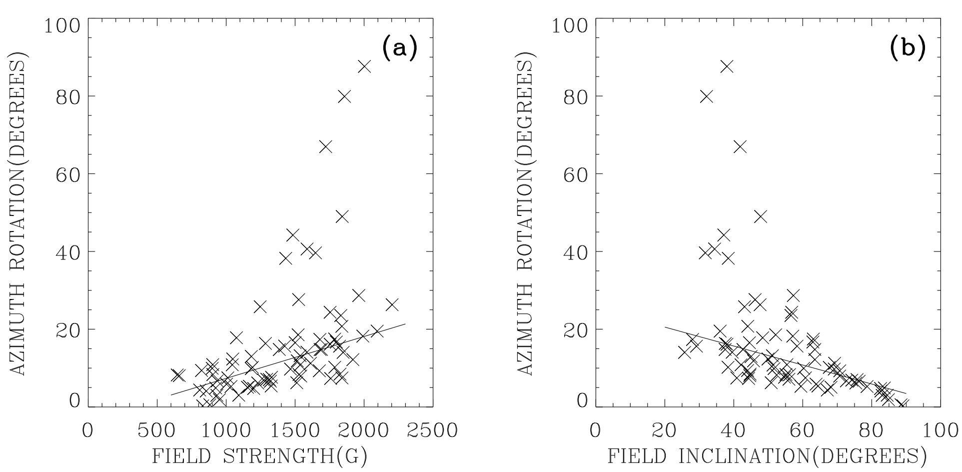

Figure 1. Correlation plots of field strength and field inclination

Highlights of Astronomy, Vol. 13
International Astronomical Union, 2003
O. Engvold, ed.

On a Cyclic Variation of the Hemispheric Helicity Rule.

A. A. Pevtsov

National Solar Observatory, Sunspot, NM 88349, U.S.A.

M. J. Hagyard

Space Science Department, NASA MSFC, AL 35812, U.S.A.

Z. Blehm

Montana State University, Bozeman, MT 59717, U.S.A.

J. E. Smith

Space Science Department, NASA MSFC, AL 35812, U.S.A.

R. C. Canfield

Montana State University, Bozeman, MT 59717, U.S.A.

T. Sakurai

National Astronomical Observatory, 2-21-1 Ohsawa, Mitaka-shi, Tokyo 181-8588, Japan

M. Hagino

Meisei University, 2-590 Nagabuchi, Ohme-shi, Tokyo 198-8655, Japan

Abstract.

We report the result of a study of magnetic helicity in solar active regions during 1980-2000. Using the vector magnetograms from four instruments (Haleakala Stokes Polarimeter, Marshall Space Flight Center, Mitaka Solar Flare Telescope and Okayama Observatory Solar Telescope) we calculated the force-free parameter α and computed a slope $d\alpha/d\varphi$ as the linear fit of α vs. latitude φ, using annual subsets of data. The hemispheric helicity rule can be expressed in terms of this slope as $d\alpha/d\varphi < 0$. We find that each instrument exhibits change in sign of $d\alpha/d\varphi$ for some years. However, we do not see consistency between different instruments in regards to years disobeying the rule. We show that this inconsistency can be attributed to insufficient numbers of active regions in annual subsets of data. We conclude that the present data sets do not allow to make statistically significant inference about possible cyclic variation of the hemispheric helicity rule.

For further discussion see Hagyard et al., 2003, ApJ, submitted.

Highlights of Astronomy, Vol. 13
International Astronomical Union, 2003
O. Engvold, ed.

The search for correlation between BiSON SMMF data and CME events

William J. Chaplin, Andrew M. Dumbill, Yvonne P. Elsworth, George R. Isaak, Clive P. McLeod, Brek A. Miller

School of Physics and Astronomy, University of Birmingham, Edgbaston, Birmingham B15 2TT, UK

Roger New, Balázs Pintér

School of Science and Mathematics, Sheffield Hallam University, Howard Street, Sheffield S1 1WB, UK

Abstract. We present first attempts to compare the Birmingham Solar-Oscillations Network (BiSON) high precision solar mean magnetic field (SMMF) data of four years with the occurrence of CMEs (coronal mass ejections) as recorded by LASCO on board SOHO. The BiSON magnetic measurement technique is given in Chaplin et al. (2003a). Particularly interesting results of recent SMMF high-cadence observations have come from studies of correlation between the SMMF determined by MDI and the occurrence of CMEs (Boberg and Lundstedt 2000 and Boberg et al 2002). Two frequency ranges, centered on 13 and 90 minutes, have been identified as possibly correlating with CME occurrence.

We have used BiSON SMMF data from two sites to investigate CME related SMMF signals to try to confirm the MDI results. To search methodically through our data set we have developed two correlation techniques suited to short (up to 32 minutes) and long (up to 3 hours) period wavelets, respectively. For short periods we analyzed SMMF data in the vicinity of CMEs, and for long periods we compared SMMF results for days with and without recorded CMEs. In neither period range have we yet clearly identified correlations between SMMF power excesses and CME onsets. For the details of the techniques and the results see Chaplin et al. (2003b).

References

Boberg F., Lundstedt H., Geophysical Research Letters, 2000, 27, 3141

Boberg F., Lundstedt H., Hoeksema J.T., Scherrer P. H., Liu W., Journal of Geophysical Research, 2002, 107, A10, 1318

Chaplin, W.J., Dumbill A.M., Elsworth Y., Isaak G. R. McLeod C.P., Miller, New R., Pintér B. 2003a, MNRAS, 343, 813

Chaplin, W.J., Dumbill A.M., Elsworth Y., Isaak G. R. McLeod C.P., Miller, New R., Pintér B. 2003b, in preparation

Highlights of Astronomy, Vol. 13
International Astronomical Union, 2003
O. Engvold, ed.

Eruption of a Quiescent Filament on Feb. 18, 2003

Xingming Bao and Hongqi Zhang

National Astronomical Observatories, Chinese Academy of Sciences, Beijing 100012, China

An eruptive process of a quiescent filament on Feb. 18, 2003 that initiated a CME was recorded by the full disk Hα telescope in HSOS (Huairou Solar Observing Station) and by the Solar and Heliospheric Observatory (SOHO). The eruption revealed a typical process of energy release and dense plasma ejection caused by magnetic instability. Filament eruptions, flares and CMEs are believed to be the same magnetic eruption and reconnection event in three different stages. This feature was shown more clearly during eruption of the quiescent filament because of the simple and regular magnetic line-of-sight field in photosphere compared to active regions with complex magnetic configurations. The filament was located near the solar northwest limb (N 30-40, W 40-80) on Feb. 18, 2003 with height about 11000 km. It began to erupt at 02:00 UT. Bright ribbons appeared at the magnetic feet of the filament in EIT/195 at 02:30 UT. The post-eruption loops formed at 04:00 UT and lasted about 6 hours. The CME appeared on EIT/C2 images at 02:30UT with an Ω shape, just the same as the filament erupted. The speed of mass ejected of the filament was about 250km/s. We also notice that the height of the filament increased and the magnetic fields with opposite polarity moved towards each other before the filament erupted. The filament eruption reveals that the filament may be held in the corona by the twisted magnetic fields which also keep the cool plasma from escaping the solar surface. If the twisted field was broken by some magnetic instabilities, the filament would erupt. The presence of post-eruption loops implies a transition process from non-potential (twisted) to potential field magnetic configuration in the filament.

Highlights of Astronomy, Vol. 13
International Astronomical Union, 2003
O. Engvold, ed.

The current helicity parameter H_c is more sensitive than α_{best} to Faraday rotation

Shudong Bao

National Astronomical Observatories, Chinese Academy of Sciences, Beijing 100012, China

Observations have indicated that the net helicity sign of active regions is predominantly negative in the northern hemisphere and positive in the southern (see Table 1). From Table 1, we find that the hemispheric sign rule of helicity parameter $\alpha_{\rm best}$ does not change with another solar cycle; but the helicity parameter $H_{\rm c}$ seems to show a weak opposite hemispheric preference for Huairou data in the solar cycle 23 and no preference for Mees data. How to explain such a phenomenon? We think one reason may be from the action of Faraday rotation. Faraday rotation will cause a counterclockwise rotation of the azimuth for a positive polarity field and vice versa. During the cycle 22, the polarity of leading sunspots is dominantly negative in the northern hemisphere and positive in the southern. The effect of Faraday rotation, which is determined mostly by a leading polarity sunspot, has a positive contribution to the percentage of current helicity signs in active regions and leads to the increase of the strength of the hemispheric sign rule. In the cycle 23, the polarity of most leading sunspots is positive in the northern hemisphere and Faraday rotation will decrease the percentage of current helicity signs. Consequently, the strength of the hemispheric rule should be weakened. On the other hand, $H_{\rm c}$ is more susceptible to Faraday rotation than $\alpha_{\rm best}$ because it is mainly related to the areas where the line-of-sight field is strong. Therefore, if the effect of Faraday rotation is not completely removed in our observations, the hemispheric sign rule showed is weak in the cycle 23 than in the cycle 22 (for $\alpha_{\rm best}$), even opposite (for $H_{\rm c}$).

Table 1. Hemispheric distribution of current helicity sign in solar cycles 22 and 23.

Reference	Cycle	Hemisph.	$\alpha_{\rm best}$ Negative	$\alpha_{\rm best}$ Positive	$H_{\rm c}$ Negative	$H_{\rm c}$ Positive	No. Obs.	Data Source
Pevtsov et al. 1995	22	North	25(76%)		. . .		33	Mees
		South		25(69%)		. . .	36	
Bao & Zhang 1998	22	North	152(76%)		168(84%)		199	Huairou
		South		159(71%)		177(79%)	223	
Bao et al. 2000	23	North	26(59%)		14(32%)		44	Huairou
		South		28(65%)		21(49%)	43	
Pevtsov et al. 2001	23	North	88(63%)		70(50%)		140	Mees
		South		86(70%)		70(57%)	123	

References

Bao, S. D., Ai, G. X., & Zhang, H. Q. 2000, JA&A, 21, 303

Bao, S. D., & Zhang, H. Q. 1998, ApJ, 496, L43

Pevtsov, A. A., Canfield, R. C., & Latushko, S. M. 2001, ApJ, 549, L261

Pevtsov, A. A., Canfield, R.C., & Metcalf, T. R. 1995, ApJ, 440, L109

JD4

Astrophysical Impact of Abundances in Globular Clusters

Chairpersons: F. D'Antona and R. Gratton

Editors: F. D'Antona (Chief-Editor) and G. Da Costa

Highlights of Astronomy, Vol. 13
International Astronomical Union, 2003
O. Engvold, ed.

Summaries of Papers Presented at Joint Discussion Session 4: Astrophysical Impact of Abundances in Globular Cluster Stars

G. S. Da Costa

Research School of Astronomy & Astrophysics, The Australian National University, Mt. Stromlo Observatory, via Cotter Rd, Weston, ACT 2611, Australia

F. D'Antona

INAF Osservatorio di Roma, via di Frascati 33, 00040 Monteporzio, Italy

R. G. Gratton

INAF Osservatorio Astronomica di Padova, vicolo dell'Osservatorio 5, 35142 Padova, Italy

Abstract. In this contribution we give summaries of the oral and poster papers presented in Joint Discussion Session 4, *Astrophysical Impact of Abundances in Globular Cluster Stars*, at the XXVth IAU General Assembly. The full text of the papers can be found in Volume 75, issue 2, of the MEMORIE della Societá Astronomica Italiana (Journal of the Italian Astronomical Society; see the web address: <sait.oat.ts.astro.it>).

2. Foreword

Globular Clusters (GCs) are a basic tool for a number of important astrophysical problems – star formation, stellar evolution, stellar populations and cosmology to name but a few. The advent of new large telescopes is allowing detailed comparisons between the properties of stars in GCs and those in the halo field, a necessary comparison to obtain fundamental cluster parameters (e.g. age and distance) which, in turn, allow GCs to be used as probes of the properties of galaxies.

A proposal to hold a Joint Discussion session on the chemistry of GC stars was accepted by the IAU as part of the program of the XXVth General Assembly. The aim of the Joint Discussion was to give an updated overview of both observations and theory and to give insight into the following areas:

• The early chemical evolution of GCs, particularly as regards the mechanism(s) of formation of GCs, the role of self-enrichment, and possible pollution within clusters. Here observations go hand-in-hand with increased understanding of the details of stellar evolution: from the massive stars that explode as supernovae, through the intermediate mass stars whose Asymptotic Giant Branch evolution may contribute to the observed abundance anomalies, to the low mass we observe in GCs today.

• The physical processes that affect the surface chemistry of low mass stars. Here new observations of main sequence stars in GCs can provide tests of the microscopic diffusion of light elements and metals, a process that can affect the age determination of GCs. Similarly, observations of extensive samples of red giant stars have the potential to reveal the presence of rare but significant objects of peculiar chemical composition, whose explanation may provide new insights.

Consequently, the program of the JD was built around four topics:
1) Observational results and emerging abundance patterns, with a focus also on the reliability of abundance determinations. In this context, a round-table discussion, chaired by B. Barbuy, was held in which possible abundance determination errors, stemming from the assumptions made in modeling stellar atmospheres, were discussed.
2) Models relevant to the observed chemical patterns, particularly, the explosive nucleosynthesis of massive stars, the more quiescent nucleosynthesis of intermediate-mass AGB stars and their role in forming the abundance and abundance spreads in GCs.
3) Physical processes and surface chemistry. Here abundances in main sequence stars constrain the role of atomic diffusion and radiative accelerations, while abundances in red giants constrain 'standard' and 'non-standard' mixing processes. Lithium abundances are also a key topic in this area. A second round-table discussion on these subjects was chaired by D. Vandenberg.
4) Formation and evolution of globular clusters. This section featured specific talks on GC formation and talks on possible mechanisms for producing observed abundance anomalies as part of the GC formation process. This included the popular idea that a second stellar generation formed in GCs directly from the ejecta of massive AGB stars. A third round-table discussion on these topics was chaired by R. Cayrel.

The meeting was evidently popular with IAU-GA participants, as the sessions were well attended and much lively discussion occurred. All participants left with many new ideas and suggestions for future work.

The SOC for the Joint Discussion was made up of F. D'Antona (Italy, Co-Chair), R. Gratton (Italy, Co-Chair), B. Barbuy (Brazil), G. Cayrel (France), G. Da Costa (Australia), P. Denissenkov (Russia), R. Kraft (USA), J. Lattanzio (Australia), G. Meylan (USA), K. Nomoto (Japan), J. Truran (USA) and D. VandenBerg (Canada). G. Da Costa acted as the local liaison contact. All involved in the Joint Discussion were very grateful to the IAU-GA local organizers for their assistance in making the meeting run smoothly.

3. Summaries of Oral Presentations

This section contains summaries of the oral contributions in the order in which they were presented during the Joint Discussion. In each case the first named author was the presenter. Unfortunately, Bob Kraft was unable to attend the meeting and his paper was presented by Chris Sneden.

Abundance Trends of Alpha and Fe-Peak Elements in Globular Clusters
Christopher Sneden

Abstract. A fairly large fraction of Galactic globular clusters have been subjected to some sort of high spectral resolution abundance analysis in the past two decades. Several clusters have enjoyed the scrutiny of large numbers (>20) of their giant stars at very high resolution (R > 40,000) and signal-to-noise (>100), and such investigations have even begun to probe the fainter subgiant cluster members. Other clusters have seemed to be of lesser interest, having only studies of a few of their brighter members reported in the literature. This brief overview will consider the abundance trends of some key element groups, including the alpha, Fe-peak, neutron-capture, and proton-capture elements. Some comparison with field stars will be attempted to illustrate where stellar population differences between clusters and the field seem to occur. Suggestions for renewed observational attention will be drawn to specific clusters whose chemical origin appears to be substantially different than the general Galactic halo.

Abundances in Scarcely Evolved Stars in Globular Clusters
R. G. Gratton

Abstract. Abundances for stars on the main sequence and early subgiant branch (i.e. less evolved than the Red Giant Branch Bump) in globular clusters are reviewed. Emphasis is given to those elements that are involved in the Na-O and Mg-Al anticorrelations. Results obtained in the last few years clarified that very deep mixing (if any) cannot be the only cause of the abundance anomalies found in globular cluster stars. The new scenarios, calling for pollution by material processed in an earlier generation of stars, are briefly presented; the issues related to the lithium abundances are briefly commented.

Lithium Abundances in Globular Clusters
P. Bonifacio

Abstract. Warm metal–poor dwarf stars display a constant Li abundance, whichever their effective temperature or metallicity: the so-called "Spite Plateau". If this constant value represents the primordial Li abundance the Universal baryonic density may be derived by comparison to nucleosynthesis calculations. In recent years there has been an active debate on whether these stars have indeed preserved their pristine Li or whether it has been depleted by some stellar phenomenon. Since the Globular Clusters (GCs) are a homogeneous single-age population they are an ideal testing ground for any theory which predicts Li depletion. Recent observations of NGC 6397 ([Fe/H]~ -2.0) with the VLT/UVES show that there is no dispersion in Li abundances in excess of what expected from observational errors and that the Li content is the same as that of field stars. A re-analysis of extant data of M 92 ([Fe/H] ~ -2.3) shows that the intrinsic dispersion must be less than ~ 0.2 dex. On the other hand for the

more metal–rich GC 47 Tuc ([Fe/H]~ -0.7) VLT/UVES observations of 4 Turn Off (TO) stars suggest that a real dispersion in Li abundances exists. The conclusion is that the mechanism(s) which alter the Li abundance in TO stars are metallicity dependent and apparently ineffective at low metallicity.

On the Question of a Metallicity Spread in Globular Cluster M22 (NGC 6656)

I. I. Ivans, C. Sneden, G. Wallerstein, R. P. Kraft, J. E. Norris, J. P. Fulbright, & G. Gonzalez

Abstract. Results from early photometric and spectroscopic studies for M22 showed a metallicity spread similar to, albeit significantly smaller than, that found in ω Cen, the most massive cluster in our Galaxy. Numerous studies of M22 over the last few decades have yielded conflicting results: depending upon the sample and analysis techniques, some authors find no significant variations whereas others find metallicity variations of $\sim$0.5 dex. In our investigation of a sample of $\sim$30 stars, we are employing high resolution high signal-to-noise spectra and a variety of spectroscopic approaches in determining the stellar metallicities. In this contribution, we report some of the preliminary results from our investigation of the question of metallicity variations in M22, employing a set of models derived by applying chemical constraints.

The Metallicity and Age Ranges in ω Centauri

Laura M. Stanford, Gary S. Da Costa, John E. Norris, & R. D. Cannon

Abstract. We present a metallicity distribution and an age-metallicity relation for the globular cluster ω Centauri based on photometry and spectra of members at the Main Sequence Turnoff (MSTO) region of the color-magnitude diagram. The age-metallicity relation was determined by two independent methods. These preliminary results show that the formation of the cluster took place over an extended period of at least 4 Gyrs with the more metal-rich stars being younger. We find no metal-rich old or metal-poor young stars in our sample of 446 ω Cen members.

A Comparison of Globular Cluster and Field Halo Stars

Robert P. Kraft

Abstract. Abundances of the light elements O, Na, Mg, and Al in giants of four globular clusters having [Fe/H] $\sim$ –1.6, are compared with halo field giants having [Fe/H] between –1.0 and –2.5. The last named reflect the abundances expected in Type II supernova ejecta. Abundance anomalies among these elements, resulting from proton capture synthesis, increase in severity along a "sequence" corresponding to "halo field", NGC 7006, M3, NGC 6752 and finally M13. The results are discussed in terms of deep mixing vs primordial scenarios as well as impact on the so-called second parameter problem.

General Discussion I: At What Stage is the Abundance Determination Problem?

Beatriz Barbuy (Discussion Chair)

Abstract. This open session concentrates on the major problems of abundance determinations, and for this, the effective temperature determination is discussed by Mike Bessell, the use of FeI and FeII lines and excitation and ionization equilibrium is discussed by Verne Smith. Roger Cayrel discusses the use of 1-D model atmospheres with different values of the mixing length parameter, and its impact on OI lines. Martin Asplund discusses the results of using 3-D model atmospheres and NLTE effects.

The Temperature Scale of Globular Cluster Stars

Michael S. Bessell

Abstract. The empirical temperature scale for Pop I A-K stars has been well established for over 20 years from application of stellar intensity interferometry, lunar occultation, infra-red flux method and Michelson interferometry. Line-blanketed model atmospheres and a better understanding of the handling of convection now produce synthetic colors that are in excellent agreement with this empirical temperature scale. Model atmosphere colors and fluxes for higher and lower abundances than solar can be used confidently to derive temperatures for the globular cluster stars.

Globular Cluster Abundances in the Light of 3D Hydrodynamical Model Atmospheres

Martin Asplund

Abstract. The new generation of 3D hydrodynamical model atmospheres have been employed to study the impact of a realistic treatment of stellar convection on element abundance determinations of globular cluster stars for a range of atomic and molecular lines. Due to the vastly different temperature structures in the optically thin atmospheric layers in 3D metal-poor models compared with corresponding hydrostatic 1D models, some species can be suspected to be hampered by large systematic errors in existing analysis. In particular, 1D analysis based on minority species and low excitation lines may overestimate the abundances by > 0.3 dex. Even more misleading may be the use of molecular lines for metal-poor globular clusters. However, the prominent observed abundance (anti-)correlations and cluster variations are largely immune to the choice of model atmospheres.

Oxygen Abundance and Convection

C. Van'tVeer, & R. Cayrel

Abstract. The triplet IR lines of O I near 777 nm are computed with the Kurucz's code, modified to accept several convection models. The program has been run with the MLT algorithm, with l/H = 1.25 and 0.5, and with the Canuto-Mazzitelli and Canuto-Goldman-Mazzitelli approaches, on a metal-poor turnoff-star model atmosphere with Teff = 6200 K, log g = 4.3, [Fe/H]= –1.5. The results show that the differences in equivalent widths for the 4 cases do not exceed 2 per cent (0.3 mA). The convection treatment is therefore not an issue for the oxygen abundance derived from the permitted lines.

Population III Supernovae and their Nucleosynthesis

K. Nomoto, K. Maeda, H. Umeda, N. Tominaga, T. Ohkubo, J. Deng, & P. A. Mazzali

Abstract. Stars more massive than $\sim$ 20 - 25 $M_{\odot}$ form a black hole at the end of their evolution. Stars with non-rotating black holes are likely to collapse "quietly" ejecting a small amount of heavy elements (Faint supernovae). In contrast, stars with rotating black holes are likely to give rise to very energetic supernovae (Hypernovae). We present distinct nucleosynthesis features of these two types of "black-hole-forming" supernovae. Nucleosynthesis in Hypernovae is characterized by larger abundance ratios (Zn,Co,V,Ti)/Fe and smaller (Mn,Cr)/Fe than normal supernovae, which can explain the observed trend of these ratios in extremely metal-poor stars. Nucleosynthesis in Faint supernovae is characterized by a large amount of fall-back. We show that the abundance pattern of the recently discovered most Fe-poor star, HE0107-5240, and other extremely metal-poor carbon-rich stars are in good accord with those of black-hole-forming supernovae, but not pair-instability supernovae. This suggests that black-hole-forming supernovae made important contributions to the early Galactic (and cosmic) chemical evolution. Finally we discuss the nature of First (Pop III) Stars.

The Role of AGB Stars

John Lattanzio, Amanda Karakas, Simon Campbell, Lisa Elliott, & Alessandro Chieffi

Abstract. We give a brief summary of the abundance anomalies seen in globular cluster stars, and try to review how and if AGB stars could be responsible. The abundance anomalies are clearly indicative of hot H burning, such as is expected during hot bottom burning in intermediate mass AGB stars. Nevertheless, we conclude that a quantitative fit is very hard to obtain using current AGB models.

Today's AGB Stars and the Role of Binaries

Pavel A. Denissenkov

Abstract. Recent observations of the star-to-star abundance variations well below the bump luminosity in globular clusters have raised the weight of the primordial scenario. So far, intermediate-mass AGB stars have been considered as the most likely primordial sources of these abundance variations. I present some arguments against this idea and propose alternative sources. These are RGB and/or AGB stars a little bit more massive than the present-day MSTO stars that had experienced enhanced extra mixing in the past. In this case the more preferable way of polluting the lower mass MS stars by nuclearly processed material would be mass transfer in binaries rather than stellar winds from single stars.

New AGB Models to Explore the Spread of Abundances in Globular Clusters

Paolo Ventura, Francesca D'Antona, & Italo Mazzitelli

Abstract. Following the line of thought that the inhomogeneities in composition of GC stars are due to contamination from the ejecta of the massive AGBs which evolved in the first 100-200Myr, we must study in detail the production of elements during the AGB evolution. The study requires computation of complete stellar models including nuclear processing by Hot Bottom Burning, coupled with non- instantaneous mixing for as many elements as possible. These models are still subject to many uncertainties, so that the additional hypothesis that the spreads in abundances are not random, but can be attributed to the existence of several different generation of stars directly formed from AGB ejecta, provides a powerful tool to constrain the efficiency of Hot Bottom Burning and the role of the third dredge up. We show that many difficulties are still present in this scenario, in particular our recent models confirm that the anticorrelation Na–O is not well explained. If the spreads are indeed due to different stellar generations, however, we can use the abundance anomalies to understand better the AGB models.

Processes at the Turnoff

Georges Michaud, Olivier Richard, & Jacques Richer

Abstract. Stellar evolution models taking into account the atomic diffusion of 28 species, have been calculated for Pop II stars of 0.5 to 1.2 $M_\odot$ with [Fe/H] from -4.31 to -0.71. Overabundances are expected in some turnoff stars with $T_{eff} \geq 5900$ K. They depend strongly on the metallicity of the cluster. At the metallicity of M 92, they reach a factor of 10 for many species, at 12 Gyr, but a factor of at most 2, at 13.5 Gyr. Series of models were also calculated with turbulence to determine to what extent it reduces predicted abundance anomalies. The level of abundance anomalies observed in turnoff stars may then determine a level of turbulence. Even in the presence of turbulence however,

allowance for diffusive processes leads to a 10%-12% reduction in age at a given turnoff luminosity. For M 92 an age of 13.5 Gyr is determined.

Mixing along the Red Giant Branch
Achim Weiss, & Corinne Charbonnel

Abstract. We review canonical mixing in low-mass stars on the Red Giant Branch, the evidence for additional – extra – mixing based on observations of chemical abundance trends and anomalies, discuss the connection with the Red Giant bump and with proton-nucleosynthesis, and the current understanding of the connection between extra-mixing and differential rotation. New developments concerning the sequence of events leading to the observed abundances are included, too.

General Discussion II: On Current Stellar Models
Don A. VandenBerg (Discussion Chair)

Abstract. Given the emphasis at this meeting on stellar models that treat diffusive and deep-mixing processes, as well as on recent computations for the AGB phase, a panel of experts was organized to further discuss the comparisons between theory and observations, the limitations of current models, and anticipated future advances. G. Michaud provided further insights on which stars are expected to show the largest abundance anomalies due to gravitational settling and radiative accelerations, and on the role of turbulent mixing. A. Weiss emphasized the importance of fully understanding diffusive processes and of investigating the still largely untested consequences of such processes (and deep mixing) for the late evolutionary phases of stars. S. Vauclair reported on the possible interaction between meridional circulation currents and diffusion, which could potentially explain why the observed abundance anomalies are less than those predicted by diffusive models. P. Denissenkov briefly reviewed several of the main problems that need to be solved in order to achieve an understanding of the observed abundances in giant stars, including the identification of the physical mechanism of deep mixing and an understanding of how the rotation profile in stars evolves. F. D'Antona outlined the reasons why she believes that massive AGB stars are the source of the material that produces the observed abundances in globular cluster stars (via pollution), including, in particular, the constraints provided by the observed Li abundances. Finally, J. Lattanzio commented that deep mixing is likely restricted to the upper giant branch and that some kind of primordial mechanism must be found to explain the abundance anomalies in less evolved stars: he also reminded us of some difficulties with the AGB scenario. Short contributions from each of the above are included in this paper.

Formation of Stars in Clusters

Bruce Elmegreen

Abstract. Models of star formation in clusters and some of their observational constraints are reviewed. The formation of old globular cluster stars probably proceeded in a similar fashion to the formation of stars in today's young massive clusters, considering their similar IMF's, stellar densities, and masses. The dominant mechanism for star formation would then be collapse following energy dissipation and gravitational instabilities in a compressible turbulent medium. The formation of the halo globulars themselves occurred in a peculiar environment, however, where the microwave background temperature was higher than it is today by a factor of 3 to 10, the pressure from the potential well of the protogalaxy was larger than in today's galaxy disks by a factor of > 100, the mean magnetic field was probably lower by at least an order of magnitude without an active dynamo, the metallicity was lower by $\sim 1/40$, and non-thermal radiation from QSOs and other nuclear activity was important. These differences must have had several important consequence for star formation even though the basic physical processes were the same. The most important consequence seems to be that the epoch of globular cluster formation was the first time in the history of the Universe when cooling was strong enough and the microwave temperature small enough to produce a thermal Jeans mass that was less than a solar mass given the typical pressure of the environment. This small thermal Jeans mass allowed the cluster to remain bound over a Hubble type without severe mass loss from stellar winds and supernovae, and it allowed most of the stars in the cluster to shine for a Hubble time without turning off the main sequence. Other star and cluster formation from earlier times could not have produced such long-lasting objects as the halo globular clusters. Globular clusters are the result of a selection effect for survival over a Hubble time.

Globular Cluster Formation from Cloud-Cloud Collisions

T. Shigeyama, & T. Tsujimoto

Abstract. Hydrodynamic evolution of supernova remnants in collided proto-cluster clouds is investigated in the frame work of a supernova-driven star formation scenario. It is found that the relative velocity of proto-clouds must be greater than a certain value, which is a function of the mass of each proto-cloud, to produce a stellar cluster with little dispersion of [Fe/H] ratios among the member stars. The metallicity distribution function for globular clusters in the Galactic halo is calculated from a simple model. This calculation shows that cloud-cloud collisions can reproduce the observed metallicity distribution function for globular clusters. Before cloud-cloud collisions, each cloud has been enriched with heavy elements according to a supernova-driven star formation scenario that reproduces the observed abundance distribution function for the Galactic halo field stars.

Globular Cluster Abundance Anomalies: Clues from the Main Sequence

G. S. Da Costa, Russell Cannon, Barry Croke, & John Norris

Abstract. We present an analysis of spectra of a large sample of main sequence stars in the globular cluster 47 Tuc observed with the 2dF multi-fibre instrument on the Anglo-Australian Telescope. The spectra confirm that anti-correlated variations in the strengths of the CN and CH bands exist among the main sequence stars in this cluster. Further, the ratio of CN-strong to CN-weak stars on the main sequence is identical, to within the statistics, to the value for the red giant branch. This strongly implies that evolutionary (mixing) processes do not play a significant role in generating the abundance anomalies observed in this cluster. We also find that the strengths of the sodium-D lines in the spectra of these main sequence stars correlate positively with the cyanogen band strength index. We then compare our 47 Tuc results to those for main sequence stars in M71, a globular cluster of comparable abundance to 47 Tuc, and to those for main sequence stars in the more metal-poor globular cluster M13.

The Horizontal Branch Morphology in Globular Clusters: Consequences for the Self-Pollution Model

Francesca D'Antona

Abstract. The Joint Discussion 4 of the Sydney IAU General Assembly takes place at a very interesting stage for Globular Cluster (GC) astrophysics, when it is becoming clear that many –if not all– of the inhomogeneities in the chemical composition of GC stars are due to some mechanism of primordial enrichment. The best candidate for "self-pollution" is identified with the matter lost in winds of low velocity from Asymptotic Giant Branch (AGB) stars, especially of high mass, evolving during the first phases of the life of the Clusters, and cycling their envelope material through the hot-CNO cycle at the bottom of their convective envelopes (Hot Bottom Burning – HBB). Recognition that Globular Clusters showing large chemical anomalies are also peculiar in their Horizontal Branch (HB) star distributions, led D'Antona et al. (2002) to suggest that extended blue tails are directly linked to enhanced helium in the matter, processed through HBB, from which these stars are born. Here we show that other HB peculiar morphologies –such as the lack of stars in the RR Lyrae region, in clusters like NGC 2808, whose red and blue side of the HB are both well populated– can be attributed to the helium enrichment of the matter from which the stars populating the whole blue HB in this cluster were born. This interpretation lends credit to the idea that the GC stars are formed in two main generations, the first one having the composition of the primordial gas cloud, the second one formed *directly* from the AGB ejecta over a span of time lasting $\sim 2 \times 10^8$ yr. This hypothesis provides a useful and conceptually simple key not only to interpret some –but not all– HB peculiarities, but also to understand the distribution of abundance anomalies. If the model is correct, in the end we can use the abundance anomalies to falsify (or calibrate) our AGB models.

General Discussion III: Chemistry and Self–Pollution Mechanisms
R. Cayrel (Discussion Chair)

Abstract. Round table 3 was devoted to the origin of chemical anomalies found in a significant fraction of stars in GCs, but not in field metal-poor stars of similar metallicity. Formerly a hot topic was if such anomalies, studied only in giant stars, bright enough to allow reliable abundance determinations, were generated in the course of the evolution of the star, or inherited at the birth of the star. The ESO Large Program led by R. Gratton has demonstrated, without ambiguity, that the most famous of these "anomalies", the O-Na anticorrelation, was already present in turn-off (TO) stars, therefore already there at the birth of the star. This does not preclude that some modifications occur along the red giant branch, as described, for example, already in Charbonnel (1994), but those are well identified and do not include the O-Na anticorrelation, but affect mostly ^{12}C,^{13}C, ^{14}N and Li. More recently, models including rotation in the evolution (see for example talks by Charbonnel and Weiss at JD 4) have been produced. The most promising process for explaining the O-Na anticorrelation is the hot-bottom-burning process (HBB) in TP-AGBs, Ventura et al. (2001). The problem remaining is the transfer of the processed matter to an unevolved star. Here, several routes exist, and so far no consensus has been reached on those which are dominant. Roundtable 3 was expected to supply a live discussion between the proponents of the various ideas emitted on this subject. Unfortunately, in the time allotted, the only thing which appeared possible was to suggest tests for evaluating the coherency of the various proposals, against the widest set of observational constraints. For example, the HBB produces an enrichment in helium, potentially affecting the isochrones. Very accurate observations could try to detect this side-effect. Transfer of mass from an AGB to an unevolved companion is an efficient way of pollution. But it is then expected that the remaining binary shows a variable radial velocity (unless the pair has been disrupted afterwards...). At the other extreme, the mass loss of AGBs may have been large enough to have produced a second generation in a GC (see F. d'Antona contribution). But let us leave their role to our participants...

The AGB Contamination Scenario
Achim Weiss

Abstract. *Proposed tests.* The primordial scenario suggested by D'Antona, Gratton, and others, which assigns the observed ONa-anticorrelation and the Mg- and Al-anomalies in cluster red giants to processes in thermally pulsing, hot bottom-burning AGB stars of an earlier generation, has many attractive features. The models also make clear predictions concerning the initial composition of those stars we see today as red giants. These predictions should be tested with stellar models using the predicted initial composition, which is helium-enriched. One can, for example, check, whether the subgiant branch, during which the effectiveness of the hydrogen-shell (i.e. the abundance of CNO) is important, or the location and extent of the bump are affected; whether there are photometric

differences between "normal" and "AGB-contaminated" stars, even if so far the isochrones appear to be indistinguishable. Observationally, a determination of the luminosity function and the distribution of stars of both types towards the tip of the RGB should be done, because the initial helium content will affect both. It is also necessary to investigate closer the nucleosynthesis of AGB stars of interest, because I think that no agreement has been reached here concerning the production/destruction of certain elements (Na, Mg and its isotopes) as function of mass, metallicity, etc. We need to be able to define robust results, which can guide future observations.

Contribution to JD4 Round Table Discussion 3
G. S. Da Costa

Abstract. In my contribution to the roundtable discussion I drew attention to what I see as two key questions relevant to the debate concerning the relative importance of processes occurring early in the life of a globular cluster ("primordial processes") and processes occurring in the stars we observe today ("mixing processes"). These are: (1) In a given cluster, is the total abundance of C+N+O constant from star-to-star, even though the individual C, N and O abundances vary substantially? We don't have a definite answer here but it is a vital question since constant C+N+O is a necessary outcome of any mixing process. (2) In a given cluster, is it really reasonable to imagine that all the 'second generation' stars can be formed from the ejecta of AGB stars? At this meeting we have frequently heard the suggestion that the Nitrogen- and Sodium-rich, Carbon- and Oxygen-poor stars may have been formed from the mass lost by thermally-pulsing upper-AGB stars. I think we are now in a position where we could attempt to quantitatively evaluate this question for a cluster like 47 Tucanae. It may be that such a requirement can only be filled with a rather unusual mass function for the 'first generation', a point first made long ago by Smith & Norris (1984).

Abundance Anomalies and Lithium in Globular Clusters
P. Bonifacio

Abstract. Since Li is destroyed at temperatures above 2.5×10^6K its abundance may be a useful diagnostic for the nuclear history of the material observed in a stellar atmosphere. It is therefore interesting to note what are the correlations (if any) between Li abundances and abundance anomalies.

A Discussion of Self-Pollution Mechanisms
P. A. Denissenkov

Abstract. Intermediate-mass AGBs and low-mass stars having just passed the helium-flash are both potential contributors to chemical variations in GC stars. Both mechanisms face the difficulty of the short time available between sweeping the generated gas at each crossing of the galactic plane by the GCs.

Can we Build up Second Generation Stars in GCs Directly from the Ejecta of AGBs?
Francesca D'Antona

Abstract. My contribution to the round table on chemistry and self-pollution mechanisms examines the consequences behind the hypothesis of globular clusters are made up by a first stellar generation plus a second, long stage of star formation, lasting some 200Myr, directly from the ejecta of AGB stars.

4. Poster Paper Summaries

This section gives summaries of the poster papers.

B. Barbuy, J. Meléndez, S. Ortolani, M. Zoccali, E. Bica, A. Renzini, V. Hill, Y. Momany, D. Minniti, & M. Rich: Abundance Analysis of the Bulge Globular Clusters NGC 6553 and NGC 6528

A detailed abundance analysis of 5 giants of the metal-rich bulge globular cluster NGC 6553 was carried out using high resolution infrared spectra in the H band, obtained at the Gemini-South 8m telescope. High resolution spectra of 3 stars in the bulge globular cluster NGC 6528 were obtained at the 8m VLT UT2-Kueyen telescope with the UVES spectrograph. The present analysis provides a metallicity [Fe/H] $= -0.15 \pm 0.2$ and $[\alpha/\mathrm{Fe}] \approx +0.2$ for NGC 6528, and [Fe/H] $= -0.20 \pm 0.10$ and an oxygen overabundance of [O/Fe] $= +0.20$ for NGC 6553, resulting in an overall metallicity $Z \approx Z_{\odot}$ for both clusters.

Uta Fritze – v. Alvensleben: Stellar Abundances in Young and Intermediate Age GCs

Globular Cluster (**GC**) formation seems to be a widespread mode of star formation in extreme starbursts triggered by strong interactions and mergers of massive gas-rich galaxies. We use our detailed chemically consistent evolutionary synthesis models for spiral galaxies to predict stellar abundances and abundance ratios of those second generation GCs as a function of their age or formation redshift. Comparison with observed spectra of young star clusters formed recently in an ongoing interaction (NGC 4038/39) and a merger remnant (NGC 7252) are encouraging. Abundances and abundance ratios (and their respective spreads) among young and intermediate cluster populations and among the red peak GCs of elliptical/S0 galaxies with bimodal GC color distributions are predicted to bear a large amount of information about those clusters' formation processes and environment. Not only the bright young clusters but also representative populations of "old" GCs in E/S0 galaxies are readily accessible to MOS on 10m class telescopes.

Jennifer A. Johnson: A Survey for CH Stars in Globular Clusters

To determine the frequency of CH stars in metal-poor globular clusters, I have begun a survey using intermediate-band photometry and low-dispersion spectroscopy. In the preliminary analysis of one cluster, M 30, I have found that the photometry successfully selects stars with strong G-bands, while the low-dispersion spectra isolate those stars with the correct metallicities and radial velocities to be cluster members. In the M 30 sample, I have found three stars that have stronger G-bands than normal cluster stars of the same luminosity.

L. Sbordone, P. Bonifacio, G. Marconi, & R. Buonanno: Chemical Abundances in Terzan 7 from UVES spectra

We present abundances for Mg, Si, Ca, Fe, and Ni for 3 giants in the sparse globular cluster Terzan 7, physically associated with the Sagittarius Dwarf Spheroidal Galaxy (Sgr dSph), which is presently being tidally disrupted by the Milky Way. Sgr dSph shows signs of a prolonged and peculiar star formation history, (low α content, high metallicity, significant Na, Co, Ni underabundance). Our data, obtained with VLT-UVES, show a mean [Fe/H]$= -0.57$, solar-scaled α elements ([α/Fe]$\sim$0) and a significant Ni underabundance ([Ni/Fe]$= -0.2$). These results are strikingly resembling what we find in the body of the Sgr dSph. This enforces the membership of Terzan 7 to the Sgr dSph system. In fact, a clear chemical pattern can be traced in the [α/Fe] vs [Fe/H] plane including the Sgr dSph, the associated clusters Ter 7 and M54, the clusters Pal 5 and Pal 12, and the young globular Ru 106. This last system is also known to show a similar Ni underabundance, never found elsewhere in the Milky Way. Note that Pal 12 and Pal 5 are believed to have been originated inside the Sgr dSph system, while Ru 106 is suspected to have been also accreted from another merging episode.

Takuji Tusujimoto, & Toshikazu Shigeyama: Star Formation History of Omega Centauri

The star formation history of the globular cluster Omega Centauri is investigated in the context of an inhomogeneous chemical evolution model in which supernovae induce star formation. The proposed model explains recent observations for Omega Cen stars and divides star formation into three epochs. The formation of Omega Cen is also discussed in the framework of globular cluster formation triggered by cloud-cloud collisions. In this scenario the relative velocity of clouds in the collision determines the later chemical evolution in the clusters. A head-on collision of proto-cluster clouds with a low relative velocity would have converted less than 1% of gas into stars and promoted the subsequent chemical evolution by supernova-driven star formation. This is consistent with present observed form of Omega Cen. In contrast the other Galactic globular clusters are expected to have formed from more intense head-on collisions and the resultant clouds would have been too thin for supernovae to accumulate enough gas to form the next generation of stars. This explains the absence of chemical evolution in these other globular clusters.

JD5

White Dwarfs:
Galactic & Cosmological Probes

Chairperson: H. Shipman

Editors: H. Shipman (Chief-Editor) and E.M. Sion

No manuscripts received.

JD6

Extragalactic Globular Clusters & Their Host Galaxies

Chairpersons: T. Bridges and D. Forbes

Editors: T. Bridges (Chief-Editor) and D. Forbes

Highlights of Astronomy, Vol. 13
International Astronomical Union, 2003
O. Engvold, ed.

M31's Disk System of Globular Clusters

Heather Morrison, Paul Harding and Denise Hurley-Keller

Dept of Astronomy, Case Western Reserve University, 10900 Euclid Ave, Cleveland OH 44106

Kathy Perrett

Department of Astronomy and Astrophysics, University of Toronto, Toronto, ON, Canada M5S 3H8

Abstract.
Globular cluster systems are often thought to be associated with violent formation events such as galaxy mergers or the formation of large bulges. However, formation in relatively ordered regions such as thin disks may also be an important process which has been overlooked.

Recent high-quality spectroscopic studies of the M31 globulars show that a significant number of the clusters projected on its disk belong to a rapidly rotating thin disk. This contrasts strongly with the Milky Way system, which is composed of a halo and thick disk system and has no known thin disk globulars. It is also likely that M31 has experienced no minor mergers since the globular cluster formation epoch, as such a merger would have heated the globulars into a thick disk system. The metallicity distributions of the disk and non-disk clusters are quite similar.

1. Introduction

M31 is a remarkably poorly understood system, despite its convenient location close to the Milky Way. In the past few years two high-quality kinematic studies of old population tracers (globular clusters and planetary nebulae (PN))have been published, with velocity errors of order 10 km/s. The globular velocities come from the study of Perrett et al (2002) and the PN data from Hurley-Keller et al (2003). These low velocity errors allow sensitive searches for systems with cold kinematics such as thin disks and dwarf galaxies. Here we describe our detection of a thin disk subsystem of globular clusters in M31.

2. Thin Disk Kinematics

The signature of disk kinematics is clear in a "position-velocity" plot such as Figure 1, where narrow strips parallel to the major axis are shown with velocity plotted against distance along the major axis. A completely cold disk with zero velocity dispersion will show a narrow diagonal line in this figure, with the only deviations due to variations in distance from the major axis (which affects the amount of circular velocity projected along the line of sight). A more realistic disk (such as those studied by Bottema 1993, whose properties were used to construct the model panels in the Figure) will have additional velocity dispersion which will make the feature less narrow but still recognizable.

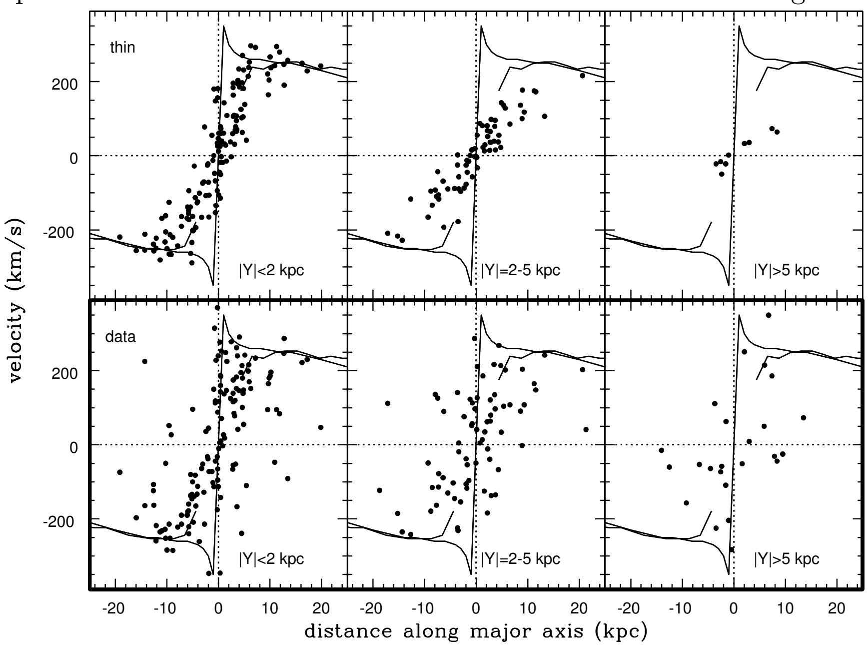

Figure 1. Velocity of globular clusters in M31 with velocity errors less than 20 km/s (lower panels), compared to a realistic thin disk model (upper panels), against major axis distance X. Data are split by distance Y from the major axis. A significant number of objects, particularly those close to the major axis, have thin disk kinematics.

Particularly for clusters within 2 kpc of the major axis, we see a subsystem with disk kinematics as well as a group with hotter kinematics. We find that 40% of the clusters projected on M31's disk belong to the disk subsystem. Disk clusters are found over the entire radial range of the M31 stellar disk. Studies of the age of these clusters will constrain the epoch of disk formation in M31, but it seems likely from existing work that they are old, suggesting that M31 had a large thin disk in place quite early.

References

Bottema, R. 1993, A&A, 275, 16

Perrett, K. M., Bridges, T. J., Hanes, D. A., Irwin, M. J., Brodie, J. P., Carter, D., Huchra, J. P., & Watson, F. G. 2002, AJ, 123, 2490

Hurley-Keller, D., Morrison, H.L., Harding, P. and Jacoby, G. 2003, submitted to ApJ

Highlights of Astronomy, Vol. 13
International Astronomical Union, 2003
O. Engvold, ed.

The Evolution of NGC 5128: Globular Clusters and Field Stars

Eric W. Peng

Physics and Astronomy, Rutgers University, Piscataway, NJ, 08854, USA

Abstract. As the nearest giant elliptical galaxy, NGC 5128 (Centaurus A) is an excellent place to use globular clusters (GCs) and host galaxy field stars to study galaxy evolution. We have performed a detailed investigation of this galaxy, comparing field star kinematics with the metallicities, ages, and kinematics of GCs. We used our sample of 780 planetary nebulae (PNe) to trace the kinematics of the field star population. Our survey for GCs bring the total number of confirmed GCs to 215. Using spectra of the brightest GCs to determine ages, we find that the metal-rich GCs have a mean age of approximately 4–5 Gyr, and that their kinematics are similar to those of the PNe. The metal-poor GCs have old ages similar to the Galactic GCs, and show a weaker kinematic correlation with the field stars. It is possible that NGC 5128 was formed by the merger of two or more disk galaxies at the time that the metal-rich clusters were formed.

1. Introduction

Globular clusters represent the fossil record of vigorous star formation that marks the evolutionary history of their host galaxies. Detailed investigations of these cosmic markers can provide leverage on the chemical and dynamical history of spheroidal stellar populations. Equally important are studies of the field stars that make up the bulk of a galaxy. One of the best galaxies for conducting an in-depth study is the nearby (3.5 Mpc) post-merger elliptical NGC 5128 (Centaurus A). We have conducted a *UBVRI* survey of the NGC 5128 GC system, and an [OIII] survey of its planetary nebula (PN) system, which trace the kinematics of the field stars. Spectroscopic follow-up provided radial velocities for both populations, bringing the total number of confirmed GCs to 215, and the total number of confirmed PNe to 780.

2. GC Colors, Ages, Kinematics, and Formation

The GC color distribution of NGC 5128 is distinctly bimodal. For old clusters, these trends in color are attributed to differences in metallicity. Spectroscopy, however, allows us to gain some leverage on GC ages. In Figure 1, we plot the age-sensitive Hβ index (Worthey et al. 1994) and the metallicity-sensitive $[MgFe]'$ index defined by Thomas, Maraston, & Bender (2003). The metal-poor clusters are consistent with being a universally old population (12–15 Gyr old). The bulk of the metal-rich GCs, however, appear to be significantly younger, having ages from 1–8 Gyr. We confirm the large rotation of the PNe, showing

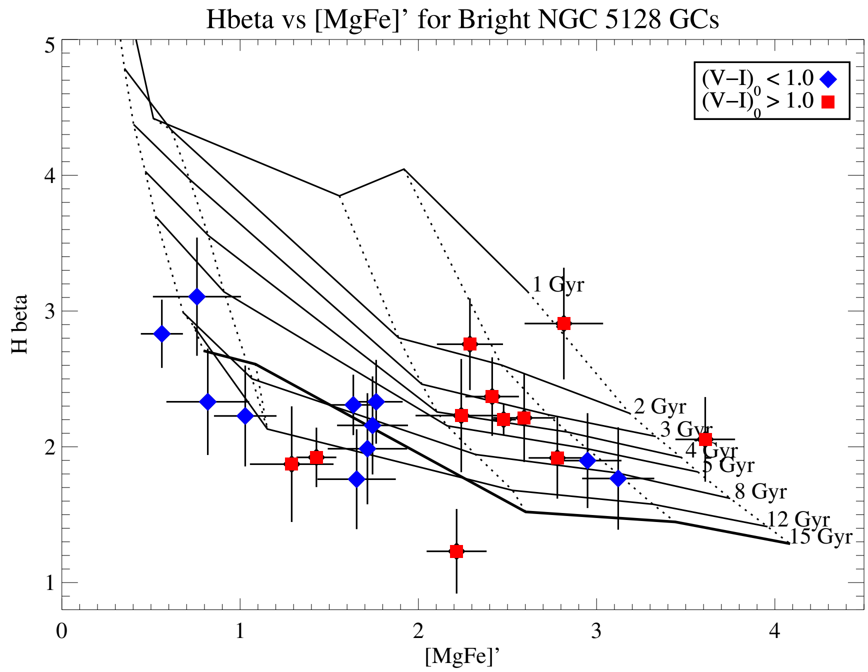

Figure 1. Hβ and $[MgFe]'$ Lick/IDS index measurements on the model grids from Thomas et al. (2003). Lines of constant metallicity (dotted) have values [m/H] = [-2.25, -1.35, -0.33, 0.0, +0.35] (left to right) at [α/Fe] = 0. Lines of constant age (solid) have values from 1–15 Gyr. This figure shows the index measurements for 23 bright, $(S/N)_{H\beta} > 40$, GCs.

that the rotation stays flat along the major axis at a level of 100 km/s out to 80 kpc. The metal-rich GCs have a velocity field that is similar to the PNe, exhibiting rotation at the level of 50 km/s, while the metal-poor clusters show less rotation. The kinematic association of the metal-rich GCs and the PNe, as well as the age determinations, point to a possible major merging event between two disk galaxies approximately 4–5 Gyr ago. This scenario is consistent with the results of merger simulations, which can produce strong rotation and young star clusters in the remnant.

References

Thomas, D., Maraston, C., & Bender, R. 2003, MNRAS, 339, 897

Worthey, G. 1994, ApJS, 95, 107

Highlights of Astronomy, Vol. 13
International Astronomical Union, 2003
O. Engvold, ed.

The Dynamical Mass of the Young Cluster W3 in NGC 7252: Heavy-Weight Globular Cluster or Ultra Compact Dwarf Galaxy?

Claudia Maraston, N. Bastian, R. P. Saglia, Markus Kissler-Patig, François Schweizer, Paul Goudfrooij

MPE, Giessenbachstraße, 85748 Garching, Germany
Universitäts-Sternwarte, Scheinerstraße 1, 81679 München, Germany

Abstract. We have measured the dynamical mass of the highly luminous star cluster W3 in the young merger remnant galaxy NGC 7252. The value is $M_{\rm dyn} = (8 \pm 2) \times 10^7 M_\odot$, and represents the highest dynamically-confirmed mass for an extra-galactic star cluster so far. The dynamical mass is in excellent agreement with the luminous mass (Maraston et al. 2001). This results from the use of stellar population models that include correctly the brightest AGB stellar phase, dominant in young stellar populations. To classify W3, we employ the *fundamental plane* of stellar systems (Bender, Burstein & Faber 1992), for the first time in these kinds of studies. We find that W3 lies far from typical Milky Way globular clusters, but it is also far from the heavyweights ωCen in the Milky Way and G1 in M31, because it is too extended for its mass, and from dwarf elliptical galaxies because it is much more compact for its mass. Instead W3 lies close to the ultra-compact Fornax objects (Drinkwater et al. 2003) and to the compact elliptical M32, possibly shedding light on the still mysterious nature of these objects. A previously deserted region of the fundamental plane starts to be populated.

Extreme star bursts seen in galaxy mergers are able to produce star clusters with masses up to $10^7 M_\odot$, that are suggested to evolve into galactic globular clusters (GC). However some objects seem to escape such notice, because their luminosity-estimated masses are much larger than those of the most massive GCs. The most extreme case is a star cluster in the young ($t \lesssim 1$ Gyr) merger remnant galaxy NGC 7252, for which the luminous mass was found to be nearly $10^8 M_\odot$ (Schweizer & Seitzer 1998; Maraston et al. 2001). Therefore it is important to check the dynamical mass (Maraston et al. 2003). To this aim, the internal velocity dispersion of the object has been measured from a high-resolution, high S/N optical spectrum obtained with UVES/VLT, by means of the FCQ method (Bender 1990). We use a *composite* stellar template in which the luminosity contributions of the individual stars are those of the stellar population model that matches the spectra and colors of W3 ($t \sim 300$ Myr, $Z \sim 0.5\ Z_\odot$, $[\alpha/Fe] \sim 0$; Maraston et al. 2001). Our result is the astonishingly high velocity dispersion $\sigma = 45 \pm 5$ km/s, that combined with the large cluster size $R_{\rm eff} = 17.5 \pm 1.8$ pc, translates into a dynamical virial mass for W3 of $(8 \pm 2) \times 10^7 M_\odot$. In order to classify this object, we use the *fundamental plane* (Figure 1), on which we place the new UCDGs and the massive Local Group star clusters ωCen and G1. W3 lies far from the average line of galactic GCs and from ωCen and G1. Instead, a connection might exist with the UCDGs and with the compact elliptical M32.

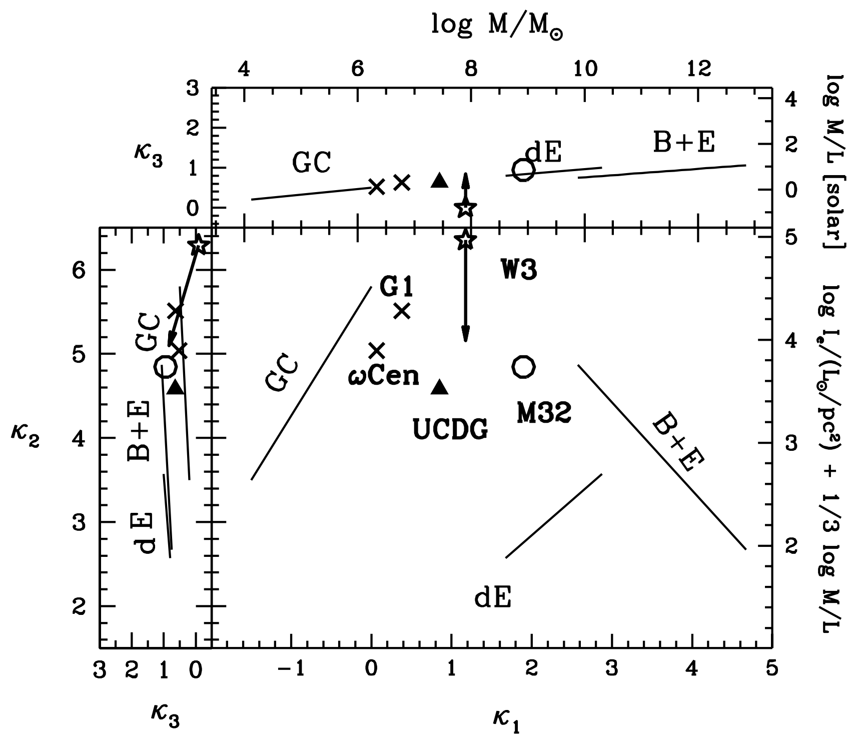

Figure 1. The fundamental plane of stellar systems - bulges plus ellipticals B+E, dwarf ellipticals dE, globular clusters GC (Burstein et al. 1997) in the version containing massive star clusters and Ultra Compact Dwarf Galaxies (UCDGs) (Maraston et al. 2003). κ_1 is the mass of an object, while κ_2 can be interpreted as a concentration factor in the sense that objects with higher values of κ_2 are more concentrated for a given mass. κ_3 is the mass-to-light ratio. The arrow from W3 indicates its position when faded to 10 Gyr due to stellar evolution. Note that dynamical mass losses are not taken into account (see discussion in Maraston et al. 2003).

References

Bender, R. 1990, A&A, 229, 441

Bender, R., Burstein, D., Faber, S.M. 1992, ApJ, 399, 462

Burstein, D., Bender, R., Faber, S.M., Nolthenius, R. 1997, AJ, 114, 1365

Drinkwater, M.J., et al., 2003, Nature, 423, 519

Maraston C., Bastian, N., Saglia, R. P., Kissler-Patig M., Schweizer, F., Goudfrooij, P. 2003, A&A, *accepted*

Maraston C., Kissler-Patig, M., Brodie, J., et al. 2001, A&A, 400, 823

Schweizer, F., Seitzer, P. 1998, AJ, 116, 2206

Highlights of Astronomy, Vol. 13
International Astronomical Union, 2003
O. Engvold, ed.

Extreme Globular Cluster Systems

John P. Blakeslee

Department of Physics and Astronomy, Johns Hopkins University
Baltimore, MD, USA (jpb@pha.jhu.edu)

Abstract. The superior resolution and large format of the Advanced Camera for Surveys (ACS) on the Hubble Space Telescope (HST) make it a powerful new tool in the study of extra-galactic globular cluster (GC) systems. We summarize some early results on GC populations from the ACS GTO program, concentrating on the extreme cases of the isolated dwarf NGC 2915 and the core of the massive lensing cluster Abell 1689.

1. Introduction

ACS has been delivering superb quality images since soon after its installation on *HST* in March 2002. The earliest ACS science included observations of merging galaxies such as "the Tadpole" (UGC 10214). While Tran et al. (2003) concluded that the bright young star clusters in the Tadpole were unlikely to be young GCs, the ACS science team has a continuing program to study star cluster formation in some star-burst galaxies, including NGC 1569, which is known to harbor massive young clusters that are consistent with being young globulars. Our team has a number of other programs that, while not explicitly designed for studying extra-galactic GCs, have proven to be extremely interesting for this purpose. We discuss two such cases in what follows.

2. "New" Old Globulars in a Dark Matter Dominated Dwarf

NGC 2915 is an isolated dwarf galaxy about 4.2 Mpc away. While the optical morphology appears to be that of a blue compact dwarf, it is surrounded by a massive HI spiral disk with an extent more than 5 times greater than the optical light (Meurer et al. 1996). This HI disk allows for dynamical probing of the dark matter halo to large radii, and the results indicate that NGC 2925 is one of the most dark-matter dominated galaxies known, having $M/L_B \sim 80$.

Our 3-band ACS Wide Field Camera images reveal a significant old halo population, including the three globular clusters shown in Figure 1. These objects have colors similar to those of old, metal-poor Galactic globulars. They are 1–2 mag brighter than the mean of the Galactic GC luminosity function, but fainter than the brightest Galactic GCs such as ω Cen. If we were just extremely lucky with our one ACS pointing and happened to capture all the NGC 2915 GCs in a single frame, then we calculate a specific GC frequency $S_N \sim 1$ for this galaxy. However, if we extrapolate according to a more typical power-law GC distribution, then we find a number almost an order of magnitude larger, making NGC 2915 a "high-S_N" galaxy. This result is in line with the high gas fraction and M/L ratio, and the apparent scaling of GC population sizes with these quantities, rather than with luminosity, in elliptical galaxies.

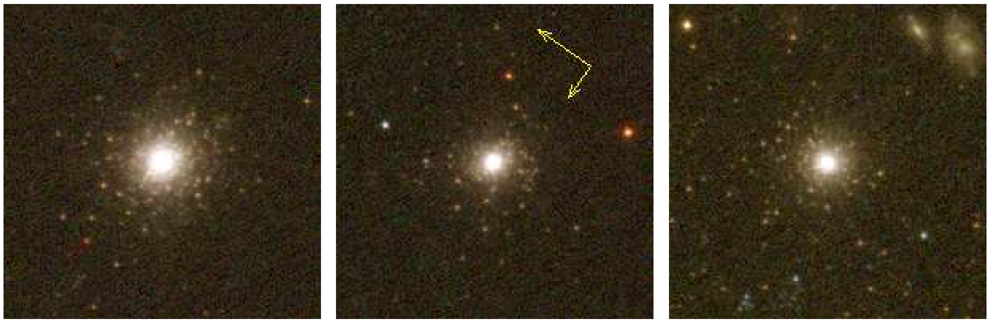

FIG. 1. NGC 2915 globulars newly discovered with ACS.

We can speculate about the future evolution of S_N in NGC 2915: whether it will evolve towards typical low values through quiescent star formation in the HI disk, whether it will remain high or increase through loss of the HI and fading of the stellar light, or how it might change through dissipative merging and starbursts. This may prove a key galaxy for understanding the evolving relationship between GC systems, their host galaxies, and the larger environment.

3. Abell 1689: The Biggest Globular Population Yet?

At the other extreme, we have found a teeming GC population in the core Abell 1689 $z = 0.18$, the most powerful cluster lens in the sky. Rich GC systems were known around many cD galaxies, but all at $z < 0.1$. Besides being the most distant studied to date, extrapolation of the counts indicates this cluster has on the order of 10^5 GCs in its center, or 2-3 times that of any other system and ~ 7 times the number found around M87, the prototypical "high-S_N" central cluster galaxy. I caution that these results are highly preliminary and we are working to improve the analysis, but it is clearly an extremely rich system.

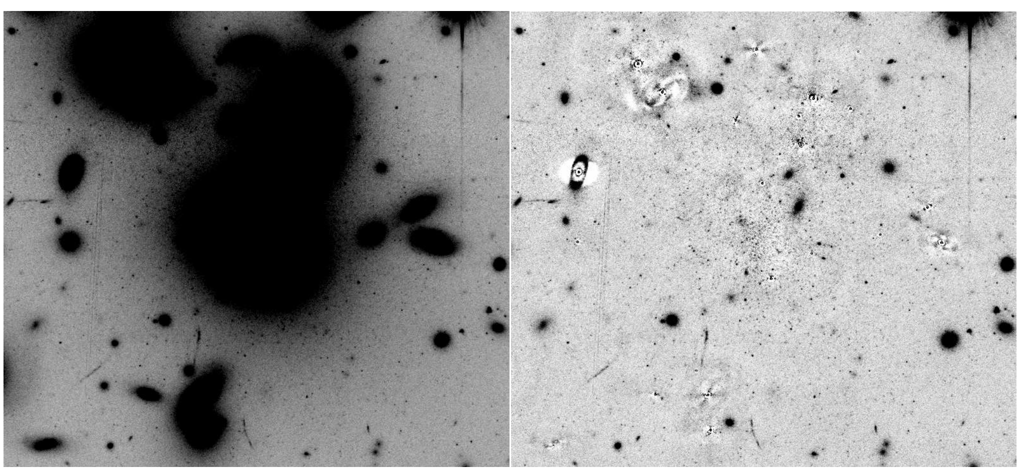

FIG. 2. ACS image of A1689 core (left); faint point sources visible following subtraction (right).

These results are all thanks to the devoted efforts of many ACS IDT members.

References

Meurer, G. R. et al. 1996, ApJ, 111, 1551.
Tran, H. et al. 2003, ApJ, 585, 750.

Highlights of Astronomy, Vol. 13
International Astronomical Union, 2003
O. Engvold, ed.

Globular Clusters in Early-Type Galaxies with GMOS

Terry Bridges, Mike Beasley, Favio Faifer, Duncan Forbes, Juan Forte, Karl Gebhardt, Dave Hanes, Ray Sharples, Steve Zepf

AAO, Swinburne, UNLP/CONICET, Swinburne, UNLP/CONICET, U. of Texas, Queen's U., Durham, Michigan State U.

Abstract. We present recent results from our long-term Gemini/GMOS study of globular clusters (GCs) in early-type galaxies. To date, we have obtained photometry and spectroscopy for GCs in NGCs 3379, 4649, 524, 7332, and IC 1459. We find a clear bimodality in the NGC 4649 GC color distribution, with the fraction of blue/red clusters increasing with galacto-centric radius. We derive ages and metallicities for 22 GCs in NGC 3379, finding that most of the clusters appear old (10−15 Gyr); however, there is a group of 4 metal-rich, younger clusters with ages of 2−6 Gyr. The NGC 3379 GC velocity dispersion decreases with radius, as does the inferred (local) mass-to-light ratio: there is *no* evidence for a dark matter halo in NGC 3379 based on our GC data.

1. Introduction

Globular clusters (GCs) are excellent probes of the dynamics, dark matter content, star-formation histories, and chemical enrichment of early-type galaxies. We have embarked upon a major programme using the Gemini Multi-Object Spectrograph (GMOS) on the 8m Gemini telescopes to obtain photometry and spectroscopy of GCs in ~ 12 early-type galaxies, covering a range of galaxy type, luminosity, and environment. In this paper we present some of the first results from this programme.

2. Data

We have been using GMOS on Gemini North (since 2002A) and South (since 2003B) to obtain spectroscopy for 30−100 GCs in each of NGCs 3379, 4649, 524, 7332, and IC 1459. GMOS pre-imaging in the g', r', and i' filters for 2−3 fields per galaxy (400−800 sec in each filter) is used to select GC candidates for follow-up spectroscopy and for photometric analysis of the GC systems. The GMOS images have been reduced using IRAF/DAOPHOT, with photometric calibration from HST photometry kindly supplied by Soeren Larsen. Final GC candidate lists are determined after rejection of resolved objects, and objects with colors outside the range of Galactic GCs. GMOS multi-slit spectroscopy has been obtained for one or more fields in each galaxy, with 25−50 slits per field/mask (depending on the richness of the GC system), and exposure times of 8−10 hours per mask. Spectroscopic data reduction is done using the IRAF/GMOS package.

3. Globular Cluster Photometry in NGC 4649

NGC 4649 is a luminous (M_V=−22.4) Virgo elliptical. We present preliminary photometric results for ∼ 2000 unresolved objects with i' < 25 and 0.5 < (g'-i') < 1.5 (see Forbes et al. (2004) for a fuller account, and Bridges et al. (2004) for NGC 4649 GC spectroscopy). The NGC 4649 GC colour distribution is clearly bimodal, with peaks at (g'-i') = ∼ 0.9 and 1.15. The fraction of blue/red clusters increases with radius, as found in other early-type galaxies.

4. Globular Cluster Spectroscopy in NGC 3379

NGC 3379 is a less luminous elliptical in the nearby Leo group. We have spectra for 22 NGC 3379 GCs in a 10 hour GMOS exposure with 5 Å resolution and coverage from ∼ 4000−7000 Å . **Figure 1** shows the ages and metallicities of 18 GCs, based on the comparison of line-strengths with stellar population synthesis models. Most of the GCs are old, with ages > 10 Gyr, but there is a group of ∼ 4 metal-rich, younger GCs with ages of 2−6 Gyr. **Figure 2** shows that both the GC velocity dispersion (top panel) and the local M/L (bottom panel) decrease outwards. A preliminary analysis (see Beasley et al. 2004) shows that *there is no evidence for a dark-matter halo in NGC 3379*, a very interesting result also seen in the PNe kinematics (Romanowsky et al. 2003, Science, 301, 1696).

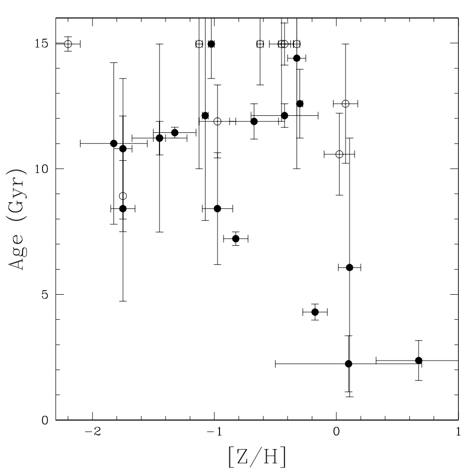

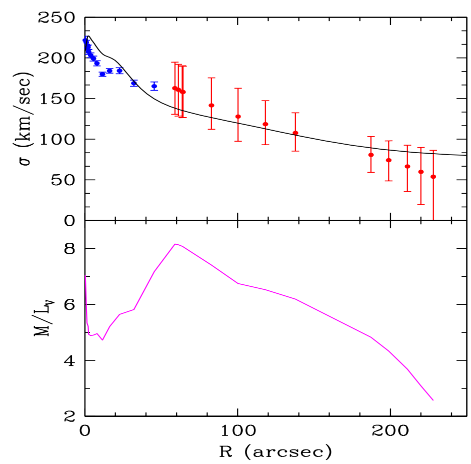

Figure 1 (left): Ages/metallicities for NGC 3379 GCs (filled circles) and MW GCs (open circles), from our GMOS spectra. **Figure 2 (right):** *Top:* velocity dispersion of NGC 3379 stars (small errors) and GCs (larger errors); the solid line is a constant M/L fit. *Bottom:* The local M/L for NGC 3379.

Acknowledgments. We are very grateful to Søren Larsen for all of his help with our photometric calibration, and to the Gemini staff, particularly Inger Jørgensen, for obtaining such nice data for us.

Highlights of Astronomy, Vol. 13
International Astronomical Union, 2003
O. Engvold, ed.

Intergalactic Globular Clusters

Michael J. West

Department of Physics & Astronomy, University of Hawaii, Hilo, Hawaii 96720, USA

Patrick Côté

Department of Physics & Astronomy, Rutgers University, Piscataway, NJ 08854, USA

Henry C. Ferguson

Space Telescope Science Institute, 3700 San Martin Drive, Baltimore, MD 21218, USA

Michael D. Gregg

Department of Physics, University of California, Davis, CA 95616, USA; and IGPP, Lawrence Livermore National Laboratory, Livermore, CA 94550, USA

Andrés Jordán

Department of Physics & Astronomy, Rutgers University, Piscataway, NJ 08854, USA

Ronald O. Marzke

Department of Physics & Astronomy, San Francisco State University, San Francisco, CA 94132, USA

Nial R. Tanvir

Department of Physical Science, University of Hertfordshire, Hatfield AL10 9AB, UK

Ted von Hippel

Department of Astronomy, University of Texas, Austin, TX 78712, USA

Abstract. We confirm and extend our previous detection of a population of intergalactic globular clusters in Abell 1185, and report the first discovery of an intergalactic globular cluster in the nearby Virgo cluster of galaxies. The numbers, colors and luminosities of these objects can place constraints on their origin, which in turn may yield new insights to the evolution of galaxies in dense environments.

1. Introduction

There are several reasons to believe that a population of intergalactic globular clusters (IGCs) should exist outside of galaxies:

(1) The Jeans mass at recombination was $\sim 10^5 - 10^6$ solar masses, and hence globular cluster sized objects could have formed wherever the local density of matter was high enough.

(2) Many galaxies may have met their demise over a Hubble time as a result of collisions and tidal disruption. Globular clusters are likely to survive the disruption of their parent galaxy, resulting in the gradual accumulation of a population of IGCs. Intergalactic stars, planetary nebulae, supernovae and HII regions have already been found; it would be surprising if there were no IGCs.

(3) The existence of IGCs might explain high specific frequencies, bimodal globular cluster metallicity distributions and other current puzzles in the study of globular cluster systems.

Jordán et al. (2003) reported a tentative detection of IGCs in the center of the rich galaxy cluster A1185 ($z = 0.032$) based on I-band images obtained with WFPC2 on the Hubble Space Telescope.

2. What's New?

We (Côté, Jordán, Marzke, West) recently obtained very deep, multicolored (V and I) images of the same A1185 field using HST with the new ACS. The goals of these new observations are to 1) detect the peak of the assumed universal Gaussian-like globular cluster luminosity function (which should occur at $I \sim 27.3$ at A1185's distance) and thereby confirm that these candidate IGCs are bona fide globular clusters and 2) use color information to infer their metallicities. Preliminary analysis indicates that we are reaching sufficiently faint magnitudes to reliably detect the luminosity function turnover. The number and colors (metallicities) of IGCs will provide constraints on the number and types of galaxies that have been destroyed or stripped over a Hubble time.

Using the Keck telescope, we (Ferguson, Gregg, Tanvir, von Hippel, West) recently measured the redshift of a candidate IGC in the nearby Virgo galaxy cluster that was found serendipitously on an HST image obtained for another project. Preliminary data reductions show that this object, which is slightly resolved in the HST image and appears to be a distant globular cluster, has a recessional velocity of ~ 470 km/s, and hence is most likely in the Virgo cluster. Its apparent magnitude, $m_V \sim 21.2$, is consistent with it being a bright globular cluster. Using telescopes on Mauna Kea we have since obtained optical and NIR colors of this object, as well as a medium-resolution spectrum that should yield its velocity dispersion. These data are presently being analyzed.

Acknowledgments. MJW acknowledges support from NSF grant AST 02-05960 and HST grant HST-GO-09438.01-A.

References

Jordán, A., West, M.J., Côté, P. & Marzke, R.O. et al. 2003, AJ, 125, 1642

Highlights of Astronomy, Vol. 13
International Astronomical Union, 2003
O. Engvold, ed.

A Tale of Giants Stealing from Dwarfs

Duncan A. Forbes
Centre for Astrophysics & Supercomputing, Swinburne University, Hawthorn VIC 3122, Australia

1. Disrupting Dwarf

Cold Dark Matter simulations predict 10-100× more dwarf satellite galaxies than are observed. Some of these 'missing satellites' may have been accreted, along with their globular clusters (GCs), by giant galaxies (Cote et al. 1998). But examples of dwarfs in the early stages of disruption have remained elusive.

However images of the Tadpole galaxy by the ACS on HST contained a background spiral with a candidate 'disrupting dwarf' (ie two tails were seen coming from the dwarf). A 1hr Keck spectrum of the spiral (V = 18) and dwarf (V = 23) confirmed the physical association and gave a redshift of 0.15. We fit Sersic profiles to the surface brightness and found the dwarf has properties similar to a dE galaxy with blue central colors (Forbes et al. 2003).

Comparison with simulations suggests the original dwarf had a disk, ie a dIrr galaxy (Mayer et al. 2001). As it orbits, tails of stars are pulled off by tidal forces and the galaxy is accreted due to dynamical friction. As the starburst fades and it continues to lose stars it may resemble a dSph galaxy. The disrupted stars eventually add a metal-poor population to the giant galaxy halo. We would also expect the dwarf to contain some 25 GCs but these would have V > 29 and hence too faint to be seen in the ACS image. This observation illustrates the transformation of a dIrr to dE and possibly dSph via tidal stripping, and may help explain the dwarf galaxy morphology-density relation. *Dwarfs can be transformed from one type into another if they get too close to a giant.*

2. Blues

In the last few years it has become clear that the mean color of the *red* (metal-rich) GCs in giant galaxies is strongly correlated with host galaxy mass (eg Forbes & Forte 2001; Larsen et al. 2001). Strader, Brodie & Forbes (2003) using high quality data, extended to include dwarf galaxies, have found a 6σ correlation for *blue* (metal-poor) GCs of the type $Z \sim L^{0.15}$ (the slope is about half that for the red GCs). This implies that, like the red GCs, the blue GCs know about the potential they live in. Dwarf galaxies' GCs have a mean V–I of ~ 0.88 whereas giants have V–I ~ 0.94. This places strong limits on the number of accreted dwarf galaxy GCs that can be part of the blue GC subpopulation in giant galaxies. *Dwarfs make up only a small part of the diet of giants.*

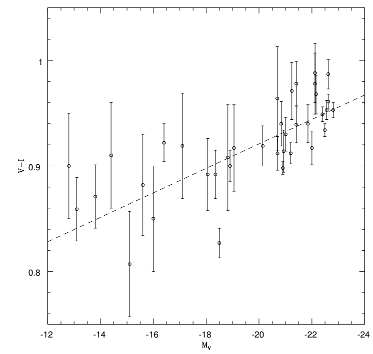

Figure 1. Mean V–I color for the blue (metal-poor) GC systems of galaxies versus the host galaxy luminosity. A 6σ correlation is seen. Giant galaxies' GC systems can not simply be the accretion of many dwarf galaxy GC systems.

3. Tidal stripping of GCs

Another potential source of GCs for giant galaxies is to acquire them, via tidal stripping, from nearby galaxies. In this case, GCs, and possibly some field stars, are acquired, but in general the donor galaxy remains as a separate entity. Perhaps the best case for tidal stripping is that of NGC 1399 and NGC 1404 in the Fornax cluster. There is amble evidence for an ongoing interaction between the two galaxies and NGC 1404 reveals a low specific frequency of $S_N \sim 2$ (eg Forbes, Brodie & Grillmair 1997). Building on the ground-breaking work of Muccio and collaborators in the 1970s, Bekki et al. (2003) have modeled this process. Starting with an $S_N = 5$, Bekki et al. could reproduce the value of 2 by tidal stripping. They found an extended GC system and an eccentric orbit for NGC 1404 was required. The kinematics of the stripped GCs can, in principle, be used to probe the cluster-wide potential. A trend for S_N to increase with cluster-centric distance is predicted and mildly supported by current data (Forbes, Brodie & Grillmair 1997). *Giants steal GCs from dwarfs and sometimes eat the dwarf too (but most of the time the dwarf gets away).*

4. References

Bekki, K., Forbes, D., Beasley, M., Couch, W., 2003, MNRAS, in press
Cote, P., Marzke, R., & West, M., 1998, ApJ, 501, 554
Forbes, D., Brodie, J., Grillmair, C., 1997, AJ, 113, 1652
Forbes, D., Forte, J., 2001, MNRAS, 322, 257
Forbes, D., Beasley, M., Bekki, K., Brodie, J., Strader, J., 2003, Science, 301, 5637
Larsen, S., Brodie, J., Huchra, J., Forbes, D., Grillmair, C., 2001, AJ, 121, 2974
Mayer, L., et al. 2001, ApJ, 559, 754
Strader, J., Brodie, J., Forbes, D. 2003, ApJL submitted.

Highlights of Astronomy, Vol. 13
International Astronomical Union, 2003
O. Engvold, ed.

The ACS Virgo Cluster Survey

Patrick Côté

Rutgers University, 136 Frelinghuysen Road, Piscataway, NJ 08854

Michael J. West

University of Hawaii, Hilo, HI 96720

Abstract. We describe the ACS Virgo Cluster Survey, an HST imaging survey of early-type galaxies in the Virgo Cluster. Multi-color ACS images for one hundred member galaxies, spanning a range of 450 in luminosity, are being used to study the central regions of these galaxies, their globular cluster systems, and the three-dimensional structure of Virgo itself. In terms of depth, spatial resolution, sample size and homogeneity, this represents the most comprehensive imaging survey to date of early-type galaxies in dense environments.

1. Introduction

The Virgo Cluster is the largest and most massive concentration of galaxies in the Local Supercluster. Not surprisingly, it has played a central role in understanding how galaxies form and evolve in dense environments, providing invaluable information on the extra-galactic distance scale, the nature of galactic nuclei, the local velocity field, and the shape and universality of the galactic luminosity function. In the study of early-type galaxies, Virgo has played an especially pivotal role since it contains, by far, the largest concentration of elliptical and lenticular galaxies in the local universe.

2. Survey Strategy and Sample Selection

With our colleagues (see below), we are carrying out an imaging survey of early-type galaxies in the Virgo Cluster using ACS Wide Field Camera. While the full list of science drivers is too lengthy to describe in detail here, our primary scientific objectives include: (1) the measurement of distances for the full sample of galaxies using the method of surface brightness fluctuations; (2) a comprehensive isophotal analysis for each program galaxy, including the measurement of nuclear surface brightness and color profiles; and (3) the measurement of luminosities, colors, concentration indices, half-light radii, and ages for thousands of globular clusters belonging to our program galaxies.

The sample consists of one hundred early-type (E, E/S0, S0, dE, dE,N, and dS0) galaxies, drawn from the Virgo Cluster Catalog of Binggeli et al. (1985). Each galaxy is a confirmed member of Virgo based on its measured radial velocity. The program galaxies span the range $9.31 \leq B_T \leq 15.97$, corresponding to a factor of ~ 450 in luminosity.

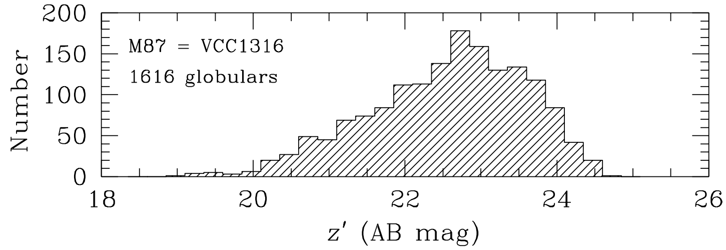

Figure 1. Globular cluster luminosity function for M87 from the ACS Virgo Cluster Survey.

The first data were obtained in December 2002, and the final images are expected to be in hand by April–June 2004. The dataset for each galaxy consists of two 375 sec exposures in the F475W (g′) bandpass, two 560 sec exposures in the F850LP (z′) bandpass, and a single 90 sec F850LP exposure. This filter combination provides roughly a 50% increase in color baseline relative to F555W and F814W, a commonly used WFPC2 filter combination. The approximate limiting magnitude in both band passes is $V \sim 25.7$ for a point-source signal-to-noise ratio of five. By observing each galaxy for just a single HST orbit, we are therefore able to sample the brightest $\sim 90\%$ of the globular cluster luminosity function in each galaxy (see Fig 1).

3. Reductions and Data Products

A PYTHON-based calibration/reduction pipeline has been written to: align and combine the images; generate "background" images using multi-resolution wavelet filtering; detect objects; and measure object magnitudes and colors. Note that globular clusters at the distance of Virgo are marginally resolved on our images (WFC scale $= \simeq 3.8$ pc pixel^{-1}). For the globular clusters belonging to our program galaxies — identified on the basis of their colors and luminosities — we also derive structural parameters (i.e., half-light radii, concentration indices) by fitting psf-convolved, Michie-King models to their two-dimensional profiles. A complete discussion of the pipeline will be presented in Jordán et al. (2004), and additional information about the survey in general may be found at http://www.physics.rutgers.edu/∼pcote/acs/

Acknowledgments. The ACS Virgo Cluster Survey is a collaborative effort between P. Côté, J.P. Blakeslee, L. Ferrarese, A. Jordán, S. Mei, D. Merritt, M. Milosavljević, E. Peng, J. Tonry, and M. West.

References

Binggeli, B., Sandage, A., & Tammann, G.A. 1985, AJ, 90, 1681

Jordán, A., Côté, P., Blakeslee, J.P., Ferrarese, L., Mei, S., Merritt, D., Milosavljević, M., Peng, E., Tonry, J.L., & West, M.J. 2003, ApJ, submitted.

Highlights of Astronomy, Vol. 13
International Astronomical Union, 2003
O. Engvold, ed.

The Fundamental Plane of Globular Clusters

Dean E. McLaughlin

Space Telescope Science Institute, 3700 San Martin Drive, Baltimore, MD 21218 USA

Abstract. The fundamental plane of globular clusters can be expressed as a particular scaling of cluster energy vs. mass: $E_b \sim M^2$. New calculations of energy and mass for a large sample of young clusters in the Magellanic Clouds may shed light on the origins of this scaling.

The fundamental plane of globular clusters (GCs) is typically defined in terms of velocity dispersion, radius, and surface brightness (Djorgovski 1995; Burstein et al. 1997). Comparisons in this parameter space show that GCs do not follow the same structural relations as early-type galaxies and bulges: while the radii of the latter depend on their masses, GC sizes do not; and while ellipticals follow the Faber-Jackson relation, $M \sim \sigma^4$, GCs instead obey $M \sim \sigma^2$ or so (e.g., Djorgovski & Meylan 1994).

These scalings for GCs, $R \sim M^0$ and $\sigma \sim M^{0.5}$, are manifestly equivalent to a scaling between binding energy and total mass: $E_b \sim M^2$, as McLaughlin (2000) has confirmed by direct calculation. McLaughlin further shows how this energy-mass relation combines with a constant mass-to-light ratio in Galactic GCs to produce *all* other correlations between *any* set of GC observables, including the more traditional expressions of the fundamental plane. GCs in M31, M33, and NGC 5128 appear to follow the same mass-energy relation (Barmby et al. 2002; Larsen et al. 2002; Harris et al. 2002). On the other hand, the Faber-Jackson relation suggests $E_b \sim M^{1.5}$ for E galaxies and bulges.

The advantage of viewing the fundamental plane in terms of energy is that the processes of GC formation and dynamical evolution are ultimately ones of energetics. It is therefore significant that a scaling such as $E_b \sim M^2$ is much steeper than what is expected to have held in gaseous protoclusters ($E_b \sim M^{1.5}$ again, quite generically; see, e.g., McLaughlin & Pudritz 1996). It has been argued, though only heuristically, that the steeper $E_b(M)$ slope might have been imprinted during the birth of GCs, rather than over a Hubble time of dynamical evolution (McLaughlin 2000; Ashman & Zepf 2001).

To check this idea empirically, we (D. E. McLaughlin & R. P. van der Marel, in preparation) have calculated the masses and energies of Magellanic Cloud star clusters spanning a wide range of ages, from tens of Myr to 13 Gyr. Figure 1 shows our results. The values of E_b and M here follow from fitting structural models to the star-count data of Mackey & Gilmore (2003a, b) and applying mass-to-light ratios derived from the population-synthesis code PEGASE (Fioc & Rocca-Volmerange 1997). The apparent change of slope in E_b vs. M around $M \sim 1 - 2 \times 10^5\ M_\odot$ is a new feature, unrecognized in analysis of old and relatively massive GCs. Whether it is primarily an effect of age or of mass is not yet clear—though it is especially intriguing that it occurs at about the same

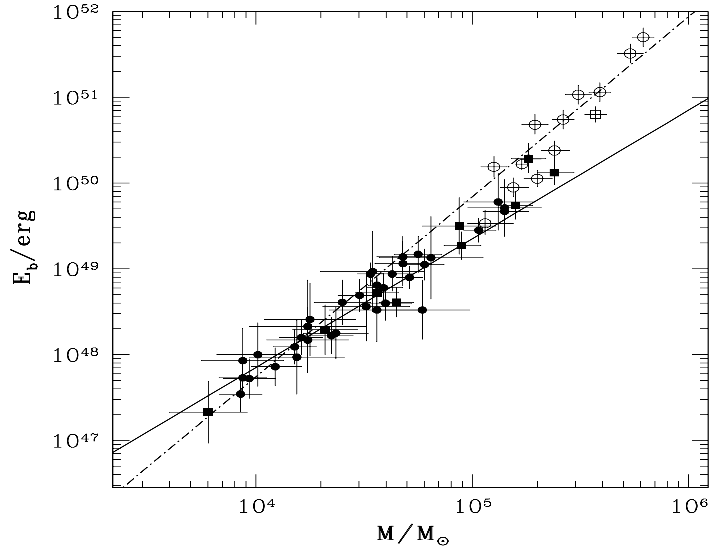

Figure 1. Binding energy vs. total mass for star clusters in the Magellanic Clouds. Filled circles: 36 young LMC clusters ($\tau \sim 10^7 - 10^{10}$ yr). Open circles: 12 old LMC globulars. Filled squares: 9 young SMC clusters. Open square: one old SMC globular. Solid line: $E_b \sim M^{1.5}$, as expected for gaseous protoclusters. Broken line: $E_b \sim M^{2.1}$, roughly as found for old GCs in the Milky Way, M31, M33, and NGC 5128.

mass scale which marks the turnover of the globular cluster luminosity function. Although it must be noted that the result depends critically on the cluster mass-to-light ratios predicted by the PEGASE code, understanding it may eventually provide important new insight into the overall properties of GCs as a class.

Acknowledgments. I am grateful to the American Astronomical Society for support in the form of an International Travel Grant.

References

Ashman, K. M., & Zepf, S. E. 2001, AJ, 122, 1888

Barmby, P., Holland, S., & Huchra, J. P. 2002, AJ, 123, 1937

Burstein, D., Bender, R., Faber, S., & Nolthenius, R. 1997, ApJ, 114, 1365

Djorgovski, S. 1995, ApJ, 438, L29

Djorgovski, S., & Meylan, G. 1994, AJ, 108, 1292

Harris, W. E., Harris, G. L. H., Holland, S. T., & McLaughlin, D. E. 2002, AJ, 124, 1435

Fioc, X., & Rocca-Volmerange, Y. 1997, A&A, 326, 950

Larsen, S. S., Brodie, J. P., Sarajedini, A., & Huchra, J. P. 2002, AJ, 124, 2615

Mackey, A. D., & Gilmore, G. 2003a, MNRAS, 338, 85

Mackey, A. D., & Gilmore, G. 2003b, MNRAS, 338, 120

McLaughlin, D. E. 2000, ApJ, 539,618

McLaughlin, D. E., & Pudritz, R. E. 1996, ApJ, 469, 194

Highlights of Astronomy, Vol. 13
International Astronomical Union, 2003
O. Engvold, ed.

HST Observations of Young Stellar Clusters in Nearby Galaxies

Søren S. Larsen

European Southern Observatory, Karl-Schwarzschild-Str. 2, D-85748 Garching bei München, Germany

Abstract. The HST data archive contains images of several nearby spirals, suitable for detailed studies of the properties of individual star clusters and their surroundings. By combining structural information derived from HST images with ground-based photometry, it is possible to study cluster properties as a function of age and mass. While both the core and effective radii of young clusters correlate with mass, the slopes of these relations are shallower than for a constant-density relation, implying that the mean density increases with cluster mass. This must be accounted for in theories for cluster formation.

1. Introduction

While the rich cluster systems in galaxy mergers and starbursts have been studied intensively over the past decade, it is sometimes overlooked that even some "normal", undisturbed spiral galaxies can form highly luminous, young star clusters (Larsen & Richtler 1999; Paper I). Within a distance of 10 Mpc, there are several examples of spirals with rich cluster systems which have been imaged with HST/WFPC2, allowing the properties and environments of individual star clusters to be studied in great detail. By combining the HST images with ground-based photometry, it is possible to look for trends in structural parameters with cluster age and mass, providing potentially valuable clues to the physics of cluster formation and subsequent dynamical evolution.

2. Cluster structure versus mass and age

We have recently scanned the HST archive for images of galaxies included in the original survey from Paper I. A total of 17 galaxies were found to have adequate HST data (Larsen 2004). The constraint that the clusters have to be visible on ground-based images is not as severe as it might appear at first, since a high S/N in the HST images is required anyway to measure accurate structural parameters. By fitting "Moffat" models of the form $P(r) \propto [1 + (r/r_c)^2]^{-\alpha}$, it is possible to constrain both the core radius r_c and the shape of the luminosity profile at large radii, parameterized by the slope α. While these profiles have no physical motivation, they have been shown to fit LMC clusters well (Elson et al. 1987). For $\alpha = 1$, they are identical to a King (1962) model with infinite concentration parameter.

The left panel in Fig. 1 shows the distribution of envelope slopes for clusters in four age bins. There is a clear tendency for many of the youngest clusters to have extended outer envelopes. This may reflect the density structure of the

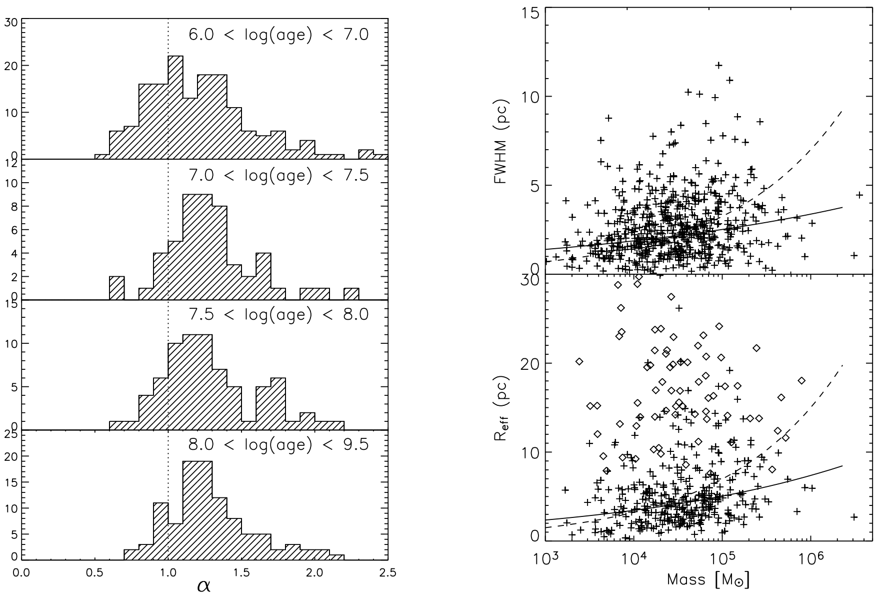

Figure 1. Left: Distribution of envelope slopes for clusters in four age bins. Right: FWHM and half-light radius versus mass.

parent molecular cloud cores, or be a hint that some of these clusters are unbound and expanding. Older clusters gradually evolve towards a King-like profile. In the right-hand panel, the FWHM and half-light radii are shown versus cluster mass. In each panel, the constant-density relation (size $\propto M^{1/3}$) is shown with a dashed line, while the solid lines indicate a fit to the data. For the half-light radii, only clusters with $1 < \alpha < 5$ were included in the fit (clusters with $\alpha < 1$ have poorly defined half-light radii and are shown with diamond symbols). Although both relations show substantial scatter, the fits are significantly shallower than for the constant-density relation. This conclusion is robust to selection effects, which would be expected to produce a bias against extended, low-mass objects.

The main limitation in this study is the difficulty of detecting low-mass clusters older than a few times 10^7 years. This situation is expected to improve when new ACS data become available.

References

Elson, R. A. W., Fall, S. M. & Freeman, K. C. 1987, ApJ, 323, 54

King, I. R. 1962, AJ, 67, 471

Larsen, S. S. & Richtler, T. 1999, A&A, 345, 59

Larsen, S. S. 2004, A&A, in preparation

Highlights of Astronomy, Vol. 13
International Astronomical Union, 2003
O. Engvold, ed.

Star Cluster Formation in Extreme Starburst Environments

Richard de Grijs

Department of Physics & Astronomy, The University of Sheffield, Hicks Building, Hounsfield Road, Sheffield S3 7RH, UK

Abstract. The currently available empirical evidence on the star formation processes in the extreme, high-pressure environments induced by galaxy encounters, mostly based on high-resolution *Hubble Space Telescope* imaging observations, strongly suggests that star *cluster* formation is an important and perhaps even the dominant mode of star formation in the starburst events associated with galaxy interactions.

1. Gravitational Interaction Induced Star (Cluster) Formation

Close encounters between gas-rich galaxies often have devastating effects on the state of their interstellar medium (ISM), in particular of the ISM of either the smaller or of the most gas-rich of the interacting galaxies (e.g., de Grijs et al. 2001, 2003). The ram pressure caused by the time-varying gravitational potential induced by the interaction causes free-floating giant molecular clouds in the affected galaxy's ISM to collapse and enter a phase of violent star formation. This process is particularly well illustrated by the ongoing interaction between NGC 6745 and its small northern companion galaxy, "NGC 6745c" (cf. de Grijs et al. 2003), where dynamical and kinematic evidence from HI observations obtained with the Very Large Array support the scenario that the small companion galaxy has traveled from the south east across the eastern edge of the main galaxy to its current location north of the main galaxy, in its wake leaving a frenzy of very violent and active star, and in particular star *cluster*, formation.

In de Grijs et al. (2003b) we used the ages, masses and metallicities of the rich young star cluster system in NGC 6745, based on the analysis of multi-passband archival *Hubble Space Telescope (HST)* observations, to derive its cluster formation history and subsequent evolution. We derive a median age, and thus an estimate of the starburst duration, of ~ 10 Myr. NGC 6745 contains a significant population of high-mass "super star clusters (SSCs)", with masses in the range $6.5 \lesssim \log(M_{\rm cl}/{\rm M}_\odot) \lesssim 8.0$. We caution, however, that these massive SSC candidates may not be gravitationally bound objects, but more diffuse star forming regions or aggregates of multiple unresolved clusters instead. Nevertheless, we measure an effective radius for the most massive object ($M_{\rm cl} \simeq 5.9 \times 10^8 {\rm M}_\odot$) of only $R_{\rm eff} \sim 16$ pc. However, this object appears very elongated, or may in fact be a double cluster. We should keep in mind, of course, that this high mass estimate is a strong function of the (low) metallicity assumed; if we had assumed solar metallicity for this object, the derived age would have been significantly smaller ($\sim 10 - 20$ Myr vs. ~ 1 Gyr), and the mass could be smaller by a factor of $\gtrsim 10$. Even so, if we could confirm this mass estimate spectroscopically, either of the subcomponents would be the most massive cluster known to date, significantly exceeding cluster W3 in NGC 7252, which has a mass of about $(3-18)\times 10^7 M_\odot$, depending on the age, metallicity and IMF assumed (Schweizer & Seitzer 1998; Maraston et al. 2001).

The suggestion that such massive objects (either star clusters, or extended star-forming regions) form preferentially in the extreme environments of interacting galaxies, is supported quantitatively by our analysis (de Grijs et al. 2003a) of pixel-by-pixel colour-magnitude and colour-colour diagrams of the Mice and Tadpole interacting galaxies (NGC 4676 and UGC 10214, respectively), based on a subset of the (archival) *HST* Advanced Camera for Surveys Early Release Observations, which provide a powerful technique to explore and deduce the star and star cluster formation histories of galaxies at moderate distances. In each interacting system we found some 40 bright young star clusters, with a characteristic mass of $\sim 3\times 10^6 M_\odot$, which are spatially coincident with blue regions of active star formation in their tidal tails and spiral arms. We showed that star cluster formation is a major mode of star formation in galaxy interactions, with $\gtrsim 35\%$ of the active star formation in encounters occurring in star clusters. In particular, the tidal tail of the Tadpole system is dominated by blue star-forming regions, which occupy some 60% of the total area covered by the tail and contribute $\sim 70\%$ of the total flux in the F475W filter (decreasing to $\sim 40\%$ in F814W).

Finally, in the nearby (ultra)luminous infrared galaxy NGC 6240, we detect a population of massive young star clusters, with tentative evidence (based on statistical considerations) that the more massive clusters are found closer to the galaxy's double (or perhaps triple) nucleus and the most intense starburst region (Pasquali, de Grijs, & Gallagher 2003).

Thus, the currently available empirical evidence, mostly based on high-resolution *HST* imaging observations, strongly suggests that star cluster formation is an important and perhaps even the dominant mode of star formation in the starburst events associated with galaxy interactions.

Acknowledgments. I acknowledge invaluable collaborations with Peter Anders, Nate Bastian, Uta Fritze-v. Alvensleben, Jay Gallagher, Henny Lamers, and Anna Pasquali.

References

de Grijs, R., O'Connell, R.W., Gallagher, J.S., III 2001, AJ, 121, 768

de Grijs, R., Lee, J.T., Mora Herrera, M.C., Fritze-v. Alvensleben, U., Anders, P. 2003a, New Astron., 8, 155

de Grijs, R., Anders, P., Bastian, N., Lynds, R., Lamers, H.J.G.L.M., O'Neil, E.J., Jr. 2003b, MNRAS, 343, 1285

Maraston, C., Kissler-Patig, M., Brodie, J.P., Barmby, P., Huchra, J.P. 2001, A&A, 370, 176

Pasquali, A., de Grijs, R., Gallagher, J.S., III 2003, MNRAS, in press (astro-ph/0306446)

Schweizer, F., Seitzer, P. 1998, AJ, 116, 2206

Highlights of Astronomy, Vol. 13
International Astronomical Union, 2003
O. Engvold, ed.

From Young to Old: Spectral Models for Star Cluster Systems

Uta Fritze - v. Alvensleben, Peter Anders

Universitätssternwarte Göttingen, Geismarlandstr. 11, 37083 Göttingen, Germany

Richard de Grijs

Department of Physics & Astronomy, University of Sheffield, Hicks Building, Hounsfield Road, Sheffield S3 7RH, UK

Abstract. Evolutionary synthesis models for star clusters of various metallicities, including gaseous emission during the lifetime of the ionizing stars, are used to model star cluster systems comprising two populations: an old metal-poor globular cluster (GC) population similar to that of the Milky Way halo, and a second GC population of arbitrary metallicity. We investigate the time evolution of color distributions and luminosity functions for the two GC populations and compare with observations of E/S0 galaxies. We show that multi-passband data for GC populations give clues to the relative ages and metallicities of the two subpopulations, and help constrain formation scenarios for their parent galaxies.

1. Motivation

GCs are among the oldest objects known, their ages being used to constrain the age of the Universe and the Hubble constant. HST detections of rich systems of bright, blue, young and compact star clusters in numerous interacting and star-burst galaxies came as a surprise raising the question if, and eventually how many of those young compact clusters could be progenitors of old GCs. This motivated us to calculate a new set of evolutionary synthesis models for the spectral and photometric evolution of star clusters from very young to very old ages, and extend them to star cluster systems – complemented by dynamical models for evolution, survival and destruction of clusters in galactic potentials.

2. Modeling Star Clusters and Star Cluster Systems

Our evolutionary synthesis models using Padova stellar isochrones, **including the thermal-pulsing AGB phase**, model atmosphere spectra, and gaseous emission (**lines and continuum**) for star clusters of different metallicities, provide the time evolution of spectra, luminosities (U, ..., K), M/L-ratios and colors in many filter systems. Including the TP-AGB phase is important for age-dating clusters on the basis of $V - I$ (Schulz et al. 2002). Gaseous emission gives important contributions to broad band fluxes (up to 65 %) at young ages ($\leq 6 - 20$ Myr, depending on metallicity) (Anders & Fritze - v. A. 2003). Theoretical calibration colors $\leftrightarrow$ [Fe/H] agree well with empirical calibrations for ~ 12 Gyr old Milky Way GCs with [Fe/H] ≤ -0.5, get significantly non-linear beyond

[Fe/H] $= -0.5$, and change completely for clusters younger than 12 Gyr.
The age-metallicity-extinction degeneracy – worst for optical colors, with optical-NIR colors giving better separation in metallicity and UV-optical colors better separation in extinction – requires a multi-wavelength analysis to disentangle individual star cluster properties. An ASTROVIRTEL project (PI R. de Grijs, CoIs UFvA, G. Gilmore) provides us with this kind of data. They are compared to a grid of model Spectral Energy Distributions for 5 metallicities, $-1.7 \leq$ [Fe/H] $\leq +0.4$, ages from 4 Myr through 14 Gyr, and extinction values $0 \leq \mathrm{E(B-V)} \leq 1$, by means of a dedicated analysis tool (Anders et al. 2003a) to yield individual cluster ages, metallicities, E(B−V), masses, and their 1 σ uncertainties (e.g. Anders et al. 2003b). Extensive tests with artificial clusters and varying numbers of filters show that: 1) *a priori* assumptions can be very misleading; 2) a long wavelength baseline and good photometric accuracy are essential, and 3) there are good and bad passband combinations: the U-band is important for ages, extinctions and metallicities of **young** clusters and the NIR for metallicities of **old** clusters (cf. Anders et al. *this volume*). Under the simplifying assumptions that a secondary GC population has comparable richness and intrinsic widths of its color distributions (=**CD**s) and luminosity functions (=**LF**s) to those of the uniform blue peak GC population in E/S0 galaxies or the Milky Way halo, we investigate for which combinations of age and metallicity the CDs and LFs show detectable bimodality and look similar to what is seen in E/S0 galaxies (Fritze - v. Alvensleben, *submitted*). We find that: 1) it is not clear *a priori* if the red peak GCs are older or more metal-rich than the blue peak clusters, and 2) many combinations (age/metallicity), ranging from (age = 13 Gyr, [Fe/H]= −0.4) through (age = 2.5 Gyr, [Fe/H]= +0.4), can explain the peak $\langle \mathrm{V-I} \rangle_{\mathrm{red}} = 1.2$ observed e.g. in NGC 4472, NGC 4486, NGC 4649 (Larsen et al. 2001) with, however, significantly different $\langle \mathrm{V-K} \rangle = 3.1$ for the former and $\langle \mathrm{V-K} \rangle = 3.6$ for the latter. Hence, K-band observations will tell the difference and give decisive clues to the galaxies' (violent) formation histories.

Acknowledgments. We gratefully acknowledge support by ASTROVIRTEL, funded by the European Commission under HPRI-CT-1999-00081.
UFvA & PA gratefully acknowledge partial travel support from IAU and DFG.

References

Anders, P., Fritze - v. Alvensleben, U., 2003, A&A, 401, 1063

Anders, P., Bissantz, N., Fritze - v. Alvensleben, U., de Grijs, R. 2003a, MNRAS, *in press*, astro-ph/0309356

Anders, P., de Grijs, R., Fritze - v. Alvensleben, U., Bissantz, N. 2003b, MNRAS, *in press*, astro-ph/0309153

Larsen, S. S. *et al.* 2001, AJ, 121, 2974

Schulz, J., Fritze - v. Alvensleben, U., Möller, C., Fricke, K. 2002, A&A, 392, 1

Highlights of Astronomy, Vol. 13
International Astronomical Union, 2003
O. Engvold, ed.

Stellar Population Models with Variable Element Abundance Ratios

Daniel Thomas, Claudia Maraston, Ralf Bender

MPE, Giessenbachstraße, 85748 Garching, Germany
Universitäts-Sternwarte, Scheinerstraße 1, 81679 München, Germany

Abstract. We present a comprehensive set of new generation stellar population models of Lick absorption line indices, which for the first time include element abundance ratios different from solar. We computed the 21 Lick indices CN_1, CN_2, Ca4227, G4300, Fe4383, Ca4455, Fe4531, $C_2$4668, Hβ, Fe5015, Mg_1, Mg_2, Mg_b, Fe5270, Fe5335, Fe5406, Fe5709, Fe5782, Na D, TiO_1, and TiO_2, in the wavelength range $4000 \lesssim \lambda \lesssim 6500$ Å. Models are provided with: $[\alpha/Fe] =$ 0.0, 0.3, 0.5, $[\alpha/Ca] = -0.1$, 0.0, 0.2, 0.5, and $[\alpha/N] = -0.5$, 0.0; ages from 1 to 15 Gyr; total metallicities from 1/200 to 3.5 solar ($-2.25 \leq [Z/H] \leq 0.67$).

The models are based on the evolutionary synthesis technique described in Maraston (1998). The α/Fe enhanced mixtures are obtained by increasing the abundances of α-group elements and by decreasing the abundances of the Fe-peak elements, such that total metallicity is conserved. The impact from these element abundance variations on the absorption line indices is taken from Tripicco & Bell (1995), using an extension of the method introduced by Trager et al. (2000). Most importantly, we take into account that the empirical stellar libraries used to compute model indices follow the chemical enrichment history of the Milky Way, and are therefore biased towards super-solar α/Fe ratios at sub-solar metallicities. We corrected for this bias, so that the models presented here have well-defined α/Fe ratios at all metallicities.

We take particular care at calibrating the models with galactic globular clusters, for which ages, metallicities, and element abundance ratios are known from independent sources. Our α/Fe enhanced models with $[\alpha/Fe] = 0.3$ (and 12 Gyr age) perfectly reproduce the positions of the globular cluster data in the Mg_1-$\langle$Fe$\rangle$ diagram up to solar metallicities (see also Maraston et al. 2003). The total metallicities for the sample clusters that we derive from these indices are in excellent agreement with the Zinn & West (1984) metallicity scale. We point out that the latter most likely reflects total metallicity rather than iron abundance, because it is obtained essentially by averaging the abundances derived from the Mg triplet near 5175 Å and the Fe blend at 5270 Å. This aspect needs to be emphasized, as with the α/Fe enhanced models we are now in the position to distinguish total metallicity [Z/H] and iron abundance [Fe/H].

By means of our calibrated α/Fe enhanced models, we confirm that the index [MgFe], suggested by González (1993) to balance α/Fe ratio effects, is almost independent of α/Fe. As it modestly decreases with increasing α/Fe, however, we define the slightly modified index $[\mathrm{MgFe}]' \equiv \sqrt{Mg_b\ (0.72 \cdot \mathrm{Fe5270} + 0.28 \cdot \mathrm{Fe5335})}$ which is completely independent of α/Fe, and hence an even better tracer of total metallicity. We further show that the linear correlation between Mg_2 and metallicity at old ages derived empirically by Brodie & Huchra (1990) is valid up to $\sim$1/3 solar metallicity, but underpredicts Mg_2 indices at metallicities above that threshold.

It turns out to be hard to find indices that correlate with α/Fe as well as the intensively studied indices Mg_1, Mg_2, and Mg_b. Promising alternatives are the blue indices CN_1 and CN_2 that also increase with increasing α/Fe ratio, mainly because of an anti-correlation with Fe abundance. With the caveat that CN_1 and CN_2 are additionally sensitive to C and Nabundances, they can be regarded to be complementary to the indices Mg_1, Mg_2, and Mg_b. Alternatives to the iron indices Fe5270 and Fe5335, the strengths of which decrease with increasing α/Fe ratio, are easier to find. The best cases are the indices Fe4383, Fe4531, Fe5015, and Fe5709.

The indices CN_1, CN_2, and Ca4227 of globular clusters are very interesting, particular cases. We find that the relatively strong CN features observed in globular clusters require models in which nitrogen is enhanced by a factor three relative to the α-elements, hence $[\alpha/N]$ = -0.5. This is in agreement with early suggestions by D'Antona (2003), that stars in globular clusters are nitrogen enriched by a previous generation of stars. The good calibration of other indices like Mg_1, Mg_b or $\langle Fe \rangle$ is not affected by a variation of the $[\alpha/N]$ ratio, as these indices are not sensitive to nitrogen abundance. We note that an enhancement of carbon abundance, instead, would lead to serious inconsistencies with Mg_1. Interestingly, also Ca4227 is sensitive to nitrogen abundance, and the globular cluster data of this index are also best reproduced by the model with increased nitrogen abundance.

To conclude, the stellar population models presented here make it possible, for the first time, to study in detail individual element abundance ratios of unresolved stellar populations (Thomas et al. 2003b). In particular, total metallicity is now a well-defined quantity.

The models are published in Thomas et al. (2003a). Tables are available electronically via anonymous ftp at `ftp.mpe.mpg.de` in the directory `people/dthomas/SSPs`. They are also available via WWW by going to `ftp://ftp.mpe.mpg.de/people/dthomas/SSPs`.

References

Brodie J., Huchra J., 1990, ApJ, 362, 503
D'Antona, F. 2003, this volume
Gonz'alez, J. J. 1993, PhD thesis, University of Santa Cruz
Maraston C. 1998, MNRAS, 300, 872
Maraston C., Greggio L., Renzini A. et al. 2002, A&A, 400, 823
Trager S. C., Faber S. M., Worthey G., González J. J. 2000, AJ, 119, 164
Tripicco M. J., Bell R. A. 1995, AJ, 110, 3035
Thomas, D., Maraston, C., Bender, R. 2003a, MNRAS, 339, 897
Thomas, D., Maraston, C., Bender, R. 2003b, MNRAS, 343, 279
Zinn R., West M. J. 1984, ApJS, 55, 45

Highlights of Astronomy, Vol. 13
International Astronomical Union, 2003
O. Engvold, ed.

Formation of Globular Clusters in Galaxy Mergers

Kenji Bekki, Warrick J. Couch

School of Physics, University of New South Wales, Sydney, NSW, 2052, Australia

Duncan A. Forbes and M. A. Beasley

Centre for Astrophysics & Supercomputing, Swinburne University of Technology, Hawthorn, VIC, 3122, Australia

Abstract. Our numerical simulations first demonstrate that the pressure of ISM in a major merger becomes so high ($> 10^5$ k_B K cm^{-3}) that GMCs in the merger can collapse to form globular clusters (GCs) within a few Myr. The star formation efficiency within a GMC in galaxy mergers can rise up from a few percent to $\sim$ 80 percent, depending on the shapes and the temperature of the GMC. This implosive GC formation due to external high pressure of warm/hot ISM can be more efficient in the tidal tails or the central regions of mergers. The developed clusters have King-like profiles with an effective radius of a few pc. The structural, kinematical, and chemical properties of these GC systems can depend on the orbital and chemical properties of major mergers.

1. Implosive formation of globular clusters

Several authors have suggested that very high pressure of ISM expected in major galaxy merging can be responsible for the rapid (triggered) collapse of GMCs and the subsequent GC formation (e.g., Elmegreen & Efremov 1997; Bekki et al. 2002). We numerically investigate the key questions on this GC formation scenario: whether or not the star formation efficiency within a GMC under such high pressure ISM can be as high as that (> 50 %, e.g., Hills 1980) required for the bound cluster formation. Figure 1 shows that the high pressure of the ISM can continue to strongly compress the cloud without losing a significant amount of gas from the cloud. As the strong compression proceeds, the internal density/pressure of the cloud can rise so significantly that a GC can form from the gas of a starburst (See the caption of Fig.1 for the detail of this).

References

Bekki, K., Forbes, D. A., Beasley, M. A., & Couch, W. J. 2002, MNRAS, 335, 1176 Elmegreen, B. G., & Efremov, Y. N., 1997, ApJ, 480, 235 Hills, J. G. 1980, ApJ, 235, 986

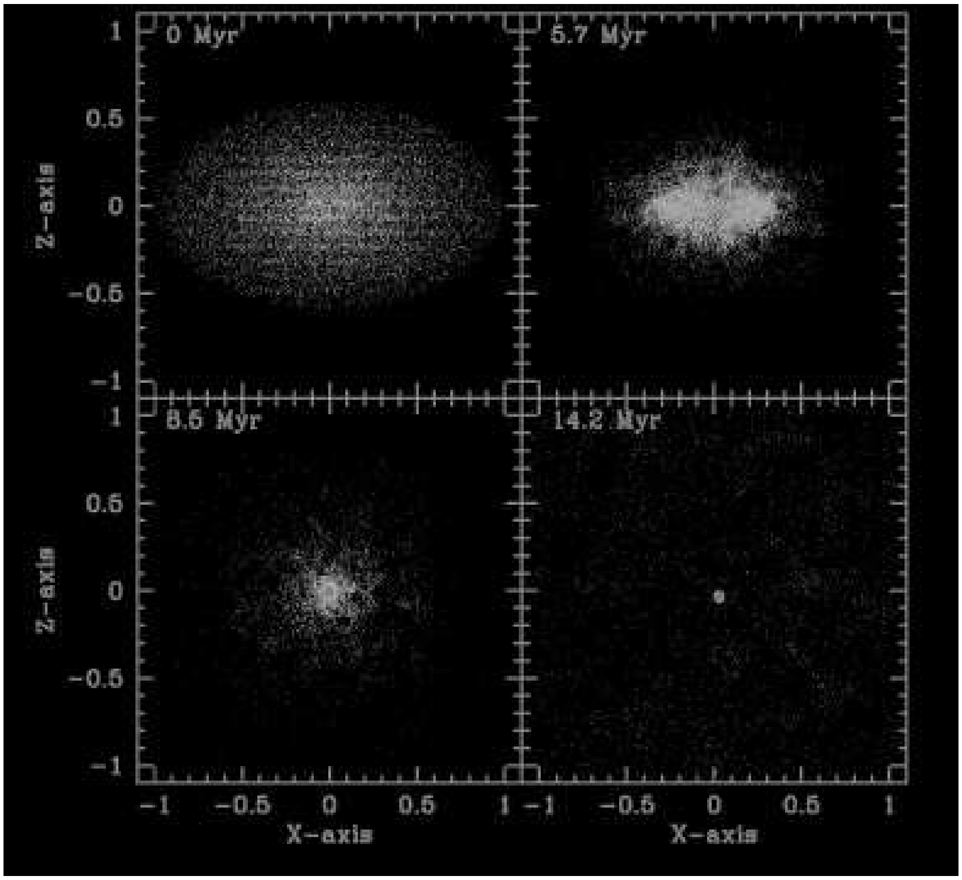

Figure 1. Time evolution of a GMC embedded by high pressure ISM for gaseous components (cyan) and for new stars formed from the gas (magenta). For clarity, the surrounding high pressure warm/hot ISM with $P \sim 10^5$ k_B K cm^{-3} is not shown. The mass and the size of the initial GMC is $10^6 M_\odot$ and 97 pc, respectively. The oblate shape of the cloud is assumed in this model (the long-to-short-axis-ratio is set to be 0.6). The initial sound velocity of the gas in GMC is $\sim$ 5 km s^{-1}, for which the GMC can not collapse owing to its self-gravity (if the surrounding ISM's density and pressure are as low as those observed in disk galaxies). One frame measures 200 pc on a side. Note that a very compact GC is formed owing to strong external compression of the GMC by the hot, high pressure ISM. About 80 % of the initial gas is converted into new stars within a few Myr so that the developed compact stellar system with the effective radius of a few pc can be strongly bounded even after the removal of the remaining gas. Due to the rapid, dissipative collapse, the gaseous density of the cloud dramatically rises and consequently star formation begins in the central regions of the cloud. The star formation rate increase significantly to 1.5 $M_\odot$ yr^{-1} (8 Myr after the start of the cloud's collapse). Because of the "implosive" formation of stars from strongly compressed gas, the developed stellar system is strongly self-gravitating and compact. This result implies that high external pressure from the ISM is likely to trigger the formation of bound, compact star clusters rather than unbound, diffuse field stars (astro-ph/0308263 for color version).

Highlights of Astronomy, Vol. 13
International Astronomical Union, 2003
O. Engvold, ed.

Dynamical Evolution of Globular Cluster Systems

E. Vesperini

Department of Physics and Astronomy, Michigan State University, East Lansing, MI, USA

Abstract. I present the results of a number of simulations of the dynamical evolution of globular cluster systems (GCS) in elliptical galaxies including the effects of two-body relaxation, dynamical friction, stellar evolution and the effects of the tidal field of the host galaxy. The results of detailed models for the evolution of the M87 GCS are also presented. A significant number of clusters are disrupted by evolutionary processes and the properties of many of the clusters which survive are effected by dynamical evolution. In spite of large differences in the efficiency of evolutionary processes in different galaxies, the final galaxy-to-galaxy variation of the GCS mean mass and its radial variation within individual galaxies in my simulations are small and consistent with observations. The effects of dissolution of low-concentration clusters due to mass loss through stellar evolution are also discussed and are shown to play an important role in the evolution of a power-law GCS mass function (GCMF), similar to that observed in young cluster systems in merging galaxies, towards a final GCMF with properties consistent with observations.

1. Introduction

A number of theoretical studies have shown that, due to the effects of two-body relaxation, tidal shocks, stellar evolution, the structure and the stellar content of globular clusters evolve and that, during the evolution, clusters lose mass and eventually dissolve (see e.g Meylan & Heggie 1997 for a review). Although many of the effects predicted by theoretical investigations of the dynamical evolution of globular clusters have been confirmed by observational studies, there are a number of observational findings concerning the global properties of GCS which are apparently in conflict with what one would expect if dynamical evolution played an important role in shaping the current GCS properties. In particular, observations show that the overall shape of the GCMF and the mean mass of clusters in galaxies with different structure are very similar to each other and that, within individual galaxies, the mean cluster mass does not significantly depend on the galacto-centric radius. Since the efficiency of evolutionary processes depends on the structure of the host galaxy and, within individual galaxies, on the distance from the center of the host galaxy, these observational findings have sometimes been interpreted as an indication that evolutionary processes did not play an important role in determining the properties of GCS. In order to explore this issue I have a carried out a large number of simulations to study the dynamical evolution of GCS in elliptical galaxies with different properties. I summarize below the main results concerning the GCMF evolution; further details can be found in Vesperini (2000), Vesperini (2001), Vesperini & Zepf (2003) and Vesperini et al. (2003).

2. Results

1) For a log-normal initial GCMF similar to that observed in old GCS, the final values of the mean mass and the galaxy-to-galaxy variation of the mean mass, from simulations of the evolution of GCS in elliptical galaxies with properties equal to those observed, are perfectly consistent with observations. In most galaxies dynamical evolution is important and evolutionary processes lead to the disruption of a significant fraction of the initial population of clusters. Although the efficiency of evolutionary processes and the fraction of surviving cluster depend on the properties of the host galaxy, the galaxy-to-galaxy variation of the final mean mass is small and consistent with observations. The radial variation of the final mean mass within individual galaxies is small and in agreement with observational data.
2) In simulations with a power-law initial GCMF, evolutionary processes transform the power-law GCMF into a bell-shaped GCMF similar to that of old GCS, but the final mean cluster masses are for most galaxies smaller than those observed, and the galaxy-to-galaxy-variation and the radial variation of the mean mass are large and not consistent with observations.
3) The results of detailed models for the evolution of the M87 GCS show that, for a power-law initial GCMF, the final values of the GCS mean mass and its radial variation are consistent with observations if a strongly anisotropic initial GCS velocity distribution is adopted, but the final kinematical properties of these models are characterized by a strong radial anisotropy inconsistent with observational kinematical data. A number of models starting with a bell-shaped (in $\log M$) initial GCMF similar to that of old GCS have final properties satisfying all the observational constraints available on the GCMF, the kinematics and the spatial distribution of the M87 GCS.
4) A number of simulations including a distribution of initial concentrations for individual clusters, and including the dissolution of low-concentration clusters induced by mass loss due to stellar evolution have been carried out. The results of these simulations show that dissolution of low-concentration clusters can significantly affect the initial number of clusters in a GCS, alter the initial GCMF, and play an important role in the evolution of a power-law initial GCMF towards a final GCMF with properties consistent with observations.

References

Meylan, G., & Heggie, D.C., 1997, A&A Rev., 8, 1

Vesperini, E. 2000, MNRAS, 318, 841

Vesperini, E. 2001, MNRAS, 322, 247

Vesperini, E., & Zepf, S. E., 2003, ApJ, 587, L97

Vesperini, E., Zepf, S. E., Kundu, A., & Ashman, K. M., 2003, ApJ, 593, 760

Highlights of Astronomy, Vol. 13
International Astronomical Union, 2003
O. Engvold, ed.

Multi-Color Observations of Young Star Clusters

Peter Anders, Uta Fritze - v. Alvensleben

Universitäts-Sternwarte Göttingen, Geismarlandstrasse 11, 37083 Göttingen, Germany

Richard de Grijs

Department of Physics & Astronomy, The University of Sheffield, Hicks Building, Hounsfield Road, Sheffield S3 7RH, UK

Abstract. We present a new set of evolutionary synthesis models of our GALEV code, specifically developed to include the gaseous emission of presently forming star clusters, in combination with an advanced tool to compare large model grids with multi-color broad-band observations of YSC systems. Tests and first applications are presented.

1. Models & Applications

We have further refined the Göttingen evolutionary synthesis code GALEV by including the effect of gaseous emission. The emission contributes significantly to the integrated light of stellar populations younger than 3×10^7 yr (Anders & Fritze - v. Alvensleben 2003). The updated models are available from **http://www.uni-sw.gwdg.de/~galev/panders/**.
The tool to compare large model grids with multi-color broad-band observations was tested extensively using artificial clusters (Anders et al. 2003a) and broad-band observations of star clusters in NGC 3310 (de Grijs et al. 2003a).
Here we focus on the dwarf starburst galaxy NGC 1569, in which we detect and analyze a sample of star clusters significantly larger than done before. Our derived cluster properties are consistent with literature values. We find a surprising dependence of the (cluster) mass function on cluster ages (Anders et al. 2003b).

2. References

Anders, P., Fritze - v. Alvensleben, U. 2003, A&A, 401, 1063
Anders, P., Bissantz, N., Fritze - v. Alvensleben, U., de Grijs, R. 2003a, MNRAS, *submitted*
Anders, P., de Grijs, R., Fritze - v. Alvensleben, U., Bissantz, N. 2003b, MNRAS, *submitted*
de Grijs, R., Fritze - v. Alvensleben, U., Anders, P., Gallagher, J. S., Bastian, N., Taylor, V. A., Windhorst, R. A. 2003a, MNRAS, 342, 259

Highlights of Astronomy, Vol. 13
International Astronomical Union, 2003
O. Engvold, ed.

Formation of ω Centauri from an Ancient Nucleated Dwarf Galaxy

Kenji Bekki

School of Physics, University of New South Wales, Sydney, NSW, 2052, Australia

K. C. Freeman

Mount Stromlo and Siding Spring Observatories, The Australian National University, Private Bag, P.O. Weston Creek, ACT 2611, Australia

Abstract. We present a self-consistent dynamical model in which ω Cen is formed from an ancient nucleated dwarf galaxy merging with the first generation of the Galactic thin disc in a retrograde manner with respect to the Galactic rotation. Our numerical simulations demonstrate that during merging between the Galaxy and the ω Cen's host dwarf with $M_{\rm B} \simeq -14$ mag and its nucleus mass of $10^7\ M_{\odot}$, the outer stellar envelope of the dwarf is nearly completely stripped whereas the central nucleus can survive from the tidal stripping because of its compactness. The developed naked nucleus is orbiting the young Galactic disc in a retrograde manner with its apocenter and pericenter distances of ~ 8 kpc and ~ 1 kpc, respectively, and thus have orbital properties similar to those of ω Cen. The Galactic tidal force can induce radial inflow of gas to the dwarf's center and consequently triggers moderately strong nuclear starbursts in a repetitive manner. This result implies that efficient nuclear chemical enrichment resulting from the later starbursts can be closely associated with the origin of the observed relatively young and metal-rich stars in ω Cen. Dynamical heating by the ω Cen's host can transform the young thin disc into the thick one during merging.

1. Prediction of dynamical and chemical properties of the Galactic stellar halo formed from the ω Cen host.

Since the details of the models and the results are given in Bekki & Freeman (2003), only one important model prediction is described here. We predict that if ω Cen was previously the nucleus of a nucleated dwarf galaxy with orbital parameters given by Bekki & Freeman (2003), the Galactic stellar halo stripped from the host shows crowding around $L_{\rm z} \sim -500$ and $L_{\rm xy} \sim 300$ kpc km s^{-1}, which reflects the orbital evolution of the dwarf. Here $L_{\rm z}$ represents angular momentum component in the z direction and $L_{\rm xy}$ is $(L_{\rm x}^2 + L_{\rm y}^2)^{1/2}$.

Highlights of Astronomy, Vol. 13
International Astronomical Union, 2003
O. Engvold, ed.

Dynamical Evolution of Globular Cluster Systems in Clusters of Galaxies: The Case of NGC 1404 in the Fornax Cluster

Kenji Bekki, Warrick J. Couch

School of Physics, University of New South Wales, Sydney, NSW, 2052, Australia

Duncan A. Forbes and M. A. Beasley

Centre for Astrophysics & Supercomputing, Swinburne University of Technology, Hawthorn, VIC, 3122, Australia

Abstract. We investigate, via numerical simulations, the tidal stripping and accretion of globular clusters (GCs). In particular, we focus on creating models that simulate the situation for the GC systems of NGC 1404 and NGC 1399 in the Fornax cluster, which have poor (specific frequency $S_{\rm N} \sim 2$) and rich ($S_{\rm N} \sim 10$) GC systems respectively. We initially assign NGC 1404 in our simulation a typical $S_{\rm N}$ (~ 5) for cluster ellipticals, and find that its GC system can only be reduced through stripping to the presently observed value, if its orbit is highly eccentric (with orbital eccentricity of > 0.5) and if the initial scale length of the GCs system is about twice as large as the effective radius of NGC 1404 itself. These stripped GCs can be said to have formed a 'tidal stream' of intra-cluster globular clusters (ICGCs) orbiting the center of Fornax cluster (many of which would be assigned to NGC 1399 in an imaging study). The physical properties of these GCs (e.g., number, radial distribution, and kinematics) depend on the orbit and initial distribution of GCs in NGC 1404. Our simulations also predict a trend for $S_{\rm N}$ to rise with increasing cluster-centric distance - a trend for which there is some observational support in the Fornax cluster. We demonstrate that since the kinematical properties of ICGCs formed by tidal stripping in the cluster tidal field depend strongly on the orbits of their previous host galaxies, observations of ICGC kinematics provides a new method for probing galaxy dynamics in a cluster.

1. Observable evidence for the tidal stripping scenario for low $S_{\rm N}$ cluster ellipticals

We suggest that the following three are the observable evidences: First is *the ratio of* $S_{\rm N}$ *within* $1 - 2R_{\rm e}$ *to that within 5–10* $R_{\rm e}$. The second is the formation of an elongated or flattened distribution (or "tidal stream") of ICGCs along the orbit of their previous host galaxy. The third is the statistical correlation between the distance of an elliptical galaxy from the center of a cluster and the $S_{\rm N}$ of the galaxy (more details are given by Bekki et al. 2003 MNRAS accepted).

Highlights of Astronomy, Vol. 13
International Astronomical Union, 2003
O. Engvold, ed.

Formation of Star Clusters in the LMC and SMC

Kenji Bekki, Warrick J. Couch

School of Physics, University of New South Wales, Sydney, NSW, 2052, Australia

Duncan A. Forbes and M. A. Beasley

Centre for Astrophysics & Supercomputing, Swinburne University of Technology, Hawthorn, VIC, 3122, Australia

Abstract. We demonstrate that single and binary star clusters can be formed during cloud-cloud collisions triggered by the tidal interaction between the Large and Small Magellanic clouds. We run two different sets of self-consistent numerical simulations which show that compact, bound star clusters can be formed within the centers of two colliding clouds due to strong gaseous shocks, compression, and dissipation, providing the clouds have moderately large relative velocities ($10 - 60$ km s^{-1}). The impact parameter determines whether the two colliding clouds become a single or a binary cluster. The star formation efficiency in the colliding clouds is dependent upon the initial ratio of the relative velocity of the clouds to the sound speed of the gas. Based on these results, we discuss the observed larger fraction of binary clusters, and star clusters with high ellipticity, in the Magellanic clouds.

1. Young GC formation in colliding gas clouds.

The details of numerical methods and models for GC formation in colliding gas clouds are given by Bekki et al. (2003, submitted to ApJ), therefore we here describe the results briefly. Strong gas compression and dissipation during the collision leads to an elongated slab-like structure formed at around $T = 17.1$ Myr, where T represents the time elapsed since the two clouds began to collide. As the dissipative merging proceeds, the density of gas becomes very high in the shocked regions which are originally the central regions of the two clouds ($T = 22.8$ Myr). Two compact clusters are formed in these high-density gas regions and begin to orbit each other ($T = 22.8$ Myr). This result implies that the orbital angular momentum of the two gas clouds is efficiently converted into that of the binary star clusters during the dissipative cloud-cloud collision. The star formation is akin to an instantaneous "starburst" with a maximum star formation rate of 0.095 $M_{\odot}$ yr^{-1}, and 40 % of the gas is converted into stars within 10 Myr. We do not observe any new stellar particles escaping from the parent clouds because they are initially in the deepest potential well (i.e., the center of the clouds). Thus a single star cluster with a very smooth and homogeneous mass distribution would finally form.

Highlights of Astronomy, Vol. 13
International Astronomical Union, 2003
O. Engvold, ed.

2dF Spectroscopy of Globular Clusters in M104

Terry Bridges, Steve Zepf, Katherine Rhode, Ken Freeman

Anglo-Australian Observatory; Michigan State University; Yale University; Australian National University

Abstract. We have found 56 new globular clusters in M104 from 2dF multi-fiber spectroscopy, doubling the number of confirmed clusters, and extending the spatial coverage to 50 kpc radius. We find no significant rotation in the total sample, or for subsets split by color or radius. However, there are hints that the blue clusters have a higher rotation than the red clusters, and for counter-rotation of clusters at large radius. We find a total mass of M $\sim 1\times10^{12}$M$_\odot$ and a (M/L)$_B$ =30 out to 50 kpc radius, which is strong evidence for a dark matter halo in M104.

1. Data

Globular cluster (GC) candidates were selected from KPNO mosaic BVR imaging (Rhode & Zepf 2003, in preparation). We obtained a sample of 585 candidates with $19 < V < 21.5$, after color cuts and image classification. In April 2002, we used the 2dF multi-fiber spectrograph on the AAT to obtain spectra for 200 candidates, which yielded 56 confirmed GCs.

2. Globular Cluster Kinematics and Dark Matter in M104

The velocity dispersion of the total sample is $\sim$ 200 km/s, with no significant difference between the blue and red GCs. A smoothed velocity dispersion profile shows that σ decreases from $\sim$ 225 km/s near the galaxy center to $\sim$ 125 km/s at 50 kpc radius.

The smoothed velocity profile shows rotation of $\sim$ 50 kpc; this is not statistically significant, however, and we place a 95% upper limit on rotation of 110 km/s for the total sample. We have looked for rotation amongst the blue and red GCs separately, and also for GCs at small and large radius (separated at $10'$= 25 kpc). There is no significant rotation for any subsample. However, there are hints that the blue GCs have higher rotation than the red GCs, and that there is more rotation at large radius. Interestingly, the GCs at large radius may be counter-rotating with respect to the GCs and stars at smaller radius, but again this is not significant.

We have used the Projected Mass Estimator, assuming isotropic orbits, to find a total mass of 1.2×10^{12} M$_\odot$ and a (M/L)$_B$ = 30 at 50 kpc radius. This is strong evidence for a dark matter halo in M104.

A fuller account of this work may be found in Bridges et al. (2003).

Highlights of Astronomy, Vol. 13
International Astronomical Union, 2003
O. Engvold, ed.

Abundances in LMC and SMC Globular Clusters

Jennifer A. Johnson

DAO/HIA/NRC, 5071 West Saanich Road, Victoria, BC, V9E 2E7, Canada

Inese I. Ivans

California Institute of Technology, MS 105-24,,Pasadena, CA, 91125, USA

Peter B. Stetson and James E. Hesser

DAO/HIA/NRC, 5071 West Saanich Road, Victoria, BC, V9E 2E7, Canada

Michael Bolte

UCO/Lick Observatory, University of California, Santa Cruz, CA 95064, USA

Abstract. We present results for abundances in four old Magellanic Cloud clusters based on high-resolution spectroscopy of individual giants.

1. Abundances

We present abundances for four old LMC and SMC clusters based on high-resolution spectra of 2-3 red giants per cluster taken with the Magellan telescope. We find that in the two clusters close to the LMC bar, NGC 1898 and NGC 2019, the [Si/Fe] ratio is enhanced by ~ 0.5 dex relative to solar, while [Ca/Fe] and [Ti/Fe] are between 0 and 0.2 dex, similar to what is seen in the inner halo Milky Way clusters. In contrast, [Ca/Fe] is 0.3 dex in the outer LMC cluster Hodge 11 and and the SMC cluster NGC 121, which is the canonical value for the old outer halo Milky Way clusters. The [Fe/H] values found are in good agreement with those previously derived from the slopes of the red giant branches. Finally, the [Fe/H] and [α/Fe] ratios are compared to the results from integrated spectra of these clusters.

Highlights of Astronomy, Vol. 13
International Astronomical Union, 2003
O. Engvold, ed.

Perhaps They are not Globular Clusters After All

A. M. Karick

School of Physics, University of Melbourne, Victoria 3010, Australia

Abstract. Our 2dF Fornax Cluster Spectroscopic Survey (FCSS) and follow-up work in the Virgo Cluster have shown that the cores of both galaxy clusters contain a previously-unknown class of object, ultra-compact dwarf (UCD) galaxies. We present high resolution spectroscopy and deep multicolor imaging to show that these enigmatic objects are dynamically distinct from both globular clusters (GCs) and nucleated dwarf galaxies (dE,Ns). Our hypothesis for their origin may explain the observed high "specific frequency" of GCs in central cluster galaxies.

1. Dynamical Analysis and Stellar Populations

Internal velocity dispersions of the UCDs and a comparison dE,N (FCC303) have been measured using the VLT and Keck Telescopes (Drinkwater et al.2003). The velocity dispersions of the UCDs range from 24 to 37 km s^{-1}, considerably higher than those of Galactic GCs. The UCDs lie well off the globular cluster $L \propto \sigma^{1.7}$ relation in a previously unoccupied region. This supports the "galaxy threshing" model in which the UCDs are the remnant nuclei of infalling dE,Ns which have been tidally disrupted by the cluster cD galaxy (Bekki et al. 2001). Removing the halo of the dE,N galaxy reduces the total luminosity by about a factor of 100 but barely changes the central velocity dispersion. We obtained deep multicolour imaging (u,g,r,i) of the core of the Fornax Cluster taken with the CTIO MOSAIC camera. The colours of the UCDs were compared with a sample of NGC 1399 globulars (Mieske et al. 2003) and the nuclei of cluster dE,Ns. Preliminary analysis suggests that the UCDs have colours similar to the nuclei of the brightest dE,Ns and GCs.

Acknowledgements
This work was done in collaboration with M. J. Drinkwater, M. D. Gregg and M. Hilker.

References

Bekki, K., Couch, W.J., Drinkwater, M. J., 2001, ApJ, 552, L105

Drinkwater, M. J., Gregg, M. D., Hilker, M., Bekki, K., Couch, W. J., Ferguson, H. C., Jones, J. B., Phillipps, S., 2003, Natur, 423, 519

Mieske, S. Hilker, M. Infante, L., 2002, A&A, 383, 823

Highlights of Astronomy, Vol. 13
International Astronomical Union, 2003
O. Engvold, ed.

Self-Induced Formation of Metal-Rich Globulars in Bulges?

Valery V. Kravtsov

Sternberg Astronomical Institute, Universitetski pr. 13, Moscow, 119992, Russia

Abstract. Taken together, the latest key observations assume that (i) **old** metal-rich globular cluster populations (MRGCPs) in bulges were able to form due to an increased self-induced star formation rate (SFR) in their host galaxies, while galaxy merging played an additional role; (ii) massive star cluster populations (MSCPs) in irregulars may be young, less prominent counterparts of the old MRGCPs in spheroids.

1. Formation of MRGCPs in sheroids and MSCPs in irregulars

Data on high redshift galaxies and QSOs, super-massive black holes, redshift evolution of QSO emissivity, elemental abundances, etc. assume that more massive spheroids have shorter formation time scales (e.g., Granato et al. 2001). The metallicity distribution functions (MDFs) for the disk stars of the LMC and for the old red giants in the halos of the elliptical NGC 5128 and spiral M31 are virtually identical (Harris & Harris 2001). Surprisingly, the most probable metallicities of the MSCPs in the LMC and other irregulars lie between $0.004 < z < 0.008$ (as do metallicities of MRGCPs and metal-rich components of the MDFs), irrespective of the presence or absence of signs of interaction (Billett et al. 2002; de Grijs et al. 2003, among others). In addition, for a sample of BCD galaxies Hopkins et al. (2002) find a positive correlation between galaxy metallicity (oxygen abundance) and SFR. These findings imply that the formation of both the MRGCPs in spheroids and MSCPs in irregulars may be preferentially related to a certain stage of the host's (chemical?) evolution, during which there is an increase in the host galaxy SFR.

Acknowledgments. Many thanks are due to the organizers and the IAU for a travel grant, without which my attendance at the GA would have been impossible.

References

Billett, O. H., Hunter, D. A., & Elmegreen, B. G. 2002, AJ, 123, 454
de Grijs, R. et al. 2003, MNRAS, 343, 1285
Granato, G. L. et al. 2001, MNRAS, 324, 757
Harris, W. E., & Harris, G. L. H. 2001, AJ, 122, 3065
Hopkins, A. M., Schulte-Ladbeck, R. E., & Drozdovsky, I. O. 2002, AJ, 124, 862

Highlights of Astronomy, Vol. 13
International Astronomical Union, 2003
O. Engvold, ed.

The Spectra of Bright Near-IR Clusters in M82

A. Lançon[(1)], M. Mouhcine[(1)], E. Chané[(1)], L.J. Smith[(2)], J.S. Gallagher[(3)], N. Förster Schreiber[(4)], W. Vacca[(5)], R. de Grijs[(6)], R.W. O'Connell[(7)]

(1) Observatoire de Strasbourg (UMR 7550), France; (2) University College London, UK; (3) University of Maddison, Wisconsin, USA; (4) Leiden University, The Netherlands; (5) NASA Ames Research Centre, USA; (6) Sheffield University, UK; (7) University of Virginia, USA

Abstract. Based on new spectra spanning wavelengths from 0.8 to 2.4 μm, we study the properties of bright near-IR clusters in M82. We focus on age and extinction, which are critical parameters when one uses dynamical masses to constrain the stellar IMF. The modelling of red supergiant evolution by various authors leads to very significant differences in synthetic cluster spectra. Near-IR fluxes alone therefore do not rule out a normal IMF for cluster F, previously found to be deficient in low mass stars. Combined optical and near-IR studies are being undertaken.

The spectra of four bright near-IR clusters and of the nucleus of M82 were obtained with SpeX on IRTF (NASA/Hawaii). Synthetic spectra of cluster populations were constructed using the evolutionary tracks of the Padova group, a standard IMF, and the BaSeL library of stellar spectra, into which new SpeX supergiant spectra were inserted. Note that at solar metallicity the $T_{\rm eff}$ distribution of the red supergiants populating the Padova isochrones peaks around 3900 K (M stars contribute relatively little), while the predominant $T_{\rm eff}$ is cooler with the tracks of the Geneva group (at least for a range of ages). Tracks including rotation are different again.

We built χ^2-maps in age-extinction space for all targets and find that:
(1) all targets are dominated by red supergiants, including cluster F and the previously overlooked cluster observed in the Eastern "fossil starburst" region;
(2) with the Padova tracks, age discrimination is strong between 5 and 10 Myr, but weak between 12 and 60 Myr; for cluster F, our best fit is at 10 Myr with A_V=1.9, which would make the dynamical mass of Smith & Gallagher (2001, MNRAS 326, 1027) consistent with a normal IMF; their age of $\sim$60 Myr is however not excluded;
(3) estimated ages depend strongly on the assumed metallicity and stellar rotation; work with a variety of tracks is necessary.
More robust constraints on age, intrinsic luminosity and thus the IMF will be obtained by using optical and near-IR spectra jointly. This will also constrain red supergiant evolution models.

Highlights of Astronomy, Vol. 13
International Astronomical Union, 2003
O. Engvold, ed.

Evolution of Globular Cluster Populations in Compact Galaxy Groups

S. Leon, J. Perea, A. Del Olmo

Instituto de Astrofísica de Andalucía (CSIC), Granada, Spain

E. Athanassoula

Observatoire de Marseille, Marseille, France

G. Bergond

MSU Physics and Astronomy Dept.,Lansing , USA

G. Meylan

Space Telescope Science institute, Baltimore, USA

C. Garcia Gomez

Universitat Rovira i Virgili, Tarragona, Spain

Abstract. The redistribution of globular clusters within compact groups of galaxies is followed through N-body simulations. Particular emphasis is given to the globular clusters released in the Intra-Group Medium (IGM) and to the final configuration of the evolution.

1. Simulations and Results

We follow the evolution of the GCs in compact groups with 5 Milky Way-like galaxies. The simulations have been done on a PC cluster using the GADGET code. The different runs have the same initial spatial distribution, and only the individual galaxy velocities are changed with increasing virial (2T/V) parameter. The GCs are distributed according to a radial density profile which fits the Galactic population (Djorgovski & Meylan, 1994). Up to 50% of the initial GC population is lost by the host galaxies after few Gyrs. The GCs loss is sensitive to the initial GC concentration. The final radial distribution of GCs is flatter than the initial one with a drop of the radial slope of 0.2-0.4 for the galaxies that merge, whereas for interacting galaxies the radial distribution can become slightly steeper. The specific frequency SN in most of the runs is decreasing down by 20 % at the most. An important population of GCs is released in the IGM: 200-550 GCs are populating the IGM, with an extension to 200-300 kpc from the center of the group. The distribution of GCs is similar to what is found in the particular case of HCG90, with tidal tails and following the diffuse emission distribution.

Highlights of Astronomy, Vol. 13
International Astronomical Union, 2003
O. Engvold, ed.

Globular Cluster Formation in Galaxy Mergers

Yuexing Li[1,2], Mordecai-Mark Mac Low[2,1], and Ralf S. Klessen[3]

[1]*Columbia Univ, NY;* [2]*AMNH, NY, USA;* [3]*AIP, Potsdam, Germany*

Abstract. We present preliminary results of a high resolution simulation of globular cluster formation in a galaxy merger using GADGET (Springel et al. 2001). A barotropic equation of state (Li et al 2003) is implemented to include effects of cooling and heating. After one orbital period, a dozen proto-globular clusters are identified in the tidal tails.

1. Simulation

We simulate an equal-mass, head-on merger of two identical disk galaxies moving on parabolic orbits. Each galaxy has a dark matter halo, a stellar disk, and a gas disk (Springel 2000) . The mass of the galaxy is $M_{200} = 3 \times 10^{10} M_{\odot}$, of which gas is 10%. The total particle number is $N_{tot} = 1.4 \times 10^5$, the mass resolution is $2.3 \times 10^6 M_{\odot}$, and the spatial resolution is 1 pc.

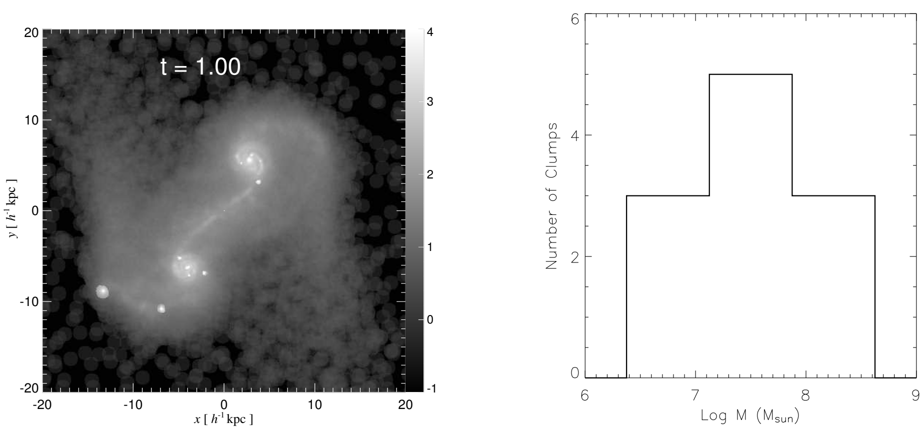

Figure 1. Proto-globular clusters identified in tidal tails and bridges, and their mass histogram derived with a clump-finding algorithm.

Acknowledgments. We acknowledge support from V. Springel, Kade Fellowship, NSF AST99-85392, NASA NAG5-13028, and the Emmy Noether of Deutsche Forschungsgemeinschaft (KL1358/1).

References

Li, Y., Klessen, R., & Mac Low, M-M, 2003, ApJ, 592, 975
Springel, V., Yoshida N. & White, S. 2001, New Astronomy 6, 79
Springel, V. 2000, MNRAS 312, 859

Highlights of Astronomy, Vol. 13
International Astronomical Union, 2003
O. Engvold, ed.

Multicolor Photometry and Age Estimates of Globular Clusters in M31

Jun Ma

National Astronomical Observatories, Chinese Academy of Sciences, Beijing, 100012, P. R. China

Abstract. We present CCD multicolor photometry for 172 globular clusters (GCs), taken from the Bologna catalog (Battistini et al. 1987), in the nearby spiral galaxy M31. The observations were performed by using the National Astronomical Observatories 60/90 cm Schmidt Telescope in 13 intermediate-band filters, which covered a range of wavelength from 3800 to 10000 Å. This provides a multicolor map of M31 in pixels of 1.7×1.7 arcminutes. By aperture photometry, we obtain the spectral energy distributions (SEDs) for these GCs. Using the relationship between the Beijing-Arizona-Taiwan-Connecticut (BATC) intermediate-band system used for the observations and the UBVRI broad-band system, the magnitudes in the B and V bands are derived. The computed V and B–V are in agreement with the values given by Battistini et al. (1987) and Barmby et al. (2000). Finally, by comparing the photometry of each GC with theoretical stellar population synthesis models of Bruzual & Charlot (1996, hereafter BC96), we estimate ages of the sample GCs for different metallicities. The BC96 models provide the evolution in time of the spectrophotometric properties of simple stellar populations for a wide range of stellar metallicity. The results show that nearly all our sample GCs have ages more than 10^9 years, and most of them are around 10^{10} years old. At the same time, we find that GCs fitted by the metal-poor model are generally older than ones fitted by the metal-rich model.

Acknowledgments. This work has been supported by the National Key Basic Research Science Foundation (NKBRSF TG199075402).

References

Barmby, P., & Huchra, J. P. 2000, ApJ, 531, 29

Battistini, P., Bònoli, F., Braccesi, A., Federici, L., Fusi Pecci F., Marano, B., & Börngen, F. 1987, A&AS, 67, 447

Bruzual, A. G., & Charlot, S. 1996, unpublished

Highlights of Astronomy, Vol. 13
International Astronomical Union, 2003
O. Engvold, ed.

Search for Formation Criteria of Globular Cluster Systems

S.N.Nuritdinov[1,2], K.T.Mirtadjieva[1,2] and I.U.Tadjibaev[1]

[1] *National University of Uzbekistan, Tashkent 700174, Uzbekistan*
[2] *Ulugh Beg Astronomical Institute, Tashkent 700052, Uzbekistan*

The research of early evolution stages and formation of galaxies requires creation of appropriate non-linear theory. The formation process of globular cluster systems (GCS) covers the long period of time as probably one begins from a dark matter state. So far it is difficult to simulate formation of GCS and galaxies ab initio. That's why it is necessary to construct exact analytically solvable models of non-linear non-stationary early stages of evolution of self-gravitating systems and revealing the instabilities on a background of non-equilibrium states. The formation and evolution of GCS at early stage of collapsing dark matter (or protogalaxy) can be explained by instability of the modes of the high oscillation degrees (Nuritdinov et al., 2000), which corresponds to rather small-scale perturbations of the density of collapsing system. The mode degree defines on the average the number of clusters. We study of the mode behavior of oscillations of high degrees, solving the non-stationary dispersion equation (NDE), for example,

$$(1+\lambda cos\psi)\frac{d^2\gamma_\tau}{d\psi^2}+\lambda\sin\psi\frac{d\gamma_\tau}{d\psi}+\gamma_\tau=(1+\lambda cos\psi)^3(\lambda+cos\psi)^{N-\tau}\cdot\sin^{\tau-1}\psi A(\psi)$$

at $N >> 1$, where $\lambda = 1-(2T/|U|)_0$, $(2T/|U|)_0$ is the virial ratio at $\psi = 0$ and $A(\psi)$ is unknown function of time.

Searching for an exact formation criteria of the GCS demands finding an exact asymptotic of the NDE. Using the asymptotic for the Legandre function $P_N(e)$ at $N >> 1$ we found a numerical solution of the NDE.

We have concluded:

- GCS formation takes place in the background of collapsing dark matter only for very special conditions of $(2T/|U|)_0 << 1$.

- In spite of the fact that the modes of high degree are small- scale in comparison of the ellipsoidal mode $(2;2)$, their maximal increments are close in many cases.

- At very large values of N the instability increment is decreased.

- The analysis of special cases of the NDE shows that it is necessary to find an exact asymptotic in the case $N \to \infty$ taking into account the rotation effect.

Highlights of Astronomy, Vol. 13
International Astronomical Union, 2003
O. Engvold, ed.

Young Stellar Clusters in the ULIRG IRAS 17208-0014

Naveen A. Reddy, Shardha Jogee, & Nick Scoville

Caltech MS 105-24, Pasadena, CA 91125

Abstract. High resolution studies reveal that luminous young stellar clusters and their associations are ubiquitous within 1 kpc of ULIRGs, and could be the precursors to globular clusters. We have undertaken a study of the ages, masses, extinction, and dust properties of the clusters found in the brightest ULIRG in the extended IRAS BGS Sample, IRAS 17208−0014, using it as a unique system in which to study the formation and evolution of clusters in gas-rich mergers. Using NICMOS *JHK* and WFPC2 *I*−band images, we have compared the near-IR colors of the clusters with those expected from a Bruzual & Charlot model. There are a few clusters whose colors can be explained by moderate values of extinction $(1-3 \text{ mag})$, but others require some contribution from hot $(400-1000 \text{ K})$ dust. We derive ages of a few tens of Myr and masses from 10^6 to 10^7 $M_\odot$. These clusters may be supermassive compared to globular clusters, or could be unresolved associations of clusters.

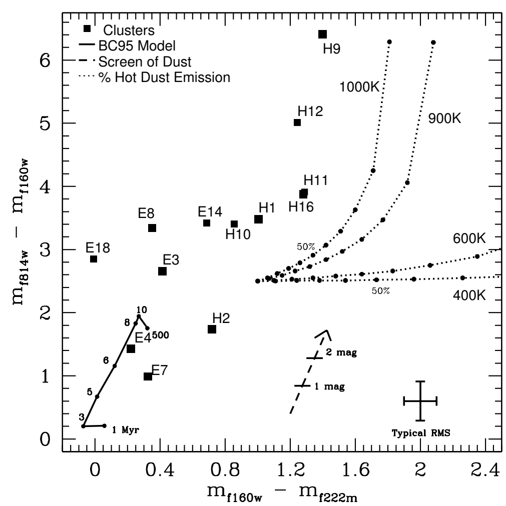

Figure 1. Color-color diagram showing the cluster colors, those which can be ascribed to extinction alone (prefixed by E), and those which may require a contribution from hot dust (prefixed by H). Also shown are curves corresponding to various dust temperatures, a reddening vector, and the Bruzual & Charlot model colors for a stellar population evolving from an instantaneous burst of star formation.

Highlights of Astronomy, Vol. 13
International Astronomical Union, 2003
O. Engvold, ed.

SUBARU/FOCAS Globular Clusters Survey around M82

Yoshihiko Saito, Masanori Iye, Nobunari Kashikawa, Koji S. Kawabata

National Astronomical Observatory Japan (NAOJ), 2-21-1, Osawa, Mitaka, Tokyo, 181-8588 Japan

Michitoshi Yoshida

Okayama Astrophysical Observatory, NAOJ, Kamogata, Okayama, 719-0232 Japan

Youichi Ohyama, Toshiyuki Sasaki, Tadafumi Takata, George Kosugi, Kentaro Aoki

Subaru Telescope, NAOJ, 650 North A'ohoku Place, Hilo, Hawaii, 96720 USA

1. Motivation

Recently, a number of possible young globular clusters (GCs) have been found in some merging/interacting galaxies or starburst galaxies. On the other hand, it is well known that GCs are numerous in giant elliptical galaxies many of which are thought to be formed via major merger of galaxies. These facts lead us to a thought that the formation process of GCs could accompany galaxy – galaxy interaction followed by starburst. The archetypical starburst galaxy M82 is an ideal target to study the relation between galaxy interaction, starburst, and GC formation.

2. Summary

We carried out search of GCs in M82, by taking advantage of high-resolution imaging and deep spectroscopic capabilities provided by FOCAS on the Subaru telescope. We applied a scheme for searching for GCs in disk/irregular galaxies that combines color selection, spectral analysis, and profile analysis for identifying GCs. Especially, the profile analysis is a key method for this scheme. We cannot identify GCs only from color selection and spectral analysis around nearby galaxies having low receding velocity, because we cannot distinguish late-F – early-G type stars in our Galaxy from those GCs. In the central 6 arc-minutes diameter region of M82, we found two bona fide GCs and 8 young GC candidates in our first attempt at searching for GCs in M82. The estimated total number of bona fide GCs is about 10 corresponding to the expected number from the initial luminosity of M82. We conclude that M82 has a GC system similar to our Galactic specific frequency before the interaction, and newly born GCs should be formed by the tidal interaction with M81.

Highlights of Astronomy, Vol. 13
International Astronomical Union, 2003
O. Engvold, ed.

Chemical Abundances in the Sagittarius Galaxy: Terzan 7

Gražina Tautvaišienė

Vilnius University Institute of Theoretical Physics and Astronomy, Gostauto 12, Vilnius 2600, Lithuania

George Wallerstein

University of Washington, Box 351580, Seattle, WA 98195-1580

Doug Geisler

Universidad de Concepción, Casillo 160-C, Concepción, Chile

Guillermo Gonzalez

Iowa State University, Ames, IA 50011

Corinne Charbonnel

Geneva Observatory, CH-1290 Sauverny, Switzerland

Abstract. Abundances of 21 chemical elements have been determined in three red giants in Terzan 7 using high-resolution spectra obtained with the UVES spectrograph on the ESO 8.2 m Kueyen telescope. The mean [Fe/H]$= -0.61 \pm 0.07$. The relative elemental abundance ratios indicate a close similarity of Terzan 7 to its host galaxy.

1. Comparison of Terzan 7 with the Sagittarius system

We have found that 3 red giants in Terzan 7 (S16, S34 and S35) have a mean [Fe/H]$= -0.61 \pm 0.07$(s.d.) and a corresponding age of about 6 Gyr. At a given metallicity the stars exhibit lower [α/Fe]$= 0.08 \pm 0.04$ ratios than stars in the Milky Way galaxy. The mean ratio [O/Fe]$= 0.24$ shows that the stars have not suffered from the oxygen deficiency. The mean values of [Na/Fe]$= -0.15$ and [Al/Fe]$= -0.14$ present no evidence for the Na and Al excesses. Within the iron-group and for light *s*-process species Y and Zr we see no significant departures from the solar ratios. The heavier *s*-process elements Ba, La, and Ce show an excess of 0.32 dex while the almost pure *r*-process element Eu shows an excess of 0.53 dex. The similarity of relative abundances in Terzan 7 and stars of the same metallicity in its host galaxy indicates that this cluster could be a natural product of galactic evolution. Obviously some galaxies are capable of forming globular clusters after the initial burst of star cluster formation. The chemical evolution of the Sagittarius dwarf spheroidal galaxy looks very similar to the evolution of the Large Magellanic Cloud.

JD7

The Sun & the Heliosphere as an Integrated System

Chairpersons: G. Poletto and S.T. Suess

Editors: G. Poletto (Chief-Editor) and S.T. Suess

Highlights of Astronomy, Vol. 13
International Astronomical Union, 2003
O. Engvold, ed.

JD 7: The Sun and the Heliosphere as an Integrated System

Giannina Poletto

INAF - Arcetri Astrophysical Observatory, Largo Fermi, 5, 50125 Firenze, Italy

Steven T. Suess

NASA-MSFC, MS SD50, Huntsville, AL 35812, USA

Abstract. We summarize here the oral contributions given at the Joint Discussion (JD) 7 *The Sun and the Heliosphere as an Integrated System*, held on July 17, 2003, in Sydney, as part of IAU XXV and give a list of posters presented at the JD.

1. Introduction

As knowledge of the Sun and the heliosphere grows, it is becoming not only possible but preferable to view the global structure, the interaction with the local interstellar medium, and changes over a solar cycle as the behavior of an integrated system. This consideration motivated Joint Discussion 7, which was meant both to summarize the state of art at the time of IAU *XXV* and to solicit interest in this kind of approach. The Joint Discussion was arranged in four sections, two on processes that, beginning from the Sun's interior, model and shape the heliosphere (*From the Transition Region to the Corona and Beyond* and *From the Sun to the Interstellar Medium*), one on elemental abundances and particles in the corona and the heliosphere (*Energetic Particles, Energetic Neutral Atoms and Composition*) and one on forthcoming solar and heliospheric space missions. In the following we give a brief summary of the contributions presented at the JD in each section. An extended discussion of the topics covered by JD is expected to appear in a comprehensive book on the Sun and the Heliosphere which will be edited by us and printed by Kluwer in year 2004. Posters which were exhibited as part of the Joint Discussion are listed at the end of this summary.

2. Program

2.1. Scientific Program

Session I: From the Sun to the Interstellar Medium	
Chair: H. Cane	*Invited Speaker*
Ulysses at Solar Maximum: Selected Highlights	R. Marsden
Hydrogen Walls: Mass Loss of Dwarf Stars and the Young Sun	J. L. Linsky, B. E. Wood, and G. P. Zank
Radio Emission from the Outer Heliosphere and Beyond	I. Cairns
MHD Turbulence in the Heliosphere	B. Bavassano
Session II: From the Transition Region to the Corona and beyond	
Chair: G. Poletto	*Invited Speaker*
The Magnetic Field from the Sun to the Interstellar Medium	S. Solanki
The 3D Solar Wind over the Solar Cycle Observed by IPS	M. Kojima M. Tokumaru, K. Fujiki, M. Hirano, B. V. Jackson, P. Hick, K. Hayashi, and T. Ohmi
The Chromosphere-Corona Coupling and the Solar Wind	O. Lie-Svendsen
The Bastille Day Event: from Solar Surface to the Far Heliosphere	J. Zhang
Session III: Energetic Particles, Energetic Neutral Atoms, and Composition	
Chair: B. Fleck	*Invited Speaker*
Elemental Abundances in the Solar Corona	J. Raymond
The Heliospheric Interface: Theory and Observations	V. Izmodenov
Propagation of Energetic Particles to High Latitudes	T. Sanderson
Particles in the Heliosphere: An Overview	R. Wimmer -Schweingruber
Session IV: New Missions	
Chair: S. Suess	*Invited Speaker*
Novel Solar and Heliospheric Research with Solar Orbiter	E. Marsch
The International Living With a Star Program	H. Opgenoorth, M. Guhathakurta, and R. Marsden

2.2. Scientific Organizing Committee

The JD Scientific Organizing Committee included: I. Cairns (Local Liaison, Australia), B. Fleck (The Netherlands), R. Forsyth (U.K.), G. Poletto (Co-Chair, Italy), H. Cane (Australia), R. Lallement (France), S. T. Suess (Co-Chair, U.S.A.), A. V. Usmanov (Russia), J. X. Wang (China), H. Washimi (Japan), T. Zurbuchen (U.S.A.).

3. From the Sun to the Interstellar Medium

3.1. Ulysses at Solar Maximum: Selected Highlights

The original objective of Ulysses was to "investigate for the first time as a function of heliographic latitude the properties of the solar wind, the structure of the Sun/wind interface, the heliospheric magnetic field, solar radio bursts and plasma waves, solar X-rays, solar and galactic cosmic rays, and both interstellar and interplanetary neutral gas and dust." The 6.2 year orbit, inclined by 80 degrees to the heliographic equator, with an aphelion of 5.4 AU and perihelion of 1.34 AU, has allowed Ulysses to meet this original objective and go on to make fundamental contributions and discoveries related to the 3D heliosphere and also to the Sun, Jupiter, the local interstellar medium, the Milky Way, and the origins of gamma ray bursts. Orbit I was completed in 1998, covering solar sunspot minimum, and Orbit II is nearing completion. Orbit III will then provide coverage during the second half of the 22 year solar magnetic cycle. R. Marsden (European Space Agency, Noordwijk, The Netherlands) reviewed existing Ulysses' results and what Ulysses will be doing over the coming 4 years.

Solar wind plasma measurements during Orbit II illustrate the difference between the simple bimodal structure at solar minimum and the variable flows seen at all latitudes around solar maximum. This is graphically displayed in the solar wind speed "dial plot" shown in Figure 1. In spite of large differences in solar wind statistics, if only the peaks in solar wind speed are considered these peak speeds show the same latitudinal dependence as the peak speeds at minimum, implying some rotation effect. The dynamic pressure at the recent solar maximum was only 50%-75% that at the last maximum, implying a smaller distance to the termination shock. Orbit II also expanded the determination of the different compositions and ionization states that occur in different types (slow, fast, transient) wind states.

Interplanetary magnetic field measurements in Orbit II go along with the plasma measurements at solar maximum in exhibiting alternating polarities to the highest latitudes, although the pattern is not random. A dipole-like character still dominates even at solar maximum and the dipole axis appeared to be approximately equatorial. Open flux was measured to be independent of latitude at maximum, as it was at minimum, and approximately equal to the open flux at the preceding sunspot minimum (Smith et al., 2003). This was discovered by extrapolating the radial magnetic field measured during the two fast latitude scans to a fixed radius and making the comparison.

Energetic particle events from the Sun, from interplanetary shocks, and from Jupiter that are seen near Earth are also seen at Ulysses, regardless of the position of Ulysses relative to the Earth. There is furthermore, to a greater or lesser degree, a disappearance of latitudinal, longitudinal, and radial gradients in particle fluxes near solar maximum. There is also virtually no latitudinal gradient in cosmic rays at solar maximum. This situation cannot be easily explained by existing models of energetic particle motion in the heliosphere. The drifts of charged particles is reversing in the second half of the solar magnetic cycle and it is hoped that measurements made then will produce a better understanding of what is leading to the easy latitudinal transport of particles.

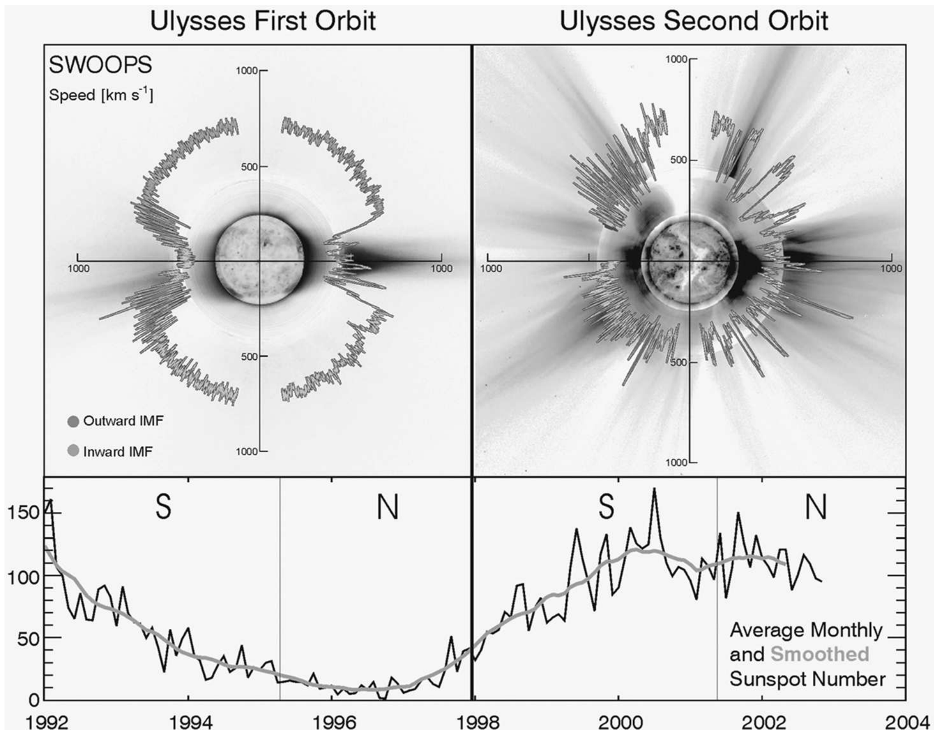

Figure 1. Polar plots of solar wind speed as a function of heliographic latitude for Ulysses' first two orbits. Sunspot number (bottom panel) shows that the first orbit occurred through the solar cycle declining phase and minimum while the second orbit spanned solar maximum. Both are plotted over solar images characteristic of (left) solar minimum (8/17/96) and (right) maximum (12/07/00); from the center outward images are from SOHO/EIT (Fe XII 195 Å), the Mauna Loa K-coronameter, and SOHO/LASCO/C2. (McComas et al., 2003)

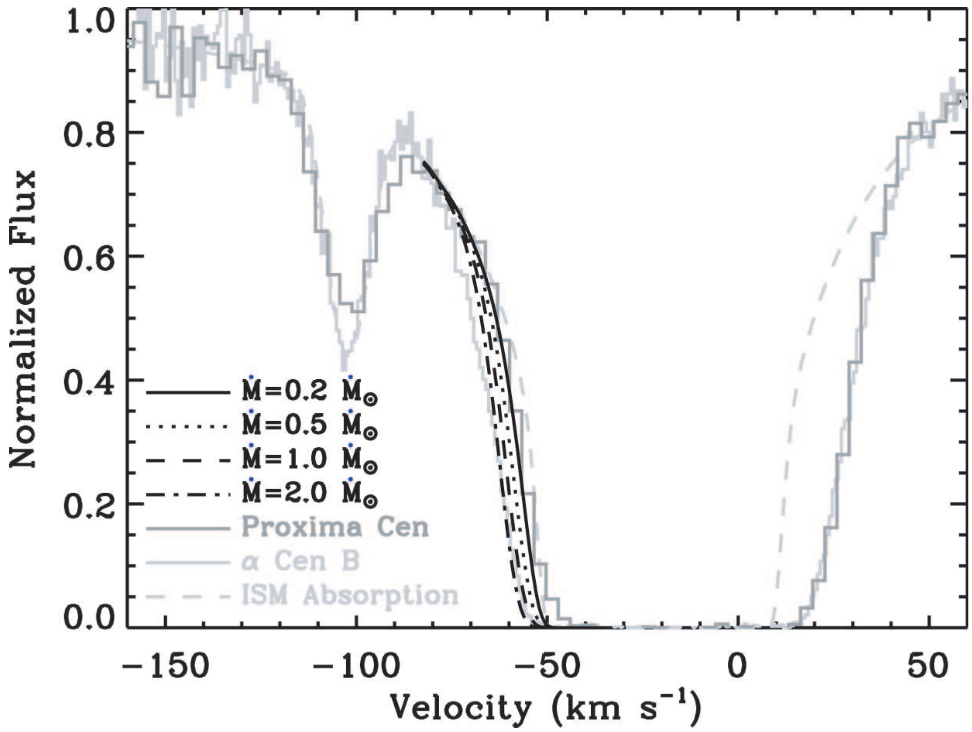

Figure 2. Empirical Lyman-α profiles for Proxima Cen and Alpha Cen B. The light-gray dashed line shows the interstellar absorption profiles of deuterium and metal lines. The extra absorption on the red side is heliospheric. The extra absorption on the blue side (different for the two stars) is astrospheric. Also shown are predictions of models for different mass loss rates. (from J. L. Linsky & B. E. Wood, *Space Telescope Sci. Inst. Newsletter*, in press, December 2003)

3.2. Hydrogen Walls: Mass Loss of Dwarf Stars and the Young Sun

The collision of an ionized stellar wind with the partially-ionized warm gas in the interstellar medium creates a population of hot decelerated neutral hydrogen atoms. This "hydrogen wall" produces a blue-shifted absorption component in the stellar Lyman-α emission line that has now been detected in HST spectra of six dwarf stars. Figure 2 shows the Ly-α profiles for two of these stars. The blue side of the Ly-α absorption (-70 to -50 km/s) is different for these two nearby stars, leading to the estimates of the mass loss rates. The physics of this interaction, its understanding, based on similar processes occurring around the heliosphere, and progress in the observational program were reviewed by J. Linsky (Joint Inst. for Laboratory Astrophysics, Colorado, USA). Comparisons of the observed Lyman-α line profiles with theoretical models lead to the first very sensitive measurements of mass loss rates, as small as 4×10^{-15} $M_\odot$/year, for solar-like dwarf stars. The range of mass loss rates determined so far is $0.2\dot{M}_\odot \leq \dot{M} \leq 30\dot{M}_\odot$. The speed of the local interstellar plasma relative to the stellar wind source has been $25 \leq V_{ISM} \leq 130$ km/s, where the heliosphere is moving at $\sim$25 km/s.

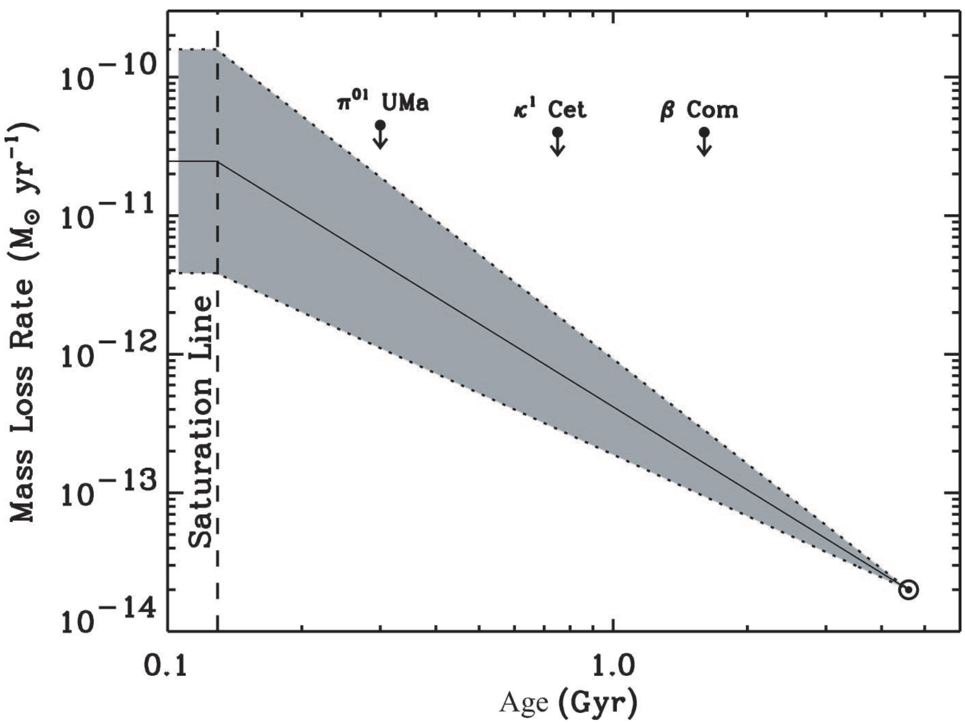

Figure 3. The mass loss history of the Sun, based on empirical mass loss rates for dwarf stars of different ages and X-ray surface fluxes. The upper limits are based on radio nondetections of three solar-like stars (Gaidos et al., 2000). (from J. L. Linsky & B. E. Wood, *Sky & Telescope*, in press, December 2003)

The observational program of Linsky and his colleagues provides the first observational data (other than for the Sun) with which to test theories for winds of solar-like dwarf stars. It shows an empirical correlation of stellar mass loss rate with X-ray surface flux that allows prediction of the mass loss rates of other stars and inference of the solar wind flux at earlier times, when the solar wind may have been as much as 1000-fold more massive. The solar prediction is shown in Figure 3. Important ramifications exist for the history of planetary atmospheres in the solar system - that of Mars in particular, and for exoplanets around stars.

In reference to the heliosphere, the volume of space dominated by the solar wind and its magnetic field, the regions dominated by these stellar winds and leading to their hydrogen walls, are called astrospheres. This naturally leads to a full set of corresponding terminology, including astropauses which divide stellar wind plasma from local interstellar plasma, bow and termination shocks, and inner and outer astrosheaths between the astropauses and the associated bow and termination shocks (Figure 2).

The models presently used to interpret the Lyman-α absorption normally assume the simplest possible wind: spherical symmetry and a speed of 400 km/s (Wood et al., 2000). As data accumulates on astrospheres, it will become possible to test these assumptions to examine, for example, whether the bimodal

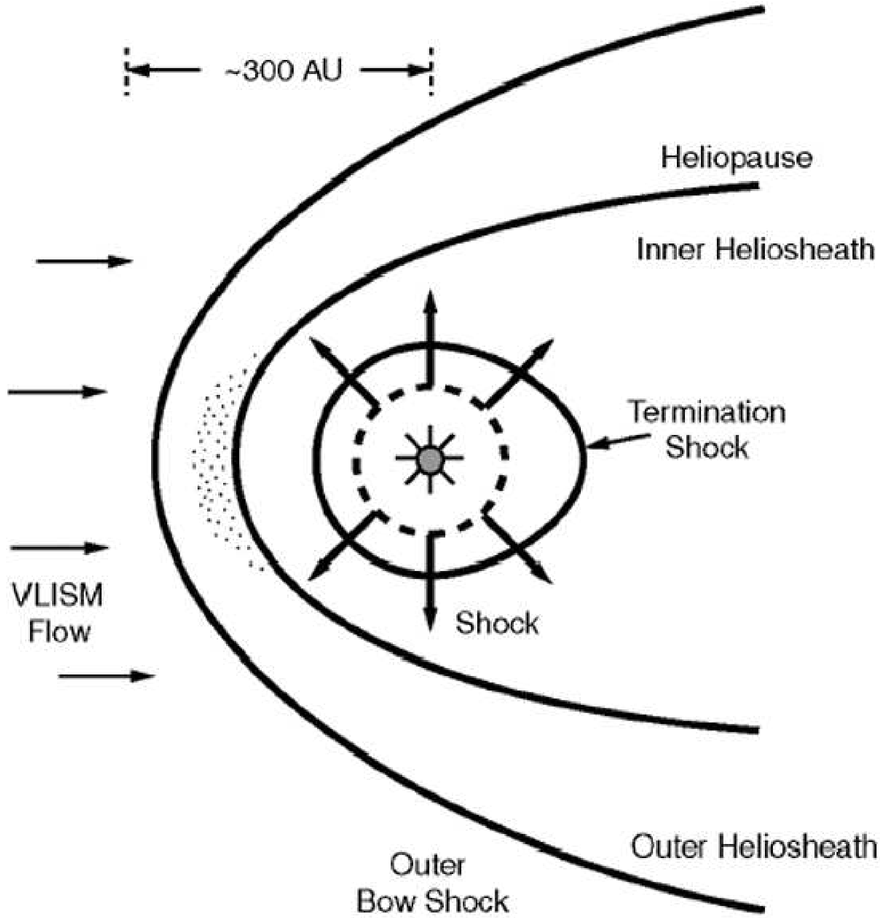

Figure 4. Plasma boundaries associated with the local interstellar medium - solar wind interaction. Stippling shows where lower-hybrid drive is predicted to occur, while the dashed line shows a GMIR shock moving toward the heliopause (Cairns and Zank, 2002).

nature seen in the solar wind around solar minimum (Figure 1) is more typical of dwarf star winds.

3.3. Radio Emission from the Outer Heliosphere and Beyond

The Voyager spacecraft have observed episodic bursts of radio emissions near 2-3 kHz that are generated beyond the inner heliosphere. These are believed to occur when shock waves driven by global merged interaction regions (GMIRs) reach the vicinity of the heliopause (see Gurnett et al., 1993). It is presently thought that the heliopause, which divides solar wind plasma from local interstellar plasma, lies roughly 150 AU from the Sun so that it takes a few years for GMIRs to pass through the heliosheath and reach the heliopause (Figure 4).

The Voyagers are traveling in a direction which is within a few tens of degrees of the upstream direction relative to motion of the heliosphere through

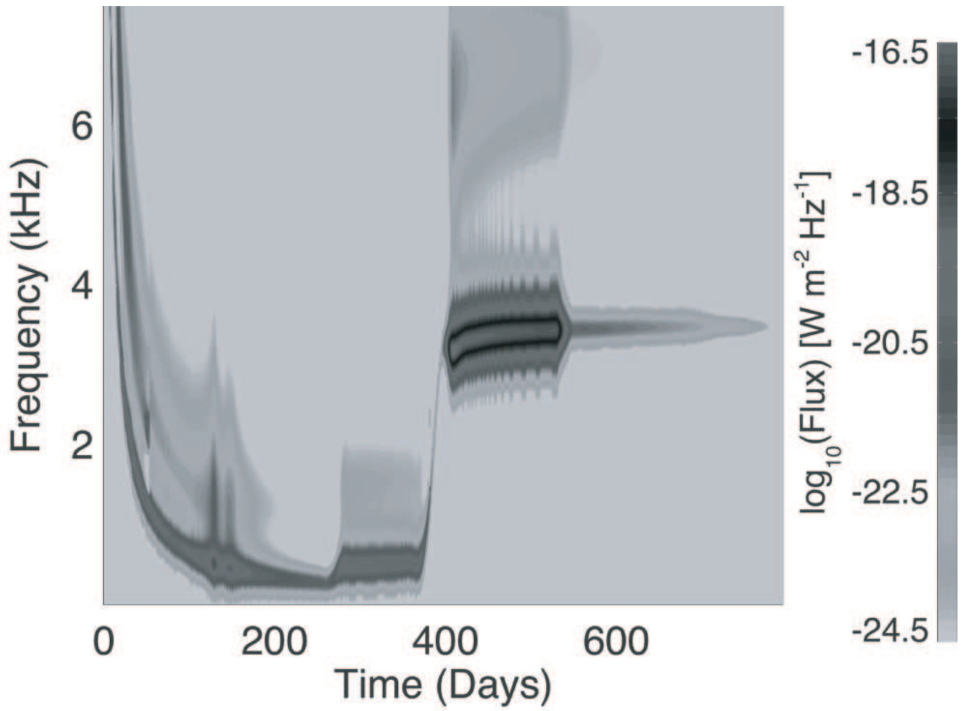

Figure 5. Theoretical prediction for the dynamic radio spectrum (J. Mitchell, I. Cairns, & P. A. Robinson, JD 07 Poster Paper).

the local interstellar medium and are expected to soon encounter the termination shock. They are the only spacecraft that are far enough from the Sun to be able to detect such low-frequency emission originating in the outer heliosphere or beyond. Amplitude and time-of-flight measurements and use of occasional spacecraft roll testing to study modulation of the signal, indicate the source is in the vicinity of the nose of the heliosphere. More concisely, the source seems to start at the nose and migrate away along a line lying near the galactic plane.

Voyager observations and theories for the source region, generation processes, and propagation of the radiation were reviewed in this presentation by I. Cairns (Univ. of Sydney, Australia). Special foci were the successes of the current GMIR model for the radiation and a new theory which specifically addresses the turn-on and generation of the radiation in the outer heliosheath, near the heliopause nose, and the propagation of the radiation into the inner heliosphere.

The theoretical model (Cairns & Zank, 2002) predicts that the radiation is generated in the fore-shock region. It turns on when a GMIR shock enters a region primed with a supra-thermal electron tail beyond and near the heliopause nose. The tail is produced by "lower hybrid-drive" associated with pick-up ions. The model source mechanism explains how the supra-thermal electron tail increases the emitted radio flux and predicts that emission is predominantly at the fundamental plasma frequency (Figure 5). There is also a suggestion that the local galactic magnetic field lies mainly near the galactic plane (Figure 6).

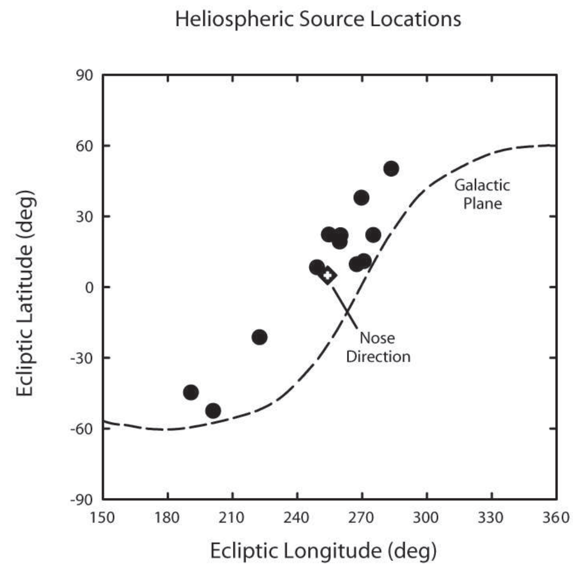

Figure 6. The direction to the low frequency radio source locations and the nose of the heliopause, suggesting the direction of the magnetic field in the local interstellar medium (Kurth et al., 2003).

The hypothesized source mechanism depends on interstellar neutral atoms being ionized in the vicinity of the heliospheric bow shock and then charge-exchanging with shocked solar wind plasma. One of the posters (Mitchell et al.) for this JD provided details on this source mechanism.

3.4. MHD Turbulence in the Heliosphere

The heliospheric plasma is an excellent laboratory to study the behavior of collisionless MHD turbulence. This is a topic of fundamental importance for both plasma physics and astrophysics and has been reviewed here by B. Bavassano (CNR, Italy). In the 1970s and 1980s decades impressive advances were made in the knowledge of turbulent phenomena in solar wind, although spacecraft observations were confined within a small latitude belt near the solar equator. In the 1990s, with the Ulysses mission, investigations have been extended to the high-latitude heliosphere. This has allowed studies of how the MHD turbulence evolves in polar solar wind, a plasma flow in which the effects of large-scale inhomogeneities are considerably less important than in low-latitude wind, at least near solar minimum when stable high speed wind dominates the polar heliosphere. With this new laboratory, important new results have been obtained. In the review, observations of turbulence evolution in polar wind were discussed and compared to those typical of the low-latitude solar wind.

Equatorial solar wind turbulence appears to normally have a strongly Alfvénic character, as determined by the coherence between solar wind plasma flow vector and magnetic field vector fluctuations. The power density spectrum of the fluctuations displays a characteristic -5/3 power law above a well-determined frequency which, in turn, moves downwards to lower frequencies with increasing distance from the Sun. Alfvénic modes are commonly described in terms of "Elsässer variables" (Marsch, 1991) $\mathbf{z}_{\pm}$ describing outward (+) and inward (-) waves.

It was realized very early that the solar wind is expanding at speeds in excess of the local Alfvén speed beyond $\sim 5 - 30 R_{\odot}$. The radius at which the Alfvén speed is exceeded is known as the Alfvén radius, r_A. Outside r_A both the $\mathbf{z}_+$ and the $\mathbf{z}_-$ modes originating inside r_A are carried away from the Sun. Any inward mode beyond r_A must be of local origin, and therefore a consequence of nonlinear interactions or interaction of outward modes with the ambient gradients in the wind. Outward modes have been found to dominate in all regions. However, the difference decreases with increasing distance to show there are local sources of inward modes. These results all were gathered near the heliographic equator in a region of mixed solar wind states.

Figure 1 shows that the polar wind around solar sunspot minimum is fast and steady, as compared to wind near the heliographic equator. This presented the opportunity to study how Alfvénic turbulence evolves under undisturbed conditions. Power spectra in the solar minimum polar wind indicate a -5/3 spectrum similar to that measured in the equatorial wind, and that the spectrum also evolves towards lower frequency with increasing distance. A specific difference is that this spectral evolution with distance is slower than in low-latitude wind. A related result is that the predominance of outward modes continues to greater distances at high latitudes.

It is concluded that solar wind turbulence, in addition to having solar sources, is locally generated at velocity shear layers. Empirical results also show that the presence of magnetic field reversals speeds up spectral evolution. This process may have a relevant role in increasing the rate of turbulence evolution in low-latitude solar wind where fast-slow stream structures and reversals of the magnetic polarity are common. In the polar wind, where velocity gradients are weak, other mechanisms have to exist and parametric decay has been proposed. This is presently one of the main areas of investigation.

4. From the Transition Region to the Corona and Beyond

4.1. The Magnetic field from the Sun to the Interstellar Medium

The behavior of the magnetic field from the interior of the Sun out to the interplanetary medium has been reviewed by S. Solanki (Max Planck Institute for Aeronomy, Germany) who began by describing the recent observational evidence about large scale flow fields and the internal rotation velocity of the Sun, which supports an overshoot-layer dynamo scenario. Magnetic flux tubes in the overshoot region reach the surface of the Sun when subject to undular instability and emerge with properties (tilt angle, latitude of emergence) that are observed in active regions (Caligari et al. 1995). Numerical MHD simulations of the magnetic field dynamics in plage regions are being developed and reproduce reasonably well the observed morphological patterns and measured quantities (Vögler & Schüssler 2003).

Solanki proceeded then to discuss how the magnetic field acts as the coupling agent between higher and lower solar layers, the latter being responsible for the structure and energetics of the overlying levels. A beautiful example of this is offered by 3-D numerical simulations that show how displacements of the photospheric footpoints of magnetic loops result in a magnetic dissipation strong enough to heat and maintain loops at coronal temperatures (Gudiksen & Nordlund 2002). Observational evidence of electric current sheets at coronal base have been obtained via He I 10830 Å line data.

At high coronal altitudes the magnetic field can be modeled by extrapolating photospheric values under different assumptions: the reconstructed coronal field is then compared with LASCO white light images. Far away from the Sun, the interplanetary field configuration had been predicted by Parker. More recently, Fisk extended Parker's model taking into account the misalignment between the magnetic and the rotation axis as well as the loop footpoint motions. The model better reproduces the cosmic rays behavior (Fisk 1996).

A relevant question to ask is whether the changing magnetic fields at the solar surface are the source of the variability of the solar irradiance and whether this variability accounts for the earth climate changes. Solar variability can be reconstructed by properly modeling the quiet sun, the sunspots and faculae evolution over time. However, climate changes, as recorded by the temperature increase measured after 1970, cannot be ascribed to changes in the solar irradiance, which is at most responsible for a fraction of the order of $\approx 30\%$ of the observed behavior (Krivova et al. 2003, Solanki & Krivova 2003).

4.2. The 3D Solar Wind Over the Solar Cycle Observed by IPS

M. Kojima (STE Lab., Nagoya Univ., Japan), reported on the 3-D solar wind properties over the solar cycle, as derived from interplanetary scintillation measurements (IPS), in a review co-authored by M. Tokumaru, K. Fujiki and M. Hirano (STE Lab., Nagoya Univ., Japan), B. V. Jackson and P. Hick (CASS, Univ. of San Diego, USA), K. Hayashi (W.W. Hansen Experimental Physics Lab., Stanford Univ., USA) and T. Ohmi (Science and Technology Dept., CTI Co., Ltd.). Because interplanetary scintillation observations integrate along the line-of-sight, data need to be analyzed with a tomographic technique in order to retrieve the three dimensional wind parameters (see, e.g. Hayashi et al. 2003). Kojima showed that the solar wind speeds derived from a recently developed IPS tomographic technique compare well with *in situ* values measured by Ulysses. Figure 7 illustrates IPS results over 14 Carrington rotations and gives corresponding Ulysses values.

With this method, Kojima and collaborators have been able to study the solar cycle dependence of the solar wind properties, such as the speed of the wind, the asymmetry of fast wind, the origin of the slow wind, the bimodal character of the wind. IPS studies show also that the Nolte et al. (1976) claim (later supported by Neugebauer et al. 1998) that the smaller a coronal hole, the lower the solar wind speed originating from the hole, is only a first approximation to a more complex behavior. For instance, slow wind may emanate from a small coronal hole close to an active region, at solar minimum, as well as it

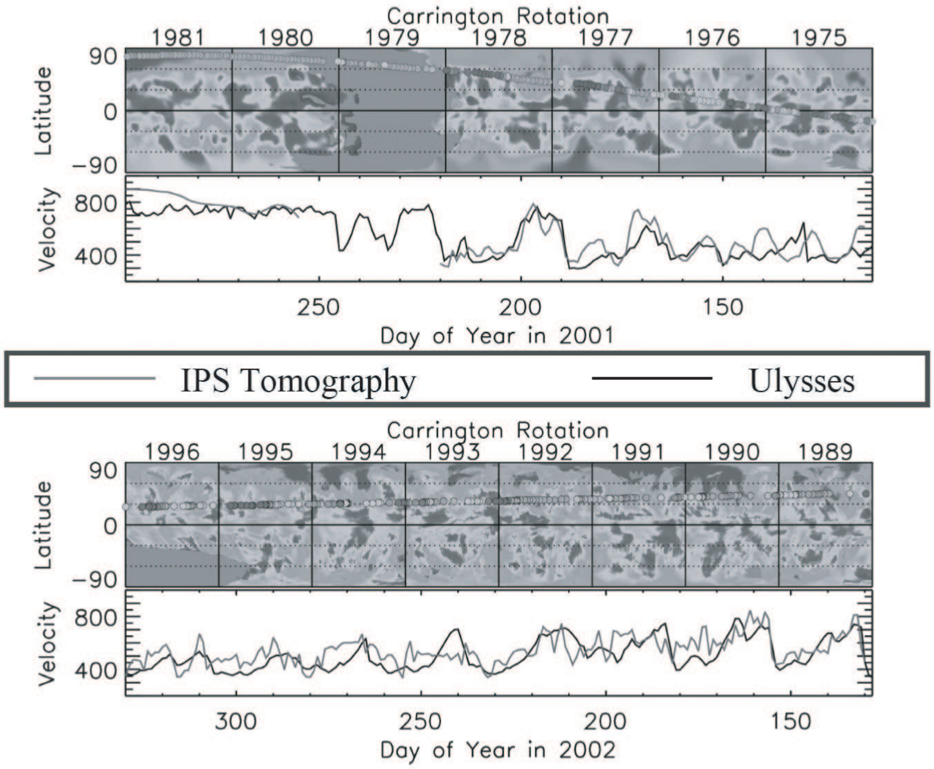

Figure 7. Solar wind speed measured over 7 Carrington rotation in years 2001 and 2002 as derived from IPS tomography are compared with speeds measured *in situ* by Ulysses.

emanates from a small polar hole, at solar maximum (Ohmi et al. 2001, Ohmi et al. 2003). Also, during the ascending phase of the solar cycle, wind streams originating from holes that shrink from a large to a smaller area do not change their speed. Obviously, the same behavior occurs in descending phases of the solar cycle.

Impressive solar wind "images", giving the distribution of the solar wind speed all over the solar surface, throughout the solar cycle, may be built from IPS data. The solar cycle in solar wind may be compared with conventional images of the solar cycle in magnetic fields or in solar X-rays, as directly observed by, for instance, NAO and Yohkoh instrumentation, respectively. These maps provide an immediate first-order answer to questions such as the sources of slow/fast wind, the percentage of solar surface they occupy, and their dependence on the solar activity distribution.

On the basis of the measured wind speed, it has been possible to reconstruct the profile of the solar wind speed *vs.* latitude. Depending on the phase of the solar cycle, the fast wind latitudinal velocity gradient $dV/d\theta$ varies between zero and 4 $kms^{-1}deg^{-1}$. The bimodal character of the wind, already identified in Ulysses observations, is reproduced quite well by IPS measurements. The bimodality holds in the ascending and descending phase of the solar activity cycle and not only at minimum activity (Kojima et al. 2001).

It is well known that the wind speed seems to correlate well with the expansion factor of its source region f (see, e.g. Wang and Sheeley 1990) and/or to its photospheric magnetic field B (see, e.g., Fisk 1996). On the basis of the wind speeds measured by IPS, of the average magnetic field measured at photospheric levels over the wind originating region and of the flux expansion rate calculated from potential extrapolations, Kojima showed that neither the Wang and Sheeley, nor the Fisk assumption, are valid. The correlation factor between the wind speed and the magnetic field is on the order of 0.4 — 0.5, while the correlation factor between the speed and the $1/\sqrt{f}$ factor suggested by Wang and Sheeley is ≈ 0.7. However, the correlation factor rises to 0.91 ± 0.1, when the wind speed is compared to B/f values.

Also time—dependent phenomena, like coronal mass ejections (CMEs), can be studied via IPS measurements, adopting the time-dependent tomography algorithm developed to this purpose (see e.g. Jackson et al. 2003). This new program will be applied also to the study of the evolution of co-rotating heliospheric structures. Preliminary results are very promising and will be used for reconstructing in three dimensions the evolution and interaction of interplanetary structures.

4.3. The Energy Balance from the Chromosphere to the Corona and its Effect on Solar Wind Properties

While Solanki's talk focused on the role of magnetic fields from the Sun to the interplanetary space, O. Lie-Svendsen (Norwegian Defencer Research Establishment) showed how the flow of energy between the chromosphere and the corona controls solar wind properties. That the solar atmosphere is the source of the solar wind and the heliospheric plasma is obvious, but the coupling occurs via processes which are not yet well known. In particular, one should understand how energy is fed into the coronal and solar wind plasma and how the upper chromosphere reacts to the downward energy flow from the hot corona.

Lie-Svendsen illustrated results from a solar wind model which has its lower boundary in the chromosphere and its upper boundary at 1 AU. The model, based on the 16—moment transport equations developed by Demars & Schunk (1979), uses the gyrotropic approximation to these equations deriving densities, the drift speed along the magnetic field, the temperatures and the heat flux densities parallel and perpendicular to the magnetic field, for each particle species. Details of the model characteristics (e.g., terms adopted in the description of coronal and chromospheric heating) can be found in Lie-Svendsen, Hansteen, & Leer (2002), Lie-Svendsen, Hansteen, Leer & Holzer (2002).

The study addresses the questions of how the energy transport between the lower atmospheric levels and the corona, as well as the energy deposition in the transition region, affect the solar wind characteristics out to 1 AU. Both a radial and a super-radial geometry are considered and the properties of the resulting two solar wind "modes", namely fast and slow solar wind, are illustrated in Figure 8. It should be pointed out that the use of higher order transport equations, and the description of the collisionless plasma, has been crucial in establishing the characteristics given in the figure, and also revealed how the altitude inter-

Two solar wind "modes"

	slow	fast
geometry	radial	rapidly expanding
downward heat flux absorbed by	*radiation*	*enthalpy flux*
wind speed	slow	high
solar wind mass flux	high	low
coronal density	high	low
heat flux	classical	non-classical
transition region pressure	high	low
mass flux limited by	coronal heating	transition region heating (supply from chromosphere/transition region)
coronal He abundance	high	low
He mass flux limited by	coronal energy	supply from chromosphere (a problem!)

Figure 8. Main properties of slow and fast wind as derived in the model presented by Lie-Svendsen (see text).

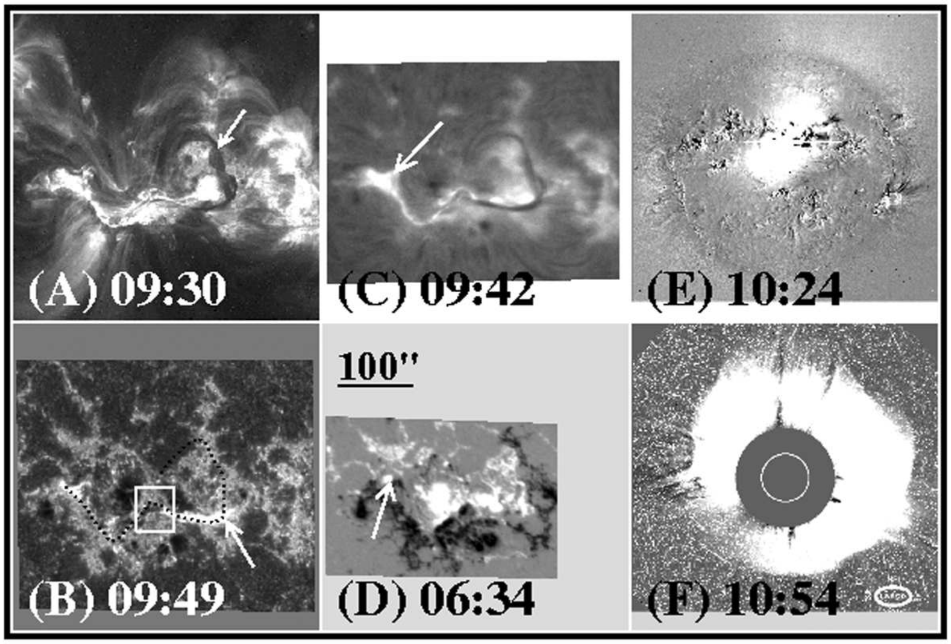

Figure 9. The Bastille day event scenario: (A), (B) *TRACE* images in, respectively, 195 and 1600 Å (C) H_α filtergram about 20 minutes before the X5.7 flare occurrence, (D) line of sight magnetogram of the Bastille event region, from Huairou Solar Observing Station, (E) running difference of SOHO EIT images at the time of flare maximum, (F) running difference of LASCO C2 images at the time it first detection in C2 (Zhang et al., 2001).

val (somewhere in the transition region or low corona), where plasma changes from being collisional to being collisionless, although fairly limited, has a large influence on the solar wind mass flux: a good example of the solar-heliospheric connection! However, additional work may be necessary to insure that the model realistically describes the proton velocity distribution in the extended corona, as the model assumes a not too large departure from a bi-Maxwellian function.

4.4. The Bastille Day Event: From Solar Surface to the Far Heliosphere

An example of a solar event whose effects have been detected and measured out to ≈ 60 AU has been presented by J. Zhang (National Astronomical Observatory, Chinese Academy of Sciences), who summarized the observations of the so called *Bastille Day Event*, from the solar surface to the outer interplanetary space. This event occurred on July 14, 2000, and his manifestations include a giant filament eruption, a large flare (X5.7/3B) and an earth-directed coronal mass ejection. Figure 9 shows pre and post flare images of the Bastille event region as imaged by different experiments (Zhang et al. 2001).

Observations of the magnetic evolution of the active region (NOAA 9077) where the flare occurred revealed multiple cancellation events (or slow reconnection events) in the vicinity of the filament bridging the region. These observations provide evidence of the role played by slow reconnection in generating the global instability responsible for the events seen in the region. Over a more extended area, a large transequatorial filament, and loop arcade, appear to be associated with the CME.

Yan et al. (2001) and Deng et al. (2001) have been able to reconstruct the magnetic configuration of the region above the photosphere via a non linear force free field extrapolation of the vector magnetic fields measured at the Huairou Solar Observing Station (HSOS). From the evolution of the non-potentiality of the region these authors conclude that energy gradually propagated from the lower to the higher solar layers and the stored energy caused first the filament eruption and then the flare occurrence. The temporal profile of the longitudinal current, helicity and total energy stored in the region over a time interval of a few days centered on July 14 is also given.

A variety of radio signatures were associated to the 14 July event. In particular the flare event produced an intense, long duration Type III-like radio emission, associated with electrons accelerated deeply in the corona (Reiner et al. 2001). The CME was the source of Type II radio emission, whose frequency drift indicated a significant CME deceleration, as it moved from the corona to the interplanetary medium.

Near 1 AU the solar wind structure associated with the Bastille event consisted of a large speed stream observed on July 15 and a few small streams. Over a period of 6 days the wind speed increased from 400 to 1100 kms^{-1} and the field from 10 nT to 60 nT. An interaction region, bounded between a pair of forward and reverse shock has also been identified (Whang et al. 2001). The CME-driven shock arrived at *Voyager 2*, at ≈ 63 AU on January 12, 2001, with a speed jump of 60 kms^{-1}. These observations provided a good opportunity to study the shock propagation from the inner to the outer heliosphere: MHD simulations showed that the CME shock changed dramatically in strength and propagation speed as it moved outward (Wang et al. 2001). The leading forward shock has decayed while all other shocks and discontinuities apparently dissipated by the time they would have reached Voyager 2. The merged interaction region had expanded to at least 10 days in length.

The response of the Earth's inner magnetosphere to the Bastille CME has been recorded by the IMAGE spacecraft, which made images in the Energetic Neutral Atoms (ENA) produced by charge exchange between the hot magnetospheric ions and the cold geocoronal neutral hydrogen. These images showed that as the B_z component of the interplanetary magnetic field became positive the ring currents became closed and symmetric (Brandt et al. 2001). A large polar cap absorption event, lasting about 3 days, has also been observed at the Zhongshan station, in Antarctica (Liu et al., 2001) and large geopotentials had been induced over oceanic distances (Lanzerotti et al. 2001).

Optically, the Bastille day event was the fourth event in solar cycle 23 that had an optical importance of 3B. Although larger events had been observed in other solar cycles, it was undoubtedly an extremely large event and it provided a good opportunity to study the different manifestation of large events throughout the solar atmosphere and the heliosphere. We point out also that the study of the return period of such events is relevant for the prediction of natural hazards in space weather.

5. Energetic Particles, Energetic Neutral Atoms, and Composition

5.1. Elemental Abundances in the solar Corona

J. Raymond (Harvard-Smithsonian Center for Astrophysics, Cambridge, USA) reviewed our present knowledge of elemental Abundances in the solar corona and pointed out how many analyzes of astrophysical observations assume "solar elemental abundances" without recognizing the large variations of abundances within the solar atmosphere. However, abundances in the solar corona are modified with respect to those in the photosphere in (at least) two systematic ways. First, the abundances of elements whose neutral species have an ionization potential below about 10 eV are enhanced relative to elements whose atoms have higher ionization potentials. This First Ionization Potential (FIP) effect has been studied for many years, and it is typically a factor of 3 or 4 enhancement. The second effect is a reduction of the abundances of all elements relative to hydrogen. It has been less well studied because hydrogen lines or continuum are not found in the wavelength ranges of many instruments, or else the lines are optically thick or formed at different temperatures. Recent studies of line/continuum ratios in solar flares and of UV line intensities above the solar limb have begun to remedy this problem, and depletions of order a factor of 3-10 are commonly observed. They are attributed to gravitational settling.

Abundances also have important physical consequences. The radiative cooling rate is directly proportional to the abundances at temperatures up to about 10^7 K, where bremsstrahlung begins to dominate. The mean particle weight can affect flow dynamics, and Hansteen et al (1998) have studied the effects of helium on the fast solar wind. Moreover, preferential acceleration of oxygen is observed in the fast solar wind and attributed to cyclotron damping of plasma waves (Cranmer et al. 1999). While the oxygen abundance is too small to have much of an effect on the overall dynamics of the wind, analogous preferential heating of helium could have major consequences.

Most coronal abundance determinations rely upon ratios of collisionally excited emission lines. One can obtain the relative abundances of two elements by choosing spectral lines such that the product of excitation rate and ionic concentration has the same temperature dependence for both lines. A common example is the Ne VI and Mg VI lines near 400 Å which has the additional advantage that the wavelengths are so close that the instrumental radiometric calibration uncertainty also cancels out. In the X-ray range, O VIII Lyα and the nearby lines of Fe XVII are formed at similar temperatures. There is never a perfect match of temperature response, and time-dependent ionization could distort the derived abundances, but in general these methods give reliable relative abundances within the uncertainties in the atomic rates.

To carry the analysis a step further, one can obtain absolute abundances if one of the elements being compared is hydrogen. This can be difficult, in that there are no lines of hydrogen shortward of 912 Å. The bremsstrahlung continuum is largely formed by hydrogen, and it can be measured shortward of about 10 Å. Absolute abundances in solar flares can be derived by measuring the equivalent widths of lines such as Ca XIX λ3.18, provided that that ion dominates at the temperature of the flare plasma and that the continuum is not contaminated by fluorescence due to X-rays at shorter wavelengths (Fludra &

Schmelz 1999; Phillips et al. 2003). For observations of the corona above the limb, the hydrogen Lyman lines can be compared with lines of other elements. The analysis is somewhat different in the Lyman lines that include strong contributions from radiative scattering, but results have been obtained for coronal holes, active regions and streamers (Raymond et al. 1997; Feldman et al. 1998; Laming & Feldman 2002; Ko et al. 2002; Bemporad et al. 2003)

Overall the observations show a FIP enhancement that varies not only from one region to another, but also increases with time within individual active regions as they evolve (Widing & Feldman 2001). The gravitational settling effect seems to be observed in the closed field regions of active region streamers and equatorial streamers at solar minimum.

Various explanations have been proposed for the FIP effect, but all agree that it must occur in the chromosphere (see review by Henoux 1998). Models include diffusion (Peter 1998), rising magnetic fields and injection of enriched material by reconnection (Arge & Mullan 1998). Gravitational settling has a characteristic time scale of about 1 day. In a steady state, gravitational settling would predict much smaller abundances than observed (Lenz, Lou & Rosner 1998), suggesting continual mixing of fresh material.

5.2. The Heliospheric Interface: Theory and Observations

Sun is moving through warm (∼6500 K) and partly ionized local interstellar cloud (LIC) with velocity ∼26 km/s. The charged component of interstellar medium interacts with the solar wind (SW) forming the heliospheric interface, the SW/LIC interaction region (Figures 4, 10). Both the solar wind and interstellar gas have a multi-component nature that creates a complex behavior of the interaction region. The current state of art in the modeling of the heliospheric interface was reviewed by V. Izmodenov (Moscow State University, Russia). Modern models of the interface take into account effects of the solar wind and interstellar plasma components (protons, electrons, pickup ions, interstellar helium ions and solar wind alpha particles), interstellar neutral component (H atoms), interstellar and heliospheric magnetic fields, galactic and anomalous cosmic rays, latitudinal and solar cycle variations of the solar wind. New results of self-consistent time-dependent kinetic/gas-dynamic model of the heliospheric interface were reported. Predictions of the theoretical models were compared with available remote diagnostics of the heliospheric interface - backscattered solar Lyman-α radiation, pickup ions, deceleration of the solar wind at large heliocentric distances, heliospheric absorption of stellar light, anomalous cosmic rays (ACRs) and heliospheric neutral atoms (ENAs).

Remote diagnostics of the interface region include observations of pickup ions created from interstellar atoms, solar Lyman-α radiation that is backscattered from interstellar neutral atoms, and the kilohertz radio emission discussed above in §3.3, where models of the radio emission were described. Global interactions are the focus here. The models are typically either multifluid or kinetic hybrid, but not both, and are often not well determined in that they still make somewhat different predictions. They are, however, uniform in predicting that the effect of interstellar neutrals is large, reducing the radius of the termination shock from 200 to ∼ 100 AU. These neutrals are also the source of the hydrogen wall (§3.2, Figure 10(b)). The models show that the heliotail extends far

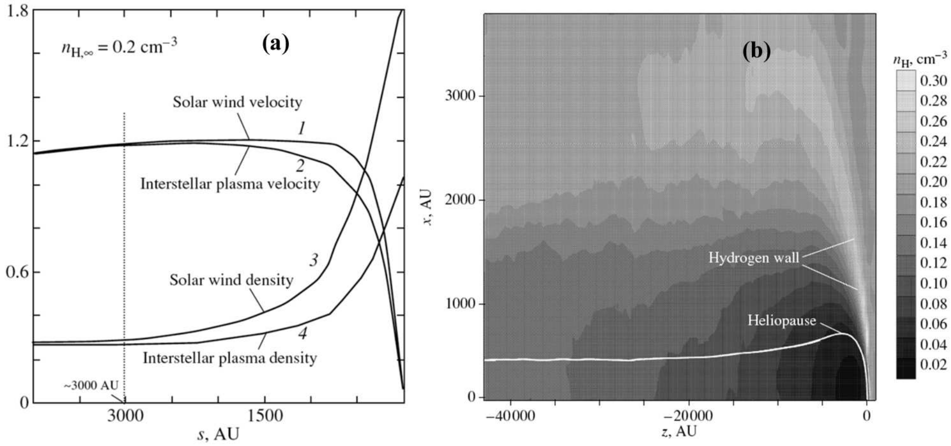

Figure 10. (a) Density and flow speed in the interstellar medium and far down the heliotail, showing when the two finally merge. The velocities and densities are normalized to their interstellar values (Izmodenov & Alexashov, 2003). (b) The two-dimensional density distribution of hydrogen atoms in the heliospheric interface. At heliocentric distances $\sim 40,000$ AU, the atomic density is close to its value in the unperturbed interstellar medium. The hydrogen wall, the increase in the density of hydrogen atoms in front of the heliopause, is clearly seen. The intensity of the hydrogen wall decreases with increasing heliocentric distance.

out to $\sim 2000 - 3000$ AU where the heliopause finally disappears due to charge exchange effects. The heliotail does not disappear, but extends indefinitely in models without neutral interstellar hydrogen (Figure 10(a)).

Other model predictions are that the heliosphere, overall, breathes in and out with the solar cycle, as the solar wind dynamic pressure changes (§3.1, Figure 11). The distance to the termination shock varies by ~ 20 % and shock waves between the heliopause and bow shock can sometimes be induced in the simulations.

The models are now being used to investigate modulation of galactic cosmic rays (GCRs) in the inner and outer heliosheaths and their general access to the heliosphere. GCRs are found to have only a minor effect on the termination shock. Conversely, the models indicate that GCRs have an important effect on the boundary region and, in turn, are strongly modulated in the boundary region.

5.3. Propagation of Energetic Particles to High Latitudes

Trevor Sanderson (European Space Agency, Noordwijk, The Netherlands) illustrated how the Ulysses mission has taught us that the heliosphere can no longer be considered as a uniform entity - that any study of the propagation and acceleration of particles in the heliosphere must take into account the three-dimensional structure. The starting point for this discussion was again the bimodal structure of the solar wind around solar sunspot minimum, illustrated in Figure 1. The propagation of energetic particles at low latitudes in low speed solar wind is

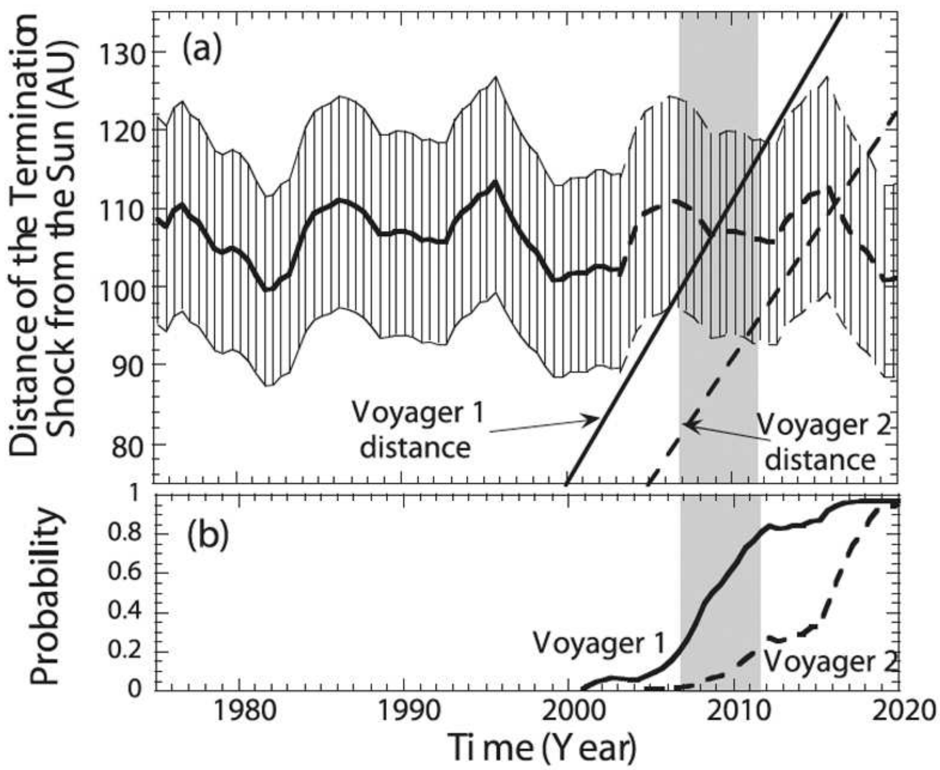

Figure 11. (a) Mean, with 1-σ, of the termination shock distance (in astronomic units) as a function of time, at 30° from the upwind direction (Izmodenov et al., 2003). (b) Probability of termination shock crossing for Voyager 1 and Voyager 2 as a function of time.

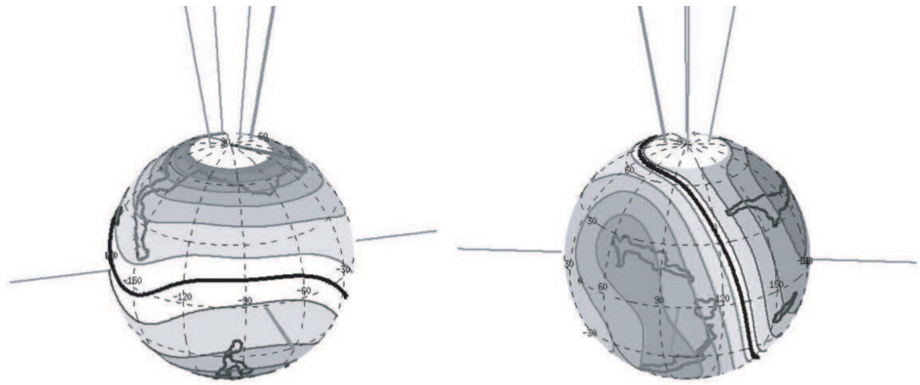

CR1925, 29 July 1977 CR1965, 24 July 2000

Figure 12. Source surface maps of the coronal magnetic field strength and direction.

influenced by the presence of small scale structures such as discontinuities and large scale structures such as CIR's, CME's, and transient stream interaction regions. High latitude wind near solar minimum differs considerably. It is high speed, contains large amplitude Alfvén waves and a relative deficit of CIR's and CME's. Low latitude energetic particle events interacting and originating from these structures were then described (e.g., Lanzerotti & Sanderson, 2001). Based on ISEE-3 35-1600 keV ion observations, typical behavior is for: (i) Upstream ion flux to increase as a shock approaches. (ii) Upstream ions to resonate with upstream waves. (iii) Ion flux to peak $\sim$ 6 hours after the shock. (iv) Ion flux to drop within CMEs. (v) Ion distributions to be bi-directional within a CME.

Around solar sunspot maximum, solar wind conditions are considerably different (Figure 1). The streamer belt is highly inclined, coronal holes are small, and there is little high speed wind near the ecliptic plane (Figure 12). During the second high latitude pass of Ulysses, near solar maximum, several energetic particle events at high latitude and in high speed solar wind flow were observed, with energies extending from $\sim$ 1 to $\sim$ 100 MeV. The high speed wind arose from small coronal holes that were beginning to form just after solar maximum. These particle events, observed for the first time under such conditions, give us the opportunity to study particle propagation within the substantially different conditions of the fast and slow solar wind. Sanderson presented a detailed analysis of particle time-intensity profiles and anisotropies in the relatively homogeneous plasma of the high speed flow. He compared these events with events observed in the slow solar wind, and discussed this in the context of current propagation models. These high latitude events, all associated with CMEs in the high speed wind, presented a different character than corresponding low latitude events: (i) The ion flux peaks at the leading edge of the CME, not at the shock. (ii) The ion flux is higher within the CME. (iii) There are no bi-directional ions within the CMEs. These high latitude CMEs are usually 'over-expanding' and will be a target of study during the third Ulysses orbit.

5.4. Particles in the Heliosphere: An Overview

While J. Raymond's talk focused on elemental abundances in the solar corona, and gave estimates of the present solar abundances, R. Wimmer-Schweingruber (Institut für experimentelle und angewandte Physik, Kiel, Germany) dealt with an historical perspective of solar and heliospheric abundances. This is a fascinating subject, which has the capability of creating cross-cultural exchanges between "astronomers" and geophysicists. Solar abundances may vary during the Sun lifetime: we know that the Sun formed from an interstellar medium, $\approx 4.5\ 10^9$ years ago, and processes, like supernovae explosions, and events, like embodying planets at an early stages of its life, have an impact on solar abundances. Knowledge of solar abundances thus may provide us with information about the composition of the primitive nebula - an essential issue for the understanding of planetary system formation and evolution.

Helioseismology data provide a means to get information about inhomogeneities in the composition of the interior of the Sun via a comparison between measured and predicted oscillation modes (we remind the reader that the speed of sound depends, among various factors, on the mean molecular weight of the plasma). These analysis suggested that the photopsheric abundance of elements heavier than H decreased by ≈ 10 % over the sun lifetime, because of the gravitational settling of heavier elements. This reduction is too small to be tested by photospheric abundance measurements and Wimmer-Schweingruber described an alternative way to check the predicted variation by a comparison between abundances in meteorites and in the solar wind (Turcotte & Wimmer-Schweingruber 2002).

Chondritic meteorites are assumed to keep a record of the composition of the pre-solar nebula. Abundances in meteorites thus give a fairly accurate description of solar abundances and can be measured with a higher accuracy (3 - 10 %) than photospheric abundances (which are known with an uncertainty of at least 25 - 30 % , this being the uncertainty of atomic parameters alone). A comparison between meteoritic and photospheric abundances is given in Figure 13. Wimmer-Schweingruber then showed that abundances in fast wind, because of their small First Ionization Potential (FIP) effect, are best suited for a comparison with meteoritic abundances and that the isotopic composition of fast wind is best representative of the plasma feeding the wind.

Another means to test the predicted behavior of solar abundances with time calls for an analysis of lunar soil. Heber et al. (2003) have analyzed lunar samples of different solar wind antiquities, that is samples exposed to solar wind in different epochs. Results from the Heber et al. work seem to indicate a time evolution of the $^3He/^4He$ ratio in solar wind, which might be interpreted as an effect of gravitational settling of the heavier ^4He or of some mixing of ^3He produced by incomplete H burning beneath the convection zone. However, a more thorough analysis revealed the increase of the $^3He/^4He$ ratio to be an artifact and the authors conclude that lunar samples point to a constant $^3He/^4He$ ratio in solar wind over the past ≈ 4 Gyr.

At a greater depth than used for measuring solar wind particles, lunar soil shows the presence of particles more energetic than found in solar wind, which, in spite of being dubbed *SEP* (Solar Energetic Particles) are much more abundant than today's solar energetic particles and cannot be ascribed to en-

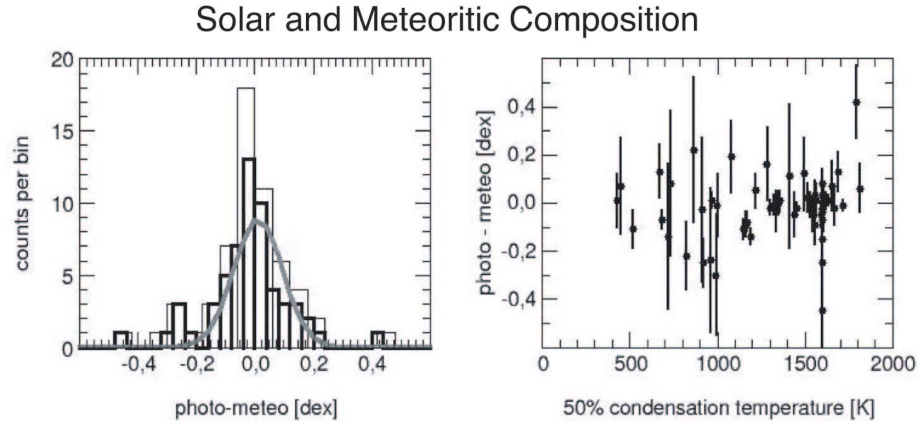

Figure 13. Comparison between meteoritic and photospheric abundances normalized to Mg. Right panel: the logarithm of the abundance ratio X/Mg in meteorites divided by its corresponding photospheric value is plotted vs. 1/2 the condensation temperature. Left panel: the same as the left panel plotted as a histogram and fitted by a Gaussian with a standard deviation of 0.084 dex.

hanced solar activity in the past. This *SEP* component, according to Wimmer-Schweingruber, has a non-solar origin and can be ascribed to interstellar pick-up ions (PUI) ionized and accelerated in the heliopshere. This interpretation of the *SEP* population opens up the possibility of using the lunar soil as an historical record of the galactic environment the Sun has encountered during its lifetime (Wimmer-Schweingruber & Bochsler 2001, 2003). New instruments that measure the composition of the solar wind and of supra-thermal and energetic particle populations have greatly increased our knowledge and understanding of PUI sources and their evolution. Within the past few years, two important sources of supra-thermal pick-up ions have been discovered, the inner and outer source, which appear to be related to interstellar and interplanetary dust particles.

6. New Missions

6.1. Novel Solar and Heliospheric Research with Solar Orbiter

Solar Orbiter (SO) is an ESA mission that will be launched into a heliocentric orbit in 2012. E. Marsch (Max-Planck-Institute for Aeronomy, Germany) described the scientific rationale for and the experimental approach to SO.

SO will carry out both in situ and remote measurements. It will measure in-situ the properties of fields and particles in the unexplored near-Sun heliosphere in three dimensions. It will remotely investigate fine-scale structures and events in the magnetically coupled layers of the Sun's atmosphere. During portions of the orbit, SO will effectively corotate with the Sun and identify through this corotation links between activity on the Sun's surface and the resulting evolution of the inner heliosphere. During the high latitude portions of its orbit, SO will observe the Sun's polar regions and the equatorial projection corona. Finally, the

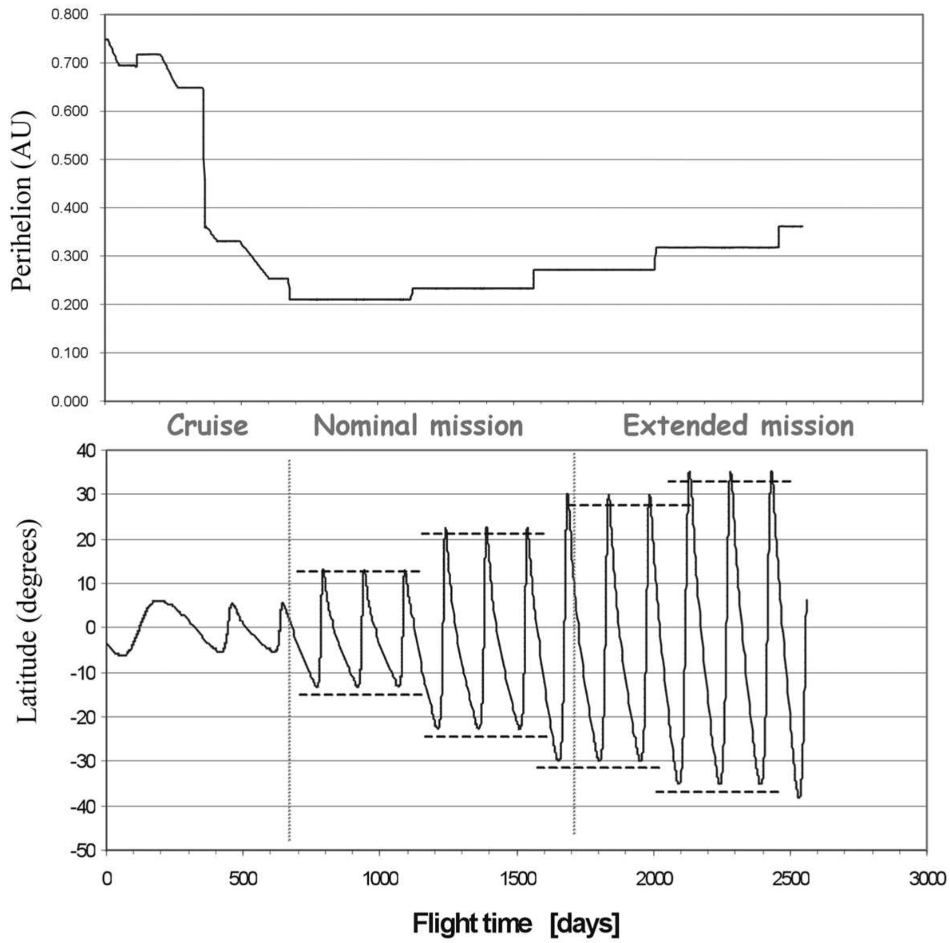

Figure 14. Perihelion distance and helio latitude achieved by the Solar Orbiter orbit over the lifetime of the mission, measured in days after launch.

unique virtue of the SO mission is that it will render possible the first close-up observations made from a near-Sun platform.

The experiment complement of SO is designed to fully exploit the heliospheric location of the platform. At closest approach (0.2 AU perihelion, Figure 14) to the Sun, optical observations with 35 km pixels at all wavelengths and radiance measurements resolving filling factors will be made. The out-of-ecliptic (up to 38° helio latitude) orbits will allow the magnetic field and magnetoconvection in the Sun's polar region to be observed directly and will provide synoptic views of the equatorial streamer belt. Corotation of the spacecraft with the Sun will enable us to disentangle spatial from temporal effects.

The fundamental questions addressed by the mission are: Why does the sun vary and how does the solar dynamo work? What are the fundamental processes at work in the solar atmosphere and heliosphere? What are the links between the magnetic field dominated regime in the solar corona and the particle regime in the heliosphere? Addressing these questions will further make SO a valuable addition to the International Living With a Star Program that is discussed in §6.2.

6.2. The International Living With a Star Program

The International Living With a Star (ILWS) Program will provide an umbrella for forging international coordination, cooperation, and bi-lateral and multi-lateral agency collaborations in studies of: How and why does the Sun vary? How does the Earth respond (and vary)? What are the impacts on humanity? The mission statement is to "Stimulate, strengthen, and coordinate space research to understand the governing processes of the connected Sun-Earth system as an integrated entity." This will be achieved through a systems approach that will quantify the physics, dynamics, and development of the Sun-Earth connected system through the entire range of conditions occurring in the 11 year solar cycle. To do this, it incorporates space missions, additional data sources, data dissemination, and supporting theory and modeling. Membership presently includes Canada, Europe, the USA, and Russia. R. Marsden (European Space Agency, Noordwijk, The Netherlands), in collaboration with H. Opgenoorth (European Space Agency, Noordwijk, The Netherlands) and L. Guhathakurta (NASA, USA), presented ILWS for this consortium.

ILWS expects to accomplish the following:

- Delineate key processes involved in the generation and propagation of solar and geomagnetic disturbances.
- Characterize & quantify the dynamics and evolution of the solar interior, surface, and corona.
- Characterize and quantify the dynamics of the Earth's upper upper atmosphere and current systems, electric fields, and particle populations in the near-Earth space.
- Characterize and quantify global dynamics that cause enhanced magnetospheric radiation zones and satellites to transit these zones.

The missions included in ILWS are shown in Figure 15. These are selected on the basis of the systems approach, instrumentation, and ability to complement measurements made on other missions. The time line at the bottom shows the initiation of ILWS this year and its continuation past the middle of the next decade.

The ILWS mission fleet is a consequence of circumstances rather than planning. Therefore, there are obvious shortfalls. Specifically,

- There is insufficient spacecraft coverage to sample simultaneously all critical regions & phenomena of the complex, time-varying geo-space environment.
- Solar wind is to be sampled at only a few points.
- There is inadequate measurement of solar high energy phenomena (e.g. flares and energetic particles) currently planned for the next solar maximum.
- There is a gap in the measurement of solar irradiance.

ILWS will address these shortfalls in planning for the Solar Orbiter, Solar Sentinels, and long-range mission strategy. The planning will be designed to continually clarify opportunities and possibilities and incorporate community participation in ILWS planning and priority setting.

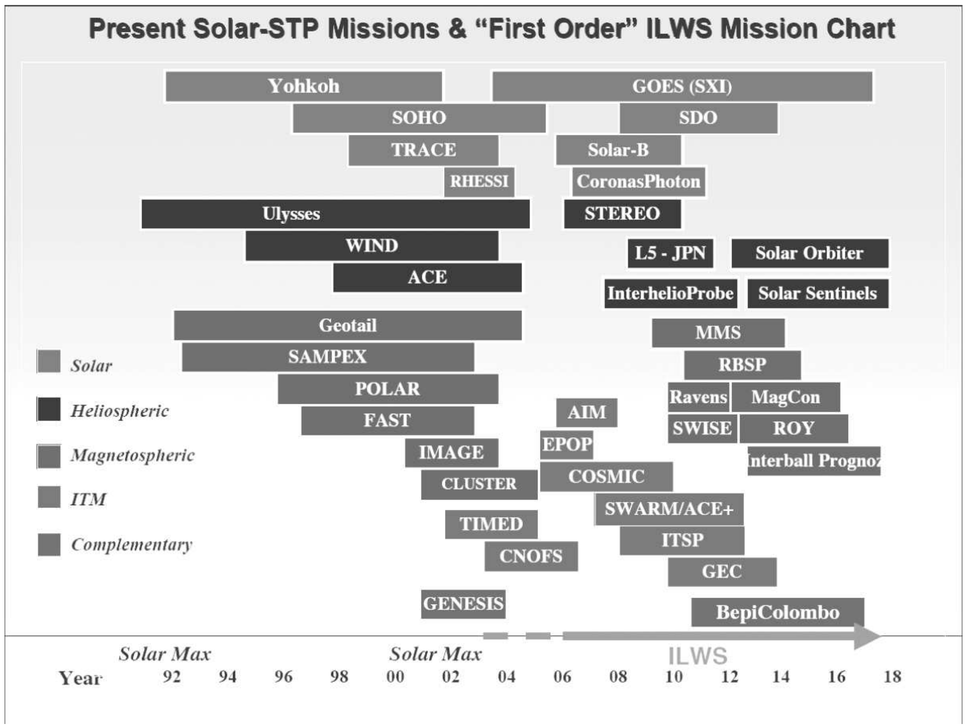

Figure 15. Chart showing existing, planned, and proposed missions that are part of the ILWS Mission.

7. Poster Papers

Title	*Authors*
Magnetic solar cycle related heliospheric density anomalies	S. Ananthakrishnan, P. Janardhan, V. Balasubramanian
The solar flare myth	H. V. Cane
Stereo observations of the Sun and interplanetary medium, space triangulation, and the problems of creation of the long-life solar stereoscopic observatory - Russia	V. M. Grigoriev, P. G. Papushev, S. A. Chuprakov, M. S. Chubey, G. I. Eroshkin, V. N. L'vov, and V. V. Pashkevich
Analysis of the Faraday rotation in the measurement of transverse magnetic field	J. Dun and H. Zhang
Tomography of heliospheric features developed for SMEI (*Invited*)	B. V. Jackson, P. P. Hick, and A. Buffington
Is the chromosphere heated by oscillations? (*Invited*)	W. Kalkofen
Type II bursts: dynamic spectra and source locations	S. A. Knock, I. H. Cairns, and P. A. Robinson
Radio emission from upstream of the Earth's bowshock	Z. Kuncic, I. H. Cairns, S. Knock, and P. A. Robinson
Nonlinear electrostatic decay of beam-driven Langmuir waves	B. Li, A. J. Willes, P. A. Robinson, and I. H. Cairns
Dynamics and entry of small dust grains near the heliosphere	I. Mann and A. Czechowski
Dynamic spectra for 2-3 kHz radio emission	J. Mitchell, I. Cairns, and P. A. Robinson
Regimes of stochastic wave growth in space plasmas	P. A. Robinson, B. Li, and I Cairns
North-south offset of heliospheric current sheet and its causes	P. Zhao, J. T. Hoeksema, and P. Scherrer
First steps to solar feature catalogues	V. V. Zharkova

References

Arge, C.N., & Mullan, D. J. 1998, Sol. Phys. 182, 293

Bemporad, A., Poletto, G., Suess, S. T., Ko, Y. K., Parenti, S., Riley, P., Romoli, M., & Zurbuchen, T. 2003, ApJ, 593, 1146

Brandt, P. C., Mitchell, D. G., Roelof, E. C., & Burch, J. L. 2001, Sol. Phys. 204, 377.

Caligari, P., Moreno-Insertis, F., & Schussler, M. 1995, ApJ, 441, 886.

Cairns, I. H., & Zank, G. P. 2002, GRL, 29(7), 47.

Cranmer, S.R., et al. 1999, ApJ, 511, 481

Demars, H., & Schunk, R. 1979, J. Phys. D, 12, 1051.
Deng, Y., Wang, J., Yan, Y., Zhang, J. 2001, Sol. Phys., 204, 11
Feldman, U., Schüle, U., Widing, K.G., & Laming, J.M. 1998, ApJ, 505, 999
Fludra, A., & Schmelz, J.T. 1999, A&A, 348, 286
Fisk, L. A. 1996, JGR, 101, 1011.
Gaidos, E. J.,Güdel, M., & Blake, G. A. 2000, GRL, 27, 501.
Gudiksen, B. V. & Nordlund, Å 2002, ApJ, 572, 113.
Gurnett, D. A., Kurth, W. S., Allendorf. S. C., & Poynter, R. L. 1993, Science, 262(5131), 199.
Hayashi, K., Kojima, M., Tokumaru, M., & Fujiki, K. 2003, JGR, 108,
Hansteen, V., Leer, E., & Holzer, T.E. 1997, ApJ, 482, 498
Henoux, J.-C., 1998, Space Sci. Rev., 85, 215
Jackson, B. V, Hick, P., & Buffington, A. 2003, in SPIE Conf. Proc. 4853, ed. S. L. Keil & S. V. Avakya (Bellingham, WA: SPIE Press), 23.
Izmodenov, V., Gloeckler, G., & Malama, Y. 2003, GRL, 30(7), 1351.
Izmodenov, V., & Alexashov, D. 2003, Astr. Lett., 29, 58.
Ko, Y.-K., Raymond, J., Li, J., Ciaravella, A., Michels, J., Fineschi, S., & Wu, R. 2002, ApJ, 578, 979
Kojima, M., Fujiki, K., Ohmi, T., Tokumaru, M., Yokobe, A., & Hakamada, K. 2001, JGR, 106(A3), 15677, SSH2-1.
Krivova, N. A., Solanki, S. K., Fligge, M., & Unruh, Y. C. 2003, A&A, 399, L1.
Kurth, W. S., & Gurnett, D. A. 2003, JGR, 108(A10), LIS 2-1.
Laming, J.M., & Feldman, U. 2003, ApJ, 591, 1257
Lanzerotti, L. J., Meford, L. V., Maclennan, C. G., Kraus, J. S., Kappenman, J., & Radasky, W. 2001, Sol. Phys., 204, 351.
Lanzerotti, L., J., & Sanderson, T. 2001, in The Heliosphere Near Solar Minimum: The Ulysses Perspective, ed. A. Balogh, R. G. Marsden, & E. J. Smith (Chichester, UK: Praxis Publishing), 259.
Lenz, D., Lou, Y,-Q, & Rosner, R. 1998, ApJ, 504, 1020
Liu, R-Y., Hu, H-Q., Xu, Z-H., Sato, N., & Fraser, B. J. 2001, Sol. Phys., 204, 307.
Lie-Svendsen, O., Hansteen, V. H. & Leer, E. 2002, JGR, 107(A10), SSH18-1.
Lie-Svendsen, O., Hansteen, V. H., Leer, E. & Holzer, T. E. 2002, ApJ 566, 562.
Marsch, E. 1991, in Physics of the Inner Heliosphere vol. 2 ed. R. Schwenn & E. Marsch (Heidelberg: Springer-Verlag), 159.
McComas, D. J., Elliott, H. A., Schwadron, N. A., Gosling, J. T., Skoug, R. M., & Goldstein, B. E. 2003, GRL, 30, 24.
Neugebauer, M., Forsyth, R. J., Galvin, A. B. et al. 1998, JGR, 103, 14587.
Nolte, J. T., Krieger, A. S., Timothy, A. F., et al. 1976, Sol. Phys. 46, 303.
Ohmi, T., Kojima, M., Yokobe, A., Tokumaru, M., Fujiki, K., & Hakamada, K. 2001, JGR, 106, 24923.
Ohmi, T., Kojima, M., Fujiki, K., Tokumaru, M., Hayashi, K., & Hakamada, K. 2003, GRL, 30, 62.
Peter, H. 1998, A& A, 335, 691
Phillips, K. J. H., Sylwester, J., Sylwester, B., & Landi, E. 2003, ApJL 589, 113
Raymond, J.C., et al. 1997, Sol. Phys., 175, 645
Reiner, M. J., Kaiser, M. L., Karlický, M., Jiřička, K. & Bougeret, J.-L. 2001, Sol. Phys., 204, 123
Smith, E. J., et al., 2003, GRL, in press.

Solanki, S. K., & Krivova, N. A. 2003, JGR, 108, SSH7-1.
Turcotte, S. & Wimmer-Schweingruber, R. F. 2002, JGR, 107, SSH5-1
Vögler, A. & Schüssler, M. 2003, AN, 324, 399
Wang, C., Richardson, J. D., & Burlaga, L. 2001, Sol. Phys., 204, 413
Wang, Y.-M. & Sheeley, N. R. 1990, ApJ, 355, 726.
Whang, Y. C., Burlaga, L. F., Ness, N. F., & Smith, C. W. 2001, Sol. Phys., 204, 253
Widing, K.G., & Feldman, U. 2001, ApJ, 555, 426
Wood, B. E., Müller, H.-R., & Zank, G. P. 2000, ApJ, 542, 493.
Yan, Y., Aschwanden, M. J., Wang, S., & Deng, Y. 2001, Sol. Phys., 204, 27
Zhang, J., Wang, J., Deng, Y., & Wu, D. 2001, ApJ, 548, L99.

JD8

Large Telescopes & Virtual Observatory: Visions for the Future

Chairpersons: F. Genova and Ding-qiang Su

Editors: F. Genova (Chief-Editor) and Xiangqun Cui

Highlights of Astronomy, Vol. 13
International Astronomical Union, 2003
O. Engvold, ed.

Joint Discussion 8: Large Telescopes and Virtual Observatory: Visions for the Future

Editors

Françoise Genova

CDS, Observatoire de Strasbourg, 11 rue de l'Universié, 67000 Strasbourg, France

Cui Xiangqun

National Astronomical Observatories/NIAOT, Chinese Academy of Sciences

Abstract. Very Large scale telescopes and virtual observatories have in common to be global facilities, which will enable entirely new types of sciences and will require new technical and operational philosophies. Joint discussion 8 was built with a series of invited reviews to set the long term vision and challenges, and specific projects or technical topics were presented in the poster session which was also a very important part of the meeting. To keep track of all the contributions, these proceedings contain the abstracts of all papers, invited reviews and accepted contributed posters, with a few extended abstracts.

1. Introduction

Joint Discussion 8, *Large Telescopes and Virtual Observatories: Visions for the future*, was held on July 17 and 18, 2003, in Sydney during General Assembly XXV. The Scientific Organizing Committee was J. Andersen (IAU), J.B. Breckinridge (USA), R.D. Cannon (Australia), O.B. Dluzhnevskaia (Russia), F. Genova (France, Co-Chair), R. Gilmozzi (ESO), R.J. Hanisch (USA), Iye M. (Japan), A. Kembhavi (India), R.P. Norris (Australia), P.J. Quinn (ESO), L.M. Stepp (USA), and Su D.-Q. (China, Co-Chair). A copy of the oral presentations is available on-line at `http://cdsweb.u-strasbg.fr/misc/jd_08.html`.

2. Invited Review Papers

2.1. Large Telescopes

Science drivers for Ground-based Future Giant Telescope (FGT) and Next Generation Space Telescope (NGST)

- **Cosmology, Large-Scale Structure, and Galaxy Formation**
  R. Gilmozzi - European Southern Observatory

  The next generation of future giant telescopes, with projects ranging from 30m to 100m and combining several-fold increases in sensitivity and resolution, will provide a totally new view of the Universe in the optical and near infrared, and will create important synergies with space observatories (e.g. JWST, XEUS) and ALMA.

  I will discuss possible science cases in cosmology, large scale structure and galaxy formation, showing the potentialities of various FGT sizes as well as the scientific requirements that the science cases put on the designs.

  The scientific topics will include the re-ionization epoch, the distribution of dark matter, the emergence of large scale structures, the supernova rate at high redshift, the evolution of the cosmological parameters, the structure and evolution of high redshift galaxies.

- **Formation of Stars and Planetary Systems**
  S. Strom - National Optical Astronomy Observatory, and L.M. Stepp

  We discuss the capabilities of next generation telescopes for addressing key problems in star and planet formation and the characterization of mature planets. Areas to be addressed include: (1) the formation of high mass stars and the origin of the stellar initial mass function; (2) the search for forming planets during the disk accretion phase; (3) new frontiers in exo-planet study. In each case we describe key measurements needed to enable major advances in understanding and the requirements they place on instrumentation and telescope system performance.

Ground-based Future Giant Telescope (FGT)

- **FGT Projects and Their Technological Challenges**
  L.M. Stepp - AURA New Initiative Office

  Around the world more than a dozen optical/infrared telescopes of the 6-10 meter class have been constructed in the past fifteen years. Astronomers and telescope designers are now focusing their attention on the design of even more powerful facilities described as future giant telescopes (FGTs). Many design concepts have been proposed; several of these concepts have received a significant amount of planning and analysis. This paper describes the main FGT projects and discusses the differences among their design concepts.

  Construction of FGTs will be challenging because of their large size and more demanding specifications for image quality, and because the affordability of these telescopes depends on finding ways to build them at costs significantly below the level predicted by conventional cost-scaling relations. This paper describes the key technological challenges faced by each type of design, and shows that many of these challenges are common to all of the concepts.

- **Progress in adaptive optics and multi-conjugated adaptive optics**
  R. Ragazzoni - INAF, Arcetri and MPIA, Heidelberg

  As single Natural Guide Star Adaptive Optics for 8-10m class telescope turned out recently to become reality and to produce astrophysical result, it is time to review which is the status of the matter, especially in the framework of Extremely Large Telescopes. This will obviously lead to the point of which is the progress status of Multi-Conjugated Adaptive Optics, a technique that, employing more than one Deformable Mirror, promises to achieve diffraction limited capabilities on a much larger Field of View. Today there are several projects in this framework aiming to produce images over a Field of View of about two arc min in size. I note here just three: the MCAO for GEMINI that should employ five laser guide stars that will generate artificial stars to be used as references; the Multi-conjugated Adaptive optics Demonstrator by ESO that will employ two different kind of wavefront sensors, both using three to eight natural reference stars, and NIRVANA, that is a two stage MCAO on the Large Binocular Telescope, used as an interferometer. All of these efforts has clearly an eye on the possible extension of the adopted techniques to Extremely Large Telescopes where, thanks to the larger pupil, some of the conceptual problems are easier to attack. The opinion of the writer is that there is today a wide range of attacks to the problem of achieving AO on ELTs and that in a couple of years, as some of the mentioned technique will be tested on the sky, a more detailed and effective road-map will be traced.

Future Giant Telescope in Space (NGST)

- **The James Webb Space Telescope**
  J.P. Gardner - NASA's Goddard Space Flight Center

  The James Webb Space Telescope (JWST) will be a large (6m) cold (50K) telescope launched to the second Earth-Sun Lagrange point. It is the successor to the Hubble Space Telescope and is a partnership of NASA, ESA and CSA. It's science goals are to detect and identify the first galaxies to form in the universe, to trace their assembly into the Hubble Sequence, and to study stellar and planetary system formation. JWST will have three instruments: The Near InfraRed Camera (NIRCam) and the Near InfraRed multiobject Spectrometer (NIRSpec) will cover the wavelength range 0.6 to 5 microns and the Mid InfraRed Instrument (MIRI) will do both imaging and spectroscopy from 5 to 28 microns.

- **Advanced technologies for future space telescopes and instruments**
  P. Gondoin - European Space Agency

  Astronomical space missions to be launched by the European Space Agency (ESA) include the Planck mission to image the anisotropies of the cosmic background radiation field, the Herschell sub-millimeter space observatory, the Eddington asteroseismology and planet finding mission, the NIRSpec multi-object spectrometer and the Gaia astrometry mission. A brief description of the scientific objectives and model payloads of some of these missions will be given. These provide guidelines for the technologies to be developed within the next years in the field of astronomical optics for space applications. The Darwin IR space interferometer and the XEUS high energy astrophysics mission currently under study by ESA indicate that future space observatories could consist of telescopes arrays operating in interferometric modes and of very large telescopes assembled into orbit. These future space observatories could make use of innovative technologies such as integrated optics or super-conductive tunnel junctions detectors with intrinsic spectral resolution.

Towards the Global Multi-wavelength Observatory

- **Future giant radio telescopes**
  H. Butcher - ASTRON - No abstract

- **International Collaboration in Astronomy**
  R.T. Schilizzi - Square Kilometre Array Projec)

  A number of the current major ground-based telescopes are international in funding and organisation, but most are not. Astronomical ambitions concerning the next generation of ground-based instruments are so substantial, and the costs so high, that international collaboration and funding may be the only way to realize the goals. I will examine a number of different models for international collaboration from astronomy and elsewhere, and draw some conclusions about their applicability for the next generation of telescopes.

- **Conclusion: IAU and Commission 9 roles in FGT**
  Su D.-Q. - National Astronomical Observatories/NIAOT, Chinese Academy of Sciences

  Looking back, from 1609 Galileo inventing the astronomical telescope to 1993, in 384 years, there were only two astronomical telescopes with aperture larger than 5m: the Russia 6m telescope and U.S.A. 5m Hale telescope. But from 1993 to the present, in only ten years, ten telescopes with aperture more than 8m have operated for astronomical observation. How great progress this is! These telescopes are ground-based telescopes and work in optical and IR waveband. Similar unprecedented achievements have also been obtained in radio telescopes and space missions. All these telescopes and instrumentation enable astronomers to study celestial bodies from the whole electromagnetic spectrum.

  By using various existent telescopes and instrumentation some events in the early universe have been observed. More than one hundred Jupiter-like planets have been found. These stimulate the astronomers and popular people strongly to hope to observe more events in the early universe including the first generation of galaxies to be assembled and to shine in the dark universe i.e. to see the dawn of modern universe, to research star and planet formation, to study black hole, to explore the earth-like planets in nearby stars. Telescopes much larger than existent 8-10m ground-based telescopes and 2.4m HST, and various other telescopes are needed for these researches. The progress in technology creates the possibility to build various much larger telescopes. Here let me only cite ground-based telescope as an example: the success of segmented- mirror Keck telescope created a possibility to build much larger telescopes, and the progress of adaptive optics showed the diffraction-limited image could be obtained at least in IR waveband. By using larger ground-based telescope not only more light energy could be collected, but also the higher resolution can be obtained. Many Future Giant Telescope projects have been put forward and are being developed, such as ground-based 100m OWL, 30m GSMT and CELT, Euro-50; space-based JWST, Herschel, Darwin, TPF, XEUS; radio waveband ALMA, SKA, and many others.

Now every two years SPIE holds astronomical telescopes and instrumentation conferences. This may be the main reason why for many years IAU Commission 9 has had almost no science meeting in these areas. IAU is the most important organization of the international astronomical community. Telescopes, instrumentation, and techniques are an important part of astronomy. New telescope projects are driven by astronomical goals. I think IAU should also hold astronomical telescopes and instrumentation conferences. These conferences should lean toward science goals, and they could make astronomers understand the recent development of telescopes and techniques. These meetings will be complementary with the SPIE meetings. Now IAU leaders have taken a serious about this. Dr. Andersen, the former IAU General Secretary, as a representative of IAU attend the SOC of JD8 and Prof. Ekers, the President-Elect of IAU, will give the closing talk for JD8 tomorrow. JD8 is a new beginning. I hope from now on there will be more symposia or colloquia on telescopes and instrumentation sponsored by IAU. And I hope IAU will achieve great successes in promoting the international collaboration on Future Giant Telescopes.

2.2. Virtual Observatories

Rationale, organization and science highlights

- **The Basis for the Virtual Observatory: History and Context**
  E.J. Schreier - Associated Universities, Inc. and STScI

  The International Virtual Observatory has been a concept in the making for several decades. Its realization depended on the convergence of several different technologies. Astronomy has had the advantage of requiring - and thus either driving or adapting - the state of the art in the relevant technologies, and doing so in advance of many other disciplines. As a result, the Virtual Observatory serves as a model for other disciplines. This paper will review the developments - sociological as well as technical - that made the Virtual Observatory first a possibility and then a reality as the technologies matured. It will also discuss the synergism of the VO concept currently being implemented with other forefront developments in astronomy.

- **The International Virtual Observatory Alliance**
  A. Kembhavi - Inter-University Centre for Astronomy and Astrophysics

Over the last few years, Astronomical Virtual Observatory (VO) projects have been initiated in several countries. The aim of these projects is to make astronomical data, gathered in all ways and in all places, available to every person who may need it, along with appropriate software for data access, analysis visualization and interpretation. The VO projects largely work in their own ways and with their own priorities, shaped by scientific interests and available resources.

For the VO concept to be successful, these efforts have to be meshed together seamlessly, through inter-operability standards, new data formats which take into account emerging technology, and software developed in forms which are largely independent of platforms and operating systems. It is also necessary to develop computing grids, which will cross national and project boundaries, and can be accessed by any researcher who wishes to use the data mountains. This process of integration and assimilation is to be fostered through international alliances spanning various VO efforts. I will describe in my talk formal alliances, like the International Virtual Observatory, as well as specific bilateral and multilateral collaborations between individuals, institutions or projects, and the VO related products that have been launched through these collaborations.

- **Science highlights: Star clusters and ASTROVIRTEL**
  P. Anders - Universitäts-Sternwarte Göttingen, and R. de Grijs - Extended abstract

  We introduce the potential of star cluster astronomy as a robust tracer of galaxy formation and evolution, and discuss the importance and relevance of linked multi-passband data archives (e.g., through the Virtual Observatory initiative) for its success. As an example, we present first results of a study utilizing the tools provided by the ASTROVIRTEL project built as a direct outcome of our approved proposal 'The Evolution and Environmental Dependence of Star Cluster Luminosity Functions', and incorporated in the QUERATOR data mining facility.

  As a result of the wealth of available observational data in the Hubble Space Telescope and ESO archives, the mining and retrieval of which were facilitated by the ASTROVIRTEL project, considerable feedback onto our stellar population models resulted in an iterative learning process: our models needed to be extended to cover the full parameter space spanned by our observed cluster parameters, and efficient tools to compare the observations with our model grid were developed. Both are finished, and the scientific phase of the project, i.e., the analysis of the large data volume, has started. Essentially, our data analysis tools allow us to determine the basic physical parameters (age, metallicity, extinction, mass) of each individual cluster in a given galaxy. From this we derive the required information about when and under which conditions the star clusters were formed.

  From the outset, this approach applied to our first example object, the dwarf starburst galaxy NGC 1569, resulted in a number of surprises. While the burst of star cluster formation in this galaxy appears to be shorter than the burst of general star formation in the field (as derived from the resolved stellar population), the average masses of the star clusters decrease as the burst of star cluster formation proceeds. This burst temporally coincides with the close passage of an intergalactic HI cloud. This suggests, therefore, that star cluster formation occurs predominantly during violent episodes of star formation. The change in the star cluster mass function is most likely related to the changing conditions of the interstellar matter from which the clusters were built.

`http://archive.eso.org/querator/`

- **Science highlights: Automated Classification of X-Ray Sources**
  R.J. Hanisch - Space Telescope Science Institute, and A.A. Suchkov, R.L. White, T.A. McGlynn, E.L. Winter, M.F. Corcoran, W. Voges

  ClassX is a Virtual Observatory prototype project aimed at the semi-automated classification of unidentified X-ray sources. ClassX draws from numerous on-line object catalogs using VO standard protocols to collect multi-wavelength position, flux, and source extent information. These data are used to train oblique decision tree classifiers. With ClassX we find large candidate populations of massive stars and T-Tauri stars, more than five times more numerous than the respective populations identified in the ROSAT WGACAT catalog. Many O-F5 and K-M candidates are found along sight lines to the LMC and SMC. A number of O-F5 and K-M candidates are bright IR sources with J-K excesses of 2 magnitudes and more, suggesting thermally emitting, hot circumstellar dust disks indicative of a pre-main sequence population. ClassX finds about twice as many new X-ray binary star candidates than in WGACAT, concentrated in the direction of the LMC and SMC. Many of these likely XRBs have harder X-ray spectra, suggesting a new class of previously unknown, extreme types of these objects. We also see that among extra-galactic objects, quasars are the most likely candidates for previously unidentified WGACAT sources, exceeding the population of galaxies and AGNs by factors of two to three.

- **The VO and Ground-Based Data**
  J. Huchra - Harvard-Smithsonian Center for Astrophysics

  The era of extremely large, public databases in astronomy is upon us. Such databases are opening the field to new research and new researchers. However it is important to be sure the resources are available to properly archive ground-based astronomical data, and include the necessary quality checks and calibrations.

  A Virtual Observatory without proper archives will have limited usefulness. This also implies that with limited resources, not all data can or should be archived. NASA already has a very good handle on US space-based astronomical data. Agencies and organizations that operate astronomical facilities, particularly ground based observatories, need to plan and budget for these activities now.

  We should not underestimate the effort required to produce high quality data products that will be useful for the broader community. Currently the best way to “fill” archives is with data from surveys. That will continue to be the case for most ground based observatories.

- **The Theoretical Virtual Observatory**
  S. White - Max Planck Institute for Astrophysics

  A functioning virtual observatory will require easy and transparent access not only to diverse observational databases, but also to the tools needed to analyze, visualize and interpret them. For the large statistical datasets produced by modern, multi-wavelength surveys, this almost always requires the use of equally large, artificially generated “mock” surveys. These are used to calibrate observational biases introduced, for example, by flux or resolution limits, and to study how differing physical effects are manifest in the observational plane (for example how the observable clustering of galaxies is affected by merging, by collision-induced starbursts, by harassment, etc). Such mock catalogues are almost always produced from large-scale supercomputer simulations, so the “virtual observer” of the future will need access to such theoretical datasets or to the computer codes and resources needed to create them. At the MPA and within the Virgo Super-computing Consortium we have for several years publically released both supercomputer code and large, simulated datasets. I will review how this experience can help in the design of the theoretical component of a virtual observatory.

- **Science highlights: Discovery of Brown Dwarfs with Virtual Observatories**
  J.D. Kirkpatrick, presented by G.B. Berriman - Infrared Processing and Analysis Center, R.J. Hanisch, A. Szalay, R. Williams

  We describe how to use cross-matching between the 2MASS and SDSS source catalogs to find brown dwarf candidates that are cooler and more distant than those discovered to date in the individual surveys. Our eventual goal is use the cross-matching to discover brown dwarf candidates from the large numbers of usually spurious single-band detections in each survey. A pilot study conducted for the NVO illustrates the power and promise of the method. This study searched for brown dwarf candidates that were detected only in the z-band in SDSS and in the J band in 2MASS. In our first trial we cross-matched all 2MASS Second Incremental Data Release (IDR2) sources falling within 3 arc sec of an SDSS Early Data Release (EDR) source. The cross-match covered an area of roughly 150 square degrees and contains 326020 matches. Further filtering through a conservative z-J color cut recovered the known brown dwarfs in that area - a T dwarf (SDSS 1346-0031) and a late-L dwarf (SDSS 1326-0038) while also uncovering three more excellent brown dwarf candidates. One of these (2MASSI J0104075-005328) has been spectroscopically identified as an L5 dwarf.

- **Science Highlights: Science from the AVO 1ST Light: the High Redshift Universe**
  N.A. Walton - Institute of Astronomy, University of Cambridge, and M.G. Allen

The Astrophysical Virtual Observatory science working group defined a number of key science drivers for which the AVO should develop capabilities. At the AVO's Jan 2003 'First Light' event, the AVO prototype data access and manipulation tool was demonstrated. In particular its use in enabling discovery in deep multi wavelength data sets was highlighted. In this presentation I will describe how the AVO demonstrator has enabled investigation into the high redshift universe, and in particular its use in discovering rare populations of high redshift galaxies from deep Hubble and ground based imaging data obtained through the Great Observatories Origins Deep Survey (GOODS) programme.

Round table Discussion

The round table discussion was chaired by O. Malkov and Ohishi M.. Ohishi M. introduced the discussion, and then several papers were presented, dealing with different aspects of the VO. Two talks presented emerging VO projects in Australia (D. Barnes, abstract in the Poster section) and in South Africa (P. Woudt). T. Dorokhova discussed the important topic of Thesaurus is astronomy (paper presented by F. Genova, abstract in the Poster section). Tatematsu K. presented a user point of view on the "VO for diverse interests". G.T. Rixon discussed the GRID paradigm.

Conclusions

- **How Will the VO Affect Astronomy?**
  G. Gilmore - Institute of Astronomy, University of Cambridge

  The Virtual Observatory is in that optimistic yet dangerous phase of development where everyone believes it will solve all problems, but not really force any involuntary changes on the way astronomy is done. The same statements were made about the Internet a few years ago... Progress in astronomy has depended on individual insight, and has also typically been led by small groups with the best technology and greatest resources. More commonly today, multi-partner collaborations with at least significant public funding develop the largest projects, with rapid public data access an obligation. The/a/one goal of the astrophysical virtual observatory is to provide the analysis tools and practical access to those data to a very wide community. When this is achieved, as it will be, given the excellence and enthusiasm of those involved, astronomy will be one step towards solving its people-problem: the whole community will be able to think about the best data. This threatens PIs, imposes huge strains on funding, makes it harder for groups to do well by resource control, will potentially restructure the present link between excellence and place of research, and will force all of us to try harder. Excellent.

- **Summary: Commission 5 role in the VO**
  F. Genova - Centre de Données astronomiques de Strasbourg

  Astronomy is a small discipline, with few commercial constraints and a long tradition of data conservation and of partnership to define standards, with FITS as a figurehead. Information networking is already an everyday tool for astronomers, which can for instance access bibliographic information from ADS, SIMBAD, NED, from the electronic journals, from the VizieR catalogue and table database, and from observatory archives, and can also surf easily from one information service to the other. The next step is now to integrate information, including large surveys, theory, ... The Virtual Observatory is *an enabling and coordinating entity to foster the development of tools, protocols, and collaborations necessary to realize the full scientific potential of astronomical databases in the coming decade* (NVO White Paper, June 2000). It is science driven, not technology driven (although it aims at making the best usage of Information Technologies for building tools for astronomers). VO projects arose from active and experienced groups, which cooperated at the international level from the very beginning. The Virtual Observatory is one of the very few truly global endeavors of astronomy. Each project pursues its own goals (as accepted by its financing agencies), with a common goal, giving transparent access to data and tools for users from all around the world - which should bridge gaps in data and information access and accessibility. They all work together to define inter-operability standards. New teams (even small teams) from other countries are welcome to participate, publish their data, create new tools to be used in the general frame, join the IVOA inter-operability working groups, etc

IAU Commission 5 (Documentation and Astronomical Data) has been eager to take into account the rapid evolution of data dissemination since the advent of the Internet, by implementing a dedicated Working Group, first called *Data Centres and Networks*, which became *Data Centres, Networks and Virtual Observatories* in 2000, and will be *Virtual Observatory* from the General Assembly on.

2.3. Closing talk: Big telescopes, big data, more science (R.D. Ekers - UAI, ATNF)

R. Ekers, IAU President, agreed to present Joint Discussion 8 concluding remarks. He explained that the IAU executive combined the requests for a meeting on large telescopes with a request from the Virtual Observatory community into this single Joint Discussion. He commented on the differences in approach between these two groups, but also the need for both to work closely together, and on his hope that IAU can facilitate this interaction.

He illustrated the following points from his experience in radio-astronomy: both hardware and software developments are needed to exploit the potential of new facilities; one needs to include projection of new capabilities when designing instruments; different approaches are used in the management of hardware and software projects in astronomy, which in part lead to the very different issues and approaches which have been discussed in the two halves of the JD8 meeting. He listed important topics pleading for diminishing the separation between the IVO and the telescope building communities: learning from each other; the need for the IVO to understand the impact of new hardware technologies, and for technology developers to understand the IVO since this new paradigm might effect optimum hardware design. This is a difficult challenge because of the need to extrapolate expected performances into the future to build the optimum strategy. Difference in times scales also have to be taken into account with complex software taking longer to develop than the time scales for computer hardware developments.

IVO developments can play a key role in the broader applications of shared databases. Fortunately for astronomers the stars and galaxies have no privacy requirements and so we can develop tools to link and explore multi-wavelength databases in a much easier environment than for example in epidemiological studies where databases have to be linked through peoples names. Developments in IVO can be used to help solve the far more difficult epidemiology problems.

R. Ekers reminded us that the IAU mission is to promote the science of astronomy worldwide. The IVO is a visionary project which has to be international to succeed and has a natural and supportive home in the IAU.

3. Poster papers

3.1. Large Telescopes

Future Giant Large Telescopes and Sites

- **Status of the Southern African Large Telescope (SALT)**
  D.A. Buckley - Southern African Large Telescope

  SALT is well over half way to completion. By the end of 2003, all major subsystems, including the commissioning instrument, will be in place and the commissioning of them begun. Tests of a subset of the mirror array, including the Shack-Hartmann alignment instrument, the mirror actuators, capacitive edge sensors and active control system will also have started. Finally, the first on-sky tests involving the complete light path, from object to detector, will be completed.

  This paper describes the status of the SALT project, due for completion by the end of 2004, including the major science drivers and first-generation instruments. These are confined to the visible spectrum, but optimized for UV performance, with capability from $\tilde{3}$20-900 nm. Instruments will have access to an 8 arcmin diameter science field and will be seeing limited. The telescope design necessitates queue-scheduled observing, ideal for survey science and time resolved studies of astrophysical phenomena, an important aspect of the overall SALT science drivers. Special efforts are being made to ensure such a capability by employing frame transfer CCDs. Initial instrument capabilities include broad and narrow band imaging, long-slit and multi-object spectroscopy, polarimetry, Fabry-Perot imaging spectroscopy and high resolution fibre-fed spectroscopy.

- **Two Chinese Telescope Projects Based on Active Optics**
  Su D.-Q. - National Astronomical Observatories/NIAOT, Chinese Academy of Sciences, and Nan R.

  Two special telescopes are being developed in China, which cannot be realized in traditional ways. One is the Large Sky Area Multi-object Fiber Spectroscopic Telescope (LAMOST). It has a 4m aperture and 5 degree FOV, with a reflecting Schmidt optical system. Three main parts: the reflecting correcting plate, the focal surface and the spherical mirror lie on the ground along north to south. During observation only the alt-azimuth mounting of reflecting plate and the focal surface do the tracking rotations. In this situation the shape of correcting plate should be changed with the change of sky area. LAMOST has been approved by Chinese Government. Another is the radio telescope FAST, Five Hundred Meter Aperture Spherical Telescope. It will be sited in a Karst hole like Arecibo 305m telescope. The main difference between FAST and Arecibo is: during the observation the illuminated area (300m diameter) of FAST will be changed from spherical surface into a paraboloid. Thus spherical aberration correcting system is unnecessary and a simple feed can be put in its focus. It extremely reduces the weight and complexity on the cable. The feasibility study has been financed by the Chinese Academy of Sciences and completed successfully in 2002.

- **A Configuration for Chinese Future Giant Telescope (CFGT)**
  Cui X. - National Astronomical Observatories/NIAOT, Chinese Academy of Sciences, and Su D.-Q., Wang, Y.-N.

  In this paper a preliminary configuration for Chinese Future Giant Telescope (CFGT) is proposed. It is a 30m telescope using segmented primary mirror alt-azimuth mounting. The primary mirror is aspherical f-ratio 1.2 and it consists of 1095 submirrors. This telescope includes Nasmyth coude and a wide field of view optical systems. There are some characteristics in CFGT: (1) Partial annular submirrors are used;(2) One of coude planar mirrors is aspherical and the better image quality is obtained for such a coude system. (3) A pair of lens-prism is used in wide field of view system. The better image quality is obtained and atmospheric dispersion is corrected.

  We believe China has got the potential to build a 30m telescope even if China has not build 8-10m telescope, because:(1) The economics has been developing very fast in recent 25 years; (2) We are obtaining experiences and technologies from national project LAMOST;(3) A glass factory in Shanghai has got experience to manufacture the zero thermal expansion mirror blank VO2 for about 25 years; (4) We have specially bought an annular polishing machine for the large number of submirrors' polishing; (5) Site exploration on Qinghai-Tibet Plateau for future giant optical/infrared telescope has started.

- **Canadian Efforts Towards a Future Large Telescope**
  D. Crabtree - National Research Council Canada, and S. Roberts, R. Carlberg, D. Halliday

  A Very Large Optical Telescope (VLOT) was identified as a high priority project in the Canadian Long Range Plan for Astronomy that was published in early 2000. The VLOT concept is for a 20-m segmented mirror telescope that could replace the CFHT on Mauna Kea. Technical studies and some design work have been undertaken by both NRC-HIA and AMEC Dyanamic Structures over the past two years. VLOT effort is now funded at the \$1M (Cdn) per year level. This presentation will describe the Canadian work to date.

- **Next Generation CFHT: Concepts and Optical Performance**
F. Zamkotsian - Laboratoire d'Astrophysique de Marseille, and K. Dohlen, D. Burgarella, M. Ferrari

The Canada-France-Hawaii Telescope (CFHT) community is engaged in studies for the replacement of the present 3.6m telescope, until recently considered one of the best telescopes in the world, by a world-class research facility at the beginning of next decade. The motivation to design and build a new telescope is driven by the astronomers need to observe fainter sources. The basis of the next generation CFHT (NG-CFHT) is therefore to increase the size of the primary mirror up to 20-30m. Beyond this photon quest the way we use the photons is also very important.

We propose to develop a NG-CFHT which is able to handle and take advantage of parallel observing with several instruments simultaneously. New technologies e.g. active and adaptive wavefront control Micro Opto Electro Mechanical Systems (MOEMS) will permit an optimization of the telescope performance. We present different optical concepts based on a segmented primary with 8 large 8m-class aspheric petals. Optical performance is evaluated through PSF calculation for the different concepts.

- **The Case for Small Telescopes in the Age of Giants**
T.D. Oswalt - Florida Institute of Technology

The closures of 1-4m telescopes at several international facilities over the past decade have been cause for lament in the astronomical community. However the future of small telescopes in the dawning era of giants should be quite bright if creative steps are taken. This paper will address some of the scientific and productivity issues that argue persuasively that a strong partnership between small efficient telescopes and the new generation of giant telescopes is essential. For example, among a host of functions that can best be performed by small telescopes are the development of innovative approaches to operations instrumentation, and unique research projects. To accomplish these, it will be essential to improve the operational efficiency of existing small facilities via more frequent use of standard off-the-shelf technology, optimization of individual telescopes for special projects, increased use of active and adaptive optics, automation, and remote access. A selection of scientific initiatives will be presented that are ideally suited for new (or renovated) small telescopes.

- **Magdalena Ridge Observatory Project Overview**
B.E. Laubscher - Los Alamos National Laboratory, and D. Buscher, M.J. Chang, M.L. Cobb, C.A. Haniff, R.F. Horton, A.M. Jorgensen, D. Klinglesmith, G. Loos, G., R.J. Nemzek, S. Restaino, V. Romero, E. Ryan, W. Ryan, S. Teare, L. Trusdell, D. Voelz, D. Westfahl

The Magdalena Ridge Observatory (MRO) is a project with the goal of building a state of the art observatory on Magdalena Ridge, west of Socorro, New Mexico. This observatory will be sited above 3700 meters and will consist of a 10-element, 400-meter baseline optical/infrared imaging interferometer and a separate, 2.4-meter telescope with fast response capability. The MRO consortium members include New Mexico Institute of

Mining and Technology, University of Puerto Rico, Mew Mexico Highlands University, New Mexico State University and the Los Alamos National Laboratory. The University of Cambridge is a joint participant in the current design phase of the interferometer and expects to join the consortium. We will present an overview of the optical interferometer and single telescope designs and review their instrumentation and science programs.

- **Mt. Maidanak and Plateau Suffa as a Candidate Sites for FGT**
  S. Egamberdiev - Ulugh Beg Astronomical Institute of the Uzbek Academy of Sciences, and S. Ilyasov

  The astroclimate studies at Mt. Maidanak, located at a distance of about 120 km south of Samarkand, Uzbekistan, carried out in co-operation with ESO, Universities of Nice and Moscow in 1996-2002 indicated that it is one of the most favorable sites world-wide for astronomical observations. Not only this fact but also an exceptional geographical location, very complementary to the main international facilities of Chile, Canaries and Hawaii, makes Mt.Maidanak very attractive for observational programs requiring continuous monitoring of astronomical objects. Recent results of site testing at Mt. Maidanak as well as summary of results obtained in frame of collaborative programs with advanced western institutions will be presented. In the 80s the Suffa plateau located at a distance of about 200 km south-west of Tashkent was selected for construction of observatory with 70m radiotelescope (RT-70) for submm range as a main instrument. Just before the end of the SU, about 60% of facilities including 105 m high pillar of the RT-70 were constructed. Now an Uzbek-Russian intergovernment Agreement on constructing the radio observatory has been signed and at present both governments show increasing interest on finalizing this project.

- **Mt. Dushak-Erekdag Observatory as a potential site for the Future International Observatory**
  T.N. Dorokhova - Astronomical Observatory of Odessa National University, and N.I. Dorokhov

  The Mt. Dushak-Erekdag Observatory (Central Asia, Turkmenistan, the longitude 58° E, the latitude +38°) is located just in the "longitudes' gap" of asteroseismological networks. Our observations during many years have shown that the sky seeing at the site is one of the best in Central Asia: a low light pollution, high and stable sky transparency, over 200 usable nights per year. The altitude is above 2000 m. Characteristics of the locality have such fortunate combination of the features which makes this site unique for building of FGTs. We present the project of the Future International Observatory at the Mt. Dushak-Erekdag.

New Techniques and Methods

- **LAMA - a Novel Concept for a Very-Large Optical Telescope**
  P. Hickson - University of British Columbia, and K.M. Lanzetta, A. Crotts, M. Shara, B. Truax, B., J.K. Webb

We report preliminary results of a conceptual design study for a next-generation ground-based telescope. The Large-Aperture Mirror Array (LAMA) would be a multi-aperture telescope employing rotating liquid-metal primary mirrors. Tracking systems, comprised of articulating aspheric mirrors traversing the focus of each primary mirror, would allow this telescope to point and track within an 8-degree diameter region. Light from all primary mirrors would be combined at a common focus. Adaptive optics, in conjunction with phase-tracking and a Fizeau beam combiner, would allow the telescope to achieve milli-arcsecond resolution in fields surrounding natural guide stars. With an effective area equivalent to that of a 50-meter telescope, LAMA could reach sub-nanoJansky flux levels in targeted areas. Equipped with a multi-band optical-infrared camera and a high-resolution spectrograph, it would be a powerful tool for exploring the distant and local universe, stellar systems and extra-solar planets.

- **Status of Active Optics Methods and Applications to FGTs**
  G. Lemaitre - Laboratoire d'Astrophysique de Marseille, and M. Ferrari, K. Døhlen, F. Zamkotsian

  A short review of today state of the art in active optics techniques will be presented. The two mains topics addressed by these techniques will be considered and detailed. Active optics processes applied during optical manufacturing have many advantages for the realization of aspherics or extreme optics (stress polishing techniques). Examples of realization will be given. The high potential of active techniques for in-situ control of large mirrors shape has been fully demonstrated with the results obtained with the VLT project. Another example of this clever solution for mirror shape control is the original LAMOST project. Considering the technological challenges raised by the future generation of giant telescopes FGTs ranging from 20 to 100m, the active optics techniques can be a solution to many of the foreseen difficulties. The advantages of active optics will be emphasized in the perspective of the realization of FGTs and improvement of their performances.

- **Active Optics Concept for Hyper Telescopes**
  K. Dohlen - Laboratoire d'Astrophysique de Marseille, and P. Dargent, M. Ferrari, G. Lemaitre

  The Hyper Telescope (HT) based on densified sparse pupils is one of the instrumental concepts under study for future large-baseline interferometers. Its compatibility with stellar coronography makes it interesting for exo-planet search and characterization. Baselines considered for first-generation HTs are of the order of 100 m but one can envisage kilometric arrays capable of unprecedented angular resolution. The focal plane instrumentation, including aberration correction and pupil densification optics, is included in an instrument space craft (ISC) located in the primary focus.

  In this paper we present optical and mechanical concepts for combined aberration correction and pupil densification using multi-mode deformable mirror (MDM) and mechanically amplified piezo actuator technologies. Among the advantages of such a system over large monolithic corrector optics is the relaxation of piston alignment requirements between primary segments.

- **MOEMS, Micro-Optics for Future Astronomical Instrumentation**
  F. Zamkotsian - Laboratoire d'Astrophysique de Marseille, and P. Lanzoni, A. Liotard, K. Dohlen

  Scientific breakthroughs often follow technological breakthroughs permitting to make significant steps forward. Astronomical research of the next decade is related to the quest for our Origins: How did Galaxies form? How did Stars and Planetary Systems form? Can we detect Life in other Planets? The science requirements provided by those topics are very constraining for future astronomical instrumentation calling for multiplexing capabilities and high spatial and spectral resolutions.

  In Laboratoire d'Astrophysique de Marseille we are engaged since several years in the development of micro-optical components so called Micro-Opto-Electro-Mechanical Systems (MOEMS). Based on the micro-electronics fabrication process the major advantages of these components are their compactness scalability and specific task customization using elementary building blocks. We are studying programmable slit masks for Multi-Object Spectroscopy (MOS) and micro-deformable mirrors for next generation Adaptive Optics (AO) systems.

  We will present our work on modeling and characterization of the micro-mirror array (MMA) for generating reflective slits and the micro-shutter array (MSA) for generating transmissive slits for MOS application. We will also discuss our recent developments of micro-deformable mirrors in our collaboration with micro-opto-electronics laboratories. We are involved in JWST VLT2 NG-CFHT and OWL studies.

- **Mach-Zehnder Phasing Sensor for ELTs**
  K. Dohlen - Laboratoire d'Astrophysique de Marseille, and L. Montoya-Martinez

  Segmented mirror technology has been successfully applied to 10m class telescopes (Keck, HET, GTC) and its application to future extremely large telescopes (20m NG-CFHT, 30m CELT, 50m EURO50, 100m OWL) is required. Extensive use of adaptive optics in these telescopes puts stringent specifications on wavefront error allowing typically of the order of lambda/20 to segmentation errors. Several phasing metrology schemes adaptable to these giant telescopes are under development.

  We investigate a novel technique based on the Mach-Zehnder interferometer with a spatial filter in one arm. Atmospheric turbulence is tolerated in this setup if the spatial filter has the size similar to that of the seeing disk. The resulting interference pattern only contains the high-frequency spatial information including information about the piston step height.

  We describe the theoretical analysis of this system and show simulated and experimental results. Different error sources are analyzed in order to provide a preliminary idea of the merits of this technique compared with other phasing techniques.

- **New Method for Stellar CCD Photometry**
  A. El-Bassuny Alawy - National Research Institute of Astronomy and Geophysics

  The ALAWY stellar CCD photometry method (Alawy 2001 Ap&SS 277 473) is outlined. Further development has been done to handle the case of uneven background brightness employing simple numerical technique. Several CCD frames of different specifications have been adopted to test the method. The result obtained is excellent in view of the accordance between magnitudes derived and the published ones.

- **Simulating Interferograms for Testing Big Dimensions Optics**
  A. Rodriguez-Hernandez - INAOE, and J. Castro-Ramos

  Based on two interferometric modern techniques, Electronic Speckle Pattern Interferometry and Fringe Projection Technique, we have realized simulations of interferograms for both rough aspherics surfaces around five microns and five meters in diameter up. Experimental interferometric setup is proposed and developed software with which we reached our goal is explained.

- **The Limit Magnitude for the Next Extremely Large Telescopes**
  Z. Benkhaldoun - LPHEA Cadi Ayyad University, and T. El Halkouj, R.G. Petrov, M. Lazrek, Y. El Azhari

  This work consists in determining the limit magnitude of co-phasing for an interferometer made of N telescopes simultaneously co-phased on a natural star, then to compare it with that for a mono-pupil of the same collecting surface. We showed that the simultaneous co-phasing telescopes made an interferometer less powerful than if its surface is divided into a greater number of pupils. The configuration of cophasing in which the groups of pupil are organized in hierarchical structure are studied to decrease this disadvantage. The limit magnitudes are founded on an estimate of the signal to noise ratio (SNR) of (or for) sensor of fringes taking into account the noise of photons, thermal noise and detector noise reading, for conditions of seeing given, supposing all bases are larger than external scale of optical turbulence.

- **2-CLEAN DSA Method for Simulation and New Systems Projecting**
  M. Agafonov - Radiophysical Research Institute, NIRFI

  In [1,2,and 3] we have presented the 2-CLEAN DSA Method for tomographic and astronomical image reconstruction. This technology can help simulate and create new systems. The basic principles in modern tomography and in astronomy are the necessity to take into account the physical character of the problem and the demand to start the instrument projecting after the algorithm has been created and examined. The latter, unfortunately, was not used in medicine earlier and because of great number of projections the radiation dose was sufficient. Radioastronomy has made a considerable contribution to the solution of some important problems that are the same for radioastronomy and tomography [4], which, as it seems to us, it can be proud of. We present the technology of simulation for creating of tomographical or astronomical systems by few projections of knife beams, for optical slits systems with having the opportunity to investigate in a wide space frequency range. 1. Agafonov M.I. ASP Conf. Ser. v.125 ADASS VI p.202, 2. ASP Conf. Ser. v.145 ADASS VII p.58 3. Agafonov M.I. Few Projections Astrotomography: 2-CLEAN DSA Reconstruction, 4. IAU00446 & Radioastronomical approach to Few Projections Tomography. IAU00450. See also abstracts IAU GA 2003, JD09.

- **New Solutions, Innovative Materials for Giant Telescopes**
  G. Marchiori - European Industrial Engineering, and F. Rampini, L. Ghedin, S. de Lorenzi, A. Zanon, L. Giagomel

  The VLT 8-m ground-base telescopes, successfully realized and commissioned, are now producing science.

  The European Prototype for ALMA project is manufactured and now under erection.

  Based on these experiences, EIE will present his status of the new solutions for mirror cell structures and for telescope buildings.

- **The Impact of Radio Interference on Future Radio Telescopes**
  D.A. Mitchell - The University of Sydney, School of Physics, and G.J. Robertson, R.J. Sault

  While future radio telescopes will require technological advances from the communications industry, interference from sources such as satellites and mobile phones is a serious concern. In addition to the fact that the level of interference is growing constantly, the increased capabilities of next generation instruments make them more prone to harmful interference. These facilities must have mechanisms to allow operation in a crowded spectrum. In this report some of the factors which may limit the effectiveness of these mechanisms are investigated. Radio astronomy is unique among other observing wavelengths in that the radiation can be fully sampled at a rate which completely specifies the electromagnetic environment. Knowledge of phases and antennae gain factors affords one the opportunity to attempt to mitigate interference from the astronomical data. At present several interference mitigation techniques have been demonstrated to be extremely effective. However the observational scales of the new facilities will push the techniques to their limits. Processes such as signal decorrelation, varying antenna gain and instabilities in the primary beam will have a serious effect on some of the algorithms. In addition the sheer volume of data produced will render some techniques computationally and financially impossible.

- **Feed Designs for the Lovell and MKII/Defford Telescopes**
  Su Y. - National Astronomical Observatories, Chinese Academy of Sciences

  In order to remain competitive with, eMERLIN requires the development of four new feed designs to cover the 4 to 8 GHz band, for the Lovell Telescope, MkII and Defford, Cambridge, and the E-Systems Telescopes. The need, in each case, for good return loss and constant beam width across an octave band presents a set of difficult challenges. The prototype Lovell and MKII/Defford feeds have been designed, manufactured and tested, both in the laboratory and on the telescopes.

- **Multi-Band Film Lens Antennas for Radio Telescope Satellites**
  Ujihara H. - National Astronomical Observatory in Japan, and Chikada Y., Nakahira K.T.

  Large reflector antenna is a conventional way to achieve high sensitivity of radio telescopes, but keeping accurate reflector surface becomes more difficult in higher frequency or larger antenna aperture. Radio telescopes with lens antenna would be less sensitive to surface errors and pointing accuracy than with reflector antennas, however, no practical studies have ever been done about large lens antennas. We developed Film Lens Antenna (FLA), which has very low insertion loss and mass. This is fundamentally Fresnel lens antennas with unique phase shifter films which were newly developed and which cause FLA to have a simple plane structure with a few films. Therefore it is especially useful for a main antenna of a satellite like "HALCA" which is a radio astronomical satellite for the first Space-VLBI mission.

  We can design transparent phase shifter films with arbitrary phase shifts to $\pm$ 180 degrees to make efficient lens. We made 90-cm FLAs for 22GHz based on our previous numerical works and measured its efficiency as 40%. This is a satisfactory result as a first step of FLA to gigantic aperture radio telescopes. Also we designed and measured multi-band films toward more practical FLA which can simultaneously receive 86GHz, 43GHz, 22GHz for example.

- **Spherical Dish Huge Array from Radio to IR**
  Sawano A. - Waseda University, Institute for astrophysics, and Okubo R., Takefuzi K., Yoshimura N., Ichikawa H., Matsumura N., Kuniyoshi M., Takeuchi H., Asuma K., Daishido T.

  Eight element 20m spherical dish array was constructed as a digital interferometer for searching radio transient sources and pulsars. Wavelength ratio to IR is 10000. We investigate the possibility in extending wavelength to IR. In spherical dish all segment mirrors have identical iso-curvature, which makes it possible to use mass-produced system. In our spherical dish array, 36x2x8 = 576 segment mirrors are used. Present surface accuracy of 2mm rms must be reduced to 0.01 mm in IR, which requires smaller segment mirrors. Aberration correcting asymmetrical Gregorian sub-reflector is used in the present radio observation watching to five degrees from zenith and focus is at bottom in each dish. Thus the sky from +32 deg to +42 deg zone in declinations is observable. Only Az rotation of sub-reflector and feed horn are required. Four box PCs reading sixteen Az rotary encoder outputs of the sub-reflectors and the feed horns control them to rotate. Main PC watching all system is connected with the box PCs by RS485 cables. Total construction cost of the present eight element array in radio waves was $1.2M. Present digital phase correction system might be useful in future digital adaptive optics system in IR Spherical Dish Huge Array.

3.2. Virtual Observatories

Status reports of Virtual Observatory projects

- **The Australian Virtual Observatory Project: 2003 and Beyond**
  D.G. Barnes, The University of Melbourne

  The Australian Virtual Observatory is funded in 2003 to bring a number of premiere Australian astronomy archives on-line and to begin prototyping virtual observatory tools and processing pipelines relevant to Australian astronomers. We are exploring the use of a commercial database to publish source catalogs such as HIPASS and SUMSS, both with VOTable export capabilities. Meanwhile, the catalog of quasars from the 2dF galaxy redshift survey will be published using the Canadian Virtual Observatory resources, and the CSIRO is hosting a cross-divisional project to place the entire archive of observations with the AT Compact Array on-line with a sophisticated search interface honoring data providence and proprietary periods. In terms of virtual observatory tools, a joint project is underway with AstroGrid to grid-enable an existing high-performance volume rendering application, making it available to users without requiring special hardware or software, and the ATNF is building on its expertise in visualization to develop a Java-based interface to existing AIPS++ display tools.

- **Science and the Virtual Observatory**
  D. Schade - National Research Council Canada, and P. Dowler

  The Canadian Virtual Observatory (CVO) is the cornerstone of a budding international partnership that delivers high quality scientific content and capabilities to the astronomical community. We have developed a uniform astronomical data model to characterize all types of observational data across the entire electromagnetic spectrum; this model enables users to find archive data based on the content and the quality without letting the technology get in the way. We have also developed general purpose source and object catalogs to store information extracted from the data using standard techniques and algorithms. These catalogs are explorable with a variety of scientific tools, from a web interface for simple tasks to a programmatic interface for sophisticated analysis involving client and server side processing. Finally, all of the data processing and analysis tasks we have executed or will execute are viewable via our processing catalog; links between object and source catalogs, processing catalogs, and observation catalogs allow users to examine the complete pedigree of every single derived value. Thus, the entire system is open to peer review which is the cornerstone of science.

- **Grid Based Chinese Virtual Observatory System Design**
  Cui C. - National Astronomical Observatory of China, and Zhao Y.

  Chinese Virtual Observatory (China-VO) project is a consortium initiated by Chinese National Astronomical Observatory and Large Sky Area Multi-Object Fiber Spectroscopic Telescope project. A three-layer architecture of the China-VO is described, which depends upon the Open Grid Services

Architecture being developed by the Global Grid Forum. The fabric layer mainly consists of astronomical datasets with corresponding metadata and data access services. The resource layer includes a large scale of services for grid resource management, data interoperation, data mining, security, logical name space, and so on. The application layer consists of user interfaces and other client services. In the China-VO system, all the functional components are SOAP Grid service implementations.

Chinese National Grid (CNGrid) will be the testbed for the China-VO. How to interact with other CNGrid components is also discussed.

- **LAMOST Project and the Chinese Virtual Observatory.**
  Zhao Y. - National Astronomical Observatories, and Cui C.

  Chinese Virtual Observatory (China-VO) is a consortium initiated by National Astronomical Observatories of China and Large Sky Area Multi-Object Fiber Spectroscopic Telescope (LAMOST) project. The LAMOST project will survey more than ten million galaxies and stars to get their spectra after the telescope constructed. The huge volume of data set from LAMOST spectroscopic sky survey is very valuable for researches on wide field and large sample astronomy. An important task for China-VO is to make LAMOST scientific data services as VO-enabled. The input catalogs for the LAMOST spectroscopic survey will benefit from the abundant international astronomical archives interconnected through China-VO. The progress and roadmap of China-VO project will be introduced.

- **VO and Chinese Current Status, Developments**
  Lin, G.

  VO will produce huge and deep affect on astronomy. Chinese astronomer is facing to VO's chance and challenge. In this paper, the author discusses relationships between Chinese current status, development in network, large telescopes, data and computer equipments and VO from macroscopical point of view. The author thinks CVO (China VO) will not only make contribution to Chinese astronomers but also to world astronomers.

- **Introduction of the Korean Virtual Observatory (KVO)**
  Kim S. C. - Korea Astronomy Observatory, and Sung H.-I., Kim B.G., Chun M.-Y., Park J.-H., Cho S.-H., Byun Y.-I., Koo B.-C.

  The Korean Astronomical Data Center (KADC) in Korea Astronomy Observatory (KAO), the national observatory of the Republic of Korea, has started its mission in 2002 and performed the principal axis in giving birth to the Korean Virtual Observatory (KVO) in February 2003. We have commenced building the KVO. About twenty members of astronomers and computer scientists took part in the KVO and we have annual fund of 100,000 USD till 2005. As a first mission of the KVO, we are constructing an initial version of KVO using data produced by telescopes in Korea, such as those from Taeduk 14m radio telescope, Bohyunsan Optical Astronomy Observatory 1.8m telescope, YSTAR (Yonsei Survey Telescopes for Astronomical Research)-NEOPAT (Near Earth Object PATrol) project, and Galactic plane CO survey (l=60-180) project using the Seoul National University 6m radio telescope. Data from telescopes that will be built in the near future (e.g., Korean VLBI Network; KVN) and data from satellites being launched by international cooperation (e.g., Far-ultraviolet IMaging Spectrograph - FIMS - or Galaxy Evolution Explorer - GALEX) will also be used. We will show and discuss key aspects in building the KVO, including general plans and technical issues.

- **The Astrophysical Virtual Observatory AVO**
  P.J. Quinn - European Southern Observatory, and P. Benvenuti, P. Diamond, M. Dolensky, F. Genova, A. Lawrence, Y. Mellier

  The Astrophysical Virtual Observatory Project (AVO) is conducting a research and demonstration programme on the scientific and requirements and technologies necessary to build a VO for European astronomy. The Phase A program focuses its effort in three areas: First, a detailed description of the science requirements for the AVO is constructed following the experience gained in a smaller-scale science demonstration program called ASTROVIRTEL. Second, the difficult issue of data and archive inter-operability is addressed by new standards definitions for astronomical data and trial programmes of "joins" between specific target archives within the project team. Finally, the necessary GRID and database technologies are assessed and tested for use within a full AVO implementation. This already resulted in an AVO prototype system displayed at the common demo booth of the International Virtual Observatory Alliance (IVOA).

- **The German Astrophysical Virtual Observatory.**
  W. Voges - Max-Planck-Institut für extraterrestrische Physic, and M. Steinmetz, H.-M. Adorf, H. Enke, G. Lemson

  The German Astrophysical Virtual Observatory (GAVO; `www.g-vo.org`) is a project led by the Max-Planck-Institut für extraterrestrische Physik, Garching, and the Astronomisches Institut Potsdam with the aim of triggering and coordinating Virtual Observatory activities in Germany. The long-term goal of GAVO consists in establishing a technologically advanced platform that supports astronomical research. GAVO pursues this goal by facilitating the exploitation of heterogeneous, distributed data archives from astronomical observations and from large-scale astrophysical simulations.

  A pilot project was proposed to the German Bundesministerium für Bildung und Forschung and, in October 2002, received funding for an initial period of 18 months. The main objectives of the GAVO pilot project are: (1) the federation of distributed, heterogeneous public astronomical archives; (2) the exploitation of GRID-computing for the next generation of large astrophysical simulations and as a platform independent system for distributed data analysis and cross-correlation; (3) the implementation of an advanced classification, tool called the "Next Generation Search Engine". Additionally GAVO supports database curators in the process of publishing their data in a VO-compliant form. GAVO participates in the activities of the IVOA, and actively cooperates with other virtual observatory projects as well as industrial partners.

- **Japanese Virtual Observatory Project**
  Ohishi M. - National Astronomical Observatory of Japan, and Mizumoto Y., Yasuda N., Shirasaki Y., Tanaka M., Masunaga Y.

  The Japanese Virtual Observatory (JVO) project has been commenced as an observatory's project since April 2002. The JVO aims to provide federated astronomical databases (especially SUBARU, Nobeyama and ALMA) and data analysis environment through the Grid technology. The project has been performed under collaboration with the NAOJ, the Ochanomizu University and Fujitsu Ltd. Furthermore we have been collaborating with many information scientists in Japan, whose research interests are on the Grid technology. We already defined a unified query language to access astronomical databases the JVO QL, and constructed a prototype of the JVO to confirm if the JVOQL really works on a federated database through Grid technology. In the near future JVO will be connected with other VOs in the world through the International Virtual Observatory Alliance. We plan to demonstrate the JVO prototype at the IVOA demo booth.

- **Current Status of the Russian Virtual Observatory**
  O.Y. Malkov - Institute of Astronomy, and O.B. Dluzhnevskaya, E.Y. Kilpio, A.A. Kilpio, D.A. Kovaleva

  The Russian Virtual Observatory (RVO) has been officially recognized as one of the key projects of the Scientific Council on Astronomy of the Russian Academy of Sciences since December 2001.

  The ultimate goal of the RVO initiative is to integrate resources of astronomical data accumulated in Russian observatories and institutions, and to provide Russian data to the rest of the world.

  One of the principal goals of the project is to provide Russian researchers with on-line access to the rich volumes of data and metadata that have been and will continue to be produced by astronomical survey projects.

  RVO architecture, main tasks and roadmap are discussed in the presentation.

- **Astrogrid, the Virtual Observatory, and what it Isn't**
  A. Lawrence - Institute for Astronomy, University of Edinburgh

  The Virtual Observatory should do for astronomical databases what the WWW did for documents - to make them transparently available from your desktop, and easy to manipulate with a standard set of tools. The UK AstroGrid project aims at an early working implementation of this idea. The analogy with the Web is actually quite close. Our philosophy is that the VO should not be a software monolith or a bureaucratic structure, but simply an enabling framework. First and foremost this means a set of standards - not just for data, but for metadata, data exchange protocols, provenance, and so on. The programme of standards is developing internationally. AstroGrid itself aims to build a set of open source software components, analogous to Apache in the web world. We will build a first concrete working example, but the intention is actually that anybody can customize and adapt these components to build their own system. I will describe progress on building these components so far.

- **AstroGrid - Constructing the UK's Virtual Observatory**
  N.A. Walton - Institute of Astronomy, University of Cambridge, and A. Lawrence, A.E. Linde

  The UK AstroGrid Project (`http://www.astrogrid.org`) is one of three major world-wide projects (along with the European AVO and US-VO projects) which are creating an astronomical Virtual Observatory. This will be a set of co-operating and inter-operable software systems that:

  - allow users to interrogate multiple data centers in a seamless and transparent way;
  - provide powerful new analysis and visualization tools;
  - give data centers and providers a standard framework for publishing and delivering services using their data.

  AstroGrid's long term vision is not one of a single software package, but rather of a framework which enables data centers to provide competing and co-operating data services, and software providers to offer compatible analysis and visualization tools. Our presentation will describe (and illustrate with live demonstrations) how AstroGrid is developing a standardized framework to allow such creative diversity, which will:

  - improve the quality, efficiency, ease, speed, and cost-effectiveness of on-line astronomical research
  - make comparison and integration of data from diverse sources seamless and transparent
  - remove data analysis barriers to interdisciplinary research
  - to make science involving manipulation of large datasets as easy and as powerful as possible.

- **The U.S. National Virtual Observatory**
  R.J. Hanisch - Space Telescope Science Institute

  The U.S. National Virtual Observatory project is a development effort aimed at implementing the framework for an eventual Virtual Observatory facility. Project activities include the development of metadata standards, resource and service registries, table and image access protocols, interfaces to the computational grid, and access to VO resources for education and public outreach. Select science prototypes are used to guide technical development and demonstrate the capabilities of the VO framework for enhancing research. The US NVO project works closely with international VO partners through the International Virtual Observatory Alliance.

  The US NVO project is funded by the National Science Foundation under Cooperative Agreement AST0122449 with The Johns Hopkins University.

New projects, ideas, techniques and standards

- **Report of ALMA-Japan Activities for Virtual Observatory**
  Tatematsu K. - National Astronomical Observatory of Japan, and Nakanishi K., Sawada T., Kandori R., Morita K., Sunada K.

The Japanese side of the Atacama Larger Millimeter/submillimeter Array (ALMA-Japan) is making its efforts for Virtual Observatory, which will be one of the key functionalities of the ALMA Regional Support Center in Japan. We summarized our science requirements and science cases with priority ranking for VO from our expertise in radio astronomy at Nobeyama Radio Observatory, NAOJ. We are working on development of pipelines for the existing radio telescopes and near-infrared telescope to assess the data qualities which are suitable for pipeline data retrieval for Virtual Observatory. Because the average ALMA data rate is as high as 380 TB/yr, the data abstraction (i.e. making catalogue) of 3 dimensional data including diffuse line emission will be a key technology for efficient Virtual-Observatory astronomy with ALMA. We like to report the status report of our activity. The program is being carried out in collaboration with Astronomical Data Analysis Center, NAOJ.

- **Architecture of the AVO Prototype**
  M. Dolensky - European Southern Observatory, and M.G. Allen, K. Andrews, T. Boch, F. Bonnarel, S. Derriere, P. Fernique, M. Hill, M. Leoni, A.E. Linde, A. Micol, B. Pirenne, A.M.S.R. Richards, A. Schaaff, G. Tissier, N.A. Walton, A. Wicenec

  Europe's Astrophysical Virtual Observatory (AVO) developed a prototype system and continues to improve it. A board of 50 scientists - the AVO science working group - is advising the project team with the goal of maximizing the scientific return.

  In order to implement their recommendations a number of VO key technologies come into play. Each of the software components of the AVO prototype is developed and maintained by a different team in a different country. All modules work stand-alone, but can be integrated as shown at the IVOA demo booth. The AVO prototype consists of a browser backed by image and catalogue servers, a web service for the extraction of source catalogues and a utility for analyzing the spectral energy distribution of selected objects. The three components communicate in VOTable format - an XML dialect for Astronomy. Parameters (meta data) are mapped to Unified Content Descriptors (UCD). UCDs are about to become the standard way for expressing meta data in a VO. Finally, the integrated meta data browser is based on the IDHA data model.

- **Collaborative Astrophysical Research in AIRE**
  Zhou J. - Center for Astrophysics, Tsinghua University, and Qi R., Yang Y., Nie J.

  To study the complex universe effectively, collaboration among astrophysicists is necessary. The proposed AIRE (Astrophysical Integrated Research Environment) is to help astrophysicists do collaborative research efficiently. The AIRE consists of three main parts: a Data Archive Center (DAC) which collects and manages public astrophysical data; a web-based Data Processing Center (DPC) which enables astrophysicists to process the data in a central server at any place and anytime; and a Collaborative Astrophysical Research Project System (CARPS) with which astrophysicists in different fields can exchange their ideas and organize international virtual research groups. A few examples will be demonstrated in this talk.

- **Design of the W.M. Keck Observatory Single Dish Archive**
  B. Berriman - California Institute of Technology, and N. Tahir-Kheli, T. Bida, A. Conrad, P. Kurpis, H. Tran

  The W. M. Keck Observatory will deploy an archive of observations made with the telescope operating in Single Aperture mode. When complete, the archive will enable scientific discovery through fusion of data from multiple instruments, and will enable detailed performance analysis of the Keck instruments. The archive will provide access to observations made on multiple instruments that meet complex criteria based on position in the sky and the attributes of the data (wavelength range, spectral resolution, etc). Its design takes advantage of emerging or proposed standards for describing and distributing complex data sets. By late 2004, the archive will serve observations made with the High Resolution Echelle Spectrometer (HIRES). The archive leverages a highly modular design implemented at the NASA/IPAC Infrared Science Archive (IRSA), in which thin front-end interfaces sit on top of an component based infrastructure.

- **Space-Time Coordinate Metadata for the Virtual Observatory**
  A.H. Rots - Smithsonian Astrophysical Observatory

  Space-time coordinate metadata is at the very core of understanding astronomical data and information. This aspect of data description requires very careful consideration. The design needs to be sufficiently general that it can adequately represent the many coordinate systems and conventions that are in use in the community. On the other hand the most basic requirement is that the space-time metadata for queries, for resource descriptions, and for data be complete and self-consistent. Among other things, it is important to keep space and time coordinates together - not only to account for relativistic effects but also to allow transformations and accommodate ephemerides information; to provide information, not only on the observation's coordinates, but also those of the telescope; to handle celestial as well as solar system coordinates; and to support the description of regions. The development of a complete description has been underway for about a year. At this point we are ready to present the definitive description of this metadata structure expressed as an XML schema.

  This work has been supported by NASA contract NAS 8-39073 (CXC) and by the University of Strasbourg.

- **Organisation of Datasets in Virtual Observatories**
  M.G. Allen - CDS, Observatoire de Strasbourg, and F. Bonnarel, T. Boch, P. Fernique, M. Louys, AVO Team

  Browsing and providing access to large local and distributed datasets is an important aspect of enabling Virtual Observatories. We present an example implementation of a meta-data tree in the Astrophysical Virtual Observatory prototype tool. This is a dynamically built "meta-data tree" containing information on image datasets, based on the IDHA data model. This meta-data representation of the GOODS dataset in the AVO demo, allows efficient data browsing and selection. This capability is being developed in the framework of the CDS Aladin image browser, and AVO prototypes.

- **The unique classification systems UDC52 and Astronomy Thesaurus**

  T.N. Dorokhova - Astronomical Observatory of Odessa National University, and N.I. Dorokhov, O.B. Dluzhnevskaya

  Two systems for arrangement and ranking of an astronomical information are presented for discussion.

  1. UDC52 as class for astronomy of the Universal Decimal Classification. The UDC is one of the oldest and well-arranged language-independent classification scheme The Russian agency VINITI took an active part in the UDC development during almost half of century. As a result of this work every astronomical publication in the Russia, Ukraine and some other Former Soviet Union countries connects traditionally with definite classes and subclasses of UDC52 till present time. The revision of UDC52 was undertaken by G.Wilkins for the task of IAU Commission 5 but this project does not progress now.

  2. The Astronomy Thesaurus Project with the Multi-Lingual Supplement which was realized by R.M. and R.R. Shobbrook in cooperation with the librarians of different countries on the instructions of the IAU, Commission 5. We are presently carrying out the translation of the Astronomy Thesaurus into Russian and also into Ukrainian as an addition to the Multi-Lingual Supplement. This advisable list of terms with the definite hierarchy and relationship have demonstrated its usability for building and development of the NASA ADS retrieval service and for the revision of UDC52.

  Unfortunately, recently both of these perfectly arranged systems are not updated. The situation can be corrected with the attention and efforts of the World astronomical community. Both systems can be useful and advantageous for the Project of Virtual Observatory providing the reliable storage and retrieval of the information. Hopefully, that such project will promote involving a bulk of Russian and Ukrainian astronomical publications and data archives into existing World Data Networks.

- **XML in the Virtual Observatory**

  R.G. Mann - Institute for Astronomy, University of Edinburgh, and R. Baxter, P. Buneman, D. Byrne, R. Hutchison, C. Koch, T. Wen, M. Westhead

  XML is the lingua franca in the Web (and Grid) services world and so will play a major role in the construction of the Virtual Observatory. Its great advantages are its flexibility, platform-independence, ease of transformation and the wide variety of existing software that can process it. An obvious disadvantage in its use as an astronomical data format is its verbosity; the number of bytes taken up writing the XML tags can easily outnumber those constituting the actual astronomical data. This becomes prohibitively inefficient when large amounts of data are stored in XML, and the developers of VOTable sought to circumvent this, by allowing for the use of binary data, either in the VOTable document itself or in an external file linked from it. The verbosity of XML in this regard is a problem in many other disciplines, and computer scientists are developing more generic solutions to that found in the VOTable specification. In this paper we describe several of these projects currently underway in Edinburgh, which focus on the compression and querying of XML, and a technology for representing the structure of a binary file in XML, enabling it to be read as if it were XML.

- **COSMO.LAB: Software for Stereographic Viewing**
  H.R. de Ruiter - Osservatorio Astronomico di Bologna

  A Virtual Observatory will have to deal with the problem of easy and quick data display. Most astronomical catalogs contain multi-dimensional data, but the common visualization packages only allow for displaying two dimensions at a time. This is now a severe and unnecessary limitation: modern day computer technology permits true 3D visualization at very low cost. A new software package (Cosmo.Lab) which can run under different operating systems (Linux, MSWindows) has been developed that makes stereographic vision easy, fast and user-friendly. The project, funded by the European Union, is at present in an advanced stage of completion. The software is able to handle very large data sets and manipulate the data (zooming, rotation, etc.) in real time. It can read gridded data as well as object lists extracted from astronomical catalogs. One of the strong points is the portability of the package on many different computer platforms ranging from (costly) virtual 3D theaters to (very cheap) personal computers. Finally we should mention that Cosmo.Lab is free ware, i.e. it can be freely down loaded from the Web page of CINECA. At request a CD-ROM is also available.

- **Automated Online Data Analysis by Artificial Neural Networks**
  H.P. Singh - Department of Physics, Sri Ventkateswara College, and R. Gupta

  Artificial neural networks (ANN) have been successfully used recently for automated stellar spectral classification of the UV, visible and the IR spectral databases. We propose to build an ANN based online data analysis pipeline in collaboration with VO India for the new INDO-US stellar spectral library of nearly 1300 stars from 3500-9500Åobserved from the KPNO Coude feed by Valdes et al. (2003). The paper discusses important ingredients of such a pipeline.

- **Object Classification with GAIA and Virtual Observatories**
  C.A. Bailer-Jones - Max-Planck-Institut für Astronomie

  The GAIA Galactic Survey Mission will be launched in 2010 by the European Space Agency to obtain microarcsecond precision astrometry and radial velocities of stars across the entire Galaxy. The resulting six dimensional phase space database (3 spatial, 3 velocity co-ordinates) will be supplemented by 15 band optical photometry at many tens of epochs. This large complex database - comprising all one billion objects in the sky brighter than 20th magnitude - will be the basis for numerous scientific projects - such as investigating the merger history and chemical evolution of our Galaxy mapping its star formation history and searching for extra-solar planets - to significantly improve our understanding of stellar and galactic astrophysics. But to achieve this, an accurate classification of everything in the database (including QSOs, galaxies and solar system objects) will be required, as will a detailed determination of stellar parameters (effective temperatures, radii, metallicities etc.). I shall discuss various multidimensional data techniques which are being developed to address these problems. A number of the challenges we face are common to those faced by the Virtual Observatory projects, including combination of inhomogeneous data, object matching, efficient mining for objects types and variable criteria for object selection.

- **AstroGrid and the VOs: Science and Use in the ELT ERA**
  N.A. Walton - Institute of Astronomy, University of Cambridge

  In the new era of Extremely Large Telescope's (ELT), new science discoveries will come from the linkage of multi-wavelength data sets from a wide range of the 'best in class' facilities, e.g. James Webb Space Telescope (JWST), ALMA, ESO's OWL, etc. AstroGrid and the Virtual Observatory (VO) initiatives are providing the technical infrastructure to enable the seamless integration, mining and dissemination of these data.

  This presentation will highlight how major science programmes, such as the hunt and investigation of earth like planets, will be facilitated by the use of Virtual Observatory systems in linking these, large, distributed, multi-sourced information and data streams.

  VO's will also impact on instrument design and use. By obtaining data from a multitude of sources, simultaneously through integrated VO-Observatory operations, specific ELT instruments could be designed to be much more specific in which data they acquire. A future operating model could see data acquisition programmes routinely delivering simultaneous data streams (e.g. rapid, multi facility observations of Gamma Ray Bursters) from instruments on e.g. ELT, ALMA, JWST, via the VO.

- **ASTROVIRTEL - a Precursor of the Virtual Observatory**
  P. Benvenuti - ESA/ESO, and A. Micol, F. Pierfederici, B. Pirenne

  ASTROVIRTEL, a small support programme for the utilization of large astronomical archives, is completing its 3rd Cycle. The experience in supporting a number of selected science projects has been very useful for deriving scientific requirements for the Virtual Observatory. A summary of the lessons learned is presented.

- **VO and KP for Massive Planetary Data Sets**
  P.A. Yanamandra-Fisher - Jet Propulsion Laboratory

  The concept for a National Virtual Observatory (NVO) is being realized for astrophysical data sets. A similar need exists for massive large planetary data sets from planetary missions and ground-based observations. Data returned from missions are organized into information data repositories such as the Planetary Data System (PDS) for NASA mission data; Space Telescope Science Institute (STScI) for Hubble Space Telescope (HST) data; SIRTF Science Center (SSC) for SIRTF, and other similar sites. However no such dedicated repository exists for the terabits of data collected by ground-based observers in support of various missions. Coordination of these data sets and providing analysis tools is necessary to allow the planetary astronomy community access for research and cross-correlative analysis. Towards this goal, we are developing a prototype suite of algorithms for ground-based data collected by our team in support of NASA's GALILEO and CASSINI missions to integrate multi-spectral and multi-instrument data. We have an end-to-end data pipeline from initial data processing to absolute calibration and products in between. Our goal is to develop a knowledge portal for content and an ancillary virtual observatory in support of established planetary data warehouses.

- **Adding Theory to the Virtual Observatory**
  S.T. Maddison - Swinburne University, and G.F. Lewis

  The Virtual Observatory is an ambitious plan to bring the world of astronomical data to everyone within a few simple keystrokes. There is significant international interest and funding for this project for which the observational component is very well established. The inclusion of theoretical data and models has yet to be tackled, and it is clear from the breadth of theoretical research that the Theory VO faces a lot of challenges. A unique component of the VO may be the provision of virtual telescopes, allowing mock observations of a synthetic universe. On behalf of the Australian National Institute for Theoretical Astrophysics, we present the current ideas and views of the Australian theoretical community concerning the implementation of theory as an integral part of the international virtual observatory.

- **Extending the Time Dimension of the IVO**
  R.E.M. Griffin - Dominion Astrophysical Observatory, Herzberg Institute for Astrophysics

  Most of the scientific visions for the International Virtual Observatory are focusing on digital datasets from major surveys, current or planned. Here we urge the inclusion of astrometric and spectroscopic datasets of historic observations.

  Despite their unprecedented high quality, modern observations are telescoped into brief time intervals that cannot contain the information on slow changes that is vital for refining orbits, proper motions or evolution studies. Whether we research supernova precursors, NEO orbits, post-helium-flash stars or long-period binaries, access to historic observations is of paramount importance. Such observations exist, but they are photographic and are presently not easily accessible. Digitizing projects, now fully feasible, can bring their information into the public domain and into the IVO. Re-working the past does not imply re-doing the science of the day; observations can be re-used for science never contemplated by the original observers.

The inclusion of data from 30-100+ years ago will furnish an important extra dimension to the new 3D research of the cosmos promised by the IVO. Some plate-scanning has already commenced. The creation of accessible digital datasets from historic observations is a minuscule operation compared to the IVO which they will undoubtedly enhance. It deserves and seeks the IVO's support.

- **The Contribution of the Wide-Field Plate Database to the International Virtual Observatory**
  M. Tsvetkov - Sofia Sky Arcive Data Center, Institute of Astronomiy, Bulgarian Academy of Sciences

  The development for the period 2000-2003 of the Wide-Field Plate Database (WFPDB, `http://www.skyarchive.org`) as an initiative of the IAU Working Group on Sky Surveys, hosted by Commission 9, is presented. The new version of the Catalogue of the Wide-Field Plate Archives contains descriptive information for practically all existing professional wide-field photographic observations stored in 365 archives around the world. The total number of plates, made since the end of the 19th century by the help of more than 200 telescopes, is over 2 000 000. Currently the WFPDB provides access to the information for about 640 000 plates from 117 plate archives, i.e. about 30% of the estimated archive total number. Following the directions of the Centre de Données Astronomiques de Strasbourg (CDS) and International Virtual Observatory (IVO) the WFPDB contains the digitized plate preview images, as well as digitized plate row data obtained by the new generation of the flatbed scanners. The WFPDB team continues to enlarge the database with submitted or retrieved information from the photographic plates, which enable the astronomical community to complement "the digital sky" with data going more than 100 years back in time.

- **Bamberg Southern Photographic Patrol Survey: Incorporation in the WFPDB**
  M. Tsvetkov - Sofia Sky Archive Data Center, Institute of Astronomy, Bulgarian Academy of Sciences, and K. Tsvetkova, A. Borisova, D. Kalaglarski, R. Bogdanovski, U. Heber, I. Bues, H. Drechsel, R. Knigge

  The description, cataloging and incorporation into the Wide Field Plate Database (WFPDB, `http://www.skyarchive.org`) of the Dr. Remeis-Observatory Bamberg Southern Photographic Patrol Survey (22 000 plates) is presented. The survey was carried out with 22 cameras (each with d=10 cm), Zeiss camera (d=7cm), and the Harvard telescopes Metcalf (10=94) and Ross B (3=93). The plates were obtained in the period 1963-1976 in Boyden Observatory (South Africa), Mount John University Observatory -Lake Tekapo (New Zealand) and San Miguel Observatory (Argentina) and are stored at present in the Observatory stacks. The observational programme was supported by the Deutsche Forschungsgemeinschaft (DFG) and carried out under the supervision of W. Strohmeier (1965, Kleine

Veroeff. der Remeis-Sternwarte Bamberg, Bd. IV, No. 40, p. 302). Digital CCD preview images of the plates by observational zones are, for the first time, included into the WFPDB providing access to them for the worldwide astronomical community. Special attention is paid to the sub-survey in the LMC region. The digitization of plates at the Bamberg Observatory will become possible soon with the installation of an EPSON Expression 1640XL flatbed scanner granted by DFG.

- **Digitization of Archives of Astronomical Plates**
  A. Omizzolo - Vatican Observatory Research Group, and B. Cesare, C. Blanco, B. Bucciarelli, A. di Paola, R. Nesci

  The photographic plate archives of telescopes around the world contain a veritable treasury of astronomical data. Unfortunately the emulsion is a volatile support and full exploitation of the scientific content is more and more difficult. A large-scale two-year project to digitize the archive of plates of the Italian Astronomical Observatories and of the Specola Vaticana has been started in 2002 with funds from the Ministry of the University and Research, following a pilot program funded by the University of Padova in 2001. Identical systems, composed by a high quality commercial scanner plus dedicated personal computers and acquisition software (developed initially at DLR Berlin) have been installed in all participating Institutes. Three main goals make up the total project: to provide high quality photometric sequences with the Campo Imperatore telescopes to be used on the scanned plates, to perform astrometric measures taking advantage of the large span of time covered by the plates, and to distribute the digitized information to all interested researchers via the international Web. This paper presents some of the activities carried out and results obtained so far.

JD9

Astrotomography

Chairpersons: M. Richards and L. Morales Rueda

Editors: A. Collier Cameron (Chief-Editor), A. Schwope and S. Vrielmann

Highlights of Astronomy, Vol. 13
International Astronomical Union, 2003
O. Engvold, ed.

Joint Discussion 9: Astrotomography

Andrew Collier Cameron

School of Physics and Astronomy, University of St Andrews,North Haugh, St Andrews, SCOTLAND KY16 9SS

Axel Schwope

Astrophysikalisches Institut Potsdam,An der Sternwarte 16, D-14482 Potsdam, GERMANY

Sonja Vrielmann

Hamburger Sternwarte, Universität Hamburg, Gojenbergsweg112, 21029 Hamburg, GERMANY

Abstract. Even in the new millenium, many astronomical objects cannot be resolved spatially with any available telescope. Most stars are too small and galaxies are too far away to be imaged directly or in detail in the foreseeable future. However, advances in data-analysis techniques allow us now to create detailed indirect images using tomographic methods. These images provide unprecedented insights into fundamental processes that drive the evolution of stars and galaxies, such as accretion and magnetic-field generation, on length scales that are of great physical importance but which are otherwise inaccessible.

Joint Discussion 09 was held on two half-days during the General Assembly. The main proceedings will be published in full in a special issue of *Astronomische Nachrichten*, to which the reader is referred, early in 2004. Here we give only a brief listing of subjects addressed and the titles of talks presented at the meeting.

2. Introductory talks and general principles

Astrotomography is a generic term for indirect mapping techniques that can be applied to a huge variety of astrophysical systems, ranging from planets via single stars and binaries to active galactic nuclei. These techniques use the temporal variability and velocity structure of continuum and line emission from astrophysical objects, to infer the spatial distribution of emitting material.

Astrotomography takes advantage of the fact that we can observe a rotating object from different angles, and exploit light travel-time effects across structures of finite size. A series of n-dimensional images of a full cycle can be fed into a computer in order to yield a$(n+1)$-dimensional picture of the object. These methods allow us to obtain for the first time micro-arcsecond resolution images of surfaces of accretion discs and stellar objects. Overview talks covering both the range of science that can be addressed with these techniques, and ways of maximizing the information return from a minimal set of observations, included:

Micro-arcsecond astrotomography (K. Horne)
Few-projections astrotomography (M. Agafonov)

3. Cataclysmic variables and X-ray binaries

Tomographic studies of cataclysmic variables (CVs) adopt four methodically different strategies to discern structure within the accretion disc, along the stream or on the surface of the white dwarf or the red dwarf star. The first, Eclipse Mapping, uses the cool secondary star as an occulting mask, to deduce the spectral emission of the accretion disc at various locations from spectrophotometric variations recorded as the eclipse proceeds. The second approach, Doppler Tomography, entails taking densely-sampled sequences of intermediate- to high-resolution spectra covering one or more full orbital cycles, in order to pin down the locations of individual emitting structures in velocity space. The third technique, Stokes Imaging, maps the cyclotron emission on the surface of the white dwarf by modeling polarimetric observation. Finally, Roche Tomography, models the emissivity on the surface of the red companion, similar to stellar surface mapping (see Section 3.).

Eclipse Mapping studies of CVs have verified the presence of accretion discs and streams, establishing models for the accretion physics. Doppler Tomography has revealed the location of accretion streams and the existence of tidally induced spiral shock waves in accretion discs. Stokes Imaging revealed the shape, size and location of the accretion spots on the white dwarf's surface. And finally, Roche Tomography confirmed thick disc rims shielding the donor star surface from irradiation by the hot inner disc. Talks given in this subject area included:

Eclipse mapping (R. Baptista)
Doppler tomography, including modulated tomography (D. Steeghs)
Roche tomography of CV secondaries (C. Watson)
Doppler mapping of CVs (L. Morales Rueda)
Indirect Imaging of polars (A. Schwope)
Stokes imaging of magnetic CVs (S. Potter)
Selected magnetic CVs (G. Tovmassian)
Mapping the accretion disk of Her X-1 (D. Leahy)
Tomography of X-ray binaries (S. Vrtilek)

4. Stellar surface imaging

Doppler tomography has been in use for two decades to discern the distributions of surface brightness, elemental abundances and magnetic polarities. In any star rotating fast enough that the rotational Doppler effect is the dominant line-broadening mechanism, surface inhomogeneities produce bump-like irregularities in the profiles of spectral lines. As the star rotates, these bumps migrate through the profile, following sinusoidal paths through a trailed spectrogram. The amplitude, phase and modulation of the sinusoid reveals the location of the feature on or (in the case of prominences and accretion streams) above the stellar surface.

The analysis of cool stars has revealed not only that their surface are covered with large cool spots but also with changing magnetic field patterns, and that both are affected by surface differential rotation similar to what we see on the Sun. Eclipse mapping and Doppler tomography of Algols has also provided detailed insights into the trajectories of the accretion streams, and their emitting properties. Topics covered by talks in this area included:

Stellar surface imaging, including magnetic imaging (G. Hussain)
Differential rotation of stars (P. Petit)
Eclipse mapping of Algols (G. Peters)
Doppler tomography of Algols (M. Richards)
Surface images of the short-period contact binary, AE Phe (J. R. Barnes)
Tomography of stellar non-radial pulsations (S. Berdyugina)
The atmosphere of V471 Tau (F. Walter)

5. Echo-mapping of active galactic nuclei, X-ray binaries and exoplanets

Echo mapping, or reverberation mapping, was developed to analyze the structure and velocity field of the microarcsecond-scale emission-line regions in active galactic nuclei or quasars via time delays between continuum and emission-line variations caused by reflection and re-processing of radiation. In both X-ray binaries and active galactic nuclei, a compact irradiating source varies in brightness on time scales that are short compared to the light-travel time across the region in which line-emitting gas responds to the variations in the central engine. By monitoring changes in both the brightness and velocity structure of emission lines formed in AGN and XRBs, it is possible to measure both the location and velocity field of the emitting gas. A related tomographic technique, used for searching for starlight reflected from extra-solar planets, relies on the orbital Doppler shift of the planet.

Echo-mapping is beginning to yield information on accretion-disc structure. To date, application of this technique has yielded sizes of the emission-line regions and demonstrated radial ionization stratification, and has led to measurements of the masses of the super-massive black holes that power these sources. The next generation of reverberation mapping experiments, using dedicated facilities, will resolve finer-scale structures, such as temperature-radius profiles, and settle definitively the origin of the emission-line gas and clarify how quasars are fueled. The three talks given on echo-mapping and related techniques were:

Echo mapping of active galactic nuclei (B. Peterson)
Echo mapping of X-ray binaries (K. Horne)
Tomographic studies of exoplanet atmospheres (A. Collier Cameron)

JD10

Evolution in Galaxy Clusters: A Multiwavelength Approach

Chairpersons: L. Feretti and R.W. Hunstead

Editors: R.W. Hunstead (Chief-Editor), L. Feretti, B. Gibson and P. Nulsen

Highlights of Astronomy, Vol. 13
International Astronomical Union, 2003
O. Engvold, ed.

Evolution in Galaxy Clusters: A Multi-Wavelength Approach

Joint Discussion 10, 17–18 July 2003

Organizing Division: X

Participating Divisions: VIII and XI

SOC members: R. Hunstead (Australia, chair), L. Feretti (Italy, co-chair), R. Carlberg (Canada), W. Couch (Australia), B. Gibson (Australia), G. Kauffmann (Germany), L. Lubin (USA), G. Miley (The Netherlands), P. Nulsen (Australia), T. Ohashi (Japan), P. Thomas (UK)

As the largest virialized systems in the universe, clusters of galaxies are astrophysical laboratories for studying a wide variety of phenomena. These range from the properties of individual galaxies, to the intra-cluster medium through which they move and the violent events that accompany cluster mergers. Observational data span the entire electromagnetic spectrum from X-ray through UV to optical, infrared and radio. Each wavelength region reveals a different facet of the underlying astrophysics that governs the gas and galaxies.

In this context, we felt it was timely to schedule a Joint Discussion about clusters and their evolution within the IAU General Assembly in Sydney. The multi-wavelength theme emphasized the above mentioned synergies, and linked the exciting new observational data from ground-based and space observatories to the most recent analytical and numerical simulations.

Joint Discussion 10 focused on some recent highlights of cluster research: (i) cluster formation, with discussion of the optical and X-ray data, substructure, mergers and accretion; (ii) cluster galaxies, with emphasis on the star-formation histories and radio galaxy populations; and (iii) the intra-cluster medium, with the recent results on the gas cavities, cooling flows, non-thermal processes and the interaction between thermal and relativistic plasma. Since it was only a 1.5-day meeting, the number of oral contributions was limited to 10 invited and 12 contributed talks. Other contributions were presented as Posters, and a short presentation of each poster was given during the oral session.

In the following sections we present an abbreviated version of the program, followed by the texts of 8 of the 10 invited talks, the abstracts of the contributed talks, and the list of posters.

We thank all the participants for their contributions to a productive and successful meeting.

Dick Hunstead
Luigina Feretti

Highlights of Astronomy, Vol. 13
International Astronomical Union, 2003
O. Engvold, ed.

Clusters in the Optical

Lori M. Lubin

Department of Physics, University of California, One Shields Avenue, Davis, CA 95616

Abstract.
I present a brief review of studies of galaxy clusters in the optical. Clusters of galaxies were historically detected in the optical, and this selection provided the first large, statistical samples of clusters. I describe how these samples have been instrumental in characterizing the properties of the local cluster population, tracing large scale structure, and constraining cosmology. More sophisticated cluster detection techniques in the optical have now made it possible to detect large numbers of clusters up to $z \sim 1.4$. I describe these advances and discuss how large-area and deep surveys are being used to determine the evolution in the global cluster properties and the properties of cluster galaxy populations.

1. The Historical Selection

1.1. Original Catalogs

Clusters of galaxies were historically detected in the optical pass bands. G.O. Abell and F. Zwicky compiled the first catalogs of galaxy clusters at redshifts of $z \lesssim 0.2$ by searching by eye for surface density enhancements in the Palomar Sky Survey plates (Abell 1958; Zwicky et al. 1961). The Abell and Zwicky catalogs contained over 2700 and 9000 clusters, respectively. Further improvements on the surface density enhancement technique utilized automatic detection in digitized sky plates, for example the Edinburgh-Durham Cluster Catalog (EDCC; Lumsden et al. 1992) and the Automated Plate Measuring Survey (APM; Dalton et al. 1994a). These surveys provided statistical samples of poor to the richest clusters in the nearby universe and have been used to determine the properties of the cluster population. Typical cluster properties include Abell richness (30–300 galaxies), radius (1–2 h^{-1} Mpc), velocity dispersion (400–1400 km s^{-1}), mass within an Abell radius (0.1–3 $\times 10^{15}$ h^{-1} $M_\odot$), blue luminosity (0.6–6 $\times 10^{12}$ h^{-2} $L_\odot$), mass-to-blue light ratio (~ 300 h $M_\odot/L_\odot$), and number density of richness class 1 and above clusters ($\sim 6 \times 10^{-6}$ h^3 Mpc^{-3}).

Rich clusters are also efficient tracers of the large scale structure of the Universe. Consequently, the large-area cluster catalogs provided one of the first means to quantify the clustering of clusters. This clustering was expressed in terms of superclusters (e.g., Bahcall & Soneira 1984) or the cluster-cluster correlation function which stays positive out to ~ 100 h^{-1} Mpc (e.g., Dalton et al. 1994b; Bahcall et al. 2003a).

1.2. Cosmological Constraints

Because clusters are the most massive systems in the universe, their global properties place strong constraints on cosmology – specifically the mass density of the universe, Ω_m, and the normalization of the power spectrum, σ_8. Many different measurements of cluster optical properties can be used to constrain these cosmological parameters, including the mass-to-light ratio on large scales, the cluster mass function, and the cluster-cluster correlation function. As been known for many years, all of these cluster observations suggest that $\Omega_m = 0.1 - 0.4$ (e.g., Bahcall & Cen 1993; Bahcall, Lubin & Dorman 1995; Bahcall et al. 2003a).

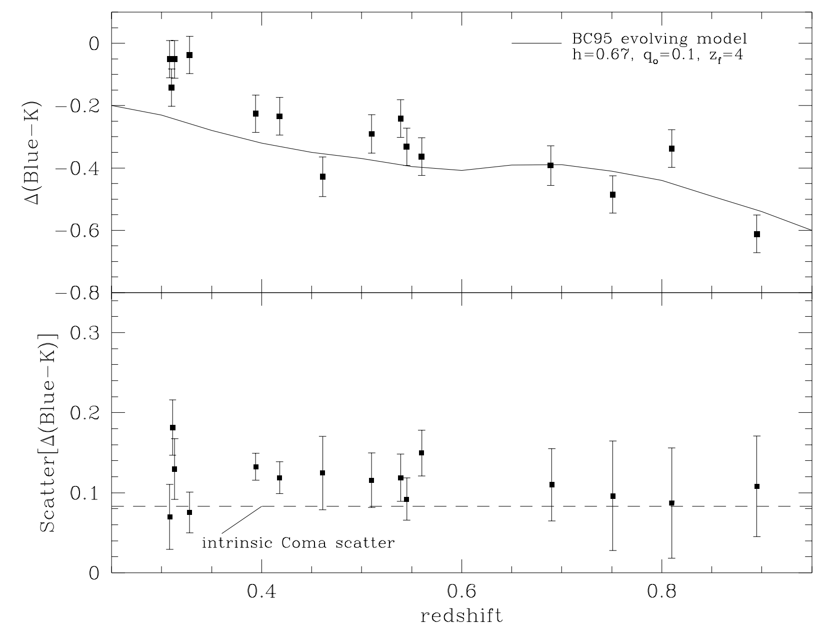

Figure 1. (*Top*) Color of the red sequence (relative to the rest-frame color of the Coma) versus cluster redshift. Solid line indicates the expected color evolution from the 1995 version of the Bruzual & Charlot (1993) evolving model of a single burst of star-formation at $z_f = 4$. (*Bottom*) Color scatter in the red sequence versus cluster redshift. Dashed line indicates intrinsic scatter in the Coma cluster. This figure is taken from Dickinson (1996).

2. Modern Cluster Finding Techniques

Detection of galaxy clusters in the optical has significantly improved with the introduction of large-area imaging surveys which employ sophisticated, automated techniques whose contamination and completion rates can be easily quantified. Improving on the EDCC and APM surveys, adaptive-kernel density mapping and automatic detection of surface brightness fluctuations of cluster overdensities are being used in the Northern Sky Optical Cluster Survey (Gal et al. 2003;

5800 deg^2; $z < 0.3$) and the Las Campanas Distant Clusters Survey (Gonzalez et al. 2001; 69 deg^2; $0.3 < z < 1$). The Palomar Distant Cluster Survey (Postman et al. 1996; 5 deg^2; $0.2 \leq z \leq 1.2$) was the first survey to employ a matched filter algorithm that used both galaxy position and brightness to detect objectively clusters up to $z \sim 1.2$. This algorithm and its derivatives have been used for cluster detection in the Sloan Digital Sky Survey (Bahcall et al. 2003b; 400 deg^2; $0.05 \leq z \leq 0.3$), the ESO Imaging Survey (Scodeggio et al. 1999; 17 deg^2; $0.2 \leq z \leq 1.2$), and the Deep Range Survey (Postman et al. 2002; 16 deg^2; $0.2 \leq z \leq 1.2$).

Another technique exploits the fact that the early-type galaxy population in clusters forms a distinct locus in the color-magnitude (CM) diagram. This sequence is distinguished by extremely red colors and a tight CM relation. So far, all massive clusters up to redshifts of $z \sim 1.3$ exhibit a reasonably-strong red sequence in the CM diagram (e.g., Stanford, Eisenhardt & Dickinson 1995, 1997; Lubin et al. 1998, 2003; van Dokkum et al. 2000, 2001; Blakeslee et al. 2003). As such, the Red-Sequence Cluster Survey (RCS; Gladders & Yee 2000) utilizes the form and color of this distinct feature to optimize cluster detection over the blue field population. The RCS covers 100 deg^2 and expects to detect over 1000 clusters at redshifts of $0.1 < z < 1.4$.

3. Cluster Evolution

Using the increasing numbers of high-redshift clusters, it is now possible to study the evolution of massive clusters and their galaxy populations.

One of the obvious global properties to measure as a function of time is the number of clusters. In a low-Ω universe, density fluctuations evolve and freeze out at early times, producing little evolution at recent times, i.e. redshifts of $z < 1$. In a flat ($\Omega = 1$) universe, fluctuations start growing only recently, thereby producing strong evolution at recent times. Optical surveys have revealed only a mild decline in the co-moving volume density of rich (Abell richness class 1 and above) clusters out to $z \sim 1$. The existence of massive clusters at these redshifts again favors a low Ω_m Universe (Postman et al. 1996, 2002; Carlberg et al. 1997; Bahcall & Fan 1998).

By charting the change in the color of the red sequence (see §2), it is possible to determine how the stellar populations in early-type galaxies have evolved from $z \sim 1$ to the present day. Figure 1 shows the evolution in the color and color scatter of the red sequence for 15 clusters between $z \sim 0.3$ and $z \sim 0.9$. The broad-band color distribution of the early-type galaxy population shows significant bluing; the observed trend is consistent with passive stellar evolution of a relatively well synchronized initial starburst occurring at $z \gtrsim 2$ (e.g. Stanford, Eisenhardt & Dickinson 1995, 1997), although continuing star-formation in a fraction of the galaxies is not strongly constrained (van Dokkum & Franx 2001).

Even though clusters of galaxies at high redshift still contain a large number of early-type galaxies, the fraction of early-type galaxies is evolving with time. This trend was first observed as the progressive bluing of cluster's galaxy population with redshift (Butcher & Oemler 1984). Butcher & Oemler found that the fraction of blue galaxies in a cluster is an increasing function of redshift (see Figure 2), indicating that clusters at redshifts of $z \sim 0.5$ are significantly bluer than their low–redshift counterparts. At redshifts of $z \sim 0.4$, the fraction of blue galaxies is $\sim 20\%$, compared to $< 5\%$ locally. High-angular-resolution HST images have revealed that most of these blue galaxies are either "normal" spirals or have peculiar morphologies, resulting in late-type fractions which are 3 to 5 times higher than the average current epoch cluster (e.g., Dressler et al. 1994, 1997; Couch et al. 1994).

This trend continues to $z \sim 1.3$ (Lubin et al. 1998, 2002, 2003; van Dokkum et al. 2000, 2001; Blakeslee et al. 2003). Figure 2 shows the evolution of the early-type fraction with cluster redshift. At $z \sim 1$, this fraction is lower by a factor of 1.5 – 2.0, compared to local clusters. Consequently, the fraction of late-type (spiral, irregular, and peculiar) galaxies increases with redshift. This evolution implies that early-type galaxies are forming out of the excess of late-type galaxies over this ~ 7 Gyr time scale. The key question now is what physical process associated with the cluster environment is responsible for the observed evolution.

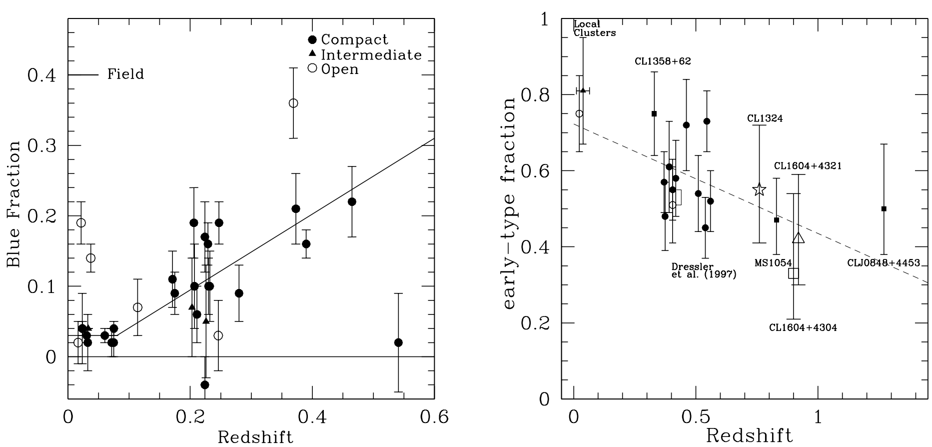

Figure 2. (*Left*) Cluster blue fraction versus redshift. Different symbols represent clusters of different concentrations. This figure is taken from Butcher & Oemler (1984). (*Right*) Early-type fraction versus cluster redshift. Data points are taken from Dressler (1980a); Dressler et al. (1997); Andreon 1998, Lubin et al. (1998, 2002, 2003); Fabricant, Franx & van Dokkum (2000); and van Dokkum et al. (2000, 2001). The dashed line indicates best-fit least-squares line. This figure is taken from Lubin et al. (2003).

4. Conclusions

Detecting and examining clusters of galaxies in the optical has provided a wealth of information over the last 40+ years. Optical selection provided the first large, statistical samples of galaxy clusters. These samples have been used to define the local cluster population, study structure on scales up to ~ 100 Mpc, and to constrain the cosmological world model. Sophisticated, automated cluster finding techniques are now extending cluster catalogs up to redshifts of $z \sim 1.4$.

Optical observations of the ever-increasing numbers of moderate-to-high redshift clusters have been critical in studying in detail how clusters and their galaxy populations have evolved with time.

References

Abell, G.O. 1958, ApJS, 3, 211

Andreon, S. 1998, ApJ, 501, 533

Bahcall, N.A. & Soneira, R.M. 1984, ApJ, 277, 27

Bahcall, N.A. & Cen, R. 1993, ApJ, 407, 49

Bahcall, N.A. & Fan, X. 1998, ApJ, 504, 1

Bahcall, N.A., Lubin, L.M., & Dorman, V. 1995, ApJ, 447, 81

Bahcall, N.A. et al. 2003a, ApJ, in press

Bahcall, N.A. et al. 2003b, ApJ, in press

Blakeslee, J. et al. 2003, ApJ, in press

Bruzual, A. & Charlot, S. 1993, ApJ, 405, 538

Butcher, H. & Oemler, A. 1984, ApJ, 285, 426

Carlberg, R.G. et al. 1997, ApJ, 485, 13

Couch, W.J., Ellis, R.S., Sharples, R.M. & Smail, I. 1994, ApJ, 430, 121

Dalton, G.B. et al. 1994a, MNRAS, 269, 151

Dalton, G.B. et al. 1994b, MNRAS, 271, 47

Dickinson, M. 1996, in HST and the High Redshift Universe, Proceedings of the 37th Herstmonceux Meeting, eds. N. Tanvir et al.

Dressler, A. 1980, ApJS, 42, 565

Dressler, A., Oemler, A., Butcher, H.R., & Gunn, J.E. 1994, ApJ, 430, 107

Dressler, A. et al. 1997, ApJ, 490, 577

Fabricant, D., Franx, M., & van Dokkum, P. 2000, ApJ, 539, 577

Gal, R.R. et al. 2003, AJ, 125, 2064

Gladders, M.D., & Yee, H.K.C. 2001, AJ, 120, 2148

Gonzalez, A.H. et al. 2001, ApJ, 536, 561

Lubin, L.M., Oke, J.B., & Postman, M. 2002, AJ, 124, 1905

Lubin, L.M. et al. 1998, AJ, 116, 584

Lubin, L.M. et al. 2003, AJ, in preparation

Lumsden, S.L. et al. 1992, MNRAS, 258, 1

Postman, M. et al. 1996, AJ, 111, 615

Postman, M. et al. 1996, ApJ, 579, 93

Scodeggio, M. et al. 1999, A&AS, 137, 83

Stanford, S.A., Eisenhardt, P.R.M. & Dickinson, M. 1995, ApJ, 450, 512

Stanford, S.A., Eisenhardt, P.R.M. & Dickinson, M. 1997, ApJ, 492, 461

van Dokkum, P.G. et al. 2000, ApJ, 541, 95

van Dokkum, P.G. et al. 2001, ApJ, 552, L101

van Dokkum, P.G. & Frank, M. 2001, ApJ, 552, 90

Zwicky, F. et al. 1961, Catalog of Galaxies and Clusters of Galaxies (California Institute of Technology), vols. 1-6

Highlights of Astronomy, Vol. 13
International Astronomical Union, 2003
O. Engvold, ed.

Mergers and Non-Thermal Processes in Clusters

Craig L. Sarazin

Department of Astronomy, University of Virginia, P. O. Box 3818, Charlottesville, VA 22903-0818 USA

Abstract. Clusters of galaxies generally form by the gravitational merger of smaller clusters and groups. Mergers drive shocks in the intra-cluster gas which heat the intra-cluster gas. Mergers disrupt cluster cooling cores. Mergers produce large, temporary increases in the X-ray luminosities and temperatures of cluster; such merger boost may bias estimates of cosmological parameters from clusters. Chandra observations of the X-ray signatures of mergers, particularly "cold fronts," will be discussed. X-ray observations of shocks can be used to determine the kinematics of the merger. As a result of particle acceleration in shocks and turbulent acceleration following mergers, clusters of galaxies should contain very large populations of relativistic electrons and ions. Observations and models for the radio, extreme ultraviolet, hard X-ray, and gamma-ray emission from non-thermal particles accelerated in these shocks are described.

1. Introduction

Major cluster mergers are the most energetic events in the Universe since the Big Bang. In these mergers, the subclusters collide at velocities of $\sim$2000 km/s, releasing gravitational binding energies of as much as $\gtrsim 10^{64}$ erg. Figure 1a shows the Chandra image of the merging cluster Abell 85, which has two subclusters merging with the main cluster (Kempner, Sarazin, & Ricker 2002). The relative motions in mergers are moderately supersonic, and shocks are driven into the intracluster medium. In major mergers, these hydrodynamical shocks dissipate energies of $\sim 3 \times 10^{63}$ erg; such shocks are the major heating source for the X-ray emitting intracluster medium. Merger shocks heat and compress the X-ray emitting intracluster gas, and increase its entropy. We also expect that particle acceleration by these shocks will produce nonthermal electrons and ions, and these can produce synchrotron radio, inverse Compton (IC) EUV and hard X-ray, and gamma-ray emission.

2. Thermal Effects of Mergers

Mergers heat and compress the intracluster medium. Shocks associated with mergers also increase the entropy of the gas. Mergers can help to mix the intracluster gas, possibly removing abundance gradients. Mergers appear to disrupt the cooling cores found in many clusters; there is an anticorrelation between cooling core clusters and clusters with evidence for strong ongoing mergers (e.g., Buote & Tsai 1996). The specific mechanism by which cooling cores are disrupted is not completely understood at this time (e.g., Ricker & Sarazin 2001).

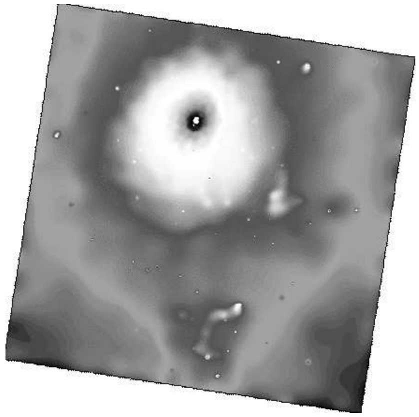

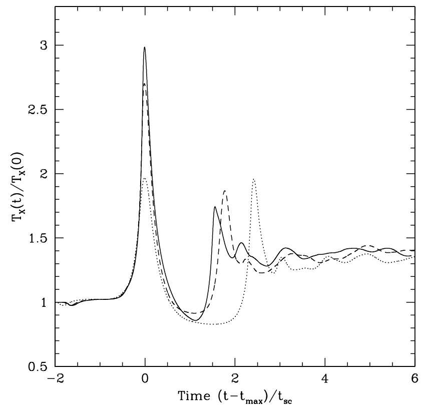

Figure 1. (a) The Chandra X-ray image of the merging cluster Abell 85 (Kempner et al. 2002). Two subclusters to the south and southwest are merging with the main cluster. (b) The X-ray emission-averaged temperature in a pair of equal mass clusters undergoing a merger (Ricker & Sarazin 2001; Randall et al. 2002)

The heating and compression associated with mergers can produce a large, temporary increase in the X-ray luminosity (up to a factor of $\sim$10) and the X-ray temperature (up to a factor of $\sim$3) of the merging clusters (Figure 1b; Ricker & Sarazin 2001; Randall, Sarazin, & Ricker 2002). Very luminous hot clusters are very rare objects in the Universe. Although major mergers are also rare events, merger boosts can cause mergers to strongly affect the statistics of the most luminous, hottest clusters. Simulations predict that many of the most luminous, hottest clusters are actually merging systems, with lower total masses than would be inferred from their X-ray luminosities and temperatures (Randall et al. 2002). Since the most massive clusters give the greatest leverage in determining Ω_M and σ_8, these values can be biased by merger boosts.

One of the most dramatic results on clusters of galaxies to come from the Chandra X-ray observatory was the discovery of sharp surface brightness discontinuities in the images of merging clusters (Figure 1a). These were first seen in Abell 2142 (Markevitch et al. 2000) and Abell 3667 (Vikhlinin, Markevitch, & Murray 2001b). Initially, one might have suspected these features were merger shocks, but X-ray spectral measurements showed that the dense, X-ray bright "post-shock" gas was cooler, had lower entropy, and was at the same pressure as the lower density "pre-shock" gas. This would be impossible for a shock. Instead, these "cold fronts" are apparently contact discontinuities between gas which was in the cool core of one of the merging subclusters and surrounding shocked intracluster gas (Vikhlinin et al. 2001b). The cool cores are plowing rapidly through the shocked cluster gas, and ram pressure sweeps back the gas at the front edge of the cold front. In a few cases (e.g., 1E0657−56; Markevitch et al. 2003), bow shocks are seen ahead of the cold fronts.

Cold fronts and merger shocks provide a number of classical hydrodynamical diagnostics which can be used to determine the kinematics of the merger (Vikhlinin et al. 2001b; Sarazin 2002). Most of these diagnostics give the merger Mach number $\mathcal{M}$. The standard Rankine-Hugoniot shock jump conditions can

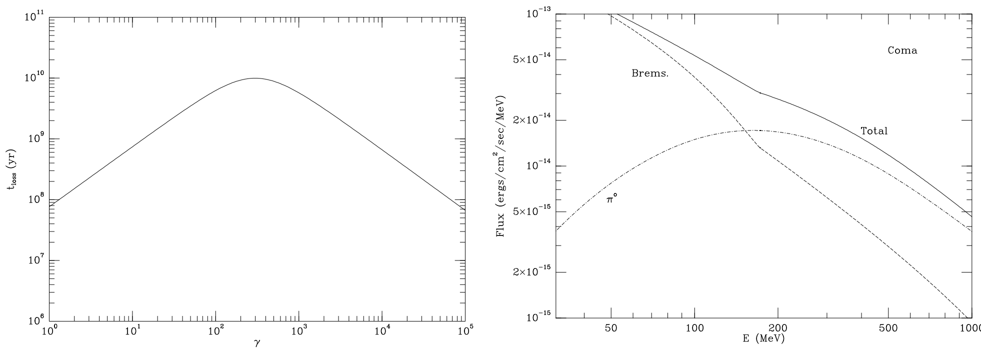

Figure 2. (a) The lifetimes of relativistic electrons in a typical cluster as a function of their Lorentz factor γ (Sarazin 1999a). (b) The gamma-ray emission spectrum from a model for relativistic particles in the Coma cluster (Sarazin 1999b). Emission from electrons (Brems.) and ions (due to π^o decays) are shown separately.

be applied to merger shocks; for example, the pressure discontinuity is

$$\frac{P_2}{P_1} = \frac{2\gamma}{\gamma+1}\mathcal{M}^2 - \frac{\gamma-1}{\gamma+1}\,, \tag{1}$$

where P_1 and P_2 are the pre- and post-shock pressure, and $\gamma = 5/3$ is the adiabatic index of the gas. For bow shocks in front of cold front, the shock may be conical at the Mach angle, $\theta_m = \csc^{-1}(\mathcal{M}_1)$. The ratio of the pressure at the stagnation point in front of a cold front to the pressure well ahead of it is given by

$$\frac{P_{\rm st}}{P_1} = \begin{cases} \left(1 + \frac{\gamma-1}{2}\mathcal{M}^2\right)^{\frac{\gamma}{\gamma-1}}\,, & \mathcal{M} \le 1\,, \\ \mathcal{M}^2 \left(\frac{\gamma+1}{2}\right)^{\frac{\gamma+1}{\gamma-1}} \left(\gamma - \frac{\gamma-1}{2\mathcal{M}^2}\right)^{-\frac{1}{\gamma-1}}\,, & \mathcal{M} > 1\,. \end{cases} \tag{2}$$

If the motion of the cold front is supersonic, the stand-off distance between the cold front and the bow shock varies inversely with $\mathcal{M}$. For major mergers, these kinematic diagnostics generally indicate that mergers are mildly transonic $\mathcal{M} \approx 2$, corresponding to merger velocities of $\sim$2000 km/s.

Mergers also provide a useful environment for testing the role of various physical processes in clusters. For example, the very steep temperature gradients at cold fronts imply that thermal conduction is suppressed by a large factor ($\sim 10^2$; Ettori & Fabian 2000; Vikhlinin, Markevitch, & Murray 2001a), presumably by magnetic fields. The smooth front surfaces of some cold fronts suggest that Kelvin-Helmholtz instabilities are being suppressed, also probably by magnetic fields. Recently, Markevitch et al. (2003) have used the relative distributions of dark matter, galaxies, and gas in the dramatic merging cluster 1E0657−56 (Figure 1b) to argue that the collision cross-section per unit mass of the dark matter must be low, $\sigma/m \lesssim 1$ cm^2/g, which excludes most of the self-interacting dark matter models invoked to explain the mass profiles of galaxies.

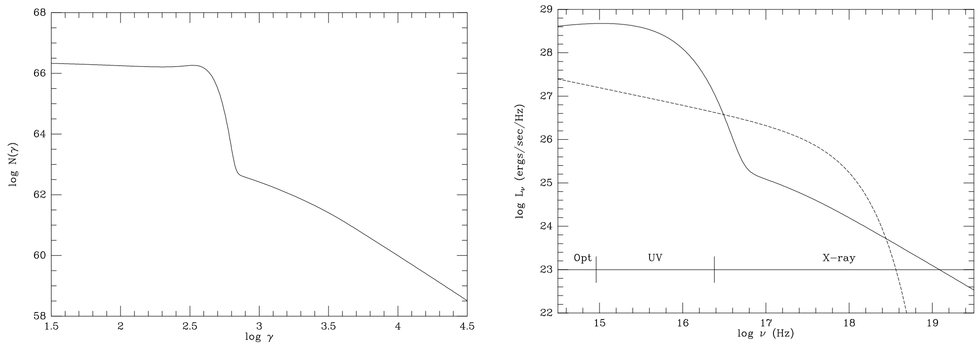

Figure 3. (a) The energy spectrum of relativistic electrons in a model for a merging cluster (Sarazin 1999a). The large population at $\gamma \sim 300$ are due to many previous mergers, while the tail to high energies is due to the current merger. (b) The IC spectrum produced by the model in (a). For reference, the dashed line is thermal bremsstrahlung at a typical cluster luminosity.

3. Non-Thermal Effects of Mergers

High speed astrophysical shocks in diffuse gas generally lead to significant acceleration of relativistic electrons. For example, typical supernova remnants have blast wave shock velocities of a few thousand km/s, which are comparable to the speeds in merger shocks. (However, the Mach numbers in merger shocks are much lower.) The ubiquity of radio emission from Galactic supernova remnants implies that at least a few percent of the shock energy goes into accelerating relativistic electrons, with more probably going into ions. If these numbers are applied to strong merger shocks in clusters, one would expect that relativistic electrons with a total energy of $E_{\rm rel,e} \sim 10^{62}$ erg would be accelerated, with even more energy in the relativistic ions. Thus, merging clusters should have huge populations of relativistic particles.

Clusters should also retain some of these particles for very long times. The cosmic rays gyrate around magnetic field lines, which are frozen-in to the gas, which is held in by the strong gravitational fields of clusters. Because clusters are large, the timescales for diffusion are generally longer than the Hubble time. The low gas and radiation densities in the intracluster medium imply that losses by relativistic ions are very slow, and those by relativistic electrons are fairly slow. Figure 2a shows the loss timescale for electrons under typical cluster conditions; electrons with Lorentz factors $\gamma \approx 300$ and energies of $\approx$150 MeV have lifetimes which approach the Hubble time, as long as cluster magnetic fields are not too large ($B \lesssim 3\ \mu$G). As a result, clusters should contain two populations of primary relativistic electrons (Figure 3a): those at $\gamma \sim 300$ which have been produced by mergers over the lifetime of the clusters; and a tail to higher energies produced by any current merger.

The lower energy electrons will mainly be visible in the EUV/soft X-ray range (Figure 3b). Such emission has been seen in clusters, although its origin is uncertain and may well be thermal, as Jonathan Mittaz described in this session. More energetic electrons, with energies of many GeV, produce hard X-ray IC emission and radio synchrotron emission. Diffuse radio sources, not associated with radio galaxies, have been observed for many years in merging clusters.

Centrally located, unpolarized, regular sources are called "radio halos", while peripheral, irregular, polarized sources are called "radio relics". Recent Chandra observations seem to show a direct connection between radio halos and merger shocks in clusters (Markevitch & Vikhlinin 2001). The same higher energy electrons will produce hard X-ray IC emission. Recently, such emission appears to have been detected with BeppoSAX and RXTE, although the detections are relatively weak and controversial [see Rossetti & Molendi (2003) and the poster by Fusco-Femiano et al. in this session].

I believe one of the most exciting possibilities for the future is the detection of clusters in hard gamma-ray radiation (Figure 2b). Essentially, all models for the nonthermal populations in clusters predict that they should be very luminous gamma-ray sources, particularly at photon energies of $\sim$100 MeV (Sarazin 1999b; Blasi & Gabici 2003). The emission at these energies is partly due to electrons with energies of 150 MeV, which should be ubiquitous in clusters. One nice feature of this spectral region is that emission is produced both by relativistic electrons (bremsstrahlung and IC) and relativistic ions (through the production of π^o particles which decay into gamma-ray photons; see Figure 2b). Thus, one can determine both population is clusters. Models suggest that GLAST and AGILE will detect $\sim$40 nearby clusters.

Acknowledgments. This work was supported by the National Aeronautics and Space Administration through Chandra Award Numbers GO1-2123X, GO2-3159X, and GO3-4160X, and *XMM/Newton* Award Numbers NAG5-10075 and NAG5-13088.

References

Blasi, P., & Gabici, S. 2003, preprint (astro-ph/0305251)

Buote, D. A., & Tsai, J. C. 1996, ApJ, 458, 27

Ettori, S., & Fabian, A. C. 2000, MNRAS, 317, L57

Kempner, J., Sarazin, C. L., & Ricker, P. R. 2002, ApJ, 579, 236

Markevitch, M., et al., 2000, ApJ, 541, 542

Markevitch, M., et al., 2003, ApJ, submitted (astro-ph/0309303)

Markevitch, M., & Vikhlinin, A. 2001, ApJ, 563, 95

Randall, S. W., Sarazin, C. L., & Ricker, P. M. 2002, ApJ, 577, 579

Ricker, P. M., & Sarazin, C. L. 2001, ApJ, 561, 621

Rossetti, M., & Molendi, S. 2003, preprint

Sarazin, C. L. 1999a, ApJ, 520, 529

Sarazin, C. L. 1999b, in Diffuse Thermal and Relativistic Plasma in Galaxy Clusters, ed. H. Böhringer, L. Feretti, & P. Schuecker (Garching: MPE Rep. 271), 185

Sarazin, C. L. 2002, in Merging Processes in Clusters of Galaxies, ed. L. Feretti, I. M. Gioia, & G. Giovannini (Dordrecht: Kluwer), 1

Vikhlinin, A., Markevitch, M., & Murray, S. M. 2001a, ApJ, 549, L47

Vikhlinin, A., Markevitch, M., & Murray, S. M. 2001b, ApJ, 551, 160

Highlights of Astronomy, Vol. 13
International Astronomical Union, 2003
O. Engvold, ed.

Stellar Populations, Butcher-Oemler Effect, Star Formation in Clusters

Bianca M. Poggianti

Osservatorio Astronomico di Padova-INAF, Italy

Abstract. In this brief overview of the stellar populations of galaxies in clusters I highlight some of the most recent results, including the downsizing of the k+a population and the star formation–local density relation. I conclude discussing some open questions regarding the interpretation of the observational results, and speculating on the current meaning of the words "primordial" and "environmental".

1. Introduction

Studying the evolutionary histories of galaxies in clusters has always been an endeavor to understand how galaxies (all galaxies) came to be as we observe them. In recent years, this quest can be better described as an effort to comprehend how galaxies formed and evolved in a "changing" environment. In fact, the common framework for these studies is now a hierarchical universe, in which galaxies can and often do change environment during their evolution. When a galaxy infalls into a cluster, it can do so as a single isolated galaxy, as a pair, as part of a group or as a member of another merging cluster. A galaxy can experience very different environmental conditions throughout its evolution. A major challenge for today's research is to identify the effects produced by the various environments on the observable properties of galaxies. It is especially hard to discriminate between minor and major influences. If all environments are potentially expected to have *some* impact on their galaxies, we would like to discern secondary effects ("cosmetics") from the primary causes that determine how galaxies are.

In this search we can rely on some objective and measurable properties, such as mass in stars and gas, their chemical content, their motion within the galaxy and the structures they design. The star formation activity is one of the most outstanding characteristics. Though a precise measurement of the current and past star formation activity is no easy task for any galaxy, star formation affects the accessible observables, such as colors and spectra, in such a manifest way that is often the most immediate evidence for evolution.

In this contribution I focus on the build-up of the stellar populations in cluster galaxies and on the evolution with redshift of their star formation activity. The subject has been very rich in results and papers published during the past 25 years, and it is impossible to give an exhaustive summary in a short text. I will therefore only touch upon some of the issues, and highlight just a couple of the most recent results. Overviews on the evolution of the stellar populations in cluster galaxies can be found in Ellingson (2003), Poggianti (2003a) and several reviews in the 3rd volume of the Carnegie Observatories Astrophysics Series: Clusters of Galaxies: Probes of Cosmological Structure and Galaxy Evolution (eds. J.S. Mulchaey, A. Dressler, and A. Oemler (Pasadena: Carnegie Observatories, http://www.ociw.edu/ociw/symposia/series/symposium3/proceedings.html).

2. Where it all started....and where we are

The Butcher-Oemler effect is the excess of galaxies bluer than the color-magnitude red sequence in clusters at $z > 0.1 - 0.2$ as compared to the richest nearby clusters (Butcher & Oemler 1984).

The origin of the scatter in the fraction of blue galaxies from cluster to cluster at any given redshift, and the consequent search for correlations between the blue fraction f_B and the global cluster properties (Smail et al. 1998, Margoniner et al. 2001, Metevier et al. 2000); the trend with redshift of f_B in optical and X-ray selected cluster samples and the dependence on cluster selection (Andreon & Ettori 1999, Ellingson et al. 2001, Kodama & Bower 2001, Fairley et al. 2002); the change in galaxy colors with cluster-centric distance (Pimbblet et al. 2002); the nature of the galaxies giving rise to the Butcher-Oemler effect (De Propris et al. 2003); these are some of the aspects related to the Butcher-Oemler effect that are still subject of ongoing investigation, witnessing the interest in fully understanding the consequences and the cause of the seminal Butcher & Oemler findings.

Put in a slightly different way, the Butcher-Oemler effect is the presence of large numbers of blue galaxies in rich clusters more distant than those in the local universe. This higher average level of activity in the past has been confirmed and greatly clarified by spectroscopic surveys and by Hubble Space Telescope morphological studies of galaxies in distant clusters (Couch et al. 1994, 1998, Dressler et al. 1997, Balogh et al. 1997, 1998, 1999, Poggianti et al. 1999, van Dokkum et al. 1999, 2000, Fabricant et al. 2000, Ellingson et al. 2001, Postman et al. 2001, Smail et al. 2001, Lubin et al. 2002).

No matter how the evolution in the populations of cluster galaxies is observed, if using the blue colors, the spectral features or the proportion of spiral versus early-type galaxies: all the three types of observations contribute to delineate a picture in which the evolution of galaxies in clusters is strong, given that a large fraction of them at $z = 0$ have evolved from star-forming, late-type galaxies to passively evolving, early-type galaxies within a relatively short period of time (Kodama & Smail 2001, van Dokkum & Franx 2001).

At least three phenomena likely play a role in this evolution (Poggianti et al. 1999, Ellingson et al. 2001, Kodama & Bower 2001): the declining infall rate of galaxies onto clusters at lower z predicted by hierarchical cosmological models (Bower 1991, Kauffmann 1995); the evolution with z of the average star formation rate (SFR) in the "field" galaxies that infall into clusters; and the decline of star formation in the cluster galaxies likely due to some physical process (or processes) that acts when galaxies infall in the denser environment. In fact, though the universe as a whole seems to evolve towards a progressively lower star formation activity in the Madau plot, such a trend appears to be accelerated in clusters (Kodama & Bower 2001).

The past star formation activity as seen from the absorption lines The most cited result obtained from spectra of galaxies in distant clusters is the presence of "k+a" spectra, with no emission lines and strong Balmer lines in absorption indicating a vigorous star formation activity that was terminated at some point during the last 1–1.5 Gyr (Dressler & Gunn 1983, Couch & Sharples 1987). Since such spectra unequivocally identify post-starburst or post-starforming galaxies, their excess in distant clusters as compared to the field at similar redshifts is strong, if not the strongest, evidence that star formation is truncated by the dense environment (Dressler et al. 1999, but see Balogh et al. 1999 for a different view). K+a galaxies have been thoroughly discussed elsewhere (e.g. Poggianti 2003b and references therein), but it is worth highlighting here a very recent result from Tran et al. (2003). On the basis of the galaxy velocity dispersions and radii, these authors find that the descendants of the k+a's observed at $z \sim 0.8$ must be among the most massive early-type galaxies in clusters today, while the maximum luminosity and galaxy velocity dispersion of cluster k+a galaxies decrease towards lower redshifts. Another result pointing in the same direction is presented in Poggianti et al. (2003), where we analyzed the luminosity distribution of k+a galaxies in the Coma cluster: no k+a as luminous as in the distant clusters is observed, while k+a's are found to be a significant fraction of the dwarf galaxy population.

The ongoing star formation activity as seen from the emission lines In the absence of a significant AGN ionizing radiation, emission lines are present in a spectrum only when there is ongoing star formation activity.

In agreement with the other photometric and spectroscopic signs of current activity, a significant fraction of even the most luminous galaxies in distant clusters have been observed to have emission lines indicating they are actively forming stars (Dressler et al. 1999, Postman et al. 2001), though the fraction of emission line galaxies remains lower in clusters than in the field at all redshifts.

Whether the star formation activity in clusters is enhanced in some of the infalling galaxies, and how relevant this is for the global cluster populations is still debated. Besides considerations based on optical observations in favor and against cluster-triggered starbursts, a striking result comes from dust-free wavelengths: the large numbers of Luminous Infrared starburst galaxies detected by ISOCAM in distant clusters seem to be too high to be consistent with simple accretion of starburst galaxies from the field (Duc et al. submitted, Coia et al. submitted).

Finally, several works have been recently devoted to the study of the emission line trend with clustercentric radius. Balogh et al. (1997, 1998) have shown how the mean equivalent width of [O II] increases radially in distant clusters, failing to reach the mean field value even as far out as several Mpc from the cluster centre. An extension of these radial studies has been carried out using the large datasets of the 2dF (Lewis et al. 2002) and Sloan (Gomez et al. 2003) spectroscopic surveys. As shown in Fig. 1, the mean EW(Hα) increases at lower projected local surface density of galaxies (and, correspondingly, larger distance from cluster centre) down to a density of ~ 1 galaxy per Mpc^2, and approaches the field value at ~ 3 times the virial radius of the cluster.

The mean EW, or SFR, used in these studies is the mean over all galaxies (with and without emission lines, of any morphological type), including the pas-

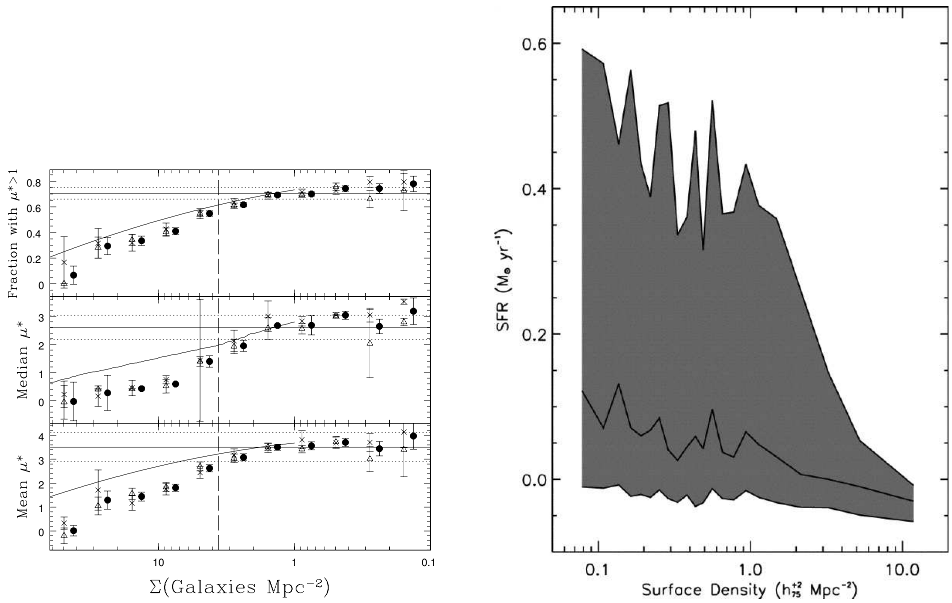

Figure 1. **Left** - From Lewis et al. 2002 (2dF): μ^*, the star formation rate normalized to L^*, is proportional to the EW(Hα). Its trend as a function of the local galaxy density is shown for all clusters (solid points) and for clusters with σ greater than or less than 800 km s^{-1} (triangles and crosses, respectively). The horizontal solid line represents the field value. **Right** - From Gomez et al. 2003 (Sloan): the shaded area represents the distribution of star formation rates, corrected for extinction. The median is shown as a solid line. The top of the shaded area is the 75^{th} percentile, while the bottom is the 25^{th} percentile.

sive early-type galaxies that dominate the cluster cores and the highest density regions. A mean total EW decreasing with density and towards the cluster centre is therefore not surprising in this respect. Whether the trend of mean EW *simply* reflects a different morphological mix as a function of local density, and whether it can be *fully* explained by the morphology-density relation (Dressler et al. 1997) is still unclear (Lewis et al. 2002, Gomez et al. 2003).

The *origin* of the observed EW trend remains in my opinion one of the most interesting questions to be answered, together with the origin of the morphology-density relation and the relation between the two. A systematic variation of galaxy properties with the environment does not necessarily imply a “transformation” due to an environmental process beginning to act on a galaxy when this enters an environment for the first time. In principle, one cannot exclude that the correlation of star formation with local density can be partly or fully explained as an “imprinting” on the galaxy star formation history established in the early universe as a function of the local density. For example, the most massive ellipticals in the densest regions today (the cluster cores), that formed most of their stars at very high redshifts, were in the densest regions also at $z > 3$ and it is then, by those conditions, that their star formation history was decided. These galaxies contribute to the shape of the EW-density relation today as some of the galaxies with EW=0 (devoid of SF), and it is therefore logical to conclude that at least *part* of the SF-density relation has been established very early on. Similarly, the morphology-density (MD) relation must have a "primordial" component, since at all redshifts the most massive early-type galaxies are found in the highest density regions. However, the MD relation as we observe it today is not *fully* established at high redshift, because we observe how it evolves in clusters, with late type spirals being transformed into early-type galaxies (Dressler et al. 1997, Lubin et al. 2002).

It is probably time for the astronomical community working on clusters to reconsider the meaning of words such as "primordial" and "environmental". By "primordial", do we mean anything that took place at $z > 3$, or anything that was already engraved in the galaxy "destiny" by the early conditions in the location where they formed their first stars? And by "environmental", do we mean any physical process that affects galaxies once they enter a "new" environment, implying that their evolution would have been different if they did not become part of it? Or do we consider an effect environmental any time it has to do with something external to the galaxy itself? In this case, what do we consider as the "galaxy itself"? Anything that will be part of that galaxy by $z = 0$? Can a process be considered an environmental effect even if it only affected the galaxy at $z > 3$? Re-thinking the definition of the words "primordial" and "environmental" is not just a semantic exercise, it is probably useful to make progress in an era in which we believe galaxies can change environment, but today's environment is not necessarily unrelated with the environments of yesterday.

Acknowledgments. I thank the IAU and the organizers of this Joint Discussion on clusters for their kind invitation and for generously supporting my participation with a IAU travel grant.

References

Andreon, S., Ettori, S., 1999, ApJ, 516, 647

Balogh, M.L., Morris, S.L., Yee, H.K.C., Carlberg, R.G., Ellingson, E., 1997, ApJ, 488, L75

Balogh, M.L., Schade, D., Morris, S.L., Yee, H. K. C., Carlberg, R. G., Ellingson, E., 1998, ApJ, 504, L75

Balogh, M. L., Morris, S. L., Yee, H. K. C., Carlberg, R. G., & Ellingson, E., 1999, ApJ, 527, 54

Bower, R.G., 1991, MNRAS, 248, 332

Butcher, H. & Oemler, A., 1984, ApJ, 285, 426

Couch, W. J., & Sharples, R. M. 1987, MNRAS, 229, 423

Couch, W. J., Ellis, R. S., Sharples, R.M., Smail, I. 1994, ApJ, 430, 121

Couch, W. J., Barger, A.J., Smail, I., Ellis, R. S., Sharples, R.M. 1998, ApJ, 497, 188

De Propris, R., Stanford, S.A., Eisenhardt, P.R., Dickinson, M., 2003, ApJ in press (astro-ph 0307545)

Dressler, A., & Gunn, J. E. 1983, ApJ, 270, 7

Dressler, A., Oemler, A., Jr., Couch, W. J., Smail, I., Ellis, R. S., Barger, A., Butcher, H., Poggianti, B. M., Sharples, Ray M., 1997, ApJ, 490, 577

Dressler, A., Smail, I., Poggianti, B. M., Butcher, H., Couch, W. J., Ellis, R. S., & Oemler, A. 1999, ApJS, 122, 51

Ellingson, E., Lin, H., Yee, H. K. C., & Carlberg, R. G. 2001, ApJ, 547, 609

Ellingson, E., 2003, in Matter and Energy in Clusters of Galaxies, eds. S. Bowyer and C.-Y. Hwang, ASP Conf.Series vol.301, p.221

Fabricant, D., Franx, M., van Dokkum, P., 2000, ApJ, 539, 577

Fairley, B.W., Jones, L.R., Wake, D.A., Collins, C.A., Burke, D.J., Nichol, R.C., Romer, A.K., 2002, MNRAS, 330, 755

Gomez, P.L., Nichol, R.C., Miller, C.J., et al., 2003, ApJ, 584, 210

Kauffmann, G., 1995, MN, 274, 153

Kodama, T., & Bower, R. G. 2001, MNRAS, 321, 18

Kodama, T., Smail, I. 2001, MNRAS, 326, 637

Lewis, I., Balogh, M., De Propris, R. et al., 2002, MNRAS, 334, 673

Lubin, L. M., Oke, J. B., & Postman, M. 2002, AJ, 124, 1905

Margoniner, V.E., de Carvalho, R.R., Gal, R.R., Djorgovski, S. G., 2001, ApJ, 548, 143

Metevier, A.J., Romer, A.K., Ulmer, M. P. 2000, AJ, 119, 1090

Pimbblet, K.A., Smail, I., Kodama, T., Couch, W., Edge, A.C., Zabludoff, A.I., O'Hely, E., 2002, MNRAS, 331, 333

Poggianti, B. M., Smail, I., Dressler, A., Couch, W. J., Barger, A. J., Butcher, H., Ellis, R. S., & Oemler, A., 1999, ApJ, 518, 576

Poggianti B.M., 2003a, Ap&SS 285, 121

Poggianti B.M., 2003b, in Carnegie Observatories Astrophysics Series, vol.3: Clusters of Galaxies: Probes of Cosmological Structure and Galaxy Evolution (eds. J.S. Mulchaey, A. Dressler, and A. Oemler (Pasadena: Carnegie Observatories, http://www.ociw.edu/ociw/symposia/series/symposium3/proceedings.html).

Poggianti, B.M., Bridges, T.J., Komiyama, Y., Yagi, M., Carter, D., Mobasher, B., Okamura, S., Kashikawa, N., 2003, ApJ in press (astro-ph 0309449)

Postman, M., Lubin, L. M., Oke, J. B. 2001, AJ, 122, 1125

Smail, I., Edge, A.C., Ellis, R. S., Blandford, R.D., 1998, MNRAS, 293, 124

Smail, I., Kuntschner, H., Kodama, T., Smith, G. P., Packham, C., Fruchter, A. S., & Hook, R. N. 2001, MNRAS, 323, 839

Tran, K.-V.H., Franx, M., Illingworth, G., Kelson, D.D., van Dokkum, P., 2003, ApJ in press (astro-ph 0309460)

van Dokkum, P. G., Franx, M., Fabricant, D., Kelson, D. D., & Illingworth, G. D. 1999, ApJ, 520, L95

van Dokkum, P. G., Franx, M., Fabricant, D., Illingworth, G. D., & Kelson, D. D. 2000, ApJ, 541, 95

van Dokkum, P.G., Franx, M., 2001, ApJ, 553, 90

Highlights of Astronomy, Vol. 13
International Astronomical Union, 2003
O. Engvold, ed.

Radio Sources as Probes of Distant Clusters

Joanne Baker

Astrophysics Department, Keble Road, Oxford, OX2 0BA, UK

Jordi Barr

Astrophysics Department, Keble Road, Oxford, OX2 0BA, UK

Malcolm Bremer

Physics, University of Bristol, Tyndall Avenue, Bristol BS8 1TL, UK

Abstract. Powerful radio sources are efficient probes of dense regions throughout the universe, including clusters of galaxies. The status of cluster searches around radio sources is reviewed, including new evidence that cluster environments affect radio morphology.

1. Introduction

Powerful active galactic nuclei (AGN) — including radio sources — are efficient tracers of dense regions in the universe. The massive ellipticals that host them should be sited in high-density peaks in the galaxy distribution, including clusters. Galaxy mergers in dense environments may also explain the triggering and fueling of the AGN.

Visible out to the highest redshifts, luminous AGN signpost the first forming structures. Counting distant clusters constrains the amount of matter in the universe, Ω_m, that ultimately controls the rate at which massive systems collapse (Bahcall & Fan 1998). Detecting even small numbers of massive clusters at high redshift implies Ω_m is low, less than one.

It is much more efficient to use AGN to locate distant clusters than to carry out a blind survey, although both ways have different biases. Galaxies and intra-cluster gas rapidly become faint at great distances, and are swamped by foreground objects. So blind surveys are difficult beyond $z \sim 1$.

Although both types may live in clusters, radio-loud AGN have many distinct advantages over radio-quiet ones. Dust does not dim the radio emission, whose intrinsic jet power and orientation can be inferred directly. Extended radio lobes also sample the surrounding gas, and intra-cluster medium (ICM) (e.g. Blanton et al. 2003).

McLure & Dunlop (2001) argue that powerful radio sources at high redshift trace the progenitors of rich clusters today. This follows from the similar space density of powerful radio sources at $z \sim 2.5$ and Abell clusters locally, implying virtually all nearby clusters hosted a powerful radio galaxy in the past. In addition to having massive hosts, powerful (Jy) radio sources have massive central black holes ($M_{bh} \sim 10^9 M_\odot$), and so are key targets for investigating galaxy and black hole formation and evolution.

More numerous weak (mJy) radio sources can also be mapped on the sky to reveal large galaxy structures, including clusters and superclusters (e.g. Cotter et al. 2002; Brand et al. 2003).

To date, many clusters have been identified around radio sources, including systems at the highest redshifts ($z > 4$). But the wider question of how cluster environments affect AGN and their elliptical hosts remains. Also, it is not obvious how to link the $z > 2$ 'protoclusters' with lower redshift clusters and AGN environments.

2. Clusters around radio sources at $z > 2$

Galaxy overdensities have been reported around a handful of high-redshift radio galaxies, at $z = 2-5$. These so-called 'protoclusters' comprise mainly overdensities of tens of star-forming galaxies, visible in Lyα emission (e.g. Venemans et al. 2002), ultraviolet spectral breaks (e.g. Lacy & Rawlings 1996), or sub-millimeter emission (e.g. Ivison et al. 1999; Smail et al. 2003).

An excess of X-ray sources, but no diffuse cluster gas component, has been seen in one $z = 2.2$ field (Carilli et al. 2002).

Typically, the high-redshift radio galaxies found in clusters have unusually clumpy hosts and small, asymmetric radio sources (e.g. Pentericci et al. 1997; 1998).

3. Clusters around radio sources at $z < 2$

AGN environments have been surveyed systematically out to $z = 0.7$, but less so beyond this. Most cluster searches around moderate redshift AGN simply count galaxies within some radius of the AGN. Large studies have characterized AGN environments in this way (Yee & Green 1987; Ellingson et al. 1991; Hill & Lilly 1991; Wold et al. 2000; Hall et al. 1998, 2001), and individual rich fields have been identified out to $z \sim 2$ (Sanchez & Gonzalez-Serrano 1999; Chapman, McCarthy & Persson 2000).

Incorporating simple color information — selecting extremely red objects around AGN — is one way to alleviate foreground confusion in fields at $z \sim 1$ (e.g. Stern et al. 2003).

Diffuse cluster ICM is detectable around powerful radio sources out to $z \sim 1$ (e.g. Crawford & Fabian 2003; but see Donahue, Daly & Horner 2003) but is generally too faint to see at higher redshifts, where microwave background photons scattered by the radio lobes may dominate (e.g. Fabian et al. 2003)

In summary, AGN inhabit a range of environments, mostly of moderate richness (Abell class 0) but sometimes very rich (Abell class 2 or 3). Relatively few of these clusters have had their masses established by X-ray detections of ICM and/or weak lensing measurements (e.g. Wold et al. 2002; Crawford & Fabian 2003).

Although early studies proposed evolution in quasar environments from $z = 0.7$ to the present day (Yee & Green 1987; Ellingson et al. 1991; Hill &

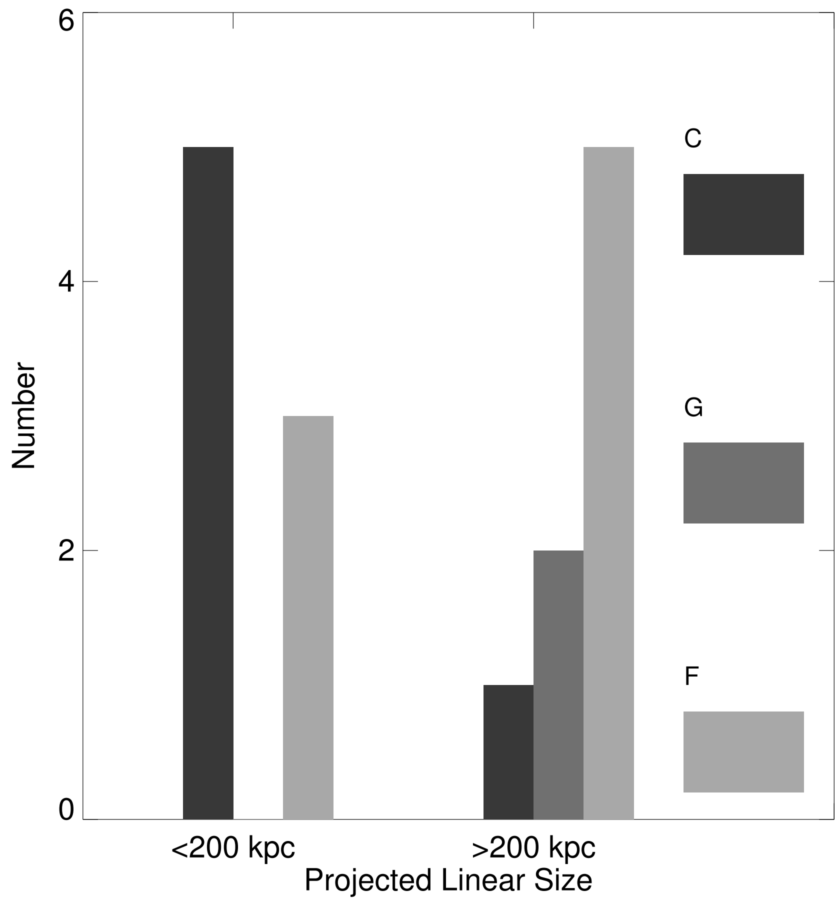

Figure 1. Bar chart showing numbers of radio sources in clusters (c), groups (g) and field (f) environments as a function of radio linear size (D) split at 200 kpc. See Barr et al. (2003).

Lilly), evidence that environment correlates strongly with AGN properties is weak (Wold et al. 2000).

There is a clear need for systematic studies at $z > 0.7$ to push into the epoch where clusters are still coalescing from sub-clumps.

4. A new survey of quasars at $z \sim 1$

Barr et al. (2003) imaged the fields of 21 steep-spectrum powerful radio quasars with $0.6 < z < 1.1$, drawn from a complete redshift-limited subset of the Molonglo Quasar Sample (Kapahi et al. 1998). The fields were imaged in at least two optical filters chosen to straddle the redshifted 4000Å break feature, selecting the passively-evolving elliptical galaxies that populate cluster cores.

Some fields were also targeted with narrow-band (FWHM 7Å) imaging around the wavelength of redshifted [O II] emission line with the TAURUS Tunable Filter (TTF) at the AAT. This traces strongly star-forming galaxies at the quasar redshift.

Galaxy clustering was measured in two ways (i) by counting galaxies around the quasar, in the same way as previous $z < 0.7$ studies, and (ii) counting only red galaxies with the colors expected for passively-evolving, old stellar populations at the quasar redshift.

Red galaxy overdensities were seen in 8/21 fields. Foreground systems (overdensities with the wrong colors) were spotted in two cases, illustrating the weakness of single filter counting statistics. The overdensity centroids lay typically within $10'' - 20''$ of the quasar — but not on it — and extended over typically $100''$, being frequently elongated.

Looking at the radio morphologies, small (linear size $D < 200$ kpc), and asymmetric, radio sources were most often located in clusters (5/8 small sources compared with 1/8 larger sources in clusters).

In the 6 fields targeted with TTF, 47 emission-line galaxy candidates were detected, with star formation rates 1–100 $M_\odot\,\mathrm{yr}^{-1}$ and very faint ($I(AB) > 23$) continua. Emission-line galaxy candidates cluster around the quasars, but less strongly than the red galaxies, suggesting the morphology-density relation is in place at $z \sim 1$.

5. Conclusion

Powerful radio sources — especially small, asymmetric ones — are often located in clusters of galaxies that are seen out to the highest redshifts.

At redshifts $z > 0.7$, they are best located using multicolor and/or narrow-band techniques, along with X-ray and sub-millimeter observations.

More work is needed on a systematic basis to measure the masses of these systems (e.g. diffuse X-rays, spectroscopy and weak lensing techniques) and to understand links between AGN and their environments.

Acknowledgments. JCB acknowledges support from a Royal Society University Research Fellowship.

References

Bahcall, N, Fan X. 1998, ApJ, 504, 1
Barr, J., et al. 2003, MNRAS, in press (astro-ph: 0308128)
Blanton, L., et al., 2003, AJ, 125, 1635
Brand, K., et al. 2003., MNRAS, 344, 283
Carilli, C., et al. 2002, ApJ, 567, 781
Chapman, S., McCarthy P., Persson S. 2000, AJ, 120, 1612
Cotter, G., et al. 2002, MNRAS, 331, 1
Crawford, C., Fabian, A. 2003, MNRAS, 339, 1163
Donahue, M., Daly R., Horner D. 2003, ApJ, 584, 643
Ellingson, E., Yee, H., Green R. 1991, ApJ, 371, 49
Fabian A., Sanders, J., Crawford C., Ettori, S. 2003, MNRAS, 341, 729

Hall, P., et al. 2001, AJ, 121, 1840
Hall, P., Green, R. 1998, ApJ, 507, 558
Hill, G., Lilly, S. 1991, ApJ, 367, 1
Ivison, R., et al. 2000, ApJ, 542, 27
Kapahi, V., et al. 1998, ApJS, 118, 327
Lacy M., Rawlings S. 1996, MNRAS, 280, 888
McLure, R., Dunlop, J. 2001, MNRAS, 327, 199
Pentericci, L., et al. 1998, ApJ, 504, 139
Pentericci, L., et al. 1997, å, 326, 580
Sanchez, S., Gonzalez-Serrano, J. 1999, å, 352, 383
Smail, I., et al. 2003, ApJ, 583, 551
Stern, D., Holden, B., Stanford, S., Spinrad, H. 2003, AJ, 125, 2759
Venemans, B., et al. 2002, ApJ, 569, L11
Wold, M., et al. 2002, MNRAS, 335, 1017
Wold, M., Lacy, M., Lilje, P., Serjeant, S. 2000, MNRAS, 316, 267
Yee, H., Green, R. 1987, ApJ, 319, 28

Highlights of Astronomy, Vol. 13
International Astronomical Union, 2003
O. Engvold, ed.

X-ray Cavities and Cooling Flows

Paul E. J. Nulsen

School of Engineering Physics, University of Wollongong, Wollongong NSW 2522, Australia, and Harvard-Smithsonian Center for Astrophysics, 60 Garden St, Cambridge, MA 02138, USA

Brian R. McNamara

Department of Physics and Astronomy, Ohio University, Athens, OH 45701, USA

Laurence P. David

Harvard-Smithsonian Center for Astrophysics, 60 Garden St, Cambridge, MA 02138, USA

Michael W. Wise

Massachusetts Institute of Technology, Center for Space Research, 70 Vassar St, Building 37, Cambridge, MA 02139, USA

Abstract. Recent data have radically altered the X-ray perspective on cooling flow clusters. X-ray spectra show that very little of the hot intra-cluster medium is cooler than about 1 keV, despite having short cooling times. In an increasing number of cooling flow clusters, the lobes of a central radio source are found to have created cavities in the hot gas. Generally, the cavities are not overpressured relative to the intra-cluster gas, but act as buoyant bubbles of radio emitting plasma that drive circulation as they rise, mixing and heating the intra-cluster gas. All this points to the radio source, i.e., an active galactic nucleus, as the heat source that prevents gas from cooling to low temperatures. However, heating due to bubbles alone seems to be insufficient, so the energetics of cooling flows remain obscure. We briefly review the data and theory supporting this view and discuss the energetics of cooling flows.

1. Introduction

The radiative cooling time of the hot intergalactic gas close to the centers of about 70 percent of rich clusters of galaxies is significantly shorter than the Hubble time. These systems are known as cooling flows (Fabian 1994). Over the lifetime of a cooling flow cluster, radiative losses have a significant impact on the gas unless the radiated heat is replaced. Cooling gas is compressed in order to maintain hydrostatic equilibrium, causing inflow near to the cluster center and the deposition of large quantities of cool gas. X-ray data from *Chandra* and *XMM-Newton* confirm central cooling times as short as 10^8–10^9 y in many clusters (e.g. David et al. 2001), highlighting the significance of radiative losses. However, 100–1000 $M_\odot\ y^{-1}$ of cold gas should be deposited by cooling flows (e.g. White, Jones & Forman 1997) and very little evidence is found of this gas. Many forms of cool gas (e.g. Crawford et al. 1999; Edge 2001) and recent star formation (e.g. Mittaz et al. 2001) have been found at the centers of cooling flow clusters, but the amounts fall well short of those expected. Cooling flows also occur in groups and isolated elliptical galaxies (Mathews & Brighenti 2003).

X-ray spectra from the Reflection Grating Spectrograph (RGS) on *XMM-Newton* show that there is very little gas cooler than about 1 keV in cluster cooling flows. If the late stages of cooling are isobaric as expected, then the luminosity in a line is $L_{\rm line} = \dot{M}(5k/(2\mu m_{\rm H}) \int_0^{T_{\rm max}} \Lambda_{\rm line}(T)/\Lambda(T)\, dT$, where $\dot{M}$ is the deposition rate of cooled gas, Λ is the cooling function and $\Lambda_{\rm line}$ the part of the cooling function due to the line. This prediction is quite robust for low temperature lines, but RGS data show that some low energy lines are at least an order of magnitude weaker than expected (e.g. Peterson et al. 2003).

2. Radio Lobe Cavities in Cooling Flows

Burns (1990) found that 70 percent of cD galaxies in cooling flow clusters are radio loud, compared to 25 percent overall. Observations with *Chandra* reveal a growing list of clusters where radio lobes at the cluster center have created cavities in the hot intra-cluster gas. Some examples are Perseus (Böhringer et al. 1993; Fabian et al. 2000), Hydra A (McNamara et al. 2000), Abell 2052 (Blanton et al. 2001), RBS797 (Schindler et al. 2001), MKW3S (Mazzotta et al. 2002) and Abell 4059 (Heinz et al. 2002).

Contrary to expectation, there is little evidence of shocks driven by expanding radio lobes in most systems (but see Kraft et al. 2003; Fabian et al. 2003). Furthermore, the coolest X-ray emitting gas surrounds the cavities in many systems (e.g. Nulsen et al. 2002). It would be very surprising to find the lowest entropy gas close to the origin of a strong shock. Lastly, the equipartition pressure of the radio lobes is typically about one tenth of the surrounding gas pressure. All this argues that the radio lobes are at nearly the same pressure as the surrounding gas.

The cool gas around the cavities is surprising. Nulsen et al. (2002) argued that this is not due to shock induced cooling or magneto-hydrodynamic shocks in Hydra A. However, in a temperature map, they found a plume of cool gas extending from the center to beyond the radio lobe cavities in Hydra A. This suggests that repeated radio outbursts have produced buoyant bubbles (cavities) that drive outflow along the radio axis, lifting some low entropy gas from the cluster center. Numerical simulations support this model (Brüggen et al. 2002).

3. Energetics

The question of what prevents gas from cooling to low temperatures in cooling flows remains a major issue. The heat required to make up for radiative losses from the region where the cooling time is shorter than the age of a cluster is typically 10^{44}–10^{45} erg s^{-1}. Also, a significant amount of gas at the cluster center must be maintained with cooling times of 10^8–10^9 y. This is very difficult to achieve without a process that involves feedback.

Radio lobes are powered by an AGN, which is likely fueled by cooled and cooling gas. If the mechanical energy input due to the cavities is appreciable, this provides a feedback mechanism linking cooling and AGN heating. We consider the energy input by the bubbles, using Hydra A for illustration (David et al. 2001). The work of creating a bubble in local pressure equilibrium is $pV \simeq 2.8 \times 10^{59}$ erg for the SW cavity of Hydra A. The free energy of a bubble is the sum of this and its thermal energy, giving the enthalpy $\gamma pV/(\gamma - 1)$, where γ is the ratio of specific heats. We double this again to allow for the NE bubble. If the cavity is dominated by relativistic plasma, then $\gamma = 4/3$ and the total free energy of the two cavities in Hydra A $\simeq 2.2 \times 10^{60}$ erg. If all of this is thermalized within the cooling flow region of Hydra A, then it can prevent gas from cooling for 2.3×10^8 y.

Churazov et al. (2002) argue that the enthalpy of a rising adiabatic bubble decreases with pressure, and the loss goes into heating the gas. A bubble rises as the ICM falls in around it, converting potential energy to kinetic energy, which is then dissipated in the bubble's wake. The potential energy released when a bubble of volume V rises a distance δR is $\delta E = \rho V g \, \delta R$, where ρ is the density of the ICM and g the acceleration due to gravity. From the equation of hydrostatic equilibrium, $\rho g = -dp/dr$, so that $\delta E = -V dp/dr \, \delta R = -V \, \delta p$. For an adiabatic bubble, $pV^\gamma =$ constant, and this result is readily integrated, giving the energy dissipated over a finite length of wake, $\Delta E = H_0 - H$, where the enthalpy depends on the pressure through $H = H_0 (p/p_0)^{(\gamma-1)/\gamma}$. For Hydra A, with $\gamma = 4/3$, about half of the free energy is dissipated in the cooling flow region. If the bubble is non-adiabatic, more energy is deposited in the core.

While Hydra A is a very powerful FRI radio source, its cavities are not exceptional. Indeed, the existence of "ghost" cavities (e.g. McNamara et al. 2001) tells us that radio lifetime can be shorter than bubble lifetime and we should not expect a strong correlation between bubble energy and radio power. There may also be other energy inputs from an AGN, including direct injection of relativistic particles, uncollimated outflows, or Compton heating.

It is generally difficult to heat from the center of a cluster without creating a well mixed, isentropic core (Fabian et al. 2001; Brighenti & Mathews 2003). Slow heating drives steady convection. Fast heating drives a shock, causing entropy inversion, then convection and mixing. Mixing is less thorough if energy is deposited off center, forming bubbles. However, to prevent the bulk of the lowest entropy gas from cooling to low temperatures, most gas must be heated substantially at some stage and so take part in large-scale convection, tending to disrupt observed abundance gradients (e.g. David et al. 2001).

Zakamska & Narayan (2003) have shown that thermal conduction can balance radiative losses in some, but not all, cooling flows. However, since it involves no feedback, maintaining cool gas by thermal conduction requires very fine tuning (e.g. Bregman & David 1988). Also, thermal conductivity must be suppressed to explain observed structures in several clusters. It has been argued that these are special cases, but this is harder to accept for the large scale suppression found by Markevitch et al. (2003).

Even when suppressed by a factor of 10 or more, thermal conduction can balance radiative losses in the outer parts of cluster cooling flows. Thus, thermal conduction may augment AGN heating in clusters. In that case, AGN heating need only account for radiative losses from near to the cluster center. Thermal conduction falls rapidly with temperature, and so is less likely to be significant in groups and isolated elliptical galaxies. On the other hand, their energetics are less demanding, since a single AGN outburst can disrupt the hot interstellar medium of an isolated elliptical (e.g. Finoguenov & Jones 2001).

It has long been argued that major mergers can completely disrupt a cooling flow (McGlynn & Fabian 1984) and a variety of mechanisms have been proposed to tap the energy of mergers to prevent gas from cooling (e.g. Motl et al. 2003). However, in minor mergers and infall, most energy is deposited in the outer parts of clusters. Stable stratification, and the huge density and pressure contrast from center to edge are obstacles to getting energy from the outer regions deposited in the cluster core. Furthermore, without feedback it is very difficult for such a process to maintain short cooling times in the cluster core. As for thermal conduction, these effects may augment AGN heating.

4. Discussion and Conclusions

There is good evidence of AGN heating in cooling flows, but it remains unclear whether it is significant for cooling flows as a whole. Since AGN heating is linked to cooling by feedback, this process can plausibly explain how gas can be maintained with short cooling times in cooling flows. AGN heating probably needs to be augmented in order to account for global energetics of cooling flows. Many details of the heating process remain obscure. In particular, it is unclear how a cluster can be heated from its center without producing a constant entropy core and mixing out observed abundance gradients.

To end on a speculative note, AGN outbursts also occur in isolated elliptical galaxies, where they can prevent the cooling of hot gas more readily than in clusters. If so, AGN feedback inhibits cooling, hence star formation, in almost any system dominated by hot gas. In that case, the effect of AGN feeback is imprinted on the galaxy luminosity function.

Acknowledgments. This work was partly supported by the Australian Research Council and by NASA grant NAS8-01130.

References

Blanton, E. L., Sarazin, C. L., McNamara, B. R., & Wise, M. W., 2001, ApJ, 558, L15

Böhringer, H., Voges, W., Fabian, A. C., Edge, A. C., & Neumann, D. M. 1993, MNRAS, 264, L25

Bregman, J. N., & David, L. P. 1998, ApJ, 326, 639

Brighenti, F., & Mathews, W. G. 2003, ApJ, 587, 580

Brüggen, M., Kaiser, C. R., Churazov, E., & Enßlin, T. A. 2002, MNRAS, 331, 545

Burns, J. O. 1990, AJ, 99,14

Churazov, E., Sunyaev, R., Forman, W., & Böhringer, H. 2002, MNRAS, 332, 729

Crawford, C. S., Allen, S. W., Ebeling, H., Edge, A. C., & Fabian, A. C. 1999, MNRAS, 306, 857

David, L. P., Nulsen, P. E. J., McNamara, B. R., Forman, W. R., Jones, C., Ponman, T., & Robertson, B., Wise, M. 2001, ApJ, 557, 546

Edge, A. C. 2001, MNRAS, 328, 762

Fabian, A. C. 1994, ARA&A, 32, 277

Fabian, A. C. et al. 2000, MNRAS, 318, L65

Fabian, A. C., Mushotzky, R. F., Nulsen, P. E. J., Peterson, J. R. 2001, MNRAS, 321, 20P

Fabian, A. C. et al. 2003, MNRAS, in press (astro-ph/0306036)

Finoguenov, A., & Jones, C. 2001, ApJ, 547, L107

Heinz, S., Choi, Y.-Y., Reynolds, C. S., & Begelman, M. C. 2002, ApJ, 569, L79

Kraft, R. P., Vázquez, S. E., Forman, W. R., Jones, C., Murray, S. S., Hardcastle, M. J., Worrall, D. M., & Churazov, E. 2003, ApJ, 592, 129

Markevitch, M. et al. 2003, ApJ, 586, L19

Mathews, W. G., & Brighenti, F. 2003, ARA&A, 41, 191

Mazzotta, P., Kaastra, J. S., Paerels, F. B., Ferrigno, C., Colafrancesco, S., Mewe, R., & Forman, W. R. 2002, ApJ, 567, L37

McGlynn, T. A., & Fabian, A. C. 1984, MNRAS, 208, 709

McNamara, B. R. et al. 2000, ApJ, 534, L135

McNamara, B. R. et al. 2001, ApJ, 562, L149

Mittaz, J. P. D. et al. 2001, A&A, 365, L98

Motl, P. M., Burns, J. O., Loken, C., Norman, M. L., & Bryan, G. 2003, ApJ, in press (astro-ph/0302427)

Nulsen, P. E. J., David, L. P., McNamara, B. R., Jones, C., Forman, W. R., Wise, M. 2002, ApJ, 568, 163

Peterson, J. R., Kahn, S. M., Paerels, F. B. S., Kaastra, J. S., Tamura, T., Bleeker, J. A. M., Ferrigno, Jernigan, J. G. 2003, ApJ, 590, 207

Peres, C. B., Fabian, A. C., Edge, A. C., Allen, S. W., Johnstone, R. M., White, D. A. 1998, MNRAS, 298, 416

Schindler, S., Castillo-Morales, A., De Filippis, E., Schwope, A., Wambsganss, J. 2001, A&A, 376, L27

White, D. A., Jones, C., Forman, W.R. 1997, MNRAS, 292, 419

Zakamska, N. L., & Narayan, R. 2003, ApJ, 582, 162

Highlights of Astronomy, Vol. 13
International Astronomical Union, 2003
O. Engvold, ed.

Radio Halo and Relic Sources in Galaxy Clusters

Kinwah Wu

Mullard Space Science Laboratory, University College London, Holmbury St Mary, Surrey RH5 6NT, United Kingdom

Melanie Johnston-Hollitt

Leiden Observatory, P.O. Box 9513, NL-2300 RA, Leiden, The Netherlands

Richard Hunstead

School of Physics, University of Sydney, NSW 2006, Australia

Abstract. We review briefly the general properties of halo and relic sources in galaxy clusters. We also present a polarized radiative transfer algorithm which is useful for calculations of polarized radio emission from halos, relics and active galaxies in a magnetized intra-cluster medium.

1. Introduction

Radio halos and relics are diffuse sources which appear to be peculiar to galaxy clusters. They are generally believed to be associated with the clusters themselves rather than with individual active galaxies. Typically they have low surface brightness and steep radio spectra, indicating the emission is non-thermal and optically thin. Halos are spatially extended, with sizes of ~ 500 kpc, comparable with the cores of galaxy clusters. They tend to have a round morphology, show little or no polarization, and permeate the cluster centers. Relics are also spatially extended, but they are elongated and are usually located at the cluster periphery. In contrast to halos, emission from relic sources is strongly polarized. (For a review of radio halos and relics, see e.g. Giovannini & Feretti 2002a). Both radio halos and relics are rare, currently being detected in only about 5% of clusters. However, the detection rate increases with cluster mass and among the clusters with X-ray luminosity of 10^{45} erg s^{-1} or above, 1/3 show radio halos or relics (Giovannini & Feretti 2002b).

Several important aspects of these cluster radio sources were found recently. First, there is a linear relation in the point-to-point spatial distribution of radio and X-ray emission of halos (Govoni et al. 2001). Second, the radio power of relic sources at 1.4 GHz increases with the X-ray temperature of the cluster (Colafrancesco 1999; Liang et al. 2000). Third, the radio power of halos at 1.4 GHz is correlated with the cluster dipole power ratio (Buote 2001). The first two findings indicate a close connection between the non-thermal electrons for radio synchrotron radiation and the thermal electrons that emit keV X-rays. They also suggest that more massive clusters are more powerful radio sources. The dipole power ratio, which is a measure of the degree of departure of a cluster from its virial state, can be caused by core disruption when a violent merging event occurs. The third finding thus implies that the formation of radio halos is a consequence of cluster merging.

A possible scenario is that cluster merging leads to the formation of shocks and turbulence, which in turn accelerate (and/or reaccelerate) electrons to ultra-high energies, and result in radio synchrotron emission. (See e.g. Sarazin 2001, for a review of merger shocks and non-thermal emission from clusters.) The details of this mechanism, such as how halos and relics are induced by merging and how to accelerate the pool of non-thermal charged particles, are unclear. Nevertheless, observations continue to accumulate data, and our understanding of these sources also grows with the data base. Many interesting phenomena associated with individual sources have been found in newer observations. Among these are the imaging observations of the Mpc-scaled relics such as those found in A3667 (Röttgering et al. 1997) and A2256 (Miller et al. 2003, and references therein).

To understand how the polarized radiation interacts with intra-cluster media, we have developed a polarized radiative transfer algorithm which calculates the emission from the halos, relics or active galaxies in the clusters. We now briefly discuss the algorithm and show some results of our calculations.

2. Polarized Radiative Transfer in Cluster Environments

Radio sources in galaxy clusters could be halos, relics or resident active galaxies. The clusters have very tangled magnetic fields (e.g. Dolag 2001; Carilli & Taylor 2002) which may alter the properties of the radio radiation from these sources significantly. In particular, de-polarization and Faraday rotation/mixing are important (Burn 1966; Tribble 1991), and we need to take into account these effects when we interpret the fine features in spectral-polarization imaging observations (such as that seen in clusters like A3667 and A2256).

The polarized radiative transfer equation reads

$$\hat{D} I_\alpha \;=\; -\kappa_{\alpha\beta} I_\beta + \epsilon_\alpha \ ,$$

where $I_\alpha = (I, Q, U, V)$ are the four Stokes parameters, $\hat{D} = c^{-1}(\partial/\partial t) + \hat{k}\cdot\nabla$ is the time and spatial differential operator, ϵ_α are emission coefficients and $\kappa_{\alpha\beta}$ is the transfer matrix. (Here c is the speed of light and $\hat{k}$ is the unit propagation vector of the light ray.) The anti-Hermitian part of $\kappa_{\alpha\beta}$ contains the absorption coefficients, and the Hermitian part contains the Faraday rotation/mixing coefficients (see Pacholczyk 1977).

In our calculations, we divide the cluster into many small cells with constant density, constant magnetic field and an homogeneous electron energy distribution. The radiative transport in each cell is determined by the equation above. We use a ray-tracing algorithm, which solves the transfer equation in the cells in succession along the rays. The resulting Stokes parameters are then used to construct the spectral-polarization images of the cluster.

For the study of the intra-cluster medium with random magnetic fields (such as those with a power-law spectrum in their distribution) or with embedded sources with complex structures on different scales, very fine cell sizes are needed in order to achieve good accuracy. This demands a computational algorithm which can solve efficiently the transfer equation, in which the four Stokes parameters are coupled. Instead of directly integrating the equation we seek a semi-analytic approach. By means of the transformations $I'_\alpha = \Lambda_{\alpha\sigma} I_\sigma$, $\epsilon'_\alpha = \Lambda_{\alpha\sigma}\epsilon_\sigma$ and $\kappa'_{\alpha\beta} = (\Lambda_{\alpha\sigma}\kappa_{\sigma\tau}\Lambda^{-1}_{\tau\beta})$ we obtain another radiative transfer equation

$$\hat{D}I'_\alpha \quad = \quad -\kappa'_{\alpha\beta} I'_\beta + \epsilon'_\alpha \ .$$

We diagonalize $\kappa'_{\alpha\beta}$ by choosing a suitable $\Lambda_{\alpha\sigma}$ and obtain four decoupled differential equations, each corresponding to a component in I'_α. These equations have analytic solutions. We now just need to solve for I' using a set of complex algebraic equations. After carrying out an inverse transform of I'_α we obtain the four Stokes parameters that describe the polarization and the spectrum of the radiation.

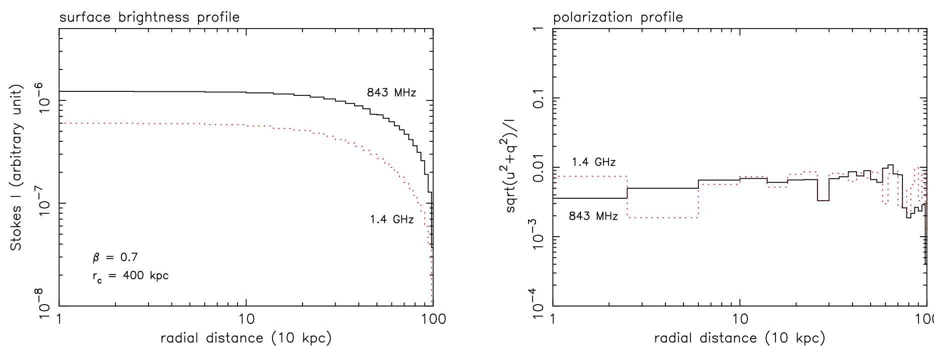

Figure 1. Surface brightness (left) and linear polarization (right) profiles of a model cluster at 843 MHz and 1.4 GHz. The cluster parameters are $\beta = 0.7$ for the density profile and core radius of 400 kpc. The energy spectral index of the electrons is 0.7. The absorption and Faraday coefficients are adopted from Jones and O'Dell (1977).

Figure 1 shows an example of a surface brightness profile and a polarization profile of a model cluster at 843 MHz and 1.4 GHz obtained from the calculations. The model cluster has a β density profile and it is permeated by a random magnetic field with a flat (approximately white noise) distribution. We note that existing calculations of polarized radiation from magnetized intra-cluster media simply sum the local contribution of the four Stokes parameters, which is a good approximation when the medium is optically thin to absorption and Faraday rotation/mixing. The algorithm that we use takes full account of transfer effects, thus allowing us to calculate emission from a clumpy medium with embedded sources, which could have opacities many orders of magnitude greater than the medium.

3. Mpc-scaled Relics: A3667, a well studied case

As mentioned in Section 1, relics and halos are generally rare; to date some 30 to 40 cases are known. Unfortunately, most of these diffuse radio sources have not been studied in the detail required to obtain a deep insight into their structure and origin. Present generation telescope arrays do not have the surface brightness sensitivity to record accurately their full extent and polarization structure. An exception is A3667 which is both bright and highly polarized and has been studied in some detail.

A3667 is a rich, X-ray luminous galaxy cluster at $z = 0.055$ (Sodré et al. 1992). The ROSAT X-ray image reveals that it has a slightly elongated shape (see Röttgering et al. 1997). The cold gas front at the center (Vikhlinin et al. 2001) suggests that the cluster was disturbed quite recently. The NW region of the cluster was mosaic imaged at 1.4 and 2.4 GHz using the Australia Telescope Compact Array (ATCA) by Röttgering et al. (1997), and the rest of the region by Johnston-Hollitt (2003). The cluster was also imaged at 843 MHz with the Molonglo Observatory Synthesis Telescope (MOST) of Sydney University. In both the MOST and ATCA images for the entire cluster region, two remarkable arc-like diffuse radio regions are clearly visible. In addition, low resolution images reveal that there might also be a small central halo (Johnston-Hollitt 2003).

The average spectral index of the northern radio arc is $\alpha = -1.0 \pm 0.2$, where $S_\nu \propto \nu^\alpha$. There is a moderate spectral-index gradient across the arc, with the flattest spectrum appearing toward the very north where the emission is most diffuse. The southern arc shows a more prominent spectral-index gradient along the major axis of A3667, with the flattest spectra at the outermost parts of the arc.

The emission from the arcs is strongly linear polarized at both 1.4 and 2.4 GHz. The percentage polarization of the northern arc varies from 10 to 40%, and the polarization appears correlated with the brightest filaments. The percentage polarization of the southern arc is at the 30–50% level. The polarization angles show complex spatial patterns, but there is no obvious correlation with the spatial distribution of the intensity. More detailed discussions of the observations, analysis, results and interpretation can be found in Johnston-Hollitt (2003) and Johnston-Hollitt et al. (2003, in preparation).

The combination of these detailed data, particularly the radio polarimetry, make A3667 an ideal platform for exploring polarized radiative transfer and testing the new code described in Section 2.

References

Buote, D. A. 2001, ApJ, 553, L15

Burn, B. J. 1966, MNRAS, 133, 67

Colafrancesco, S. 1999, in Proc. Workshop Diffuse Thermal and Relativistic Plasma in Galaxy Clusters, ed. H. Böhringer et al. (Garching: MPE), 269

Carilli, C. L., & Taylor, G. B. 2002, ARA&A, 40, 319

Dolag, K. 2001, in Proceedings of XXI Moriond Conference: Galaxy Clusters and the High Redshift Universe Observed in X-rays, ed. D. Neumann & J. T. T. Van

Giovannini, G., & Feretti, L. 2002a, in Merging Processes in Galaxy Clusters, ed. L. Feretti et al. (Dordrecht: Kluwer), 197

Giovannini, G., & Feretti, L. 2002b, HiA, 12, 513

Govoni, F., Ensslin, T. A., Feretti, L., & Giovannini, G. 2001, A&A, 369, 441

Johnston-Hollitt, M. 2003, PhD Thesis, University of Adelaide

Jones, T. W., & O'Dell, S. L. 1977, ApJ, 214, 522

Liang, H., Hunstead, R. W., Birkinshaw, M., & Andreani, P. 2000, ApJ, 544, 686

Miller, N. A., Owen, F. N., & Hill, J. H. 2003, AJ, 125, 2393

Pacholcyzk, A. G. 1977, Radio Galaxies (Oxford: Pergamon)

Röttgering, H. J. A., Wieringa, M. H., Hunstead, R. W., & Ekers, R. D. 1997, MNRAS, 290, 577

Sarazin, C. L. 2001, in Proceedings of XXI Moriond Conference: Galaxy Clusters and the High Redshift Universe Observed in X-rays, ed. D. Neumann & J. T. T. Van (astro-ph/0105458)

Sodré, L., Capelato, H. V., Steiner, J. E., Proust, D., & Mazure, A. 1992, MNRAS, 259, 233

Tribble, P. C. 1991, MNRAS, 253, 147

Vikhlinin, A., Markevitch, M., & Murray, S. S. 2001, ApJ, 551, 160

Highlights of Astronomy, Vol. 13
International Astronomical Union, 2003
O. Engvold, ed.

Non-thermal Activity and Particle Acceleration in Clusters of Galaxies

Vahe' Petrosian

Stanford University, Stanford, CA 94305-4060

Abstract. Evidence for non-thermal activity in clusters of galaxies is well established from radio observations of synchrotron emission by relativistic electrons, and new windows (in EUV and Hard X-ray ranges) have provided more powerful tools for its investigation. The hard X-ray observations, notably from Coma, are summarized and results of a new RXTE observations of a high redshift cluster are presented. It is shown that the most likely emission mechanism for these radiations is the inverse Compton scattering of the cosmic microwave background photons by the same electrons responsible for the radio radiation. Various scenarios for acceleration of the electrons are considered and it is shown that the most likely model is episodic acceleration by shocks or turbulence, presumably induced by merger activity, of high energy electrons injected into the inter-cluster medium by galaxies or active galactic nuclei.

1. Introduction

The intra-cluster media (ICM) of several clusters of galaxies, in addition to the well studied thermal bremssstrahlung (TB) emission in the 2 to 10 keV soft X-ray (SXR) region, show growing evidence for non-thermal activity, first observed in the form of diffuse radio radiation (classified either as relic or halo sources) and more recently, at extreme ultraviolet (0.07–0.4 keV; EUV) and hard X-ray (20–80 keV; HXR) regions. In the next section I will give a brief review of the status of these observations and present new yet unpublished HXR observation of another cluster, and in §3 I will compare the merits of different emission mechanisms proposed for their production. Even though the presence of non-thermal electrons in the ICM was established decades ago, very little theoretical treatment of the acceleration mechanism was carried out (see e.g. Schlickeiser, Siervers & Thiemann 1987) until the discovery of the EUV and HXR radiations. Given the meager amount of data, detailed calculations of the energy sources and the exact mechanisms of the acceleration may be premature. Consequently, I will emphasize the general physical characteristics and not the numerical details of the problem. It turns out that one can put significant and meaningful constraints on the general aspects of the acceleration mechanism. I will describe these in §4.

2. Observations

The first cluster observed to have **diffuse radio emission** was the Coma cluster and recent systematic searches have identified more than 30 clusters with halo or relic sources. The rate of occurrence of these sources increases with cluster redshift z, SXR luminosity or temperature T (Giovannini & Feretti 2000). There is little doubt that this radiation is due to synchrotron emission in a magnetic field of strength $B \sim \mu$G by a population of relativistic electrons of Lorentz factor $\gamma \sim 10^4$. In the case of Coma the electron spectra may be represented by a broken power law (Rephaeli 1979) or a power law with an exponential cutoff (Schlickeiser et al. 1987).

Extreme UV (0.07–0.4 keV) radiation was detected by the *Extreme Ultraviolet Explorer* from Coma (Liu et al. 1966) and some other clusters. A cooler ($kT \sim 2$ keV) component and inverse Compton (IC) scattering of cosmic microwave background (CMB) photons by relativistic ($\gamma \sim 10^3$) electrons are two possible ways of producing this excess radiation. Some of the observations and the emission process are still controversial (Bowyer & Hwang 2003). I will not discuss this emission any further here.

The third evidence for non-thermal activity comes from the observations of excess **HXR** emission in the 20 to 80 keV range by instruments on board the *Beppo*SAX and *RXTE* satellites. Each of these observatories has detected HXR excess from Abell 2256 once and Coma twice, although the second *Beppo*SAX observation shows a weaker signal (Fusco-Femiano et al. 1999 and Rephaeli et al. 1999, 2002). HXR detections have also been reported in Abell clusters 754, 2199, 2319 and 3667 all in the redshift range $0.023 < z < 0.056$. Most of these excesses can be best fitted with a fairly hard spectrum (photon power-law index $\alpha \sim 2$). Recently, detection of non-thermal X-rays (albeit at lower energies) have been reported from a poor cluster IC 1262 (Hudson et al. 2003). In Figure 1 I show the HXR spectrum and its characteristics for the cluster RXJ0658−5557 with a considerably higher redshift ($z = 0.296$) obtained by *RXTE*. These observations encompass a wide range of temperature, redshift and luminosity, indicating that HXR emission may be a common property of all clusters with significant diffuse radio emission.

Figure 2 (left panel) shows the photon flux at all wavelengths from Coma, where in addition to the above mentioned radiations, we show the gamma-ray upper limit from EGRET on board *CGRO* (Sreekumar et al. 1996), and the equivalent flux for the CMB and optical radiation density present in the cluster. (To these should be added the contribution from Far IR background radiation.) Similarly, an equivalent flux has been indicated for the static magnetic field of $\sim 1\mu$G, which is the size of the field strength deduced in several clusters (Eilek 1999, Clarke et al. 2001). The observed Faraday rotation of the Coma cluster can be interpreted as indicating a uniform magnetic field along the line of sight of $\sim 0.3\mu$G. However, the field lines are most likely chaotic. Kim et al (1990) and Clarke et al. (2003) estimate a mean magnetic field of $\sim 2-3\mu$G. It should be noted, however, that the interpretation of these observations is controversial (see Rudnick & Blundell 2002).

3. Radiation Mechanisms

The HXR emission could be produced via IC scattering of CMB photons by the same population of relativistic electrons responsible for the radio emission (see e.g. Sarazin & Lieu 1998) shown by the solid lines in Figure 2 (right panel).

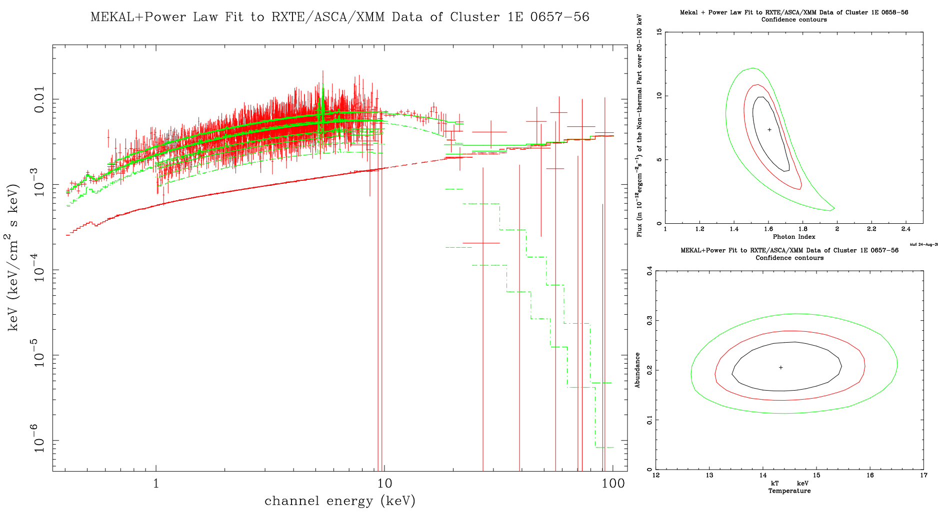

Figure 1. **Left panel:** Thermal plus a power law fit to 300ks RXTE and ASCA+SMM observations of the cluster RXJ0658−5557, and the 68, 90 and 99% confidence levels of the photon power-law index vs. 20–100 keV flux and temperature vs hydrogen column density. From Petrosian, Madejski and Luli, in preparation.

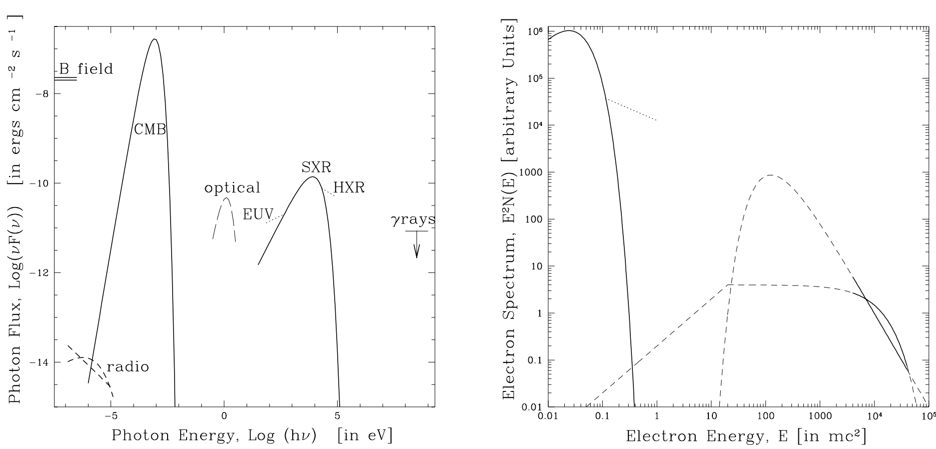

Figure 2. **Left Panel:** Schematic presentation of the $\nu f(\nu)$ flux of the electromagnetic fields in the ICM of Coma cluster including the B field. The two short dashed lines show two different fits to the radio data. **Right Panel:** Schematic spectra of the thermal ($T = 10^8$ K) and two non-thermal electrons responsible for the radio emission (solid lines). The dashed lines show maximal extrapolations of spectra so that one avoids unacceptably high rate of heating of the ICM plasma. The dotted line is the electron spectrum for the NTB model. This clearly exceeds the heating limit.

However, simple arguments show that this scenario requires a field strength $B_\perp < 0.2\mu$G, which is much smaller than values of several μG deduced from Faraday rotation mentioned above and equipartition arguments. Consequently, several workers have proposed non-thermal bremsstrahlung (NTB) for the HXR emissions (Enßlin et al. 1999, Sarazin & Kempner 2000, Blasi 2000). The dotted line in Figure 2 (right panel) shows the spectrum of the required electrons. However, as shown by Petrosian (2001, **P01**), the NTB process faces a serious difficulty, which is hard to circumvent. This is because compared to Coulomb losses the bremsstrahlung yield is very small: $Y_{\rm br} \sim 3 \times 10^{-6}(E/25{\rm keV})^{3/2}$ (see Petrosian 1973). Thus, for a HXR luminosity of 4×10^{43} erg s^{-1} (for Coma), a power of $L_{\rm HXR}/Y_{\rm br} \sim 10^{49}$ erg s^{-1} is fed into the ICM, increasing its temperature to $T \sim 10^8$ K after 3×10^7 yr or to 10^{10} K in a Hubble time! Therefore, *the NTB emission phase, if any, must be very short lived.*

This inefficiency of the NTB appears more serious than the inefficiency of the IC relative to the synchrotron process. There are several arguments which indicate that a higher B field can be tolerated in the IC model (see **P01**). Briefly, this discrepancy can be alleviated by i) a more realistic electron spectral distribution (e.g. Exponential spectral break beyond $\gamma \sim 10^4$); ii) a non-isotropic pitch angle distribution (Epstein 1973); and iii) spatial inhomogeneities (Goldschmidt & Rephaeli 1993, Govoni et al. 2003). Finally, the Faraday rotation measures may give a somewhat biased view of the B field by selecting clusters with the highest values of B while the EUV or HXR observations favor clusters with low values of B. The cluster RXJ 0658−5557 was chosen for observations because it was estimated that it should have relatively high IC flux of $\sim 7 \times 10^{-12}$ erg cm^{-2} s^{-1} which is what is observed. This increases our confidence in the validity of the IC model.

4. Acceleration Mechanism

It turns out that the acceleration mechanism of electrons can also be constrained significantly, even though we have very limited data. This mechanism should produce the relativistic electron spectra shown in Figure 2 (right panel). The lifetimes of these electrons are longer than their crossing time, $T_{\rm tr} \sim 3 \times 10^6$ yr. Therefore, these electrons will escape the cluster and radiate most of their energy outside it unless there exists some scattering agent with a mean free path $\lambda_{\rm scat} \sim 1$ kpc to trap the electrons in the ICM for at least a time scale of $T_{\rm esc} = (R/\lambda_{\rm scat})T_{\rm tr} \sim 3 \times 10^9$ yr, for cluster size $R \sim 1$Mpc. **Turbulence** can be this agent and can play a role in stochastic acceleration directly, or indirectly in acceleration by **shocks**. Both shocks and turbulence can presumably be produced during merger events. Several lines of argument point to an ICM which is highly turbulent. The possible scenarios of acceleration by turbulence and/or shocks are explored in **P01** leading to the following conclusions: i) The seed electrons cannot be the ICM thermal electrons for the same reason that the NTB fails as a source of HXRs, namely because it will lead to excessive heating of the ICM. Therefore, we require injection of high energy (> 50 MeV) electrons into the ICM, presumably from galaxies or AGNs. ii) The short lifetimes of the relevant electrons with respect to $T_{\rm esc}$ and the small $\lambda_{\rm scat}$ imply a continuous and *in situ* acceleration process. iii) A *steady state* model seems natural but it leads to a flatter spectrum than required unless the turbulence has an unreasonably steep spectrum. iv) *Time Dependent Models* can produced the desired spectra but only for a short period ($\sim 3\times10^8$ to 10^9 yr) implying an *episodic acceleration process* induced by merger activity.

Acknowledgment: This work is partially supported by the NASA grant NAG5 13031. I would like to thank my collaborators G. Madejski and K. Luli for permission to present our unpublished data here and note that many authors have contributed significantly to the subject of this paper whose work I could not fully acknowledge because of space limitations.

References

Blasi, P. 2000, ApJ, 532, L9

Bowyer, S. & Hwang, C-Y. (eds) 2003, ASP Conf. Ser. 301

Clarke, T. E. et al. 2001, ApJ, 547, L111

Clarke, T. E. 2003 in ASP Conf. Ser. 301, eds. S. Bowyer & C-Y Hwang, 185

Eilek, Jean 1999, eds. H. Böhringer, L. Feretti & P. Schucker, MPR Rep. 271

Enßlin, T. A., Lieu, R., & Biermann, P. 1999, A&A, 344, 409

Epstein, R. I. 1973, ApJ, 183, 593

Fusco-Femiano et al. 1999, ApJ, 513, L21 and 2000, ApJ, 534, L7

Giovannini, G., & Feretti, L. 2000, NewA, 5, 535

Goldschmidt, O. & Rephaeli, Y. 1993, ApJ, 411, 518

Govoni et al. 2003, in ASP Conf. Ser. 301, eds. S. Bowyer & C-Y Hwang, 501

Hudson, D. S., Henriksen, M. J. & Colafrancesco, S. 2003, ApJ, 583, 706

Kim, K. T. et al. 1990, ApJ, 355, 29

Lieu, R. et al. 1996, Science, 274, 1335

Petrosian, V. 1973, ApJ, 186, 291

Petrosian, V. 2001, ApJ, 557, 560

Petrosian, V., Madejski, G. & Luli, K. 2003, in preparation

Rephaeli, Y. 1979, ApJ, 227, 364

Rephaeli, Y. et al. 1999, ApJ, 511, L21 and 2002, ApJ, 579, 587

Rudnick, L. & Blundell, K. M. 2003, ApJ, 588, 143

Sarazin, C. L., & Lieu, R. 1998, ApJ, 494, L177

Sarazin, C. L., & Kempner, J. C. 2000, ApJ, 533, 73

Schlickeiser, R., Sievers, A., & Thiemann, H. 1987, A&A, 182, 21

Sreekumar, P. et al. 1996, ApJ, 464, 628

Highlights of Astronomy, Vol. 13
International Astronomical Union, 2003
O. Engvold, ed.

Magnetic Fields in Galaxy Clusters

Federica Govoni

Dip. Astronomia, Univ. Bologna, Via Ranzani 1, Bologna, Italy

Matteo Murgia

Ist. di Radioastronomia del CNR, Via Gobetti 101, Bologna, Italy

Abstract. Magnetic fields in galaxy clusters can be investigated using a variety of techniques. Recent studies including radio halos, Inverse Compton hard X-ray emissions and Faraday rotation measure, are briefly outlined. A numerical approach for investigating cluster magnetic fields strength and structure is presented. It consists of producing simulated rotation measure, radio halo images, and radio halo polarization, obtained from 3-dimensional multi-scale cluster magnetic field models, and comparing with observations.

1. Magnetic Field Measures

A complete description of the astrophysical processes in cluster of galaxies requires knowledge of magnetic fields. The most detailed evidence for this component comes from the radio observations:
• Some clusters of galaxies exhibit diffuse non-thermal synchrotron radio halos, associated with the intra-cluster medium, which extend up to Mega-parsec scales. Using minimum energy assumptions, it is possible to estimate an equipartition magnetic field strength averaged over the entire halo volume. These estimates give equipartition magnetic field strengths of $\simeq$0.1 to 1 μG (e.g. Bacchi et al. 2003).
• In a few cases, clusters containing a radio halo show an excess emission. This emission could be interpreted in terms of Inverse Compton scattering of the cosmic microwave background photons with the relativistic electrons responsible for the radio halo emission. In this case, the measurements of the magnetic field strength (e.g. Fusco-Femiano et al. 1999, Rephaeli et al. 1999) inferred from the ratio of the radio to X-ray luminosities are consistent with the equipartition estimates.
• Indirect measurements of the magnetic field intensity can also be determined in conjunction with X-ray observations of the hot gas, through the study of the Faraday Rotation Measure (RM) of radio sources located inside or behind clusters. By using a simple analytical approach, magnetic fields of $\sim 5-30$ μG, have been found in cooling flow clusters (e.g. Allen et al. 2001; Taylor & Perley 1993) where extremely high RMs have been revealed. On the other hand, significant magnetic fields have also been detected in clusters without cooling flows: the RM measurements of polarized radio sources through the hot intra-cluster medium leads to a magnetic field of $2-8$ μG which fluctuates on scales as small

as $2 - 15$ kpc. (e.g. Feretti et al. 1995, Feretti et al. 1999, Clarke et al. 2001, Govoni et al. 2001, Taylor et al. 2001, Eilek & Owen 2002).

The magnetic field strength obtained by RM studies is therefore higher than the value derived from the radio halo data and from Inverse-Compton X-ray studies. However, as pointed out by Carilli & Taylor (2002) and references therein, all the aforementioned techniques are based on several assumptions. For example, the observed RMs have been interpreted, until now, in terms of simple analytical models which consider single-scale magnetic fields. On the other hand, magneto-hydrodynamic cosmological simulations (Dolag et al. 2002) suggest that cluster magnetic fields may span a wide range of spatial scales with a strength that decreases with distance from the cluster center.

We developed a numerical approach for investigating the strength and structure of cluster magnetic fields. It consists of comparing simulated rotation measure, radio halo images, and radio halo polarization, obtained from 3-dimensional multi-scale cluster magnetic field models, with observations (Murgia et al. 2003, submitted).

2. Simulated Rotation Measures

The RM is related to the thermal electron density, $n_{\rm e}$, and magnetic field along the line-of-sight, $B_{\|}$, through the cluster by the equation:

$$\mathrm{RM} = 812 \int_0^L n_{\rm e} B_{\|} \mathrm{d}l \quad \mathrm{rad\ m}^{-2} \tag{1}$$

where $B_{\|}$ is measured in μG, $n_{\rm e}$ in cm^{-3} and L is the depth of the screen in kpc.

We consider a multi-scale magnetic field model with a three-dimensional power spectrum: $|B_k|^2 \propto k^{-n}$. Different power spectrum index will generate different magnetic field configurations and therefore will give rise to very different simulated RM images.

Fig. 1 (top) shows simulated RM images with different values of the index n for a typical cluster of galaxies (see caption for more details). RM images, such as those we simulate, cannot be observed for real clusters of galaxies. However, it is relatively easy to measure the RM dispersion and mean ($\sigma_{\rm RM}$ and $\langle\mathrm{RM}\rangle$) in limited regions by observing radio sources located at different projected distances from the cluster center. Fig. 1 (bottom) shows the simulated profiles of $\sigma_{\rm RM}$ (left), $|\langle\mathrm{RM}\rangle|$ (center), and $|\langle\mathrm{RM}\rangle|/\sigma_{\rm RM}$ (right), as a function of the distance from the cluster center. While both $\sigma_{\rm RM}$ and $|\langle\mathrm{RM}\rangle|$ increase linearly with the cluster magnetic field strength, the ratio $|\langle\mathrm{RM}\rangle|/\sigma_{\rm RM}$ depends only on the magnetic field power spectrum slope for a given range of fluctuation scales. This means that the comparison of RM data of radiogalaxies embedded in a cluster of galaxies with simulated profiles, can infer the strength and the power spectrum slope of the cluster magnetic field. The comparison of our simulations with data (Murgia et al. 2003, submitted), indicates magnetic field strengths a factor of $\sim$2 lower than that predicted by the single-scale magnetic field approximation widely used in the literature, and a rather flat spectral index $n \simeq 2$.

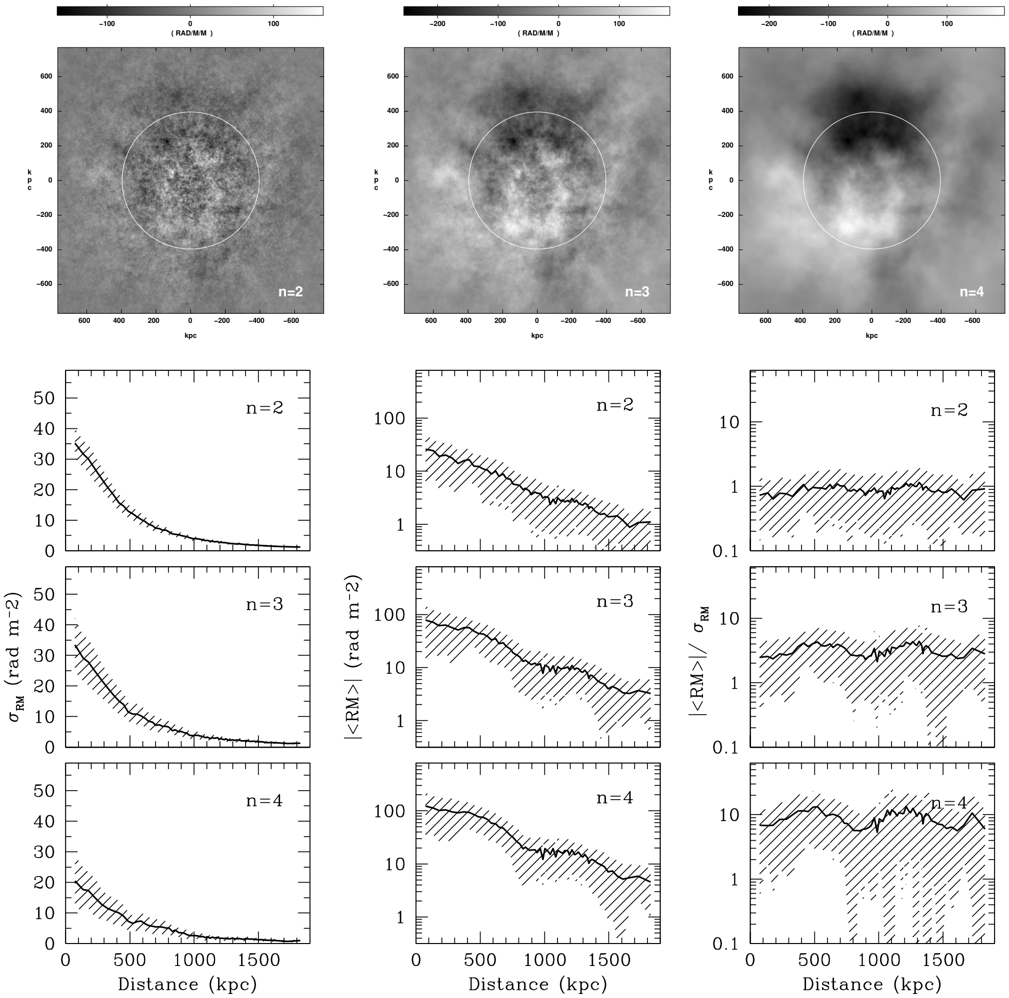

Figure 1. **Top**: simulated RM images for magnetic field power spectrum spectral index $n = 2, 3, 4$. The electron gas density of the cluster follow a standard β-model with a core radius r_c=400 kpc (indicated by a circle in the figure) a central density $n_e(0)$=10^{-3} cm^{-3} and β=0.6. The three power spectra are normalized to have the same total magnetic field energy which is distributed over the range of spatial scales from 6 kpc up to 770 kpc. The field at the cluster center is $\langle \mathbf{B} \rangle_0 = 1$ μG and its energy density decreases from the cluster center according to $B^2 \propto n_e(r)$. **Bottom**: radial profiles ($\sigma_{\rm RM}$, $|\langle {\rm RM} \rangle|$ and $|\langle {\rm RM} \rangle|/\sigma_{\rm RM}$ respectively) obtained from the RM simulations described above. The profiles have been obtained by averaging the simulated RM images in regions of 50×50 kpc^2, which is a typical size for radio galaxies.

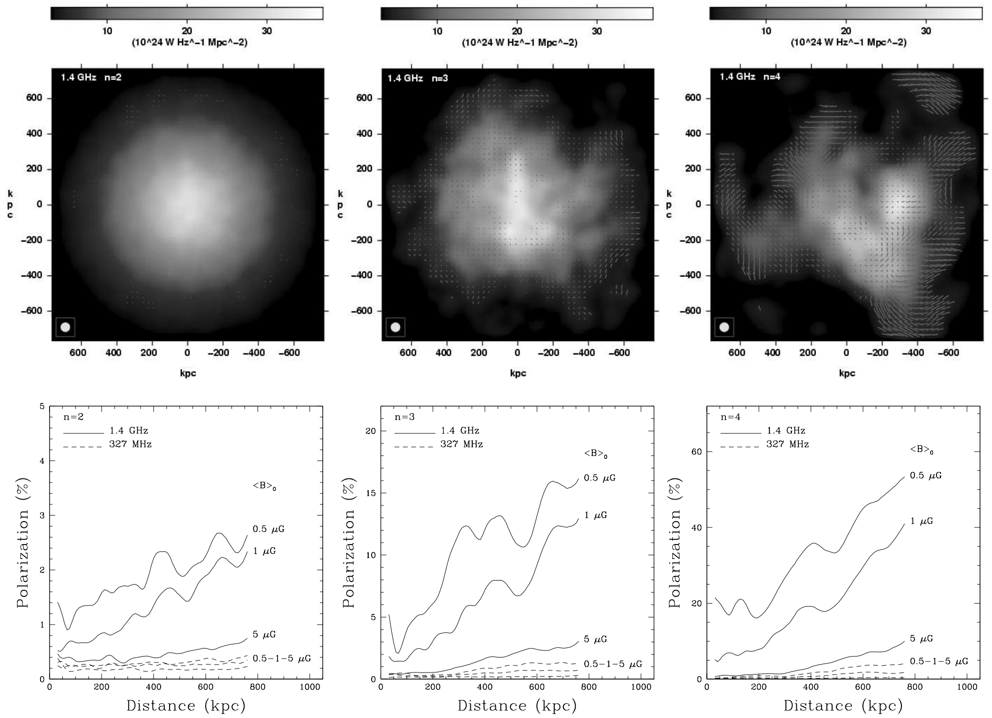

Figure 2. Simulated halo brightness and polarization for cluster at a distance of $z = 0.05$ as it would be observed with a beam of $45''$ ($H_0 = 50\,\mathrm{km\,s^{-1}Mpc^{-1}}$). **Top**: simulated halo images at 1.4 GHz for different values of the magnetic field power spectrum slope n and $\langle B\rangle_0 = 1\ \mu$G; the vectors lengths are proportional to the degree of polarization, with 100 percent corresponding to 100 kpc on the sky. Field directions are those of the E-vector. **Bottom**: radially averaged profiles of the polarization percentage at 327 MHz and 1.4 GHz for three values of the magnetic field strength, namely $\langle B\rangle_0 = 0.5$, 1 and 5 μG.

3. Simulated Radio Halo Images and Radio Halo Polarization

Radio halo observations may provides important information about the cluster magnetic field structure since different values of the power spectrum spectral index will generate very different total intensity and polarization brightness distributions for the radio halo emission.

So far, polarization emission from radio halos has not been detected. The current upper limits to the polarization at 1.4 GHz, for beams of about $45''$, are a few percent ($3 - 4\%$).

We simulated the expected total intensity and polarization brightness distribution at 1.4 GHz and 327 MHz, as it would be observed with a beam of $45''$, for different values of the magnetic field strength and power spectrum index, by introducing in the 3-dimensional magnetic field an isotropic population of relativistic electrons.

Fig. 2 (top) shows simulated radio halo brightness and polarization percentage distributions at 1.4 GHz (see caption for more details). Fig. 2 (bottom) shows the expected fractional polarization profiles at 1.4 GHz and 327 MHz for the different values of the average magnetic field strength and power spectrum spectral index. Our results indicate that a power spectrum slope steeper than $n = 3$ and a magnetic field strength lower than $\sim 1\,\mu$G result in a radio halo polarization percentage at a frequency of 1.4 GHz that is far in excess of the current observational upper limits at $45''$ resolution. This means that, in agreement with the RM simulations, either the power spectrum spectral index is flatter than $n = 3$ or the magnetic field strength is significantly higher than $\sim 1\mu$G. The halo depolarization at 327 MHz is particularly severe and the expected polarization percentage at this frequency is always below 1%. Moreover we also found that the magnetic field power spectrum slope has a significant effect in shaping the radio halo. In particular, flat power spectrum indexes ($n < 3$) give rise to very smooth radio brightness images (under the assumption that the radiating electrons are uniformly distributed).

4. Conclusions

The numerical approach presented here demonstrates how the dispersion and mean of the RM measured in radio galaxies embedded in a cluster of galaxies can be used to constrain not only the strength but also the power spectrum slope of the intra-cluster magnetic fields. Moreover, the study of the polarization properties of a large scale radio halo, if it is present in a cluster, can be used to improve the estimates based on the RM analysis.

Acknowledgment. We thank L. Feretti, G. Giovannini, D. Dallacasa, R. Fanti, G.B. Taylor and K. Dolag for their collaboration.

References

Allen S.W., Taylor G.B., Nulsen P.E.J., et al., 2001, MNRAS 324, 842
Bacchi M., Feretti L., Giovannini G., & Govoni, F., 2003, A&A 400, 465
Carilli C.L., Taylor G.B., 2002, ARA&A, 40, 319
Clarke T.E., Kronberg P.P., Böhringer H., 2001, ApJ 547, L111
Dolag K., Bartelmann M., Lesch H., 2002, A&A 387, 383
Eilek J.A., Owen F.N., 2002, ApJ, 567, 2002
Feretti L., Dallacasa D., Giovannini G., Tagliani A., 1995, A&A 302, 680
Feretti L., Dallacasa D., Govoni F., et al., 1999, A&A 344, 472
Fusco-Femiano R., dal Fiume D., Feretti L., et al., 1999, ApJ 513, L21
Govoni F., Taylor G.B., Dallacasa D., et al., 2001b, A&A 379, 807
Rephaeli Y., Gruber D., Blanco P., 1999, ApJ 511, L21
Taylor G.B., Perley R.A., 1993, ApJ, 416, 554
Taylor G.B., Govoni F., Allen S., Fabian A.C., 2001, MNRAS 326, 2

Highlights of Astronomy, Vol. 13
International Astronomical Union, 2003
O. Engvold, ed.

Contributed Papers for JD10: Abstracts

A Detailed Study of the Massive Lensing Cluster Cl 0024+16

R. S. Ellis (Caltech), T. Treu (Caltech), J-P. Kneib (OMP)

Abstract. We present a comprehensive study of galaxies and dark matter to the turn-around radius (5 Mpc) in the lensing cluster Cl 0024+16 ($z = 0.40$). We directly study the transformation of field galaxies as they fall into the potential determined quantitatively from weak lensing signals. Our analysis exploits a mosaic of 38 WFPC2 images and ground-based imaging and spectroscopy using CFHT, Keck and Palomar. Correlations between morphology, star formation rate and environmental location are interpreted using known infall time scales. The dark matter distribution, revealed for the first time over such a wide dynamical range in density, is compared directly with the numerical simulations and with that observed for the stellar light. In-depth studies of more clusters, sampling a wide range in environmental density, will yield valuable insights into the origin of the morphology-density relation observed today.

Galaxy Groups: New Insights from Chandra and XMM

J. M. Vrtilek (CFA), E. J. O'Sullivan (CFA), L. P. David (CFA), T. J. Ponman (Birmingham), W. R. Ponman (CFA), C. Jones-Forman (CFA), D. E. Harris (CFA)

Abstract. Groups and poor clusters are the locus of most galaxies in the present-day Universe and the building blocks from which clusters form. They accordingly occupy a significant place in the continuum of structure between isolated galaxies and rich clusters. Owing to the lower temperature of their intracluster gas, X-ray emission from groups produces strong lines from a broader range of elements than do hotter clusters. Here, we employ Chandra and XMM images of several X-ray bright groups (including HCG 62, NGC 741, and MKW 4) to examine issues of current interest in the study of both groups and clusters: the distribution of heavy elements, the presence and nature of X-ray cavities and their relation to radio observations, the presence of cooling cores, and X-ray signatures of recent galaxy interactions. This work has been supported in part by NASA grants GO0-1037X, GO1-2138X, and GO2-3186X.

Cluster Properties via Sunyaev-Zel'dovich Effect

Asantha Cooray (Caltech) California Instiute of Technology

Abstract. We will discuss the role played by the Sunyaev-Zel'dovich (SZ) effect in understanding the physical properties of the intra-cluster medium. While the SZ effect has been considered widely for its cosmological purposes, when combined with multi-wavelength observations, the SZ effect data can also be used to understand the nature and evolution of the ICM including its thermal structure and the presence of non-thermal plasma. We also discuss future opportunities on this aspect involving observations from the planned South Pole Telescope, Planck mission, and various other attempts to image the SZ effect in galaxy clusters using wide-field bolometer arrays and other techniques. We will also explore the connection between gas in clusters and the general intergalactic

medium and how one can use detailed wide-field SZ maps, beyond those towards individual clusters, to study such possibilities.

ACS Observations of Three Rich Galaxy Clusters at High Redshift

J. P. Blakeslee (JHU), M. Postman (STScI), P. Rosati (ESO), H. Ford (JHU), G. Illingworth (UCSC), M. Franx (Leiden), C. Gronwall (PSU), B. Holden (UCSC)

Abstract. Our Advanced Camera for Surveys (ACS) cluster survey aims to establish new and detailed constraints on the formation and evolution of clusters and their member galaxies. We have used the ACS Wide Field Camera to obtain multi-band imaging of several X-ray selected clusters near $z \sim 1$. These clusters include MS1054−0321 and CL0152−1357, both at $z = 0.83$, and CL1252−2927 at $z = 1.24$. Each was observed in a mosaic of 4 partially overlapping pointings, with the central 1 arc min imaged to the greatest depth. CL1252−2927 is one of the most distant clusters known, yet it appears to be a relaxed, centrally concentrated system with a well-defined red sequence of evolved galaxies in the color-magnitude (CM) diagram. Monte Carlo simulations with the latest population models suggest an age scatter of about 30% for the ellipticals, with a mean age of at least 2.5 Gyr, for a formation epoch $z > 2.7$. The slope and scatter in the elliptical CM relation show little or no evidence for evolution out to $z = 1.2$. However, the clusters at $z = 0.83$ show signs of ongoing dynamical evolution, including irregular structure and significant merging, although they also show prominent red sequences.

The Role of Dwarf Galaxies in Galaxy Cluster Evolution

Christopher Conselice (Caltech)

Abstract. Although they are the faintest galaxies in clusters, dwarf galaxies, especially dwarf ellipticals, are a key component for understanding the evolution of cluster galaxies, as well as clusters themselves. These dwarfs dominate clusters in number, and potentially contain a significant fraction of the cluster's dark matter. They are also potentially the remnants of larger infalling Butcher-Oemler galaxies stripped of their mass through dynamical cluster processes. We will present observational results that show that dwarfs in nearby clusters could be the remnants of much of early galaxy formation in clusters and discuss how these objects can account for many observed properties of clusters such as intergalactic light.

Ultra-compact Dwarf Galaxies: New Constituents of Clusters

M. J. Drinkwater (U Queensland), M. D. Gregg (UCD), M. Hilker (Bonn), W. J. Couch (UNSW), H. C. Ferguson (STScI), B. Jones (Nottingham), S. Phillipps (Bristol)

Abstract. In the course of our all-object Fornax Cluster Spectroscopic Survey, using the Anglo-Australian Telescope's 2dF spectrograph, we discovered a new population of physically small ultra-compact dwarf (UCD) galaxies. Unresolved from the ground, these objects have been overlooked by previous galaxy surveys although clearly visible on 30-year-old sky survey plates. We present high-resolution imaging (HST) and spectroscopy (VLT and Keck) of the Fornax UCDs. They are qualitatively different from both globular star clusters and all

known galaxy types: we have discovered an entirely new class of galaxy. The data are consistent with our hypothesis that UCDs are the remnant nuclei of nucleated dwarf galaxies which have been tidally stripped by the central galaxy of the cluster. We suggest that part of the huge globular clusters populations around central cluster galaxies are really UCDs and not globular clusters at all. Based on our UCD formation hypothesis, we predicted that a similar population would exist in the Virgo Cluster. In just 3 hours of 2dF service time we measured redshifts of 900 objects towards the Virgo Cluster and identified 9 UCDs. UCDs appear to be a common product of galaxy evolution in the cluster environment.

The Evolution of Active Galaxies in Clusters

Philip Best (IfA Edinburgh)

Abstract. Recent deep studies at radio, sub-mm and X-ray wavelengths of both low and high ($z \sim 1$) redshift clusters are reviewed, to investigate the active galaxy content of these clusters. These results show that clusters, especially at intermediate and high redshifts, contain a significant population of powerful active galaxies, which would not be identified as such by either imaging or spectroscopy at optical wavelengths. Studies of this active galaxy population are on-going, and offer the opportunity to shed light on the triggering, fueling and suppression of active and star–forming galaxies, as well as on the evolutionary status of the high redshift clusters themselves.

Chandra X-ray Observations of 5 Radio Galaxies with $z = 2$–2.6

D. E. Harris (SAO), R. Overzier (Leiden), C. L. Carilli (NRAO), J. Kurk (Leiden), G. K. Miley (Leiden), L. Pentericci (MPIA Heidelberg), H. Rottgering (Leiden), and W. van Breugel (LLNL)

Abstract. We report on Chandra observations of 20 ks each on the high redshift radio galaxies 0156−252, 0406−244, 0828+193, 2036−254, and 2048−272. These data were obtained to evaluate the amount of hot gas around the radio galaxies (none was found, $M <$ few $\times 10^{12}$ $M_\odot$); to determine if there is an over-density of AGN in the fields surrounding the radio galaxies (preliminary results are negative); and to ascertain if some of the X-ray emission could be non-thermal (we detected emission consistent with the IC/CMB process for hotspots/lobes in 4 of the 5 targets). In 4 cases the nucleus of the host galaxy is detected, and for 3 targets there is off-nuclear emission aligned with the radio axes. One extended X-ray source was detected adjacent to a radio galaxy. If it were at the same redshift, it would be of order 100 kpc in diameter with $L_X = 10^{44}$ erg s^{-1}. The work at SAO was partially supported by NASA grant GO2-3139B and contract NAS8-39073.

Cooling Cores and Radio Mini-Halos

M. Gitti (Innsbruck; IRA-CNR Bologna), G. Brunetti (IRA-CNR Bologna), G. Setti (Bologna), L. Feretti (IRA-CNR Bologna)

Abstract. We have recently developed a model for the origin of radio minihalos, observed in some cooling flow clusters, as due to synchrotron emission from relativistic electrons re-accelerated by MHD turbulence. The MHD turbulence, naturally present in the ICM, is assumed to be frozen into the compressed

thermal ICM and thus amplified in the cooling region. Here we present the application of this model to the mini-halo candidates observed in the Perseus cluster and in A2626. A very good agreement between the model and observations is found for the three observables: surface brightness profile, integrated spectrum and radial spectral steepening. Our results showed that a relic population of relativistic electrons can be efficiently re-accelerated by MHD turbulence, with the necessary power being only a small fraction of the maximum power that can be extracted by the cooling flow. Observationally, we notice that the strongest radio mini-halos are found in association with the most powerful cooling flows, and that cooling flow powers are orders of magnitude larger than the integrated radio power.

Abell 754: Low Frequency Observations of a Merging Cluster

T. E. Clarke (U Virginia), N. Kassim (NRL), T. Ensslin (MPIA Garching), D. Neumann (CEA Saclay)

Abstract. In the hierarchical model of structure formation, discrete sources form from the collapse of initial density enhancements and subsequently grow through gravitational effects. Clusters of galaxies are thought to form at the intersection of large scale filaments and are expected to undergo a number of merger events. These mergers are highly energetic (10^{63}–10^{64} erg) and provide significant energy input into the intra-cluster medium (ICM) through shocks and turbulence which can lead to amplification of magnetic fields and acceleration of relativistic particles, thus triggering synchrotron emission in the ICM. We present results from a low frequency VLA study of the merging cluster Abell 754. Optical and X-ray data reveal that this cluster has undergone a major merger event. The radio data reveal two clear regions of diffuse synchrotron emission, one concentrated in the cluster center and the other located on the edge of a bar-like structure found in the X-rays. We discuss the spectral index of the relativistic particles and compare the radio and X-ray emission of Abell 754. Comparing the spatial and spectral distribution of the relativistic particles to the X-ray temperature maps provides additional information on the nature of the complex merger within this cluster.

Cluster Soft Excess Emission in the XMM/Newton Era

Richard Lieu (Alabama), Jonathan Mittaz (Alabama)

Abstract. In the XMM Newton era, research on the topic of cluster soft excess takes a sharp upward turn. The phenomenon is clearly confirmed for many clusters, moreover its thermal warm gas origin is established for the outer parts of five clusters through the detection of O VII emission at the cluster redshift. Since this line is not present in the inner soft excess spectra, the warm gas may reside in filaments projecting from a cluster and accounting in total for a lot of 'missing baryons'. Nonetheless, the mystery of the inner soft excess, which is bright enough to remain clearly visible even in the cooling flow regions where the hot intra-cluster medium is very luminous, can only be explained as inverse Compton emission. By using the clusters A1795 and AS1101 as test cases, we modeled the central soft excesses with a power law and in this way evaluated the *observed* cosmic rays pressure. In each case the parameter values indicate that the pressure is at least sufficient for equipartition between cosmic

rays and gas. Thus there is compelling evidence that the soft excess emission in clusters centers and the cooling flow riddle are really one and the same problem.

Deep WSRT 0.35–1.4 GHz Imaging of the Perseus Cluster

Ger de Bruyn (ASTRON) & Michiel A. Brentjens (Gröningen)

Abstract. We present new radio observations at 0.35 GHz of the Perseus cluster taken in Dec 2002 with the new wide-band correlator at the WSRT. The data have been combined with existing, extremely high dynamic range observations at 1.4 GHz, to analyze the diffuse synchrotron emission from the existing radio galaxy population, the halo from NGC1275 and its cooling flow and the intra-cluster medium extending to 1 Mpc radius. The relation between the radio and X-ray morphologies can be compared in detail. We have also detected widespread polarized emission which we interpret as due to a combination of Galactic foreground emission and Thomson scattered emission from the central radio source off the hot cluster gas. Our wide-band data furthermore allow us to study the radial dependence of the cluster and foreground Rotation Measure.

POSTERS*

CLUSTER FORMATION

Clusters at $z > 1$ observed with XMM and Chandra —*Christophe Adami*
Spectroscopy of the ESO distant cluster survey (EDISCS) —*Claire Halliday*
The ellipticity of galaxy clusters —*Piotr Flin*
The morphological decomposition of Abell 868 —*Simon Driver*
The ACS Virgo cluster survey —*Michael West*
The XMM LSS survey—initial spectroscopic results —*Jon Willis*
Galaxy overdensities in the Shapley Supercluster —*Lin-wen Chen*
Galaxy clusters and cosmology —*Thomas Reiprich*
MACS: the evolution of very massive clusters out to $z = 0.7$ —*Harald Ebeling*
MACS J0717.5+3745: a merging massive cluster at $z = 0.55$ —*Elizabeth Barrett*
Temperature structure and point sources in Abell 1650 —*Koujun Yamashita*
Merging clusters as unidentified 3EG sources —*Wataru Kawasaki*
Arc statistics in galaxy clusters —*Masamune Oguri*
The Asiago-ESO/RASS QSO survey —*Alessandro Omizzolo*
High-z clusters traced by groups of radiosources —*Garret Cotter*
MHD simulations of the formation of cold fronts —*Naoki Asai*

CLUSTER GALAXIES

Origin of E+A galaxies in clusters —*Kenji Bekki*
Stellar population gradients of early-type galaxies in Coma —*Daniel Thomas*
The local Butcher-Oemler effect —*Roberto De Propris*
Extremely red objects at $z < 1.5$ —*Marian Suran*
Rings in radio galaxies: a multiwavelength approach —*Nectaria Gizani*
The kinematics of spirals in distant galaxy clusters —*Jochen Heidt*
A survey of nearby clusters with the INT —*Michael Pracy*
Dying radio galaxies in clusters —*Paola Parma*
Radio and FIR properties of nearby X-ray cluster galaxies —*Naveen Reddy*
Large scale radio jets in the galaxy cluster Abell S0102 —*Miroslav Filipovic*
Cen A and its interaction with the X-ray-emitting ISM —*Diana Worrall*
Evolutionary synthesis for galaxy transformation in clusters —*Uta Fritze-v. Alvensleben*

INTRACLUSTER MEDIUM

Optical spectrocopy of the cooling flow cluster 2A 0335+096 —*Richard Gelderman*
XMM-Newton detection of the WHIM in clusters —*Jelle Kaastra*
Detailed radio and optical observations of A3667 —*Melanie Johnston-Hollitt*
Spectral index of the radio halos in A665 and A2163 —*Luigina Feretti*
Measuring cluster magnetic fields —*Nectaria Gizani*
Simulating magnetic fields in galaxy clusters —*Klaus Dolag*
Simulations of clusters of galaxies with thermal conduction —*Viktor Ziskin*
Non-thermal hard X-ray excess in the Coma cluster —*Roberto Fusco-Femiano*

* Displayed posters only; to save space, only first authors are given here

JD11

Dynamics and Evolution of Dense Stellar Systems

Chairpersons: F. Combes and D. Richstone

Editors: F. Combes (Chief-Editor), P. Hut and D. Richstone

Highlights of Astronomy, Vol. 13
International Astronomical Union, 2003
O. Engvold, ed.

MODEST: Modeling Stellar Evolution and (Hydro)dynamics

Piet Hut

Institute for Advanced Study, Princeton, NJ 08540, USA

Abstract. Simulations of dense stellar systems currently face two major hurdles, one astrophysical and one computational. The astrophysical problem lies in the fact that several major stages in binary evolution, such as common envelope evolution, are still poorly understood. The best we can do in these cases is to parameterize our ignorance, in a way that is reminiscent of the introduction of a mixing length to describe convection in a single star, or an alpha parameter in modeling an accretion disk. The hope is that by modeling a whole star cluster in great detail, and comparing the results to the wealth of observational data currently available, we will be able to constrain the parameters that capture the unknown physics. The computational problem is one of composition: while we have accurate computer codes for modeling stellar dynamics, stellar hydrodynamics, and stellar evolution, we currently have no good way to put all this knowledge together in a single software environment. A year ago, a loosely-knit organization was founded to address these problems, MODEST for MOdeling DEnse STellar systems, with nine working groups and a series of meetings that are held every half year. This report reviews the first year of this initiative. Much more detail can be found on the MODEST web site `http://www.manybody.org/modest.html` .

1. Introduction

Large-scale computer simulations in astrophysics require teamwork. Gone are the days that an individual graduate student could write from scratch all the software needed to model a complex astrophysical system. Whether a simulation requires a state-of-the-art stellar evolution code, hydrodynamics code or stellar dynamics code, it has become standard practice to use a 'legacy code'. One may write some modifications and additions, but it is hard to compete with the tens of person-years that have gone into some of the standard codes.

As a result, codes have steadily grown in complexity within separate disciplines in astrophysics, but until recently little effort has been invested to make these legacy codes compatible across different areas of astrophysics. In the area of dense stellar systems, the topic of this meeting, the result has been that we have access to very detailed codes that can model the evolution of individual stars, other codes that can handle collisions between stars, and yet other codes that can follow the motion of the whole ensemble of stars. However, none of these codes come even close to being able to talk with each other.

To let different codes talk together, similar requirements hold as for humans trying to communicate between cultures and across language barriers: each person needs to adapt to some extent to the customs of the other culture, and there needs to be a dictionary to translate between the languages.

The first requirement reads like a medical oath: *first of all, do no harm*, *i.e.* do not cause the combined codes to halt. It is better that a large-scale simulation is allowed to come to completion, with messages in a log file indicating where serious errors may have been made, than to have the simulation halt at each bend of the road, when one of the modules is not optimally happy.

The second requirement boils down to the definition of specific interfaces, and a willingness in the community to adopt a standard definition. Producing such a definition requires a fair amount of care, flexibility and vision, to avoid the danger of saddling a field with a standard that can hinder future progress.

In the next few pages, I summary recent efforts to let codes cross the boundaries of stellar evolution, stellar dynamics and stellar hydrodynamics, in order to enable next-generation large-scale simulations of dense stellar systems.

2. MODEST-1: New York

It was the goal of the MODEST-1 meeting to begin addressing this problem of letting codes talk to each other. The workshop was held at the Hayden Planetarium in the Museum for Natural History in New York City, in June 2002. The MODEST acronym was coined during this meeting, and it can stand not only for MOdeling DEnse STellar systems, but also for MODifying Existing STellar codes. The latter description stresses the desirability to start with what is already available, and to find ways to put it all together, rather than to try to write a kitchen-sink type over-arching super code from scratch.

The format of the meeting was unconventional. The organizers, Piet Hut and Mike Shara, polled whether there was enough interest to warrant a workshop, and then sent out an email with the following note: "this will be a work-workshop, not a lectures-workshop. Believe it or not, we have not a single scheduled lecture! We are curious to see how this format will work out. Hopefully we will actually get a lot of work done, together as well as in smaller groups."

We did. The 34 participants met for five days, splitting up in topical groups and reporting their results back to the group on a daily basis. Major progress was made in defining and starting to tackle the two main requirements listed above, that of culture and translation. Within a few weeks of the meeting, 10 of the participants had written a review paper, in lieu of proceedings, which was posted on astro-ph, and subsequently published (Hut et al. 2003).

Also immediately following the workshop a web site was established at `http://www.manybody.org/modest.html` , as a place to accumulate general information, demos, toy models, links to more detailed models and simulation software, *etc.* At the same time an email list was started, with occasional announcements of major events and progress reports. The web site contains instructions for subscribing to this email list.

As a result of the great enthusiasm displayed during the first workshop, it was decided to hold similar meetings frequently enough so as to enable ongoing projects to be critiqued at each meeting. Such peer-review feedback is essential for the health of any really large-scale project, and therefore a frequency of two meetings per year was chosen as an optimal compromise. While individual projects could of course use more frequent reviews, getting the main players together every half year was already seen as quite a challenge. It was a challenge that was met, it turns out, judging from the attendance of each of the following two workshops, between 30 and 40 people, comparable to that of MODEST-1.

3. MODEST-2: Amsterdam

MODEST-2 was organized by Simon Portegies Zwart en Piet Hut, at the University of Amsterdam, Holland, in December 2002. This workshop followed a similar format: there were no scheduled talks. Instead, individual participants sometimes showed a couple view graphs, to illustrate a particular point. Also, during the first day a number of specific topics of interest were formulated, and speakers were invited to give an impromptu brief introduction to each topic. In this way, eight short talks were delivered by participants outlining how their own work was fitting into the MODEST framework, what they wanted to get out of participation in MODEST, what the most relevant questions were for their area, and what they had accomplished since MODEST-1.

During the previous workshop in New York, a broad discussion had been started concerning the question when to use full-blown stellar evolution codes and when to use approximate recipes. This discussion was continued in Amsterdam. The conclusions reached were similar, but more refined in detail: to use recipes for single stars; a mix of recipes and codes for interacting binaries; and 'life' stellar evolution codes for merger products. Given the very many ways that stars can form from single or even repeated mergers, there is just no way that we can expect to construct a grid of model tracks to anticipate the specific needs for evolving such merger products. Not only will the chemical compositions be different from standard values, but incomplete mixing of the progenitor stars will add a full functional amount of degrees of freedom.

Another outcome of this workshop was the organization of eight working groups, listed below (the ninth working group was added during MODEST-3). The main MODEST web site now contains pointers to these working groups. While Steve McMillan is the webmaster for the main web site, the following people are the contact persons for the web sites of the individual working groups:

Working Group	Contact Person
Star Formation	Ralf Klessen
Stellar Evolution	Onno Pols
Stellar Dynamics	Rainer Spurzem
Stellar Collisions	Marc Freitag
Simulating Observations of Simulations	Simon Portegies Zwart
Data Structures	Peter Teuben
Validation	Douglas Heggie
Literature	Melvyn Davies
Observations	Giampaolo Piotto

The highlights of the workshop appeared on astro-ph within a few weeks after concluding the meeting, and were published as a review (Sills et al. 2003).

4. MODEST-3: Melbourne

The third workshop was held at Monash University in Melbourne, Australia, and was organized by Rosemary Mardling and Piet Hut. The meeting was held in early July 2003, in the three days before the General Assembly assembled in Sydney. In contrast to the previous two workshops, we experimented with a more traditional style of scheduled presentations (For the detailed program with speakers, titles, and abstracts, see the MODEST-3 web site `http://www.manybody.org/modest/Workshops/modest-3.html`).

These talks filled the first two days of the meeting. In the morning of the third day, each of the working groups reported about their progress, and a ninth working group was added to focus on observations. The afternoon featured an open discussion. One of the outcomes was a series of proposals for extending the web site, by including a page for job opportunities and another page for project proposals. Examples of the latter can be notes from people who have observational data sets, for which they invite theoreticians to join them in simulations of the systems observed; or simulators who have large data sets for which they invite students to join them in analyzing the results.

After all the informal discussions during the first two workshops, this meeting with more formal talks played a complementary role, as a one-time occasion to inform people from all three fields (evolution, dynamics, hydrodynamics) about the main activities in the other fields. Subsequent workshops will return to the old format of more free-wheeling discussions, starting with MODEST-4, in January 2004 at Geneva Observatory, located between Geneva and Lausanne in Switzerland.

5. Future Meetings and Activities

The MODEST initiative has grown in one year from an initial informal meeting into a broad framework to facilitate collaborations across boundaries between various disciplines within computational astrophysics. So far, these collaborations have taken on the form of sharing codes, defining and building code interfaces, developing demos, writing review papers, applying for joint grants, and starting joint research projects. Future workshops may coincide with the organization of MODEST summer schools and other teaching activities, as well as outreach projects aimed at the general public. MODEST is an open forum: we invite anyone interested in simulations of dense stellar systems to join us.

References

Hut, P., Shara, M.M., Aarseth, S.J., Klessen, R.S., Lombardi, J.C., Makino, J., McMillan, S., Pols, O.R., Teuben, P.J., & Webbink, R.F. 2003, New Astronomy 8, 337

Sills, A., Deiters, S., Eggleton, P., Freitag, M., Giersz, M., Heggie, D., Hurley, J., Hut, P., Ivanova, N., Klessen, R.S., Kroupa, P., Lombardi, J.C., McMillan, S., Portegies Zwart, S., & Zinnecker, H. 2003, New Astronomy 8, 605

Highlights of Astronomy, Vol. 13
International Astronomical Union, 2003
O. Engvold, ed.

Black Hole Binary Mergers

Junichiro Makino

Department of Astronomy, School of Science, The University of Tokyo, 7-3-1 Hongo, Bunkyo-ku, Tokyo 113-0033, Japan

Abstract.
I overview the current understanding of the evolution of massive black hole (MBH) binaries in the center of the host stellar system. One of the main questions is whether the stellar dynamical effect can make the MBH binary hard enough that they can merge through gravitational wave radiation. So far, theories and numerical simulations suggested otherwise, since the hardening time scale becomes very long once "loss cone" is depleted. I'll present the result of recent simulations on this hardening time scale, and discuss its implication on the formation history of massive black holes.

1. Introduction

There are now plenty of evidences that many, if not most, of giant ellipticals contain massive central black holes (Magorrian et al. 1998). Also, it has been suggested that the black hole mass $M_{\rm BH}$ shows tight correlation with the spheroidal mass and the central velocity dispersion (Gebhardt et al. 2000; Ferrarese & Merritt 2000). The most straightforward explanation of such correlation is that massive galaxies are formed by merging of less massive galaxies, and that the central black hole also grows through merging (Kauffmann & Haehnelt 2000). This merging scenario naturally explains the observed correlations.

This merging scenario has additional important characteristic that it nicely explains the observed structure of the central region of massive elliptical galaxies. High-resolution observations by HST revealed that the "cores" of the giant elliptical galaxies are not really cores with flat volume density, but very shallow cusps expressed as $\rho \propto r^{-\alpha}$, where ρ is the volume luminosity density and r is the distance from the center, with power index $\alpha = 0.5 \sim 1$ Gebhardt et al. (1996), Byun et al. (1996). Makino & Ebisuzaki (1996) performed the simulation of repeated mergers of galaxies with central black holes. They found that the structure of the merger converges to one profile. The merger product has a central cusp around the black hole with slope approximately -0.5, and the total mass of the stars in the cusp region is around the mass of the black hole binary. Nakano & Makino (1999b), Nakano & Makino (1999a) showed, by combination of simple N-body simulation and an analytic argument, that this shallow cusp is explained by the fact that distribution function of stars has a lower cutoff energy E_0. Their analytic argument naturally explains the observed correlation between the cusp radius and the black hole mass.

One remaining problem is what will happen to the binary black hole. Begelman et al, (1980) [hereafter BBR] predicted that the hardening of the BH binary would be halted once it ejected all the stars in its "loss cone". Early numerical simulations Makino et al. (199), Mikkola & Valtonen (1992) could not cover the range of the number of particles (relaxation time) wide enough to see the change in the time scale. Recent studies Makino (1997), Quinlan & Hernquist (1997), Chatterjee et al. (2003), Milosavljevic & Merritt (2001) reported the results, which are not only mutually inconsistent but also inconsistent with the theoretical prediction. BBR predicted that after the stars in the loss cone is depleted, the hardening time scale would be the relaxation time scale of the parent galaxy, since in the relaxation time scale stars would diffuse into the loss cone. The results of numerical simulation ranges from no dependence on the relaxation time scale (Milosavljevic & Merritt 2001), to some dependence with upper limit in the time scale (Quinlan & Hernquist 1997; Chatterjee et al. 2003), and finally to weaker-than-linear dependence (Makino 1997).

Thus, it has been an open question whether or not the loss-cone depletion occurs. Some even argued that numerical simulations would not help in determining the fate of a BH binary. Here, we present the result of our resent N-body simulations with up to 1M particles, where we saw a clear sign of the loss-cone depletion.

2. Numerical method and Initial Models

The details of the model is given elsewhere (Makino & Funato 2003). We performed N-body simulations using direct summation method on GRAPE-6 (Makino et al 2002). Gravitational interaction between field particles is softened, while that involves BH particles is not.

The initial galaxy model is a King model with non-dimensional central potential of $W_0 = 7$. We use the Heggie unit, where the mass M and the virial radius R_v of the initial galaxy model and gravitational constant G are all unity. The mass of black hole particles is $M_{BH} = 0.01$. They are initially placed at $(\pm 0.5, 0, 0)$ with velocity $(0, \pm 0.1, 0)$.

The largest calculation (1 million particles and up to $t = 400$) took about one month, on a single-host, 4-processor-board GRAPE-6 system with the peak speed of 4 Tflops.

3. Results

Figure 1 shows the time evolution of the specific binding energy (per reduced mass) E_b of the black hole binary. It is clear that the hardening time scale becomes longer as we increase N (and thereby the relaxation time).

To quantitatively evaluate the dependence of the hardening rate on the number of particles, we calculated the hardening rate β (see figure 1). When $E_b = -1$, the hardening rate is almost independent of N. However, as the binary becomes harder, β decreases, and the decrease is larger for larger N. Thus, the hardening rate β for large values of $|E_b|$ shows strong dependence on the number of particles N. For $E_b = -7$, the hardening rate β is almost proportional to $1/N$. In other words, we obtained the result which is consistent with the theory. The hardening time scale is proportional to the relaxation time scale of the parent galaxy.

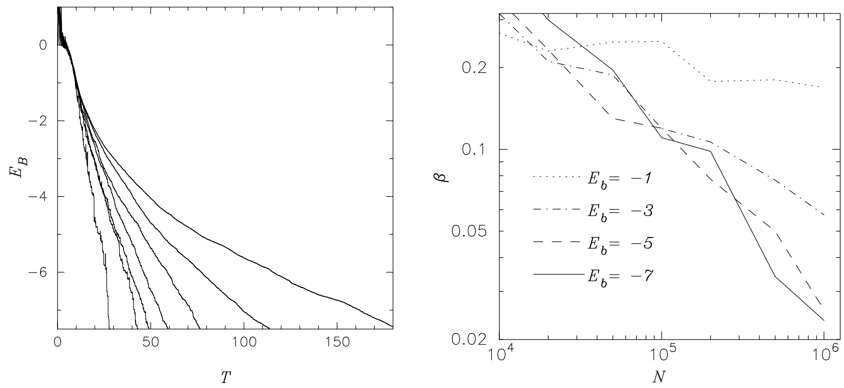

Figure 1. (Left) the evolution of the specific binding energy E_b of the binary black hole. Curves are result with $N = 10K$, 20K, 50K, 100K, 200K, 500K and 1M (left to right). For all calculations, the softening length is $\epsilon = 0.01$. (Right) the hardening rate $\beta = |\Delta E_b/\Delta t|$ plotted as a function of the number of particles N. Dotted, dash-dotted, dashed and solid curves denote the values measured from the time at which $|E_b|$ reached 1, 3, 5 and 7, respectively. The end time is the time at which $|E_b|$ reached initial value +0.5.

4. Discussions

Our present result is consistent with the theory of loss-cone depletion and its refilling in thermal time scale, while previous numerical results are not. What caused this difference?

Makino (1997) obtained the dependence much weaker than linear from simulations with $N = 2,048$ to 266,144. If we compare his figure 1 and our figure 1, the reason is obvious. The value of the binding energy at which the dependence is measured was rather small. In other words, Makino (1997) did not cover long enough time.

Quinlan & Hernquist (1997) performed simulations very similar to the ones presented here. They found that the hardening rate was practically the same for $N = 10^5$ and $N = 2 \times 10^5$. We do not really understand why they obtained this result. They used the SCF method by Hernquist & Ostriker (1992) and they varied the masses of particles depending on their initial angular momenta. We suspect this combination might have complicated the dependence of the hardening time scale on the number of particles. Chatterjee et al (2003) might have similar problem.

Milosavljevic & Merritt (2001) performed three runs with 8K, 16K and 32K stars, and found that the hardening rate was independent of the number of particles. As suggested in their paper, this result is simply because the loss cone was not depleted in their simulation, primarily because N was too small. So their result is not inconsistent with ours.

As first suggested by BBR and confirmed by a number of followup works, if the hardening time scale of the black hole binary is proportional to the relaxation time scale of the parent galaxy, the evolution time scale of a typical binary black hole in an elliptical galaxy exceeds the Hubble time by many orders of magnitude. In other words, the binary is unlikely to merge through encounters with field stars and gravitational wave radiation.

Our result strongly suggests that the hardening time scale is indeed determined by the relaxation time scale, for large enough N and after the binary becomes sufficiently hard. Thus, our result imply that gravitational interaction with field stars is insufficient to let the binary merge.

If the binary black hole has long lifetime, it is quite natural to assume that some of the host galaxies which contain binary black holes would further merge with another galaxy with a central massive black hole or a binary. Simple estimate assuming the thermal distribution of the eccentricity Makino & Ebisuzaki (1994) suggests that, during repeated three body interactions, the eccentricity of the binary can reach a very high value, resulting in quick merging through gravitational wave radiation. Thus, strong triple interaction of three super-massive black holes may be common.

References

Begelman, M. C., Blandford, R. D., & Rees, M. J. 1980, Nature, 287, 307

Byun, Y.-I., et al. 1996, AJ, 111, 1889

Chatterjee, P., Hernquist, L., & Loeb, A. 2003, preprint.

Ferrarese, L., & Merritt, D. 2000, ApJ, 539, L9

Gebhardt, K., et al. 2000, ApJ, 539, L13

Gebhardt, K., et al. 1996, AJ, 112, 105+

Kauffmann, G., & Haehnelt, M. 2000, MNRAS, 311, 576

Hernquist, L., & Ostriker, J. P. 1992, ApJ, 386, 375

Magorrian, J., et al. 1998, AJ, 115, 2285

Makino, J. 1997, ApJ, 478, 58

Makino, J., & Ebisuzaki, T. 1994, ApJ, 436, 607

—. 1996, ApJ, 465, 527

Makino, J., et al. 2002, preprint

Makino, J., & Funato, Y. 2003, preprint

Makino, J., et al. 1993, PASJ, 45, 303

Mikkola, S., & Valtonen, M. J. 1992, MNRAS, 259, 115

Milosavljević, M., & Merritt, D. 2001, ApJ, 563, 34

Nakano, T., & Makino, J. 1999, ApJ, 525, L77

—. 1999, ApJ, 510, 155

Quinlan, G. D., & Hernquist, L. 1997, New Astronomy, 2, 533

Highlights of Astronomy, Vol. 13
International Astronomical Union, 2003
O. Engvold, ed.

Can Bars be Destroyed by Central Mass Concentrations?

E. Athanassoula

Observatoire de Marseille, 2 place Le Verrier, 13248 Marseille cedex 04, France

W. Dehnen

Department of Physics & Astronomy, University of Leicester, Leicester LE1 7RH, UK

J. C. Lambert

Observatoire de Marseille, 2 place Le Verrier, 13248 Marseille cedex 04, France

Abstract. We use N-body simulations to follow the evolution of bars in the presence of a central mass concentration (CMC). We find that the bar amplitude decreases in response to the CMC, but the bar is not totally destroyed unless the CMC mass is several percent of that of the disc. More centrally concentrated CMCs are more efficient. The bar evolution does not stop after the CMC has fully grown, but continues well after that time.

1. Introduction

Both strong bars and CMCs can be found in a large fraction of disc galaxies. Examples of the latter can be black holes or central concentrations of molecular gas. It is thus necessary to study the dynamics of cases where both bars and CMCs are present in the same disc. Initially this was attempted by studying the orbits of individual particles in rigid potentials which have both a CMC and a bar component (Hasan & Norman 1990, Hasan, Pfenniger & Norman 1993). Such studies aim towards an understanding of the stability of the individual periodic orbits, which is necessary in order to assess the possible building blocks from which a bar can be built. They can not, however, give quantitative information on how a bar will evolve in the presence of a black hole. Thus these works were followed by N-body simulations, either 2D (Norman, Sellwood & Hasan 1996, Hozumi & Hernquist 1998), or 3D but with mainly rigid haloes (Norman et al 1996, Shen & Sellwood 2003). Here we will present results of N-body simulations in which both the disc and the halo are live, i.e. composed of particles.

2. Results

The initial conditions for our simulations were taken from one of the simulations of Athanassoula (2003). These started with an exponential disc of unit mass and scale length. This sets the units of mass and length. For the model described here we chose a halo with a core radius half the disc scale length and a mass five times that of the disc. A bar grows spontaneously in this simulation and evolves by emitting angular momentum, which is absorbed by the outer disc and the halo (Athanassoula 2003). For the simulations we present here we use as initial conditions a time at which the bar has grown quite strong. At that time we introduce gradually a CMC, which for simplicity is modeled by a Plummer sphere. We have tried a number of growth times (T_{grow}), of final CMC masses (M_{CMC}), and of CMC scale lengths (R_{CMC}). In this section we will discuss some results obtained with $T_{grow} = 100$, $R_{CMC} = 0.01$ and $M_{CMC} = 0.1$ or 0.05, all measured in computer units. Results for other parameter values will be very briefly mentioned in the next section and a complete account of our results will be given elsewhere. The evolution was followed with a treecode (Dehnen 2000, 2002).

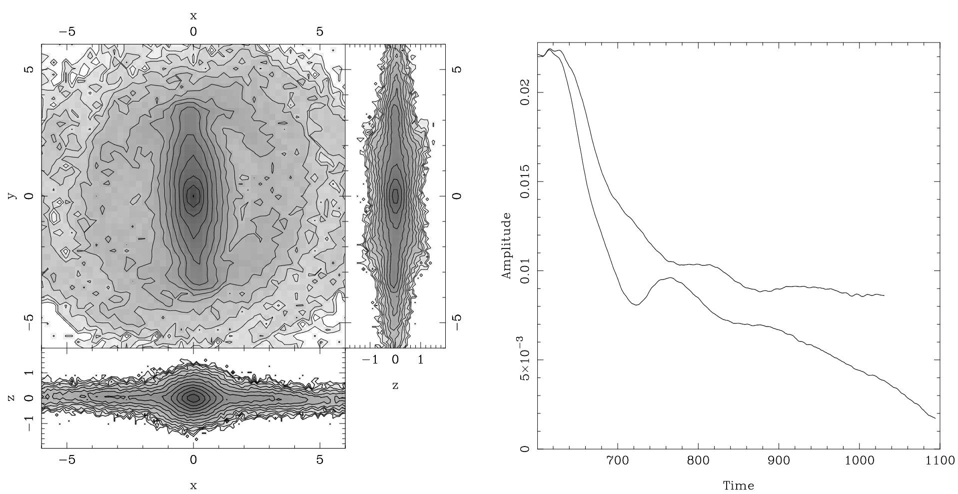

Figure 1. The left panel shows the three orthogonal views of the disc component at the time the CMC is introduced. The right panel shows the bar strength for the two simulations discussed in section 2, as a function of time.

The left panel of Fig. 1 shows the three orthogonal views of the disc component at the time the CMC is introduced. Seen face-on, the bar is reminiscent of the strong bars observed in real galaxies. It is long and thin and its isodensities have a rectangular-like shape in the outer parts (Athanassoula & Misiriotis 2002). Seen edge-on and side-on, i.e. with the line of sight along the bar minor axis, it displays a characteristic peanut shape.

Fig. 2 shows the disc component 440 computer time units after the CMC has been initially introduced. Note that in the calibration introduced by Athanassoula (2003) the unit of time is 1.4 $\times 10^7$ yrs, so that 440 computer units correspond roughly to 6 Gyrs. In the simulation with $M_{CMC} = 0.05$ the bar is still present, but is considerably shorter and less thin. Its isodensities are more elliptical-like and in the innermost parts they are near-circular. Seen side-on, it is now boxy. For $M_{CMC} = 0.1$ the bar has nearly disappeared (indeed it does so even more at later times of that simulation) and seen edge-on it has an oblate shape.

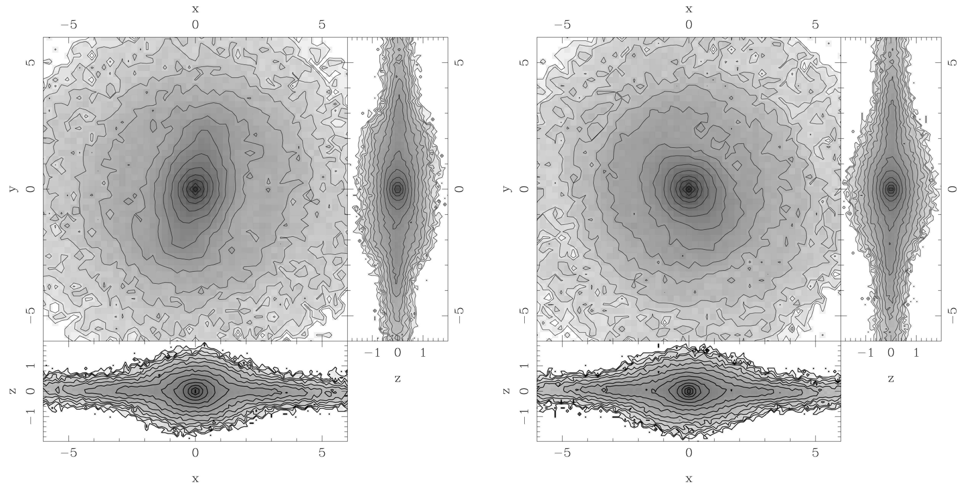

Figure 2. Three orthogonal views of the disc component towards the end of the simulations. The left panel corresponds to the simulation with M_{CMC} = 0.05 and the right one to the simulation with M_{CMC} = 0.1.

The strength of the two bars (here simply defined as the maximum of the m=2 Fourier component of the density in arbitrary units) is compared as a function of time in the left panel of Fig. 1. The time is given in computer units. We note that in the first 20 to 30 time units the bar strength stays roughly constant. This is followed by a phase of sharp decrease, which lasts roughly 100 time units. This is followed by a third phase, where the bar still decreases, but now considerably less fast. This plot, and many similar ones for other simulations, shows clearly that the decrease of the bar amplitude does not stop after the CMC has reached its maximum mass, but continues well after that time.

Fig. 3 shows the amplitude of the $m = 2$ component of the density as a function of radius and of time. At the time when the CMC is introduced the $m = 2$ component is small in the innermost regions and grows outwards to reach a maximum, and then decreases. At later times the amplitude of the $m = 2$ decreases. This is achieved from the centermost and the outermost parts simultaneously. This is consistent with what was seen in Fig. 2, which showed that the innermost contours become rounder and the length of the bar decreases considerably. All this is much clearer for the case with $M_{CMC} = 0.1$, but can also be seen for $M_{CMC} = 0.05$. Similar plots (not shown here) for the $m = 4$ component show that this component decays much faster than the $m = 2$ one. As a result, the isodensities become elliptical-like before the bar disappears.

3. Summary and Discussion

The main results from a number of simulations (not shown here) are that :

- CMCs with larger masses and/or smaller scale lengths are more efficient in destroying the bar.

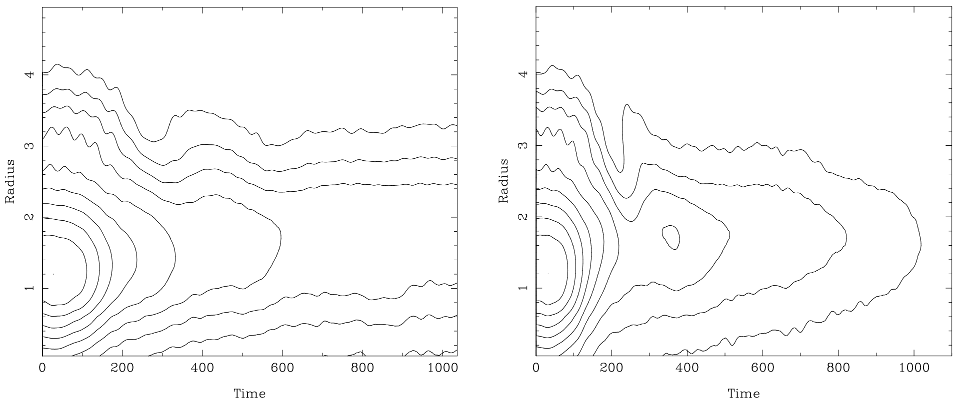

Figure 3. Amplitude of the $m = 2$ component of the density as a function of radius and of time. The left panel corresponds to the simulation with M_{CMC} = 0.05 and the right one to the simulation with $M_{CMC} = 0.1$.

- The mass and the scale length of the CMC necessary to destroy the bar depend on the bar model.
- For all models we tried, a CMC mass of at least several percent of the disc mass is necessary in order to destroy the bar.
- The final result does not depend much on the CMC growth time
- The evolution does not stop after the CMC has reached its maximum mass.

These and further results will be discussed further elsewhere, where we will present also comparisons with previous analysis and with observations.

References

Athanassoula E. 2003, MNRAS, 341, 1179
Athanassoula E., & Misiriotis, A. 2002, MNRAS, 330, 35
Dehnen, W. 2000, ApJ, 536, L39
Dehnen, W. 2002, J. Comp. Phys., 179, 27
Hasan, H., & Norman, C. 1990, ApJ, 361, 69
Hasan, H., Pfenniger, D., & Norman, C. 1993, ApJ, 409, 91
Hozumi, S., & Hernquist, L. 1998, astro-ph 9806002
Norman, C., Sellwood, J. A., & Hasan, H. 1996, ApJ, 462, 114
Shen, J., & Sellwood, J. A. 2003, astro-ph 0303130

Highlights of Astronomy, Vol. 13
International Astronomical Union, 2003
O. Engvold, ed.

The Formation and Evolution of Star Clusters and Galaxies

Stephen E. Zepf

Dept. of Physics and Astronomy, Michigan State University, East Lansing, MI 48824, USA

Abstract. This paper addresses the questions of what we have learned about how and when dense star clusters form, and what studies of star clusters have revealed about galaxy formation and evolution. One important observation is that globular clusters are observed to form in galaxy mergers and starbursts in the local universe, which both provides constraints on models of globular cluster formation, and suggests that similar physical conditions existed when most early-type galaxies and their globular clusters formed in the past. A second important observation is that globular cluster systems typically have bimodal color distributions. This was predicted by merger models, and indicates an episodic formation history for elliptical galaxies. A third and very recent result is the discovery of large populations of intermediate age globular clusters in several elliptical galaxies through the use of optical to near-infrared colors. These provide an important link between young cluster systems observed in starbursts and mergers and old cluster systems. This continuum of ages of the metal-rich globular cluster systems also indicates that there is no special age or epoch for the formation of the metal-rich globular clusters, which comprise about half of the cluster population. The paper concludes with a brief discussion of recent results on the globular cluster - low-mass X-ray binary connection.

1. Globular Cluster Formation

A natural starting point for the discussion of galaxies and globular cluster systems is the formation of globular clusters (GCs). Any model of the formation of globular cluster systems and their host galaxies that does *not* include a consideration of how the globular clusters themselves form is necessarily incomplete. Fortunately, nature has provided us nearby examples of GC formation, most dramatically revealed in HST images (e.g. Whitmore et al. 1999, Zepf et al. 1999). The formation of globular clusters in galaxy mergers was predicted by Ashman & Zepf (1992) and Schweizer (1987) and then confirmed by many subsequent HST observations. Moreover, as discussed at this meeting by Bruce Elmegreen, these observations are providing an important testing ground for theoretical work on GC formation (e.g. Elmegreen 2002, Ashman & Zepf 2001).

2. Key Properties of Globular Cluster Systems

A second key point is the bimodality typical of the color distributions of early-type galaxies. The bimodality of early-type galaxy globular cluster systems was first discovered about ten years ago (Zepf & Ashman 1993), and has now been confirmed to be typical by extensive studies of archival HST data (Kundu &

Whitmore 2001, Larsen et al. 2001). The data show that roughly half of the GCs are blue (metal-poor) and half are red (metal-rich, i.e. very roughly solar or somewhat less). There is little or no trend of the red/blue ratio with galaxy luminosity or globular cluster number (e.g. Rhode & Zepf 2003).

The observed bimodality in the cluster systems of elliptical galaxies has important implications for the formation of globular clusters and galaxies. Firstly, bimodality was predicted by Ashman & Zepf (1992) to result from elliptical galaxy formation by mergers of disk galaxies, mostly at $z \gtrsim 1$, and so the observation was in agreement with an earlier theoretical prediction. Moreover, regardless of the specific model, bimodality requires an episodic formation history for elliptical galaxies, and not a single formation event. Secondly, most of these events also have to occur at least ~ 8 Gyr ago in order for the metal-rich GCs to become red enough to produce the color bimodality from the metallicity bimodality. However, even if most of the major formation events take place at $z \gtrsim 1$, some will take place more recently, and to make the picture complete, we should be able to identify and characterize these. This has recently been achieved, as discussed in the following section.

3. Intermediate Age Globular Cluster Systems

The discovery of intermediate age globular cluster systems in elliptical galaxies is important because it links the young systems observed in mergers to the traditional old GC systems. A key observational advance has been the use of optical to near-infrared colors to break the age-metallicity degeneracy to identify intermediate age, $\sim$ solar metallicity globular clusters (which are effectively indistinguishable from lower metallicity, older clusters in optical colors alone).

The breakthrough in identifying intermediate age clusters came in two ways. Puzia et al. (2002) discovered a large population of intermediate age globular clusters in the otherwise fairly normal elliptical galaxy NGC 4365. Subsequent spectroscopy of a subset of the Puzia et al. clusters confirmed the effectiveness of their optical to near-infrared technique (Larsen et al. 2003). While Puzia et al. (2002) demonstrated that some quiescent ellipticals had a major formation event in their not so distant past, Goudfrooij et al. used similar techniques to identify a major intermediate-age globular cluster population in the disturbed galaxy NGC 1316. More recently, Hempel et al. (2003) found a significant intermediate-age cluster population in NGC 5846. Both Puzia et al. and Hempel et al. also find galaxies without intermediate age populations, as expected since the common bimodal systems are probably not intermediate-age. However, the presence of intermediate age systems shows that the age distribution of cluster systems is continuous from very young to very old, with all ages present. The formation of these clusters traces out the starburst histories of their host ellipticals, which appears to be complex and to occur over a significant range of times.

4. Globular Cluster - Low-Mass X-Ray Binary Connection

Since this is a dynamics session, and GCs are fertile ground for the study of stellar dynamics, it is relevant to note that the dynamical interactions between stars play an important role in understanding X-ray emission from elliptical galaxies. This is because roughly half of all X-ray binaries seen in Chandra images are located in GCs (see upcoming review by Verbunt & Lewin 2003 and references therein). Moreover, the dynamical formation of X-ray binaries in GCs may be the dominant process in early-type galaxies, since sources not now in GCs may have been formed there and ejected or been in clusters that were disrupted (e.g. Maccarone, Kundu, & Zepf 2003). The study of the GCs hosting low-mass X-ray binaries also provides constraints on the physics of X-ray binary formation and evolution. In particular, there is a strong metallicity dependence and no strong age dependence (Kundu et al. 2003 and references therein).

Acknowledgments. I thank my many collaborators on the projects described here, and also my postdocs and graduate students Arunav Kundu, Katherine Rhode, Enrico Vesperini, Gilles Bergond, and Chris Waters. Financial support is acknowledged from LSTA grant NAG5-11319 and Chandra and HST programs.

References

Ashman, K.M., & Zepf, S.E. 1992, ApJ, 384, 50

Ashman, K.M., & Zepf, S.E. 2001, AJ, 122, 1888

Elmegreen, B.G. 2002, ApJ, 577, 206

Goudfrooij, P., et al. 2001, MNRAS, 322, 643

Hempel, M., et al. 2003, A&A, 405, 487

Kundu, A., & Whitmore, B.C. 2001, AJ, 121, 2950

Kundu, A., Maccarone, T.J., Zepf, S.E., & Puzia, T.H. 2003, ApJL, 589, 81

Larsen, S.S., et al. 2001, AJ, 121, 2974

Larsen, S.S., et al. 2003, ApJ, 585, 767

Maccarone, T.J., Kundu, A., Zepf, S.E. 2003, ApJ, 586, 814

Puzia, T.H., Zepf, S.E., Kissler-Patig, M., Hilker, M., Minniti, D., & Goudfrooij, P. 2002, A&A, 391, 453

Rhode, K.L., & Zepf, S.E. 2003, AJ, submitted

Schweizer, F. 1987, in Nearly Normal Galaxies, ed. S.M. Faber (Berlin: Springer), 18

Whitmore, B.C., Zhang, Q., Leitherer, C. Fall, S.M., Schweizer, F., & Miller, B.W. 1999, AJ, 118, 1551

Zepf, S.E., & Ashman, K.M. 1993, MNRAS, 264, 611

Zepf, S.E., Ashman, K.M., English, J., Freeman, K.C., & Sharples, R.M. 1999, AJ, 118, 752

Highlights of Astronomy, Vol. 13
International Astronomical Union, 2003
O. Engvold, ed.

Formation and Evolution of Massive Black Holes in Star Clusters

Holger Baumgardt

Institute of Advanced Physical and Chemical Research RIKEN, 2-1 Hirosawa, Wako-shi, Saitama 351-019, Japan

Junichiro Makino

Department of Astronomy, School of Science, The University of Tokyo, 7-3-1 Hongo, Bunkyo-ku, Tokyo 113-0033, Japan

Simon Portegies Zwart

Astronomical Institute "Anton Pannekoek" and Section Computational Science, University of Amsterdam, Kruislaan 403, 1098 SH Amsterdam, The Netherlands

Abstract. We present results of N-body simulations on the formation of massive black holes by run-away merging in young star clusters and the later dynamical evolution of star clusters containing massive black holes. We determine the initial conditions necessary for run-away merging to form a massive black hole and study the equilibrium profile that is established in the cluster center as a result of the interaction of stars with the central black hole. Our results show that star clusters which contain black holes have projected luminosity profiles that can be fitted by standard King models. The presence of massive black holes in (post-)core collapse clusters is therefore ruled out by our simulations.

1. Introduction

It has long been suspected that black holes with masses of a few hundred to a few thousand solar masses exist in the centers of some star clusters. Nevertheless observational evidence for their presence has been slow to accumulate. One of the best candidates to harbor a black hole is MGG-11, a young star cluster in the star-burst galaxy M82. Matsumoto et al. (2001) and Kaaret et al. (2001) have performed X-ray imaging of the central kpc of M82 and found an ultraluminous X-ray source with a luminosity that corresponds to a mass of more than 700 $M_{\odot}$ if the object is accreting at the Eddington rate. Optical follow-up observations have shown that the position of the X-ray source coincides with that of MGG-11. McCrady et al. (2003) have obtained surface photometry and spectroscopy for a sample of star clusters in M82 and found that MGG-11 is deficient in low-mass stars. In addition, the cluster also had the smallest half-mass radius of all clusters in their study. Both findings imply that MGG-11 has a short relaxation time, so it seems possible that runaway collision of the most massive cluster stars could have formed a black hole.

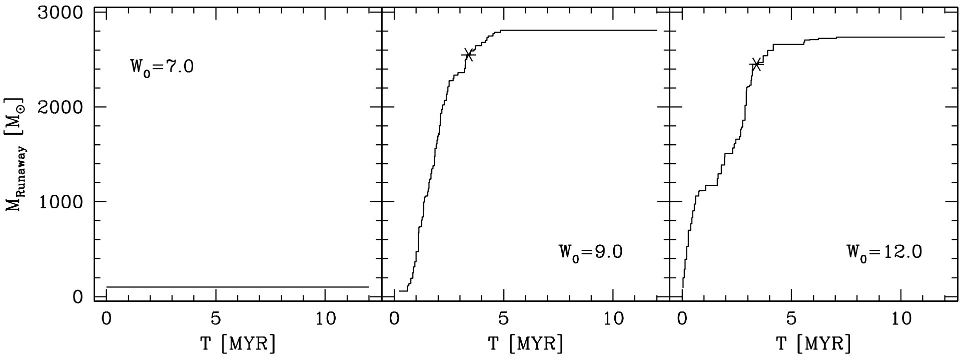

Figure 1. Mass of the most massive star for three clusters starting from King models with different central concentrations. Clusters with central concentrations $W_0 \geq 9.0$ go into core-collapse quickly enough so that runaway merging leads to the formation of a star with several thousand solar masses. Asterisks mark the time of collapse of the runaway star to a black hole.

2. Simulations of run-away merging

In order to test if run-away merging can happen in MGG-11, we simulated the cluster evolution by N-body simulations. Our clusters contained $N = 131.072$ stars which initially followed a Salpeter IMF between 1.0 and 100 $M_\odot$. This leads to a total cluster mass and mass-to-light ratio which is in agreement with the observations. Since the density profile is not well known, we simulated clusters starting from King profiles with central concentrations in the range $7.0 \leq W_0 \leq 12.0$. The simulations were run for $T = 12$ Myrs, which is compatible with the age of MGG-11 as found by McCrady et al. (2003). The initial half-mass radii of our clusters were adjusted such to match the observed cluster radius $r_{hp} = 1.2$ pc after $T = 12$ Myrs.

Fig. 1 shows the mass of the most massive star as a function of time for three different clusters. For a $W_0 = 7.0$ King model, the merger rate remains low throughout the simulation since the central density is low initially and the core collapse time is longer than the lifetime of the most massive cluster stars (about 3 Myrs). Hence the cluster starts expanding due to stellar evolution mass-loss before it can go into core-collapse and no run-away merging occurs.

King $W_0 = 9.0$ and $W_0 = 12.0$ models go into core-collapse quickly enough to concentrate a large fraction of their heavy mass stars in the center. Due to their large radii and masses collisions happen predominantly between the massive stars and lead to the formation of a super-massive star with a mass of more than 2000 $M_\odot$ before going supernova. After the star is turned into a black hole, the merging activity declines. We conclude that an intermediate-mass black hole could have formed in MGG-11 if the initial cluster concentration was larger than $W_0 \approx 9.0$. Since this is a typical concentration for globular clusters, it seems entirely possible that an intermediate mass black hole has formed in MGG-11.

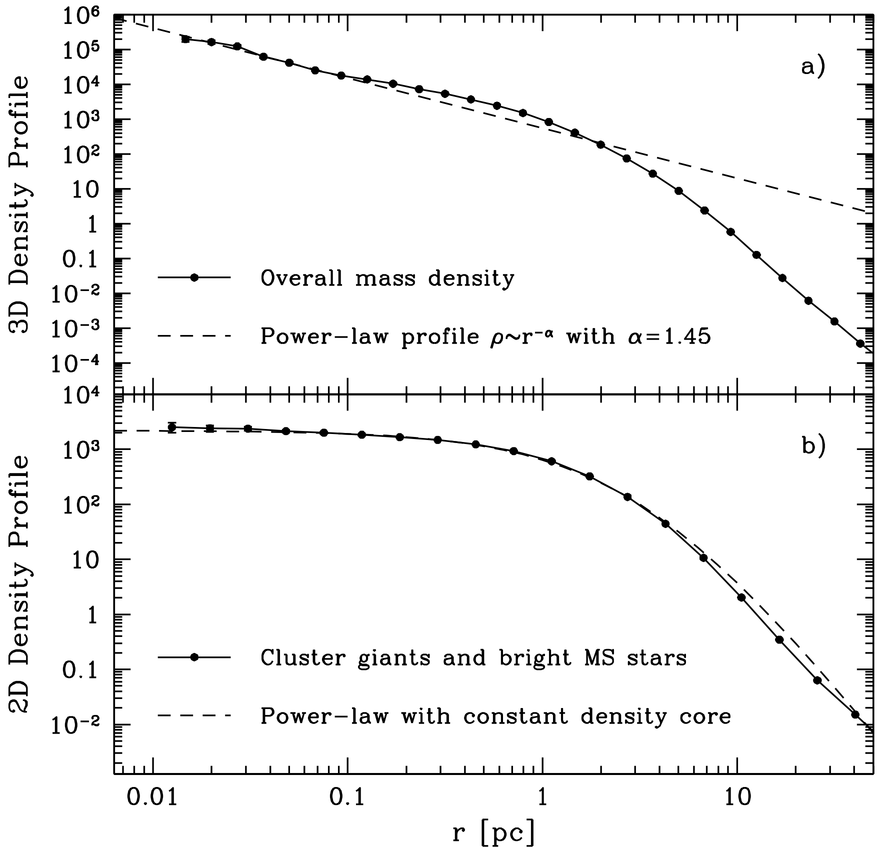

Figure 2. Density profile after T=12 Gyrs of a star cluster containing $N =$ 131.072 stars and a central massive black hole of 1000 $M_\odot$. In the center, a power-law profile with slope $\alpha = 1.45$ is established in three dimensions (Fig. 2a). This leads to an almost flat luminosity profile in projection (Fig. 2b).

3. Dynamical evolution of star clusters with massive central black holes

After its formation, a massive black hole is likely to stay in the center of its parent cluster because it is too heavy to be expelled through close three-body interactions with other cluster stars. One might therefore expect that some galactic globular clusters contain massive black holes. Possible ways to detect them include the emission of gravitational waves if the black hole is in a tight binary with another black hole or neutron star, or the comparison of the central light and velocity profile with kinematical models. In order to study how star clusters with massive black holes evolve, we simulated the evolution of multi-mass clusters containing a 1000 $M_\odot$ black hole in their center. The studied clusters started with a Kroupa (2001) IMF between 0.1 and 30$M_\odot$ and contained between 16.384 and 131.072 cluster stars. The simulations were performed for a duration of 12 Gyrs. Fig. 2 shows the final density profile for the cluster which started with $N = 131.072$ stars.

In three dimensions, the central density profile follows a power-law distribution $\rho \sim r^{-\alpha}$ with slope $\alpha = 1.45$. This is slightly flatter than the results obtained from Fokker-Plank and Monte Carlo simulations: $\alpha = 1.75$ (Bahcall & Wolf 1976, Cohn & Kulsrud 1978). One reason is that in the Fokker-Plank and Monte Carlo simulations the black hole was assumed to be at rest in the cluster center while in a real globular cluster it moves around in the center as a result of encounters with passing unbound stars. This leads to a flattening of the central profile. The projected distribution of bright stars is shown in Fig. 2b. It can be seen that the bright stars have a more or less constant density core. A cluster with a massive black hole in its center would therefore appear as a standard King profile cluster to an observer. We obtain the same results for clusters with other particle numbers.

4. Conclusions

We have performed simulations of the formation of massive black holes in star clusters and the later dynamical evolution of such systems. The ultra-luminous X-ray source in M82 might be an intermediate mass black hole formed through runaway merging of stars in a star cluster during the first 3 million years after cluster formation. We expect that star clusters with massive black holes will develop power-law cusps with relatively shallow slopes. It seems unlikely that massive black holes can be present in core-collapse clusters like M15, since in such clusters the central luminosity profile increases too steeply. Clusters with high central densities which appear to have a near constant density core might however be good places to look for massive black holes. A more detailed discussion of our results will be published in forthcoming papers (Portegies Zwart et al. 2003, Baumgardt et al. 2003).

References

Bahcall, J. N, Wolf, R. A. 1976, ApJ, 209, 214
Baumgardt, H., et al. 2003, in preparation
Cohn, H., Kulsrud, R., M. 1978, ApJ, 226, 1087
Kaaret, P., et al. 2001, MNRAS, 321, L29
Kroupa P., 2001, MNRAS, 322, 231
Matsumoto, H., et al. 2001, ApJ, 547, L25
McCrady, N., Gilbert, A. M., Graham, J. R. 2003, ApJ submitted, astro-ph/0306373
Portegies Zwart, S., et al. 2003, in preparation

Highlights of Astronomy, Vol. 13
International Astronomical Union, 2003
O. Engvold, ed.

A Physicist's View of Stellar Dynamics: Dynamical Instability of Stellar Systems

V.G.Gurzadyan

Yerevan Physics Institute, Armenia and Department of Physics, University of Rome 'La Sapienza', Italy

Abstract. I argue that the widely adopted framework of stellar dynamics survived since 1940s, is not fitting the current knowledge on non-linear systems. Borrowed from plasma physics when several fundamental features of perturbed non-linear systems were unknown, that framework ignores the difference in the role of perturbations in two different classes of systems, in plasma with Debye screening and gravitating systems with no screening. Now, when the revolutionary role of chaotic effects is revealed even in planetary dynamics i.e. for nearly integrable systems, one would expect that for stellar systems, i.e. non-integrable systems, their role have to be far more crucial. Indeed, ergodic theory tools already enabled to prove that spherical stellar systems are exponentially instable due to N-body interactions, while the two-body encounters, contrary to existing belief, are not the dominating mechanism of their relaxation. Chaotic effects distinguish morphological and other properties of galaxies. Using the Ricci curvature criterion, one can also show that a central massive object (nucleus) makes the N-body gravitating system more instable (chaotic), while systems with double nuclei are even more instable than those with a single one.

1. On the current framework of stellar dynamics

Since this is a Joint Discussion at IAU General Assembly, I allow myself to start from some general but also provocative remarks; for detailed refs see (Allahverdyan, Gurzadyan 2002). The current framework of stellar dynamics is the one summarized in Chandrasekhar's book of 1942. That framework was borrowed earlier from the plasma physics when many features of perturbed non-linear systems were unknown. This resulted in the ignorance of the drastic difference in the role of perturbations for two different classes of systems, plasma and gravitating systems: with Debye screening and justified cutoff of perturbations for the former, and long range interaction and no screening for the latter. Correspondingly, the two-body (Rutherford) scatterings, i.e. neglecting the perturbations of other particles of the system, were *a priori* assumed as the universal mechanism of relaxation of stellar systems,[3] even though it failed to explain even elliptical galaxies, the most well-mixed systems in the Universe, predicting time scales exceeding their age (Zwicky paradox).

Does the framework of stellar dynamics fit the current knowledge of the non-linear systems? To address this question maximally briefly, I will concentrate

[3]The two-body relaxation is postulated also in kinetic (diffusion coefficients) and other approaches to stellar dynamics.

only on nearly integrable systems, linked with planetary dynamics and on non-integrable ones, i.e. on the class of systems, the stellar systems belong to.

Nearly integrable systems. I will illustrate the scale of changes occurred since 1940s mentioning two works, the Kolmogorov theorem (1954) and Fermi-Pasta-Ulama (FPU, 1955) experiment.

Done practically at the same time, at the different sides of the iron curtain, in Moscow and Los Alamos, both works came to contradict the views held almost during half a century, since Poincare's theorem on the perturbed Hamiltonian systems. Kolmogorov theorem (now the main theorem of Kolmogorov-Arnold-Moser (KAM) theory) had tremendous impact on the study of dynamical systems, including the dynamics of the Solar system. FPU has inspired numerous studies (including the discovery of solitons), however in spite of much efforts, the dynamics of that 64-particle nonlinearly interacting one-dimensional system remains not completely understood up to now. Maybe this lesson has to be taken into account also for stellar dynamics.

Non-integrable systems. After the discovery of the metric invariant by Kolmogorov (1958), KS-entropy, and introduction of K-systems (Kolmogorov, 1959), 'an unexpected discovery' (to quote Arnold) was made in 1960s (Anosov, Sinai, Smale) on the structural stability of exponentially instable systems. The emerged ergodic theory provided the classification of non-integrable systems by their statistical properties, with corresponding criteria and tools, though the latter not always were easy to apply for a given physical system. Those achievements enabled to attack several long standing problems such as the relaxation of Boltzmann gas, and served as the framework for the study of chaos during the following decades.

KAM theory ideas when applied in planetary dynamics by Laskar, Tremaine and others revealed the fundamental role of chaos in the evolution of the Solar system, predicting the possible escape of Mercury from its orbit due to chaotic variations of the eccentricity, chaotic variations of the obliquity of Mars and the stabilization of the same effect by the Moon in the case of Earth (Laskar). So, if already for planetary systems i.e. for nearly integrable systems, the chaotic effects due to small perturbations of planets lead to such unexpected results, how can stellar systems, i.e. non-integrable many-dimensional systems avoid the influence of chaos due to the perturbations of N particles?

Ergodic theory tools were applied in stellar dynamics in (Gurzadyan, Savvidy 1984, below GS), where the spherical systems were shown to be exponentially instable systems and the time scale of tending to micro-canonical state (the relaxation time) was estimated using the standard Maupertuis re-parameterization for the geodesic flow, as follows from the theorems of ergodic theory.[4]

More important, the results in GS and in (Pfenniger 1986) (using the Lyapounov formalism) came to reveal that, the plasma analogy in the linear (!) sum of scattering angles at subsequent two-body scatterings is irrelevant for a long-

[4]The Maupertuis re-parameterization of the affine parameter (time) of the geodesics corresponds to the conservation of total energy of the system. Numerical experiments without such re-parameterization performed first by Miller in 1964, repeated later by Heggie, Hut, Kandrup and others, therefore violate the energy conservation condition and have no link with the mentioned statistical properties and relaxation of the system.

range non-linear system's dynamics, and N-body scatterings do contribute to the statistical properties and hence in the relaxation of stellar systems. Particularly, the formula derived in GS for the relaxation time scale due to non-linear effects provided enough time for the relaxation of elliptical galaxies. By now that formula is supported by numerical simulations, alternative theoretical derivation, observational data on globular clusters and elliptical galaxies; see refs in (Allahverdyan, Gurzadyan 2002).

There are preliminary indications from deep surveys on the existence of elliptical galaxies at redshifts $z > 4$, i.e. of 10 per cent of their present age. If confirmed, this fact would moreover require more rapid mechanism of relaxation than the two-body one. The chaotic effects are not only responsible for the relaxation and evolution of globular clusters and elliptical galaxies, but also they are indicators of the morphological type and other properties of galaxies. How many decades are needed to realize the necessity of replacement of the 'plasma' framework of stellar dynamics and abandoning of the two-body relaxation myth?

2. Relative instability of stellar systems

I will now briefly discuss the problem of relative instability of stellar systems, concentrating particularly on the role of central massive objects, in view of recent progress in their studies in the cores of galaxies and globular clusters. The results are obtained by means of the above mentioned ergodic theory formalism.

In accord to the criterion introduced in (Gurzadyan, Kocharyan 1988) among two systems the one with smaller negative Ricci curvature r_u has to be considered as more instable. For N-body gravitating systems the Ricci curvature equals

$$r_u(s) = -\frac{(3N-2)}{2}\frac{W_{ik}u^i u^k}{W} + \frac{3}{4}(3N-2)\frac{(W_i u^i)^2}{W^2} - \frac{(3N-4)}{4}\frac{|\nabla W|^2}{W^3}, \qquad (1)$$

where

$$W = E - V, \quad V = -G\sum_{i<j}^{N} m_i m_j / r_{ij},$$

and

$$W_i = \frac{\partial W}{\partial r^i}, \quad W_{ik} = \frac{\partial^2 W}{\partial r^i \partial r^k}, \quad |\nabla W|^2 = \sum_i (\frac{\partial W}{\partial r_i})^2,$$

m_i denote the masses, u is the velocity of geodesics with affine parameter s in the configuration space. The minimal values of the Ricci curvature have to be compared within given interval of the affine parameter. The contribution of direct impacts of stars, i.e. when two stars get the same coordinates, is neglected in Eq.(1), as they are rare events for real stellar systems.

The idea is based on the average description of the exponential deviation of geodesics in the configuration space with sign-indefinite curvature tensor. The latter condition appears to be fulfilled for N-body gravitating systems thus indicating the diversity of possible configurations with very different properties, from semi-regular planetary systems to mixing spherical systems. The $r_u(s)$ is related with the Ricci tensor *Ric* by the following expression

$$r_u(s) = \frac{Ric(u,u)}{u^2}.$$

This criterion has a principal difference from that of Lyapounov exponents, since provides local in time characteristics of the system and hence does not require 'infinite' iterated computations.

Numerical experiments using this criterion have been performed for various N-body configurations by Bekarian, El-Zant, Melkonian, Kocharyan and others. It is natural to see that, for example, disk configurations with rotational momentum are more regular than spherical ones. More rigorous consideration based on Arnold's theorem (1966) on one-parametric groups of manifolds with right-invariant Riemannian metric enables one to conclude that the Galactic disk does not possess the property of mixing (and hence the corresponding relaxation time scale), as spherical stellar systems do.

The following classification for the systems of our interest by the increase of statistical properties is emerging from numerical experiments:

1. Spherical systems;
2. Systems with a massive central object (nucleus);
3. Systems with double nuclei.

The role of a massive center, with similar conclusions, has been studied using other methods by van Albada, Norman, Rauch, Tremaine and others. We now see that double (or binary) massive objects, like those apparently observed in galaxies Markarian 273, Arp 220, have to make the system even more chaotic, i.e. with further increase in the rate of evolution driving effects (Bekarian, Melkonian 2000).

The topics mentioned above on the role of non-linear effects in stellar dynamics gain more importance in view of ever increasing possibilities of numerical experiments (Makino 2003).

References

Allahverdyan A.E., Gurzadyan V.G.: 2002, Nuovo Cimento, 117B, 947
Bekarian K.M., Melkonian A.A.: 2000, Astron.Lett. 26, 1
Gurzadyan V.G., Savvidy G.K.: 1984, Sov.Phys.Doklady, 29, 520 (GS)
Gurzadyan V.G., Kocharyan A.A.: 1988, Sov.Phys.Doklady, 33, 494
Makino J.: 2003, talk at this Joint Discussion
Pfenniger D.: 1986, A & A, 165, 74

Highlights of Astronomy, Vol. 13
International Astronomical Union, 2003
O. Engvold, ed.

Formation of Young Star Clusters

Bruce Elmegreen

IBM Research Division, T.J. Watson Research Center, PO Box 218, Yorktown Hts., NY, 10598, USA, bge@watson.ibm.com

Abstract. Turbulence, self-gravity, and cooling convert most of the interstellar medium into cloudy structures that form stars. Turbulence compresses the gas into clouds directly and it moves pre-existing clouds around passively when there are multiple phases of temperature. Self-gravity also partitions the gas into clouds, forming giant regular complexes in spiral arms and in resonance rings and contributing to the scale-free motions generated by turbulence. Dense clusters form in the most strongly self-gravitating cores of these clouds, often triggered by compression from local stars. Pre-star formation processes inside clusters are not well observed, but the high formation rates and high densities of pre-stellar objects, and their power law mass functions suggest that turbulence, self-gravity, and energy dissipation are involved there too.

1. Many Scales of Star Formation

Star formation has many scales. Giant star complexes extend for ~ 500 pc along spiral arms and disperse in the inter-arm regions. The clouds that form them are usually visible in HI surveys, and their cores are visible in CO surveys (Grabelsky et al. 1987). These clouds are mildly self-bound by gravity (Elmegreen & Elmegreen 1987; Rand 1993), so they are like any other star-forming clouds: virialized, supersonically turbulent, and producing stars in perhaps several generations with an efficiency of $\sim 10\%$. The star formation process is confined to the densest cores of these clouds, where gravity is strong and thermal pressure is weak. Between these extremes of scale, the gas temperature decreases and the molecular content increases, but the physical processes that cause stars to form in aggregates do not change much. These processes are a combination of multi-scale and repetitive compressions from supersonic turbulence and self-gravity, energy dissipation through shocks and magnetic diffusion, and collapse from overwhelming gravitational forces. Some of the complexity of star-formation dynamics is shown in the simulations by Bate, Bonnell, & Bromm (2003).

2. Scale-dependent Morphologies

Corresponding to the many scales of star formation, self-gravitating clouds have a wide range of masses, from $\sim 10^7$ $M_\odot$ to less than 1 $M_\odot$ in our Galaxy. What a cloud produces is called a star cluster only if its mass exceeds ~ 100 $M_\odot$ (Lada & Lada 2003). Other than this, there is no characteristic or dominant mass for clouds or clusters, only power law distributions, so most star-forming regions are similar except for size. Size determines velocity dispersion and density for a common background pressure, and density variations lead to important morphological differences through two dimensionless ratios: the dynamical time divided by the evolution time of stars, and the dynamical time divided by the shear time in the local galaxy. The largest clouds take a short time, in relative terms, to form most of their stars: just 1 or 2 dynamical times like nearly every other cloud. But these largest clouds take a long time, in absolute terms, to do this, ~ 40 My in the case of Gould's Belt, and by then the oldest populations have lost their most massive members to stellar evolution, making the complexes look relatively dull (Efremov 1995). The largest clouds are also the most severely affected by shear, making them look like flocculent spiral arms or spiral arm spurs (Kim & Ostriker 2002). These morphological differences disguise the fact that the physical processes of star and cluster formation are very similar on all scales.

Galactic-scale stellar dynamical processes can lead to the collection of gas into spiral density waves and resonance rings. Then the largest clouds are somewhat uniformly distributed along the length of the stellar structure with a characteristic separation equal to ~ 3 times the arm or ring thickness. What happens here is that clouds form by asymmetric gravitational instabilities with a converging flow along the length of the structure. Typically shear and galactic tidal forces are low in these regions, allowing the clouds to form in gas that would otherwise be stable (Rand 1993; Elmegreen 1994). -1.0cm

3. Power Spectra

When there are no galactic-scale structures, the gas appears completely scale-free, as in the Large and Small Magellanic Clouds (Stanimirovic et al. 1999; Elmegreen, Kim, & Staveley-Smith 2001). Power spectra of the emission or absorption from this gas have power laws with a slope similar to that for velocity power spectra in incompressible turbulence, namely ~ -2.8 in two-dimensions (Stützki et al. 1998; Dickey et al. 2001). Incompressible turbulence has the Kolmogorov spectrum with a slope of $-8/3$. Why the *column density* structure in a medium that is supersonically turbulent should have about the same power spectrum as the *velocity* structure in incompressible turbulence is somewhat of a mystery, unless it is partly coincidence. The power spectrum of turbulent velocities varies by only a small amount, from $-8/3$ to -3 (in 2D), as the motion varies from incompressible to shock-dominated. Thus even the most extreme cloud formation scenarios, where all clouds are shock fronts, would have a power spectrum similar to incompressible turbulence. In addition, some of the gas structure could result from entrainment of many tiny clouds in the larger-scale turbulent velocity field (Goldman 2000). Entrainment means density is a passive scalar, and then density power spectra are the same as velocity power spectra. Third, expanding shells make dense gas, and these introduce a -3 component to the power spectrum because of their sharp edges. The result is a mixture of processes and innate power spectra. This is why widely diverse morphologies ranging from flocculent dust spirals in galactic nuclei (Elmegreen, Elmegreen, & Eberwein 2002) to shells and holes in the LMC or SMC (Kim et al. 1999; Stanimirovic et al. 1999; Elmegreen et al. 2001; Lazarian, Pogosyan, & Esquivel 2002) all have about the same overall power spectrum.

4. Stars Follow the Gas

Stellar structures, such as clusters and flocculent spiral arms, have hierarchical geometries (Feitzinger & Galinski 1987; Gomez et al. 1993; Elmegreen & Elmegreen 2001; Zhang, Fall, & Whitmore 2001) and power-law power spectra (Elmegreen, Elmegreen, & Leitner 2003; Elmegreen et al. 2003) that are nearly identical to those of the gas. Star formation also has a duration that scales with the region size in the same way as the turbulent crossing time scales with size (Efremov & Elmegreen 1998). These similarities between star formation and turbulent gas imply that star formation follows the gas to first order, i.e., that turbulence controls the star formation density, rate, and morphology. This control apparently extends to small scales too, perhaps down to individual binary stars (Larson 1995), as the protostars in clusters sometimes have their own hierarchical structure (Motte, André, & Neri 1998; Testi et al. 2000). The large formation rates and high densities of embedded protostars also suggest that turbulence compresses the gas in which they form (Elmegreen & Shadmehri 2003).

5. Triggering

Closer examination shows a second-order effect: a fairly high fraction of star formation is triggered inside pre-existing clouds by external pressures unrelated to the clouds and to the pressures of the current generation. These processes are revealed by the wind-swept appearance of many cluster-forming clouds (e.g., de Geus 1992; Bally et al. 1987) and by the proximity of cluster-forming cores to external HII regions (Yamaguchi et al. 1999; Walborn et al. 1999; Heydari et al. 2001; Yamaguchi et al. 2001a,b; Deharveng et al. 2003). Probably supersonic turbulence and entrainment in a multi-phase ISM produce the basic cloudy structure, and then pressure fluctuations in the environment trigger star formation in these structures (Elmegreen 2002). There would still be star formation without the triggers, but with a smaller rate per cloud because of the lower cloud densities, and a higher number of active clouds because of the more dispersed nature of the dense sub-regions. The influence of pressurized triggering on the star formation rate in a galaxy is not known, but the universal scaling of star formation rate with average column density (Kennicutt 1998) suggests that any direct influence is weak. Star formation is probably saturated to the maximum rate allowed in a compressibly turbulent medium (Elmegreen 2002).

6. Size of Sample Effects

The stochastic nature of turbulence is also reflected in the formation of star clusters, which show a random size-of-sample effect with regard to maximum mass. This appears in several ways: the most massive stars in a cluster increase with the cluster mass (Elmegreen 1983), the most massive clusters in a galaxy increase with the number of clusters (Whitmore 2003; Billett et al. 2002; Larsen 2002), and the most massive clusters in a logarithmic age interval increase with age (Hunter et al. 2003). In all cases, the slopes of these increases are determined exclusively by the mass function through the size of sample effect: bigger regions sample further out in the tail of the distribution and have more massive most-massive members. There is apparently no physical effect that has yet been found to determine the most massive member of a population. This is true even for individual stars (Massey & Hunter 1998; Selman et al. 1999) although stellar radiation pressure and winds could limit the stellar mass once it gets large enough (Yorke & Sonnhalter 2002; but see McKee & Tan 2003).

Similarly, the ISM pressure should limit the cluster mass, considering that a cluster is recognized only if its density exceeds a certain value (depending on the sensitivity of the observation), and the density, mass and pressure are related by the virial theorem with a boundary condition. Nevertheless, this pressure limit for massive clusters has not been seen yet. It would appear as a drop-off at the upper end of the cluster mass function in a very large galaxy (sampling lots of clusters) with a low pressure (such as a giant low-surface brightness galaxy). Most galaxies have their sample-limiting mass comparable to or less than their pressure-limiting mass. Dwarf star-burst galaxies are an extreme example of this because they have very few clusters overall and yet some high pressure regions. Dwarf galaxies do indeed have an erratic presence of massive clusters, some of which may be related to galaxy interactions (Billett et al. 2002).

7. Summary

Most stars form in clusters (Carpenter 2000; Lada & Lada 2003) and many of these clusters are close enough to high-pressure regions to look triggered. Triggering seems necessary because the dynamical pressures inside clusters are several orders of magnitude larger than the ambient interstellar pressure. The high pressure state of a cluster is an obvious remnant of its birth, but clues to the origin of the pressure are lost once the gas disperses and the stellar orbits mix. *The primary distinction between the formation of standard "open clusters" and the mere aggregation of stars in a compressibly turbulent medium is probably this last step of triggering.* HII regions did not compress gas to make Gould's Belt, but they did compress gas to make the Trapezium cluster in Orion.

The masses and positions of the clouds that are compressed into clusters seem to be the result of interstellar turbulence and shell formation. Turbulence structures the gas in two ways: by direct compression through random large-scale flows, and by moving pre-existing clouds around passively. This duality of processes follows from the multi-phase nature of the ISM and from the presence of self-gravity. Combine these with pervasive pressure bursts from massive stars and the result is a mode of star formation dominated by dense clusters.

References

Bally, J., Langer, W.D., Stark, A.A., & Wilson, R.W. 1987, ApJ, 312, L45

Bate, I.A., Bonnell, M.R., & Bromm, V. 2003, MNRAS, 339, 577

Billett, O.H., Hunter, D.A., & Elmegreen, B.G. 2002, AJ, 123 1454

Carpenter, J.M. 2000, AJ, 120, 3139

de Geus, E.J. 1992, A&A, 262, 258

Deharveng, L., Zavagno, A., Salas, L. et al.: 2003, A&A, 399, 1135

Dickey J., McClure-Griffiths N., Stanimirovic S. et al: 2001 ApJ 561, 264

Efremov, Y.N. 1995, AJ, 110, 2757

Efremov, Y.N., & Elmegreen, B.G. 1998, MNRAS, 299, 588

Elmegreen, B.G. 1983, MNRAS, 203, 1011

Elmegreen, B.G. 1994, ApJ, 433, 39

Elmegreen, B.G. 2002, ApJ, 577, 206
Elmegreen, B.G. & Elmegreen, D.M. 1987, ApJ**320**, 182
Elmegreen, B.G. & Elmegreen, D.M. 2001, AJ, 121,1507
Elmegreen, B. G., Kim, S., & Staveley-Smith, L. 2001, ApJ, 548, 749
Elmegreen, B.G. & Shadmehri, M. 2003, MNRAS, 338, 817
Elmegreen, D.M., Elmegreen, B.G., & Eberwein, K.S. 2002, ApJ, 564, 234
Elmegreen, B.G., Elmegreen, D.M., & Leitner, S.N., 2003, ApJ, 590, 271
Elmegreen, B.G., Leitner, S.N., Elmegreen, D.M., & Cuillandre, J.-C. 2003, ApJ, in press
Feitzinger, J. V. & Galinski, T. 1987, A&A, 179, 249
Goldman, I. 2000, ApJ, 541, 701
Gomez, M., Hartmann, L., Kenyon, S. J., & Hewett, R. 1993, AJ, 105, 1927
Grabelsky, D.A., Cohen, R.S., May, J. et al: 1987, ApJ, 315, 122
Heydari, M., Charmandaris, V., Deharveng, L. et al.: 2001, A&A, 372, 495
Hunter, D., Elmegreen, B.G., Dupuy, T., Mortonson, M. 2003, ApJ, in press
Kennicutt, R.C. 1998, ApJ, 498, 541
Kim, S., Dopita, M.A., Staveley-Smith, L., Bessell, M.S. 1999, AJ, 118, 2797
Kim, W.-T. & Ostriker, E.C. 2002, ApJ, 570, 132
Lada, C.J. & Lada, E.A. 2003, ARAA, in press.
Larsen, S. S. 2002, AJ, 124, 1393
Larson, R.B. 1995, MNRAS, 272, 213
Lazarian, A., Pogosyan, D., & Esquivel, A. 2002, ASP Conf. Proc. 276, Seeing Through the Dust, p. 182
Massey, P. & Hunter, D.A. 1998, ApJ, 493, 180
McKee, C.F. & Tan, J.C. 2003, ApJ, 585, 850
Rand, R.J. 1993, ApJ, 410, 68
Selman, F., Melnick, J., Bosch, G., & Terlevich, R. 1999, A&A, 347, 532
Stanimirovic S., Staveley-Smith L., Dickey J. et al: 1999 MNRAS 302, 417
Stützki, J., Bensch, F., Heithausen, A. et al.: 1998, A&A, 336, 697
Walborn, N.R., Barbá, R.H., Brandner, W. et al.: 1999, AJ, 117, 225
Whitmore, B. C. 2003, in STScI Symp. 14, A Decade of HST Science, ed. M. Livio, K. Noll, & M. Stiavelli (Baltimore: STScI), in press
Yamaguchi, R., Saito, H., Mizuno, N. et al.: 1999, PASJ, 51, 791
Yamaguchi, R., Mizuno, N., Onishi, T. et al.: 2001a, ApJ, 553, 185
Yamaguchi, R., Mizuno, N., Onishi, T. et al.: 2001b, PASJ, 53, 959
Yorke, H.W. & Sonnhalter, C. 2002, ApJ, 569, 846
Zhang, Q., Fall, S. M., & Whitmore, B. C. 2001, ApJ, 561, 727

Highlights of Astronomy, Vol. 13
International Astronomical Union, 2003
O. Engvold, ed.

"Super" Star Clusters

Richard de Grijs

Department of Physics & Astronomy, The University of Sheffield, Hicks Building, Hounsfield Road, Sheffield S3 7RH, UK

Abstract. The production of "super star clusters" (SSCs; luminous, compact star clusters) seems to be a hallmark of intense star formation, particularly in interacting and star-burst galaxies. Their sizes, luminosities, and mass estimates are entirely consistent with what is expected for young Milky Way-type globular clusters (GCs). SSCs are important because of what they can tell us about GC formation and evolution (e.g., initial characteristics and early survival rates). They are also of prime importance as probes of the formation and (chemical) evolution of their host galaxies, and of the initial mass function in the extreme environments required for cluster formation. Recent evidence lends support to the scenario that Milky Way-type GCs (although more metal rich), which were once thought to be the oldest building blocks of galaxies, are still forming today.

1. "Super" or normal?

One of the main contributions to date of the *Hubble Space Telescope (HST)* to the field of stellar populations in nearby galaxies has been the discovery of numerous dense stellar objects resembling star clusters with properties similar to those predicted for the progenitors of the old globular cluster (GC) population in the Milky Way and other nearby galaxies.

These objects are often confusingly referred to as "super star clusters" (SSCs), by virtue of their high luminosities and compact sizes. They have been found in a wide variety of galactic environments, ranging from quiescent dwarf and irregular or amorphous galaxies to large, gas-rich spiral galaxies involved in large-scale gravitational interactions and mergers, and in the star-burst events associated with them (see de Grijs, O'Connell, & Gallagher 2001 for an overview). However, the question arises of whether these objects are indeed "super" star clusters, in terms of either their integrated luminosity or their total mass. If they are indeed the progenitors of Milky Way-type GCs, assuming that they have the potential to survive for a Hubble time, then their high luminosities at their correspondingly young ages (of up to ~ 1 Gyr, in general) are simply conform the expectations of any modern flavor of simple stellar population theory.

Indeed, the mass distributions of most of these young star cluster populations do not extend significantly beyond that of the Milky Way GC population (which is generally used as a benchmark), with a few exceptions (e.g., NGC 7252-W3: Schweizer & Seitzer 1998, Maraston et al. 2001; NGC 6745: de Grijs et al. 2003c; some of the Antennae clusters, e.g., Mengel et al. 2002), although their existence might simply be due to stochastic effects. Nevertheless, the latter objects may therefore truly be super*massive* objects. With the exception of these few clusters, one should perhaps not consider the overall mass distribution of a given cluster population compared to that of the almost universal GC mass function in a wide variety of galaxies hosting such old objects, but instead consider these remarkable clusters in the context of their own parent population. This exercise leads us to realize that in a number of (predominantly) dwarf and irregular galaxies the overall cluster population is host to a few clusters that are significantly more massive than any of the other clusters (although not necessarily more massive than the high-mass wing of the Milky Way GC system), such as observed in NGC 1705 (NGC 1705-I, Ho & Filippenko 1996), NGC 1569 (SSCs A and B; see, e.g., Hunter et al. 2000, and Anders et al 2003 for comparative analysis in the context of the galaxy's overall cluster population), and M82 (M82-F; e.g., Smith & Gallagher 2001). Therefore, the assignation "super" appears to be merely a relative qualification.

In view of the confusing nomenclature, I will henceforth refer to these objects as *Young Massive Star Clusters (YMCs)*.

2. Survival to old age?

Although YMC populations are often assumed to be GC-type progenitors, their survival for a Hubble time is by no means guaranteed. In fact, this depends crucially on the slope of the stellar initial mass function (IMF) governing these clusters. High-resolution spectroscopy can – for the nearest YMC systems – be utilized to derive dynamical mass estimates and, combined with integrated luminosity measurements from e.g. *HST* imaging, one can derive mass-to-light (M/L) ratios for a small number of clusters at a time. In their comparison of the M/L ratios at the corresponding ages for a handful of the brightest YMCs, Smith & Gallagher (2001) and Mengel et al. (2002) showed convincingly that a number of them appear to have IMF slopes that are significantly too shallow for the clusters to survive for any longer than roughly the next Gyr. Thus, these objects are unlikely to become GC analogues.

Instead of going through the cumbersome exercise of measuring individual M/L ratios, one can approach this problem statistically, by analyzing the potential of a given cluster population to survive for a Hubble time. The currently most popular models for the dynamical evolution of star clusters predict that the power-law Cluster Luminosity Functions (CLFs) characteristic of YMC systems will be transformed rapidly into the universal Gaussian CLFs of old Milky Way-type GC systems. In a recent paper (de Grijs, Bastian, & Lamers 2003a; see also de Grijs, Bastian, & Lamers 2003b), we provided the first evidence for a turn-over in the intermediate-age, approximately 1 Gyr-old CLF in the center of the nearby star-burst galaxy M82, which very closely matches the universal CLFs of old Milky Way-type GC systems. This is likely to remain virtually unchanged for a Hubble time. We also showed that with the very short characteristic cluster disruption time-scale governing the center of M82 (de Grijs et al. 2003b), its cluster mass distribution will evolve towards a higher characteristic mass scale than for the Galactic GCs by the time it reaches a similar age. We argue, therefore, that this evidence, combined with the similar cluster sizes (de Grijs et al. 2001), lends strong support to a scenario in which the current central M82 cluster population will eventually evolve into a significantly depleted old Milky Way-type GC system dominated by a small number of high-mass clusters. This implies that GC progenitors, which were once thought to be the oldest building blocks of galaxies, are still forming today in galaxy interactions and mergers. However, they will likely be more metal-rich than the present-day old GC systems. This connection between young or intermediate-age star cluster systems and old GCs lends strong support to the hierarchical galaxy formation scenario.

M82's proximity, its shortest known cluster disruption time-scale of any galaxy, and its well-defined peak of cluster formation make it an ideal candidate to probe the evolution of its star cluster system to fainter luminosities, and thus lower masses, than has been possible for any galaxy before.

Acknowledgments. I acknowledge invaluable collaborations with Peter Anders, Nate Bastian, Uta Fritze–v. Alvensleben, Jay Gallagher, and Henny Lamers.

References

Anders, P., de Grijs, R., Fritze–v. Alvensleben, U., Bissantz, N. 2003, MNRAS, submitted

de Grijs, R., O'Connell, R.W., Gallagher, J.S., III 2001, AJ, 121, 768

de Grijs, R., Bastian, N., Lamers, H.J.G.L.M., 2003a, ApJ, 583, L17

de Grijs, R., Bastian, N., Lamers, H.J.G.L.M., 2003b, MNRAS, 340, 197

de Grijs, R., Anders, P., Bastian, N., Lynds, R., Lamers, H.J.G.L.M., O'Neil, E.J., Jr. 2003c, MNRAS, 343, 1285

Ho, L.C., Filippenko A.V. 1996, ApJ, 472, 600

Hunter, D.A., O'Connell, R.W., Gallagher, J.S., III, Smecker-Hane, T.A. 2000, AJ, 120, 2383

Maraston, C., Kissler-Patig, M., Brodie, J.P., Barmby, P., Huchra, J.P. 2001, A&A, 370, 176

Mengel, S., Lehnert, M.D., Thatte, N., Genzel, R. 2002, A&A, 383, 137

Schweizer, F., Seitzer, P. 1998, AJ, 116, 2206

Smith, L.J., Gallagher, J.S., III 2001, MNRAS, 326, 1027

Highlights of Astronomy, Vol. 13
International Astronomical Union, 2003
O. Engvold, ed.

Young Star Clusters: Progenitors of Globular Clusters!?

Peter Anders, Uta Fritze - v. Alvensleben

Universitäts-Sternwarte Göttingen, Göttingen, Germany

Richard de Grijs

Department of Physics & Astronomy, The University of Sheffield, UK

Abstract. Star cluster formation is a major mode of star formation in the extreme conditions of interacting galaxies and violent starbursts. Young clusters are observed to form in a variety of such galaxies, a substantial number resembling the progenitors of globular clusters in mass and size, but with significantly enhanced metallicity. From studies of the metal-poor and metal-rich star cluster populations of galaxies, we can therefore learn about the violent star formation history of these galaxies, and eventually about galaxy formation and evolution. We present a new set of evolutionary synthesis models of our GALEV code, with special emphasis on the gaseous emission of presently forming star clusters, and a new tool to compare extensive model grids with multi-color broad-band observations to determine individual cluster masses, metallicities, ages and extinction values independently. First results for young star clusters in the dwarf starburst galaxy NGC 1569 are presented. The mass distributions determined for the young clusters give valuable input to dynamical star cluster system evolution models, regarding survival and destruction of clusters. We plan to investigate an age sequence of galaxy mergers to see dynamical destruction effects in process.

1. Models & tests

We use our evolutionary synthesis code to study the basic physical parameters of star clusters in interacting galaxies and violent starbursts. The main ingredients are: stellar isochrones from the Padova group for metallicities in the range -1.7 $\leq$ [Fe/H] $\leq +0.4$, a stellar initial mass function (usually assumed to be Salpeter-like), the library of stellar spectra by Lejeune et al. (1997, 1998), and gaseous emission (both lines and continuum). From the integrated spectrum we derive magnitudes in a large number of filter systems. The gaseous emission contributes significantly to the integrated light of stellar populations younger than 3×10^7 yr both in terms of absolute magnitudes and derived colors (see Fig. 1 and Anders & Fritze - v. Alvensleben 2003). The updated models are available from **http://www.uni-sw.gwdg.de/~galev/panders/**

While star clusters can easily be approximated as simple stellar populations (SSPs; with all stars having the same age, metallicity and extinction), more complicated star formation / metallicity evolution histories of galaxies can be studied by superimposing appropriate SSPs.

We developed a tool to compare our evolutionary synthesis models with observed cluster SEDs to determine the cluster parameters age, metallicity, internal extinction and mass independently. Using artificial clusters with various input parameters (with SEDs taken directly from the evolutionary synthesis

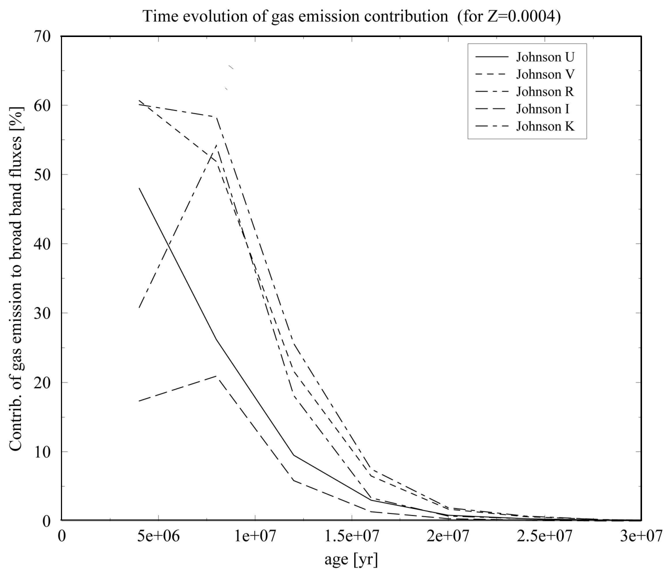

Figure 1. Contribution of gaseous emission to various standard Johnson magnitudes for metallicity Z = 0.0004 as a function of time.

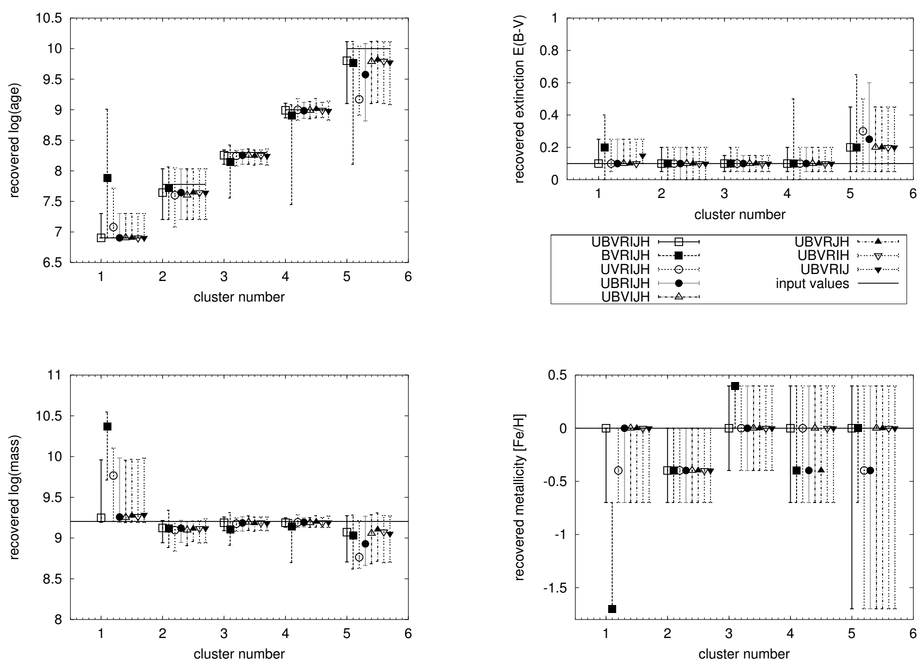

Figure 2. Dispersion of recovered properties of artificial clusters, assuming availability of *UBVRIJH* and using passband combinations consisting of 6 out of the available 7 pass bands for the analysis, as indicated in the legend. Input parameters for the artificial clusters are: solar metallicity, E(B-V) = 0.1 mag, ages = 8, 60, 200 Myr, 1, 10 Gyr.

models) we systematically studied the impact of the choice of pass bands, of finite observational photometric uncertainties, and *a priori* assumptions on our analysis results. One example of these tests is shown in Fig. 2. Additional tests were performed using broad-band observations for star clusters in NGC 3310 (de Grijs et al. 2003a,b), confirming the results from the artificial cluster tests. Due to the young age of this cluster system these additional tests are restricted to ages younger than approx. 200 Myr. From our tests we conclude that:

1. At least 4 pass bands are necessary to determine the 3 free parameters age, metallicity and extinction, and the mass by scaling the SED, independently.
2. The most important pass bands are the U and B bands; for systems older than roughly 1 Gyr the V band is equally important.
3. NIR bands significantly improve the results by constraining the metallicity efficiently.
4. A wavelength coverage as long as possible is desirable. Best is UV through NIR, thus tracing the pronounced kink/hook in the SEDs around the B band.
5. Large observational errors and/or wrong *a priori* assumptions may lead to completely wrong results.

2. The case of NGC 1569

As a first application the dwarf starburst galaxy NGC 1569 was chosen. Our sample enlarges the number of observed star clusters in this galaxy by a factor of 3. Our results for the physical parameters are in agreement with previous results of the starburst history in NGC 1569 in general, and of the two prominent "super star clusters" in particular, regarding age, mass and metallicity. In addition, we find a surprising change in the cluster mass function with age: The clusters formed during the onset of the burst (approx. 25 Myr ago) seem to exhibit an excess of massive clusters as compared to clusters formed more recently. Using various statistical methods we show the robustness of this result (Anders et al. 2003b).

3. References

Anders, P., Fritze - v. Alvensleben, U. 2003, A&A, 401, 1063
Anders, P., Bissantz, N., Fritze - v. Alvensleben, U., de Grijs, R. 2003a, MNRAS, *submitted*
Anders, P., de Grijs, R., Fritze - v. Alvensleben, U., Bissantz, N. 2003b, MNRAS, *submitted*
de Grijs, R., Fritze - v. Alvensleben, U., Anders, P., Gallagher, J. S., Bastian, N., Taylor, V. A., Windhorst, R. A. 2003a, MNRAS, 342, 259
de Grijs, R., Anders, P., Bastian, N., Lynds, R., Lamers, H.J.G.L.M., O'Neil, Jr., E.J. 2003b, MNRAS, 343, 1285
Lejeune, T., Cuisinier, F., Buser, R. 1997, A&AS, 125, 229
Lejeune, T., Cuisinier, F., Buser, R. 1998, A&AS, 130, 65

Highlights of Astronomy, Vol. 13
International Astronomical Union, 2003
O. Engvold, ed.

A New Scenario for the Formation of Massive Stellar Clusters

Jan Palouš

Astronomical Institute, Academy of Sciences of the Czech Republic, Boční II 1401, 141 31 Praha 4, Czech Republic

Guillermo Tenorio-Tagle, Sergiy Silich

Instituto Nacional de Astrofísica Optica y Electrónica, AP 51, 72000 Puebla, México

Gustavo A. Medina-Tanco

Instituto Astronômico e Geofísico, USP, Av. Miguel Stéfano 4200, 04301-904 Sao Paulo, Brazil

Casiana Muñoz-Tuñon

Instituto de Astrofísica de Canarias, E 38200 La Laguna, Tenerife, Spain

Abstract. A new scenario is proposed, in which the continuous creation of stars results into a highly concentrated massive (globular cluster-like) stellar system. We assume that the collapse of a massive cloud leads to the formation of first stars. Their winds and terminal supernova explosions create a standing, small radius, cold and dense shell, where the next stars form. The shell is in steady state location, which is due to a detailed balance established between the ram pressure from the collapsing cloud, the gravitational force exerted on the shell and the ram pressure of the stellar wind from the forming cluster. In this contribution we show that the standing shell remains stable against Rayleigh - Taylor instability, and discuss future prospects of this work.

1. Introduction

Our model invokes pressure-bounded, self-gravitating, isothermal cloud, which may become gravitationally unstable if sufficiently compressed (Ebert 1955; Bonner 1956) during galaxy versus galaxy collision, when the interstellar pressure increases by several orders of magnitude above its average value. The gravitational instability allows a large cloud ($M_{\rm c} \sim 10^4 - 10^6$ M$_\odot$) to enter its isothermal ($T_{\rm c} \sim 100$ K) collapse phase (Larson 1969), thereby developing a density and velocity structure with the following characteristics:

1. A central region of constant density (the plateau), where the infall velocity increases linearly from zero at the center, to a maximum value $v_{\rm max}$ at the boundary.

2. A region of increasing size and constant maximum infall velocity, $v_{\rm max}$, where the density falls off as R^{-2} (the skirt).

As the collapse proceeds and the density in region 1 becomes larger, the knee region in the density distribution, that separates zones 1 and 2, moves closer to the center of the configuration with an increasing speed. As the density in the plateau region increases, unstable fragments begin to form, and the first stellar generation is created in the 3D converging. From then onwards, stellar winds and supernova explosions will begin to have an important impact on the collapsing cloud. For this to happen however, massive stars ought to form in sufficient numbers as to jointly stop the infall at least in the most central regions of the plateau. Otherwise, individual stars, despite their mechanical energy input rate, will unavoidably be buried by the in-falling cloud, delaying the impact of feedback until more massive stars form.

2. The Factory

We assume that the first generation of massive stars is able to regulate itself by displacing and storing the high-density matter left over from star formation into a cool expanding shell, thereby limiting the number of sources in the first generation of stars. The shell will be driven by the momentum injected by the central wind sources and the stellar winds and radiation, which have been considered to interrupt the star formation, are trapped inside of the shell. The energy deposited by the first generation of massive stars causes the accumulation of the in-falling cloud into the standing shell, which becomes gravitationally unstable, creating the star forming factory. This model is described in greater details by Tenorio-Tagle et al. (2003).

In order to keep the shell at its standing location, the ram pressure exerted by the wind sources has to balance the in-falling gas ram pressure and the gravitational force exerted on the shell by the increasing mass of the central star cluster (see Fig. 1):

$$4\pi R_{\rm k}^2 \rho_{\rm w} v_{\rm w}^2 = 4\pi R_{\rm k}^2 \rho_{\rm k} v_{\rm max}^2 + \frac{G M_{\rm sh} M_{\rm sc}}{R_{\rm k}^2}, \qquad (1)$$

where $R_k,\ \rho_k$ are the radius and the density at the knee and $\rho_w,\ v_w$ are the density and velocity of the stellar wind. The central star cluster mass is

$$M_{\rm sc} = 4\pi R_{\rm k}^2 \rho_{\rm k} v_{\rm max} t, \qquad (2)$$

and the mass of the shell is

$$M_{\rm sh} = 4\pi R_{\rm k}^2 \Sigma_{\rm sh}, \qquad (3)$$

where $\Sigma_{\rm sh}$ is the shell surface density and t is the evolutionary time. Inserting (2) and (3) into eq. (1) we get

$$\rho_w v_w^2 = \rho_k v_{max}^2 + 4\pi G \rho_k \Sigma_k v_{max} t. \qquad (4)$$

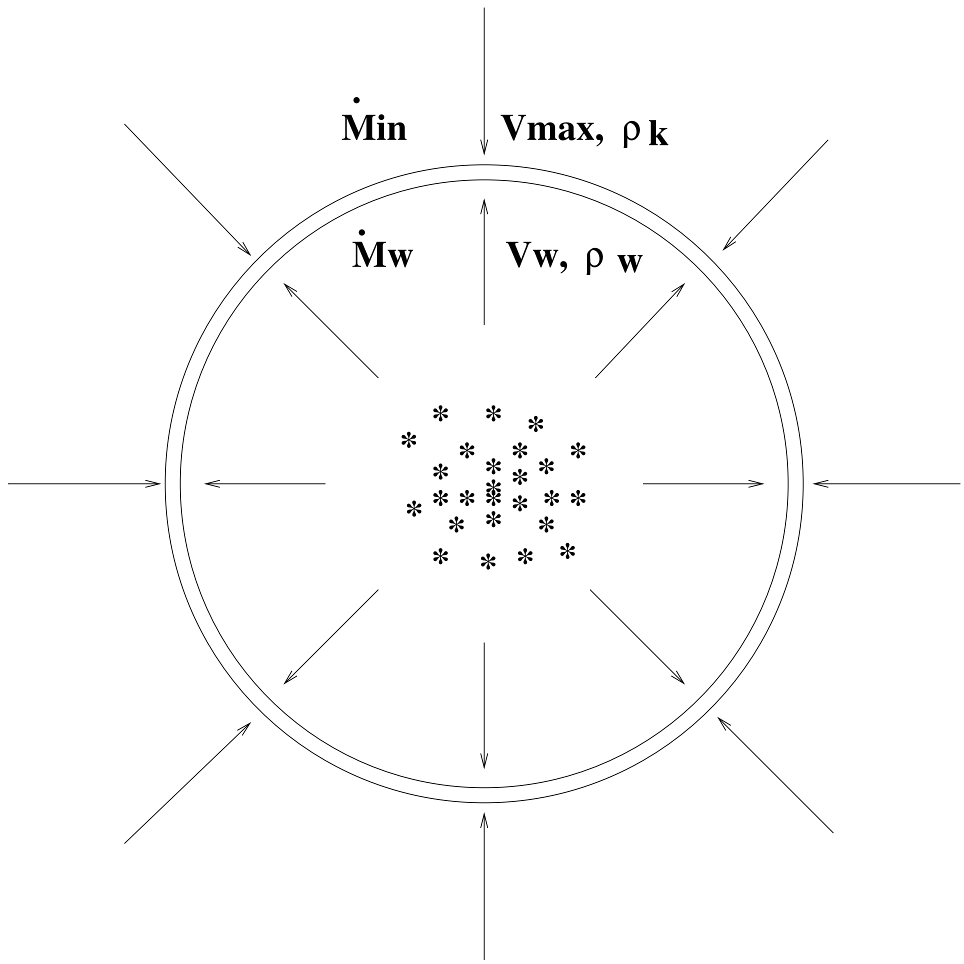

Figure 1. The standing shell inside of a collapsing cloud

The first and the second terms on the right-hand side of Eq. (4) show that after

$$t \geq v_{\rm max}/(4\pi G \Sigma_{\rm sh}) \approx 10^4 - 10^5 {\rm yr} \tag{5}$$

the infall ram pressure becomes negligible compared to the gravitational pull provided by the forming cluster. Thus the shell becomes gravitationally bound with its mechanical equilibrium simply given by the equation

$$4\pi R_{\rm k}^2 \rho_{\rm w} v_{\rm w}^2 = \frac{G M_{\rm sh} M_{\rm sc}}{R_{\rm k}^2}. \tag{6}$$

The density of the shocked wind is larger than that of the shocked in-falling cloud, which shows that the shell remains stable against Rayleigh - Taylor modes.

3. Future prospects

The influence of the density and the velocity perturbations from spherically symmetric infall of the collapsing cloud is one issue to be solved in the future. Another important issue to be addressed is the rotation and angular momentum distribution in the collapsing cloud leading to large scale deviations from the spherical symmetry, and how this asymmetry influences the forming stellar cluster.

References

Bonner, W. B. 1956, MNRAS, 116, 351

Ebert, R. 1955, Z. Astrophys., 36, 222

Larson, R. B. 1969, MNRAS, 145, 271

Tenorio-Tagle, G., Palouš, J., Silich, S., Medina-Tanco. G. A. & Muñoz-Tuñon, C. 2003, A&A, in press, astro-ph/0308340

Highlights of Astronomy, Vol. 13
International Astronomical Union, 2003
O. Engvold, ed.

Mass Loss, Kinematics, & Evolution of Super Star Clusters in the Antennae

Andrea M. Gilbert

Max-Planck Institut für extraterrestrische Physik, Postfach 1312, D-85748 Garching, Germany

James R. Graham

University of California, Berkeley, CA 94720-3411, USA

Abstract. The youngest super star clusters (SSCs) in the merging Antennae Galaxies (NGC 4038/39) drive supersonic mass-loaded outflows from the HII regions in which they are embedded. High-resolution K-band Keck/NIRSPEC spectroscopy reveals broad, spatially extended Brγ emission in 16 targets. Simple wind models for the line profiles provide good fits and imply cluster mass-loss rates of up to 1.5 $M_\odot$/year and terminal velocities of up to 205 km s^{-1}. The emission-line clusters (ELCs) that drive these outflows constitute at least 15% of the star formation rate in the Antennae, and their high star formation efficiencies imply that they will probably evolve into bound SSCs. The youngest ELC outflows, which are driven primarily by stellar winds, very efficiently entrain ambient matter. The cluster winds transfer or dissipate a large fraction of their energy and momentum in a hot or cool medium that does not emit Brγ. ELCs are the individual engines that power galactic-scale superwinds, viewed in their earliest evolutionary stage.

1. Emission-Line Clusters in the Antennae

Star formation in starbursts creates massive young super star clusters (SSCs) that are not often found in more quiescent environments. Their high masses and stellar densities resemble those of globular clusters (GCs), though their ages are measured in Myr rather than Gyr. This suggests an evolutionary sequence in massive star-forming regions: GCs may evolve from SSCs, whose precursors are ultra-dense compact H II regions detected in radio surveys (e.g. Johnson et al. 2003 and references therein). In order to study their nebular kinematics, we conducted a K-band spectroscopic survey of a sample of the youngest SSCs in the nearby merger NGC 4038/39, the Antennae Galaxies, whose large SSC population is well-studied (e.g. Whitmore & Zhang 2002). We discovered broad, supersonic Brγ lines in Keck/NIRSPEC echelle spectra of 16 of 17 targets (Gilbert 2002). The Brγ profiles are well resolved (spectral resolution was 12 km s^{-1}), have widths of 60–105 km s^{-1} FWHM, and exhibit high-velocity non-Gaussian wings (Fig. 1) We refer to these broad-line SSCs as emission-line clusters (ELCs). Turner et al. (2003) also found an ELC in NGC 5253.

Giant extra-galactic H II regions (GHIIRs) are characterized by supersonic line widths as large as the lowest ELC widths (Smith & Weedman 1970) as well as large sizes ($d > 100$ pc) and Lyman continuum fluxes of order Q = 10^{51} s^{-1}. ELCs are typically more compact ($d \sim 40 - 80$ pc) and brighter, with Q = $10^{51} - 10^{53}$ s^{-1}. GHIIR recombination line fluxes are positively correlated

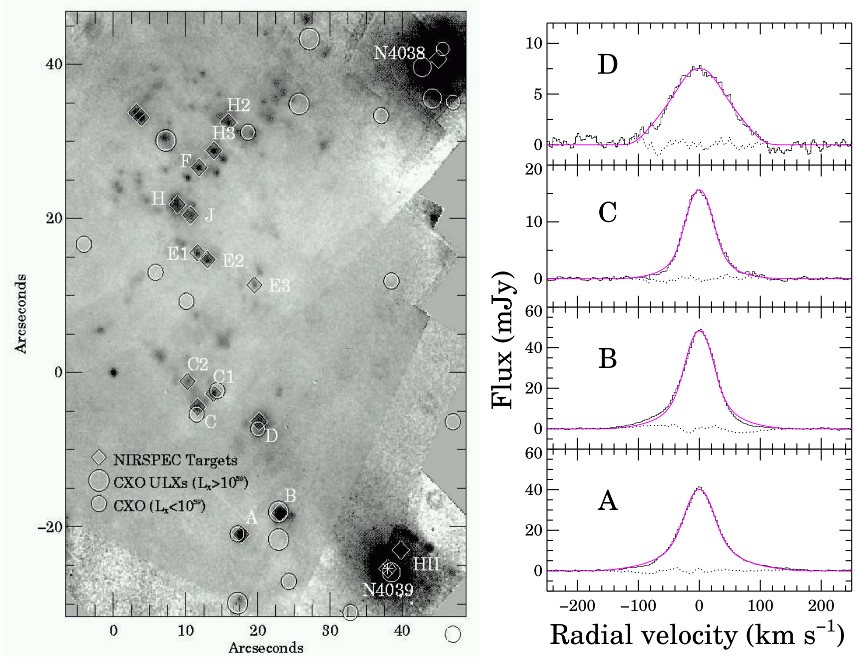

Figure 1. Left: K-band mosaic of the central region of the Antennae identifies ELCs and positions of Chandra sources (Zezas et al. 2002). Right: Supersonic Brγ profiles of four ELCs with over-plotted wind models and fit residuals.

with their line widths (e.g. Fuentes-Masip et al. 2000), and ELCs display the same correlation, extending it to larger line fluxes and widths (Gilbert 2002). GHIIRs and ELCs excite similar quantities of gas ($10^5 - 10^6$ M$_\odot$) but the mean emissivity-weighted gas density in an ELC is several orders of magnitude higher than that in GHIIRs (Gilbert 2002). This may be due to higher pressure in the interstellar medium (ISM) of a merger than in a typical galactic disk.

Brγ line fluxes and K magnitudes imply ELC ages of 3–8 Myr and masses of $10^5 - 10^7$ M$_\odot$ with the help of Starburst99 models (Leitherer et al. 1999). IR spectroscopy and radio recombination line fluxes yield $A_K = 0.2 - 1.1$ mag for some ELCs (Gilbert 2002 and references therein). Comparing the virial line widths (from ELC masses and sizes) with observed ones suggests that much of the gas in ELC outflows is unbound.

A massive stellar cluster produces X-rays due to colliding stellar winds and X-ray binaries (XRBs). A model for the X-ray emission of an ELC produces values comparable with Chandra fluxes near Eddington for ELCs with likely X-ray counterparts (Fig. 1; Zezas et al. 2002), but not for the ULX that appears coincident with ELC B and thus must be a more exotic object, e.g. beamed XRB or intermediate-mass black hole (Gilbert 2002).

2. Mass-Loaded Outflows from Emission-Line Clusters

In order to determine the mass-loss rates of ELCs, we model their supersonic Brγ profiles with a semi-empirical β-wind law. This velocity law is predicted and

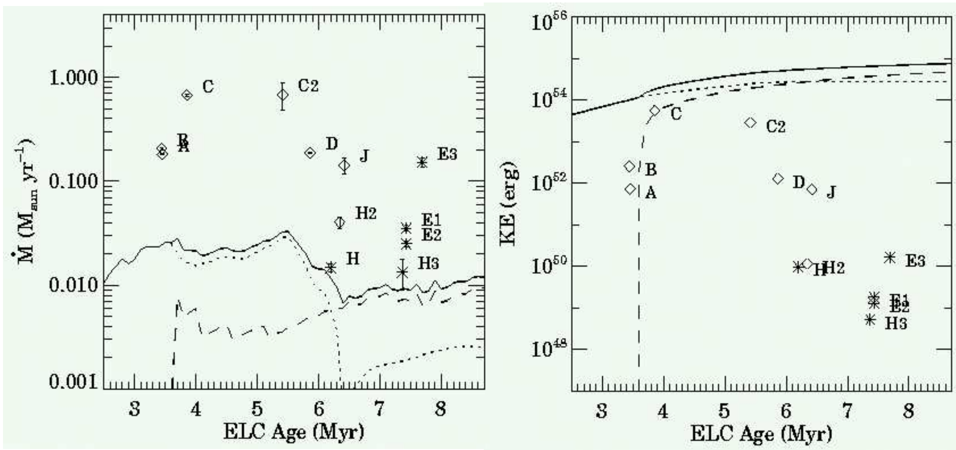

Figure 2. Mass-loss rates (left) and kinetic energy (right) measured for ELC outflows (points, normalized to a 10^6 $M_\odot$ cluster). Curves are predictions from Starburst99 models (Leitherer et al. 1999) for a cluster's stellar winds (dotted), SNe (dashed), and their sum (solid). ELC outflows display much higher $\dot{M}_{\rm HII}$ and lower KEs than models predict, suggesting efficient mass loading and thermalization of KE.

observed for radiation-driven wind lines of hot stars (Kudritzki & Puls 2000), but we find that it also provides an excellent semi-empirical model for our data. We parameterized the line profile models with six unknowns: inner and outer wind radii r_0 and r_1, mass-loss rate $\dot{M}_{\rm HII}$, the power-law slope β for the velocity law $v(r) = v_\infty \left(1 - b\frac{r_0}{r}\right)^\beta$ where $b \equiv 1 - [v(r_0)/v_\infty]^{\frac{1}{\beta}}$, adopted for the line-emitting gas, and the terminal velocity of the wind v_∞. The Doppler broadening parameter of the gas for a Gaussian line profile, $v_D = \sqrt{2}\sigma = \sqrt{2kT/\mu} = 16.3$ km s^{-1}, is fixed at that of a 10^4 K plasma. We fixed the wind velocity at r_0, v_0, equal to v_D, since it tends to be comparable with v_D and has little effect on the profile (Kudritzki & Puls 2000). Assuming a constant mass-loss rate ($\dot{M}_{\rm HII} = 4\pi r^2 \rho v$), the velocity law and $\dot{M}_{\rm HII}$ prescribe a density law $\rho(r)$ for the emitting gas. With this recipe we can compute the Brγ flux from the flow as a function of radial velocity, and compare the resulting line profile with the observed one. The predicted line profiles have broad non-Gaussian wings and provide excellent fits to the observed line profiles (Fig. 1).

The mass loss rates values derived from the β model range over $0.006 - 1.5$ $M_\odot$ yr^{-1}. The most powerful ELC outflow has an observed mass-loss rate that is equivalent to the combined winds of about 10^6 O stars or 10^4 WR stars. At an age of 3 Myr a 10^6 $M_\odot$ cluster has about 350 WR stars and 4500 O stars for a Salpeter IMF ($1-100$ $M_\odot$, Starburst99 model), which provide a total mass-loss rate in wind ejecta that is nearly two orders of magnitude lower than inferred from our Brγ profile models. We detect much more out-flowing photoionized gas than is ejected directly from stars; thus *ELC outflows efficiently entrain matter.* This effect is also observed in starburst superwinds (e.g. NGC 1569, Martin, Kobulnicky, & Heckman 2002), which are powered by the joint energy input from many clusters into the ISM.

The terminal velocities of ELC outflows range from a few times the sound speed up to 200 km s^{-1}, significantly less than terminal velocity of a single O star wind, a few 1000 km s^{-1}. This provides another indication that we are not directly observing mass loss from hot stars. The low terminal velocities may be due to the interaction in close quarters of many individual winds, photo-evaporative flows, (in older clusters) supernova explosions, and ultimately the collision with ambient neutral gas that the outflow encounters and entrains.

The discrepancy between observed $\dot{M}_{\rm HII}$ and predicted stellar mass loss due to winds and supernovae (SNe) decreases with increasing cluster age, shown in Fig. 2 for all ELCs (normalized to a mass of 10^6 $M_\odot$). Either older ELCs entrain matter less efficiently, or they have swept away most of their reservoir of neutral gas. Fig. 2 also displays the measured and predicted kinetic energies (KEs) of the outflows. In Brγ we detect only a small fraction of the KE available from winds and SNe; the rest must reside in a hotter and/or cooler medium. Stellar wind shocks generate X-rays, and Chandra observations reveal possible counterparts for some ELCs (e.g. Zezas et al. 2002). Efficient thermalization of mechanical energy in a starburst is a necessary condition for generating a large-scale superwind, the earliest phase of which may be taking place in the Antennae.

The star-formation rate (SFR) in our small sample of ELCs is 4 $M_\odot$ yr^{-1} (nearly half of this in a single ELC), so ELCs comprise at least 15% of the total SFR in the Antennae. A simple estimate of ELC star-formation efficiencies gives values of 30–70%, suggesting that they stand a good chance of becoming bound SSCs, which in turn may evolve into GCs (Gilbert 2002).

References

Fuentes-Masip, O., et al. 2000, AJ, 120, 752
Gilbert, A. M. 2002, Ph.D. Thesis (University of California, Berkeley)
Johnson, K. E., Indebetouw, R., & Pisano, D. J. 2003, AJ, 126, 101
Kudritzki, R. & Puls, J. 2000, ARA&A, 38, 613
Leitherer, C., et al. 1999, ApJS, 123, 3
Martin, C. L., Kobulnicky, H. A., & Heckman, T. M. 2002, ApJ, 574, 663
Smith, M. G. & Weedman, D. W. 1970, ApJ, 161, 33
Turner, J. L., et al. 2003, Nature, 423, 621
Whitmore, B. C., & Zhang, Q. 2002, AJ, 124, 1418
Zezas, A., Fabbiano, G., Rots, A. H., & Murray, S. S. 2002, ApJ, 577, 710

Acknowledgments. We thank the Hawaiian community for the opportunity to observe on Mauna Kea and the staff of the Keck Observatory for assistance therein. This work was supported in part by a NASA GSRP Fellowship and NSF grants AST-0205999 and AST-9876783.

Highlights of Astronomy, Vol. 13
International Astronomical Union, 2003
O. Engvold, ed.

Contributed Papers for JD11: Abstracts

The Dynamical Evolution of Globular Clusters in the Galaxy

Wu, Zhen-yu & Shu, Cheng-gang (National Astronomical Observatories, Chinese Academy of Sciences)

Abstract. Given various initial conditions, the dynamical evolution of globular clusters in our Galaxy is investigated in detail by means of Monte Carlo simulations. Four dynamic mechanisms in the present paper are considered. They are the stellar evaporation in the tidal field, the stellar evolution during the early evolutionary stage, the tidal shocks due to clusters passing through the bulge and disk, and the dynamical friction. Comparing with the current observations, which include the number density distribution in space, mass function, etc., the so-called standard modes for both the power law and Gaussian cluster initial mass functions are selected among many runs of simulations. The deviation from the standard modes, which is resulted from the change of the parameter for the initial conditions, is discussed in detail. The discussion of the model parameters is also presented although they are adopted as the typical values based on previous work. Based on our simulations, some relevant discussions about the mass contributions to the Galactic central region and stars in the halo due to the dynamic evolution of globular clusters are also qualitatively presented.

A Hybrid Monte Carlo Tool to Simulate Dense Stellar Systems

Giersz, Mirek; Spurzem, Rainer & Lin, Doug (Nicolaus Copernicus Astronomical Center, Polish Academy of Sciences)

Abstract. Spherically symmetric star clusters containing a large amount of primordial binaries or planetary systems are studied using a hybrid method, consisting of a gas dynamical model for the single stars and a Monte Carlo treatment for relaxation of binaries and their interactions with other stars and binaries. Each binary encounter is investigated by means of a highly accurate direct few-body integrator (adopted from NBODY6++). The evolution of individual binary and planetary orbital parameters can be directly followed and the cross sections for interesting physical processes involved binaries can be computed. Cross sections are obtained from a sampling of several hundred thousands of scattering events as they occur in a real cluster evolution including mass segregation of binaries, gravothermal collapse and re-expansion, binary burning phase and gravothermal oscillations. For the first time we are able to present empirical cross sections for eccentricity variation of binaries in close three- and four-body encounters. It is found that a large fraction of four-body encounters results in merging. We are also able, for the first time, to follow the changes of orbital parameters of primordial planetary systems in the course of cluster evolution.

General Solution for Hydrodynamical Equations

Otarod, Saeed & Ghanbari, Jamshid (Razi University)

Abstract. We will apply a new mathematical method (introduced by the authors) to solve the nonlinear hydrodynamical equations Governing the opti-

cally thin interstellar media in one dimension. Although a simple example have been chosen, But it is very instructive. In this simple example we will discuss about cases that we way substitute an ordinary equation for continuity equation. we also will prove that the same can be done to equation of motion and energy equation. As a conclusion we will show that the results of this research can have a wide application in all areas of Physics and nonlinear mathematics. It seems that in many cases we are not obliged to make use of numerical calculations and a great number of nonlinear important physical equations can be solved analytically in their most general form.

Dynamical Friction on Star Clusters Near the Galactic Center

Kim, Sungsoo & Morris, Mark (Kyung Hee University, Korea)

Abstract. Numerical simulations of the dynamical friction suffered by a star cluster near the Galactic center have been performed with a parallelized tree code. Gerhard (2001) has suggested that dynamical friction, which causes a cluster to lose orbital energy and spiral in towards the galactic center, may explain the presence of a cluster of very young stars in the central parsec, where star formation might be prohibitively difficult owing to strong tidal forces. The clusters modeled in our simulations have an initial total mass of 10^5-10^6 Msun and initial galacto-centric radii of 2.5-30 pc. We have identified a few simulations in which dynamical friction indeed brings a cluster to the central parsec, although this is only possible if the cluster is either very massive (10^6 Msun), or is formed near the central parsec (¿ 5 pc). In both cases, the cluster should have an initially very dense core (10^6 Msun pc^{-3}). The initial segregation of massive stars into the cluster core can help achieve the requisite density, and can help account for the observed distribution of HeI stars in the central parsec.

Distribution, Orbits and Dynamics of Globular Clusters

Zhou, Hongnan & Huang, Keliang (Physics Dept. of Nanjing Normal University, Nanjing, China)

Abstract. We have compiled the samples of the 29 F globular clusters from Harris?s ?Catalog of parameters for Milky Way globular clusters? (1999) and other sources. According to the azimuth coordinates, distances from Sun, radial velocities and proper motions of the sample clusters, we have integrated orbits assuming three different galactic potential models and have calculated orbital parameters. The uncertainties associated with the orbital parameters are produced by Monte Carlo simulation, the relationship between the distributive morphologies of the orbital parameters and the initial observational errors as well as the different galactic potential models are discussed. We investigate the effect of the orbital motion on the internal dynamics of clusters samples, the results of our investigation show that the two-body relaxation is more important than tidal shocking.

Diagnostics of Accretion Disc in AGN

Borah, Surendra Nath & Duorah, Hira Lal (DKD College & Dergaon)

Abstract. The active galactic nuclei (AGN) are the most luminous objects in the universe. Total power radiated by an AGN is greater than the total power emitted by all the stars in the host galaxy.The direct diagnostics of the conditions within AGNs come from radiations produced by a wide variety of mechanisms including high energy gamma ray processes, atmospheric re processing, dust emissions, and synchrotron radiation. In addition to optical and X-ray photons,the emission includes MeV, GeV and also TeV gamma rays. We have considered that AGNs are powered by an accretion disc around a supermassive black hole of 10^{08} solar mass. The structure and heights from the central plane of an accretion disc around such a black hole depends on the composition of disc material,accretion rate, self gravity,and magnetic field in the accreting material. We have considered three types of composition of the disc material: 1. X= 0.600; Y= 0.380; Z= 0.020, 2. X= 0.700; Y= 0.280; Z= 0.020, 3. X= 0..800; Y= 0.199; Z= 0.001, X,Y,and Z represent hydrogen,helium and metal abundances respectively and the three accretion rates are 0.01,0.001, 0.005 solar mass per year respectively. The result shows that the disc height decreases as the accretion rate decreases.

Towards the Formation Problem of Dense Stellar Systems

Nuritdinov, S. & Mirtadjieva, K. (Astron. Department, National University of Uzbekistan)

Abstract. Two possible formation models of dense stellar systems (DSS) are considered. According to one of these models cold initial conditions can stimulate a collapse and bring to the DSS at least in central region of the system. The stability problem of the collapse is also studied. New asymptotic unknown in cosmology is found. In the frame of other model it is revealed the regions on the diagram "virial ratio - rotation parameter", which are connected with the formation of the DSS.

Close Encounters and a Black Hole in the Globular Clusters

Ashurov, Abdikul (Ulugh Beg Astronomical Institute of the Uzbek Academy of Sciences)

Abstract. It is known that the presence of a black hole in the globular cluster (GC) affects the stellar density profile and the central stellar dynamics. In this paper a problem of the dynamical evolution under close encounters in the GC, where a black hole is present, is considered. Since the evolution temp depends on the rate of the stellar encounters, an exact expression for the probability of encounters with given changes of energy integral and angular momentum per unit mass is determined assuming an anisotropic field star distribution function. It is used as a core of the collisional term of the Boltzman's equation. A behavior of the probability density in a globular cluster with and without a black hole has been studied for Plummer and King-Michie models in the isotropic and anisotropic cases. Because of this method takes weak as well as close encounters into account, it is more general method than Fokker-Planck one.

Massive Star Cluster Birth and the Morphology of Galaxies

Kroupa, Pavel (University of Kiel)

Abstract. Most stars form in embedded star clusters with low star formation efficiencies. When the gas is expelled a large fraction of the stellar population expands outwards into the field of the host galaxy. The implications this process

has on the morphological appearance of galaxies will be addressed using the example of thickened galactic disks.

The Masses and Stellar Content of Nuclear Star Clusters

Ho, Luis (Carnegie Observatories)

Abstract. Central nuclear star clusters are very common in late-type spiral galaxies; approximately80contain such clusters. Central star clusters may be related to the formation of seed massive black holes and the secular build up of bulges. However, very little is known about their physical properties, including their ages, chemical composition, and mass. We present deep high-resolution spectra of nuclear star clusters to determine their internal velocity dispersions and virial masses, and medium-resolution spectra to determine their stellar ages and metallicities. These fundamental parameters will help elucidate the nature of these objects and their relation to the global evolution of galaxies.

The Initial Mass Function of Star Cluster Systems

Fritze - v. Alvensleben, Uta; De Grijs, Richard & Anders, Peter (Universitaetssternwarte Gö ttingen, Germany)

Abstract. It is well-established that the Globular Cluster (GC) System of the Milky Way has lost about 50population over a Hubble time. Details about the initial distributions of GC masses, concentrations, metallicities, positions and orbits are difficult to reconstruct. Since star cluster formation appears to be the dominant mode of star formation in massive interacting gas-rich starburst galaxies, this allows us to at least assess the initial Mass Function (MF) of such star cluster systems "observationally". Luminosity functions are strongly distorted with respect to MFs due to age-spread effects in combination with strongly age-dependent M/L-ratios for young star clusters. Hence, we developed techniques to independently determine individual cluster ages, metallicities, and extinctions from a UV-optical-NIR comparison of model and observed spectral energy distributions, from our ASTROVIRTEL-project (European HST archive research). Initial star cluster MFs and MFs for cluster systems of older ages are presented. We anticipate that our results will provide valuable input and boundary conditions for dynamical GC evolution and destruction models.

Radiation-Hydrodynamic Formation of Massive Black Hole

Kawakatu, Nozomu & Umemura, Masayuki (Center for Computational Physics, University of Tsukuba)

Abstract. A novel mechanism to build up a massive black hole is proposed based on the relativistic radiation-hydrodynamic model. In the present scenario, the mass of a black hole is predicted to be in proportion to the bulge mass, and it is found that the BH-to-Bulge mass ratio is basically determined by the nuclear energy conversion efficiency from hydrogen to helium(=0.007). Also, we find that the radiation drag works effectively in forming a BH even in a small spheroidal system, but the mass of BH in globular cluster is closely related to its star

formation history. In addition, we reveal relationship between the morphology of galaxy and the mass of black hole.

Morphology of Galactic Open Clusters

Chen, Chin-wei & Chen, Wen-ping (Graduate institute of Astronomy, National Central University)

Abstract. Thirty six open clusters were selected from the 2MASS database on the basis of the latest open cluster catalogue (Dias et al 2002). The morphological parameters such as eccentricity, orientation were obtained via isodensity elliptic fitting. Most star clusters are elongated, and the eccentricity is correlated with z as an indication of the influence of the Galactic disk. The morphology shows clear evidence of competing internal dynamics and external Galactic disturbances when a cluster becomes 10 Myr old.

The Initial Violent Dynamics of Globular Clusters

Miocchi, Paolo & Capuzzo Dolcetta, Roberto (Universita' di Roma, Dipartimento di Fisica)

Abstract. In order to investigate some relevant aspects of globular clusters formation, we studied numerically the dynamics of a self-gravitating stellar system of the size of a typical globular cluster, starting from non-equilibrium and 'cold' initial conditions. Such conditions are, indeed, those expected after the formation of the stellar system, i.e. after the complete exhaustion of primordial gas through the gas-star phase transition which occurred on the star-formation time scale. Our (preliminary) results allow to draw some meaningful conclusions about the evolution of the distribution function toward a meta-stable state, by mean of the quick 'violent relaxation' of the whole system (core formation, mass segregation, anisotropy...). To this virialized state follows the, well known, further evolution caused by star-star encounters. We underline that the initial 'violent' dynamics can be well investigated by mean of codes (like our own tree-code) which are efficient in the representation of the time evolution driven by the quick mean-field variations, even if the individual 2-body close interactions (which are not really relevant in this phase) are not followed in detail.

Globular Cluster Merging in the Inner Galactic Region

Capuzzo-Dolcetta, Roberto A; Di matteo, Paola and Paolini Stefano (Dep. of Physics, University of Roma La Sapienza)

Abstract. The dynamics of the encounter of two globular clusters, made up of 10^5 stars each, in the bulge of an elliptical galaxy, has been followed up to 15 orbital periods ($1.7{*}10^7$ years) by mean of a direct summation code. Aim of these simulations is to understand whether the merging of a group of globular clusters in a unique stellar system is possible in the central regions of galaxies, before the strong coupled bulge-nucleus [Image] tidal actions destroy them. As a matter of fact, three dynamical mechanisms act in competition during the merging of two globular clusters. The galactic tidal action tends, on one side, to break up clusters before they form a unique self-gravitating system; on the other side, the same tidal force has also the effect to convert translational kinetic energy into internal random motion, thus leading, slowly, clusters to inner

galactic regions. Additionally, the dynamical friction caused by the stellar field decelerates significantly the cluster orbital decay. Due to the non-linearity of the interactions among these mechanisms, reliable results can be achieved just via detailed numerical simulations, as those we present here.

Statistical Study of Blue Straggler Properties in GGC

De Angeli, Francesca & Piotto, Giampaolo (Astronomy Department of Padova University)

Abstract. In this poster we report on the most significant results from a statistical analysis of the main properties of globular cluster blue straggler stars (BSS) extracted from the HST snapshot database of photometrically homogeneous color-magnitude diagrams (Piotto et al. 2002). The BSS relative frequency presents a significant anticorrelation with the collisional rate and with the cluster total absolute luminosity.

Dynamical Friction Acting on a Dissolving Globular Cluster

Fellhauer, Michael (Institut für Theoretische Physik und Astrophysik)

Abstract. We want to investigate with high-resolution N-body calculations the strength of the dynamical friction acting on a globular cluster sinking into the dense center of the Milky Way. On its way to the center of the Galaxy the cluster looses mass efficiently due to tidal forces and it is still unclear how this mass-loss affects the time-scale of dynamical friction. The ultimate aim of this study is to investigate if and how quickly globular clusters sink to the center of the Milky Way and deposit their stars there.

Blue Stragglers in M67: Evidence of Primordial Triples?

Kiseleva-Eggleton, Ludmila & Eggleton, Peter (St. Mary's College of California)

Abstract. At present there are between 18 and 40 (depending on the criteria used) identified blue stragglers (BS hereafter) in M67. Among these BSs are single stars, single-lined (SB1 hereafter) and double-lined spectroscopic binaries, eclipsing binaries and even a triple system S1082. There are three main channels that allow binaries to produce BSs: (*i*) very close binaries → semi-detached binaries → contact binaries → merger into a single star; (*ii*) moderately close binaries → semi-detached binaries (Algols) → post-Algols; (*iii*) collision of the components of a close binary, when perturbed dynamically by another star or binary. The first and second can produce binary BSs, and the first and third can produce single BSs. EV Cnc (S1036) - a BS eclipse - looks like a good example of channel (i), part-way through the contact phase and heading for a merger. Unfortunately the eclipses are shallow, and so it is hard to analyze definitively, e.g. whether it is in contact, semi-detached or even detached. The same mechanism might account for some single BSs as well. We should probably expect comparable numbers, as the merger time scale is roughly the magnetic-braking time scale, and this appears to be comparable to the nuclear time scale at these low masses. S1284 (a sort-period SB1 with $P = 4.2$d, $e = 0.26$) is a possible candidate for channel (ii), although the eccentricity is remarkable. Perhaps it suffered a moderate dynamical encounter that de-cirularized the orbit once mass transfer was finished. Four known SB1s have $P \sim 850 - 5000$d. It is hard to believe that these wider SB1s are the remains of mass transfer. We expect very

non-conservative Roche-lobe overflow (RLOF) in the wider binaries, so that the gainer is not able to become very much bluer than the loser was originally. At $P \sim 3000 - 5000$d we expect little or no mass transfer. The mechanism of dynamically-forced collisions with mergers seems the most promising (or least unpromising) for such systems. But it means presumably that the BSs which are now wide SB1s were **previously triple**. One BS (S1082) is currently triple; not only that but *two* of the three components are BSs! Perhaps what we need in this case is a collision between two triples. The close pair in each was forced into collision, one star was ejected, and one of the two third bodies remained in a fairly close orbit around one of the merged pairs. Although triples can be produced in a cluster by dynamical interactions, such triples usually are destroyed again later. We need a population of **primordial triples**, where the outer orbit is sufficiently small ($\sim 1 - 30$yr) that the triple can survive a long time. Such systems constitute $1 - 3\%$ of the solar neighborhood. This does not seem enough to have much influence in producing BSs. But triples ought to tend to migrate towards the center of a cluster and so should be particularly prone to interact with binaries and with each other. They also have larger interaction cross-sections.

An N-Body Model of the Hyades

Madsen, Søren (Lund Observatory)

Abstract. The three-dimensional structure and kinematics of the Hyades cluster as seen by Hipparcos are compared with realistic N-body simulations using the NBODY6 code. Stars are selected from the model in a way that resembles the Hipparcos observations of the cluster. Attempts to detect a correlation between the velocity dispersion and cluster radius or stellar mass using observational data from the Hipparcos and Tycho-2 Catalogues are inconclusive, but the fit of the N-body model to the observations of the cluster structure indicates that the current cluster velocity dispersion decreases from 0.35 km/s at the cluster center to a minimum of 0.20 km/s at 8 pc radius (2-3 core radii), from where it slightly increases outwards. A clear negative correlation between dispersion and stellar mass is seen in the central part of the cluster but is almost absent beyond a radius of 3 pc. With GAIA astrometry it will be possible to investigate the structure, velocity field, IMF, binary properties etc. of the entire entire Hyades (excluding sub-stellar objects). This detailed dynamical knowledge suggests that the Hyades can be used as a calibrator for N-body models in the future.

An Overview (Introductory Notes on Dense Stellar Systems)

Spurzem, Rainer (Astronomisches Rechen-Institut)

Abstract. An Overview on Dense Stellar Systems is given - relevant time scales for young massive or old globular star clusters are reviewed and compared to the different conditions in dense galactic nuclei, possibly with one or more massive black holes. It is discussed, how our physical knowledge depends on the advancement of computing and simulation techniques and the underlying physical methods. Different methods, such as direct N-body, gaseous or Fokker-

Planck models are discussed and compared and recent theoretical developments are highlighted.

The Wake of a Body Moving Through a Stellar Distribution

Sweatman, Winston L & Heggie, Douglas C. (Massey University)

Abstract. We calculate the change in density within a uniform distribution of field stars which is caused by a dense body plunging through with a constant velocity. Starting with the simplest case in which the field stars are initially stationary this leads to an infinite density along the axis of the wake. Introducing a small thermalisation within the field stars removes this infinity whilst leading to similar results off the path of the dense body. Results are in good agreement with those previously derived. A uniform approximation can be made for the density in the thermalized case and this can be used to deduce the force exerted on the moving star due to the drag caused by the accretion wake.

The Mass Function of Galactic Clusters and its Evolution

De Marchi, Guido (European Space Agency)

Abstract. We show that we can obtain a good fit to the main sequence mass functions of a large sample of Galactic clusters (young and old) with a tapered Salpeter power law distribution function with an exponential truncation. The average value of the power-law index is very close to Salpeter (2.3), whereas the peak mass is in the range 0.1-0.5 Msolar and does not seem to vary in a systematic way with the present cluster parameters such as metal abundance and central concentration. A remarkable correlation with age, however, is seen in that older disc clusters have higher peak mass, although this trend does not extend to globular clusters, whose peak mass is lower than that of old disc clusters. We attribute this trend to the onset of mass segregation following early dynamical interactions in the loose cluster cores. Differences between globular and younger clusters may depend on the initial environment of star formation, which in turn affects their total mass. Mass functions of field populations such as the solar neighborhood and Galactic bulge are consistent with the hypothesis that they were built up over time by contributions from many functions of this type with different peak masses.

Density Waves in Gaseous Mini-Disks of NGC 4501 and NGC6951

Orlova, Natalia; Korchagin, Vladimir; Moiseev, Aleksei & Theis, Christian (Institute of Physics, Rostov State University)

Abstract. We studied the gaseous mini-disks of the central regions of NGC 4501 and NGC 6951. Taking into account the observed properties of the molecular gas in the central region we built equilibrium models for both galaxies. These models are characterized by a gas-rich, self-gravitating central region which is close to marginal stability measured by the Toomre parameter Q. The minimum Q-values are 1.2 and 0.8 for NGC 4501 and NGC 6951, respectively. In agreement with the expectation from linear analysis, our hydrodynamical simulations showed that both mini-disks are gravitationally unstable. Moreover, different to extended galactic disks multi-armed modes are dominant instead of low-m

modes. This yields in a flocculent morphology which is in good agreement with the observed structures for both galaxies.

The Survival of Substructure in Clumpy Clusters

Goodwin, Simon & Whitworth, Anthony (Cardiff University)

Abstract. Initially fractal star clusters undergo a dramatic phase of dynamical evolution. Significant amount of substructure can remain in the clusters, especially if the initial velocity field is correlated with the density structures. As observations show that many star clusters are born clumpy, simulations with smooth initial conditions may be missing an important phase of cluster evolution.

The Distribution of Stars in the Outer Part of Clusters

Lee, Kang Hwan & Lee, Hyung Mok (Astronomy Program, SEES, Seoul National University)

Abstract. We have performed N-body simulations to study the tidal tails of the Galactic globular clusters. The Galactic potential in our model is contributed by central bulge, outer halo, and exponential disk. These components are assumed to be invariant in time in the frame. We investigate the cluster of multi-mass models with a power-law initial mass functions starting with different initial masses, initial number of particles, and different galacto-centric distances as well as ellipticities of orbit. We have examined the general evolution of the clusters, the shape of outer parts of the clusters, density profiles and the direction of tidal tails. We also have performed the wide field CCD photometry of two Galactic globular clusters (M92 and NGC 7492) to examine the dynamical status of the clusters. The observations were made with the 3.6 m Canada-France-Hawaii Telescope (CFHT), using CFH12K camera. The effects of the dynamical evolution of the cluster have been investigated by means of a completeness-corrected luminosity function and mass function and radial density profile and surface density map.

Case C Mass Transfer in the Evolution of Black Hole Binaries

Lee, Chang-Hwan & Brown, Gerald E. (Pusan National University, Korea)

Abstract. Earlier works have shown that if the Fe core in a pre-supernova star is to be sufficiently massive to collapse into a black hole, earlier in the evolution of the star the He core must be covered (clothed) by a hydrogen envelope during He core burning and removed only following this, in, e.g. common envelope evolution. This is classified as Case C mass transfer. In this work we argue for Case C mass transfer on the basis of binary evolution. The giant progenitor of the black hole will have a large radius about 1000 solar radius at the end of its super-giant stage. Its lifetime at that point will be short, about 1000 yrs, so it will not expand much further. Thus, the initial giant radius for Case C mass transfer will be constrained to a narrow band about 1000 solar radius. This have the consequence that the final separation following common envelope evolution will depend nearly linearly on the mass of the companion which becomes the donor after the He core of the giant has collapsed into the black hole. We show

that the reconstructed pre-explosion separation of the black hole binaries fit well the linear relationship.

Nuclear Starbursts and AGN Evolution

Dopita, Michael (Research School of Astronomy and Astrophysics, Aust. Nat. University)

Abstract. The environments of Active Galactic Nuclei (AGN) are often also the regions of greatest gas concentration and star formation in galaxies. The symbiotic relationship between the circum-nuclear gas, the associated star formation and the inflow, jets and photoionization associated with the AGN provides for very rich gas-phase physics. I will discuss some of these aspects insofar as they relate to the temporal evolution of both the nuclear star formation region and of the AGN.

Formation of Massive Black Holes Via IMBHs

Funato, Yoko (University of Tokyo)

Abstract. We propose a possible way of forming massive black holes (MBHs) from stellar mass black holes (SBHs) through intermediate mass black holes (IMBHs). We assume that the SBHs can be formed from massive stars. Although this is possible, it was thought to be difficult that SBHs merge into massive black holes. When SBHs have to be born in a star cluster, they concentrate in the center of the cluster. After concentration, they cannot grow through merging since they are ejected the from the cluster due to sling shots. When the star cluster is enough large and the potential of the center of the cluster is enough deep to enclose SBHs, the SBHs cannot concentrate into the center for the largeness of the cluster. The situation seems a dead end for SBHs born in star clusters. However, the discovery of an IMBH in a star cluster in M82 suggests that there is a possible way to form a MBH from SBHs through IMBHs. Here we show that it is possible for the IMBHs born in star clusters to merge and to form a MBH from the point of view of dynamical evolution of star clusters in a host galaxy.

Evolution of Dense Star Clusters Near the Galactic Center

McMillan, Steve & Portegies Zwart, Simon (Drexel University)

Abstract. We use direct N-body simulations to study the internal evolution and orbital decay of dense star clusters near the Galactic center. These clusters sink toward the center due to dynamical friction with the stellar background, and may go into core collapse before being disrupted by the Galactic tidal field. Collisions in the collapsed cluster core may lead to the formation of a single super-massive star. When the cluster eventually dissolves, it may deposit the remnant of this super-massive star, as well as a disproportionately large number of other massive stars, within the innermost parsec of the Galactic nucleus. Comparing the results of N-body models to the observed spatial distribution

and kinematics of IRS16, a group of young He I stars near the Galactic center, we argue that this association may have formed in this way.

An Intermediate-Mass Black Hole in the Dwarf Galaxy Pox 52
Barth, Aaron (California Institute of Technology)

Abstract. Do dwarf elliptical and dwarf spiral galaxies contain central black holes with masses below 10^6 solar masses? Beyond the Local Group, dynamical searches for black holes in this mass range are very difficult, but the detection of accretion-powered nuclear activity could be used to infer the presence of a black hole. The nearby dwarf spiral galaxy NGC 4395 hosts a faint Seyfert 1 nucleus with a likely black hole mass in the range 10^4-10^5 solar masses, and for more than a decade it has been the only known example of a Seyfert 1 nucleus in a dwarf galaxy. I will present new Keck spectra of the dwarf galaxy POX 52, which demonstrate that it has a Seyfert 1 spectrum nearly identical to that of NGC 4395. Its velocity dispersion is 37 km/s, suggesting a possible black hole mass of order 10^5 solar masses. I will discuss the prospects for systematic searches for nuclear activity in dwarf galaxies and the implications for black hole demographics.

Stellar Disc Near SgrA*-A Remnant of a Dense Accretion Disc
Levin, Yuri & Beloborodov, Andrei (CITA)

Abstract. We analyze recently measured 3-D velocities of massive stars in the Galactic center. We show that a thin disc of massive stars revolves around SgrA*, and we argue that these stars are a remnant of a dense accretion disc which existed a few million years ago.

JD12

Solar & Solar-Like Oscillations: Insights & Challenges for the Sun and Stars

Chairpersons: T. R. Bedding and J. Leibacher

Editors: T. R. Bedding and J. Leibacher (Chief-Editor)

Highlights of Astronomy, Vol. 13
International Astronomical Union, 2003
O. Engvold, ed.

Asteroseismology: From Dream to Reality

D. W. Kurtz

Centre for Astrophysics, University of Central Lancashire, Preston PR1 2HE, UK

Abstract. With the resounding success of Helioseismology in determining the interior structure and rotation of the Sun, and in providing unprecedented studies of the interaction of pulsation and magnetic fields in the solar atmosphere, astronomers have been delighted, after decades of disappointing attempts, with the recent discovery of solar-like oscillations in ξ Hya, β Hyi, α Cen, η Boo and ν Ind. There is now true seismology of a variety of solar-like stars. Asteroseismology also studies stars with a wide variety of interior and surface conditions. For two decades asteroseismic techniques have been applied to many pulsating stars across the HR Diagram. This review describes for non-specialists pulsation modes in stars and discusses a selection of some of the successes already accomplished in asteroseismology.

1. Introduction to asteroseismology

In 1926 in the opening paragraph of his now-classic book, *The Internal Constitution of the Stars*, Sir Arthur Eddington lamented, "What appliance can pierce through the outer layers of a star and test the conditions within?" While he considered theory to be the proper answer to that question, there is now an observational answer: asteroseismology.

Asteroseismology uses the normal oscillation eigenmodes of a star to probe its interior conditions. In the simplest case, where the star can be approximated as spherically symmetric, these modes are described by spherical harmonics. The two main driving forces that cause stellar pulsations are stochastic excitation and the κ-mechanism. Stochastic excitation occurs when the star's eigenmodes resonate with the time scales of the convective motions; this is the case in the Sun and solar-like oscillators. All other known pulsating stars are driven by variable opacity in H, He and sometimes metals, primarily Fe.

There are two main sets of solutions to the equations of motion for a pulsating star, and these lead to two types of pulsations modes: p modes and g modes. For the p modes, or pressure modes, pressure is the primary restoring force for a star perturbed from equilibrium by one of the above driving mechanisms. These p modes are acoustic waves and have gas motions that are primarily vertical. For the g modes, or gravity modes, buoyancy is the restoring force and the gas motions are primarily horizontal.

For the spherically symmetric case, the spherical harmonics that describe the pulsation have three quantum numbers: n, the radial overtone, is the number of radial nodes, each of which is a concentric shell inside the star; ℓ, the degree, gives the number of surface nodes for the mode; m, the azimuthal order, specifies how many of the surface nodes are lines of longitude; for $\ell > |m|$ the rest of the surface nodes are lines of latitude ($-\ell \leq m \leq +\ell$).

Modes with $\ell = 0$ are called radial modes. The star pulsates spherically symmetrically. For known types of pulsating stars these are p modes; e.g. Cepheids and RR Lyrae stars pulsate in radial modes. Modes with $\ell > 0$ are called non-radial modes and may be either p modes or g modes. It is easiest to picture how asteroseismology probes the interiors of stars by imagining a non-radial p mode: A sound wave travels from the surface down into the star along a ray path that is not directed at the center of the star; the wave has an increasing sound speed as it goes deeper, mostly because of increasing temperature and density, hence is refracted back towards the surface of the star where almost all of the energy of the mode is reflected. Modes of different ℓ penetrate to different depths in the star – each mode measuring the integral of the sound speed over its path. The volume of the star that each p mode samples is called the acoustic cavity. With enough modes, as in the Sun, it is possible to invert the observational data to derive the interior sound speed distribution. That can then constrain tightly temperature, density, chemical composition, and rotation as a function of depth.

There are two other important properties of p modes and g modes: 1) as n, the radial overtone increases the frequencies of the p modes increase, but the frequencies of the g modes decrease; 2) the p modes are most sensitive to conditions in the outer part of the star, whereas g modes are most sensitive to the core conditions.

The prime goal of asteroseismology is to study pulsating stars with rich enough frequency spectra to allow inversion of the observations to derive the atmospheric and interior physics of the stars. Thus there is great interest in the study of the newly-discovered solar-like oscillators (the subject of JD12) for this purpose. Other types of pulsating stars have far fewer pulsation modes than the Sun, but the physical conditions in those stars are, in many cases, very different from the Sun and asteroseismology is leading to new, broad understanding of stellar structure.

Some types of stars of interest to asteroseismology are discussed in the following sections to give a flavor of asteroseismic discoveries being made. The solar-like oscillators are discussed in detail by Bedding & Kjeldsen (2003) and Bouchy & Carrier (2003). A basic introduction to the theory of stellar pulsation can be found in the monograph by Cox (1980) and non-radial pulsation is discussed in detail in the monograph by Unno et al. (1989).

2. roAp stars

The roAp stars have been observed photometrically since their discovery over 20 years ago. Frequency analysis of their light curves have yielded rich asteroseismic information on the degrees of the pulsation modes, distortion of the modes from normal modes, magnetic geometries, and luminosities. The latter, in particular, are derived asteroseismically and have been shown to agree well with Hipparcos luminosities (Matthews et al. 1999). New theoretical work on the interaction of pulsation with both rotation and the magnetic field by Bigot & Dziembowski (2002) has presented an entirely new look at the oblique pulsator model of these stars: They find that the pulsation axis is inclined to both the magnetic and rotation axes, and the pulsation modes are complex combinations of spherical harmonics that result in modes that, in many cases, can be traveling waves looking similar to (but are not exactly) sectoral (meaning $|m| = \ell$) m modes. This unique geometry of the pulsation modes in roAp stars allows us to examine their non-radial pulsation modes from varying aspect as can be done with no other type of star.

High-resolution spectra of the roAp stars γ Equ, α Cir and HR 3831 (Ryabchikova et al. 2002; Kochukhov & Ryabchikova 2001) show the extreme stratification effects of abundances and the short vertical wavelength of the pulsation modes in these stars. Lines of Pr and Nd show significant radial velocity variations, while most other lines in the spectrum show none. A plausible interpretation of this phenomenon is that those ions are concentrated in a thin layer by the effects of radiative diffusion, and that this layer lies high in the atmosphere near a vertical anti-node of the pulsation mode. This is consistent with previous observations of strong line-depth dependence (atmospheric height dependence) of the pulsation amplitude in the Hα line (Baldry et al. 1999; Baldry & Bedding 2000), and the strong drop-off of photometric amplitude with increasing wavelength explained by Medupe & Kurtz (1998).

Kurtz, Elkin & Mathys (2003) have resolved the pulsation modes in the roAp star HD 166473 into standing waves and overlying evanescent traveling waves. They have shown for this star that the pulsation modes are standing waves of constant phase in the layers in which the core of the Hα line forms, while they are traveling waves moving outward through the layers above that where the Pr lines form. This is first direct view of outwardly traveling waves in the magneto-acoustic reflective boundary layer in any pulsating star other than the Sun. They also provide the first detailed observational evidence to test new theories of Cunha & Gough (2000) and Bigot et al. (2000) of the complex behavior of the magneto-acoustic modes of the roAp stars in this important boundary layer. Cunha (2001), on the basis of this theory, predicted a solution to a long-standing problem in understanding the asteroseismology of the roAp star HR 1217 that was later observationally confirmed using the Whole Earth Telescope (Kurtz et al. 2002). The time is now ripe for substantial new theoretical developments based on the new kinds of observations being made on roAp stars.

3. White dwarf variables

White dwarfs are g-mode pulsators and are the current champions of asteroseismology. They have more frequencies detected than any other type of pulsating star, other than the Sun, and theory has been more successful in extracting astrophysical information for them than for any other kind of pulsator. There are three main regions of white dwarf pulsation: The DOV, DBV and DAV stars, where the nomenclature is D = white dwarf; V = pulsating variable; and O, B and A refer to spectra that resemble O, B and A stars in the presence of He and H lines.

The best studies of pulsating white dwarfs have been carried out by the Whole Earth Telescope (WET). The WET web site contains a wealth of information and references to published papers from many extended coverage (Xcov) campaigns. An outstanding example is their study of the DOV star PG 1159-035 (Winget et al. 1991) where they found 101 independent pulsations modes. Models yielded a mass of $M = 0.586 \pm 0.003\,\mathrm{M}_\odot$; independent tests using distances determined from parallaxes and the mass-radius relation indicate that the quoted precision is probably correct. The periods in PG 1159 are in the range $385 \leq P \leq 1000\,\mathrm{s}$; they are high-overtone ($n \gg \ell$) g-mode pulsations, as is the case for other pulsating white dwarfs. Asymptotic theory gives a clear prediction of period spacing for such stars, and deviations from that are used to derive the compositional stratification in their atmospheres, i.e. the mass of the surface He and/or H layers – possibly even resolving He^3 and He^4 layers (Wolff et al. 2002). PG 1159 clearly shows $\ell = 1$ and 2 modes, but not $\ell = 3$. The magnetic field strength is less than 6000 G – a very small value for a white dwarf star where field strengths are often MG. Clearly asteroseismology of white dwarf stars is highly successful in extracting astrophysically interesting information.

One of the more striking properties of white dwarfs being studied by asteroseismology now is the C/O interior composition and the potential crystallization of the core in the most massive of the DAV stars in stars such as BPM 37093 (Montgomery et al. 1999) into earth-sized "diamonds". Metcalfe (2003) has even used seismic models of two white dwarfs to measure the $^{12}\mathrm{C}\,(\alpha,\gamma)\,^{16}\mathrm{O}$ reaction rates, finding a value consistent with laboratory reaction rates.

4. Sub-dwarf B variables

It has been only 7 years since the discovery the EC 14026 stars, the sdBV stars. This group was discovered observationally (Stobie et al. 1997) at the same time that its existence was predicted theoretically (Charpinet et al. 1996). The sdBV stars are low-ℓ, non-radial p-mode pulsators with $65\,\mathrm{s} \leq P \leq 500\,\mathrm{s}$, and amplitudes from 1 mmag up to 0.3 mag. They are all multiperiodic with 2 to 50 modes. Driving is caused by the κ-mechanism operating on a metal line opacity bump in a layer where Fe has been radiatively levitated and concentrated. They are Extreme Horizontal Branch stars that have been stripped of their H envelopes, leaving behind an approximately 0.5–$\mathrm{M}_\odot$ He star wrapped in a miniscule H-rich atmosphere with a mass no greater than $10^{-4}\,\mathrm{M}_\odot$. They are all in binary systems. Now there is a second group of sdBV stars that pulsate with periods around one hour (Green et al. 2003); these are g-mode pulsators that are slightly separated from the p-mode EC 14026 stars in the HR Diagram.

One of the most exciting of the EC 14026 stars is PG 1336-035. It is an sdBV star in an eclipsing binary with an orbital period of 2.4 hr and with an M dwarf companion of similar radius to the sdBV star. WET devoted two campaigns to this star. During primary eclipse as the M star passes in front of the sdBV star, the pulsation amplitude changes as parts of the non-radial modes are selectively covered. Removal of the eclipse light curve to study these amplitude changes suggests that the pulsation axis may be the tidal axis between the two stars. While there is a wealth of theoretical discussion of tidally induced and modulated stellar pulsation, there have been few observations to test the theory, giving PG 1336 great promise for that.

Another exciting sdBV star, the subject of WET Xcov23 is KPD 1930+2752, an ellipsoidal variable with over 44 periods, and an orbital period of 2.28 hr. The companion is unseen and exceeds the mass of KPD 1930+2752. In fact, the projected orbital velocity of 349 km s^{-1} implies a total mass for the system of *at least* 1.47 $M_{\odot}$ – greater than the Chandrasekhar limit! Gravitational radiation is expected to cause the system to merge in about 200 Myr making KPD 1930+2752 the first good candidate of a Type Ia supernova (SNe Ia) double-degenerate progenitor.

For application of asteroseismology it is necessary to have clear mode identifications of n, ℓ and m for each mode. The combination of line profile and radial velocity studies from spectroscopy and concurrent photometry is best for this. Now in addition to the photometric WET there is the Multi-site Spectroscopic Survey Telescope (MSST). A large campaign by the MSST in 2002 was awarded 113 nights of spectroscopic time to observe the sdBV star PG1605+072 in conjunction with 127 hours of photometric observations obtained by WET in Xcov22. This outstanding data set is still under analysis and promises rich results.

Asteroseismology of sdBV stars was explored for 1.5 days at the recent meeting, "Extreme Horizontal Branch Stars and Related Objects", held in 2003 June at Keele University; recent reviews and latest results can be found in the proceedings (Ap&SS, in press).

5. β Cep stars

The β Cep stars are (primarily) p-mode main sequence pulsators of spectral type B0–B2. They have large convective cores which makes them interesting targets for asteroseismology, because of the uncertainty of modeling such cores. Although they are multi-periodic, they are not known to have large numbers of pulsation modes such as are found for solar-like or white dwarf oscillators. Nevertheless, much can be learned from just a few modes, and there have been major recent asteroseismic successes for some β Cep stars.

Aerts et al. (2003a) studied 21 years of multi-color photometry for the β Cep star HD 129929 (V836 Cen). They identified an $\ell = 1$ triplet, a doublet they attributed to two m modes of an $\ell = 2$ quintuplet and an $\ell = 0$ radial mode, all with frequencies in the range of 6–7 d^{-1}. The models that best fitted the observed frequencies had a core overshooting parameter of $\alpha_{over} = 0.1$ and non-rigid rotation, with the core rotating four times faster than the surface. If this result stands the test of time, it is the first detection of differential rotation with depth in a star other than the Sun.

For mode identification Handler et al. (2003) and Aerts et al. (2003b) have obtained extensive photometric and spectroscopic data sets for the β Cep star ν Eri: 600 hr of differential photometry on 148 nights and 2442 spectra for line profile and radial velocity studies obtained on 118 nights. The frequencies are in the 5–8 d^{-1} range and there is some suggestion from the lowest frequencies of the presence of g modes, as well as p modes. If this is confirmed it will make ν Eri a slowly pulsating B star, as well as a β Cep star.

6. Conclusion

There are many other kinds of pulsating stars that are being studied asteroseismically: The δ Sct stars have, in some cases, dozens of detected p modes. The γ Dor stars are early F, g-mode pulsators with prospect for g-mode studies of cores of stars not very different from the newly discovered solar-like oscillators. Slowly pulsating B stars are mid-to-late B stars pulsating in g modes. All periodically pulsating stars have tremendous promise for new looks at stellar interiors as we hone our theoretical understanding and obtain previously undreamed of observations. Asteroseismology is truly Eddington's "appliance" to see inside the stars. The dream is now a reality.

References

Aerts, C. et al. 2003a, Science, 300, 1926

Aerts, C. et al. 2003b, MNRAS, in press

Baldry, I. K., & Bedding, T. R. 2000, MNRAS, 318, 341

Baldry, I. K., Viskum, M., Bedding, T. R., Kjeldsen, H., & Frandsen, S. 1999, MNRAS, 302, 381

Bedding, T. R., & Kjeldsen, H. 2003, Publ. Astr. Soc. Australia, 20, 203

Bigot, L., & Dziembowski, W. A. 2002, A&A, 391, 235

Bigot, L. et al. 2000, A&A, 356, 218

Bouchy, F., & Carrier, F. 2003, Ap&SS, 284, 21

Charpinet, S., Fontaine, G., Brassard, P., & Dorman, B. 1996, ApJ, 471, L103

Cox, J. P. 1980, Theory of Stellar Pulsation, Princeton University Press

Cunha, M. S. 2001, MNRAS, 325, 373

Cunha, M. S., & Gough, D. 2000, MNRAS, 319, 1020

Green, E. M. et al. 2003, ApJ, 583, L31

Handler, G. et al. 2003, MNRAS, in press

Kochukhov, O., & Ryabchikova, T. 2001, A&A, 374, 615

Kurtz, D. W., Elkin, V. G., & Mathys, G. 2003, MNRAS, 343, L5

Kurtz, D. W. et al. 2002, MNRAS, 330, L57

Medupe, R., & Kurtz, D. W. 1998, MNRAS, 299, 371

Metcalfe, T. S. 2003, ApJ, 587, L43

Matthews, J. M., Kurtz, D. W., & Martinez, P. 1999, ApJ, 511, 422

Montgomery, M. H., Klumpe, E. W., Winget, D. E., & Wood, M. A. 1999, ApJ, 525, 482

Ryabchikova, T. et al. 2002, A&A, 384, 545

Stobie, R. S. et al. 1997, MNRAS, 287, 848

Unno, W., Osaki, Y., Ando, H., Saio, H., & Shibahashi, H. 1989, Nonradial Oscillations of Stars, Tokyo: University of Tokyo Press, 1989, 2nd ed.

Winget, D. E. et al. 1991, ApJ, 378, 326

Wolff, B., Koester, D., Montgomery, M. H., & Winget, D. E. 2002, A&A, 388, 320

Highlights of Astronomy, Vol. 13
International Astronomical Union, 2003
O. Engvold, ed.

Physics of Solar-like Oscillations

Jørgen Christensen-Dalsgaard

Teoretisk Astrofysik Center, Danmarks Grundforskningsfond, and Institut for Fysik og Astronomi, Aarhus Universitet, DK-8000 Aarhus C, Denmark

Abstract. The physics of solar and stellar oscillations determine their observable characteristics. I provide a brief overview of the properties of solar-like oscillations, excited by stochastic processes, in other stars. In addition, I consider the current state of investigations of such oscillations, as well as the prospects for an improved understanding of their physics and the properties of the pulsating stars.

1. Introduction

Oscillations of isolated stars may be caused by two fundamentally different mechanisms: intrinsic instability and stochastic excitation. In the former case, the star acts as a heat engine, converting thermal energy into mechanical energy through a proper phasing of local heating and compression; this is the case, for example, in the classical instability strip populated by the Cepheids, RR Lyrae stars and δ Scuti stars. In the latter case, the stellar oscillations are intrinsically damped, but excited by other processes, typically turbulent flows; this happens in the Sun where the near-surface convection, with nearly sonic speeds, causes emission of acoustic waves which excite the modes of oscillation. Oscillations excited in this manner by convection may be considered solar-like; as discussed below, they are expected to be present in all stars with vigorous near-surface convection and hence occur in both solar-like stars and stars quite unlike the Sun.

As discussed by Kjeldsen & Bedding in this volume, solar-like oscillations have been observed in a variety of stars in recent years, including both main-sequence stars and highly evolved giants. Further extensive data are expected in the near future, both from continuing ground-based observations and from several space missions under way. Thus it is important to consider the physical properties of the oscillations, and in particular how the observed characteristics reflect the properties of the stars and may be used to probe these properties.

2. Basic properties of solar-like oscillations

Only a very brief discussion of the properties of stellar oscillations can be provided here. For more details, Unno et al. (1989) and Gough (1993) may be consulted, for example.

2.1. Mode Properties

A mode of stellar oscillation is characterized by the degree ℓ and azimuthal order m which determine the properties of the mode as a function of co-latitude and longitude, and the radial order n which depends on the variation with distance r to the center. Here ℓ determines the total number of nodal lines on the stellar surface, while m determines the number of nodes around the equator. From stellar observations, averaging light over the stellar disk typically suppresses the signal from all but the modes of the lowest degree, with $\ell \leq 3$.

The behavior of a mode in the radial direction is determined by the restoring forces: pressure forces caused by compression and rarefaction, and buoyancy forces caused by horizontal density differences being affected by gravity. These forces can be described in terms of two characteristic frequencies, varying through the star: the acoustic (or Lamb) frequency S_ℓ and the buoyancy (or Brunt-Väisälä) frequency N. S_ℓ is determined by $S_\ell = \sqrt{\ell(\ell+1)}c/r$, where c is the adiabatic sound speed, $c^2 = \Gamma_1 p/\rho$, where p is pressure, ρ is density, and $\Gamma_1 = (\partial \ln p/\partial \ln \rho)_{\rm ad}$ is the adiabatic exponent. N is given by

$$N^2 = g\left(\frac{1}{\Gamma_1}\frac{\mathrm{d}\ln p}{\mathrm{d}r} - \frac{\mathrm{d}\ln \rho}{\mathrm{d}r}\right) , \tag{1}$$

where g is the gravitational acceleration. In regions where $N^2 > 0$, N is the frequency of a gas element of small horizontal extent oscillating under the effect of buoyancy. Regions where $N^2 < 0$ are convectively unstable, buoyancy giving rise to accelerating direct motion leading to convective energy transport.

Asymptotic analysis shows that the eigenfunction of a mode oscillates as a function of r if its angular frequency ω satisfies one of two conditions: either $\omega > S_\ell, N$ or $\omega < S_\ell, N$. In the first case pressure dominates the restoring force and the mode has the nature of a standing acoustic wave; in the second case restoring is dominated by buoyancy and the mode has the character of a standing gravity wave. The former modes are known as acoustic, or p, modes whereas the latter modes are known as gravity, or g, modes.

The observed modes of solar-like oscillation typically have the character of high-order acoustic modes. These satisfy a simple asymptotic relation for the frequencies, usually written in terms of the cyclic frequency $\nu = \omega/2\pi$:

$$\nu_{nl} \sim \Delta\nu \left(n + \frac{\ell}{2} + \alpha\right) , \tag{2}$$

to lowest order of approximation, where α is a surface phase. Hence the spectrum is uniformly spaced in order, by the large separation $\Delta_{n\ell} = \nu_{n\ell} - \nu_{n-1\,\ell} \sim \Delta\nu \simeq (2\int_0^R \mathrm{d}r/c)^{-1}$, i.e., the inverse of the sound travel time across a stellar diameter. Also, modes of the same $n + \ell/2$ are degenerate to this approximation. Corrections to Eq. (2) give rise to a departure from this degeneracy, characterized by the small separation $\delta_{n\ell} = \nu_{n\ell} - \nu_{n-1\,\ell+2}$.

In the core of evolved stars the buoyancy frequency attains very high values, due to the strong central condensation and the resulting high value of g, often enhanced by a steep gradient in the hydrogen abundance (e.g., outside a convective core). In such cases the buoyancy frequency in the core may exceed typical values for the observed frequencies. Here, therefore, a mode can show g-mode-like behavior in the core and p-mode-like behavior in the envelope.

A very useful characteristic of a mode is its mode mass $M_{\rm mode}$ defined by $M_{\rm mode} = \int_V \rho|\delta\mathbf{r}|^{\mathbf{2}}\mathrm{d}\mathbf{V}/|\delta\mathbf{r}_{\rm ph}|^{\mathbf{2}}$ where the integration is over the volume V of the star; here $\delta\mathbf{r}$ is the displacement and $|\delta\mathbf{r}_{\rm ph}|$ is its surface norm. This relates the surface rms velocity $|\mathbf{V}_{\rm ph}|$ to the total energy $\mathcal{E}$ of the mode through $\mathcal{E} = M_{\rm mode}|\mathbf{V}_{\rm ph}|^2$. Evidently, modes trapped in the deep interior of a star, such as g modes, tend to have a high value of $M_{\rm mode}$; one may then suspect that they are less likely to be excited to large amplitudes.

Rotation introduces a dependence of the frequencies on m. For slow rotation this *rotational splitting* is proportional to the rotation rate; this is a good approximation in the solar case. For rapidly rotating stars, however, effects of higher order in the rotation rate must be taken into account, substantially complicating the frequency spectrum (e.g., Soufi et al. 1998).

2.2. Mode excitation

As discussed in the introduction, solar-like oscillations are intrinsically damped but excited stochastically by near-surface convection. Thus the mode energies are determined by a balance between the energy input, which typically depends only on the frequency, and the damping rate (e.g., Goldreich et al. 1994; Samadi et al. 2003; see also Stein et al., this volume). Very roughly, the resulting energy is predominantly a function of frequency; at a given frequency the dependence of the surface amplitude on mode properties is then determined by the mode inertia as $|\mathbf{V}_{\rm ph}| \propto M_{\rm mode}^{-1/2}$.

Stochastic excitation produces a characteristic frequency variation of the surface amplitude, leading to the largest amplitudes in the solar case near periods of 5 minutes. At low frequencies the modes have low amplitude in the region of efficient excitation, compared with the overall amplitude, leading to small surface amplitudes. Also, driving is most efficient for modes whose periods match the time scale of the near-surface convection, in the solar case 5 – 10 minutes. At high frequency, at and above the so-called acoustical cut-off frequency, the modes are no longer reflected at the photosphere and suffer substantial energy loss through running waves. For stars that are not too highly evolved this places the largest amplitudes in the frequency range corresponding to high-order acoustic modes, confirming the applicability of the asymptotic Eq. (2).

Christensen-Dalsgaard & Frandsen (1983) made a very rough estimate of the amplitude expected for stochastically excited modes in a variety of stars, based on an early analysis by Goldreich & Keeley (1977). Later estimates by Houdek et al. (1999) largely confirmed the earlier results. These estimates are now being tested by data on solar-like oscillations. Interestingly, the observed amplitude for Procyon, which is somewhat hotter than the Sun, is lower by a factor of roughly three than the prediction (e.g., Barban et al. 1999).

3. Diagnostic potential of solar-like frequencies

The asymptotic relation in Eq. (2) defines the basic structure of the spectrum of solar-like oscillations and provides the basis for the simplest analysis of observed frequencies, in the determination of the large and small frequency separations. Indeed, the regular spacing of the frequency spectrum, together with the characteristic distribution of power with frequency, are the two main signatures of the presence of solar-like oscillations. The large separation provides an average of the entire structure of the star; for stars on or near the main sequence it may be taken as a measure of stellar mass. On the other hand, the small separation is sensitive to the structure of the core of the star; in particular, $\delta_{n\ell}$ is reduced with increasing stellar age. This suggests illustrating the two separations in a two-dimensional diagram, similar to the classical Hertzsprung-Russell diagram (e.g., Christensen-Dalsgaard 1984, 1988; Ulrich 1986). Assuming that other parameters of a star are known, such as its composition, the observed location of the star in this diagram determines its mass and evolutionary state (but see also Gough 1987).

Although the small separation is determined principally by conditions in the core, it retains some sensitivity to overall structure, including detailed properties of the stellar envelope. Roxburgh & Vorontsov (2003) showed that ratios such as $r_{nl} = \delta_{n\ell}/\Delta_{n\ell}$ are entirely determined by the core conditions and hence provide a much cleaner probe of the age of the star or other aspects of its core structure.

The oscillation frequencies evidently contain information beyond the large and small separations. In particular, the asymptotic description assumes a smooth model, on the scale of the eigenfunction variations. Sharp features give rise to detectable oscillatory signals in the frequencies. In the solar case this signal has been used to investigate the properties of the base of the convective envelope, where the sudden change from adiabatic to sub-adiabatic temperature gradient causes a similarly sharp change in the gradient of the sound speed (e.g., Basu et al. 1994; Monteiro et al. 1994; Roxburgh & Vorontsov 1994). Also, the decrease of Γ_1 in the region of second helium ionization causes a localized change in the sound speed, with a detectable signature in the frequencies which provides a measure of the helium content of the solar envelope (e.g., Vorontsov et al. 1991; Antia & Basu 1994; Pérez Hernández & Christensen-Dalsgaard 1994). Similar analysis may become possible in the stellar case, once data of sufficient quality have been obtained (e.g., Lopes et al. 1997; Pérez Hernández & Christensen-Dalsgaard 1998; Monteiro et al. 2000; Miglio et al. 2003).

4. Asteroseismology of evolved stars

After the star leaves the main sequence, following the exhaustion of hydrogen at the center, the buoyancy frequency in the deep interior increases strongly as a result of the contraction of the core. As discussed above, modes in the observed range of frequency may then have a dual character, with p-mode properties in the envelope and g-mode properties in the interior. In most cases the mode is dominated by one of the two possible regions of oscillatory behavior; if this is the g-mode region the resulting mode mass is typically so high that the mode is unlikely to be observed. However, some modes can have substantial amplitudes in both regions; this results in a modest mode mass, and hence a potentially detectable amplitude, while the g-mode behavior causes significant departures from the simple asymptotic relation, Eq. (2). An example of such behavior may be present in the sub-giant η Bootis which was found by Kjeldsen et al. (1995) to show solar-like oscillations; computed frequencies (e.g., Christensen-Dalsgaard et al. 1995; Guenther & Demarque 1996; Di Mauro et al. 2003) show clear departures from Eq. (2) for $\ell = 1$, at mode masses indicating that the modes might be observable. Interestingly, there is some evidence that the observed frequencies show similar behavior; this would be a first indication that properties of the buoyancy frequency can be probed with solar-like oscillations.

The estimates of mode amplitudes indicate that larger amplitude may be expected in more evolved stars, particularly for red giants. Some indications for solar-like oscillations were found in the K0 giant α UMa from observations made with the WIRE satellite (Buzasi et al. 2000) although the interpretation of the data was later questioned (Dziembowski et al. 2001). Frandsen et al. (2002) found clear evidence for solar-like oscillations in the G7 giant ξ Hya, with an envelope of power strongly reminiscent of the solar case, albeit with an amplitude maximum at a period of around 3 hours. This star is probably in the core helium burning stage, with an extremely condensed core. It is likely, as discussed by Dziembowski et al. (2001), that the resulting very rapid variation of the eigenfunctions in the region of g-mode behavior causes strong damping of non-radial modes, such that only modes with $\ell = 0$ are excited to observable amplitudes. Indeed, the observed uniform spacing of the frequencies corresponds to the full large separation $\Delta\nu$ for the most plausible models, rather than half this value as would be observed if both $\ell = 0$ and 1 modes were observed.

For even more luminous red giants the predicted amplitudes are quite substantial but the periods are very long, of order weeks or months, making observations extremely time consuming. For the extreme case of asymptotic giant branch stars literally decades of observations are required to identify the frequency structure and other properties of the oscillations. It was argued by Christensen-Dalsgaard et al. (2001) that data on semi-regular variables, obtained through very extensive efforts by the American Association of Variable Star Observers showed statistical properties consistent with stochastic excitation of a solar-like nature. Thus it seems plausible that solar-like oscillations can be observed throughout the red part of the Hertzsprung-Russell diagram, extending to quite extreme cases very different from the Sun. The full diagnostic potential of these data still needs to be explored, however.

Acknowledgments. This work was supported in part by the Danish National Research Foundation through its establishment of the Theoretical Astrophysics Center.

References

Antia, H. M., & Basu, S. 1994, ApJ, 426, 801

Barban, C., Michel, E., Martic, M., Schmitt, J., Lebrun, J. C., Baglin, A., & Bertaux, J. L. 1999, A&A, 350, 617

Basu, S., Antia, H. M., & Narasimha, D. 1994, MNRAS, 267, 209

Buzasi, D., Catanzarite, J., Laher, R., Conrow, T., Shupe, D., Gautier III, T. N., Kreidl, T., & Everett, D. 2000, ApJ, 532, L133

Christensen-Dalsgaard, J. 1984, in Space Research Prospects in Stellar Activity and Variability, eds A. Mangeney & F. Praderie (Paris: Paris Observatory Press), 11

Christensen-Dalsgaard, J. 1988, in IAU Symp. 123, Advances in helio- and asteroseismology, eds J. Christensen-Dalsgaard & S. Frandsen (Dordrecht: Reidel), 295

Christensen-Dalsgaard, J., & Frandsen, S. 1983, Solar Phys., 82, 469

Christensen-Dalsgaard, J., Bedding, T. R., & Kjeldsen, H. 1995, ApJ, 443, L29

Christensen-Dalsgaard, J., Kjeldsen, H., & Mattei, J. A. 2001, ApJ, 562, L141

Di Mauro, M. P., Christensen-Dalsgaard, J., Kjeldsen, H., Bedding, T. R., & Paternò, L. 2003, A&A, 404, 341

Dziembowski, W. A., Gough, D. O., Houdek, G., & Sienkiewicz, R. 2001, MNRAS, 328, 601

Frandsen, S., Carrier, F., Aerts, C., et al. 2002, A&A, 394, L5

Goldreich, P., & Keeley, D. A. 1977, ApJ, 212, 243

Goldreich, P., Murray, N., & Kumar, P. 1994, ApJ, 424, 466

Gough, D. O. 1987, Nature, 326, 257

Gough, D. O. 1993, in Astrophysical fluid dynamics, Les Houches Session XLVII, eds J.-P. Zahn & J. Zinn-Justin (Amsterdam: Elsevier), 399

Guenther, D. B., & Demarque, P. 1996, ApJ, 456, 798

Houdek, G., Balmforth, N. J., Christensen-Dalsgaard, J., & Gough, D. O. 1999, A&A, 351, 582

Kjeldsen, H., Bedding, T. R., Viskum, M., & Frandsen, S. 1995, AJ, 109, 1313

Lopes, I., Turck-Chièze, S., Michel, E., & Goupil, M.-J. 1997, ApJ, 480, 794

Miglio, A., Christensen-Dalsgaard, J., Di Mauro, M. P., Monteiro, M. J. P. F. G., & Thompson, M. J. 2003, in Asteroseismology across the HR diagram, eds M. J. Thompson, M. S. Cunha & M. J. P. F. G. Monteiro, (Dordrecht: Kluwer), 537

Monteiro, M. J. P. F. G., Christensen-Dalsgaard, J., & Thompson, M. J. 1994, A&A, 283, 247

Monteiro, M. J. P. F. G., Christensen-Dalsgaard, J., & Thompson, M. J. 2000, MNRAS, 316, 165

Pérez Hernández, F., & Christensen-Dalsgaard, J. 1994, MNRAS, 269, 475

Pérez Hernández, F., & Christensen-Dalsgaard, J. 1998, MNRAS, 295, 344

Roxburgh, I. W., & Vorontsov, S. V. 1994, MNRAS, 268, 880

Roxburgh, I. W., & Vorontsov, S. V. 2003, A&A, in the press.

Samadi, R., Nordlund, Å, Stein, R. F., Goupil, M. J., & Roxburgh, I. 2003, A&A, 403, 303

Soufi, F., Goupil, M. J., & Dziembowski, W. A. 1998, A&A, 334, 911

Ulrich, R. K. 1986, ApJ, 306, L37

Unno, W., Osaki, Y., Ando, H., Saio, H., & Shibahashi, H. 1989, Nonradial Oscillations of Stars, 2nd Edition (Tokyo: University of Tokyo Press)

Vorontsov, S. V., Baturin, V. A., & Pamyatnykh, A. A. 1991, Nature, 349, 49

Highlights of Astronomy, Vol. 13
International Astronomical Union, 2003
O. Engvold, ed.

Challenges in Stellar Models from Helioseismology to Asteroseismology

Sylvaine Turck-Chièze, Phu Anh Phi Nghiem

SAp/DAPNIA/DSM/CEA CE Saclay, 91191 Gif sur Yvette, France

Laurent Piau

SAp/DAPNIA/DSM/CEA CE Saclay, 91191 Gif sur Yvette, France, ULB/IAA CP 226, Boulevard du Triomphe, B-1050 Bruxelles, Belgium

Abstract. Experience in helioseismology provides guidance for modeling challenges in asteroseismology. It guides choices of targets and conditions of observation. The main objectives are the interplay between rotation and convection and the knowledge of the internal magnetic field. Progress on the structure of the outer layers is crucial to avoid mode identification problems.

1. Introduction

Stellar modeling has been recently improved by a better understanding of many physical phenomena; e.g. the interaction of photons with complex plasmas or the way stars lose mass and rotate. Additional progress has been achieved by a better determination of stellar composition, distance, and geometry. Seismic investigation of stellar interiors will give us a real insight and consequently will contribute to answering outstanding questions concerning on convection, magnetic field and rotation. Currently, the absence of a proper description of such phenomena limits our understanding of early and late stages of evolution, and the objective is to directly introduce them in stellar structure equations.

In this review, we anticipate from the solar case the potential progress for solar-like stars, including young or massive stars. Of course, the Sun is a unique object as we can detect a large number of modes. For solar-like stars, the detection will be limited to low-degree acoustic modes. But the richness of our experience in helioseismology allows us to deduce from the understanding of the mode characteristics the way to achieve a real insight from the surface to the core if we have the opportunity to achieve the required accuracy.

2. The Solar Experience

The investigation of the stellar interior with seismic probes (Ballot et al. 2003a,b) depends on the ability to identify the observed modes, to get a sufficient number of them (from 20 to 50 at least) and to have a sufficient length of observations (typically several months). In these conditions, the extension of convective zones and helium content are accessible. Moreover, we notice that the correct extraction of the rotation profile (Couvidat et al. 2003a) in the radiative zone benefits from limited instrumental perturbations at low frequencies to approach the range of mixed modes. A major lesson from helioseimic data is that we can considerably improve the quality of the information if we integrate the signal for several years at low frequencies (Turck-Chièze et al. 2001; Couvidat et al. 2003b), in reducing the stellar activity effect together with the role of the stochastic excitation, encouraging seismic observations during exoplanet observations which will cover several successive years. Due to the high quality of the solar seismic information, which allows an extraction of the sound speed at the level of 10^{-4} down to $0.06R_{\odot}$, a deep understanding of the physical ingredients such as nuclear reaction rates, opacities and surface composition has been possible, which is directly useful for asteroseismology.

3. Future Major Challenges

The knowledge of the metallicity through only the iron composition is not sufficient and the composition of carbon, nitrogen and mainly oxygen is necessary to interpret the sound speed profile. These elements play a crucial role at the base of the convective zone and just below, so the detailed knowledge of the composition helps to disentangle competition between radiation and convection.

In the possible cases, we will determine the edge of external convective zones of solar-like stars, and deduce strong constraints on convective phenomena using several stellar calibrators. The aim is to go beyond the mixing length approximation and the notion of over or undershooting. This is one of the important issues for asteroseismology. For this objective, hydrodynamical 3D simulations will be of great utility (Brun & Toomre, 2002), if we can observe the internal behavior of stars with different surface rotation. It will be extremely exciting to really understand the role of the rotation in convective layers, by looking at a large number of clusters of different ages. Progress will come from the study of young clusters with higher rotation rates for which we are waiting confrontation with present modeling (Piau & Turck-Chièze 2002; Piau, Ballot & Turck-Chièze 2003).

In simulating the perturbed characteristics of the modes (stochastic excitation and variability along stellar cycle), we are confident that we can extract the depth of outer convective zone at a level of several percent, and the determination of photospheric helium content; this will be critical for a good estimate of the stellar ages of solar like stars of different metallicities, thanks also to the precise determination of stellar diameters for nearby observed stars. We hope also to make progress on the magnetohydrodynamic role of the interlayer between radiation and convection. Any improvements in computer performance will be immediately used to simulate such still inaccessible regions of stars. Today's tachocline parameters must be replaced by a real understanding of the processes in action. Another very important goal consists of improving determinations of the frequencies of the modes, which is important for the identification of the observed peaks and consequently it will help in going towards higher masses and other areas of the HR diagram. This progress supposes a correct introduction of the turbulence, which is mainly concentrated in the solar case in the outer 1000 km, and of the external magnetic field.

4. The surface magnetic field

For many years, the high precision achieved in the measurement and the calculation of solar acoustic frequencies has shed light on the detailed disagreement between them, which varies much more with frequency than with the mode degree ℓ. For low values of ℓ, this discrepancy can be considered to be independent of ℓ, and reaches several tens of μHz at high frequencies. Since Woodard & Noyes (1985), it has been well known that frequency variations with the solar cycle present qualitatively the same properties: independent of ℓ for $\ell = 0$ - 10, reaching a maximum of several tenths of μHz at high frequencies.

These specific behaviors are attributed to very near-surface effects. Indeed, for low values of ℓ, the wave vector becomes nearly radial. But until now, despite numerous studies, it has been difficult to build up a scenario that can give rise to the frequency changes capable of reproducing the observations. The most concrete result was obtained very recently by Li et al. (2003), where the frequency variations with the cycle were relatively well reproduced, with a combination of turbulent pressure and magnetic field.

Nghiem (2002a) developed a semi-analytical calculation using a boundary condition directly implying the stellar structure studied without any other hypothesis on this structure. Such an approach, despite its reduced precision compared to the numerical methods, could be pertinent in the study of near surface layers. It consists in examining pure acoustic waves traveling in a locally homogeneous gas sphere. At the surface, these waves are reflected when the environment is no longer homogeneous, that is when its characteristic length, identified here with the pressure scale height H_p, is of the same magnitude as the wavelength. So the external cavity limit r_2 is the radial position obeying the following equation: $\frac{1}{k_r}\frac{\omega^2}{c_0^2} = \frac{2\pi}{11.3H_p}$. k_r the radial wave number which is equal to ω/c_0 at the surface for low ℓ. When comparing the observations and the resulting eigenfrequencies obtained with a solar model of Brun, Turck-Chièze & Zahn (1999), an ℓ-independent discrepancy can be seen, characteristic of surface effects, but different from the classical figure, due to the relaxing of the isothermal atmosphere approximation.

A conventional inversion method is used to search for a sound speed change. But that cannot be a solution; on the contrary, a change in H_p with c_0 constant, or almost constant, will lead to a net change of r_2 and thus a frequency change independent of ℓ. The magnetic field is a good candidate satisfying this latter condition. Because the magnetic pressure induces a change in H_p as well as the sound speed, but the latter is compensated by the Alfven speed. The effect on the gas pressure and the sound speed of an horizontal field B_h is:

$$p_1 - p_0 = -\frac{B_h^2}{8\pi} \text{ ; and } \mathrm{c}_1^2 - \mathrm{c}_0^2 = (\mathrm{p}_0 - \mathrm{p}_1)(\frac{2-\Gamma_1}{\rho_0}) \qquad (1)$$

and a change from B_h to $B_h + \delta B_h$ leads to:

$$p_2 - p_1 = -\frac{B_h \delta B_h}{4\pi} - \frac{\delta B_h^2}{8\pi} \text{ ; and } \mathrm{c}_2^2 - \mathrm{c}_1^2 = (\mathrm{p}_1 - \mathrm{p}_2)(\frac{2-\Gamma_1}{\rho_0}) \qquad (2)$$

where the indices $0, 1, 2$ refer to the cases without magnetic field, with magnetic field, and with a magnetic field change. In this study, the adiabatic coefficient Γ_1

and the density ρ_0 remain unchanged, provided that the hydrostatic equilibrium is maintained with the same total pressure. The above equations clearly show that the determination of the variation δB_h depends on the determination of B_h.

To determine the surface magnetic field, we calculate first the eigenfrequencies with the above mentioned method, applied to the solar structure of our solar model. By comparing with the LOWL observed frequencies of Jiménez-Reyes (2001) near the minimum and maximum of magnetic activity, i.e. in 1996-1997 and 1999-2000, we can infer B_h and δB_h. The results are the following. We are able to extract an order of magnitude of the magnetic field and of its variation through the solar cycle, down to about 0.995 increasing from 0 to 10 kG for the permanent magnetic field, and down to 0.997 increasing from 0 to 100 G for the variation of this magnetic field. Below, the magnetic pressure is so small in comparison with the gas pressure, that we can deduce nothing from the absolute values of the frequencies. Near the surface, the introduction of a turbulent pressure term does not modify these conclusions as the impact of this term is very localized.

Despite some questionable approximations used here, the B_h profile shows magnetic field values at roughly the same range as the ones estimated from measurements, and the δB_h profile is not very different from the one infered in Li et al. (2003).

This method may be extended to other stars in the future and provides input for stellar models to improve the identification of the detected modes.

References

Ballot, J., Turck-Chièze, S., García, R. A., & Nghiem, P. 2003a, in Asteroseismology across the HR diagram, ed. M. Thompson, M. Cunha, & M. Monteiro, 497

Ballot, J., Turck-Chièze, S., & García, R. A. 2003b, A&A, submitted

Brun, A. S., Turck-Chièze, S. & Zahn, J.-P. 1999, ApJ, 525, 1032

Brun, A. S., Toomre, J. 2002, ApJ, 570, 865

Couvidat, S., García, R. A., Turck-Chièze, S., Corbard, T., Henney, C. J., & Jiménez-Reyes, S. 2003, ApJ, 597, L77

Couvidat, S., Turck-Chièze, S, & Kosovichev, A. 2003, ApJ, 599,

Jiménez-Reyes, S. J. 2001, Ph.D. Thesis, Univ. La Laguna, Spain

Kosovichev, A. G. 1995, Proc. of Fourth SOHO workshop, ESA SP-376, 165

Li, L. H., Basu, S., Sofia, S., Robinson, F. J., & Demarque, P. 2003, ApJ, 591, 1267

Nghiem, P. A. P. 2002, Proc. of SOHO12/GONG+2002, ESA SP-517, 353

Piau, L. & Turck-Chièze, S. 2002, ApJ, 566, 419

Piau, L., Ballot, J., & Turck-Chièze, S. 2003, A&A, submitted.

Turck-Chièze, S., et al. 2001, ApJ, 555, L69

Woodard, M. F. & Noyes, R. W. 1985, Nature, 318, 449

Highlights of Astronomy, Vol. 13
International Astronomical Union, 2003
O. Engvold, ed.

Observations of Solar-Like Oscillations

Hans Kjeldsen

Teoretisk Astrofysik Center, Institut for Fysik og Astronomi, Aarhus Universitet, DK-8000 Aarhus C, Denmark

Timothy R. Bedding

School of Physics A28, University of Sydney, NSW 2006, Australia

Abstract. The solar-like oscillations are oscillations that are expected to be excited by near-surface convection. Apart from the Sun itself, we now have a number of stars where p-mode solar-like oscillations have been detected. In this paper we present a short presentation of those recently discovered oscillations.

1. Introduction

The oscillations in the Sun are believed to be excited by convection near the solar surface, and we therefore expect that all stars that have a outer convection zone will display solar-like oscillations. A detailed discussion of solar-like oscillations, their detection and properties can be found in a recent review in Bedding & Kjeldsen (2003), and we will therefore not discuss all of the details of solar-like oscillations in the present paper. In the description below we will concentrate on two aspects related to observations of solar-like oscillations; the global properties of the p-mode excess power and the oscillations detected in α Cen A.

2. P-Mode Power in Solar-Type Stars

Detailed model calculations of solar and solar-like oscillations as well as observations of high-order p-mode oscillations in a number of stars, show that the frequencies of low-degree (ℓ) and high-order (n) oscillations can be approximated by the asymptotic relation:

$$\nu_{n,\ell} \;=\; \Delta\nu(n + \frac{1}{2}\;\ell + \epsilon) - \ell(\ell+1)D_0 \tag{1}$$

This relation show that the structure of p-modes can be characterized by a set of so-called separations. The large separation ($\Delta\nu$) is the distance between modes with same degree (but different order), while the small separations reflect differences between modes with different order (and different degree). The following small separations can be defined:

$$\delta\nu_{02} = \nu_{n,\ell=0} - \nu_{n-1,\ell=2} = 6\;D_0 \tag{2}$$

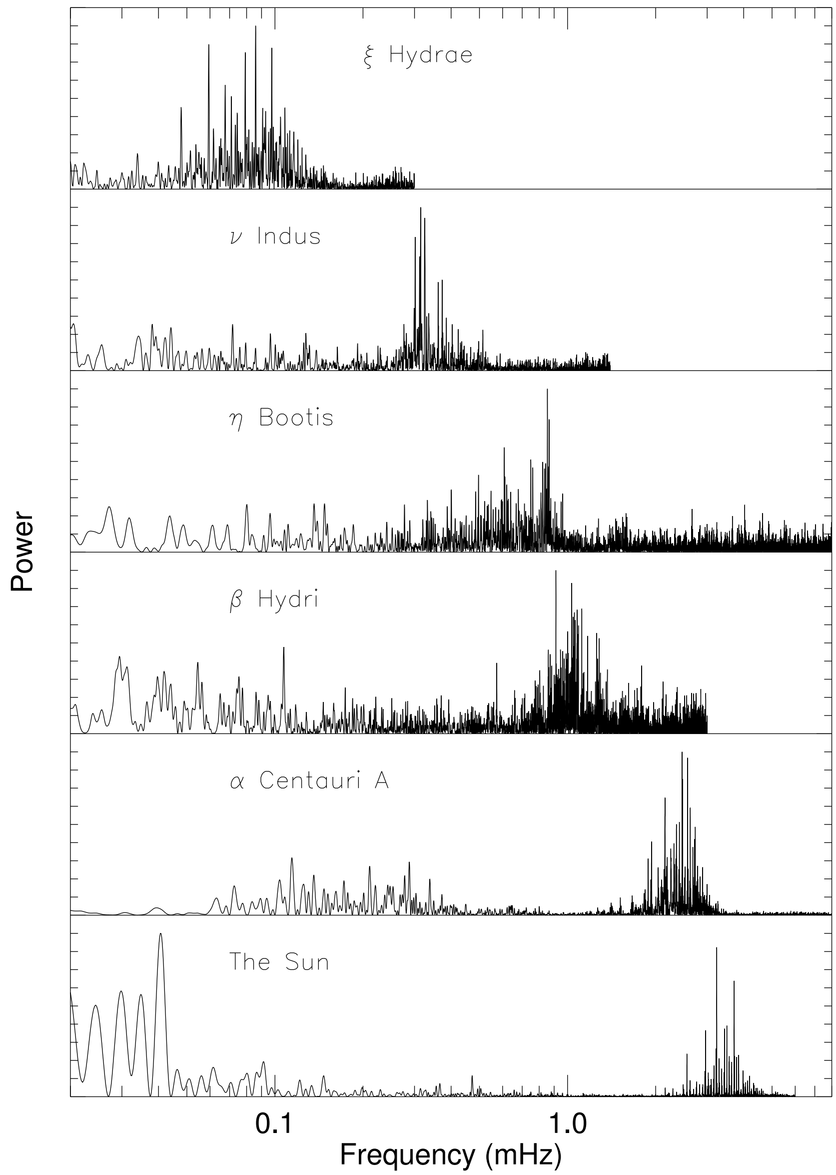

Figure 1. Observed power spectra of oscillations in the Sun and in 5 other stars. For details of the observations see Bedding & Kjeldsen (2003). The frequency is shown on a logarithmic scale and, as one can see, oscillations are found at a significantly lower frequency in evolved stars like ξ Hydrae, ν Indus, η Bootis and β Hydri than observed in α Cen A and the Sun. The reason for this is that the peak p-mode power is proportional to the acoustic cutoff frequency in the stellar atmospheres.

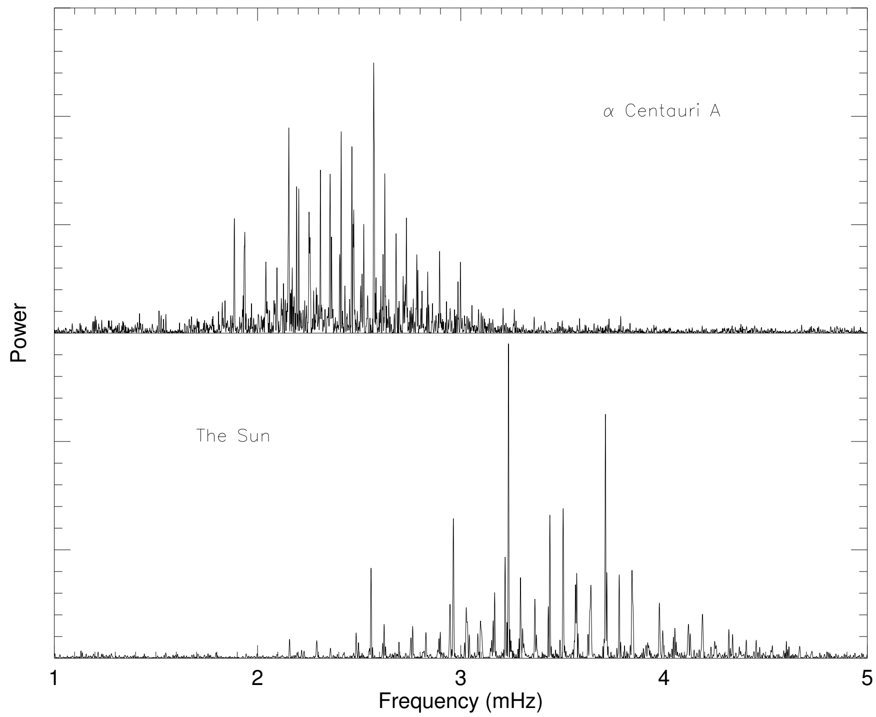

Figure 2. Power spectrum of time series of velocity measurements for the star α Centauri A and the Sun. The details of the power spectrum indicate that α Cen A is significantly more evolved than the Sun. The large separation for the Sun is about 135 μHz and the small separation ($\delta\nu_{02}$) is about 9 μHz. For α Cen A the same values are 106 μHz for the large separation and 5.5 μHz for the small separation ($\delta\nu_{02}$). Based on the value for the large separation, we can estimate the density of α Cen A to be 0.61 times solar (0.86 g/cm^3). The α Cen A power spectrum in this figure is from Butler et al. (2003) and the solar spectrum from full-disk velocities from the GOLF instrument on SoHO (Gabriel et al. 1997). The velocities for the α Centauri A time series show a scatter that is well below 1 m/s per data point for data taken at the UVES spectrograph (using an iodine absorption cell for wavelength referencing) at VLT (UT2) at a sampling rate of two data points per minute. This accuracy is in fact higher than the one obtained using the GOLF instrument. The observations of α Cen A result in a noise level in the Fourier amplitude spectrum of 1.9 cm/s and as such, these observations represent the most accurate velocities ever measured on any star (apart from our Sun).

$$\delta\nu_{13} = \nu_{n,\ell=1} - \nu_{n-1,\ell=3} = 10\ D_0 \tag{3}$$

The small separations reflect details of the structure of the star while the large separation to first order is a measure of the stellar density (see e.g. Kjeldsen & Bedding 1995). The small separations will decrease during the Hydrogen core burning phase of the stellar evolution and one will therefore potentially be able to determine stellar ages by detailed measurements of the small separations (see e.g. Brown et al. (1994); Gough (2003); and Christensen-Dalsgaard in this volume).

Observing solar-like oscillations is difficult because of the low amplitude (peak amplitudes for individual modes are in most cases below 1 m/s). The frequency of low-degree high-order modes are in most cases between 0.5 and 4 mHz making observations insensitive to low-level night-to-night variations. The first star (apart from the Sun) where solar-like p-mode excess power was found is Procyon (α CMi), an F5 subgiant. Evidence for oscillations was presented as early as 1991 by Brown et al. Since then detections have been claimed in a number of stars, some of them shown in figure 1. For details on the individual stars, see Bedding & Kjeldsen (2003).

3. Seismology of α Cen A

The star α Cen A is a nearby star with the same spectral type as the Sun and it is therefore an obvious target for trying to detect solar-like oscillations. Using the CORALIE spectrograph, Bouchy & Carrier (2001 and 2002) detected p-modes similar to those seen in the Sun. New observations using the UVES instrument (on VLT) and the UCLES spectrograph (on AAT) confirm the frequencies detected by Bouchy & Carrier (see figure 2).

Acknowledgments. This work was supported in part by the Danish National Research Foundation through its establishment of the Theoretical Astrophysics Center.

References

Bedding, T. R., & Kjeldsen, H. 2003, PASA, 20, 203
Bouchy, F. & Carrier, F. 2001, A&A, 374, L5
Bouchy, F., & Carrier, F. 2002, A&A, 390, 205
Brown, T. M., Gilliland, R. L., Noyes, R. W. & Ramsey, L. W. 1991, ApJ, 368, 599
Brown, T. M., Christensen-Dalsgaard, J., Weibel-Mihalas, B. & Gilliland, R. L. 1994, ApJ, 427, 1013
Butler et al. 2003, ApJ Letters, submitted
Gabriel, A. H., et al. 1997, Solar Phys., 175, 207
Gough, D. O., 2003, Ap&SS, 284, 165
Kjeldsen, H., & Bedding, T.R. 1995, A&A, 293, 87

Highlights of Astronomy, Vol. 13
International Astronomical Union, 2003
O. Engvold, ed.

Excitation of P-Modes in the Sun and Stars

Robert Stein, Dali Georgobiani, Regner Trampedach

Michigan State University, East Lansing, MI 48824, USA

Hans-Günter Ludwig

Lund Observatory, Box 43, 22100 Lund, Sweden

Åke Nordlund

Astronomical Observatory / NBIfAFG, Juliane Maries Vej 30, Dk-2100 Copenhagen Ø, Denmark

Abstract. P-mode oscillations in the Sun and stars are excited stochasticly by Reynolds stress and entropy fluctuations produced by convection in their outer envelopes. The excitation increases with increasing effective temperature (until envelope convection ceases in the F stars) and also increases with decreasing gravity.

1. Introduction

Acoustic (p-mode) oscillations have been observed in the Sun and several other stars. They are excited by entropy (non-adiabatic gas pressure) fluctuations and Reynolds stress (turbulent pressure) fluctuations produced in envelope convection zones. Expressions for the excitation rate have been derived by several people (Goldreich & Keeley 1977; Balmforth 1992; Goldreich, Murray & Kumar 1994; Nordlund & Stein 2001; Samadi & Goupil 2001). Evaluation of these expressions depends on knowing the properties of convection. To obtain analytic results it is necessary to make drastic approximations to the convection properties. Using results of numerical simulations of the near surface layers of a star it is possible to calculate the excitation rate of p-modes for the Sun and other stars without the need to make such approximations.

2. Excitation Rate

The excitation rate can be derived by evaluating the PdV work of the non-adiabatic gas and turbulent pressure (entropy and Reynolds stress) fluctuations on the modes. Since excitation is a stochastic process, the work must be averaged over the relative phase between the mode and the pressure. The result (Nordlund & Stein 2001) is

$$\frac{\Delta\langle E_\omega\rangle}{\Delta t} = \frac{\omega^2 \left|\int_r dr \delta P_\omega^* \frac{\partial \xi_\omega}{\partial z}\right|^2}{8\Delta\nu E_\omega} \ . \tag{1}$$

Here, δP_ω is the time Fourier transform of the non-adiabatic total pressure,

$$\delta P^{\mathrm{nad}} = \left(\delta \ln(P_{\mathrm{gas}} + P_{\mathrm{turb}}) - \Gamma_1 \delta \ln \rho\right)(P_{\mathrm{gas}} + P_{\mathrm{turb}}) \ . \tag{2}$$

The non-adiabatic total (gas plus turbulent) pressure is calculated directly from the simulation at each 3D location at each saved time. It is then averaged over horizontal planes and interpolated to the Lagrangian frame at each time. $\Delta\nu = 1/$(total time interval) is the frequency resolution with which δP_ω is computed. ξ_ω is the mode displacement eigenfunction. The mode energy is

$$E_\omega = \frac{1}{2}\omega^2 \int_r dr \ \rho \ \xi_\omega^2 \left(\frac{r}{R}\right)^2 \ . \tag{3}$$

The mode eigenfunctions are evaluated from a complete envelope model, obtained by fitting the mean simulation radial structure to a deeper one-dimensional adiabatic convective envelope.

3. The Simulations

We simulate a small portion of the photosphere and the upper layers of the convection zone by solving the equations of mass, momentum and energy conservation. Spatial derivatives are calculated using third order splines vertically and 5th order compact derivatives horizontally on a non-staggered grid. Time advance is a third order leapfrog scheme (Hyman 1979; Nordlund & Stein 1990). The equation of state includes ionization and excitation of hydrogen and other abundant elements and the formation and ionization of H_2 molecules. Radiative energy exchange is found by solving 3D, LTE, non-gray radiation transfer. Horizontal boundaries are periodic. Vertical boundaries are transmitting, with the entropy of the in-flowing fluid at the bottom of the domain specified.

4. Convection

Convection is driven by radiative cooling in the thin thermal boundary layer at the solar surface. It consists of cool, low entropy, filamentary, turbulent, downdrafts that plunge through a warm, entropy neutral, smooth, diverging, laminar upflow. The low entropy downflows are the site of most of the buoyancy work that drives the convection (Stein & Nordlund 1998).

5. Solar Excitation Rate

Excitation of p-modes peaks at some intermediate frequency. For the Sun, this is 3-4 mHz. The excitation behavior at low frequency is controlled by the behavior of the eigenmodes. Excitation decreases at low frequencies because the mode mass increases and the mode compression decreases as the frequency decreases.

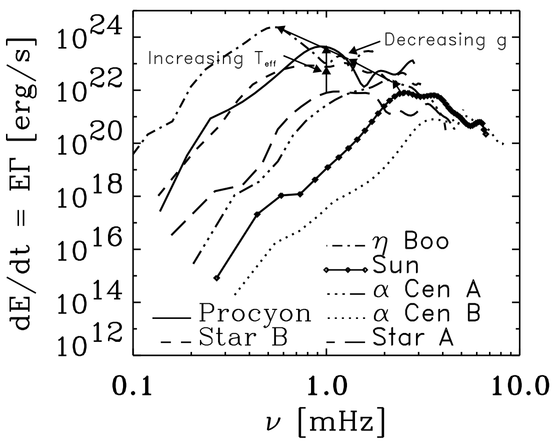

Figure 1. Excitation spectra of stars with varying surface gravity and effective temperature. Excitation increases with increasing effective temperature (until convection ceases) and decreasing surface gravity.

The excitation behavior at high frequencies is controlled by the behavior of the convection. Excitation decreases at high frequencies because the gas and turbulent pressure fluctuations are produced by the convective motions and convective power is concentrated at low frequencies. Most p-mode excitation occurs in the low entropy, turbulent downdrafts and at the edges of granules, close to the surface where the convective velocities and entropy (non-adiabatic gas pressure) fluctuations are largest. At low frequencies the mode driving is spread out over a larger depth range and as the frequency increases the excitation becomes more and more concentrated close to the surface (Stein & Nordlund 2001).

6. Stellar Excitation Rates

Simulations of convection in other stars have been used to calculate their p-mode excitation rates. As the surface gravity of the stars decreases the excitation rate increases and shifts to lower frequency (Fig. 1), and as the effective temperature of the stars increases (until surface convection ceases in F stars) the excitation rate increases with the peak frequency remaining the same (Fig. 1). Figure 2 shows a contour plot of the total (frequency integrated) excitation as a function of surface gravity and effective temperature. The increase in excitation with decreasing gravity and increasing effective temperature can be understood using the approximate mixing length expression for the convective flux solved for the convective velocity

$$V_z = \left[\frac{F_{\rm conv} R_{\rm gas}}{2\rho C_P \mu}\right]^{1/3} , \tag{4}$$

where $F_{\rm conv}$ is the convective flux, $R_{\rm gas}$ is the gas constant, ρ is the density, C_P is the specific heat at constant pressure, and μ is the mean molecular weight of the plasma. Smaller gravity (more giant) stars have lower density, so larger con-

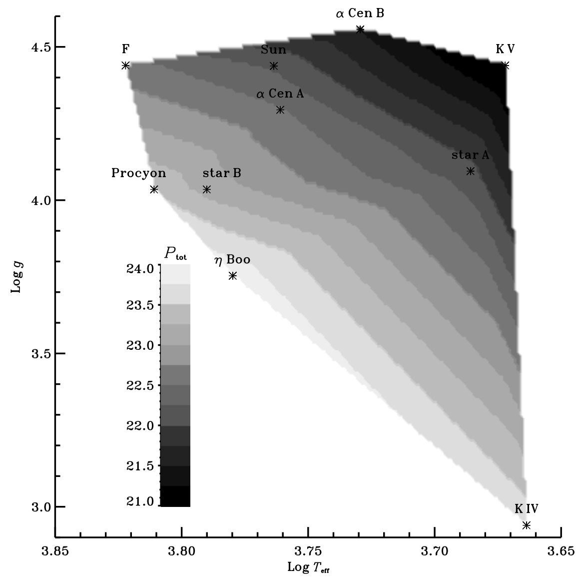

Figure 2. Total excitation (logarithmic scale) increases with increasing effective temperature (until convection ceases) and decreasing surface gravity.

vective velocities and larger Reynolds stresses and entropy fluctuations. Higher effective temperature stars have a larger emerging flux and hence also larger convective velocities.

Acknowledgments. This work was supported in part by NASA grants NAG 5 9563 & NAG 5 12450 and NSF grant 0205500.

References

Balmforth, N. J. 1992, MNRAS, 255, 639

Goldreich, P. & Keeley, D. A. 1977, ApJ, 211, 934

Goldreich, P., Murray, N., & Kumar, P. 1994, ApJ, 424, 466

Hyman, J. 1979, in Adv. in Comp. Meth. for PDE's, vol 3, ed. R. Vichnevetsky & R. S. Stepleman, (New Brunswick: IMACS), 313

Nordlund, Å. & Stein, R. F. 1990, Comp. Phys. Commun., 59, 119

Nordlund, Å. & Stein, R. F. 2001, ApJ, 546, 576

Samadi, R. & Goupil, M.-J. 2001, A&A, 370, 136

Stein, R. F. & Nordlund, Å. 1998, ApJ, 499, 914

Stein, R. F. & Nordlund, Å. 2001, ApJ, 546, 585

Highlights of Astronomy, Vol. 13
International Astronomical Union, 2003
O. Engvold, ed.

Helio- and Asteroseismic Analysis Methods

Jesper Schou

Stanford University, HEPL Annex A201, Stanford, CA 94305-4085, USA

Abstract. Over the past couple of decades increasingly sophisticated analysis algorithms have been developed in helioseismology. Here I will describe some of these with an emphasis on those most relevant to asteroseismology and some of the lessons learned. I will also discuss some of the properties of stellar oscillations and how those affect the analysis.

1. Overview

Helioseismic analysis methods have become increasingly complex as the quality of the data, our understanding of the physics and the available computing power have increased. In section 2 I will briefly review some of these methods.

With the increase in quantity and quality of asteroseismic data (see reviews by Kurtz and Kjeldsen in these proceedings), it is natural to investigate how the helioseismic experience can be applied to the asteroseismic case and where new techniques need to be developed. I will briefly review this in Section 3.

2. Helioseismic Data Analysis

The analysis techniques are generally classified as either global or local. The former are effectively defined as those treating the oscillations as a sum of normal modes. I will review the typical steps in the global methods in the following subsections. For more details see Schou (1992) or Hill et al. (1996). The local methods are reviewed by Haber and Hill in these proceedings.

2.1. Spherical Harmonic Transform

The first step is to isolate the individual spherical harmonics. This is generally done by mapping the images to heliographic coordinates, multiplying by the spherical harmonic and integrating the result. However, only part of the solar surface is observed, and thus the spherical harmonics will not be perfectly isolated, causing so-called leaks. While those can be calculated, imperfections in our knowledge of the image geometry or mode physics will lead to errors.

2.2. Temporal Fourier Transform

The next step is to Fourier transform the time series of each spherical harmonic coefficient. While this is simple, a number of problems exist. In particular it is necessary to remove bad points and to prevent data gaps from causing spectral

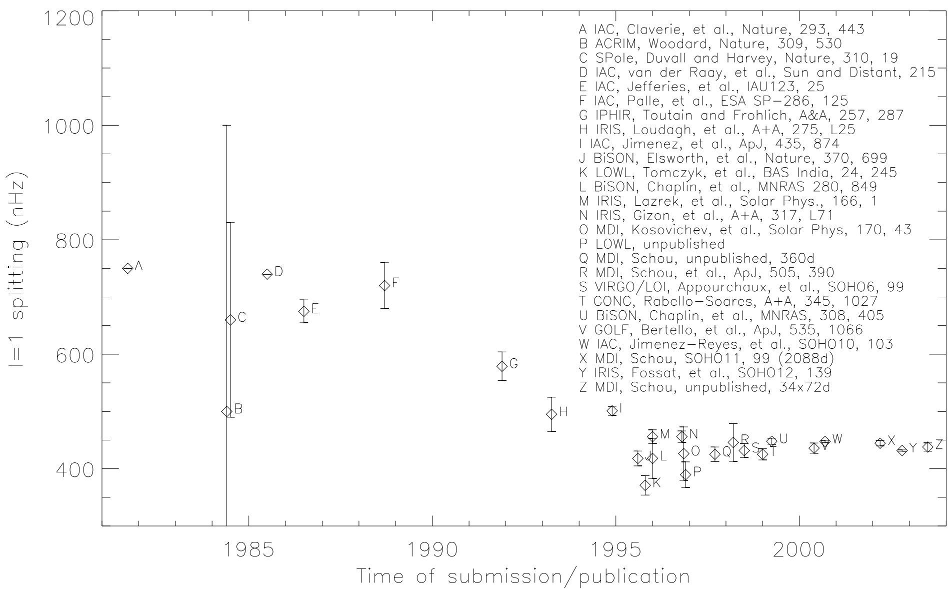

Figure 1. Splittings for $\ell = 1$ (averaged over the available n) as a function of time of submission/publication/generation. Each data point is identified by the experiment and a reference is given.

artifacts. This is typically done by a combination of detrending and gap filling. Due to the large dynamic range in the spectra, it is essential to do this carefully.

2.3. Parameter Estimation

Finally the mode parameters need to be estimated from the spectra. This is, by far, the most complicated part of the analysis. Depending on the modes being studied the methods are categorized as either peakbagging or ridge fitting.

Peakbagging Here, modes with different spherical harmonic degree ℓ can be separated in the spectra, while the azimuthal orders m may or may not be separated. The methods differ in which effects are taken into account and which parameters are fitted versus modeled. Some of the differences are illustrated by the algorithms used by the MDI and GONG projects (see Schou et al. 2002 and Basu et al. 2003 for a more detailed comparison).

The GONG method (Anderson et al. 1990; Hill et al. 1996) fits each (n, l, m) (n is the radial order) separately; the fit is done in the power spectra, no leakage matrix is used and the parameters from a fit of a mode is not used to constrain the properties of that same mode when it appears as a leak.

The MDI method (Schou 1992) is more complex. All m values at each (n, l) are fitted simultaneously, a leakage matrix is used, the leak parameters are constrained and the fit is done in the Fourier domain. However, while using a leakage matrix and constraining the leak parameters should improve the fits, inaccurate leaks can affect the fitted parameters.

Ridge Fitting As leak spacings decrease and line widths increase, modes merge into ridges. While fitting those is fairly easy, it is difficult to relate the fitted parameters to those of the underlying modes, as this requires an accurate leakage matrix. For details see Rhodes et al. (2001) and Korzennik et al. (2003).

3. Asteroseismic Data Analysis

While parts of the asteroseismic analysis techniques, such as the Fourier transforms and peakbagging are similar to those used in helioseismology, other aspects, detailed below, are quite different. For a review see Appourchaux (2003).

3.1. Time series problems

Among the challenges here are low S/N, short time series, low duty cycle, uneven data quality and uneven sampling when combining data from different sites. An example of the problems encountered is shown in Figure 1. The systematic trend in the $\ell = 1$ splitting is most likely not solar in origin, rather it is probably caused by a bias in the estimates for short time-series of spatially unresolved data, such as those available early on for the Sun and those currently available for other stars. While this bias is fairly well understood Figure 1 does illustrate that it is essential to understand the properties of the analysis methods.

3.2. Mode Identification Difficulties

Another problem is to identify the modes. For the Sun the basic parameters are well known, modes can be observed to high ℓ, the spectrum is fairly simple and the identities thus easy to determine. For other stars this is not the case, as illustrated in Figure 2, which shows the tentative identifications of peaks in a WIRE spectrum of α Cen A originally reported by Schou and Buzasi (2001) and the identifications based on additional data (Bouchy & Carrier 2002).

Another set of problems is caused by the complex behavior of the frequencies in some stars caused by the simultaneous presence of modes of different character (e.g. p, f, and g modes). The different modes may have very different line widths or amplitudes and some modes may not be excited to a measurable amplitude or be invisible due to geometric effects. Rapid rotation can also lead to non-linearities and even more confusion.

3.3. Miscellaneous

Other problems encountered include such things as large inherent frequency variations and confusion or frequency changes caused by binary stars. Also a number of decisions have to be made, such as deciding on the number of stars observed versus duration and how the HR diagram should be covered.

4. Conclusion

While some of the above may sound discouraging, the situation is actually quite encouraging. Several ground-based experiments are delivering data, WIRE and MOST have been or are operating in space and other projects, such as COROT, Kepler and Eddington are in various stages of planning or under construction.

Regarding the data analysis it is important to understand the physics, the instrument and the data analysis methods. Hopefully the lessons learned in

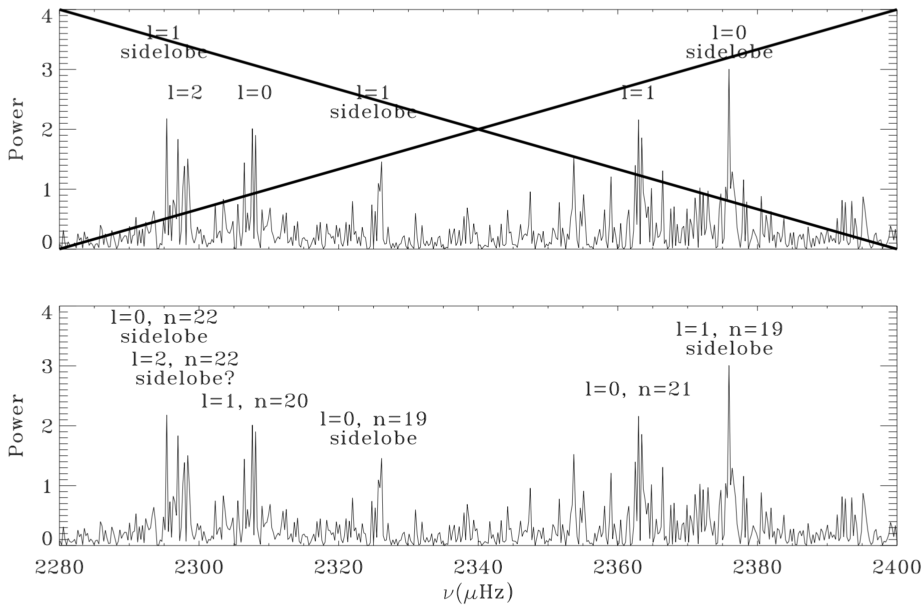

Figure 2. Spectra of α Cen A as observed by WIRE (Schou & Buzasi 2001). Top: original mode identifications. Bottom: revised.

helioseismology will be valuable for asteroseismology and allow for rapid progress to be made.

Acknowledgments. This work was supported by NASA through grants NAG5-10483 and contract NAS5-02139.

References

Anderson, E. R., Duvall, Jr., T. L. & Jefferies, S. M. 1990, ApJ, 364, 699

Appourchaux, T. 2003, Ap&SS, 284, 109

Basu, S., et al. 2003, ApJ, 591, 432

Bouchy, F. & Carrier, F. 2002, A&A, 390, 205

Hill, F., et al. 1996, Science, 272, 1292

Korzennik, S. G., Rabello-Soares, M. C. & Schou, J. 2003, ApJ, submitted (astro-ph/0207371)

Rhodes, E. J., Jr, et al. 2001, ApJ, 561, 1127

Schou, J. 1992, PhD Dissertation, University of Aarhus, Denmark

Schou, J. 1998, SOHO 6/GONG 98, ESA SP-418, 47

Schou, J. & Buzasi, D. L. 2001, SOHO 10/GONG 2000, ESA SP-464, 391

Schou, J., et al. 2002, ApJ, 567, 1234

Highlights of Astronomy, Vol. 13
International Astronomical Union, 2003
O. Engvold, ed.

Observational Results of Full-Disc Helioseismology

Roger New

School of Science and Mathematics, Sheffield Hallam University, Howard Street, Sheffield S1 1WB, UK

Abstract. Ever since the discovery of the low-degree p modes was announced by Claverie et al. (1979), full-disc helioseismology – seismology of the Sun based on the study of sunlight integrated across the entire disc – has contributed very significantly to our understanding of the deep solar interior and the origin and nature of the oscillation modes which probe it. This paper touches on the principal observational techniques used for full-disc helioseismology and outlines key results and their implications.

1. Introduction

In a Sun-as-a-star view, the amplitudes of oscillation modes with degree, ℓ, greater than 4 average very nearly to zero. Hence the particular value of full-disc helioseismic data is that they are optimized for the study of low-ℓ modes. Such modes are vital to inform our understanding of the Sun at depths below about 0.4 R, because the lower the degree of a p mode, the deeper in the Sun is its lower turning point. In addition to studies of the deep interior, full-disc data have been used to investigate the mode physics of low-ℓ oscillations and their solar cycle dependence, to investigate the excitation and damping mechanisms of the modes and to study the background velocity continuum. Finally, a full-disc view can inform the developing field of asteroseismology.

Historically the first extensive helioseismic data sets came from the full-disc ground-based networks, BiSON (Chaplin et al. 1996) and IRIS (Fossat 1995). Observations from the early 1990's are still routinely used in studies requiring extended data sets, for example to enhance mode detection, improve precision or to study solar cycle effects (for example, Chaplin et al. 2000; Salabert et al. 2003), and some studies can be performed with the less well-filled data from earlier epochs and from measurements from single sites.

2. Techniques

Full-disc helioseismic observations are carried out both in velocity and intensity, where the amplitude of the strongest p mode is of the order of 15 cm s^{-1} and a few ppm respectively. The small full-disc Doppler shift in a suitable Fraunhofer line can be determined by use of a resonant scattering spectrometer (RSS) (Grec at al. 1976, Brookes et al. 1978). In current operation, the instruments of the BiSON ground-based network (Chaplin et al. 1996) and the GOLF instrument on the ESA/NASA satellite SOHO (Gabriel et al. 1995) are different implementa-

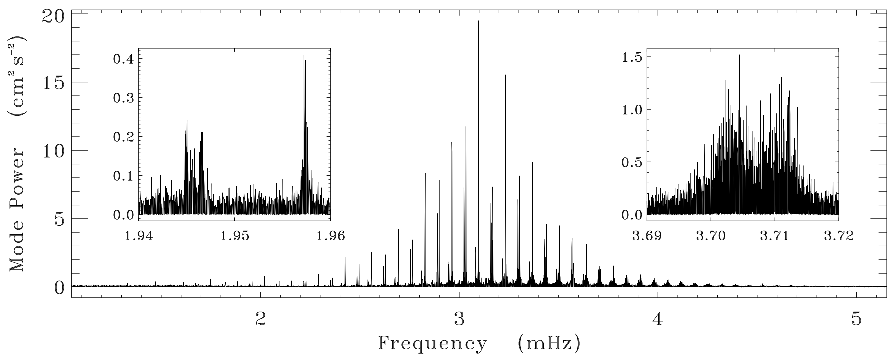

Figure 1. Low-ℓ p-mode spectrum of 3456 days of BiSON data. Each inset panel shows one $\ell = 0$ and one $\ell = 2$ mode. Rotational splitting of the low frequency $\ell = 2$ mode is evident.

tions of the principles of the RSS. The intrinsic stability of the basic technique and careful instrument design means that modes with amplitudes lower than 10 mm s^{-1} can be observed in spectra of long data-sets.

Although extremely difficult from the ground due to the influence of the atmosphere, full-disc intensity measurements made by space-borne irradiance monitors have made a significant contribution to helioseismology. Pioneering observations were performed using the ACRIM instrument on the Solar Maximum Mission satellite (Woodard 1984), by IPHIR on PHOBOSII (Fröhlich et al. 1988), and the current VIRGO package on SOHO has full-disc (SPM) and low-resolution (LOI) intensity instruments (Fröhlich et al. 1995).

In addition to full-disc data, resolved-Sun low-ℓ results, such as those from MDI, GONG and ECHO have great value – as will be alluded to in Section 4.

3. The Low-ℓ Spectrum and the Deep Solar Interior

Figure 1 illustrates two important features of the p-mode spectrum. Firstly, the mode amplitude falls off at both low and high frequency and, secondly, mode widths increase (by about 2 orders of magnitude) over the visible spectrum.

Near the center of the p-mode spectrum the frequency uncertainties can be as low as a few ppm and the intrinsic narrowness of the lower frequency modes allows their central frequencies to be determined to better than 10 nHz, even though the modes have low amplitudes (García et al. 2001; Chaplin et al. 2002a). More extended observation will improve this precision as the uncertainty scales as $T^{-1/2}$, where T is the data-set length. The high precision already achieved makes the frequencies of the low-ℓ p modes a very effective probe of the deep interior. Although, for a given ℓ, modes of higher frequency (and, therefore, higher radial order, n) penetrate deeper into the Sun, it is often the narrow, low-n, modes which can be used most easily to test models. See Goode (2001) for illustration and discussion.

Low-degree oscillation frequencies have been of great value in testing models of structure and dynamics of the deep interior. Firstly, well before the recent results from the Sudbury Neutrino Observatory confirmed the existence of neutrino oscillations, the level of agreement between "standard" solar model predictions and observed low-ℓ p mode frequencies suggested that there would not be an "astrophysical" solution to the solar neutrino problem (see, for example, Chaplin et al 1997a). The agreement between calculated and observed frequencies is not, however, exact, and much theoretical effort is being focused on models with modified stratification near the core (Guzik et al 2000; Turck-Chièze et al. 2001; Gough 2003). For observers, the challenge is to produce ever more precise mode frequencies to better inform the model tests. This requires more extended observations and more detailed investigation of solar cycle variations.

Secondly, full-disc helioseismology has contributed significantly to understanding of the rotation of the deep interior, providing compelling evidence for a slowly (i.e. approximately surface rate) rotating core (see the review by Thompson et al. (2003)). The rotational splitting of the $\ell > 0$ p modes (evident in the low frequency example in Figure 1) causes the individual $\ell + m$ even components (the only ones detectable in a full-disc view from Earth-orbit) to be separated by about 800 nHz. This is very much less than the line width of the modes at the higher frequency end of the spectrum. Great care is required to extract reliable estimates of rotational splittings from power spectra, and, again, low-n modes are of great value because of their intrinsically small line width.

Two problems need to be flagged at this point. Firstly, p-mode parameters, including frequency, are functions of solar activity. It is becoming ever more important when using p-mode frequencies to test core models, and multiplet splittings to study rotation, that allowance is made for the activity level extant during the period of observation (Dziembowski & Goode 1997). The phenomenology of solar cycle variations has been studied in detail in recent years (see Howe et al. (2003) and references therein) and cycle-dependent asymmetries have been reported in the $\ell = 2$ multiplets used for rotation studies (Chaplin et al. 2003). Techniques for de-trending the data need further development.

Secondly, the peak profiles in the frequency spectrum are asymmetric. Fitting procedures have been developed which allow for, and determine the extent of, such asymmetries, returning more reliable estimates of the central frequencies of the modes, but recent comparisons between BiSON and GONG data show that the asymmetries are not yet fully understood (Howe et al. 2003).

4. Mode Parameters and the Solar Cycle

Although they can be determined with much poorer fractional uncertainty than central frequencies, there is also much important information to be gained from the widths and "strengths" of the p-mode profiles. Useful science can be obtained by studying peak heights over short time scales and by extracting peak heights and widths from analysis of power spectra of long time series.

The former analysis allows a test of the theory that p modes are generated by stochastic turbulence in the outer layers of the convection zone. Kumar et al. (1988) predicted that the distribution of mode powers, determined on a time scale short compared to the mode lifetimes, would follow negative exponential statistics. A number of studies (Chaplin et al. 1997b; Chang & Gough 1998;

Foglizzo et al. 1998) have shown this to be very largely the case, but longer data sets would help confirm the nature of a small number of extreme events.

More detailed information can be gained from the fitting of peak shapes to power spectra of long time series. Based on evidence that the modes are stochastically excited, fitting procedures generally employ maximum likelihood techniques to optimize the mode heights, widths, splittings, asymmetries and, where appropriate in ground based data, sideband leakage. Such analysis is not trivial and a wide range of studies have been carried out testing different strategies on real data, testing the data "pipelines" with simulated data and comparing results obtained from contemporaneous data from different instruments (for example, Thierry et al. 2001; Schou et al. 2002; Howe et al. 2003).

A number of points of consensus have been arrived at. Firstly, the variation of line width with frequency has been characterized and is in reasonable agreement with models of p-mode damping based on turbulent convection (Houdek et al. 2001). Secondly, the mode widths and powers are seen to change through the solar cycle. The widths increase by of the order of 20% near the center of the spectrum, while amplitudes fall by about 50% (Chaplin et al. 2000). To within the precision of present data, the width and power variations are consistent with increasing mode damping at high activity, while the energy supply rate from the stochastic source remains constant (Chaplin et al. 2002b; Jiménez et al. 2002).

References

Brookes, J. R., Isaak, G. R., & van der Raay, H. B. 1978, MNRAS, 185, 1

Chang, H-Y., & Gough, D. O. 1998, Solar Phys., 181, 251

Chaplin, W. J., Elsworth, Y., Isaak, G. R., Lines, R., McLeod, C. P., Miller, B. A., New, R., & van der Raay, H. B. 1996, Observatory, 116, 32

Chaplin, W. J., Elsworth, Y., Isaak, G. R., McLeod, C. P., Miller, B. A., & New, R. 1997a, ApJ, 480, L75

Chaplin, W. J., Elsworth, Y., Howe, R., Isaak, G. R., Lines, R., McLeod, C. P., Miller, B. A., & New, R. 1997b, MNRAS, 287, 51

Chaplin, W. J., Elsworth, Y., Isaak, G. R., Miller, B. A., & New, R. 2000, MNRAS, 313, 32

Chaplin, W. J., Elsworth, Y., Isaak, G. R., Miller, B. A., & New, R. 2002a, MNRAS, 330, 731

Chaplin, W. J., Elsworth, Y., Isaak, G. R., Miller, B. A., New, R., & Toutain, T. 2002b, ApJ, 582, L115

Chaplin, W. J., Elsworth, Y., Isaak, G. R., Miller, B. A., New, R., Thierry, S., Boumier, P., & Gabriel, A. H. 2003, MNRAS, 343, 343

Claverie, A., Isaak, G. R., McLeod, C. P., van der Raay, H. B., & Roca Cortés, T. 1979, Nature, 282, 591

Dziembowski, W. A., & Goode, P. R. 1997, A&A, 317, 919

Foglizzo, T., García, R. A., Boumier, P., Charra, J., Gabriel, A. H., Grec, G., Robillot, J-M., Roca Cortés, T., Turck-Chièze, S., & Ulrich, R. K. 1998, A&A, 330, 341

Fossat, E. 1995, in ASP Conf. Ser. Vol. 76, GONG'94: Helio- and Astero-Seismology, eds., R. K. Ulrich, & E. J. Rhodes Jr., 387

Fröhlich, C., Bonnet, R. M., Bruns, A. V., Delaboudinière, J. P., Domingo, V., Kotov, V., Rashkovsky, D. N., Toutain, T., Vial, J. C., & Wehrli, C. 1988, in ESA SP Vol.286, Seismology of the Sun and Sun-like Stars, ed. E. J. Rolfe, 359

Fröhlich, C., Romero, J., Roth, H., Wehrli, C., Andersen, N. B., Appourchaux, T., Domingo, V., Telljohann, U., Berthomieu, G., Delache, P., Provost, J., Toutain, T., Crommelnyk, D., Chevalier, D., Fichot, A., Däppen, W., Gough, D., Hoeksema, T., Jimenéz, A., Gómez, M. F., Herreros, J., Roca Cortés, T., Jones, A. R., Pap, J., & Willson, R. C. 1995, Solar Phys., 162, 101

Gabriel, A. H., Grec, G., Charra, J., Robillot, J-M., Roca Cortés, T., Turck-Chièze, S., Bocchia, R., Boumier, P., Cantin, M., Cespédes, E., Cougrand, B., Crétolle, J., Damé, L., Decaudin, M., Delache, P., Denis, N., Duc, R., Dzitko, H., Fossat, E., Fourmond, J. J., García, R., Gough, D., Grivel, C., Herreros, J. M., Lagardère, H., Moalíc, J. P., Pallé, P. L., Pétrou, N., Sanchez, M., Ulrich, R., & van der Raay, H. B. 1995, Solar Phys., 162, 61

García, R., Régulo, C., Turck-Chièze, S., Bertello, L., Kosovichev, A. G., Brun, A. S., Couvidat, S., Henney, C. J., Lazrek, M., Ulrich, R. K., & Varadi, F. 2001, Solar Phys., 200, 361

Goode, P. R. 2001, Solar Phys., 200, 343

Gough, D. O. 2003, Ap&SS, 285, 341

Guzik, J. A., Neuforge-Verheeke, C., Young, A. C., Epstein, R. I., Poulin, F. M., & Schissel, J. R. 2000, Solar Phys., 200, 305

Grec, G., Fossat, E., & Vernin, J. 1976, A&A, 50, 221

Houdek, G., Chaplin, W. J., Appourchaux, T., Christensen-Dalsgaard, J., Däppen, W., Elsworth, Y., Gough, D. O., Isaak, G. R., New, R., & Rabello-Soares, M. C. 2001, MNRAS, 327, 483

Howe, R., Chaplin, W. J., Elsworth, Y., Hill, F., Komm, R., Isaak, G. R., & New, R. 2003, MNRAS, 588, 1204

Jiménez, A., Roca Cortés, T., & Jiménez-Reyes, S. J. 2002, Solar Phys.,209, 247

Kumar, P., Franklin, J., & Goldreich, P. 1988, ApJ, 328, 879

Salabert, D., Jiménez-Reyes, S. J., & Tomczyk, S. 2003,A&A, 408,729

Schou, J., Howe, R., Basu, S., Christensen-Dalsgaard, J., Corbard, T., Hill, F., Komm, R., Larsen, R. M., Rabello-Soares, M. C., & Thompson, M. J. 2002, ApJ, 567, 1234

Thierry, S., Boumier, P., Gabriel, A. H., & GOLF team 2001, in ESA SP Vol. 464, SOHO10/GONG Workshop: Helio- and Asterosiesmology at the dawn of the Millennium, eds, A. Eff-Darwich, P. Palle, & A. Wilson, 119

Thompson, M. J., Christensen-Dalsgaard, J., Miesch, M. S., & Toomre, J. 2003, Annual Rev. Astron. Astrophys., 41, 599

Turck-Chièze, S., Nghiem, P., Couvidat, S., & Turcotte, S. 2001, Solar Phys., 200, 323

Woodard, M., 1984, Nature, 309, 530

Highlights of Astronomy, Vol. 13
International Astronomical Union, 2003
O. Engvold, ed.

Seismology of Solar Internal Rotation

Takashi Sekii

Solar Physics Division, National Astronomical Observatory of Japan, Mitaka, Tokyo 181-8588, JAPAN

Abstract. Helioseismologists have been highly successful in revealing how the solar interior differentially rotates, through observations of rotationally split eigen p modes of the Sun. What we currently know about the internal rotation of the Sun is reviewed, and outstanding issues are discussed.

1. Introduction

The 22-year solar activity cycle is believed to be caused by an interplay between magnetic field and internal flows, of which differential rotation seems to constitute the main component. The surface differential rotation of the Sun has been known for a long time, but observational study of the internal differential rotation was not possible until the era of helioseismology. Realistic numerical simulation is extremely difficult, owing to the large Reynolds number in the solar convection zone. Thus helioseismology provides an essential tool in probing the internal dynamics of our star. Seismological study of solar internal rotation is important not only in advancing our understanding of the solar cycle, but also in posing constraints on theory of the dynamical evolution of stars.

2. Rotational splitting

Rotation affects wave propagation in the Sun, thereby modifying frequencies of eigenmodes mainly via advection. The Sun is a slow rotator in the sense that the rotational period is much longer than the global dynamical time scale. Linear perturbation theory is therefore applicable. The frequency shift of a mode is then $m\times$(average rotation rate), where m is the azimuthal order of the mode. Observed shifts indicate that average rotational periods are of the order of a month, as is observed on the surface, justifying the linear treatment. The way the average is taken, expressed by a sensitivity function, differs from mode to mode. The sensitivity function, called *splitting kernel*, is calculable from an equilibrium model. Given a distribution of angular velocity, therefore, one can calculate the rotational shift of eigenfrequency for any eigenmode. This is sometimes called the forward problem. The inverse problem, then, is to find the underlying angular velocity distribution from an observed set of rotational shifts.

3. Inversion

Since the forward problem is linear, the inverse problem can also be formulated as a linear problem. For discussion for linear inversion methodology see, e.g., Sekii (1997). Modern experiments, such as the GONG project and the SOHO satellite, have produced splitting data of unprecedented quality, which have subsequently been inverted to obtain angular velocity in the solar interior (Thompson et al. 1996; Schou et al. 1998). It was found that, throughout the convection zone, latitudinal differential rotation is similar to that of the surface. Near the base of the solar convection zone there is a shear layer, beneath which there is no strong differential rotation i.e. the rotation profile is consistent with that of a rigid rotation.

4. Tachocline

The position of the shear layer near the base of the convection zone, called *tachocline* (Spiegel and Zahn 1992), coincides with a sound speed anomaly found from sound speed inversions (Gough et al. 1996). This may be evidence for extra mixing caused by the shear (Gough & McIntyre 1998), which circulates back the gravitationally settled helium to the convection zone, thereby reducing the local mean molecular weight. The dynamics of the tachocline is becoming one of the hottest topics in astrophysical fluid dynamics (e.g. Garaud 2003). Howe et al. (2000) examined temporal variation of the layer and reported a 1.3-year periodicity.

5. Rotation in the convection zone

In classical numerical simulations of the solar convection zone, as presented by Glatzmaier (1985), Taylor-Proudman type columnar rotation is produced in the low- to mid-latitudes. By ignoring the inertia term in the fluid equation of motion for a stationary flow, it can be shown that the z-gradient of rotational velocity is proportional to $\sin\chi$, where z runs parallel to rotation axis and χ is the angle between density gradient and pressure gradient. For a barotropic fluid, χ vanishes and so does the z-gradient (Taylor-Proudman theorem). Helioseismic results show that this is not the case, and that the departure from the columnar rotation is in the sense of a warm pole. From the departure, we can estimate the angle χ and even compute the nominal latitudinal gradient of temperature T along the constant pressure surface, by assuming the ideal gas equation of state. The result is that the relative temperature gradient $\partial \log T/\partial\phi$, where ϕ is colatitude, is of the order of 10^{-7} (Sekii 2003). The number is so small basically because the rotation is so slow. This departure must have been caused by terms ignored in the equation, such as the Reynolds stress. According to Elliott (2003), however, Reynolds stress alone cannot explain the departure.

6. Implication on dynamo

Classical α–ω dynamo models required a large radial gradient of angular velocity in the solar convection zone. According to the current view, however, there is no such gradient. This led to the idea of dynamo action in the tachocline region (Choudhuri 1990; Parker 1993). Dikpati & Charbonneau (1998) were the first to carry out kinematic dynamo calculation by using the helioseismologically inferred rotation rate. Such models tend to produce butterfly diagrams with eruption too far from the equator. Nandy & Choudhuri (2002) suggested that meridional flow penetrating into the radiative zone can solve the problem. This is of course so-called flux-transport dynamo.

Hathaway et al. (1996) found a surface pole-ward flow of up to 20m/s from GONG data. With time-distance technique applied to MDI data, Giles et al. (1997) found that such a flow persists down to the depth of 30Mm below the photosphere. In both cases, the flow was detected up to a latitude of around 60°. The biggest unanswered question concerns the properties of the counter flow, particularly in the context of a flux-transport dynamo. If the overall circulation satisfies anything like $|\rho v| \sim$ const. (cf. Gough & Sekii 1998), then the counterflow velocity will be very small and difficult to detect.

7. Polar Region

Rotation inversions of MDI data indicated the presence of a jet, as well as an extra amount of slowing down towards the pole, in the high-latitude region (Schou et al. 1998). Global mode splitting is rather insensitive to this region, which renders it difficult to confirm these findings. Local-helioseismology may be the way, especially if the Sun can be viewed from a high-latitude. Such a proposition has indeed been made, for the Solar Orbitor mission (Gizon et al. 2001). The success of the local approach however has so far been confined to the near-surface layers and it remains to be seen how deep we can go with this new approach.

8. Deep interior

Without g-mode splitting data, we have to rely on low-degree p modes for investigation of deep core rotation. For low-degree modes, full disc, Sun-as-a-star observation seems to have an advantage over spatially resolved observation (and is more relevant to stellar case) but there is a problem of line blending: splitting measurement tends to be biased when line widths are comparable to rotational shifts. Also, there is an issue of poor localization due to lack of odd parity modes. Without these modes, the sensitivity function for combinations of $\ell = 1$ modes, for example, have a different angular profile from the one from $\ell = 2$ modes. Therefore, the rotation rate sampled by dipole modes and by quadrupole modes are difficult to disentangle.

9. Near Future

Helioseismology has played a crucial role in revealing the dynamics of the solar interior. In the bulk of the solar convection zone we now know enough to tell that classical dynamo models do not work, which has inspired new models. Deep interior and polar region have been illusive and they may remain so for a while. Local helioseismology will give us further clues for the entire dynamical picture and this *may* not be confined to the surface layers alone.

Kawaler, Sekii & Gough (1999) looked at data from the WET campaign on pulsating white dwarfs PG1159 (Winget et al. 1991) and GD358 (Winget et al. 1994), to find evidence for differential rotation. Recently, Aerts et al. (2003) reported evidence for non-rigid rotation in a β-Cephei variable HD129929. Application to stars has begun, which is challenging but doubtlessly worthwhile.

References

Aerts, C. et al. 2003, Science, 300, 1926

Choudhuri, A. R. 1990, ApJ, 355, 733

Dikpati, M., & Charbonneau, P. 1999, ApJ, 518, 508

Elliott, J. R. 2003, in Stellar Astrophysical Fluid Dynamics, ed. M. J. Thompson & J. Christensen-Dalsgaard (Cambridge University Press), 315

Garaud, P. 2003, in Stellar Astrophysical Fluid Dynamics, ed. M. J. Thompson & J. Christensen-Dalsgaard (Cambridge, Cambridge University Press), 131

Giles, P. M. et al. 1997, Nature, 390, 52

Gizon, L., et al. 2001, in Solar Encounter: The First Solar Orbitor Workshop, ed. B. Battrick & H. Sawaya-Lacoste (Noordwijk, ESA), 227

Glatzmaier, G. 1985, ApJ, 291, 300

Gough, D., & McIntyre, M. E. 1998, Nature, 394, 755

Gough, D. O., & Sekii, T. 1998, in Sounding Solar and Steller Interiors, ed. G. Berthomieu, J. Provost and F. X. Schmider (Nice, Observatoire de la Côte d'Azur), 93

Gough, D. O. et al. 1996, Science, 272, 1296

Hathaway, D. et al. 1996, Science, 272, 1306

Howe, R. et al. 2000, Science, 287, 2456

Kawaler, S. D., Sekii, T., & Gough, D. O. 1999, ApJ, 516, 349

Nandy, D., & Choudhuri, A. R. 2002, Science, 296, 1671

Parker, E. N. 1993, ApJ, 408, 707

Schou, J. et al. 1998, ApJ, 505, 390

Sekii, T. 1997, in Sounding Solar and Steller Interiors, ed. G. Berthomieu, J. Provost & F. X. Schmider (Dordrecht, Kluwer Academic), 189

Sekii, T. 2003, in Stellar Astrophysical Fluid Dynamics, ed. M. J. Thompson & J. Christensen-Dalsgaard (Cambridge, Cambridge University Press), 263

Spiegel, E. A., & Zahn, J.-P. 1992, A&A, 265, 106

Thompson, M. J. 1996, Science, 272, 1300

Winget, D. E. et al. 1991, ApJ, 378, 326

Winget, D. E. et al. 1994, ApJ, 430, 839

Highlights of Astronomy, Vol. 13
International Astronomical Union, 2003
O. Engvold, ed.

Local Helioseismology – What Does It Really Tell Us?

Frank Hill

National Solar Observatory, PO Box 26732, Tucson Arizona USA 85726-6732

Abstract. The three major local helioseismology methods of time-distance, ring diagrams, and acoustic holography are briefly summarized along with their advantages and disadvantages. Useful tests with artificial data are outlined, and current data comparisons briefly described.

1. Introduction

The subfield of local helioseismology is now 15 years old. In its brief history, it has yielded maps of flows beneath the solar surface, images of active regions on the far-side of the Sun, and inferences about the sound speed below sunspots. However, there has not yet been a systematic study of the consistency among results obtained with the three major local methods of time-distance, acoustic holography, and ring diagrams. In addition, realistic numerical simulations of data suitable for testing the methods have proven difficult to construct. This paper gives a brief overview of the methods, comparing them from a heuristic point of view. It also discusses the types of tests that would be desirable, and presents the latest results from a data-based comparison exercise now underway.

2. Ring Diagrams

Ring diagrams (Hill 1988) are constructed by computing the three-dimensional power spectrum in a local area on the solar surface. Slicing the spectrum at constant temporal frequency ν reveals the solar oscillation signal as a set of concentric rings. The offset of the rings in horizontal wavenumber components k_x and k_y is a measure of the subsurface flow. The analysis is typically done with a "dense-pack" of 189 areas of diameter 15° and spacing of 7.5° in heliographic coordinates. The ring offset is then inverted to infer the flows as a function of depth below each area.

The advantages of the method are that it is straightforward; the effective averaging over the area reduces the random errors; the inversion is easy to perform; and the resolution kernels of the inversion are simple to interpret. The disadvantages are the relatively low spatial resolution; it is mainly limited to near-surface layers; and the results may be sensitive to the absorption of p modes by sunspots.

3. Time-Distance

The time-distance method (Duvall et al. 1993) is very similar to the methods of terrestrial seismology. An acoustic source emits sound which travels along the ray paths prescribed by the solar structure and the properties of the acoustic emission. The observed relationship between the distance from the source and the acoustic travel time is a measure of conditions below the surface. The waves can be reflected multiple times within their thermal cavity. Time-distance diagrams are constructed either from the $\ell - \nu$ diagram, or from velocity cross-correlations. A typical analysis period is 8 hours.

The one *major* advantage of time-distance is the high spatial resolution of less than 1 arc min that can be achieved with the method. There are a number of disadvantages – the inversion is difficult; the averaging kernels are hard to interpret; it is limited primarily to near-surface layers; the errors in the results cannot be simply estimated; and the height of formation of the spectral line used for the observations can introduce additional time delays in localized areas.

4. Holography

Acoustic holography (Lindsey & Braun 1990) is completely analogous to optical holography. The method analyzes the pattern of interference of acoustic waves that are either emitted from sources or are scattered from subsurface inhomogeneities. The observed interference pattern is computationally regressed through a solar model to infer the structure below the surface. The method can control the depth of the focal plane to bring structures into view.

The advantages of the method are the high spatial resolution that can be achieved; the ability to infer the local sound speed; and the ability to probe very deeply. Indeed, holographic images of the far side of the Sun are now routinely made and have proven valuable for solar activity and space weather forecasting. The disadvantages are the difficulty of removing the influence of the surface on the results; the absence of averaging kernels and error estimates; and the difficulty of inferring velocity fields.

5. General Limits

All three methods have four common limitations. Perhaps the most worrisome is that the basic assumption of the response of the wave field to the flows is theoretically and numerically unverified. This shortcoming should be resolved soon as several efforts to simulate the observations are underway. A second disadvantage is that the methods are insensitive to the vertical component of the velocity field. Since the waves must travel both downward and upward, the effects of vertical flows cancel out to first order and only second-order effects survive.

All of the methods are limited by a trade-off between depth and spatial resolution. Since fewer modes reach deeper depths, the best horizontal spatial resolution is achieved near the surface and degrades with depth. Finally, the spherical surface of the Sun causes the horizontal spatial Nyquist wavenumber to decrease near the limb. This foreshortening limits the local results to near disk center.

6. Tests

In the absence of theoretical and numerical confirmation of the methods, work has shifted to comparisons of methods on common data sets and to comparison of data sets with common methods. The Local Helioseismology Comparison (LoHCo) group has been formed for this purpose. This group has compared ring-diagram flow fields from GONG and MDI data sets; ring-diagram and time-distance flows from a common MDI data set; time-distance travel times from GONG and MDI; and both near- and far-side holography on GONG and MDI. The results can be simply summarized: there is large-scale agreement between methods and data sets, with differences in the details. More specifically, the results concerning rotation and torsional oscillations are robust, but the inferences about counter-cell meridional flows, flows below sunspots, and changes in the tachocline are less so. Not surprisingly, the noise level in the observations plays a role, particularly when it is a function of spherical harmonic degree.

The major drawback of observational comparisons is that the actual structure of the Sun is unknown. Thus, an unsuspected systematic error common to all methods could dominate the results and lead to unjustified complacency. This has motivated a number of efforts to simulate the observations including a known solar internal structure or flow field. The full numerical simulation is quite formidable, as it requires a physically self-consistent wave field and flow field. Several approximations to the problem are currently in progress, such as the construction of the wave field from an artificial ring-diagram spectrum without attempting self-consistency. Even this “physics-lite” approach is valuable, particularly with a zero flow field as a null test.

7. Conclusion

Local helioseismic methods can provide images of velocity fields and sound speed structures in the outer solar layers. These images provide important information on the origin of the solar activity cycle and the solar internal dynamics. However, much remains to be done in the testing and verification of these methods.

References

Duvall, T.L. Jr., Jefferies, S.M., Harvey, J.W., & Pomerantz, M.A. 1993, Nature, 362, 430

Hill, F. 1988, ApJ, 333, 996

Lindsey, C., and Braun D.C. 1990, Solar Phys, 126, 101

Highlights of Astronomy, Vol. 13
International Astronomical Union, 2003
O. Engvold, ed.

Solar Meridional Flows: Recent Findings

Deborah A. Haber & Bradley W. Hindman
JILA and Dept. of Astrophysical and Planetary Sciences, University of Colorado, Boulder, CO 80309-0440, USA

Abstract. We report new measurements of the sun's global meridional circulation within the near-surface shear layer for the years 1996 to 2003. The flows are obtained using the local helioseismic technique of ring analysis applied to MDI Dynamics Program data. The most recent estimates of the solar p-angle correction to this data have been incorporated. Previously published accounts that the solar meridional circulation possesses multiple cells within the northern hemisphere (Haber et al. 2002) are not contradicted by the new findings. We do find, however, that with the inclusion of the p-angle correction, cross-equator flows have been eliminated.

1. Introduction

The meridional circulation deduced using local helioseismology techniques such as ring analysis and time-distance tomography reveals asymmetries between the northern and southern hemispheres (Giles 1999; Haber et al. 2000, 2002; Zhao & Kosovichev 2003). The asymmetries manifest themselves as a southward flow across the equator on the order of 6 m s^{-1}, as multiple meridional cells in the northern hemisphere from 1998 to the present, or as faster flows in the southern hemisphere.

There has been general agreement that a southward flow across the equator is seen in the MDI data (e.g., Schou & Bogart 1998; Basu & Antia 2000; Haber et al. 2000, 2002). However, some researchers have suggested that this cross-equator flow arises from a misidentification of the Sun's rotational axis. There are not any fundamental theoretical reasons why the meridional flow should vanish at the equator. But the orientation of the MDI CCD chip with respect to the solar north pole is only known to a few tenths of a degree. A small error in the measurement of the p-angle can lead to mixing of the large differential rotation signal into what is identified as meridional flow.

Haber et al. (2002) and Giles (1999) both saw reversal of the meridional flow in a submerged zone in the northern hemisphere starting in 1998, while in the southern hemisphere the meridional flow remained polewards at all depths. This finding has not been universally reported (Chou & Dai 2001). These discrepant findings may result from the use of instruments with different (or minimal) p-angle errors, or they may arise from differences in the depth dependence of the averaging kernel sensitivities.

2. Meridional Flow Observations With and Without Corrections

There now exist measurements of the MDI p-angle offset acquired by cross-correlating MDI data with coeval GONG data whose p-angle was calibrated using Mercury transits of the Sun (Toner 1999). The results of these comparisons have shown that the north pole of the MDI images diverges from the nominal solar rotation axis by 0.2°, yielding an error of ~ 7 ms^{-1} in the meridional flow. An additional effect that should be considered is an error in the determination of the Carrington elements. Giles (1999) performed a fit to time-distance measurements of the meridional flow for two years of MDI data and discovered that $\Delta i = -(0.091 \pm 0.012)^\circ$ and $\Delta\Omega = -(0.18 \pm 0.10)^\circ$ where i is the inclination of the solar equator to the ecliptic and Ω is the longitude of the ascending node of the solar equator on the ecliptic plane.

The observations reported here were generated using the ring analysis technique described briefly in Hill's review of local helioseismology appearing in this volume (2003) and in Haber et al. (2002). Figure 1 shows the longitudinally and temporally averaged meridional flows at a depth of 11.6 Mm for the years 1996 to 2003. Both the original processing of the full MDI Dynamics Programs

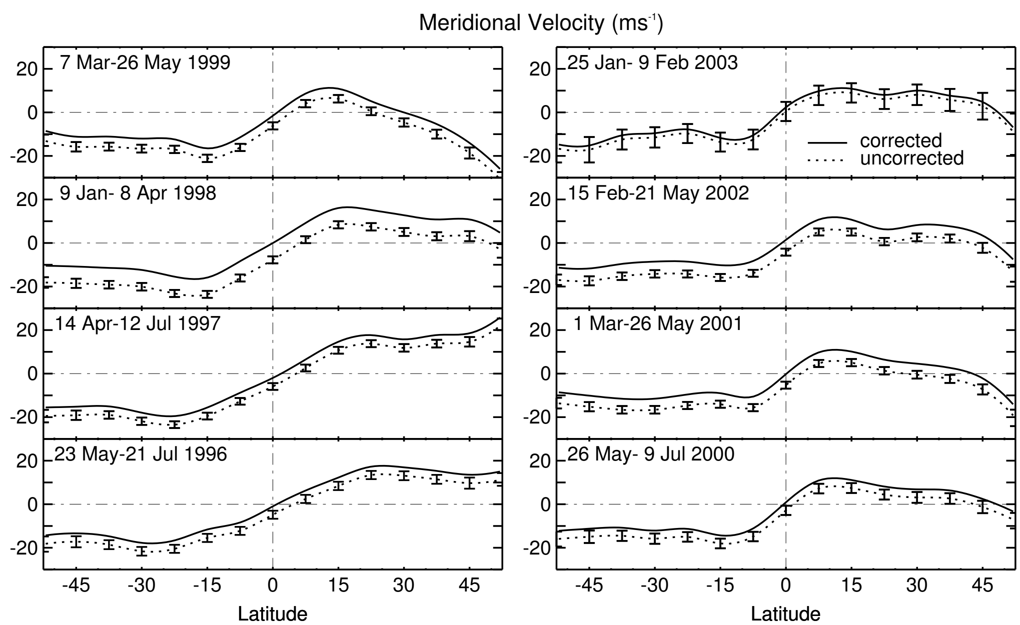

Figure 1. Mean meridional flows determined from longitudinal and temporal averages over the dense-pack mosaic for the full MDI Dynamics period from each of the past 8 years for the uncorrected data (dashed line) and the corrected data (solid line). The results of the inversions at a depth of 11.6 Mm are shown with 10 σ error bars, where σ is the formal error. Notice that the velocity at the equator tends to be smaller for the corrected data and that the latitude at which the meridional flow becomes negative in the northern hemisphere is higher than in the uncorrected case.

and the same data corrected for the p-angle and possible misidentification of the Carrington elements are shown. Figure 2 presents (a) the uncorrected and (b) the corrected meridional circulation over the years 1998 to 2003 as a function of latitude and depth. The extent of the additional meridional cell is more clearly portrayed in this representation. We see that the submerged meridional cell with reversed flow in the northern hemisphere still exists after the data has been

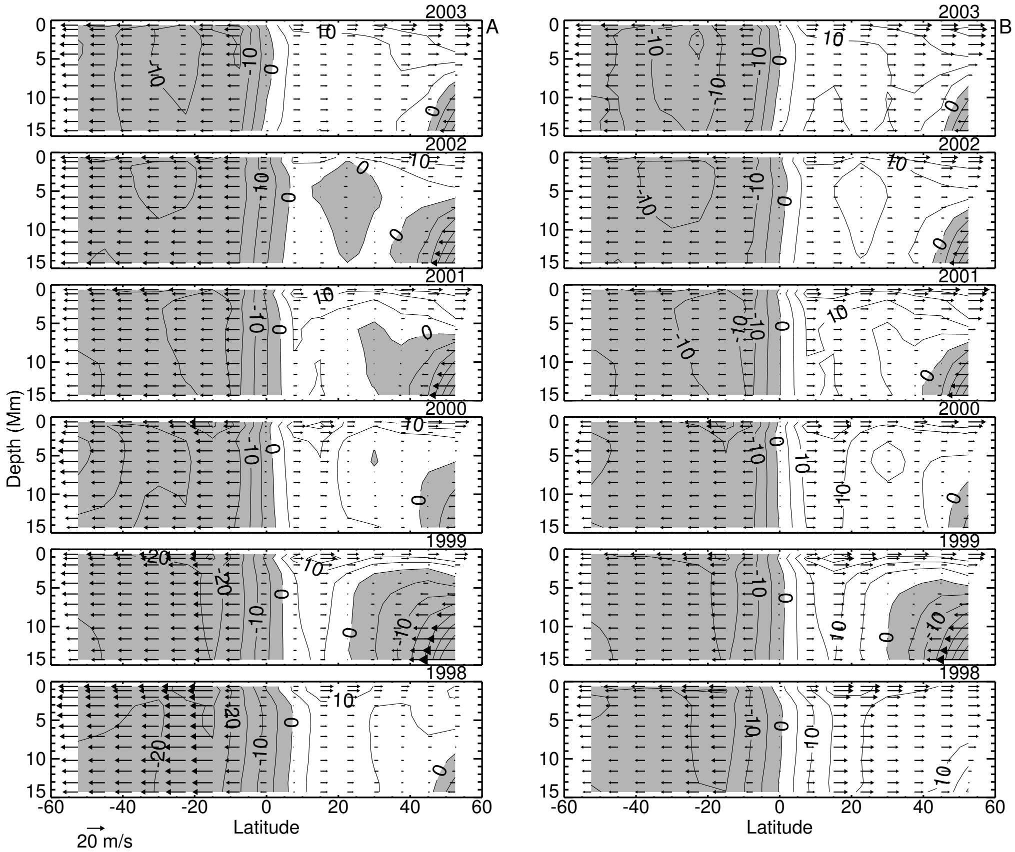

Figure 2. The longitudinally and temporally averaged meridional flow as a function of latitude and depth: (*a*) uncorrected and (*b*) corrected for the misidentified p-angle and Carrington elements. The meridional flows are indicated with both contours and arrows, with the negative contours corresponding to southerly flow (shaded in grey). The submerged cell of reversed circulation in the northern hemisphere appears in both the corrected and uncorrected data.

corrected. Albeit this cell appears at greater depths and higher latitudes than previously reported. In any case, the meridional flow in the northern hemisphere became very different from that in the southern hemisphere as magnetic activity rose with the advancing solar cycle.

3. Discussion

It is clear that with the corrections as they are now known, the submerged cell in the northern hemisphere is still present and the meridional flow at depth in this hemisphere is still much less uniform than it is in the southern hemisphere. The southward flow across the equator, however, is almost completely eliminated.

These corrections, however, are still preliminary. The correction of the MDI p-angle has so far been analyzed for only two days of data spaced 6 months apart in 1999. Both measurements gave a value of 0.2° but it would be useful to analyze the other measurements that have been taken since that time. Likewise, the analysis carried out by Giles (1999) was for the two years of data that were available at the time, but since (as he pointed out) the signal that he was analyzing has a yearly period and 8 years of MDI data are now in hand, it would also be useful to look at this correction again.

Acknowledgments. We would like to thank Jesper Schou for useful discussions and for sending us the data corrections as currently known. This research was supported by NASA through grants NAG 5-11920 and NAG 5-12491 and by NSF through grant ATM-0219581. SOHO is a project of international cooperation between ESA and NASA.

References

Basu, S. & Antia, H. M. 2000, Solar Phys., 192, 469

Chou, D.-Y. & Dai, D.-C. 2001, ApJ, 559, L175

Giles, P. 1999, Ph.D. Thesis, Stanford University

Haber, D. A., Hindman, B. W., Toomre, J., Bogart, R. S., Thompson, M. J., & Hill, F. 2000, Solar Phys., 192, 335

Haber, D. A., Hindman, B. W., Toomre, J., Bogart, R. S., Hill, F., & Larsen, R. M., 2002, ApJ, 570, 855

Hill, F. 2003, this volume

Schou, J. & Bogart, R. 1998, ApJ, 504, L131

Toner, C. 1999, private communication

Zhao, J. & Kosovichev, A. 2003, ApJ, submitted

Highlights of Astronomy, Vol. 13
International Astronomical Union, 2003
O. Engvold, ed.

Observations and Interpretation of Subsurface Magnetic Structures

P. S. Cally

Centre for Stellar and Planetary Astrophysics, School of Mathematical Sciences, Monash University, Victoria, Australia 3800

A. D. Crouch

Department de Physique, Université de Montreal, Canada

Abstract. Immediate subsurface local solar structures – flow, magnetic, and thermal – especially those associated with active regions, are of considerable interest, and are potentially accessible using high ℓ helioseismology. In recent years, classical modal seismology has been supplemented with new approaches, such as time-distance helioseismology, Hankel analysis, and acoustic holography. Results from time-distance helioseismology on shallow subsurface wave speed are at odds with those from the other methods. A simple model is presented which yields good agreement with the observed Hankel phase shifts of p modes passing through sunspots.

1. Introduction

The subsurface structure of solar active regions has been the subject of conjecture for decades. But now, the advent of various local helioseismic techniques has opened up the possibility of probing sunspots and their surrounds using observations of surface velocities. Three specific techniques – Time-Distance Helioseismology (TD), Acoustic Holography (AH), and Hankel Analysis – have made particular contributions. The foundations of these three approaches are quite different, and taking information from each can give us a more detailed picture than can be gleaned from any one technique alone. Importantly, they also serve as checks on each other, and the purpose of this paper is, in part, to point out a discrepancy between TD on the one hand and AH and Hankel analysis on the other concerning wave propagation speeds in the immediate subsurface layers of sunspots.

Perhaps the best developed active region seismology program is based on TD methods (Kosovichev, Duvall & Scherrer 2000; Kosovichev 2002; and Zhao & Kosovichev 2003). Time-distance helioseismology in its basic form inverts surface cross-covariance data using a ray-theoretic description of the propagation of disturbances in the solar interior. Variations of travel time are used to infer the positions and magnitudes of regions of enhanced propagation speed, and comparisons of travel times in opposite directions reveal details of flow patterns. TD has for example mapped inflows surrounding spots at the surface, and outflows several Mm down, forming a cell pattern which is undoubtedly implicated in keeping the spot together over time-scales of weeks. The other major result from these TD studies is the inference of a wave speed deficit in the first ~ 4 Mm beneath a spot, and an excess from there down to around 10 Mm.

However, both Hankel analysis (Braun 1995) and holography (Braun & Lindsey 2000a,b) clearly infer wave speed increases at shallow depth, as well as substantial wave absorption. In this paper, we focus on the best available Hankel analysis data, in concert with recent theoretical results from Crouch & Cally (2003), in an attempt to build a simple model which explains these features. Finally, we speculate on the reasons for the discrepancy with TD.

2. Hankel Data

Hankel analysis (Braun, Duvall & LaBonte 1987; Braun et al. 1992; and Braun 1995) is the only one of the three techniques which is based on global p modes. It is also the only one which has not yet been married with an inversion method to directly image the subsurface layers. Nevertheless, when regarded as a forward technique, it can certainly provide useful information, and potentially rule out many models. The major result from Hankel analysis of sunspots is that they both partially absorb p modes incident upon them, and shift their phases forward on emergence.

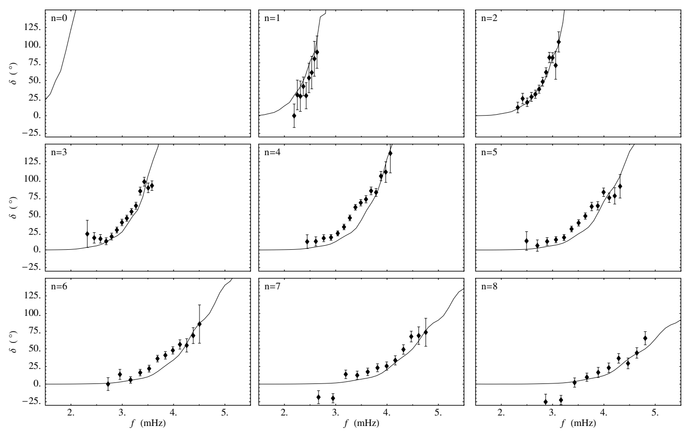

Figure 1. Hankel phase shift δ (degrees) as a function of frequency for radial orders 0 to 8 ($n = 0$ refers to the f-mode). The points with error bars are for the active region NOAA5254 and are taken from Braun (1995) (the errors on the f-mode frequency shifts are too large for that data to be useful) . The curves are from the model of §3

There are several effects which disguise the true absorption, for example the presence of acoustic glories around spots which produce enhanced emission at some frequencies. For this reason, we regard the phase shift as a more direct measure of the influence of a sunspot. In Fig. 1 phase shift δ is plotted as a function of frequency f for one of the active regions discussed in Braun (1995), with each panel referring to a different radial order n of p-mode. Two features are particularly instructive: (i) for each n, the phase shift increases with frequency; (ii) this rising curve shifts rightward with increasing n. The interpretation is clear. For fixed n, increasing frequency corresponds to increasing spherical harmonic degree ℓ and to decreasing lower turning point depth. Hence, the higher frequency modes are trapped ever closer to the surface. Consequently, we interpret the rise in δ with f as indicating an increased wave travel speed compared to the quiet sun immediately below the active region. For higher radial order n, the p modes extend deeper for fixed f, and so it is necessary to increase f further in order to bring the mode up into the enhanced speed region. This explains the rightward shift with n. However, our interpretation appears to be at odds with the TD result.

3. Simple Model

The Sun's p modes are substantially altered in the presence of strong magnetic field. For example, if we superpose a uniform vertical magnetic field on a simple polytropic model (Cally, Bogdan & Zweibel 1994), the horizontal wavenumber k of the modes for fixed frequency typically reduces, resulting in an increased horizontal phase speed. In addition, k acquires an imaginary part, indicating decay with horizontal distance x. This is due to coupling to the magneto-acoustic slow wave, which siphons off much of the p-mode's energy and directs it downwards along the magnetic field lines into the interior. This mechanism is capable of explaining the observed absorption of f modes in sunspots, but is too weak for the p modes, especially beyond the first one or two radial orders.

Recently, Crouch & Cally (2003) have recalculated the eigenvalue wavenumbers for *inclined* uniform magnetic field. It is found that absorption is greatly enhanced at moderate inclination angles, with the peak effect being at around 30° from the vertical, depending on frequency and radial order. As shown in Cally et al. (2003), such inclined field produces ample absorption to explain the observations (indeed, too much at frequencies beyond a few mHz, though this can be explained by reference to acoustic glories and the other mechanisms which serve to mask the true extent of absorption).

Using the inclined-field eigenvalue wavenumbers, Cally et al. (2003) developed a simple model which postulates that these eigenvalues can be used locally as a crude measure of both phase shift (through the real part of k) and absorption (imaginary part). In so doing, many complications are ignored, but this model is built as an attempt to understand the *essence* of the physics involved, and in particular to determine the simplest description which can give at least qualitatively correct results. Work is currently underway to improve on some of these approximations, most notably by adopting a more realistic model than the polytrope used in the eigenvalue calculations.

The upshot of the model is that, for given "sunspot" radius R, magnetic field inclination θ, and field strength parameter L (this is the depth in the polytrope at which the sound and Alfvén speeds coincide), plots of phase shift δ and absorption coefficient α against frequency can be produced for each radial order n. To determine R it is best to first compare with the m-specific data. Here m is the cylindrical order (through $\exp[im\theta]$) of the modes. Direct (axisymmetric) incidence of p modes on a circular spot corresponds to $m = 0$, with higher m being associated with increasingly glancing incidence. The data indicates that δ has a steep shoulder at m of order 10, beyond which there is effectively no shift. Detailed fits of our model to this data indicate that R should be chosen to be around 25 to 30 Mm for the active region NOAA5254. This is substantially larger than the observed penumbral radius of 18 Mm, but is in accord with other estimates of the p-mode scattering radius.

Having settled on $R = 27.5$ Mm, θ and L are adjusted to give the best fits to the observational phase shift data (binned over small m). An example of such a fit is given in Fig. 1 and corresponds to $L = 0.58$ Mm and $\theta = 35°$. The agreement is remarkable. This encourages us to believe that the essential physics of the interaction between p modes and sunspots is being captured in this model, despite its simplicity. However, the precise values of the optimal L and θ are likely to be revised when more realistic solar models are used to calculate the eigenvalues. We also point out that Cally, Crouch & Braun (2003) present a "shell" model in which concentric shells in the sunspot are given different L and θ, which allows more detailed fine tuning. We defer extensive treatment of this model till the more realistic eigenvalue tables are available.

4. Discussion

The sunspot model, despite its simplicity, clearly gives excellent agreement with the Hankel phase shift data, and also provides ample absorption. However, at this stage it cannot be used to quantitatively probe sunspot interiors, largely because it is based on a polytropic models rather than something more realistic.

Both the Hankel and Acoustic Holography approaches are based on viewing a sunspot from the outside. On the other hand, it would appear that TD results for wave travel speeds in the shallow layers of a spot are based on ray paths which begin and end in the spot. Since the TD raypath formalism does not as yet adequately address magnetic field, we are concerned that this may result in errors. In addition, it is not clear how substantial fast-to-slow mode conversion in these layers will affect TD inversions. Perhaps these are the reasons for the wave speed discrepancy between TD and the other methods.

References

Braun, D. C. 1995, ApJ, 451, 859
Braun, D. C., Duvall, T. L. & LaBonte, B. J. 1987, ApJ, 319, L27
Braun, D. C., Duvall, T. L., LaBonte, B. J., Jefferies, S. M., Harvey, J. W. & Pomerantz, M. A. 1992, ApJ, 391, L113
Braun, D. C. & Lindsey, C. 2000a, Solar Phys., 192, 285
Braun, D. C. & Lindsey, C. 2000b, Solar Phys., 192, 307
Cally, P. S., Bogdan, T. J. & Zweibel, E. G. 1994, ApJ, 437, 505
Cally, P. S., Crouch, A. D. & Braun, D. C. 2003, MNRAS, in press
Crouch, A. D. & Cally, P. S. 2003, Solar Phys., 214, 201
Donea, A.-C., Lindsey, C. & Braun, D. C. 2000, Solar Phys., 192, 321
Kosovichev, A. G. 2002, Astron. Nachr., 323, 186
Kosovichev, A. G., Duvall, T. L. & Scherrer, P. H. 2000, Solar Phys., 192, 159
Zhao, J. & Kosovichev, A. G. 2003, ApJ, 591, 446

JD13

Extragalactic Binaries

Chairpersons: A. Gimenez and I. Ribas

Editors: A. Gimenez (Chief-Editor) and I. Ribas

Highlights of Astronomy, Vol. 13
International Astronomical Union, 2003
O. Engvold, ed.

Joint Discussion 13 on Extragalactic Binaries

Ignasi Ribas

Dep. d'Astronomia i Meteorologia, Av. Diagonal, 647, 08028 Barcelona, Spain

Alvaro Giménez

Research and Scientific Support Department, ESA, ESTEC, Postbus 299, 2200 AG Noordwijk, The Netherlands

Abstract. In this paper we discuss the impact of extragalactic binaries on astrophysics and briefly summarize the oral papers presented in Joint Discussion 13.

1. Introduction: Extragalactic binaries

Less than a decade ago about 4000 close binaries were known in the Galaxy with an additional 200 or so systems identified in the Magellanic Clouds and M31. Now, over 10 000 close binary stars (CBS), mostly eclipsing binaries, are known. The vast majority of these CBS were discovered during the last several years alone, and many more are expected to be detected within the next few years. Most of these stars were found as spin-offs of microlensing surveys. Interestingly, over half of the currently-known CBS are found outside our Galaxy, primarily in the Magellanic Clouds. Two major areas of research, albeit complementary, are being currently addressed with this formidable database:

- Accurate distance measurements to the Local Group galaxies are crucial to calibrating the Cosmic Distance Scale and to determining the age and evolution of the Universe. As the first rungs on the cosmic distance ladder, these galaxies serve as calibrators for distance indicators which reach far beyond the bounds of the Local Group. The Large Magellanic Cloud (LMC), in particular, has been exploited for this purpose because of its proximity to the Milky Way and the relative brightness of its young population. Eclipsing binaries have been proven to make excellent "standard candles" that can potentially resolve the controversy and yield an accurate distance to the LMC, and to other Local Group galaxies. Also, binaries with Cepheid components are exceedingly interesting as they can yield simultaneous determinations of the Cepheid P–L zero point and the distance to the galaxy in which they reside.

- Every type of star is represented as a member of a close binary. This includes main sequence (as well as pre-main sequence) stars, giants, and supergiants, with the entire possible range of spectral types and masses represented. Moreover, white dwarfs, neutron stars, and black holes have

> been found as members of CBS. These binaries continue to play vital roles in many areas of modern astrophysics. Extragalactic binaries, and in particular systems belonging to the Local Group, can be used to probe the structure and evolution of stars in environments with chemical histories that differ significantly from those of the solar neighborhood. For example, studying massive, metal deficient stars in the LMC ($\sim$1/2 solar) and SMC ($\sim$1/5 solar) is like using a "time machine" for studying the low-metallicity massive old disk O- and B-type stars that once populated our Galaxy about 5–10 billion years ago.
>
> In addition, extragalactic eclipsing binaries yield essential fundamental data on masses, radii, and luminosities of stars (the mass-luminosity law), as well as the much needed checks of the evolutionary models for these extreme metal abundances, which are widely used in stellar population synthesis calculations. These data are crucial to understanding all stars, as well as the clusters and galaxies in which they reside, and the basic physical laws that govern their behavior. Local Group binaries can also be used to address other astrophysically important issues, such as the structure and dynamics of these galaxies and the enrichment of the interstellar medium.

Thus, extragalactic CBS provide laboratories for studying the combined effects of chemical composition (i.e., stellar opacities, convective overshooting, and stellar winds) on the structure and evolution of stars. Semi-detached O/B systems will provide data for more in-depth studies of mass exchange and mass loss during binary evolution than is possible from Milky Way binaries alone. Thus, the study of CBS in the Local Group galaxies is critically important to stellar astrophysics, galaxy formation and structure, and will improve the cosmic distance scale.

These encouraging prospects and the significant amount of work that has already been carried out in the field out prompted us to organize a Joint Discussion in the IAU General Assembly in Sydney. In the remainder of this paper we briefly summarize the main points of the meeting and give some ideas about possible future research directions.

2. Summary of the meeting and future prospects

The Joint Discussion was divided in three sessions focusing on different aspects of extragalactic binary star research, namely: I) Introduction and survey results, II) Binaries as distance indicators, and III) Astrophysics with extragalactic binaries.

Session I started with a general introduction on some general aspects related to extragalactic CBS by E. F. Guinan (with the most necessary historical perspective), followed by overview presentations of the Local Group galaxies by M. L. Mateo and the long-lasting problem of the distance to the LMC by D. R. Alves. Special attention was given to the smaller galaxies in the Local Group, some with very interesting star formation histories, which certainly contain numerous CBS awaiting discovery and investigation. With regard to the LMC distance, the thorough comparison presented clearly indicates a decrease in the spread of recent results thus pointing towards a imminent resolution of the secular debate on the so-called "short" and "long" distance scales. Interestingly, the average of the estimations seem to converge to a value close to the "canonical" value of 18.5 for the distance modulus.

The remainder of the first session focused on the results from the MACHO, OGLE and DIRECT surveys. Besides statistical studies, the representatives of the different groups, K. H. Cook for MACHO, A. Udalski for OGLE, and L. M. Macri for DIRECT, reviewed the methods and instrumentation used to obtain light curves that meet the requirements for the determination of accurate elements. Also, efforts to further observe and analyze some of the most promising candidates were discussed. If an exciting result presented at the Joint Discussion had to be singled out, this would be perhaps the announcement by the OGLE group of three candidate RR Lyr type variables in LMC eclipsing binaries. The analysis of these objects (if confirmed as such) will provide a unique opportunity to obtain absolute dimensions of RR Lyr variables for the first time, as well as an accurate determination of the period-luminosity zero point.

One of the fields within extragalactic CBS research that has driven most of the recent attention is the use of eclipsing binaries as distance indicators. Session II was entirely devoted to this exciting topic with several presentations discussing the methods, results and suitability of different eclipsing binary types. The first oral paper within this session by J. V. Clausen provided a thorough review of the methods used to estimate distances to detached systems and a detailed study of the errors sources. Also, the importance of multicolor photometry as well as ultraviolet observations for the determination of effective temperatures (one of the most critical pieces of information) were pointed out. It was recognized by several of the speakers in the Joint Discussion that the most demanding data set in CBS studies continues to be the acquisition of accurate radial velocity curves. The use of large telescopes (NTT, AAT, VLT) and space facilities (HST) has been necessary to provide reliable data. The results of an analysis of SMC eclipsing binaries were presented by R. W. Hilditch. This study represents a pioneering work based on a somewhat different approach of using a multi-object spectrograph (2dF at AAT) with relatively low resolution. The accuracy achieved in the derived distance, however, proves this as one of the most efficient observational programs. From the results presented at the Joint Discussion, double-lined eclipsing binaries nowadays provide a distance modulus to the LMC of 18.42 ± 0.05 mag and to the SMC of 18.90 ± 0.04 mag.

Distance determinations using semi-detached binaries and contact binaries were discussed by R. E. Wilson and S. M. Rucinski, respectively. Albeit still awaiting definite proof, these CBS may have some specific advantages over detached binaries. For example, semi-detached systems permit accurate determinations of the component's relative dimensions although their distorted shapes make temperature and radial velocity measurements a more difficult task. The case of contact binaries is different because it is possible to define an analogous relationship to the Cepheid's period-luminosity law. The accuracy reached in galactic systems is still somewhat modest but the prospects are definitely worth considering. Future eclipsing binary searches in the LMC should soon reach a limiting magnitude that will permit the discovery of numerous W UMa-type binaries and this distance determination method will reach full applicability.

Key systems among eclipsing binaries as distance indicators are those having a Cepheid variable as a component. Most notably, they permit simultaneous determination of the distance to the LMC and the calibration of the Cepheid period-luminosity relationship. A few systems of this kind are known in the LMC, two of which were discussed by D. Welch. In spite of them not being fundamental mode pulsators the prospects from the work in progress are very good but complications in the light curve solution from intrinsic variability require a very careful job. Session II also included presentations by Y. W. Kang and A. Pigulski, who described their ongoing programs to observe and characterize eclipsing binaries in the LMC, mostly discovered from the EROS and OGLE surveys. The ultimate goal of both projects is to determine the absolute dimensions of the binary components and carry out distance estimations.

The final session of the Joint Discussion, Session III, focused on the application of extragalactic CBS to study aspects related to stellar astrophysics. In this respect, V. S. Niemela presented the efforts of her group to observe and analyze high-mass binaries in the LMC and SMC. The relative brightness of these O-type CBS has allowed their observation even with moderately-sized telescopes. Some of the stars in binaries with the known highest mass have been studied within this program and a calibration of the mass-luminosity relationship is in progress. In the second talk of the session, I. Ribas presented some results on the first steps towards using extragalactic eclipsing binaries as astrophysical laboratories. The aspects covered were the establishment of the mass-luminosity law, detailed comparison with stellar models (with consequences on the convective overshooting parameter), studies of stellar atmospheres, analysis of the the interstellar medium along the line of sight and use of eclipsing binaries to probe the structure of the host galaxies. Also, very good astrophysical insights can be gained from statistical studies such as those presented by P. North and C. Alcock based on the OGLE and MACHO databases. In the the first case, the statistical analysis of the sample permits the investigation of tidal evolution in the LMC and to assess the value of the critical radius for circularization in CBS. Similarly, C. Alcock discussed aspects related to the use of the MACHO database for statistical purposes and analyzed the distribution of orbital elements among eclipsing binaries.

Session III was completed with two presentations on supernovae by B. P. Schmidt and S. Van Dyk. The study of Type Ia supernovae (SNe) are certainly the most important contribution, albeit often neglected, of CBS research to cosmology. The intensive observation of SNe Ia has provided us with the surprising picture of an accelerating flat universe dominated by dark energy. B. P. Schmidt gave a comprehensive review of the role of SNe Ia in our current view of the Universe and also discussed efforts to better characterize the progenitors to these important binaries. This is a crucial aspect because currently we only have a phenomenological picture based on the shape of the light curve and a better physical understanding of what becomes a SN Ia would be most useful. Finally, S. Van Dyk presented a review of SNe and the role of binarity in each of the types. Apparently, binary systems are the likely progenitors of a very significant fraction of core-collapse SNe. To gather the necessary evidence, observational efforts have been directed towards a better characterization of SNe and their progenitors with encouraging results thus far.

With regard to future prospects, discussed in the closing talk by A. Giménez, it was emphasized that distance determination is not the only goal. The results obtained thus far prove that a new field of stellar astrophysics can be now studied outside our own galaxy. Photometry is basically available but significant work is still required to obtain spectroscopy and to better characterize CBS. Also, even deeper photometry is needed to uncover fainter LMC/SMC binaries with A-type components and also binaries with pulsating components are definitely worth searching for. More and better ground-based observations are needed, requiring large telescopes for spectroscopy and interferometry (VLT, Keck, Magellan) and state-of-the-art instruments (e.g. multi-object via fiber-fed spectrographs). Ongoing and new surveys, including data mining of available catalogs (e.g. MACHO or OGLE) will provide additional candidates and data but more attention should be paid to well-calibrated surface brightness estimates (eventually using interferometry). Concerning space-based instruments, important results are expected from global astrometry as given by ESA mission GAIA (leading to a 20% accuracy for LMC individuals). On the other hand, interferometry from space, as expected to be available for example from SIM, will permit to resolve the photocenter motion of LMC and SMC long-period binaries and will open a new era of dynamical orbit determination through astrometry in extragalactic binaries.

In the remainder of these proceedings we include the title, author information and abstracts (often somewhat extended versions) of all oral contributions presented at the meeting. The full papers will be published by Elsevier in a special New Astronomy Reviews issue with I. Ribas and A. Giménez as guest editors. The authors wish to express their gratitude to the members of the Scientific Organizing Committee, J. V. Clausen, K. H. Cook, E. F. Guinan, R. W. Hilditch, V. S. Niemela, J. D. Pritchard, K. Z. Stanek, and A. Udalski, for their support and their contribution to make the Joint Discussion a success. Finally, we would like to thank, on behalf of the organizers of JD13, all speakers as well as the audience for a very enlightening and useful Joint Discussion (despite the allocation of number 13).

Highlights of Astronomy, Vol. 13
International Astronomical Union, 2003
O. Engvold, ed.

Seeing Double in the Local Group: Extragalactic Binaries

Edward F. Guinan

Dept. of Astronomy & Astrophysics, Villanova University, 800 Lancaster Ave., PA 19085, USA

Photographic surveys of the Magellanic Clouds and the M31 carried decades ago discovered ∼200 close binaries. In most cases the photographic light curves are good enough only to identify the stars as close (mostly eclipsing) binaries and to estimate orbital periods and binary type. Except for a few cases, little useful information may be obtained from these stars except to be reassured that eclipsing binary (EB) systems are present in other galaxies. However a major advance occurred with the advent of high quantum efficient CCDs. Because of this an explosion in the number of known extragalactic binaries occurred during the 1990s as offshoots of photometric microlensing surveys such as EROS, MACHO, and OGLE. Now over 10 000 extragalactic EBs have been identified. Also, photometric surveys of M31 and M33 (e.g. DIRECT) are discovering many more 19–20th mag eclipsing/close binaries. Over the next decade it is expected that ∼1 million new binary systems will be identified in these galaxies. In this overview I will discuss recent advances and future expectations in the studies of extragalactic binaries

Highlights of Astronomy, Vol. 13
International Astronomical Union, 2003
O. Engvold, ed.

Binary Stars in the Local Group: The Playing Field

Mario L. Mateo

Department of Astronomy, University of Michigan, 821 Dennison Building, Ann Arbor, MI 48109-1090, USA

As an introduction to the stage on which Extragalactic Binaries exist I will present an overview of the stellar populations of the Local Group Galaxies. This will highlight the (few) similarities in the star formation histories of Local Group galaxies as well as the better-known variety that has been uncovered in recent studies. In the few cases where this is possible, the direct role of binaries in the interpretation of the star forming histories of these galaxies will be described. The possible role of binaries in helping to shape the star-formation history will be described more generally with some emphasis on the sorts of observations that can be carried out to investigate this more fully.

Highlights of Astronomy, Vol. 13
International Astronomical Union, 2003
O. Engvold, ed.

A Review of the Distance and Structure of the Large Magellanic Cloud

David R. Alves

Columbia Astrophysics Lab., 550 W. 120th St., New York, NY, USA

The debate about the distance to the Large Magellanic Cloud (LMC) has an epic history full of controversial and dramatic claims (i.e., see review by Walker 2003), and yet in recent years a standard distance modulus has emerged due primarily to the completion of the *Hubble Space Telescope* (*HST*) Key Project to measure the Hubble constant (Freedman et al. 2001). The adopted standard distance modulus, $\mu_0 = 18.5 \pm 0.1$ mag, yields $H_0 = 71 \pm 10$ km s^{-1} Mpc^{-1} (total error) in excellent agreement with that derived from the *Wilkinson Microwave Anisotropy Probe*: $H_0 = 72 \pm 5$ km s^{-1} Mpc^{-1} (Spergel et al. 2003), which lends considerable support to its accuracy.

The average of 14 recent measurements of the distance to the LMC implies a true modulus of 18.50 ± 0.02 mag, and demonstrates a trend in the past 2 years of convergence toward a standard value. Table 1 is a summary of the distance results by method. Where both random (r) and systematic (s) errors are given, I adopt their arithmetic sum as the total error, and I use this to weight the average. I exclude one result, and two are assigned new error bars as noted in parenthesis. Last, I adopt the average distance modulus for the 4 eclipsing binary estimates as one result. Note that the eclipsing binaries yield a consistent mean distance, but their scatter is twice as large as their average measurement error. The reduced chi-squared is about 0.3 for the final average, and thus the adopted error bars are probably too conservative (the average uncertainty is ± 0.08 mag).

The recent results for the LMC distance demonstrate a remarkably high level of consistency. The possibility that a consensus on the LMC distance has been reached seems much more plausible now than it did at the conclusion of the *HST* Key Project only two years ago. A great American sports journalist once said famously, "The opera ain't over till the fat lady sings," to make a point that the outcome of a series of games was not yet determined. *Regarding the convergence of published LMC distance results, I suggest to you that the fat lady has begun to sing.*

There is no standard model for LMC structure, at least not yet, but in a series of recent papers a new understanding has emerged (van der Marel et al. 2002). It has been established that the photometric major axis of the LMC disk is about 50° away from the line-of-nodes (along which the disk is at a constant distance equal to the center-of-mass distance), and thus the LMC is intrinsically elongated. Several independent estimates for the center of the LMC are consistent with the optical center; the exception is the center derived from the velocity field of H I gas. The velocity field of carbon stars and simple equilibrium models indicate that the LMC disk is thick like the Galactic thick

Table 1. LMC distance moduli in the past 2 years

Method	μ_0	Method	μ_0
Red Clump	$18.493 \pm 0.033_r \pm 0.03_s$	Mira	18.48 ± 0.08
Red Clump	$18.471 \pm 0.008_r \pm 0.045_s$	Main Sequence (excl.)	$18.5 - 18.7$
Red Clump	18.54 ± 0.10	Main Sequence	18.58 ± 0.08
Cepheid	18.48 (± 0.1)	SN 1987A	18.46 ± 0.12
Cepheid	$18.55 \pm 0.02_r$ (± 0.1)	EB (HV 982)	18.51 ± 0.05
Cepheid	18.54 ± 0.29	EB (EROS 1044)	18.38 ± 0.08
RR Lyrae	18.50 ± 0.07	EB (HV 5936)	18.18 ± 0.09
RR Lyrae	$18.43 \pm 0.06_r \pm 0.16_s$	EB (HV 982)	18.63 ± 0.08
RR Lyrae	18.55 ± 0.07	Eclipsing binaries (ave.)	18.46 ± 0.08
RR Lyrae	18.48 ± 0.08		
	Wtd. ave.	**18.50±0.02 (s.d.=0.04)**	

disk and flared. The vertical exponential scale height of carbon stars attains a value of about 1 kpc at locations 5–6 degrees from center, and is only about 100 pc in the central bar region.

The LMC is the nearest example besides the Milky Way of a disk galaxy that has a stellar halo (Minniti et al. 2003). Although the LMC has a halo, it does not have a bulge, and in this way it is similar to M33. It not known whether or not the Population II distance indicators like RR Lyrae variables are distributed in the same way as the young and intermediate-age stellar populations which represent the bulk of the LMC disk, and hence whether or not geometric inclination-corrections appropriate for the disk should apply. However, the kinematics of the halo and disk stars in the LMC are distinct.

Finally, I note that the warps in the LMC disk recently discovered using the color and magnitude of the red clump (Olsen & Salyk 2002) are suspiciously found in regions of high reddening, and could be caused by a change in the mix of young and old red clump stars which would bias the reddening correction. Old and intrinsically redder red clump stars, if they exist, could be distributed in a different manner than the young (disk) clump stars, and thus it is possible for the population mix of the clump to vary in unexpected ways across the LMC.

References

Freedman, W. L., et al. 2001, ApJ, 553, 47

Minniti, D., Borissova, J., Rejkuba, M., Alves, D. R., Cook, K. H., & Freeman, K. C. 2003, Science, 301, 1508

Olsen, K. A. G., & Salyk, C. 2002, AJ, 124, 2045

Spergel, D. N., et al. 2003, ApJS, 148, 175

van der Marel, R. P., Alves, D. R., Hardy, E., & Suntzeff, N. B. 2002, AJ, 124, 2524

Walker, A. R. 2003, in "Stellar Candles for the Extragalactic Distance Scale," Lecture Notes in Physics (Springer), eds. D. Alloin and W. Gieren (astro-ph/0303011)

Highlights of Astronomy, Vol. 13
International Astronomical Union, 2003
O. Engvold, ed.

Binary Star Research Using the MACHO Database

Kem H. Cook

Lawrence Livermore National Laboratory, 7000 East Avenue, Livermore, CA 94550, USA

The MACHO Collaboration has produced a variable star catalog of the Magellanic Clouds which is a rich source of eclipsing binary systems. I will review the techniques that have been used by MACHO for identifying eclipsing binaries in a relatively automated fashion which is necessitated by the more than 230 000 variable light curves cataloged. We have identified about 6000 eclipsing binaries using these techniques. These systems have periods ranging from hours to more than 1000 days. I will survey the binary star data from MACHO and highlight its use in investigating topics spanning the physics of supersoft gamma-ray sources to the distance of the Large Magellanic Cloud and point to future directions of research using this public resource.

Highlights of Astronomy, Vol. 13
International Astronomical Union, 2003
O. Engvold, ed.

Eclipsing Binaries in the Magellanic Clouds

Andrzej Udalski

Warsaw University Observatory, Al. Ujazdowskie 4, 00–478 POLAND

We present results of a search for eclipsing binaries in the Magellanic Cloud fields covering central parts of these galaxies. The data were collected during the second phase of the Optical Gravitational Lensing Experiment survey (OGLE-II) in 1997–2000. In total, about 1500 and 3000 eclipsing stars were found in the Small and Large Magellanic Cloud, respectively (Udalski et al. 1998, Wyrzykowski et al. 2003). The photometric data of all objects are available to the astronomical community from the OGLE Internet archive (`http://sirius.astrouw.edu.pl/~ogle/`). OGLE-II data contain a full variety of classical eclipsing objects of all types: Algol EA-type, β-Lyr EB-type and W UMA EW-type stars. Large samples of stars allow to study in detail statistical properties of eclipsing objects. OGLE data also contain many very unusual eclipsing stars. Examples include eclipsing variable B-type stars (Mennickent et al. 2003), many spotted stars or eclipsing stars with a Cepheid as a component (Udalski et al. 1999). Recently three objects from the LMC revealing simultaneously RR Lyr and eclipsing binary type variability were discovered (Soszyński et al 2003). If the follow-up observations confirm that both components are physically bound and not optical blends these stars will provide a unique opportunity of direct determination of physical parameters of RR Lyr pulsating stars.

The OGLE-III project, which began regular observations of the Magellanic Clouds in June 2001, is still in the early phases. Up to the end of June 2003 about 100–250 epochs were collected for the LMC fields and about 200 epochs for the SMC fields. The LMC and SMC fields cover now practically the entire galaxies. Photometry of more than 30 million stars from both MC is obtained in real time. The new data pipeline system based on image subtraction technique provides now photometry with mmag accuracy for the brightest stars. We believe that in the time scale of a few years the vast majority of eclipsing stars from the Magellanic Clouds down to ≈ 20 mag will be detected by the OGLE-III survey and photometry will be released to the astronomical community.

References

Mennickent, R. E., Pietrzyński, G., Diaz, M., & Gieren, W 2002, A&A, 399, 47

Soszyński, I., Udalski, A., Szymański, M., Kubiak, M., Pietrzyński, G., Woźniak, P., Żebruń, K., Szewczyk, O., & Wyrzykowski, Ł. 2002, AcA, 53, 93

Udalski, A., Soszyński, I., Szymański, M., Kubiak, M., Pietrzyński, G., Woźniak, P., & Żebruń, K. 1998, AcA, 48, 563

Udalski, A., Soszyński, I., Szymański, M., Kubiak, M., Pietrzyński, G., Woźniak, P., & Żebruń, K. 1999, AcA, 49, 223

Wyrzykowski, Ł., Udalski, A., Kubiak, M., Szymański, M., Żebruń, K., Soszyński, I., Woźniak, P., Pietrzyński, G.& Szewczyk, O. 2003, AcA, 53, 1

Highlights of Astronomy, Vol. 13
International Astronomical Union, 2003
O. Engvold, ed.

DIRECT DEBs in M31 and M33

Lucas M. Macri

Hubble Fellow, National Optical Astronomy Observatory, 950 N Cherry Avenue, Tucson, AZ 85719, USA

The DIRECT project (as in "direct distances") started in 1996 with the long-term goal of obtaining distances to two important galaxies in the cosmological distance ladder – M31 and M33 – using detached eclipsing binaries (DEBs) and Cepheids. These two nearby galaxies are the stepping stones in most of the current effort to understand the evolving universe at large scales. Not only are they essential to the calibration of the extragalactic distance scale, but they also constrain population synthesis models for early galaxy formation and evolution. However, accurate distances are essential to make these calibrations free from large systematic uncertainties.

Detached eclipsing binaries have the potential to establish distances to M31 and M33 with an unprecedented accuracy of better than 5% and possibly to better than 1%. Current uncertainties in the distances to these galaxies are in the order of 10 to 15%, as there are discrepancies of 0.2-0.3 mag between various distance indicators. Detached eclipsing binaries (Paczyński 1997) offer a single-step distance determination to nearby galaxies (Fitzpatrick et al. 2003) and may therefore provide an accurate zero-point calibration for other distance indicators, including Cepheids.

The DIRECT project obtained time-series observations of M31 and M33 during 170 nights between 1996 September 6 and 2000 January 2 using the Fred L. Whipple Observatory 1.2-m telescope. Additional observations were carried out during 36 nights in 1996 and 1997 at the Michigan-Dartmouth-MIT Observatory 1.3-m telescope. In 1996 and 1997, images were obtained using a camera with $\sim 11' \times 11'$ field of view. In 1998 and 1999, data were collected using a camera with a $\sim 22' \times 22'$ field of view.Observations were obtained mainly in the V and I bands, with some additional data in the B band. The total area covered by the observations was $\sim 0.5\Box^\circ$ in M31 and $\sim 0.3\Box^\circ$ in M33.

Most of the fields have been analyzed and published (Bonanos et al. 2003; Kaluzny et al. 1998; Kaluzny et al. 1999; Macri et al. 2001c; Mochejska et al. 1999; Stanek et al. 1998; Stanek et al. 1999). These publications contain a total of ~ 130 eclipsing binaries, ~ 600 Cepheid variables, and ~ 500 miscellaneous variables.

Additional publications related to the DIRECT project include: the discovery of cessation of pulsations in a long-period Cepheid in M33 (Macri et al. 2001a); the study of the influence of unresolved blends on the Cepheid Distance Scale (Mochejska et al. 2000; Mochejska et al. 2001a); a catalog of globular clusters in M31 and M33 (Mochejska et al. 1998); ancillary stellar catalogs and additional short-period variables (Macri et al. 2001b; Mochejska et al. 2001b; Mochejska et al. 2001c; Mochejska et al. 2001d).

Four promising detached eclipsing binary systems have been discovered in the DIRECT fields; two in M31 and two in M33. As a first step in their follow-up, higher quality light curves were obtained through observations conducted at the Kitt Peak National Observatory 2.1-m telescope in 1999 and 2001. Recently, a program was started to measure radial velocities of the DEBs using the Echelle Spectrograph and Imager (ESI) at Keck Observatory. We have also obtained out-of-eclipse near-infrared observations of the DEBs in M33 using the Gemini North 8-m telescope, to increase the wavelength baseline of our coverage and obtain a better measurement of $E(B-V)$ for these systems.

References

Bonanos, A. Z., Stanek, K. Z., Sasselov, D. D., Mochejska, B. J., Macri, L. M., & Kaluzny, J. 2003, AJ, 126, 175

Fitzpatrick, E. L., Ribas, I., Guinan, E. F., Maloney, F. P., & Claret, A. 2003, ApJ, 587, 685

Kaluzny, J., Stanek, K. Z., Krockenberger, M., Sasselov, D. D., Tonry, J. L., & Mateo, M. 1998, AJ, 115, 1016

Kaluzny, J., Mochejska, B. J., Stanek, K. Z., Krockenberger, M., Sasselov, D. D., Tonry, J. L., & Mateo, M. 1999, AJ, 188, 346

Macri, L. M, Sasselov, D. D. & Stanek, K. Z. 2001a, ApJ, 550, L159

Macri, L. M., Stanek, K. Z., Sasselov, D. D., Krockenberger, M., & Kaluzny, J. 2001b, AJ, 120, 861

Macri, L. M., Stanek, K. Z., Sasselov, D. D., Krockenberger, M., & Kaluzny, J. 2001c, AJ, 120, 870

Mochejska, B. J., Kaluzny, J., Krockenberger, M., Sasselov, D. D., & Stanek, K. Z. 1998, AcA, 48, 445

Mochejska, B. J., Kaluzny, J., Stanek, K. Z., Krockenberger, M., & Sasselov, D. D. 1999, AJ, 118, 2211

Mochejska, B. J., Macri, L. M., Sasselov, D. D., & Stanek, K. Z. 2000, AJ, 120, 810

Mochejska, B. J., Macri, L. M., Sasselov, D. D., & Stanek, K. Z. 2001a, astro-ph/0103440

Mochejska, B. J., Kaluzny, J., Stanek, K. Z., & Sasselov, D. D. 2001b, AJ, 122, 1383

Mochejska, B. J., Kaluzny, J., Stanek, K. Z., Sasselov, D. D., & Szentgyorgyi, A. H. 2001c, AJ, 121, 2032

Mochejska, B. J., Kaluzny, J., Stanek, K. Z., Sasselov, D. D., & Szentgyorgyi, A. H. 2001d, AJ, 122, 2477

Paczyński, B. 1997, in The Extragalactic Distance Scale, ed. M. Livio, M. Donahue & N. Panagia (Cambridge: Cambridge Univ. Press), 273

Stanek, K. Z., Kaluzny, J., Krockenberger, M., Sasselov, D. D., Tonry, J. L., & Mateo, M. 1998, AJ, 115, 1894

Stanek, K. Z., Kaluzny, J., Krockenberger, M., Sasselov, D. D., Tonry, J. L., & Mateo, M. 1999, AJ, 117, 2810

Highlights of Astronomy, Vol. 13
International Astronomical Union, 2003
O. Engvold, ed.

Eclipsing Binaries as Precise Standard Candles and Distance Indicators

Jens Viggo Clausen

Niels Bohr Institute for Astronomy, Physics, and Geophysics, Astronomical Observatory, Copenhagen University, Denmark

Double-lined eclipsing binaries are (still) our main source for accurate information on stellar masses, radii, and luminosities. Also, they offer very direct distance determinations, useful within the Milky Way and for Local Group Galaxies. I will briefly review the methods involved and discuss critically their advantages and limitations. Furthermore, past and recent highlights will be presented.

Highlights of Astronomy, Vol. 13
International Astronomical Union, 2003
O. Engvold, ed.

Eclipsing Spectroscopic Binaries in the SMC

Ron W. Hilditch

School of Physics and Astronomy, University of St Andrews, North Haugh, St Andrews, Fife KY16 9SS, UK

Tim J. Harries

School of Physics, University of Exeter, Stocker Road, Exeter EX4 4QL, UK

Ian D. Howarth

Department of Physics and Astronomy, University College London, Gower Street, London WC1E 6BT

The OGLE survey of the SMC has discovered ~1500 eclipsing binaries thereby providing an excellent platform to study the evolution of close binary systems through case A and case B mass-exchange processes. The complementary spectroscopic radial-velocity studies of these binaries are now in progress and are revealing many interesting systems which challenge current theoretical models of close binary star evolution. These studies also provide excellent direct determinations of distances to these binary stars leading to an improved understanding of the mean distance to the SMC and its 3-D structure. Comparisons between these binary-star distances and other methods of determining the mean distance to the SMC will also be made.

Highlights of Astronomy, Vol. 13
International Astronomical Union, 2003
O. Engvold, ed.

Semi-detached Binaries as Probes of the Local Group

Robert E. Wilson

Astronomy Department, University of Florida, Gainesville FL 32611 USA

The SMC I band light curves of the OGLE project show a curious absence of familiar Algols. Comparitive statistical work for SMC and Milky Way Algols might uncover an evolutionary explanation, presumably connected with chemical composition, or may point to observational selection or even merely perception. As background, LMC and SMC abundances of nitrogen, oxygen, and neon are lower than in our Galaxy by respective factors of about 2.5 and 6, raising the issue of metallicity effects on semi-detached (SD) statistics - specifically on SD light curves and numbers of SDs. Lobe overflow is a *triggered* process, with both system age and structural configuration at triggering dependent on composition.

On another topic, the EB distance scheme's main attraction is directness, as *no calibration of any kind is involved*, allowing distance estimates for individual binaries. *If there were only one EB, in principle we could find its distance.* Only geometric and radiative properties are utilized and evolution is essentially irrelevant. Only the best conditioned EB's are needed for distances to Local Group galaxies, as GAIA will observe EB's in enormous numbers. The value of total-annular eclipses is well known, although luminosity ratios from spectra or SED's restore much of the information otherwise missing in partial eclipse cases. Among several continuing difficulties are third light, aliasing of radii, and observational selection.

Most workers on EB distances to Local Group galaxies actively select well detached binaries (WDB), presumably regarding them as the simplest morphological type. Tacit issues would be 1) whether WDB's simplicity helps with light curve solutions, 2) whether it helps with absolute scaling, and 3) whether WDB's really are relatively simple. The answer to item 1 is *no* - irradiation and static tides are solved problems at the level required for light curve solutions. Relevant to item 2 is a need for improvements in binary spectrum synthesis – the analog of a light curve program for SED's, with solution of the inverse problem for SED's just as one now does for light curves. We also need to convert from relative to absolute theoretical flux correctly. For item 3 one must distinguish among several kinds of simplicity. *Physical* simplicity (few parameters) is the issue for fitting problems. *Application of physics removes free parameters* so - in the way that matters for general solutions and for distances - *SD and over-contact binaries are simpler than WDB's.*

Essentially all SD binaries have sensibly circular orbits because of strong tides. Three parameters are thereby saved, as eccentricity, e, is known, argument of periastron, ω, is inconsequential, and the contact star's rotation is synchronous. Although e and ω are readily found for DB's, every free parameter increases uncertainty by complicating the correlation matrix. The role of mass ratio ($q = m_2/m_1$) is very important for SD and even more important for overcontact (OC) light curves. The situation can be seen in the connection between q and relative (mean) radii, $r_{1,2} = R_{1,2}/a$. There is *no* connection for DB's, except for upper limits on $r_{1,2}$, whereas a known or assumed q immediately fixes *one* radius for an SD and nearly fixes *both* radii for an OC. Complete eclipses are required for strong photometric mass ratios ($q_{\rm ptm}$) for the same reason that complete eclipses are needed for strong measures of $r_{1,2}$, since q estimates essentially come from radius estimates. Note that $q_{\rm ptm}$'s arise from lobe-related radii that are found from eclipses, contrary to a common misconception that they come from tidal deformation inferred mainly from outside-eclipse variation. Eclipses carry most of the information coded into EB light curves, so it follows that observing time is used efficiently where fractional eclipse width is relatively large. Fractional eclipse width is statistically larger for SD's than for DB's and even larger for OC's because it increases with $r_1 + r_2 = (R_1 + R_2)\, a$. Aliasing of radii can impede selection of survey binaries (say from GAIA) for subsequent intensive observation with large aperture telescopes and is reduced for SD's *vis a vis* DB's. Observing radial velocities (RV) for the dim SD secondaries is not easy, with limiting magnitudes for velocities being much brighter than for light curves. A partial remedy is to go to the infra-red where the low temperature secondaries are relatively bright. The most realistic circumvention may be to use spectra for primary star velocities only and complete our mass information with the help of q_{ptm}'s.

The common W UMa OC's are too dim for useful RV observation outside the Milky Way with present technology and luminous OC's are very rare. Circular orbits and synchronous rotation are guaranteed for OC's, thus saving four fitting parameters (e, ω, and two rotations). OC solutions are especially strong because *two* radii must fit into the lobe configuration, compared to one for SD's and none for DB's. Complete eclipses are reasonably common for W UMa's, although not common for high luminosity OC's. Rigorously correct scaling of theoretical flux is important for the distance problem. Distant flux scales with polar normal intensity, and the remaining problem is to find the scaling constants for the components - just two numbers. If a light curve program computes all relative quantities self-consistently, then

$$F_d^{\rm abs} = 10^{-.4\,A} \left[F_{\rm a,1}^{\rm prog} \left(I_1^{\rm abs}/I_1^{\rm prog} \right) + F_{\rm a,2}^{\rm prog} \left(I_2^{\rm abs}/I_2^{\rm prog} \right) \right] [a/d]^2 \,, \qquad (1)$$

where subscripts *abs* and *prog* refer to absolute flux (F) or normal intensity (I), subscripts d and a are observer distance and standard program distance respectively, and subscripts 1 and 2 are for stars 1 and 2. Absolute I's come from a stellar atmosphere program and program F's and I's come from the program. Observations give F_d^{abs} and semi-major axis a comes from a light/velocity solution. One has all needed quantities except d (and perhaps A), so the relation can be inverted to find d (or $d\,[A]$). To find $I_1^{\rm abs}$ and I_2^{abs} we need polar effective temperatures, $T_{\rm pole}$, which can be estimated by analysis of spectra or SED's.

Highlights of Astronomy, Vol. 13
International Astronomical Union, 2003
O. Engvold, ed.

Contact Binaries of the W UMa Type as Distance Tracers

Slavek M. Rucinski

David Dunlap Observatory, University of Toronto P.O. Box 360, Richmond Hill, Ontario, Canada L4C 4Y6

Contact binary stars of the W UMa-type (also known as W) are unique objects: The luminosity, produced almost exclusively in the more massive component is efficiently distributed through the common envelope so that the surface brightness is practically identical over the whole visible surface of the binary. Mass ratios are known to span the whole wide range, from almost unity to very small values, as small as $q = 0.066$. Typically, the primary component provides the luminosity, while both components provide the radiating area. The range of the primary masses is moderate and corresponds to Main Sequence spectral types from middle A to early K and roughly maps into the orbital-period range of about 1.5 days to 0.22 days.

With their special properties, the contact binaries of the W UMa type form a distinct group of objects, very easy to find and identify in massive stellar variability programs, even in short-duration ones, thanks to the short orbital periods and large amplitudes of photometric variations. Contact binaries are not as convenient as detached binaries for distance determinations. Although described by fewer parameters than detached binaries, they have more complex geometry. Thus, the contact binaries are more like pulsating stars and – with still many uncertainties about their structure and adherence to the strict Roche model – do require empirical luminosity calibrations.

The rationale for the existence of a period - luminosity relation is based in the strong geometric constraints imposed by the common equipotential envelope which permit to consider an equivalent of the $Q = P\sqrt{\rho}$ relation for contact binary systems. By defining the mean density of the whole configuration, $\rho = (M_1 + M_2)/V$, by eliminating a^3 using the Kepler law and by expressing the quantities in familiar units, one obtains the "pulsation equation", $P\sqrt{\rho} = Q(q, F) = \sqrt{0.079/v(q, F)}$, with P in days and ρ in g/cm^3 (q is the mass ratio and F characterizes the degree of contact, $F = 0$ for inner contact at L_1 and $F = 1$ for outer contact, opening up at L_2). The similarity of contact binaries to pulsating stars is not accidental as the underlying physical time scale, of the pulsation or of the orbital revolution, is the same familiar dynamical time scale.

The full calibration equation:

$$\begin{aligned} M_V &= -10 \log T_{eff} + B.C.(T_{eff}) - 10/3 \log P \\ &\quad -5/3 \log M_1 - 5/3 \log(1 + q) - 2.5 \log s(q, F) + const \end{aligned}$$

can be simplified for situations when only photometric data are available to

$$M_V = C_1 * colour + C_2 \log P + C_3$$

where *colour* is any of the available color indices. The currently best calibrations utilizing de-reddened $B-V$ and $V-I$ color indices are:

$$\begin{aligned} M_V &= -4.44 \log P + 3.02\,(B-V)_0 + 0.12 \\ M_V &= -4.43 \log P + 3.63\,(V-I)_0 - 0.31 \end{aligned}$$

There are several sources of uncertainties in the current calibrations. The trigonometric parallaxes from the Hipparcos mission introduce errors typically < 0.25 mag. In addition, some of the binaries are unrecognized triple systems with an associated offset in brightness, loss in accuracy and even entirely false data for the parallaxes. The main source of errors is in the photospheric spots on individual binaries. These binaries are very active and almost always show spots. A brightness calibration must simply assume some sort of an average. When a simple mean weighted error is considered, then the deviations are characterized by $\sigma M_V \simeq 0.35$ mag. Monte–Carlo simulations indicate that within the main range of the applicability, the typical errors are $\sigma M_V \simeq 0.25$ mag.

As with any calibration for pulsating stars, one must establish the metallicity dependence of the period–color–luminosity relation. It has been found that there exists no discernible trend in the deviations from the predicted values of M_V as a function of [Fe/H]. Although the contact binaries with low metallicity content are structurally different than the disk population ones, there exists no need to introduce the metallicity corrections in M_V at the current level of accuracy. Population II contact binaries are bluer and smaller i.e. have shorter orbital periods then the disk–population Main Sequence systems, but the shifts in the color–magnitude diagram are practically horizontal in M_V. This is a preliminary result which must be checked again as the data become more accurate.

Since the M_V calibrations utilizing de-reddened color indices $B-V$ or $V-I$ and the periods can predict individual values to about ± 0.25 mag, about a thousand systems are needed to reduce the group uncertainty to the level of ± 0.01. Such large numbers will be discovered in the nearby galaxies once the surveys pass the threshold of $M_V \simeq 3-5$ which, for the Local Group typically corresponds to $V > 23-25$. The current calibrations involve de-reddened color indices and thus remain sensitive to the reddening corrections. The widespread availability of the K-band data suggests calibrations based on the $V-K$ or $I-K$ indices; this is a matter of the current work.

Highlights of Astronomy, Vol. 13
International Astronomical Union, 2003
O. Engvold, ed.

Cepheid Variables in Ecliping Binary Systems

Douglas Welch

Department of Physics and Astronomy, McMaster University,
Hamilton, ON L8S 4M1, Canada

Microlensing surveys of the Large and Small Magellanic Clouds have revealed the existence of Type I and II Cepheid variable stars in eclipsing binary systems. In this review I will summarize the state of the known published and unpublished observations of these systems describe what has been learned to date and discuss what the prospects are for extracting additional information from the known systems using future observations. This review will also discuss the known state of searches for RR Lyrae stars in both spectroscopic and eclipsing binaries and suggest strategies for future success in detecting such systems.

Highlights of Astronomy, Vol. 13
International Astronomical Union, 2003
O. Engvold, ed.

Improved Light Curves of LMC Eclipsing Binaries

Young Woon Kang, Kyungsoo Hong

Department of Astronomy, Sejong University, Seoul, 143-747, Korea

Woo-Baik Lee, Ho-Il Kim

Korea Astronomy Observatory, Taejon, 305-348, Korea

Kyu-Dong Oh

Department of Earth Sciences, Chonnam National University, Kwangju, 500-757, Korea

We present accurate BV light curves and continuum energy curves of the EROS eclipsing binaries in the Large Magellanic Cloud to find accurate binary parameters as well as their distances. The observations have been carried out using the 2.1 meter telescope in CASLEO Argentina during Feb. 1–10, 2003. We have concentrated CCD direct observations upon EROS field 1 and 2 to improve the accuracy of light curves of eclipsing binaries in the fields. The spectroscopic observations have been also carried out using the simple dispersion method to get continuum energy curves between wavelengths of 4000–8000 Å for several EROS eclipsing binaries. At first, we determined a combined temperature of both components of each binary system using the continuum. Then, the combined temperature was resolved using the first estimation of the light curve solution. Finally, we determined the photometric solutions of several binaries in the Large Magellanic Cloud.

Highlights of Astronomy, Vol. 13
International Astronomical Union, 2003
O. Engvold, ed.

Detached Binaries in the Large Magellanic Cloud

G. Michalska, & A. Pigulski

Wrocław University Observatory, Kopernika 11, 51-622 Wrocław, Poland

Analysis of the radial-velocity and light curves of detached eclipsing binaries allows to derive stellar masses and radii and, in consequence, enables to find their distances. The method has been already applied to several LMC binaries, but in order to have the distance to the LMC determined with good accuracy, the parameters need to be known for a larger number of systems. As a first step we present results of the analysis of the photometry of over eighty detached binaries in the LMC selected from the OGLE-II catalog of 53 000 variable star candidates. If possible, we combine the OGLE-II data with the photometry from other projects (MACHO and EROS). As a result, we present the list of brightest eclipsing binaries in the LMC suitable for distance determination.

Highlights of Astronomy, Vol. 13
International Astronomical Union, 2003
O. Engvold, ed.

Massive Binaries in the Magellanic Clouds

Virpi S. Niemela

Facultad de Cs. Astronmicas y Geofsicas, Universidad Nacional de La Plata, Paseo del Bosque s/n, 1900 La Plata, Argentina

We present results of our ongoing observing program on search and studies of massive stars (O and WR type) in binary systems in our neighbor galaxies, the Magellanic Clouds. Radial velocity orbits are presented for two new binaries, one in the Small Magellanic Cloud and another in the Large Magellanic Cloud, and improved orbits for previously known systems. We compare orbital parameters of selected binaries containing O and WR type components. We also discuss the present status of knowledge for massive binary stars in the Magellanic Clouds and the problems encountered in their orbital studies such as stellar winds the ubiquitous tendency to be born in multiple systems.

Highlights of Astronomy, Vol. 13
International Astronomical Union, 2003
O. Engvold, ed.

Extragalactic Eclipsing Binaries: Astrophysical Laboratories

Ignasi Ribas

Dept. d'Astronomia i Meteorologia, Univ. Barcelona, Av. Diagonal, 647, E-08028 Barcelona, Spain

Eclipsing binaries (EBs) have long been known for providing accurate stellar fundamental properties, such as masses and radii. These are obtained from the modeling of light and radial velocity curves and, with input data of good quality, uncertainties of a few percent in the components' physical properties are now routinely achieved. Additionally, a number of other observables are determined for eclipsing binaries using techniques similar to those employed for single stars: Effective temperatures from multi-wavelength photometric analysis and chemical abundances from detailed spectroscopic modeling. Thus, EB systems provide a complete characterization of the physical properties of their components, with the added constraint that both stars should have identical age. Also worth mentioning is the ubiquity of EB systems among all kinds of stars. Main sequence stars, variable stars, giants, supergiants, and compact objects, to name a few, are found as members of EBs. This makes EBs excellent "laboratories" for stellar astrophysics. A number of studies have exploited this fact and carried out detailed analysis of galactic EB systems (e.g. Andersen et al. 1991; Clausen 1991; Claret & Giménez 1993; Schröder et al. 1997; Guinan et al. 2000). A few areas where EBs play a crucial role in astrophysics are stellar structure and evolution, tidal evolution, stellar atmospheres, binary evolution in interactive systems, ...

A new perspective has opened in the last decade with the advent of powerful telescopes, detectors and analysis techniques, which have permitted the acquisition of accurate data of EBs in Local Group galaxies. With this comes the possibility of performing detailed stellar astrophysical studies beyond our Galaxy. Worth noting is the great benefit that has experienced this field from the release of the microlensing survey catalogs, which have resulted in a database of thousands of new eclipsing binaries with light curves of excellent quality. Extragalactic EBs provide a unique opportunity to study stars that have formed and evolved in environments with chemical histories that may differ from those of the solar neighborhood. For example, the LMC and SMC are populated with low-metallicity, young massive stars that are no longer found in our Galaxy.

The use of extragalactic EBs as distance indicators has been thus far the main thrust for their study but increasing interest in the astrophysical aspects has developed in the last few years. One straightforward application is the definition of a mass-luminosity (M–L) law. But, to accomplish this, a representative sample of stars are needed and just a handful of EBs currently have physical properties accurate enough, still insufficient for a first establishment of a M–L law outside our Galaxy. More productive thus far has been the study of individual EB systems with the goal of evaluating stellar structure and evolution models. Especially well-suited for such purpose is the LMC EB HV 2274, which has similar components in a moderately evolved stage (close to the TAMS). Ribas et al. (2000) analyzed HV 2274 and performed a critical study of stellar models both using the H-R diagram and the apsidal motion rate (which contains information of the internal structure of the stars). From that, the authors were able to constrain the elusive convective overshooting parameter for metal-poor massive stars. Another example of using extragalactic EBs as astrophysical laboratories was given by Fitzpatrick et al. (2003). In that case, the spectroscopic study of the semi-detached LMC EB HV 5936 provided insight into the atmospheric properties (most notably helium abundance) of the mass-losing component.

These are just a few examples of EBs used as astrophysical laboratories, where the physical properties of the stars themselves were subject of study. Also interesting is the possibility of using extragalactic EBs as probes. For example, the properties of the interstellar medium along the line of sight (strength of the 2175 Å bump or the far-UV rise) can be analyzed from spectrophotometric observations spanning a wide wavelength range (e.g. Ribas et al. 2002). Even more tantalizing is the prospect of using a large ensemble of EBs across a galaxy to study its line of sight distribution. Since the distance can be accurately determined ($\sim$3%) for each EB system individually, once the "mean" distance of the galaxy is subtracted, the residuals may trace the spatial distribution of the young stellar population.

With some five ongoing projects aimed at the determination of physical properties of Local Group EBs (mostly in the LMC), the future of this field looks bright and significant progress is expected in the coming years. In addition, some projects are now focusing on galaxies other than the LMC, such as the SMC, M31 and M33, and opening new grounds for study. Also promising is the possibility of exploring the realm of stars with lower masses (late B- and A-type), which, with a magnitude of about 18 in the LMC, are within the grasp of current instrumentation.

References

Andersen, J., Clausen, J. V., Nordström, B., Tomkin, J., & Mayor, M. 1991, A&A, 246, 99

Claret, A., & Giménez, A. 1993, A&A, 277, 487

Clausen, J. V. 1991, A&A, 246, 397

Fitzpatrick, E. L., Ribas, I., Guinan, E. F., Maloney, F. P., & Claret, A. 2003, ApJ, 587, 685

Guinan, E. F., Ribas, I., Fitzpatrick, E. L., et al. 2000, ApJ, 544, 409

Ribas, I., Fitzpatrick, E. L., Maloney, F. P., Guinan, E. F., & Udalski, A. 2002, ApJ, 574, 771

Ribas, I., Guinan, E. F., Fitzpatrick, E. L., et al. 2000, ApJ, 528, 692

Schröder, K.-P., Pols, O. R., & Eggleton, P. P. 1997, MNRAS, 285,696

Highlights of Astronomy, Vol. 13
International Astronomical Union, 2003
O. Engvold, ed.

Circularization in B-type Eclipsing Binaries in Both Magellanic Clouds

P. North

Laboratoire d'Astrophysique, EPFL, Observatoire, CH-1290 Chavannes-des-Bois, Switzerland

J.-P. Zahn

LUTH, Observatoire de Paris-Meudon, F-92195 Meudon, France

Making use of detached eclipsing binaries with B-type components discovered by the OGLE and MACHO teams in the SMC and in the LMC, we give the value of the fractional radius above which circularization occurs. This critical radius is around 0.24 to 0.26, regardless of the mass, surface gravity or metallicity, and is consistent with that found by Giuricin et al. (1984) for galactic binaries. These empirical facts are shown to be consistent with Zahn's (1975) theory of tidal dissipation. This work confirms and extends that of North & Zahn (2003), thanks to a sample of 448 binaries taken from the recent OGLE catalogue of 2580 eclipsing binaries in the LMC (Wyrzykowski et al. 2003) and a more homogeneous interpretation of the lightcurves of the 148 SMC binaries.

As a by-product of this study, we provide approximate stellar parameters of the average component of 148 binaries in the SMC and of up to 353 binaries (some of which might be non-detached) in the LMC, under the assumption of equal components, known distance and average absorption towards the Magellanic Clouds. These parameters are available at the address `http://obswww.unige.ch/~north/DEBs/`.

References

Giuricin, G., Mardirossian, F., & Mezetti, M. 1984, A&A, 134, 365
North, P., & Zahn, J.-P. 2003, A&A, 405, 677
Wyrzykowski, L., Udalski, A., Kubiak, M., et al. 2003, AcA, 53, 1
Zahn, J.-P. 1975, A&A, 41, 329

Highlights of Astronomy, Vol. 13
International Astronomical Union, 2003
O. Engvold, ed.

Orbital Elements of MACHO Project Eclipsing Binary Stars

Charles Alcock

Department of Physics and Astronomy, University of Pennsylvania, 209 South 33rd Street, Philadelphia, PA 19104, USA

Large scale photometric surveys can deliver very large numbers of eclipsing binary stars. It is not presently possible to obtain radial velocity information for more than a small fraction of these. We have made some progress in the estimation of the statistical distributions of orbital elements (including semi-major axis and eccentricity) in the MACHO Project catalog of eclipsing binary stars. We see the well-known tendency to circularization in short period orbits and also detect late tidal circularization during the giant phase. The extension of these techniques to newer surveys will also be discussed.

Highlights of Astronomy, Vol. 13
International Astronomical Union, 2003
O. Engvold, ed.

Review of SN Ia Progenitors

Brian P. Schmidt

The Research School of Astronomy and Astrophysics, The Australian National University, Mount Stromlo and Siding Spring Observatories, via Cotter Road, Weston Creek PO 2611, Australia

Type Ia Supernovae have taken on a leading role in measuring extra-galactic distances providing key information about the Hubble Constant and providing evidence of an accelerating Universe. Unfortunately these conclusions are based on an empirical relationship between SN brightness and light curve shape rather than any deep physical understanding. A key ingredient to gaining physical understanding lies in understanding what becomes a SN Ia progenitor. Essentially all models require a binary system to push a white dwarf higher in mass. I will review the current attempts observational and theoretical to pin down the nature of these important astrophysical objects.

Highlights of Astronomy, Vol. 13
International Astronomical Union, 2003
O. Engvold, ed.

Extragalactic Binaries as Core-Collapse Supernova Progenitors

Schuyler D. Van Dyk

IPAC/Caltech, 100-22, Pasadena, CA 91125

Core-collapse supernovae (SNe) come in a variety of subtypes. The SNe II-plateau (II-P) show a long plateau in their light curves, as well as classical P Cygni Balmer line profiles in their spectra. The SNe II-linear (II-L) show a linear decline in their light curves after maximum, and the blue absorption trough in the Balmer lines is missing, leaving only broad emission profiles. The SNe II-narrow (IIn) show a narrow profile atop a broad base to the Balmer emission. The SNe Ib exhibit no hydrogen lines, but prominent He lines instead. The SNe Ic also show no H, but also weak or no He, with their spectra dominated by intermediate-mass elements. The SNe IIb start out appearing as SNe II(P), but in time evolve spectrally to resemble SNe Ib, with a later resumption of broad Balmer profiles, as in the case of SN 1993J (see Filippenko 1997 for a review of SN types). The progression from SNe II-P, II-L, IIn, IIb, Ib, through Ic may be due to the degree of stripping of the H-rich stellar envelope. Binary star systems are likely the progenitors of many core-collapse SNe. In fact, we might expect $\gtrsim$ 40–50% of all such SNe to arise from binaries (e.g., De Donder & Vanbeveren 1998).

Observational evidence supports the binary nature of the progenitors of some core-collapse SNe. One constraint on the binary nature of SNe Ib/c may come from their centimeter-wavelength radio emission. This synchrotron emission arises as the SN blastwave interacts with a dense, pre-SN wind-established, circum-stellar medium (CSM), leading to particle acceleration and compression of magnetic fields. In the case of SNe Ib/c, any dense CSM may require the presence of an interacting binary companion (Van Dyk et al. 1992; although see Chevalier 1998; yet also see Chevalier 2002). However, the association of two extreme SNe Ic, 1998bw and 2003dh, with long-duration γ-ray bursters implies, if the collapsar model is correct (e.g., MacFadyen & Woosley 1999), that some SNe Ic may arise from (single) very massive stars, possibly in the Wolf-Rayet phase. This is consistent with SNe Ib/c possibly being preferentially associated with massive star formation regions (Van Dyk et al. 1999), implying that SNe Ib/c arise from more massive progenitors than SNe II, further supporting the Wolf-Rayet model.

Various anomalies of and the famous circum-stellar ring structure around the peculiar Type II-P SN 1987A in the LMC can be explained by an accreting or merging binary system (e.g., Podsiadlowski 1992). The SN IIb 1993J in M81 has been proposed to be a binary KO I + OB? system (e.g., Aldering, Humphreys, & Richmond 1994). The radio emission for this SN implies a CSM density profile shallower than expected for a spherically symmetric progenitor wind, which might occur as a result of binary interaction. It is not clear from recent

HST ACS images of a now much fainter SN 1993J that the blue companion has been detected.

The ∼8% modulations in the radio light curves for the Type II-L SN 1979C in M100 imply a quasi-periodic, ∼ 1575 d, variation in the pre-SN wind. This suggests that the progenitor was in a highly-eccentric, long-period ($P \sim 4000$ yr), interacting, massive (10 $M_{\odot}$ + 15 $M_{\odot}$) VV Cephei-like (RSG+OB) binary system (Weiler et al. 1992), This picture is supported by a full 2-D hydrodynamic simulation of the system (Schwarz & Pringle 1996). Similar bumps and dips in the radio light curves for the Type IIb SN 2001ig in NGC 7424 (Ryder et al. 2003), a SN quite similar to SN 1993J, imply modulations in the wind with $P \sim 600$ yr; this is generally far longer than stellar pulsation time scales, but is perhaps consistent with thermal pulse (C/He flashes) periods in 5–10 $M_{\odot}$ asymptotic giant branch stars. However, such time scales are also consistent with modulation in the colliding winds in an interacting WR+OB binary system.

References

Aldering, G., Humphreys, R. M., & Richmond, M. 1994, AJ, 107, 662

Chevalier, R. A. 1998, ApJ, 499, 810

Chevalier, R. A. 2003, in From Twilight to Highlight – The Physics of Supernovae, ESO/MPA/MPE Workshop, eds. W. Hillebrandt & B. Leibundgut (ESO: Garching), in press

De Donder, E., & Vanbeveren, D. 1998, A&A, 333, 557

Filippenko, A. V. 1997, ARA&A, 35, 309

MacFadyen, A. I., & Woosley, S.E. 1999, ApJ, 524, 262

Podsiadlowski, P. 1992, PASP, 104, 717

Ryder, S. D., et al. 2003, in prep

Schwarz, D. H., & Pringle, J. E. 1996, MNRAS, 282, 1018

Van Dyk, S. D., et al. 1992, ApJ, 409, 162

Van Dyk, S. D., et al. 1999, AJ, 118, 2331

Weiler, K. W., et al. 1992, ApJ, 399, 672

Highlights of Astronomy, Vol. 13
International Astronomical Union, 2003
O. Engvold, ed.

Joint Discussion 13: Abstracts

Status of the International Celestial Reference Frame:

Alan L. Fey (U.S. Naval Observatory, 3450 Massachusetts Avenue NW, Washington DC, 20392-5420, USA); Jean Souchay (Observatoire de Paris, DANOF, 61, avenue de l'observatoire, 75014 Paris, France)

Abstract. We present a brief report on the status of the International Celestial Reference Frame. There have been two extensions (updates) of the ICRF since its initial definition in 1998. The primary objectives of extending the ICRF were to provide positions for the 109 extragalactic radio sources observed since the definition of the ICRF and to refine the positions of candidate and other sources using additional observations. A secondary objective was to monitor sources to ascertain whether they continue to be suitable for use in the ICRF. Positions of the ICRF defining sources have remained unchanged. Improved positions and errors for the candidate and other sources were estimated and reflect the changes in the data set and the analysis. The 109 new sources were added with ICRF coordinates. We also discuss current efforts toward ICRF maintenance and the International Celestial Reference System Product Center.

Potential Refinement of the ICRF:

Chopo Ma (NASA Goddard Space Flight Center, Code 926, Greenbelt, MD 20771, USA)

Abstract. The ICRF analysis and data represented the state of the art in global, extragalactic, X/S band microwave astrometry in 1995. Similar analysis has been used to extend the ICRF with subsequent data consistent with the original catalog. Since 1995 there have been considerable advances in the geodetic/astrometric VLBI data set and analysis that would significantly improve the systematic errors, stability, and density of the next realization of the ICRS when the decision is made to take this step. In particular, data acquired since 1990, including extensive use of the VLBA, are of higher quality and astrometric utility because of changes in instrumentation, schedule design, and networks as well as specifically astrometric intent. The IVS (International VLBI Service for Geodesy and Astrometry) continues a systematic extension of the astrometric data set. Sufficient data distribution exists to select a better set of defining sources. Improvements in troposphere modeling will minimize known systematic astrometric errors while accurate modeling and estimation of station effects from loading and nonlinear motions should permit the re-integration of the celestial and terrestrial reference frames with Earth orientation parameters though a single VLBI solution. The differences between the current ICRF and the potential second realization will be described.

The CRF Solution by the Geoscience Australia IVS Analysis Center:

Oleg Titov (GPO Box 378, Canberra, ACT, 2601, Australia)

Abstract. The Geoscience Australia IVS Analysis Center is working for improvement of the ICRF. The catalogue of 659 radio-source positions estimated from a 23-year set of the VLBI data (1980-2003) in a homogeneous solution

(TRF, CRF, EOP) has been obtained using the OCCAM software. Statistical analysis of the results shows that the median accuracy of the source positions is 0.2-0.3 mas in both coordinates. The long-term apparent motions of two quasars: 0923+392 (4C39.25) and 2145+067 are also analyzed.

Contribution of stable sources to ICRF improvements:
A.-M. Gontier & Martine Feissel-Vernier (Observatoire de Paris, SYRTE, 61, avenue de l'observatoire, 75 014 Paris France)

Abstract. A set of stable compact radio sources is proposed for the future maintenance of the ICRF axes, based on time series analysis of VLBI-derived coordinates of extragalactic radio sources. The selection scheme makes a combined use of statistical and deterministic tests. It identifies 199 stable sources, to be compared to the current 212 defining sources. Their consideration for the maintenance of the frame axes is expected to improve the frame stability by a factor of five, reaching the level of less than 10 microarcseconds in the medium term. The improved stability and internal consistency of the frame also enhances the quality of the Earth orientation determinations.

Astrometric Microlensing and Degradation of Reference Frames:
Mizuhiko Hosokawa (Communications Research Laboratory, Tokyo, 184-8795, Japan); Kouji Ohnishi (Nagano National College of Technology, Nagano, 381-8550, Japan); Toshio Fukushima (National Astronomical Observatory, Mitaka, Tokyo, 181-8588, Japan)

Abstract. We have pointed out that the positions of extragalactic radio sources fluctuate on the order of a micro arcsecond (μas) because of astrometric microlensing by stars and MACHOs in our galaxy (Hosokawa *et al.* 1997). This means that the kinematical reference frames based on the positions of extragalactic radio sources will be degraded by this kind of fluctuation. Recently, we have shown that in the case of the extragalactic sources in the direction close to the Galactic Center, the optical depth of 10 μas fluctuation is about a quarter for the standard model of our galaxy (Hosokawa *et al.* 2002). Further, macro scale astrometric gravitational lensing by the collective mass of the Galactic Center appears in a different manner. In this paper we discuss the type, the magnitude and the time scale of the degradation of reference frames due to the astrometric gravitational lensing. For the astrometric gravitational lensing event of a few μas caused by each star, the event duration is expected to be several years. On the other hand, the induced motion due to macro scale astrometric gravitational lensing is practically regarded as secular.

Extending the ICRF to Higher Radio Frequencies: 24 & 43 GHz:
Christopher S. Jacobs (Jet Propulsion Laboratory, California Institute of Technology, 4800 Oak Grove Drive, Pasadena, CA 91109, USA); Patrick Charlot, David Gordon, Gabor Lanyi (Chopo Ma, Charles Naudet, Ojars Sovers, Liwei Zhang, and the KQ VLBI Survey Collaboration)

Abstract. Astrometric observations of active galactic nuclei have been used to construct quasi-inertial global reference frames, most notably the International Celestial Reference Frame (ICRF) which now forms the basis for all as-

trometry including deep space navigation. The ICRF was defined using X- (8.4 GHz) and S-band (2.3 GHz) observations collected over 20+ years. There are several motivations for extending this work to higher frequencies, namely, to construct a more stable frame based on more compact sources, to provide calibrators for phase referencing, and to support spacecraft navigation at higher frequencies.

Survey observations using the Very Long Baseline Array at K-band (24 GHz) and Q-band (43 GHz) have been undertaken to pursue these goals. Three observing sessions have covered the full 24 hours of right ascension and declination down to −30 deg. The resulting catalog of 80+ sources has K-band median formal position uncertainties of < 200 micro-arcseconds. The Q-band positional uncertainties are about 1.5 times larger. Group delay residuals were excellent at approximately 20 psec weighted RMS. Comparison of the K-band frame to the S/X-band ICRF shows systematic errors which we will discuss.

The research performed at JPL-Caltech and GSFC was done under contract with NASA.

Densification of the ICRF/HCRF in Visible Wavelengths:
Sean E. Urban (U.S. Naval Observatory, 3450 Massachusetts Ave. NW, Washington DC, 20392-5420, USA)

Abstract. With the release of the Hipparcos Catalogue and the IAU resolution designating its 100,000 star subset as the HCRF, the optical reference frame increased 20-fold in the number of stars over the FK5. For many applications, even these 100,000 stars are inadequate in spatial density and limiting magnitude. However, Hipparcos is dense enough and deep enough to reduce many astrometric catalogs directly; the resulting data can be used to densify the HCRF and extend its magnitude limit. The initial major densification efforts of the HCRF utilized the Tycho data, culminating in the Tycho-2 Catalogue of 2.5 million stars. Over the last few years, several groups have been working toward even greater densification. Some resulting catalogs, such as the CMC 13, M2000, and SPM 2.0 are zonal, covering selected areas of the sky. Others, such as UCAC, USNO-B, and GSC 2.3 aim at global coverage but with varying degrees of accuracy and magnitude regimes. Others, namely DENIS and 2MASS, are extending the HCRF into the near IR realm. The current state of many of these projects, and what is expected in the next few years in terms of densification of the optical frame, is presented.

Extending the ICRF into the Infrared: 2MASS−UCAC Astrometry:
Norbert Zacharias (U.S. Naval Observatory, 3450 Massachusetts Ave. NW, Washington DC, 20392-5420, USA); Howard L. McCallon, Eugene Kopan & Roc M. Cutri (IPAC, Caltech, MS 100-22, 770 S. Wilson Ave., Pasadena, CA 91125, USA)

Abstract. An external comparison between the infrared 2MASS and the optical UCAC positions was performed, both being on the same system, the ICRS. About 48 million sources in common were identified. Random errors of the 2MASS catalog positions are about 60 to 70 mas per coordinate for the K_S = 4 to 14 range, increasing to about 100 to 150 mas for saturated and very faint stars. Systematic position differences between the 2 catalogs are very small, about 5 to 10 mas as a function of magnitude and color, with somewhat larger

errors as a function of right ascension and declination. The extension of the ICRF into the infrared has become a reality.

JD14

Formation of Cometary Material

Chairperson: W.F. Huebner

Editors: W.F. Huebner (Chief-Editor), P. Ehrenfreund and H.-U. Keller

Highlights of Astronomy, Vol. 13
International Astronomical Union, 2003
O. Engvold, ed.

Apparent Inconsistencies in the Formation of Cometary Matter

W. F. Huebner

Southwest Research Institute, P. O. Drawer 28510, San Antonio, TX 78228-0510, USA.

H. U. Keller

Max-Planck-Institut für Aeronomie, D-37191 Lindau, Germany.

Abstract. The Joint Discussion (JD14) is intended to focus attention on several apparent inconsistencies found in comet observations when compared with observations of collapsing interstellar clouds, star-forming regions, and models of the solar nebula. The JD is not intended to resolve these problems, for that a one-day discussion is too short. It rather is intended to draw attention to the inconsistencies to be discussed and resolved in future workshops.

1. Enumeration of Some Inconsistencies

Observations of comets reveal information about the structure and composition of their nuclei. They in turn, provide clues about the thermodynamic conditions and composition of the solar nebula in the region where comet nuclei formed. Most neutral molecular species identified in comets, coming directly from comet nuclei, have also been identified in the gas phase in the interstellar medium (ISM). However, the relative abundances of ice species are the important quantities that should be compared, not the gaseous species. Abundances of species in the ISM vary with location and abundances in the coma of a comet are not necessarily the same as the abundances of ices in the nucleus (Huebner & Benkhoff 1999).

The D/H ratios in molecules have been measured in a few Oort-cloud comets (Halley, Hale-Bopp, Hyakutake). They are consistent with values expected from interstellar chemistry. This suggests that if interstellar molecules were incorporated in comet nuclei, they were not chemically transformed in the solar nebula accretion shock in the region where these nuclei formed. The question arises if the accretion shock was absent or too weak in the region where comets formed, or can the same molecules found in the ISM reform in the solar nebula? No reliable measurements of the D/H ratio exist for Kuiper-belt comets. A key question concerns the abundances of various ices on interstellar grains.

The hydrogen ortho-to-para ratio in cometary H_2O and NH_2 suggest that comet nuclei formed at low temperatures [1P/Halley at $\sim$ 50 K: Mumma, Weaver, & Larson 1987; C/1999 S4 (LINEAR) at $\sim$ 28 K: Kawakita et al. 2001]. CO has been detected in many comets, but N_2, CH_4, and Ar are found only in trace amounts. Yet, CO is less volatile than N_2 and more volatile than CH_4 and Ar.

Evidence for amorphous water ice in comets is circumstantial. It is based on models for the release of gases trapped in amorphous water ice to explain the heliocentric distance dependence of some observed gaseous species abundances in comet comae. However, it is thought that amorphous water ice cannot form in the solar nebula (SN) even though temperatures are low enough. The condensation rate in the SN is too slow so that H_2O molecules have time to reorient themselves to form crystalline ice (Kouchi et al. 1994). Thus, the question arises about additional evidence for amorphous vs. crystalline water ice in collapsing clouds, ISM, and Comets.

The discovery of large, highly saturated complex molecules of biological importance in collapsing clouds and the ISM is increasing. There are still many unidentified spectral lines in comet comae. Do some of them belong to complex molecules? How complex can we expect molecules to be in comets? Can complex molecules form in the SN?

Detection of crystalline silicate grains in comet comae indicates that some dust has been exposed to temperatures of about 900 K. One theory suggests that turbulent mixing and heating of dust in the inner solar nebula followed by transport into the comet-forming zone may be responsible for crystallization. However, this also requires heating the gas that entrains and transports the dust. Heating the gas would change its interstellar composition. Are comet coma observations consistent with such high-temperature exposures? What evidence exists for amorphous and crystalline silicates in collapsing clouds, the ISM, dark interstellar clouds (DISCs), and comets? Are there alternative mechanisms for formation of crystalline silicate grains?

Silicates and GEMS (submicron-sized glassy silicates) bear evidence of exposure to large doses of ionizing radiation. They appear to be similar to the inferred properties of interstellar grains. Can these properties also be acquired in the SN?

Recently it has been pointed out that the composition of comet nuclei is not consistent with the solar composition of icy planetesimals (SCIPs) responsible for the formation of Jupiter (Owen & Encrenaz 2003). Has the composition of comet nuclei changed over time? Is the composition of Kuiper-belt comets different from Oort-cloud comets? From the formation of comet nuclei, what inherent differences can we expect in structure and composition of Kuiper belt comets vs. Oort cloud comets (other than cosmic ray effects)? Did SCIPs that formed the core of Jupiter possibly come from a companion cloud to the SN? Was such a companion cloud too small to form a star but cold and dense enough to form comet nuclei that have a different composition? Can we find such comets?

Models of collapsing clouds and of star-forming regions are used as analogs of the SN. In such models, the physics (e. g., turbulence and shocks) and chemistry are not separable. How can SN models be constraint by observations of comets? What are the extent, strength, and effect of the accretion shock in the SN? How does it influence the gas and dust composition of the SN? How strong are the effects of the SN accretion shock on gas and dust in the comet-forming region?

Laboratory work relevant to the above topics is very important but can be difficult: Higher densities must be assumed in the laboratory to account for time-compression. The interstellar radiation field varies with location. Physical effects such as turbulence are difficult to simulate. Relative abundances are difficult to determine because they depend on properties of various species and their state variables such as gases or ices.

2. Prospects for the Resolution of the Inconsistencies

This Joint Discussion is intended to focus attention on the conflicting evidence of survival of the low-temperature interstellar molecules in the SN in spite of the accretion shock, the detection of crystalline features in cometary dust, and on observations, models, and laboratory experiments that help to clarify the issues at hand. The following presentations were made in the Joint Discussion to focus attention on these challenging issues.

References

Huebner, W. F., & Benkhoff, J. 1999, Space Sci.Rev.90, 117

Kawakita, H., Watanabe, J., Ando, H., Aoki, W., Fuse, T., Honda, S., Izumiura, H., Kajino, T., Kambe, E., Kawanomoto, S., Noguchi, K., Okita, K., Sadakane, K., Sato, B., Takada-Hidai, M., Takeda, Y., Usuda, T., Watanabe, E., & Yoshida, M. 2001, Science 294, 1089

Kouchi, A., Yamamoto, T., Kozasa, T., Kuroda, T., & Greenberg, J. M. 1994, A&A290, 1009

Mumma, M. J., Weaver, H. A., & Larson, H. P. 1987, A&A187, 419

Owen, T., & Encrenaz, T. 2003, Space Sci.Rev.106, 121

Highlights of Astronomy, Vol. 13
International Astronomical Union, 2003
O. Engvold, ed.

Large Interstellar and Cometary Biomolecules

Lewis E. Snyder

Department of Astronomy, University of Illinois, 1002 W. Green, Urbana, Illinois 61801, USA

Abstract. The relevance of hot molecular cores (HMCs) to the solar nebula has been strengthened as evidence emerges for a hot core phase in low mass star formation regions. Consequently, interferometric studies of large highly saturated molecules of biological interest (biomolecules) in HMCs have been extended to comets. A key goal is the interferometric detection and mapping of large biomolecules, which could be formed along chemical pathways similar to those for HMC species.

1. Galactic Star Formation Regions and Hot Molecular Cores

Much progress has been made toward understanding the formation of solar-type stars by focusing on low-mass regions (Mundy, Looney, & Welch 2000). However, the most interesting and complex chemistry of molecules of biological interest (biomolecules) has been observed in hot molecular cores (HMCs) mainly in regions of massive star formation. Complex saturated molecules have been reported for only one low-mass young stellar object, IRAS 16293-2422 (Cazaux et al. 2003). Because of their relatively large sizes and column densities, high-mass HMCs provide an environment in which the chemical pathways for many biomolecules can be directly inferred from observations. The chemistry in HMCs is more complex than that detected so far in the cold dark clouds, which have been the targets of most low-mass studies. Large, highly saturated molecules have been mostly detected in HMCs. Examples include ethyl cyanide, methyl formate, methanol, dimethyl ether, acetone, glycolaldehyde, and acetic acid. The high temperatures in HMCs permit a chemistry to take place that ordinarily would not occur in cold dark clouds (Ehrenfreund & Charnley 2000). The rich, active chemistry of HMCs is confined to small regions near the heating sources, and so molecular detections are enhanced by telescopes that have high spatial resolution, such as interferometric arrays. There are many gaps in our knowledge about the evolutionary progression from a high-mass HMC to a primordial solar nebula. For example, detailed data are needed for HMC sizes, masses, structures, kinematics, and temperatures. Much of this can be obtained through high spatial resolution studies of large, highly saturated molecules in HMCs. Coincidentally, many of these large species are also of biological interest, which makes the potential connection to the solar nebula even more interesting.

2. Current Research on Large Molecules in HMCs

Over the last few years, interferometric array measurements have revealed a hot core of unusually high column density embedded within the more extended molecular cloud in Sgr B2(N). It is called the Large Molecule Heimat source, or Sgr B2(N-LMH), due to its extraordinarily high column densities of large, highly saturated molecules, including many of pre-biotic interest (Snyder et al. 1994; Miao & Snyder 1997). The interferometric array measurements were made with synthesized beams that ranged from $1''$ to $14''$ in width. Given the distance to Sgr B2 of 7.1 kpc (Reid 1993), an angular resolution of $1''$ corresponds to a physical scale of $\sim$ 7500 AU, or $\sim$ one-tenth the size of the Oort cometary cloud. A consistent set of beam-averaged column densities measured with the BIMA Array, all at a few arcseconds angular resolution, has been summarized by Snyder et al. (2002) for several large dust generated molecular species in Sgr B2(N-LMH): $2.9(3)\times 10^{16}$ cm^{-2} for acetone; $0.6(1)\times 10^{16}$ cm^{-2} for acetic acid; $1.1(3)\times 10^{16}$ cm^{-2} for formic acid; $4.6(1)\times 10^{16}$ cm^{-2} for ethyl cyanide; and $11.2(10)\times 10^{16}$ cm^{-2} for methyl formate. Note the relatively high column density of acetic acid. Acetic acid is of possible pre-biotic importance because its structure is only separated by an NH_2 fragment from glycine, the simplest amino acid. In Sgr B2(N-LMH), its column density is $\sim$ 20 times less than that of its isomer, methyl formate. This suggests that large molecules in the pre-solar nebula are not formed from randomly assembled constituent atoms.

Because it is important to learn how well the astrochemistry found in Sgr B2(N-LMH) really represents the astrochemistry of HMCs in the disk of the Galaxy, searches for new sources of large molecules outside the galactic center region have been conducted by Remijan et al. (2002; 2003). As a result, acetic acid has been detected in the high-mass sources W51e2 and G34.3+0.2. In the 3 known high-mass sources, the acetic acid column density appears to be $\sim$ 15-100 times below the abundance of its isomer methyl formate, $\sim$ 2-10 times below the abundance of formic acid, and $\sim$ 2-10 times below the abundance of ethyl cyanide. (Cazaux et al. (2003) detected only one line of acetic acid in IRAS 16293-2422, which makes the relative abundance determination difficult in this source.)

3. Comets

Bockelée-Morvan et al. (2000) conducted an extensive study of Comet C/1995 O1 (Hale-Bopp) with the Caltech Submillimeter Observatory, the IRAM 30 m, and the Plateau-de-Bure interferometer, all in autocorrelation mode. They observed 16 molecular species, including 3 which are likely to be made either abundantly or exclusively by grain chemistry: formaldehyde, methanol, and methyl formate (MeF). The detection of methyl formate provides the first clear chemical link between the chemistry of comets and that of biomolecules observed in high-mass hot molecular cores. Bockelée-Morvan et al. (2000) calculated a molecular abundance relative to H_2O of 0.08% for methyl formate and Q(MeF) $= 2.8 \times 10^{28}$ s^{-1}. The upper limits from BIMA Array observations are more than 3 times higher. If the same molecular formation chemistry active in HMCs applies to Comet Hale-Bopp, to find acetic acid (AcA) it would have been necessary to reach Q(AcA) = (3-20) $\times$ 10^{26} s^{-1}. The BIMA Array limit for Hale-Bopp at 3 mm wavelength was 5 $\times$ 10^{28} s^{-1}, or 25 times greater than the best possible case for detecting acetic acid (Snyder et al. 2003).

4. Conclusions

HMCs in high-mass star formation regions produce large biomolecules which now are starting to be found in HMCs in low-mass regions. Among these large biomolecules, only methyl formate has been found in a comet (Hale-Bopp). However, if the chemistry of comets follows the chemistry of HMCs, methyl formate may provide a connection to acetic acid and even to glycine in comets. The BIMA Array results from Hale-Bopp miss the sensitivity required to image cometary methyl formate by at least a factor of 3. This situation will change with the construction of the Combined Array for Research in Millimeter-wave Astronomy (CARMA) at a new high site near Owens Valley Observatory in California. At wavelengths near 1 mm, there will be a gain of at least an order of magnitude in sensitivity, which should introduce a new era in the imaging of large cometary biomolecules.

Acknowledgments. We acknowledge support from the Laboratory for Astronomical Imaging at the University of Illinois, NSF AST 99-81363, NSF AST 02-28953, and NASA NAG 5-4292.

References

Bockelée-Morvan, D., et al. 2000, A&A, 353, 1101

Cazaux, S., et al. 2003, ApJ, 593, L51

Ehrenfreund, P., & Charnley, S. B. 2000, ARA&A, 38, 427

Miao, Y., & Snyder, L. E. 1997, ApJ, 480, L67

Mundy, L. G., Looney, L. W., & Welch, W. J. 2000, in Protostars and Planets IV, eds. V. Mannings, A. Boss, & S. Russell (U. Arizona Press), 355

Reid, M. J. 1993, ARA&A, 31, 345

Remijan, A. J., Snyder, L. E., Fridel, D. N., Liu, S. Y., & Shah, R. 2003, ApJ, 590, 314

Remijan, A., Snyder, L. E., Liu, S.-Y., Mehringer, D., & Kuan, Y.-J. 2002, ApJ, 576, 264

Snyder, L. E., Kuan, Y.-J., & Miao, Y. 1994, in The Structure and Content of Molecular Clouds, ed. T. Wilson & K. Johnston (Springer-Verlag), 187

Snyder, L. E., et al. 2003, in preparation

Snyder, L. E., et al. 2002, ApJ, 578, 245

Highlights of Astronomy, Vol. 13
International Astronomical Union, 2003
O. Engvold, ed.

Processed and Unprocessed Ices in Circumstellar Disks

Klaus Pontoppidan & Ewine van Dishoeck

Leiden Observatory, P. O. Box 9513, 2300 RA Leiden, Netherlands

Emmanuel Dartois

IAS, Bât 121, Université Paris XI, 91405 Orsay Cedex, France

Wing-Fai Thi

Astronomical Institute "Anton Pannekoek", University of Amsterdam, Kruislaan 403, 1098 SJ Amsterdam, Netherlands

Abstract. We present 3-5 μm VLT-ISAAC spectroscopy showing the presence of methanol ices in edge-on disks of young embedded stars. Examples include the disks of L1489 IRS in Taurus and CRBR 2422.8-3423 in Ophiuchus, the last of which has the highest column density of solid CO known toward a YSO. Several additional low-mass sources in the Serpens and Chameleon molecular clouds exhibit abundant solid methanol although it is not clear if the ice is associated with a disk or with the envelope. These are the first detections of solid methanol in the disks and circumstellar environments of embedded young low-mass stars providing evidence that complex molecular species previously observed only in the solid state toward high-mass star forming regions are also present near solar-type young stars. The constraints on the formation mechanisms of methanol and the chemical evolution of ices as the material is incorporated into circumstellar disks are discussed.

1. Introduction

The presence of abundant ices in the interstellar medium has long been firmly established and its connection to the ices present in solar system comets has been the subject of some discussion. Most of the major constituents of interstellar grain mantles have now been firmly identified, mostly due to the ISO mission and extensive laboratory work. However, only recently have attempts been made to observe the ices in the context of their astrophysical environments. Models indicate that ices may undergo significant transformation when material from a protostellar envelope is incorporated into a disk, either through shock evaporation (Charnley, this volume) and recondensation or through growth of ice mantles under different densities and temperatures than those of the quiescent interstellar medium (e.g., Aikawa et al 2003).

In this contribution, new direct observations of ices in circumstellar disks are described and compared to ices more likely to be associated with circumstellar envelopes and quiescent molecular cloud material.

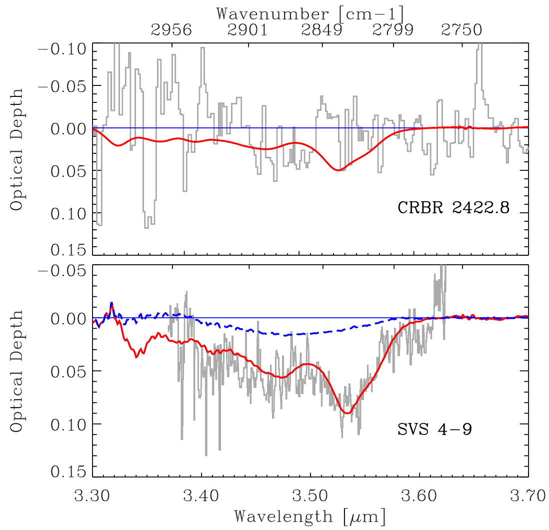

Figure 1. Top: Upper limit of the methanol 3.53 μm band toward the edge-on disk CRBR 2422.8-3423 ($N(CH_3OH)/N(H_2O) \leq 0.06$). Bottom: VLT-ISAAC detection of methanol toward a YSO (SVS 4-9) which probes dense envelope material and an outflow rather than a disk ($N(CH_3OH)/N(H_2O) = 0.25$). The dashed curves show a template for the 3.47 μm feature. The solid curves show a sum of the 3.47 μm template and a laboratory spectrum of an $H_2O : CH_3OH : H_2CO$=1:1:1 mixture at 10 K.

2. Observations of ices in disks

Mid-infrared spectroscopy of nearly edge-on circumstellar disks around young stars probe a line of sight passing through the cold disk mid-planes where ices are expected to exist. As part of a 3-5 μm spectroscopic survey of more than 40 young low mass stars (van Dishoeck et al. 2003) a small selection of sources with edge-on disks have been included. Previously, the stretching mode of solid CO at 4.67 μm have been analysed in this manner for the low mass edge-on disk sources L1489 IR (Boogert et al. 2002) and CRBR 2422.8-3423 (Thi et al. 2002).

Here we present the results from a search for solid methanol toward these two sources. Methanol (CH_3OH) is believed to be formed primarily in the solid state through successive hydrogenation of CO. The formation efficiency of this species is particularly interesting due to its significant role in the gas-phase formation of more complex organic molecules. In Fig. 1 a VLT-ISAAC spectrum of the 3.53 μm region of CRBR 2422.8-3423 is presented showing a non-detection of solid methanol with an upper limit of 6% with respect to water ice. For comparison a strong methanol band observed toward the low mass YSO SVS 4-9 in the Serpens cloud core is shown below (Pontoppidan et al. 2003).

In Fig. 2 the same spectral region is shown of L1489. The band is clearly dominated by the "3.47 μm feature", which is unrelated to the methanol band. The presence of this band makes it difficult to determine the abundance of solid methanol even if the spectrum is of high quality. The spectrum of another low mass source, IRS 42, is also shown as an example of a good upper limit

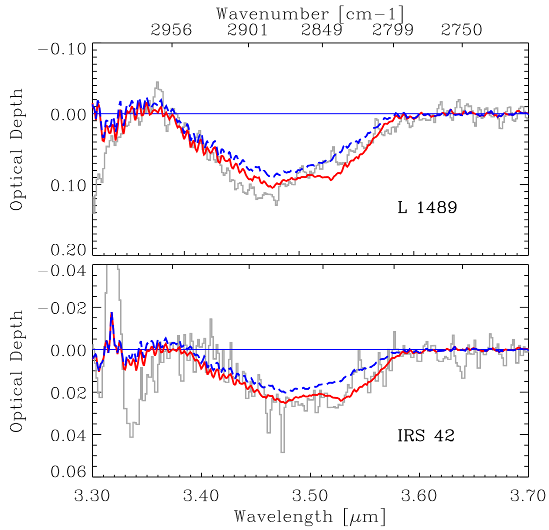

Figure 2. Same as Fig. 1. Top: The deep 3.47 μm feature of the edge-on disk source L1489. The solid curve corresponds to a methanol content of 5%. Bottom: A comparison with IRS 42 in the Ophiuchi cloud core thought to probe mostly quiescent molecular cloud material. The solid curve corresponds to a methanol content of 4%.

of $\lesssim$ 4% methanol with respect to water. We find in general that about 10% of our observed lines of sight contain ice with 20% or more methanol, while only upper limits of 2-10% methanol are available for the rest. This implies that the methanol content of specific grain mantles may vary with an order of magnitude, depending on the environment. We have not found firm evidence of abundant methanol in the circumstellar disk material observed so far, but our upper limits are still consistent with cometary abundances. If methanol-rich ices from protostellar envelopes have been included in these disks, the methanol must have been diluted or destroyed during the process of disk-formation.

References

Aikawa, Y., Ohashi, N. & Herbst, E. 2003, ApJ, 593, 906

Boogert, A. C. A., Hogerheijde, M. R. & Blake, G. A. 2002 ApJ, 568, 761

van Dishoeck, E. F., Dartois, E., Pontoppidan, K. M. et al. 2003, ESO Messenger, 113, 49

Pontoppidan, K. M., Dartois, E., van Dishoeck, E. F., Thi, W.-F. & d'Hendecourt, L. 2003, A&A, 404, 17

Thi, W. F., Pontoppidan, K. M., van Dishoeck, E. F., Dartois, E. & d'Hendecourt, L. 2002, A&A, 394, 27

Highlights of Astronomy, Vol. 13
International Astronomical Union, 2003
O. Engvold, ed.

Ortho-To-Para Ratio of Cometary Water and Ammonia

Hideyo Kawakita

Gunma Astronomical Observatory, 6860-86 Nakayama, Takayama, Agatsuma, Gunma 377-0702, Japan

Jun-ichi Watanabe, Reiko Furusho, Tetsuharu Fuse

National Astronomical Observatory of Japan, 2-21-1 Osawa, Mitaka, Tokyo 181-8588, Japan

Abstract. Since the time that the ortho-to-para ratio (OPR) of cometary water was first Determined from observations of Comet Halley, the real meaning of OPR has not been discussed in detail. Here we review the OPRs of water and ammonia and discuss the possibilities that the OPRs were modified in the coma or the nucleus. Our conclusion indicates that the OPRs were not altered after comet nucleus formation, i.e., the OPRs reflect the temperatures in the solar nebula or the pre-solar molecular cloud.

Molecule that have protons at symmetric positions like H_2O, NH_3, and CH_4, can be distinguished into different nuclear spin species ("ortho" and "para", or E, A, and F species) according to the relative orientations of molecular proton spins. The radiative or collisional transitions between ortho and para species are forbidden in the gas phase and the conversion speed between them is probably very slow even in the solid (Mumma et al. 1993; Crovisier 2000). Therefore, even though the rotational distribution of a molecule in the gas phase can be easily changed according to the surrounding environment, the ortho-to-para abundance ratio (OPR) retains the old value. If the OPR was determined in thermal equilibrium, the nuclear spin temperature (Mumma et al. 1987) which is the rotational excitation temperature to reproduce the observed OPR value, is used to infer the temperature condition when the nuclear spins were last equilibrated.

The first determination of the nuclear spin temperature of water in Comet Halley showed about 29 K which was derived from the near infrared observation of the 2.7 μm vibrational bands by the Kuiper Airborne Observatory (Mumma et al. 1987). Three comets were observed in the same vibrational bands after Comet Halley: Comet Wilson with the KAO (Mumma et al. 1993) and Comets Hale-Bopp and Hartley 2 with ISO (Crovisier 2000). Because these water emission bands were hampered by the telluric water vapor, it is difficult to increase the number of samples. The obtained nuclear spin temperature is about 28 — 35 K except for Comet Wilson, which showed > 50 K (this value is considered as the result of cosmic ray damage in the Oort cloud).

Recently, a new technique to derive the OPR of water from ground-based observations has been developed by Dello Russo et al. (2002). They use the vibrational hot band of water. Since the water molecule in the telluric atmosphere is not pumped as much to the vibrational excited levels, the water hot band emissions are not absorbed significantly by the telluric atmosphere. They demonstrated the technique for water OPRs derived from the high-dispersion near infrared spectra of comets (Dello Russo et al. 2002). Their OPR values correspond to spin temperatures of 23 – 26 K.

For another molecule, Kawakita et al. (2001) demonstrated that the OPR of ammonia can be derived from the high-dispersion spectrum of NH_2, which is a photo-dissociation product of ammonia in a comet coma. Based on the same technique, the OPRs of ammonia in four comets have been derived so far (Kawakita et al. 2004). The nuclear spin temperatures of ammonia range from 26 to 32 K in four comets. The nuclear spin temperatures of ammonia are similar to the water values. There are some comets for which the nuclear spin temperature of both ammonia and water were obtained, and the ammonia value is consistent with the water value in each comet. This fact is considered as evidence that the OPRs of water and ammonia were determined in thermal equilibrium (Kawakita et al. 2004). Otherwise, the OPRs of water and ammonia are generally different according to the structures of molecules.

On the other hand, in the case of methane, Gibb et al. (2003) and Weaver et al. (1997) reported the lower limit of the nuclear spin temperature of CH_4 in several comets (25 — 50 K). The nuclear conversion speed of CH_4 may be faster than for water or ammonia and the methane values obtained in the comets were probably affected by the temperature of the nucleus surface (Weaver et al. 1997).

The OPRs of cometary molecules might evolve with time after comet nuclei formed. First, the OPRs might re-equilibrate to the interior temperatures of comet nuclei during their long stay in the Oort cloud or the Kuiper belt. Secondly, the OPRs might re-equilibrated to the surface temperatures of nuclei during sublimation of molecules. Finally, the OPRs might be changed by proton transfer chemical reactions in the inner coma (the nuclear spin temperature reflects the kinetic temperature of the inner coma gas in this case). Here, we check the possibility of these processes based on the present data for water and ammonia molecules (we do not consider methane here).

The nuclear spin temperatures of water and ammonia are about 30 K (except for Comet Wilson as described above) although the orbital periods of the comets vary from only 6 years to several tens of thousands years. Because it is unlikely that the interior temperatures of comet nuclei are the same for all comets, the OPRs didn't equilibrate to their interior temperatures (as pointed out earlier with respect to the OPRs of water by Irvine et al. 2000).

Regarding the second scenario, the observed nuclear spin temperatures of comets are nearly the same and not correlated to the heliocentric distances during their observation. This means that the OPRs did not re-equilibrate to the surface temperatures of the nuclei (the surface temperature depends strongly on the heliocentric distance).

Finally, the possibility of changing the OPR values by the proton transfer reactions in the inner coma is considered. Although the reaction rates of such proton transfer reactions are proportional to the gas density in the inner coma (namely, proportional to gas production rates), there is no correlation between the nuclear spin temperatures and the water production rates during the observations of OPRs. Moreover, the OPRs of ammonia in the inner coma are nearly constant with respect to the nucleocentric distances based on the NH_2 observations. These facts indicate that the OPRs were not altered by chemical reactions. The calculation of inner coma chemistry by Rodgers & Charnley (2002) also supports this conclusion.

Thus, the OPRs of cometary water and ammonia are considered to be fixed in thermal equilibrium, and to be unaltered after the cometary nuclei formed in the solar nebula. Since the nuclear spin temperature must be considered as the physical temperature where the molecules formed or condensed on the cold grain, the OPRs of water and ammonia show that the cometary materials formed or condensed at the temperature of 25 — 35 K in the solar nebula or in the pre-solar molecular cloud. Correlation between the nuclear spin temperature and the molecular abundances should be discussed in future work.

This work is financially supported by the Ministry of Education, Culture, Sport, Science, and Technology of Japan under Grant No. 15740127 (H. Kawakita) and No. 15654078 (J. Watanabe).

References

Crovisier, J. 2000, in *Proc. of IAU Symp. 197*, Minh, Y. C. & van Dishoeck, E. F., Eds., 461

Dello Russo, N., DiSanti, M. A., Magee-Sauer, K., Gibb, E., & Mumma, M. J. 2002, BAAS, 34, 854

Gibb, E. L., Mumma, M. J., Dello Russo, N., Disanti, M. A., & Magee-Sauer, K. 2003, Icarus 165, 391

Irvine, W. M., Schloerb, F. P., Crovisier, J., Fegley,Jr., B., & Mumma, M. J., 2000, in *Protostars and Planets IV*, Mannings, V., Boss, A. P., & Russell, S. S., Eds. (Univ. Arizona Press, Tucson, 2000), 1159

Kawakita, H., et al. 2001, Science, 294, 1089

Kawakita, H., Watanabe, J., Furusho, R., Fuse, T., Capria, M. T., De Sanctis, M. C., & Cremonese, G. 2004, ApJ, in press

Mumma, M. J., Weaver, H. A., & Larson, H. P. 1987, A&A, 187, 419

Mumma, M. J., Weissman, P. R., & Stern, S. A. 1993, in *Protostars and Planets III*, Levy, E. H. & Lunine, J. I., Eds. (Univ. Arizona Press, Tucson, 1993), 1177

Rodgers, S. D., & Charnley, S. B. 2002, MNRAS, 330, 660

Weaver, H. A., Brooke, T. Y., Disanti, M. A., Mumma, M. J., Tokunaga, A., Chin, G., A'Hearn, M. F., Owen, T. C., & Lisse, C. M. 1997, BAASociety, 29, 1041

Highlights of Astronomy, Vol. 13
International Astronomical Union, 2003
O. Engvold, ed.

Material Processing of Interstellar Dust in Comets

Hiroshi Kimura & Ingrid Mann

Institut für Planetologie, Westfälische Wilhelms-Universität, Wilhelm-Klemm-Straße 10, D-48149, Münster, Germany

Abstract. To better understand the processing of pristine materials in comets, we compare the composition of cometary and interstellar dust. We suggest that the deficit of N in comet dust bears evidence for the processing of the organic refractory mantle of pre-solar interstellar dust, unless it arises from the protosolar disk chemistry. The amorphous silicate core, in contrast, seems to be protected against processing due to the presence of the organic refractory mantle.

1. Introduction

The processing of pre-solar interstellar materials incorporated into comet nuclei is a key parameter for understanding the formation and evolution of comets. Here we compare the element composition of cometary and interstellar dust to seek evidence for material processing.

2. Composition of Pristine Materials

Cometary dust: The elemental composition of dust from comet Halley was measured in situ aboard VeGa-1, VeGa-2, and Giotto (Kissel et al. 1986a, 1986b). Kissel & Krueger (1987) claimed that the data are better interpreted by the predominance of silicate-core, organic-mantle grains, similar to the pre-solar interstellar dust model (see Greenberg 1998). Jessberger, Christoforidis, & Kissel (1988) found that comet dust is a mixture of refractory organics, called CHON, and Mg-rich silicates, deriving the elemental abundances of Halley's dust from the most reliable data (see Fig. 1a). Laboratory analysis of interplanetary dust particles (IDPs), collected in the stratosphere, would provide detailed composition of comet dust. Cluster IDPs are likely of cometary origin because of their pristine nature inferred from enhanced D/H ratios (Messenger 2000). These cometary IDPs contain sub-micron glass with embedded metal and sulfides (GEMS) within a matrix of amorphous carbonaceous material (Bradley 1994). GEMS may be pre-solar interstellar silicates preserved in comets and the amorphous carbonaceous material seems to be transformed from pre-solar interstellar organics that carry the high D/H ratio (Keller, Messenger, & Bradley 2000). The bulk compositions of 3 GEMS measured by Bradley (1994) and 5 GEMS by Bradley & Ireland (1996) are averaged to determine the elemental abundances of GEMS (see Fig. 1b).

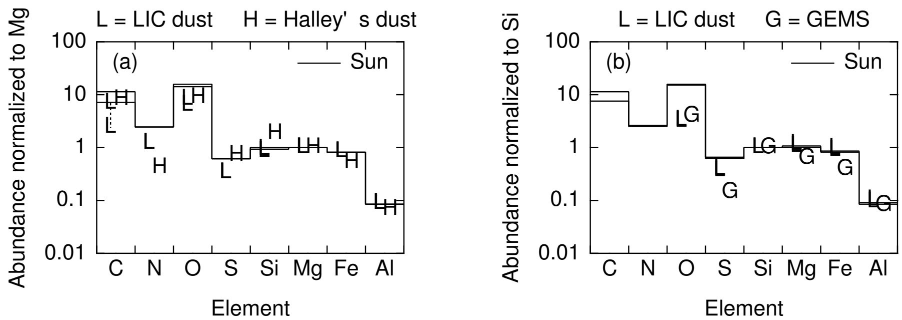

Figure 1. Elemental abundances of solar photosphere, (a) dust in the Local Interstellar Cloud (LIC) and dust in Comet Halley, normalized to Mg, and (b) silicate component in the LIC dust and glass with embedded metal and sulfides (GEMS) in interplanetary dust particles, normalized to Si.

Interstellar dust: We assume that siliceous and carbonaceous materials in present-day interstellar dust provide a reference composition of pre-solar interstellar dust. The solar system currently lies inside the Local Interstellar Cloud (LIC) filled mainly with warm partially ionized hydrogen atoms (Linsky et al. 1993; Lallement et al. 1995). Measurements of UV absorption lines through the LIC by Hubble Space Telescope gives the elemental abundances of LIC gas (Kimura, Mann, & Jessberger 2003b). The elemental abundances of LIC dust are derived from comparison between the gas-phase abundances and the solar photospheric abundances (Kimura, Mann, & Jessberger 2003c). The similarity in the compositions between LIC and Halley's dust justifies our assumption mentioned above (see Fig. 1a). This similarity also allows us to stoichiometrically assign the elements to $MgAl_2O_4$, FeNi, Mg_2SiO_4, $MgSiO_3$, FeS, and CHON, based on our best knowledge of possible major compositions for comet dust. Further information on the composition of LIC dust comes from analysis of impact data measured in situ by Ulysses (Mann & Kimura 2000, 2001). The data on the velocity and mass of LIC dust places constraints on acting forces that depend on the dust composition (Mann 1996; Landgraf et al. 1999). Solar radiation pressure on LIC dust estimated from the data suggest that the LIC contains aggregate particles consisting of silicate-core, organic-mantle, and submicron grains (Kimura et al. 2003c).

3. Results and Discussion

Organic refractory mantle: Figure 1a shows that comet dust contains only 1/3 of N compared to interstellar dust despite the similarity in the overall composition. The N depletion in comet dust might be related to gas-grain chemistry in the comet-forming regions of the solar nebula (Charnley & Rodgers 2002). Alternately, it may indicate the processing that transformed organic refractory into amorphous carbonaceous material, the amount of which depends on the degree of processing. In fact, light scattering properties of comet dust are well explained if 2/3 of carbonaceous materials is in the form of amorphous carbon and 1/3 in the form of organic refractory (Kimura, Kolokolova, & Mann 2003a).

This supports the idea that the organic refractory mantles of comet dust are partially processed into amorphous carbon, but this issue requires further studies.

Amorphous silicate core: Figure 1b shows the similarity in the composition between GEMS and the silicate component of interstellar dust except for S, which is more than a factor of two depleted in GEMS. The S abundance in the silicate component of interstellar dust would be lowered if the majority of S is contained in the organic refractory. However, the correlation of S and Fe in dust from Comet Halley and the similarity of the S abundances in Halley's and LIC dust do not support this idea (see Jessberger et al. 1988). The S depletion in GEMS may be better explained by the partial loss of S due to atmospheric-entry heating (Greshake et al. 1998). If this is the case, there is no evidence for processing of the amorphous silicate core of pre-solar interstellar dust after its incorporation in comets. This possibly indicates that the core has been protected from alteration by its organic refractory mantle.

Acknowledgments. We would like to thank Elmar K. Jessberger and Iris Weber for useful discussions. This research is supported by the German Aerospace Center *DLR* (Deutschen Zentrum für Luft- und Raumfahrt) under the projects "Kosmischer Staub: Der Kreislauf interstellarer und interplanetarer Materie" (RD-RX-50 OO 0101-ZA) and "Mikro-Impakte" (RD-RX-50 OO 0203).

References

Bradley, J. P. 1994, Science, 265, 925

Bradley, J., & Ireland, T. 1996, in ASP Conf. Ser. Vol. 104, Physics, Chemistry, and Dynamics of Interplanetary Dust, ed. B. Å. S. Gustafson & M. S. Hanner (San Francisco: ASP), 275

Charnley, S. B., & Rodgers, S. D. 2002, ApJ, 569, L133

Greenberg, J. M. 1998, A&A, 330, 375

Greshake, A., Klöck, W., Arndt, P., Maetz, M., Flynn, G. J., Bajt, S., & Bischoff, A. 1998, Meteorit. Planet. Sci., 33, 267

Jessberger, E. K., Christoforidis, A., & Kissel, J. 1988, Nature, 332, 691

Keller, L. P., Messenger, S., & Bradley, J. P. 2000, J. Geophys. Res., 105, 10397

Kimura, H., Kolokolova, L., & Mann, I. 2003a, A&A, 407, L5

Kimura, H., Mann, I., & Jessberger, E. K. 2003b, ApJ, 582, 846

— 2003c, ApJ, 583, 314

Kissel, J., & Krueger, F. R. 1987, Nature, 326, 755

Kissel, J., et al. 1986a, Nature, 321, 280

— 1986b, Nature, 321, 336

Lallement, R., Ferlet, R., Lagrange, A. M., Lemoine, M., & Vidal- Madjar, A. 1995, A&A, 304, 461

Landgraf, M., Augustsson, K., Grün, E., & Gustafson, B. Å. S. 1999, Sci., 286, 2319

Linsky, J. L., et al. 1993, ApJ, 402, 694

Mann, I. 1996, Space Sci.Rev., 78, 259

Mann, I., & Kimura, H. 2000, J. Geophys. Res., 105, 10317

— 2001, Space Sci.Rev., 97, 389

Messenger, S. 2000, Nature, 404, 968

Highlights of Astronomy, Vol. 13
International Astronomical Union, 2003
O. Engvold, ed.

From Interstellar Matter To Comets: A Laboratory View

Pascale Ehrenfreund & Oliver Botta

Leiden Observatory, P O Box 9513, 2300 RA Leiden, The Netherlands.

Abstract. Comets, formed in the cold outer parts of the solar system, provide a record of pristine material from the parent interstellar cloud. The investigation of outgassing curves from bright comets has provided a relationship to the abundances of interstellar ices and gas phase molecules. However, being porous and stratified in various layers of different densities and temperatures, the outgassing characteristics of comets can not always be directly reconciled with the interstellar composition. This is due to the structure of the nuclear ice component, which contains different coexisting ice phases, clathrates, and trapped gases. Ices, silicates and carbonaceous compounds - studied through astronomical observations and by laboratory simulations - serve as reference material to obtain information on cometary bulk material. A major fraction of cosmic carbon in the interstellar medium, comets and meteorites seems to be incorporated into complex aromatic networks, which are difficult to observe and to identify spectroscopically. However, recent measurements of the macromolecular structure and soluble organic species in carbonaceous meteorites provide a powerful tool to investigate the link of small bodies in the solar system.

1. Introduction

Cometary nuclei are formed in outer solar system environments and are porous aggregates of ice and refractory material. In 1986 several spacecraft performed a close fly-by of Comet Halley in order to perform in situ measurements that revealed the structure and composition of this comet. Since then observations of volatiles in the cometary coma over large parts of the electromagnetic spectrum are a crucial tool to obtain indirect information on the composition of cometary nuclei. Revealing the composition of comets provides clues to the formation of our solar system (e.g. Irvine et al. 2000).

2. Laboratory simulations

Ices, silicates and carbonaceous material - the major building blocks of the cometary nucleus - can be studied through astronomical observations and by laboratory simulations. Simulating interstellar dust and ice in the laboratory - the precursor material of comets - allows us to gain insights into the physical and chemical properties of cometary bulk material. Interstellar dust consists of micron-sized carbon or silicon grains which accrete ice layers in dense interstellar clouds, where the temperature is generally as low as 10K. In such cold environments atoms and molecules efficiently adsorb from the gas phase on dust surfaces. Small molecules and atoms can diffuse along the grain surface or within the ice, as do larger molecules when the temperature on the surface increases. Reactions will occur when two atoms, molecules, ions or radicals collide. In the absence of energy barriers this leads to the formation of new and usually more complex compounds. Thermal and energetic processing enhances the rate of reactions within the ice layers covering dust particles. At increased temperature, sublimation of newly formed species from the grain surface leads to further chemical evolution in the gas phase.

Table 1. Average interstellar ice abundances measured toward high-mass, low-mass protostars and in cometary comae. In contrast to cometary observations, there is no evidence for the presence of C_2H_6, C_2H_2, HCN nor S-bearing species (apart from tiny abundances of OCS) in interstellar ices. H_2CO and HCOOH have still to await a more firm detection.

Ice species	high-mass protostars	low-mass protostars	comets
H_2O	100	100	100
CO	1-20	1-60	5-20
CO_2	20	15-40	2-10
CH_4	1-4	-	0.2-1.2
CH_3OH	1-35	1-25	0.3-2
H_2CO	3	-	0.2-1
OCS	0.05-0.18	<0.08	0.5
NH_3	<5	-	0.6-1.8
C_2H_6	<0.4	-	0.4-1.2
HCOOH	3	-	0.05
O_2	<20	-	0.5 ul

Laboratory simulations of low temperature ices are achieved by condensing ices as pure gas or gas mixtures in a high-vacuum chamber on the surface of a cooled (10K) substrate. Most of the abundant ice species do have specific molecular vibrational transitions with energies corresponding to absorptions between 2.5 and 25 μm and can therefore be studied by infrared spectroscopy in transmission or reflection. Thermal processing by step-wise warming of the substrate and UV irradiation, using microwave-excited hydrogen flow lamps, allow the simulation of some of the environmental conditions prevailing in interstellar clouds. Such laboratory studies strongly increased our understanding of extraterrestrial ice chemistry (Ehrenfreund et al. 2003). Also experiments on surface diffusion, reaction and desorption behavior of icy species contributed to this success. Currently 36 ice absorption features attributed to 16 different molecules have been identified, leading to a detection rate of $\sim$ 1 infrared band per year. The ISO satellite strongly increased our knowledge on interstellar icy species, but also high resolution studies in telluric windows using large ground-based telescopes show exciting results (Pontoppidan et al. 2003). Table 1 shows a current overview of abundances measured for interstellar ices and for cometary volatiles. Carbonaceous chondrites are the most pristine types of meteorites and therefore provide a record of the physical and chemical conditions in the early solar system. These meteorites contain up to 5 weight % organic carbon, most of which is locked in insoluble kerogen-like material. Distinct organic compounds that have been identified in carbonaceous chondrites range from simple soluble species such as amino acids to polycyclic aromatic hydrocarbons (PAHs) and fullerenes (for a recent review see Botta & Bada 2002). The composition of soluble species, e.g. amino acids provide a powerful tool to investigate the link of small bodies in the solar system (Botta et al. 2002). The macromolecular material in these meteorites has recently been characterized (Sephton et al. 2000, Gardinier et al. 2000). However, its link to the interstellar aromatic network is yet to be understood. The organic inventories of carbonaceous meteorites display large and variable enrichments in deuterium, ^{13}C and ^{15}N which is indicative of their retention of an interstellar heritage.

3. Conclusion

The observations of low-mass stars, using ground and spaced-based telescopes and a broader consensus on cometary diversity will provide a better view on the interstellar-cometary connection in the future. Theoretical models indicate that bulk material in cometary nuclei contains coexisting ice phases, possibly clathrates and trapped gases. Furthermore the bulk material is stratified in density and porosity. Laboratory experiments identified different phase transitions within amorphous water ice which during cometary evolution will strongly influence the trapping and outgassing of volatiles. Therefore it remains questionable if the outgassing pattern of comets should essentially mimic the interstellar ice composition and if processing of interstellar matter within the solar nebula can ever be traced as such. The large fraction of solid aromatic networks assumed in the interstellar medium and measured in meteoritic material has to be present in comets. In order to understand the processes which led to the formation of our solar system and comets a comet rendezvous or comet sample return mission is mandatory.

References

Botta, O., Bada, J. L. 2002, Survey in Geophysics, 23, 411

Botta, O. et al. 2002, OLEB 32, 697

Ehrenfreund, P. et al. 2003, Planet. Space Sci. 41, 473

Gardinier, A. et al. 2000, Earth Planet. Sci. Lett., 184, 9

Irvine, W. M. et al. 2000 In PPIV (Mannings, V., Boss, A., Russell, S. Eds.) 1159-1200. University of Arizona Press, Tucson.

Pontoppidan, K.M. et al. 2003 A&A, 408, 981

Sephton, M. et al 2000 Geochim. Cosmochim. Acta 64, 321

Highlights of Astronomy, Vol. 13
International Astronomical Union, 2003
O. Engvold, ed.

Implications of Ice Morphology for Comet Formation

M. P. Collings, J. W. Dever, M. R. S. McCoustra

School of Chemistry, University of Nottingham, University Park, Nottingham, U.K., NG7 2RD.

H. J. Fraser

Raymond and Beverly Sackler Laboratory of Astrophysics, Leiden Observatory, University of Leiden, Niels Bohr Weg 2, 2300 RA, Leiden, Netherlands.

Abstract. Laboratory surface science under ultra-high vacuum (UHV) conditions allows us to simulate the growth of ices in astrophysical environments. Using the techniques of temperature programmed desorption (TPD), reflection-absorption infrared spectroscopy (RAIRS) and micro-balance methods, we have studied binary ice systems consisting of water (H_2O) and variety of other species including carbon monoxide (CO), at astrophysically relevant conditions of temperature and pressure. We present results that demonstrate that the morphology of water ice has an important influence on the behavior of such systems, by allowing processes such as diffusion and trapping that can not be understood through a knowledge of the binding energies of the species alone. Through an understanding of the implications of water ice morphology on the behavior of ice mixtures in the interstellar environment, additional constraints can be placed on the thermodynamic conditions and ice compositions during comet formation.

A commonly applied description of the structure of the ice mantles accreted on interstellar dust grains is the 'onion layered' model (Allamandola et al 1999, Ehrenfreund et al 1998). In this model, the dust grain is surrounded by an inner layer of hydrogenated (polar) ice, which in turn is coated with an outer layer of non-hydrogenated (apolar) ice. Since the composition of each layer is dominated, respectively, by water (H_2O) and carbon monoxide (CO), our laboratory representation of this model is a film of H_2O upon which a film of CO is subsequently deposited.

We have demonstrated previously that the desorption characteristics of CO are strongly dependent on the morphology of the underlying water film (Collings et al 2003a, b). As the water ice undergoes an irreversible phase change from a high density to a lower density amorphous structure during thermal processing, CO molecules become trapped within pores as pathways to the surface are sealed off. Such CO entrapment can occur even when the CO is initially in a separate layer, since the molecules in the solid CO film become mobile and diffuse into the porous water film at less than 15 K, well below the temperature at which the sublimation of solid CO becomes significant. Trapped CO is released as the water film crystallizes and again as the water desorbs.

Using a stochiastic integration software package, we have developed a kinetic simulation incorporating the phase changes of the water ice and diffusion of CO to accurately reproduce the complex desorption traces of the CO/H_2O system in laboratory experiments (Collings et al 2003b). The simulation can then be adapted to suit astrophysical time scales, and hence provide a prediction of the desorption behavior of ice mantles during the formation of the pre-solar nebula. Current models of desorption in the pre-solar nebula tend to treat the non-hydrogenated layer in isolation, allowing it to sublime entirely at roughly 20 K. The results displayed in figure 1 predict that (at the film thickness simulated) some 15 to 25 % of the CO in the outer layer will become trapped in the low density amorphous ice. This portion of CO will be retained in any amorphous water ice that is subsequently incorporated in cometary material, and is available for chemical reaction in the warm ice.

The kinetic parameters for the desorption processes, determined through a combination of laboratory experiment and simulation, are also of great worth in the analysis of other significant scenarios, for example, condensation in the solar nebula. The condensation coefficient, α (fraction of incident molecules condensed), is given by

$$\alpha = S - R/Z_W,$$

where S is the sticking probability, R is the rate of desorption of the species, and Z_W is the rate at which gas phase molecules of the species impinge on the surface, which is a function of temperature and pressure. For CO impinging on a water ice surface at low temperature, it is reasonable to assume that the sticking probability is unity. Figure 2 shows a plot of the gas phase pressure against temperature at which α is zero, for a condensation of amorphous and crystalline water ice, solid CO, and 5 % CO in water ice, which have been calculated using desorption kinetics that we have measured by experimentation and simulation (Fraser et al 2001, Collings et al 2003b). These curves effectively mark the 'vapor pressure' for the process - condensation occurs above (and to the right) of the curve. These plots demonstrate that at realistic pressures, the condensation of CO can only occur at temperatures below about 40 K, below the temperatures typically quoted for comet formation.

In conclusion, the morphology of water ice, through the entrapment of volatile species such as CO within its porous structure, is a highly significant factor influencing the composition of interstellar ices incorporated into comets. An understanding of the kinetics of desorption processes provides a link between experiments performed under laboratory conditions and the behavior of ices in astrophysical environments.

Acknowledgments. This research was performed with the financial support of Particle Physics and Astronomy Research Council (PPARC) U.K., the Leverhulme Trust and the University of Nottingham. The authors gratefully acknowledge the advice of David A. Williams and Serena Viti. MPC thanks the Sir Eric Rideal Trust and the IAU Travel Bursaries for support in attending this meeting.

References

Allamandola, L. J., Bernstein, M. P., Sandford, S. A., & Walker, R. L. 1999, Space Sci.Rev., 90, 219

Collings, M. P., Dever, J. W., Fraser, H. J., McCoustra, M. R. S., & Williams, D. A. 2003a, ApJ, 583, 1058

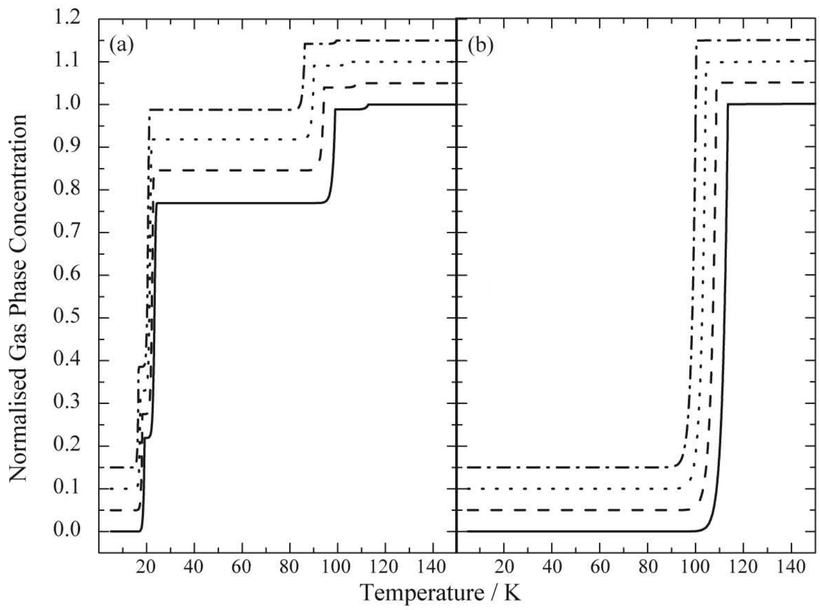

Figure 1. Normalized gas phase concentrations (offset for clarity) of (a) CO, and (b) H_2O, as a function of temperature as predicted by a kinetic simulation for heating rates of 1 K year^{-1} (solid), 1 K decade^{-1} (dashed), 1 K century^{-1} (dotted) and 1 K millenium $^{-1}$ (dot-dashed).

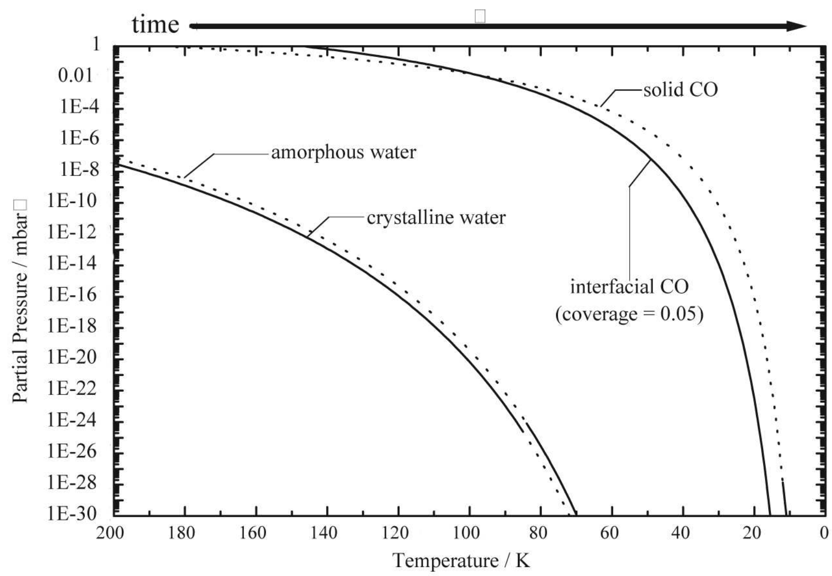

Figure 2. Plots of the pressure and temperature conditions for which condensation = desorption for amorphous and crystalline water ice, solid CO ice, and CO adsorbed with a coverage of 0.05 on water ice (gas phase temperature and dust temperature are assumed to be equal). Dotted curves show where certain species can not be formed; i.e., water ice is crystalline when condensed above ∼ 80 K and amorphous when condensed below 80 K; solid CO is mobile above ∼ 15 K and will diffuse into the porous water ice.

Collings, M. P., Dever, J. W., Fraser, H. J., & McCoustra, M. R. S. 2003b, A&SS, 285, 1

Ehrenfreund, P., Dartois, E., Demyk, K, & d'Hendecourt, L. 1998, A&A, 339, L19

Fraser, H. J., Collings, M. P., McCoustra, M. R. S., & Williams, D. A. 2001, MNRAS, 327, 1165

Highlights of Astronomy, Vol. 13
International Astronomical Union, 2003
O. Engvold, ed.

Cometary Silicates: Interstellar and Nebular Materials

Diane H. Wooden

NASA Ames Research Center, MS 245-3, Moffett Field, CA 94035-1000, USA

Abstract. Evidence for interstellar material in comets is deduced from IR spectra, in situ measurements of Comet Halley, and chondritic porous interplanetary dust particles (CP IDPs). IR spectra of comets reveal the spectrally active minerals: amorphous carbon, amorphous silicates, and (in some comets) crystalline silicates. Evidence suggests amorphous silicates are of interstellar origin while crystalline silicates are of nebular origin.

10 μm spectra of comets and sub-micron amorphous silicate spherules in CP IDPs have shapes similar to absorption spectra through lines-of-sight in the ISM. Thermal emission models of cometary IR spectra require Fe-bearing amorphous silicates. Fe-bearing amorphous silicates may be Fe-bearing crystalline silicates formed in AGB outflows that are amorphized through He^+ ion bombardment in supernova shocks in the ISM.

Crystalline silicates in comets, as revealed by IR spectra, and their apparent absence in the ISM, argues for their nebular origin. The high temperatures (>1000 K) at which crystals form or are annealed occur in the inner nebula or in nebular shocks in the 5 – 10 AU region. Oxygen isotope studies of CP IDPs show only 1% by mass of the silicate crystals are of AGB origin. Together this suggests crystalline silicates in comets are probably primitive grains from the early solar nebula.

1. Introduction

Comets are frozen reservoirs of early solar nebula materials. During their perihelion passages, comets release volatile gases and dust particles into their comae. Cometary silicate mineralogy is deduced from IR spectra, in situ flyby mass spectrometry, and laboratory studies of cometary interplanetary dust particles. Analysis of cometary silicates suggests amorphous silicates are interstellar and crystalline silicates are formed or processed in the solar nebula (Wooden 2002).

2. Silicate Mineralogy of Comets from IR Spectroscopy

Long period and a few short period comets have broad silicate emission features. Some long period comets have crystalline silicate peaks: 11.2-11.4 μm from Mg-rich crystalline olivine, and (in Comet Hale-Bopp) 9.2 μm from Mg-rich crystalline ortho-pyroxene (Harker et al. 2002). Utilizing discrete mineral grains, thermal emission models of Comet Hale-Bopp show one-third of the sub-micron silicates are crystalline (Harker et al. 2002).

3. Interstellar Fe-bearing Amorphous Silicates

The 10 μm absorption features seen along lines-of-sight through the interstellar medium are broad and attributed to amorphous silicates. In particular, Fe-bearing amorphous olivine fits the interstellar extinction curve (Li & Draine 2002). Fe-bearing amorphous olivine and pyroxene fit the absorption feature in the line-of-sight to the Galactic Center (Kemper, Vriend, & Tielens 2003).

Aggregates of Fe-bearing amorphous silicates, Mg-rich silicate crystals, and carbonaceous materials constitute chondritic porous interplanetary dust particles (CP IDPs) of probable cometary origin (Fig. 1a) (Bradley et al. 1999b). The amorphous silicates in CP IDPs are 0.1 – 0.25 μm silicate spherules with embedded nanophase Fe and FeS and are called GEMS (Glass with Embedded Metal and Sulfides) (Bradley et al. 1999a). Properties of GEMS have been attributed to ion bombardment in the interstellar medium (Bradley 1994). Laboratory experiments show He^+ ion bombardment of crystalline olivine destroys the crystalline structure and reduces the FeO bonds in the mineral to Fe, transforming the Fe-bearing crystal into a highly porous, Mg-rich amorphous silicate with embedded nanophase Fe (Carrez et al. 2002). Absorption spectra of GEMS match the interstellar feature (Bradley et al. 1999a). Fe-bearing amorphous silicates in comets are probably from the interstellar medium.

4. Nebular Mg-rich Crystalline Silicates

In the interstellar medium, the fraction of crystalline silicates is very low (<5% Li & Draine 2002; <0.5% Kemper et al. 2003), and is insufficient to account for the fraction deduced for comets. Mg-rich crystals (such as in Fig. 1c) may condense from nebular gases at ∼1400 K (Grossman 1972). Alternatively, Mg-rich crystals may be Mg-rich amorphous silicates annealed into crystals (∼900–1200 K). Crystals annealed in the hot inner regions of the young (<30,000 yr) solar nebula may be subsequently spread throughout the disk through turbulent dissipation (Bockelée-Morvan et al. 2002). Alternately, annealing may occur in nebular shocks in the 5 – 10 AU region (Harker & Desch 2002). Laboratory experiments show Mg-rich amorphous olivine silicate smokes anneal into forsterite crystals (Fig. 1b) within a matrix of polycrystalline forsterite, crystalline and amorphous silica, and MgO (Fabian et al. 2000). Submicron sized particles with morphologies shown in Fig. 1b, c produce resonances of Mg-rich crystalline olivine.

5. Challenges

• Oxygen isotopic nanoSIMS measurements of 1031 subgrains of 9 CP IDPs show that six grains (<1% by mass) have a very large anomalies and are stardust. One of the six pre-solar grains is a forsterite crystal, and two are GEMS (Messenger et al. 2003). If GEMS are interstellar, then why do most not show extreme anomalies? Future higher accuracy measurements of subgrains with modest anomalies will contribute to our understanding of the reservoir of materials that contributed to the solar system.
• Mg-rich crystals are annealed from Mg-rich amorphous silicates; annealing does not change the stoichiometry. However, amorphous silicates appear to have Fe. What is the source of Mg-rich amorphous silicates?
• CP IDPs contain discrete Mg-rich crystals (Fig. 1a; Bradley et al. 1999b) which do not appear morphologically similar to annealing products (Fig. 1b).

Acknowledgments. DHW thanks Drs. Don Brownlee and John Bradley.

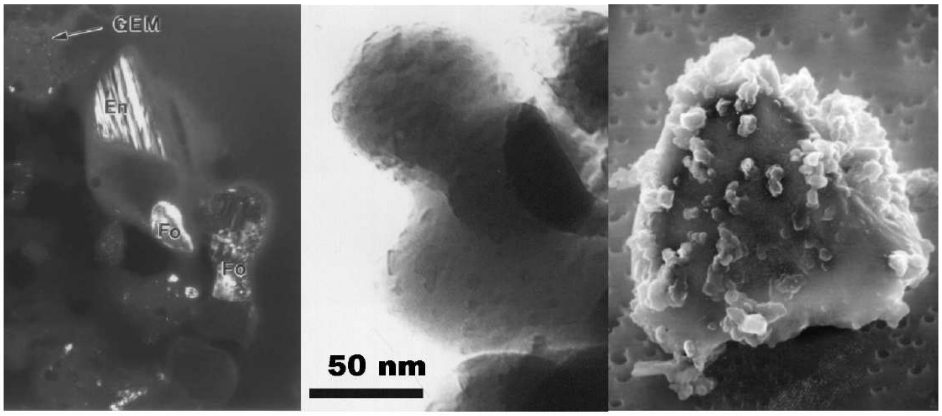

Figure 1. a. (Left) SEM view ($\sim$0.5 μm wide) of a cometary CP IDP showing GEMS and Mg-rich silicate crystals (Fo and En). b. (Middle) Amorphous pure-Mg olivine smoke annealed at 1206 K for 1 hr contains Forsterite crystals within an amorphous and polycrystalline matrix. c. (Right) 10 μm Forsterite crystal IDP with GEMS attached. (Refs.: a, c: Fig. 4, 11, Bradley et al. 1999b; b: Fig. 11, Fabian et al. 2000.)

References

Bockelée-Morvan, D., Gautier, D., Hersant, F., Huré, J.-M., Robert, F. 2002, A&A, 384, 1107

Bradley, J. P. 1988, Geochim. Cosmochim. Acta, 52, 889

Bradley, J. P. 1994, Science, 265, 925

Bradley, J. P., Keller, L. P., Gezo, J., Snow, T., Flynn, G. J., Brownlee, D. E., & Bowey, J. 1999a, Lunar Planet. Sci., 30, Abs. No. 1835 The 10 and 18 Micrometer Silicate Features of GEMS: Comparison with Astronomical Silicates

Bradley, J. P., Keller, L. P., Snow, T. P., et al., Hanner, M. S., Flynn, G. J.,Gezo, J. C., Clemett, S. J., Brownlee, D. E., & Bowey, J. E. 1999a, Science, 285, 1716 An infrared spectral match between GEMS and interstellar grains

Bradley, J. P., Snow, T. P., Brownlee, D. E., & Hanner, M. S. 1999b in Solid Interstellar Matter: The ISO Revolution, Les Houches Workshop, ed. L. d'Hendecourt, C. Joblin, & A. Jones (EDP Sciences and Springer-Verlag), 297

Carrez, P., Demyk, K., Cordier, P., Gengembre, L., Grimblot, J., d'Hendecourt, L., Jones, A. P., & Lerouz, H. 2002, Meteorit. Planet Sci., 37, 1599

Fabian, D., Jäger, C., Henning, Th., Dorschner, J., & Mutschke, H. 2000, A&A, 364, 282

Grossman, L. 1972, Geochim. Cosmochim. Acta, 38, 47

Harker, D. E., & Desch, S. 2002, ApJ, 565, L109

Harker, D. E., Wooden, D. H., Woodward, C. E., & Lisse, C. M. 2002, ApJ, 580, 579

Kemper, F., Vriend, W. J., & Tielens, A. G. G. M. 2003, ApJ, in preparation.

Li, A., & Greenberg, J. M. 1997, A&A, 323, 566

Li, A., & Draine, B. T. 2002, ApJ, 564, 803

Wooden, D. H. 2002, Earth Moon Planets, 89, 247

Highlights of Astronomy, Vol. 13
International Astronomical Union, 2003
O. Engvold, ed.

Light Scattering as a Clue to Cometary Dust Structure

A. Chantal Levasseur-Regourd, E. Hadamcik & J. Lasue

Univ. Paris6 / Aéronomie CNRS-IPSL, BP 3, 91371 Verrières, France

Abstract. The linear polarization of comets depends upon the cometary dust physical properties, as well as upon the phase angle and the wavelength. The observed similarities and discrepancies provide drastic constraints on the physical properties of the dust. A series of measurements of light scattering properties on clouds of particles and of the aggregates they form under microgravity conditions should allow the interpretation of the observations in terms of physical properties of the dust.

1. Introduction

Images of IPDs collected in the Earth's stratosphere suggest that cometary dust particles are built up of aggregates of submicron-sized grains (Jessberger et al. 2001). Analysis of simultaneous local light scattering and impact data during 1P/Halley flyby indicates that the dust density was very low, possibly of about 100 $kg\ m^{-3}$ (Fulle et al. 2000). However, the actual physical properties of cometary dust particles and their changes within different cometary comae regions are unknown. Estimating them would provide constraints on their formation processes, and suggest strategies for future missions to comets.

Remote observations of the light emitted and scattered by the dust are available for numerous comets, leading to information on the temperature and composition of the dust, as well as on its light scattering properties. The latter observations provide clues to the physical properties of the dust particles.

2. Properties of light scattered by cometary dust

Solar light scattered by low concentration dust comae is partially linearly polarized. The polarization neither depends upon the Sun and Earth distances, nor upon the concentration, but only varies with the phase angle α, the wavelength λ, and the dust physical properties. High resolution polarization images actually reveal halos corresponding to a lower polarization around the nucleus and jet-like structures with a polarization higher than the average (Levasseur-Regourd 1999, Hadamcik and Levasseur-Regourd 2003). Polarization data also allow us to compare data obtained on a comet at different times and on different comets.

The phase angle dependence corresponds to smooth $P_\lambda(\alpha)$ phase curves, with a small negative branch below about 20° and a wide positive branch with a near 90° to 100° maximum. Classes of comets are pointed out by these phase curves. Comets with a low maximum (of about 10% to 15%, depending upon the wavelength), comets with a high maximum (of about 25% to 30%), and comet 1995 O1 Hale-Bopp, the polarization of which was the highest (Levasseur-Regourd 1999). Comets with a high maximum in polarization usually present a significant silicate emission feature that could be induced by submicron-sized grains in low-density aggregates (Levasseur-Regourd et al. 1996, Hanner 2003).

The $P_\alpha(\lambda)$ curves are linear, at least in the visible domain and for phase angles in the 20° to 90° range. The rate of increase of the wavelength dependence varies with the object, and is actually higher for Hale-Bopp than for Halley. The polarization slope always increases with increasing wavelength, although an opposite effect may take place in the inner coma of bright comets, as illustrated by data recently retrieved from the OPE experiment on board Giotto (Fig. 1).

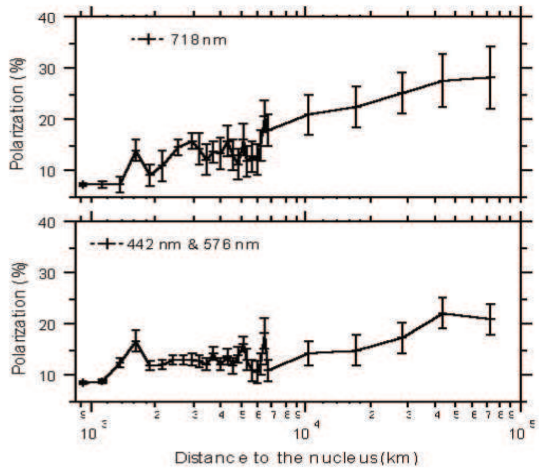

Figure 1. Variation of P ($\alpha = 73°$) with distance to Halley nucleus along Giotto trajectory. Above 7000 km, P is higher in red than in blue, while the effect is opposite in the innermost coma (with good S/N ratio).

3. Laboratory simulations under microgravity conditions

Drastic constraints on the properties of the dust are provided by the phase and wavelength dependences (Levasseur-Regourd and Hadamcik 2003). They need to be interpreted through numerical and/or experimental simulations. A series of experimental simulations under microgravity conditions (on board aircraft, rockets or spacecraft) is being developed. Such experiments avoid sedimentation of the dust and may allow (with sufficient microgravity duration) the formation of realistic particles through aggregation/fragmentation and condensation/evaporation processes (Levasseur-Regourd et al. 1998, Ehrenfreund et al. 2003).

The PROGRA^2 experiment provides polarization measurements on illuminated levitating dust samples at different phase angles, in the laboratory as well as during parabolic flights (Worms et al. 1999). The already available data base indicates, amongst other results, that cometary dust properties are reproduced by low-density aggregates of submicron-sized grains (Hadamcik et al. 2002). The

CODAG-SRE experiment provides a monitoring of the brightness and polarization phase curves of levitating dust samples (Levasseur-Regourd et al. 1999). The ESA MASER-8 rocket flight allowed us to demonstrate the feasibility of such measurements while ballistic aggregation processes were taking place.

The ICAPS (Interactions in Cosmic and Atmospheric Particles Systems) has been proposed for the initial Columbus utilization phase on board the ISS. It should, amongst other objectives, simulate aggregation processes and formation of regoliths during long microgravity flights, and translate the light scattering observations in physical properties of the dust. It is now in phase B at ESA and a precursor rocket experiment (so-called ICAPS-SRE) will take place in 2004-2005. This MASER-10 experiment will be used to test critical ICAPS subsystems, with a Light Scattering Unit performing measurements over a large number of phase angles (including the near backscattering region) and three wavelengths. It will monitor the formation of bi-disperse aggregates of micron-sized grains of high and low albedos.

In conclusion, comets observations suggest the existence of very fluffy dust aggregates. Differences have been observed in the dust light scattering properties, e.g. structure of the comae, polarization phase curves maxima and minima, polarization colors. The series of experimental simulations should provide, in the coming years, a unique approach to derive the physical properties of the dust particles from their light scattering properties.

Supports of Programme National de Planétologie for the observations, and of CNES and ESA for the laboratory simulations, are acknowledged.

References

Ehrenfreund, P., Fraser, H. J., Blum, J., et al. 2003, PSS, 51, 473

Fulle, M., Levasseur-Regourd, A. C., McBride, N., & Hadamcik, E. 2000, AJ, 119, 1968

Hadamcik, E., Renard, J. B., Worms, J. C., Levasseur-Regourd, A. C., & Masson, M. 2002, Icarus 155, 497

Hadamcik, E., & Levasseur-Regourd, A. C. 2003, JQSRT, 79-80, 661

Hanner, M. S. 2003, JQSRT, 79-80, 903

Jessberger, E. K., Stephan, T., Rost, et al. 2001, in Interplanetary Dust, ed. E. Grün et al. (Berlin: Springer), 253

Levasseur-Regourd, A. C. 1999, Space Sci.Rev., 90, 163

Levasseur-Regourd, A. C., Hadamcik, E., & Renard, J. B. 1996, A&A, 313, 327

Levasseur-Regourd, A. C., Cabane, M., Haudebourg, V., & Worms, J. C. 1998, Earth Moon Planets, 80, 343

Levasseur-Regourd, A. C., Cabane, M., Chassefière, E., Haudebourg, V., & Worms, J. C. 1999, ASR, 23, 1271

Levasseur-Regourd, A. C., & Hadamcik, E. 2003, JQSRT, 79, 903

Worms J. C., Renard, J. B., Hadamcik, E., Levasseur-Regourd, A. C., & Gayet, J. F. 1999, Icarus, 142, 281

Highlights of Astronomy, Vol. 13
International Astronomical Union, 2003
O. Engvold, ed.

The Nature of Diatomic Sulfur in Comets

D. C. Boice

Southwest Research Institute, 6220 Culebra Road, San Antonio, Texas 78238-5166, USA

Céline Reylé

Observatoire de Besancon, BP 1615, 25010 Besancon, France

Diatomic sulfur was first discovered in comets during the close approach to Earth of comet IRAS-Araki-Alcock (C/1983 H1). The spatial distribution of S_2 was restricted to within a few hundred kilometers of the nucleus, consistent with S_2 being a parent molecule. This molecule has been detected in comets Hyakutake (C/1996 B2), Lee (C/1999 H1), and recently in Ikeya-Zhang (C/2002 C1), leading to the conclusion that S2 is ubiquitous in comets.

The nature of the source of S_2 in comets is not known. It has been proposed that S_2 formed by irradiation of sulfur-bearing molecules in interstellar grain mantles, implying that the grains were never heated above about 30 K at any time before or after their inclusion in the nucleus. Alternative mechanisms to produce S_2 have been put forth including, solar wind sputtering of coma grains and via fast chemical reactions in the inner coma. We will explore these formation mechanisms within the context of a global comet model including coma chemistry and molecular fluorescence and discuss the relevance of S_2 to the total sulfur budget.

Support for this work was provided by the NSF Planetary Astronomy Program and the Université de Franche-Comté.

Highlights of Astronomy, Vol. 13
International Astronomical Union, 2003
O. Engvold, ed.

Solar Composition of Icy Planetesimals: A New Source For Comet Nuclei?

Tobias Owen

Institute for Astronomy, University of Hawaii, 2680 Woodlawn Drive, Honolulu, Hawaii 96822 USA

The enrichment of heavy elements on Jupiter appears to require the existence of a new class of icy planetesimal that exhibits solar relative abundances.

Prior to the Galileo probe mission, observations of methane in Jupiter's atmosphere had revealed that C/H was approximately three times the solar ratio. This enrichment was thought to be the result of the delivery of heavy elements by icy planetesimals, which were assumed to be essentially identical to comets. However, comets are notoriously deficient in nitrogen (e.g., Geiss 1987; Krankowsky 1991) and recent upper limits on argon in three comets (Weaver et al. 2002) indicate that this element is also sub-solar relative to O. Hence it was assumed that Jupiter would exhibit the same deficiency in argon and nitrogen relative to carbon (Pollack and Bodenheimer 1989; Owen & Bar-Nun 1995). Yet the mass spectrometer on the Galileo Probe clearly showed that Ar, Kr, Xe, N, C, and S are all enriched in Jupiter's atmosphere by the same factor of 3 ± 1 (Niemann et al. 1998; Owen et al. 1999).

The only measured elements that were not found to be enriched were helium, which precipitates out in the deep interior, and neon, which dissolves in the helium droplets (Roulston & Stevenson 1997). The oxygen abundance could not be measured because the probe did not go deep enough to reach levels of Jupiter's atmosphere where water—the main oxygen reservoir—was well mixed.

These results define the need for a new class of icy planetesimal, one that exhibits the solar composition of all elements less volatile than hydrogen, helium and neon. If these solar composition icy planetesimals (SCIPs) built the cores of all of the giant planets, they must have been the most abundant form of solid matter in the early solar system (Owen & Encrenaz 2003). How did they form?

The deficiency of nitrogen in comets is ascribed to the fact that this element is expected to be present primarily in the form of N_2 , in both the interstellar medium from which the solar system originated and in the outer solar nebula, the home, if not the birthplace, of the comets. N_2 is highly volatile and does not readily condense on itself or get trapped by forming ice, as graphically demonstrated by the presence of nitrogen compounds in dark, interstellar clouds in which CO is highly depleted (e.g., Caselli et al. 2003). Laboratory experiments on the trapping of argon, N_2, and CO in forming amorphous ice also reveal this difference in behavior (Owen & Bar-Nun 1995).

Thus in order to deliver nitrogen and argon to Jupiter, the icy planetesimals that carried them must have formed at low temperatures—below 27 K if the condensing water vapor formed amorphous ice, and below 38K if it made clathrate hydrates. Evidently, low temperature is the key to making these SCIPs.

There seem to be two possibilities. Either they were made as amorphous ice in the ISM and then transported into the solar nebula without subliming, or they were made as clathrate hydrates from crystalline ice that condensed within the nebula. In the latter case, they will exhibit ≥ 9 times solar oxygen, in order to have enough water molecules to build the crystal cages that trap the molecules. Jupiter would then exhibit at least 9 times the solar value of O/H, instead of the 3 times enrichment predicted for the amorphous case (Gautier et al. 2001a, b).

Could there be fragments of SCIPs in our population of comets? To find them we need to look for solar values of Ar/O and N/O, and interstellar values of N_2/O, which we could only expect in dynamically new comets coming in from the Oort cloud for the first time. The easiest observation is a search for the predicted high abundance of N_2, in the form of N_2^+ in the ion tails of these comets. It is important to note, however, that the ratio N_2^+/CO^+, which is commonly measured, contains the ambiguity of the CO abundance, which is known to vary from comet to comet (Crovisier & Bockelée-Morvan 1999). Thus it is critical to obtain CO/H_2O in the comet and to derive N_2/H_2O for comparison with expected interstellar values. Although N_2 is not observed directly in the ISM, up to 90% of the total nitrogen may be in this form, based on studies of N_2H^+ and NH_3 (van Dishoeck et al. 1993).

References

Caselli, P., et al. 2003, presented at this conference.

Crovisier, D., & Bockelée-Morvan, D. 1999, Space Sci.Rev., 90, 19

Gautier, D., Hersant, F., Mousis, O., & Lunine, J. I. 2001a, ApJ, 550, L227

Gautier, D., Hersant, F., Mousis, O., & Lunine, J. I. 2001b, ApJ, 559, L183

Geiss, J. 1987, A&A, 187, 859

Krankowsky, D., 1991, in Comets in the Post-Halley Era, eds. R. L. Newburn, M. Neugebauer, & J. Rahe (Dordrecht: Kluwer), 855

Niemann, H. B., et al. 1998, J. Geophys. Res., 103, 22831

Owen, T., & Bar-Nun, A. 1995, Icarus, 116, 215

Owen, T., & Encrenaz, Th. 2003, Space Sci.Rev., 106, 121

Owen, T., Mahaffy, P., Niemann, H. B., Atreya, S., Donahue, T., Bar-Nun, A., & de Pater, I. 1999, Nature, 402, 269

Pollack, J. B., & Bodenheimer, P. 1989, in Origin and Evolution of Planetary and Satellite Atmospheres, eds. S. K. Atreya, J. B. Pollack, & M. S. Matthews (Tucson: Univ. Arizona Press), 564

Roulston, M. J., & Stevenson, D. J. 1997, EOS Trans., AGU 76 (46) Fall Meeting Suppl. F, 343

van Dishoek, E. F., Blake, G. A., Draine, B. T., & Lunine, J. I. 1993, in Protostars and Planets III, eds. E. H. Levy & J. I. Lunine (Tucson: Univ. Arizona Press), 163

Weaver, H. A., et al. 2002, ApJ, 576, L95

Highlights of Astronomy, Vol. 13
International Astronomical Union, 2003
O. Engvold, ed.

Models of Collapsing Clouds and Star-Forming Regions as Analogs of the Solar Nebula

Paola Caselli

INAF–Osservatorio Astrofisico di Arcetri, Largo E. Fermi 5, I–50125 Firenze, Italy

Abstract. To fully understand the formation and the evolution of the Solar Nebula, the physical and chemical characteristics of the "pre-solar" cloud should be known. Here, I review recent findings on the study of starless and pre-stellar cores, pointing out the importance of molecular freeze out in the chemical and dynamical evolution of star forming regions.

1. Introduction

Stars like our Sun form inside gas and dust condensations of molecular clouds, called dense cores. These objects are observed throughout our Galaxy, but particular attention is devoted to nearby (< 200 pc) dense cores, which are embedded in molecular cloud complexes, such as Taurus and Ophiuchus (e.g. Myers 1999; Evans 1999). Their proximity to Earth makes them the ideal targets on which to carry out accurate and detailed studies.

It is well known that roughly one half of the nearby dense cores are associated with young stellar objects (or protostars; Beichman et al. 1986), which actively interact with the surrounding medium, altering the chemical composition and physical structure of the parent cloud with their strong collimated winds (bipolar outflows) and radiation. The other half of dense cores are starless and, although some of them may be in equilibrium and never form a star (see, e.g., Lada et al. 2003), a fraction (recently estimated to be $\sim 5\%$; Crapsi et al., in prep.) is thought to be on the verge of star formation, with clear evidence for centrally concentrated density profiles (e.g. Ward–Thompson et al. 1999) and contraction (Tafalla et al. 1998; Williams et al. 1999; Caselli et al. 2002a). Any information on the physical and chemical structure of these objects, called *pre-stellar cores*, will provide clues on the initial conditions of the star formation process and the material composition out of which stars as well as circumstellar disks, planets and comets will form.

Here, I will review recent progress in the study of starless and pre-stellar cores, the initial conditions in the process of star formation. Their chemical and physical properties will be described in an attempt to link "pre-solar" clouds to star–disk systems, for a better understanding of Solar Nebula evolution.

2. From *starless* to *protostellar* cores

In their evolution toward the formation of a young stellar object, dense cores with sizes of about 0.1 pc and molecular hydrogen number density of a few $\times$

10^4 cm^{-3} (e.g. Caselli et al. 2002b), change their density distribution until the so–called "pivotal" state is reached (e.g. Shu et al. 1987). This stage is considered the starting point for protostellar accretion and evolution.

There is much debate nowadays about how the "pivotal" stage is reached. The classical picture (see e.g. Ciolek & Mouschovias 1995) is that of a system contracting quasi–statically through ambipolar diffusion (the contraction motion of neutral particles in dense cores of low ionization, relative to the magnetic field and the ionized component). Another school of thought is represented by Hartmann et al. (2001; see also Mac Low & Klessen 2003), who claim that cloud cores form faster than predicted by ambipolar diffusion models and that star (and cloud) formation takes place in a few (and not tens of) million years, due to the presence of supersonic turbulence generated by big explosions (such as supernovae). The two pictures imply different chemical and physical histories, so that it is crucial to understand which model is closer to reality. This is currently under investigation.

A series of detailed studies of starless cores, based on observations of molecular lines, have been carried out in the past few years (e.g. Willacy et al. 1998; Caselli et al. 1999; Bergin et al. 2002; Caselli et al. 2002a,c; Tafalla et al. 2002; Lee et al. 2003). From these studies, coupled with millimeter continuum dust emission observations (e.g. André et al. 2000), it is now clear that the sample of starless cores is not homogeneous and an evolutionary trend is present.

Some starless cores (e.g. B68, L1512) appear quiescent and close to hydrostatic equilibrium (Lada et al. 2003; Lee et al. 2003), with central densities of a few times 10^5 cm^{-3} , and no evidence of contraction. They appear to be "chemically evolved", with large abundances of "late–time" molecules (such as NH_3 and N_2H^+) and clear signatures of molecular (mainly CO and CS) freeze out. Other objects (e.g. L1521E) have similar density structures but are chemically young (Hirota et al. 2002), suggesting that they are recently formed.

Another category of starless cores is represented by objects such as L1498 and L1517B, which present a more complex kinematic structure, likely due to material accretion onto the core and core contraction (Tafalla et al. 2002). They have central densities of $\sim 10^5$ cm^{-3} and constant temperatures of $\sim$10 K. CO and CS disappear from the gas phase at gas densities of a few $\times\ 10^4$ cm^{-3}, N_2H^+ maintains a constant abundance throughout the core, whereas the NH_3 abundance increases toward the center (Tafalla et al. 2003). The different amount of depletion for CO and the two N–bearing species can be reproduced by gas–grain chemical models which account for the different binding energies of CO and N_2 (the *common* parent species of N_2H^+ and NH_3) onto dust grain surfaces (Bergin & Langer 1997). The differing behavior of N_2H^+ and NH_3 is still not fully understood, although very low binding energies of ammonia precursors help in reproducing the observed trend (Caselli & Aikawa, in preparation).

Other objects (e.g. L1544, L1521F) seem to be close to the "pivotal" stage, with about ten times larger central densities, more centrally concentrated density profiles, and with clear signs of contraction in the central few thousand AU (Caselli et al. 2002c; Crapsi et al., in prep.). These condensations, being on the verge of star formation, should be more properly called *pre-stellar* cores. They stand out in having large degrees of CO depletions and deuterium fractionations (see also Bacmann et al. 2003), and show line broadening in the central few thousands AU, likely due to inward motions (Caselli et al. 2002c). The recent strong detection of H_2D^+ in the central ~ 2500 AU of L1544 (Caselli et al. 2003) had strong implications for the chemical structure of pre-stellar cores. In fact, the large H_2D^+ abundance ($[H_2D^+]/[H_2] \simeq 10^{-9}$) inferred from observations is consistent with the central few thousands AU being completely deprived of species heavier than helium.

Therefore, the material out of which the "protostellar nebula" will form is essentially composed of H_2 and dust grains covered with thick icy mantles. Assuming "classical" dust particles with radius 0.01 μm and 10^6 sites for adsorption of gaseous species (e.g. Tielens & Allamandola 1987), it is easy to show that a complete freeze out of molecules implies dust grains covered by about one hundred layers of ice. The consequent increase in grain size has consequences for the dust properties, including the emissivity (Ossenkopf & Henning 1994). In particular, thick icy layers are expected to boost grain coagulation (Ossenkopf 1993), so that large and fluffy aggregates probably form *before* becoming part of the protoplanetary disk. How this affects the evolution of the Solar Nebula is unknown and it awaits further investigation.

Interestingly, very young protostars (the so–called Class 0 sources; André et al. 1993) appear to have chemical characteristics (and kinematics) similar to pre-stellar cores, including molecular depletion (Belloche et al. 2002), reinforcing the idea that pre-stellar cores are indeed evolving toward stellar birth and can be considered as initial conditions in the process of star formation. Moreover, Class 0 sources possess a disk (see also Harvey et al. 2003), embedded (and formed) in the molecular depleted region. Finally, the presence of a rich chemistry on dust grain surfaces during the pre-stellar phase of evolution of a molecular cloud core is testified to by the recent discovery of complex organic molecules (hard to form in the gas phase) in the warm (~ 100 K) gas surrounding the Class 0 source IRAS 16293-2422 (Cazaux et al. 2003). Molecular species such as ethyl cyanide C_2H_5CN are thought to be formed on grain surfaces during the cold pre-stellar phase and, after protostellar formation, released in the gas phase. These findings furnish stringent constraints on current chemical models of protoplanetary disks.

References

Andre, P., Ward-Thompson, D. & Barsony, M. 1993, ApJ, 406, 122

Andre, P., Ward-Thompson, D. & Barsony, M. 2000, in Protostars and Planets IV, ed. V. Mannings, A. P. Boss, & S. S. Russel (Tucson: Univ. Arizona Press), p. 59

Bacmann, A., Lefloch, B., Ceccarelli, C., Steinacker, J., Castets, A. & Loinard, L. 2003, ApJ, 585, L55

Beichman, C. A., Myers, P. C., Emerson, J. P., Harris, S., Mathieu, R., Benson, P. J. & Jennings, R. E. 1986, ApJ, 307, 337

Belloche, A., Andre', P., Despois, D. & Blinder, S. 2002, A&A, 393, 927

Bergin, E. A., Alves, J., Huard, T. & Lada, C. J. 2002, ApJ, 570, L101

Bergin, E. A. & Langer, W. D. 1997, ApJ, 486, 316

Caselli, P., Benson, P. J., Myers, P. C. & Tafalla, M. 2002b, ApJ, 572, 238

Caselli, P., van der Tak, F. F. S., Ceccarelli, C. & Bacmann, A. 2003, A&A, 403, L37

Caselli, P., Walmsley, C. M., Tafalla, M., Dore, L. & Myers, P. C. 1999, ApJ, 523, L165

Caselli, P., Walmsley, C. M., Zucconi, A., Tafalla, M., Dore, L. & Myers, P. C. 2002a, ApJ, 565, 331

Caselli, P., Walmsley, C. M., Zucconi, A., Tafalla, M., Dore, L. & Myers, P. C. 2002c, ApJ, 565, 344

Cazaux, S., Tielens, A. G. G. M., Ceccarelli, C., Castets, A., Wakelam, V., Caux, E., Parise, B. & Teyssier, D. 2003, ApJ, 593, L51

Ciolek, G. E. &, Mouschovias, T. Ch. 1995, ApJ, 454, 194

Evans, N. J., II 1999, ARA&A, 37, 311

Hartmann, L., Ballesteros-Paredes, J. & Bergin, E. 2001, ApJ, 562, 852

Harvey, D. W. A., Wilner, D. J., Myers, P. C. & Tafalla, M. 2003, ApJ, in press

Hirota, T., Ito, T. & Yamamoto, S. 2002, ApJ, 565, 359

Lada, C. J., Bergin, E. A., Alves, J. F. & Huard, T. L. 2003, ApJ, 586, 286

Lee, J.-E., Evans, N. J., II, Shirley, Y. L. & Tatematsu, K. 2003, ApJ, 583, 789

Mac Low, M. -M. & Klessen, R. S. 2003, Rev. Mod. Phys., in press

Myers, P. C. 1999 in The Physics and Chemistry of the Interstellar Medium, Proceedings of the 3rd Cologne-Zermatt Symposium, Eds.: V. Ossenkopf, J. Stutzki and G. Winnewisser & G. Winnewisser, GCA-Verlag Herdecke, p. 227

Ossenkopf, V. 1993, A&A, 280, 617O

Ossenkopf, V. & Henning, Th. 1994, A&A, 291, 943O

Shu, F. H., Adams, F. C. & Lizano, S. 1987, ARA&A, 25, 23

Tafalla, M., Mardones, D., Myers, P. C., Caselli, P., Bachiller, R. & Benson, P. J. 1998, ApJ, 504, 900

Tafalla, M., Myers, P. C., Caselli, P. C. & Walmsley, C. M. 2003, A&A, submitted

Tafalla, M., Myers, P. C., Caselli, P. C., Walmsley, C. M. & Comito, C. 2002, ApJ, 569, 815

Tielens, A. G. G. M. & Allamandola, L. J. 1987, in Physical Processes in Interstellar Clouds, ed. G. E. Morfill & M. Schloer (Dordrecht: Reidel), p. 333

Ward-Thompson, D., Motte, F. & Andre, P. 1999, MNRAS, 305, 143

Willacy, K., Langer, W. D. & Velusamy, T. 1998, ApJ, 507, L171

Williams, J. P., Myers, P. C., Wilner, D. J. & di Francesco, J. 1999, ApJ, 513, L61

Highlights of Astronomy, Vol. 13
International Astronomical Union, 2003
O. Engvold, ed.

The Structure Of The Solar Nebula From Cometary Composition

D. Bockelée-Morvan

Observatoire de Paris, 5 place Jules Janssen, F-92195, Meudon, France

F. Hersant

Institut für Theoretische Astrophysik, Tiergartenstr. 15, D-69121, Heidelberg, Germany

D. Gautier

Observatoire de Paris, France

J.-M. Huré

Observatoire de Paris and Université de Paris 7, France

Abstract. This paper presents an interpretation of cometary compositional data in the frame of an evolutionary 2D turbulent model of the Solar Nebula: D/H ratios, crystalline silicates and N_2/CO deficiency.

A number of models of the Solar Nebula have been published, but most of them are weakly constrained. Observational data acquired these last years improve the situation. It is currently admitted that accretion of matter in circumstellar disks is driven by turbulence (although its origin is still controversial). Among observational evidences are non-thermal velocity dispersions, UV and visible luminosity excesses in T Tauri stars and disk lifetime. Turbulence has been considered for a long time as responsible for angular momentum redistribution in the Solar System. Since the exact calculation of the turbulence at all scales requires an unrealistically large amount of computer time, modelers simplify the problem thanks to a prescription for turbulent viscosity that is proportional to the speed of sound and half-thickness H of the disk, with α as the proportionality factor (Shakura & Sunyaev 1973). On this basis, Hersant, Gautier, & Huré (2001) developed an evolutionary two-dimensional turbulent model for the solar nebula. This model is defined by three parameters: the initial accretion rate $\dot{M}_0$, the initial radius of the disk R_0 and the α parameter. The temporal evolution of the temperature T, surface density Σ, pressure P and height H throughout the nebula are computed using the decay of the mass accretion rates versus age observed for T Tauri stars (Hartmann 2000).

However, the large range of possible input parameters lead to a considerable number of different evolving Solar Nebulae. Solar system data, especially the isotopic composition of comets and of primitive meteorites, introduce strong additional constraints. The D/H ratio has been measured in H_2O in Comets Halley, C/1996 B2 (Hyakutake) and C/1995 O1 (Hale-Bopp), and in HCN in Comet Hale-Bopp. The D/H ratio in OH has been measured in LL3 meteorites (for a review of all measurements, see Robert, Gautier, & Dubrulle 2000). From the analysis of these data, Drouart et al. (1999) and Hersant et al. (2001) obtained important conclusions: (i) a major part of water ices (strongly enriched in deuterium), falling from the pre-solar cloud on the nebula disk, vaporized outwards to 20–30 AU; as long as water did not condense, it subsequently exchanged its deuterium with H_2 of the nebula, which D/H ratio was equal to the protosolar value ($\sim 2\times10^{-5}$); (ii) the decrease of the initial D/H was much more efficient in the hot inner nebula than in the outer nebula where comets formed from icy grains; (iii) the material of the inner part of the nebula mixed by turbulent diffusion with that of the outer nebula; (iv) the D/H ratios measured in water in the Oort cloud comets are relics of the value reached in H_2O at the epoch when the gas condensed to form the pre-cometary ices; (v) a minor part of water ices either accreted late in the life of the nebula, or arrived late in the region of meteorite formation: their D/H ratio, higher than the value measured in comets, must be relics of that in the interstellar medium (ISM). Indeed, highly D-enriched phases coexist with less enriched (reprocessed) components in LL3 meteorites.

From their analysis, Drouart et al. (1999) and Hersant et al. (2001) showed that the D/H ratio measured in water in comets, and in the reprocessed part of OH in LL3 meteorites, constrains the temporal evolution of the radial distributions of temperature and density throughout the nebula. This considerably reduce possible values of $\dot{M}_0$, R_0 and α, namely: $2\times10^{-6} < \dot{M}_0 < 10^{-5}$ solar mass per year, $12.8 < R_0 < 39$ AU, $0.006 < \alpha < 0.04$ according to Hersant et al. (2001). Interestingly enough, values of D/H in HCN measured in Comet Hale-Bopp are reproduced with the same evolution schemes (Mousis et al. 2000; Hersant et al. 2001).

These models also succeed in the interpretation of the presence of crystalline silicates in comets. Their detection (see Crovisier et al. 2000; Wooden et al. 1999) was unexpected because silicates detected so far in the ISM are amorphous and that the crystallization requires temperatures much higher than expected in the outer nebula. Bockelée-Morvan et al. (2002) proposed that amorphous silicates coming from the outer regions were annealed in the inner hot nebula. Using the nebula models of Hersant et al. (2001) which fit cometary D/H ratios, they were able to reproduce the mass ratio of crystalline silicates over amorphous silicates observed in Comet Hale-Bopp, as a result of the subsequent mixing of the silicate variety formed in the inner nebula with the amorphous variety present in the region of formation of Oort cloud comets.

Another interesting product of the turbulent models of Hersant et al. (2001) is that they can be used to interpret the strong deficiency of N_2 with respect to CO observed in several Oort cloud comets. When the nebula cooled down, H_2O condensed in crystalline form at temperatures of about 150 K. As cooling further proceeded, the nebula reached temperature/pressure conditions for which various volatiles (H_2S, CH_4, CO, N_2, and noble gases) may be trapped in the form of clathrate hydrates (Iro et al. 2003). NH_3 is trapped as an hydrate. The trapping of CO and N_2 occurs, in principle, at similar temperatures. However, if the amount of available ice is not sufficient to trap both CO and N_2, the clathration of CO drastically dominates that of N_2. Iro et al (2003) have calculated that clathrate hydrates of N_2 cannot form if the H_2O/H_2 ratio (at the epoch of condensation of water) is less than 2.8 times the solar O/H ratio. In other words, N_2 was trapped in cometary grains only in regions where icy grains accumulated. The same approach is valid for argon. This noble gas has not been detected in any comet so far.

In the framework of the same clathration theory, the uniform enrichment in C, N and noble gases measured in Jupiter results from the clathration of volatiles (including CO, CH_4, N_2, NH_3, Ar, Kr and Xe) in the feeding zone of the planet, and from the accumulation of ices around 5 AU (Gautier et al. 2001). The theory of clathration also permitted Hersant, Gautier, & Lunine (2003) to predict that enrichments in Saturn, Uranus and Neptune should be strongly different (especially for noble gases) from those observed in Jupiter.

References

Bockelée-Morvan, D., Gautier, D., Hersant, F., Huré, J-M., & Robert, F. 2002, A&A, 384, 1107

Crovisier, J., Brooke, T. Y., Leech, K. Bockele-Morvan, D., Lellouch, E., Hanner, M. S., Altieri, B., Keller, H. U., Lim, T., Encrenaz, P., Salama, A., Griffin, M., de Graauw, T., van Dishoeck, E., & Knacke, R. F. 2000, in Thermal emission spectroscopy and analysis of dust disks, and regoliths, eds. M. L. Sitko, A. L. Sprague, & D. K. Lynch, Astron. Soc. Pac.. Conf. Ser., 196, 109

Drouart, A., Dubrulle, B., Gautier, D., and Robert, F. 1999, Icarus, 140, 129

Gautier, D., Hersant, F., Mousis, O., & Lunine, J. I. 2001, ApJ, 550, L227, ERRATUM: ApJ, 559, L183

Hartmann, L. 1998, Accretion Processes in Star Formation, Cambridge Univ. Press. (Cambridge, UK)

Hartmann, L. 2000, Space Sci.Rev., 92, 55

Hersant, F., Gautier, D., & Huré, J. M. 2001, ApJ, 554, 391

Hersant, F., Gautier, D., & Lunine, J. I. 2003, Planet. Space Sci. (in press)

Iro, N., Gautier, D., Hersant, F., Bockelée-Morvan, D., & Lunine, J. I. 2003, Icarus, 161, 511

Mousis, O., Gautier, D., Bockelée-Morvan, D., Robert, F., Dubrulle, B., & Drouart, A. 2000, Icarus, 148, 513

Robert, F., Gautier, D., & Dubrulle, B. 2000, Space Sci.Rev., 92, 201

Shakura, N. I., & Sunyaev, R. A. 1973, ApJ, 24, 337

Wooden, D. H., Harker, D. E., Woodward, C. E., Butner, H. M., Koike, C., Witteborn, F. C., & McMurtry, C. W. 1999, ApJ, 517, 1034

Highlights of Astronomy, Vol. 13
International Astronomical Union, 2003
O. Engvold, ed.

Chemistry of Collapse and Disk Accretion

S. B. Charnley & S. D. Rodgers

Space Science Division, NASA Ames Research Center, Moffett Field, CA 94035, USA

Abstract.
Recent results relevant for the survival and chemical alteration of interstellar material at the nebular accretion shock are summarised.

1. Introduction

A key issue for the ISM-comet connection is to determine under what conditions volatile interstellar matter could survive the accretion shock and arrive, largely unmodified, in the protosolar nebula (see Ehrenfreund & Charnley 2000). That is, in which regions of the nebula are infalling gaseous molecules and solid ice mantles processed, survive the shock, and simply recondense as ices of similar composition in the post-shock flow? It is also of great interest to quantify the processing in that material which does experience chemical changes. However, there have been no detailed studies of how the accretion process affects the volatile interstellar molecules, apart from those seeking to establish conditions for vaporization (e.g. Neufeld & Hollenbach 1994). We have therefore begun an extensive study aimed at understanding precisely how interstellar molecules, and their isotopic fractionation ratios, are modified as they collapse towards a protostellar disk, pass through the accretion shock, and subsequently take part in nebular chemistry (see also Markwick & Charnley in this volume).

Detailed chemical collapse calculations show that heating of the infalling gas by radiation from the protostar/disk leads to evaporation of molecular ices, and thence to strong spatial and temporal molecular abundance gradients in the protostellar core (Rodgers & Charnley 2003). These calculations indicate that, soon after an 'inside-out' collapse (Shu 1977) has started, infall time-scales become shorter than most chemical time-scales. This results in material from the cool envelope collapsing onto the central protostar without significant chemical alteration. We have extended this into a two-stage model. The first stage is a rotating collapse to allow the composition of accreted interstellar material to be studied as a function of entry position on the nebular disk (Cassen & Moosman 1981). In this short contribution we present some preliminary results from our modeling of the second stage: chemistry at the accretion shock.

2. Accretion Shock Chemistry

We initially consider a simple scenario. As cold interstellar gas and ice-mantled dust grains collapse onto the luminous protostar/disk system they are heated and the ice molecules evaporate (e.g. Chick & Cassen 1997). We take the pre-shock chemical composition to be that corresponding to the general composition of interstellar ice mantles. At the accretion shock, the gas is heated and compressed and we follow the post-shock chemistry of volatile material as it cools and recondenses onto dust grains. For the shock calculations we use a steady interstellar J-shock chemical code (Charnley et al. 1988), based on the model of Hollenbach & McKee (1979) suitably modified to treat the more extreme conditions of the accretion shock problem (e.g. 3-body reactions, gas-grain interaction, collisional dissociation of H_2). The chemical network is that of Charnley (1997) but with additional high-temperature reactions from the literature (e.g. for methanol).

3. Results & Discussion

For a given mass accretion rate, the accretion shock is fully dissociative closer to the protostar. Slow shock speeds and low pre-shock densities favor the survival of the most volatile material; these conditions occur in the outer disk. At these and intermediate disk radii, the shock is only partially-dissociative and so a key parameter for the chemistry is the H/H_2 ratio in the post-shock gas. This can increase by many orders of magnitude from its value in quiescent dense gas.

Figure 1 shows the post-shock chemistry for three shock speeds impacting on gas in the outer disk. As expected, the slowest shock produces little chemical change. This preliminary calculation shows that CO and H_2O can survive the accretion shock and in fact increase in abundance. Any chemical erosion of H_2O to OH and O by H atom abstraction reactions is overwhelmed by hydrogenation reactions with H_2. The abundances of some molecules, like CH_4 and CO_2, are eroded in such a J-shock but can partially recover. Other molecules, such as H_2S, CH_3OH, OCS and H_2CO are completely destroyed. The post-shock chemistry is highly nonlinear. At the intermediate shock speed the methane abundance actually rises because CH_3OH is being broken into CH_3 and OH; at these post-shock temperatures the reaction of CH_3 with H_2 is faster than its destruction by H atoms.

In future work we plan to perform a comparative study of the chemistry in dense C-shocks (e.g. Charnley & Kaufman 2000) since the physical conditions in these shocks may be more benign to molecule survival. We will also make detailed models of specific shock chemistries. This project will eventually allow us, for example, to assess how interstellar deuterium fractionation signatures were altered upon incorporation into the protosolar nebula.

This work was supported by NASA's Origins of Solar Systems and Long Term Space Astrophysics Program's with funds allocated by NASA Ames under Interchange No. NCC2-1412.

References

Cassen, P. & A. Moosman 1981, Icarus 48, 353

Chick, K. M. & Cassen, P. 1997, ApJ, 477, 398

Charnley, S. B. 1997, ApJ, 481, 396

Charnley, S. B., Dyson, J. E., Hartquist, T. W. & Williams, D. A. 1988, MNRAS231, 269

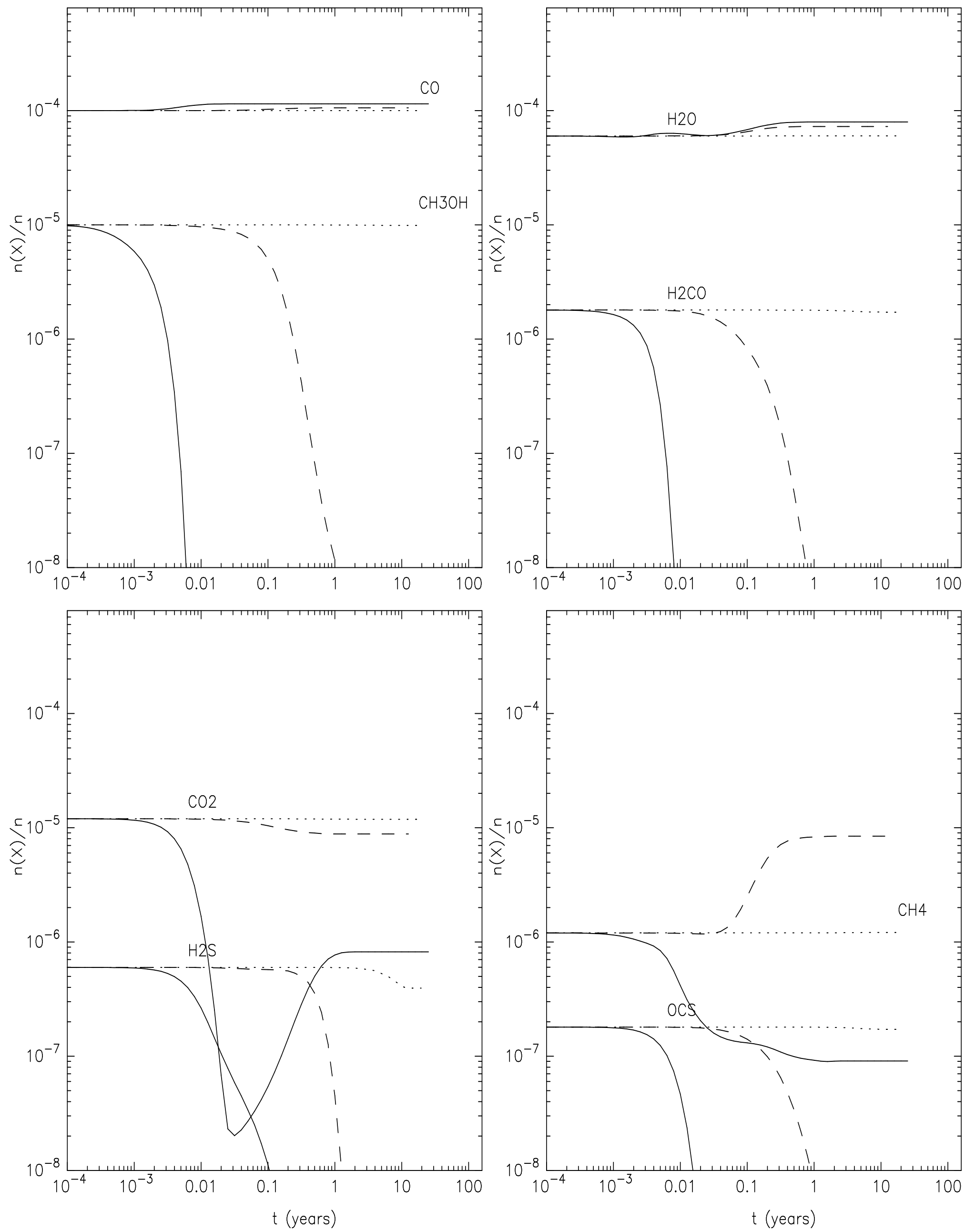

Figure 1. Post-shock chemical evolution of interstellar volatiles at the outer disk accretion shock for a pre-shock gas density of $2 \times 10^6 \mathrm{cm}^{-3}$ and shock speeds of 5 kms^{-1} (dotted curves), 8 kms^{-1} (broken curves), and 10 kms^{-1} (solid curves)

Charnley, S. B., & Kaufman, M. J. 2000, ApJ, 529, L111
Ehrenfreund, P., & Charnley, S. B., 2000, ARA&A, 38, 427
Hollenbach, D. & McKee, C. F. 1979, ApJS, 41, 555
Neufeld D. & Hollenbach D. J. 1994, ApJ, 428, 170
Rodgers, S. D., & Charnley, S. B. 2003, ApJ, 585, 355
Shu, F. H. 1977, ApJ, 214, 488

Highlights of Astronomy, Vol. 13
International Astronomical Union, 2003
O. Engvold, ed.

Chemistry in Protoplanetary Disks

Yuri Aikawa

Department of Earth and Planetary Sciences, Kobe University, Kobe 657-8501, Japan

Abstract. Molecular evolution is calculated in migrating fluid parcels in a protoplanetary disk considering gas-phase and grain-surface reactions. Radial distribution of molecules is obtained, which depends on ionization rate, temperature and/or desorption rate in the disk. If the temperature is high enough (> 20 K) or non-thermal desorption is efficient enough to sublimate dominant species such as CO in the comet forming regions, the desorbed species are transformed to less volatile species and again incorporated into ice mantles. Chemistry in these outer disks is similar to that in molecular clouds; it produces both oxidized and reduced species with a high D/H ratio.

1. Introduction

Chemistry in the protoplanetary disk is a key to understand the evolution from interstellar matter to planetary matter. Spectroscopic observation of disks detected several molecules and determined their relative abundances in the gas phase (Dutrey et al. 1997; van Zadelhoff et al. 2001; Aikawa et al. 2003; Qi et al. 2003) and ice mantles (Thi et al. 2002). But the current observations are sensitive only to the regions outside 100 AU owing to the poor angular resolution. Comets are unique probes in planet-forming regions until we get new facilities such as ALMA. In this contribution I solve the chemical reaction network in the disk, and obtain ice composition in the comet-forming region at $R = 5 - 20$ AU. The model is basically the same as Aikawa & Herbst (1999), but the current work adopts updated disk model and includes grain-surface reactions.

2. Model

A steady accretion disk model by D'Alessio et al. (1999) is adopted. They solve energy transfer (including the irradiation from the central star and gravitational energy released by accretion) to determine vertical structure of the disk at each radius. In the midplane of comet-forming region, the temperature is $\sim 30 - 60$ K and gas density is $\sim 10^{11} - 10^{12}$ cm^{-3}.

Chemical reaction network is solved as an initial value problem. The initial composition of gas and ice is given by calculating contraction of a molecular cloud core. Then we follow migrating fluid parcels in the disk towards the central star. The network includes gas-phase reactions, gas-dust interaction (adsorption and desorption), and modified-rate grain-surface reactions (Stantcheva et al. 2001). Gas-phase reaction includes cosmic ray ionization. Since the attenuation length of the cosmic-ray ionization (96 g cm^{-2}) is larger than the column density to the midplane at $R = 5$ AU, the interstellar ionization rate $\sim 10^{-17}$ s^{-1} would be available in the disk. If the cosmic ray is scattered by magnetic fields of the central star, decay of ^{26}Al could be the main ionization source with the ionization rate of 6×10^{-19} s^{-1} (Umebayashi & Nakano 1981). The ionization rate by X rays from the central star is $> 10^{-17}$ s^{-1} within the surface layer of $\leq 10^{24}$ cm^{-2} at $R = 5$ AU (Igea & Glassgold 1999). If ions and radicals produced in the upper layers can diffuse into the midplane, column density at $R = 5$ AU (column-density averaged) ionization rate is $\sim 10^{-18}$ s^{-1}. I investigate models with ionization rates of 10^{-18} s^{-1} and 10^{-17} s^{-1}.

3. Results

3.1. Temporal Evolution and Radial Distribution

Fluid parcels of interstellar matter fall onto the disk at $R \sim 250$ AU, and migrate to $R = 5-20$ AU in 3×10^6 yr. Molecular abundances vary with time, and newly formed ice accretes onto grains, which are already covered by interstellar ice. Although the density is high, the chemistry in these outer radii is qualitatively similar to cloud chemistry. Figure 1 (a) shows radial distribution of molecules at 3 Myr, which corresponds to a typical life time of classical T Tauri stars. At $R \geq 15 AU$ ice composition is almost constant, which is determined in the stage of molecular cloud and migration in the outer radius, and is basically similar to interstellar ice. At $R \leq 15$ AU radial variation is more significant. For example, H_2S ice is transformed to SO ice after sublimation. HCN ice is more abundant in the inner radius. Just like hot core chemistry, the evaporation of simple species such as CO and H_2S triggers the new gas-phase reactions; the larger and less volatile species are formed and adsorbed onto ice mantle again.

3.2. If the Gas is Initially Hot

causes diffusion in the disk, and thermally processed material in inner hot regions might migrate to outer regions. Such diffusion or shock heating in the comet-forming regions is suggested from the existence of crystalline silicate in the disks and comets. Here I assume that the matter is initially processed at high temperature and left in the cold comet-forming region. Considering the equilibrium at high temperature, initial composition is assumed to be CO, N_2 and water. At $t = 0$, the matter is put at the radius of $3 - 25$ AU. Molecules observed in comets – such as hydrocarbons, NH_3, CO_2 and deuterated water – become abundant within a time scale of 10^6 yr. Figure 1 (b) shows radial distribution of molecules at 3 Myr. The abundance varies with radius according to the temperature gradient in the disk.

3.3. Implications for Comets

If chemistry is inactive in comet forming regions, variation of comet composition is caused only by evaporation, and comets formed in outer radius have larger abundance of all molecular species. On the other hand, if chemistry is active in the comet-formic regions, as shown in this work, some species become more abundant in comets formed in inner regions. A'Hearn et al. (1995) found that carbon chain species are depleted in Jupiter-Family comets, dynamical origin of

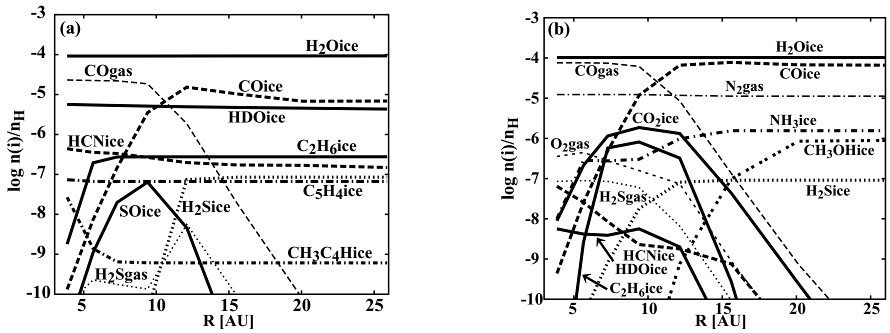

Figure 1. (a) Radial distribution of molecules in a steady accretion disk model at 3 Myr. The ionization rate is assumed to be 1.3×10^{-17} s^{-1}. (b) Radial distribution of molecules at 3 Myr. Initial composition is CO gas, N_2 gas, and H_2O ice. Ionization rate is assumed to be 1.3×10^{-18} s^{-1}.

which are in outer radius than that of the Halley-type comets. It may indicate the second case is appropriate for the Solar Nebula.

Acknowledgments. Y. A. is supported by a Grant-in-Aid for Scientific Research (14740130) and "The 21st Century COE Program of Origin and Evolution of Planetary Systems" of Ministry of Education, Culture, Sports, Science and Technology (MEXT) of Japan.

References

A'Hearn, M., Millis, R. L., Schleicher, D. G., Osip, D. J., & Birch, P. V. 1995, Icarus, 118, 223

Aikawa, Y., & Herbst, E. 1999, ApJ, 526, 314

Aikawa, Y., Momose, M., Thi, W. F., van Zadelhoff, G. J., Qi, C., Blake, G. A., & van Dishoeck, E. F. 2003, PASJ, 55, 11

D'Alessio, P., Calvet, N., Hartmenn, L., Lizano, S., & Canto, J. 1999, ApJ, 527, 893

Dutrey, A., Guilloteau, S., & Guelin, M. 1997, A&A, 317, L55

Igea, J., & Glassgold, A. E. 1999, ApJ, 518, 848

Qi, C., Kessler, J. E., Koerner, D. W., Blake, G. A., & Sargent, A. I. 2003, ApJ, in press

Stantcheva, T., Caselli, P., & Herbst, E. 2001, A&A, 375, 673

Thi, W. F., Pontoppidan, K. M., van Dishoeck, E. F., Dartois, E., d'Hendecourt, L. 2002, A&A, 394, 27

Umebayashi, T., & Nakano, T. 1981, PASJ, 33, 617

van Zadelhoff, G. J., van Dishoeck, E. F., Thi, W. F., Blake, G. A. 2001, A&A, 377, 566

Highlights of Astronomy, Vol. 13
International Astronomical Union, 2003
O. Engvold, ed.

Disk Chemistry and Cometary Composition

A. J. Markwick & S. B. Charnley

Space Science Division, NASA Ames Research Center, Moffett Field, CA 94035

Abstract. We describe a theoretical study of protoplanetary disk chemistry. By considering physical conditions similar to that of the protosolar nebula, we attempt to assess the contribution made by material from the cooler nebular regions to cometesimal composition. Calculations are presented which determine the spatial and temporal chemistry of the gas and dust within the 5-40 AU comet-forming region of the nebula. We show that there is little radial variation in the solid-state distribution of some molecules which could potentially be parents of the carbon-chain species observed in comets. We conclude that the apparent variation in abundance of C_2 and C_3 between long- and short-period comets is the result of chemical processing during their lifetimes and not differences in composition at the time of formation.

1. Introduction

Short-period comets formed in the nebula roughly where they reside today ($\sim 30-1000$ AU) and comprise the Kuiper Belt. On the other hand, long-period comets formed closer to the protosun ($\sim 5-40$ AU), but dynamical effects led them to be ejected from there into the Oort Cloud (radii $\sim 10^3 - 10^5$ AU). There is an apparent variation in the coma abundances of C_2 and C_3 between each comet population, with the short-period comets being more depleted in these molecules (A'Hearn et al. 1995). As C_2 and C_3 are coma photoproducts (Helbert et al. 2000), any differentiation between the comet families must be due to chemical differences in the nuclear ices of the two populations. Possible nuclear parents are C_2H_2 (acetylene) and CH_3CCH (methyl acetylene). The origin of this differentiation could lie either in the protostellar disk chemistry which occurred during their formation (nature), or in the chemical-processing histories (photolysis, radiolysis, heating) of each family (nurture). Using a model of the chemistry in the protostellar disk, we might hope to discriminate between these two possibilities.

2. The Model

The model we have developed is constructed in two stages. First, the physical structure (density, temperature) of the disk is computed. This calculation includes the combined heating effects of viscous dissipation and irradiation by the central object, as well as a 2D treatment of the radiative transfer (Nomura 2002). The structure ($0 < r < 100$ AU) of a steady α-disk is produced for a central solar-mass object with mass accretion rate 10^{-7} solar masses per year.

Figure 1 shows the associated temperature and density distributions. These results are then used as input for a comprehensive chemical model, described in Markwick et al. (2002). Briefly, the reaction network comprises around 250 species and 2500 reactions of various types including photoprocesses and gas-grain interaction. The latter allows molecules to freeze out onto dust particles and be thermally evaporated as conditions allow. Note that this model does not include any reactions between species on the grain surfaces, except the formation of molecular hydrogen and some ion-grain recombination reactions. This is because there are conceptual problems in attempting to treat surface reactions in such a deterministic model. The model integrates the chemical rate equations at each point for which physical structure is available, and so 2D gas-phase molecular distributions can be produced (see Millar et al. 2003). In this work, we consider only the mid-plane abundances of solid-phase species, which we assume will be incorporated directly into cometary ices as they form.

3. Results and Discussion

Figure 2 shows the variation of some solid-phase carbonaceous species in the mid-plane of the disk. The region between 10 and 40 AU is a significant fraction of the comet-forming region and, encouragingly, we see that, due to the temperature structure of the mid-plane, molecules in the ice are abundant there. If we are to adopt the 'nature' perspective described above, then we might expect to see a difference in the carbon-chain abundances between 10 and 40 AU. However, Figure 2 shows that there is no variation in the abundances of these species in the region of interest. The same result is true for all species with 2 and 3 carbon atoms in the model: there is no variation between 10 and 40 AU. The reason for this is quite straightforward. The gas-grain interaction in the model is described by 'freeze-out'. This is a balance between sticking collisions between molecules and grains, and the return of these molecules by evaporation from grain surfaces. Thermal desorption depends on the nebular dust (and gas) temperature, T, and on the binding energy of the molecule to the dust grain, E_b, a material property. The temperature structure in the mid plane is such that the thermal desorption rate ($\propto \exp[-E_b/kT]$) effectively switches the solid-state abundances between negligible and significant: binding energies are simply not low enough to allow a variation across the comet-forming region, where the temperature varies by only about 10 K. Hence, using the model described here, we conclude that any differences in carbon-chain composition between long- and short-period comets arise due to their different processing histories (see Stern 2003).

This work was supported by NASA's Origins of Solar Systems Program with funds allocated by NASA Ames under Interchange No. NCC2-1412. AJM is a National Research Council postdoctoral research associate.

References

A'Hearn M. et al., 1995, Icarus 118, 223

Helbert, J., Rauer, H., Boice, D., Huebner, W. F., 2000, BAAS, 32, 1071

Markwick A. J., Ilgner M., Millar T. J., Henning Th., 2002, A&A, 385, 632

Millar T. J., Nomura H., Markwick A. J., Ap&SS, in press

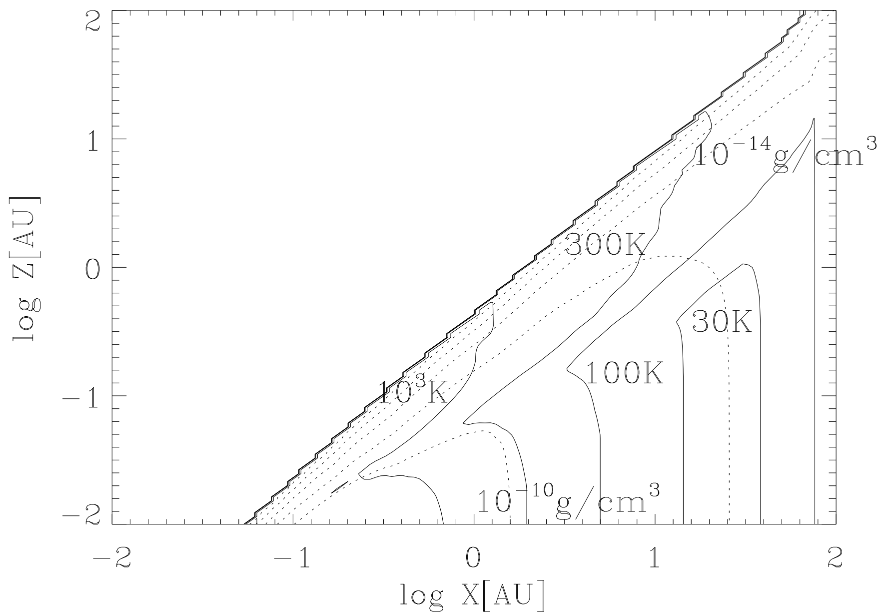

Figure 1. The two-dimensional structure of the disk for $r < 100$ A.U.

Nomura H., 2002, ApJ, 567, 587
Stern, S. A. 2003, Nature 424, 639

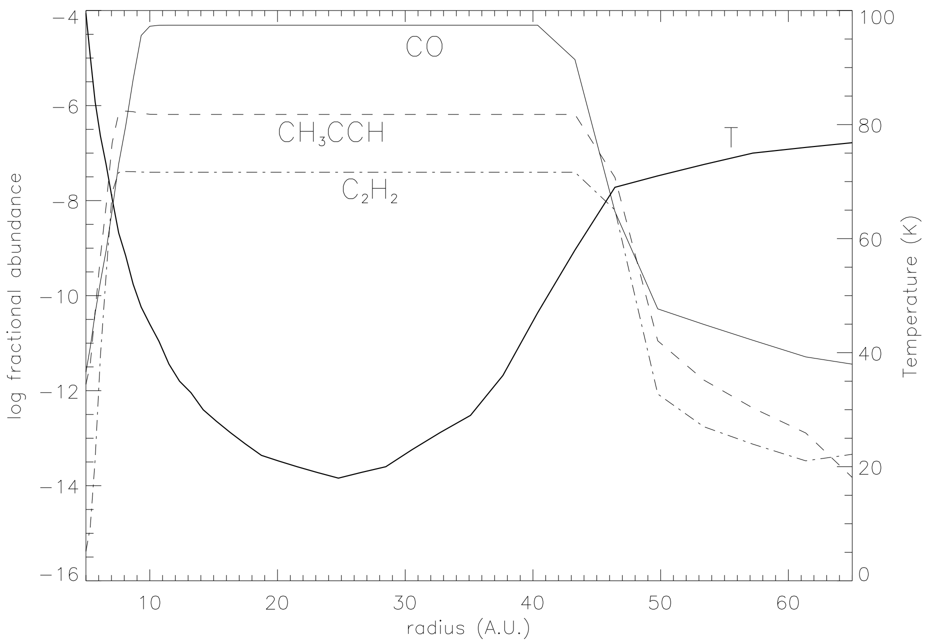

Figure 2. The mid-plane variation of the relative solid-phase abundances of C_2H_2 and CH_3CCH. The abundances are scaled to be the fractional abundance relative to gas-phase H_2. Also shown is the temperature structure of the mid plane.

Highlights of Astronomy, Vol. 13
International Astronomical Union, 2003
O. Engvold, ed.

A Mechanism of Crystallization of Cometary Silicates

Tetsuo Yamamoto & Takeshi Chigai

Department of Earth and Planetary Sciences, Nagoya University, Nagoya 464-8602, Japan

Abstract. We propose a new mechanism of crystallization of cometary silicate. The crystallization is due to heat released by chemical reactions in the organic refractory mantle of Greenberg's model of cometary dust induced by moderate heating by solar radiation. It is shown that the strength of the crystalline feature observed in the comets can be reproduced by the present mechanism of crystallization.

1. Introduction

Since the first identification of crystalline silicate feature in Comet Halley in the wavelength region of 8 to 13 μm (Bregman et al. 1987; Campins & Ryan 1989), the crystalline silicate features have been observed in dust in several other comets as well as in dust in various kinds of objects (see Hanner 1999 for a review). It has been proposed that cometary crystalline silicate was formed by annealing of amorphous silicate or direct condensation in a hot (> 1000 K) region of the primordial solar nebula. On the other hand, the molecular composition observed in cometary comae requires cold amorphous dust preserving interstellar volatile composition in its icy mantle. To reconcile both requirements, it has been considered that cometary silicates are a mixture of crystalline and amorphous silicates, each of which are of different origin.

In this article, we propose a new mechanism that makes both of the preservation of interstellar volatiles and the presence of crystalline silicate possible without mixing.

2. The Crystallization Mechanism

The crystallization mechanism proposed here is based on the Greenberg model of cometary dust (Greenberg 1982; Greenberg & Zhao 1988), which is composed of a silicate core, an organic mantle and an outer icy mantle. When the dust is released as a comet approaches the Sun, the icy mantle sublimes quickly and the remaining organic mantle and silicate core are heated to temperatures of several hundred K depending on the heliocentric distance. Note that the composition of the icy mantle preserved the interstellar composition. Although the dust temperatures of several hundred K are insufficient to crystallize amorphous silicate itself, it will trigger reactions among reactive molecules in the organic mantle because of the increase in the reaction rates due to the temperature rise. The energy released will heat the surface of the silicate core and flows into the

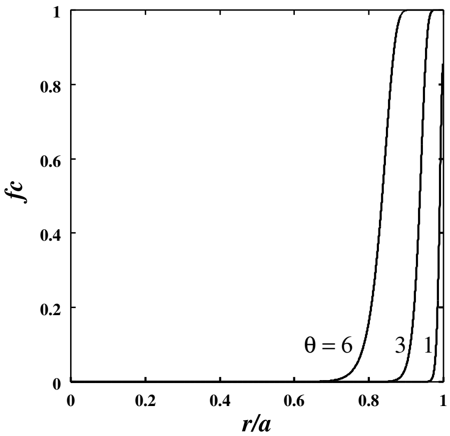

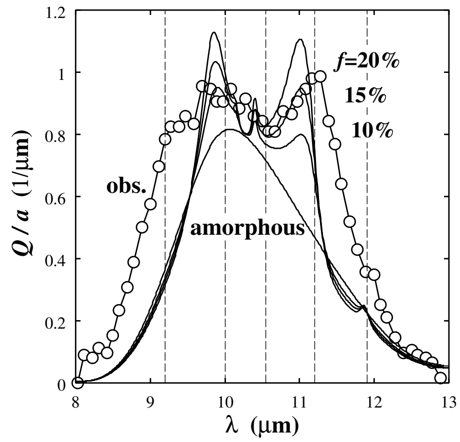

Figure 1. (Left) Degree of crystallinity f_c as a function of distance r from the center of a silicate core of radius a. See text for θ.

Figure 2. (Right) Comparison of the emissivity spectra of partially crystallized silicate grains with that of Comet Halley (Campins & Ryan 1989). The volume fraction of crystalline region is denoted by f.

core. This leads to crystallization of the amorphous silicate core from the surface towards the interior.

3. Results

The crystallization process proposed above is described by the rate equation of crystallization (Haruyama et al. 1993) and by the equation of heat conduction in an originally amorphous silicate core together with the initial condition of the instantaneous heat source on the silicate core surface. In the present model, the degree of crystallinity is determined by only one parameter θ defined by $\theta = k\Omega n_r h_r E_r / c_p (\pi \chi A)^{1/2} E_c$, where n_r is the number density of reactive molecules in the organic refractory mantle of thickness h_r, E_r is the amount of energy released per reaction, χ is thermal diffusivity of amorphous silicate, A is a time constant on the order of a period of lattice vibration, c_p is specific heat per unit cell, and E_c is activation energy of crystallization of amorphous silicate. The quantity of the largest uncertainty is n_r, which is estimated to be 10^{21} to 10^{22} cm^{-3} corresponding to the concentrations of reactive molecules of 1 to 10 % in the organic refractory. Possible values of θ are then estimated to be 0.6 to 6. Figure 1 shows the crystallization degree as a function of radial distance from the center of an originally amorphous silicate core, indicating that substantial crystallization occurs near the silicate core surface if $\theta > 1$. The volume fraction of the crystallized region in the silicate core is 2 to 40 % for $0.6 \leq \theta \leq 6$.

Does this degree of crystallinity explain the observed strength of the crystalline silicate feature? We focus on the strength of the major peaks at 10.0 and 11.2 μm due to crystalline olivine, and make Maxwell-Garnett calculations of the infrared spectra of the partially crystallized silicate grains (Greenberg et al. 1996). We used the complex refractive indices given by Scott & Duley (1996) for amorphous forsterite and those by Sogawa et al. (1999) for crystalline forsterite. The spectra for various volume fractions of the crystalline region are compared with the observed spectrum of Comet Halley (Campins & Ryan 1989) in Fig. 2 in terms of the emissivity Q. It is seen that the observed strengths of the main peaks of forsterite at 10.0 and 11.2 μm are realized for the crystalline volume fraction around 10 to 20 % in volume. The crystalline fraction that fits best to the observed spectra is about 15 %. Note that these crystalline fractions are in the range of those (2 to 40 %) expected from the present mechanism of crystallization.

4. Concluding Remarks

We have proposed a chemical heating model as a mechanism of crystallization of cometary silicate, and have shown that the chemical heating mechanism leads to the crystallization degree needed to explain the observed strength of the cometary crystalline features. It should be pointed out that the present crystallization mechanism needs neither high temperature to crystallize amorphous silicate nor mixing of amorphous and crystalline silicates, and furthermore can preserve volatiles of the interstellar composition. The mechanism will work for crystallization of grains in the objects other than comets as well as those in protoplanetary disks, if the θ-values of the grains there are large enough to induce crystallization and if moderate heating is available to trigger the chemical heating in the organic refractory mantles on the amorphous silicate cores. The experimental work is hoped to examine the present model.

Acknowledgments. We wish to dedicate this paper to the late Professor J. M. Greenberg, who encouraged us at an early stage of the present study.

References

Bregman, J. D., Campins, H., Witteborn, F. C., Wooden, D. H., Rank, D. M., Allamandola, L. J., Cohen, M., & Tielens, A. G. G. M. 1987, A&A, 187, 616

Campins, H., & Ryan, E. V. 1989, ApJ, 341, 1059

Greenberg, J. M. 1982, in Comets, ed. L. L. Wilkening, (Tucson: Univ. Arizona Press), 131

Greenberg, J. M., & Zhao, N. 1988, Nature, 331, 124

Greenberg, J. M., Li, A., Yamamoto, T., & Kozasa, T. 1996, in ASP Conf. Ser., 104, Physics, Chemistry, & Dynamics of Interplanetary Dust, eds. B. Å. S. Gustafson & M. S. Hanner, (San Francisco: ASP), 497

Hanner, M. S. 1999, Space Sci.Rev., 90, 99

Haruyama, J., Yamamoto, T., Mizutani, H., & Greenberg, J. M. 1993, J. Geophys. Res., 98, 15079

Scott, A., & Duley, W. W. 1996, ApJS, 105, 401

Sogawa, H., Kozasa, T., Koike, C., & Suto, H. 1999, in Proc. ISAS Lunar Planet. Symp., 32, eds. H. Mizutani & M. Kato, (Japan; ISAS), 179

Highlights of Astronomy, Vol. 13
International Astronomical Union, 2003
O. Engvold, ed.

Crystallization Of Silicate Particles By Shock Waves

Taishi Nakamoto

Center for Computational Physics, University of Tsukuba, Tsukuba 305-8577, Japan

Hitoshi Miura

Center for Computational Physics, University of Tsukuba, Tsukuba 305-8577, Japan

Abstract. Crystalline silicate dust particles have been found in some comets, though progenitors of those dust particles are thought to be amorphous. Here, the origin of the crystalline particles was investigated based on the shock-wave heating mechanism. We find that appropriate shock waves can crystallize amorphous dust particles and conditions of these shock waves (shock velocity and pre-shock gas density) are clarified.

The gas density in the solar nebula and the shock velocity that may be induced in comet forming regions by some mechanisms were discussed. It was suggested that comets formed in a region closer than about 20 AU to the Sun can contain the crystalline particles, whereas comets formed in a further region can hardly have them.

1. Introduction

Crystalline silicate dust particles have been found in some long period comets (Hanner *et al.* 1994). However, progenitors of those particles are thought to be amorphous. Thus, amorphous silicates are expected to be crystallized by some mechanism in the solar nebula or in comets, though the mechanism is not clearly understood.

Harker and Desch (2002) proposed that the shock-wave heating mechanism may be responsible for the crystallization of dust particles in comets. However, they showed the possibility of the mechanism for only a limited number of cases. It is still not clear to what extent the mechanism can be applied or if there are limitations to the mechanism.

Here, we propose that shock-wave heating can crystallize amorphous dust particles in comet forming regions. If there are appropriate shock waves, dust particles are heated and crystallized. Shock-wave heating has been investigated as a mechanism that formed chondrules in meteorites (e.g., Hood & Horanyi 1991; Iida *et al.* 2001). It seems that shock wave heating works not only in meteorite-forming regions, but also in comet-forming regions.

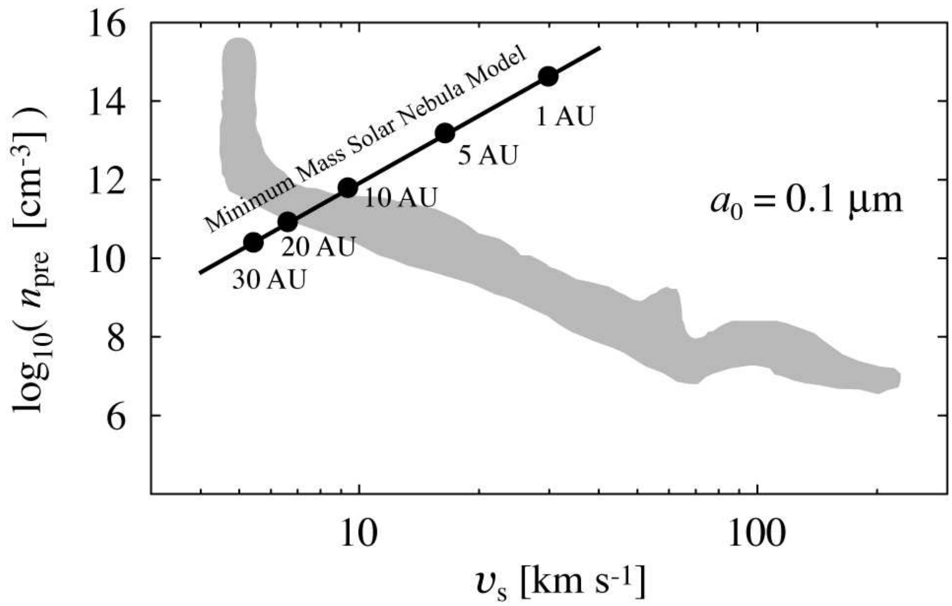

Figure 1. Conditions of shock waves for silicate crystallization.

2. Shock-Wave Heating Model

Basic mechanism of the shock wave heating is as follows. Let us suppose a shock wave passes a gas medium containing dust particles with a dynamical equilibrium, i.e., they do not have a relative velocity. Then the gas is accelerated and obtains some amount of velocity, while dust particles tend to remain in the initial position. The relative velocity between dust particles and gas causes drag heating. If the intensity of heating is high enough, dust particles can be crystallized.

We have developed the numerical model that simulates 1-dimensional plane-parallel steady shock flow including dust particles. In this model, the dynamics of the gas flow and the dust particles are treated in detail. Details of the model are described in Iida et al. (2001) and Miura & Nakamoto (2003).

Crystallization of dust particles is evaluated by the silicate evolution index (SEI) provided by Hallenbeck, Nuth, & Nelson (2000). This index was derived by a series of experiments of annealing. We calculate the SEI along the thermal history of the dust particle and evaluate if the particle is crystallized or not.

3. Silicate Crystallizing Shock Waves

We have carried out numerous calculations with various shock velocities and pre-shock gas densities and examined if those shock waves can crystallize the dust particles or not. Results for the initial particle radius $a_0 = 0.1\mu$m are summarized in Figure 1. Gray colored region represents shock wave conditions with which dust particles are crystallized properly.

4. Origin of Crystalline Dust in Comets

In order to clarify the origin of crystalline particles in comets, we should specify the nature of shock waves that might have crystallized dust particles in comet forming region. However, it is not easy to estimate the gas density and the flow velocity in the comet forming region in the solar nebula. One possible shock generation mechanism is the accretion flow from the parent molecular cloud core that generates shock waves at the surface of the disk. In this case, the velocity of the shock is expected to be of the order of $\sqrt{2}\,V_{\rm K}$, where $V_{\rm K}$ is the Kepler velocity of the disk. Since the shock velocity is high enough, the dust particles can be crystallized by those shock waves, if the gas density is adequate. On the other hand, some shock waves might be generated in the disk by some other mechanisms, such as the density waves induced by the gravitational instability (Wood 1984; Harker & Desch 2002), eccentric motion of planetesimals (Hood 1998), or another unknown mechanism. If this is the case, the shock velocity should be of the order of or less than $V_{\rm K}$. Here we assume that the solar nebula is represented by the minimum mass solar nebula model (Hayashi, Nakazawa, & Nakagawa 1985) and draw a line in Fig. 1 which shows the relation between the mid-plane gas density and the Kepler velocity. Then, we can see from Fig. 1 that the shock waves generated in a region $R \lesssim 20$ AU can crystallize dust particles, whereas shock waves in $R \gtrsim 20$ AU cannot. This suggests that comets that formed in the inner region of the disk ($R \lesssim 20$ AU), can be recognized as long period comets containing crystalline dust particles, while comets formed in the outer region of the disk ($R \gtrsim 20$ AU), such as the Jupiter-family comets, should not have crystalline dust particles if radial mixing due to diffusion does not take place in the disk.

Acknowledgments. TN was supported by Grant-in-Aid for Young Scientists (B) (14740284) of Japan Society for the Promotion of Science. HM was supported by the Research Fellowship of Japan Society for the Promotion of Science for Young Scientists.

References

Hallenbeck, S. L., Nuth, J. A., & Nelson, R. N. 2000, ApJ, 535, 247

Hanner, M., Lynch, D. K., & Russell, R. W. 1994, ApJ, 425, 274

Harker, D. E. & Desch, S. J. 2002, ApJ, 565, L109

Hayashi, C., Nakazawa, K., & Nakagawa, Y. 1985, in Protostars & Planets II, eds. D. C. Black & M. S. Matthews (Univ. of Arizona Press, Tucson), 1100

Hood, L. L. 1998, Meteor. Planet. Sci., 33, 97

Hood, L. L. & Horanyi, M. 1991, Icarus, 93, 259

Iida, A., Nakamoto, T., Susa, H., & Nakagawa, Y. 2001, Icarus, 153, 430

Miura, H. & Nakamoto, T. 2003, submitted to Icarus

Wood, J. A. 1984, Earth Planet. Sci. Lett. 70, 11

Highlights of Astronomy, Vol. 13
International Astronomical Union, 2003
O. Engvold, ed.

Collisional Simulations Of Cometary Nuclei

Sin-iti Sirono

Earth and Environmental Sciences, Nagoya University, Building E, Nagoya 464-8602, Japan

Abstract. Collisional simulations of cometary nuclei (icy dust aggregates) are conducted. Conditions for sticking are determined as a function of the impact velocity and mechanical properties of nuclei. Possible collisional outcomes in three evolutionary stages of icy-dust aggregates are discussed.

Comet nuclei are porous and believed to be aggregates of icy-dust grains (Greenberg 1982). There are three stages where collisions between icy-dust aggregates are important; 1) formation of Oort cloud (collisions between cometary nuclei; $V_{\mathrm{impact}} \sim 100\,\mathrm{m\,s^{-1}}$), 2) evolution of Kuiper belt objects (collisions between icy planetesimals; $V_{\mathrm{impact}} \sim 10 - 100\,\mathrm{m\,s^{-1}}$), and 3) formation of icy planetesimals (collisions between icy dust aggregates; $V_{\mathrm{impact}} \sim 10\,\mathrm{m\,s^{-1}}$). It was shown that the extent of fragmentation strongly affects the stages 1) (Stern & Weissman 2001) and 2) (Stern & Colwell 1997). In the stage 3), sticking of a dust aggregate is crucial for the formation of planetesimals. In this report, I investigate collisions between aggregates composed of icy dust grains and clarify conditions for sticking.

I performed collisional simulations of dust aggregates using an SPH code (Benz & Asphaug 1994). Details of simulations will appear soon (Sirono 2003, submitted to Icarus). In this code, a dust aggregate is treated as a continuum medium. This enables us to simulate aggregates of any large sizes up to $\sim$ 10km. This limit comes from ignorance of gravity force in this simulation.

There are two important mechanical properties of an aggregate to be included in the simulation. One is elasto-plastic deformation and the other is healing of fractures. An aggregate deforms elastically for sufficiently small external stresses. However, plastic deformation proceeds by re-arrangement of grains if a large stress is applied. A boundary between elastic and plastic deformation defines a yield surface, which is a hypersurface in a three dimensional space of principal components of a stress tensor. A stress tensor can be decomposed into two terms: hydrostatic pressure and deviatory stress. When pressure reaches compressive strength $\Sigma(\rho)$, irreversible compaction occurs and when pressure reaches tensile strength $-T(\rho)$, tensile fragmentation starts. For the deviatory part, we adopt the von Mises yielding criterion. If the second invariant of deviatory stress becomes larger than the square of yield strength Y^2, irreversible shear deformation takes place (Benz & Asphaug 1994). Here I assumed $\Sigma(\rho)$ and $T(\rho)$ vary as power laws of ρ as $\Sigma(\rho) = \Sigma_0\rho^6$ and $T(\rho) = T_0\rho^5$, and $Y(\rho)$ is given by $Y(\rho) = \sqrt{2T(\rho)\Sigma(\rho)/3}$.

When stress reaches the yield surface, fragmentation of an aggregate begins. The degree of fragmentation is expressed by the damage parameter D increasing

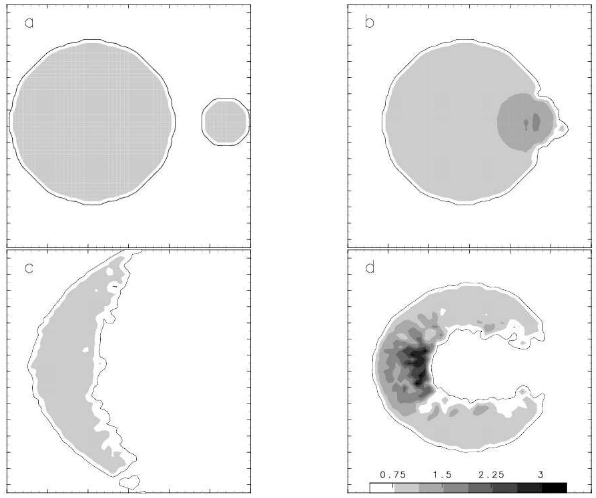

Figure 1. Density distributions of representative collisions. (a) Initial arrangement of an impactor (small sphere) and a target (large sphere). Size ratio is 10:3. (b) Sticking collision. $\Sigma_0 = 10^{-3}$, $T_0 = 10^{-2}$, and $M = 0.13$. (c) Catastrophic disruption. $\Sigma_0 = 10^{-2}$, $T_0 = 10^{-3}$, and $M = 0.13$. (d) Formation of a deep hole. $\Sigma_0 = 10^{-4}$, $T_0 = 10^{-3}$, and $M = 0.4$.

from 0 to 1 as reducing the strengths and elastic moduli by a factor of $1 - D$. When D reaches 1, the region cannot sustain any tensile and shear stresses.

A typical size of a composing grain is μm (Greenberg 1982). Because of its large surface to mass ratio, surface cohesion of a grain is effective. In this case, the damage due to the fracture can be restored by reconnection between grains followed by compaction of an aggregate. If this "healing effect" is effective, the damage parameter D can be reduced as compaction proceeds. I conducted both cases of simulations, with and without the healing effect.

The input parameters are the initial normalized compressive strength Σ_0, normalized tensile strength T_0 (both quantities are normalized with bulk modulus of an aggregate), and the impact velocity M which is normalized with the sound speed of an aggregate. In addition to these parameters, the impact angle is varied to simulate off-center collisions.

Figure 1 summarizes representative results of simulations. The gray contours of the figures shows density distribution of an aggregate and the scale is shown in the bottom of Fig 1d. The initial arrangement of a target (large sphere) and an impactor (small sphere) is shown in Fig 1a. A sticking case is shown in Fig 1b. The parameters are $\Sigma_0 = 10^{-3}$, $T_0 = 10^{-2}$, and $M = 0.13$. Note that the compressive strength is larger than tensile strength in this case. On the other hand, if the tensile strength is larger than the compressive strength, the outcome is catastrophic disruption as shown in Fig 1c. In this collision, the parameters are $\Sigma_0 = 10^{-2}$, $T_0 = 10^{-3}$, and $M = 0.13$. The healing effect is included in all three simulations shown in Fig 1. If the healing effect is not included, it was found that the outcome is catastrophic disruption even if the strength parameters are the same to those of Fig 1b.

An interesting outcome can be seen in Fig 1d. A deep hole is formed. The parameters are $\Sigma_0 = 10^{-4}$, $T_0 = 10^{-3}$, and $M = 0.4$. The aggregate is weaker and the impact velocity is higher than those of Fig 1b and c. The impactor perfectly sticks to the target. Behind the impactor, a hole is formed along the impactor path. Although we cannot identify in the figure, substantial amount of fragments is produced from the surface of the hole and floats inside the target. We might observe no apparent fragmentation like this simulation when the impactor hits the comet Tempel 1 in the Deep Impact mission (http://deepimpact.jpl.nasa.gov/) if the mechanical properties of the comet is highly compressive.

A set of conditions for sticking has been found by conducting simulations for various parameter values:

- $T_0 > \Sigma_0$
- $Y_0 > \Sigma_0$
- $M \lesssim 0.04$
- Healing effect.

If one of the parameters of a collision does not meet these conditions, an outcome of the collision will be cratering or catastrophic disruption. The third condition ($M \lesssim 0.04$) comes from the results of oblique impacts. If only head-on collision is concerned, the condition is $M \lesssim 0.13$.

The important parameter is the impact velocity M normalized with the sound speed of an aggregate. A possible range of bulk modulus of an icy aggregate is $8 \times 10^6\,\mathrm{erg\,cm^{-3}}$ at packing fraction of 0.1 (=90% porosity) to $4 \times 10^8\,\mathrm{erg\,cm^{-3}}$ at packing fraction of 0.3 (Sirono & Greenberg 2000). From these values, the sound speed varies from $9\,\mathrm{m\,s^{-1}}$ to $360\,\mathrm{m\,s^{-1}}$. Coming back to the three important stages of aggregate collisions and impact velocities noted in the beginning, we can draw the following conclusions.

- Formation of Oort cloud: Catastrophic disruption ($0.3 < M < 11$)
- Evolution of Kuiper belt objects: Catastrophic disruption ($0.03 < M < 11$)
- Formation of icy planetesimals: Sticking is possible ($0.03 < M < 1.1$)

References

Benz, W., & Asphaug, E. 1994, Icarus, 107, 98
Greenberg, J. M. 1982, in Comets, ed. L. L. Wilkening, 131
Stern, S. A., & Colwell, J. E. 1997, AJ, 114, 841
Stern, S. A., & Weissman, P. R. 2001, Nature, 409, 589
Sirono, S. & Greenberg, J. M. 2000, Icarus, 145, 230

Highlights of Astronomy, Vol. 13
International Astronomical Union, 2003
O. Engvold, ed.

Impacts onto Cometary Nuclei

Jacek Leliwa-Kopystynski

Institute of Geophysics, Warsaw University, Pasteura 7, 02-093 Warsaw, Poland; and Space Research Center of PAS, Bartycka 18A, 00-716 Warsaw, Poland

It is expected that the Deep Impact mission will hit the Comet Tempel 1 nucleus in July 4, 2005. So, modeling of the impacts onto icy/mineral granular and porous materials, and therefore low-dense media, are very relevant. A model of result of the impact onto icy-mineral-porous target is presented on the basis of many series of impact experiments performed in the laboratories. Experimental results are extrapolated to the Deep Impact scale and farther on, to the planetary scale of collisions, e.g., to impacts of the meteorites on comet nuclei. Crucial for modeling are the parameters of the medium forming the nucleus. The most important of them are the ice to total mass ratio and the porosity. Both are virtually unknown, so they are discussed within the large ranges. Self-references. Icarus, 131, 210-222, 1998; Planet. Space Sci., 48, 1437-1446, 2000; Icarus, 158, 516-531, 2002.

JD15

Elemental Abundances in Old Stars & Damped Lyman-Alpha Systems

Chairpersons: P.E. Nissen and M. Pettini

Editors: P.E. Nissen (Chief-Editor) and M. Pettini

Highlights of Astronomy, Vol. 13
International Astronomical Union, 2003
O. Engvold, ed.

Introduction to Joint Discussion 15: "Elemental Abundances in Old Stars and Damped Lyman-alpha Systems"

Poul E. Nissen

Department of Physics and Astronomy, University of Aarhus, Denmark

Max Pettini

Institute of Astronomy, University of Cambridge, UK

Different chemical elements are manufactured by stars of different masses and at different stages of evolution. The way that relative element abundances change with the overall metallicity is not only the empirical basis on which our knowledge of nucleosynthetic yields rests. Such measurements also provide vital clues to the origin of different stellar populations in the Milky Way Galaxy; to the star formation histories of nearby galaxies; and, as recognized most recently, to the nature of galaxies at high redshift seen in absorption against background quasars, such as the damped Lyman-alpha systems (DLAs).

Efficient high-resolution spectrographs on the new generation of 8-10 m class telescopes, such as HIRES on Keck I, UVES on the VLT, and HDS on the Subaru telescope, are producing stellar and DLA spectra of unprecedented quality in the visible and near UV region. Many research groups throughout the world are pursuing ongoing surveys of metal-poor stars and DLAs. This wealth of new data is advancing fast our knowledge of elemental abundances in a variety of astrophysical environments, both local and at high redshift, and providing new information on such fundamental problems as nucleosynthesis of the elements, chemical evolution of galaxies, formation of the first stars and galaxies, and the nature of the damped Lyman-alpha systems.

Astronomers working with stellar and DLA spectra share many common interests and face similar difficulties in the analysis and interpretation of their results. Examples are the derivation of reliable abundances from the observed spectra, the determination of elemental abundances as a function of stellar age and redshift, and the impact of the new data on current theories of nucleosynthesis and galaxy formation and evolution. And yet up to now there have been only limited opportunities for the Galactic and extragalactic communities to meet in a joint discussion. The IAU General Assembly in Sydney provided an ideal and most timely occasion for such a joint discussion. The following proceedings contain the invited review talks presented at JD15 and abstracts of contributed papers and posters.

Highlights of Astronomy, Vol. 13
International Astronomical Union, 2003
O. Engvold, ed.

Comparing Chemical Abundances of the Damped Lyα Systems and Metal-Poor Stars

Jason X. Prochaska

UCO/Lick Observatory, UC Santa Cruz, Santa Cruz, CA, 95064

Abstract. I briefly draw comparisons between the fields of damped Lyα and metal-poor stellar abundances. In particular, I examine their complementary age-metallicity relations and comparisons between the damped Lyα and dwarf galaxy abundance patterns. Regarding the latter, I describe a series of problems concerning associating high z damped Lyα systems with present-day dwarfs.

1. Introduction

I wish to first acknowledge the wisdom of the organizers for bringing the damped Lyα and metal-poor stellar abundance communities together in a Joint Discussion aimed at heightening communication and collaboration between the two fields. While previous conferences on chemical abundances have included members of each group, talks were generally organized such that we have talked to one another instead of with one another. From the perspective of a DLA researcher, the preceding 50 years of stellar abundance research is invaluable for drawing interpretations on nucleosynthesis from DLA observations. I suspect that as DLA abundance studies become a mature field, the stellar community will similarly gain from observations of these young, metal-poor galaxies.

The organizers charged me with reviewing the fields to open the JD. In Sydney, I briefly compared the observations, techniques of analysis, and major systematic uncertainties in each field. I then described a few areas of research where the fields clearly intersect and where a joint analysis impacts on theories of chemical evolution, nucleosynthesis, and galaxy formation. In this proceeding I present an even more brief summary.

2. Observations and Analysis

Presently, the data for damped Lyα and metal-poor stellar abundance research is acquired with the same telescopes on the same instruments and with comparable spectral resolution. Ionic transitions are analyzed in a similar fashion: integrated equivalent widths or column densities are derived from isolated, 'clean' lines while spectral synthesis or line-profile fitting techniques are applied to blended and crowded regions. The derivation of elemental abundances from the ionic measurements, however, follows different paths. For stellar abundances, one introduces a stellar atmosphere derived from the spectroscopic and/or photometric observations of the star. The atmosphere is typically parameterized by three parameters – temperature, gravity, and microturbulence – and one solves the radiative transfer equations to predict equivalent widths and/or spectral profiles. The uncertainties attributed to this modeling (e.g. non-LTE corrections; see M. Asplund's contribution) generally dominate the statistical errors associated with the observations.

With the DLA systems, one must consider ionization corrections to convert the measured ionic column densities into elemental abundances. In practice, the corrections are generally assumed to be small. This assumption is supported by theory and observation, although with exception (see Vladilo et al. 2001; Prochaska et al. 2002). The most important systematic error in the DLA analysis is dust depletion; the DLA observations provide gas-phase abundances which may significantly underestimate the true abundances of refractory elements like Fe, Cr, and Ni which deplete from the gas-phase onto dust grains (e.g. Jenkins 1987). This effect dominates the uncertainty of DLA abundance studies and plays a central role in nearly all interpretations drawn from the observations.

3. Age-Metallicity Relation (AMR)

One research area where the two fields nicely complement each other is in describing an age-metallicity relation (AMR). Stellar research has focused primarily on Galactic disk stars and therefore probes the chemical enrichment history of a single galaxy over the past ≈ 10 Gyr. Because of the uncertainties of isochrone fitting, it is difficult to determine absolute ages with meaningful precision for ages > 10 Gyr. In contrast, the DLA observations reveal the AMR of the population of high z galaxies which dominate the H I content of the universe. Therefore, the DLA trace the 'cosmic' mean metallicity in neutral gas (e.g. Prochaska et al. 2003). The ages of the DLA systems are precisely calculated by combining their cosmological redshift with the 'concordance cosmology' (e.g. Spergel et al. 2003). The challenge with DLA studies is pursuing the AMR to $z < 1.7$ because space-bourne UV observations are required to observe the Lyα profile. Therefore, the DLA and stellar abundance measurements complement one another both temporally (spanning nearly the entire history of the universe) and spatially (examining a single galaxy to a population of galaxies).

For very different reasons, the AMR's measured from Galactic stars and the DLA systems have had controversial histories. Indeed, my own studies have contributed to the controversy surrounding the AMR derived for the DLA systems (see also Kulkarni, this proceedings). In this case, the analysis has been limited by uncertainty relating to small sample size; even with 50 DLA systems there was no statistically significant evolution in the cosmic metallicity. Similarly, the AMR of the Galactic disk remains a point of great debate with competing groups arguing for and against any trend of metallicity with age (Edvardsson et al. 1993; Rocha-Pinto et al. 2000; Feltzing, Holmberg, & Hurley 2001; Ibukiyama & Arimoto 2002). It remains unclear to me whether the debate revolves around sample bias or age determinations.

These uncertainties aside, it is illustrative to compare AMR's taken from the two fields of research. In Figure 1, I present a census of DLA age-metallicity observations overplotted with one estimate of the Galactic AMR (Rocha-Pinto et al. 2000) and rough estimates for the age and metallicity of the Galactic bulge, thick disk, and halo stellar components. Clearly, the DLA systems at

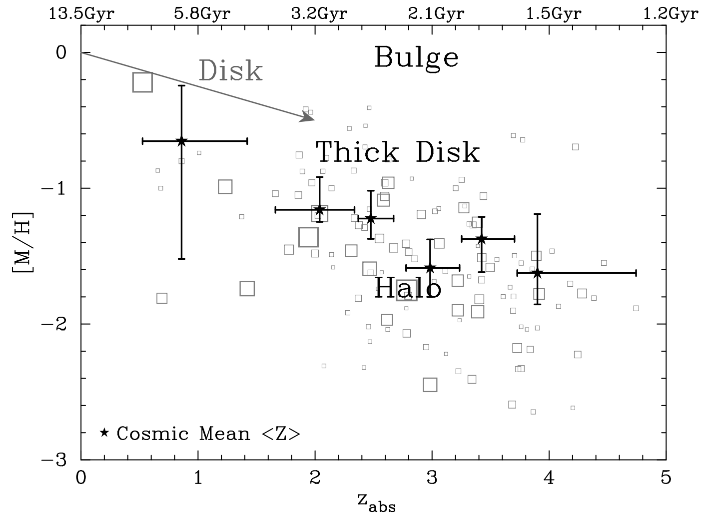

Figure 1. Age-metallicity relations for the DLA systems (summarized by the individual and binned data points) and the Galactic disk (solid arrow). The rough locations for the Galactic thick disk, halo, and bulge are also shown in the figure.

$z > 2$ are distinct in both metallicity and age from the Galactic disk AMR. As first noted by Pettini et al. (1997), the majority of DLA metallicities lie between the peaks of the distributions for the thick disk and halo populations. This indicates the majority of gas associated with the DLA systems at $z > 2$ may feed the formation of the thick disk and halo populations but has insufficient metallicity at these epochs to produce the majority of disk stars.

As the AMR's are refined and extended to include additional stellar populations and local galaxies as well DLA systems at $z < 1$, one will gain further insight into the nature of the DLA systems and their connection to modern galaxies. Future surveys will reveal whether a sample of metal-rich DLA exist at $z \sim 1.5$ which can be identified as the gas reservoirs of spiral disk formation. The identification of this gas is an important aspect of tracing the history of disk formation. In addition, age-metallicity measurements for high z galaxies (e.g. LBG, ERO's) will allow comparisons with the DLA and stellar populations, illuminating the processes of galaxy enrichment during the early universe.

4. DLA systems, Dwarf Galaxies, and the Galactic Halo

One of the most exciting aspects of connecting the fields of DLA and stellar abundance research is to draw comparisons between abundance patterns of local stellar populations and those observed in the early universe. Indeed, this was the focus of several talks and posters of this JD (e.g. Tolstoy, Bonifacio, Dessauges-Zavadsky). A principal challenge to drawing such comparisons is uncertainty in the DLA abundance patterns related to differential depletion. This point is well illustrated by Figure 2 where I present gas-phase Si/Fe ratios against metallicity for a sample of 56 DLA systems with echelle observations. As noted by Prochaska & Wolfe (2002), the metal-poor DLA systems exhibit

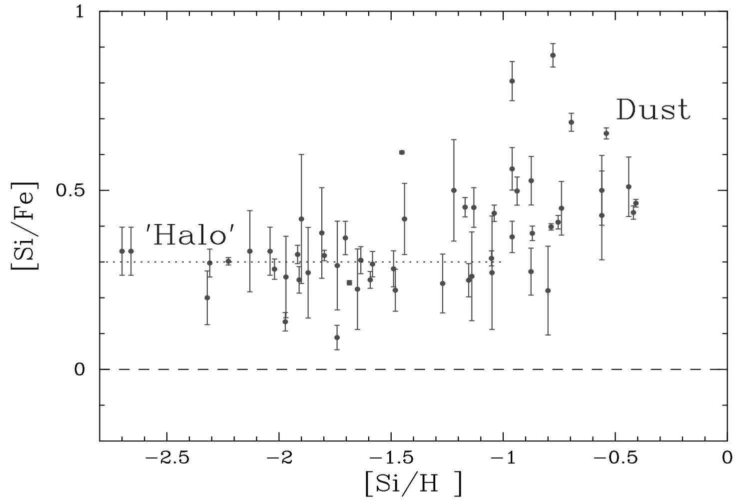

Figure 2. Gas-phase Si/Fe measurements for 56 DLA systems observed with echelle spectroscopy. At low metallicity, the Si/Fe values exhibit a 'plateau' at [Si/Fe] $\approx +0.3$ dex which matches the nominal value for the Galactic halo (dashed line; McWilliam et al. 1995). At higher metallicity, however, the Si/Fe values increase because of the effects of differential depletion (Fe is more readily depleted from the gas-phase onto dust grains).

[Si/Fe] values comparable to the Galactic halo with remarkably small scatter (particularly given that each data point represents a unique galaxy with its own specific chemical enrichment history). This Si/Fe plateau suggests the metal-poor DLA systems have been predominantly enriched by Type II supernovae, perhaps in the same manner as the Galactic halo. At higher metallicity, however, the Si/Fe ratios *increase*, in contradiction with any empirical or theoretical trends of chemical evolution. The rise in Si/Fe is explained by differential depletion; higher metallicity DLA systems have significant dust-to-gas ratios and a substantial fraction of their Fe is locked into dust grains. If one explains the rising Si/Fe ratios in terms of differential depletion, it raises the possibility that the enhancement of Si/Fe at all metallicity is dominated by differential depletion. Presumably, this interpretation would require an uncomfortable degree of fine-tuning to reproduce a [Si/Fe] plateau at [Si/H] < -1 which matches the nucleosynthetic enhancement of Si/Fe observed for the Galactic halo, yet more peculiar coincidences exist.

Presently, the majority of both communities favor imposing significant depletion corrections to the observed DLA abundances (e.g. Vladilo 2002). To estimate the corrections, one must assume the intrinsic value for the relative abundance of a refractory and non-refractory element and also assume a differential depletion pattern. Standard practice is to adopt an empirical depletion pattern based on ISM observations (e.g. Savage & Sembach 1996) and to assume [Zn/Fe] ≈ 0 intrinsically (i.e. attribute any departures from solar as depletion). Under this assumption, one finds that the majority of the DLA systems show nearly solar relative abundances at nearly all metallicity and redshift where Zn is observed. This leads to the conclusion that the relative abundances of the metal-poor DLA do not match Galactic metal-poor stars, specifically the enhanced α/Fe ratios observed for these stars (note the contradiction with my interpretation of Figure 2). Instead, these researches argue the DLA abundance patterns more closely resemble recent results for dSph and dIrr galaxies (e.g. Shetrone et al. 2001; Venn et al. 2003; Tolstoy et al. 2003).

At first glance, the correspondence between the DLA systems and dwarf galaxies is a comforting picture. In hierarchical cosmology, galaxies at $z \sim 2$ are actively merging to build-up our present-day galaxies. The DLA systems are identified with 'protogalactic clumps' within dark matter halos (Haehnelt et al. 1998; Maller et al. 2001) whose masses might be comparable to modern dSph and dIrr galaxies. For the following reasons, however, I contend that connecting the DLA systems to modern dwarf galaxies is premature and potentially in great conflict with hierarchical cosmology. Consider:

• In hierarchical cosmology, the majority of DLA systems will not evolve into present-day dwarf galaxies.

In order to explain the kinematic characteristics observed for the DLA systems (Prochaska & Wolfe 1997) within the paradigm of hierarchical cosmology, the 'protogalactic clumps' identified as DLA systems must arise predominantly in galaxies with $v_c > 125$ km/s (e.g. Maller et al. 2001). Furthermore, these clumps are actively merging with one another to build up the central galaxy of the dark matter halo. In this scenario, only a small fraction of the DLA population (presumably the low mass tail) could serve as the progenitors of present-day dwarfs; the majority will be merged into larger galaxies by $z \sim 1$. Therefore, any correspondence between the abundance patterns of the $z \sim 2$ DLA systems and present-day dwarfs may have to be considered a coincidence.

• Where is the gas enriched by Type II SN?

An important challenge raised by observers studying the elemental abundances of dSph in the Local Group is that these stars exhibit abundances which are very different from those measured for the Galactic halo (specifically, the Galactic halo within a few kpc of the Sun). This apparently contradicts the favored scenario for the formation of the Galactic halo in hierarchical cosmology, i.e., it formed from the accretion of dwarf satellites during the first few Gyr of the universe. One possible (and fashionable) resolution of this problem is that the dwarf galaxies which exist today (i.e. those which have not yet merged with the Milky Way) have had different chemical enrichment histories from those which merged to form the Galactic halo. As noted above, however, in CDM cosmology it is the DLA systems which correspond to the merging dwarfs. This identification leads to a more significant conflict regarding the origin of Galactic metal-poor stars. If we interpret the DLA abundance patterns as matching present-day dwarf galaxies, one is left with the problem: "Where is the gas enriched by Type II SN in the early universe which fueled the formation of the metal-poor stars of the Milky Way?"

• Ages, SFR, Zn, etc.

There are a number of other issues which may contradict or at least complicate the dwarf/DLA connection: (1) the ages of the DLA galaxies are too young to be consistent with the slow, steady SFH generally associated with dIrr galaxies; (2) SFR's derived for the DLA systems from the C II* absorption are typical of those expected for spiral disk galaxies (Wolfe, this proceedings); (3)

the DLA galaxies are gas-rich whereas the dSph galaxies are gas-poor. To link the two populations, one may require that the duty cycle for star formation in the dSph galaxies was significantly longer than the starburst behavior suggested by their stellar populations; and (4) the reported agreement between DLA and dwarf abundance patterns hinges on the assumption that [Zn/Fe]=0 intrinsically. If [Zn/Fe] is even +0.2 dex, then the DLA observations would be in good agreement with the Galactic halo abundance patterns. I note that several new issues related to the [Zn/Fe]=0 presumption were raised at the JD by Nissen, Asplund, and Israelian.

These issues aside, comparisons of the DLA and metal-poor stellar abundance patterns offer a powerful and insightful means of studying nucleosynthesis and galaxy formation. I am confident that ongoing studies of stellar populations in the Milky Way and Local Group as well as more comprehensive analysis of the DLA systems (e.g. Prochaska, Howk, & Wolfe 2003; Dessauges-Zavadsky, this proceeding) will lead to new puzzles and discoveries over the next years.

References

Edvardsson, B., Andersen, J., Gustafsson, B. et al. 1993, A&A, 275, 101

Feltzing, S., Holmberg, J., & Hurley, J.R. 2001, A&A, 377, 911

Haehnelt, M.G., Steinmetz, M. & Rauch, M. 1998, ApJ, 495, 647

Ibukiyama, A. & Arimoto, N. 2002, A&A, 394, 927

Jenkins, E.B. 1987, in Interstellar Processes, ed. D.J. Hollenbach and H.A. Thronson, Jr. (Boston: D. Reidel Publishing Company), p. 533

Maller, A.H., Prochaska, J.X., Somerville, R.S., & Primack, J.R. 2001, MNRAS, 326, 1475

McWilliam, A., Preston, G.W., Sneden, C., & Searle,L. 1995, AJ, 109, 2757

Pettini, M., Smith, L.J., King, D.L., & Hunstead, R.W. 1997, ApJ, 486, 665

Prochaska, J.X., Howk, J.C., O'Meara, J.M. et al. 2002, ApJ, 571, 693

Prochaska, J.X., Gawiser, E., Wolfe et al. 2003, ApJ, 595, L9

Prochaska, J.X., Howk, J.C., & Wolfe, A.M. 2003, Nature, 423, 57

Prochaska, J.X. & Wolfe, A. M. 1997, ApJ, 486, 73

Prochaska, J.X. & Wolfe, A.M. 2002, ApJ, 566, 68

Rocha-Pinto, H.J., Scalo, J., Maciel, W.J., & Flynn, C. 2000, A&A, 358, 869

Savage, B. D. and Sembach, K. R. 1996, ARA&A, 34, 279

Shetrone, M., Côté, P., Sargent, W.L.W. 2001, ApJ, 548, 592

Spergel, D.,N., et al. 2003, ApJS, 148, 175

Tolstoy, E., Venn, K.A., Shetrone, M. et al. 2003, AJ, 125, 707

Venn, K.A., Tolstoy, E., Kaufer, A. et al. 2003, AJ, 126, 1326

Vladilo, G., Centurión, M., Bonifacio, P., & Howk, J.C. 2001, ApJ, 557, 1007

Vladilo, G. 2002, A&A, 391, 407

Highlights of Astronomy, Vol. 13
International Astronomical Union, 2003
O. Engvold, ed.

Uncertainties in Stellar Abundance Analyses

Martin Asplund

Research School of Astronomy and Astrophysics, Mt Stromlo Observatory, Cotter Rd, ACT 2611, Australia

Abstract.
Over the last half-century quantitative stellar spectroscopy has made great progress. However, most stellar abundance analyses today still employ rather simplified models, which can introduce severe systematic errors swamping the observational errors. Some of these uncertainties for late-type stars are briefly reviewed here: atomic and molecular data, stellar parameters, model atmospheres and spectral line formation.

1. Introduction

In view of the central role stellar abundance analyses play in the endeavours to decipher the formation and evolution of stars, galaxies and indeed the Universe as a whole, minimizing systematic errors should be of utmost importance. Certainly, there are many potential fallacies that can be made in the process of going from an observed stellar spectrum to the extracted chemical composition of the star, all which deserve very careful consideration. Unfortunately, this is an area which often has not received the attention its importance warrants. Instead, still today most elemental abundance analyses of late-type stars rely on very simplified models for the stellar atmospheres and the spectral line formation processes. Unfortunately, the progress in modelling has not kept up with the dramatic improvements on the observational side over the last couple of decades, leaving the error budget normally dominated by systematic uncertainties.

Due to page restrictions this review focus only on the uncertainties in the derived elemental abundances introduced during the numerical analyses. Potential observational pitfalls such as signal-to-noise, resolving power, fringing, scattered light, continuum placement and blends can certainly also be major sources of error, but are not discussed here. Furthermore, the review is limited to late-type stars as they have traditionally been the most widely used beacons when tracing Galactic chemical evolution. The reader is referred to Werner et al. (2002) for an account of current hot star modelling, which is becoming increasingly important when probing environments beyond our own Galaxy.

2. Atomic and molecular data

The most obvious input data needed to derive elemental abundances is the transition probability, normally expressed as the gf-value. While there is always a continuing need for more and better data in this respect, the *overall situation* is in fact relatively good today. Provided the stellar spectroscopists are prepared to search the physics literature and databases, there are many accurate experimental and computational gf-determinations available (e.g. http://physics.nist.gov). The Kurucz database (http://kurucz.harvard.edu) is a very valuable resource but the drawback with such a large-scale computational effort is that individual transitions can be very erroneous, in particular when involving predicted energy levels. Other necessary data (continuous opacities, line broadening, dissociation energies etc) are also *in general* in reasonably healthy shape now (e.g. Seaton et al. 1994; Barklem et al. 2000), although improvements are certainly encouraged.

As will be discussed further below, the formation of a spectral line depends in principle not only on the line itself but on all other lines also, including those of other elements. In order to compute the statistical equilibrium of a species one needs not only transition probabilities for all relevant lines but also photo-ionization and collisional cross-sections. In terms of photo-ionization there has been marked improvements recently with the advent of large opacity calculations like the Opacity Project and Iron Project (e.g. Seaton et al. 1994). For elements up to the Fe-peak the situation is now fairly healthy for late-type stars. The most pressing uncertainty in non-LTE studies today is the cross-sections for collisional excitation and ionization with electrons and hydrogen atoms. The Opacity Project has partly addressed the case of electron collisions but most calculations largely rely on classical recipes like van Regemorter's (1963) formula. The situation for inelastic H collisions is even worse with the approach of Drawin (1968) mostly used. The few existing experimental and quantum mechanical calculations suggests, however, that the Drawin recipe over-estimates the cross-sections by about three orders of magnitude, at least for Na and Li (e.g. Fleck et al. 1991; Barklem et al. 2003). Whether this is true for all elements is not known. Clearly there is a great need for more quantum mechanical calculations addressing this fundamental problem.

3. Stellar parameters

We will here limit the discussion to methods more universally used, noting that in special situations other more accurate options are available (interferometry, eclipsing binaries etc).

Of the fundamental stellar parameters, $T_{\rm eff}$ is normally the most crucial in order to obtain accurate abundances. There exists a multitude of methods to determine $T_{\rm eff}$ of varying model dependence and reliability. Of these, the infrared flux method (IRFM, Blackwell & Shallis 1977) is often advocated as the best. IRFM is based on the ratio of bolometric flux ($\propto T_{\rm eff}^4$ and reddening- and model-independent) with an IR monochromatic flux ($\propto T_{\rm eff}$ and essentially reddening- and model-independent). If the problem of collecting sufficiently accurate (spectro-)photometry can be overcome, IRFM should yield temperatures to better than 50 K (Alonso et al. 1996). Photometric $T_{\rm eff}$ determinations can be almost as good when using colours like $V-K$ and $b-y$ (corrected for interstellar reddening if significant), in particular if calibrated to an IRFM- or interferometric temperature scale (Bessell et al. 1998). As always with theoretical colours, the zero-point is an outstanding issue.

In principle, hydrogen Balmer lines should be sensitive thermometers but practical problems unfortunately limit their usefulness, not the least observational. The Balmer lines are formed in deep atmospheric layers where convective energy transport is important for setting the temperature structure. The classical mixing length theory for convection in 1D models is unlikely to capture all aspects in this transition from convection to radiation, as will be further discussed below. The line broadening, including self-broadening, of the H lines have recently been improved (Barklem et al. 2002) but these results have not yet been fully disseminated into the wider astronomical community, leading to unnecessary additional errors. At solar metallicities H lines could in the best cases yield $T_{\rm eff}$ to within about 100 K but the uncertainties become progressively worse for metal-poor stars. The use of, for example, excitation balance of Fe I and other lines and various line-depth ratios can achieve highly precise *relative* temperatures for similar stars, but due to possible non-LTE and 3D effects can not be expected to give accurate *absolute* values. In summary, $T_{\rm eff}$ can under favourable circumstances be determined to within 100 K, which corresponds to abundance errors of typically 0.1 dex.

The surface gravities are often the most poorly constrained parameter. With the advent of the Hipparcos astrometry the situation has improved dramatically, at least for the stars sufficiently nearby to show measurable parallaxes. Knowing the parallax, the observed magnitude can be converted to a surface gravity: $\log g/g_{\odot} = \log\mathcal{M}/\mathcal{M}_{\odot} + 4\cdot\log T_{eff}/T_{\rm eff,\odot} + 0.4\cdot(M_{\rm bol} - M_{\rm bol,\odot})$. The uncertainty is normally dominated by the parallax error going into $M_{\rm bol}$ but if $\Delta\pi/\pi < 0.2$, $\log g$ can be determined to within 0.2 dex (e.g. Nissen et al. 1997). The Strömgren c_1-index and isochrone-fitting can also be employed to estimate $\log g$ but are more uncertain. The pressure-sensitive wings of strong lines, such as the Mg Ib triplet (Blackwell & Willis 1977) is a good gravity-meter with the caveat of potential systematic errors due to non-LTE and 3D effects, which have not yet been fully assessed. One of the most commonly used techniques is to force ionization balance between neutral and ionized species such as Fe I/Fe II and Ti I/Ti II. In the absence of any of the above-mentioned procedures, this is a viable option but it must be realised that the result may be very severe errors in $\log g$. Due to over-ionization of neutral minority species (e.g. Fe I) compared with the LTE predictions, this method typically underestimates the gravity by up to 0.5 dex or even more (Thevenin & Idiart 1999). For pressure-sensitive spectral features like molecular lines this can obviously be disastrous. A good habit is to ratio two equally gravity-sensitive species like C I, O I, S I and Fe II to obtain abundance ratios (e.g. Nissen et al. 2002, 2003; Akerman et al. 2003).

In view of the potentially large non-LTE effects and 3D effects on Fe I lines discussed below, the preferred choice for the metallicity determinations is no doubt Fe II lines, which are largely immune to such problems (e.g. Thevenin & Idiart 1999; Asplund et al. 1999). This should yield [Fe/H] values accurate to typically within $0.1 - 0.2$ dex, depending on how well $T_{\rm eff}$ and $\log g$ can be constrained. The alternative method of relying on colours, in particular Strömgren photometry, normally gives reasonable results with uncertainties $\lesssim 0.3$ dex when properly calibrated. Any error in [Fe/H] naturally directly propagates into the derived [X/Fe] ratios, re-enforcing the need for a simultaneous [Fe/H] determination together with the other elements rather than relying on literature values.

4. Stellar model atmospheres

The vast majority of abundance analyses of late-type stars rely on model atmospheres which are 1D, time-independent and hydrostatic, which assume LTE and treat convection with the rudimentary mixing length theory. Even a casual glance at the solar surface reveals that these assumptions and approximations are very disputable. The question is whether this propagates into significant systematic errors in the derived abundances. Recently, realistic 3D time-dependent hydrodynamical simulations of stellar surface convection and atmosphere with a detailed treatment of radiative transfer and state-of-the-art equation-of-state and opacities have become available for solar-type stars (e.g. Nordlund & Dravins 1990; Stein & Nordlund 1998; Asplund et al. 1999; Asplund & García Pérez 2001). They successfully reproduce a wide range of observational diagnostics (granulation topology, helioseismology, intensity brightness contrasts, spectral line shapes, shifts and asymmetries etc). It therefore appears that one can place a fairly high degree of confidence in their ability to describe the real stellar atmospheres, in spite of the simplifications necessary in order to carry out the simulations, most notably in terms of numerical resolution and radiative transfer. A notable achievement is that the traditional free parameters of stellar spectroscopy (mixing length parameters, micro- and macroturbulence) have become obsolete with 3D models, greatly reducing the uncertainties.

This new generation of 3D hydrodynamical model atmospheres have started to be applied to stellar abundance analyses. For the Sun, this has caused a very substantial reduction ($0.2 - 0.3$ dex) in the solar C, N and O abundances (Allende Prieto et al. 2001, 2002; Asplund et al. 2003b). For the first time, all different diagnostics (permitted, forbidden and molecular lines) give concordant abundances. The new results are also supported by the excellent agreement between observed and predicted line shapes and center-to-limb variations. Other, less temperature-sensitive elements like Si and Fe only show small ($\lesssim 0.05$ dex) 3D abundance corrections (Asplund et al. 2000). The exact 3D effects depend on the ionization stage, excitation potential and strength of the line in question.

The most dramatic differences with standard 1D analyses appear at low metallicities. Due to much lower temperatures in the optically thin layers in the metal-poor 3D models as a result of the shift in balance between expansion cooling and radiative heating, many spectral features are greatly affected (Asplund et al. 1999). In particular molecular lines, but also low excitation lines and neutral minority species, tend to have large negative 3D abundance corrections in metal-poor stars (i.e. 1D analyses *over-estimate* the abundances). As a result, Fe I lines are very unreliable but Fe II lines, which are formed in deeper atmospheric layers where the differences between 3D and 1D models are much smaller, are quite robust. In some cases additional 3D non-LTE effects can conspire to give final results quite close to the 1D non-LTE case, as for Li (Asplund et al. 2003a), but this is obviously not generally true. In the absence of detailed 3D non-LTE calculations, we advise against using Fe I and such species. Extreme caution must be exercised when relying on resonance and other low excitation lines (Al, Mg, Sr, Ba, Eu etc) in halo stars, where the systematic errors may well be $-0.3..-0.5$ dex. The largest errors, however, occur for molecular lines (Fig. 1) for which the 1D analyses can overestimate the abundances by up to 1.0 dex at [Fe/H] $= -3$ (Asplund & García Pérez 2001; Asplund 2003). Needless to say,

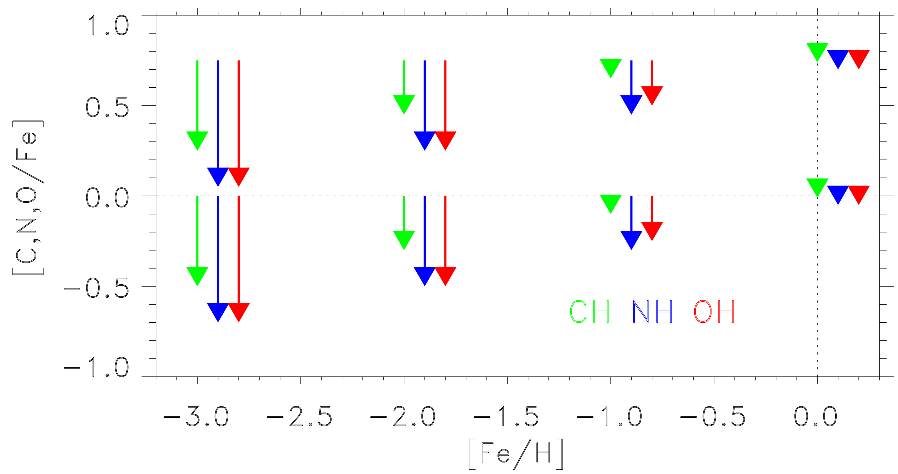

Figure 1. The typical 3D abundance corrections *relative to the Sun* for CH, NH and OH (A-X) lines reveal a strong metallicity dependence.

such large systematic errors can have a profound impact on the interpretations in terms of stellar nucleosynthesis and Galactic chemical evolution.

5. Spectral line formation

Spectral line formation essentially always occurs as a non-equilibrium process: under typical atmospheric conditions radiative rates dominate over collisional rates and the radiation field departs from the Planck function. *Non-LTE line formation* is therefore neither special nor unusual, while *LTE line formation* is: LTE is an extreme assumption, not a cautious middle-ground. Of course, in many incidences the different line formation processes are such that LTE-based abundances are indeed good approximations but that must always be confirmed a posteriori by detailed non-LTE calculations (e.g. Fe II). In general, non-LTE effects become progressively worse for higher T_{eff} (higher J_ν) and lower $\log g$ (less collisions) and [Fe/H] (less e^- collisions and stronger UV radiation field).

In spite of the availability of efficient and user-friendly non-LTE codes such as MULTI (Carlsson 1986), not enough work has been devoted to this important area. Amazingly, detailed non-LTE studies of solar-type and metal-poor stars have been undertaken for only a dozen elements or so. Typical non-LTE abundance corrections for halo stars are $0.2 - 0.3$ dex of either sign (e.g. Be II, O I, Mg I, K I, Ca I, Fe I, Sr II, Ba II) but significantly larger in cases like Al I and B I (Kiselman 1994). It is true that the poorly known H collision cross-sections introduce uncertainties (e.g. Korn et al. 2003) but calculations with and without the classical Drawin (1968) recipe should bracket the expected non-LTE effects; as already mentioned, the available evidence suggests that the Drawin formula over-estimates the H collisions by about three orders of magnitude.

The lack of non-LTE calculations for the majority of elements severely hampers our understanding of stellar nucleosynthesis and galactic chemical evolution. For example, it is not known whether the recently discovered upturn in [C/O] at the lowest [Fe/H] is due to C production in Pop III stars or can be explained by differential non-LTE effects between C I and O I (Akerman et al. 2003). Clearly, there is huge need for more non-LTE investigations for more elements.

Acknowledgments. I thank the organizers (Poul Erik Nissen and Max Pettini) and the other JD15 participants for creating a stimulating meeting. This talk is available at http://www.mso.anu.edu.au/~martin/talks/Sydney03_jd15).

References

Akerman, C.J., Carigi, L., Nissen, P.E., et al. 2003, A&A, in press
Allende Prieto, C., Lambert, D.L., & Asplund, M. 2001, ApJ, 556, L65
Alonso, A., Arribas, S., & Martinez-Roger, C. 1996, A&AS, 117, 227
Asplund, M., 2003, ApJL, submitted
Asplund, M., Carlsson, M., & Botnen, A.V. 2003a, A&A, 399, L31
Asplund, M., & García Pérez, A.E. 2001, A&A, 372, 601
Asplund, M., Grevesse, N., Sauval, A.J., et al. 2003b, A&A, submitted
Asplund, M., Nordlund, Å., Trampedach, R., & Stein, R.F. 1999, A&A, 346, L17
Asplund, M., Nordlund, Å., Trampedach, R., & Stein, R.F. 2000, A&A, 359, 743
Barklem, P.S., Belyaev, B.K., & Asplund, M. 2003, A&A, in press
Barklem, P.S., Piskunov, N., & O'Mara, B.J. 2000, A&AS, 142, 467
Barklem, P.S., Stempels, H.C., Allende Prieto, C., et al. 2002, A&A, 385, 951
Bessell, M.S., Castelli, F., & Plez, B. 1998, A&A, 333, 231
Blackwell, D.E., & Shallis, M.J. 1977, MNRAS, 180, 177
Blackwell, D.E., & Willis, R.B. 1977, MNRAS, 180, 169
Carlsson, M. 1986, Uppsala Astronomical Report No. 33
Drawin, H.W. 1968, Z. Physik, 211, 404
Fleck, I., Grosser, J., Schnecke, A., et al. 1991, JPhysB, 24, 4017
Kiselman, D. 1994, A&A, 286, 169
Korn, A.J., Shi, J., & Gehren, T. 2003, A&A, 407, 691
Nissen, P.E., Chen, Y.Q., Asplund, M., & Pettini, M. 2003, A&A, submitted
Nissen, P.E., Høg, E., & Schuster, W.J. 1997, in: ESA *Hipparcos* Symp., 225
Nissen, P.E., Primas, F., Asplund, M., & Lambert, D.L. 2002, A&A, 390, 235
Nordlund, Å., & Dravins, D. 1990, A&A, 228, 155
Seaton, M.J., Yan, Y., Mihalas, D., & Pradhan, A.K., 1994, MNRAS, 266, 805
Stein, R.F., & Nordlund, Å. 1998, ApJ, 499, 914
Thévenin, F., & Idiart, T. 1999, ApJ, 521, 753
van Regemorter, H. 1962, ApJ, 136, 906
Werner, K., et al. 2002, in: Stellar atmosphere modelling [astro-ph/0209535]

Highlights of Astronomy, Vol. 13
International Astronomical Union, 2003
O. Engvold, ed.

Stellar Abundances in Local Group Galaxies

Eline Tolstoy

Kapteyn Institute, Univ. of Groningen, the Netherlands

Kim Venn

Macalester College & Univ. of Minnesota, USA

Abstract. Here we describe some of our latest results from measuring detailed abundances in Local Group dwarf galaxies with the VLT. Combining spectroscopic abundances with Color-Magnitude diagrams allows the effective *measurement* of detailed chemical evolution with time in these galaxies. Although there are not yet significant numbers of individual stars observed in local group dwarf galaxies, the uniformity of the abundance patterns of the majority of stars in galaxies with very different star formation histories must hint at general properties of all star formation in these small systems.

1. The Fossil Record of the Early Universe

Low mass stars, such as those found on the Red Giant Branch (RGB), have long lifetimes, often comparable to the age of the Universe, and they have retained much of their original chemical composition in their atmospheres. These stars are thus very useful because they are fossils containing a direct measure of abundances and their evolution since the earliest times. This is what Freeman & Bland-Hawthorn (2002) have neatly termed *Chemical Tagging*.

The spectroscopic abundance measurements of individual stars on the RGB by definition break the age-metallicity degeneracy in determining the star formation histories of galaxies from Color-Magnitude Diagrams (CMDs). High resolution spectra give a much more accurate measure of the metallicity than can be obtained from CMD analysis alone. If we believe that theoretical stellar evolution tracks are reasonably accurate, then we can determine ages for all the stars for which we have measured a metallicity. These ages range from the earliest star formation in the Universe to 1−2 Gyr from the present day. Thus they enable a measurement of the chemical evolution variations within dwarf galaxies over almost the entire age of the (star-forming) Universe. With a large enough sample of stars we can determine the influence of gas and metal infall and outflow in the galaxy. We can determine the relative importance of different enrichment processes over time (e.g., Supernovae Ia and II, AGB stars, stellar winds and the like). We can re-examine our understanding of the nucleosynthesis of the elements, especially those that have many possible formation sites, *e.g.,* Ti, Mg/Ca, Cu/Fe, Zn/Fe, Y/Ba, Ba/Eu, Mg/Eu.

It is also possible to measure accurate abundances of relatively young stars in nearby galaxies to determine how the ongoing star formation we observe directly today in dwarf galaxies relates to past star formation. Dwarf galaxies can have extremely low metallicities and therefore enable us to study star formation in a regime which is more common at high-redshift.

As well as allowing us a better understanding of star formation and the effects it has on individual systems, spectroscopic abundances allow a comparison between the chemical signatures of stars found in dwarf galaxies with stars found in other environments, such as our Galaxy. This allows us to examine the theory that larger galaxies like our own were built up from small, dwarf galaxy sized clumps. It is clear from direct observations of the Universe at all redshifts that galaxies frequently merge with each other. Looking at the differences in properties of stars in small and large galaxies provides additional constraints on the likelihood and time scale of these merger events.

Dwarf galaxy size objects are believed to be the first structures to form in the early universe and thus they are potentially the sites of the formation of the first stars. Of course we have no guarantee that these first structures *were* actually dwarf galaxies that have survived until today but there is no evidence against this either. All dwarf galaxies for which sufficiently detailed observations exist have ancient stellar populations, which are most directly observed by the presence of a blue Horizontal branch in their CMD and/or an RR Lyr variable star population. There are a number of scenarios as to how the first stars may have formed, each with a distinct chemical signature for which we can test.

2. Measuring Chemical Evolution

There are several different approaches to measuring stellar abundances in nearby galaxies. Each has their own regime of validity and interest, and all contain the inherent assumption that the stellar abundances we observe are representative of the abundance of the gas out of which the stars were initially formed.

For the nearest dwarf galaxies, out to about 200 kpc from us, we can obtain high resolution spectra of individual RGB stars. This provides the most direct information about the chemical evolution of the host galaxy over the longest time baseline. These types of observations have been made with UVES (e.g., Shetrone et al. 2003; Tolstoy et al. 2003; Hill et al. 2000) and also at Keck with HIRES (e.g., Shetrone et al. 2001). High resolution spectra allow the determination of the abundance of a wealth of different chemical elements often from more than one spectral line. In each UVES spectrum, for example, there are around 100 lines of iron (Fe I and Fe II), there are also lines from α-elements (e.g., O, Ca, Mg, Ti), Fe-peak elements (V, Cr, Mn), and neutron capture elements (e.g., Y, Ba, La, Eu). Several of these elements are also frequently observed in high resolution absorption spectra of high-redshift damped Lyman-alpha (DLA) systems (e.g., Zn, Cr, Mn). Direct comparison can also be made with extensive spectroscopic surveys of stars in the Milky Way (e.g., Edvardsson et al. 1993; McWilliam et al. 1995; Fulbright 2002).

It is also possible to take lower resolution spectra of more simple metallicity indicators. For example the Ca II triplet at $\lambda\lambda$8500, 8544, 8665 Å is a well calibrated [Fe/H] indicator (e.g., Cole et al. 2000, 2003) which allows us to trace [Fe/H] with time using RGB stars. This has been successfully applied to several nearby galaxies, and allows us to survey galaxies out 1.5 Mpc, or almost

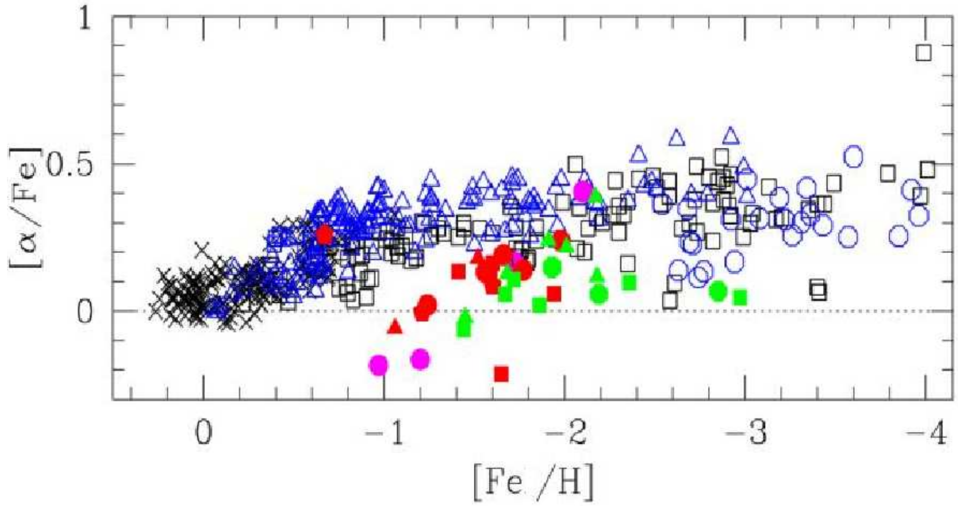

Figure 1. α-Element abundances from Shetrone et al. (2001) and Tolstoy et al. (2003) plotted versus [Fe/H] as filled symbols which represent the individual stars observed in Carina, Leo I, Sculptor, Fornax, Draco, Ursa Minor and Sextans dSphs. The crosses are Galactic disk star measurements from Edvardsson et al. (1993); the open squares are halo data from McWilliam et al. (1995) and the open circles and triangles are Galactic stars from Ryan et al. (1995) and Fulbright (2002). This plot highlights the differences between the α-element abundances observed in our Milky Way and in dwarf galaxies.

the entire volume of the Local Group (e.g., M31: Reitzel & Guhathakurta 2002; LMC: Olszewski et al. 1991, Cole et al. 2000; Fornax, Sculptor & NGC 6822: Tolstoy et al. 2001). Although this abundance measurement is quite basic (only providing information on Fe) many measurements can efficiently be made and this method can benefit greatly from multi-object instruments (e.g., VIMOS and FORS on VLT and DEMOS on Keck). In fact the wavelength range of the Ca II triplet is < 200Å, so a narrow band filter can enhance the multiplexing power of slit mask instruments many fold.

It is also possible to observe Blue Supergiants (BSGs) at high resolution to obtain more detailed abundance information for young stars in galaxies out to 1.5 Mpc distance. BSGs are much brighter than RGB stars, but they are also much younger. This means that they provide us with an accurate measurement of the *present day* metallicity in the galaxies where they are observed but they do not provide a *direct* measurement of chemical evolution, although they are of course the end product of galaxy evolution. Long observations with UVES at VLT (or HIRES on Keck) are typically required for these abundance studies. There have been several galaxies studied to date (e.g., M31, NGC 6822, WLM: Venn et al. 2000, 2001, 2003; Sextans A: Kaufer et al. 2003). These measurements can, of course, only be made in galaxies with recent star formation, i.e. dwarf irregulars rather than dwarf spheroidals where most of the detailed RGB abundances have been measured. Dwarf Irregulars are typically somewhat more massive than dSph and have arguably had an evolution less disturbed by close proximity to our Galaxy. These abundances can also be compared to H II

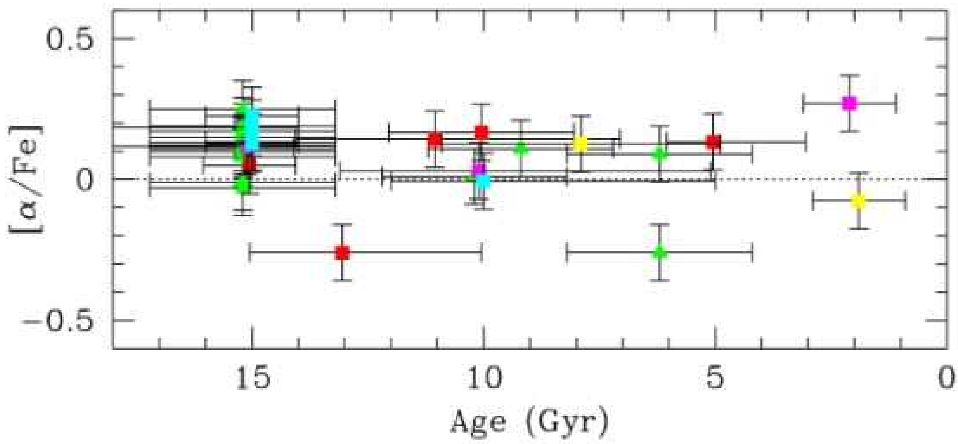

Figure 2. α-element abundance plotted against time. The age of each star is determined from an isochrone of the measured metallicity at the best fitting age. The objects plotted here are stars from the same galaxies listed in Figure 1. There is no obvious trend with age.

region metallicities, determined from emission line analysis of ionized gas. Both measures of current chemical enrichment in a galaxy are generally in agreement with each other, although some enigma remain (e.g., Venn et al. 2003).

3. Interpreting the Abundance Patterns

One of the, perhaps, most surprising results of the measurement of abundance ratios in RGB in dwarf spheroidal galaxies is that the α elements are typically found to be around solar and there is no apparent correlation between age and star formation history and α-abundance (see Figures 1 & 2). If we were to take the Milky Way as a template (e.g., Gilmore & Wyse 1991), for their [Fe/H] and especially for the oldest stars in each system we would expect dwarf spheroidals to have higher [α/Fe] than the average trend which is observed in Figure 1.

Although the number of stars with high resolution abundances in any given dwarf spheroidal to date is on average very small (around 5), the [α/Fe] measured is consistently low for all dSph despite widely varying ages, [Fe/H] and star formation histories. This suggests that for dSph the Galaxy is probably not the best template to interpret the observed abundances. It seems that low α-abundance need not mean stars which have been made from material which was enriched by SNIa explosion. It is possible for a low-α enrichment pattern to exist from very early on in the star formation history of a galaxy *before there has been any time for SNIa enrichment* (Tolstoy et al. 2003), unless we have significantly overestimated the SNIa time scale at low metallicities (not impossible). It is also possible to invoke AGB wind enrichment, as another mechanism to diminish [α/Fe], and account for the over-abundance of s-process elements (e.g., Ba, Y). However, the time scale for this to occur is also thought to be at least a giga-year after the onset of star formation and so this would have to occur more rapidly than current predictions suggest (also not impossible) to fully explain our observations.

It is also possible that the dwarf galaxies we observed may have an *effectively* truncated Initial Mass Function, in the sense of a lack of very high mass stars. This is not too hard to envisage as these dwarf galaxies are small systems with extremely low star formation rates throughout their history. They may not typically form very high mass molecular clouds, and thus the probability that a galaxy will form many (or even any) high mass stars is statistically low. This could explain the abundance patterns seen. In addition to the low α-element abundances observed, the enhanced abundance of the r-process element Eu, for example, is consistent with the scenario of predominantly low mass SNII in a slow evolving environment.

It is also possible that blow-out has played a significant role in the chemical evolution of these galaxies going back to the earliest times. But it would have to be quite selective (predominantly expelling α-elements for example), and consistent over a range of different galaxy masses (and types). Blowing up a small galaxy is "easy" in theory, (e.g., Mori, Ferrara & Madau 2001) but it is not so easy to find direct evidence of blow-out in a small galaxy with the confidence that the gas currently seen flowing out will never return (e.g., Martin et al. 2002). Determining if gas and/or metals will leave a galaxy for good is very sensitive to the structure of the ISM in a galaxy and whether or not it contains a significant gaseous halo, and how high the star formation rate can be at any given time.

It is also interesting to note that [α/Fe] measured in massive (young) BSG stars in dIrr galaxies is also low and thus unlike the Milky Way at the same [Fe/H] (e.g., Venn et al. 2001, 2003; Kaufer et al. 2003). Another class of object with low α-abundance measurements are damped Lyman-alpha systems (e.g., Nissen et al. 2003, submitted). That is not to say that they are necessarily dwarf galaxies but it appears that their chemical evolution has been similar to that of dwarf galaxies in the Local Group.

Looking at Figure 1 it is rather clear that significant numbers of stars from dwarf galaxies cannot be included in a merging formation scenario for our Galaxy *at any epoch*. Thus, dwarf galaxies *are not obvious hierarchical fragments*. The only way this aspect of standard hierarchical galaxy formation scenario can be retained is if the dwarf galaxies merged to form larger objects like the Milky Way *very* early in the Universe, before the majority of their stars were formed, while they were still gas rich.

4. In Summary

The results of our observations of high resolution abundances of a handful of individual stars in nearby dwarf galaxies suggest that the evolution of [Fe/H] with time is consistent with a closed box chemical evolution scenario, although the evidence is not very definitive with the current small samples. The role of outflows remains unclear. We note that, despite wide variations in star formation histories and [Fe/H] in dwarf galaxies, the [α/Fe] abundances are very similar and typically Galactic-disk-like solar values for the majority of the stars we observe. The iron peak elements observed are similar to the Galactic halo, but occur at *higher* [Fe/H]. Dwarf galaxies are thus not obvious hierarchical fragments. Their slow evolution apparently leads to distinctly different abundance patterns from those seen in the Milky Way.

To put our tentative results on a firmer basis requires spectra of many more stars in dwarf galaxies. We have in VLT/FLAMES the ideal instrument for this kind of study. We have put together a programme with the Dwarf Abundance Radial-velocity Team (DART, http::/www.astro.rug.nl/~dart) to use FLAMES to make detailed observations at high resolution of abundances of more than a hundred stars in each of three nearby dwarf spheroidal galaxies (Sculptor, Fornax and Sextans). This promises dramatic new data sets in the near future to answer many of the unresolved issues discussed here.

Acknowledgments. ET gratefully acknowledges salary and travel funds from a fellowship of the Royal Netherlands Academy of Arts and Sciences.

References

Cole A.A., Smecker-Hane T.A. & Gallagher J.S. 2000, AJ, 120, 1808
Cole, A.A. et al. 2003, MNRAS, in press (astro-ph/0309614)
Edvardsson B., Andersen J., Gustafsson B., et al. 1993, A&A, 275, 101.
Freeman, K. & Bland-Hawthorn, J. 2002, ARA&A, 40, 487
Fulbright, J.P. 2002, AJ, 123, 404
Gilmore G. & Wyse R.F.G. 1991, ApJL, 367, 55
Hill V., Franois P., Spite M., Primas F. & Spite F. 2000, A&A, 364, L19
Kaufer, A., Venn, K.A., Tolstoy E., & Pinte C. 2003, submitted to AJ
Martin, C.L., Kobulnicky, H.A., & Heckman, T.M. 2002, ApJ, 574, 663
McWilliam, A., Preston, G.W., Sneden, C. & Searle, L. 1995, AJ, 109, 2757
Mori, M., Ferrara, A. & Madau, P. 2002, ApJ, 571, 40
Olszewski, E.W., Schommer, R.A., et al. 1991, AJ, 101, 515
Reitzel, D.B. & Guhathakurta, P. 2002, AJ, 124, 234
Ryan, S.G., Norris, J.E., & Beers, T.C. 1996, ApJ, 471, 254
Shetrone M.D., Côté P. & Sargent W.L.W. 2001, ApJ, 548, 592
Shetrone, M., Venn, K.A., Tolstoy, E., et al. 2003, AJ, 125, 684
Tolstoy, E., Irwin, M.J., Cole, A.A., Pasquini, L., et al. 2001, MNRAS, 327, 918
Tolstoy, E., Venn, K.A., Shetrone, M., et al. 2003, AJ, 125, 707
Venn, K.A., McCarthy, J.K., Lennon, D.J., et al. 2000, ApJ, 541, 610
Venn K.A., Lennon D.J., Kaufer A., et al. 2001, ApJ, 547, 765
Venn, K.A., Tolstoy, E., Kaufer, A., et al. 2003, AJ, 126, 1326

Highlights of Astronomy, Vol. 13
International Astronomical Union, 2003
O. Engvold, ed.

The Early Chemical Evolution of Dwarf Irregular Galaxies

Gerhard Hensler[1,2], Simone Recchi[1,2], Joachim Köppen[2,3], Andreas Rieschick[2]

[1)] *Institute of Astronomy, University Observatory, Türkernschanzstr. 17, A–1080 Vienna, Austria*
[2)] *Institute of Theoretical Physics and Astrophysics, University of Kiel, Olshausenstr. 40, D–24098 Kiel, Germany*
[3)] *UMR 7550, Observatoire Astronomique de Strasbourg, 11 rue de l'Universit, F–67000 Strasbourg, France*

Abstract. Investigations have been performed to understand the age of dwarf irregular galaxies from the point of view of their presently low chemical abundances and the enhanced star-formation rate. While for a few objects, like e.g. I Zw 18, their assumed relative youth can be verified by models taking a double-starburst behavior into account, those dIrrs with old underlying stellar populations have passed the regime of observed N/O-O values within almost 2 Gyrs after their formation even with gas loss by means of supernova-driven galactic winds. Therefore alternative processes like gas infall must be invoked.

1. Introduction

Dwarf galaxies (DGs) serve as cornerstones for understanding the evolution of galaxies as well as for determining the basic cosmological model. On the one hand, they are invoked to be the building blocks for the accumulation of galaxy mass in the hierarchical CDM cosmology, while, on the other hand, their evolutionary paths from the formation to their fading and even their requested disappearance differ substantially. They seem to form at all cosmological epochs, by different processes and from different sources. Because of their low binding energy their evolution is strongly affected by internal and external energetic events thus leading to a wide variety of morphological types.

Dwarf elliptical galaxies e.g. are an extremely common and astrophysically interesting class of galaxies, because they seem to have formed preferably in dense environments. Objects of their extension to lower masses, the dwarf spheroidals (dSphs), are at present only detectable within the local group, where they appear as satellite galaxies in the vicinity of the large spiral galaxies (gSs), M31 and the Milky Way. Although their gas is easily evacuated by accumulated supernova explosions so that many dSphs have ceased their star formation (SF) showing only an intermediate-age stellar population (Hodge 1989, Grebel 1997), also more recent SF events have occurred in some objects. Those have experienced two to three short and episodic SF epochs interrupted by longer periods of quiescence. There does not exist a fully homogeneous picture of their evolution, because in some dSphs the metallicity increases with time, indicating that gas was partly kept in the system, while this is not the case in others.

Equivalently, the gas-rich variant of DGs, dwarf irregulars (dIrrs), show at present a large variety of SF rates from low to extraordinarily high values as e.g. in starbursts (SBDGs). Another mystery of dIrrs are their unusual abundances. As already demonstrated by Pagel (1985) some dIrrs, though with O abundances below 1/10 solar, show also low N/O ratios of up to 0.7 dex smaller than in gSs, with a large scatter and no significant correlation with O/H. Their regime of N/O-O values overlap with those of H II regions in the outermost disk parts of gSs at around 12+log(O/H) = 8.0 ... 8.5 (van Zee, Salzer, & Haynes 1998a). These two effects, namely, high SF rates that cannot be maintained for a Hubble time, and low metallicities challenge the picture of dIrrs to be unevolved systems in the early stage after their formation.

More detailed observations during the past years, however, have unveiled old underlying stellar components in most dIrrs like e.g. in NGC 1569 (Heckman et al. 1995) or NGC 1705 (Meurer et al. 1992). The newly formed stellar associations are often very massive and compact, called super star clusters (SSCs). Two possibilities are plausible to reduce the metal abundances in the presence of old stellar populations: loss of metal-enriched gas or infall of metal-poor to even pristine intergalactic gas. Garnett (2002) and van Zee (2001) have shown that the effective yield in dIrrs decreases for low-mass galaxies, what means that their element abundances, in particular O measured in H II regions, are smaller than those released by a stellar population and confined in a closed box. Nevertheless, three fundamental questions remain open: 1) Where would a forming dIrr be located in the N/O-O diagram during its early evolution? 2) If dIrrs are old can they still reach the observed N/O-O regime? And 3) Which physical process triggers such enormously high SF rates, while it is expected that due to the low gravitational trough SF should work extremely self-regulated in DGs (Köppen, Theis, & Hensler 1995, 1998)?

2. The Early Phases of dIrr Chemical Evolution

To study the first question we have performed *chemo-dynamical* numerical models of dIrrs' evolution. The *chemo-dynamical* prescription properly takes the energetics and dynamics of different gas phases, their mutual interactions and those of the star-gas coupling into account. The *chemo-dynamical* formulation in 1d and 2d dynamics with the "materialistic" and "energetic" equations is described e.g. in Theis, Burkert, & Hensler (1992) and Samland, Hensler, & Theis (1997), respectively. Its effects by application to dIrrs are various and demonstrated e.g. in Hensler, Rieschick, & Köppen (1999), Rieschick & Hensler (2000), Hensler & Rieschick (2002), Rieschick & Hensler (2003).

Our model starts from $10^{10}\,M_\odot$ baryonic mass with a Plummer-Kuzmin distribution over a radius of 20 kpc and a Dark Matter halo of $10^{11}\,M_\odot$ distributed according to Burkert (1995). The angular momentum is set according to the spin parameter λ=0.05. These initial conditions are chosen to represent a protogalactic gas cloud that has been ionized by the metagalactic radiation field until its cooling dominates and it collapses dissipatively. In addition, only the initial stellar mass function has to be fixed as a free parameter, because the other processes are determined by self regulation and formulated in accordance to results from empirical or theoretical studies.

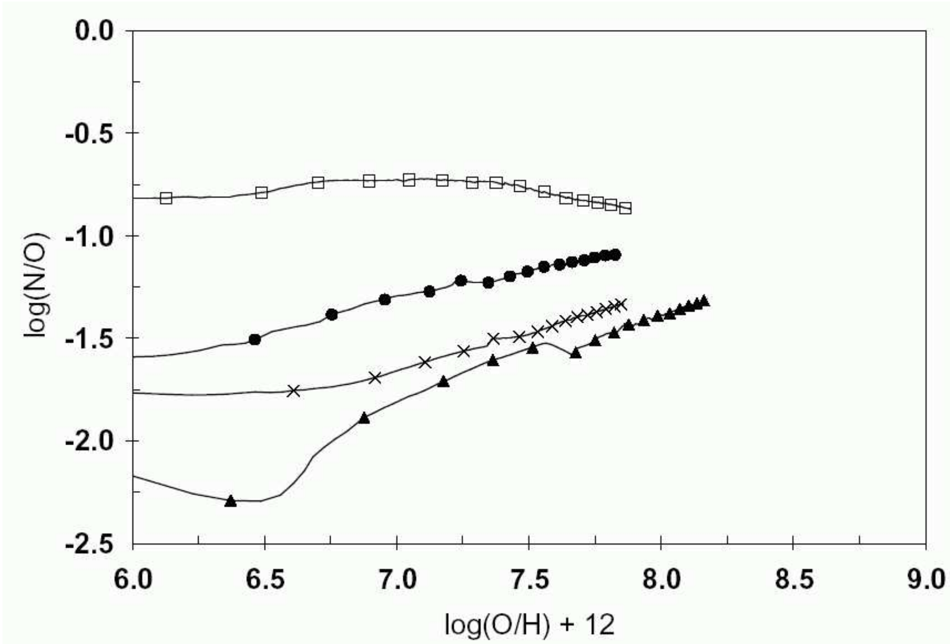

Figure 1. The N and O enhancement during the early evolution (2 Gyrs) for different regions of a representative dIrr that assembles a disk of $10^9\,M_\odot$: galactic disk (filled dots), central 1.5 kpc (open squares), a 5 kpc sphere without the disk (triangles), whole model galaxy (crosses).

Fig. 1 show the abundance evolution in different regions of the model for the first 2 Gyrs. One can discern that the central region reaches already solar values very rapidly, while the disk enhances O to 12+log(O/H) $\approx$ 7.8 at log(N/O) between -1.5 and -1.0. The curve smallest in N/O demonstrates that the halo is most O rich reaching 12+log(O/H) $\approx$ 8.2.

Conclusively, this *chemo-dynamical* model shows that dIrrs even with expulsion of O to the halo should evolve rapidly to the right-hand side in the N/O-O diagram only touching the observed regime of dIrrs at their upper N/O values. This evolutionary path is thus almost equal to the evolutionary tracks published for damped Lyα systems by Henry, Edmunds, & Köppen (2000). For the present conditions of dIrrs this means, that if they contain an old stellar population that has polluted the ISM with the elements under consideration and even with different effective yields due to gas loss by galactic winds, they are expected not to be located in the observed range of N/O-O.

3. The Evolution of I Zw 18

I Zw 18 was considered until recently as one of the best candidates for a truly "young" galaxy. However, recent HST observations were deep enough to resolve faint stars and thus to reveal an older stellar population. Quoting Östlin (2000) "We can thus conclude that all these different studies on independent sets of data in various spectral regions give the same answer: that I Zw 18 is an old

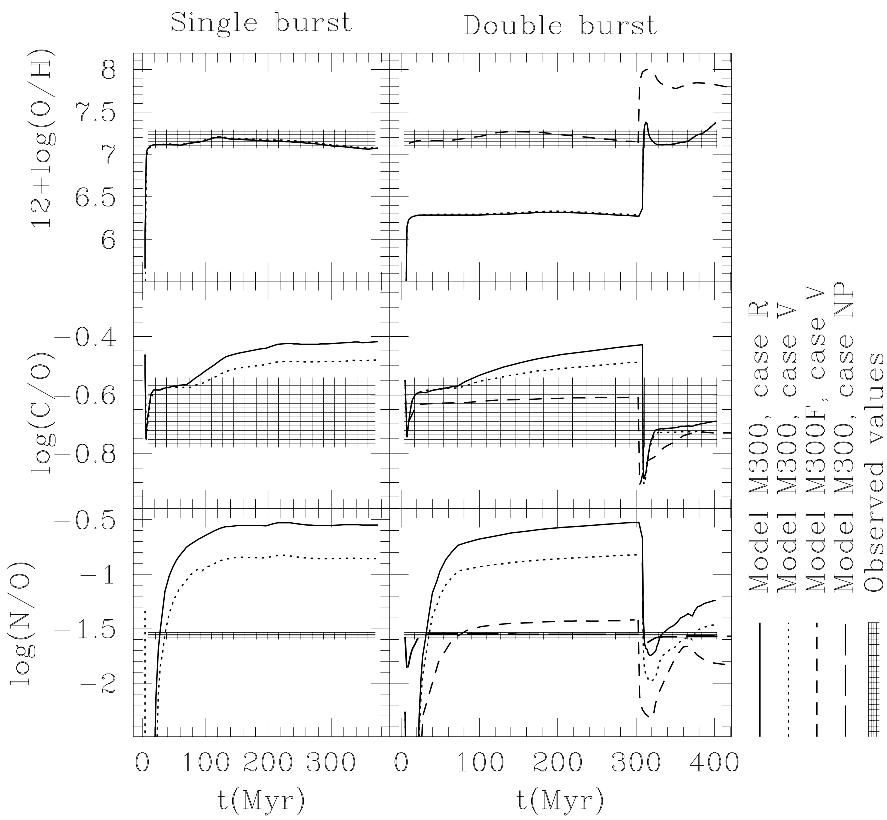

Figure 2. C, N, O evolution for the single-burst model (left panels) and double burst ones (right panels). Both sets of yields from intermediate-mass stars from Renzini & Voli (1981) (case R) and from van den Hoek & Groenewegen (1997) (case V) are implemented. Dashed line is a model with a flat (x=0.5) IMF, whereas all the other models assume a Salpeter IMF. Also shown, in the bottom-right panel, the evolution of N/O for a model (model NP) in which we assumed an "ad hoc" production of primary N in massive stars. The superimposed dashed areas represent the observational values found in literature for IZw18.

galaxy". But, "how old is old?". To address this question, we performed 2-D *chemo-dynamical* simulations of a model resembling I Zw 18, in order to put constraints on the past SF history of this object. Our models consider two possible evolutionary scenarios: bursting vs. continuous SF.

Two instantaneous bursts of SF are separated by a quiescent period of 300 Myr. Owing to the low luminosity of the first burst, a galactic wind does not develop. After 300 Myr, most of the gas mass in the central region is cold and dense, thus the onset of a second burst is likely. This second burst creates a strong galactic wind and the metals produced are easily channeled along the galactic chimney. We tested different chemical evolution yields and different IMFs. We conclude that, in order to reproduce the abundances and abundance ratios observed in I Zw 18, the age of the second burst of SF should be not more than 7 Myr (Fig. 2). Details about this set of calculations can be found in Recchi et al. (2002). Also remarkable is that most of the metal-enriched gas locked inside the galactic region (i.e. the region in which stars are present) cools in a relatively short time-scale, at variance with previous similar estimates.

We adopt the SF rate as suggested by Aloisi, Tosi & Greggio (1999), namely constant for almost 300 Myr with $6\times 10^{-3}\,M_\odot\ y^{-1}$, and superimpose a second, more vigorous burst of $3\times 10^{-2}\,M_\odot\ y^{-1}$, lasting for 5 Myr. The favored age of the last burst is, assuming this SF history, around 15 Myr. As discernible in Fig. 2 the model N/O is larger than observed. This is due to the fact that the last burst of SF is only 5 times more intense than the average SFR and lasts for only 5 Myr. The O production is not enough to compensate the N coming from intermediate-mass stars. There are indications (Chiappini et al. 2003) that the sets of yields of van den Hoek & Groenewegen (1997) overestimate N. Recent models of stellar evolution with rotation (Meynet & Maeder 2002) predict less N, although they do not take into consideration the third dredge-up. These models are much more promising in order to reproduce the chemical evolution of metal-poor systems.

We test also the effect of a cloudy medium, in which gas exchange processes by means of condensation and evaporation are acting between the cloud and the surrounding diffuse medium and to how it changes the chemical evolution. The time-scale for a complete evaporation of clouds is around 30 Myr. Only clouds outside the central region can survive after the first tens of Myr. In these models thus less energy is available to drive the galactic wind, but the difference with the "smooth" models is still small.

In conclusion, we can state that the last burst of SF in I Zw 18 is very young (less than 15 Myr), in agreement with other estimates (Hunt et al. 2003; Mas-Hesse & Kunth 1999). Stars older that 300 Myr are not required in order to reproduce the chemical composition of the neutral and ionized medium.

4. The Rejuvenation of dIrrs by Gas Infall

Instead of reducing the element abundances by means of galactic winds driven by different episodes of SBs (e.g. in the models by Garnett (1990), Pilyugin (1992), Marconi, Matteucci, & Tosi (1994)) it is also plausible that infall of gas reduces the abundances. Moreover, the SF triggered by gas infall would fit into this scenario. This seems to be proven observationally, because of the growing evidence that most SBDGs are surrounded by large H I reservoirs (e.g. NGC 4449: Hunter et al. 1998; I Zw 18: van Zee et al. 1998b). At least, their exist two clear indications that such gas like in the case of He 2-10 collides with the luminous stellar body of the dIrr producing several knots of SSCs (Kobulnicky et al. 1995) or like in NGC 1569 falls in (Stil & Isreal 2003) where two massive star clusters are ignited. This infall scenario has to be elaborated (Hensler et al. 1999; Hensler et al. 2003).

5. Acknowledgments

Parts of this project are supported by the Deutsche Forschungsgemeinschaft (DFG) under grants no. HE 1487/23 (AR) and HE 1487/28 (SR). SR acknowledges financial support from the Alexander von Humboldt Foundation. The attendance of the GA2003 in Sydney was enabled for GH by a DFG travel grant no. HE 1487/31. GH also thanks the organizers of JD 15 for their invitation.

References

Aloisi, A., Tosi, M., & Greggio, L. 1999, AJ, 118, 302
Burkert, A. 1995, ApJ, 447, L25
Chiappini, C., Romano, D., & Matteucci, F. 2003, MNRAS, 339, 63
Grebel, E. 1997, Rev. Modern Astron., 10, 29
Garnett, D.R. 1990, ApJ, 360, 142
Garnett, D.R. 2002, ApJ, 581, 1019
Heckman, T.M., Dahlem, M., Lehnert, M.D., et al. 1995, ApJ, 448, 98
Henry, R.B.C., Edmunds, M.G., & Köppen, J. 2000, ApJ, 541, 660
Hensler, G. & Rieschick, A. 2002, in ASP Conf. Ser. Vol. 285, Modes of Star Formation, ed. E. Grebel & W. Brandner, (San Francisco: ASP), 341
Hensler, G., Rieschick A., & Köppen, J. 1999, in ASP Conf. Ser. Vol. 187, The Evolution of Galaxies on Cosmological Timescales, ed. J. Beckman & T.J. Mahoney, (San Francisco: ASP), 214
Hensler, G., Köppen, J., Hirche, S., Pflamm, J., & Rieschick, A., 2003, in Symp. 217, ed. P.-A. Duc et al., in press
Hodge, P.W. 1989, ARA&A, 27, 139
Hunt, L., Thuan, T.X., & Izotov, Y.I. 2003, ApJ, 588, 281
Köppen, J., Theis, C., & Hensler, G. 1995, A&A, 296, 99
Köppen, J., Theis, C., & Hensler, G. 1998, A&A, 328, 121
Mas-Hesse, J.M., & Kunth, D. 1999, A&A, 349, 765
Marconi, G., Matteucci, F., & Tosi, M. 1994, MNRAS, 270, 35
Meurer, G.R., Freeman, K.C., Dopita, M.A., et al. 1992, AJ, 103, 60
Meynet, G., & Maeder, A. 2002, A&A, 390, 561
Östlin, G. 2000, ApJ, 535, L99
Pagel, B.E.P. 1985, in "Production and Distribution of C,N,O Elements", ed. I.J. Danziger, F. Matteucci, & K. Kjär, 155
Pilyugin, L.S. 1992, A&A, 260, 58
Recchi, S., Matteucci, F., D'Ercole, A., & Tosi, M. 2002, A&A, 384, 799
Rieschick, A., & Hensler, G. 2000, in ASP Conf. Ser. Vol. 215, Proc. III. Haro Conf., Cosmic Evolution and Galaxy Formation: Structure, Interactions, and Feedback, ed. J. Franco et al., (San Francisco: ASP), 130
Rieschick, A., & Hensler, G. 2003, A&A, submitted
Samland, M., Hensler, G., & Theis, Ch. 1997, ApJ, 476, 544
Stil, J.M. & Isreal, F.P. 2003, A&A, 392, 473
Theis, Ch., Burkert, A., & Hensler, G. 1992, A&A, 265, 465
van den Hoek, L.B., & Groenewegen, M.A.T. 1997, A&AS, 123, 305
van Zee, L. 2001, AJ, 121, 2003
van Zee, L., Salzer, J.J., & Haynes M.P. 1998a, ApJ, 497, L1
van Zee, L., Westphal, D., Haynes M.P., & Salzer, J.J. 1998b, AJ, 115, 1000

Highlights of Astronomy, Vol. 13
International Astronomical Union, 2003
O. Engvold, ed.

Nucleosynthesis in Population III Supernovae

K. Nomoto, K. Maeda, H. Umeda, N. Tominaga

Department of Astronomy, School of Science, University of Tokyo, Bunkyo-ku, Tokyo 113-0033, Japan

Abstract. Stars more massive than $\sim 20-25\ M_\odot$ form a black hole at the end of their evolution. Stars with non-rotating black holes are likely to collapse "quietly" ejecting a small amount of heavy elements (Faint supernovae). In contrast, stars with rotating black holes are likely to give rise to very energetic supernovae (Hypernovae). Nucleosynthesis in Hypernovae is characterized by larger abundance ratios (Zn,Co,V,Ti)/Fe and smaller (Mn,Cr)/Fe than normal supernovae, which can explain the observed trend of these ratios in extremely metal-poor stars. Nucleosynthesis in Faint supernovae is characterized by a large amount of fall-back. We show that the abundance pattern of the recently discovered most Fe-poor star, HE0107-5240, and other extremely metal-poor carbon-rich stars are in good accord with those of black-hole-forming supernovae, but not pair-instability supernovae. This suggests that black-hole-forming supernovae made important contributions to the early Galactic (and cosmic) chemical evolution as the First (Pop III) Supernovae.

1. Hypernova Branch and Faint Supernova Branch

Among the important developments in recent studies of core-collapse supernovae are the discoveries of two distinct types of supernovae (SNe): 1) very energetic SNe (Hypernovae), whose kinetic energy (KE) exceeds 10^{52} erg, about 10 times the KE of normal core-collapse SNe (hereafter $E_{51} = E/10^{51}$ erg), and 2) very faint and low energy SNe ($E_{51} \lesssim 0.5$; Faint supernovae, e.g., Zampieri, et al. 2003). These two types of supernovae are likely to be "black-hole-forming" supernovae with rotating or non-rotating black holes. Figure 1 shows E and the mass of ^{56}Ni ejected, $M(^{56}\mathrm{Ni})$, as functions of the main-sequence mass $M_{\rm ms}$ of the progenitor star obtained from fitting the optical light curves and spectra (Nomoto et al. 2003ab; Zampieri et al. 2003).

2. Hypernovae and Zn, Co, Mn, Cr

In core-collapse supernovae/hypernovae, iron-peak elements are produced in two distinct regions, which are characterized by the peak temperature, $T_{\rm peak}$, of the shocked material. For $T_{\rm peak} > 5 \times 10^9$K, material undergoes complete Si burning whose products include Co, Zn, V, and some Cr after radioactive decays. For $4 \times 10^9\mathrm{K} < T_{\rm peak} < 5 \times 10^9$K, incomplete Si burning takes place and its after decay products include Cr and Mn.

Nucleosynthesis with very large explosion energies has the following characteristics (Nakamura et al. 2001):

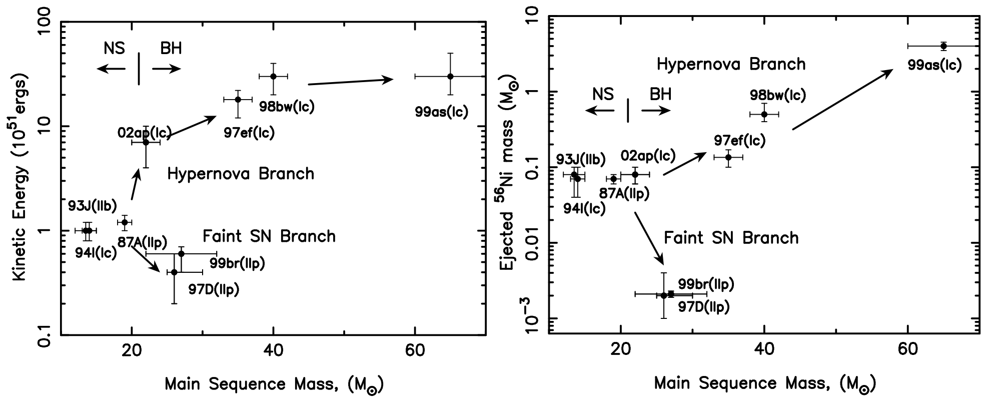

Figure 1. The explosion energy and the ejected ^{56}Ni mass as a function of the main sequence mass of the progenitors for several supernovae/hypernovae (Nomoto et al. 2003ab).

(1) Both complete and incomplete Si-burning regions shift outward in mass compared with normal supernovae, so that the mass ratio between the complete and incomplete Si-burning regions becomes larger. As a result, higher energy explosions tend to produce larger [(Zn, Co, V)/Fe] and smaller [(Mn, Cr)/Fe], which can explain the trend observed in very metal-poor stars (Umeda & Nomoto 2002, 2003b).

(2) In the complete Si-burning region of hypernovae, elements produced by α-rich freezeout are enhanced. Hence, elements synthesized through capturing of α-particles, such as ^{44}Ti, ^{48}Cr, and ^{64}Ge (decaying into ^{44}Ca, ^{48}Ti, and ^{64}Zn, respectively) are more abundant.

At early epochs the Galaxy was not yet chemically well-mixed, so that [Fe/H] may well be determined by a single SN event (Audouze & Silk 1995). Hypernovae with larger E are likely to induce the formation of stars with smaller [Fe/H], because the mass of interstellar hydrogen swept up by a hypernova is roughly proportional to E (Ryan et al. 1996; Shigeyama & Tsujimoto 1998) and the ratio of the ejected iron mass to E is smaller for hypernovae than for normal supernovae.

In the observed abundances of halo stars, there are significant differences between the abundance patterns in the iron-peak elements below and above [Fe/H]~ -2.5 to -3.

(1) For [Fe/H]$\lesssim -2.5$, the mean values of [Cr/Fe] and [Mn/Fe] decrease toward smaller metallicity, while [Co/Fe] increases (McWilliam et al. 1995; Ryan et al. 1996).

(2) [Zn/Fe]~ 0 for [Fe/H] $\simeq -3$ to 0 (Sneden, Gratton, & Crocker 1991), while at [Fe/H] < -3.3, [Zn/Fe] increases toward smaller metallicity (Primas et al. 2000; Blake et al. 2001).

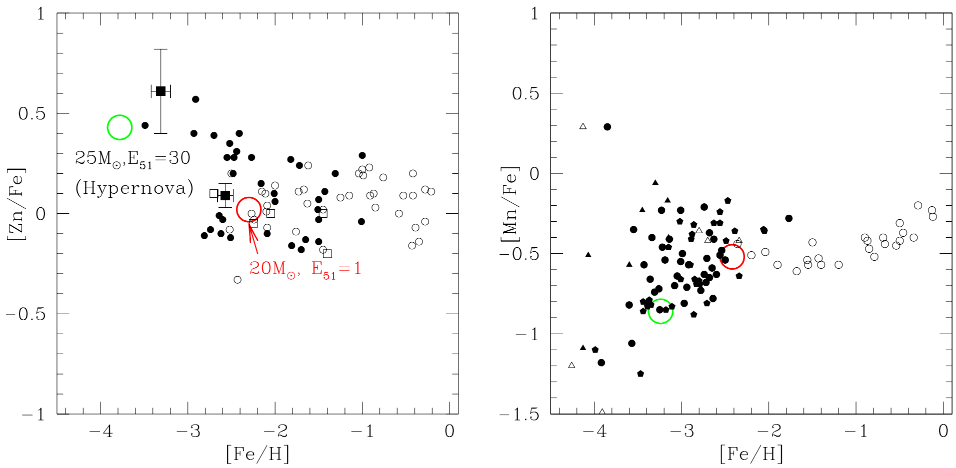

Figure 2. Observed abundance ratios of [Zn, Mn/Fe] vs [Fe/H] compared with the ($20M_\odot$, $E_{51} = 1$) and ($25M_\odot$, E_{51}=30) models (large open circles).

The larger [(Zn, Co)/Fe] and smaller [(Mn, Cr)/Fe] in the supernova ejecta can be realized if the mass ratio between the complete Si burning region and the incomplete Si burning region is larger, or equivalently if deep material from the complete Si-burning region is ejected by mixing or aspherical effects. This can be realized if (1) E is larger to move the outer edge of the complete Si burning region to larger M_r, or (2) asphericity in the explosion is larger.

A large explosion energy E enhances α-rich freezeout, which results in an increase of the local mass fractions of Zn and Co, while Cr and Mn are not enhanced (Umeda & Nomoto 2002, 2003b). Therefore, hypernovae could explain the large Zn and Co abundances and the small Mn and Cr abundances observed in very metal-poor stars (Fig. 2).

3. Extremely Metal-Poor (EMP) Stars

Recently the most Fe deficient and C-rich low mass star, HE0107-5240, was discovered (Christlieb et al. 2002). This star has [Fe/H] $= -5.3$ but its mass is as low as 0.8 $M_\odot$. This would challenge the recent theoretical arguments that the formation of low mass stars, which should survive until today, is suppressed below [Fe/H] $= -4$ (Schneider et al. 2002).

The important clue to this problem is the observed abundance pattern of this star. This star is characterized by very large ratios of [C/Fe] = 4.0 and [N/Fe] = 2.3, while the abundances of elements heavier than Mg are as low as that of Fe (Christlieb et al. 2002). Interestingly, this is not the only extremely metal poor star to exhibit large C/Fe and N/Fe ratios, but several other such stars have been discovered (Aoki et al. 2002).

3.1. The Most Fe-Poor Star HE0107-5240

We consider a model in which C-rich EMP stars are produced in the ejecta of (almost) metal-free supernova mixed with extremely metal-poor interstellar

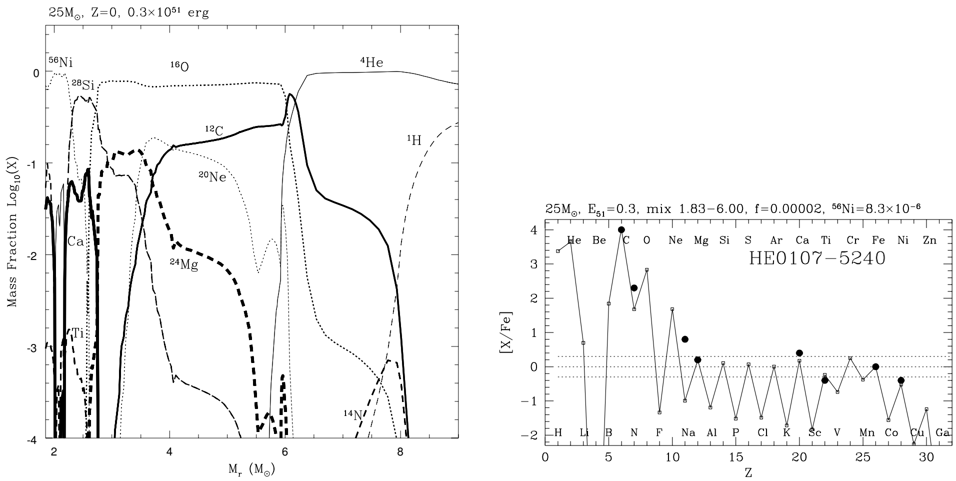

Figure 3. (left) The abundance distributions for the 25 $M_\odot$ model with the explosion energy $E_{51} = 0.3$. (right) Elemental abundances of the C-rich most Fe deficient star HE0107-5240 (filled circles), compared with a theoretical supernova yield (Umeda & Nomoto 2003a).

matter (Umeda & Nomoto 2003a). In Figure 3 (right) we show that the elemental abundances of one of our models are in good agreement with HE0107-5240, where the progenitor mass is 25 $M_\odot$ and the explosion energy $E_{51} = 0.3$.

In this model, explosive nucleosynthesis takes place behind the shock wave that is generated at $M_r = 1.8\ M_\odot$ and propagates outward. The resultant abundance distribution is seen in Figure 3 (left), where M_r denotes the Lagrangian mass coordinate measured from the center of the pre-supernova model (Umeda & Nomoto 2003a). The processed material is assumed to mix uniformly in the region from $M_r = 1.8\ M_\odot$ and 6.0 $M_\odot$. Almost all materials below $M_r = 6.0$ $M_\odot$ fall back to the central remnant and only a small fraction ($f = 2\times\ 10^{-5}$) is ejected from this region. The ejected Fe mass is $8 \times 10^{-6}\ M_\odot$.

The CNO elements in the ejecta were produced by pre-collapse He shell burning in the He-layer, which contains 0.2 $M_\odot$ of ^{12}C. Mixing of H into the He shell-burning region produces $4 \times 10^{-4}\ M_\odot$ of ^{14}N. On the other hand, only a small amount of heavier elements (Mg, Ca, and Fe-peak elements) are ejected and their abundance ratios are the average in the region of $M_r = 1.8 - 6.0$ $M_\odot$. The sub-solar ratios of [Ti/Fe] $= -0.4$ and [Ni/Fe] $= -0.4$ are the results of the relatively small explosion energy ($E_{51} = 0.3$). With this "mixing and fallback", the large C/Fe and C/Mg ratios observed in HE0107-5240 are well reproduced (Umeda & Nomoto 2003a). The "mixing and fall-back" effect may also be effectively realized in non-spherical explosions accompanying energetic jets (e.g., Maeda et al. 2002, 2003; Maeda & Nomoto 2003).

In this model, (N, Na)/Fe appear to be underproduced. However, N and Na can be produced inside the EMP stars through the C-N cycle, and brought up to the surface during the first dredge up stage while becoming a red giant star (Boothroyd & Sackmann 1999; Iwamoto et al., in preparation).

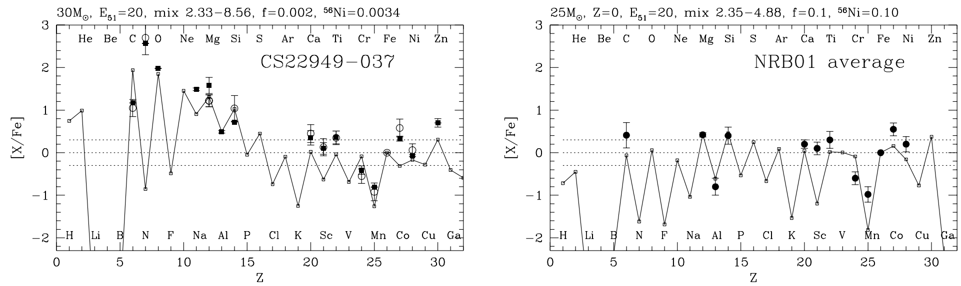

Figure 4. (left) Elemental abundances of CS 22949-037 (open circles for Norris et al. 2001, and solid squares for Depagne et al. 2002), compared with a theoretical supernova yield. (right) Averaged elemental abundances of stars with [Fe/H] = -3.7 (Norris et al. 2001) compared with a theoretical supernova yield (Umeda & Nomoto 2003ab).

3.2. Carbon-rich EMP stars: CS 22949-037 and CS 29498-043

The "mixing and fallback" scenario is commonly required to reproduce the abundance pattern of typical EMP stars. In Figure 4 (left) we show a model, which is in good agreement with CS22949-037 (Umeda & Nomoto 2003a). This star has [Fe/H] = -4.0 and is also C, N-rich (Norris, Ryan, & Beers 2001; Depagne et al. 2002), though the C/Fe and N/Fe ratios are smaller than in HE0107-5240. The model is the explosion of a 30 $M_\odot$ star with $E_{51} = 20$. In this model, the mixing region ($M_r = 2.33 - 8.56\ M_\odot$) is chosen to be smaller than the entire He core ($M_r = 13.1\ M_\odot$) in order to reproduce the relatively large Mg/Fe and Si/Fe ratios.

A similar degree of the mixing, but for a more massive progenitor, would also reproduce the abundances of CS29498-043 (Aoki et al. 2002).

We assume a larger fraction of ejection than in HE0107-5240, 2%, from the mixed region for CS22949-037, because the C/Fe and N/Fe ratios are smaller. The ejected Fe mass is 0.003 $M_\odot$. The larger explosion energy model is favored to explain the large Zn/Fe, Co/Fe and Ti/Fe ratios (Umeda & Nomoto 2002).

3.3. EMP Stars with a Typical Abundance Pattern

Similarly, the "mixing and fall back" process can reproduce the abundance pattern of the typical EMP stars without enhancement of C and N. Figure 4 (right) shows that the averaged abundances of [Fe/H] = -3.7 stars in Norris et al. (2001) can be fitted well with the model of 25 $M_\odot$ and $E_{51} = 20$ but with a larger fraction ($\sim 10\%$) of the processed materials in the ejecta. This yield (Umeda & Nomoto 2003b) is recommended as the averaged core-collapse SN yield to be used in chemical evolution models.

4. The First Stars

We have shown that the ejecta of black-hole-forming supernovae from $20 - 130$ $M_\odot$ stars can well account for the abundance pattern of EMP stars. In contrast, the observed abundance patterns, such as the large C/Fe observed in HE0107-5240 and other C-rich EMP stars, cannot be explained by pair-instability supernovae (PISNe) of $130-300\ M_\odot$ stars (Umeda & Nomoto 2002; Heger & Woosley 2002). The abundance ratios of iron-peak elements ([Zn/Fe] < -0.8 and [Co/Fe] < -0.2) in the PISN ejecta cannot explain the large Zn/Fe and Co/Fe observed in typical EMP stars nor in CS22949-037.

We thus propose that the first generation supernovae were the explosion of $\sim 20 - 130\ M_\odot$ stars and that some of them produced C-rich, Fe-poor ejecta. Then small mass stars with even [Fe/H] < -5 can form from the mixture of such a supernova ejecta with the (almost) metal-free interstellar medium, since the gas can cool efficiently thanks to the enhanced C and O abundances ([C/H]~ -1).

References

Aoki, W., Ryan, S.G., Beers, T.C., & Ando, H. 2002, ApJ, 567, 1166

Audouze, J., & Silk, J. 1995, ApJ, 451, L49

Blake, L.A.J., et al. 2001, Nucl. Phys. A, 688, 502

Boothroyd, A.I., & Sackmann, I.-J. 1999, ApJ, 510, 217

Christlieb, N., et al. 2002, Nature, 419, 904

Depagne, E., et al. 2002, A&A, 390, 187

Heger, A., & Woosley, S.E. 2002, ApJ, 567, 532

Maeda, K., Nakamura, T., Nomoto, K., et al. 2002, ApJ, 565, 405

Maeda, K., & Nomoto, K. 2003, ApJ, 598, in press (astro-ph/0304172)

Maeda, K., Mazzali, P.A., Deng, J., Nomoto, K., et al. 2003, ApJ, 593, 931

McWilliam, A., Preston, G.W., Sneden, C., & Searle, L. 1995, AJ, 109, 2757

Nakamura, T., et al. 2001, ApJ, 555, 880

Nomoto, K., et al. 2003a, in *IAU Symp 212*, p.395 (astro-ph/0209064)

Nomoto, K., et al. 2003b, in *Stellar Collapse* (astro-ph/0308136)

Norris, J.E., Ryan, S.G., & Beers, T.C. 2001, ApJ, 561, 1034

Primas, F., et al. 2000, in *The First Stars*, eds. A. Weiss, et al. (Springer), 51

Ryan, S.G., Norris, J.E., & Beers, T.C. 1996, ApJ, 471, 254

Schneider, R., Ferrara, A., Natarajan, P., & Omukai, K. 2002, ApJ, 571, 30

Shigeyama, T., & Tsujimoto, T. 1998, ApJ, 507, L135

Sneden, C., Gratton, R.G., & Crocker, D.A. 1991, A&A, 246, 354

Umeda, H., & Nomoto, K. 2002, ApJ, 565, 385

Umeda, H., & Nomoto, K. 2003a, Nature, 422, 871

Umeda, H., & Nomoto, K. 2003b, ApJ, submitted (astro-ph/0308029), http://supernova.astron.s.u-tokyo.ac.jp/~umeda/data.html

Zampieri, L., et al. 2003, astro-ph/0310057

Highlights of Astronomy, Vol. 13
International Astronomical Union, 2003
O. Engvold, ed.

Evolution of Metals and Stars in Damped Lyman-alpha Galaxies

Varsha P. Kulkarni

University of South Carolina, Dept. of Physics and Astronomy, Columbia, SC 29208, U.S.A.

Abstract. Damped Lyman-alpha absorbers in quasar spectra provide a unique tool to directly measure the abundances of elements in galaxies at redshifts $0 < z < 5$, and hence probe the chemical evolution of galaxies over $> 90\%$ of the age of the Universe. Since cosmic chemical evolution models predict the global metallicity of galaxies to increase with time, it is of great interest to determine whether DLAs actually show such a trend. We discuss statistical analysis of existing DLA Zn data to examine the metallicity-redshift relation, and a comparison of the observed data with models of cosmic chemical evolution. We also describe efforts to expand the DLA abundance sample at $z < 1.5$, where the current data are particularly sparse. Finally, we discuss emission-line imaging studies of the absorber galaxies and compare constraints on their star formation rates with models based on the global star formation history.

1. Introduction

The damped Lyman-alpha (DLA) absorption systems in quasar spectra have high H I column densities $N_{\rm HI} \geq 2 \times 10^{20}$ cm^{-2}, and contain most of the neutral gas in galaxies, nearly enough to form all of the stars visible today (Wolfe et al. 1995). DLAs are therefore expected to shed light on the history of star formation and heavy element production in galaxies. Furthermore, DLAs are selected only by the presence of high H I column density, regardless of the apparent brightness of the underlying galaxy. Therefore they are expected to offer a relatively unbiased representation of normal galaxies.

The exact nature of DLAs and their relation to present-day galaxies is not quite clear. But DLAs are presently our principal source of information about the chemical content of normal high-z galaxies, since spectroscopic studies have yielded abundances for a large range of elements in a substantial number of DLAs. Several emission-line imaging searches for DLAs have also tried to constrain the star formation rates in these objects. The combination of spectroscopic and imaging information can make DLA observations a powerful tool for understanding the history of element production and star formation in galaxies.

2. Evolution of Metallicity

2.1. Constraints from the Existing Data

Several studies of element abundances in DLAs have been carried out using data from 4-m and 8-m class optical telescopes (e.g., Meyer, Welty, & York 1989; Lu et al. 1996; Kulkarni et al. 1996; Kulkarni, Fall, & Truran 1997; Pettini et al. 1994, 1997; Prochaska & Wolfe 1999, 2000; Prochaska et al. 2001, 2003; and references therein). Zn is considered a good probe of the total (gas + solid phase) metallicity in DLAs because Zn tracks Fe in most Galactic stars, it is undepleted on interstellar dust grains, and the lines of the dominant ionization species Zn II are often unsaturated. The N_{HI}-weighted mean metallicity,

$$\overline{Z} = \frac{\Sigma N(\mathrm{Zn\,II})_i / \Sigma N(\mathrm{H\,I})_i}{(\mathrm{Zn/H})_\odot} Z_\odot, \tag{1}$$

is a good measure of the global mean metallicity (Kulkarni & Fall 2002).

Most cosmic chemical evolution models ranging from analytical studies to hydrodynamical simulations predict the global metallicity to rise from nearly zero at high z to nearly solar at $z = 0$ (e.g., Malaney & Chaboyer 1996; Pei & Fall 1995; Pei, Fall, & Hauser 1999; Somerville et al. 2001; Tissera et al. 2001). The present-day mass-weighted mean metallicity of local galaxies is indeed nearly solar (e.g., Kulkarni & Fall 2002). If DLAs trace an unbiased sample of normal galaxies, their interstellar mean metallicity may also be expected to rise with time. It is therefore of great interest to ask whether or not DLAs actually show this trend. Surprisingly, there has been great debate about this issue, with most studies advocating no evolution in the global mean metallicity (Pettini et al. 1997, 1999; Prochaska & Wolfe 1999; Vladilo et al. 2000; Prochaska & Wolfe 2000; Savaglio 2000; Prochaska et al. 2001; Prochaska & Wolfe 2002).

We have examined this question by compiling 57 DLA Zn measurements for $0.4 < z < 3.4$ from the literature (36 detections and 21 limits; Kulkarni & Fall 2002). We applied a variety of statistical techniques, including a binned linear χ^2 fit to $\overline{Z}$ vs. z, an unbinned $N(\mathrm{H\,I})$-weighted nonlinear χ^2 fit to an exponential relation, survival analysis to treat limits on Zn, and a comparison of data with chemical evolution models. Fig. 1 shows the $N(\mathrm{HI})$-weighted mean metallicity $\bar{Z}$ vs. redshift relation. Treating limits with survival analysis, the slope of the metallicity-redshift relation is -0.26 ± 0.10, consistent at the $\approx 2 - 3\,\sigma$ level both with model predictions (-0.25 to -0.61) and with no evolution. Recently, Prochaska et al. (2003) have reported a similar value for this slope (-0.26 ± 0.07) using Zn data in 11 DLAs together with Fe, Si, S, or O data for 114 other DLAs. These studies suggest that there may be some metallicity evolution in DLAs.

2.2. Improving the Statistics at $z < 1.5$

The main reason for the large uncertainty in the slope of the metallicity-redshift relation is the small number of measurements, especially at $z < 1.5$. Most previous DLA Zn studies have focused on $z > 1.5$ because the Zn II $\lambda\lambda$ 2026, 2062 lines lie in the ultraviolet (UV) for $z < 0.6$, and the Lyman-α line lies in the UV for $z < 1.6$. For $0.6 < z < 1.3$, the Zn II lines can be accessed with ground-based telescopes, but lie at blue wavelengths where most spectrographs have lower sensitivity. It is very important to obtain more data at $z < 1.5$, because this regime spans $\sim 70\%$ of the age of the Universe (for $\Omega_m = 0.3$, $\Omega_\Lambda = 0.7$). The low-z data have great leverage on the slope of the metallicity-redshift relation, and can clarify the relation of DLAs to present-day galaxies.

To improve the statistics of the metallicity-redshift relation at intermediate redshifts, we have recently started a survey of element abundances for DLAs

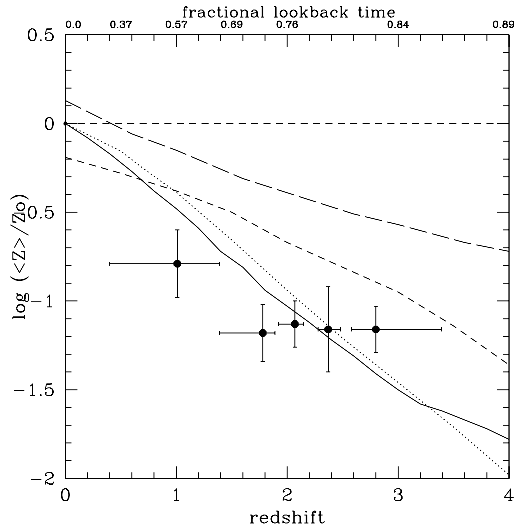

Figure 1. N(HI)-weighted mean Zn metallicity vs. redshift for DLAs (Kulkarni & Fall 2002). Vertical error bars denote 1 σ uncertainties. Horizontal bars denote redshift spreads in each bin. Short-dashed, dotted, solid, and long-dashed curves show, respectively, the mean metallicity in models of Malaney & Chaboyer (1996), Pei & Fall (1995), Pei et al. (1999), and Somerville et al. (2001). The nonlinear scale on the top x-axis denotes fractional look-back time for $\Omega_m = 0.3$ and $\Omega_\Lambda = 0.7$.

at $0.6 < z < 1.5$ using the blue channel spectrograph on the Multiple Mirror Telescope (MMT). These spectra have resolution of ≈ 75 km s^{-1}, while the S/N near the Zn II λ 2026 line is 25–130 for most objects. A wide range of Zn II line strengths is seen among the DLAs in our sample (Khare et al. 2003).

We are also carrying out a study of element abundances in DLAs at $0.1 < z < 0.5$ with the Hubble Space Telescope. Most of these have log $N_{\rm HI} > 20.9$ and are relatively important in determining the $N_{\rm HI}$-weighted mean metallicity at low redshifts. The observations are being obtained with the Space Telescope Imaging Spectrograph (STIS) CCD and near-UV Multi-Anode Micro-channel Array (MAMA), at dispersions of 0.09 or 0.15 Å, and are being analyzed with IRAF/STSDAS. Together, our MMT and HST data have so far doubled the $z < 1.5$ DLA Zn sample. These and future data at $z < 1.5$ will help to clarify whether or not the global mean metallicity in DLAs shows evolution.

3. Star Formation History

Closely related to the history of metal production is the history of star formation. The cosmic star formation history has been estimated on the basis of deep galaxy imaging surveys such as the Canada-France Redshift Survey (Lilly et al. 1996) and the Hubble Deep Field (HDF; Madau et al. 1996, 1998). It is interesting to compare the star formation history of DLAs to the global star formation history.

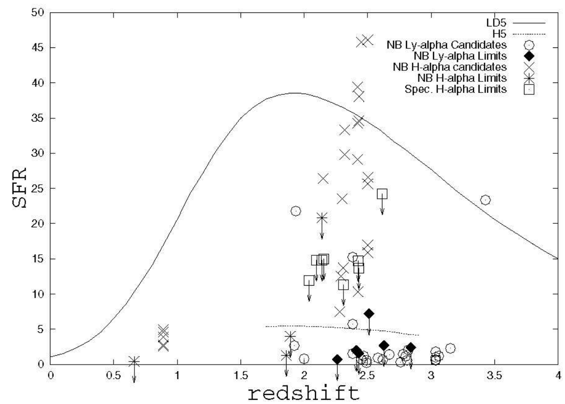

Figure 2. Measurements of SFRs (in $M_\odot$ yr^{-1}) for quasar absorption selected objects, based on narrow-band imaging and spectroscopic searches for Ly-α and H-α emission lines. See text for further details.

3.1. Emission-line Imaging Studies of DLAs

One way to estimate the star formation rates (SFRs) in DLAs is by direct imaging in emission lines such as Ly-α or H-α commonly found in star-forming regions. The H-α line, although intrinsically weaker than Ly-α, is less susceptible to effects of dust attenuation. However, the imaging of DLAs is in general difficult because of the possibility of a small angular separation between the quasar and the foreground absorbing galaxy. High-resolution studies with the Hubble Space Telescope have been carried out for some DLAs. For the low-z DLAs, a variety of morphologies has been observed. For high-z DLAs ($z \geq 1.5$), the situation remains unclear. Most attempts to detect and spectroscopically confirm high-z DLA galaxies with $z_{\rm abs} < z_{\rm em}$ have been unsuccessful.

To detect the underlying galaxies and measure their SFRs, we are carrying out deep imaging studies of high-redshift absorbers using HST and ground-based facilities. With the Near Infrared Camera and Multi-Object Spectrograph (NICMOS) on the HST, we have obtained diffraction-limited continuum and H-α images of DLAs with $z \approx 1.9$, at a FWHM of 0.15-0.17$''$ (Kulkarni et al. 2000, 2001). The highly stable and reproducible point spread function (PSF) of the HST NICMOS enabled us to search for absorbing galaxies as close as $\sim 0.2''$ from the quasar. After careful PSF subtraction, only a few compact features were seen, which did not show excess emission in H-α compared to the continuum. The non-detections imply 3 σ upper limits on the SFRs of $1.3 - 4.0$ M$_\odot$ yr^{-1}. These limits are much tighter than those reached previously (e.g., with ground-based spectroscopy of Bunker et al. 1999). A similar conclusion has also been reached by Bouché et al. (2001) for a $z \approx 0.7$ DLA.

Recently, we have obtained deep Ly-α images of quasar absorber fields at $z = 2.3 - 2.6$ using the NASA Goddard Space Flight Center's Fabry Perot (FP) imager at the Apache Point Observatory (APO) 3.5 m telescope (Kulkarni et al. 2003). The FP serves as a tunable narrow-band filter (400-700 km s^{-1} FWHM). In integrations of 400-720 minutes per object, we are reaching 3 σ flux sensitivity of 1.0×10^{-17} erg s^{-1} cm^{-2}, allowing some of the best existing SFR constraints.

3.2. Comparison with Global Star Formation History

Fig. 2 shows a compilation of SFRs vs. redshift data for quasar absorbers from our NICMOS studies and other emission-line studies in the literature. All measurements are normalized to $q_0 = 0.5$ and $H_0 = 70$ km s^{-1} Mpc^{-1}. The curves show the predictions of Bunker et al. (1999), for the cross-section-weighted SFR for large proto-spiral disks (LD5) and sub-galactic pieces in a hierarchical scenario (H5). These calculations are based on the closed-box global SFR model of Pei & Fall (1995), which agrees with the luminosity density of galaxies from the deep imaging surveys such as the HDF.

Many of the data points in Fig. 2 are for candidates that have not been confirmed spectroscopically. But it is clear that the SFRs of a large fraction of the absorption-selected objects lie far below the model predictions. Thus there appears to be a dichotomy between the absorption and emission pictures of the star formation history of galaxies. This discrepancy seems related to the "missing metals problem" noted by Wolfe et al. (2003). Using C II* absorption, they estimate SFRs per unit area in DLAs to be comparable to the Galactic value, but find the predicted metal density to be far higher than the observations. One possibility is that the SFRs appear to be low because of dust attenuation, which could also make the metallicity-redshift relation appear flatter than it really is (e.g., Kulkarni & Fall 2002 and references therein). Another possibility is that star formation occurs in compact regions. Further spectroscopic and imaging studies, including large samples of radio-selected quasars, are essential to better understand how important dust selection effects are and where DLAs lie in the overall history of metal production and star formation in galaxies.

4. Acknowledgments

It is a pleasure to thank my collaborators Drs. S. M. Fall, D. G. York, J. M. Hill, B. Woodgate, P. Palunas, P. Khare, J. Lauroesch, J. W. Truran, D. E. Welty, and Ms. D. Thatte. I am grateful for support from the National Science Foundation grant AST-0206197, NASA / Space Telecope Science Institute grant GO-9441.01 and from the Univ. of South Carolina Research Foundation. Finally, I thank the organizers of this very fruitful Joint Discussion for inviting me.

References

Bouché, N., Lowenthal, J. D., Charlton, J. C., Bershady, M. A., Churchill, C. W., & Steidel, C. C. 2001, ApJ, 550, 585

Bunker, A. J., Warren, S. J., Clements, D. L., Williger, G. M., & Hewitt, P. C. 1999, MNRAS, 309, 875

Khare, P. A., Kulkarni, V. P., Lauroesch, J. T., York, D. G., Crotts, A. P. S., & Nakamura, O. 2003, to be submitted

Kulkarni, V. P., Huang, K., Green, R. F., Bechtold, J., Welty, D. E., & York, D. G. 1996, MNRAS, 279, 197

Kulkarni, V. P., Fall, S. M. and Truran, J. W. 1997, ApJ, 484, L7

Kulkarni, V. P., Hill, J. M., Schneider, G., Weymann, R. J., Storrie-Lombardi, L. J., Rieke, M. J., Thompson, R. I., & Jannuzi, B. 2000, ApJ, 536, 36

Kulkarni, V. P., Hill, J. M., Schneider, G., Weymann, R. J., Storrie-Lombardi, L. J., Rieke, M. J., Thompson, R. I., & Jannuzi, B. 2001, ApJ, 551, 37

Kulkarni, V. P., & Fall, S. M. 2002, ApJ, 580, 732

Kulkarni, V. P., Palunas, P., Woodgate, B., & York, D. G. 2003, to be submitted

Lilly, S. J., Le Fevre, O., Hammer, F., & Crampton, D. 1996, ApJ, 460, L1

Lu, L., Sargent, W. L. W., Barlow, T. A., Churchill, C. W., & Vogt, S. S. 1996, ApJS, 107, 475

Madau, P., Ferguson, H. C., Dickinson, M. E., Giavalisco, M., Steidel, C. C., & Fruchter, A. 1996, MNRAS, 283, 1388

Madau, P., Pozzetti, L., & Dickinson, M. 1998, ApJ, 498, 106

Malaney, R. A., & Chaboyer, B. 1996, ApJ, 462, 57

Meyer, D. M., Welty, D. E., & York, D. G. 1989, ApJ, 343, L37

Pei, Y. C., & Fall, S. M. 1995, ApJ, 454, 69

Pei, Y. C., Fall, S. M., & Hauser, M. G. 1999, ApJ, 522, 604

Pettini, M., Smith, L. J., Hunstead, R. W., & King, D. L. 1994, ApJ, 426, 79

Pettini, M. Smith, L. J., King, D. L., & Hunstead, R. W. 1997, ApJ, 486, 665

Pettini, M., Ellison, S. L., Steidel, C. C., & Bowen, D. V. 1999, ApJ, 510, 576

Prochaska, J. X., & Wolfe, A. M. 1999, ApJS, 121, 369

Prochaska, J. X., & Wolfe, A. M. 2000, ApJ, 533, L5

Prochaska, J. X. et al. 2001, ApJS, 137, 21

Prochaska, J. X., & Wolfe, A. M. 2002, ApJ, 566, 68

Prochaska, J. X. et al. 2003, ApJ, 595, L9

Savaglio, S. 2000, IAUS, 204, E24

Somerville, R. S., Primack, J. R., & Faber, S. M. 2001, MNRAS, 320, 504

Tissera, P. B., Lambas, D. G., Mosconi, M. B., & Cora, S. 2001, ApJ, 557, 527

Vladilo, G., Bonifacio, P., Centurión, M., & Molaro, P. 2000, ApJ, 543, 24

Wolfe, A. M. et al. 1995, ApJ, 454, 698

Wolfe, A. M., Gawiser, E., & Prochaska, J. X. 2003, ApJ, 593, 235

Highlights of Astronomy, Vol. 13
International Astronomical Union, 2003
O. Engvold, ed.

The Star Formation History of Damped Lyman Alpha Systems

Arthur M. Wolfe

University of California, San Diego, CASS, 9500 Gilman Drive, La Jolla, CA, 92093-0424

Abstract. The C II* technique for measuring star formation rates (SFRs) in damped Lyα systems (DLAs) is described. We measure cooling rates of the gas from the strength of C II* 1335.7 absorption lines, and infer heating rates by assuming the gas is heated by the grain photoelectric mechanism. Since the heating rates depend on the intensity of FUV radiation, we deduce the SFRs per unit area, which are comparable to the value in the Milky Way disk. From DLA statistics we obtain the SFRs per unit comoving volume at z=[1.6,4.5], which are similar to the rates in Lyman Break Galaxies. Implications such as the presence of a two-phase medium, metal production, and feedback processes are described. The model is tested and found to be consistent with observations.

1. Introduction

In this talk I describe a new technique for measuring SFRs in protogalaxies. The technique differs from traditional methods, which rely on the detection of starlight (e.g. Steidel et al. 1999). Rather, it relies on feedback between radiation emitted by newly formed stars and the surrounding interstellar gas. Specifically, we detect the gas in absorption against background QSOs in the C II* 1335.7 transition, which measures the rate at which the gas is heated. Therefore, the sample of protogalaxies is cross-section weighted rather than luminosity weighted. As a result the SFRs we obtain are not limited to the most luminous objects, but instead refer to a more representative portion of the protogalactic mass distribution.

Our sample of protogalaxies is comprised of DLAs, a population of high-z layers of neutral gas, which dominate the neutral gas content of the universe at z=[0,5], and contain sufficient gas to account for a significant fraction of visible stars in modern galaxies (e.g. Storrie-Lombardi & Wolfe 2000). For these reasons the DLAs are widely regarded to be the progenitors of modern galaxies (Peebles 1993).

2. The C II* Technique

Assume neutral gas in DLAs is heated by the same grain photoelectric mechanism that heats the ISM (Bakes & Tielens 1994). In that case the heating rate per H atom is given by $\Gamma_d = 10^{-24}\kappa\epsilon G_0$ erg s^{-1} H^{-1}, where κ is the dust-to-gas ratio relative to the Milky ISM, ϵ is the grain photoelectric heating efficiency, and G_0=$4\pi J/1.6\times10^{-2}$ ergs cm^{-2} s^{-1} where J is the FUV mean intensity (Bakes &

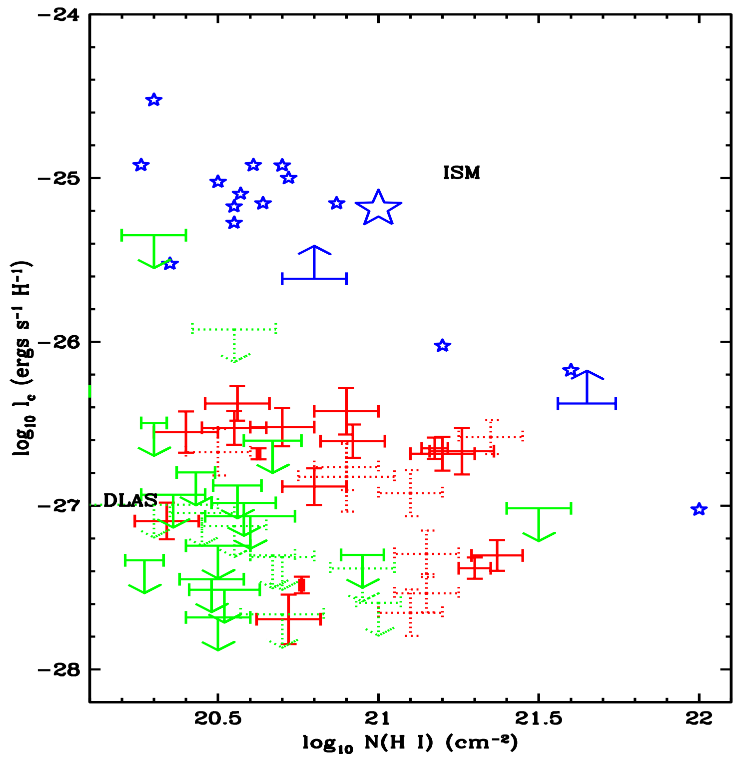

Figure 1. l_c versus N(H I). Data points with error bars show positive detections, and $2-\sigma$ upper and lower limits. Solid and dashed data points correspond to HIRES and ESI data respectively. Small stars depict detections toward H I clouds in the ISM. The large star is the spontaneous emission rate per H atom averaged over the ISM

Tielens 1994). Because of their low dust content, plane parallel layers comprising DLAs are optically thin to FUV radiation. Therefore, J is proportional to the line integral $\int \rho_L ds$ where the source function ρ_L is the luminosity density of starlight in DLAs. Thus, J is proportional to the projected luminosity per unit area, which is proportional to $\dot{\psi}_*$ since FUV radiation comes from short-lived upper main-sequence stars. Consequently, a measurement of J determines $\dot{\psi}_*$. Because ϵ has been calculated (Bakes & Tielens 1994) and it is straightforward to determine κ, we can obtain $\dot{\psi}_*$ provided we measure the heating rate.

We determine the heating rate by equating it to the cooling rate. In the ISM, cooling is dominated by [C II] 158 μm emission, which results from the transition between the $^2P_{3/2}$ and $^2P_{1/2}$ fine-structure states. Let the density-weighted cooling rate averaged along the line-of-sight be given by $l_c = N(\mathrm{CII}^*) h\nu_{ul} A_{ul}$ $/N(\mathrm{HI})$ erg s^{-1} H^{-1} (Pottasch 1979) where $h\nu_{ul}$ and A_{ul} are the energy and spontaneous emission coefficient for the fine-structure transition, and N(C II*) is the column density of C$^+$ ions in the $^2P_{3/2}$ state. We obtain l_c from UV spectroscopy by inferring N(C II*), from C II* 1335.7 absorption lines arising from the $^2P_{3/2} \rightarrow {}^2D_{3/2}$ transition and N(H I) from the damped Lyα line. Using the HIRES and ESI spectrographs on the Keck 10 m telescopes we have determined l_c for 50 DLAs. The results shown in Figure 1 indicate that l_c for the main body of DLA detections is about 1/30 of l_c for the ISM. The ratio of the two heating rates is simply explained if the DLA and ISM gas are heated by the same grain photoelectric effect. Moreover, if G_0 and ϵ in DLAs assume the same values as in the ISM, the ratio of the heating rates equals the ratio of the dust-to-gas ratios, κ, which according to Pettini et al. (1994) is remarkably close to 1/30. This suggests that $\dot{\psi}_*$ in DLAs is similar to that in the ISM and that the DLA heating rates are lower only because of the paucity of dust.

We checked this hypothesis by computing the thermal equilibria of gas heated by cosmic rays, X-rays, and FUV radiation, and which cools via excitation of fine-structure transitions of abundant low ions, Lyα radiation, and grain radiative recombination (see Wolfire et al. 1995; Wolfe, Prochaska, & Gawiser 2003; hereafter WPG): we assumed the ratio of X-ray and cosmic ray heating rates to $\dot{\psi}_*$ to be the same as in the ISM. The resulting equilibria admit two thermally stable phases: a warm neutral medium (WNM) and a cold neutral medium (CNM). By assuming the CNM and WNM are in pressure equilibrium at a unique pressure, P_{eq}, we infer the stable densities, n_{CNM} and n_{WNM}, and quantities such as temperature, ionization fraction, and l_c for each phase. We find that while [C II] 158 μm emission is the dominant coolant in the CNM, it is only a small fraction of the total cooling rate in the WNM.

For these reasons we considered two models in which CNM and WNM gas are in pressure equilibrium at $P = P_{eq}$: a CNM model in which the QSO sightline intersects comparable column densities of CNM and WNM gas, and a WNM model in which only the WNM gas is encountered. We constructed 2-phase models for each of the DLAs in our sample. For a DLA with a given metallicity, [M/H], and κ we solve the transfer equation for G_0 corresponding to a selected $\dot{\psi}_*$ for a uniform disk and vary $\dot{\psi}_*$ until the predicted l_c at n_{CNM} or n_{WNM} agrees with the observed l_c (see WPG for details). The results show no evidence for evolution of $\dot{\psi}_*$ in either model for z=[1.6, 4.5]. Furthermore, the mean SFR per unit area, $<\dot{\psi}_*>$, is comparable to the Milky Way rate for the CNM model, but, as expected, is much higher for the WNM model.

3. Global SFRs and Implications

We deduce the SFR per unit comoving volume, $\dot{\rho}_*(z)$, a quantity with cosmological significance, by combining $< \dot{\psi}_*(z) >$ for a given redshift bin with an expression for the incidence of DLAs per unit absorption distance, $d\mathcal{N}/dX$. The redshift dependence of $\dot{\rho}_*(z)$ implies a luminosity density history that gives rise to background radiation. The bolometric background intensity generated by the WNM model exceeds the 95 % confidence upper limits placed on the background intensity (e.g. Hauser & Dwek 2001) and is therefore ruled out (Wolfe, Gawiser, & Prochaska 2003; hereafter WGP). The resulting $\dot{\rho}_*(z)$ for the surviving CNM model are shown in Figure 2. The approximate agreement between $\dot{\rho}_*(z)$ determined for DLAs and Lyman Break Galaxies (LBGs) is either a coincidence

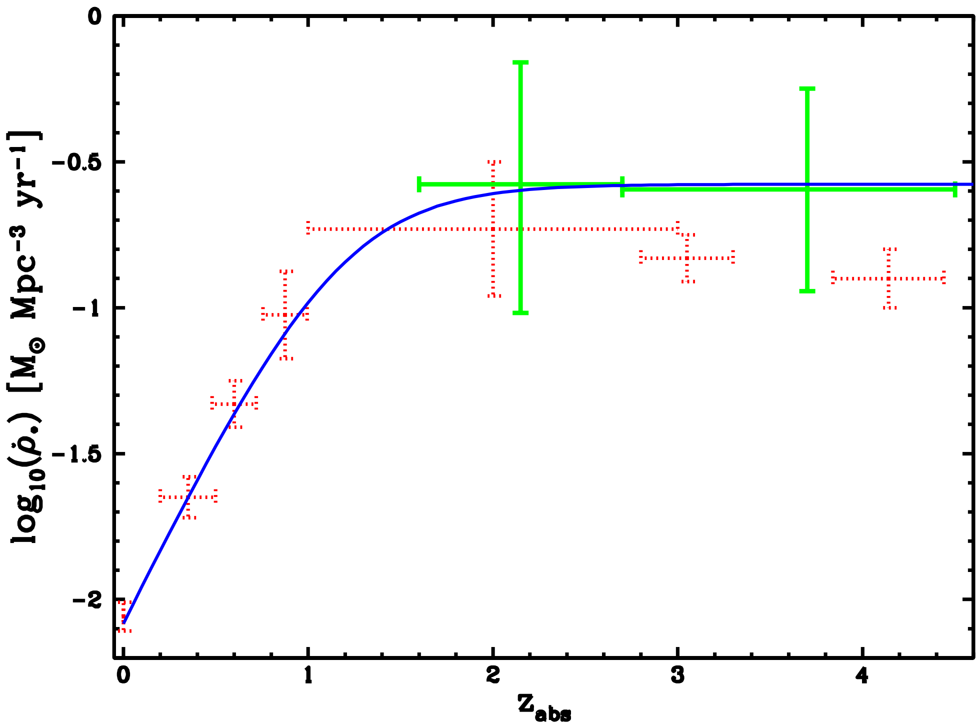

Figure 2. Solid data points depict $\dot{\rho}_*$ and 68% confidence errors for consensus CNM model. Dotted data points are from galaxies detected in emission: two highest redshift points are for LBGs (see WPG). Smooth curve is eyeball fit to consensus CNM model and galaxy data. Cosmology with $\Omega_{\rm M}$=1.0,Ω_Λ=0.0, and h=0.5 assumed. Note, the DLA data points include systematic errors not included in the galaxy data.

or indicates a connection between DLAs and LBGs. This question is currently under investigation.

Our results have several implications (see WGP). First, time integrals of the $\dot{\rho}_*(z)$ curve in Figure 2 result in the densities of stars and metals at a given redshift. Although the mass of stars produced by z=0 is consistent with the masses of stellar populations in modern galaxies, the mass of metals produced by z=2.5 is more than a factor of 20 higher than is observed in DLAs at that redshift. This generic problem also appears in CDM models (Nagamine et al. 2003) and in semi-analytic models (e.g. Somerville et al. 2001), but is absent in the models of Pei et al. (1999), which account for selection biases due to dust. We suggest that star formation confined to a centrally located "bulge" region offers a possible solution to this dilemma. In this scenario, rapid metal enrichment occurs in a compact bulge, an old but metal-rich population (Wyse et al. 1997), while FUV radiation leaks out of the bulge to heat the spatially extended H I gas detected in absorption. WGP find that the $\dot{\rho}_*(z)$ predicted for the bulge scenario is the same as for star formation throughout a uniform disk.

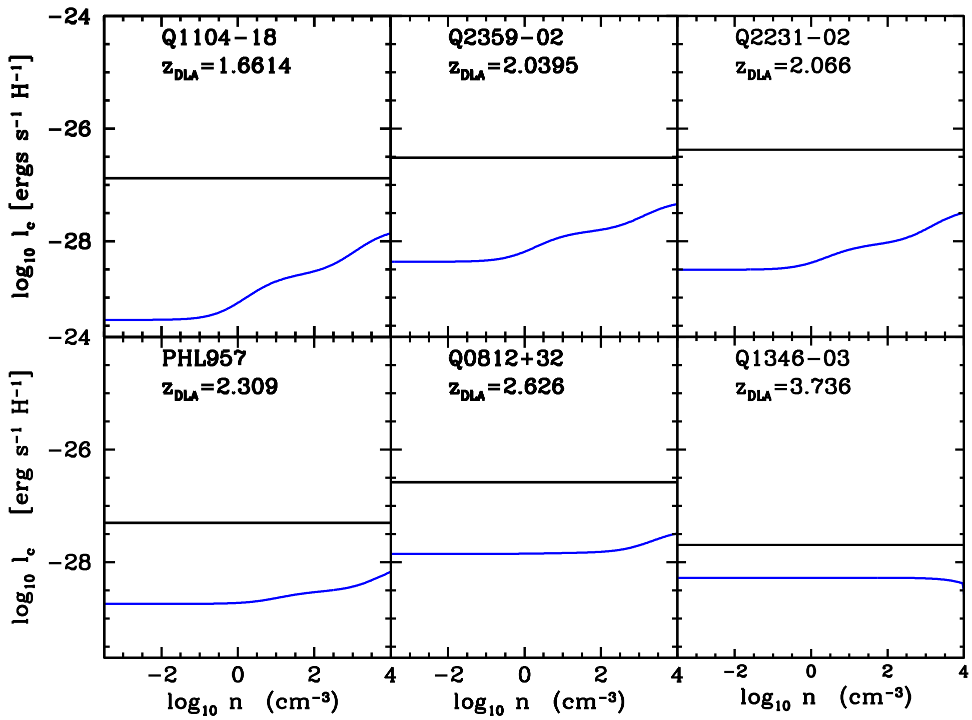

Figure 3. l_c versus density for 6 DLAs heated by FUV background radiation alone. CMB excitation dominates at low n, grain photoelectric heating dominates at intermediate n, and C I photoionization heating dominates at highest n. Measured l_c, depicted as horizontal lines, have typical 1-σ error bars of $\pm$ 0.2 dex.

Second, WGP searched for evidence of feedback and found tentative evidence in two cases. They found evidence, at 2-σ significance, for a correlation between $\dot{\psi}_*$ and [Si/H], which, if confirmed, would be consistent with similar correlations found in nearby galaxies (Garnett et al. 1997), and which is predicted in CDM models for galaxy formation (Nagamine et al. 2003). WGP also found a more significant correlation ($>$ 3-σ significance) between $\dot{\psi}_*$ and low-ion line width, Δv_{low}. Because $\dot{\psi}_*$ is a global quantity integrated over the star forming region of the DLA, such a correlation would imply Δv_{low} is also global, which would indicate Δv_{low} corresponds to the virial velocity of the dark matter halo enclosing the gas. If confirmed, this would be a valuable diagnostic of numerical models for star formation in DLAs, which predict how $\dot{\psi}_*$ depends on halo mass (Springel & Hernquist 2003). At the same time WGP found no evidence for a correlation between $\dot{\psi}_*$ and N(H I) nor $\dot{\psi}_*$ and high-ion line width.

WGP tested the C II* model, by showing that the observed l_c could not be due to radiative excitations from the high-redshift CMB. Nor can it arise from heating by the grain photoelectric effect or C I photoionization if the radiation source is the FUV background. Fig. 3 shows the observed l_c lies above the predicted cooling rates in all cases. Therefore, in contrast to the Lyα forest, an internal source of heat is required for DLAs. WGB also demonstrated a highly significant correlation between l_c and κ. This is predicted if C II* absorption arises in CNM gas heated by the grain photoelectric effect for a given SFR. It is not naturally predicted for heating by cosmic rays or soft X-rays.

More recently, we tested the CNM model by searching for evidence of Si II* 1264.3 absorption. Because this transition arises from a $^2P_{3/2}$ state 410 K above the ground state, it can only be detected in WNM gas where $T >> 400$ K. If C II* and Si II* absorption arise in WNM gas, the optical depth ratio τ(Si II*)/τ(C II*) reaches a maximum value of 0.025. Howk et al. (2003) find this ratio is significantly smaller than 0.025 and that $T < 400$K for a high-z DLA. This test is independent of the heating mechanism, and only depends on collision strengths and radiative recombination coefficients for the C II* and Si II* transitions. It provides unambiguous evidence for CNM gas in a high-z DLA.

Acknowledgments. The author wishes to thank his collaborators J. X. Prochaska, E. Gawiser, and J. C. Howk for their contributions to this research which is supported by NSF grants AST 0071257 and AST0307824.

References

Bakes, E. L. O. & Tielens, A. G. G. M. 1994, ApJ, 427, 822

Garnett, D. R., Shields, G. A., Skillman, E. D., Sagan, S. P., & Dufour, R. J., 1997, ApJ, 489, 63

Howk, J. C., Wolfe, A. M., & Prochaska, J. X. 2003, in preparation

Hauser, M. G., & Dwek, E. 2001, ARA&A, 39, 249

Nagamine, K., Springel, V., & Hernquist, L. 2003, astro-ph/0305409

Peebles, P. J. E. 1993, Principles of Physical Cosmology, Princeton: Princeton University Press, p. 562

Pei, Y. C., Fall, S. M., & Hauser, M. G. 1999, ApJ, 522, 604

Pettini, M., Smith, L. J., Hunstead, R. W., & King, D. L. 1994, ApJ, 426, 79

Pottasch, S. R., Wesselius, P. R., & van Duinen, R. J. 1979, A&A, 77, 189

Somerville, R. S., Primack, J. R. & Faber, S. M. 2001, MNRAS, 320, 540

Springel, V. & Hernquist, L. 2003, MNRAS, 339, 312

Steidel, C.C., Adelberger, K. L., Giavalisco, M., Dickinson, M., & Pettini, M. 1999, ApJ, 519, 1

Storrie-Lombardi, L. J., & Wolfe, A. M. 2000, ApJ, 543, 552

Wolfe, A. M., Prochaska, J. X., & Gawiser, E. 2003, ApJ, 593, 215 (WPG)

Wolfe, A. M., Gawiser, E., & Prochaska, J. X. 2003, ApJ, 593, 125 (WGP)

Wolfire, M. G., Hollenbach, D., McKee, C. F., Tielens, A. G. G. M., & Bakes, E. L. O. 1995, ApJ, 443, 152

Wyse, R. F. G., Gilmore, G., & Franx, M. 1997, ARA&A, 35, 637

Highlights of Astronomy, Vol. 13
International Astronomical Union, 2003
O. Engvold, ed.

JOINT DISCUSSION JD15: ABSTRACTS

The Evolution of the C/O ratio in Metal-Poor Halo Stars

C.J. Akerman[1], *L. Carigi*[2], *P.E. Nissen*[3], *M. Pettini*[1], *M. Asplund*[4] [1]Institute of Astronomy, Cambridge, UK; [2]Instituto de Astronomía, UNAM, México; [3]University of Aarhus, Denmark; [4]MSSSO, Australia.

Abstract. We report new measurements of carbon and oxygen abundances in 34 dwarf and subgiant Galactic halo stars with metallicities [Fe/H] = −0.7 to −3.2. We observed four permitted lines of C I near 9100 Å and the O I 7774 Å triplet, all recorded at high signal-to-noise ratios with the UVES echelle spectrograph on the ESO VLT. The line equivalent widths were analyzed with the 1D, LTE, MARCS model atmosphere code to deduce C and O abundances; corrections due to non-LTE and 3D effects are discussed. Our survey has uncovered tentative evidence to suggest that, as the oxygen abundance decreases below [O/H] = −1, [C/O] may not remain constant at [C/O] =−0.5, as previously thought, but increase again, possibly approaching near-solar values at the lowest metallicities. With the current dataset this is no more than a 3 sigma effect and it may be due to metallicity-dependent non-LTE corrections to the [C/O] ratio which have not been taken into account. However, its potential importance as a window on the nucleosynthesis by Population III stars is a strong incentive for future work, both observational and theoretical, to verify its reality. (see Akerman et al. 2003, A&A, in press; astro-ph/0310472)

Subaru HDS Studies of Carbon-Rich, Very Metal-Poor Stars

W. Aoki[1], *S.G. Ryan*[2], *J.E. Norris*[3], *T. Beers*[4], *S. Tsangarides*[2], *H. Ando*[1]
[1]National Astronomical Observatory of Japan, Tokyo; [2]The Open University, UK; [3]MSSSO, Australia; [4]Michigan State University, USA.

Abstract. Recent surveys of metal-poor stars have discovered a large number of carbon-rich objects. To investigate the origin of the carbon excesses, detailed abundance studies were made for 33 carbon-rich, metal-poor stars based on high-resolution spectra obtained with the Subaru Telescope (a part of the results was reported by Aoki et al. 2002, ApJ, 580, 1149) and the Anglo-Australian Telescope (Aoki et al. 2002, ApJ, 567, 1166). 24 stars in our sample (approximately 70%) show large excesses of *s*-process elements (e.g., Ba). A correlation between C and Ba abundances in these objects suggests production of carbon and *s*-process elements in the same site, probably in thermally pulsing AGB stars, and the dilution of the yields. The other 9 objects have low (or normal) Ba abundance. One of them (CS29498-043) has extremely low iron abundance ([Fe/H]=−3.7) and significant over-abundances of Mg and Si (Aoki et al. 2002, ApJ, 576, L141). This chemical nature is suggestive of supernovae production in which relatively little material escaped from the region surrounding the iron core. The other 8 carbon-rich, Ba-normal stars simply show an excess of C (or excesses of C and N). Some models (e.g., supernovae with extreme mixing in the explosion, He-flash in low-mass red-giants) are proposed to explain the carbon-enhancement in these stars.

Rapid Neutron Capture Process in Supernovae

R. Baruah[1], *K. Duorah*[2], *H.L. Duorah*[2] [1]Department of Physics, HRH Prince of Wales Inst. of Engg. and Technology, India; [2]Department of Physics, Gauhati University, India.

Abstract. The rapid neutron capture process is one of the major nucleosynthesis processes responsible for the synthesis of heavy nuclei beyond iron. Approximately half of the heavy elements with mass number $A > 70$ and all of the actinides in the solar system are believed to have been produced in the r-process. We have studied the r-process in supernovae for production of heavy elements beyond $A = 45$. The supernova envelopes at temperatures $T > 10^9$ K and neutron density $n \sim 10^{24}$ cm^{-3} are considered to be one of the most potential site for the r-process. The primary goal of the calculations is to fit the global abundance curve for solar system r-process isotopes by varying time dependent parameters such as temperature and neutron density. The neutron capture paths are obtained at different Q_n values ranging from 0.52 MeV to 5.07 MeV. We have studied the abundance distributions corresponding to temperatures ranging from 1.2×10^9 K to 2.8×10^9 K and neutron density from 10^{24} cm^{-3} to 10^{32} cm^{-3}. With temperature and density conditions of $T = 2.8 \times 10^9$ K and $n = 10^{24}$ cm^{-3} a nucleus of mass 252 was theoretically found. It was found that abundances at Q_n from 0.52 to 4.9 MeV give significant results. As we increase the neutron density, the computed abundance curves were found to approach the observed one in a more significant way. The beta decay of $_{21}Sc^{45}$ (normalization to $A = 45$) was found to govern most of the abundance curves.

The Metallicity Distribution Function of Halo Stars

T.C. Beers[1], *N. Christlieb*[2] [1]Michigan State University, USA; [2]Hamburger Sternwarte, Germany.

Abstract. Over the past two decades, a worldwide effort to obtain medium-resolution spectroscopic confirmation of candidate low-metallicity stars in the halo and thick disk of the Galaxy has produced ∼8000 1-2 Å observations of stars selected from the HK objective prism survey of Beers and colleagues. More recently, the Hamburg/ESO prism survey of Christlieb and collaborators has produced a larger, and better understood, selection of metal-poor candidates that explore a much larger volume of the Galaxy than was available to the HK survey. We summarize the final derived Metallicity Distribution Function (MDF) of the HK survey objects, and compare it with that obtained from the first several years of the HES follow-up effort. In particular, we investigate whether there is evidence for a change in the nature of the MDF as a function of distance from the Galactic center, which could have profound implications for the nature of the formation and evolution of the Milky Way, and for galaxy formation in general.

HERES: The Search for *r*-process Enhanced, Metal-Poor Stars

T.C. Beers[1], *N. Christlieb*[2], *M.S. Bessell*[3], *V. Hill*[4], *P.S. Barklem*[5], *S.G. Ryan*[6], *S. Rossi*[7], *A. Korn*[8] [1]Michigan State University, USA; [2]Hamburger Sternwarte, Germany; [3]MSSSO, Australia; [4]Observatoire de Paris-Meudon, France; [5]Uppsala Observatory, Sweden; [6]The Open University, UK; [7]IAG, Brazil; [8]München Sternwarte, Germany.

Abstract. In recent years, a handful of extremely metal-deficient stars have been identified that exhibit moderate to large enhancements of their abundance ratios (relative to Fe) of elements associated with the astrophysical r-process, enabling detections of radioactive species such as U and Th. Our understanding could be greatly improved by increasing the numbers of known r-process-enhanced, metal-poor stars, as well from building the sample to the point where meaningful measures of the frequency of the phenomenon, especially as a function of metallicity, could be ascertained. We describe the present status of HERES – The Hamburg/ESO R-process Enhanced Star survey. This survey is based upon "snapshot" high-resolution VLT/UVES spectra of large numbers of giants with [Fe/H] < -2.5. Spectra of sufficient quality to detect the presence of the Eu II line (4019 Å), a distinctive neutron-capture feature, have now been obtained for some 150-200 extremely metal-deficient giants chosen from the Hamburg/ESO survey. We discuss the number of moderate- and highly r-process enhanced stars discovered, update our estimate of the frequency of their detection, and present a discussion of the distribution of ~ 20 other easily measured elements in each of these stars (e.g., C, Ca, Mg, Si, Co, Ni, Sr, Ba, etc.).

Carbon Abundances of Metal-Poor Stars in the Galactic Halo

T.C. Beers[1], *S. Rossi*[2], *C. Sneden*[3], *N. Christlieb*[4], *J. Rhee*[5], *S.G. Ryan*[6], *T. Sevastianenko*[1], *B. Marsteller*[1] [1]Michigan State Univ., USA; [2]IAG, Brazil; [3]Univ. of Texas, USA; [4]Hamburger Sternwarte, Germany; [5]Univ. of Virginia, USA; [6]Open University, UK.

Abstract. Very metal-deficient stars that exhibit enhancements of their carbon abundances are of crucial importance for understanding a number of issues: The nature of stellar evolution among the first generations of stars, the shape of the Initial Mass Function, and the relationship between carbon enhancement and neutron-capture processes, in particular the astrophysical s-process. One fundamental result from recent objective-prism surveys dedicated to the discovery of metal-deficient stars is that the frequency, and perhaps, the level, of carbon enhancement increases greatly with declining metallicity. Most previous discoveries of these important stars have been serendipitous, as the stars were initially targeted because of their apparently low overall metallicity, and it was only discovered later that carbon was strongly enhanced. To more completely explore this phenomenon, we have undertaken spectroscopic follow-up of a published list of metal-deficient candidates from the Hamburg/ESO prism survey that show clearly strong carbon features directly on the survey plates. We have already obtained spectra for some 350 of the 413 stars in the sample, and will report on their observed properties, including estimates of their [Fe/H] and [C/Fe], their radial velocities, and their spatial distribution.

Cu and Zn Abundances in Metal-Poor Stars

G. Bihain[1], *R. Rebolo*[1], *G. Israelian*[1] [1]Instituto de Astrofisica de Canarias, Spain.

Abstract. We present Cu and Zn abundances for a sample of 38 FGK stars, mostly dwarfs, spanning a metallicity range between solar and [Fe/H] $= -3$. LTE

abundances were obtained using Kurucz's model atmospheres and the near-UV lines of Cu I 3273.95 Å and Zn I 3302.58 Å observed at high spectral resolution. The trend of [Zn/Fe] vs. [Fe/H] is essentially solar for [Fe/H] > -2.0 and then slightly increases at lower metallicities to an average value of $<$[Zn/Fe]$>$ $= +0.18$, whereas the [Cu/Fe] trend is approximately constant down to [Fe/H] ~ -1 and then decreases at lower metallicities reaching a plateau around [Cu/Fe] ~ -0.95 for [Fe/H] < -2.5. We compare our results with previous work on these elements and briefly discuss them in terms of nucleosynthesis processes. A paper will be submitted to A&A.

Lithium Abundances in Extremely Metal-Poor Stars

P. Bonifacio[1], *P. Molaro*[1], *T. Sivarani*[1], *M. Spite*[2], *F. Spite*[2], *R. Cayrel*[2], *P. François*[2], *V. Hill*[2], *B. Plez*[3], *T. C. Beers*[4], *J. Andersen*[5], *B. Barbuy*[6], *E. Depagne*[7], *B. Nordström*[5,8], *F. Primas*[7] [1]INAF–OA Trieste; [2]Observatoire de Paris-Meudon; [3]GRAAL–Université de Montpellier; [4]Michigan State University; [5]Astronomical Observatory, Copenhagen; [6]Universidade de São Paulo; [7]European Southern Observatory; [8]Lund Observatory, Sweden.

Abstract. We present preliminary lithium abundances for 21 turnoff stars in the range $-3.6 <$[Fe/H]< -2.5, observed with VLT/UVES. Effective temperatures were derived by fitting the wings of the Hα lines. In 5 stars, Li is depleted by modest to large factors, while the remaining 16 stars define a very tight relation in the [Fe/H]–A(Li) plane. The sample has mean lithium abundance A(Li)=2.30 with a dispersion of 0.08 dex. The relation exhibits a significant slope (0.17 ± 0.05), which cannot be simply interpreted as due to Li production in the early Galaxy: extrapolation to [Fe/H]$=-5.0$ implies A(Li)=1.94, while the A(Li) implied by the WMAP baryonic density is A(Li)=2.66 and the minimum abundance predicted by BBN is A(Li)=2.05. More likely explanations of the steep slope are: 1) systematic errors in our analysis, 2) observational bias, or 3) metallicity-dependent atmospheric effects which alter the Li abundance. The data also show trends of increasing [Fe/H] and A(Li) in the apparently brighter stars, which could be partly due to observational bias. Accordingly, we defer a full discussion of the slope of the [Fe/H]–A(Li) relation until these effects are fully understood.

Spin Temperature in High Redshift DLAs

J. Chengalur[1], *N. Kanekar*[2] [1]National Center for Radio Astrophysics, Pune University, India; [2]Kapteyn Institute, University of Groningen, The Netherlands.

Abstract. We present results from recent deep searches for H I 21cm absorption in high redshift Damped Lyman-alpha systems (DLAs). 21cm observations, coupled with measurements of the total H I column density from the Lyman-alpha line, allow one to estimate the average spin temperature T_s of the neutral hydrogen in the DLA. In most astrophysical circumstances, the spin temperature is the same as the kinetic temperature, for a single homogeneous H I cloud. In a heterogeneous medium, the average spin temperature allows one to estimate the fractional H I content in different temperature phases (i.e. WNM and CNM). We discuss the variation in the average spin temperature with redshift, as well as morphology of the optical counterpart. Dwarf galaxies are known to contain a

larger fraction of their atomic gas in the WNM phase, so variations of the average spin temperature with morphological type of the optical counterpart could be expected. Finally, we present preliminary results of a new survey which attempts to relate the spin temperature of an absorber to its metallicity, i.e. its [Zn/H] ratio. (See Kanekar & Chengalur 2003, A&A, 399, 857 for more details.)

D/H in a New Lyman Limit Absorber towards Q1937–1009

N.H. Crighton[1], *J. Webb*[1] [1]Department of Astrophysics, University of New South Wales, Australia.

Abstract. Initial results from the WMAP satellite have constrained the cosmological baryon density with an uncertainty of 4%. We can now test our understanding of both Big Bang nucleosynthesis and subsequent stellar nucleosynthesis by comparing this precise result with predictions for the baryon density from abundances of light elements produced in BBN. The discrepancy between the predicted baryon density from He^4 and Li^7 measurements and the density predicted from deuterium and WMAP already shows that there are problems either with the interpretation of the data or the model we are fitting to it. Currently the handful of extra-galactic deuterium abundance (D/H) measurements broadly agree with the WMAP baryon density, but there is significant scatter amongst these values. While the scatter can be explained by underestimated systematic effects, it may also be hinting at an early source of nucleosynthesis or other non-standard scenarios. We present a measurement of D/H in a new Lyman limit absorption system towards QSO 1937–1009. Several different models of the velocity structure of the system require D/H to be significantly lower than that measured in other absorption systems. If true, this may imply that the scatter in D/H measurements is real, and not only a result of systematic errors.

Fluorine in the Galaxy and the Large Magellanic Cloud

K. Cunha[1], *V. Smith*[2], *K. Hinkle*[3] [1]Observatorio Nacional - MCT, Brazil; [2]Univ. of Texas, El Paso, USA; [3]NOAO, Tucson, USA.

Abstract. The behavior of fluorine with metallicity has not yet been probed in any stellar population. To date, fluorine abundances have only been measured in a few K and M giant stars with near-solar metallicities in our Galaxy. The origins of fluorine are still uncertain and could be due to perhaps three sources: 1) neutrino-induced nucleosynthesis happening in core-collapse supernovae, 2) asymptotic giant branch stars undergoing He-burning thermal pulses, or 3) mass-loss from He burning regions in Wolf-Rayet stars. In this work we present first results for fluorine abundances in a sample of red giants from the Galactic disk, M4, Omega Centauri, and the LMC from spectra obtained with Phoenix on Gemini South. The observed IR spectra contain HF molecular lines. If fluorine is produced with Wolf-Rayet stars, its yield is predicted to be a strong positive function of metallicity. In such a case, fluorine abundances derived in DLA systems could test for chemical evolution driven by Wolf-Rayet stars.

Probing the DLA Nature and Star Formation History

M. Dessauges-Zavadsky[1,4], *F. Calura*[2], *J.X. Prochaska*[3], *S. D'Odorico*[4], *F. Matteucci*[2]

[1]Geneva Observatory, Switzerland; [2]Dept. of Astronomy, University of Trieste, Italy; [3]UCO/Lick observatory, USA; [4]European Southern Observatory, Germany.

Abstract. By combining UVES-VLT spectra of four DLAs toward Q0100+13, Q1331+17, Q2231−00 and Q2343+12 with HIRES-Keck spectra, we covered the total optical spectral range. This large wavelength coverage allowed us to measure the column densities of 21 ions and abundances of 15 elements − N, O, Mg, Al, Si, P, S, Cl, Ar, Ti, Cr, Mn, Fe, Ni, Zn. This comprehensive set contrasts with the majority of DLAs for which only a handful of ions and elements is observed, and is yet necessary to constrain the photoionization and dust depletion effects to derive the intrinsic abundances of DLAs. Our analysis revealed that the DLA toward Q2343+12 requires important ionization corrections. We thus had access to the complete series of intrinsic abundances in three DLAs only and we could constrain their star formation history, age and star formation rate by a detailed comparison with the chemical evolution models of Calura, Matteucci & Vladilo (2003, MNRAS 340, 59) for spiral and irregular/starburst galaxies. Our results show that the galaxies associated with these DLAs at $z_{\rm abs} = 1.7-2.5$ are either outer regions of spiral disks or starburst/irregular galaxies with ages from 0.05 to 3.5 Gyr and with moderate star formation rates $-2.1 < \log \dot{\Psi}_* < -1.5$ $M_\odot$ yr^{-1} kpc^{-2} (see Dessauges-Zavadsky et al. 2003, A&A, submitted).

Damped Systems Associated with a Galaxy Cluster at z=2.38

P.J. Francis[1], *G. Williger*[2] [1]The Australian National University; [2]John Hopkins Univ., USA.

Abstract. We have found a unique cluster of three damped Lyman-alpha systems at redshift 2.38, seen in absorption against three background QSOs. One of the damped systems lies in the center of a rich galaxy cluster – indeed it lies less than 150 kpc from a pair of giant elliptical galaxies. Despite this dense environment, the gas is cold and has a metallicity of only –2.7 dex. Another damped system lies roughly 10 co-moving Mpc away in the middle of a void. Despite this low density location, it has a much higher metallicity: around –1.5 dex. We conclude that there is no strong correlation between the environment of damped systems and their metallicities at high redshifts. Damped systems in the middle of clusters can have very low metallicities, while damped systems in voids can be substantially enriched.

Heavy Elements in a Sample of Extremely Metal-Poor Giants

P. François[1], *E. Depagne*[1], *R. Cayrel*[1], *V. Hill*[1], *F. Spite*[1], *M. Spite*[1], *B. Plez*[2], *B. Barbuy*[3], *T. Beers*[4], *P. Bonifacio*[5], *J. Andersen*[6], *F. Primas*[7], *S. Thirupathi*[1], *B. Nordström*[6,8], *P. Molaro*[5] [1]Observatoire de Paris-Meudon; [2]GRAAL–Université de Montpellier; [3]Universidade de São Paulo; [4]Michigan State University; [5]INAF–OA Trieste; [6]Astronomical Observatory, Copenhagen; [7]European Southern Observatory; [8]Lund Observatory, Sweden.

Abstract. The abundances of the neutron capture elements (Sr, Ba, La, Ce, Eu ...) are studied in a sample of more than 30 extremely metal-poor giants ([Fe/H]< -2.7) observed at the VLT with the high resolution spectrograph

UVES. The S/N ratio of the spectra is high and it is generally possible to measure very weak lines ($W > 1\,\mathrm{m\AA}$). The trends of the ratios [Sr/Fe], [Ba/Fe] .. with metallicity are shown and the scatters compared to the scatter observed for iron–peak elements. Consequences for the formation of these elements and the Galactic evolution are discussed.

Constraints on Early Galactic Enrichment from a Large Sample of Extremely Metal-Poor Stars Observed with VLT+UVES

V. Hill[1], *R. Cayrel*[1], *M. Spite*[1], *B. Plez*[2], *F. Spite*[1], *P. François*[1], *E. Depagne*[3], *J. Andersen*[4], *B. Barbuy*[5], *T. Beers*[6], *P. Bonifacio*[7], *P. Molaro*[7], *B. Nordström*[4,8], *F. Primas*[3] [1]Observatoire de Paris-Meudon; [2]GRAAL–Université de Montpellier; [3]European Southern Observatory; [4]Astronomical Observatory, Copenhagen; [5]Universidade de São Paulo; [6]Michigan State University; [7]INAF–OA Trieste; [8]Lund Observatory, Sweden.

Abstract. The overall results from an large effort conducted at ESO-VLT+UVES to measure abundances in a sample of extremely metal-poor stars (EMPS) from high-resolution and high signal-to-noise spectra are presented. More than 70 EMPS with [Fe/H]< -2.7 were observed, equally distributed between turnoff and giants stars, and very precise abundance ratios could be derived thanks to the high quality of the data. Among the results, the abundances of the elements from C to Zn of the 35 extremely metal-poor giants of the sample (Cayrel et al., 2003, A&A, in press), are presented, including the much debated abundance of oxygen in the early galaxy (we present [OI] line measurements down to [O/Fe]$=-3.5$), and the trends of alpha elements, iron group elements and zinc. The remarkably small scatter around these trends is also discussed, together with its implications on the early Galactic enrichment. More specific topics covered by this large effort (and large team) are addressed in devoted posters presented at this JD: Bonifacio et al., François et al., Spite et al.

Molecules in Damped Lyα Systems: Spatial Distribution

H. Hirashita[1], *A. Ferrara*[2], *K. Wada*[3], *P. Richter*[4] [1]Graduate School of Science, Nagoya University, Japan; [2]SISSA, Trieste, Italy; [3]National Astronomical Observatory of Japan, Tokyo; [4]Osservatorio Astrofisico di Arcetri, Firenze, Italy.

Abstract. To interpret H_2 (hydrogen molecule) quasar absorption line observations in damped Ly-alpha clouds (DLAs), we model the H_2 spatial distribution within a DLA. Based on numerical simulations of disk structures with parameters similar to those derived for such absorbers, we calculate the H_2 distribution as a function of ultraviolet background (UVB) intensity and dust-to-gas ratio. For typical values of these two quantities we find that the area in which the H_2 fraction exceeds 10^{-6} (typical observational detection limit) only covers $< 10\%$ of the disk surface, i.e., H_2 has a very inhomogeneous, clumpy distribution even at these low abundance levels. This explains the relative paucity of H_2 detections in DLAs. We also show the dependence of the covering fraction of H_2 on dust-to-gas ratio and UVB intensity and we comment on the physics governing the H_2 chemical network at high redshift. We finally comment on our implication on the statistics of the H_2 column density distribution. (See Hirashita, H., Ferrara, A., Wada, K., & Richter, P. 2003, MNRAS, 341, L18)

Subaru/HDS Studies of r-process Elements in Metal-Poor Stars
S. Honda[1], *W. Aoki*[1], *T. Kajino*[1], *H. Ando*[1], *T.C. Beers*[2] [1]National Astronomical Observatory, Japan; [2]Michigan State University, USA.

Abstract. We have obtained high-quality spectra of 22 very metal-poor stars with Subaru/HDS, in order to conduct detailed abundance studies of the neutron-capture elements including Th. As has been found by previous abundance studies, the star-to-star scatter in the abundances of neutron-capture elements is very large. The abundance patterns of the heavy neutron-capture elements ($56 \leq Z \leq 70$) in seven objects with moderate to large excesses of the neutron-capture elements are similar to that of the solar system r-process component. These results strongly suggest that the heavy neutron-capture elements in these objects are primarily synthesized by the r-process. On the other hand, the abundance ratios of the light neutron-capture elements ($38 \leq Z \leq 46$) exhibit a rather large dispersion. Our results support previous suggestions that the light neutron-capture elements are likely to have been produced in different astrophysical sites from those associated with the production of the heavier ones. The abundances of Th in a number of these stars are slightly higher than the values expected from the solar system r-process pattern. The Th/Eu ratio, which has been commonly used for nuclei cosmo-chronometry, exhibits a dispersion of about 0.3 dex in our sample.

Synthetic Lick Indices as a Function of Stellar Abundance Ratios
M.L. Houdashelt[1], *S.C. Trager*[2], *G. Worthey*[3] [1]Johns Hopkins Univ., Baltimore, USA; [2]Kapteyn Astronomical Inst., The Netherlands; [3]Washington State Univ., USA.

Abstract. Tripicco & Bell (1995) used synthetic stellar spectra to characterize the sensitivities of the optical Lick indices to changes in the abundances of specific elements. These results allowed Trager et al. (2000; hereafter TFWG) to estimate the chemical abundances in elliptical galaxies from the differences between the Lick indices observed in these galaxies and those predicted by the evolutionary synthesis models of Worthey (1994). For this poster, we have calculated two new evolutionary synthesis models, one of which incorporates the TFWG chemical abundances, while the other uses standard solar abundances. We compare the integrated Lick indices from these two models and find general agreement with the differences predicted by TFWG. The only Lick indices that vary by more than two times the observational errors in these models are the CN indices, $C_2$4668, the Mg indices, and Na D. To examine the potential of using spectral features at redder wavelengths to further refine the TFGW abundances, we have also compared the integrated models between 0.6 and 1.0 μm. However, we find no spectral features that vary by more than 1% between these two models in this wavelength regime.

Abundance Ratios in Ba-Poor Stars
J. Johnson[1], *M. Bolte*[2] [1]Dominion Astrophysical Observatory, Canada; [2]UCO/Lick Observatory, USA.

Abstract. We present abundance ratios for four stars with $[Fe/H] < -3.0$ and $[Ba/Fe] < -1.0$. These include three stars from the sample of McWilliam et al.

(1995) which only had upper limits. These observations will be used to define the lower envelope of [Ba/Fe] abundances in the very metal-poor stars in the Galaxy. Also, the abundance ratios of the light elements will be compared to predictions of Type II SNe ejecta and to those in Ba-rich stars to see if the stars that do not make the *r*-process can be identified.

Type Ia Supernova Progenitors and Elemental Abundance Ratios

C. Kobayashi[1] [1]Max-Planck-Institute for Astrophysics, Garching, Germany.

Abstract. Elemental abundance ratios are much related to the progenitor model of Type Ia supernovae (SNe Ia). We make a comparison of the lifetime distribution function derived from several models of SNe Ia, and evaluate the SN Ia models from several observational constraints. With our single-degenerate model, the SN Ia rate in the system with [Fe/H] ≤ -1 is supposed to be very small. Such metallicity effects may conflict with [α/Fe] observed in the Damped Lyα systems (DLAs) and dwarf spheroidal galaxies (dSphs). However, both theoretically and observationally, SNe Ia should increase [Mn/Fe]. From the abundance pattern from O to Zn, we argue that low [alpha/Fe] observed in the DLAs and dSphs is caused not by SNe Ia but by low-mass supernovae (13–15 $M_\odot$), because their [Mn/Fe] is as low as in the Milky Way halo stars.

The Composition at the Outer Edge of the Galaxy

D.A. Lubowich[1], *G. Brammer*[2], *H. Roberts*[3], *T. J. Millar*[4], *J. M. Pasachoff*[5], *C. Henkel*[6], *P. Ruffle*[4] [1]Hofstra University, Hempstead, NY, USA; [2]STScI, Baltimore, USA; [3]Ohio State University, USA; [4]UMIST, Manchester, UK; [5]Williams College, Williamstown, USA; [6]Max-Planck Institut für Radioastronomie, Bonn, Germany.

Abstract. We present cm and mm-wave observations of a molecular cloud at the outer edge of the Galactic disk (kinematic galactocentric distance of 28 kpc). We detected CO, ^{13}CO, ^{18}CO, CS, CN, SO, HCN, HNC, C_2H, HCO^+, $H^{13}CO^+$, HCS^+, NH_3, H_2CO, C_3H_2 and CH_3OH, while ^{17}CO, ^{34}CS, SiO, SiS, N_2H^+, DCN, DNC, DCO^+, SO_2 and HC_3N were not detected. From the NH_3, H_2CO, and CS data we derived a kinetic temperature of $T_{\rm kin} \sim 20$ K and a density of $n(H_2) \sim 5{\times}10^3$ cm^{-3}. The lines from N-containing molecules that we detected were weak and we did not detect the usually strong N_2H^+ or HC_3N lines. Using our 5300 chemical reaction network we calculated that this cloud is depleted in N by $\sim 24\times$ and metallicity is reduced by $5\times$ (similar to dwarf irregular galaxies or damped Lyman alpha systems) relative to the solar neighborhood. This unique composition probably results from the infall of halo gas enriched in O, C, and S from a burst of massive star formation shortly after the Galaxy formed. This activity would have produced both O and S which are produced by massive stars; C which is produced by massive and intermediate mass stars; but less N abundance because the secondary element N is produced primarily from low mass stars. Thus the edge cloud probably results from infalling halo gas that was not significantly processed during the last 10 Gyr.

The mystery of CH stars frequency at low metallicity

S. Lucatello[1], R.G. Gratton[1], E. Carretta[1], T.C. Beers[2], N. Christlieb[3], J.G. Cohen[4] [1]INAF, Osservatorio Astronomico di Padova, Italy; [2]Michigan State University, USA; [3]Hamburger Sternwarte, Germany; [4]Palomar Observatory, USA.

Abstract. One of the results of the spectroscopic HK and the Hamburg/ESO surveys of metal-poor stars is the high frequency of C-enhanced stars among very metal poor stars. This is still unexplained, as well as the mechanisms responsible for the production of C in the few C-enhanced extremely metal poor (CEMP) stars studied so far with high resolution, high S/N spectroscopy. The results of the follow-up works to date seem to suggest that there are different kinds of CEMP stars, exhibiting, besides the C-enhancement, *s*- and *r*-process element enhancements, as well as normal n-capture elements abundances; and hence possibly as many C production mechanisms. To shed light on such mechanisms, a wider sample of CEMP stars is crucial. We present the preliminary results of abundance analysis of UVES and HIRES spectra of a sample of 10 CEMP stars, suggesting that there is no definite trend of [Pb/Ba] with [Fe/H], contrary to what was supposed on the basis of the Aoki et al. (2002) sample, and also at odds with the the predictions of the shell nucleosynthesis models. Moreover, the coupling of our results with those published in the literature show a clear correlation between [Pb/Ba] and [N/Fe], especially when considering the more metal poor stars ([Fe/H]< -2 dex), suggesting that the most extreme *s*-process signatures are present in stars with high N abundances. This is somewhat surprising, as N is a poison for the *s*-process and a high content of such element is expected to inhibit the *s*-process.

Sulphur and Zinc Abundances in Halo and Disk stars

P.E. Nissen[1], Y.Q. Chen[2], M. Asplund[3], M. Pettini[4] [1]University of Aarhus, Denmark; [2]National Astronomical Observatories, Beijing, P.R. China; [3]MSSSO, Australia; [4]Institute of Astronomy, Cambridge, UK.

Abstract. High resolution spectra of 34 halo population dwarf and subgiant stars have been obtained with VLT/UVES and used to derive sulphur abundances from the $\lambda\lambda 8694.0, 8694.6$ and $\lambda\lambda 9212.9, 9237.5$ S I lines. In addition, iron abundances have been determined from 19 Fe II lines and zinc abundances from the $\lambda\lambda 4722.2, 4810.5$ Zn I lines. The abundances are based on a classical 1D, LTE model atmosphere analysis, but effects of 3D hydrodynamical modeling on the [S/Fe], [Zn/Fe] and [S/Zn] ratios are shown to be small. We find that most halo stars with metallicities in the range $-3.2 <$ [Fe/H] < -0.8 have a near-constant [S/Fe] $\simeq +0.3$; a least square fit to [S/Fe] vs. [Fe/H] shows a slope of only -0.04 ± 0.01. Among halo stars with $-1.2 <$ [Fe/H] < -0.8 the majority have [S/Fe] $\simeq +0.3$, but two stars (previously shown to have low α/Fe ratios) have [S/Fe] $\simeq 0.0$. For disk stars with [Fe/H] > -1, [S/Fe] decreases with increasing [Fe/H]. Hence, sulphur behaves like other typical α-capture elements, Mg, Si and Ca. Zinc, on the other hand, traces iron over three orders of magnitude in [Fe/H], although there is some evidence for a small systematic Zn overabundance ([Zn/Fe] $\simeq +0.1$) among metal-poor disk stars and for halo stars with [Fe/H] < -2.0. (See Nissen et al. 2003, A&A, submitted)

Metallicities and Ages in the Galactic Disk

B. Nordström[1,2], *J. Andersen*[1], *J. Holmberg*[1], *B. Jørgensen*[2] [1]Niels Bohr Institute, Copenhagen, Denmark; [2]Lund Observatory, Sweden.

Abstract. Metallicities, ages, and full Galactic orbits have been derived for a complete, kinematically unbiased sample of 14.000 F and G dwarfs in the Solar neighborhood. The observational data are Strömgren *uvby* photometry, Hipparcos/TYCHO astrometry, and extensive new radial-velocity observations from which duplicity information is available for all the stars as well. The sample is magnitude complete to $V \sim 8.5$ and volume complete to 40 pc. Special attention has been given to developing and testing a new algorithm for age determination of field stars from theoretical isochrones, with particular emphasis on deriving realistic error estimates also for the oldest stars, and on identifying the stars for which no meaningful ages can in fact be derived. The results challenge traditional views of the chemical enrichment history of the Galactic disk. Full details are given in Nordström et al. (A&A 2003, in prep.).

Sub-Damped Lyman-alpha Systems: Implications for the Cosmological Evolution of Metals

C. Péroux[1], *M. Dessauges-Zavadsky*[2], *S. D'Odorico*[2], *T. Kim*[2,3], *R.G. McMahon*[3] [1]Osservatorio di Trieste, Italy; [2]European Southern Observatory, Germany; [3]Institute of Astronomy, Cambridge, UK

Abstract. Damped Lyα Systems (DLAs), with $N(\mathrm{H\,I}) > 2 \times 10^{20}$ cm^{-2}, observed in the spectra of quasars have allowed us to quantify the chemical content of the Universe over cosmological scales. Such studies can be extended to lower column densities, in the sub-DLA range ($10^{19} < N(\mathrm{H\,I}) < 2 \times 10^{20}$ cm^{-2}), which are systems believed to contain a large fraction of the neutral hydrogen at $z > 3.5$. We use a homogeneous sample of sub-DLAs from the ESO UVES archives presented in Dessauges-Zavadsky et al. (2003, MNRAS, 345, 447), to analyze their chemical content in conjunction with a compilation of abundances from 72 DLAs taken from the literature. In particular, we analyze the H I column density-weighted mean abundance which is believed to be an indicator of the Universe's metallicity. The results suggest a slightly stronger evolution of this quantity in the sub-DLA range. Therefore these systems might be associated with a different class of objects which better trace the overall chemical evolution of the Universe. Finally, the elemental ratios in sub-DLAs are similar with those from DLAs. The metallicities are compared with two different sets of models of galaxy evolution in order to provide constraints on the morphology of quasar absorbers. Further details of this study can be found in Péroux et al. (2003, MNRAS, 345, 480).

Sgr dSph: a Bridge between Dwarf Galaxies and DLAs?

L. Sbordone[1,2], *P. Bonifacio*[3], *G. Marconi*[1], *L. Pasquini*[4], *V. Hill*[5] [1]European Southern Observatory, Santiago, Chile; [2]Dipartimento di Fisica, Universita di Roma, Italy; [3]INAF–OA, Trieste, Italy; [4]European Southern Observatory, Germany; [5]Observatoire de Paris-Meudon, France.

Abstract. We present abundances for 12 giants in the Sagittarius Dwarf Spheroidal Galaxy (Sgr dSph) obtained from VLT-UVES spectra. Moving on a

short period, polar orbit around the Milky Way, the Sgr dSph is undergoing tidal disruption and will eventually dissolve in the Galactic Halo. Our sample appears dominated by a Fe-rich, α-element-poor and young population, indicative of a long chemical processing of the dSph gas during a slow, probably bursting star formation history. This population is the most metal-rich ever observed in a dwarf galaxy of the local group, and has the lowest α-element content. The "extreme" composition observed in the Sgr dSph may be attributed to an unusually prolonged star formation, related to its strong interaction with the MW. Placing the known abundances of the LG dwarfs on the [α/Fe] vs. [Fe/H] plane allows now to recognize a well defined evolution sequence. The "dwarf sequence" resembles the one followed by the MW disc star, but at a consistently lower [α/Fe] ratio for each given [Fe/H]. Conversely, it is apparently superimposed to the one followed by many of the Damped Lyman alpha systems.

Bimodal Metallicity Distribution Function of OLD Stars

T. Shigeyama[1], *T. Tsujimoto*[1], *Y. Yoshii*[1] [1]National Astronomical Observatory, University of Tokyo, Japan.

Abstract. The external pollution of the first stars in the Galaxy is investigated. The first stars were born in clouds composed of the pristine gas without heavy elements. These stars accreted gas polluted with heavy elements while they still remained in the cloud. As a result, it is found that they exhibit a distribution with respect to the surface metallicity that is easily distinguished from the metallicity distribution of Population II stars. This metallicity distribution function strongly suggests that the recently discovered most metal-deficient star HE0107–5240 with [Fe/H]=-5.3 was born as a metal-free star and accreted gas polluted with heavy elements. Future observations for a number of metal-deficient stars with [Fe/H]< -5 will be able to prove or disprove this external pollution scenario.

CS 29497-030: Lead in the Early Galaxy

T. Sivarani[1], *P. Bonifacio*[1], *P. Molaro*[1], *R. Cayrel*[2], *M. Spite*[2], *F. Spite*[2], *B. Plez*[3], *J. Andersen*[4], *B. Barbuy*[5], *T. C. Beers*[6], *E. Depagne*[7], *V. Hill*[2], *P. François*[2], *B. Nordström*[4,8], *F. Primas*[7] [1]INAF–OA, Trieste; [2]Observatoire de Paris-Meudon; [3]GRAAL–Université de Montpellier; [4]Astronomical Observatory, Copenhagen; [5]IAG, Universidade de São Paulo; [6]Michigan State University; [7]European Southern Observatory; [8]Lund Observatory, Sweden.

Abstract. We present an abundance analysis of the halo blue straggler CS 29497-030, based on high-resolution, high S/N spectra from the ESO VLT/UVES. The star has very low metallicity ([Fe/H]=-2.8), large overabundances of C, N, and O ([C/Fe]=+2.38, [N/Fe]=+1.88, and [O/Fe]= +1.67), and large enhancements of heavy *s*-process elements. Most strikingly, the Pb enhancement ([Pb/Fe]=+3.5) is the highest yet observed in very metal-poor *s*-process rich stars. The occurrence of several very metal-poor stars with large overabundances of heavy *s*-process elements, e.g Ba, La, Ce, Nd, and particularly Pb, suggests that the *s*-process was operating at early times in the Galaxy, at least locally. This appears to contradict the long-accepted view that the neutron capture elements in low-metallicity stars originate from the *r*-process only. However,

like some (but not all) similar stars, CS 29497-030 is a binary (P=342d), and the Pb and other *s*-process elements could have been synthesized in the envelope of a former AGB companion, perhaps significantly later than the formation of the star itself. Full details of our analysis and discussion are reported in Sivarani et al. (A&A accepted).

Abundance of Nitrogen in the Early Galaxy from the NH Band at 336nm

M. Spite[1], *B. Plez*[2], *V. Hill*[1], *F. Spite*[1], *R. Cayrel*[1], *P. François*[1], *E. Depagne*[3], *J. Andersen*[4], *B. Barbuy*[5], *T. Beers*[6], *P. Bonifacio*[7], *P. Molaro*[7], *B. Nordström*[4,8], *F. Primas*[3] [1]Observatoire de Paris-Meudon; [2]GRAAL–Université de Montpellier; [3]European Southern Observatory; [4]Astronomical Observatory, Copenhagen; [5]Universidade de São Paulo; [6]Michigan State University; [7]INAF–OA Trieste; [8]Lund Observatory, Sweden.

Abstract. As part of the ESO Large Programme "First Stars", high-resolution, high-S/N spectra of 35 extremely metal-poor giants selected from the HK survey (Beers et al. 1992, 1999) have been obtained at the VLT. The spectra were analyzed with the LTE spectral line code "Turbospectrum" and OSMARCS model atmospheres (Gustafsson et al. 1975, Plez et al. 1992, Asplund et al. 1997). Element abundances from C to Zn are presented in Cayrel et al. (2003, A&A, in press), but nitrogen abundances from the CN band are lacking for most of the stars. We have used the NH band at 336nm to determine nitrogen abundances for all our stars. The dispersion in the relations of [N/Fe] vs. [Fe/H] (and [C/Fe] vs. [Fe/H]) is very large, However, a group of stars displays very low values of C/N, suggesting that their atmospheres are mixed with internal layers where the CN cycle has converted C to N. Supporting this theory, the relation (C+N) vs. [Fe/H] is flat, and the dispersion around the mean value is much smaller. For unmixed stars with [Fe/H]< -3.4, [N/Fe] is close to $+0.1$ and [N/O] close to -0.6, suggesting these ratios for the primordial production of N.

Behavior of Sulfur Abundances in Halo Stars Observed with HIDES at OAO

M. Takada-Hidai[1], *Y.-j. Saito*[2], *Y. Takeda*[3], *S. Honda*[3], *K. Sadakane*[4], *H. Izumiura*[5], *S. Masuda*[5] [1]Liberal Arts Education Center, Tokai University, Japan; [2]Physics Department, Tokai University, Japan; [3]National Astronomical Observatory of Japan, Tokyo; [4]Osaka Kyoiku University, Kashihara, Japan; [5]National Astronomical Observatory of Japan, Okayama .

Abstract. LTE and non-LTE (NLTE) abundances of sulfur of 21 metal-poor stars (mainly halo stars) and one normal star were explored in the metallicity range of
$-3 <$[Fe/H]< 0, using high-resolution ($\sim$ 50000), high-signal-to-noise ($\sim$ 100–450) spectra of S I lines with the multiplet numbers of 1 and 6, which were observed with the 1.88 m telescope equipped with the High Dispersion Echelle Spectrograph (HIDES) at the Okayama Astrophysical Observatory (OAO). Equivalent widths of S I(1) (9212, 9228, 9237 Å) and S I(6) (869 3.9, 8694.6 Å) lines were analyzed to obtain the abundances. Iron abundances were determined from

Fe II lines and used to investigate the behavior of S against Fe. Our main results are: (1) The LTE abundances of S I(6) are systematically smaller than those of S I(1) with the average difference of 0.07 ±0.09 dex. (2) The NLTE corrections for S I(6) abundances are in the range from −0.01 to −0.05 dex with the average of −0.03 dex, while those for S I(1) are from −0.14 to −0.33 dex with the average of −0.22 dex. Consequently, NLTE abundances of S I(6) are systematically larger than S I(1) with the average of 0.13 dex ±0.14 dex. (3) As for the behavior of NLTE [S/Fe], it forms a plateau with the average of [S/Fe]= +0.49 ± 0.12 dex in the range of $-3 <$ [Fe/H]≤ -1.

Chemical Evolution of MgII Absorption Systems

T. Tsujimoto[1], *N. Kobayashi*[1], *M. Iye*[1], *Y. Yoshii*[1] [1]National Astronomical Observatory, University of Tokyo, Japan.

Abstract. Based on the [Mg/Fe] ratios for the high-z Mg II absorption systems obtained by the near-infrared camera and spectrograph for the Subaru 8.2 m Telescope, we construct the chemical evolution model for these high-z objects. It is found that host galaxies for these systems formed within a short time scale of a few hundred million years, suggesting that they are progenitors of modern-day dwarf galaxies. The elemental abundance relation between stars and gas in dwarf galaxies will also be discussed.

The Heavy Element Abundance Pattern in Lead Stars

L. Začs[1], *R. Spelmanis*[1], *F. Musaev*[1] [1]Department of Physics, University of Latvia.

Abstract. A quantitative understanding of evolution of nuclei heavier than iron in the Galaxy has so far been a challenging problem. Only recently have the observational data grown in number and precision to allow a direct comparison with theoretical predictions. In order to reconstruct the evolutionary history of neutron-capture elements in the Galaxy, one must disentangle the *s*- and *r*-process contributions of all their isotopes and follow their abundances as a function of Galactic age. A new series of abundance analysis of lead star candidates is presented here starting with spectroscopy of the lead-rich star HD196944 ([Fe/H] = −2.45; [hs/ls] = +0.8). High resolution CCD spectra in a large spectral region from 3 500 to 10 000 Å have been used to determine detailed abundance patterns for a large number of species. The results are compared with available spectroscopic observations of stars at different metallicities in both the Galactic halo and the disc and with calculations of neutron-capture nucleosynthesis.

JD16

The International Celestial Reference System: Maintenance & Future Realization

Chairpersons: D.McCarthy and F. Mignard

Editors: R. Gauma, D.McCarthy (Chief-Editor) and J. Souchay

Highlights of Astronomy, Vol. 13
International Astronomical Union, 2003
O. Engvold, ed.

Summary of IAU Joint Discussion 16, "The International Celestial Reference System, Maintenance and Future Realizations

Dennis D. McCarthy

U.S. Naval Observatory, Washington, DC 20392, USA

Abstract. The IAU Joint Discussion 16 (JD16) was held in conjunction with the XXVth General Assembly in July, 2003. Papers related to the maintenance of the International Celestial Reference System were presented in the one-day session, and these were followed by discussion that pointed out the need for standard nomenclature. This issue was addressed by the formation of a Division 1 Working Group on the subject. JD16 also pointed out the requirement for a dynamical expression for precession which was addressed by the creation of a Division 1 Working Group on Precession and the Ecliptic. It also showed that although plans are being implemented to provide reference frames for the future, there is a need for improved coordination of astrometric observations. Finally it should be noted that the discussion pointed out the concern for the future organization of IAU Division 1.

1. Introduction

The international Astronomical Union (IAU) Joint Discussion 16 (JD16) was held in connection with the XXVth General Assembly of the IAU in Sydney, Australia in July 2003. The title of the meeting was "The International Celestial Reference System, Maintenance and Future Realizations." The International Celestial Reference System (ICRS) has recently been redefined with the adoption of an International Celestial Reference Frame (ICRF) and revised concepts and models to access the system. The ICRF is a radio reference frame and the current realization in optical wavelengths is the HIPPARCOS Catalogue. Maintenance and improvement of the ICRF requires continuing, coordinated observations.

Extension and densification of the system to other wavelengths remains as a work to be accomplished. It is also necessary at this time to anticipate the maintenance and extension of the ICRF to meet future needs. The models currently used in the definition of the system also require maintenance to ensure that they are able to meet improving observational accuracy in all wavelengths. The potential significant improvement of reference frames from the results of future space astrometry missions requires planning for the long-term realization of the ICRS. These topics were addressed by a series of invited and contributed presentations

2. Presentations

Session 1 of JD 16 was entitled "The International Celestial Reference Frame." It was introduced with a paper by A. Fey and J. Souchay entitled "Status of the International Celestial Reference Frame." C. Ma presented a paper, "Potential refinement of the ICRF" outlining plans to improve the frame. This was followed by a review of recent work done in the Geoscience Australian IVS analysis center by O. Titov. A. M. Gontier and M. Feissel provided a presentation "Contribution of stable radio sources to ICRF improvements" showing the importance of source position stability to the astrometric observations. M. Hosokowa completed the session with a paper that he prepared in conjunction with his colleagues entitled "Astrometric microlensing and degradation of reference frames" that pointed out the limitations on accuracy imposed by microlensing.

Session 2, "Extension of the International Celestial Reference Frame" contained presentations dealing with providing realizations of the reference system in other wavelengths. C. Jacobs in a paper that he prepared with his colleagues entitled "Extending the ICRF to higher radio frequencies: 24 and 43 GHz" pointed out the advantages to moving to higher frequencies. S. Urban followed with a presentation "Densification of the ICRF/HCRF in visible wavelengths" showing plans to improve the reference frame of most concern to the astronomical community. Extension to the infrared was discussed in the paper by N. Zacharias *et al.* entitled "Extending the ICRF into the infrared: 2MASS-UCAC astrometry." C. Pinigin *et al.* presented a paper,"About progress of the link optical-radio systems," and P. Charlot finished the session with a paper, "Source structure" describing recent work in characterizing source structure.

Session 3 dealt with models needed to analyze the astrometric observations that are used to produce the ICRF. V. Dehant in a paper "Geophysical nutation model" described the geophysical background of the recently adopted IAU 2000 precession-nutation model. P. Wallace provided practical implementation procedures in his paper, "Practical consequences of improved precession-nutation model." The philosophy and status of the International Earth Rotation and Reference System Service (IERS) Conventions was described in a presentation by D. McCarthy and G. Petit. T. Fukushima showed a new determination of precession formulas and M. Soffel *et al.* discussed the relativistic concerns with the ICRS in their paper entitled "ICRS, ITRS and the IAU resolutions concerning relativity." J. Vondrak described a reference frame provided largely by historical observations in visual wavelengths made to determine the Earth's orientation in his paper "Earth orientation catalogue - An improved reference frame." I. Platais closed the session with his paper "Astrometry with large un-astrometric telescopes" that outlined work that could be done to improve the ICRF that made use of instrumentation not usually used to make astrometric observation.

The final session was devoted to Space-Based Astrometry and Dynamical Reference Frames. It was introduced with a review of the status of space-based astrometric missions by R. Gaume. F. Mignard followed with a review of recent work on GAIA in his paper "Future space-based celestial reference frame," and the Radio Astron project was described in a presentation by W. Zharov and colleagues. F. Mignard presented a paper by J. Kovalevsky entitled "Misleading proper motions of galactic objects at the mas level." The relationship of modern dynamical ephemerides to the ICRS was covered by M. Standish in his paper "Relating the dynamical frame and the ephemerides to the ICRF."

3. Posters

The work of JD16 was enhanced by a large number of poster contributions. These are listed below.

Wang Wen-Jun, "Celestial three-pole rotations of the Earth."
Hu Hui, "Optical positions of 55 radio stars."
W. Dick, "The ICRS and the IERS information system."
V. Martin, "Ground-based astrometry: optical-radio connection."
P.C. Rocha Poppe, "Relativistic reference systems transformations."
E. Khrutskaya, "Pul-3 catalog of 58483 stars on the Tycho-2 system."
I. Kumkova, "ICRS-ITRS connection consistent with IAU(2000) resolutions."
E. Pitjeva, "The planetary ephemerides EPM and their orientation to ICRF."
M. Stavinschi, "Report of the WG: Future development of ground-based astrometry."
B. Bucciarelli,"Astrometric measurements of radio-stars optical counterparts."
M. Stavinschi, "Reference frames and ground-based astrometry."
S. Lambert, "Coupling between the Earth's rotation rate and nutation."
G. Bourda, "Temporal gravity field and modelisation of Earth rotation."
G. Damljanovic, "ICRF densification via Hipparcos-2MASS cross identification."
F. Mitsumi, "On the construction of radio reference frame using VERA."
A. Fey, "Extending the ICRF to higher frequencies: imaging results."
P. Fedorov, "The star positions and proper motions of stars around ERS."
T. Yano, "Japanese astrometry satellite mission - JASMINE project."
M. Zacharias, "The USNO extragalactic reference frame link program.
A. Kahrin, "An-all wave classification and principle astrometry problem."
D. Boboltz, "Testing the Hipparcos/ICRF link using radio-stars."
J. Souchay, "Numerical approach to the free rotation of celestial bodies."
G. Kaplan, "Another look at non-rotating origins."
O. Roopesh, "IDV sources as ICRF sources: viability and benefits."
O. Roopesh, "USNO/ATNF astrometry and imaging of southern ICRF sources."
F. Bustos, "CDD-based astrometric measurements of photographic plates."
M. Crosta, "Relativistic satellite attitude in the realization of space-borne astrometric catalogues."

4. Discussion

An open discussion prepared and led by P. K. Seidelmann followed the scheduled presentations. Notes from that discussion were taken by N. Zacharias and they form the basis of the following. To initiate the discussion, a list of reference system issues was presented to the participants. These are listed below along with relevant comments by participants.

Items for Discussion

a. Precession-nutation Model

New precession theory?
What angles - Newcomb or Williams?
What nutation model?
An abbreviated nutation theory with less accuracy?
Include geodesic precession and nutation?
Is it a BCRS or GCRS model?

b. Future of Equinox

Introduce Earth Rotation Angle?
Revise definition of ERA?
Dual system by IERS?
Dual system in almanacs?
Transition period specified?
For how long? 2004? Indefinitely?

c. Definition of equinox

Inertial or rotating

d. Introduce Conventional ecliptic

How defined, through x axis of ICRF? by node angle and obliquity?
For what purpose?
With what accuracy?

F. Mignard emphasized that the ecliptic moves and will change with time. D. McCarthy pointed out that this is a subject for the Working Group on precession and that a precise definition of the ecliptic is needed for planetary precession.

e. Terminology issues

CIO and TIO or CEO and TEO?
Stellar angle or Earth Rotation Angle?
right ascensions from equinox only?
right ascensions from CIO?
other terms?

C.Hohenkerk remarked that some concepts seem odd, and that the user is not concerned “which” RA,Dec is used, as long as there is some RA, Dec.

f. Unification of Lists of Constants

IAU Best Estimates
IAU 1976 Astronomical Constants
IERS Best Estimates
IUGG List of Constants
JPL DE 405 Constants
Astronomical Almanac Constants Used
Are all these necessary?

A joint IAU/IUGG committee?

g. Redefinition of UTC
UTC tied to UT1?
Use of "mean solar time"?
Leap seconds or not?

h. Implementation Issues
Who are the users?
What do users need?
What is really used by the IERS?
What is necessary for almanacs offices?
Standardized software?
Documentation required?
Dual availability for how long?
What to do now?

i. Roles of Organizations
WG on Reference systems of IAU Div I
IERS
IAU Comm 5
Others involved?

j. Possible Procedure
IAU /IUGG? WG on Reference Systems with subgroups established now
Dec 2004 WG proposals circulated
Mid 2005 Colloquium for discussion of proposals and draft resolutions
2006 Clarifying resolutions

k. Education Plan
Clear and convincing presentation of reference systems and justifications
Dissemination of information with proposals in Dec 2004
Distribution of 2005 Colloquium Proceedings
Wide distribution of any proposed resolutions well before IAU GA in 2006

In the general discussion following the presentation of the items for discussion K. Johnston said that some issues might not be solved earlier than 2006. P. Wallace argued that we need to get away from the "one-or-the-other" concept and that algorithms are now available for both paradigms so the user can choose. C. Jacobs noted that users need more education so that they can decide how complex they need to go for a given goal in accuracy. P. Wallace replied that there is a misconception that the "new paradigm is more complex," and that this was not true. The non-rotating origin procedure is simpler in concept; like spherical trigonometry and vectors: they are both there to choose. A participant said that this is difficult at the moment, that there is a need for education, and that currently we don't even know what to call things. K. Johnston suggested that there is no need for the general astronomers to make a change because current procedures are sufficient for their requirements. It is only the IERS and space astrometry applications that are concerned about sub-milliarcsecond accuracies and need to use the new more accurate system. It was pointed out that this was true, but people needed to realize that the basic values were coming from new definitions and methods.

Division I Organization

At that point there was a break in the discussion, and T. Fukushima, President of Division I, presented some details regarding the future structure of Division I in the context of this discussion. He said that the ICRS WG has been dissolved because it was too large, with too many sub-tasks. As follow-up for two of the sub-tasks, two new Working Groups were being established. These are (1) precession and the ecliptic chaired by J. Hilton and (2) nomenclature in fundamental astronomy chaired by N. Capitaine.

The new IAU structure puts more emphasis on the Divisions and the Commissions are now dynamic, with a finite life time. It is possible to terminate commissions and to create new commissions upon request by the Division and approval by the IAU Executive Committee. Working groups can be established by approval of the Division, without Executive Committee contact. The approval process is fast, and can be done by e-mail, with no need to wait for a General Assembly.

Fukushima initiated a special committee for the re-organization of Division I. Members are T. Fukushima (chair), F. Mignard, I. Platais, G. Petit, and K. Seidelmann. For the 2003-2006 period (*i.e.* before the special committee issues their recommendations), the proposal for ICRS related issues is that Celestial Reference Frame issues will be directed to Commission 8 and that IERS related issues will be directed to Commission 19. A general discussion followed about the roles of Commissions 8 and 19.

A. Fey asked about the current members of the ICRS WG and whether their expertise would be lost until a re-organization was accomplished. Following some discussion T. Fukushima responded that the "WG ICRS" will continue to exist for the next six months. During that time a re-arrangement can be organized by e-mail.

5. Conclusion

The Joint Discussion pointed out the need for standard nomenclature. This issue was addressed by the formation of a Division 1 Working Group on nomenclature. It also pointed out the requirement for a dynamical expression for precession which was addressed by the creation of a Division 1 Working Group on Precession and the Ecliptic. JD 16 also showed that although plans are being implemented to provide reference frames for the future, there is a need for improved coordination of astrometric observations. Finally it should be noted that the discussion pointed out the concern for the future organization of IAU Division 1. The proceedings will be published and distributed by the U.S. Naval Observatory.

Highlights of Astronomy, Vol. 13
International Astronomical Union, 2003
O. Engvold, ed.

Joint Discussion JD16: Abstracts

Status of the International Celestial Reference Frame:

Alan L. Fey (U.S. Naval Observatory, 3450 Massachusetts Avenue NW, Washington DC, 20392-5420, USA); Jean Souchay (Observatoire de Paris, DANOF, 61, avenue de l'observatoire, 75014 Paris, France)

Abstract. We present a brief report on the status of the International Celestial Reference Frame. There have been two extensions (updates) of the ICRF since its initial definition in 1998. The primary objectives of extending the ICRF were to provide positions for the 109 extra-galactic radio sources observed since the definition of the ICRF and to refine the positions of candidate and other sources using additional observations. A secondary objective was to monitor sources to ascertain whether they continue to be suitable for use in the ICRF. Positions of the ICRF defining sources have remained unchanged. Improved positions and errors for the candidate and other sources were estimated and reflect the changes in the data set and the analysis. The 109 new sources were added with ICRF coordinates. We also discuss current efforts toward ICRF maintenance and the International Celestial Reference System Product Center.

Potential Refinement of the ICRF:

Chopo Ma (NASA Goddard Space Flight Center, Code 926, Greenbelt, MD 20771, USA)

Abstract. The ICRF analysis and data represented the state of the art in global, extragalactic, X/S band microwave astrometry in 1995. Similar analysis has been used to extend the ICRF with subsequent data consistent with the original catalog. Since 1995 there have been considerable advances in the geodetic/astrometric VLBI data set and analysis that would significantly improve the systematic errors, stability, and density of the next realization of the ICRS when the decision is made to take this step. In particular, data acquired since 1990, including extensive use of the VLBA, are of higher quality and astrometric utility because of changes in instrumentation, schedule design, and networks as well as specifically astrometric intent. The IVS (International VLBI Service for Geodesy and Astrometry) continues a systematic extension of the astrometric data set. Sufficient data distribution exists to select a better set of defining sources. Improvements in troposphere modeling will minimize known systematic astrometric errors while accurate modeling and estimation of station effects from loading and nonlinear motions should permit the re-integration of the celestial and terrestrial reference frames with Earth orientation parameters though a single VLBI solution. The differences between the current ICRF and the potential second realization will be described.

The CRF Solution by the Geoscience Australia IVS Analysis Center:

Oleg Titov (GPO Box 378, Canberra, ACT, 2601, Australia)

Abstract. The Geoscience Australia IVS Analysis Center is working for improvement of the ICRF. The catalogue of 659 radio-source positions estimated from a 23-year set of the VLBI data (1980-2003) in a homogeneous solution

(TRF, CRF, EOP) has been obtained using the OCCAM software. Statistical analysis of the results shows that the median accuracy of the source positions is 0.2-0.3 mas in both coordinates. The long-term apparent motions of two quasars: 0923+392 (4C39.25) and 2145+067 are also analyzed.

Contribution of stable sources to ICRF improvements:
A.-M. Gontier & Martine Feissel-Vernier (Observatoire de Paris, SYRTE, 61, avenue de l'observatoire, 75 014 Paris France)

Abstract. A set of stable compact radio sources is proposed for the future maintenance of the ICRF axes, based on time series analysis of VLBI-derived coordinates of extragalactic radio sources. The selection scheme makes a combined use of statistical and deterministic tests. It identifies 199 stable sources, to be compared to the current 212 defining sources. Their consideration for the maintenance of the frame axes is expected to improve the frame stability by a factor of five, reaching the level of less than 10 microarcseconds in the medium term. The improved stability and internal consistency of the frame also enhances the quality of the Earth orientation determinations.

Astrometric Microlensing and Degradation of Reference Frames:
Mizuhiko Hosokawa (Communications Research Laboratory, Tokyo, 184-8795, Japan); Kouji Ohnishi (Nagano National College of Technology, Nagano, 381-8550, Japan); Toshio Fukushima (National Astronomical Observatory, Mitaka, Tokyo, 181-8588, Japan)

Abstract. We have pointed out that the positions of extragalactic radio sources fluctuate on the order of a micro arcsecond (μas) because of astrometric microlensing by stars and MACHOs in our galaxy (Hosokawa *et al.* 1997). This means that the kinematical reference frames based on the positions of extragalactic radio sources will be degraded by this kind of fluctuation. Recently, we have shown that in the case of the extragalactic sources in the direction close to the Galactic Center, the optical depth of 10 μas fluctuation is about a quarter for the standard model of our galaxy (Hosokawa *et al.* 2002). Further, macro scale astrometric gravitational lensing by the collective mass of the Galactic Center appears in a different manner. In this paper we discuss the type, the magnitude and the time scale of the degradation of reference frames due to the astrometric gravitational lensing. For the astrometric gravitational lensing event of a few μas caused by each star, the event duration is expected to be several years. On the other hand, the induced motion due to macro scale astrometric gravitational lensing is practically regarded as secular.

Extending the ICRF to Higher Radio Frequencies: 24 & 43 GHz:
Christopher S. Jacobs (Jet Propulsion Laboratory, California Institute of Technology, 4800 Oak Grove Drive, Pasadena, CA 91109, USA); Patrick Charlot, David Gordon, Gabor Lanyi Chopo Ma, Charles Naudet, Ojars Sovers, Liwei Zhang, and the KQ VLBI Survey Collaboration

Abstract. Astrometric observations of active galactic nuclei have been used to construct quasi-inertial global reference frames, most notably the International Celestial Reference Frame (ICRF) which now forms the basis for all as-

trometry including deep space navigation. The ICRF was defined using X- (8.4 GHz) and S-band (2.3 GHz) observations collected over 20+ years. There are several motivations for extending this work to higher frequencies, namely, to construct a more stable frame based on more compact sources, to provide calibrators for phase referencing, and to support spacecraft navigation at higher frequencies.

Survey observations using the Very Long Baseline Array at K-band (24 GHz) and Q-band (43 GHz) have been undertaken to pursue these goals. Three observing sessions have covered the full 24 hours of right ascension and declination down to -30 deg. The resulting catalog of 80+ sources has K-band median formal position uncertainties of < 200 micro-arcseconds. The Q-band positional uncertainties are about 1.5 times larger. Group delay residuals were excellent at approximately 20 psec weighted RMS. Comparison of the K-band frame to the S/X-band ICRF shows systematic errors which we will discuss.

The research performed at JPL-Caltech and GSFC was done under contract with NASA.

Densification of the ICRF/HCRF in Visible Wavelengths:
Sean E. Urban (U.S. Naval Observatory, 3450 Massachusetts Ave. NW, Washington DC, 20392-5420, USA)

Abstract. With the release of the Hipparcos Catalogue and the IAU resolution designating its 100,000 star subset as the HCRF, the optical reference frame increased 20-fold in the number of stars over the FK5. For many applications, even these 100,000 stars are inadequate in spatial density and limiting magnitude. However, Hipparcos is dense enough and deep enough to reduce many astrometric catalogs directly; the resulting data can be used to densify the HCRF and extend its magnitude limit. The initial major densification efforts of the HCRF utilized the Tycho data, culminating in the Tycho-2 Catalogue of 2.5 million stars. Over the last few years, several groups have been working toward even greater densification. Some resulting catalogs, such as the CMC 13, M2000, and SPM 2.0 are zonal, covering selected areas of the sky. Others, such as UCAC, USNO-B, and GSC 2.3 aim at global coverage but with varying degrees of accuracy and magnitude regimes. Others, namely DENIS and 2MASS, are extending the HCRF into the near IR realm. The current state of many of these projects, and what is expected in the next few years in terms of densification of the optical frame, is presented.

Extending the ICRF into the Infrared: 2MASS−UCAC Astrometry:
Norbert Zacharias (U.S. Naval Observatory, 3450 Massachusetts Ave. NW, Washington DC, 20392-5420, USA); Howard L. McCallon, Eugene Kopan & Roc M. Cutri (IPAC, Caltech, MS 100-22, 770 S. Wilson Ave., Pasadena, CA 91125, USA)

Abstract. An external comparison between the infrared 2MASS and the optical UCAC positions was performed, both being on the same system, the ICRS. About 48 million sources in common were identified. Random errors of the 2MASS catalog positions are about 60 to 70 mas per coordinate for the K_S = 4 to 14 range, increasing to about 100 to 150 mas for saturated and very faint stars. Systematic position differences between the 2 catalogs are very small, about 5 to 10 mas as a function of magnitude and color, with somewhat larger

errors as a function of right ascension and declination. The extension of the ICRF into the infrared has become a reality.

Progress on Linking Optical-Radio Reference Frames Using CCD Ground-Based Telescopes:

N.Maigurova, G.Pinigin, Yu.Protsyuk (Nikolaev Astronomical Observatory, Observatorna 1, Nikolaev, 54030 UKRAINE); R.Gumerov (Kazan State University, Kremlevskaya 18, Kazan, 420008 RUSSIA); Z.Aslan & I.Khamitov (Turkish National Observatory TUG, Antalya, 07058 TURKEY); W.Jin, Z.Tang, S.Wang (Shanghai Astronomical Observatory, Nandan Road 80, Shanghai, 200030 CHINA)

Abstract. Results of the Joint Project between observatories from China, Russia, Turkey and Ukraine on improvement of linking optical and radio reference frames are discussed. The 300 extra-galactic radio sources (ERS) observation program is extended due to the increase of observations in the southern hemisphere up to $-40°$ declination. At present, observations of more than 150 ERS were used for reduction. The intermediate internal estimation of the link between optical and radio reference frames showed values near zero within an accuracy of about 6 *mas* by using secondary reference stars from UCAC2. A comparison of presented results with those of other investigations was made.

Extragalactic Source Structure:

Patrick Charlot (Observatoire Aquitain des Sciences de l'Univers–CNRS/UMR 5804, BP 89, 33270 Floirac, France)

Abstract. The compact extra-galactic radio-emitting objects used to define the I nternational Celestial Reference Frame (ICRF) are only imperfect fiducial points in the sky on milliarcsecond scales. Many sources show frequency- and time-dependent extended emission structures with varied morphologies that are explained in the framework of unified theories of active galactic nuclei. Such theories are also useful to make predictions about the expected source morphology at optical and IR wavelengths. Various imaging surveys are now available to evaluate the source compactness and astrometric suitability on a statistical basis. Additionally, exploratory work is being conducted to correct for the effect of source structure in actual astrometric analysis by using hundreds of source maps, as available from ongoing structure monitoring. Recent progress in these areas are reviewed in the framework of future possible ICRF realizations.

Geophysical Nutation Model:

Véronique Dehant (Royal Observatory of Belgium, Ringlaan 3, B-1180 Brussels, Belgium)

Abstract. The nutation model that has been adopted by the IAU in 2000 is the semi-analytical model MHB2000 of Mathews et al. (2002, JGR 107(B4), DOI: 10.1028/ 2001JB000390). We show how robust this model is and examine the information about the interior of the Earth that has been derived. The observations used to derived the parameters of MHB2000 as well as the amplitude of the Free Core Nutation (FCN) are examined in terms of their stability and precision. Additional contributions from the external geophysical fluids (atmosphere, ocean) are also studied and shown to be non-negligible.

Practical Consequences of the Improved Precession-Nutation Models:
Patrick T. Wallace (Space Science & Technology Dept., CLRC / Rutherford Appleton Laboratory, Chilton, Didcot, OX14 4HH, United Kingdom)

Abstract. The IAU 2000 precession-nutation models are classical in form, unlike the associated Earth rotation model. The counterpart of GST in the new system is "Earth Rotation Angle", which is directly proportional to UT1 and is reckoned with respect to a kinematically-defined "non-rotating origin", the CEO. Though essential for interpreting Earth-rotation at VLBI accuracies and simplifying the computation of (h, δ), the introduction of the CEO has aroused considerable controversy. The new models came into use for VLBI analysis at 2003 January 1, and subsequent IERS Bulletins provide $(\delta X, \delta Y)$ relative to the IAU 2000 celestial pole in addition to the existing $(\delta\Delta\psi, \delta\Delta\epsilon)$ corrections to IAU1976/80. The almanac offices face interesting choices of how to present the new quantities and which, if any, of the existing tabulations can be omitted. Most astronomers will, however, be little affected. In parallel with developing the new canonical models, considerable efforts have been made also to provide classical equivalents of similar accuracy, to give users a choice of when (or whether) to adopt the new methods. The models, both new and classical, have been implemented as Fortran subroutines and published through the IERS website. An extended set of routines has been released through the IAU SOFA initiative.

IERS Conventions:
Dennis D. McCarthy (U.S. Naval Observatory, 3450 Massachusetts Ave. NW, Washington DC, 20392-5420, USA); Gerard Petit (Bureau International des Poids et Mesures, Paris, France)

Abstract. The International Celestial Reference Frame (ICRF) is currently a radio reference frame accessed through Very long Baseline Interferometry (VLBI) and refined with technique-dependent improvements described in this Joint Discussion. An important component of the International Celestial Reference System (ICRS) that is the basis for this frame is the set of conventional models and procedures that are used to define the system. The International Earth Rotation and Reference System Service (IERS) Conventions Center, provided jointly by the U.S. Naval Observatory (USNO) and the Bureau International des Poids et Mesures (BIPM), produces the IERS Conventions that contain the models and procedures needed to realize and access the ICRS. The key elements of the Conventions related to the ICRS are outlined, and recent improvements are

highlighted. Improvements in the IERS Conventions (models and procedures) should play a role by globally improving IERS products.

New Precession Formula:

Toshio Fukushima (NAO Japan, 2-21-1, Ohsawa, Mitaka, Tokyo, 181-8588, Japan)

Abstract. We adapted J.G. Williams' expression of the precession and nutation using the 3-1-3-1 rotation (Williams 1994) to an arbitrary inertial frame of reference. The modified formulation avoids a singularity caused by finite pole offsets near the epoch. By adopting the planetary precession formula numerically determined from DE405 (Harada and Fukushima 2003) and by using a recent theory of the forced nutation of the non-rigid Earth, SF2001 (Shirai and Fukushima 2001), we analyzed the celestial pole offsets observed by VLBI for 1979-2000 (McCarthy 2000, private communication) and determined the best-fit polynomials of the luni-solar precession angles. Then we translated the results into the classic precession quantities and evaluated the difference in them due to the difference in the ecliptic definition. The combination of these formulas and the periodic part of SF2001 serves as a good approximation of the precession-nutation matrix in the ICRF.

ICRS, ITRS, and the IAU Resolutions Concerning Relativity:

Mike Soffel & Sergei Klioner (Lohrmann-Observatorium, Institut fur Planetare Geodasie, Technische Universitat Dresden, Mommsenstrasse 13, D-01062 Dresden, Germany)

Abstract. The IAU2000 Resolutions concerning relativity introduce two celestial reference systems, a barycentric one, BCRS with coordinates (t,x), and a geocentric one, GCRS with coordinates (T,X). The two sets of coordinates are related by 4-dimensional space-time transformations. So far the relations of the BCRS and GCRS with the ICRS and ITRS have NOT been discussed. This will be done here. It is argued that the ICRS is a special representation of the BCRS, and the ITRS-coordinates differ from the GCRS ones by a time dependent rotation of spatial coordinates plus possible scale factors. This implies that also the ICRS- and the ITRS- coordinates are related by a generalized Lorentz-transformation.

Earth Orientation Catalogue - An Improved Reference Frame:

Jan Vondrák & Cyril Ron (Astronomical Institute, Academy of Sciences of the Czech Republic, Boční II, 14131 Prague 4, Czech Republic)

Abstract. Optical observations of latitude/universal time variations of nearly five thousand stars (made during the twentieth century at 33 observatories in Earth orientation programmes) are used, in combination with the Hipparcos and Tycho catalogues and their combination with ground-based observations (ARIHIP), to derive a new improved star catalogue called the Earth Orientation Catalogue (EOC). The first version of the catalogue, EOC-1, based on the observations with instruments observing in local meridian, is now finished. The improved proper motions and/or positions are more convenient for long-term extrapolation of apparent places than those of the original Hipparcos and Ty-

cho Catalogues. The catalogue EOC is planned to be used for another new re-analysis of Earth orientation parameters based on optical astrometry observations in the 20th century.

Astrometry With Large Un-Astrometric Telescopes:
Imants Platais (Department of Physics and Astronomy, Johns Hopkins University, Baltimore, MD 21218, USA)

Abstract. Over the last few decades the number of large-sized telescopes has grown dramatically. These new telescopes were designed to produce sharp images of stars and galaxies and are not necessarily optimized for astrometric measurements. Despite this and some other limitations cutting-edge astrometry can be done with such instruments. Space-based CCD imagers can easily break the 1-mas precision limit, while ground-based telescopes are currently limited to accuracies of 3-5 mas. It is expected that the Large Synoptic Survey Telescope will produce a 15 petabyte imaging database down to $V = 28$ and over 30,000 square degrees of the sky, which opens new horizons for astrometry.

Status of Space-Based Astrometric Missions:
Ralph Gaume (U.S. Naval Observatory, 3450 Massachusetts Ave. NW, Washington DC, 20392-5420, USA)

Abstract. Since the highly successful Hipparcos space-based astrometry mission, a number of follow-up programs have been proposed to accomplish a wide variety of scientific goals. Due in part to funding pressure and technical challenges, the status of these missions has changed on a nearly continuous basis (proposal, selection, descope, cancellation, rescope, reproposal). The status, capabilities, operational concept, science goals, schedules, and technical challenges of the current set of space-based astrometric missions will be discussed.

Realization of the Inertial Frame with GAIA:
François Mignard (OCA/CERGA, av. Copernic, F06130 Grasse, France)

Abstract. The European Space Agency astrometry mission Gaia scheduled for a launch in mid-2010 will observe thousands of extra-galactic sources together with nearly one billion stars. With a target accuracy of 10 microarcseconds at $V = 15$ and 50 microarcseconds at $V = 18$, this will open a new era in the realization of the primary reference frame. The very principles of this direct realization in the visible are outlined in this paper together with a discussion of modeling problems or intrinsic limitations due to the galactic rotation, source instability or the occurrence of gravitational lensing.

Astrometric Goals of the RadioAstron Mission:
Vladimir E. Zharov, Igor A. Gerasimov, Konstantin V. Kuimov (Sternberg State Astronomical Institute, 13, Universitetskij prospect, 119992 Moscow Russia);

Aleksander E. Rodin & Yury P. Ilyasov (Puschino Radio Astronomy Observatory, 142290 Puschino Russia)

Abstract. The high-apogee elliptical orbit of the RadioAstron international mission impacts precision astrometry on the level of about a microsecond of arc (μas). Optimal launch of the RadioAstron mission could be on March 2006. The RadioAstron program is the next generation of the radioastrometry programs. According the RadioAstron program, initiated by the Astro Space Center of Lebedev Physical Institute of Russian Academy of Science (supervisor N.S.Kardashev) in collaboration with other institutes of Russia and abroad, the satellite SPECTR carrying a 10-meter radio telescope will be launched in a highly eccentric orbit with eccentricity $e = 0.853$. Apogee distance will be 350 000 km. It is planned that the VLBI observations will be conducted with the largest ground-based radio telescopes. The period of revolution of the satellite will be about 9.5 days, and observational time during one revolution can be about 9 days. Observations can be made at P, L, C, and K frequency bands with a bandwidth of 32 MHz. For the shortest wavelength 1.35 cm and baseline of about 350 000 km resolving power of order of 8 μas can be achieved. It is planned to solve both astrophysical and astrometry problems during a total expected lifetime of the satellite of three years. The main astrometric goal of the mission is the realization of a new International Celestial Reference Frame based on measurements of the coordinates of ~ 100 defining sources with microarcsecond accuracy. Observations of some pulsars on the space-ground interferometers and by the timing technique will allow us to connect kinematical and dynamical systems with unprecedented accuracy. Coordinates of ground radio telescopes will be determined with respect to the geocenter.

Misleading Proper Motions of Galactic Objects at the Microarcsecond Level:

Jean Kovalevsky (Observatoire de la Cote d'Azur, Avenue Copernic, 06130 Grasse, France)

Abstract. At the microarcsecond (muas) level of accuracy of observations foreseen by the GAIA program, the effects of the curvature of stellar orbits around the center of the galaxy cannot be neglected. The curvature of the solar system barycentric motion induces a time dependent component of the aberration, which reaches, in some regions of the sky, 4 muas per year. In the case of stars, it is combined with a similar effect due to the curvature of the galactocentric orbit of the star, which may reach 600 muas per year for a star situated at 50 parsecs from the center of the galaxy, and much larger closer to it. The formulae permitting us to compute these apparent proper motions are given together with the maps describing this effect within the galaxy. They disappear if one uses a galactocentric rather than a barycentric reference frame. The advantages and difficulties of this frame are discussed.

Relating the Dynamical Reference Frame and the Ephemerides to the ICRF:
E. M. Standish (CalTech/Jet Propulsion Laboratory; 301-150; Pasadena, CA 91109, USA)

Abstract. In the past, the motions of solar system bodies were used to establish a non-rotating "inertial" reference system, often referred to as "the dynamical reference frame". With the establishment of the ICRF, the use of a dynamical reference frame has become obsolete in this context.

Planetary ephemerides, on the other hand, continue to play vital roles in a number of other applications, such as spacecraft navigation, mission design, etc. For present-day ephemerides, the accuracies of the inner planet positions are 1 *km* or less in all coordinates, including the orientation of the system onto the ICRF. Certain quantities are much better known over specific time intervals (e.g., Earth-Mars distance over the past few decades, throughout which it has been accurately measured). The outer planet positions are significantly less well-known, being established during the present era by CCD observations to about $0\overset{''}{.}05$ or so, but quickly deteriorating for decades away from the present.

The ICRS and the IERS Information System:
Wolfgang R. Dick, Bernd Richter, & Wolfgang Schwegmann (IERS Central Bureau, BKG, Richard-Strauss-Allee 11, 60598 Frankfurt am Main, Germany)

Abstract. This paper discusses the role of the International Earth Rotation and Reference Systems Service (IERS) for the International Celestial Reference System (ICRS) with emphasis on the IERS Information System, consisting of data, publications, documentation, and other information in printed and online form. Plans for a new database-driven information system are outlined.

ICRS — ITRS Connection Consistent with IAU (2000) Resolutions:
Irina Kumkova (Institute of Applied Astronomy RAS, 10, Kutuzov emb, St.Petersburg, 191186 RUSSIA); Michael Stepashkin (Saint-Petersburg Institute for Informatics and Automatics RAS)

Abstract. Algorithms of direct and reverse relativistic 4-dimensional transformation of barycentric and geocentric celestial reference coordinate systems (BCRS and GCRS) according to IAU Resolution B1(2000) are developed. Transformation between BCRS and GCRS is considered as a part of general process of linking the International Celestial Reference System to the International Terrestrial Reference System, provided by the International Earth Rotation and Reference System Service.

Reference Frames and Ground-Based Astrometry:
Magda Stavinschi (Astronomical Institute of the Romanian Academy, Str. Cutitul de Argint 5, RO-040558 Bucharest, Romania, E-mail: magda@aira.astro.ro)

Abstract. We try to analyze the contribution to the extension of optical reference frame to faint stars in crowded fields, the production of input catalogues for future space projects, re-observation of existing catalogues for proper motion determination, link of optical and radio reference frames, position of radio-source optical counterparts, stellar catalogues, etc. It is one of the tasks of the WG on The Future Development of Ground-Based Astrometry.

The Future Development of Ground-Based Astrometry:
Magda Stavinschi (Astronomical Institute of the Romanian Academy, Str. Cutitul de Argint 5, RO-040558 Bucharest, Romania, E-mail: magda@aira.astro.ro); Jean Kovalevsky (Observatoire de la Côte d'Azur - CERGA, av. Copernic, F-06130 Grasse, France, E-mail: Jean.Kovalevsky@obs-azur.fr)

Abstract. This WG was created following the decision of Division 1 at the XXIVth IAU GA at Manchester. During the three years it was chaired by M. Stavinschi (Romania) and Jean Kovalevsky (France). Members are Daffydd Wyn Evans (UK), Carlos Lopez (Argentina), Dan Pascu (USA), Antonio Pugliano (Italy), Manuel Sanchez (Spain), Ramakhrisna Teixeira (Brazil), and Arthur Upgren (USA).

Astrometric Measurements of Radio Sources Optical Counterparts. OATo Campaign: Some Final Results:
B. Bucciarelli, M.T. Crosta, M.G. Lattanzi, G. Massone, R. Morbidelli (Astronomical Observatory of Torino, I-10025, Italy); W. Jin, Z. Tang (Astronomical Observatory of Shanghai, 200030 China); G. Deiana, A. Poma, S. Uras (Astronomical Observatory of Cagliari, I-09012, Italy)

Abstract. We present photographically determined positions of a sub-set of 20 radio sources from a larger sample collected by OATo during a dedicated campaign, as described in this paper. Targets are from the list of extra-galactic objects adopted by the IAU for the realization and maintenance of the ICRF. The results obtained so far are in agreement with the VLBI-determined radio positions at a significance level of better than 100 microarcseconds.

Coupling Between the Earth's Rotation Rate and Precession-Nutation:
Sébastien Lambert (SYRTE - UMR8630/CNRS, Observatoire de Paris, 61 avenue de l'Observatoire, 75014 Paris, France)

Abstract. For different Earth models, we computed the effects of variations in the Earth's rotation rate on precession-nutation. In the case of a refined model with elastic mantle and decoupled liquid core, we found a major contribution of -136.56 μas and 6.18 μas on the 18.6-year nutation respectively in longitude and in obliquity, and a decrease of -3222.80 μas/century on the precession rate in longitude.

ICRF Densification Via HIPPARCOS-2MASS Cross-Identification:
Goran Damljanović (Astronomical Observatory, Volgina 7, 11160 Belgrade, Ser-

bia and Montenegro); Jean Souchay (Observatoire de Paris, DANOF, 61, avenue de l'observatoire, 75 014 Paris, France)

Abstract. We developed a cross-identification programme of stars of any two catalogues, and applied it to HIPPARCOS and 2MASS. It found 37940 common stars, after selecting a rejection criterion, that we set to a 3σ value. The procedure was more than 68.5% successful by using the data of catalogues. There were 117955 HIPPARCOS stars, and 162195232 2MASS Second Incremental Data Release ($\sim$ 47% of the sky) ones in our basic selection. Then, we calculated a preliminary systematic error ($\sim 0\overset{''}{.}10$) of differences $\Delta\alpha$ and $\Delta\delta$ of detected common stars, included it into the programme, and the cross-identification was near 80% successful.

Extending the ICRF to Higher Radio Frequencies - First Imaging Results:

A. L. Fey, D. A. Boboltz (U.S. Naval Observatory - 3450 Massachusetts Avenue NW, Washington DC, 20392-5420, USA); P. Charlot (Observatoire Aquitain des Sciences de l'Univers - CNRS/UMR 5804, BP 89, 33270 Floirac, France); E. B. Fomalont (National Radio Astronomy Observatory - 520 Edgemont Road, Charlottesville, Virginia 22903–2475, USA); G. E. Lanyi, L. D. Zhang (Jet Propulsion Laboratory - California Institute of Technology, 4800 Oak Grove Drive, Pasadena, CA 91109-8099, USA); and the K-Q VLBI Survey Collaboration

Abstract. We present first imaging results and preliminary source structure analysis of 108 extra-galactic objects observed using the Very Long Baseline Array (VLBA) at 24 GHz and 43 GHz as part of a joint NASA, USNO, NRAO and Bordeaux Observatory program to extend the ICRF to higher radio frequencies.

Japan Astrometry Satellite Mission — The JASMINE Project:

Taihei Yano, Naoteru Gouda, Yukiyasu Kobayashi, Takuji Tsujimoto Yukitoshi Kan-ya (National Astronomical Observatory, Mitaka, Tokyo 181-8588, Japan); Yoshiyuki Yamada (Graduate School of Science, Kyoto University, Sakyo-ku, Kyoto 606-8502, Japan); Hiroshi Araki, Seiichi Tazawa, Kazuyoshi Asari,Seiitsu Tsuruta, Hideo Hanada, Nobuyuki Kawano (National Astronomical Observatory, Mizusawa, Iwate 023-0861, Japan)

Abstract. JASMINE is the name of a Japanese infrared (z-band: 0.9 μm, or K-band: 2.2μm) scanning astrometric satellite, planned to be launched between 2013 and 2015. The main objective of JASMINE is to study the fundamental structure and evolution of the disk and the bulge components of the Milky Way Galaxy. Its important objective is to investigate stellar physics. In order to accomplish the objective, JASMINE will measure parallaxes, positions and proper motions with a precision of 10 microarcsec (μas) at z =15.5mag or K=12mag.

The USNO Extragalactic Reference Frame Link Program:

Marion I. Zacharias (USRA, 1101 17th St. NW, Suite 1004, Washington DC, USA and U.S. Naval Observatory, 3450 Mass. Ave. NW, Washington DC, 20392, USA); Norbert Zacharias, & Theodore J. Rafferty (U.S. Naval Observatory, 3450 Mass. Ave. NW, Washington DC, 20392, USA)

Abstract. The objective of this project is to improve the link between the radio and optical reference frames over the initial Hipparcos effort. The alignment of the radio-optical systems is important for absolute proper motions and source identification across the wavelength spectrum. There are 717 ICRF+extensions radio sources. The U.S. Naval Observatory (USNO) extra-galactic reference frame link program includes all applicable ($\approx$ 600) sources with optical counterparts. Furthermore, USNO is involved in the extra-galactic link of the Space Interferometry Mission (SIM) and plans for a new astrometric, ground-based, 1-meter class telescope.

Testing the Hipparcos/ICRF Link Using Radio Stars:

D. A. Boboltz, A. L. Fey, K. J. Johnston, N. Zacharias & R. A. Gaume (U.S. Naval Observatory, 3450 Massachusetts Avenue NW, Washington DC, 20392-5420, USA)

Abstract. We have undertaken an effort to verify and improve the radio/optical frame link through connected element interferometer astrometry of radio stars. In our first epoch, we observed 19 radio stars using the Very Large Array in A-configuration plus the Pie Town Very Long Baseline Array antenna (VLA+PT). Differences in right ascension and declination were computed between our VLA+PT data and the Hipparcos positions updated to our epoch (2000.94). A weighted least-squares fit to the position differences was performed and the three rotation angles between the radio and optical frames were determined. We found that the two frames are aligned to within the formal errors of approximately 3 milliarcseconds per axis. Presented here are the results of this work and the plans for future work.

Another Look at Non-Rotating Origins:

George H. Kaplan (U.S. Naval Observatory, 3450 Massachusetts Ave. NW, Washington DC, 20392-5420, USA)

Abstract. Two "non-rotating origins" were defined by the IAU in 2000 for the measurement of Earth rotation: the Celestial Ephemeris Origin (CEO) in the ICRS and the Terrestrial Ephemeris Origin (TEO) in the ITRS. Universal Time (UT1) is now defined by an expression based on the angle θ between the CEO and TEO. Many previous papers, e.g., Capitaine, Guinot, & McCarthy (2000), developed the position of the CEO in terms of a quantity s, the difference between two arcs on the celestial sphere. A similar quantity s' was defined for the TEO.

As an alternative, a simple vector differential equation for the position of a non-rotating origin on its reference sphere is presented here. The equation can be easily numerically integrated to high precision. This scheme directly yields the unit vector of the CEO in the ICRS, or that of the TEO in the ITRS, as a function of time. This simplifies the derivation of the main transformation matrix between the ITRF and the ICRS. The directness of the development may have pedagogical and practical advantages for the vast majority of astronomers who are unfamiliar with the history of this topic.

IDV Sources as ICRF Sources: Viability and Benefits:

Roopesh Ojha (Australia Telescope National Facility, CSIRO, PO Box 76, Epping, NSW 1710, Australia); Alan L. Fey (U.S. Naval Observatory, 3450 Massachusetts Ave. NW, Washington DC, 20392-5420, USA); David L. Jauncey (Australia Telescope National Facility, CSIRO, PO Box 76, Epping, NSW 1710, Australia); Kenneth J. Johnston (U.S. Naval Observatory, 3450 Massachusetts Ave. NW, Washington DC, 20392-5420, USA); James E. Lovell & Lucyna Kedziora-Chudczer (Australia Telescope National Facility, CSIRO, PO Box 76, Epping, NSW 1710, Australia)

Abstract. Radio sources that exhibit rapid variability in their light curves, as a result of radio wave propagation through turbulent electron density fluctuations in the interstellar medium, appear to be the most compact sources in the sky. In particular, the most variable weak sources, might be the most point-like and, thus, some of the best candidates for densification of the International Celestial Reference Frame (ICRF) and consequent improvement in its accuracy. Further, the advent of the Mk IV/V VLBI system will make use of weaker sources easier. We will discuss the viability of this idea and state the benefits that might flow from this approach.

USNO/ATNF Astrometry and Imaging of Southern Hemisphere ICRF Sources:

Roopesh Ojha, David L. Jauncey (Australia Telescope National Facility, CSIRO, PO Box 76, Epping, NSW 1710, Australia); Alan L. Fey, Kenneth J. Johnston (U.S. Naval Observatory, 3450 Massachusetts Ave. NW, Washington DC, 20392-5420, USA); Richard G. Dodson, Simon D. Ellingsen, Peter M. McCulloch (University of Tasmania, Hobart, Australia); George D. Nicolson, Jonathan F. H. Quick (Hartebeesthoek Radio Astronomy Observatory, Krugersdorp, South Africa); John E. Reynolds, Anastasios K. Tzioumis & Warwick E. Wilson (Australia Telescope National Facility, CSIRO, PO Box 76, Epping, NSW 1710, Australia)

Abstract. The USNO and the ATNF are collaborating in a continuing VLBI research program in southern hemisphere source imaging and astrometry. The goals of this program are two fold: to image all southern hemisphere ICRF sources at least twice for structure monitoring and to search for new astrometric sources for densification of the ICRF. All 184 existing ICRF sources south of -20 degrees, have been observed for imaging at least once. Imaging and a second epoch of observations are underway. In order to identify new extra-galactic radio sources to be added to the ICRF, survey observations of selected ATCA calibrator sources have been interspersed among the imaging observations. These survey observations have, to date, identified a total of 29 possible astromet-

ric targets. Dedicated astrometric VLBI experiments have been scheduled to determine accurate positions for these sources.

CCD-Based Astrometric Measurements of Photographic Plates:

I. H. Bustos Fierro & J. H. Calderon (Observatorio Astronomico, Universidad Nacional de Cordoba, Rep. Argentina)

Abstract. A methodology for the astrometric measurement of photographic plates making use of a scientific grade CCD camera was developed and tested on a Carte du Ciel plate. In order to measure a complete CdC plate a mosaic of f64 frames with partial overlap in both coordinates was made. With the aim of evaluating the accuracy of stellar centroids a MAMA-based digitization of the same plate was employed as a pattern. We found a noticeable radial distortion produced by the optical system of the camera that was corrected. The reduction to celestial coordinates was performed by means of the block-adjustment technique, using Tycho-2 as a reference catalog. Differences with Tycho-2 suggest that the errors of CCD-based positions obtained ftom the CdC plate are between 0.20 and 0.25 arcseconds. These positions are intended to be employed in the determination of proper motions at few mas/yr level, therefore allowing densification of the proper motion system in regions of interest of the sky up to photographic magnitude 14.5 (for CdC plates), using a relatively low cost device available at our own observatory.

Relativistic Satellite Attitude: Joining Local and Global Reference Frames for the Realization of Space-Borne Astrometric Catalogues:

Donato Bini (Istitute "M. Picone", C.N.R., and I.C.R.A., Rome, Italy); Beatrice Bucciarelli, Maria T. Crosta, Mario G. Lattanzi, and Alberto Vecchiato (Turin Astronomical Observatory, Pino Torinese, Turin, Italy); Fernando de Felice (Department of Physics, University of Padova, Padova, Italy)

Abstract. The definition of the satellite rest frame plays a fundamental role in the relativistic treatment of space observations. We find a mathematical representation of this frame which is an analytical solution accurate to $(v/c)^3$ and corresponds to the expected attitude of the astrometric satellite Gaia. We named this frame *attitude frame* since it takes into account the satellite's actual orbital motion and attitude law, both computed in global BCRS coordinates. Moreover, we show that the running time on Gaia is compatible with IAU resolution B1.5 (2000).

JD17

Atomic Data for X-Ray Astronomy

Chairperson: A.K. Pradhan

Editors: A.K. Pradhan, Sultana Nahar, and P.L. Smith (Chief-Editor)

Highlights of Astronomy, Vol. 13
International Astronomical Union, 2003
O. Engvold, ed.

IAU XXV JD17: Atomic Data For X-Ray Astronomy

Anil K. Pradhan and Sultana N. Nahar

Department of Astronomy, The Ohio State University, Columbus, OH 43210, USA

Peter L. Smith

Harvard Smithsonian Center for Astrophysics, Cambridge, MA 023138, USA

Abstract. The Joint Discussion on Atomic Data For X-ray Astronomy addressed all aspects of X-ray astronomy: (I) New Observations, (II) Atomic Theory, (III) Laboratory Measurements (IV) Numerical Simulations, (V) Databases. There were 22 invited presentations and approximately 40 contributed papers. Following papers are brief summaries of the proceedings.

A detailed description of the aims and contents of JD17 are given at: www.astronomy.mps.ohio-state.edu/~pradhan/Iau/iau.html. The SOC consisted of: N. Brickhouse (USA), H. Hasan (USA), J. Houck (USA), A. Fabian (UK), J. Kaastra (Netherlands), F. Keenan (UK), S. Kahn (USA), T. Kallman (USA), H. Netzer (Israel), A.K. Pradhan (USA, Chair), P.L. Smith (USA), K.Yamashita (Japan).

Acknowledgments. The SOC would like to thank the Executive Committee and the Secretariat of the IAU for approving the JD, local arrangements in Sydney, for several travel grants to invited speakers. The chair (AKP) would especially like to thank Dr. Hans Rickman for great and prompt assistance in all of these.

Highlights of Astronomy, Vol. 13
International Astronomical Union, 2003
O. Engvold, ed.

Probing X-ray Emitting Plasma with High Resolution Chandra and XMM-Newton Spectra

Julia C. Lee

Chandra Fellow, MIT Center for Space Research, 77 Massachusetts Ave. NE80-6073, Cambridge, MA. 02139 USA

Abstract. Highlights of interesting astrophysical discoveries are reviewed in the context of high resolution X-ray spectroscopy made possible with *Chandra* and *XMM-Newton* , and its relevance to atomic physics calculations and measurements is discussed. These spectra have shown that the overlap between astrophysics and atomic physics is stronger than ever, as discoveries of new X-ray lines and edge structure is matching the need for increasingly detailed theoretical calculations and experimental measurements of atomic data.

1. X-ray spectral probes of astrophysical systems at high resolution

High resolution X-ray spectroscopy provides a powerful new tool for advancing our understanding of the physical environments of energetic astrophysical systems. As demonstrated with *Chandra* and *XMM-Newton* spectral studies, the scientific impact is far reaching, encompassing studies of stars, supernova remnants (SNR), X-ray binaries (XRBs), active galactic nuclei (AGN), clusters, and the interstellar and intergalactic medium (respectively ISM and IGM). To give a flavor for some of the newly X-ray discovered spectral features and their relevance to spectral modeling and calculations, I will draw mostly on examples from observations of AGN and XRBs with which I have been involved. See Paerels & Kahn (2003) for a complete review of *Chandra* and *XMM-Newton* results.

1.1. Narrow emission and absorption lines

Narrow (i.e. barely resolved) emission and absorption lines are nearly ubiquitous in the astrophysical sources seen at high resolution. From the lines strengths alone, we can deduce much about the conditions of the plasma, which range from the "X-ray cold" where fluorescent emission and photoionzation prevail to the "X-ray hot" where collisional ionization dominates. From the view of atomic calculations and spectral modeling, the parameterization of the emitters and absorbers are at an advanced state as demonstrated by high resolution spectral studies of the photoionized plasma in Seyfert galaxies (e.g., Sako et al. 2000; Ogle et al. 2000; Branduardi-Raymont et al. 2001; Collinge et al. 2001; Lee et. l2001, 2002a; Kaspi et al. 2000, 2001, 2002; Brinkman et al. 2002; Kinkhabwala et al. 2002; Blustin et al; Sako et al. 2003). Specific features which demonstrate the power of high resolution spectroscopy come from the detection of high order (low oscillator strength) resonance absorption lines (i.e. higher than Lyman γ) which are the mark of high optical depth clouds (e.g., Lee et al. 2001; Kaspi et al. 2002). Commonly used atomic codes include [5]`Cloudy:` Ferland et al. (1998), [6]`XSTAR:` Kallman & Bautista (2001) and [7]`photoion:` Kinkhabwala et al. (2003).

Strong evidence for non-equilibrium collisionally ionized plasma can be seen in SNRs observed with *Chandra*and *XMM-Newton*. One of the best examples is 1E 0102.2-7219 where spectral-line images reveal progressive ionizations in the remnant attributed to a reverse shock (Flanagan et al. 2003b; and Fig. 5 of Flanagan et al. 2003a).

1.2. P-Cygni Profiles, Line Variability, Doppler Shifts, and Spatial-Spectral Doppler mapping

Outflows have been seen in many different forms in *Chandra* and *XMM* spectra. Key spectroscopic signatures include (1) Doppler-shifted absorption and/or emission lines which provide information on the kinematics and geometry of the outflow, (2) P-Cygni profiles (red-shifted/rest-frame emission from material out of the line-of-sight, accompanied by blue-shifted absorption lines from the foreground, line-of-sight part of the wind) as seen in both X-ray binaries (e.g. Circinus X1: Brandt & Schultz 2000; Schultz & Brandt 2002) and AGN (e.g. NGC 3783: Kaspi et al. 2001; 2002), and (3) more subtle variability effects (e.g. the micro-quasar GRS 1915+105: Lee et al. 2002b). Of these, the most remarkable are those which show relativistic velocities (e.g. the BHC SS 433 where $v_{\rm jet} \sim 0.27c$, Marshall, Canizares & Schultz 2002), and more recently also seen in QSOs and Narrow line Seyfert galaxies. From the X-ray measurements of these lines and shifts, a great deal can be learned about the X-ray portion of the flow. For example, based on the line broadening, information about the flow opening angle can be deduced while density diagnostics using observed He-like lines can provide important limits on the mass flow rate. For some of the brighter SNRs, spatial-spectral Doppler mapping can be used to reveal the 3-D structure of the SNR (e.g. 1E 0102, Fig 6 of Flannagan et al. 2003a) – see Dewey (2002) for technique; for Cassiopeia A, see Willingale et al. (2002).

1.3. Inner Shell lines

'Low' ionization (in the X-ray sense) lines such as O III-VI or Fe VI-XVII are typically only seen in other wave-bands (e.g. UV), but photoexcitation of the ion's inner shell electron followed by auto-ionization causes resonance lines to appear in the X-ray band. These lines have been detected in the X-ray spectra of AGN: (1) the broad structure between $\sim 15.5 - 17$ Å ($\sim 0.72 - 0.8$ keV) known as the 'unresolved transition array' (UTA) of inner-shell 2p-3d resonance absorption lines in weakly ionized M-shell Fe VI-XII (for calculations, see Behar, Sako & Kahn 2001) was first detected in the Seyfert galaxy IRAS 13349+2438 (Sako et al. 2001) and since seen in NGC 3783 (Kaspi et al. 2002), (2) similarly, the K-L resonance absorption (inner shell 1s-2p transition) of Li-like oxygen

[5]http://www.nublado.org/

[6]http://heasarc.gsfc.nasa.gov/docs/software/xstar/xstar.html

[7]http://xmm.astro.columbia.edu/research.html

for calculations, see Pradhan 2000) was also first discovered in a Seyfert galaxy (MCG-6-30-15: Lee et al. 2001). Since then, lower ionization oxygen lines have also been seen in this source (Sako et al. 2003; Lee et al. in prep), and inner shell lines of Si VII-XII and S XII-XIV have been reported in NGC 3783 (Kaspi et al. 2002). Low ionization oxygen lines have also been detected in the X-ray binaries and attributed to the line-of-sight ISM or that intrinsic to the source (e.g., Paerels et al. 2001; Takei et al. 2002; Juett, Schultz & Chakrabarty 2003).

For highly extincted extragalactic sources where a UV spectrum cannot be seen, the inner shell lines can eventually provide a powerful alternative for studying the "lukewarm" part of the partially ionized gas in the AGN environment (i.e. the warm absorber). For ISM studies, these lines provide an important diagnostic for the abundance distributions in our local Universe.

1.4. Edge Structure (XAFS) and Shifts

Photoelectric edges are seen as prominent spectral features in X-ray spectra of sources with significant absorption, from which we can deduce the optical depth and hydrogen column of the absorbing medium. However, based on the edge discontinuity alone, we cannot distinguish between gas versus dust phase absorption. In some cases, dust has been inferred as the source of an Fe L photoelectric edge at ~ 17.7 Å (~ 0.7 keV) (e.g., Lee et al. 2001, 2002a). However, the most direct probe of dust is if the X-ray Absorption Fine Structure (XAFS), which probes material in solid form can be extracted from high resolution data of bright highly absorbed XRBs. Tentative detections of these features have been reported in the *Chandra*spectrum of GRS 1915+105 (Lee et al. 2002b).

2. Concluding Thoughts

The wealth of high resolution *Chandra*and *XMM-Newton* spectra accumulated over the course of the last $\sim$ four years has provided us with a very rich laboratory for probing the details of astrophysical plasma. While the atomic physics calculations appear to be well suited to model the high resolution X-ray data in hand, much of the detailed modeling has been parametric. Our next step should be to take the wealth of atomic and satellite data and connect it to the detailed models of the astrophysical sources themselves.

Acknowledgments. I thank Claude Canizares for his generosity & insightful discussions. I also thank the MIT CXC & HETGS members. I am grateful for the financial support of the Chandra fellowship grant PF2–30023, issued by the Chandra X-ray Observatory Center which is operated by SAO for NASA under contract NAS8–39073.

References

Behar, E., Sako, M., & Kahn, S. M., 2001, ApJ, 563, 497
Blustin, A. J., et al., 2003, A&A, 403, 481
Brandt, W. N., & Schulz, N. S., 2000, ApJ, 544, L123
Branduardi-Raymont, G., Sako, M., Kahn, S. M., Brinkman, A. C., Kaastra, J. S., & Page, M. J., 2001, A&A, 365, L140
Brinkman, A. C., Kaastra, J. S., van der Meer, R. L. J., Kinkhabwala, A., Behar, E., Kahn, S. M., Paerels, F. B. S., & Sako, M., 2002, A&A, 396, 761
Collinge, M. J., et al., 2001, ApJ, 557, 2

Dewey, D., 2002, in High Resolution X-ray Spectroscopy with XMM-Newton and Chandra

Ferland, G. J., Korista, K. T., Verner, D. A., Ferguson, J. W., Kingdon, J. B., & Verner, E. M., 1998, PASP, 110, 761

Flanagan, K. A., et al., 2003a, in X-Ray and Gamma-Ray Telescopes and Instruments for Astronomy. Edited by Joachim E. Truemper, Harvey D. Tananbaum. Proceedings of the SPIE, Volume 4851, pp. 45-56 (2003)., 45

Flanagan, K. A., Canizares, C. R., Dewey, D., Houck, J. C., Fredericks, A. C., Schattenburg, M. L., Markert, T., & Davis, D., 2003b, ApJ, submitted

Juett, A. M., Schulz, N. S., & Chakrabarty, D., 2003, ApJ, submitted

Kallman, T., & Bautista, M., 2001, ApJS, 133, 221

Kaspi, S., et al., 2002, ApJ, 574, 643

Kaspi, S., et al., 2001, ApJ, 554, 216

Kaspi, S., Brandt, W. N., Netzer, H., Sambruna, R., Chartas, G., Garmire, G. P., & Nousek, J. A., 2000, ApJ, 535, L17

Kinkhabwala, A., Behar, E., Sako, M., Gu, M. F., Kahn, S. M., & Paerels, F., 2003, ApJ, submitted

Kinkhabwala, A., et al., 2002, ApJ, 575, 732

Lee, J. C., Canizares, C. R., Fang, T., Morales, R., Fabian, A. C., Marshall, H. L., & Schulz, N. S., 2002a, in X-ray Spectroscopy of AGN with Chandra and XMM, 9

Lee, J. C., Fang, T., Kallman, T., Canizares, C. R., Fabian, A., R., G. R., & Marshall, H. L., ApJ, in preparation

Lee, J. C., Ogle, P. M., Canizares, C. R., Marshall, H. L., Schulz, N. S., Morales, R., Fabian, A. C., & Iwasawa, K., 2001, ApJ, 554, L13

Lee, J. C., Reynolds, C. S., Remillard, R., Schulz, N. S., Blackman, E. G., & Fabian, A. C., 2002b, ApJ, 567, 1102

Marshall, H. L., Canizares, C. R., & Schulz, N. S., 2002, ApJ, 564, 941

Ogle, P. M., Marshall, H. L., Lee, J. C., & Canizares, C. R., 2000, ApJ, 545, L81

Paerels, F., et al., 2001, ApJ, 546, 338

Paerels, F. B., & Kahn, S. M., 2003, Annual Review of Astronomy and Astrophysics, 41, 291

Pradhan, A. K., 2000, ApJ, 545, L165

Sako, M., et al., 2001, A&A, 365, L168

Sako, M., et al., 2003, ApJ, in press

Sako, M., Kahn, S. M., Paerels, F., & Liedahl, D. A., 2000, ApJ, 543, L115

Schulz, N. S., & Brandt, W. N., 2002, ApJ, 572, 971

Takei, Y., Fujimoto, R., Mitsuda, K., & Onaka, T., 2002, ApJ, 581, 307

Willingale, R., Bleeker, J. A. M., van der Heyden, K. J., Kaastra, J. S., & Vink, J., 2002, A&A, 381, 1039

Highlights of Astronomy, Vol. 13
International Astronomical Union, 2003
O. Engvold, ed.

The First Results from "Solar X-ray Spectrometer (SOXS)" Mission

Rajmal Jain, Hemant Dave, P. Sreekumar*, A. B. Shah, N. M. Vadher, K. S. B. Manian, G. P. Ubale, V. M. Shah, K. J. Shah, S. L. Kayasth, V. D. Patel, Sumit Kumar and M. R. Deshpande

Physical Research Laboratory, (Dept. of Space, Govt. of India)
Navrangpura, Ahmedabad - 380 009, India

Abstract. "Solar X-ray Spectrometer (SOXS)" mission on-board GSAT-2 Indian spacecraft was launched on 08 May 2003 by GSLV-D2 and deployed in geostationery orbit to study the X-ray emission from solar flares with high spectral and temporal resolution. The SOXS consists of two independent payloads viz. SOXS Low Energy Detector (SLD) payload, and SOXS High Energy Detector (SHD) payload. The SLD consists of two solid state detectors Si PIN and CZT, which cover the energy range from 4-60 keV, while the SHD has NaI(Tl)/CsI(Na) sandwiched phoswich detector that covers energy range from 20 keV to 10 MeV. We present very briefly the science objectives and instrumentation of SLD payload. After the successful In-orbit Tests (IOT), the first light was fed into SLD payload on 08 June 2003 when the solar flare was already in progress. We briefly present the first results from the SLD payload.

Highlights of Astronomy, Vol. 13
International Astronomical Union, 2003
O. Engvold, ed.

The Iron Project and the RmaX Project

Anil K. Pradhan

Department of Astronomy, The Ohio State University, Columbus, OH 43210, USA (www.astronomy.mps.ohio-state.edu/∼pradhan)

Abstract. Ongoing activities under an international collaboration of atomic physicists and astrophysicists under the Iron Project and the RmaX Project, with applications to X-ray astronomy, are briefly described.

1. Introduction

The Iron Project (IP; Hummer et al.1993) is an extension of the erstwhile Opacity Project (OP; Seaton et al.1994), devoted primarily to collisional and radiative processes of the Iron-peak elements. The RmaX Project is a part of the IP aimed at X-ray astronomy. The IP/RmaX work deals with highly charged ions and inner-shell processes.

To date 55 publications on **Atomic Data From the Iron Project** have appeared in Astronomy and Astrophysics. More details are on the IP website www.usm.uni-muenchen.de/people/ip/iron-project.html, or the author's website above. Additional details are provided in reviews in this volume by Palmeri and Mendoza on the OP/IP database TIPTOPBASE, and by Nahar on "New Radiative Data" not yet generally available. The IP/RmaX collaboration consists of about 20 members from Canada, France, Germany, UK, US, and Venezuela. Some RmaX publications are also reported in the Journal of Physics B: Atomic, Molecular, and Optical Physics.

2. Methodology

The IP/RmaX calculations, like the OP, are carried out using the R-matrix method, based on the close-coupling approximation from atomic collision theory (Burke and Robb 1975; Seaton 1987). Unlike the OP radiative calculations that were in LS coupling, the IP/Rmax calculations generally take account of fine structure and some relativistic effects using the Breit-Pauli R-matrix method (BPRM; Berrington et al.1995).

3. Radiative and Collisional Calculations

One of the primary activities under the IP has been collisional calculations for all Fe ions (see references in the IP series), and radiative data for a many Fe and other ions.

Most recent collisional work has been on highly charged ions from H-like to Ne-like sequences, and K- and L-shell radiative transitions. In the following subsections we exemplify the nature of the IP/RmaX work, on various atomic processes and using the same approximation (BPRM), for the important ion Ne-like Fe XVII that gives rise to a number of well known X-ray lines (see the Grotrian diagram in Chen et al.2003).

3.1. Electron impact excitation

BPRM calculations for a benchmark study of electron scattering with Fe XVII showed extensive series of resonances that significantly enhance the effective (averaged) cross sections and rate coefficients (Fig. 1, Chen and Pradhan 2002; Chen et al.2003). These calculations resolved longstanding discrepancies between two sets of experimental measurements using Electron-Beam-Ion-Traps (EBIT) at the Lawrence Livermore National Laboratory (Brown et al.2001) and at the National Institute for Standards and Technology (NIST, Laming et al.2000). The measured and calculated cross sections and line ratios in question are due to three prominent X-ray transitions labeled 3C,3D, and 3E, to the ground level $1s^2 2s^2 2p^6\ ^1S_0$ from excited levels:
3C (λ 15.014Å) $1s^2 2s^2 2p^5 [1/2] 3d_{3/2}\ ^1P^o_1$, 3D λ 15.265Å $1s^2 2s^2 2p^5 [3/2] 3d_{5/2}\ ^3D^o_1$, and 3E λ 15.456Å: $1s^2 2s^2 2p^5 [3/2] 3d_{5/2}\ ^3P^o_1$. While the 3C is dipole allowed, the 3D and 3E are spin-forbidden inter-combination transitions. The so called '3s/3d' problem, also due to discrepancies between the two sets of EBIT measurements, has also been solved using (a) the Gaussian average, and (b) the Maxwellian average, over the cross sections in the collisional-radiative model (Chen and Pradhan, in preparation). Chen et al.(2003) discuss the factors that affect the accuracy of the collision strengths for many other transitions up to n = 4 levels in Fe XVII.

3.2. Transition probabilities

Relativistic BPRM transition probabilities for Fe XVII have been calculated for over 2.6×10^4 allowed (E1) transitions that are of dipole and inter-combination type, and about 3000 forbidden transitions that include electric quadrupole (E2), magnetic dipole (M1), electric octopole (E3), and magnetic quadrupole (M2) type, representing the most detailed calculations to date for the ion (Nahar et al.2003).

3.3. Photoionization and Electron-Ion Recombination

BPRM photoionization and recombination calculations for (hν + Fe XVII $\longleftrightarrow$ (e + Fe XVIII) have been reported by Zhang et al.(2001), using the unified method for (e + ion) recombination that includes both the radiative and the dielectronic recombination processes in an ab inito manner. Both the level-specific and the total cross sections for the two inverse processes are obtained. In an earlier work, Pradhan et al.(2001) demonstrated that the theoretical unified rates agree with experimental data from ion storage rings to within 20%. The unified and self-consistent approach to photoionization and (e + ion) recombination is reviewed by Nahar and Pradhan (2003, astro-ph/0310624).

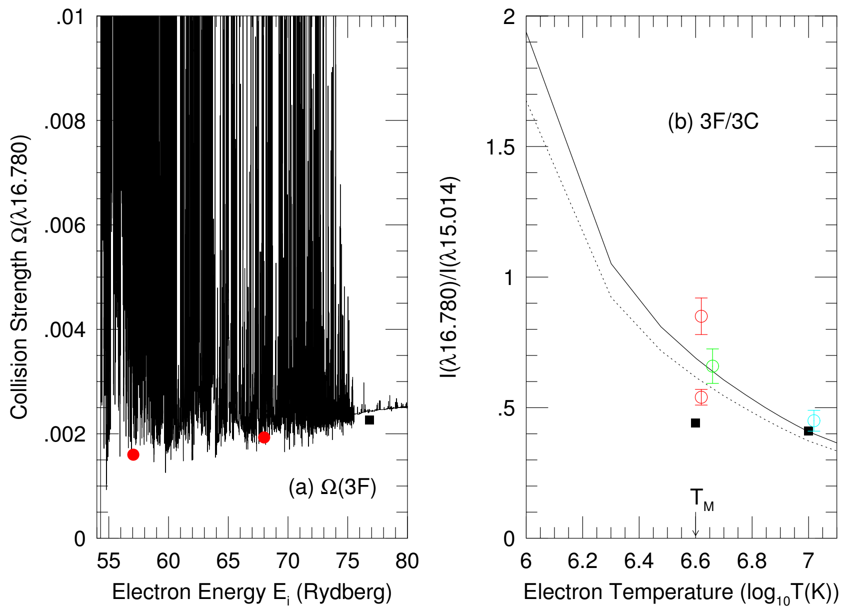

Figure 1. Enhancement of collisional rates of Fe XVII by resonances: (a) BPRM collision strength Ω for the forbidden 3F line $2s^22p^53s \rightarrow 2s^22p^6, J = 1 \rightarrow 0, \lambda 16.780\mathring{A}$; the filled circles and square are non-resonant DW calculations; (b): line ratio 3F/3C vs. T from a 89-level C-R model. The electron densities for solid-line and dot-line curves are 10^{13} and 10^9 cm^{-3} respectively. The 4 open circles with error bars are observed and experimental values: from the solar corona at T$_m$ $\sim$ 4MK, from the corona of solar-type star Capella at $\sim$ 5MK, and from the EBIT experiment at 0.9 keV (log T = 7). The filled squares are values using DW results. Owing to Maxwellian averaged rate coefficients, resonance enhancement is particularly large at low temperatures, such as in photoionized plasmas, as opposed to higher temperatures in coronal equilibrium.

3.4. Opacities, inner-shell excitation, and databases

The review by Palmeri and Mendoza on TIPTOPBASE describes recent calculations on K-shell Auger processes and the Opacity Project/Iron Project atomic and opacities databases.

4. Summary

Atomic data for a variety of processes and ions are being calculated under the Iron/RmaX projects. The R-matrix approach is capable of taking account of all important atomic effects, and produce data of definitive accuracy that can be bencmharked against state-of-the-art experiments. Self-consistent ab initio calculations for Fe XVII are presented as an example of large-scale data obtained for all collisional and radiative processes in an ion using the same basic approximation (BPRM method) and wavefunction expansions.

Acknowledgments. The work reported herein is partially supported by the NASA Astrophysical Theory Program and the Space and Astrophysics Research program.

References

Berrington, K.A., Eissner, W.B., & Norrington, P.H. 1995, CPC, 92, 290.

Brown G V, Beiersdorfer P, Liedahl D A, and Widmann K 1998 ApJ, 502, 1015

Burke, P.G. and Robb, W.D. 1975, Adv. At. Mol. Phys., 11, 143

Chen, G.X. and Pradhan, A.K. 2002 Phys.Rev.Lett, 89, 013202

Chen, G.X., Eissner, W., and Pradhan, A.K. 2003 J. Phys.B, 36, 453

Hummer D G, Berrington K A, Eissner W, Pradhan A K, Saraph H E, and Tully J A 1993, A&A, 279, 298

Laming J M et al.2000 ApJ, 545, L161

Nahar, S.N. and Pradhan, A.K. 2003, *Self-consistent R-matrix Approach To Photoionization And Unified Electron-Ion Recombination*, in "Radiation Processes in Physics and Chemistry", Elsevier (in press, Eds. R.H. Pratt and S. M. Manson), astro-ph/0310624.

Nahar, S.N., Chen, G.X., Eissner, W., Pradhan, A.K. 2003, A&A, 408, 789 (astro-ph/0302561).

Pradhan, A.K., Nahar, S.N., and Zhang, H. L. 2001, ApJ, 549,L265

Seaton, M.J. 1987, J.Phys.B, 20, 6363

Seaton, M.J., Yu, Y., Mihalas, D. and Pradhan, A.K. 1994, MNRAS, 266, 805

Zhang, H.L., Nahar, S.N., Pradhan, A.K. 2001, Phys.Rev.A, 64, 032719.

Highlights of Astronomy, Vol. 13
International Astronomical Union, 2003
O. Engvold, ed.

Atomic Physics Calculations for Iron L-line Spectra

Jacques Dubau

LIXAM, UMR8624, Université Paris-Sud, Bat. 350, 91405 Orsay Cedex, France

LUTH, Observatoire de Paris, 5 Place J. Janssen, 92190 Meudon, France

Delphine Porquet

Max-Plank-Institut für extraterrestrische Physik, Postfach 1312, D-85741, Garching, Germany

Oleg Zabaydullin

Institute of Nuclear Fusion, Russian Research Center Kurchatov Institute, 123182 Moscow, Russia

Abstract. Absorption L-lines of iron ions are observed, in spectra of Seyfert 1 galaxies by the new generation of X-ray satellites: Chandra and XMM-Newton. Lines associated to Fe^{23+} to Fe^{16+} have been already observed in emission, in the solar corona and in laboratory. Whereas, those corresponding to Fe^{15+} to Fe^{6+} have not been observed as emission lines, the upper level of the transition decaying preferentially by autoionization. Many atomic data are available for the first ion set. For the second set, some data have been recently published for n=2 to n'=3 transitions. We have recalculated them using another theoretical approach and have extended them to n'=4.

1. Introduction

The new generation of X-ray satellites (*Chandra* and *XMM-Newton*) produces very detailed spectra, thanks to a high spectral resolution combined to a high sensitivity of the spectrometers on board. For the first time, it is possible to have access to X-ray spectroscopy of extra-solar astrophysical objects: e.g., stellar coronae, Active Galactic Nuclei (AGN), X-ray binaries, etc. In particular, observations of Seyfert galaxies, show numerous lines of highly ionized elements: predominantly in absorption, for Seyfert 1 and only in emission for Seyfert 2 galaxies.

Much atomic data have already been calculated to analyze X-ray spectra of solar corona or laboratory plasmas. The well-known He-like ion diagnostics of Gabriel and Jordan (1969), have been extended from solar to non-solar coronae and also to photoionized plasmas by Porquet, Dubau (2000), Porquet et al. (2001). Besides these K-lines, Fe-L lines have also been observed in X-ray spectra, for Seyfert 1 (Sako et al. 2001, Blustin et al. 2002, Kaspi et al. 2002), and for Seyfert 2, (Kinkhabwala et al. 2002) galaxies. To analyze the "unresolved part" of the Fe-L spectra (Fe^{16+} to Fe^{6+}), atomic data for the transitions from n=2 to n'=3 have been calculated and presented as an abbreviated set, assuming a UTA (unresolved transition array) statistical model of Behar et al. (2001), i.e. mean wavelengths, statistical spectral widths of transition arrays, etc. The arguments used by the authors to justify statistical treatment is that various processes, such as turbulence, will merge lines into a broad UTA, independent of the spectral resolution of the measuring device. Comparisons of the Seyfert 1 NGC 3783 spectra with different spectral resolutions, XMM (Bustin et al. 2002), and Chandra (Kaspi et al. 2002), show that the statistical assumption is not justified at least for this object : fine details can be clearly resolved. Indeed, for such a low density plasma the number of possible absorption transitions is quite limited and as the absorption changes dramatically over the ionization stages, the use of a statistical width artificially increases the real width of the lines (Iglesias et al. 2003). We have therefore re-calculated all the atomic data of Behar et al. (2001) , extending them to n'= 4 transitions, giving a particular importance to the numerous possible autoionization channels (Dubau, Porquet, Zabaydullin, 2003).

2. Calculations of atomic parameters

2.1. Method

Wavelengths λ, oscillator strengths f and radiative transition probabilities A_r have been calculated using the SUPERSTRUCTURE code (Eissner et al. 1974) which uses a multi-configuration expansion of the wave functions. The atomic Hamiltonian includes most of the Breit Pauli relativistic corrections (one-body and two-body terms). The non-relativistic and relativistic eigenstates are obtained by diagonalizing the Schrödinger and Breit Pauli Hamiltonian respectively. The matrix transformation between both eigen-states is then used to transform non-relativistic autoionization transition matrix elements to fine- structure autoionization probabilities A_a, in the AUTOLSJ code, (TFR Group, Dubau, Loulergue 1981). The radial parts of the one electron wave-functions are calculated in scaled Thomas-Fermi-Dirac potentials, the scaling parameters, for each l orbital, being derived by minimizing the energies of some selected LS terms.

2.2. Results

Calculations have been done for 11 ions from Fe^{16+} to Fe^{6+} using the ground state configuration and the excited configurations accessible by absorption (i.e., by electric-dipole transitions). For example:

Fe^{6+}: $1s^2 2s^2 2p^6 3s^2 3p^6 3d^2$, $1s^2 2s^2 2p^5 3s^2 3p^6 3d^3$, $1s^2 2s^2 2p^5 3s^2 3p^6 3d^2 4s$, $1s^2 2s^2 2p^5 3s^2 3p^6 3d^2 4d$, $1s^2 2s 2p^6 3s^2 3p^6 3d^2 4p$.

For Fe^{23+} to Fe^{16+}, the excited configurations give bound states. Whereas for Fe^{+15} to Fe^{+6}, the excited configurations correspond to autoionizing states. As example, we provide in Table 1, the wavelengths, absorption oscillator strengths, radiative and autoionization probabilities for Fe^{14+} and Fe^{8+}. One can observe the dramatic increase in the autoionization probabilities from Fe^{14+} to Fe^{8+}.

Moreover, the number of possible autoionizing channels increases also. In particular, this explains why one does not observe the emission lines in Seyfert 2 which could correspond to the absorption lines in Seyfert 1. That is, for L-lines, the photo-excited bound states, Fe^{23+} to Fe^{16+}, decay by the reverse radiative transition whereas the photo-excited autoionizing states, Fe^{15+} to Fe^{6+}, decay preferentially by autoionization.

Table 1. Absorption oscillator strengths, wavelengths, radiative and autoionization probabilities

(from the ground level of Fe^{14+})	$1s^22s^22p^63s^2\ ^1S_0$			
to the upper level)	f (abs)	$A_r(s^{-1})$	λ(Å)	$A_a(s^{-1})$
$1s^22s^22p^53s^23d\ ^3D_1$	0.59	5.49 (+12)	15.51	7.75 (+12)
$1s^22s^22p^53s^23d\ ^1P_1$	2.55	2.44 (+13)	15.26	1.43 (+13)
$1s^22s2p^63s^23p\ ^1P_1$	0.27	3.05 (+12)	14.09	8.99 (+13)
$1s^22s^22p^53s^24d\ ^3D_1$	0.37	5.12 (+12)	12.74	8.49 (+12)
$1s^22s^22p^53s^24d\ ^1P_1$	0.41	5.80 (+12)	12.60	8.78 (+12)
$1s^22s2p^63s^24p\ ^1P_1$	0.08	1.42 (+12)	11.38	8.82 (+13)
(from the ground of Fe^{8+})	$1s^22s^22p^63s^23p^6\ ^1S_0$			
to the upper level)	f (abs)	$A_r(s^{-1})$	λ(Å)	$A_a(s^{-1})$
$1s^22s^22p^53s^23p^63d\ ^3D_1$	0.66	5.37 (+12)	16.59	4.19 (+14)
$1s^22s^22p^53s^23p^63d\ ^1P_1$	1.52	1.27 (+13)	16.33	4.77 (+14)
$1s^22s^22p^53s^23p^64d\ ^1P_1$	0.26	2.67 (+12)	14.59	4.05 (+14)
$1s^22s^22p^53s^23p^64d\ ^3D_1$	0.18	1.89 (+12)	14.39	4.00 (+14)
$1s^22s2p^63s^23p^64p\ ^1P_1$	0.06	8.52 (+11)	12.80	6.20 (+13)

References

Gabriel, A. H., & Jordan, C. 1969, MNRAS, 145, 241

Porquet, D., & Dubau, J. 2000, A&A, 143, 495

Porquet, D., Mewe, R., Dubau, J., Raassen, A.J.J., & Kaastra, J.S. 2001, A&A, 376, 1132

Sako, M., Kahn, S.M., Behar, E., Kaastra, J.S., & al. 2001, A&A, 365, L168

Blustin, A.J., Branduardi-Raymont, G., Behar, E., & al. 2002, ApJ, 574, 643

Kinkhabwala, A., Sako, M.., & Behar, E.. & al. 2002, ApJ, 575, 732

Behar, E., Sako, M., & Kahn, S.M. 2001, ApJ, 563, 497

Iglesias, C.A., Chen, M.H., Sonnad, V., Wilson, B.G. 2003, J. Q. S. R. T., 81, 227

Dubau, J., Porquet, D., Zabaydullin, O. 2003, J. Q. S. R. T., 81, 117

Eissner, W., Jones, M., & Nussbaumer, H. 1974, Comp Phys Commun, 8, 270

TFR Group, Dubau, J., & Loulergue, M.J. 1981, J. Phys B, 15, 1007

Highlights of Astronomy, Vol. 13
International Astronomical Union, 2003
O. Engvold, ed.

Iron Kα Spectra from an Atomic Modeling Perspective

Duane A. Liedahl

Department of Physics and Advanced Technologies, Lawrence Livermore National Laboratory, P.O. Box 808, L-473, Livermore, CA 94550

Abstract. In order to upgrade the diagnostic capability associated with Fe Kα spectra, we have calculated detailed atomic models that include the effects of inner-shell photoionization, autoionization, collisional excitation at relatively high particle number densities, and photoexcitation in plasmas with high X-ray and/or UV energy densities. I discuss some of the potential uses of these models in the context of compact X-ray sources.

1. Introduction

Observations and analysis of Fe Kα spectra have long been a mainstay of astrophysical X-ray spectroscopy. This will continue to be true in the future, with *Astro-E 2* and *Constellation-X* in the offing. Solar X-ray observations (Seely, Feldman, & Safranova 1986) and laboratory plasma experiments (Beiersdorfer et al. 1993) have shown that Fe Kα spectra can be extremely complex, comprising several charge states crowding a relatively narrow spectral band. This is not observed in extra-solar objects, since, to date, the data have been of poor spectral resolution. Advancements in detector capabilities, however, exemplified by the XRS on *Astro-E 2*, promise to uncover the spectral complexity in the Fe Kα spectrum in several classes of celestial X-ray source.

Owing to the poor resolving power with which Fe K spectra are measured, analyzes are typically restricted to dealing with "the iron line," even if the underlying structure is suspected to be rich; obviously, it would be ill-advised to apply a complicated spectral model to a feature that can be described with a simple Gaussian model. Unfortunately, many potentially useful plasma diagnostics become obscured by detectors with poor resolution, which, in turn, tends to inhibit the development of these diagnostics. In light of the imminent launch of *Astro-E 2*, with a resolving power ≈ 6 eV, this situation is improving, and detailed calculations of the atomic physics processes associated with Fe K spectral formation, using state-of-the-art computer codes, are now becoming available (for example, Palmeri et al. 2003).

We have used the HULLAC (Hebrew University/Lawrence Livermore Atomic Code; Bar-Shalom et al. 1988) atomic physics package to search for plasma diagnostics involving Fe K spectra. Thus far, this research has focused on the L-shell species (Fe XVII-XXIV), which is a natural follow-on to similar work on Si Kα spectra, which was motivated by an observation of the high-mass X-ray binary Vela X-1 using the high-resolution gratings on the *Chandra* satellite (Liedahl et al., in prep.). We find that the part of the Si Kα line complex formerly attributed to neutral or near-neutral species (Sako et al. 1999) is actually made up of features corresponding to Si III – Si XII. The Kα spectra of L-shell ions provide unique diagnostic capability, and provide information on plasmas that exist at an intermediate range of ionization parameter. There is the possibility that, at least in some sources, the Fe Kα complex will be observed as consisting of several charge states, some of which are L-shell ions. Not only will such detections provide corollary or corroborative information relative to Kα spectra from lower-Z elements, but Fe Kα spectra, typically possessing larger equivalent widths than lower-Z elements, might be found to contain the superior set of diagnostics.

2. Results

The main results of this research are described below. A more thorough presentation will appear in a future paper.

2.1. Density Diagnostics

A detailed treatment of the level population kinetics shows that the Kα fluorescence spectrum can be a proxy for the local electron density. Underlying the mechanism is collisional excitation from ground to low-lying meta-stable levels, which, when photoionized out of the 1s shell, leads to fluorescence lines that are distinct from those produced in the low-density limit (Jacobs et al. 1989). The critical electron densities are $\sim 10^{13}$ cm^{-3} (Liedahl et al. 1992).

2.2. Direct Photoexcitation by a Continuum Radiation Field

Sources characterized by a hard X-ray continuum, in which fluorescence following inner-shell photoionization can be important, can also host gas for which direct photoexcitation of bound levels can drive line emission. This has been shown for the case of Seyfert 2 galaxies (Kinkhabwala et al. 2002) and high-mass X-ray binaries (Wojdowski et al. 2003). Similarly, line emission from quasi-bound auto-ionizing levels can be driven by the continuum radiation field. The essential difference, as found in this work, is that photoexcitation of auto-ionizing levels can give rise to bright lines that are not strongly driven by any other process under conditions of photoionization equilibrium. Lines of this type thus provide relatively unambiguous constraints on the column densities of the relevant charge states.

2.3. Level Population Dependence of Resonant Auger Destruction

Resonant Auger destruction (Ross, Fabian, & Brandt 1996) can efficiently suppress Kα emission from L-shell ions, since, as opposed to simple resonant scattering by bound levels, when the upper level is autoionizing, the photon destruction probability per scatter is equal to the autoionization branching ratio, which often exceeds 0.5. The other quantities of interest are, of course, the line optical depths. For a given fluorescence line, the optical depth depends on the level population density of the lower level of the radiative transition, which, in turn, depends on the local electron density. Therefore, the efficacy of resonant Auger destruction depends on both the ionic column density, a macroscopic quantity, and the local electron density, a microscopic quantity. It has been found that there are bright Kα fluorescence lines from Fe L-shell ions that may survive the resonant Auger destruction process and escape to infinity. To compare with the case of Vela X-1, as mentioned above, where we clearly see Kα lines from Si L-shell ions, the fluorescing gas in that object appears to be of relatively low ionic column density. We have found a set of transitions that can survive *large* ionic column densities, such as may be found in accretion disk atmospheres, for example. The action of resonant Auger destruction can produce spectra that differ dramatically from the "zero-D" limit.

3. Concluding Remarks

Through detailed treatments of atomic level population kinetics, we have found that Fe Kα spectra are, at least on "paper," exceptionally versatile diagnostics of physical conditions in X-ray photoionized plasmas, such as are found in active galactic nuclei and X-ray binaries. Since the spectra can differ dramatically from what one might expect from an assessment of a "zero-D," isolated ion model, care must be taken in identifying individual fluorescence lines. This will clear the way for the application of the rich diagnostic potential of these ions.

Acknowledgments. D.A.L. was supported in part by the NASA Long Term Space Astrophysics Program grant S-92654-F. Work at LLNL was performed under the auspices of the U.S. Department of Energy by the University of California Lawrence Livermore National Laboratory under contract No. W-7405-Eng-48.

References

Bar-Shalom, A., Klapisch, M., & Oreg, J. 1988, Phys.Rev.A, 38, 1773

Beiersdorfer, P., Phillips, T., Jacobs, V.L., Hill, K.W., Bitter, M., & von Goeler, S. 1993, ApJ, 409, 846

Jacobs, V.L., Doschek, G.A., Seely, J.F., & Cowan, R.D. 1989, Phys.Rev.A, 39, 2411

Kinkhabwala, A., et al. 2002, ApJ, 575, 732

Liedahl, D.A., Kahn, S.M., Osterheld, A.L., & Goldstein, W.H. 1992, ApJ, 391, 306

Palmeri, P., Mendoza, C., Kallman, T.R., & Bautista, M.A. 2003, A&A, 403, 1175

Ross, R.R., Fabian, A.C, & Brandt, W.N. 1996, MNRAS, 278, 1082

Sako, M., Liedahl, D.A., Kahn, S.M., & Paerels, F. 1999, ApJ, 525, 921

Seely, J.F., Feldman, U., & Safranova, U.I. 1986, ApJ, 304, 838

Wojdowski, P.S., Liedahl, D.A., Sako, M., Kahn, S.M., & Paerels, F. 2003, ApJ, 582, 959

Highlights of Astronomy, Vol. 13
International Astronomical Union, 2003
O. Engvold, ed.

New Results in Laboratory X-ray Astrophysics

P. Beiersdorfer, H. Chen

Lawrence Livermore National Laboratory, Livermore, CA 94550

K. R. Boyce, G. V. Brown, R. L. Kelley, F. S. Porter, C. K. Stahle

NASA Goddard Space Flight Center, Greenbelt, MD 20771

J. K. Lepson, J. G. Jernigan

Space Science Laboratory, University of California, Berkeley, CA, 94720

B. J. Wargelin

Harvard-Smithsonian Center for Astrophysics, Cambridge, MA 02138

S. M. Kahn

Physics Department, Stanford University, Stanford, CA 94305

Abstract. A multi-faceted, multi-institutional laboratory astrophysics program is carried out at the Livermore electron beam ion trap facility, which is a mature spectroscopic source with unsurpassed controls and capabilities, and an unparalleled assortment of spectroscopic equipment, including a full complement of grating and crystal spectrometers and a 6x6 micro-calorimeter array. Recent results range from the calibration of x-ray diagnostics, including the Fe XVII and Fe XXV emission lines, extensive lists of L-shell ions, the first laboratory simulation and fit of a cometary x-ray emission spectrum, and the discovery of new spectral diagnostics for measuring magnetic field strengths.

1. Introduction

Addressing the atomic needs of the *ASCA* and *EUVE* missions, we initiated a laboratory astrophysics program in the the early 1990's. The need for reliable laboratory data continued with the advent of observations with *Chandra* and *XMM-Newton*, which provide both CCD-quality and high-resolution grating spectroscopic data. Our laboratory astrophysics program has various facets tailored to address the particular needs for atomic data and calibrated line diagnostics. These include measurements in the extreme ultraviolet and X-ray regions, including measurements of charge exchange, relevant to space astrophysics and planetary science research.

Our program is centered on the electron beam ion traps at the University of California Lawrence Livermore National Laboratory. In over 15 years of use, this facility has been optimized for laboratory astrophysics and provides a unique resource for assessing atomic data and addressing spectroscopic issues. A large suite of spectrometers has been developed, including high-resolution crystal and grating spectrometers and a 6x6-pixel, square-array microcalorimeter. We also make use of additional laboratory sources to address a specific astrophysical problem.

A review of laboratory X-ray astrophysics was recently given by Beiersdorfer (2003). Here we only briefly mention a few results and their implications for astrophysics.

2. Spectral Catalogues

Line lists covering the X-ray and extreme ultraviolet wavelength bands are still grossly incomplete making it difficult to identify many lines observed with *Chandra* and *XMM* or to assess line blends appropriately (Lepson et al. 2000; Beiersdorfer et al. 2000b). In response, we have embarked on an ambitious program to provide wavelengths, line identifications, and relative intensities of all relevant lines in the EUV and X-ray region. Recently, we have reported line lists for the L-shell transitions of Ar IX through Ar XVI, Fe VII through Fe IX, and Fe XVIII through Fe XXVI (Brown et al. 2002; Lepson et al. 2002; Lepson et al. 2003).

Our wavelengths are being incorporated in various spectral modeling codes, where they make a decisive difference in line identification and modeling. This was pointed out, for example, by Behar, Cottam, & Kahn (2001) in their analysis of the L-shell iron emission from Capella observed by *Chandra*. Our line lists have also resulted in new line identifications, such as that of an Ar IX line near 50 Å in Procyon (Lepson et al. 2003), as well as several revised line assignments.

Our line surveys have uncovered new spectral diagnostics. We recently discovered the first X-ray line that can be used for magnetic field measurements (Beiersdorfer et al. 2003b).

A typical spectrum showing the iron L-shell emission between 15–17 Å is shown in Fig. 1. The spectrum was recorded with our high-resolution grating spectrometer and illustrates the blending of the Fe XVII lines with lines from Fe XVI.

3. Excitation Cross Sections

Knowledge of line formation processes and accurate excitation cross sections are needed for modeling observed line intensities and for deriving plasma conditions of the sources under investigation. Focusing on the iron L-shell emission, we have reported detailed excitation cross sections for Fe XXI through Fe XXIV (Gu et al. 1999; Gu et al. 2001; Chen et al. 2002). Our measurements illustrated the importance of resonance excitation and blending with satellite lines produced by dielectronic recombination into high principal quantum numbers. Very importantly, our measurements pointed out inaccuracies in the energy scaling of the excitation rates used, for example, in the MEKAL spectral model. Contributions by dielectronic satellite lines were also studied in the K-shell spectrum of neon and reported recently (Wargelin, Kahn, & Beiersdorfer 2001).

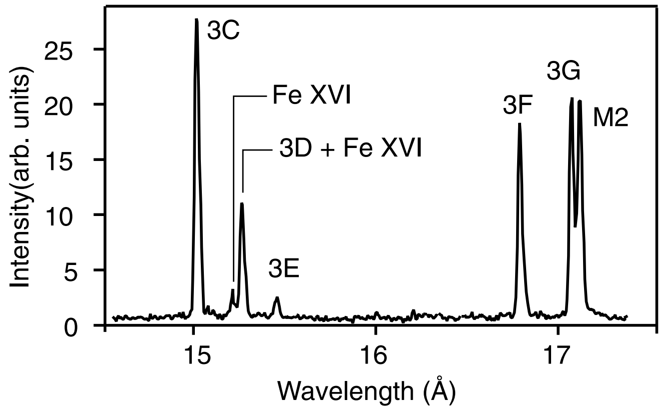

Figure 1. L-shell X-ray emission from iron. The Fe XVII line $3D$ is blended with a Fe XVI line increasing its apparent intensity relative to that of the Fe XVII line $3C$.

4. The Fe XVII spectrum

The difficulties of spectral models in predicting reliable line intensities are illustrated by the Fe XVII spectrum. Invariably, the Fe XVII emission could not be described by calculations. The discrepancies between the modeling calculations and the astrophysical spectra have been attributed to various source-specific processes, such as resonant scattering. However, this did not make sense in many instances.

We have studied the L-shell emission of neon-like ions in general and Fe XVII in particular since the beginning of our laboratory astrophysics program (Beiersdorfer et al. 1990; Beiersdorfer & Wargelin 1994). We showed that the laboratory data reproduce nicely the astrophysical spectra. To do so we used not only the Livermore electron beam ion traps but also tokamak plasmas generated at the Princeton Plasma Physics Laboratory (Brown et al. 1998; Beiersdorfer et al. 2000a; Beiersdorfer et al. 2001; Brown et al. 2001a; Brown et al. 2001b; Brown et al. 2002). Our measurements showed that the discrepancies between models and astrophysical spectra are clearly a problem with the atomic data in all but a few exceptional cases. By contrast, laboratory data obtained with a single-pixel calorimeter by Laming et al. (2000) at the National Institute of Standards and Technology seemed to confirm simple Fe XVII models and to disagree with solar and astrophysical data. We showed these conclusions to be erroneous (Beiersdorfer et al. 2002).

5. The Fe XXV spectrum

We have made extensive high-resolution crystal spectrometer measurements of the K-shell iron spectrum in the past (Brown et al. 1989; Beiersdorfer et al. 1992; Wong et al. 1995; Decaux et al. 1995; Beiersdorfer et al. 1996; Decaux et al. 1997; Jacobs, Decaux, & Beiersdorfer 1997). Most recently, we reported on K-shell line formation by inner-shell ionization (Decaux et al. 2003). We have

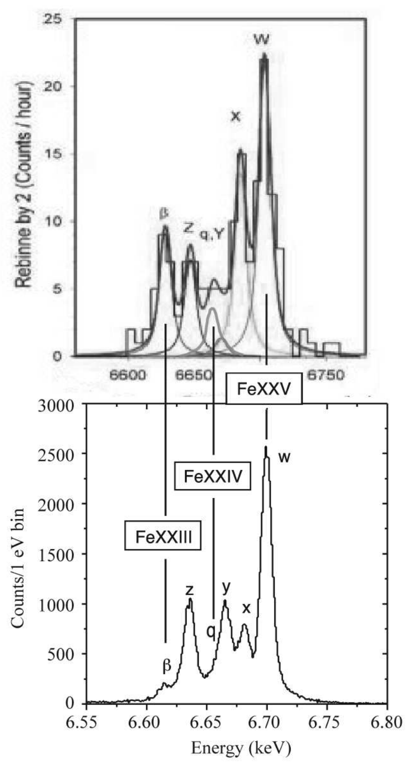

Figure 2. K-shell X-ray emission from iron. Top: Single-pixel calorimeter spectrum obtained at the National Institute of Standards and Technology [adapted from Silver et al. (2002)]. Bottom: Spectrum obtained with the 6x6 array calorimeter at Livermore. Lines β, q, and w are used to determine the relative abundances of Fe XXIII, Fe XXIV, and Fe XXV, respectively.

also used the 36-pixel microcalorimeter to measure the Fe XXV spectrum on one of the Livermore electron beam ion traps (Porter et al. 2000), as the iron K spectrum will be a focus of the upcomming *ASTRO-E2* mission. The spectrum is shown in Fig. 2 and compared to the spectrum measured with the single-pixel calorimeter by Silver et al. (2002) at the National Institute of Standards and Technology.[8]

Our spectrum shows the Fe XXV resonance line w, inter-combination lines x and y, and forbidden line z, and the Fe XXIV line q and Fe XXIII line β. The spectrum matches our crystal spectrometer data as well as the spectra obtained from other high-temperature plasmas such as tokamaks or the Sun (Bitter et al. 1979; Doschek 1990; Kato et al. 1997). The single-pixel calorimeter spectrum, however, whose L-shell branch was used in consecutive measurements to determine Fe XVII ratios mentioned above, differs remarkably from ours. The large intensity of lines w and β and small intensity of line q (blended with y) indicates a large abundance of helium-like and beryllium-like iron (Fe XXIII and Fe XXV) and little lithium-like iron (Fe XXIV). This is in contrast to any expected reasonable charge state distribution. Moreover, the $1s2p\,^3P_2 \rightarrow 1s^2\,^1S_0$ inter-combination line x is the second strongest line in this spectrum, although line formation processes do not preferentially favor this transition.

6. X-rays from Comets

Our laboratory measurements successfully simulated the X-ray emission spectrum of comet Linear S4 1999 observed with *Chandra*. We showed that charge exchange between heavy ions found in the solar wind and neutral cometary gases completely reproduces the observed emission (Beiersdorfer et al. 2003a). This laid to rest the question whether the emission is from the solar wind or from the comet itself. The laboratory simulation shows that all X-ray emission stems from the solar wind ions.

Work by the University of California Lawrence Livermore National Laboratory was performed under the auspices of the US Departments of Energy under Contract No. W-7405-Eng-48. Support from NASA's Space Research and Analysis Program and NASA's Planetary Atmospheres Program is gratefully acknowledged.

References

Behar, E., Cottam, J., & Kahn, S. M. 2001, Astrophys. J., 548, 966

Beiersdorfer, P. 2003, Ann. Rev. Astron. Astrophys., 412, 343

Beiersdorfer, P., Behar, E., Boyce, K. R., Brown, G. V., Chen, H., Gendreau, K. C., Gu, M.-F., Gygax, J., Kahn, S. M., Kelley, R. L., Porter, F. S., Stahle, C. K., & Szymkowiak, A. E. 2002, Astrophys. J. (Lett.), 576, L169

Beiersdorfer, P., Boyce, K. R., Brown, G. V., Chen, H., Kahn, S. M., Kelley, R. L., May, M., Olson, R. E., Porter, F. S., Stahle, C. K., & Tillotson, W. A. 2003a, Science, 300, 1461

[8]The latter is the same spectrum shown on the poster of the 25th Generally Assembly of the IAU Joint Discussion 17.

Beiersdorfer, P., Brown, G. V., Chen, H., Gu, M.-F., Kahn,S. M., Lepson, J. K., Savin, D. W. & Utter, S. B. 2000a, in Atomic Data Needs for X-ray Astronomy, ed. M. A. Bautista, T. R. Kallman, and A. K. Pradhan, Vol. NASA/CP-2000-209968, NASA Goddard Space Flight Center (Greenbelt, MD: NASA), 103

Beiersdorfer, P., Brown, G. V., Drake, J. J., Gu, M.-F., Kahn, S. M., Lepson, J. K., Liedahl, D. A., Mauche, C. W., Savin, D. W., Utter, S. B., Wargelin, B. J. 2000b, Revista Mexicana Astronomía y Astrofísica, 9, 123

Beiersdorfer, P., Osterheld, A. L., Chen, M. H., Henderson, J. R., Knapp, D. A., Levine, M. A., Marrs, R. E., Reed, K. J., Schneider, M. B., & Vogel, D. A. 1990, Phys. Rev. Lett., 65, 1995

Beiersdorfer, P., Phillips, T., Jacobs, V. L., Hill, K. W., Bitter, M., von Goeler, S., & Kahn, S. M. 1993, Astrophys. J., 409, 846

Beiersdorfer, P., Phillips, T. W., Wong, K. L., Marrs, R. E. & Vogel, D. A. 1992, Phys. Rev. A, 46, 3812

Beiersdorfer, P., Scofield, J. H., & Osterheld, A. L. 2003b, Phys. Rev. Lett., 90, 235003

Beiersdorfer, P., Vogel, D. A., Reed, K. J., Decaux, V., Scofield, J., Widmann, K., Hölzer, G., Förster, E., Wherhan, O., Savin, D. W., & Schweikhard, L. 1996, Phys. Rev. A, 53, 3974

Beiersdorfer, P., von Goeler, S., Bitter, M., & Thorn, D. B. 2001, Phys. Rev. A, 64, 032705

Beiersdorfer, P. & Wargelin, B. J. 1994, Rev. Sci. Instrum., 65, 13

Bitter, M., Hill, K. W., Sauthoff, N. R., Efthimion, P. C., Meservey, E., Roney, W., von Goeler, S., Horton, R., Goldman, M., & Stodiek, W. 1979, Phys. Rev. Lett., 43, 129.

Brown, C. M., Feldman, U. Doschek, G. A., Seely, J. F., LaVilla, R. E., Jacobs, V. L., Henderson, J. R., Knapp, D. A., Marrs, R. E., Beiersdorfer, P. & Levine, M. A., 1989, Phys. Rev. A, 40, 4089

Brown, G. V., Beiersdorfer, P., Chen, H., Chen, M. H., & Reed, K. J. 2001a, Astrophys. J., 557, L75

Brown, G. V., Beiersdorfer, P., Kahn, S. M., Liedahl, D. A. & Widmann, K. 1998, Astrophys. J., 502, 1015

Brown, G. V., Beiersdorfer, P., Liedahl, D. A., Widmann, K., Kahn, S. M., & Clothiaux, E. J. 2002, Ap. J. Suppl., 140, 589

Brown, G. V., Beiersdorfer, P., & Widmann, K. 2001b, Phys. Rev. A, 63, 032719

Chen, H., Beiersdorfer, P., Scofield, J. H., Gendreau, K. C., Boyce, K. R., Brown, G. V., Kelley, R. L., Porter, F. S., Stahle, C. K., Szymkowiak, A. E., & Kahn, S. M. 2002, Astrophys. J. (Lett.), 567, L169

Decaux, V., Beiersdorfer, P., Kahn, S. M., & Jacobs, V. L. 1997, Astrophys. J., 482, 1076

Decaux, V., Beiersdorfer, P., Osterheld, A., Chen, M., & Kahn, S. M. 1995, Astrophys. J., 443, 464

Decaux, V., Jacobs, V. L., Beiersdorfer, P., Liedahl, D. A., & Kahn, S. M. 2003, Phys. Rev. A, 68, 012509

Doschek, G. A. 1990, Astroph. J. Suppl., 73, 117

Gu, M.-F., Kahn, S. M., Savin, D. W., Behar, E., Beiersdorfer, P., Brown, G. V., Liedahl, D. A., & Reed, K. J. 2001, Astrophys. J., 563, 462

Gu, M., Kahn, S., Savin, D., Beiersdorfer, P., Brown, G., Liedahl, D., Reed, K., Bhalla, C., & Grabbe, S. 1999, Astrophys. J., 518, 1002

Jacobs, V. L., Decaux, V., & Beiersdorfer, P. 1997, J. Quant. Spectr. Rad. Transf., 58, 645

Kato, T., Safronova, U. I., Shlyaptseva, A. S., Cornille, M., Dubau, J., & Nilsen, J. 1997, At. Data Nucl. Data Tables, 67, 225

Laming, J. M., Kink, I., Takacs, E., Porto, J. V., Gillaspy, J. D., Silver, E. H., Schopper, H. W., Bandler, S. R., Brickhouse, N. S., Murray, S. S., Barbera, M., Bhatia, A. K., Doschek, G. A., Madden, N., Landis, D., Beeman, J., & Haller, E. E. 2000, Astrophys. J., 545, L161

Lepson, J. K., Beiersdorfer, P., Behar, E., & Kahn, S. M. 2003, Astrophys. J., 590, 604

Lepson, J. K., Beiersdorfer, P., Brown, G. V., Kahn, S. M., Liedahl, D. A., Mauche, C. W., & Utter, S. B. 2000, RevMexAA, 9, 137

Lepson, J. K., Beiersdorfer, P., Brown, G. V., Liedahl, D. A., Brickhouse, N. S., Dupree, A. K., Kaastra, J. S., Mewe, R., & Kahn, S. M. 2002, Astrophys. J., 578, 648

Porter, F. S., Audley, M. D., Beiersdorfer, P., Boyce, K. R., Brekosky, R. P., Brown, G. V., Gendreau, K. C., Gygax, J., Kahn, S., Kelley, R. L., Stahle, C. K., & Szymkowiak, A. E. 2000, Proc. SPIE, 4140, 407

Silver, E., Schnopper, H., Bandler, S., Brickhouse, N., Murray, S., Barbera, M., Takács, E., Gillaspy, J. D., Porto, J. V., Kink, I., Ratliff, P. R., Hudson, L., Laming, J. M., Madden, N., Landis, D., Beeman, J., Haller, E. E., & Schuch, R. 2002, in *Photonic, Electronic & Atomic Collisions*, ed. by J. Burgdörfer and J. S Cohen and S. Datz and C. R. Vane (Rinton Press, Princeton, 2003), p. 312

Wargelin, B. J., Kahn, S. M., & Beiersdorfer, P. 2001, Phys. Rev. A, 63, 022710

Wong, K. L., Beiersdorfer, P., Reed, K. J., & Vogel, D. A. 1995, Phys. Rev. A, 51, 1214

Highlights of Astronomy, Vol. 13
International Astronomical Union, 2003
O. Engvold, ed.

Photorecombination and Photoionization Experiments at Heavy-Ion Storage-Rings and Synchrotron-Light Sources

Stefan Schippers

Institut für Kernphysik, Justus-Liebig-Universität Giessen, Leihgesterner Weg 217, 35392 Giessen, Germany

Abstract. Recent experimental work on the photorecombination and the photoionization of astrophysically relevant atomic ions employing the merged-beams technique at heavy-ion storage-rings and synchrotron-light sources, respectively, is summarized. The resulting *absolute* photoionization cross sections and recombination rate coefficients benchmark corresponding theoretical calculations and are needed for the accurate determination of ionization equilibria in astrophysical plasmas.

1. Introduction

Photoionization (PI) and Photorecombination (PR) are basic atomic processes that govern the charge state balance in any plasma. Therefore, the accurate knowledge of these processes is a prerequisite for any plasma modeling and, hence, for any meaningful interpretation of many astrophysical observations. To date, most PI and PR cross sections used in plasma modeling stem from theoretical calculations. Their accuracy is often difficult to assess and, therefore, experimental PI and PR cross sections and rate coefficients are vitally needed as benchmarks and guidelines for the development of the theoretical methods. Moreover, in the near future, experiments will probably be the only reliable source for PR and PI cross sections of complex ions such as ions with an open M-shell (Schippers et al. 2002a; 2003a).

The measurement of PR and PI cross sections of atomic (and molecular) ions is experimentally challenging because the ion densities that can be experimentally prepared are very low — some 10^6 cm^{-3} (to be compared with $\approx 10^{13}$ cm^{-3} for gaseous and $\approx 10^{22}$ cm^{-3} for solid targets). Consequently, signal rates from electron-ion and photon-ion collision experiments are comparatively weak. In order to make up for the low ion density in such experiments an arrangement is chosen where the colliding particle beams are merged collinearly over a distance of the order of 1 m. The merged-beams arrangement (Phaneuf et al. 1999) provides a relatively large interaction volume, and the directionality of the ion beam facilitates the effective collection of the PI or PR reaction products, i. e., of ions that have changed their charge state due to either ionization or recombination. For the measurement of *absolute* PR and PI cross sections the merged-beams method was implemented at heavy-ion storage rings (Müller & Wolf 1997; Müller & Schippers 2001) and at synchrotron-light sources (West 2001; Covington et al. 2002), respectively.

2. Photorecombination of atomic ions

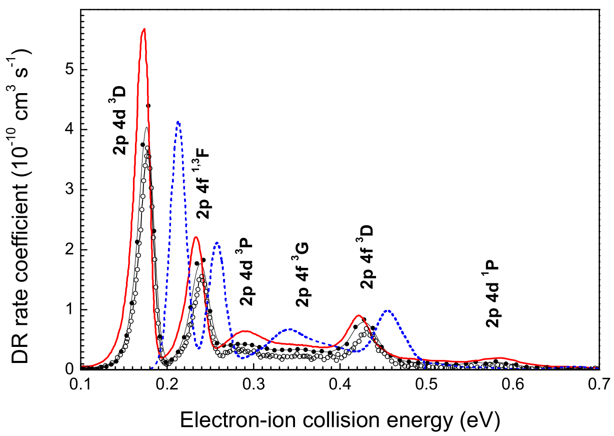

Figure 1. Dielectronic recombination (DR) of $C^{3+}(1s^2\,2s)$-ions at low energies: experiment (full symbols: Schippers et al. 2001, open symbols: Mannervik et al. 1998), many body perturbation theory (full line: Mannervik et al. 1998) and Breit-Pauli R-Matrix theory (dashed line: Pradhan et al. 2001).

The basic procedure for producing plasma rate coefficients from PR measurements at storage rings was outlined by Müller (1999). Recent examples are the PR rate coefficients of the lithium-like ions C IV (Schippers et al. 2001), O VI (Böhm et al. 2003) and Ni XXVI (Schippers et al. 2000). Figure 1 shows a comparison between measured and calculated C IV dielectronic recombination (DR) rate coefficients at low electron-ion collision energies. The two experimental results, which were obtained a two different storage-rings, agree with one another to within the 15% experimental error for the absolute cross section. This exemplifies the reliability of recombination measurements at storage rings. Mannervik et al. (1998) also calculated the C IV DR rate coefficient using relativistic many-body perturbation theory (RMBPT, Tokman et al. 2002). They pointed out that even for a light ion such as C IV, a *relativistic* treatment of the recombination process is necessary to reproduce the experimentally observed $2p\,4l$ DR resonance structure. Presently, RMBPT is only applicable to relatively simple systems and it is therefore instructive to see in how far more standard "production" codes are able to reproduce low-energy resonance positions and strength. For C IV the Breit-Pauli R-Matrix results of Pradhan et al. (2001) differ by less than 20 meV from the measured resonance positions (figure 1). It should be kept in mind, however, that there are pathological systems, e. g. Mg IX, where a mere 50 meV uncertainty of low-energy resonance positions can translate into a nearly one-order-of-magnitude uncertainty on the plasma rate-coefficient scale in a temperature range where the ion is expected to form in photoionized gases (Schippers et al. 2004). Such findings strongly emphasize the need for experimental benchmarks, especially for low-temperature PR rate coefficients.

Photorecombination measurements responding to astrophysical data needs were carried out for L-shell iron ions at the Heidelberg storage-ring TSR by Savin et al. (1997; 1999; 2002a; 2002b; 2003) who already published DR rate coefficients for the ions Fe XVIII through Fe XXII. In a series of measurements with lithium-like ions, the influence of external electromagnetic fields on DR cross sections was thoroughly investigated by Bartsch et al. (1997; 1999; 2000), Böhm et al. (2001; 2002) and Schippers et al. (2000). This work is also of astrophysical interest. It was recently summarized by Müller & Schippers (2003).

3. Photoionization of atomic ions

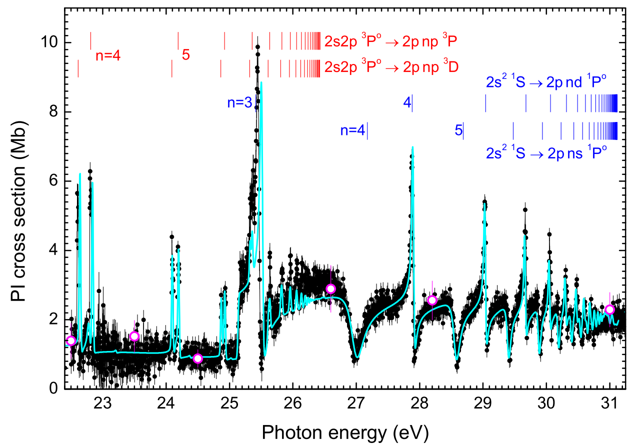

Figure 2. Photoionization of B^+-ions: experiment and Breit-Pauli R-Matrix theory (Schippers et al. 2003b). From the comparison between experiment and theory, it is concluded that 29% of the ions in the experiment were in the metastable state.

More recently, experiments aiming at measuring absolute PI cross sections of atomic ions and employing merged photon-ion beams were set up at 3rd generation synchrotron light sources. Measurements of astrophysical relevance were carried out, e. g., for singly charged boron (figure 2, Schippers et al. 2003b), carbon (Kjeldsen et al. 2001), nitrogen (Kjeldsen et al. 2002a), oxygen (Covington et al. 2001; Kjeldsen et al. 2002a; Aguilar et al. 2003a), neon (Covington et al. 2002), magnesium (Kjeldsen et al. 2000; Aguilar et al. 2003b) and iron (Kjeldsen et al. 2002b) as well as for the multiply charged ions C III (Müller et al. 2002), Ne IV (Aguilar 2003c), and Al III (Aguilar et al. 2003b).

Finally, it should be mentioned that the possibility to relate the time-inverse processes of PI and PR via the principle of detailed balance can be exploited for consistency checks between PI and PR measurements (Müller et al. 2002) and to obtain more comprehensive results than from only one experiment alone (Schippers et al. 2002b, 2003a).

Acknowledgments. The experimental work summarized in this article was carried out in close collaborations with S. Böhm, C. Brandau, S. Kieslich, W. Shi, and A. Müller (Gießen), D. W. Savin (New York), G. Gwinner, M. Schnell, D. Schwalm, and A. Wolf (Germany), H. Danared, N. Eklöw, and R. Schuch (Stockholm), A. Aguilar, A. M. Covington, E. D. Emmons, M. F. Gharaibeh, and R. A. Phaneuf (Reno).

References

Aguilar, A., et al. 2003a, ApJS, 146, 467

Aguilar, A., et al. 2003b, Phys.Rev.A, 67, 012701

Aguilar, A. 2003c, PhD Thesis, (Reno: University of Nevada).

Bartsch, T., et al. 1997, Phys.Rev.Lett, 79, 2233

Bartsch, T., et al. 1999, Phys.Rev.Lett, 82, 3779

Bartsch, T., et al. 2000, J.Phys.B, 33, L453

Böhm, S., et al. 2001, Phys.Rev.A, 64, 032707

Böhm, S., et al. 2002, Phys.Rev.A, 65, 052728

Böhm, S., et al. 2003, A&A, 405, 1157

Covington, A. M., et al. 2001, Phys.Rev.Lett, 87, 243002

Covington, A. M., et al. 2002, Phys.Rev.A, 66, 062710

Kjeldsen, H., et al. 2000, J.Phys.B, 33, 1403

Kjeldsen, H., et al. 2001, ApJS, 135, 285

Kjeldsen, H., et al. 2002a, ApJS, 138, 219

Kjeldsen, H., et al. 2002b, J.Phys.B, 35, 3655

Mannervik, S., et al. 1998, Phys.Rev.Lett, 81, 313

Müller, A., & Wolf, A. 1997, in Accelerator-based atomic physics techniques and applications, ed. J. C. Austin & S. M. Shafroth (Woodbury: AIP) 147

Müller, A. 1999, Int.J.Mass.Spectrom., 192, 9

Müller, A., et al. 2002, J.Phys.B, 35, L137

Müller A. & Schippers, S. 2001, in ASP Conf. Ser. Vol. 247, Spectroscopic Challenges of Photoionized Plasmas, ed. G. Ferland & D. W. Savin, 53

Müller, A., & Schippers, S. 2003, in The Physics of Multiply and Highly Charged Ions, Volume 1, ed. F. J. Currell (Dordrecht: Kluwer) 269.

Phaneuf, R. A., et al. 1999, Rep.Prog.Phys, 62, 1143

Pradhan, A. K., et al. 2001, Phys.Rev.Lett, 87, 183201

Savin, D. W., et al. 1997, ApJ, 489, L115

Savin, D. W., et al. 1999, ApJS, 123, 687

Savin, D. W., et al. 2002a, ApJS, 138, 337

Savin, D. W., et al. 2002b, ApJ, 576, 1098

Savin, D. W., et al. 2003, ApJS, 147, 421

Schippers, S., et al. 2000, Phys.Rev.A, 62, 022708

Schippers, S., et al. 2001, ApJ, 555, 1027

Schippers, S., et al. 2002a, Phys.Rev.A, 66, 042723

Schippers, S., et al. 2002b, Phys.Rev.Lett, 89, 193002

Schippers, S., et al. 2003a, Phys.Rev.A, 67, 032702

Schippers, S., et al. 2003b, J.Phys.B, 36, 3371

Schippers, S., et al. 2004, to be published

Tokman, M., et al. 2002, Phys.Rev.A, 66, 012703

West, J. 2001, J.Phys.B, 34, R45

Highlights of Astronomy, Vol. 13
International Astronomical Union, 2003
O. Engvold, ed.

The Ionized Gas and Nuclear Environment in NGC 3783

Hagai Netzer

School of Physics and Astronomy, Raymond and Beverly Sackler Faculty of Exact Sciences, Tel-Aviv University, Tel-Aviv 69978, Israel

Abstract.
The 900 ks *Chandra* spectrum of NGC 3783 was analyzed in various ways to study the properties of the absorbing gas. The main findings are: 1) On a time scale of 20–120 days, the source exhibits two very different spectral shapes with different softness ratios. The absorbing gas is not responding to these continuum variations. 2) Detailed photoionization modeling based on 10 silicon and sulphur lines near 5–7Å produces a satisfactory fit of the entire 3–25 Å spectrum of the source. The only discrepancy is in the central wavelength of the iron UTA feature. 3) A combination of three ionized absorbers, each split into two kinematic components, can explain the strengths of almost all the absorption lines and bound-free edges. The three components span a large range of ionization and have a total column of about 4×10^{22} cm^{-2}. Moreover, all three components are thermally stable and seem to have the same gas pressure.

1. Introduction

The barred-spiral galaxy NGC 3783 ($V \simeq 13.5$ mag., $z = 0.0097$) hosts a well-studied, type-I active galactic nucleus (AGN) with prominent broad emission lines and strong X-ray absorption features. The object has been observed extensively with almost all X-ray instruments, most recently by *Chandra* (Kaspi et al. 2002) and *XMM-Newton* (Blustin et al. 2002; Behar et al. 2003). The *Chandra* observations consist of a relatively short observation performed in 2000 January, and five longer observations performed in 2001 February – June, separated by various intervals from 2 to 120 days. Here we summarize the main findings of a detailed spectroscopic analysis of this spectrum. A more detailed work is presented in Netzer et al. (2003, hereafter N03).

2. The two-state X-ray spectrum of NGC 3783

The N03 study of the 900 ks *Chandra* spectrum reveals a a two-component continuum and large changes in softness ratio between “low” and “high” states of the central source. Crucial to the spectroscopic analysis is the fact that there are no obvious effects of the large continuum variations on the absorption spectrum and hence we can deduce lower limits on the distance of the absorbing gas. The present spectroscopic study is based on the low-state spectrum which is a combination of four 170 ks individual spectra (*Chandra* observations nos. 2090, 2091, 2092 and 2094).

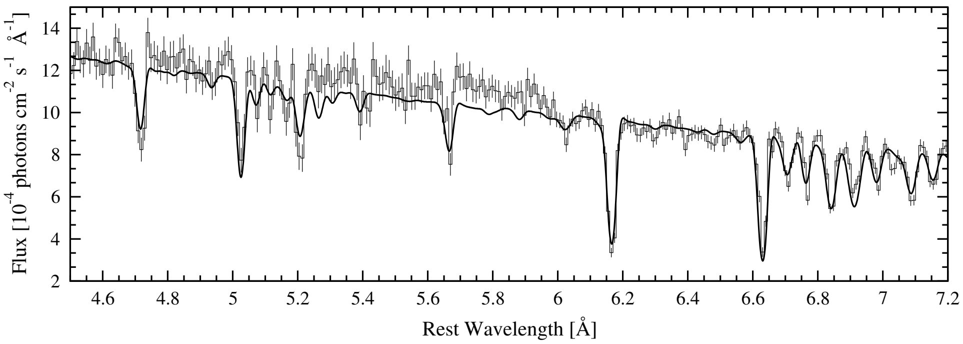

Figure 1. A comparison of the low-state NGC 3783 *Chandra* spectrum (680 ks) with the three component model described in the text.

3. Spectral analysis

The underlying idea is that the absorbing gas in NGC 3783 is photoionized by the central X-ray source and that the observed low and high-state spectra represent the physical conditions in the gas during the two phases. The principles and the ingredients of such modeling were outlined in Netzer (1996) and previous applications to the case of NGC 3783 were discussed by Kaspi et al. (2001). In the present case, the incident continuum is taken to be the broken power-law defined in Kaspi et al. (2001, Table 4) and the gas composition is "solar". The measured line profiles suggest two kinematic components per ionization component and the turbulent velocity in each is approximately 250 km s^{-1}.

3.1. The silicon and sulphur line method

We have developed a method to model the spectrum based on the EW measurements of various lines in the 5–7.1 Å band. This wavelength range contains lines from Si vii to Si xiv as well as the strongest lines of S xv and S xvi. Most of these lines are not blended. The range of ionization and excitation is very large and represents the ionization of almost all line-producing ions in the *Chandra* spectrum. The column densities of the various ions are deduced from the mesured EWs.

We searched for the best combination of photoionization models (i.e. a combination of ionization parameter, U_{OX}, and column density, N cm^2) that fit the observed 5–7Å spectrum. We found that at least three ionization components (i.e. six kinematic components) are required to fit the data to within the observational accuracy. The need for three components arise from the very large difference in ionization between the lowest (e.g. Si vii and Si viii) and the highest (e.g. S xvi) ionization lines. This requires at least one component to fit the EWs of the lowest ionization lines, one to fit the intermediate ionization lines and one for the highest ionization lines. A generic model with the required properties is the following three-component model: a low ionization component with $\log(U_{OX}) = -2.4 \pm 0.1$ and $\log(N) = 21.9 \pm 0.1$, a medium ionization component with $\log(U_{OX}) = -1.2 \pm 0.2$ and $\log(N) = 22.0 \pm 0.15$, and a high ionization component with $\log(U_{OX}) = -0.6 \pm 0.2$ and $\log(N) = 22.3 \pm 0.2$. This model is compared with the observations in Fig. 1.

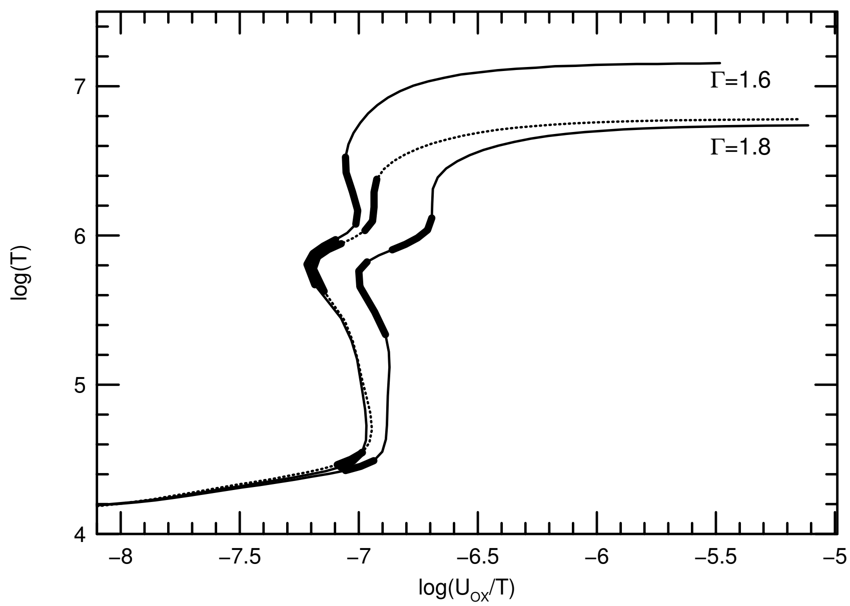

Figure 2. Thermal stability curves for a low density gas exposed to the low-state continuum of NGC 3783. The two curves marked by Γ are for a bare continuum with a 0.1–50 keV slope as marked. The dotted line is the stability curve for a gas exposed to a $\Gamma = 1.8$ continuum seen through a $\log(U_{OX}) = -2.4$ absorber. Thick sections mark the locations of the three absorbers considered in this.

The next step is to test the combination of components that fit the 5–7 Å spectrum over other wavelength bands. The results are surprisingly good and the very same combination provides a proper fit to the entire spectrum (this depends somewhat on the definition of the SED - see N03). The only significant discrepancy is in the wavelwngth of the M-shell iron UTA feature (see Behar, Sako & Kahn 2001) that indicates a lower ionization for iron compared with silicon and oxygen. We suggest that this is related to the unknown dielectronic recombination rates of M-shell iron ions (e.g. Savin et al. 2003; Gu 2003).

4. Discussion: the three component absorber

We found that three ionization components with different properties and a large range of ionization, are required to fit the spectrum of NGC 3783. Each of those components is split into two kinematic components, as implied by the observed line profiles.

A significant new aspect of our model is that the product $n_e \times T$ is similar (within a factor <2) for all three absorption components. This raises the interesting possibility that all the components are in pressure equilibrium (assuming gas pressure dominates the total pressure, i.e. radiation pressure and turbulent pressure are not important), and they all occupy the same volume of space. To test this idea, we have calculated a large number of thermal stability curves ($\log(T)$ vs. $\log(U_{OX}/T)$ changing the assumed SED and metalicity. Some results are plotted in Fig. 2. The interesting feature of the stability diagram is that all radiation fields considered here result in extended, almost vertical parts between $T \simeq 3 \times 10^4$ K and $T \simeq 2 \times 10^6$ K (the curve for $\Gamma = 1.6$ has a more extended vertical part since the higher mean energy of the radiation field results in a Compton temperature). All three ionization components required to explain the spectrum of NGC 3783 lie on the stable part of the curve. This suggest that the three can coexist in the same volume and provide important constraints on the location and density of the absorbing gas. More details on those models, as well as on the emission line spectrum and other physical properties of this gas are given in N03.

Acknowledgments. This work is supported by the Israel Science Foundation grant 545/00. I am greatful to my co-authors on N03, Shai Kaspi, Ehud Behar, W. N. Brandt, Doron Chelouche, Ian M. George, D. Michael Crenshaw, Jack R. Gabel, Frederick W. Hamann, Steven B. Kraemer, Gerard A. Kriss, Kirpal Nandra, Bradley M. Peterson, Joseph C. Shields, and T. J. Turner, for their critical comments and many useful suggestions during this large, long-term fruitful collaboration.

References

Behar, E., Sako, M., & Kahn, S. M. 2001, ApJ, 563, 497

Behar et al., 2003 (ApJ, in press; astro-ph/0307467)

Blustin, A. J., Branduardi-Raymont, G., Behar, E., Kaastra, J. S., Kahn, S. M., Page, M. J., Sako, M., & Steenbrugge, K. C. 2002, A&A, 392, 453

Gu, M. F. 2003, ApJ, 589, 1085

Kaspi, S., et al. 2001, ApJ, 554, 216

Kaspi, S., et al. 2002, ApJ, 574, 643

Netzer, H. 1996, ApJ, 473, 781

Netzer, H., et al., 2003, (ApJ, in press - N03)

Savin, D. W. et al. 2002, ApJ, 576, 1098

Highlights of Astronomy, Vol. 13
International Astronomical Union, 2003
O. Engvold, ed.

New Results on X-ray Models and Atomic Data

Jelle S. Kaastra[1], Rolf Mewe[1], & Ton Raassen[1,2]

[1]*SRON, Sorbonnelaan 2, 3584 CA Utrecht, The Netherlands*

[2]*Astronomical Institute Anton Pannekoek, Amsterdam, The Netherlands*

Abstract. We discuss the most recent developments of the spectral analysis package SPEX. We report on the progress made in updating the atomic data that are used in the spectroscopic code. We also present a set of spectral models that are used for the analysis of high-resolution X-ray spectra of photo-ionized plasmas such as occur in active galactic nuclei. These models include absorption line spectroscopy of photoionized layers. The importance and diagnostic power of inner-shell transitions is shown. We illustrate our results with several examples of observed spectra obtained with the XMM-Newton and Chandra grating spectrometers.

1. Introduction

Starting in the early seventies (Mewe 1972) we have developed a spectral code for the X-ray emission of optically thin plasmas. Milestones in this development were the Mewe-Gronenschild code (Mewe et al. 1985, 1986), the *mekal* model (Mewe et al. 1995) and the start of the *SPEX* project (Kaastra et al. 1996). The *mekal* model is a model for the calculation of emission spectra from optically thin, collisionally ionized plasmas. It is included in the popular *XSPEC* package and in a more complete form (including thermal Doppler broadening and non-equilibrium ionization (NEI) variants) in our own *SPEX* package, version 1. The *SPEX* package contains apart from the software to produce these thermal emission spectra also modules to calculate other line/continuum emission or absorption models, hydrodynamical models for supernova remnants, differential emission measure (DEM) analysis tools, spectral fitting and plotting tools, and tools to display relevant physical information of the plasma, ions or transitions.

Already at the time of the release of the *mekal* code and the *SPEX* package it became clear that updates are needed for various reasons. The advent of high-resolution X-ray spectroscopy through the launch of Chandra and XMM-Newton demanded for higher precision in wavelengths, a larger number of spectral lines to be included and more accurate atomic data. This also required more efficient use of computing power. Therefore we started updating our *SPEX* package. Version 2.0 is now available (see http://www.sron.nl/divisions/hea/spex/index.html). More background information on version 2.0 is given by Kaastra et al. (2002a).

We have made several updates of the *mekal* code that are available now in version 2.0 of *SPEX*. These include wavelength corrections according to Phillips et al. (1999), based upon Solar flare spectra; update of the line power of the strongest Fe XVII lines according to Doron & Behar (2002), and several minor corrections.

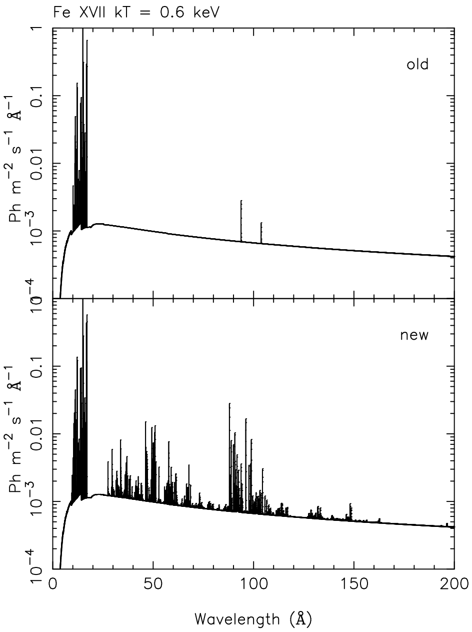

Figure 1. Fe XVII emission spectrum using *mekal* ("old") and our updated calculations ("new").

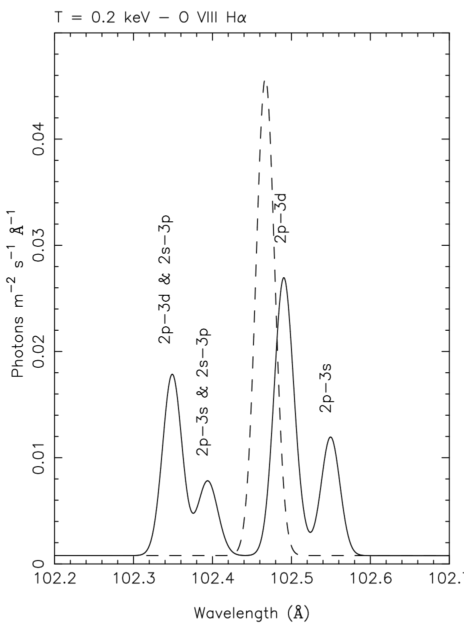

Figure 2. O VIII Hα emission spectrum using *mekal* (dashed line) and our updated calculations (solid line).

We are also working on a more ambitious project to improve and extend the atomic data for all transitions using different sources of data, such as calculations obtained using the *HULLAC* and *FAC* atomic codes and data available from the literature. For example, the *mekal* code has a subset of the strongest Fe XVII lines; the line powers used in that code were determined by scaling the old Mewe-Gronenschild temperature-dependent line powers to the level as calculated with *HULLAC* at the temperature of maximum emissivity. In our new work, we make full use of the *HULLAC* calculations (provided by D. Liedahl) for this ion and the other L-shell ions of iron. This also allows us to include many more transitions, see Fig. 1 for an example. In particular in the soft X-ray and EUV band we have many more lines now. At the harder X-rays the differences are not very large, although the inclusion of higher principal quantum numbers in our updated calculations produces more flux in specific narrow wavelength bands (cf. Brickhouse et al. 2000).

Another example of our update is given in Fig. 2. The Mekal code contains for hydrogenic ions only the Lyman α, β, γ, δ and ϵ lines, as well as Hα. We used the *FAC* code of M.F. Gu to extend the calculations to include all transitions up to $n = 10$. The figure shows the importance of the inclusion of the appropriate atomic data, since $H\alpha$ is now resolved into its 6 components.

Currently we are testing the newly included data and as soon as this has been finished they will be included in the latest *SPEX* version; we will announce this at the afore mentioned web page. Up to then, *SPEX* version 2.0 contains the updated *mekal* code.

We have also included absorption models for photo-ionized plasmas in version 2.0 of *SPEX*. For more details about these models we refer to Kaastra et al. (2002a). Examples of their application can be found in Kaastra et al. (2002b) and Steenbrugge et al. (2003).

Of particular interest in the application of these absorption models are the inner shell transitions. The importance of these lines in the context of absorption models has first been demonstrated by Sako et al. (2001) in their discovery of the Fe-M Unresolved Transition Array in a quasar spectrum. Since then, also the importance of 1s–np inner shell transitions in oxygen ions has been shown. For instance, in the Seyfert 1 galaxy NGC 5548, XMM-Newton RGS observations showed the presence of O IV–O VIII absorption lines. In fact it can be shown that for low ionization parameters and unsaturated columns, these inner shell oxygen transitions are the strongest absorption features expected in the RGS and Chandra LETGS bands (mainly due to the large cosmic oxygen abundance). Unfortunately, different atomic codes predict different wavelengths for these transitions, with differences up to the resolution of the RGS and LETGS. Laboratory measurements of the wavelengths are urgently needed.

Acknowledgments. The Space Research Organisation of the Netherlands (SRON) is supported financially by NWO, the Netherlands Organisation for Scientific Research.

References

Brickhouse, N.S., Dupree, A.K., Edgar, R.J., et al. 2000, ApJ 530, 387

Doron, R., & Behar, E. 2002, ApJ, 574, 518

Kaastra, J.S., Mewe, R., & Nieuwenhuijzen, H. 1996, in UV and X-ray Spectroscopy of Astrophysical and Laboratory Plasmas, p. 411, eds. K. Yamashita & T. Watanabe, Tokyo, Univ. Ac. Press.

Kaastra, J.S., Mewe, R., & Raassen, A.J.J., 2002a, in New Visions of the X-ray Universe in the XMM-Newton and Chandra Era, ESA SP, in press

Kaastra, J.S., Steenbrugge, K.C., Raassen, A.J.J., et al. 2002, A&A 386, 427

Mewe, R., 1972, Solar Phys. 22, 459

Mewe, R., Gronenschild, E.H.B.M., & van den Oord, G.H.J. 1985, A&A Supp 62, 197

Mewe, R., Lemen, J.R., & van den Oord, G.H.J. 1986, A&A Supp 65, 511

Mewe, R., Kaastra, J.S., & Liedahl, D.A. 1995, Legacy 6, 16

Phillips, K.J.H., Mewe, R., Harra-Murnion, L.K., et al. 1999, A&A Supp 138, 381

Steenbrugge, K.C., Kaastra, J.S., de Vries, C.P., & Edelson, R. 2003, A&A 402, 477

Highlights of Astronomy, Vol. 13
International Astronomical Union, 2003
O. Engvold, ed.

Spectral Modeling with APEC

Nancy S. Brickhouse and Randall K. Smith

Harvard-Smithsonian CfA, 60 Garden St., Cambridge, MA 02138

Abstract.
The Astrophysical Plasma Emission Code (APEC) collaboration now provides public models for X-ray spectra of collisional equilibrium plasmas. These models facilitate the diagnosis of temperature, density, elemental abundance, charge state, and optical depth. We report benchmarking studies of the APEC models from the Emission Line Project, a project to test these models using high quality stellar coronal spectra. We discuss the implications of the benchmarked atomic data for non-equilibrium collisional models as well. Finally, we discuss the extension of APEC to other applications, such as opacity models for AGN.

1. Introduction

APEC V1.3.1 (http://cxc.harvard.edu/atomdb) provides detailed spectral analysis capability for X-ray grating data. APEC line and continuum models are reasonably accurate and complete for collisional ionization equilibrium for $\lambda <$ 40 Å. Ongoing project efforts include non-equilibrium ionization modeling and opacities for X-ray photoionized plasmas. We note several issues that require better atomic data.

2. Collisionally Ionized Plasmas

Our goal is to provide calculations of populations and corresponding line emissivities for all levels $\geq n = 5$ for K- and L-shell ions and $n = 3$ for M-shell ions for the Chandra and XMM-Newton gratings. When available, accurate wavelengths from laboratory measurements replace the original theoretical wavelengths. Good spectral coverage and accurate wavelengths allow diagnostic applications even in heavily blended spectral regions (e.g. near Ne IX, Ness et al. 2003). We will soon complete the line database in the range 40 Å $< \lambda <$ 100 Å.

Published uncertainty estimates suggest that 30% accuracy in diagnostic ratios is a reasonable goal for strong lines. We note significant problems with other groups' calculations of H- and He-like line emissivities, stemming from incorrect energy extrapolations and inadequate treatment of recombination-driven cascades, (Smith et al. 2001), and our calculations should now meet this goal. The Emission Line Project is providing observational tests (Brickhouse & Drake 2000). While issues with Fe XVII are well known (Silver et al.; Beiersdorfer et al., these proceedings), similar discrepancies exist for other Fe L-shell ions as well (Fig. 1). We are now adding inner-shell transitions that become important for ionizing and recombining plasmas. Fig. 1 shows a wealth of satellite lines from

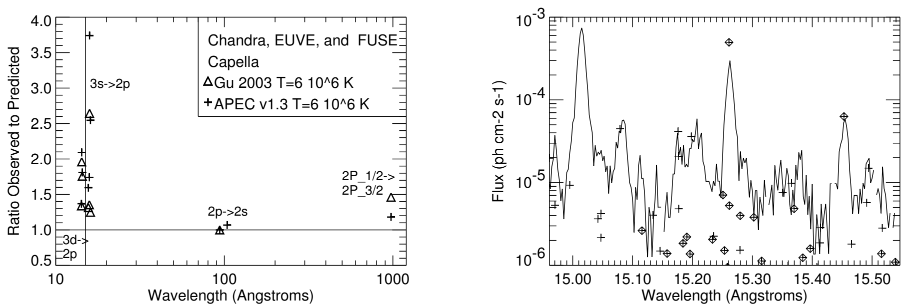

Figure 1. *Left.* Observed vs predicted line fluxes for Fe XVIII in Capella (P. Desai et al. 2003, in prep.). While the Gu (2003) calculations somewhat improve the agreement among the X-ray lines, a 40% discrepancy remains between the EUV and X-ray resonance lines. *Right.* Chandra Capella spectrum with APEC lines marked (+). Lines not due to Fe XVII DR are overplotted with ⋄ symbols.

Fe XVII that could help diagnose the ionization state; however, line-resolved calculations and laboratory wavelengths exist for only a few satellites.

3. Opacity Models

Krongold et al. (2003) have recently applied the APEC line list, plus additional inner-shell transitions, to the 900 ks Chandra summed spectrum of NGC 3783, using only a few parameters to fit more than 100 absorption features. A discrepancy exists between the best-fits to the Fe M-shell unresolved transition array (UTA) and to the Si absorption lines. To resolve this discrepancy, complete and unabbreviated models are needed.

Acknowledgments. The authors acknowledge APEC collaborators Duane Liedahl and John Raymond. Support for this project is provided by NASA NAS8-39083 to SAO for the CXC and LTSA NAG5-3559.

References

Brickhouse, N. S., & Drake, J. J. 2000, Rev. Mex. de Astronomia y Astrofisica Conf. Ser., 9, 24

Gu, M.-F. 2003, ApJ, 582, 1241

Krongold, Y., Nicastro, F., Brickhouse, N. S., Elvis, M., Liedahl, D. A., & Mathur, S. 2003, ApJ, accepted

Ness, J.-U., Brickhouse, N. S., Drake, J. J., & Huenemoerder, D. P. 2003, ApJ, accepted

Smith, R. K., Brickhouse, N. S., Liedahl, D. A., & Raymond, J. C. 2001, ApJ, 556, L91

Highlights of Astronomy, Vol. 13
International Astronomical Union, 2003
O. Engvold, ed.

The CHIANTI Database

E. Landi, K.P. Dere

Naval Research Laboratory, Washington, DC 20375, USA

P.R. Young

Rutherford Appleton Laboratory, Chilton, Didcot, OX11 0QX, UK

M. Landini

University of Florence, Largo E.Fermi 2, 51025 Firenze, Italy

H.E. Mason, G. Del Zanna

Dept. of Appl. Math. and Theor. Phys., University of Cambridge, UK

Abstract. The CHIANTI database contains assessed atomic energy levels, wavelengths, radiative transition probabilities and excitation rates necessary to calculate line emissivities and synthetic spectra of a large number of ions of astrophysical interest. CHIANTI also includes a suite of programs to carry out plasma diagnostics. In the present paper we describe the contents of the CHIANTI database, its main applications and its future developments.

1. Introduction

The launch of new space-born spectroscopic instrumentation has led to an increased need for a comprehensive and accurate database of atomic data that enables the astrophysical community to interpret the wealth of observed data now available. Over the years, we have built up the CHIANTI database in an effort to provide the astrophysical community with a database that would allow spectral analysis, plasma diagnostics and synthetic spectra calculations to be carried out at wavelengths from X-rays to the UV.

CHIANTI has been continually expanded since its first release in 1997 (Dere et al. 1997), and now includes new data for minor ions and continuum radiation (version 2 - Landi et al. 1999), data for the X-ray wavelength range (version 3 - Dere et al. 2001), and proton excitation rates and photoexcitation (version 4, Young et al. 2003). CHIANTI synthetic spectra have been compared with high-resolution spectral observations of the Sun and have been found to be complete and accurate in most cases (Young et al. 1998, Landi et al. 2002a,b, Del Zanna et al. 2002).

CHIANTI has been used extensively by the solar physics community, and has become the standard resource for atomic data for the interpretation of the solar spectrum. Also, CHIANTI has been extensively used for the analysis of data from Hubble, EUVE, FUSE, XMM, and Chandra. The accuracy and completeness of the CHIANTI database has led to the inclusion of CHIANTI emissivities in the software of current (SOHO/EIT and TRACE) and future (STEREO/SECCHI, Solar-B/XRT) broad-band imagers observing the Sun. CHIANTI is also part of the data analysis software for the SOHO/CDS spectrometer, and will be used for the Solar-B/EIS spectrometer to be launched in 2006. Because of their completeness and accessibility, CHIANTI data have been included in other spectral codes: XSTAR (Bautista & Kallman 2001), APEC/APED (Smith et al. 2001) and the Arcetri Code (Landi & Landini 2002).

CHIANTI is freely distributed by *SolarSoft* and it is also available at the web site

http://wwwsolar.nrl.navy.mil/chianti.html.

2. CHIANTI data

CHIANTI calculates line and continuum emission of optically thin plasmas, and includes the following processes:

- spectral line emission for more than 200 ions;
- radiative recombination continuum;
- bremsstrahlung continuum;
- Two-photon continuum.

Spectral line emission is calculated by solving the equations for level population under the assumption of statistical equilibrium, including electron and proton excitation, stimulated and spontaneous radiative decay and photoexcitation. All data come from the refereed literature.

The aim of the CHIANTI database is to provide a compact and easy-to-access set of data that is completely transparent to the user. CHIANTI data are stored in *ASCII* files, where the original literature sources of the data are reported at the end of each file.

3. Applications

Plasma diagnostics: CHIANTI emissivities have been used to carry out plasma diagnostics on a variety of astrophysical objects to measure plasma density, temperature, elemental abundances, velocities, emission measure, and differential emission measure in many different sources.

For example, Feldman et al. (2001) found agreement between the observed spectrum of the Jupiter-Io plasma torus and CHIANTI predictions, and estimates of the electron density and temperature made by CHIANTI complement in-situ measurements made by the Voyager and Galileo spacecrafts.

CHIANTI data have been used to measure physical properties of the solar atmosphere, in a wide variety of conditions: coronal holes (Del Zanna & Bromage 1999), quiet Sun (Landi et al. 2000), active regions (Mason et al. 1999), and flares (Landi et al. 2003). Plasma structures in the solar atmosphere, such as loops, have also been studied (i.e. Schmelz et al. 2001).

Density sensitive line pairs have been used to measure electron density in classical T-Tauri stars by Johns-Krull et al. (2000), using UV spectral lines observed with IUE and CHIANTI emissivities. Such estimates help in discriminating between different accretion shock models and allow the search for correlations between density and mass accretion rate.

CHIANTI has also been applied to X-ray and UV spectra of cool stars by a number of authors, in order to investigate the quiescent and active state of their coronae. For example, Robinson et al. (2001) measured plasma emission measure, temperature and density using CHIANTI and UV/optical observations from Hubble. Woitke & Sedlmayr (1999) used CHIANTI data for Fe II to investigate the role of iron in the energy balance in the extended atmospheres and circum-stellar envelopes of cool stars. Swartz et al. (2002) used CHIANTI to model the X-ray emission from sources detected by Chandra in M81.

Dixon et al. (2001) used O VI emissivities from CHIANTI to address the problem of the excess of EUV and soft X-ray flux present in the spectra of two clusters of galaxies, concluding that current warm gas models of the EUV excess should be revised.

Instrument calibration: In order to determine quantitative information from broad-band imagers, such as SOHO/EIT and TRACE, it is necessary to understand precisely the spectrum that is detected in each of the instruments' band passes. CHIANTI has been adopted as part of the standard EIT and TRACE calibration software to convert count rates into temperature and emission measure maps.

Comparison of line intensity ratios predicted by CHIANTI and observations from high-resolution spectrometers can provide a powerful means for determining their relative intensity calibration. Such technique has been recently applied to the SERTS rocket-borne spectrometer by Brosius et al. (1998) and Young et al. (1998). Del Zanna et al. (2001) applied CHIANTI to the calibration of SOHO/CDS, determining the relative intensity calibration of its six channels.

Atomic data assessment: The accuracy of atomic data and transition rates is crucial to reliable plasma diagnostics. The accuracy can only be assessed by comparison with observations, but direct laboratory measurements of transition rates are difficult. Comparison between CHIANTI predictions and line ratios observed by high-resolution spectrometers can be a powerful tool to investigate the accuracy of transition probabilities.

As part of the CHIANTI project we have compared CHIANTI emissivities with observations from the 1989 SERTS flight (Young et al. 1998), SUMER and CDS (Landi et al. 2002a,b). The comparisons have shown excellent agreement for the vast majority of ions, and CHIANTI accounts for all the most important lines in the EUV spectral range. Also a few ions whose atomic data need improvements were identified in these works (i.e. Fe XII). These comparisons have triggered new calculations aimed at improving the data available in CHIANTI and in the literature.

Of particular importance is the comparison between CHIANTI and the X-ray spectra observed with Chandra and XMM. Preliminary work has been carried out by Del Zanna et al. (2002), who showed that CHIANTI is able to reproduce most of the observed lines, but in the 10 to 13 Å wavelength range more work is needed to include the $n \geq 4$ transitions of highly ionized iron ions.

4. Future steps

The CHIANTI team is committed to continually update and expand the CHIANTI database in order to include more accurate data and more processes. The two main areas of development currently underway in CHIANTI are

1: Inclusion of ionization and recombination rates
2: Inclusion of data for the $n \geq 4$ transitions

Ionization and recombination rates will be included to enable CHIANTI users to investigate the effects of transient conditions often present in astrophysical plasmas. The inclusion of data for the $n \geq 4$ transitions will improve dramatically the emissivities in the X-ray range.

Acknowledgments. E. Landi is supported by NASA. K.P. Dere is supported by the Office of Naval Research. G. Del Zanna and H.E. Mason are supported by PPARC.

References

Bautista, M.A., Kallman, T.R., 2001, ApJS, 134, 139
Brosius, J.W., Davila, J.M., Thomas, R.J., 1998, ApJL, 497, L113
Del Zanna, G., Bromage, B.I.J., 1999, J. Geoph. Res., 104, 9753
Del Zanna, G., et al., 2001, A&A, 379, 708
Del Zanna, G., et al., 2002, *X-Ray Astronomy 2000*: PASP Conf. Ser. 234, Giacconi, Stella & Serio Eds.
Dere, K.P., et al., 1997, A&AS 125,149
Dere, K.P., et al., 2001, ApJS, 134, 331
Dixon, W., et al., 2001, ApJ, 550, L25
Feldman, P.D., et al., 2001, ApJ 554, L123
Johns-Krull, C.M., Valenti, J.A., Linsky, J.L., 2000, ApJ, 539, 815
Landi, E., et al., 1999, A&ASS, 135, 171
Landi, E., Mason, H.E., Lemaire, P., Landini, M., 2000, A&A, 357, 743
Landi, E., Landini, M., 2002, A&A, 384, 1124
Landi, E., Feldman, U., Dere, K.P., 2002a, ApJS, 139, 281
Landi, E., Feldman, U., Dere, K.P., 2002b, ApJ, 574, 495
Landi, E., et al., 2003, ApJ, 582, 506
Mason, H.E., Landi, E., Pike, C.D., Young, P.R., 1999, Sol.Phys., 189,129
Robinson, R.D., et al., 2001, ApJ, 554, 368
Schmelz, J.T., et al., 2001, ApJ, 556, 896
Smith, R.K., et al., 2001, ApJ, 556, 91
Swartz, D.A. et al., 2002, ApJ, 574, 382
Young, P.R., Landi, E., Thomas, R.J., 1998, A&A, 329, 291
Young, P.R., et al., 2003, ApJS, 144, 135
Woitke, P., Sedlmayr, E., 1999, A&A, 347, 617

Highlights of Astronomy, Vol. 13
International Astronomical Union, 2003
O. Engvold, ed.

Atomic Spectral Tables for the Chandra X-ray Observatory

L. I. Podobedova, D. E. Kelleher, J. Reader, and W. L. Wiese

National Institute of Standards and Technology, Gaithersburg, MD 20899-8420

Abstract. Tables of wavelengths, line classifications, and transition probabilities have been critically compiled for ionized spectra of neon (Ne V-VIII), magnesium (Mg V-X), silicon (Si VI-XII), and sulfur (S VIII-XIV) in the 20 Å-170 Å region. The tables provide basic atomic data for about 3300 transitions in support of astronomical studies from the Chandra X-ray Observatory.

1. Introduction

We have critically compiled spectral tables for higher ions of the cosmically abundant elements Ne, Mg, Si, and S in the spectral range of interest for the Low Energy Transmission Grating (LETG) of the Chandra X-ray Observatory. Our tables which include 3300 transitions will also be of use for diagnostics of plasmas found in fusion energy research devices such as tokamaks.

The wavelengths in the tables are Ritz-type values derived from experimental energy level values in the NIST Atomic Spectra Database (1999) (ASD). That is, the wave number of a particular transition is found as the difference of the values of the combining energy levels in cm^{-1}, and the wavelength in vacuum is the reciprocal of the wave number.

In compiling the transition probabilities we selected only values obtained with the most advanced theoretical and experimental methods. Our general evaluation criteria were those that have been developed at NIST (Wiese, Fuhr, & Deters 1996). We normally list here only values having estimated uncertainties of 50% or less. A few exceptions have been made for important lines. Because of the very limited amount of experimental results available for highly ionized ions, for most transitions we had to rely on theoretical data.

The most extensive source of theoretical data was the Opacity Project (2002) (OP), which has produced multiplet f-values for the spectra of many elements. However, since the OP calculations do not include spin-orbit interaction, they do not provide values for individual lines of a fine-structure multiplet. Therefore for the present work the average values for LS multiplets were decomposed into their LSJ fine structure components using LS coupling rules. For the present light atoms LS coupling should be a good approximation. For ions where this is clearly not the case we have used results of calculations that do include spin-orbit effects. Tachiev & Froese Fischer (2002) have performed calculations for Be-, B-, C-, N-, O-, F-, and Ne-like ions with the multi-configuration Hartree-Fock (MCHF) method with Breit-Pauli corrections and have made their results available on the World Wide Web. Blackford & Hibbert (1994) have carried out extensive calculations for F-like ions with the CIV3 code (CIV3 indicates Configuration Interaction code Version 3). The same method was used by Aggarwal (1998) for several C-like ions. Calculations with the many-body perturbation approach including Breit-Pauli corrections were also found to be very useful (Safronova et al. 1999; Vilkas et al. 1996). For comparative analysis data from several other sources were used in our work.

2. Graphical and Numerical Comparisons in Support of the Assessment Procedure

In order to reaffirm the uncertainty estimates of transition probabilities for the present compilation we made graphical and numerical comparisons of the results of different advanced calculations for as many transitions as possible, regardless of wavelength. Later we selected data for the Chandra spectral range 20 - 170 Å. To fit the data into systematic trends, or deviations from them, we found useful the theoretically predicted scaling of data along isoelectronic sequences. If available, we always selected data from detailed configuration-interaction calculations with intermediate coupling. As usual, these calculations are performed for transitions to the ground state or between low excited configurations. For the transitions involving high-lying configurations, only OP data are available. For the stronger transitions of many spectra, good agreement exists between the OP data and data from more detailed calculations that consider spin-orbit interactions.

The agreement among the OP calculations and different relativistic calculations gets worse for weaker transitions and for transitions between those levels where one or both are appreciably mixed due to breakdown of *LS* coupling. Large disagreements are often observed for weaker transitions when calculations for the transition probabilities of weak transitions have encountered considerable problems due to appreciable cancellations of positive and negative components of the transition integral.

Problems concerning large discrepancies in transition probabilities for fluorine-like spectra between the OP and CIV3 (Blackford & Hibbert 1994) results were recognized for some time and discussed earlier by Wiese & Kelleher (1998). At that time extended relativistic calculations for individual lines were available only from CIV3 calculations. In recent years new MCHF data became available (Tachiev & Froese Fischer 2002) which show that the agreement between MCHF and CIV3 is clearly better, but for many transitions it is still not good.

In studying the transitions for which the agreement is not good, we found that for almost all of them, one or both of the levels involved in the transition could be considered as *mixed*. By *mixed* we mean that the main contribution to the wave function of the level is less than 80%. Correspondingly, a *pure* level here means that that the main contribution to the wave function composition of this level is more than 80%.

Figure 1 shows a comparison of oscillator strengths of allowed transitions between mixed levels for the F-like ion S VIII. The ratios of CIV3 oscillator strengths (Blackford & Hibbert 1994) to the corresponding MCHF values (Tachiev & Froese Fischer 2002) are plotted on a logarithmic scale versus the MCHF oscillator strengths. The dashed lines indicate a band of 50% around a

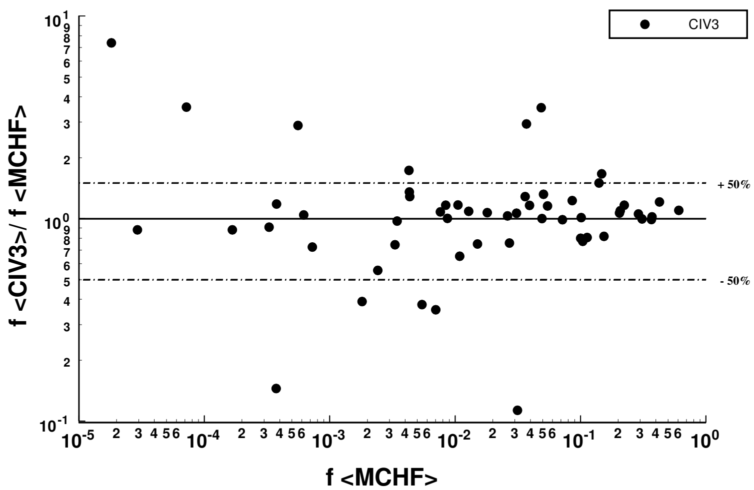

Figure 1. Comparison of oscillator strengths for S VIII for transitions with mixed levels

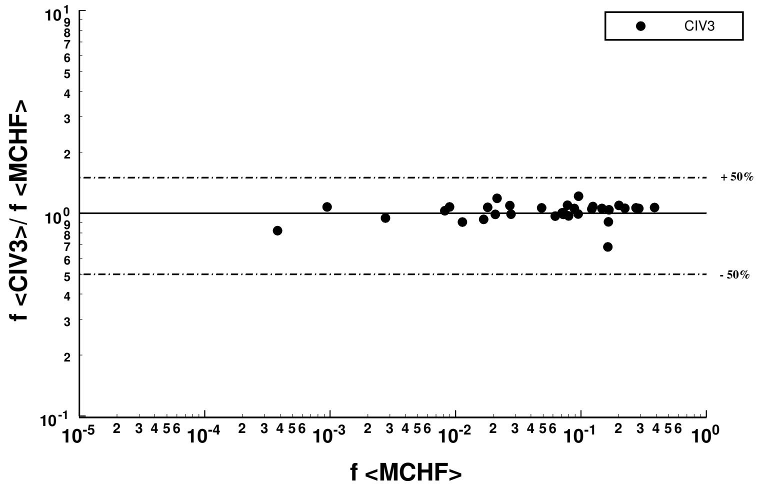

Figure 2. Comparison of oscillator strengths for S VIII for transitions with pure levels

perfect ratio of 1.00. It is seen that for most "mixed" transitions the agreement is better than 50%, which is within the range of data listed in the NIST reference tables.

For the "pure" transitions shown in Fig. 2 the agreement improves drastically. Out of 33 transitions, 31 have agreements between the CIV3 and MCHF calculations better than 10%. The others agree within 20%. The study of such cases is very valuable when we have transition probabilities available from only one source and we need to estimate their accuracy on the basis of extrapolations from comparisons with other sources in areas, where they overlap.

3. Arrangement of the tables

Atomic Spectral Data for the Chandra X-ray Observatory are presented by Podobedova et al (2003) on the world wide web. The tables are ordered for each chemical element by increasing ionization stage. Individual lines are arranged in order of wavelength, but otherwise in a format similar to the customary arrangement of the NIST ASD and the earlier NIST publications. Each transition is identified by its wavelength, the energy levels of the lower (i) and upper (k) states, the statistical weights of the levels ($g = 2J + 1$), and the level designations. All of the present values are for electric dipole transitions, E1.

For each line, the transition probability for spontaneous emission A_{ki} (in units of 10^8 s^{-1}), the oscillator strength f_{ik} (dimensionless), and log $g_i f$ are given. Also, the line strength S is given and expressed in atomic units (a.u.). Finally, the estimated accuracy and the references are given. The estimated accuracy is indicated by the following letters, which are the same as used in earlier NIST references (see, e.g., Wiese et al. 1996):

A - uncertainty less than 3%
B - uncertainty less than 10%
C - uncertainty less than 25%
D - uncertainty less than 50%
E - uncertainty greater than 50% (but typically within factors of 2-3)

4. Acknowledgments

Support for this work was provided by the National Aeronautics and Space Administration through Chandra Award EL9-1002A issued by the Chandra X-Ray Observatory, which is operated by the Smithsonian Astrophysical Observatory for and on behalf of NASA under contract NAS8-39073. Partial support was also provided by the Office of Fusion Energy Sciences of the U. S. Department of Energy. Thanks are due to Jeffrey Fuhr for supplying neon data.

References

Aggarwal, K. M. 1998, ApJS, 118, 589

Blackford, H. M. S. & Hibbert, A. 1994, ADNDT, 58, 101

NIST Atomic Spectra Database. 1999, URL http://atm.nist.gov/cgi-bin/AtData/main_asd/

Opacity Project. 2002, URL http://legacy.gsfc.nasa.gov/topbase

Podobedova, L. I., Musgrove A., Kelleher D. E., Reader J., Wiese W. L., Coursey J. S., & Olsen, K. 2003, URL http://physics.nist.gov/chandra

Safronova, U. I., Johnson, W. R., Safronova, M. S., & Derevianko, A. 1999, Phys.Scr., 59, 286. Complete data listing from private communication.

Tachiev, G., & Froese Fischer, C. 2002, URL http://www.vuse.vanderbilt.edu/~cff/mchf_collection

Vilkas, M. J., Martinson, I., Merkelis, G., Gaigalas, G., & Kisielius, R. 1996, Phys.Scr., 54, 281

Wiese, W. L., Fuhr, J. R., & Deters, T. M. 1996, JPCRD, Monograph 7, 532 pp.

Wiese, W. L. & Kelleher, D. E. 1998 in AIP Conf. Proc., 434, Atomic and Molecular Data and Their Applications, ed. P. J. Mohr & W. L. Wiese (New York: AIP), 105

Highlights of Astronomy, Vol. 13
International Astronomical Union, 2003
O. Engvold, ed.

TIPTOPbase

P. Palmeri

NASA Goddard Space Flight Center, Code 662, Greenbelt, MD 20771, USA

C. Mendoza

Centro de Física, Instituto Venezolano de Investigaciones Científicas (IVIC), PO Box 21827, Caracas 1020A, Venezuela

Abstract. An overview of the online atomic database referred to as TIPTOPbase is given, in particular its opacity server (OPserver) and current developments regarding online atomic structure calculations. Efforts to include atomic data for X-ray line modeling and to integrate TIPTOPbase within the International Virtual Observatory Alliance (IVOA) are also mentioned.

1. Introduction

TIPTOPbase is a public atomic database service for astrophysical applications that has been available on the Internet since 1993, being currently accessible from the URL `http://heasarc.gsfc.nasa.gov/topbase`. It offers the community the atomic data sets that were generated in the Opacity Project (The Opacity Project Team 1995,1996), IRON Project (Hummer et al. 1993), and more recent efforts (e.g. UKRmaX) to compute atomic data for X-ray line modeling. It lists both LS-coupling and fine-structure data, includes graphic processing, and is fully documented. We briefly describe below its present modules and some recent developments to improve data content and access capabilities.

2. TOPbase

TOPbase (Cunto & Mendoza 1992; Cunto et al. 1993) lists LS term energies, f-values, and photoionization cross sections for astrophysically abundant ions ($Z =$ 1–20 and $Z = 26$). They have been computed under the Opacity Project (Seaton 1987, The Opacity Project Team 1995, 1996) with the R-matrix method (Burke et al. 1971, Seaton 1985, Berrington et al. 1987) using multi-configuration target representations obtained with the atomic structure codes SUPERSTRUCTURE (Eissner et al. 1974) and CIV3 (Hibbert 1975). The emphasis is both on accuracy and completeness. Physical and numerical issues have been extensively discussed in the series of papers "Atomic Data for Opacity Calculations (I–XXIII)" in the *Journal of Physics B*.

3. TIPbase

TIPbase contains the atomic data sets produced in the IRON Project (Hummer et al. 1993), namely fine-structure level energies, radiative transition probabilities, electron impact excitation collision strengths and rates (effective collision strengths), photoionization cross sections, recombination coefficients, and Auger decay rates. They have been computed using the relativistic Breit–Pauli R-matrix method (Scott & Burke 1980; Scott & Taylor 1982; Berrington et al. 1995) and atomic structure codes SUPERSTRUCTURE (Eissner et al. 1974, Nahar et al. 2003) and CIV3 (Hibbert 1975). Extensive data have been calculated for ions of the iron isonuclear sequence and for the forbidden transitions (specially the infrared transitions) of the $2p^q$ and $3p^q$ (q =1–5) ions. Methods and approximations are documented in detail in the paper series "Atomic Data from the IRON Project (I–LII)" in *Astronomy & Astrophysics* and *Astronomy & Astrophysics Supplement Series*.

4. OPserver

OPserver computes with high time efficiency online Rosseland mean opacities (RMOs) and their temperature and density derivatives for a user specified temperature–density range and chemical mixture (Seaton, M.J., unpublished). The RMO for a chemical mixture M with mass density ρ and temperature T is defined as the harmonic mean (Seaton et al. 1994)

$$\kappa_{\mathrm{R}}(\rho, T, M)^{-1} = \int \frac{1}{\kappa(u)} f_{\mathrm{R}}(u) du \tag{2}$$

where $f_{\mathrm{R}}(u)$ is the Rosseland weighting function

$$f_{\mathrm{R}}(u) = \frac{15}{4\pi^4} u^4 \exp(-u)[1 - \exp(-u)]^{-2} \tag{3}$$

with $u \equiv h\nu/kT$. The monochromatic opacities are given by

$$\kappa(u) = \sum_i N_i \{\sigma_i^{\mathrm{abs}}(u)[1 - \exp(-u)] + \sigma_i^{\mathrm{scat}}(u)\} \tag{4}$$

where N_i is the number density of the ith ion and σ_i^{abs} and σ_i^{scat} its absorption and scattering cross sections. Therefore, the computation of the RMO for an arbitrary chemical mixture involves the reading of a large volume ($\sim$ 1 Gb) of ionic cross sections from secondary memory (disk) before the harmonic mean can be calculated. Data reading from disk takes up to 90% of the computing time; typical running times on the SGI Origin-2000 at the Ohio Supercomputer Center (OSC) in Columbus, Ohio, USA, are 126 s for disk reading and 14 s for computing the actual mean. On OPserver (see Figure 1), by having all the ionic cross sections permanently pre-loaded in main memory and by parallelizing the routines that take part in the calculation of the mean, the total time required to satisfy a user request on the OSC Origin-2000 is reduced to under 2 s. A small overhead for internet data transmission must be however added, but the RMO

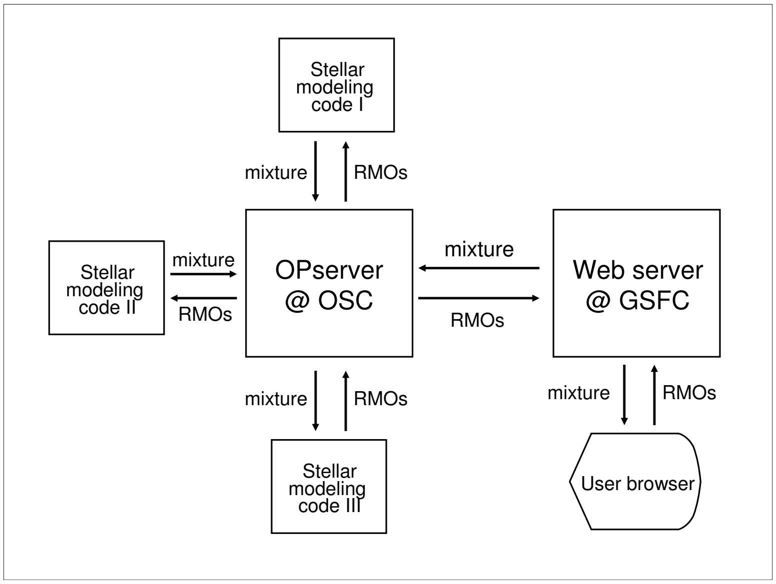

Figure 1. Online implementation of OPserver at the Ohio Supercomputer Center (OSC). User requests for Rosseland mean opacities (RMOs) for a chemical mixture can be submitted via a web page through the web server at Goddard Space Flight Center (GSFC) or from a stellar modeling code by means of linked routines.

data volume is usually small ($\sim$ 100 Kb). A user request can be performed through a web page (see Figure 1) or a stellar modeling code, say, by means of linked routines. OPserver is at present being updated with a new set of codes and monochromatic opacities that include the inner-shell contributions.

5. Online structure calculation

Since TIPTOPbase cannot always satisfy a user request for atomic data, an online implementation of the extended version of the atomic structure code SUPERSTRUCTURE (Eissner et al 1974) referred to as AUTOSTRUCTURE (Badnell 1997) is being developed that will allow the user to carry out via a web page quick calculations of acceptably accurate level energies, A-values and Auger rates for any ion. While distinct from TIPTOPbase, this service will become available in the first quarter of 2004.

6. Atomic data for X-ray line modeling

Most of the research groups that took part in the IRON Project are now involved in the computation of atomic data for X-ray applications, in particular of K and L lines in the iron isonuclear sequence. Radiative and Auger decay rates, and photoionization and electron impact excitation cross sections involving the inner shells are being studied. Lighter isonuclear sequences with $Z \leq 20$ and other systems of the iron group are also of interest. These data will progressively become available from TIPTOPbase.

7. IVOA

As from the beginning of 2004, TIPTOPbase's home will be moved from HEASARC at Goddard Space Flight Center to the Centre de Données astronomiques de Strasbourg (CDS), France, where the possibilities of integrating it within the International Virtual Observatory Alliance (`http://www.ivoa.net`) will be considered.

Acknowledgments. Technical assistance and help in the installation and tuning of the different components of TIPTOPbase from Steve Fantasia (Laboratory for High Energy Astrophysics, Goddard Space Flight Center, Maryland, USA), Paul Buerger (Ohio Supercomputer Center, Columbus, Ohio, USA), and Francois Ochsenbein (Centre de Données astronomiques de Strasbourg, France) are gratefully acknowledged.

References

Badnell, N. R. 1997, J. Phys. B, 30, 1

Berrington, K. A., Burke, P. G., Butler, K., et al. 1987, J. Phys. B, 20, 6379

Berrington K.A., Eissner W.B., Norrington P.H., 1995, Comput. Phys. Commun. 92, 290

Burke, P. G., Hibbert, A., & Robb, W. D. 1971, J. Phys. B, 4, 153

Cunto, W., & Mendoza, C. 1992, Rev. Mex. Astron. Astrofis., 23, 107

Cunto, W., Mendoza, C., Ochsenbein, F., & Zeippen, C. J. 1993, A&A, 275, L5

Eissner, W., Jones, M., & Nussbaumer, H. 1974, Comput. Phys. Commun., 8, 270

Hibbert, A. 1975, Comput. Phys. Commun., 9, 141

Hummer, D. G., Berrington, K. A., Eissner, W., et al. 1993, A&A, 279, 298

Nahar S.N. Werner, E., Chen G.X., & Pradhan, A.K., 2003, A&A 408, 789

Scott, N. S., & Burke, P. G. 1980, J. Phys. B, 13, 4299

Scott, N. S., & Taylor, K. T. 1982, Comput. Phys. Commun., 25, 347

Seaton, M.J. 1987, J. Phys. B 20, 6363

Seaton, M. J. 1985, J. Phys. B, 18, 2111

Seaton, M. J., Yu, Y., Mihalas, D., & Pradhan, A. K. 1994, MNRAS, 266, 805

The Opacity Project Team. 1995, 1996, The Opacity Project, Vols. 1, 2 (Bristol: IOPP)

Highlights of Astronomy, Vol. 13
International Astronomical Union, 2003
O. Engvold, ed.

The Astrophysical Plasma Emission Database: Progress and Plans

Randall K. Smith and Nancy S. Brickhouse

Harvard-Smithsonian Center for Astrophysics, 60 Garden St., Cambridge, MA 02138

Duane A. Liedahl

Department of Physics and Advanced Technologies, Lawrence Livermore National Laboratory, P.O. Box 808, L-41, Livermore, CA 94550

Abstract. The Astrophysical Plasma Emission Database (APED) contains atomic data for the 14 most abundant astrophysical elements, collected from the literature. Although APED was originally designed for use in calculating a collisional-equilibrium X-ray spectrum suitable for analysis of high-resolution data, it is in a general format which can be efficiently used to calculate absorption spectra, photoionization models, and non-equilibrium collisional models. We emphasize original sources; each transition, rate, and energy level in APED contains a bibliographic reference. The APED can be downloaded from `http://cxc.harvard.edu/atomdb/`, or our website WebGUIDE (`http://obsvis.harvard.edu/WebGUIDE/`) can be used to search for individual lines or transitions. We are continually working to expand APED (current version 1.3.1) and regularly issue updated collections.

1. Introduction

The goal of the Astrophysical Plasma Emission Database (APED) is to organize accurate and complete atomic data in a well-defined format that includes errors, original references, and version information as part of the electronically-available data. APED is used by a number of packages, including the Astrophysical Plasma Emission Code (APEC), which calculates the emission from a hot (10^4-10^9 K) plasma, WebGUIDE (`http://obsvis.harvard.edu/WebGUIDE/`, a web tool that creates line lists and displays data from APED, and PHASE, a photoabsorption code (Krongold et al. 2003).

APED was designed to address the needs of the high-resolution X-ray data coming from the Chandra and XMM/Newton grating spectrometers, and so focuses on the hydrogen-like, helium-like, and iron and nickel L-shell lines that form most of the X-ray emission. The data are taken from the literature (*e.g.* Sampson, Goett & Clark 1983, Jacobs et al. 1989) when available and from unpublished calculations if necessary. Some data for longer-wavelength lines was included from the CHIANTI 2.0 database as well (Landi et al. 1999)

When distributed, we combine the APED with the tables of calculated emission lines and continuum output from APEC; together, these form the atomic database ATOMDB, available at `http://cxc.harvard.edu/ATOMDB`. This site also contains documentation, software that can be used to access the ATOMDB, and any known caveats or issues with using the data.

2. Future Plans

Currently, APED includes a number of different ionization balance calculations. We plan to add ionization and recombination data so that APEC can calculate an equilibrium or non-equilibrium ionization balance as needed. In addition, we plan to add more inner-shell excitation/autoionization transitions, improve wavelengths for L-shell ions of carbon through calcium (based on lab data, *e.g.* Lepson et al. 2003), and add more dielectonic recombination lines.

3. AstroAtom

In creating APED, we have discovered that there is a gulf between atomic physicists and astrophysicists; frequently data exist in the atomic literature but are difficult for an outsider to discover. We have therefore begun a new website called "AstroAtom" (`http://cfa-www.harvard.edu/astroatom/`), which is designed to foster communication between atomic physicists and astrophysicists. The website is a joint venture of the Chandra X-ray Center and the Institute for Theoretical Atomic and Molecular Physics, and allows scientists to post abstracts, conference announcements, and questions in a search-able database.

4. Acknowledgments

The author acknowledges APED collaborators John Raymond and Priyamvada Desa. Support for this project is provided by NASA NAS8-39083 to SAO for the CXC and LTSA NAG5-3559.

References

Krongold, Y., Nicastro, F., Brickhouse, N.S., Elvis M., Liedahl,D. A. & Mathur, S. 2003, ApJ, in press

Sampson, D. H., Goett, S. J., & Clark, R. E. H. 1983, ADNDT, 29, 467

Jacobs, V. L., Doschek, G. A., Seely, J. F., & Cowan, R. D. 1989, Phys. Rev. A, 39, 2411

Landi, E., Landini, M., Dere, K. P., Young, P. R., & Mason, H. E. 1999, A&AS, 135, 339

Lepson, J. K., Beiersdorfer, P., Behar, E., & Kahn, S. M. 2003, ApJ, 590, 604

Highlights of Astronomy, Vol. 13
International Astronomical Union, 2003
O. Engvold, ed.

New Radiative Atomic Data

Sultana N. Nahar

Department of Astronomy, The Ohio State University, Columbus, OH 43210, USA

Abstract. Large amount of new radiative atomic data for I) energy levels, II) oscillator strengths (f), line strengths (S), radiative transition probabilities (A), III) photoioniztion cross sections (σ_{PI}) - total and level-specific, and IV) unified total and level-specific electron-ion recombination rate coefficients, α_R, including radiative and dielectronic recombination (RR and DR) are reported for various astrophysical applications. Most of the data are with fine structure. These data are not yet available from any databases. Photoionization and recombination data are self-consistent, using the same wave-function for both processes.

1. Introduction

Atomic parameters for radiative processes are obtained from ab initio quantum mechanical calculations using the close coupling approximation employing the R-matrix method, as developed under the OP (The Opacity Project 1995, 1996) and Iron Project (IP, Hummer et al. 1993, Berrington et al. 1995) and new theoretical developments for total electron-ion recombination using the unified method (Nahar and Pradhan 1992, 1994, Zhang et al. 1999), and large-scale theoretical spectroscopy calculations (Nahar and Pradhan 2000). Relativistic effects are included through the Breit-Pauli R-matrix (BPRM) method for most of the radiative data.

Compared to earlier results, such as those under the OP, present results include much more data in addition to σ_{PI} and f-values. Present calculations are more elaborate and extensive with the following important features:

i) wave-function expansions used for the new results are in general larger, i.e., they include more excited core states, E_t, yielding (1) more complete set of energy levels ($E_\nu = E_t$ - z^2/ν^2), (2) larger sets of f, S, A-values for bound-bound transitions, (3) more Rydberg series of resonances in the cross sections belonging to the additional core states, (4) more accurate background cross sections at higher energies.

ii) observed energies, where available, are used for the core states which provide more accurate resonance positions determined from $E_\nu = E_t$ - z^2/ν^2.

iii) calculations are carried out using finer energy mesh.

2. Bound-Bound Transitions: $X^{+n} + h\nu \leftrightarrow X^{+n*}$

Present A, f, and S-values are mainly for electric dipole (E1), i.e, dipole allowed and inter-combination ($\Delta J = 0, \pm 1$, parity change) transitions. However, forbidden transitions ($\Delta J > 1$), e.g., electric quadrupole (E2), octupole (E3), magnetic dipole (M1), quadrupole (M2), are obtained for a number of ions.

One important advantage of BPRM method is that large number of bound-bound transitions can be considered. The spectroscopic identification of the computed levels and transitions are carried out with newly developed identification procedure based on quantum defect and channel contribution analysis. Each level is assigned with a spectroscopic notation, $(C_t\ S_t\ L_t\ J_t\ \pi_t n\ell\ [K]\ s)\ \ J\ \pi$ where C denotes configuration and subscript t denotes target (or the core). The forbidden transition of type E2, E3, M1 and M2 are obtained through atomic structure calculations using updated version of SUPERSTRUCTURE (Eissner et al. 1974, Nahar et al 2003).

Data for Fe XVII (Nahar et al. 2003) is an example of new results. A total of 490 fine structure levels are obtained for this ion, compared to observed 52 levels. The calculated energies agree within 1% with the observed energies. A, f, and S-values are obtained for over 2.6×10^4 for allowed and inter-combination transitions; a comparison table of Fe XVII transitions is given below:

Table. Comparison of BPRM calculations for decay $A^{\mathrm{E1}}(j,1)$ to the Fe XVII ground state $C_1T_1 = 2\mathrm{s}^2 2\mathrm{p}^6\ {}^1\mathrm{S}_0$ with other work

C_j	T_j	$A(s^{-1})$ BPRM	$A(s^{-1})$ others
$2s^22p^53s$	${}^1P^o_1$	7.96(11)	8.28(11)^{a}, 8.01(11)^{b}, 7.75(11)^{c}, 8.30(11)^{e}, 9.40(11)‡
$2s^22p^53s$	${}^3P^o_1$	9.35(11)	9.76(11)^{a}, 9.44(11)^{b}, 9.09(11)^{c}, 9.34(11)^{e}, 8.00(11)‡
$2s^22p^53d$	${}^3P^o_1$	7.58(10)	9.19(10)^{a}, 8.27(10)^{b}, 7.77(10)^{c}, 9.00(10)^{e}, 8.89(10)‡
$2s^22p^53d$	${}^3D^o_1$	5.93(12)	6.33(12)^{a}, 5.68(12)^{b}, 5.23(12)^{c}, 6.01(12)^{e}, 5.72(12)‡
$2s^22p^53d$	${}^1P^o_1$	2.28(13)	2.24(13)^{a}, 2.64(13)^{b}, 2.44(13)^{c}, 2.28(13)^{e}, 2.52(13)‡
$2s2p^63p$	${}^3P^o_1$	4.03(11)	4.51(11)^{a}, 3.66(11)^{b}, 4.12(11)^{d}, 3.40(11)^{e}, 3.52(11)‡
$2s2p^63p$	${}^1P^o_1$	3.30(12)	3.34(12)^{a}, 3.21(12)^{b}, 3.29(12)^{d}, 3.30(12)^{e}, 3.25(12)‡

a – Safronova et al 2001, b – Bhatia & Doschek 1992, c – Cornille et al 1994, d – present MCDF, e – NIST, ‡ – SS with *all* magnetic FS-components.

Following is the list of atoms and ions for which transition probabilities (f, A, S) are available or calculations are in progress.

Fe ions: Fe I, Fe II, Fe III, Fe IV, Fe V, Fe XIII, Fe XVII, Fe XX, Fe XXI, Fe XXIII, Fe XXIV, Fe XXV
Ca ions: Ca VII, Ca XVIII
Ar ions Ar V, Ar XIII, Ar XVI, Ar XVII
S ions: S II, S III, S XIV
Si ions: Si I, Si II, Si XII
Ne ions: Ne V, Ne VIII
O ions: O II, O III, O IV, O VI
C ions: C II, CII, C IV
Li-like: N V, O VI, F VII, Na IX, Mg X, Al XI, Ti XX, Cr XXII, Ni XXVI
He-like ions (elements as for Li-like)

3. Photoionization and Recombination: $X^+ + h\nu \leftrightarrow X^{++} + \mathbf{e}$

The unified method for total electron-ion recombination developed by Nahar and Pradhan (1992, 1994) enables self-consistent sets of data for photoionization

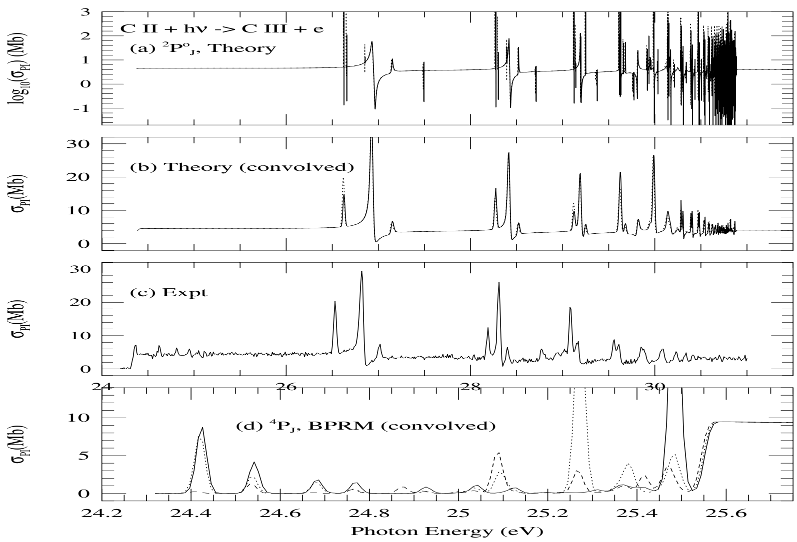

Figure 1. Comparison between theory - Nahar and experiment (Kjeldsen et al. 1999) of photoionization cross sections of C II

cross sections, σ_{PI}, and total recombination rate coefficients, $\alpha_R(T)$ for atoms and ions.

For highly charged ions, σ_{PI} and $\alpha_R(T)$ are obtained for fine structure levels including relativistic effects; radiation damping is important for Li-like and He-like ions. For complex multi-electron systems, these quantities are obtained in LS coupling. Contrary to OP data in LS coupling, present results include much more data, including partial photoionzation cross sections. Complete data sets include total and level specific photoionization cross sections and recombination rate coefficients for hundreds of levels (with n $\leq$ 10) for each ion.

Both the photoionzation cross sections and unified recombination cross sections have been benchmarked with recent sophisticated experiments. Figure 1 shows comparison of C II σ_{PI} with the measurement by Kjeldsen et al (1999). Figure 2 presents total and level-specific $\alpha_R(T)$ for Ni XXVI of interest to X-ray astrophysics.

Self-consistent sets of data for σ_{PI}, and unified recombination rate coefficients have been obtained or are in progress for over 50 ions:
Nickel: Ni II, Ni XXVI
Iron: Fe I, Fe II, Fe III, Fe IV, Fe V, Fe XIII, Fe XVII, Fe XXI, Fe XXIV, Fe XXV, Fe XXVI
Ca: Ca VII, Ca XV, Ca XVIII
Ar: Ar V, Ar XIII, Ar XVI
S: S II, S III, S XI, S XIV
Si: Si I, Si II, Si IX, Si XII
Oxygen: O I, O II, O III, O IV, O V, O VI, O VII, O VIII
Nitrogen: N I, N II, N II, N IV, N V, N VI, N VII
Carbon: C I, C II, C III, C IV, C V, C VI
C-like: F IV, Ne V, Na VI, Mg VII, Al VIII

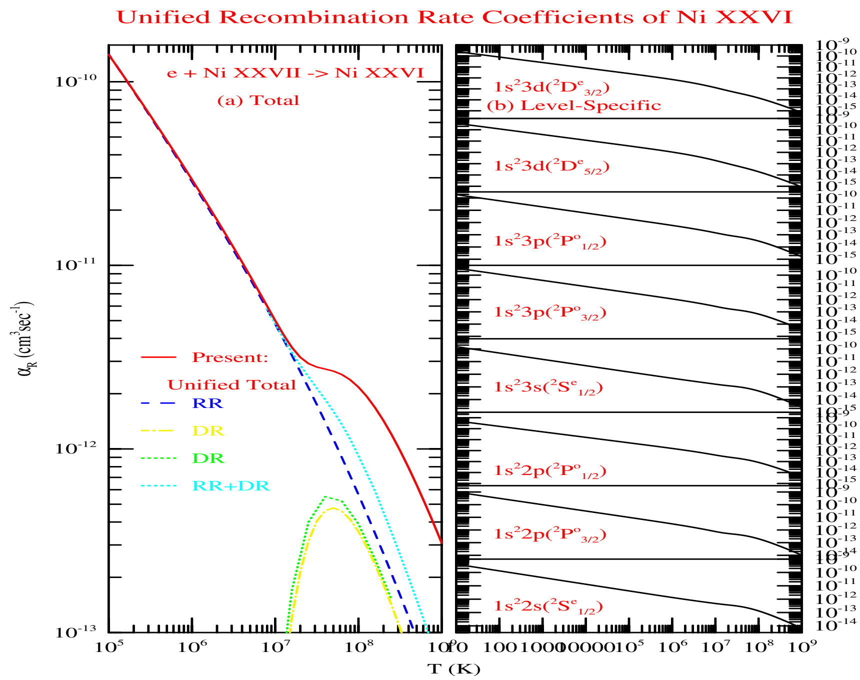

Figure 2. (a) Total unified recombination rate coefficient, α_{RC}, and (b) level-specific recombination rate coefficients of Ni XXVI.

Li-like: Ti XX, Cr XXII and others
He-like (elements as for Li-like)

Data Accessibility - Ohio State University: (i) 1. Anonymous ftp: ftp.astronomy.ohio-state.edu, (ii) http://www.astronomy.ohio-state.edu/∼ nahar, (iii) Email: nahar.1@osu.edu

Acknowledgments. Supported partially by the U.S. NSF and NASA.

References

Berrington K.A., Eissner W.B., Norrington P.H., 1995, Comput. Phys. Commun. 92, 290

Eissner W., Jones M., Nussbaumer H., 1974, Comput. Phys. Commun 8, 270

Hummer, D.G., Berrington, K.A., Eissner, W., Pradhan, A.K., Saraph, H.E., & Tully, J.A. 1993, A&A, 279, 298

Kjeldsen et al, 1999, ApJ 524, L143

Nahar S.N. 2002, Phys. Rev. A 65, 052702

Nahar S.N. & Pradhan, A.K., 1992, Phys. Rev. Lett. 68, 1488

Nahar S.N. & Pradhan, A.K., 1994, Phys. Rev. A 49, 1816

Nahar S.N. & Pradhan, A.K., 2000, Phys. Scr. 61, 675

Nahar S.N. Werner, E., Chen G.X., & Pradhan, A.K., 2003, A&A 408, 789

The Opacity Project 1 and 2, IOPP, Bristol (1995, 1996)

Zhang, H.L., Nahar, S.N. & Pradhan, A.K. 1999, J. Phys. B, 32. 1459

Highlights of Astronomy, Vol. 13
International Astronomical Union, 2003
O. Engvold, ed.

NIFS Atomic Numerical Databases

Izumi Murakami and Takako Kato

National Institute for Fusion Science, Toki 509-5292, Japan

Abstract. We have compiled the atomic and molecular numerical databases which are available through internet. The databases provide basic atomic data, such as collisional ionization and excitation cross sections, which are important for modeling and diagnosing astrophysical plasmas.

1. Introduction

Atomic data are important for modeling and diagnosing astrophysical plasmas. For instance, ion abundances are calculated with ionization and recombination rates, and spectral line intensities are estimated with transition probabilities, excitation rates, and etc. The NIFS atomic and molecular numerical databases have numerical data of cross sections and rate coefficients for collision processes between electron, ion, atom, and molecules. The data compilation was started for elements which are important for fusion plasma in 1970s first (Takayanagi & Suzuki 1976), but extended for other elements later.

2. NIFS databases

The NIFS databases consist of sub databases (DBs) categorized with the atomic processes: "AMDIS" is the DB of electron-impact ionization, excitation, and recombination cross sections and rate coefficients. Compilation of ionization and excitation rate coefficients will start soon; "CHART" is the DB of charge transfer and ionization cross sections of ion-atom/molecule collision; and there are other DBs for molecule collision processes and plasma-material interaction. These DBs are available at
`http://dbshino.nifs.ac.jp/` since 1997 and registration is required for using them (free of charge for academic research). Now more than 800 people are resisted and more than half of them are international users from 47 countries.

Atomic data are retrievable and numerical data tables and graphs are displayed in a browser. The data shown in a graph can be compared, which is useful for data evaluation. Figure 1 shows an example of the web page for data search. Data are search-able by element, ionic state, author name, and so on.

Data compilation has been done as international and domestic collaborations with atomic physicists and their help and understandings are important and necessary. We are grateful for all their help in past and future. Feedback such as data needs from the data users is also important for developing the database.

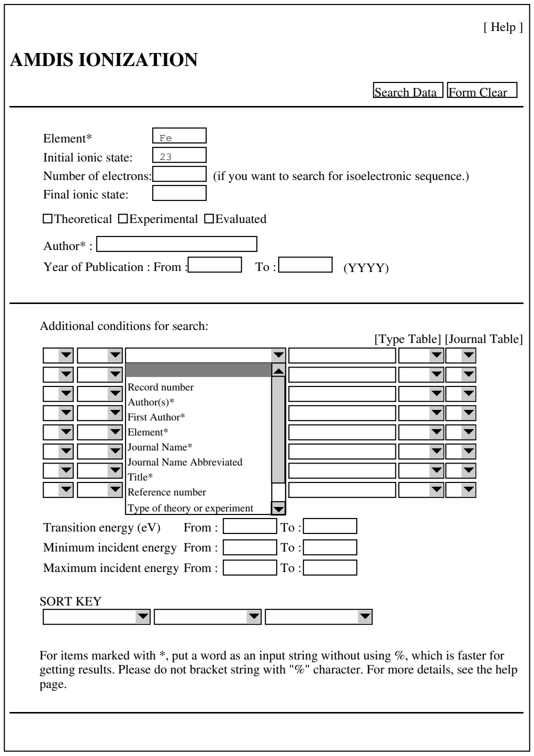

Figure 1. Example of web page image for data search of the NIFS database: AMDIS IONIZATION is the database of electron-impact ionization cross sections.

References

Takayanagi, K., Suzuki, H. 1976, IPPJ-DT-50 (Inst. Plasma Phys., Nagoya Univ.).

Highlights of Astronomy, Vol. 13
International Astronomical Union, 2003
O. Engvold, ed.

Future NASA Programs and Funding Support

Hashima Hasan

NASA Headquarters, Washington DC 20546, USA

Abstract. The future of Astronomy and Physics programs in the Office of Space Science is presented in the context of the overall NASA Strategic Plan. The highlights of the new road maps for the Origins and Structure and Evolution of the Universe science themes are given. A new initiative, Beyond Einstein, is discussed. New opportunities for technology development, building small missions, and conducting basic research and analysis to support NASA's strategic goals are outlined. The status of NASA's archives for data from its astronomy missions is presented.

Introduction

The science conducted by OSS is divided into four scientific themes.

- Astronomical Search for Origins (ASO)
- Structure and Evolution of the Universe (SEU)
- Sun Earth Connection (SEC)
- Solar System Exploration (SSE)

Road maps produced by the scientific community for each of these science themes form the basis for the Space Science Strategy. The first two science themes listed above, ASO and SEU, encompass the Astronomy and Physics program.

Astronomy and Physics Program

Astronomical Search for Origins
The science of the ASO science theme is focused around the following three research areas and the related science questions.
Emergence of the Modern Universe
-How did the cosmic web of matter organize into the first stars and planets?
-How do different galactic ecosystems (of stars and gas) form and which can lead to planets and living organisms?
Stars and Planets
-How do gas and dust become stars and planets?
-Are there planetary systems around other stars and how do their architectures and evolution compare with our own solar system?
Habitable Planets and Life
-What are the properties of giant planets orbiting other stars?
-How common are terrestrial planets? What are their properties? Which of them might be habitable?
-Is there life on planets outside the solar system?
The ASO road map defines a series of space flight missions, often supported by

ground based programs which may be required as scientific or technology precursors to a flight program. The philosophy followed by both ASO and SEU is that the science and technology feeds forward from one mission to the next.

The ASO mission, Space Infrared Telescope Facility (SIRTF), the last of NASA's Great Observatories, is scheduled for launch in August 2003. The Infrared Astronomy (SOFIA), James Webb Space Telescope (JWST), Space Interferometry Mission (SIM), Terrestrial Planet Finder (TPF) and Kepler are in development. Ground based missions in support of SIM and TPF are the Keck interferometer, and the Large Binocular Telescope Initiative (LBTI). Vision missions, such as large UV and IR telescopes, leading ultimately to a Planet Imager (PI) and Life Finder (LF) are mentioned as future possibilities.

Structure and Evolution of the Univ aunch in August 2003. Flight missions in development are the Stratospheric Observatory for erse
The SEU road map is divided into two parts. The first, *Beyond Einstein*, describes a bold new initiative which aims to address some of the unsolved questions raised by Einstein's theories. The second, *Cycles of Matter*, addresses the remaining SEU science.

The three tantalizing questions *Beyond Einstein* attempts to answer are as follows.

- What powered the big bang?
- What happens at the edge of a black hole?
- What is dark energy?

The road map proposes three inter-linked elements that work together.
Einstein Great Observatories providing breakthrough increases in capabilities to address all *Beyond Einstein* science:
-LISA: Gravitational waves from merging black holes and the early Universe
-Constellation-X: Spectroscopy close to the event horizon of black holes and place constraints on dark side of the Universe
Einstein Probes to address focused science objectives:
-Determine the nature of the Dark Energy
-Search for the signature of inflation in the microwave background
-Take a census of Black Holes of all sizes in the local Universe
A technology program, theoretical studies and an education program to inspire future generations of scientists and engineers towards the vision:
-Directly detect the gravitational waves emitted during the Big Bang
-Image and resolve the event horizon of a Black Hole

Explorer and Discovery Programs

The objective of the Explorer and Discovery programs is to provide frequent flight opportunities for world-class scientific investigations from space utilizing innovative, streamlined, and efficient management approaches within ASO, SEU and SEC space science themes for Explorer and SSE and "search for planets" component of ASO for Discovery. The programs seeks to enhance public awareness of, and appreciation for, space science and to incorporate educational and public outreach activities as integral parts of space science investigations.

The Explorer Program provides several classes of projects:
• *Medium-class Explorers (MIDEX)* - are investigations characterized by definition, development, launch service, and mission operations and data analysis costs not to exceed $180 million (FY02 $) total cost to NASA.
• *Small Explorers (SMEX)* - are investigations characterized by definition, development, launch service, and mission operations and data analysis not to exceed $120 million (FY03 $) total cost to NASA.
• *University-class Explorers (UNEX)* - are investigations characterized by definition, development, launch service, and mission operations and data analysis costs not to exceed $15.0M (FY00) total cost to NASA. (Currently on hold).
• *Missions of Opportunity (MO)* - are investigations characterized by being part of a non-NASA space mission of any size and having a total cost to NASA under $35 million (FY03). They are conducted on a no-exchange-of-funds basis with the organization sponsoring the mission. NASA solicits proposals for Missions of Opportunity with each Announcement of Opportunity (AO) issued for UNEX, SMEX, and MIDEX investigations.

The cost cap for Discovery missions is $299 million (FY01 $), with an MO option as above.

Technology Development Opportunities

Several technology development opportunities exist for investigators working in U.S. institutions. Collaboration with non-U.S. investigators is permitted on a no exchange of funds basis. The following is a sample of existing technology development programs within OSS.

Focused Technology Programs
-The primary source of advanced space observatory technology
Space Science Research and Analysis Technology Programs
-Appropriate technology source for Explorers and PI class instruments
-Limited effectiveness in supporting strategic technology needs of ASO/SEU
Partnerships With Other Agencies, e.g.
-Advanced Mirror System Demonstrator (AMSD) Partnership
-Advanced Hybrid Mirror Demonstrator (AHM) with X-Sat
Small Business Innovation Research(SBIR)/Small Business Technology Transfer (STTR)
-Continues to be a viable source of niche technologies (Cryogenic high precision deformable mirrors, for example)
Aerospace Technology(AT) Programs
-Restructuring of AT programs looks promising for Science driven technology
New Millennium Program(NMP)
- has yet to fly an astrophysics focused validation mission
-ST7/DRS will be first

Research Opportunities for Space Science (ROSS)

Scientists working in U.S. institutions have the opportunity to perform basic research to support the goals of OSS by submitting proposals in response to the ROSS solicitation. All proposals undergo a competitive peer review process before being selected for funding. The Astronomy and Physics component of ROSS can be summarized as follows.

Astronomy & Physics Research and Analysis
- Suborbital (sounding rocket and balloon payloads)
- Supporting Technology
- Laboratory Astrophysics
- Fundamental Physics
- Ground Based Astronomy (U.S. Government funded institutions only)

Astrophysics Theory Program
Long Term Space Astrophysics
Astrophysics Data Program
Origins of Planetary Systems(partially)
Astrobiology Instrument Development (partially)

NASA's Astrophysics Data Archives and Data Services

Archives:
-HEASARC (High Energy Astrophysics) at GSFC – holdings for RXTE, HETE, Chandra, etc.
-MAST (Multi-mission UV/Optical) at STScI – holdings are HST, GALEX, FUSE, etc.
-IRSA (Infra-red, submm) at Caltech – holdings are 2MASS, ISO, IRAS, soon SIRTF, etc.
-LAMBDA (Cosmic Microwave Background) at GSFC – holdings for WMAP, COBE, etc.
-MSC (Michelson Science – interferometry) at Caltech – holdings are for Keck interferometry data, etc.
Data services: **-ADS** (astrophysical Data Service) at SAO – holdings of scans of all journals and a great deal of astronomical literature.
-NED (NASA Extra-galactic Database) at Caltech – holdings of cross-correlated extra-galactic data in all wavelengths.

Acknowledgments. The contents of this paper are taken from a variety of NASA publications given in the reference section.

References

NASA's Vision http://www.gsfc.nasa.gov/nasavision/02_066.htm
NASA's Office of Space Science http://spacescience.nasa.gov/
Origins Road map http://origins.jpl.nasa.gov/library/roadmap03/
SEU Roadmap http://universe.nasa.gov/be/roadmap.html
Explorer Program http://explorers.gsfc.nasa.gov/
Discovery Program http://explorers.gsfc.nasa.gov/
OSS Research Opportunities http://research.hq.nasa.gov/code_s/code_s.cfm
Astronomy and Astrophysics Data Archives http://nssdc.gsfc.nasa.gov/astro/

Highlights of Astronomy, Vol. 13
International Astronomical Union, 2003
O. Engvold, ed.

Distinguishing Models for ACIS Data of Diffuse Emission

D.A. Leahy

University of Calgary, Alberta T2N 1N4, Canada

Abstract. Discussed here is the issue of discriminating different spectral models for diffuse emission observations with the Chandra ACIS. First background models are considered. Then standard source models such as non-ionization equilibrium and ionization equilibrium models and models with different metal abundances are considered. The datasets used are from Chandra ACIS observations of diffuse emission, in particular of the Cygnus Loop supernova remnant.

1. Introduction

Here the issue of modeling of x-ray spectra of diffuse x-ray emission is studied. With the availability of data from new instruments like the Chandra ACIS, moderately good spectral resolution studies of diffuse emission can be carried out. Previous to Chandra and XMM, only low spectral resolution data of diffuse emission was available. Dispersed spectra of diffuse emission are not yet very useful, since the spatial extent of the diffuse emission severely compromises the spectral resolution.

In this study, diffuse emission from the Cygnus Loop taken with the Chandra ACIS is studied to determine what are the limitations of current data in determining the physical properties of the diffuse x-ray emitting gas. A bright region on the south- western limb is seen in ROSAT PSPC observations of the Cygnus Loop with a high hardness ratio filament directly adjacent to a low hardness ratio filament (Aschenbach & Leahy 1999). This region was observed with the Chandra ACIS, with a field that was able to cover both filaments using the ACIS CCDs I0, I1, I2, I3 as well as cover a background region outside the Cygnus Loop with CCDs S2 and S3. The background was analyzed, then the source region was divided into several sub-regions for modeling of the diffuse emission spectrum. The use of data from a relatively old supernova remnant limits the discussion to models of thermal emission from low temperature gas ($kT <\sim 1$keV).

2. Observations and data analysis

A 10 ks exposure of the southwest V region was obtained on 2000 May 21 with the Chandra ACIS. The field of view is roughly 17 arcmin by 25 arcmin, and included the data from the six ACIS CCDs I0, I1, I2, I3, S2 and S3. All data processing was carried out using the CIAO2.3 package. Fig. 1 (left) shows a

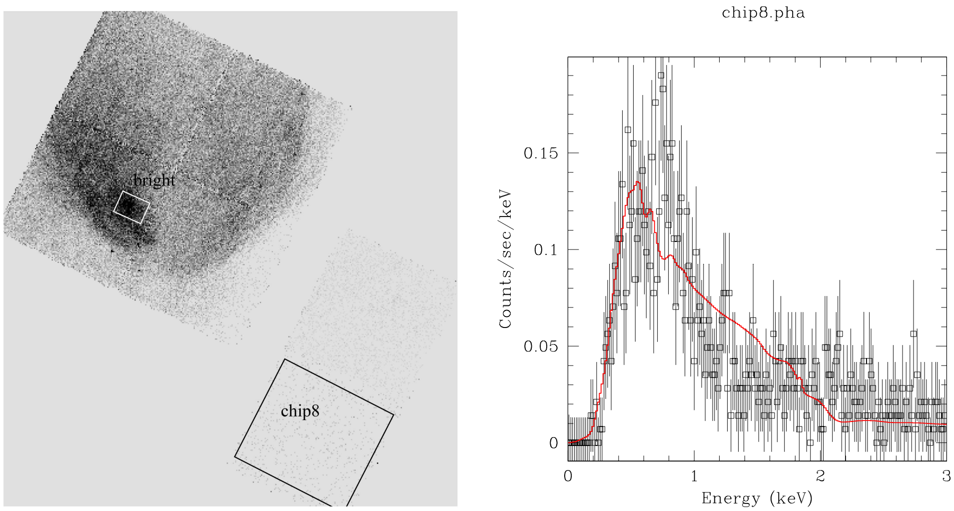

Figure 1. The Chandra ACIS image of the SW Cygnus Loop (left). The ACIS spectrum of the background region fit with the Gendreau et al. (1995) model (right).

processed image with north up. The image covers the energy band 0.3 to 1.4 keV and includes destreaking and exposure map corrections.

2.1. Background data analysis

A large region on ACIS S3 chip (as shown in Fig.1, left, labelled "chip8") was selected to yield the background spectrum. The background fitting was first carried out using pha channels 1-600 ($\sim 0-8.7$keV). Since the data for regions including Cygnus Loop emission did not show any excess above background above $\sim$ 2keV, the background fitting was redone to better match this energy range, i.e. over pha channels 1-210 ($\sim 0-3$keV). The results for the background modeling were not significantly different. The fitting was done by minimizing the Cash statistic, $C = -2 \times ln(likelihood)$).

The initial model for the background was based on the results of Gendreau et al. (1995). They modeled the x-ray background for ASCA data as a sum of two power laws, with spectral indices of 1.37 and 3.90 and a thermal plasma emission with temperature 0.16 keV. This best fit model (normalizations free) is shown in Fig. 1 (right) compared to the data: it is clearly not adequate, being systematically too low from 0.6 to 1 keV and systematically to high from 1 to 1.6 keV.

Next the mekal model(Kaastra 1992), was used to replace the xsraymond model for thermal plasma emission. To improve the systematics in the residuals it was necessary to free the power law index of the flat power law and the temperature. The result is shown in Fig. 2 (left). To improve the fit in the 0.5-0.8 keV range, the oxygen abundance was made a free parameter. This resulted in a significant improvement in the 0.5-0.8 keV residuals and gave zero amplitude to the steep power law with $\gamma = 3.9$. Thus the steep power law was removed from the model. The resulting parameters were $\gamma = 0.051$, kT=0.19 keV and O abundance=0.175$\times$ solar. This fit is shown in Fig. 2 (right). Freeing

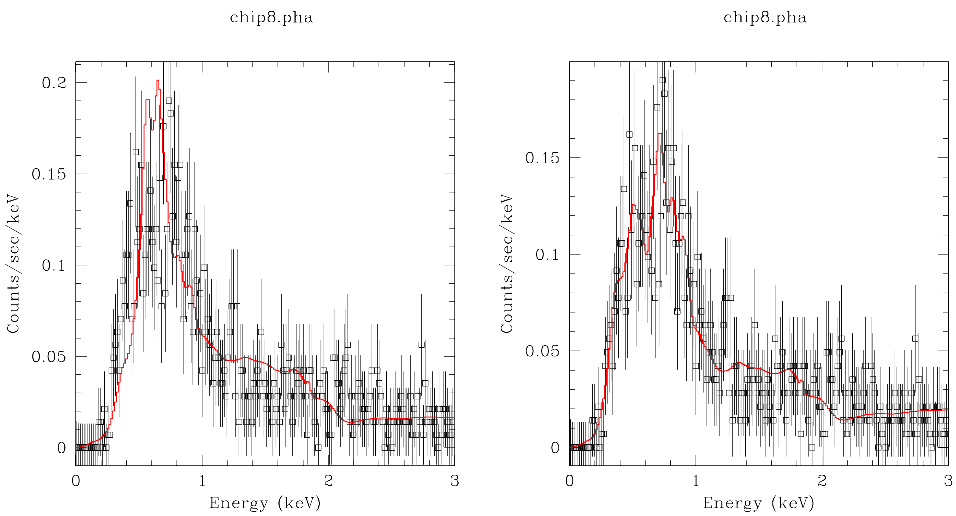

Figure 2. The ACIS spectrum of the background region fit with modified model (see text) (left). The ACIS spectrum of the background region fit with final background model (right).

abundances of other elements, including iron and neon, were tested but did not result in any significant improvement to the fit. Thus the final background model for the ACIS was determined.

2.2. Comparison of source models using ACIS spectra

The Cygnus Loop emission was spatially divided into a number of regions for spectral analysis. The brightest region (shown in Fig. 1 left) of those selected for spectral analysis was chosen as a test case for comparing source models. The best fit mekal model had kT=0.23 keV and normalization of $0.0038 \times 10^{-14}/(4\pi D^2) \int n_e n_H dV$. The fit is systematically bad 0.6-0.8 keV and around 0.9 keV. Freeing the oxygen abundance greatly improves the fit (by $\simeq 15\sigma$). Freeing the neon abundance further improves the fit (by $\simeq 7\sigma$). Freeing the iron abundance also improves the fit (by $\simeq 6\sigma$). However, freeing other element abundances individually does not further significantly improve the fit ($< 3\sigma$). Freeing the hydrogen column density gave an improvement of 3.6σ. Allowing non-equilibrium ionization did not further improve the fit.

3. Discussion

The availability of data from the different ACIS CCDs has allowed a diffuse background and a diffuse source data analysis to be carried out on the same dataset. An improved background model was derived, which has allowed a better modeling of the source data.

During the fitting process no binning of spectral channels was carried out. The fitting was done by minimizing the Cash statistic. However the χ^2 statistic was also computed for every fit. In several cases the improvement in the Cash statistic was significant but the improvement in χ^2 statistic was not. At the same time a significant improvement in the fit residuals could be seen by eye. The conclusion is that the Cash statistic is more powerful than χ^2 in distinguishing spectral fits.

The fits were carried out for a number of separate spatial regions. For the Cygnus Loop all of the spectral variation could be accounted for by variations in kT, N_H, and O, Ne and Fe abundances. None of the spectra required any non-equilibrium ionization. The ACIS data has proven sufficient to distinguish spectra of small regions in the Cygnus Loop, whereas earlier data of spatially resolved spectra, such as that from the ROSAT PSPC, could not.

Acknowledgments. This work supported by the Natural Sciences and Engineering Research Council of Canada.

References

Arnaud, K. A. 1996, in ASP Conf. Ser. 101, Astronomical Data Analysis Software and Systems V, ed. G. Jacoby & J. Barnes (San Francisco: ASP), 17

Aschenbach, B., Leahy, D., 1999, A&A, 341, 602

Gendreau, K., Mushotsky, R., Fabian, A. et al. 1995, PASJ, 47, L5

Kaastra, J. S. 1992, An X-Ray Spectral Code for Optically Thin Plasmas, (Internal SRON-Leiden Report, updated version 2.0)

Parker, R. A. R. 1967, ApJ, 149, 363

JD18

Quasar Cores & Jets

Chairpersons: D.L. Jauncey

Editors: D.L. Jauncey (Chief-Editor), K.I. Kellermann and J.V. Wall

Highlights of Astronomy, Vol. 13
International Astronomical Union, 2003
O. Engvold, ed.

X-ray and Optical Properties of Radio Jets

D.M. Worrall

Dept of Physics, University of Bristol, Tyndall Ave, Bristol BS8 1TL

Abstract. Over the last few years the high-quality imaging and spectroscopic data from *Chandra* and XMM-Newton have added greatly to our knowledge of the physics of radio jets. Supported by optical data, we are now able to understand much about jet energetics. Here I review the current state of knowledge.

1. Introduction

Chandra, XMM-Newton and HST have revitalized the study of active-galaxy radio jets. Studies using only radio data reach a natural limitation. The emission is known to be of synchrotron origin, and thus an inseparable function of the magnetic-field and electron energy densities. To progress further, the usual assumption has been that a source is "in equipartition", with these two energy densities equal, which is roughly equivalent to the source radiating at minimum energy. But this assumption was largely untested.

The electron population producing radio synchrotron emission must also lose energy by scattering ambient photons to higher energies via the inverse Compton process. If this process dominates the production of the higher-energy radiation that is measured, the electron population is probed directly. Both the electron energy density and magnetic field strength can then be estimated, and the equipartition assumption can be tested. The ambient photons may be the radio synchrotron emission itself (synchrotron self-Compton), the cosmic microwave background (CMB) radiation, or photons from the nucleus of the active galaxy.

Inverse Compton scattering is not the only mechanism which may produce radiation at energies above the radio. An electron spectrum that extends to sufficiently high energy will produce high-energy synchrotron radiation. The highest-energy electrons have correspondingly fast energy losses, and *in situ* particle acceleration may be required to ensure their supply.

Thus, once the emission mechanism of the X-ray and optical radiation is unraveled, the underlying physical processes provide insights not readily available from measuring the radio synchrotron emission alone.

X-ray detection has a further important role in probing the physics of active-galaxy radio jets, since the medium through which jets propagate is X-ray emitting. The new X-ray data provide unprecedented information on the hydrodynamical interactions between the jet and gaseous medium. This can help us understand jet content and models for jet propagation.

The high spatial resolution of *Chandra* has been key to the study of X-ray jets, and the large throughput of XMM-Newton has assisted studies of the X-ray-emitting environments. While historically the search for optical jet emission has been carried out using ground-based telescopes, a major problem has often been one of low contrast with light from the host galaxy. HST's sharp focus helps to overcome this difficulty, and it is playing a particularly important role in polarization studies.

2. Resolved X-ray Jets

For high-power radio sources, if we discount hot-spot emission, which is thought to arise from sub-relativistic flows at jet termination (but see Georganopoulos & Kazanas 2003), resolved X-ray jets are detected with *Chandra* mostly in quasars (e.g., Schwartz et al. 2000; Marshall et al. 2001; Sambruna et al. 2001, 2002; Siemiginowska et al. 2002, 2003), with the bright radio sources Pictor A and Cygnus A (Wilson et al. 2001a,b) being the galaxy exceptions. The quasar X-ray jet emission is one-sided, always on the same side as the brighter radio jet, implying that relativistic beaming is important. Two-sided X-ray emission, such as that in the quasar 3C 9 (Fabian et al. 2003) most likely does not imply the presence of counter-jet emission, but rather the more isotropic lobe, hot-spot, or cluster-related emission expected at some level in all sources and detected in many (e.g., Worrall et al. 2001b; Hardcastle et al. 2002a). Tests, using lobe and hot-spot X-ray inverse Compton emission, have generally found magnetic field strengths within a factor of a few of their equipartition (minimum energy) values (e.g., Brunetti et al. 2002; Hardcastle et al. 2002).

Currently there are at least 24 quasar X-ray jet detections. They have mostly been found through targeted programs to observe bright, prominent, one-sided radio jets. In most cases there has been no pre-existing reported optical jet detection, but there has been reasonable success in subsequent detection. The level of many detections lies below an interpolation between the radio and X-ray spectra, and so the optical flux densities are key in showing that the X-rays do not arise from synchrotron emission of a single power-law distribution of electrons (e.g., Schwartz et al. 2000; Sambruna et al. 2002). In order to avoid the total energy in particles and magnetic field being orders of magnitude above its minimum value, as would arise from a simple synchrotron self-Compton explanation, the most widely favored model is that the X-rays are produced by inverse Compton scattering of CMB photons by the electrons in a fast jet that sees boosted CMB radiation and emits beamed X-rays in the observer's frame (Tavecchio et al. 2000a; Celotti et al. 2001). The model can produce sufficient X-rays with the jet in equipartition, but only if the bulk motion is highly relativistic (bulk Lorentz factor, $\Gamma \approx 5-20$) and the jet at small angle to the line of sight. Although such a speed and angle are supported on the small scale by VLBI measurements, at least for the source which has guided this work, PKS 0637-752 (Lovell et al. 2000; Schwartz et al. 2000), the jet must remain highly relativistic hundreds of kpcs from the core (after projection is taken into account) for the X-rays to be produced by this mechanism. This conclusion, based on multi-wavelength data, has been something of a surprise, since earlier statistical studies of the structures of powerful radio sources suggested that jet velocities average only about $0.7c$ at distances of tens of kpc from the core (Wardle & Aaron 1997; Hardcastle et al. 1999).

Whether high-power jets are electron-positron, or have a significant proton content, is still somewhat unclear. For example, Tavecchio et al. (2000b) argue, based on near-equipartition models applied to the emission from quasar sub-pc-scale inner jets, that a significant proton contribution may be required to boost the kinetic power sufficiently to match the total radiated power. In contrast, Hardcastle et al. (2002a) find cases where the radio lobes would be over-pressured with respect to the ambient X-ray-emitting medium if a proton contribution were included.

Resolved X-ray jets in active galaxies with *low* radio power are detected with *Chandra* in sources covering the whole range of orientation suggested by unified schemes, suggesting that beaming is less important than in their more powerful counterparts. The more than 18 detected sources range from beamed jets in BL Lac objects (Pesce et al. 2001; Birkinshaw et al. 2002) to two-sided jets in radio galaxies (Chiaberge et al. 2003; Hardcastle et al. 2003), with most X-ray jets corresponding to the brighter radio jet (e.g., Hardcastle et al. 2001, 2002b; Harris et al. 2002a,b; Marshall et al. 2002; Worrall et al. 2001a, 2003). Several of the observations have been targeted at sources already known to have optical jets, from ground-based work or HST. However, it's easier to detect X-ray jets in *Chandra* observations than to detect optical jets in HST snapshot surveys (Worrall et al. 2001a), because there is generally better contrast with galaxy emission in the X-ray band than in the optical.

Inverse Compton models for any reasonable photon field suggest an uncomfortably large departure from a minimum-energy magnetic field in most low-power X-ray jets (e.g., Hardcastle et al. 2001). Synchrotron emission from a single electron population, usually with a broken power law, is the model of choice to fit both the radio, optical, and X-ray flux densities and the relatively steep X-ray spectra (e.g., Böhringer et al. 2001; Hardcastle et al. 2001). X-ray synchrotron emission requires TeV-energy electrons which lose energy so fast that they must be accelerated *in situ*.

It has been known for some time that the minimum pressure in low-power jets (calculated assuming an electron-positron plasma) is typically below that of the external X-ray-emitting medium (e.g., Morganti et al. 1988; Killeen et al. 1988; Feretti et al. 1995; Worrall & Birkinshaw 2000). However, this cannot be used simply to infer that the jets are launched as an electron-proton plasma to give them the extra required pressure component. Low-power jets are believed to slow down to sub-relativistic speeds within kpc distances, via significant entrainment of thermal material (e.g., Bicknell 1994), and even the most detailed hydrodynamical modeling, such as that which has been applied to 3C 31 by Laing & Bridle (2002), does not decide the issue of primary jet content.

3. Centaurus A and Particle Acceleration

The above arguments, applied to the bright northeast jet of the nearest radio galaxy, Centaurus A, find in favor of X-ray synchrotron emission (e.g., Kraft et al. 2002), and the proximity of Cen A allows us to probe its acceleration sites in the greatest possible detail. Unfortunately the dramatic dust lane spanning the galaxy masks any optical jet emission. The source is the subject of a detailed, continuing, X-ray and radio study using *Chandra*, XMM-Newton, the VLA, and the ATCA, and here I report some of the results from Hardcastle et al. (2003).

Looking first at the radio measurements, when we compare our new VLA map with archival data from 1991, we find proper motion of order 0.5c in some knots. Given that the proper motion is also apparent in the diffuse emission, we conclude that it is bulk motion rather than a pattern speed. If the jet is at about 50 degrees to the line of sight, as parsec-scale properties and other considerations suggest is reasonable, then the sub-luminal proper motion means that the strong jet-counterjet asymmetry seen on kpc scales is intrinsic and not due to beaming.

In the X-ray, we see both diffuse jet emission and much resolved structure, including substructure in some knots. Some bright X-ray knots have only weak radio emission with no indication of proper motion, but with the radio emission brightening down the jet in the direction away from the nucleus. While the radio association confirms that these X-ray knots are indeed jet related, the emission profiles are not what are expected from a simple toy model where the electrons are accelerated and then advect down the jet, with the X-ray emitting electrons losing energy faster than the radio-emitting electrons. Instead, we propose a model where there are obstacles in the jet (gas clouds or high-mass-loss stars). Both radio and X-ray-emitting electrons are accelerated in the standing shock of this obstacle, and a wake downstream causes further acceleration of the low-energy, radio-emitting, electrons. The resulting radio-X-ray offsets, averaged over several knots, could give the radio-X-ray offsets seen in more distant jets (e.g., Hardcastle et al. 2001).

What observations might help us to learn more about the acceleration processes in low-power jets? Optical polarization is one way. In M 87, Perlman et al. (1999) found evidence for strong shock acceleration at the base of bright emitting regions, in compressed transverse magnetic fields. Perlman is now leading an HST program to extend these polarization studies to other low-power radio galaxies. Variability is also an important probe of energy losses, and we are monitoring the resolved jet of Cen A in the X-ray and radio. A knot in the jet of M 87 has been observed to vary in the X-ray and optical on the time-scale of months, consistent with shock acceleration, expansion, and energy losses (Harris et al. 2003; Perlman et al. 2003).

4. Jet interactions with the X-ray-emitting medium

Most results on the interaction between jets and the X-ray-emitting medium obtained so far are for low-power sources. For example, Laing & Bridle (2003) have extended the modeling of Bicknell (1994) and use radio-jet sidedness to deduce a velocity model for twin radio jets. This model predicts the mass entrainment needed for their deceleration, and thus a density and pressure model in the ambient medium. They have applied this to 3C 31, and find that *Chandra* observations of the galaxy atmosphere (Hardcastle et al. 2002b) give an excellent match to the predicted pressure profile.

There is much current interest in the possibility of radio sources heating the interstellar and inter-cluster medium. Such heating would help to explain the weakness or absence of lines from gas cooling below 1 keV in the densest central regions of the atmospheres, as seen in reflection-grating observations with XMM-Newton (e.g., Peterson et al. 2001). The first definitive evidence for heating by a supersonically-expanding lobe is found in the inner regions of Cen A, where a rim of gas that is significantly hotter than the surrounding medium is found to cap the inner southwest radio lobe (Kraft et al. 2003). From the density and temperature measurements, we infer that gas is heated as it crosses the bow shock in front of the lobe, and then adiabatically cools from about $kT = 6.8$ keV to the $kT = 3$ keV shell that is seen. The kinetic energy in the shell exceeds the thermal energy in the nearby ambient interstellar medium, so that when the shell dissipates it will have a major effect on the interstellar medium and provide distributed heating.

There have been several reported examples where radio-emitting plasma appears to be shoving away X-ray-emitting gas, most notably Perseus A (Böhringer et al. 1993) and Hydra A (McNamara et al. 2000). 3C 66B is an interesting new example in which we see direct evidence of associated heating, as measured with XMM-Newton (Croston et al. 2003). Firstly, the group X-ray gas is hotter than expected based on a temperature-luminosity relationship for similar groups void of radio sources. Secondly, there is a region of gas which appears to have been compressed by the eastern radio lobe, and which is measurably hotter than the overall atmosphere.

5. Conclusions

The new results on radio jets which have resulted from complementary X-ray and optical observations have brought some surprises. Firstly, synchrotron X-ray jets are common in low-power sources, which implies that the intrinsic electron spectrum continues to TeV energies, and requires substantial *in situ* particle acceleration. Secondly, the detection of so many quasar X-ray jets, interpreted as due to beamed CMB photons, means that highly relativistic bulk flows exist far from the cores. This was not expected based on earlier statistical studies of radio sources. Jet theory has had some pleasing successes, such as the agreement of the X-ray pressure profile with the prediction from a hydrodynamical model for 3C 31.

There is still much observational work to be done. Firstly, there is considerable bias in the jets which have been observed in the X-ray, and we need observations of unbiased samples over broader luminosity and redshift ranges. Secondly, we need more deep X-ray observations (and refined theory) to understand jet-lobe/inter-cluster medium interactions. Finally, to study acceleration sites and processes, more detailed knot mapping and temporal monitoring is required. In combination with multi-frequency polarization measurements, such data could map the spatial distributions and follow the acceleration of the electrons responsible for the radiation in the radio to X-ray bands.

References

Bicknell, G.V. 1994, ApJ, 422, 542
Birkinshaw, M., Worrall, D.M., & Hardcastle, M.J. 2002, MNRAS, 335, 142

Böhringer, H., Voges, W., Fabian, A.C., Edge, A.C., & Neumann, D.M. 1993, MNRAS, 264, L25

Böhringer, H. et al. 2001, A&A, 365, L181

Brunetti, G., Bondi, M., Comastri, A., Setti, G. 2002, A&A, 381, 795

Celotti, A., Ghisellini, G., & Chiaberge, M. 2001, MNRAS, 321, L1

Chiaberge, M., Gilli, R., Macchetto, F.D., Sparks, W.B., & Capetti, A. 2003, ApJ, 582, 645

Croston, J.H., Hardcastle, M.J., Birkinshaw, M., & Worrall, D.M. 2003, MNRAS, in press

Fabian, A.C., Celotti, A., & Johnstone, R.M. 2003, MNRAS, 338, L7 reference Feretti, L., Fanti, R., Parma, P., Massaglia, S., Trussoni, E., & Brinkmann, W. 1995, A&A, 298, 699

Georganopoulos, M., & Kazanas, D. 2003, ApJ, 589, L5

Hardcastle, M.J., Alexander, P., Pooley, G.G., & Riley, J.M. 1999, MNRAS, 304, 135

Hardcastle, M.J., Birkinshaw, M., & Worrall, D.M. 2001, MNRAS, 326, 1499

Hardcastle, M.J., Birkinshaw, M., Cameron, R.A., Harris, D.E., Looney, L.W., & Worrall, D.M. 2002a, ApJ, 581, 948

Hardcastle, M.J., Worrall, D.M., Birkinshaw, M., Laing, R.A., & Bridle, A.H. 2002b, MNRAS, 334, 182

Hardcastle, M.J., Worrall, D.M., Kraft, R.P., Forman, W.R., Jones, C., & Murray, S.S. 2003, ApJ, 593, 169

Harris, D.E., Krawczynski, H., & Taylor, G.B. 2002a, ApJ, 578, 60

Harris, D.E., Finoguenov, A., Bridle, A.H., Hardcastle, M.J., & Laing, R.A. 2002b, ApJ, 580, 110

Harris, D.E., Biretta, J.A., Junor, W., Perlman, E.S., Sparks, W.B., & Wilson, A.S. 2003, ApJ, 586, L41

Killeen, N.E.B., Bicknell, G.V., & Ekers, R.D. 1988, ApJ, 325, 180

Kraft, R.P., Forman, W.R., Jones, C., Murray, S.S., Hardcastle, M.J., & Worrall, D.M. 2002, ApJ, 569, 54

Kraft, R.P., Vázquez, S.E., Forman, W.R., Jones, C., Murray, S.S., Hardcastle, M.J., Worrall, D.M., & Churazov, E. 2003, ApJ, 592, 129

Laing, R.A., & Bridle, A.H. 2002, MNRAS, 336, 1161

Lovell, J.E.J. et al. 2000, in Astrophysical Phenomena Revealed by Space VLBI, ed. H. Hirabayashi, P.G. Edwards & D.W. Murphy (Japan: ISAS), 215

Marshall, H.L. et al. 2001, ApJ, 549, L167

Marshall, H.L., Miller, B.P., Davis, D.S., Perlman, E.S., Wise, M., Canizares, C.R., & Harris, D.E. 2002, ApJ, 564, 683

McNamara, B.R. et al. 2000, ApJ., 534, L135

Morganti, R., Fanti, R., Gioia, I.M., Harris, D.E., Parma, P., & de Ruiter, H. 1988, A&A, 189, 11

Perlman, E.S., Biretta, J.A., Zhou, F., Sparks, W.B., & Macchetto, F.D. 1999, AJ, 117, 2185

Perlman, E.S., Harris, D.E., Biretta, J.A., Sparks, W.B., & Macchetto, F.D. 2003, ApJ, in press

Pesce, J.E., Sambruna, R.M., Tavecchio, F., Maraschi, L., Cheung, C.C., Urry, C.M., Scarpa, R. 2001, ApJ, 556, L79

Peterson, J.R. et al. 2001, A&A, 365, L104

Sambruna, R.M., Urry, C.M., Tavecchio, F., Maraschi, L., Scarpa, R., Chartas, G., & Muxlow, T. 2001, ApJ, 549, L161

Sambruna, R.M., Maraschi, L., Tavecchio, F., Urry, C.M., Cheung, C.C., Chartas, G., Scarpa, R., & Gambill, J.K. 2002, ApJ, 571, 206

Schwartz, D.A. et al. 2000, ApJ, 540, L69

Siemiginowska, A., Bechtold, J., Aldcroft, T.L., Elvis, M., Harris, D.E., & Dobrzycki, A. 2002, ApJ, 570, 543

Siemiginowska et al. 2003, ApJ, 595, 643

Tavecchio, F., Maraschi, L., Sambruna, R.M., & Urry, C.M. 2000a, ApJ, 544, L23

Tavecchio, F. et al. 2000b, ApJ, 543, 535

Wardle, J.F.C., & Aaron, S.E. 1997, MNRAS, 286, 425

Wilson, A.S., Young, A.J., & Shopbell, P.L. 2001a, ApJ, 547, 740

Wilson, A.S., Young, A.J., & Shopbell, P.L. 2001b, in ASP Conf. Ser. Vol. 250, Particles and Fields in Radio Galaxies, ed. R.A. Laing & K.M. Blundell (San Francisco: ASP), 213

Worrall, D.M., & Birkinshaw, M. 2000, ApJ, 530, 719

Worrall, D.M., Birkinshaw, M., & Hardcastle, M.J. 2001a, MNRAS, 326, L7

Worrall, D.M., Birkinshaw, M., Hardcastle, M.J., & Lawrence, C.R. 2001b, MNRAS, 326, 1127

Worrall, D.M., Birkinshaw, M., & Hardcastle, M.J. 2003, MNRAS, 343, 73

Highlights of Astronomy, Vol. 13
International Astronomical Union, 2003
O. Engvold, ed.

The Cosmic Evolution of Quasars

Carole Jackson

CSIRO Australia Telescope National Facility, PO Box 76, Epping, NSW 1710, Australia

Jasper Wall

Department of Physics & Astronomy, University of British Columbia, Vancouver, BC V6T 1Z1, Canada

Peter Shaver

European Southern Observatory, Karl-Schwarzschild-Str. 2, 85748 Garching bei München, Germany

Ken Kellermann

National Radio Astronomy Observatory, Edgemont Road, Charlottesville, VA 22903-2475, USA

Isobel Hook

Department of Physics, University of Oxford, Denys Wilkinson Building, Keble Road, Oxford OX1 3RH, UK

Abstract. The form of the quasar luminosity function and its redshift dependence to z$\sim$1 has long been established; powerful evolution is required so that by z=1 there is an increase of order 10^2 - 10^3 in the space density of the most luminous sources. However it is more difficult to deduce the form of the LF at high redshifts. In this contribution we discuss how a sample of relatively bright radio sources has been used to determine the high-redshift behavior of the radio-loud quasar luminosity function, and the particular advantages of using a radio-selected sample. Our results illustrate how radio-loud quasar samples can be an efficient probe of the high-redshift Universe.

1. Introduction

Historically, the study of the quasar luminosity function (LF) and its evolution over cosmic time has centered on large spectroscopic samples of optically-selected bright stellar objects from photographic plates. Since the ultraviolet-excess samples of the 1980s (Marshall et al. 1983, Green, Schmidt & Leibert 1986, Boyle et al. 1990) it has been known that luminous quasars have undergone strong cosmic evolution to z$\sim$2.2. The extension of the color-selection technique to six optical band passes with the large bright quasar survey yielded confirmation, first deduced by Schmidt & Green (1983), that the optical quasar LF declines in the range z = 3.5 – 4.5 (Warren, Hewett & Osmer 1994). However this decline could be induced by intervening dust absorption, rather than representing a real decline in the space density.

More recently the 2dF Quasar survey team (2Qz: Boyle et al. 2000) obtained spectra for an optically color-selected sample of more than 23,000 quasars. This huge sample yields a clear determination of the LF and its evolution between z$\sim$ 0.35 and 2.3 (Boyle et al. 2000). However, at low redshifts (z $<$ 0.35) and and at high luminosities, the quasar population is poorly sampled: low-redshift objects appear non-stellar and are rejected, whilst the high-luminosity objects have too low a space density to figure in the modest-area 2Qz survey.

The difficulty in determining the behavior of the quasar LF at redshifts between $\sim$2.3 and $\sim$4 is that quasars at these redshifts have the same colors as Galactic stars. Whilst the three-band color selection of 2Qz was highly efficient - with $\sim$50% of all targets found to be quasars - the extension of the 2Qz sample-selection technique to z $\sim$3.3 results in only 2% of the color-selected objects being quasars (Chiu et al., private communication).

To detect quasars at very high redshift, extremely red color selections can be used. From the Sloan Digital Sky Survey (SDSS, York et al. 2000, Stoughton et al. 2002), Fan et al. (2003) selected i-band drop-out objects with red z-band colors in order to find quasar candidates at z $>$ 5.7. To date Fan et al. have detected 3 quasars above z = 6.0, all with luminosities brighter than $M_{1450} = -26.8$. Their results confirm that there is apparently a much reduced space density of quasars between z = 5.7 to 7 compared to that at z = 2.2.

2. Radio-selected quasar samples

Optically-selected quasar samples trace clearly the evolution of the LF from z$\sim$0.4 to z$\sim$2. Assuming that radio-loud and radio-quiet quasars race the same phenomenon, at either side of this redshift range the subset of *radio-loud* quasars provides an efficient probe of the LF. In particular, the radio-quasar LF spans a very wide range in luminosity – over more than six magnitudes, compared to two in the optical passband – allowing straight-forward selection of both local and distant quasar samples.

At the low-to-moderate power end of the LF large samples of radio galaxies and quasars can be extracted from optically-bright galaxy catalogues to reveal their absolute *local* space density. Condon, Cotton & Broderick (2002) determined the local radio LF for galaxies in both the Uppsala Galaxy Catalog (UGC: Nilson 1973) and the NRAO VLA Sky Survey (NVSS: Condon et al. 1998). Furthermore the 2dF Galaxy Redshift Survey (2dFGRS: Colless et al, 2001) and NVSS sample of radio galaxies and quasars have been used to map the radio LF between $0.05 < z < 0.3$ (Sadler et al. 2002). The results show the extent of the local evolution in a redshift range poorly represented in optically-selected quasar samples.

At the other end of the radio LF, high-power radio quasars provide an efficient probe of the very distant Universe. Compared to the optical passband, the radio regime is un-obscured and there are no 'color' degeneracies by which bright radio-loud quasars might overlap radio properties with other known cosmic objects. In the flux-density range 100 mJy to 10 Jy and at survey frequencies of between 1 and 5 GHz almost all radio sources are radio-loud galaxies and quasars. This means that bright radio sources can be used to trace the LF of powerful radio quasars; as long as we optically-identify *all* sources in a radio-selected sample we can avoid any optical bias which might be due to intervening obscuration.

To this end we set out to obtain a completely-identified sample of radio-selected quasars, large enough to map directly their space density behavior and to decide whether the optically-selected quasar LF turnover is real or induced by dust obscuration. To ensure that our initial sample was dominated by quasars, we use the 'flat-spectrum' criterion – compact radio-loud quasars characteristically have flat, undulating or inverted spectra at GHz frequencies (Kellermann & Pauliny-Toth 1969, 1971) due to synchrotron self-absorption. The advantage of this class of source is the relative ease of determining the arcsecond radio position of the bright quasar core, and hence the ease of making a secure optical identification of the host object.

We selected our sample from the machine-readable version of the Parkes radio source catalogue (PKSCAT90: Wright & Otrupcek 1990). The catalogue contains radio and optical data for 8264 radio sources south of $+27^{\circ}$ and was compiled from a series of surveys at 2.7 GHz performed by John Bolton and colleagues between 1969 and 1979 (Bolton, Savage & Wright 1979 and references therein). PKSCAT90 also contains data from 5 GHz flux-density measurements, compiled within a few months of the original 2.7 GHz surveys. As described in detail in Jackson et al. (2002) we selected all flat-spectrum sources from PKSCAT90 with $\alpha_{2.7GHz}^{5GHz} > -0.4$, where $S \propto \nu^{\alpha}$, yielding an initial sample of 878 sources. Imaging and spectroscopy campaigns (Jackson et al. 2002; Hook et al. 2003) yielded a final sample of identifications. We found that 677/878 sources had stellar host objects (quasars and BL Lac objects). From this resulting set of quasars we selected a complete sub-sample to map the high-redshift LF.

3. Radio quasar cosmic evolution

In calculating the high redshift LF we had to allow for the fact that 'flat spectrum' radio sources in reality have curved radio spectra. This could have a large biasing effect, particularly if many sources have radio spectra which steepen at high frequencies. In our sample, a number of quasars are only marginally flat-spectrum between 2.7 GHz and 5 GHz, i.e. $-0.4 < \alpha < -0.3$. Using cataloged data at other radio frequencies we devised a methodology to predict the number of quasars expected at large redshifts based on the number seen at lower redshifts. The procedure accounts for the individual spectra of each quasar and maximizes the number of sources available to our analysis. We named this procedure, a variant of the $V_{\max}$ method, the 'single source survey' (*'sss'*, Wall et al., in preparation): each individual source is considered a 'complete survey' if it lies above the Parkes survey limit relevant to its area.

Our first *sss* analysis used only the PKS 2.7 GHz and 5 GHz survey data, and predicts 53.5 sources lying between $3 \leq z \leq 8$ if the space density found between z = 1 and 3 remained constant out to z = 8. We improved our analysis by tracing the spectral shape of each source using data from two lower-frequency surveys – Texas at 365 MHz (Douglas et al 1996) and the NVSS at 1.4 GHz (Condon et al. 1998). This modified the 'observable volume' for a number of sources up to their observed redshift. The adjustments work in both the positive and negative senses so that the overall result is only marginally amended to 54.0 sources at $3 \leq z \leq 8$. With some additional analysis based on higher-frequency radio data (Wall et al. in preparation) we concluded that our sample should have contained 40 to 50 quasars with redshifts 3 to 8, if the quasar space density between z = 1 and 3 remained constant to z = 8. In the redshift range 3 to 8 we actually found 16 quasars and we infer another 1.8 from the small (unbiased) set of candidate quasars with no spectroscopy. Given that the difference between the observed and predicted quasar number is significant at the $> 3\sigma$ level, we conclude that the space density of our radio-loud quasar sample shows a real diminution at $z > 3$. The similar high-redshift results from optically-selected samples thus are not induced by dust obscuration.

The LF results for our radio quasar sample are shown in Figures 1 and 2. The strong evolution in space density is clearly seen for the LFs of Figure 1 (left) computed in redshift bands from 0 to 2; Figure 1 (right) shows that this evolution has reached a plateau at $z = 2$, with the LFs for the ranges $2 < z < 3$ and $3 < z < 5$ lying successively lower.

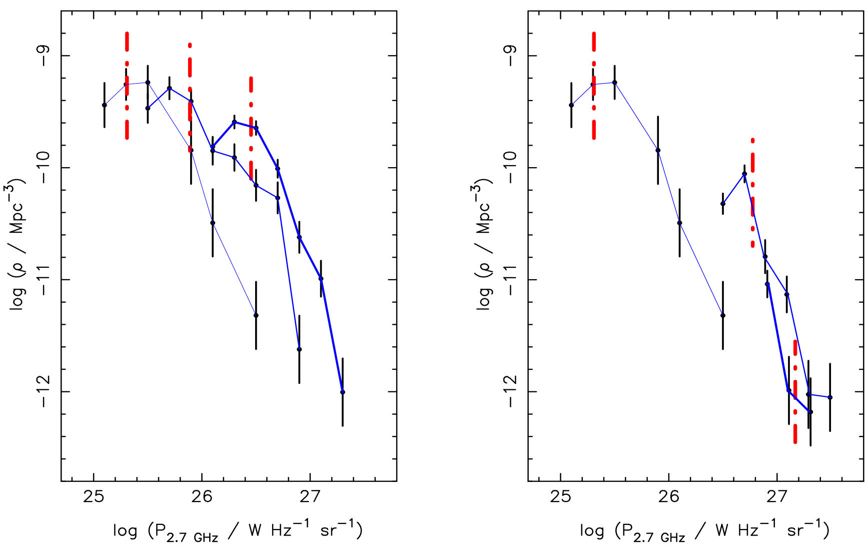

Figure 1. The radio luminosity function ($h_0 = 0.5$, $\Omega_m = 1$, $\Omega_\Lambda = 0$) for the quasars of the Parkes 0.25-Jy flat-spectrum sample, in log (number per Mpc^3 per $\Delta\log(P_{2.7\mathrm{GHz}}) = 0.2$ per Δz = 0.5). Left: computed in three redshift ranges, $0 - 0.5, 0.5 - 1.0$, and $1.0 - 2.0$; right: in redshift ranges $0 - 0.5$ (repeated from the left diagram), $2.0 - 3.0$ and $3.0 - 5.0$. Increasing line weight represents increasing redshift. Dash-dot vertical bars indicate lower limits of completeness for each redshift range, due to spectral-index spread.

The quasar LF as a function of redshift for different radio luminosities is shown in Figure 2. Numbers are small for each power range; but in general the space density is seen to decrease at redshifts greater than 2, mirroring the results from our *sss* analysis described above.

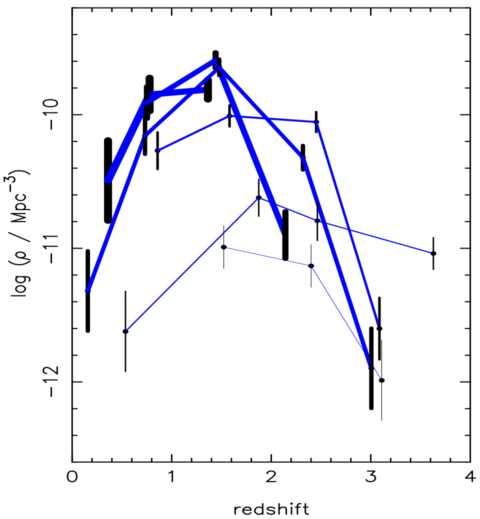

Figure 2. The space densities of Figure 1 shown as a function of redshift for 6 power ranges, log$P_{2.7} = 26.0$ to 26.2, $26.2 - 26.4$, $26.4 - 26.6$. $26.6 - 26.8$, $26.8 - 27.0$ and $27.0 - 27.2$, distinguished by decreasing line weight. Abscissa values are at the mean redshifts in each of the 5 redshift ranges in the caption to Figure 1.

4. Future quasar LF studies

Our radio-selected sample demonstrated the utility of bright radio samples to probe the high redshift quasar LF. The selection function ensured that most objects in our initial sample were quasars whose radio positions were readily measured to arcsec accuracy. Even though the quasars are radio-bright, a 4-m class telescope was required for the optical identifications and spectra.

The greatest lesson we learnt with this sample is the necessity for contemporary flux-density measurements. At GHz frequencies, a large fraction of quasars – perhaps 30% or more – are variable. It is vital to sample the population at one state, whether it is in the 'up', 'down' or 'intermediate'; and the problem is that surveys of objects obeying a steep power-law source count are dominated by objects in the 'up' state. Our use of survey data from one epoch and flux-density measurements from later epochs means that we do not have a clean sample of radio spectra from which to trace the high redshift LF. The range of our results, e.g. the prediction of 40 to 50 quasars at $3 < z < 8$, reflects the uncertainty in taking this bias into account (Wall et al. in preparation), and highlights the dangers in using different-epoch data for any study of quasar attributes. The bias may well explain the much lower significance ascribed to a redshift cutoff from a similar sample by Jarvis and Rawlings (2000).

Current and future multi-wavelength large-survey-area campaigns covering radio to X-ray pass bands (SWIRE, CDFs, ELIAS-S1, etc.) promise that much will be learnt about the quasar LF. Radio surveys and radio-selected quasar samples have a major role to play in these projects. In the course of these, to obtain single-epoch radio spectra we propose to exploit the wide field of view and multi-frequency agility of modern interferometers such as the Australia Telescope Compact Array.

The refined definition of the quasar LF will lay a foundation for understanding the physical nature of the evolution of these objects as well as the relation between radio-loud and radio-quiet quasars. More detailed knowledge of the internal quasar mechanism would provide important insights into the feedback loop with the IGM, particularly for studying the re-ionization epoch. Before this, we have to determine how best to recognize these rare objects at such epochs.

References

Bolton, J.G., Savage, A., Wright, A.E., 1979, AuJPA, 46, 1B

Boyle, B.J., Fong, R., Shanks, T., Peterson, B.A., 1990, MNRAS, 243, 1

Boyle, B.J. et al., 2000, MNRAS, 317, 1014

Colless, M.M. et al., 2002, MNRAS, 328, 1039

Condon, J.J., Cotton, W.D., Greisen, E.W., Yin, Q.F., Perley, R.A., Taylor, G.B, Broderick, J.J., 1998, AJ, 115, 1693

Condon, J.J., Cotton, W.D., Broderick, J.J., 2002, AJ, 124, 675

Douglas, J.N., Bash, F.N., Bozyan, F.A., Torrence, G.W., Wolfe, C., 1996, AJ, 111, 1945

Fan, X., et al., 2003, AJ, 125, 1649

Green, R.F., Schmidt, M., Leibert, J., 1986, ApJS, 61, 305

Hook, I.M., Shaver, P. A., Jackson, C.A., Wall, J.V., Kellermann, K.I., 2003, A&A, 399, 469

Jarvis, M.J. and Rawlings, S., 2000, MNRAS, 319, 121

Jackson, C. A., Wall, J. V., Shaver, P. A., Kellerman, K. I., Hook, I. M., and Hawkins, M. R. S., 2002, A&A, 386, 97

Kellermann, K.I., Pauliny-Toth, I.K.K., 1969, ApJ, 155, L71

Kellermann, K.I., Pauliny-Toth, I.K.K., 1971, ApJL, 8, 153

Marshall, H.L., Tananbaum, H., Avni, Y., Zamorani, G., 1983, ApJ, 269, 35

Nilson, P., 1973, Uppsala General Catalog of Galaxies (Uppsala: Uppsala Astron. Obs) (UGC)

Sadler, E.M. et al., 2002, MNRAS, 329, 2276

Schmidt, M., Green, R.F., 1983, ApJ, 269, 352

Stoughton, C. et al. 2002, AJ, 123, 485

Warren, S.J., Hewett, P.C., Osmer, P.S., 1994, ApJ, 421, 412

Wright, A.E., Otrupcek, R.E., 1990, Parkes Catalogue Australia Telescope National Facility, CSIRO

York, D. G. et al. 2000, AJ, 120, 1579

Highlights of Astronomy, Vol. 13
International Astronomical Union, 2003
O. Engvold, ed.

Central Regions of AGNs Probed by the Neutral Hydrogen

Raffaella Morganti

Netherlands Foundation for Research in Astronomy, Postbus 2, NL-7990 AA, Dwingeloo, NL

Abstract. The physical and kinematical conditions of the gas surrounding an active galactic nucleus (AGN) offer key diagnostics for understanding the processes occurring in the inner few kpc around the nucleus. Neutral hydrogen can give important insights on these regions. Apart from probing the presence of gas in relatively settled conditions (i.e. circumnuclear disks/tori) it can also trace the presence of extreme outflows. Some examples of these phenomena are briefly presented.

1. Introduction

The origin of activity in galaxies is often explained as triggered by merger and/or interaction processes. This idea is supported by morphological and kinematical evidence (e.g. Smith & Heckman 1989, Tadhunter et al. 1989, Baum et al. 1992). Torques and shocks during the merger can remove angular momentum from the gas in the merging galaxies and this provides injection of substantial amounts of gas/dust into the central nuclear regions (see e.g. Mihos & Hernquist 1996). It is, therefore, likely that in the initial phase of an AGN, this gas still surrounds (and possibly obscures) the central regions. AGN-driven outflows have powerful effects on this dense ISM. This feedback process could play an important part also in the evolution of the host galaxy as it may limit the growth of the super-massive black holes (BHs) and regulate the correlation between BH and bulge properties (see e.g. Silk & Rees 1998).

Part of the gas will end up settling into a circumnuclear disk/torus. The presence of tori is an essential ingredient for the unified schemes for active galactic nuclei. Although it has been generally assumed that the tori are composed of dusty molecular clouds, it is now clear that, under certain conditions, they can be partly formed by atomic hydrogen (Maloney et al. 1996). Nuclear (optical) disks - with size ranging from 0.1 and 1 kpc - are also detected in a large number of early-type galaxies (both radio-loud and radio-quiet). These disks (mainly detected by HST) can be seen either in ionized gas or through their strong dust absorption (van der Marel 2001, Capetti et al. 2000 and ref. therein).

All the above illustrates how important is the gas in the study of AGNs. As the gas is likely to be found in different phases (atomic, molecular and ionized), the study of all of these is crucial to obtain a complete view of the processes occurring. Neutral hydrogen is one of these components and in the nuclear regions of radio loud AGNs it has been very often detected in absorption against the stronger radio cores (see e.g. Heckman et al. 1983; van Gorkom et al. 1989;

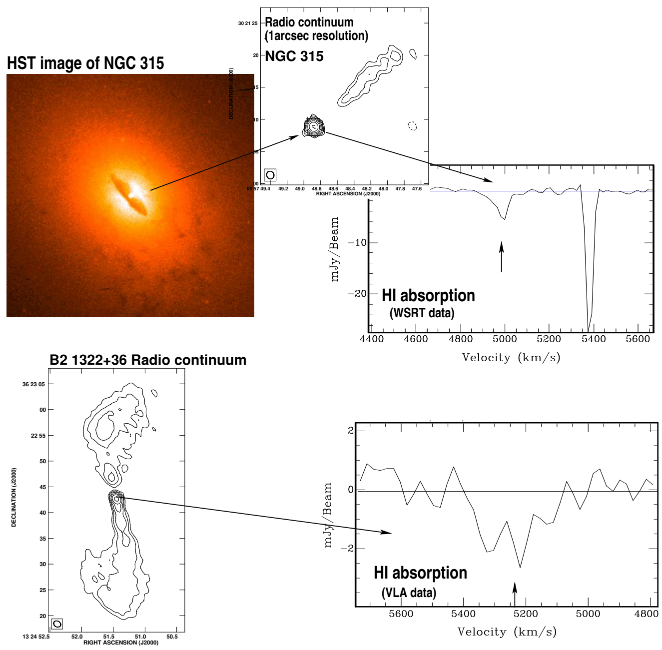

Figure 1. H I absorption detected with the WSRT and the VLA against the core of two radio galaxies: NGC 315 and B2 1322+36. The continuum images are also shown.

Morganti et al. 2001, 2002a; Vermeulen et al. 2003). From the detection of the H I we can study: *i)* the gas that is *settled* in circumnuclear disks/tori. As highlighted above, this is relevant in the context of the unified schemes for AGNs; *ii)* the *unsettled* gas that might represent the leftovers from the merger that triggered the activity. From its kinematics we can study whether it represents in-falling gas (e.g. feeding the AGN) or out-flowing gas (perhaps relevant for feedback effects). Here, I briefly discuss some of the most recent results in this area.

2. Settled gas

As described above, settled H I gas can be associated with circumnuclear disks and tori. In powerful (i.e. Fanaroff-Riley II) radio galaxies, evidence for H I associated with tori has been found, e.g., in the case of the Cygnus A. In this object, a 50 pc-scale, rotating, flattened structure has been found from the VLBI observations (Conway 1999). Due to the weakness of the radio core in these type of galaxies, this study can be done only in very few cases. More promising is the study of H I absorption in powerful compact (steep spectrum) radio sources. These sources are uniquely suited for investigations into the physics of the central engines, in particular to study the kinematics of the gas within 100 pc of the core (see e.g. Vermeulen et al. 2003). Evidence of H I associated with circumnuclear tori has been reported for some of these compact sources (see e.g. Conway 1997, Peck & Taylor 2001) with thickness of about 100 pc and column density of the order of 10^{23} cm^{-2} (with T_{spin} of several thousand K). The information derived from the H I can be particularly useful to constrain characteristics the central torus when combined with hard X-ray data. This has been done in the case of two possible Compton-thick galaxies studied by Risaliti et al. (2003).

In low luminosity radio galaxies the situation could be different. The high detection rate of optical cores, the lack of large absorption in X-ray (Chiaberge et al. 1999) and possibly also the relatively low detection rate of H I absorption (Morganti et al. 2001) suggest that the *standard pc-scale geometrically thick torus is not present* in these radio galaxies. The presence of *thin* disks has been claimed from H I observations in the case e.g. NGC 4261 (van Langevelde et al. 2000). For this object, the VLBI data suggest that the H I absorption is due to a disk of only ~1.3 pc thick projected against the counter-jet. In NGC 4261, evidence for the presence of such nuclear disk are also found in HST images. The idea of thin disks can be investigated in more detail by *correlating the presence (or absence) of H I absorption with the optical characteristics*. This has been done for a sample of radio galaxies (selected from Capetti et al. 2000) for which information about the presence of optical cores and nuclear dusty disks/lanes (from HST images) is available. Fig. 1 shows two examples of the detected objects. Interestingly, H I absorption was detected in the two galaxies that have dust disks/lanes and *no* optical cores. In these cases, the column density of the absorption is quite high ($> 10^{21}$ cm^{-2} for $T_{\rm spin} = 100$ K) and the derived optical extinction A_B (between 1 and 2 magnitudes) is such that it can, indeed, produce the obscuration of the optical cores. In the other two cases, H I absorption has been detected despite the presence of optical cores. However, the column density derived from the detected absorption is much lower ($\sim 10^{20}$ cm^{-2} for $T_{\rm spin} = 100$ K) and the derived extinction is of the order of only a fraction of a magnitude. This is, therefore, consistent with what expected if the circumnuclear disk are thin in these radio galaxies.

3. Unsettled gas

3.1. Any evidence for infall?

Evidence for in-falling gas was reported by van Gorkom et al. (1989). In a sample of radio galaxies, H I absorption was detected either close to the systemic velocity or systematically red-shifted, indicating therefore a prevalence of gas falling into the nucleus. This result does not appear to be confirmed by more recent observations. For example, the study of H I absorption in compact radio sources by Vermeulen et al. (2003) shows that there is evidence for significant gas motions and not only positive but even more negative H I velocities (up to more than 1000 km s^{-1} compared to the systemic velocity) are found. This is indicating that gas flowing out of the galaxy is also present. Indeed, clear cases of fast gas outflows have now been detected as described below.

One of the most promising case of in-falling gas was found in the radio galaxy NGC 315. A very narrow and highly red-shifted ($\sim$ 500 km s^{-1}) H I absorption (see also Fig. 1) was reported by Heckman et al. (1983) and Dressel et al. (1983). VLBI observations (Peck 1999, Morganti et al. 2002) are now

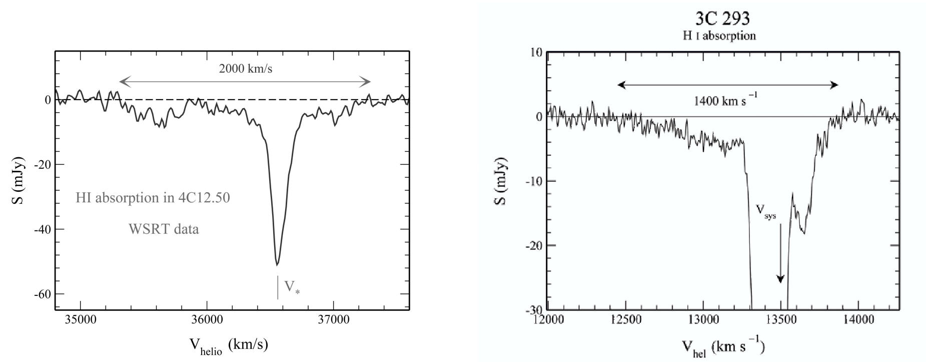

Figure 2. The H I absorption profile detected in 4C 12.50 (left) and 3C 293 (right) from the WSRT observations. The spectra are plotted in flux (mJy) against optical heliocentric velocity in $\mathrm{km\,s^{-1}}$.

showing that this absorption appears to cover a region of about 9 pc of the source, from the core to the first part of the jet. A likely explanation for this absorption is that of a cloud at large distance from the nucleus (like tidal debris) detected, in projection, against the nucleus (Morganti et al. 2002). This seems to be more favorable over the possibility of a small cloud falling into the nucleus and feeding the AGN.

3.2. Outflows

Fast nuclear outflows of ionized gas appear to be a relatively common phenomena in AGNs. It is, therefore, not too surprising to find such outflows also in radio galaxies (see Morganti et al. 2003a for a summary of recent results). However, it is extremely intriguing the discovery of a number of radio galaxies where the presence of fast outflows is associated not only with ionized but also with *neutral* gas. This finding gives new and important insights on the physical conditions of the gaseous medium around an AGN. The best examples so far are the radio galaxies 3C 293 (Morganti et al. 2003b) and 4C 12.50 and the Seyfert galaxy IC 5063 (Oosterloo et al. 2000). It is also worth noticing that outflows of ionized gas are also associated with these neutral outflows (see Morganti et al. 2003a). A number of possible hypotheses can be made about the origin of the gas outflow (e.g., star-burst winds, radiation pressure from the AGN adiabatically expanded broad emission line clouds) although at the moment the hypothesis that they are driven by the interaction of the radio jet with the ISM is favored. To investigate whether this is indeed correct, high-resolution (VLBI) studies are in progress to find the exact location of the out-flowing gas. So far these outflows have been found in objects that are either in the early-stage of their evolution (like 4C 12.50) or, perhaps, in a phase of re-started activity (as might be the case for 3C 293). Another characteristic of these galaxies is the presence of a young stellar population (from their optical spectra, see e.g. Tadhunter et al. 2002). Such a component (with ages between 0.5 and 2 Gyr) can be considered an indication that the galaxy is indeed in a *particular stage of its evolution*, when large amounts of gas/dust - likely from the merger that triggered the activity - are still present in the inner region and the radio jet is strongly interacting with it. A more systematic search for fast gas outflows in radio galaxies is now in progress (with the WSRT) and has already revealed more cases of broad, blue-shifted H I absorptions.

References

Baum S. et al. 1992, ApJ 389, 208

Capetti et al. 2000 A&A 362, 871

Chiaberge, M., Capetti, A., Celotti, A., 1999, A&A, 349, 77

Conway J.E. 1999 in *Highly redshifted radio lines*, Carilli C.L. et al. eds., ASP Conf. Series 156, 259

Conway J.E. 1997, in *2nd Workshop on GPS and CSS Radio Sources*, Snellen et al. M.N. Publ JIVE, Leiden p.198

Dressel et al. 1983, ApJL 266, L97

Heckman et al. 1983, AJ, 88, 583

Maloney P.R., Hollenbach D.J., Tielens A.G.G.M. 1996, ApJ 466, 561

Mihos J.C. & Hernquist L. 1996 ApJ, 464, 641

Morganti et al. 2003a, in *Recycling Intergalactic and Interstellar Matter*, IAU Symposium 217, eds. P.-A. Duc et al., in press (astro-ph/0310629)

Morganti R., Oosterloo T.A., Emonts B.H.C., van der Hulst J.M., Tadhunter C.N. 2003b, ApJLetter 593, L69

Morganti R. et al. 2002, *6th European VLBI Network Symposium*, Ros E. et al. (Eds.), MPIfR, Bonn, Germany p.171

Morganti R., 2002, in *Issues in Unification of Active Galactic Nuclei*, R. Maiolino et al. eds., ASP Conference Proceedings, Vol. 258 p.63 (astro-ph/0109056)

Morganti R. et al.2001, MNRAS 323, 331

Oosterloo T.A. et al. 2000, AJ 119, 2085

Peck A.B., Taylor G.B. 2001, ApJ 554, L147

Peck, A. B. 1999, *PhD Thesis*, New Mexico Inst. of Mining and Technology

Risaliti G., Woltjer L., Salvati M. 2003 A&A 401, 895

Silk J., Rees M.J. 1998, A&A 331, L1

Smith & Heckman 1989, ApJ 341, 658

Tadhunter C., Fosbury & Quinn P. 1989, MNRAS 240, 225

Tadhunter C.N. et al. 2002, MNRAS 330, 977

van Gorkom J.H. et al. 1989, AJ 97, 708

van Langevelde H.J., Pihlström Y.M., Conway J.E., Jaffe W., Schilizzi R.T. 2000, A&A 354, 45

van der Marel R. 2001, in *'Galaxies and their Constituents at the Highest Angular Resolutions'* IAU Symp. 205, Schilizzi R. et al. eds., ASP, p.154

Vermeulen et al. 2003, A&A 404, 861

Highlights of Astronomy, Vol. 13
International Astronomical Union, 2003
O. Engvold, ed.

Rapid Interstellar Scintillation of Quasar PKS 1257−326

Hayley E. Bignall

Joint Institute for VLBI in Europe, Radiosterrenwacht Dwingeloo, Postbus 2, 7990 AA Dwingeloo, The Netherlands

David L. Jauncey, James E. J. Lovell, Anastasios K. Tzioumis

CSIRO Australia Telescope National Facility, PO Box 76, Epping, NSW 1710, Australia

Jean-Pierre Macquart

Kapteyn Astronomical Institute, University of Groningen, Postbus 800, 9700 AV Groningen, The Netherlands

Lucyna Kedziora-Chudczer

Institute of Astronomy, School of Physics A28, University of Sydney, NSW 2006, Australia

Abstract. PKS 1257−326 is one of three quasars known to show unusually large and rapid, intra-hour intensity variations, as a result of scintillation in the turbulent Galactic interstellar medium. We have measured time delays in the variability pattern arrival times at the VLA and the ATCA, as well as an annual cycle in the time-scale of variability for this source. Results of the two-station time delay observations are presented here. Implications for the scintillation of this source are discussed in the light of these results, together with results from two years of monitoring with the ATCA.

1. Introduction

The flat-spectrum radio source PKS 1257−326 was first cataloged in the Sixth Part of the Parkes 2700 MHz Survey, with a measured flux density of 0.23 Jy at 2.7 GHz (Shimmins & Bolton 1974). The source is identified with an X-ray emitting, B=18.7 magnitude, quasar at $z = 1.256$ (Perlman et al. 1998). Extremely rapid flux density changes were discovered in ATCA data during 2000 (Bignall et al. 2003), making PKS 1257−326 the third known "intra-hour" radio variable, after PKS 0405−385 (Kedziora-Chudczer et al. 1997) and J1819+3845 (Dennett-Thorpe & de Bruyn 2000).

In recent years, considerable evidence has accumulated to demonstrate that interstellar scintillation (ISS) in the turbulent interstellar medium of our Galaxy is the principal mechanism responsible for the intra-day variability (IDV) seen at cm wavelengths in many flat-spectrum AGN. Two unequivocal demonstrators of ISS are (i) annual cycles in time scales of variability (e.g. Dennett-Thorpe & de Bruyn 2001; Rickett et al. 2001; Jauncey & Macquart 2001; Bignall et al. 2003), and (ii) measurement of a delay in the IDV pattern arrival times at two, widely separated telescopes (e.g. Jauncey et al. 2000; Dennett-Thorpe & de Bruyn 2002). Both of these types of observation can be used to extract information on the ISS process and on the source brightness distribution, on scales of order 10–100 microarcseconds (e.g. Macquart & Jauncey 2002). The three "extreme" rapid variables have played a key role in realizing the dominant role of ISS in radio IDV, because their variations can be well-sampled in a typical, 12-hour observing session. Furthermore, pattern arrival time delay measurements are only feasible when the variations are large and rapid enough that the IDV patterns can be located in time to a precision of tens of seconds, i.e. there must be a measurable change in flux density on time scales of order 1 minute.

Here we present results of simultaneous observations of PKS 1257−326 with the VLA and the ATCA, and discuss their implications for the ISS of this source, particularly when combined with the results of two years of ATCA monitoring.

2. Results of simultaneous observations with the VLA and the ATCA

The rapid, large-amplitude fluctuations observed in PKS 1257−326 make this source an excellent candidate for measurement of the variability pattern arrival time delay between two, widely separated telescopes. A significant delay of ~ 2 minutes was found for PKS 0405−385 (Jauncey et al. 2000), between the IDV patterns at the VLA and the ATCA, before its episode of rapid ISS ceased. J1819+3845 was observed simultaneously with the VLA and WSRT on two days in 2001 January, and the IDV pattern arrival time delay was observed to change, and in fact reverse its sign, due to the rotation of the Earth during the simultaneous observation (Dennett-Thorpe & de Bruyn 2002). In the case of J1819+3845, the VLA-WSRT baseline rotates in the plane of the sky through approximately 50° over the course of the observation, and hence a significant change in delay was observed, as the direction in which the baseline cut through the scintillation pattern changed.

PKS 1257−326 has been observed simultaneously with the ATCA and the VLA at three different times of the year. The observations in each period were made on two consecutive days, and used two frequencies simultaneously, 4.9 and 8.5 GHz. On each day, PKS 1257−326 is visible to both telescopes for 2.7 hours. The baseline vector rotates through only 20° during this time. However, the scintillation velocity changes over the course of a year due to the Earth's orbital motion, so the two-station time delay will be different at different times of the year. Repeated measurements of the time delay at different times of the year help to constrain both the velocity and spatial structure of the observed scintillation pattern, which in turn reveals information both on the source, and on turbulence in the local ISM.

The top panels in Figure 1 show VLA and ATCA data for PKS 1257−326 observed on 2002 May 14 and 2003 March 7. The frequency range covered by the data from each telescope is identical, and the 32 second decrement needed to convert the time stamps of the VLA data from IAT to UT has been applied. It is immediately apparent that on each day, the IDV patterns seen by each telescope are almost identical, and that in each case, the pattern arrives at the VLA several minutes before it reaches the ATCA. This is unequivocal evidence that

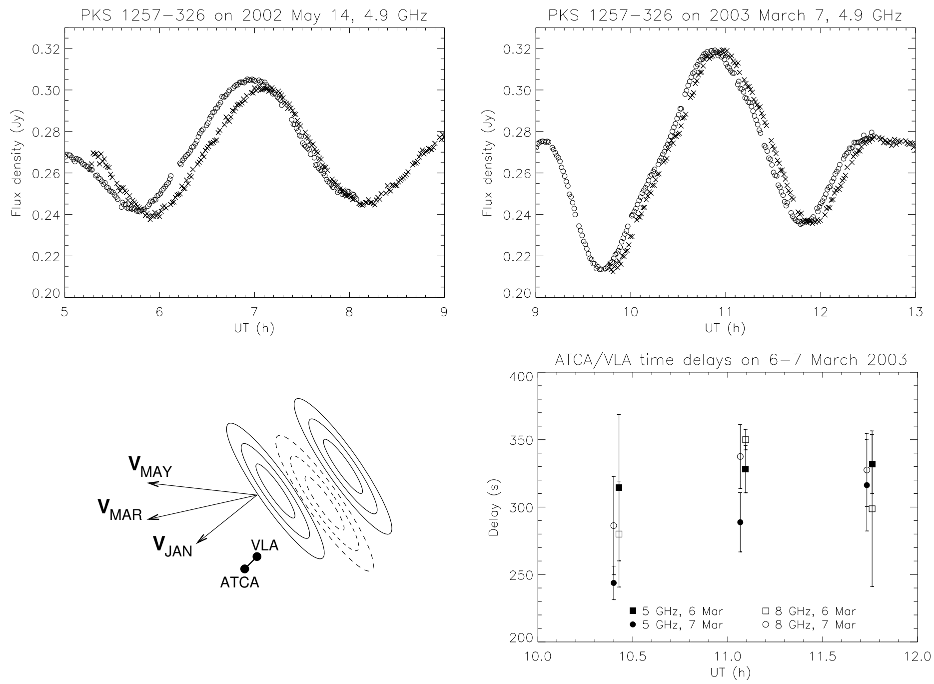

Figure 1. Top panels show simultaneous 4.9 GHz VLA and ATCA flux density measurements of PKS 1257−326, on two different days of the year. VLA data are represented by circles; ATCA data by crosses. The lower left panel shows an illustration (not to scale) of the time delay geometry. Part of the scintillation pattern is represented by elliptical contours. Arrows indicate scintillation velocity at three different times of the year when the source has been observed simultaneously with the VLA and the ATCA. The VLA-ATCA baseline is indicated. The lower right panel shows time delays calculated from the 2003 March data.

the observed rapid variations are predominantly due to interstellar scintillation. We can also immediately infer that the scintillation length scale is much larger than the $\sim 10,000$ km baseline between the two telescopes.

The time delays were clearly evident in the data after applying only a constant correction factor to data from one telescope in order to make the flux density scales comparable. However, in order to best constrain the scintillation parameters it is necessary to compare the flux densities of the scintillating component seen by each telescope with the greatest possible accuracy. As both telescopes are observing at low elevation where pointing errors and atmospheric effects are most severe, it is important to correct for these effects, as well as for any differences due to resolved structure in the source. The flux density measurements shown in Figure 1 have been calibrated using PKS 1255−316, an unresolved, non-IDV source $\sim 1^\circ$ from PKS 1257−326. The calibration source was observed every 15 minutes for ~ 1 minute at both telescopes. PKS 1257−326 itself has a few percent of its flux density in components which are extended on arc-second scales. If not subtracted, this contributes to differences in the total flux density seen by each telescope, as well as adding slight apparent variations, in addition to the IDV, due to the changing (u, v) coverage over the observation. These changes with time are more significant in the ATCA data due to the linear configuration of the array. To remove the effects of resolved source structure, we have modeled the extended components, starting with a short "snapshot" of the VLA data, and subtracted them from the visibilities for both telescopes, leaving only the central part of the source which is unresolved at both telescopes and contains the scintillating component. Flux densities are then obtained by averaging Stokes I data over all baselines. Any residual errors, after applying antenna gain corrections from PKS 1255−316 and subtracting the extended component model, are too small to have a noticeable effect on the measured pattern time delays. Data from both telescopes are directly comparable to an estimated accuracy of $\sim 0.3\%$.

In the data shown from 2002 May 14, there is evidence that the IDV patterns seen by each telescope are not exactly identical; the trough and peak in the ATCA data reach flux densities $\sim 1.5\%$ lower than those in the VLA data, which is significantly different compared with the expected measurement errors. This could be a result of a slightly different part of the scintillation pattern being seen by each telescope. The scintillation pattern can be thought of as a series of bright and dark patches or "scints", assumed to be temporarily "frozen-in", which drifts past each telescope. The time delay depends on both the velocity of the pattern with respect to the projected baseline between the two telescopes, and also on the spatial structure of the pattern. This is illustrated in the lower left panel of Figure 1. The ellipses represent contours of constant intensity in the scintillation pattern. The observed quasi-sinusoidal variations occur as the Earth passes through this pattern. If the scintillation velocity has a large component perpendicular to the baseline, which from the model discussed in Section 3 is expected to be the case in May, then a slightly different part of the pattern would be seen by each telescope. This could easily account for the observed flux density differences.

The lower right-hand panel of Figure 1 shows time delays fitted to the March data for both frequencies and both days. Delays were found by minimizing the sum of squares of the residual flux density difference, assuming that for these data, the scintillation pattern seen by each telescope is identical apart from being shifted in time. For the March data this assumption is reasonable, as no significant difference is evident in the flux density of peaks and troughs measured at each telescope. For each dataset, a running time delay was calculated using a 40-minute window of data, to test whether any change in delay was observable over the observation. The delay estimates were averaged into three UT bins, and the error bars plotted are based on the scatter in the individual delay estimates. From this preliminary analysis, it is evident that the pattern arrival time delay is almost identical at both frequencies and on both days, and does not change significantly over the course of the observations. From this we can infer that successive contours of constant intensity in the scintillation patterns are close to parallel to each other as they cross the baseline. In the data from January, the observed time delays are very similar to those in March, ~ 5 minutes, while the data from 2002 May show larger time delays, on average ~ 8 minutes at both frequencies and on both days.

3. Discussion

Two-station time delay measurements can be combined with observations of annual cycles in the characteristic time scale of variability, t_{char}, to constrain the velocity and spatial structure of the scintillation pattern, which in turn can be used to constrain the source angular size and brightness temperature, as well as the distance to the scattering material. More than a year of monitoring PKS 1257−326 with the ATCA, since early 2001, revealed a clear annual cycle in t_{char}, and subsequent observations have confirmed its continued presence. The annual cycle, reported in Bignall et al. (2003), was best fit with a screen velocity offset by ~ 5 km s^{-1} in RA from the local standard of rest, and an anisotropic scintillation pattern elongated at $\sim 55°$ to the RA axis, although the axial ratio of the "scints" was not well constrained from the annual cycle.

The model from the annual cycle is consistent with the observed time delays. In fact the time delays are consistent with the successive contours of constant intensity being *always* close to parallel to each other over the ten months between the first and last time delay measurements. One would not expect to see this unless the scints were consistently highly elongated, which could be a result of anisotropic scattering and/or anisotropic source structure. The other two rapid scintillators, PKS 0405−385 and J1819+3845, also show evidence for highly anisotropic scintillation patterns (Rickett et al. 2002, Dennett-Thorpe & de Bruyn 2003). Rickett et al. (2002) argue that the origin of the anisotropy for PKS 0405−385 is in the scattering screen rather than the source. It will be important to confirm this for PKS 1257−326, and also to determine whether highly anisotropic scintillation patterns are a common property of slower scintillators, such as those found in the Micro-Arcsecond Scintillation-Induced Variability (MASIV) Survey recently undertaken with the VLA (Lovell et al. 2003). The MASIV Survey found that sources such as J1819+3845 and PKS 1257−326 are extremely rare. Intra-hour scintillations are thought to be due to unusual, localized scattering "screens" less than ~ 30 pc from the observer, whereas more common, slower scintillations are most likely due to scattering material at distances of order 100 pc or more. Anisotropy in the scintillation pattern would strongly influence observed time scales and annual cycles in scintillating sources, and thus has important implications for extracting information via "Earth Orbital Synthesis" (Macquart & Jauncey 2002).

Acknowledgments. The Australia Telescope is funded by the Commonwealth of Australia for operation as a National Facility managed by CSIRO. The National Radio Astronomy Observatory is a facility of the National Science Foundation operated under cooperative agreement by Associated Universities, Inc.

References

Bignall, H. E., Jauncey, D. L., Lovell, J. E. J., Tzioumis, A. K., Kedziora-Chudczer, L., Macquart, J.-P., et al. 2003, ApJ, 585, 653

Dennett-Thorpe, J., & de Bruyn, A. G. 2000, ApJ, 529, L65

Dennett-Thorpe, J., & de Bruyn, A. G. 2001, Ap&SS, 278, 101

Dennett-Thorpe, J., & de Bruyn, A. G. 2002, Nature, 415, 57

Dennett-Thorpe, J., & de Bruyn, A. G. 2003, A&A, 404, 113

Jauncey, D. L., Kedziora-Chudczer, L., et al. 2000 in Astrophysical Phenomena Revealed by Space VLBI, ed. H. Hirabayashi, P. G. Edwards & D. W. Murphy (Sagamihara: ISAS), 147

Jauncey, D. L., & Macquart, J.-P. 2001, A&A, 370, L9

Kedziora-Chudczer, L., Jauncey, D. L., Wieringa, M. H., Walker, M. A., Nicolson, G. D., Reynolds, J. E., & Tzioumis, A. K. 1997, ApJ, 490, L9

Lovell, J. E. J., Jauncey, D. L., Bignall, H. E., Kedziora-Chudczer, L., Macquart, J.-P., Rickett, B. J.,& Tzioumis, A. K. 2003, AJ, 126, 1699

Macquart, J.-P., & Jauncey, D. L. 2002, ApJ, 572, 786

Perlman, E. S., Padovani, P., Giommi, P., Sambruna, R., Jones, L. R., Tzioumis, A., & Reynolds, J. 1998, AJ, 115, 1253

Rickett, B. J., Witzel, A., Kraus, A., Krichbaum, T. P., & Qian, S.J. 2001, ApJ, 550, L11

Rickett, B. J., Kedziora-Chudczer, L., & Jauncey, D. L. 2002, ApJ, 581, 103

Shimmins, A. J., & Bolton, J. G. 1974, Aust. J. Phys. astrophys. Suppl., 34, 1

Highlights of Astronomy, Vol. 13
International Astronomical Union, 2003
O. Engvold, ed.

The Jets in Micro-Quasars and Quasars: A Comparison

Ralph Spencer

Jodrell Bank Observatory, University of Manchester, Macclesfield, Cheshire SK11 9DL,UK

Abstract. The discovery of relativistic jets in radio emitting X-ray binaries in our own galaxy has led to the term 'microquasar' being coined for these objects. In this paper the properties of microquasars are compared with those of quasars and radio galaxies, with the aim of trying to see how the similarities and differences can inform us about the physical conditions and evolution of jets. GRS1915+105 and SS433 are also discussed in more detail.

1. Introduction

X-ray binary stars display a wide range of interesting phenomena particularly in X-rays and perhaps offer the best laboratory for the study of the accretion process and the physics of extreme environments. The strong X-rays indicate the existence of a deep gravitational potential well and so imply the presence of a neutron star or black hole. Radio emission has been found in ~50 of the 280 known X-ray binaries listed in the catalogues of Liu et al. (2000, 2001) of high and low mass binaries (e.g. Fender 2003). Radio emission is a strong indicator of the presence of a radio jet. If the maximum brightness temperature (neglecting beaming effects) is limited by inverse Compton radiation to 10^{12} K, then a diameter of 1 au for a source of 100 mJy at 5 GHz at a distance of 1 kpc is implied. The radio emission therefore extends beyond the likely diameter of an accretion disk around a compact object, and the variability suggests that the emitting region is ejected from the central engine. Indeed high resolution observations show that about half of the radio-emitting X-ray binaries (REXRB) have radio jets.

The first REXRB found to show apparent superluminal velocities of knots in its radio jets was GRO J1655-40 (Tingay et al. 1995). Since then a further 5 objects have been found to show features moving down the radio jet at apparent speeds >c (Fender 2003). This phenomenon, together with the presence of a jet has led to the objects being called 'Microquasars' by analogy to the more powerful (and $\sim 10^6$ times further away) quasars (Mirabel et al. 1992, Mirabel & Rodríguez 1999). The fundamental energy source is the same i.e. they are powered by accretion onto a compact object. Perhaps all REXRBs should be labeled microquasars, if indeed they all have radio jets.

2. Radio Properties

Properties of microquasars such as the radio morphology, component proper motions and other derived parameters can be compared with those of extragalactic objects covering a wide range in luminosity from the relatively nearby Active Galactic Nuclei to the distant quasars (e.g. De Young 2002). Many images of the radio emission from extragalactic sources have been published, a convenient compendium is given by the Atlas of DRAGNs by Leahy, Bridle & Strom (2000).

2.1. Morphology

The most obvious difference between REXRB and quasars is that there are no obvious extended lobes situated on either side of the REXRB for nearly all the known objects. The exceptions are the nebulae which surround SS433 (W50) (Dubner et al. 1998) and Circ X-1 (Haynes et al. 1986). These extended regions are likely to be the remains of the supernovae associated with the formation of the compact objects rather than formed by the action of the jets alone. However the 'ears' of W50 are probably formed by the precessing jets of SS433 moving out into the interstellar medium, and so perhaps can be thought of as the equivalent of lobes. Similarly the jet in Circ X-1 may be passing energy into its nebula (Fender et al. 1998), analogous to M87 where the jet appears to feed into an extended halo (Owen, Eilek & Kassim, 2000).

Similarly there are no 'hotspots', where the jets may be interacting with the interstellar medium in a working surface. Compact IRAS sources have been found aligned with GRS1915+105 (Rodríguez & Mirabel 1999), but these may be HII regions.

The morphology of REXRB jets is similar to that of the core-jet quasars like 3C345 and 3C273, etc., and also the low luminosity FRI type of radio source where the jets are brighter towards the nucleus of the object. The jet in BL Lac (Stirling et al. 2003) looks like the jets in Cyg X-1 and SS433. Indeed the precession found in BL Lac is an interesting result, suggesting a close analogy to SS433 and is worth investigating further. We should therefore think of microquasars as naked jet sources, though the energy flowing through the jet must be deposited somewhere in the interstellar medium.

2.2. Proper Motions

Measurements of the proper motion of components within microquasar jets lead to estimates of velocities ranging from ~ 0.3 to 0.98 c or more. While the high velocity objects have Lorentz factors which are not too dissimilar to those in quasars, there is an outstandingly different effect. Several objects have been detected with two-sided ejections (e.g. GRO J1655-40, GRS 1915+105) even though their velocities are high, whereas jet-dominated quasars and BL Lac objects are exclusively one-sided. Doppler boosting causes this effect for quasars, which on the whole have been selected by their radio emission. Microquasars on the other hand have been selected by their X-ray emission, the bulk of which is not Doppler boosted.

2.3. Derived Parameters

Typical jet powers in microquasars are $\sim 10^{37}$ erg sec^{-1}, compared to 10^{46} erg sec^{-1} for quasars and FRII sources, and 10^{42} erg sec^{-1} for FRI objects (Spencer, de la Force & Stirling 2001) We should therefore perhaps call REXRB Nano-Quasars! The jet powers in microquasars are an appreciable fraction of the total accretion powers available (10^{38} – 10^{39} erg sec^{-1}); the fraction may approach unity if there there is a large contribution from protons.

Jet synchrotron flux density has been shown to scale with black-hole mass ($\propto M^{1.4}$, Heinz & Sunyaev 2003, Sunyaev 2003), implying that extragalactic jets are more radio loud and therefore suffer higher energy losses than microquasar jets, i.e. lose a higher fraction of their kinetic power in the form of radiation.

The length of jets in microquasars varies from $\sim$10 au to $\sim 10^6$ au (Spencer et al. 2001). VLBI scale (10's au) "mini-jets" have been found in SS433 (Vermeulen et al. 1993) and GRS1915+105 (Dhawan, Mirabel & Rodríguez 2000) as well as large scale jets extending over 10000 au. The mini-jet sources (e.g. Cyg X-1, Stirling et al. 2001) have flat radio spectra and are rather similar to the flat spectrum core jet extragalactic sources in overall appearance. The different size scales however result in different conditions: a typical equipartition magnetic field of $\sim$ 100 mgauss for microquasars means that the electron lifetime at cm wavelengths is much longer than the dynamical time and adiabatic rather than radiative losses dominate. There is no need for particle re-acceleration along the jets of microquasars in order to maintain the jet intensity at radio wavelengths. Jets in microquasars also propagate though a dense interstellar medium and so pressure in the jet needs to be higher than in quasars in order for a jet to propagate.

3. Individual Microquasars

GRS 1915+105 shows complicated X-ray behavior and is perhaps the best laboratory for studying accretion flows. Radio flaring has been associated with X-ray outbursts, and flares are accompanied by the ejection of radio emitting components at velocities of $\sim$0.98c (Mirabel and Rodríguez 1994, Fender et al. 1999). The radio flares appear after a period of steady radio flux with a flat spectrum (the plateau state) when the X-ray emission changes from a steady low-hard state to a variable high flux soft state. Persistent mini-jets have been found when the source is in the plateau state, however this region is weaker after the strong flaring occurs.

It was possible to follow the motion of the ejected clouds in the Fender et al. (1999) observations by making images with MERLIN every 2 days. Extrapolating the positions of the components indicated an ejection date of around 1 day after the onset of the soft X-rays. Recent observations of a flaring event in July 2001 (McCormick 2003) confirm this behavior. It seems that a disk which is strong in soft X-rays is necessary for the ejection of radio clouds, but it is not required for the formation of the mini-jet.

It is interesting that the superluminal radio galaxy 3C120 also shows the ejection of radio clouds just after a restoration of high X-ray emission. Marscher et al. (2002) showed that a dip in X-rays occurred just before radio flaring. The presence of a newly formed and unstable disk seems to be necessary for the ejection of radio emitting components at relativistic velocities.

The presence of the low level compact jet in the low-hard state suggests that an underlying jet may exist at all times. The flaring could then be due to the development of a strong shock in the jet, rather than the ejection of a discrete cloud of relativistic electrons and magnetic field.

Shock in jet models (Marscher & Gear 1985) have been used to describe high radio frequency outbursts in extragalactic core-jet objects like 3C273 (e.g.

Türler, Courvoisier & Paltani 2000) rather well. The outbursts in 3C273 are remarkably similar to those on GRS 1915+105. Türler, Courvoisier & Chaty (2003) have applied the model to the May 1997 outburst on GRS 1915+105. They predict a steep electron energy spectrum and rapid expansion of the jet (i.e a trumpet shape rather than a cone). Stevens et al. (2003) found that the variability of GRO J1655-40 can also be explained using the generalized shock model. However the expanding plasma cloud model has also been used successfully to describe the June 2001 outburst in GRS 1915+105 at 23-cm wavelength (Ishwara-Chandra, Yadav & Pramesh Rao 2002). A detailed comparison of the two models applied to GRS 1915+105 is clearly needed.

SS433 is famous for its precessing jets and has shown evidence for radio emission from a component extended roughly perpendicular to the jet and centered close to the core (Paragi et al. 1999, Blundell et al. 2001). Regions of extended emission also exist in some DRAGNS where the 'back-flow' from the advancing lobes interact. To investigate this further we have undertaken 2-dimensional hydrodynamic modeling (Smponias 2003) where multiple ejections of radiating knots takes place (as seen in MERLIN and VLBI observations of the SS433 jets). It appears that the multiple bow shocks interact and heat and compress gas in the central region. The effect is more dominant when a wind is present.

4. Conclusions

Micro-quasar jets are more similar to those in FRI radio galaxies and BLLacs rather than the more luminous FRIIs. Jet formation and ejection are strongly associated with changes in X-ray state for microquasars, and as recent results on 3C120 suggest perhaps for extragalactic sources also. Shock in jet models may work for both, further progress requires frequent multi-wavelength observations. Studies of jets in both microquasars and quasars complement each other and indeed lead to further understanding of relativistic jets.

References

Blundell, Mioduszewski, A., Muxlow, T., Podriadlovski, P., & Rupen, M. 2001, ApJ, 562, L79

Dhawan, V., Mirabel, I. F., & Rodríguez, L. F. 2000, ApJ, 543, 373

De Young, D. S., 2002, The Physics of Extragalactic Radio Sources, (Chicago: University of Chicago Press)

Dubner, G. M., Holdaway, M., Goss, W. M., & Mirabel, I. F. 1998, AJ, 116, 1842

Fender, R. P., Spencer, R., Tzioumis, T., Wu, K., et al. 1998, ApJ, 506, L121

Fender, R. P., Garrington, S. T., MacKay, D. J., Muxlow, T. W. B., Pooley, G. G., Spencer, R. E., Stirling, A. M., & Waltman. E. B. 1999, MNRAS, 304, 865

Fender, R. P. 2003, in Compact X-ray Sources, ed W. Lewin & M. van der Klis (Cambridge: CUP) in press

Haynes, R. F., Komesaroff, M. M., Little, A. G., Jauncey, D. L., Caswell, J. L., Milne, D. K., Kesteven, M. J., Wellington, K. L., & Preston, R. A. 1986, Nature, 324, 233

Heinz, S., & Sunyaev, R. A. 2003, MNRAS, 343, L59

Ishwara-Chandra, C.H., Yadav, J. S., & Pramesh Rao, A., 2002 A&A, 388, L33

Leahy, J. P., Bridle, A. H., & Strom R. G. 2000, http://www.jb.man.ac.uk/atlas

Liu, Q. Z., van Paradijs, J., van den Heuvel, E. P. J. 2000, A&AS, 147, 25

Liu, Q. Z., van Paradijs, J., van den Heuvel, E. P. J. 2001, A&A, 368, 1021

Marscher, A. P., & Gear W. K. 1985, ApJ, 298, 114

Marscher, A. P., Jorstad, S. G., Gómez, J-L., Aller, M. F., Terasranto, H., Lister, M. L., & Stirling, A. M. 2002, Nature, 417, 625

McCormick, D. G. 2003, PhD Thesis, University of Manchester

Mirabel, I. F., Rodríguez, L. F., Cordier, B., Lebrun, P. J. 1992, Nature, 358, 215

Mirabel, I. F., & Rodríguez, I. F. 1994, Nature, 371, 46

Mirabel, I. F., & Rodríguez, L. F., 1999, ARA&A, 37, 409

Owen, F. N., Eilek, J. A., & Kassim, N. E. 2000, ApJ, 543, 611

Paragi, Z., Vermeulen, R., Fejes, I., Schilizzi, R., Spencer, R., Stirling, A. 1999, A&A, 348, 910

Rodríguez, L. F., & Mirabel, I. F. 1999, A&A, 340, L47

Smponias, T. 2003, PhD Thesis, University of Manchester

Spencer, R. E., de la Force, C., & Stirling, A. 2001, in IAU Symp. 205, Galaxies and their Constituents at the Highest Angular Resolution, ed R. T. Schilizzi, (San Francisco: ASP), 264

Stevens, J., Hannikainen, D., Wu, K., Hunstead, R., & McKay, D. 2003, MNRAS, 342, 623

Stirling, A. M., Spencer, R. E., de la Force, C. J., Garrett, M. A., Fender, R. P., & Ogley, R. N. 2001, MNRAS, 327, 1273

Stirling, A. M. et al. (12 authors) 2003, MNRAS, 341, 405

Sunyaev, R. A. 2003, these proceedings

Tingay, S. J., Jauncey, D. L., Reynolds, J. E., Meier, D. L., et al. 1995, Nature, 374, 141

Türler, M., Courvoisier, T. J-L., & Paltani, S. 2000, A&A, 361, 850

Türler, M., Courvoisier, T. J-L., & Chaty, S. 2003, in ASP Conf. Ser. High Energy Blazar Astronomy, (San Francisco: ASP), in press

Vermeulen, R. C., Schilizzi, R. T., Spencer, R. E., Romney, J. D., & Fejes, I., 1993, A&A, 270, 177

Highlights of Astronomy, Vol. 13
International Astronomical Union, 2003
O. Engvold, ed.

JD18: Quasar Cores and Jets - poster-paper summary

J V Wall

Department of Physics & Astronomy, University of British Columbia, Vancouver, BC V6T 1Z1, Canada

1. Introduction

Of the 17 poster papers presented at IAU25 Joint Discussion 18, three (1821, 1824, 1834) are essentially theoretical, three (1828, 1829, 1831) deal with polarization, screens and absorbers, one (1818B) considers galaxy formation and evolution, 7 (1817, 1820, 1826, 1830, 1835, 1836, 1837) describe source structure and spectra, and three (1812, 1818, 1823) deal with Intra-Day Variability (IDV).

2. Theory

Paper 1821, *Microphysics of AGN central engines* by **Zdenka Kuncic** explores the energetics and dynamics of accretion-disc coronae in AGN. A solar analogy is used to identify the mechanisms: bulk plasma heating, particle acceleration, bulk kinetic energy. Spectral signatures from the radiative cooling processes are presented. A particularly useful feature of this paper that it lays out all the physical processes involved.

Y. Lu, K.S. Cheng and S.N. Zhang in poster 1824 describe *An accretion model for the growth of the central black hole*. Their model, requiring but two parameters, shows how ionization instability produces an S-curve in the log(mass) vs log(surface density) plane. The bottom branch of the S-curve is ADIOS, advection dominated accretion, while the upper branch is rapid accretion and represents the QSOs we see now. The bulge-mass relation reported by Magorrian et al (1998) arises naturally in the model. However, time scales are such that low-mass black holes may have to grow with a different (faster) process if the accretion rate is Eddington-limited.

Paper 1834 by **S. Ramotholo** considers *Possible optical identification of gamma-ray blazars*, pointing out that detection is important in understanding particle acceleration processes. With missions HESS, GLAST, and MAGIC coming it is important to consider efficient detection methods. The peak position of synchrotron emission is crucial in determining whether a blazar will be seen at GeV or TeV energies. The paper is a combined theoretical and observational study suggesting how to determine this peak from optical observations.

3. Polarization, screens and absorbers

In paper 1828, **Nakai Naomasa** considers *Water maser disks in AGN - two types of cold absorber*. The objects in question are H_2O megamasers and the two types are distinguished by the flux ratio of high-velocity to systematic H_2O

features. The former (prototype NGC 4258) shows weak or no Fe Kα lines; the latter (prototype NGC 1068) strong Fe Kα lines. The model has the effect caused by the former having thin disks, the latter thick disks - and VLBI observations have now revealed these disks. The paper has an excellent illustration of how the Fe fluorescence works with the two disk types to give the dichotomy in line-strength ratios.

VLBA polarimetry: a Faraday screen in 3C273, paper 1829 by **R. Ojha et al.**, describes tracking the polarization of 3C273's superluminal radio components with VLBA over 6 epochs at 2-month intervals. The fractional polarization increases as a component moves out. It could be that the field becomes more ordered with distance; or that the components are moving out from behind a screen blocking polarized radiation. The observations favor the latter - but the drawback is that this now requires some kind of filamentary Faraday screen producing the same optical depth at 15 and 22 GHz, with little Faraday rotation.

W. Cotton (paper 1831) describes *Evidence for a low filling factor in the NLR of CSS QSOs*. The Compact Steep-Spectrum (CSS) sample of Fanti et al (2001) has complete linear-size measurements from VLBA observations. A plot of integrated polarization (from the NVSS) against size shows an absence of polarization at sizes < 6 kpc. Detailed examination of 3C43, 3C138, key sources in the sample, shows that some weakly polarized emission remains, despite the known amounts of ionized gas in Narrow Line Regions (NLR). The implication is that the NLR plasma has a low filling factor but high covering factor. A model in which the plasma is arranged in sheets will work, and is testable by looking for Faraday rotation at high frequencies.

4. Galaxy evolution

A possible *Radio - X-ray connection in high-z quasars on the sub-kpc scale* is discussed in 1818B by **A.P. Lobanov, L.I. Gurvits and S. Frey**. VLBA observations have revealed unusually prominent sub-kpc-scale jets at rest-frame frequencies of 7.2 GHz (with VLBA) and 25 GHz (with VSOP) for the QSOs 2215+020 and 1713+218 respectively. Both have the jets pointing toward ROSAT X-ray extensions. Both have redshifts of ~ 4. There are 71 QSOs in the current sample with $z > 3$; the authors suggest that such objects may serve as beacons for protoclusters in the early universe, providing a resource for tracing galaxy and structure development.

5. Spectra and Structure

N. Gizani and M. Garret consider *Jet misalignment in radio galaxies - the unification theory* (paper 1817). The radio sources Her A and 3C 310 are FRI/II objects of large overall double structures (arcmin scales) with ring-like features around the nucleus. The structures on VLBI scales show relatively high misalignments with the axes of the huge outer lobes of these objects. At face value this lack of alignment is troubling for unified models, which prescribe that central jet structures should lie along the ejection/lobe axis. The authors point out that the objects resemble CSS-class QSOs in this misalignment, and a relatively high-density ISM (interstellar medium) is ascribed to CSS QSOs to explain their small size by confinement of the radio lobes. If by analogy Her A and 3C 310 also have high density ISMs, then their misalignments present much less of a challenge to unified models.

X-ray measurement of energetics in lobes of radio galaxies is discussed in paper 1820 by **Naoki Isobe**. Measurements with ASCA, Chandra and XMM for a small sample of radio galaxies have mapped diffuse X-ray emission from the lobes of these radio galaxies, due to Inverse Compton scattering of CMB photons by the synchrotron electrons of the lobes. The X-ray and synchrotron radiation was compared in order to measure energy densities U_e and U_m. The following results were obtained: (1) $U_e \sim 10U_m$; (2) U_e in lobes $\propto$ luminosity of nucleus, shown to follow if jet-luminosity $\propto$ accretion; (3) U_m does not depend on luminosity of the nucleus; and (4) in several lobes, U_e is uniform but U_m is higher towards the lobe periphery.

The expanding lobe of 3C 84 is the subject of paper 1826 by **K. Asada et al**. (Note that 3C 84 is Per A, NGC 1275, etc; z = 0.0172, with extended structure dominated by the bright southern lobe.) Asada et al. have made multi-epoch observations with VSOP/HALCA, the VLBA and the full VLA; the paper presents superb maps. There is a monotonic decrease of flux, presumably due to adiabatic expansion; the southern lobe is going south at 0.3c; and some of the knots within the lobe are in motion while others are stationary. It appears as though the jet is hitting/pushing the inner edge (the northern top) of the main lobe.

A major observational program is sketched out in paper 1830 by **R. Ojha et al.**, which presents *Results from 8.4 GHz VLBI imaging of 184 southern QSOs*. This is the single largest sample of QSOs studied with VLBI; many of these QSOs have never before been examined at milliarcsec resolutions. The VLBI network used in the survey comprises the Australia Long Baseline Array together with telescopes in South Africa and Hawaii. Some early maps are shown – only half the data have been reduced, but from this it appears that $\sim$ 50% show extended structures on milliarcsec scales and $\sim$ 10% are doubles. There is much to come from this extensive observing program.

Zhi-Qiang Shen, J.M. Moran and K.I. Kellermann describe *A bent superluminal jet in the central parsecs of OV-236* (paper 1835). OV-236 is PKS 1921-293, with z = 0.325 at which 1 millarcsec = 4.6 pc; the object is compact, variable and bright at mm wavelengths. Multi-epoch multi-frequency VLBA observations were carried out at 5 and 43 GHz, 1994 to 2002; additional VLBA observations were made at 12, 15 and 86 GHz. In two VLBA images of OV-236 obtained simultaneously at 5 and 43 GHz in 2000, a misalignment of about 70^0 can be seen in the overall structure. The central 1 pc region consists of two equally compact ($\sim$ 0.1 milliarcsec) components whose relative position appears unchanged in all 7-epoch 43 GHz images over the 8 years. It is possible that they are associated with a massive binary black hole. A schematic model is drawn to show how the jet emission observed at different scales may be explained with a single smoothly-curving trajectory.

The *Radio spectra of the Parkes half-Jansky FS sample* are considered by **O.I. Wong and R.L. Webster** in paper 1836. ATCA flux-density measurements were made simultaneously at 1.4, 2.5, 4.8 and 8.4 GHz of the 323 sources in 3.9 sterad above $S_{2.7\mathrm{GHz}} = 0.5$ Jy. From these, the radio spectral-energy distributions (SEDs) were characterized. Comparison of results at different epochs showed that most SEDs move up and down flux scales at each frequency without changing spectral type. The observations permit consideration of a number of issues, e.g. long-term variability studies, development of simple models of synchrotron mechanisms, and comparison with optical and IR SEDs.

The same sample is the subject of paper 1837: *Jet vs disc: the optical output of FSRQ* by **M. Whiting et al**. The authors carried out BVRIJHK photometry for the Parkes 0.5-Jy sample. They draw a number of conclusions from decomposition of the SEDs, considering the accretion disk to emit as a (blue) power-law and the relativistic jet as a (redder) synchrotron bump. Evidence for synchrotron emission is shown by 40% of the objects, while 40% are best fit by a single power law. BL Lac objects are best fit with disc+jet model; the relatively weak emission lines of BL Lacs are thus not wholly due to swamping by a boosted jet component. The disc and broad-line region emission appears intrinsically weak, perhaps due either to a different accretion process, or to a greater amount of outflow into the jet disrupting inner regions of the disk.

6. Intra-Day Variability

Two poster papers with authorship in common consider J1819+3845, the most variable QSO: 1812, *Structure of the IDV QSO J1819+3895 from 1 microarcsec to 1 milliarcsec* by **G de Bruyn, J-P Macquart and J Dennett-Thorpe**, and 1818, *J1819+3845 as seen by VSOP* by **L I Gurvits, G de Bruyn and J Dennett-Thorpe**. The former describes combined VLBI and IDV observations and simultaneous multi-frequency modeling of the source structure, presenting the results in a fine schematic diagram. Structure scales from 100 nanoarcsec to 1 microarcsec for the scintillating component are implied, with the corresponding requirement that T_b exceeds 10^{15} K. The latter describes detection of J1819+3845 on all 78 baselines of a VLBI - HALCA experiment, with analysis using closure phases and a novel "VLBI-scintillation delay" technique.

Paper 1823 by **J. Lovell et al.** presents the *First results from MASIV*, the Micro-Arcsecond Scintillation-Induced Variability survey. In the authors' words, this is 'a 5-GHz VLA survey of the northern sky to obtain 100 - 150 scintillating flat-spectrum extragalactic sources with which to examine both the microarcsecond structure and parent populations of these sources, and to probe the turbulent interstellar medium responsible for the scintillation. Early findings: (1) The fraction of sources that scintillate and their fractional scintillation amplitude both increase for the weaker ($\sim$ 100 mJy) sources; (2) $\sim$ 20% of compact flat-spectrum sources vary on at least one epoch; (3) $\sim$ 50% show annual cycles; (4) Non-isotropic sky distribution indicates that the majority of these are tied to the ISM. A vast data-base will result from this major project, and these first results are the forerunners of much to come.

The poster papers represented a vital and integral part of Joint Discussion 18 and the organizers are very grateful to the authors for their efforts.

JD19

Physical Properties and Morphology of Small Solar System Bodies

Chairpersons: H.U. Keller and E.F. Tedesco

Editors: W.F. Huebner, E.F. Tedesco (Chief-Editor) and H.U. Keller

Highlights of Astronomy, Vol. 13
International Astronomical Union, 2003
O. Engvold, ed.

Welcome and Introduction

Edward F. Tedesco

TerraSystems, Inc., USA

1. Introduction

The purpose of JD 19 was to discuss what might (and might not) be generalized from close-up observations (fly-bys and rendezvous) when combined with remote observations (using ground-based and Earth-orbiting instruments). The organizers and participants of this Joint Discussion believe measurements from fly-by and rendezvous missions provide unique benchmarks. However, such observations are available for only a handful of objects. Thus, by leveraging close-up observations with remote observations for those few objects having both kinds of data, we will not only be able to better understand the objects visited, but also those not visited, including bodies which differ from those already studied in detail by fly-by or rendezvous missions. In addition, understanding more about types of objects not yet explored by spacecraft (e.g., NEOs, Centaurs, KBO/TNOs), besides being valuable in itself, will enable us to better plan future missions to such objects.

With the above goal in mind, approximately 150 astronomers from around the world participated in Joint Discussion 19. In addition to the 20 invited and 26 poster presentations summarized herein, numerous substantive discussions took place, many of which will undoubtedly lead to future collaborative projects.

Highlights of Astronomy, Vol. 13
International Astronomical Union, 2003
O. Engvold, ed.

Galileo's Exploration Of Small Bodies

Torrence Johnson
Jet Propulsion Laboratory, California Institute of Technology, Pasadena, CA, USA

The Galileo mission to the Jupiter system afforded the opportunity to make the first ever flyby observations of main belt asteroids. The first encounter, with 951 Gaspra, revealed an irregular, cratered surface that shows evidence of regolith optical space weathering processes. The second encounter, with 243 Ida, resulted in the discovery of the first confirmed satellite of an asteroid, Dactyl. Measurements of Dactyl's orbit also allowed a useful determination of mass and density for Ida. In addition to these pioneering asteroid observations, Galileo also made observations of Jupiter's small inner moons and found that they were the major source for material in Jupiter's tenuous ring system. During it's final data taking orbit in 2002, Galileo passed within about 250 km of the irregularly shaped satellite Amalthea. Determination of Amalthea's mass from tracking data yields a bulk density for this small body of less than 1 gm/cc, suggesting a body of relatively high porosity. This is consistent with the growing body of data on small asteroid densities and estimates of their porosity.

Highlights of Astronomy, Vol. 13
International Astronomical Union, 2003
O. Engvold, ed.

NEAR At Mathilde And Eros: An Update

Andrew Cheng

Johns Hopkins Applied Physics Laboratory, MD, USA

At the slowly rotating C-asteroid Mathilde, the Near Earth Asteroid Rendezvous (NEAR) mission imaged only one face of the body but still constrained the density to only 1.3 g/cm^3, indicating high porosity. This porosity and the approximate saturation of the surface with giant craters led to suggestions that Mathilde must be a rubble pile. At S-type Eros, NEAR measured elemental abundances and spatially resolved reflectance spectra that appear most consistent with an ordinary chondrite composition, although the Eros composition could not be identified with any known meteorite type. Imaging and altimetry data were interpreted as showing Eros to be a globally consolidated, albeit heavily fractured, collisional shard. A spectacular feature, ponding of regolith on Eros, was discovered. Continuing analyses of NEAR data suggest that Mathilde is not strengthless, and that if it is a rubble pile, large coherent components are present. Both composition and internal structure of Eros pose unresolved issues. Although almost uniform internally, Eros cannot be perfectly so. The density of 2.67 g/cm^3 is significantly less than that of ordinary chondrites and suggests significant porosity, but this may not be explained by macroscopic fracturing if these spaces can be filled with particulates.

Highlights of Astronomy, Vol. 13
International Astronomical Union, 2003
O. Engvold, ed.

Comet Halley Observed During The ESA Giotto Fly-By

H. U. Keller

Max-Planck-Institut für Aeronomie, Lindau, Germany

The major observational results of the detection of the nucleus of Comet Halley will be summarized with some emphasis on the images. A comparison to or context with ground based observations will be discussed. The paradigm set by the first observations of a cometary nucleus should be critically reviewed. The results of the VEGA missions and the recent observations of the nucleus of Comet Borrelly by DS-1 will also be considered.

Highlights of Astronomy, Vol. 13
International Astronomical Union, 2003
O. Engvold, ed.

The Deep Space 1 Encounter With Comet 19P/Borrelly

Robert M. Nelson

Jet Propulsion Laboratory, Pasadena, CA, USA

On 22 Sept 2001 at 22h 29m 33s UTC the Deep Space 1 (DS1) spacecraft encountered the comet 19P/Borrelly at a distance of 2171 km. Measurements were undertaken by two dedicated science instruments on the spacecraft and by the spacecraft's ion propulsion system diagnostic sensors (IDS). The images are the highest resolution ever obtained of a cometary nucleus and show topography and albedo differences on the surface at a resolution of 47m. The disk averaged geometric albedo is less than 0.03, among the lowest of any solar system object observed. The surface reflectance varies by a factor of three; the most absorbing areas having a normal reflectance of less than 0.01. Material is being emitted of from localized regions on the nucleus generally in the sunward direction. These regions are cylindrically shaped about 0.5 km in diameter and about 5 km in length. The cometary bow shock and other features associated with the cometary environs are asymmetrically offset from the sun-Borrelly axis. This suggests that the localized emission regions seen in the images may cause the coma to be asymmetrically offset from the sun-nucleus line. Such an offset has not been reported in previous spacecraft encounters with other comets.

Highlights of Astronomy, Vol. 13
International Astronomical Union, 2003
O. Engvold, ed.

Rosetta Asteroid Candidates

M.Antonietta Barucci

LESIA, Observatory of Paris

Marcello Fulchignoni

LESIA, Observatory of Paris

Mirel Birlan

LESIA, Observatory of Paris

Pierre Vernazza

LESIA, Observatory of Paris

Elisabetta Dotto

INAF, Osservatorio Astronomico di Roma

Alain Doressoundiram

LESIA, Observatory of Paris

Abstract. The new scenario of the Rosetta mission to comet 67/P Churyumov-Gerasimenko (launch on February 2004), includes as baseline the fly-by of one or two asteroids. Several asteroids are now possible fly-by candidates (single or double) within the available resources. Other candidates whose fly-bys require a larger Δv can be also considered if the Rosetta interplanetary orbit insertion will cost less Δv.

All the up to date available information on the possible targets are discussed in this report.

The new baseline of the Rosetta mission includes the fly-by of at least an asteroid (2009-2010) which will precede a long orbital rendez-vous with the 67/P Churyumov-Gerasimenko comet nucleus (2014). The selection of the asteroid target(s) depends on the Δv available after the Rosetta probe interplanetary orbit insertion maneuver. A few meter/sec Δv are available for the asteroid science in the pre-launch resource budget; but there is the possibility to allocate to the asteroid some of the remnant Δv, now reserved as contingency for the insertion maneuver, as soon as the Rosetta probe will be on its way toward the comet. The idea is to wait the results (in terms of Δv expenses) of the insertion maneuver and to consider the new available budget to perform the asteroid fly-by(s). For this reason it is necessary to be ready shortly after the beginning of the Rosetta interplanetary journey: an international observational campaign is started with the aim to increase at the maximum level the characterization of the possible asteroid targets of the mission.

This paper present the situation concerning the Rosetta asteroid targets choice as it is at the date of the IAU General Assembly in Sidney (July 2003). Ten main belt asteroids have been found allowing the Rosetta probe to have a single or even few double fly-bys whitin a Δv range 10-150 m/s (see table).

21 Lutetia is the largest object between these possible targets. On the basis of its visible spectra and IRAS albedo (Tedesco, 1992), it was classified as M type, but new observations in near-infrared and polarimetric data (Birlan et al. 2003) suggest that it is rather a C-type object similar to carbonaceous chondrite.

No data on *2181 Fogelin* are available in literature. Considering its absolute magnitude the diameter can be estimated in the range 12-22 km. We observed it with the IRTF/NASA on July 2003 and its near-infrared spectrum suggest a S type object (Birlan et al. 2003).

Asteroid	Diam. (km)	IRAS albedo	Extra Δv (km)	Fly-by date mm.dd.yy	Rel. Vel. (km/s)
21 Lutetia	96	0.22 ± 0.02	131	07.10.10	14.9
437 Rhodia	13	0.70 ± 0.08	87	09.17.08	11.2
1393 Sofala	–	–	113	09.11.08	6.9
1714 Sy	–	0.11 ± 0.03	11	03.06.08	8.2
2181 Fogelin	–	–	19	05.25.10	13.6
2513 Baethsle	17	0.03 ± 0.01	16	10.05.08	8.6
2867 Steins	–	–	61	09.06.08	8.6
3050 Carrera	–	–	74	07.31.08	11.2
3418 Izvekov	27	0.07 ± 0.01	14	12.04.10	11.3
5538 Luichewoo	–	–	35	04.08.09	5.6

The asteroid *437 Rhodia* is an intriguing object due to its very high IRAS albedo. The synodical period of ≥ 56 hours (Binzel, 1987) allow us to consider it within the slow rotator asteroid group.

If we consider the family members having spectra quite homogeneous (Florczak et al, 1998), we can assume that the asteroids *2513 Baethsle* and *5538 Luichewoo* belong to the S type which is characteristic of the members of the Flora family. IRAS albedo of *2513 Baethsle*, very far from the typical S-type, may indicate its “interloper” character and its appurtenance to a more primitive (C or D) asteroid class. The asteroid *3418 Izvekov* belongs to the C-type Themis family, this is in agreement with its IRAS albedo value. The visible spectrum of the asteroid *1393 Sofala* (Xu et al, 1995) indicates a S-type composition.

The final decision on the asteroid candidates will be taken after the launch. Information on all the possible target asteroids is important to be able to contribute to the best choice of the targets and to optimise the mission science return.

21 Lutetia represents one of the most interesting candidate, in fact it’s the only one which will allow us to obtain mass determination by radio science experiments, and consequently it will be possible to determine its density. Moreover, if the chondritic character of this object will be confirmed, it will cope with the scientific objectives of the mission: the exploration of the primitive bodies of the planetary system.

If Lutetia cannot be selected due to the lack of available Δv, the asteroid candidate choice has to be done favouring the objects characterized by: 1) the more primitive compositional types (C, P, D); 2) the slower fly-by relative velocity; and 3) the larger diameter.

To obtain all these information we urge the observer community to participate to the observational campaign of these objects during their 2004 opposition.

References

Binzel, R. P. 1987, Icarus, 72, 135.

Birlan, M., Barucci, M.A., Vernazza, V., Fulchignoni, M.,Binzel, R.P., Bus, S.J., Belskaia, I. and Fonasier, S. 2003, New Astronomy, in press.

Florczak, M., Barucci, M.A., Doressoundiram, A., Lazzaro, D., Angeli, C. and Dotto, E. Icarus, 133, 233.

Xu, S., Binzel, R.P., Burbine, T.H. and Bus, S.J. 1995, Icarus, 115, 1.

Tedesco, E.F. 1992, PL-TR-92-2049.

Highlights of Astronomy, Vol. 13
International Astronomical Union, 2003
O. Engvold, ed.

Muses-C As A Benchmark Mission For S-Type Asteroid Group

Akira Fujiwara

Masanao Abe

Hajime Yano

The Institute of Space and Astronautical Science, Japan

MUSES-C is launched in May 2003, and arrives in the vicinity of a near-Earth asteroid (25143)1998 SF36 in June 2005. The spectral type is S and its diameter is 300-600 m. During four months stay multi-band imaging, near-infrared spectra, and X-ray spectra will be taken at the nominal altitude of about 6km above the asteroid surface.. Sampling of the surface material will be made at two different locations. The total mass collected will be about 1 g. A miniature hopping lander on which imaging cameras are boarded will be dropped onto the surface. The sample will be returned to the earth in June 2007. These methods, the close-up global observation from the spacecraft, in situ observation from the lander, and detailed analysis of the returned sample, can, as well as ground-based observation of the targeted asteroid, provide information of surface material distribution in various scales, and also provide powerful benchmarks to interpretation of spectroscopic data obtained through ground-based observation of S-type asteroids.

Highlights of Astronomy, Vol. 13
International Astronomical Union, 2003
O. Engvold, ed.

Dawn Discovery Mission: Symbiosis with 1 AU Observations

C. T. Russell

Inst. of Geophysics and Planetary Physics & Dept. of Earth and Space Sciences, U. California, Los Angeles, USA

Abstract. The Dawn mission, the ninth in the series of NASA Discovery missions, is scheduled for launch in late May 2006 on a voyage to both Vesta and Ceres. The mission carries a framing camera, visible and infrared mapping spectrometer, gamma ray and neutron spectrometer, laser altimeter and magnetometer to understand and contrast these two very different bodies. Vesta apparently accreted dry, differentiated, and formed an iron core. Ceres apparently contains much water and ice and has remained relatively cool over its lifetime. The community of 1AU observers can help optimize the Dawn mission by improving the knowledge of Vesta and Ceres rotation axes, thus improving our knowledge of when regions and features will be best illuminated. The detection of any satellites would not just identify a potential hazard, and a secondary target of interest, but would also determine the mass of the primaries, enabling better mission planning. Characterization of the surface in any way, including identifying potential targets for detailed study, is also most welcome.

1. Introduction

The current paradigm for the formation of the solar system is that it began in a solar nebula, a rotating disk of gas and dusk about 4.6 Ga b.p. In a period that now is thought to be about 3 million years (e.g., Jacobson 2003) the dust accreted into rocks and the planetary embryos, similar in size to Vesta and Ceres. When Jupiter formed, gravitational stirring in the asteroid belt countered the accretional process, but in the inner solar system accretion continued, forming the larger terrestrial bodies, Mars, Earth, Venus and Mercury, over about 30 million years. The Earth's Moon is thought to be due to the collision of a Mars-sized object with the proto-Earth in which much of the material of the two colliding bodies remained with the Earth and a small portion remained in orbit later accreting into the present Moon. This scenario is summarized in Fig. 1.

The solar nebula itself was decidedly heterogeneous varying in physical and chemical properties as a function of heliocentric distance. Near the Sun materials that would condense and solidify at high temperature, such as iron, are believed to have been more prevalent. Further from the sun the temperature and pressure were less and lower temperature materials formed. Perhaps between Vesta at 2.34 AU and Ceres at 2.77 AU the dew line was passed and the accreted material was much richer in water and organics as the temperature dropped further, with distance as illustrated in Fig. 2.

This hypothesis is supported in the case of Vesta by the association with Vesta, of a group of meteorites, the Howardites, Eucrites and Diogenites, or HED

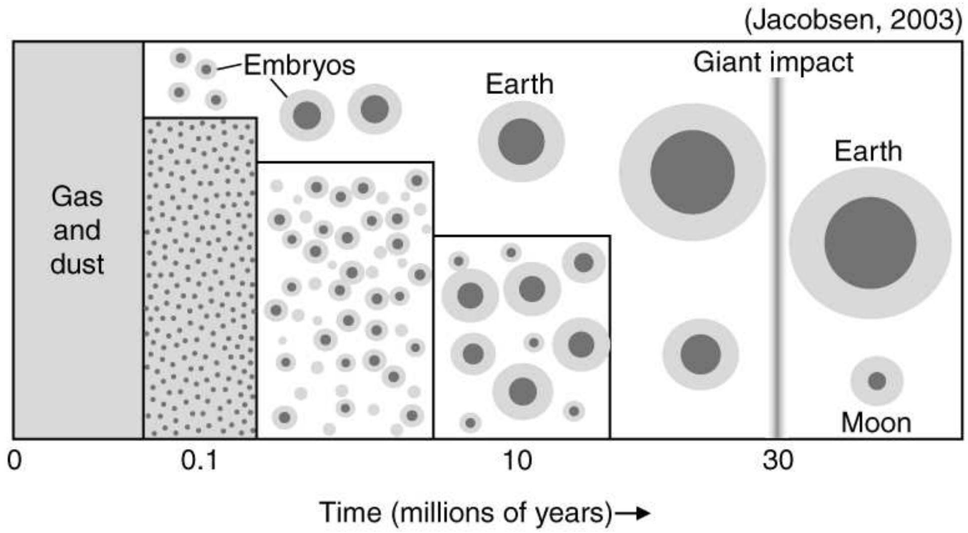

Figure 1

Figure 1. Schematic illustration of the sequence of formation of the inner solar system (after Jacobsen 2003).

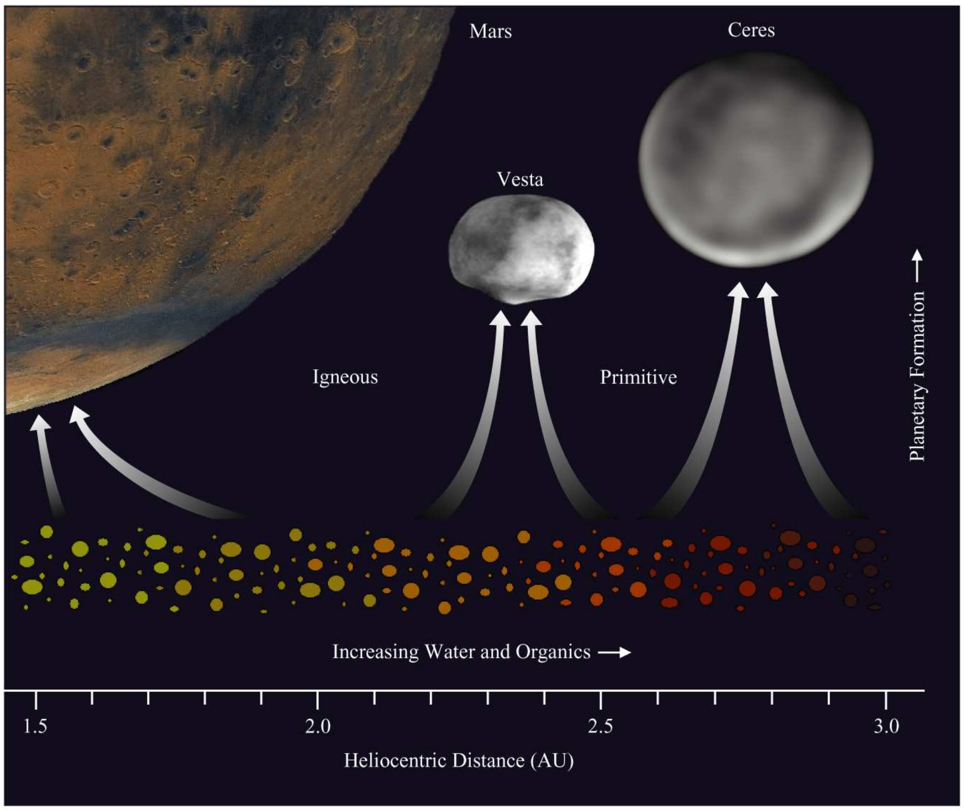

Figure 2

Figure 2. Schematic illustration of the role of the compositional gradient in the early solar nebula in affecting the composition of Mars, Vesta and Ceres (Courtesy M. Sykes, 2002).

meteorites, that constitute 5meteorites have a unique reflectance spectrum that matches the reflectance spectrum of both Vesta and those asteroids, that may be pieces of Vesta, known as vestoids. These meteorites indicate that Vesta melted, formed a central iron core, and material derived from Vesta's interior flowed across the surface similar to flows on the lunar mare. This would make Vesta the smallest known body that accreted and differentiated, the smallest of the terrestrial-type planets. Thus, studying Vesta enables us to better understand the primordial accretion and differentiation of planets. It enables us to understand the role and timing of collisions in the early solar system and what were the heat sources that contributed to planetary thermal evolution. Further Vesta data will contribute to the understanding of the generation of magnetic fields in planetary cores.

Ceres is believed to be very different than Vesta, forming a bridge between the inner rocky bodies of the inner solar system and the icy bodies of the outer solar system. Presently it is believed that Ceres began as a silicate-ice organic mixture that is melted by long-lived radio-nuclides in all but a thin ice crust. The warm water circulates, diapirs form in the ice crust, surface topography forms and reforms. Presently Ceres may be completely frozen but most probably it contains a global ocean of water. Thus Ceres is strikingly different than Vesta and enables us to study the role and emergence of water on a planetary scale and how it controlled planetary evolution. Further, the surface of Ceres may teach us much about low temperature aqueous alteration, a process we believe common in the early solar system.

2. The Mission

The spacecraft carries five instruments and obtains radiometric data for studies of Vesta's and Ceres' gravitational field. A framing camera provided by the Max-Planck-Institut für Aeronomie and DLR in Germany enables us to map the surface in seven colors plus a clear filter. A visible and infrared mapping spectrometer for the classification of the minearology of the surface has been provided by the Italian Space Agency. The Los Alamos National Laboratory is building a gamma ray and neutron spectrometer to detect the elemental compositions of the body and the presence of water. Goddard Space Flight Center is providing the laser altimeter to accurately map the size and shape of the bodies. UCLA is providing a magnetometer to map the crustal remanent magnetic field and to determine the interior electrical conductivity of the bodies. The instruments and their location on the spacecraft are given in Fig. 3.

The spacecraft is launched in late May 2006 and uses ion propulsion to assist it to reach, and then orbit, Vesta and Ceres in 2011 and 2014 respectively. The flight path is shown in Fig. 4. Once at Vesta or Ceres the spacecraft enters a series of circular orbits of varying altitude. The two principal orbits are a high altitude mapping orbit where the framing camera and the mapping spectrometer are used and a low altitude mapping orbit where the laser altimeter, gamma ray spectrometer and magnetometer obtain their prime data. The mission is led by a Principal Investigator, managed by JPL, with the spacecraft being built by Orbital Sciences Corporation.

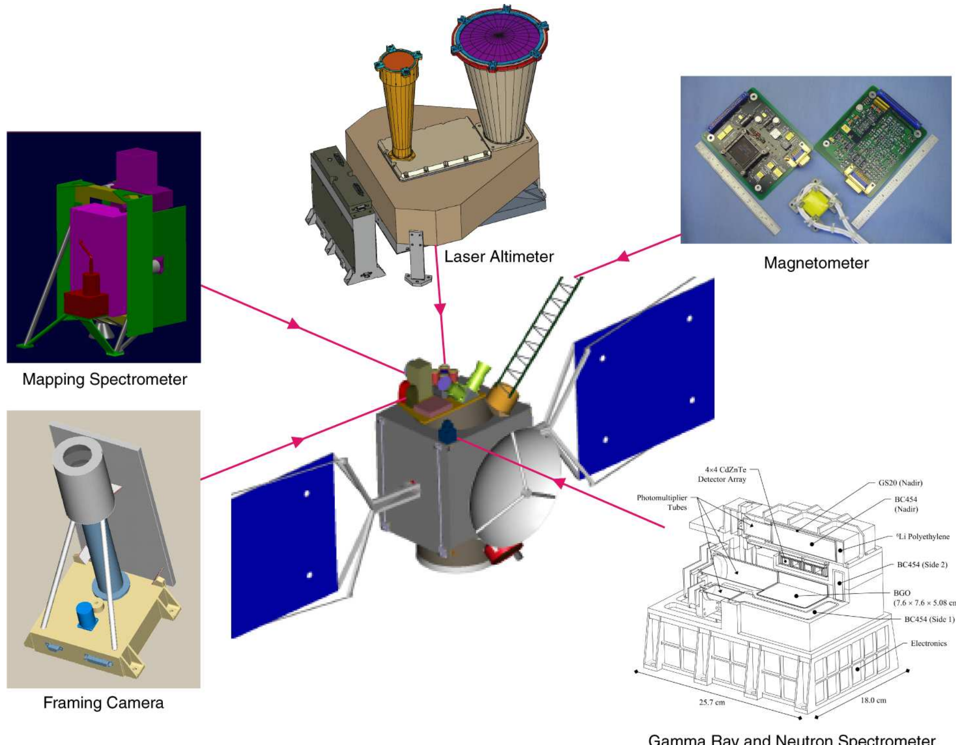

Figure 3

Figure 3. The Dawn payload.

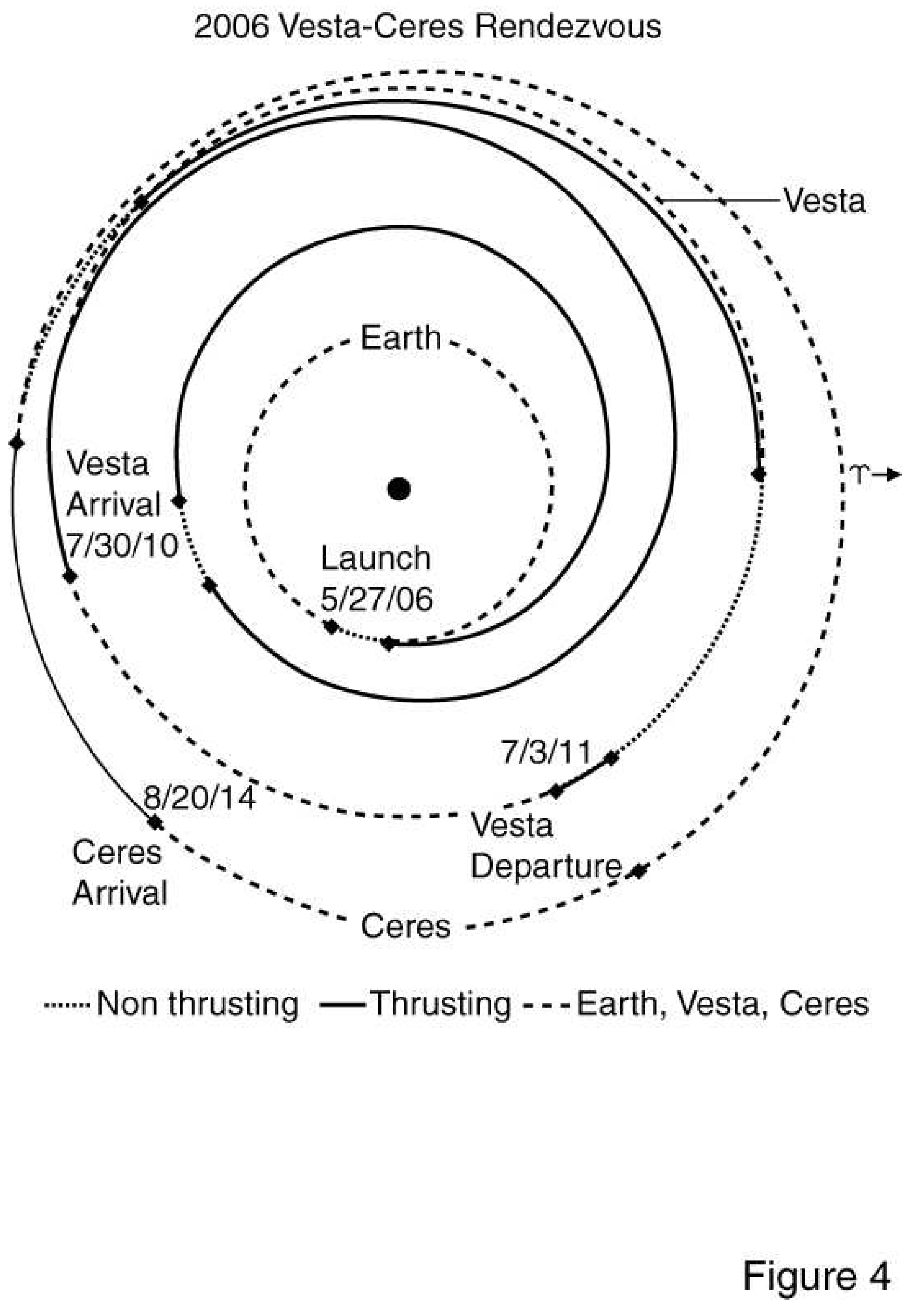

Figure 4. The Dawn trajectory.

3. Participation

There are numerous ways that the scientific community can participate meaningfully in the Dawn mission, in addition to the original selected core team. Presently, as the mission undergoes detailed design, we need to understand the illumination of the surface while the spacecraft is in orbit. This depends on an accurate knowledge of the axis of rotation of Vesta and Ceres. An improved knowledge of these directions would be most helpful to Dawn. Satellite searches would also be helpful, not simply so that Dawn could avoid hitting the satellite, but because the mass of the primary derived from the satellite's period would help definitize Dawn's trajectory analysis. Identifying features on Vesta and Ceres that need further study would be helpful. Characterizing targets of opportunity along the flight path to Vesta and Ceres is also important. Later in the program there will be a participating scientist program that will add scientists to the team as well as a data analysis program that will provide support for the analysis of data that will be rapidly entered into the public archives.

4. Concluding Remarks

Dawn is a most viable mission under active development and preparing to build hardware for a 2006 launch. It will provide exciting data to the community in 2010 and 2014. In the meantime it would benefit from the attention of the 1 AU observing community.

Acknowledgments. The Dawn mission receives its support from the German Space Agency, DLR, the Italian Space Agency, ASI, and the National Aeronautics and Space Administration under contract NASW-03006 at UCLA.

References

Jacobsen, S. B., 2003, Science, 300, 1513

Highlights of Astronomy, Vol. 13
International Astronomical Union, 2003
O. Engvold, ed.

Observations Of Small Solar System Bodies With GAIA

Francois Mignard

OCA/CERGA, France

The ESA space astrometry mission has a great potential of observation and discovery on the solar system objects. GAIA is due for launch in 2010 and the survey mission will last five years. In addition to accurate astrometry of about 1 billion stars, the mission will survey all solar system objects brighter than 20th magnitude, in astrometry and with multicolor photometry. Each object will be observed about a hundred times during the five year mission. It is expected that more than 500 000 asteroids will be repeatedly measured by the mission.

The main scientific output for the solar system physics will be a systematic search of NEOs, in particular inside the Earth orbit, a tremendous improvement in the orbit of the whole population of minor bodies, making all previous earth-based position almost obsolete in this respect, a full taxonomic classification made possible by the analysis of light over the 15 photometric bands, and the determination of ~ 100 masses of main belt objects thanks to the favorable close approaches during the period 2010-2015.

In this talk I will present the current status of the mission and the expected results for the solar system physics.

Highlights of Astronomy, Vol. 13
International Astronomical Union, 2003
O. Engvold, ed.

The ISHTAR Mission: Probing The Internal Structure Of NEOs

M. Antonietta Barucci

LESIA, Observatory of Paris

Paolo D'Arrigo

EADS Astrium, Stevenage

P. Ball

Open University

Alain Doressoundiram

LESIA, Observatory of Paris

Elisabetta Dotto

INAF, Osservatorio Astronomico di Roma

W. Kofman

Laboratoire de Planetologie de Grenoble

Roberto Orosei

IASF - INAF, Roma

Martin Patzold

Institut fur Geophysik und Meteorologie, Universitat zu Koln

Ettore Perozzi

Telespazio, Roma

Abstract. ISHTAR (Internal Structure High-resolution Tomography by Asteroid Rendezvous) is a mission developed through ESA General Studies programme. The study, led by Astrium in cooperation with several scientific institutes throughout Europe, has produced a spacecraft design capable of performing multiple asteroid rendezvous and to characterize them with a focussed set of instruments. The ISHTAR concept is centred around a Radar Tomography paylod able to probe the internal structure of a small asteroid to depths of few hundred meters, combined with a small camera for investigation of the surface properties and a radio science experiment for gravity field measurement. This combination will allow the first detailed characterization of a NEO and will give valuable insights into the origin and evolution processes that govern the NEO population. In particular, ISHTAR will be able to visit at least 2 NEOs belonging to two different spectral classes, thereby allowing us to probe the diversity of the NEO population.

1. Introduction

ISHTAR (Internal Structure High-resolution Tomography by Asteroid Rendezvous) is a mission proposed in response to ESA's recent call of ideas for NEO exploration and discovery. In particular, the focus of NEO space exploration is to collect the information necessary to develop strategies to protect our planet from future impacts (Morrison et al. 2003). The internal structure of NEOs is a key parameter in this respect, as it affects the likelihood of fragmentation when a force is applied to the asteroid.

ISHTAR will address key issues related to the threat NEOs pose to Earth: it will help assess the impact hazard, by providing the first data on the internal strength of NEOs, it will provide the basis for devising mitigation techniques, by helping to discriminate between destructive and deflective strategies and it will greatly advance our understanding of how NEOs form and collide with other planets.

2. Mission Objectives

The principal objective of the ISHTAR mission is to characterize all the physical parameters of an asteroid and in particular to investigate its internal structure. This is important to assess the impact hazard and to the development of effective mitigation strategies.

To determine how dangerous an asteroid is in case of impact, two parameters are crucial: the bulk mass, which determines the total energy of impact and the internal cohesion, which determines the likelihood of fragmentation in the atmosphere. To develop ways of deflecting or destroying an asteroid, again internal cohesion is a key parameter, because it determines the energy necessary to break it up into small fragments or the likelihood of fragmenting when trying to deflect it. Other important parameters both for scientific aim and for developing mitigation strategies are the asteroid surface properties, like depth of regolith, surface geology, spin, etc.

The main goal of ISHTAR is to determine those parameters that affect the internal cohesion of the asteroid. In particular, the radar tomographer will probe the internal structure, while the remaining payload will determine the mass, mass distribution, density and surface properties.

A high priority for the mission is to visit more than one asteroid, due to the high compositional diversity of the near-Earth asteroid population (Binzel et al. 2001). In particular, a large fraction of NEOs can be classified either as stony or carbonaceous, with significantly different density, composition and (presumably) internal structure. Therefore, the baseline ISHTAR mission is designed to visit 2 asteroids, one supposed to be similar to carbonaceous and one similar to stony material.

Finally, from a scientific perspective, knowledge of the surface mineralogy, when combined with the other key parameters listed above, would give invaluable insights into the origin and evolution of asteroids and will contribute to the study of the evolution of the solar system.

3. Payload

The Payload to assess all the key parameters mentioned earlier can be composed of a small complement of instruments, centred around a radar tomographer, essential to probe the interior of the asteroid.

The full set of instruments on board ISHTAR are:

- A Radar Tomographer to measure the internal structure
- A Radio Science Experiment to measure the asteroid gravity field (mass & mass distribution)
- A Multispectral Imager to measure the surface properties
- An IR Spectrometer to measure the surface mineralogy

The Radar Tomographer uses low-frequency radio waves that can penetrate deep inside solid rock, down to depths of hundreds or even thousands of meters. The depth of penetration is determined by the radar frequency and by the composition of the asteroid. On ISHTAR, the radar tomographer is used in a synthetic-aperture reflection mode, where the signal reflected off the asteroid is measured from a 'virtual' grid of locations around the object, allowing reconstruction of a 3D image of the asteroid interior. The spatial resolution of this 'SAR' radar is determined by the number of points in the grid and the frequency used. The ISHTAR radar tomographer, operating at two frequencies of 10 and 30 MHz, will be able to penetrate to depths of over 300m below the surface with spatial resolution of up to 10m (in length, width and depth).

The Radio Science Experiment utilizes the spacecraft communication systems to transmit and receive radio beacons from/to Earth. This will allow location of the spacecraft with respect to Earth to within a few meters and thereby reconstruction of the asteroid gravity field through the deflections in the spacecraft trajectory. The measurement is based on a Doppler Ranging technique that provides both the distance and the radial velocity of the spacecraft relative the Ground Station on Earth. The radio science experiment utilizes a dual X-band and Ka-band transmitter for the downlink signal and an X-Band receiver for the uplink. In addition an on-board Ultrastable Oscillatior (USO) provides a frequency reference. This way, ISHTAR will be able to measure the mass of the asteroid to within 0.5% and also to detect an asymmetric mass distribution in the asteroid interior.

The Multispectral Imager is based on a miniature CCD camera operating at visible wavelengths and provided with several broadband spectral filters to obtain colour information. This microcamera will map the surface of the asteroid to study its topology, geology and to measure the asteroid volume (necessary for the density determination). The camera will also be able to measure the asteroid rotation and to search for surface regolith. The ISHTAR camera will be able to resolve details of the order of 1.0 m and to determine density to within 2 % accuracy.

The IR Spectrometer will provide an IR spectrum of the asteroid surface in the wavelength region between 1.0 μm and 2.5 μm, which can be used to determine the mineralogical composition of the asteroid surface.

4. Mission and Spacecraft Design

The ISHTAR mission was designed to be sufficiently flexible to be able to access a wide range of targets. A pair of asteroids was specially selected for their scientific interest and used to size the mission, but in its current design ISHTAR is actually capable of reaching over 30 different asteroid pairs, leaving great flexibility for both target selection and choice of launch date. A Solar Electric Propulsion (SEP) system was selected as the one providing the best performance for this type of mission.

In the baseline mission ISHTAR will launch in September 2011 with a Dnepr rocket to reach asteroid (4660) Nereus after 3 years of interplanetary cruise. After a stay at Nereus of nearly 15 months during which extensive science measurements can be performed, ISHTAR will then transfer to asteroid (5797) Bivoj, which it will reach after another 2 years. After reaching Bivoj ISHTAR will repeat the same type of science measurement during a period of at least 3 months. The total mission duration is approximately 7 years. Many other possibilities are available.

While the radio science and imaging measurement can be performed at relatively high altitudes from the asteroid surface (10-20 km or more), the radar tomographer requires smaller distances, the lower the altitude the better. To avoid excessive perturbation of the spacecraft orbit by the (potentially highly irregular) asteroid gravity field, ISHTAR will still limit orbital altitude to about 2-3 km, where stable orbits exist. In fact, we have shown that even for a highly elongated asteroid with a 2:1 aspect ratio, it is possible to find stable orbits at 3 km altitude that are also synchronous with the Sun, avoiding the spacecraft going into eclipse. The good ground coverage also required by the radar can be achieved by placing ISHTAR into a near-polar orbit.

The ISHTAR spacecraft was designed to achieve its mission goals as a low-cost mission. To achieve this, the approach has been to keep the spacecraft small, while minimizing the spacecraft complexity. Whenever possible the design has used existing, 'state of the art' system, for the payload as well as the other spacecraft subsystems. In fact, all ISHTAR components are based on existing technology, with perhaps the exception of the radar tomographer, which is however still made of space-qualified components and it is an evolution of ground-based instrumentation.

Consistent with this low-cost approach, ISHTAR is baselined for an inexpensive Dnepr launcher and a launch mass of 408 kg, including 20% system margin. Note that this is well below the limit capacity of the Dnepr launcher, which is capable of delivering up to 860 kg into Earth escape. The total spacecraft dry mass is only 300 kg, with 25 kg of payload. A further mass saving of 20-30 kg is possible by the use of an Earth Gravity Assist maneuver in the mission design, which leads to significant propellant savings.

The spacecraft structure is based on an octagonal, wound monocoque structure in CFRP developed by Astrium Ltd, and capable of delivering high levels of robustness and stability at very low cost. The propulsion system utilizes 3 ion engines (1 redundant) providing up to 18 mN of thrust each. These engines require relatively large solar arrays providing 1600W of power. This, however, has the indirect advantage that plenty of power is available for telecommunications and the science instruments once ISHTAR reaches its target asteroids.

The communication systems is based on a dual X and Ka band transmitter and an X-band receiver working through a 1.0m diameter parabolic High Gain Antenna. The spacecraft is also equipped with a toroidal Medium Gain Antenna and two Low Gain Antennae, all working in X-band. This system allows downloading of science data at rates of over 1000 bps from distances of around 2.0 AU from Earth.

5. Conclusion

The ISHTAR mission has the potential to revolutionize our understanding of Near-Earth Objects and to provide us with the information needed to develop strategies to protect the Earth. The combination of instrument and multiple rendezvous will allow the first detailed physical characterization of the NEO population. The whole mission is possible within the constraint of a small spacecraft (408kg) and the financial envelope of an ESA 'flexi' mission (150 MEuros).

Within a relatively inexpensive package and a short implementation phase, ISHTAR will finally be able to answer key questions about these mysterious objects that have a long history of interaction with our planet. In so doing, ISHTAR will help us to have the means, of protecting ourselves from this NEO threat.

ISHTAR is one of the several studies (Simone, Don Quijote, Earthguard 1, Euneos, Remote Observing) financed by ESA, aimed to improve the knowledge of NEOs as potential hazardous asteroids. A mission to NEOs can be optimized merging some of these different concepts. These studies show that the scientific community is ready to endorse a mission to NEOs as soon as ESA or a national space agencies will consider it.

References

Binzel, R. P., Harris, A. W., Bus, A. W., and Burbine, T.H. 2001, Icarus, 151, 139.

Morrison, D., Harris A. W., Sommer, G., Chapman, C. R., and Carusi, A. 2003, in Asteroids III, ed. W. F. Bottke, A. Cellino, P. Paolicchi & R. B. Binzel (Univ. of Arizona Press, Tucson), 739.

Highlights of Astronomy, Vol. 13
International Astronomical Union, 2003
O. Engvold, ed.

A Target For Rosetta

Rita Schulz

Research and Scientific Support Department of ESA, ESTEC, Postbus 299, 2200 AG Noordwijk, The Netherlands

Abstract. Comet 67P/Churyumov-Gerasimenko has been chosen as the new target of the Rosetta mission. A concise overview of the basic properties of the new target comet is given.

1. Introduction

ESA's Rosetta mission is the first comet mission that will not only fly-by a comet nucleus. Rosetta will go in orbit around the nucleus to investigate its evolution along a major part of its orbit and land on it to obtain in-situ information of the surface and subsurface composition and physical properties. It was originally scheduled to launch to Comet 46P/Wirtanen in January 2003. However, as the launch had to be delayed owing to unforeseen problems with the launch vehicle, the original launch window closed and alternative mission opportunities had to be found. Comet 67P/Churyumov-Gerasimenko has now been identified as the new Rosetta target and the mission is scheduled for launch in February 2004. However, before this decision could be taken, a number of basic properties of the new target comet had to be determined to ensure that the rendezvous and landing on the nucleus will be successful. The design of the scientific instruments on board the Orbiter as well as the design of the landing scenario had been optimized to the characteristics of 46P/Wirtanen, as determined from ground. Consequently, the properties of the new target comet, particularly its size and activity had to be within the range required to guarantee the feasibility of the mission and an optimal scientific return. Comet 67P/Churyumov-Gerasimenko was therefore extensively observed between February and June 2003. The major results of these observations will be summarized here.

2. Monitoring Comet 67P/Churyumov-Gerasimenko

A huge amount of observations of Comet 67P/Churyumov-Gerasimenko was obtained in 2003, after it was announced to be the likely new target for Rosetta. The most complete monitoring was conducted at the European Southern Observatory, where the comet was observed on 11 nights between 11 February and 26 June 2003. Broad-band BVR images and low-resolution long-slit spectra were obtained at the ESO Very Large Telescope as well as the 3.6m Telescope for morphological, colour and compositional analysis of the coma and for studying the evolution of the comet's activity along the postperihelion orbit between 2.29 AU and 3.22 AU. In May 2003 the observational strategy was specifically adjusted to obtain data suitable for the analysis of the rotational properties of the nucleus. A summary of the observations is given in Table 1.

Table 1. Postperihelion Monitoring from ESO in 2003

Date	Telescope	Type of Observation	r_h [AU]
10/11 Feb	3.6m	BVR imaging + spectroscopy	2.29
8/9 Mar	3.6m	BVR imaging + spectroscopy	2.49
30 Apr - 4 May	VLT	BVR imaging + spectroscopy	2.85-2.88
3-4 June	VLT	BVR imaging	3.08
19-20 June	VLT	BVR imaging	3.18
23-26 June	VLT	BVR imaging	3.21-3.22

3. Characteristics of Major Relevance

Although they have not yet been completely evaluated the observations obtained in 2003 already resulted in a number of new findings that were vital to determine the basic characteristics of Comet 67P/Churyumov-Gerasimenko. Those most important in view to the selection of this comet as the new target for the Rosetta mission are briefly summarized. 67P/Churyumov-Gerasimenko showed a major drop of activity between 2.5 AU and 2.9 AU. The dust production rate (in $Af\rho$) decreased by more than a factor of two and the CN production rate decreased by about one third. This confirms that although the comet is more active than 46P/Wirtanen when closer to the sun (i.e. its dust production at 2.3 AU is about 1.5 times that of 46P/Wirtanen) the activity of both comets is very similar at around 3 AU, which is the heliocentric distance at which the Lander will be deployed onto the nucleus surface. The effective radius of the comet nucleus was determined to be 1.98 ± 0.02 km from HST observations obtained in March 2003 (Lamy et al., 2003). With the above information it could be confirmed that a safe landing is possible also on the nucleus of Comet 67P/Churyumov-Gerasimenko. Lamy et al. (2003) inferred a rotation period of 12.3 ± 0.27 hours on the basis of the HST observations obtained in a time interval of 12 hours. The detailed analysis of the ground based monitoring data that have been dedicated to the determination of the rotational properties is still under way. The comet displayed various distinct features in the coma as well as an anti-tail which can be used to determine, or at least constrain, some basic properties of the nucleus, such as its rotational properties and the number and location of active regions on the nucleus' surface.

4. Conclusions

Comet 67P/Churyumov-Gerasimenko is not only a suitable target for the Rosetta mission, but actually a very interesting one. In contrast to 46P/Wirtanen, this comet exhibits distinct coma features (jet structures) similar to those of Comets 1P/Halley and 19P/Borrelly, the only two comets for which images of the nucleus exist. Hence, Rosetta will be able to proof whether such structures are indeed a direct result of the nucleus being divided in active and inactive regions. Observations during previous apparition have already shown that Comet 67P/Churyumov-Gerasimenko shows a seasonal effect when it passes its perihelion. Such an effect has generally been attributed to a new active region being exposed to sunlight. The new mission scenario of Rosetta foresees a monitoring of its target not only during its preperihelion phase, but through perihelion passage and along a significant part of its postperihelion orbit. Therefore, Rosetta will not only be able to study the development of cometary activity at large distances, but also very close to the sun, i.e., when the seasonal effect occurs.

Acknowledgments. A huge amount of support was received by individual scientists and observatories in the effort to define the new target comet of the Rosetta mission. ESO and HST granted Directors Discretionary Time on short notice, which is gratefully acknowledged.

References

Lamy, P. L., Toth, I., Weaver, H., Jorda, L., & Kaasalainen, M. 2003, BAAS, 35, 970

Highlights of Astronomy, Vol. 13
International Astronomical Union, 2003
O. Engvold, ed.

The Deep Impact Project

Michael F. A'Hearn

Department of Astronomy, University of Maryland, College Park MD 20742 USA

The Deep Impact Project Team

Abstract. The Deep Impact mission aims at understanding the third dimension of a cometary nucleus, the physical and chemical properties as a function of depth below the surface. General wisdom holds that comets, because they are small and spend most of their lives far from the sun, hold primordial ices in their interiors. However, it is universally agreed that the surface layers have evolved, whether from cosmic rays while residing in the Oort cloud or from solar heating during previous perihelion passages. Clearly, in order to interpret surface observations and outgassing, we must understand how the surface layers differ from the interior. Deep Impact is the first mission to carry out a macroscopic experiment on a planetary body since the Apollo program dropped a lunar module on the moon and measured the seismic response.

1. The Mission

Deep Impact consists of two spacecraft, launched together on 30 Dec 2004 And flying together until one day before impact on 4 July 2005. On 3 July the two spacecraft separate very gently and are both on course to impact Comet 9P/Tempel 1 at 10.2 km/s, approaching at phase angle 63°. The impactor, with dry mass 360 kg, immediately goes into auto-navigation mode ensuring that it will impact the comet in an illuminated area. Images from the Impactor Targeting Sensor (ITS) are analyzed on board for navigation and transmitted to the flyby spacecraft, which transmits the images to Earth in its regular telemetry. The ITS is not expected to survive the dust in the coma unscathed, serious damage to the primary mirror being expected at some time within the last minute before impact, long after all auto-navigation has ceased. If the camera on the impactor continues to take images until impact, it will provide a series of images analogous to the series taken by the Ranger spacecraft impacting on the moon, the last having a resolution of order 20 cm.

Meanwhile, when impactor and flyby have separated by ~ 100 m, the flyby spacecraft decelerates by ~ 100 m/s and diverts by ~ 6 m/s. This allows the flyby to pass 500 km below the nucleus (as seen from the sun) and provides a window of 850 sec between impact and closest approach. The flyby has a Medium Resolution Instrument (MRI) for imaging and a High Resolution Instrtument (HRI) that uses a dichroic beamsplitter to provide both optical imaging and also $1 - 5$ μm spectroscopy. The instruments are body-mounted, the spacecraft rotating to follow the comet as it flies by. Since the largest uncertainty in the position of the comet relative to the spacecraft is the down-range distance, the flyby spacecraft measures its rotation to estimate the distance to the comet and thus predict the time of impact. This time is transmitted to the impactor and is used on both impactor and flyby to optimize the data-taking sequences.

From impact until 50 seconds before closest approach (14 min after impact), the spacecraft takes all the crucial data, including high-speed imaging and spectroscopy of the impact event itself, images of the nucleus at various resolutions and in all filters, infrared spectral maps of both the nucleus, and the innermost coma. The last images will be taken at a range of 700 km, about 50 seconds before closest approach, and the high-resolution images at this point will have a spatial scale of 1.4 meters per pixel (the point spread function is near 2 pixels).

By the time the flyby spacecraft has reached 500 km before closest approach, it has rotated 45°and the slew rate is too fast to accurately track the comet. The flyby spacecraft freezes at this position, which is designed to optimize the protection of the spacecraft and instruments from dust damage at closest approach. When the spacecraft has safely transited the inner coma, it turns again and views the other side of the nucleus.

2. The Expected Phenomena

The goal of Deep Impact is to understand the physical and chemical properties of the near-surface layers of a cometary nucleus. This enables study of the differences in composition and structure with depth and thus of the evolution of surface layers due to heating at previous perihelion passages. However, we know so little about the physical structure of the surface layers that cratering experts have a wide range of mutually inconsistent predictions based on different assumptions about which physical processes will matter. Our own team thinks that local gravity will control the formation of the late stages of the crater, i.e., that material will continue to flow out of the crater until it gets to material moving so slowly that it can not reach the rim of the crater before falling back. Other experts favor ultimate control by compression of weak (but not totally strengthless) material, while yet others predict that the strength of porous ice will control the formation of the crater. This range of physical processes, coupled with the uncertainty in key parameters such as the value of local gravity, lead to predictions for the crater diameter ranging from > 200 m down to < 10 m, our favored prediction being somewhat larger than 100m in diameter and 25 to 30m deep. The personal opinion of the PI is that the three concepts above are given in order of decreasing probability. Other predictions of the phenomenology include suggestions that the impactor will just bury itself very deeply in the nucleus (implying very low density for the nucleus), breaking a piece off the nucleus, shattering the nucleus into many pieces, and even passing all the way through the nucleus. These are also in decreasing order of probability, in the PI's personal opinion, with the most likely of these (burial of the impactor) being at least as likely as strength-dominated cratering. This wide range of possible outcomes is the primary reason that such a conceptually simple experiment as Deep Impact is an important one.

There are many other aspects to the phenomenology as well. For example, many of predictions imply an initial, very bright flash, with the strength or even the existence of the flash depending on details of the cometary structure. The true, cratering predictions (the first three above) coincide with three very different morphologies for the ejecta cone. Given that the surface of the comet is thought to be mostly inactive, the impactor will likely land in an inactive area and thus a plausible outcome is that the crater will become a new, active area. This new active area may lead to long-lasting outgassing in a jet over days, weeks or even months after the impact.

Using our prediction of crater volume and timescale, we crudely estimate, with many caveats, the the impact will eject into the coma as much material in 4 minutes as is released in a month of ambient cometary activity. If it is ejected as grains with a size distribution similar to that of ambient dust, the comet could easily become visible to the naked eye from Earth within minutes.

3. Spacecraft Instrumentation & Earth-based Observations

Although small by the standards of NASA's Great Observatories, HRI will be the largest telescope/camera ever flown on an interplanetary mission, with 2 μrad/pix. The IR spectrometer is aimed at studying the spectral reflectivity of the nucleus and dust, the thermal emission of the nucleus and dust, and the emission bands of the most abundant volatiles, H_2O, CO, and CO_2. It uses a 2-prism design for high throughput and elimination of order overlap. The very non-linear resolving power ($R = \lambda/\delta\lambda$) varies from 750 at 1.05 μm through a minimum of about 220 near 2.5 μm and back up to 400 at 4.8 μm. The filters on HRI are aimed at spectral reflectivity maps. At the time of the last images before flyby, the nucleus will be significantly larger than the field of view of HRI. The MRI has a 5× larger scale and 5× larger field of view to include the entire nucleus at the end of pre-flyby imaging. MRI includes a subset of the HRI filters and narrower-band filters to isolate emission bands and continuum. The Impactor Targeting System (ITS) is identical to MRI except that the filter wheel is omitted.

The impact will take place on 4 July 2005, at an adjustable time in the Period 06:00-06:30 UT, when the comet is at $(\alpha, \delta) = (13\text{h}38\text{m}, -9.6^\circ)$, near the star Spica. The impact will be observable high in the sky after end of nautical twilight from Hawaii and New Zealand and lower in the sky in total darkness from southwestern US and Baja California. It will be observable in daylight from Australasia. Since phenomena related to the impact are expected to continue for at least several days, Earth-based observations are desired with nearly continuous coverage from several days before impact through weeks after perihelion. The uncertainty in the predicted phenomenology emphasizes the need for observations of all possible types and at all possible wavelengths.

Further details of the mission are at http://deepimpact.umd.edu. A web page for collaborating observers will be linked in the last quarter of 2003, providing background information for observers to assist in planning observations. and allowing data entry regarding observing programs to enable individual observers to best complement other observations that are being made. We acknowledge support from NASA and from a large team of people.

Highlights of Astronomy, Vol. 13
International Astronomical Union, 2003
O. Engvold, ed.

ISO: Asteroid Results And Thermophysical Modelling

Thomas G. Müller

Max-Planck-Institut für Extraterrestrische Physik, Giessenbachstrasse, 85748 Garching, Germany

Abstract. Through a recently developed thermophysical model, observations from the Infrared Space Observatory (ISO) were combined with visual photometry, lightcurves, close-up observations and direct measurement. In this way, many applications were possible, ranging from simple diameter and albedo determination of serendipitously seen asteroids to sophisticated studies of mineralogic aspects and regolith properties, like emissivity, roughness or thermal inertia for well-known asteroids. The possibility to combine all sources of information in one single model lead also to a better understanding of thermophysical effects, like beaming or the before/after opposition effect. Thus, the mineralogic signatures can be recognized easier and asteroid data from infrared surveys and individual IR photometry can be interpreted more accurately, even in cases where shape or rotational behaviour are not known. Some well-studied asteroids are now even considered as excellent far-infrared calibrators.

1. ISO and the Thermophysical Model (TPM)

ISO (Kessler et al. 1996) observed between 1995 and 1998 more than 40 asteroids in great detail, including some complete spectra from 2 to 200 micron and large samples of photometric measurements (Müller 2003). The main goals of the about 100 hours of asteroid observing time were: the identification of surface minerals, composition, connection to meteorites and comets, surface alteration processes and the interpretation of taxonomic classes through the identification of mid-infrared features of well-known minerals and meteorites.

In parallel to the ISO mission, Lagerros (1996, 1997, 1998) developed new modelling concepts for the description of asteroids. Müller & Lagerros (1998, 2002) later on combined the modelling efforts with a large variety of thermal observations from ground-based, air-borne and space-based projects to establish a self-standing powerful thermophysical model (TPM). This TPM was the basis for the interpretation of most of the ISO asteroid observations. The key to the successful applications was its capability to combine all available information for one asteroid (e.g., spin vector, shape, size, albedo, H-G values, ...) with the full observational information coming from ISO. In that way, it is now possible to analyse regolith properties, emissivity behaviour, thermal inertia or to improve size and albedo values (e.g., Müller 2002). The TPM facilitates also the interpretation of thermal spectroscopic measurements with respect to mineralogic and meteoritic studies (e.g., Dotto et al. 2002a).

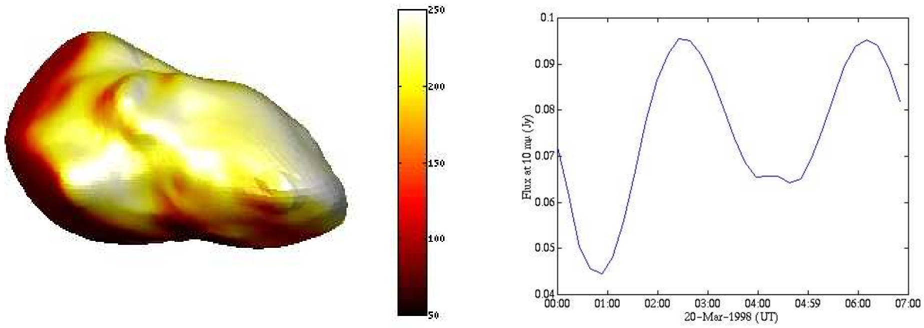

Figure 1. TPM of 951 Gaspra and a predicted thermal lightcurve at 10 μm (Credit: J. Lagerros; Shape model: Thomas et al. 1994).

2. Results and Discussion

Different examples of TPM applications are illustrated in Figs. 1 and 2. The temperature calculation (Fig. 1, left) assumes a default thermal behaviour of a regolith covered surface (Müller et al. 1999). The following TPM predictions are possible: Thermal lightcurves at any given thermal wavelength (Fig. 1, right), disk-integrated spectral energy distributions from 5 μm to the mm-wavelength range for any given time (Fig. 2, left), and multi-epoch/-wavelengths monochromatic or filter band fluxes (Fig. 2, right).

This kind of modelling in comparison with thermal infrared observations provide nice insights into the regolith properties and the emissivity behaviour of the surface material (e.g. Müller & Lagerros 1998; Müller 2002; Müller & Blommaert 2003). The infrared beaming effect, caused by surface roughness/porosity influences, can now be studied and understood (Lagerros 1996, 1998). The before/after opposition effect, caused by rotation in combination with the non-zero thermal inertia, can be calculated and treated in a correct way. The accurate description of the thermal emission for well-known large main-belt asteroids through the TPM even lead to their use as reliable photometric standards in the far-infrared, where good calibrators are scarce (Müller & Lagerros 2002, 2003).

The interpretation of ISO's spectroscopic measurements also benefited from detailed thermal continuum modelling: Dotto et al. (2000; 2002b) and Barucci et al. (2002) investigated silicate features and searched for similarities with meteoritic samples. In all three studies the TPM supported the difficult analysis of low level broad band emission structures on top of the modeled continuum.

A comparison between the Standard Thermal Model (STM; Lebofsky et al. 1986) and the TPM revealed limitations and problems of the STM in analysing multi-epoch and -wavelengths observations. Müller & Blommaert (2003) found wavelengths and phase angle dependent diameter/albedo values with the STM, whilst the TPM produced unique solutions.

References

Barucci, M. A., Dotto, E., Brucato, J. R. et al. 2002, Icarus, 156, 202

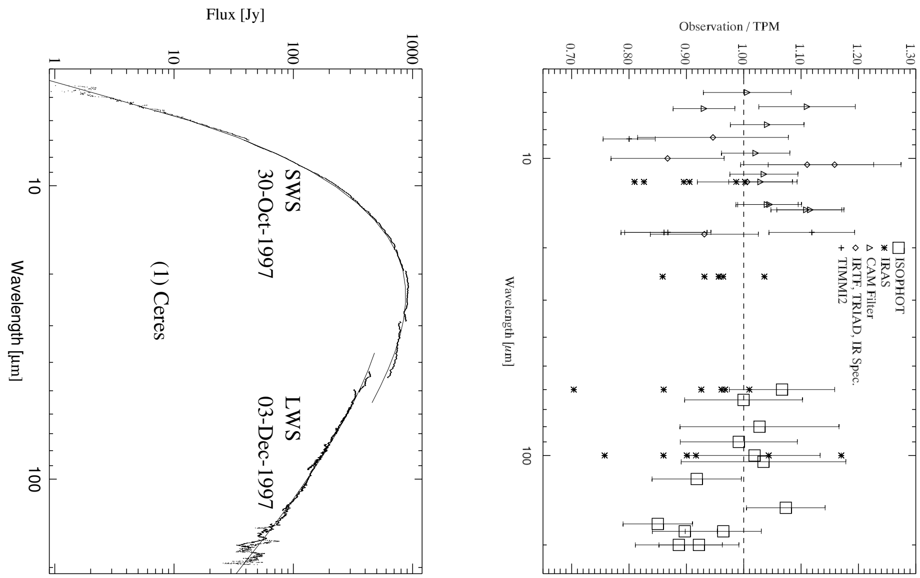

Figure 2. Left: The asteroid 1 Ceres: ISO observations and TPM predictions (solid lines) (Müller 2002). Right: 65 Cybele observation over model ratios for different photometric measurements plotted against the corresponding wavelengths (Müller & Blommaert 2003).

Dotto, E., Müller, T. G., Barucci, M. A. et al. 2000, A&A, 358, 1133

Dotto, E., Barucci, M. A., Müller, T. G. et al. 2002a, in Asteroids III, eds. W. Bottke, A. Cellino, P. Paolicchi et al., University of Arizona Press, 219

Dotto, E., Barucci, M. A., Müller, T. G. et al. 2002b, A&A, 393, 1065

Kessler, M. F., Steinz, J. A., Anderegg, M. E. et al. 1996, A&A, 315, L27

Lagerros, J. S. V. 1996, A&A, 310, 1011

Lagerros, J. S. V. 1997, A&A325, 1226

Lagerros, J. S. V. 1998, A&A332, 1123

Lebofsky, L. A., Sykes, M. V., Tedesco, E. F. et al. 1986, Icarus, 68, 239

Müller, T. G. & Lagerros, J. S. V. 1998, A&A, 338, 340

Müller, T. G., Lagerros, J. S. V., Burgdorf, M. et al. 1999, in "The Universe as Seen by ISO", eds. P. Cox & M. F. Kessler, ESA SP-427, 141

Müller, T. G. & Lagerros, J. S. V. 2002, A&A, 381, 324

Müller, T. G. 2002, Meteorit. Plan. Sci., 37, 1919

Müller, T. G. & Lagerros, J. S. V. 2003, in "The Calibration Legacy of the ISO Mission", eds. L. Metcalfe et al., ESA SP-481, 157

Müller, T. G. 2003, in "Exploiting the ISO Data Archive – Infrared Astronomy in the Internet Age", ed. C. Gry et al., ESA SP-511, 47

Müller, T. G., Blommaert J. A. D. L. 2003, A&A, in press

Thomas, P. C., Veverka, J., Simonelli, D. et al. 1994, Icarus, 107, 23

Highlights of Astronomy, Vol. 13
International Astronomical Union, 2003
O. Engvold, ed.

Ground-Based Optical Observations Of Asteroids

Alberto Cellino

INAF – Osservatorio Astronomico di Torino, strada Osservatorio 20, 10025 Pino Torinese (TO), Italy

Abstract. Many physical parameters of asteroids can be inferred from remote measurements at optical wavelengths. These observations constitute the bulk of the information we have about these objects, and nicely complement the detailed physical studies which are made possible by in situ explorations of a few selected targets. The discovery of many binary systems for which mass determinations become possible, the identification of hydration features in asteroid spectra, including unexpectedly many M-types, the detection of space-weathering phenomena affecting S-type near-Earth objects, as well as improved estimates of sizes, albedos, and spin properties for many objects are among the major results obtained in recent years by means of remote-sensing techniques. These data can be used to infer important properties of the internal structures of the asteroids.

1. Introduction

Remote observations by means of ground-based instruments and orbiting detectors have been for a long time the unique source of information about all kinds of asteroids. Starting since the successful detection of Gaspra and Ida by the Galileo spacecraft, however, automatic space probes begun to provide a wealth of new information, including images at the highest possible resolutions and a wide variety of data by means of different detectors. At present, missions aimed at collecting and bringing back to Earth direct samples of asteroidal material are under way (Hayabusa mission) and this can possibly lead to another major step forward in our understanding of asteroids.

All this does not mean, however, that in the modern era of space missions remote observations are became obsolete. In spite of the spectacular results obtainable by means of space probes, short-distance observations cannot be expected to be performed but for a tiny sample of the whole asteroid population. The data obtained by space probes are invaluable to produce detailed understanding of a few selected bodies, but equally important is the fact that in situ exploration are a wonderful tool to confirm, reject or modify some previous interpretations of remote-sensing data. In this way, an improved reliability of the conclusions based on ground-based observations can be achieved, leading to a much better understanding of asteroidal bodies.

In turn, remote-sensing data are essential for a successful planning of space missions and for the identification of the most important targets, which are normally chosen according to criteria based on available observational evidence. Ground-based observations are also usually needed as an invaluable support during and after a space mission. In this sense, we can conclude that remote sensing and in situ exploration nicely complement each other in our attempt to improve our understanding of the origin, evolution and current physical properties of the asteroid population.

In what follows, I give a forcedly short summary of some recent results of ground-based observations of asteroids at optical wavelengths, using a wide variety of techniques. Several groups in different countries are at work, and the results of all these activities open new paths of investigation, and are the basis for further developments, both on the observational and on the theoretical side, in the next years. All the new ideas which are emerging will undoubtedly influence the concepts and designs of future space missions to asteroids.

This paper is organized in different Sections, each one being devoted to recent activities and results obtained by a different technique.

2. Photometry

Lightcurve photometry has been historically one of the main tools to derive physical information since the early times of modern asteroid science.

The main goals of these observations have been traditionally the measurement of the spin period and the derivation of the spin axis direction. In spite of the presence of problems of uniqueness of the solutions, lightcurve data have long been proven to be sufficient to derive reasonable estimates of the overall shapes of the objects at least in some favourable cases, when a sufficient number of lightcurves collected at different oppositions are available. A good example of this was the computation of the overall shape of 951 Gaspra before the Galileo fly-by (Barucci et al. 1992). Even before, a general model of the flattening and albedo spot was obtained for asteroid 4 Vesta by Cellino et al. 1987. This model has been largely confirmed by direct HST images collected ten years later (Thomas et al. 1997).

The situation in the field of lightcurve inversion has significantly improved in more recent years through the development of more sophisticated mathematical techniques (Kaasalainen, Mottola and Fulchignoni 2002).

An important contribution of lightcurve studies to the general understanding of asteroid internal structures comes from an analysis of the distribution of the rotation periods as a function of the objects' sizes. As extensively discussed by Pravec, Harris and Michalowski (2002) it turns out that practically all objects, down to sizes of a few km, have spin periods below the fission limit for rubble piles. This fact is interpreted as a major proof that asteroids are not monolythic down to sizes of less than 10 km.

Further recent developments in the field of asteroid photometry include the identification of asteroid binaries through discovery of multiple periodicities (Pravec et al. 2002; Merline et al. 2002). In some cases (like asteroid 2000 DP107) lightcurve photometry has confirmed binaries originally discovered by means of radar experiments (Ostro et al. 2002).

The most recent impressive result of lightcurve photometry has been the discovery of a bimodality in the spin axis orientation of several members of the Koronis family (Slivan et al. 2003). Such a finding can have potentially important implications for our understanding of family-forming events and for the determination of family ages.

3. Spectroscopy

Asteroid spectroscopy has been traditionally the most important tool to derive qualitative information on the likely surface composition of the objects. Recently, a major observational effort has been the SMASS II spectroscopic survey (Bus & Binzel 2002; Bus, Vilas & Barucci 2002). Among the major results of this survey, we can quote a new taxonomic classification based on reflectance spectra, and the discovery that asteroid families tend to be quite homogeneous in terms of spectroscopic properties. This fact has important implications for the collisional evolution models, as pointed out by Cellino et al. (2002).

Another important result in the field of family spectroscopy has been the identification of former members of the big Eos family, which are now trapped in the 9/4 mean-motion resonance with Jupiter, and are observed during the early stages of an evolution which will decouple them from the asteroid Main Belt (Zappalà et al. 2000).

An unexpected and very important discovery has been the identification of spectroscopic bands diagnostic of hydration in the reflectance spectra of a large fraction of M-type asteroids (Rivkin et al. 2002). Since hydration is not thought to be compatible with the traditional interpretation of M-type asteroids as metal-rich stripped cores of differentiated parent bodies, these observational findings lead us to reconsider our interpretation of M-type asteroids, although other pieces of evidence, like radar data, confirm that at least in some cases we actually deal with metal-rich bodies.

Finally, a major step forward in our understanding of the origin of Ordinary Chondrites from S-type asteroids, a long debated subject, came from the discovery by Binzel et al. (2001) that S-type near-Earth asteroids tend to "fill the gap" between typical spectra of ordinary chondrites and spectra of S-type asteroids observed in the Main Belt. The interpretation is that such a diversity of spectral behaviour is likely due to different times of exposure to space-weathering phenomena. NEAs have short dynamical lifetimes, and they may be in many cases collisional debris only recently injected into resonant orbits leading them into the inner Solar System. If this is true, their surfaces may be on the average much younger than objects observed in the Main Belt. On the other hand, even if the supply of NEAs takes place over much longer time scales (dynamical diffusion, Yarkovsky effect) it is still true that the collisional lifetimes of small asteroids like the NEAs observed by Binzel et al. 2001 are shorter than those of bigger asteroids like those that are observed in the Main Belt. Thus, NEA surfaces are expected to be on the average younger and less weathered.

4. Polarimetry

Asteroid polarimetry has been used in the past to infer information about the likely properties of surface regolith, and to derive asteroid albedos and sizes (Dollfus et al. 1989) through analysis of the phase - polarization curves.

Since some years, a long-term observational campaign is carried out at the Complejo Astronomico El Leoncito (Argentina), in order to determine the albedo of relatively small asteroids (diameters below 50 km) whose sizes and albedos had been previously determined based on IRAS radiometric observations. The reason is that there is an apparent difference between the distribution of IRAS-derived albedos for objects of different sizes, and it is not clear if this is a real phenomenon, or it is an artifact of the limits in sensitivity of the IRAS detectors. Preliminary results of the polarimetric campaign show evidence of a small systematic difference between IRAS and polarimetric albedos, although important discrepancies have been found only in a couple of cases (Cellino et al. 1999, and Cellino et al. in preparation).

In addition to the above mentioned results, some observational effort is also currently devoted to the possible identification of a polarimetric "opposition effect", although the data collected so far are not yet conclusive. What seems certain, is that merging the evidence coming from polarimetric data and photometric phase curves can be important to derive improved understanding of the light scattering on asteroid surfaces (Muinonen et al. 2002; Kaasalainen et al. 2003).

5. High-resolution imaging

One of the major step forward in asteroid science in recent years has certainly been the discovery of a relevant number of binary systems. Here, we deal with results obtained by means of conventional observations at optical wavelengths, then I will not mention binary discoveries obtained by means of radar experiments (for this, see Ostro et al. 2002).

A review of binary discoveries by means of high-resolution imaging is given by Merline et al. (2002). It is clear that binaries give us unprecedented chances to derive asteroid masses, through measurements of the orbits of the binary components.

More in general, technical improvements of the detectors, and the availability of increasingly larger telescopes are steadily shifting down the size limit for which asteroids are essentially point-like sources. This certainly opens new perspectives to asteroid science. In addition to Adaptive Optics observations, also the more traditional speckle interferometry technique has been recently applied to the determination of asteroid sizes and shapes (Cellino et al. 2003).

6. Astrometry

Astrometry, with the determination of asteroid orbits, is the oldest tool of asteroid science. In recent years we have seen a huge enhancement of the asteroid discovery rate, mainly as a consequence of surveys devoted to the discovery of potentially hazardous objects (Stokes, Evans & Larson 2002). On the other hand, another independent achievement has been the development of improved dynamical models and algorithms for the computation of asteroid proper elements (Knežević, Lemaître & Milani 2002). A consequence of this, is that now we have huge data-sets of asteroid proper elements which can be used to identify asteroid families. An example of a discovery made possible by this, is the discovery of the small and apparently very young Karin family (Nesvorný et al. 2002).

7. Conclusions

The results shortly described in the above Sections show that asteroid science is currently very active, and major step forward in the understanding of the asteroid populations have been done or are imminent.

The impressive body of observational evidence obtained by means of remote observations at optical wavelengths shows that these observations are and will be absolutely needed for further advancements. Some problems are also present and deserve a careful attention in the near future. An example is the significant discrepancy between the asteroid inventory at small sizes, as resulting from visible observations from the ground (SDSS, Yoshida) and from thermal infrared observations from space (Tedesco & Désert 2002). Of course, this is a critically important point, since the inventory and size distribution of the objects are primary constraints for any attempt at modelling the overall collisional evolution of the asteroid population.

Some other contradictory evidence comes from the NEAR in situ exploration of asteroid 433 Eros. In particular, it seems that this object is a largely consolidated body (Cheng 2002), and this can be a problem in the framework of recent ideas about the internal structures of the asteroids (gravitational aggregates down to small sizes, as mentioned in the Section devoted to asteroid Photometry).

Solving these problems will require further observations, both from remote instruments and in situ.

References

Barucci, M. A., Cellino, A., De Sanctis, C., Fulchignoni, M., Lumme, K., Zappalà, V., & Magnusson, P. 2002, A&A266, 385

Binzel, R. P., Harris, A. W., Bus, S. J., & Burbine, T. H. 2001, Icarus 151, 139

Bus, S. J., Vilas, F., & Barucci, M. A. 2002, in Asteroids III, ed. W. F. Bottke, A. Cellino, P. Paolicchi & R. P. Binzel (University of Arizona Press), 169

Bus, S. J., & Binzel, R. P. 2002, Icarus 158, 146

Cellino, A., Zappalà, V., Di Martino, M., Farinella, P., & Paolicchi, P. 1987, Icarus 70, 546

Cellino, A., Gil Hutton, R., Tedesco, E. F., Di Martino, M., & Brunini, A. 1999, Icarus 138, 129

Cellino, A., Bus, S. J., Doressoundiram, A., & Lazzaro, D. 2002, in Asteroids III, ed. W. F. Bottke, A. Cellino, P. Paolicchi & R. P. Binzel (University of Arizona Press), 633

Cellino, A., Diolaiti, E., Ragazzoni, R., Hestroffer, D., Tanga, P., & Ghedina, A. 2003, Icarus 162, 278

Cheng, A. F. 2002, in Asteroids III, ed. W. F. Bottke, A. Cellino, P. Paolicchi & R. P. Binzel (University of Arizona Press), 351

Dollfus, A., Wolff, M., Geake, J. E., Lupishko, D. F., & Dougherty, L. M. 1989, in Asteroids II, ed. R. P. Binzel, T. Gehrels, & M. S. Matthews, (University of Arizona Press), 594

Kaasalainen, M., Mottola, S., & Fulchignoni, M. 2002, in Asteroids III, ed. W. F. Bottke, A. Cellino, P. Paolicchi & R. P. Binzel (University of Arizona Press), 139

Kaasalainen, S., Piironen, J., Kaasalainen, M., Harris, A. W., Muinonen, K., & Cellino, A. 2003, Icarus 161, 34

Knežević, Z., Lemaître, A., & Milani, A. 2002, in Asteroids III, ed. W. F. Bottke, A. Cellino, P. Paolicchi & R. P. Binzel (University of Arizona Press), 603

Merline, W. J., Weidenschilling, S. J., Durda, D. D., Margot, J. L., Pravec, P, & Storrs, A. D. 2002, in Asteroids III, ed. W. F. Bottke, A. Cellino, P. Paolicchi & R. P. Binzel (University of Arizona Press), 289

Muinonen, K., Piironen, J., Shkuratov, Yu. G., Ovcharenko, A., & Clark, B. E. 2002, in Asteroids III, ed. W. F. Bottke, A. Cellino, P. Paolicchi & R. P. Binzel (University of Arizona Press), 123

Nesvorný, D., Bottke, W. F., Dones, L., & Levison, H. F. 2002, Nature 417, 720

Ostro, S. J., Hudson, R. S., Benner, L. A. M., Giorgini, J. D., Magri, C., Margot, J. L., & Nolan, M. C. 2002, in Asteroids III, ed. W. F. Bottke, A. Cellino, P. Paolicchi & R. P. Binzel (University of Arizona Press), 151

Pravec, P., Harris, A. W., & Michalovski T. 2002, in Asteroids III, ed. W. F. Bottke, A. Cellino, P. Paolicchi & R. P. Binzel (University of Arizona Press), 113

Rivkin, A. S., Howell, E. S., Vilas, F., & Lebofsky, L. A. 2002, in Asteroids III, ed. W. F. Bottke, A. Cellino, P. Paolicchi & R. P. Binzel (University of Arizona Press), 235

Slivan, S. M., Binzel, R. P., Crespo da Silva, L. D., Kaasalainen, M., Lyndaker, M. M., & Krčo, M. 2003, Icarus 162, 285

Stokes, G. H., Evans, J. B., & Larson, S. M. 2002, in Asteroids III, ed. W. F. Bottke, A. Cellino, P. Paolicchi & R. P. Binzel (University of Arizona Press), 45

Thomas, P. C., Binzel, R. P., Gaffey, M. J., Storrs, A. D., Wells, E. N., & Zellner, B. H. 1997, Science 277, 1492

Zappalà, V., Bendjoya, Ph., Cellino, A., Di Martino, M., Doressoundiram, A., Manara, A., & Migliorini, F. 2000, Icarus 145, 4

Highlights of Astronomy, Vol. 13
International Astronomical Union, 2003
O. Engvold, ed.

Extended Families In The Main Belt And In The Trojan Swarms

Zoran Knezevic

Andrea Milani

Astronomical Observatory

The availability of highly accurate synthetic proper elements for a large number of asteroids made possible detailed studies of the structure of asteroid families. The entire region of the Vesta family is dominated by bodies with $D < 7$ km. The large spread of family members appears to be primarily due to Yarkovsky mobility, a strongly size-dependent. The proper elements of the asteroids the region (except close to mean motion resonances) are stable over very long time spans; thus chaotic diffusion could not play a significant role. The total volume of the family members with diameter less than 7 km amounts approximately to 6×10^4 cubic km, the volume of a crater with 100 km diameter and average depth 7 km. If the albedo feature, visible in the Hubble Space Telescope images, is really a crater its volume could be even larger. Thanks to the recently computed catalogs of proper elements for 1167 trojans, there are now confirmed dynamical families in the trojan swarms. This allows to begin to study the collisional evolution with constraints from observations.

Highlights of Astronomy, Vol. 13
International Astronomical Union, 2003
O. Engvold, ed.

Radar Observations Of Near-Earth Asteroids

Micael C. Nolan

Lance A. Benner

Greg Black

Don B. Campbell

Jon D. Giorgini

Alice A. Hine

Ellen S. Howell

Jean-Luc Margot

Steven J. Ostro
Arecibo Observatory, NAIC, USA

The recent upgrade of the Arecibo planetary radar system, combined with the huge increase in the near-Earth asteroid (NEA) discovery rate by large survey programs, has greatly increased our ability to observe these objects with radar. Radar provides size, shape, rotation, and trajectory information, and in most cases is the only ground-based technique that spatially resolves near-Earth objects. While the resolution of radar images (typically 7.5m) is not as high as for the very best spacecraft images, spacecraft can visit only a few such objects, and radar observations greatly increase our understanding of the diversity of near-Earth objects, at orders of magnitude lower cost. The single clearest result of these observations is the great variety of near-Earth objects, with binary systems, very fast and very slow rotations, spheres, "bifurcated" objects, and "shards", suggesting that a similar variety of production and delivery mechanisms deliver these objects to near-Earth orbit. Spacecraft mission planning should take into account this variety, and concentrate on broad coverage of a wide range of objects.

Highlights of Astronomy, Vol. 13
International Astronomical Union, 2003
O. Engvold, ed.

Minor Planet Binaries

Jean-Luc Margot

California Institute of Technology, Pasadena, CA, USA

The first detailed characterization of a near-Earth binary (2000 DP107) provided significant insights into the formation mechanism, orbital evolution, and physical properties of the system. Near-Earth Asteroid (NEA) binaries are tidally evolved with synchronously rotating secondaries, providing constraints on asteroid mechanical properties (tidal Q and rigidity). It is expected that radar observations will permit measurements of orbital precession, with corresponding implications for the distribution of mass within asteroids.

Several adaptive optics surveys of main-belt asteroid (MBA) binaries are underway. Apart from obtaining critical asteroid mass and density measurements, the goal is to measure the abundance of binary systems in that population and to constrain the collisional environment and the binary formation mechanism. MBA densities fall in the range 1.2-2.6, implying high porosity in main belt asteroids.

Binary Kuiper-Belt Objects (KBOs) are most likely primordial, and their abundance and properties constrain the environment in the early Kuiper belt. A carefully designed program combining ground-based observations and 25 HST visits can provide accurate orbits for 6 binary KBO systems. Such observations are likely to give the first hints on the density and internal structure of distant ice-rock bodies.

I will describe binary systems in those populations, their physical properties, and formation mechanisms.

Highlights of Astronomy, Vol. 13
International Astronomical Union, 2003
O. Engvold, ed.

ISO Observations of Comets

Dominique Bockelée-Morvan

Observatoire de Paris, France

The Infrared Space Observatory (ISO) offered us the opportunity to observe celestial bodies from 2.4 to 196 microns. A wealth of new results were obtained for comets. Spectroscopic investigations have shown band fluorescence emissions for H_2O, CO and CO_2, and rotational line emissions for H_2O. High resolution spectra of water vapor around 2.7 microns in comets C/1995 O1 (Hale-Bopp) and 103P/Hartley 2 have permitted measurement of the water rotational temperature and ortho-to-para ratio. The thermal region of the spectra showed the signatures of crystalline, Mg-rich olivine and emission features attributed to water ice. Broad band photometry of the coma allowed to investigate several properties of cometary dust, such has color temperature, size distribution and production rate. For several comets, it was possible to separate the nuclear and coma contribution in infrared images obtained from the ISO camera. Inferences concerning the nucleus size and albedo were obtained.

Highlights of Astronomy, Vol. 13
International Astronomical Union, 2003
O. Engvold, ed.

Comets

Michael F. A'Hearn
University of Maryland, USA

Earth-based observations of comets far surpass the ability of in situ observations to understand the range of cometary properties and thus provide unique insight into the relationship between comets and the formation of the solar system. Recent developments in composition have emphasized near-IR and mm-wave data, although optical and ultraviolet data still play crucial roles. Observers now realize the importance of chemistry in the coma. Surveys of nuclear sizes are beginning to provide a real size distribution and we have recent examples of breakup that provide important information on structure.

Highlights of Astronomy, Vol. 13
International Astronomical Union, 2003
O. Engvold, ed.

Radar Observations Of Comet Nuclei And Comae

Donald B. Campbell

John K. Harmon

Micael C. Nolan

Steven J. Ostro

Cornell University, Ithaca, NY, USA

Nine comets have been detected with either the Arecibo (12.6 cm wavelength) or Goldstone (3.5 cm) radar systems. Included are six nucleus detections and five detections of echoes from coma grains. The radar backscatter cross sections measured for the nuclei correlate well with independent estimates of their sizes and are indicative of surface densities in the range of 0.5 to 1.0 g cm^{-3}. Like most asteroids, comets appear to have surfaces that are very rough at scales much larger than the radar wavelength. Coma echo models can explain the radar cross sections using grain size distributions that include a substantial population of cm-sized grains. A long term goal of the cometary radar program has been the high resolution imaging of a cometary nucleus. Eleven short period comets are potentially detectable over the next two decades a few of which may be suitable for imaging. We are always waiting for the arrival of a new comet with an orbit that brings it within 0.1 AU of the earth.

Highlights of Astronomy, Vol. 13
International Astronomical Union, 2003
O. Engvold, ed.

Contributed Papers for JD19: Abstracts

Complex of Meteoroid Orbits With High Eccentricities

Svitlana V. Kolomiyets & Boris L. Kashcheyev (Kharkiv National University of Radioelectronics, Ukraine)

Abstract. In our work is demonstrated the method that can help to predict the existence of distant objects in the Solar system. This method is connected with statistical properties of a heliocentric orbital complex of meteoroids with high eccentricities. Heliocentric meteoroid orbits with high eccentricities are escape routes for dust material from distant parental objects with near-circular orbits to Earth-crossing orbits. Ground-based meteor observations yield trajectory information from which we can derive their place of possible origin: comets, asteroids, and other objects (e.g. Kuiper Objects) in the Solar system or even interstellar space [Kolomiyets, S. 2002, Abstracts ACM 2002, Berlin, 371; Kashcheyev, B. Kolomiyets, S. 2001, SP-495, 643]. Such information is important at planning space missions. We analyze elliptic meteor orbits with high eccentricities that were registered in 1972 - 1978 in Kharkiv (Ukraine). Statistical distributions of radius-vectors of nodes, and aphelia of orbits of meteoroids contain key information about position of greater bodies. We discuss the accuracy of the ground-based radar observations of faint meteors. An estimation of selectivity factors of meteor radar measurements is made on base of radiophysical and astronomical researches of meteoric substance and its interaction atmosphere of the Earth.

Meteor Showers In 1993 And 1998: On The Goniometric Data

Sergei A. Kalabanov, Vladimir V. Sidorov, Tamara K. Filimonova & Jury N. Kosenkov (Kazan State University, Russia)

Abstract. On the basis of application of a new discrete quasy-tomography approach of analysis to the goniometric data of the Kazan meteor radar it were examined acts of known meteor showers working during six months of continuous observation in 1993 and 1998 years.

The angular resolution of coordinates of radiants for all measured data is $2^\circ \times 2^\circ$. For intensive meteor showers the resolution achieved $1^\circ \times 1^\circ$. An average heliocentric velocity of a shower was calculated by averaging individual velocities after operation of an identification of a concrete set of measured data with an investigated meteor shower. Most stable annual meteor shower GEMINIDS was used as a master shower.

It is revealed, that many weak meteor showers having personal names and which should be observed within half-year in 1993 and 1998, have not detected with expected parameters. Others however were observed as though casual showers which operated within several days in immediate vicinity to expected ones, but not repeating in the same dates and with identical parameters.

The measured parameters of orbits of observed meteor showers are resulted in comparison with known lists of the basic meteor showers for northern celestial hemisphere.

Sporadic Meteor Microshowers: Data And Parameters

Vladimir V. Sidorov, Sergei A. Kalabanov & Rashid A. Ishmuratov (Kazan State University, Ukraine)

Abstract. A development of a new quasy-tomography technology of processing of the goniometric data from a meteor radar, allowed considerably to increase the angular resolution of radar measuring and its application to the data received at continuous observation within six same months 1993 and 1998 on meteor radar at KSU, has allowed to find out new astronomical objects - sporadic microshowers and to measure parameters of their orbits.

We have named microshowers as sets of the registered meteors having close velocities and their coordinates of radiants, acting during one or more days, but not repeated in identical hours and dates in two different years.

Possible sources of occurrence of such formations are discussed:

- Dust traces of small comets and the asteroids which have not been found out yet by optical astronomical tools.

- Dust traces of large meteoroids, fallen to the Earth as bolides or flown by in immediate vicinity to the Earth at the moment of time, close to the moments of display of microshowers.

- The groups of the meteor particles which have been pulled out from bodies of meteor streams by consecutive gravitational perturbation of planets, with their preserved collective properties during evolution.

Meteor Researches At KHNURE

Svitlana V. Kolomiyets, Yuri I. Voloshchuk, Boris L. Kashcheyev & Nikolay I. Slipchenko (Kharkiv National University of Radioelectronics, Ukraine)

Abstract. The Scientific-Educational Center of Radioengineering of the Kharkiv National University of Radioelectronics (KHNURE) is one of the oldest radar meteor centers, which was founded by B. L. Kashcheyev in 1958. The first automatic meteor radar system in Ukraine "MARS" is connected with our University. There are long-term observational series of meteor rates and orbital data in the Center. Fields of the KHNURE researches are: a structure of meteor showers, a determination of meteoroid orbits, an influx of cosmic rubbish in the Earth atmosphere, search of parental bodies of meteoroids, a statistic analysis of measurement results of radiometeors, an estimation of errors of meteor radar measurements, a search for real hyperbolic orbits and interstellar meteoroids. KHNURE disposes a unique electronic orbital catalogue. This catalogue contains the primary information, velocities, radiants and orbits of nearly 250,000 radiometeoroids with masses from 0.001 to 0.000001 g. The "MARS" registered these data during observations of 1972 - 1978. From these data 5160 meteor streams are singled out. New classification of streams is made in view of their structure. The study of meteor stream orbits from the KHNURE data bank allow to predict orbits of a big number of undiscovered "dangerous" NEOs.

Fluctuations In The Activity Curve Of The 2002 Leonids

Lola Herrera Ruiz, Luis R. Rubio Bellot & Miquel Serra-Ricart (Instituto de Astrofisica de Canarias, Tenerife, Canarias, Spain)

Abstract. We present observations of the 2002 Leonid meteor shower taken with four intensified video cameras from Teide Observatory (Tenerife, Spain) on November 19, 2002. The cameras, fitted with f/1.4, 85 mm objectives, were aimed at 6 °above the horizon in order to monitor the largest atmospheric volume possible. The most sensitive camera detected 1300 meteors between 0312 and 0456 UT, i.e., the period covering the European Leonid storm of 2002. The activity curve constructed from these data peaks at 0401 UT, about 9 minutes earlier than indicated by the visual observations analyzed by the International Meteor Organization. Our results thus favor the model of Lyytinen and van Flandern, who predicted the first maximum at 0402 UT. We find statistically significant oscillations in the activity curve. A Fourier analysis delivers a period of about 7 minutes. These observations confirm the discovery of Singer et al. (2000) that density fluctuations exist in the Leonid dust trails at spatial scales of 10000-30000 km. The oscillations we observe are very similar to those detected by Singer et al., the only difference being that the dust trail is 132 years older.

Geophysical Aspects Of Dergaon Meteorite

Kalpana Duorah, Sarat Phukan, Parag Phukon, Amulya Mazumdar & Hira L. Duorah (Physics Department, Gauhati University, India)

Abstract. The Astrophysics group, Gauhati University under the supervision of Dr. Kalpana Duorah collected a meteorite sample in Dergaon, Assam India having geographical location 9352/ E longitude and 26041/ 50 ″N latitude. The sample is registered by the International Meteoritic Society in their Bulletin (May 2001) as Dergaon meteorite. Preliminary analysis showed that the parent meteorite had total mass of about 50 kg out of which the collected sample was determined to be 10.2 kg. This is found to be a stony meteorite of group H 5. Electron probe Microanalysis of the sample revealed that the dominant minerals are olivine and pyroxene and subordinate amount of metal phases. The whole rock analysis has produced the element ratios Fe/Si = 0.80 and Si/Mg = 1.074. and the trace elements and the rare earth elements are obtained by the inductively coupled plasma mass spectrometry. The paper provides detailed analysis of the Dergaon Meteorite.

Meteorite Physical Properties: Implications For Asteroids

George J. Flynn (State University of New York, Plattsburgh, NY, USA)

Abstract. Meteorites are believed to be samples of asteroids. We measured the porosity of carbonaceous and ordinary chondrite meteorites by He pycnometer and imaged the porosity by computed microtomography. We found fresh samples of most ordinary chondrites have $\sim 5\%$ to 15% porosity, while carbonaceous chondrites have even higher porosity (up to 30% in Allende). This porosity occurs in three forms: extended cracks, vugs, or gaps between the matrix and the chondrules. We performed hypervelocity impact studies on chondritic me-

teorites to determine how the presence of chondrules in a more porous matrix effects fragmentation. The gaps between the chondrules and the matrix appear to enhance the ejection of whole chondrules or large chondrule fragments during hypervelocity impact, while much of the debris significantly smaller than the chondrules is chemically-distinct matrix material. We measured the speed of sound, bulk modulus, and elastic modulus of several ordinary chondrite meteorites. The speed of sound ranges from 1,100 m/sec, in a fragment of Saratov, an extremely friable ordinary chondrite, up to 4,000 m/sec in more compact ordinary chondrites. The weakest meteorites exhibit physical properties more comparable to volcanic tufts than to compact basalts. Modeling of stone asteroids needs to consider a wide range of physical Properties.

Cometary Features Of Newly Discovered Bodies

Milos Tichy, Jana Ticha & Michal Kocer (Klet Observatory, Czech Republic)

Abstract. The majority of new ground-based discoveries of comets comes from large surveys. The first step of exploration of newly discovered cometary bodies consists of the confirmatory astrometric observation and also detection of their cometary features. Only some of both professional and amateur stations do a preliminary analysis of cometary activity of a particular newly discovered body. A timely recognition of cometary features of a particular body having an unusual orbit can help in planning further observing campaigns. One of main goals of the Klet Observatory NEO astrometric follow-up program is an analysis of possible cometary activity of newly discovered unusual bodies. We present here the first results obtained with our new 1.06-m KLENOT Telescope, which we put into operation in March 2002. The CCD camera used on this telescope enables detection of comet's gas, plasma and dust activity in a more satisfactory way. *Acknowledgments:* This work was supported by grants MSMT LA163 and GACR 205/02/P114.

Observations And Investigation Of Comets In Kyiv University

Klim Churyumov (Kyiv Shevchenko National University, Kyiv, Ukraine)

Abstract. The following results of observations and investigation of comets in Kyiv Natsional Shevchenko University are discussed: a) Narrow band photometry comets, peculiarities of comet nuclei gas production rates, taxonomy of comets; b) Optical spectroscopy of comets, identification of emission lines in comet spectra, physical parameters of the comet neutral gas atmospheres, detection of the luminescent continuum in comet spectra: c) Near nucleus phenomena in comets, the dust shells in comet C/1995 O1 (Hale-Bopp); d) Large scale phenomena in comets and their theoretical modelling; e) Light curves of comets and their connection with he solar activity.

Investigation Of The Comet 19P/Borrelly Spectra

Klim I. Churyumov, Igor V. Lukýanyk & Larisa S. Chubko (Kyiv National Shevchenko University, Ukraine)

Abstract. Several hundreds of spectra and monochromatic images of Comet 19P/Borrelly were obtained with the Multi Pupil Fiber Spectrograph (MPFS) installed in the Prime Focus of the 6-m telescope of the SAO of the RAS (Nizhny Arkhyz) on Aug. 13 and 15, 2001, and with Spectral Camera with Optical

Reducer for Photometrical and Interferometrical Observations (SCORPIO) installed in the Prime Focus of the 6-m telescope of the SAO of the RAS on August 16 and 17. The observations were made 41-37 days before the New Millennium DS-1 probe approach with the comet nucleus. For detailed identification we selected the spectrum of the comet 19P/2000 Borrelly, obtained Aug. 15 , 2001. The rates of gas production (log Q) of neutral molecules from the nucleus of the comet were calculated using Haser's model for Aug.17, 2001: log Q(CN) = 25.48, Log $Q(C_3)$ = 24.29 and log $Q(C_2)$ = 24.97.

Physical Parameters Of The Comet Ikeya-Zhang Atmosphere

Klim I. Churyumov, Igor V. Lukýanyk, Alexey A. Berezhnoy, Vahram H Chavushyan, Larisa S. Chubko, Valery V. Kleshchonok, Lourdes Sandoval & Alejandro Palma (Kyiv National Shevchenko University, Ukraine)

Abstract. Physical Parameters Of The Comet Ikeya-Zhang Atmosphere Several middle-resolution optical spectra of Comet C/2002 C1 (Ikeya-Zhang) were obtained on May 5, 2002 with the help of the 2.12 - m reflector of the Guillermo Haro Astrophysical Observatory. On the basis of the intensity distribution along the slit of the spectrograph in C_2, C_3, CN emission lines we determined the velocities of expansion (v) and life times (τ) of these molecules: for C_2 (5165 Å) [201 m/s, 3.08×10^6 s]; for C_3 (4050 Å) [166 m/s, 0.075×10^6 s] and for CN (4200 Å) [157 m/s, 0.06×10^6 s].

Changes In The Spectra of Comet C/1999 S4 In July, 2000

Larisa S. Chubko (Vinnytsia Pedagogical Kotsyubynsky University, Ukraine), Klim I. Churyumov, Igor V. Lukýanyk & Ayyub S. Guliev (Kyiv National Shevchenko University, Ukraine)

Abstract. The spectra of comet C/1999 S4 (LINEAR) were obtained with the eshelle-spectrograph (and CCD) installed on the 2-m Zeiss reflector of the Shamakhy Astronomical Observatory of the Azerbajan Academy of Sciences (Mount Pirkuli) on July 21 and 23, 2000. The spectra of comet C/1999 S4 (LINEAR) were also obtained with the UAGS spectrograph (long slit and CCD) installed on the 1-m Zeiss reflector of the SAO of the RAS (Northern Caucasus, Nizhny Arkhyz) on July 23, 27 and 28, 2000. Emissions lines of the molecules C_2, C_3, CN, NH, CH, NH_2, CO, CO^+, H_2O^+ and other were identified in the spectra of comet C/1999 S4 obtained on July 21, 23 and 27, 2000 during splitting of the cometary nucleus. Changes in the spectra are discussed.

Peculiarities of Light Curves Of Some New Bright Comets

Vitaly S. Filomenko & Klim I. Churyumov (Astronomical Institute of Kharkov National University, Ukraine)

Abstract. The light curves of ten comets [C/2000 SV74 (LINEAR), C/2000 WM1 (LINEAR), C/2001 A2 (LINEAR), C/2001 OG108 (LONEOS), C/2002 C1 (Ikeya-Zhang), C/2002 F1 (Utsunomiya), C/2002 O4 (Hoenig), C/2002 V1 (NEAT), C/2002 X5 (Kudo-Fujiakawa) and 19P/ Borrelly] were constructed on the basis of visual physical observations of these comets. Photometric parameters H_{10} (Vsekhsvyatskii's absolute magnitude), H_y (absolute magnitude) and n (photometric parameter that characterizes the rate of change of cometary

brightness with heliocentric distance) were determined. The analysis of light curves showed that the parameter n of seven comets [C/2001 A2, C/2001 OG108, C/2002 C1, C/2002 F1, C/2002 O4, C/2002 V1 and 19P] undergoes abrupt changes. We found that these jumps in the rate of change of the cometary brightness were correlated with outbursts of comets. The statistically significant (reliability > 0.95) influence of the phase dependence on the visual light curves for three comets had been found. The values of phase coefficient (β) for these comets were determined: (1) C/2001 A2: $\beta = 0.086 \pm 0.027$ m/degree (before perihelion), (2) C/2001 OG108: $\beta = 0.032 \pm 0.025$ m/degree (before perihelion) and 0.052 ± 0.016 m/degree (after perihelion), (3) C/2002 V1: $\beta = -0.062 \pm 0.010$ m/degree (before perihelion).

Spatial Distribution Of The Halley Comet Dust Continuum From Data Of TKS - VEGA 2

Penka (Stoeva) Muglova, V. Guineva & R. Werner (Central Solar - Terrestrial Influences Laboratory, Bulgarian Academy of Sciences, Bulgaria)

Abstract. Spatial distribution of the solar light scattered by dust particles in Halley comet coma towards the Sun and in the near tail is investigated using spectra measured by TKS, VEGA 2. Monochromatic composed images in 5260 Åare constructed from consequently registered two-dimensional images for 9 and 10 March 1986. Radial profiles presenting the intensity as a function of the projected distance to the nucleus p are also used in the research.

Two strong jets are observed. One of them is in direction towards the Sun and expands up to $p = 19500$ km from the nucleus, and the other is perpendicular to it and reaches $p = 19000$ km. The weaker slope of the radial profile near the nucleus is explained by the greater optical depth of the inner coma or by the quick change of the scattering angle.

In antisolar direction, in the near tail, a weaker intensity of the dust continuum is observed. The intensity increasing, obtained far from the nucleus, and the radial profile maxima are probably connected with a dust shells formation due to jet activity and nucleus rotation.

Phase Dependencies Of Cometary Visual Light Curves

Vitaly S. Filomenko & Klim I. Churyumov (Astronomical Institute of Kharkov National University, Ukraine)

Abstract. Generally, the integrated flux produced by a comet on Earth is the sum of the fluxes produced by gas and dust in the cometary atmosphere and by the solid cometary nucleus. The contribution from the nucleus to the integrated comet brightness is extremely small and it can be ignored. The contributions from the gas and dust are functions of the comet heliocentric distance. But the flux from dust also depends on the phase angle. Therefore, the phase dependence of brightness can be determined in principle from the visual integrated light curves of comets whose dust-scattered radiation accounts for a considerable fraction of the total radiation. The statistical significant influence of phase dependencies on the light curves of eight comets had been found. The values of phase coefficient of these comets had been determined. For three comets the values of phase coefficient are negative. For other five comets the mean value of phase coefficients is 0.047 m/grad that practically coincides with mean value of phase coefficients of C-type asteroids (0.041 m/grad). Apparently the

phase dependencies of these comets determines by dark carbon particles in their atmospheres.

Infrared Observations In The 3-Micron Region Of Comets

Karen Magee-Sauer, Michael J. Mumma, Neil Dello Russo, Michael A. DiSanti & Erika L. Gibb (Rowan University, NJ, USA)

Abstract. The 3-micron spectral region is rich in emissions from key cometary volatile species. Spectral lines of several molecules are identified in this region, including C_2H_2, HCN, NH_3 , H_2O ("hot-band" emission), OH (prompt emission and fluorescent emission), and NH_2. These species are key to understanding several important questions in cometary science. Acetylene is an important link to the origin and processing of the natal ices in comets. The abundance of HCN and its release from the nucleus provides important information on the processing of nuclear ices from radiation and gas-phase chemistry, as well as delivery of biogenic molecules to Earth. As the fully reduced form of nitrogen, NH_3 is the key species for understanding the nitrogen chemistry of comets and thus chemistry in the region of comet formation. OH ("prompt") and H_2O emission in the spectrum provide a means of measuring water production directly. Here, we present spectra, rotational temperatures, spatial profiles, production rates, and relative abundances of molecules detected in the 3-micron region in observed comets from Hyakutake to the present. Results obtained through the CSHELL instrument at the NASA IRTF and the significant gains obtained through use of the NIRSPEC instrument at the Keck Observatory will be presented.

Results From The UMD Physical Properties Of Comets Survey

Carey M. Lisse, Michael F. A'Hearn & Yanga R. Fernandez (University of Maryland, MD, USA)

Abstract. We report on an ongoing statistical study of the emitted dust and exposed nuclei of a survey of the brightest near-Earth comets over the last 13 years. Combined thermal infrared and optical observations are analyzed using dynamical, spectral, and morphological coma models (Lisse et al. 1998, ApJ, 496, 971; Lisse et al. 1999, Icarus, 140, 189; Fernandez et al. 2000, Icarus, 147, 145) to update and improve dust emission rates (Kresak & Kresakova 1987, in Symposium on Diversity and Similarity of Comets, ESA SP-278, 739) and nucleus size estimates (Jewitt 1991, in Comets in the Post-Halley Era, eds. R. L. Newburn, M. Neugebauer, & J. Rahe, Kluwer Academic, Dordecht, 19).

Using these results, we show that 1) there is more than enough dust emitted from short period comets into bound solar system orbits to create and support the current interplanetary dust cloud (IPD); 2) that a population of dormant or extinct comets in the solar system is quite plausible; and 3) that the lifetime versus sublimation for the short period comets is much longer than their dynamical lifetime.

Deep Impact Mission Target Comet Nucleus Characterization

Karen J. Meech, Jana Pittichova, Henry Hsieh, Yan Fernandez, James M. Bauer, Michael J. Belton, Michael F. A'Hearn, Olivier R. Hainaut, Hermann Boehnhardt & Gian-Paolo Tozzi (Institute for Astronomy, Hawaii, USA)

Abstract. Comet 9P/Tempel 1 is the target of the 8th NASA Discovery Mission, Deep Impact. The focus of the ground-based observing program has been to characterize the nucleus for mission planning. We have obtained data over a full apparition from 11/97 through the present on a total of over 200 nights using 16 telescopes worldwide. The nearly 2000 images represent over 250 hours of integration. We will present the, nucleus size, heliocentric light curve, and Afrho values vs. time, and report on the status of the analysis of the rotation period. We will report on the color of the nucleus and dust coma (using BVRI filters) as a function of heliocentric distance. We have analyzed the data as a function of phase angle to infer the nucleus surface scattering properties. The comet is quite phase darkened, with a linear phase function of 0.07 mag/deg, and a negative value of G-parameter suggestive of a low albedo rough surface. We will also present a series of enhanced images to search for evidence of features (e.g. jets and other structures) in the dust coma. *Acknowledgements:* Support provided by NASA Grants NAGW-4495, NAGW-5015, NAG-54080, and NAG-59006 and through Univ. of MD subcontract Z667702 (NASA contract NASW-00004).

Korean NEO Station In South Africa

Wonyong Han, Yong-Ik Byun, Hong-Kyu Moon, Yong-Woo Kang, Hong-Suh Yim, Sunyoup Park, Young-Ho Bae & Sung Yeol Yu (Korea Astronomy Observatory, Korea)

Abstract. The joint Near Earth Object (NEO) project team of Korea Astronomy Observatory (KAO) and Yonsei University Observatory (YUO) has recently installed a 0.5-meter robotic telescope at the Sutherland Observatory in South Africa. This telescope with 2-degree FOV is operated in fully automated mode, making daily reports on discoveries NEOs and other significant luminosity variability via internet. The KAO-YUO joint team plans to install similar facility in Australia and Chile soon, making a network of survey telescopes for southern hemisphere. In spite of its small aperture size, this network will be an important tool in identifying southern NEOs, especially those in the form of comets. This paper summarizes the observatory system, data handling, and our parallel efforts to characterize NEOs with follow-up light curve investigation. *Acknowledgments:* The joint project is funded by the National Research Laboratory Program of Korean Ministry of Science and Technology (KAO) and by the Korean Research Foundation.

Observations of 2002 NY40: An Ordinary Chondrite?

Ellen S. Howell, Andrew S. Rivkin, Michael C. Nolan, Jean-Luc Margot, Gregory Black, Schelte J. Bus, Michael Hicks, William T. Reach, H. T. Jarrett & Richard P. Binzel (Arecibo Observatory, Cornell University, USA)

Abstract. The near-Earth asteroid 2002 NY40 was discovered on July 14, 2002 by the LINEAR survey. The object made a close pass by the Earth on August 18, when observations were obtained at a large range of wavelengths, from visible to radar (12.6 cm). The combination of visible and near-infrared spectroscopy gives some indication of the composition. Thermal emission in

the 3-micron region gives constraints on the visible albedo, which are confirmed independently by the radar size and visible magnitude. The lightcurve was well measured by a large number of observers, and the rotation period is well-determined at 19.99 hours. The spectrum and albedo are a very good match to an LL chondrite spectrum over the range measured. No appreciable reddening is seen in the asteroid spectrum, which suggests that the surface has not been noticeably affected by the same processes seen in many other pyroxene and olivine-rich asteroids. The radar images show that this asteroid looks like two spheroidal units joined together. Analysis and implications of these observations will be discussed.

Database For Geophysical And Geological Properties of NEOs

W. F. Huebner (Southwest Research Institute, San Antonio, TX 78228-0510, USA)

Abstract. Collisions of asteroids and comets with Earth have occurred in the past. About 150 impact structures on the Earth's continents have been identified. There may be many more impacts whose structures have eroded over time. Asteroids and comets still collide with the planets and will again collide with the Earth. These are random events. No asteroid is now known to be on a collision course with the Earth and we do not know when the next catastrophic impact might occur. Many parameters are needed to develop credible mitigation or collision avoidance strategies. We know little about geophysical properties of NEOs. Here we report on progress on the database for geophysical and geological properties of NEOs and their analog materials. The database consists of four parts: An observational database, a material properties database, a database for mission and instrument development, and a database useful for dissemination of projects and results and for public outreach. The database will be available at: http://neodata.space.swri.edu/. For atomic and molecular data see: http://amop.space.swri.edu/.

The Dynamic Estimation Of The Mass Of The Main Asteroid Belt

Elena Pitjeva (Institute of Applied Astronomy of Russian Academy of Science, Russia)

Abstract. Perturbations from asteroids affect significantly on the orbits of the inner planets and should be taken into account when high-accuracy planetary ephemerides are constructed. On the other hand, from an analysis of the motions of the major planets by processing of precise measurements of ranging to the Viking, Pathfinder, Mars Global Surveyor spacecraft and planets (1961-2002) some physical parameters of the asteroids have been obtained. The masses of several the biggest asteroids (Ceres, Pallas, Vesta, Juno) have been determined individually, masses of the most relevant 296 asteroids have been derived from their latest published diameters based on IRAS data and observations of occultations of stars by minor planets, making use of the corresponding densities. The total contribution of all remaining small asteroids is modeled as an acceleration caused by a solid ring in the ecliptic plane. As a sequence the total mass of the main asteroid belt was obtained: $M = (14 \pm 2) \times 10^{-10}$ mass of Sun. n derived expression for estimating the total number of minor planets in any unit interval of absolute magnitude H was compared with the observed distributions of the

asteroids (52224 numbered, 152451 unnumbered) and distribution of the SAM model by Tedesco et al.

ISO Observations: Results On Asteroids

Elisabetta Dotto, Maria A. Barucci, John R. Brucato, Thomas G. Mueller & Marcello Fulchignoni (INAF-Osservatorio Astronomico di Roma, Italy)

Abstract. We carried out observations of 16 asteroids with different ISO instruments (PHT-P, PHT-S and SWS) obtaining low resolution spectra up to 12 micron, high resolution spectra up to 45 micron and spectrophotometric data up to 60 micron. The aim of these observations was to investigate the physical properties of the surface of these bodies, and to improve our understanding on the processes which governed their formation and evolution. We interpreted the obtained data in terms of asteroid surface composition, comparing the observed spectra with laboratory reflectance spectra of selected mineral, mineral mixture and meteorite particulates of different grain sizes. The characterization of the material on the asteroid surfaces (presence, abundance and/or composition of minerals or chemical species) was based on the interpretation of observable diagnostic spectroscopic properties. The obtained results will be presented and discussed.

ESO-VLT Large Program On Centaurs And TNOS

Maria Antonietta Barucci, Hemann Boehnhardt & Project Team (Observatoire de Paris, LESIA, France)

Abstract. The ESO Large Program on the study of Trans-Neptunian Objects (TNOs) and Centaurs has been carried out during the last two years (April 2001-March 2003) at the Paranal (Very Large Telescope VLT) and La Silla (New Technology Telescope NTT) observatories of the European Southern Observatory (ESO) in Chile.

The aim of the Large Program was to investigate the physical properties of this population composed of cold and primitive objects.

Results has been obtained for multi-wavelength imaging, BVRI and JHK filters of 70 and 30 objects respectively, as well as for low-dispersion visible and near-IR spectroscopy of about 12 objects. The photometric results and analyses of the relative correlations between colours, photometric gradients and dynamical properties of the objects will be presented and discussed. The spectroscopic results have been interpreted with models computed using geographical mixture of organics, minerals and ices in order to constrain the surface composition. The spectra show a wide range of slopes, some are featureless with almost constant gradients over the visible-NIR range, while others show absorption signatures of ices.

The limit and the utility of the ground-based observations will be discussed together with the necessity of a space exploration.

Deep TNO Search Near Invariable Plane Using Subaru Telescope

Daisuke Kinoshita, Jun-ichi Watanabe, Naotaka Yamamoto, Tetsuharu Fuse, Seidai Miyasaka, Kyoko Muroi & An-Li Tsai (National Astronomical Observatory of Japan, Japan)

Abstract. We have carried out deep imaging observation near the invariable plane using Subaru telescope with its prime focus camera "Suprime-Cam". We have integrated single field of 0.2 sq. deg. deeply on 5, 6 October 2002, and followed up detected objects on 3 December 2002. SDSS r'-band filter was used for this observation to maximize the number of detection. The limiting magnitude is $r' = 28.0$ for signal-to-noise ratio of 5. Assuming typical color of TNO, it roughly corresponds to $R = 27.7$ mag. The aim of this observation is (1) to investigate existence or non-existence of distant TNO beyond 50 AU from the Sun and (2) to explore the faint-end of the luminosity function. All the detected TNOs have heliocentric distances ranging $38 < R_H < 45$ AU. We will report preliminary results of our deep survey.

Physical Characteristics Of Centaurs And TNOs

Alain Doressoundiram, Maria A. Barucci & Nuno Peixinho (Observatoire de Paris, France)

Abstract. Beyond the orbit of Neptune exists a population of bodies remaining from the formation of the solar system. These are the Kuiper Belt or Trans-Neptunian Objects (TNOs). Scientific interest in these bodies arises because this region of the solar system may preserve some of the most primitive materials available to direct investigation.

We have started since 1997 a multicolor photometric survey with the aim of collecting a large and homogeneous set of color data for TNOs and Centaurs objects. With this large dataset obtained mostly at CFHT and ESO, we performed relevant statistical analyses to search for compositional structures, interrelations with related populations and correlations with physical and orbital parameters.

One of the most puzzling features of the Kuiper Belt is the optical color diversity that seems to prevail among the observed TNOs. In this work, we will present results on the strong correlations found with some orbital parameters (i, e, q) for the Classical Kuiper Belt. The correlations found are important because they are diagnostic of some physical effects processing the surfaces of these icy and primitive objects. We will give a global picture of the color properties and trends within the Kuiper Belt.

The Albedo f Trans-Neptunian Object 1579 (1993SC)

Iwan P. Williams & Alan Fitzsimmons (Queen Mary, University of London, UK)

Abstract. ISO observations of the infrared emission from the Trans-Neptunian object 15789 (1993SC) were obtained in 1997 and have been published (Thomas et al. 2000, ApJ, 534, 446). Determination of the albedo, and hence the radius also requires a knowledge of the reflected (visible) radiation. In their publication, Thomas et al used ground based data obtained in 1995. Since that time ground based observations close in time to the ISO observations have been ob-

tained. The paper presents the new observations and deduced albedo based on these observations.

Detectability Of Lightcurves Of KBOs

Pedro Lacerda & Jane Luu (Leiden Observatory, Leiden, The Netherlands, & Harvard-Smithsonian CfA, Cambridge, MA, USA)

Abstract. We present a statistical study of the detectability of lightcurves of Kuiper Belt objects (KBOs). Some Kuiper Belt objects display lightcurves that appear "flat", i.e., there are no significant brightness variations within the photometric uncertainties. The lack of brightness variations may be due to (1) the objects have very nearly spherical shapes, or (2) their rotation axes coincide with the line of sight. We investigate the relative importance of these two effects and relate it to the observed fraction of "flat" lightcurves. This study suggests that the fraction of KBOs with detectable brightness variations may provide clues about the shape distribution of these objects. Although the current database of rotational properties of KBOs is still insufficient to draw any statistically meaningful conclusions, we expect that, with a larger dataset, this method will provide a useful test for candidate KBO shape distributions.

Frozen Volatiles In The Icy Satellites And KBO Objects

Jacek Leliwa-Kopystynski (Warsaw University, Physics Dept., Institute of Geophysics, Poland)

Abstract. The first physical assumption of this work is that the volatiles were transported to the growing icy/mineral objects of the Outer Solar System by means of accretion. The relative amounts of different volatiles in the accreting matter depends on the local temperature of that matter therefore, roughly, on the solar distance. The second assumption concerns degassing of the volatiles: gases instantaneously escape from the growing body if temperature of accreting matter in the moment of an impact is enough high. Discussion of the conditions related to presence of pristine-originated solidified volatiles inside of the icy satellites and the KBO objects is based (i) on the calculation of the impact-originated increase of temperature of the volatile-bearing grains of accreting material, and (ii) on the thermodynamic properties of the volatiles under consideration. It is found that the highly volatile materials are accumulated in the deep interiors and the less volatile are expected to survive everywhere, including the outer layers. The particular calculations are performed for Saturnian and Uranian icy satellites (from Epimetheus to Titania, with radii 65 - 780 km) as well as for some of KBO objects. Considered volatiles are H_20, CO_2, CO, NH_3, CH_4, N_2, and C_2H_6.

Minor Body Occultations: Statistics And Survey Requirements

Asantha Cooray (California Institute of Technology, CA, USA)

Abstract. The occultation of background stellar sources by foreground minor bodies, mainly Kuiper Belt Objects (KBOs), can be used to survey physical properties of the foreground population. We will discuss statistics related to KBO occultations and discuss what constraints can be placed on the KBO population. While the optical depth for occultation is relatively high for KBOs, lowering the number of stars one should monitor, the event duration is at the subsecond level and puts strong constraints on the instrumentation side. We discuss requirements for a reasonable ground-based survey and suggest that an array of telescopes, spread over few kilometers with imaging and timing capabilities at the level of 100 millisecond or less down to a magnitude limit of 14 in the V-band, may be used to probe the KBO population below a kilometer in size. With an array, one also probes the projected shapes of KBOs and the presence of binaries. We also discuss relative merits of a space-based experiment. If fainter stars are monitored, the diffraction fringes present in certain light curves can be used to extract physical information related to the foreground occulting body.

Existence Of The Lunar Core

Alexander Gusev & Natasha Petrova (Kazan State University, Russia)

Abstract. The question of lunar core existence is still an open question. If core existence will be verified by future direct measurements, such a core would give constraints to the model of origin of the Moon. A short review of results concerning facts of core existence is given in the report. The most advances in this study were obtained as results of the investigation of Lunar gravity and physical libration. The accumulated data about the lunar gravity are now very wealthy, but there is still a great deal to supplement the data about gravity and topography picture on the far-side. Though there are many inferential evidence of presence at the Moon of a core, nevertheless the direct experiments on detection of the core and determination of its characteristics are very important. The large prospects in the decision of this problem are opened by the RISE and ILOM projects of SELENE I, II mission. Obtained data will allow to improve the physical libration theory of the Moon and together with theoretical and observational libration data they will provide a further study of the lunar interior and, as a consequence, of its origin and evolution.

Centrifugal Librations Due To Lunar Core-Mantle Couplings

Eric Bois (Observatoire de Bordeaux L3AB, UMR CNRS/INSU 5804, France)

Abstract. We present a study of the dynamical behavior of a molten core inside the Moon related to the mantle by inertial coupling. In order to integrate the lunar core-mantle interaction in a realistic model of the Moon's rotation, we have used our SONYR (acronym of Spin-Orbit N-bodY Relativistic) model of the solar System including the Moon's spin-orbit motion. This model was previously built in accordance with the requirements of the Lunar Laser Ranging observational accuracy. We have extended this model to the spin-orbit couplings of the terrestrial planets in order to compare different dynamical behaviors of core-mantle interactions in these planets (Mercury, Venus, Earth and Mars).

Our core-mantle mechanism prove to be adequate to excite the two resonant frequencies of the lunar physical librations, namely 2.9 and 80.1 years. ignature of such a core with for instance a 1/10 homothetic ratio appears clearly on the proper rotation angle; the amplitude is then around 12 milli-arcseconds and its period 2.9 years.

Besides, we present the results obtained for various lunar nucleus radii and various initial nutations of the core relatively to the mantle. Other computations and comparisons are in progress involving Mercury, the Earth and Mars.

Mid-Infrared Spectrophotometry Of Saturn's Ring System

Padma A. Yanamandra-Fisher, Glenn S. Orton & Brendan M. Fisher (Jet Propulsion Laboratory, Pasadena, CA, USA)

Abstract. We observed Saturn's main rings at the NASA/InfraRed Telescope Facility (IRTF) from 1995 to 2003 with MIRLIN, a 10-micron camera at several diagnostic wavelengths in the 8- to 24-micron spectral window, covering one fourth of a Saturnian year, and followed the progressive march of the rings from their edge-on presentation at the equator in 1995 to their maximum opening, obscuring the northern pole of Saturn. Our preliminary results indicate that the brightness temperature of the rings peaks near 18 microns. There also exists an asymmetry between the East and West ansae of few degrees. This is similar to the near-infrared albedo asymmetry between the ansae and reflectivities at visible wavelengths. Our current efforts are aimed at modelling the ring opacities in the mid-infrared as function of changes in solar elevation angle, inclination and phase angles of the rings. In particular, the A ring had changed from being edge on in 1994 to completely unshadowed in 2003. These observations will provide constraints on thermal asymmetries and opacity of the ring. Current thermal models will be validated against these observations and previous data sets acquired by Voyager and ISO and data to be acquired by Cassini and possibly SIRTF and SOFIA.

JD20

Frontiers of High Resolution Spectroscopy

Chairperson: J. Linsky

Editor: J. Linsky

Highlights of Astronomy, Vol. 13
International Astronomical Union, 2003
O. Engvold, ed.

Introducing Joint Discussion 20 – Frontiers of High Resolution Spectroscopy

Jeffrey L. Linsky

JILA, University of Colorado and NIST, Boulder, CO 80309-0440, USA

Abstract. This paper introduces the rationale and program of Joint Discussion 20, Frontiers of High Resolution Spectroscopy, which took place on 2003 July 23–24 during the IAU General Assembly in Sydney Australia.

1. Rationale for Joint Discussion 20

Major discoveries in astrophysics are usually enabled by significant increases in observing capability – enhanced sensitivity, larger spectral coverage, higher temporal resolution, long-term monitoring, decreased noise or background, better angular resolution, and higher spectral resolution. The expectation of important future discoveries that become possible with enhanced observing capabilities is a major driver for the building of new instruments and telescopes.

In recent years we have seen a plethora of new high visibility projects that push forward the observational frontiers toward greater throughput for imaging and low-resolution spectroscopy, improved spectral coverage, and higher angular resolution. There have also been major advances in spectral resolution, although with less publicity and recognition in the astronomical community. Joint Discussion 20 was motivated by the desire the highlight the accomplishments and opportunities of high-resolution spectroscopy across the electromagnetic spectrum. The objectives of this Joint Discussion include

(1) presenting a representative sample of new results that provide insights into major questions in astrophysics by pushing the limits of high-resolution spectroscopy,

(2) speculating about major questions that could be addressed with new advances in high-resolution spectroscopy, and

(3) discussing cross-cutting technologies and data analysis techniques that may apply across the electromagnetic spectrum.

Symposia, colloquia, and workshops in astrophysics are often narrowly focused on specific phenomenola, targets, or theory. The uniqueness and virtue of the program of Frontiers of High Resolution Spectroscopy is that it cuts across many topics in astrophysics to concentrate on the common theme of high-resolution spectroscopy — what it has accomplished, and what it can accomplish with new instrumentation. The following papers describe high-resolution spectroscopy as a unique tool for understanding the physical properties of astronom-

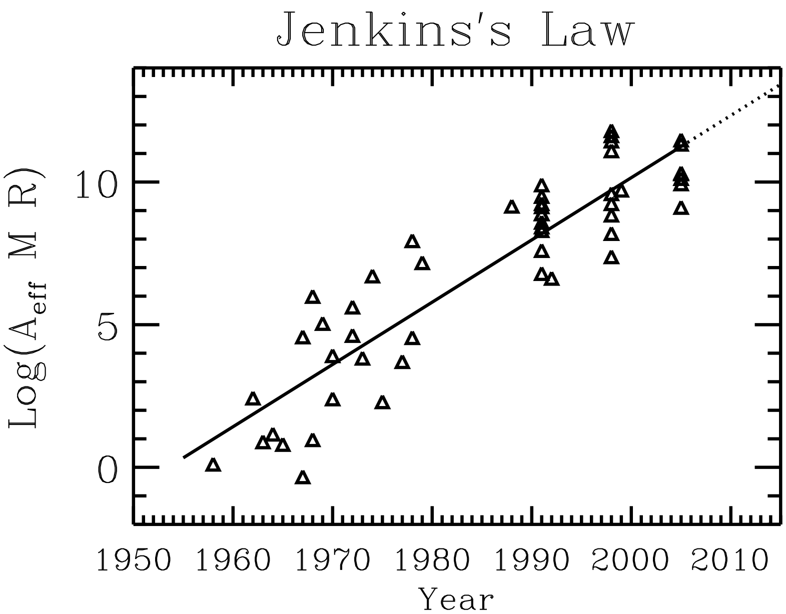

Figure 1. Jenkins's Law is a figure of merit describing the capabilities of UV spectrographs and telescopes with time. This figure is an update of a figure originally presented in Jenkins (1999) and kindly provided by the author.

ical sources — their velocity structures, temperatures, densities, and chemical compositions.

The capabilities for high-resolution spectroscopy of astronomical targets are rapidly increasing with developing technology. As described in more detail by Jenkins in his paper that follows, a useful figure of merit for high-resolution spectroscopy is the product $A_{\rm eff}MR$, where $A_{\rm eff}$ is the effective area, M is the number of independent spectral channels, and $R \equiv \lambda/\Delta\lambda$ is the spectral resolution. As shown in Figure 1, $A_{\rm eff}MR$ for UV spectrographs and telescopes is doubling every 16 months. Jenkins's law is even steeper than Moore's law for the increase in the number of transitors on a chip. Similar plots could be constructed for other wavelength regions. The challenge we face is how to harness this rapidly developing technology to astrophysical research.

2. Implementation

The program was created by the Scientific Organizing Committee: John Bally (USA), Roy Booth (Sweden), Nancy Brickhouse (USA), David Gray (Canada), Jeffrey L. Linsky (Chair, USA), Gautier Mathys (Chile), Michel Mayor (Switzerland), Roberto Pallavicini (Italy), Nikolai Piskunov (Sweden), and Alfred Vidal-Madjar (France).

The program highlighted the astronomical results obtained with high-resolution spectroscopy and other observational techniques that achieve high wavelength or velocity resolution. For example, subdiffraction limited imaging is now achievable through Doppler imaging and other tomographic techniques that require high spectral resolution data with high signal-to-noise and excellent velocity precision.

Joint Discussion 20 presented recent accomplishments and future instrument plans for high-resolution spectroscopy of astronomical sources across the electromagnetic spectrum. At all wavelengths, increased spectral resolution with high throughput is yielding new information on the chemical composition, velocity structure, and physical properties of astronomical sources. As described in the papers that follow, "high resolution" means different things in different spectral regions depending on instrumental capabilities and the properties of the targets observed. New instruments on ground-based and space telescopes will greatly increase these capabilities. The objectives of the joint discussion are to highlight these developments and to present some of the new techniques in instrumentation and data analysis that cross artificial boundaries of wavelength and scientific topic.

The following sixteen papers are short versions of the papers presented at the Frontiers of High Resolution Spectroscopy meeting spanning the electromagnetic spectrum from gamma rays to long wavelength radio astronomy.

I thank Dr. Ed Jenkins for the use of Figure 1 and NASA for support at this meeting.

References

Jenkins, E. B. 1999, in Chemical Evolution from Zero to High Redshift, eds. J. R. Walsh & M. R. Rosa (Berlin: Springer), 280

Highlights of Astronomy, Vol. 13
International Astronomical Union, 2003
O. Engvold, ed.

Gamma-ray Spectroscopy

Jürgen Knödlseder

Centre d'Etude Spatiale des Rayonnements, 9, avenue du Colonel-Roche, B.P. 4346, 31028 Toulouse Cedex, France

Abstract. Gamma-ray spectroscopy has made important progress with the observations of the OSSE and COMPTEL telescopes aboard CGRO, and has entered the domain of high-resolution spectroscopy with the launch of the SPI telescope aboard the INTEGRAL satellite. Recent science highlights in this field are presented, and an outlook is given to future promising projects.

1. Introduction

The gamma-ray domain around MeV-energies is rich in emission lines that arise from transitions following nuclear de-excitation. Each isotope obeys its own characteristic gamma-ray line pattern, hence gamma-ray spectroscopy provides a powerful tool to analyse compositions and abundances. The opaqueness of the atmosphere to gamma-rays requires the use of space based telescopes or stratospheric balloons, with the unavoidable drawback of intense cosmic-ray bombardement that leads to an overwhelming instrumental background. Extracting the generally weak celestial signal from this background is the most challenging task in the analysis of gamma-ray spectroscopy data.

The richest harvest of gamma-ray spectroscopy results comes from the OSSE and COMPTEL telescopes aboard the Compton Gamma Ray Observatory (CGRO) satellite (observing period 1991-2000), although several small satellites and balloon telescopes have also provided significant contributions. Since October 2002, ESA's INTEGRAL satellite is in orbit, and provides with SPI a high-resolution imaging gamma-ray spectrometer with unprecedented performance. The Spectrometer on INTEGRAL (SPI) is equipped with 19 cooled germanium detector crystals that are arranged in a hexagonal pattern and act as the camera of the telescope. A coded mask situated 1.71 metres above the camera modulates the incoming gamma radiation, and provides an angular resolution of $\sim 2.5^o$ within a fully coded field of view of 16^o. Typically, SPI reaches an energy resolution of $\sim$ 2.5 keV at 1 MeV with a narrow line sensitivity of $(2-3)\times 10^{-5}$ ph cm^{-2} s^{-1} for an observation time of 10^6 seconds (Roques et al. 2003). The science objectives that will be addressed by SPI are the mapping of diffuse radioactivities to explore galactic nucleosynthetic activity, the search for the origin of galactic positrons, the study of supernova and nova nucleosynthesis, the search for nuclear excitation lines, and the study of cyclotron lines. In the following section, recent science highlights that have been achieved in these domains will be presented.

2. Science Highlights

The 1.809 MeV gamma-ray line of the radio-isotope ^{26}Al (half-life 7.2×10^5 yr) is so far the best studied non-solar gamma-ray line. COMPTEL observations provided the first all-sky map of the emission and clearly demonstrated that on-going ^{26}Al nucleosynthesis is a galaxy-wide phenomenon (Oberlack et al. 1996). In particular, the gamma-ray line emission traces particularily well the distribution of the most massive stars in the Galaxy, hence it is believed that those are the nucleosynthetic sources of ^{26}Al (Knödlseder et al. 1999). Observations by the GRIS telescope (Naya et al. 1996) indicated a considerable broadening of the 1.809 MeV line that theoretically was only poorly understood. New measurements using the RHESSI solar observatory (Smith 2003a) and SPI (Diehl et al. 2003), however, show that the 1.809 MeV line is narrow, having a width that is compatible with the expected Doppler broadening that arises from the rotation of the Galaxy. Hence, high-resolution spectroscopy combined with imaging, such as provided by SPI, may allow measurements of the subtle line-shifts due to galactic rotation, and thus may provide kinematic distance information to galactic nucleosynthesis regions.

Recent RHESSI observations provided the first evidence for the detection of the 1.173 and 1.332 MeV gamma-ray lines from the radioactive decay of ^{60}Fe (half-life 1.5×10^6 yr) in the general direction of the Galactic Centre (Smith 2003b). ^{60}Fe is believed to be mainly synthesised during supernovae explosions, hence a direct study of explosive nucleosynthesis becomes feasible (in contrast, ^{26}Al also has an important hydrostatic nucleosynthesis channel). Validating the RHESSI measurements and eventually mapping the distribution of the ^{60}Fe lines are major science objectives of the INTEGRAL mission.

The first gamma-ray line detected from the interstellar medium was the 511 keV positron annihilation line (Johnson et al. 1972), yet the origin of the galactic positrons is still unclear. OSSE observations suggest at least two emission components: a prominent extended bulge, and a galactic disk. Hints of a third component, situated above the galactic disk, have gradually faded away with improvements of the data analysis techniques (Milne et al. 2003). Recent SPI observations clearly confirm the bulge emission, yet do not show any hint for a galactic disk component (Knödlseder et al. 2003). The acquired SPI exposure is probably not yet sufficient to detect the faint disk emission, and more data are needed to determine the 511 keV emission distribution in detail. Yet once known, this distribution should provide information about the underlying sources, and hopefully unveil the origin of the positrons.

3. Outlook

The Holy Grail of gamma-ray line spectroscopy, the study of nucleosynthesis in nearby extragalactic supernovae, is still beyond the sensitivity limits of existing gamma-ray telescopes. A breakthrough could come from the usage of a gamma-ray lens, a concept that has been recently validated in a first series of balloon flights in France (Halloin et al. 2003). A gamma-ray lens makes use of Bragg reflection in appropriately designed and selected cristals, which if arranged in a ring, can focus gamma-rays from a large collection area onto a small focal spot. The relatively long focal length ($\sim$ 100 m) requires a two satellite configuration in constellation, such as foreseen for other major astronomy missions (e.g., Darwin, XEUS, ...). Equipped with a small germanium detector, the lens telescope could reach sensitivities of 3×10^{-7} ph cm^{-2} s^{-1} at 847 keV, allowing for line profile studies of supernovae nucleosynthesis products that will provide crucial information for the understanding of the explosion mechanism (Isern et al. 1997).

References

Diehl, R., Knödlseder, J., Lichti, G.G., et al. 2003, A&A, in press

Halloin, H., von Ballmoos, P., Evrard, J., et al. 2003, NIM-A, 504, 120

Isern, J., Gomez-Gomar, J., Bravo, E., & Jean, P. 1997, in Proceedings 2nd INTEGRAL Workshop, St. Malo, France, eds. C. Winkler, T. Courvoisier, Ph. Durouchoux, ESA SP-382, 89

Johnson, W.N., Harnden, F.R., & Haymes, R.C. 1972, ApJ, 172, L1

Knödlseder, J., Lonjou, V., Jean, P., et al. 2003, A&A, in press

Knödlseder, J., Bennett, K., Bloemen, H., et al. 1999, A&A, 344, 68

Naya, J., Barthelmy, S.D., Bartlett, L.M., et al. 1996, Nature, 384, 44

Milne, P. 2003, in Astronomy with Radioactivities IV, in press

Oberlack, U., Bennett, K., Bloemen, H., et al. 1996, A&A, 120C, 311

Roques, J.-P., Schanne, S., von Kienlin, A., et al. 2003, A&A, in press

Smith, D. 2003a, ApJ, 589, 55

Smith, D. 2003b, in Astronomy with Radioactivities IV, in press

Highlights of Astronomy, Vol. 13
International Astronomical Union, 2003
O. Engvold, ed.

Astrophysics at X-Ray Spectral Resolution 1000

Nancy S. Brickhouse

Harvard-Smithsonian CfA, 60 Garden St., Cambridge, MA 02138

Abstract. The Chandra gratings exceed a resolving power R = 1000, but only at the longest wavelengths and with relatively low effective areas. Recent X-ray observations of cool stars illustrate the problem of line blending at different resolutions and give a good sense of what we will routinely be able to measure with Constellation-X, provided it has high enough spectral resolution. We also expect new diagnostics from weak lines and line profiles. Support for this work is provided by NASA NAS8-39083 to SAO for the CXC and LTSA NAG5-3559.

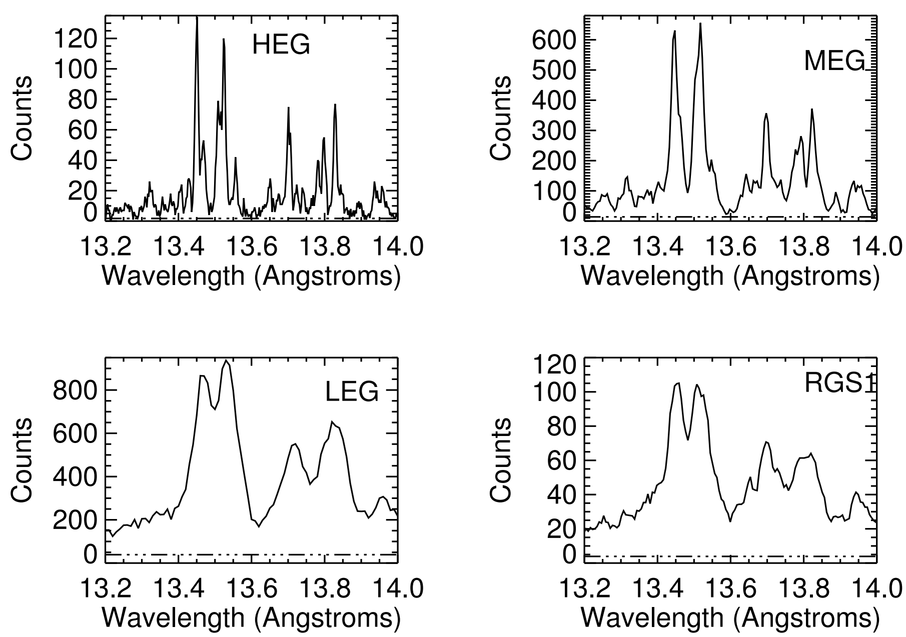

Figure 1. The Ne IX spectral region of Capella at different spectral resolution. At 13.6 Å, the HEG spectrum (154.7 ks) has resolving power R = $\lambda/\Delta\lambda \sim 1000$; MEG (154.7 ks) has R $\sim$ 500; LEG (218.5 ks) has R $\sim$ 270 and RGS (52.92 ks) has R$\sim$ 300.

1. Summary

Figure 1 shows a comparison of the Ne IX spectral region of Capella observed by Chandra and XMM-Newton (Ness et al. 2003). Although numerous strong lines are observed, the full diagnostic potential, even at R = 1000, is not realized because of the modest effective area. Figure 2 shows Lyman series lines, which can provide diagnostics for optical depth and temperature, but require high S/N. Weak lines such as Lyman series and DR satellite lines provide temperature diagnostics for non-equilibrium ionization plasmas.

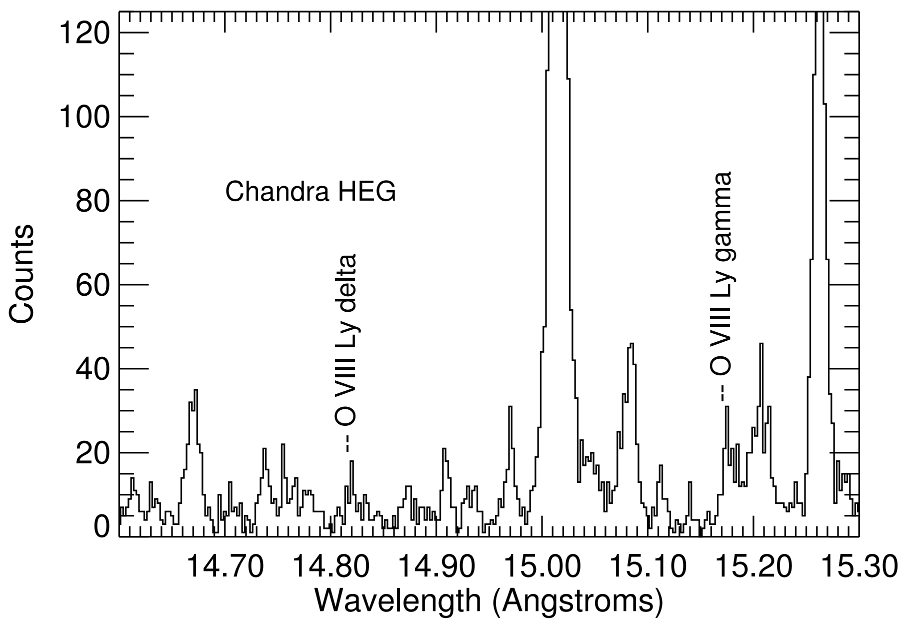

Figure 2. Capella HEG spectrum (154.7 ks) showing two weak O VIII lines. Although Ly_β (not shown) is blended with an Fe XVIII line at R=1000, the other lines appear to be relatively unblended from APEC models (Smith et al. 2001) and the observed spectrum.

Line profile diagnostics are accessible with the current gratings, but again with limited S/N at the highest resolution. While hot star winds are resolved even at low grating resolving power, motions from cool star coronae can be determined in only a few systems. Brickhouse et al. (2001) measured Doppler shifts $\sim$ 100 km s^{-1} as a function of phase and determined the locations and sizes of active regions on the contact binary 44i Boo.

The spectral resolution required for new instrumentation depends on the science case; ultimately, our goal should be to reach the thermal limit R $\sim$ 10,000 (Elvis 2001). For R between 3000 and 5000, line profiles for photoionized plasma may be resolved (Fig. 3). The Capella spectrum shows that many diagnostics are blended at R $\sim$ 1000, a problem that increases drastically at lower R.

References

Brickhouse, N. S., Dupree, A. K., & Young, P. R. 2001, ApJ, 562, L75

Elvis, M., ASP Conf. Ser. 251, New Century of X-ray Astronomy, 180

Krongold, Y., Nicastro, F., Brickhouse, N. S., Elvis, M., Liedahl, D. A., & Mathur, S. 2003, ApJ, accepted

Ness, J.-U., Brickhouse, N. S., Drake, J. J., & Huenemoerder, D. P. 2003, ApJ, accepted

Smith, R. K., Brickhouse, N. S., Liedahl, D. A., & Raymond, J. C. 2001, ApJ, 556, L91

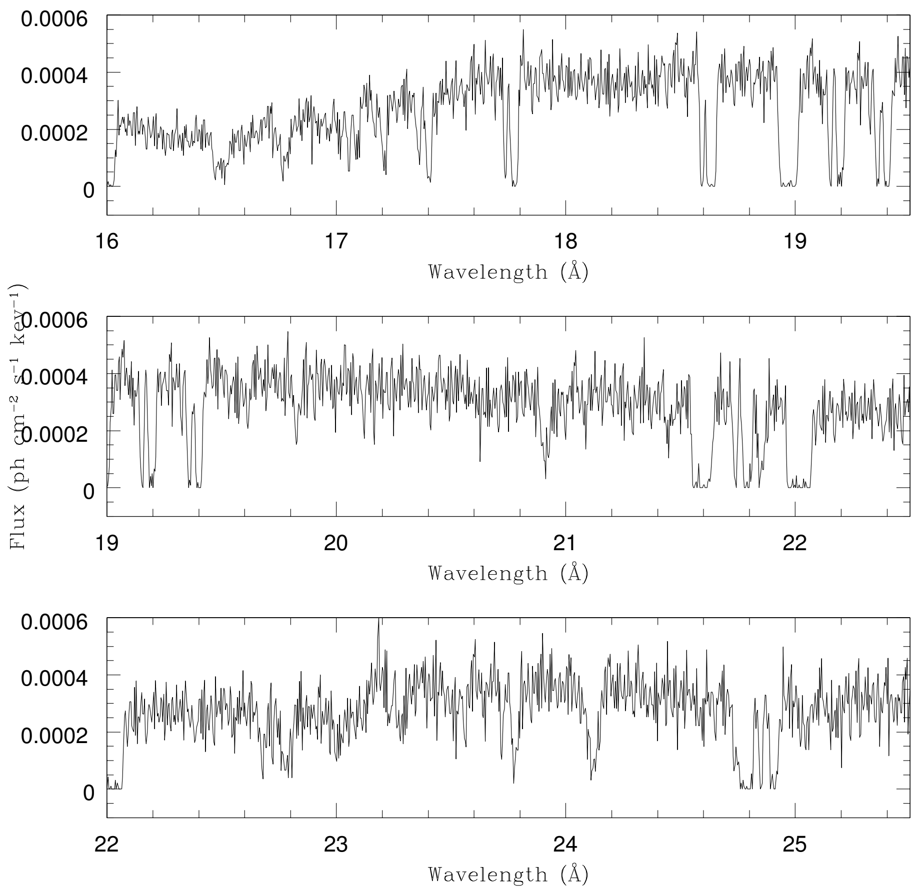

Figure 3. Simulation of NGC 3783 at R = 5000, based on Chandra observations (Krongold et al. 2003) with turbulent broadening. Note that one can distinguish between saturated and unsaturated lines at this resolution. Courtesy of Yair Krongold.

Highlights of Astronomy, Vol. 13
International Astronomical Union, 2003
O. Engvold, ed.

High Resolution X-ray Spectroscopy: Is It Interesting? Is It Possible?

Webster Cash

University of Colorado, Boulder, CO 80309-0391 USA

Abstract. The diffraction grating spectra from Chandra and XMM-Newton have given the astronomical community a huge step forward in x-ray spectroscopy of celestial sources. They have proven the scientific richness of the field. But the spectra have resolution of only 300 to 1000 - low by the standards of the visible and the ultraviolet. We discuss some of the exciting new science that can be addressed if spectral resolution of up to 10,000 (or more) can be achieved in the x-ray. We then show how practical, high efficiency, high resolution x-ray spectrographs can be built for high throughput missions like Constellation-X and XEUS.

After nearly two decades of development, the Chandra Observatory and XMM-Newton were successfully launched. Each features both imaging and spectroscopy modes in the x-ray band from 0.1 to 8 keV. Each has been spectacularly successful. The images from Chandra, featuring unprecedented subarcsecond resolution coupled with high collecting area, have revolutionized our view of the x-ray universe. But, until these two observatories were launched, professional quality x-ray spectra of celestial sources simply did not exist. All prior observatories with spectroscopic capability had very low resolution, typically below 30. Huge advances in our understanding of x-ray sources were made using this low resolution, but most of the spectral information carrying key clues to the nature of the sources was irretrievably blurred.

Chandra and XMM-Newton, with resolution of 300 up to 1500 and collecting areas in the 50 to 300 square centimeter range, reveal the true complexity of the spectra for the first time. The x-ray region, like the ultraviolet, is rich in atomic diagnostics that give basic information about the state of the emitting source and other material along the line of sight. After three years of such data, we are only scratching the surface of what is to come.

But what is needed to continue for the future? Chandra and XMM are limited by their size so more collecting area is needed. Planning is already underway for the next generation of x-ray spectrographs, most prominently for Constellation-X in the USA and XEUS in Europe. In the case of Constellation-X, the goal is to improve the collecting area of the spectrograph by an order of magnitude over XMM-Newton. XEUS, which will follow Con-X into orbit, will provide another order of magnitude yet again. These future missions will be able to reach truly faint x-ray sources.

In the visible portion of the spectrum astronomers value spectral resolution, but usually not at the expense of collecting area. As astronomy matured over the last century it became clear that spectral resolution can, if it comes at the expense of sensitivity, hinder an observation. This brings to mind the question for x-ray spectroscopy: Is high resolution interesting and if so, is it possible?

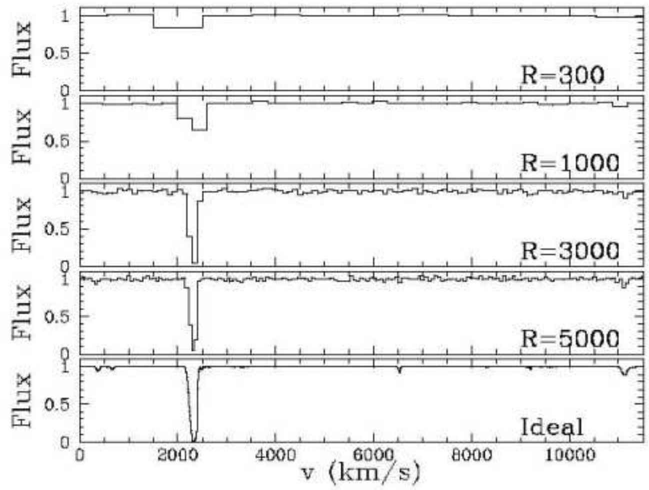

Figure 1. Simulated spectrum of the OVII line from the intergalactic medium smoothed to resolutions of 300, 1000, 3000 and 5000. It is clear that resolution of 1000 is inadequate for this problem, but 3000 appears to be sufficient. (Courtesy N. Gnedin)

What is high resolution in the x-ray band? Anything of resolution higher than is available now is usually considered to be high, meaning that as we push beyond the R=1000 limit of Chandra, we are considering high resolution.

One simple way to look at high resolution is to consider the case of absorption lines. Surely the next generation of observatories, with its huge collecting area, should be designed to resolve absorption lines from gas along the line of sight in the manner that ultraviolet astronomers have been doing for four decades. N. Gnedin has kindly provided me with a simulation of such an absorption line as shown in Figure 1. It simulates the O VII absorption line in the x-ray along a line of sight through the intergalactic medium. Since this observation is of fundamental importance to understanding the intergalactic medium and the formation of structure in the early universe, it is therefore of major importance to the future of x-ray astronomy (Hellston, Gnedin, & Miralda-Escude 1998). The figure shows simulated observations across a range of resolutions from 300 to 5000. It is clear that even resolution of 1000 is not sufficient to perform this important diagnostic: 3000 looks sufficient, and 5000 is definitely good enough.

Next one must address the feasibility of achieving these kinds of resolutions in a practical and affordable way. Unfortunately, the approach used by Chandra is unsuitable to Constellation-X and XEUS because these missions will feature large aperture, densely packed arrays of thin mirrors with spatial resolution poorer than Chandra's. XMM uses an array of reflection gratings to increase dispersion and thereby achieves spectral resolution of 300. Constellation-X is baselined on a similar configuration (Kahn et al. 1999).

Recently, at the University of Colorado, we have been studying an alternative. It again features reflection gratings, but used in the off-plane mount. This concept, as a means for achieving high spectral resolution in the x-ray with

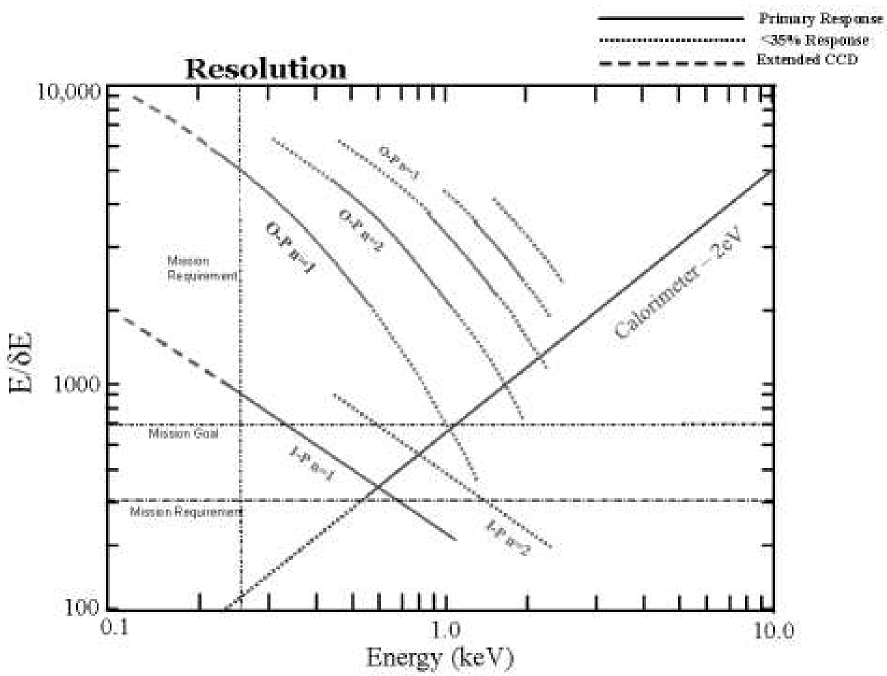

Figure 2. The diagram shows the resolution of the Constellation-X experiment as a function of spectral energy. The straight line that rises to the right is the calorimeter experiment that is optimized for work with the astrophysically significant Fe K line at 6 keV. The straight line in the lower left represents the expected performance of an in-plane reflection grating spectrograph. The curved lines show the potential for improvement represented by the off-plane mount.

modest quality telescopes, was described by Cash (1991). Development is now being supported by NASA through the Constellation-X project, and so far the results look good. Figure 2 shows the eventual possible performance of an off-plane mount grating array on Con-X (McEntaffer, Cash, & Shipley 2002). This approach has the potential to reach the really compelling resolution of 3000.

In summary, high resolution x-ray spectroscopy is very, very interesting, and appears to be achievable within the constraints of the next generation of x-ray observatories. This paper was supported by NASA grant NAG5-11850.

References

Cash, W. 1991, Appl. Opt., 30, 1749

Hellsten, U., Gnedin, N. Y., & Miralda-Escude, J. 1998, ApJ, 509, 56

Kahn, S. K., et al. 1999, Proc. Soc. Photo-Opt. Instr. Eng., 3765, 94

McEntaffer, R., Cash, W., & Shipley, A. 2002, Proc. Soc. Photo-Opt. Instr. Eng., 4851, 549

Highlights of Astronomy, Vol. 13
International Astronomical Union, 2003
O. Engvold, ed.

FUSE and the Quest for High-Resolution Spectroscopy in the Far Ultraviolet

H. Warren Moos

Department of Physics and Astronomy, The Johns Hopkins University, Baltimore, MD 21218 USA

Abstract. The Far Ultraviolet Spectroscopic Explorer (FUSE) instrument covers the spectral range 912–1187 Å with a resolving power of 15,000 to 20,000. This spectral region provides unique access for the study of many atomic and ionic species found in the interstellar medium, intergalactic medium, stars, and extragalactic objects. This paper summarizes the status of the mission and then discusses the need for higher resolution spectroscopy. Although the FUSE instrumental resolution is sufficient to separate most species, it usually it is not adequate for analyzing the gas velocity structure in detail. Implications for future missions are discussed.

1. The FUSE Mission

The Far Ultraviolet Spectroscopic Explorer (FUSE) Mission was developed and is operated by the Johns Hopkins University for NASA with participation by the Canadian Space Agency and the Centre National d'Etudes Spatiales in France. Covering the far ultraviolet from 905 to 1187 Å with a resolution $\sim 20,000$ (15 to 20 km s^{-1}), it complements the intermediate resolution capabilites of the Space Telescope Imaging Spectrograph. FUSE was launched 1999 June 24 into a 765 km circular orbit with an instrument package consisting of four coaligned prime focus telescopes, each imaged on the entrance aperture of a Rowland mount spectrograph. For a more detailed discussion of the FUSE mission see Moos et al. (2000) and Sahnow et al. (2000). The Prime Science Mission began 1999 December 1 and ended 2003 March 31. The Mission is now in the Extended Mission Phase.

The Mission has been quite successful. As of 2002 August, $\sim$ 30 million seconds of data have been obtained for more than 1700 different objects. A broad range of science has been studied ranging from solar-system planets, e.g., Krasnopolsky & Feldman (2001) to the intergalactic medium, e.g., Shull, Tumlinson, & Giroux (2003). We will not attempt to survey the rich and growing literature reporting results from this mission. Rather, we will examine the need for a mission with increased spectral resolution and the technical challenges associated with such a mission.

2. High-Resolution Spectroscopy in the Far Ultraviolet

A major limitation in the extension of far ultraviolet studies to more complex sightlines is spectral resolution. Spectroscopic studies in the far ultraviolet are

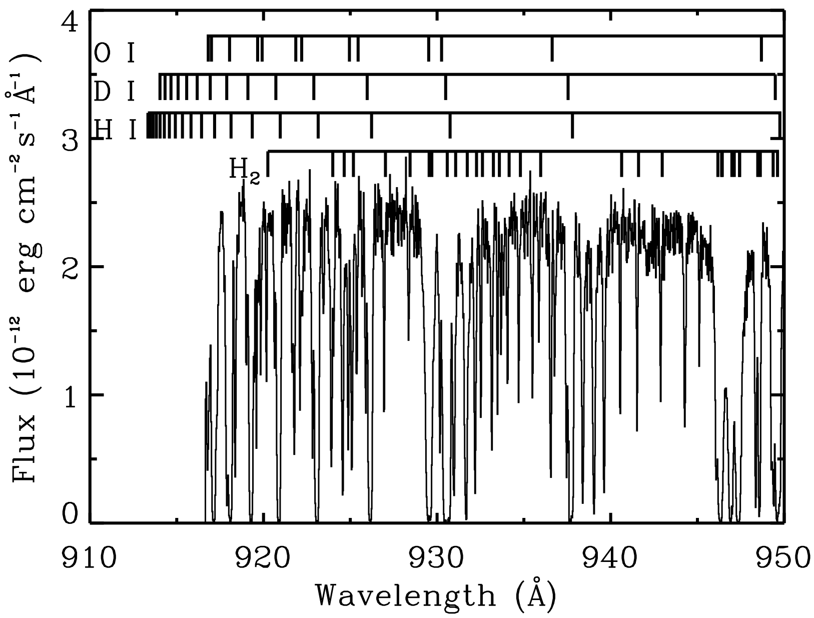

Figure 1. A portion of the FUSE spectrum of PG0038 showing numerous transitions of H I, D I, O I and H_2. At the FUSE resolution, H_2 is often blended with other species. Courtesy of C. Oliveira.

powerful because the region provides access, often unique, to diagnostic transitions in numerous atoms, ions and molecules in the interstellar medium, intergalactic medium, stars, and extragalactic objects. This spectral region is rich, containing strong transitions for H I, D I, O I, O IV, N I, N II, N III, C III, Ar I, Fe II, H_2, and many other species. However, the presence of so many transitions in this region can lead to blends. The FUSE resolution of $\sim$ 15 km s^{-1} is sufficient to remove most blends between transitions, with the notable exception of the numerous transitions of H_2, which are both a blessing and a curse. See Figure 1. However, the FUSE resolution is inadequate for understanding the velocity structure of the gas along a sight line in interstellar medium studies. Generally, moderate resolution will make it difficult to determine whether a line is saturated. In addition, for finite signal to noise, unsaturated weak lines with low b values will be hard to detect. As a result, there is increased uncertainty and less knowledge about systematic errors for complex sightlines.

Is it possible to construct a general purpose FUV observatory with spectral resolution of 1 to 3 km s^{-1}? The answer is yes, but there are significant technical challenges, both in terms of the telescope quality and the transmission of the optical system. To provide enough photons for sensitive high-resolution measurements, the size of the telescope mirror must be much larger than the 0.4 m FUSE telescopes. This leads to demands on both the optical quality and overall length of the instrument package.

First, note that for a high-resolution spectrum, the geometric area of the detector pixels must be as small as possible or the background signal from cosmic rays and scattered light will be too high for sensitive measurements. The smallest possible size of the pixel is set by the entrance aperture to the spectrograph, which in turn is set by the point spread function of the optics and the jitter in the spacecraft pointing. Thus, for a modest 1 m telescope with a focal length of 15 m, 50 μm in the focal plane (equivalent to 2 pixels) corresponds to $0.7''$. The point spread function and spacecraft pointing jitter need to be much less than this, a few times the telescope optical diffraction limit at 5000 Å ($0.12''$). This requirement is important, but does not appear to be a showstopper.

Second, note that the relatively simple FUSE design (a prime focus telescope and a Rowland circle spectrograph) with only two reflecting surfaces probably will not be adequate for reasonably high sensitivity. An instrument with a modest one meter telescope would be $\sim$ 20 m in length, too long to fit inside most launch vehicles. In addition, the FUSE instrument design carries unremovable residual abberrations that could limit the resolution and increase the background signal. In order to overcome the double disadvantages of long length and residual aberrations, a second reflection in both the the telescope and instrument are necessary.

This second reflection is perfectly acceptable if the system operates above 1000 Å, where high reflectivity coatings exist. Copernicus, for example, used a Cassegrain telescope (Rogerson et al. 1973). However, at shorter wavelengths down to the H I photoionization cut off at 912 Å, reflectivies are $\sim$ 0.3 and about one photon in a thousand falling on the telescope will be detected.

The obvious solution is to restrict instruments to wavelengths above 1000 Å, but at the cost of losing many interesting transitions including the most useful ones for D I. Alternatively, we can seek new coatings and other techniques that will permit us to work at these wavelengths. In any case, the limitations set by reflectivity must be taken into account in planning high spectral resolution missions for the far ultraviolet.

Acknowledgments. This work is based in part on data obtained for the Guaranteed Time Team by the NASA-CNES-CSA FUSE mission operated by the Johns Hopkins University. Financial support has been provided by NASA contract NAS5-32985.

References

Krasnopolsky, V. A. & Feldman, P. D. 2001, Science, 294, 1914

Moos, H. W. et al. 2000, ApJ, 538, L1

Rogerson, J. B., et al. 1973, ApJ, 181, L97

Sahnow, D. J. et al. 2000, ApJ, 538, L7

Shull, J. M., Tumlinson, J., & Giroux, M. L. 2003, ApJ, 594, L107

Highlights of Astronomy, Vol. 13
International Astronomical Union, 2003
O. Engvold, ed.

APEX, the Astrophysical Plasmadynamic EXplorer: An EUV High Resolution Spectroscopic Observatory

M Kowalski

Naval Research Laboratory, Code 7655.3, Washington, DC 20375

Abstract. APEX is a proposed Small Explorer satellite that will obtain high-resolution EUV spectra of white dwarfs, CVs, stellar coronae, and the local ISM. The APEX effective area (30-50 cm^2) and resolution (~10,000) are an order of magnitude improvement over Chandra.

APEX, a proposed mission Small Explorer mission, will investigate the density, temperature, composition, magnetic field, structure, and dynamics of hot astrophysical plasmas (log T = 5–7), which emit the bulk of their radiation at EUV wavelengths and produce critical spectral diagnostics not found at other wavelengths. With an effective area 1 cm^2 and resolution R~400, EUVE moved astronomical spectroscopy into the extreme ultraviolet. Chandra and XMM-Newton have demonstrated the promise of high-resolution X-ray spectroscopy. The termination of EUVE has left a gap in spectral coverage at EUV wavelengths that CHIPS fills only partially, as it is optimized for diffuse emission and has only moderate spectral resolution (R~150). We recently flew an APEX prototype (effective area 3 cm^2, R~3000) on a NASA sounding rocket and successfully obtained the first high-resolution EUV spectrum of an astrophysical object, the white dwarf G191-B2B (Cruddace et al. 2002). However, even higher resolution and longer observations are needed to exploit the full range of plasma diagnostic techniques developed in laboratory and solar physics, with unambiguous line identification and measurement of line profiles and Doppler shifts. APEX spans the range 90-275 Å with R~10,000 (Δv=30 km s^{-1}) and effective area 30-50 cm^2. APEX complements the Chandra, FUSE, and CHIPS missions.

APEX addresses basic questions of stellar evolution and galactic structure through high-resolution EUV spectroscopy of white dwarf stars, CVs, the local ISM, and stellar coronae. The science goals are to answer such basic questions in understanding the behavior of million-degree plasmas in the Universe.:

PRIMARY SCIENCE GOALS: (1) What is the evolutionary history of white dwarfs? (2) What are the density, temperature, ionization state, and depletion level of the local ISM? (3) Where are the emission sites in CVs, and what are their temperature, density, composition, and dynamics?

SECONDARY SCIENCE GOALS: (4) What are the structure and dynamics of stellar coronae? (5) What causes the features in the stellar differential EM distributions? (6) What is the relationship between coronal heating and flares? (7) What is the relative importance of magnetic reconnection and MHD and acoustic waves in coronal heating? (8) How do coronae evolve over stellar lifetimes? (9) How do coronal abundances differ from the photospheric abundances?

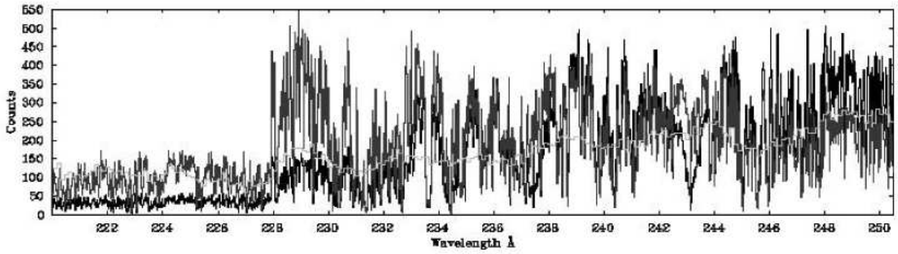

Figure 1. Simulated 4 ksec APEX exposure of the DA white dwarf Feige 24 for H layer masses of 10^{-13} (gray) and 10^{-14}(*black*) $M_\odot$. The white histogram shows the EUVE observation. Poisson noise has been added, but all fluctuations are real spectral features.

We illustrate APEX capabilities for the first goal (Fig. 1). The rapid post main sequence evolution of white dwarfs into two main types, H-rich DA and He-rich DO and DB stars, is complicated and poorly understood. Composition is determined by core nucleosynthesis, shell-burning, and stellar mass-loss. Measured abundances should reflect their evolutionary paths. However, observed patterns may be affected also by gravitational settling (diffusion), selective radiative levitation, magnetic fields, and interstellar accretion. T_{eff}, log g, and the interstellar environment influence the relative importance of these processes. Obtaining high-resolution EUV spectra of a diverse sample of white dwarfs is the key to understanding their evolution. Determination of the photospheric He content provides critical information. EUV spectroscopy of the He II Ly series (228-304 Å) provides a factor of ~100 more sensitivity than the He II lines at FUV wavelengths. Significant quantities of heavy elements are also present in the hottest white dwarf atmospheres. Studies have begun to correlate abundance patterns with evolutionary status (Barstow et al. 2003), but trends are challenged by unexpected complexities in photospheric structure. New measurements of heavy element abundances at different atmospheric depths are required to resolve questions of the radiative levitation/diffusion balance and its effect on atmospheric structure. Lines are formed at different depths in the EUV and FUV, requiring abundance measurements in both bands. High-resolution FUV spectral data are available from IUE or HST, but EUVE lacked the spectral resolution provided by APEX to determine unique heavy element abundances.

APEX is a suite of 8 spectrometers (Fig. 2), each slitless and with a figured diffraction grating (focal length 3 m) operating at near-normal incidence in a Wadsworth mount. Light enters each spectrometer through a collimated aperture, and is diffracted by a grating to form a focused spectrum of a chosen order onto a detector. All spectrometers are functionally identical, but have different wavebands defined primarily by the multilayer coating on each grating. The composite graphite structure has a diameter of 160 cm and a mass of 600 kg. The instrument requires 400 W and produces 1.2 Gb/day of science data.

To obtain high sensitivity, APEX uses large diameter (350 mm) blazed ion-etched gratings, employs multilayer coatings to enhance efficiency (Kowalski et al. 2003), and records spectra with efficient (alkali-halide photocathode)

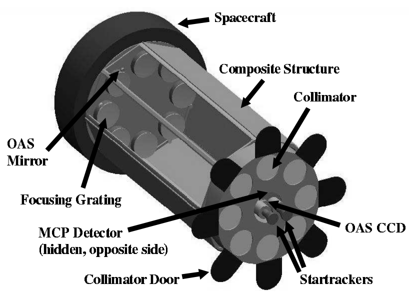

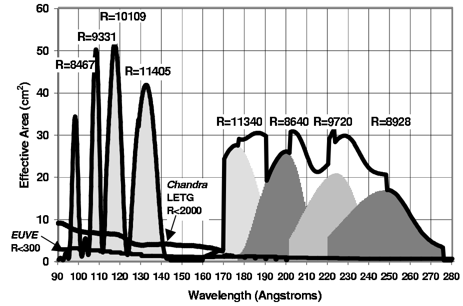

Figure 2. APEX payload. Figure 3. APEX predicted performance.

photon-counting microchannel plate (MCP) detectors with high spatial resolution (15 microns). Unlike FUSE, APEX has no slit and thus requires only modest pointing ($\sim 1'$), but accurate aspect knowledge and measurement of instrument flexure are required for high spectral resolution. Two startrackers produce precise ($< 1''$) pointing knowledge. APEX also employs two systems for measuring flexure, a pair of EUV telescopes and an optical alignment system (OAS), the latter providing continuous wavelength calibration for each spectrometer.

Predicted performance (effective area and R) is shown in Fig. 3. In summary, APEX will achieve effective areas of 30-50 cm^2 over the range 90-275 Å. At the location of important spectral lines the APEX effective area exceeds that of Chandra and EUVE by an order of magnitude. The APEX R$\sim$10,000 exceeds that of Chandra and EUVE by factors of 5 and 30, respectively.

The instrument is mounted on a 3-axis stabilized spacecraft. The Ball Aerospace and Technologies Corp. (BATC) RS-300 bus, suitably modified, meets the APEX requirements with adequate margins. The payload is launched by a Taurus vehicle, and payload size and weight fit comfortably within limits for the 2210 fairing. APEX is proposed for an August 2008 launch into a circular orbit with 500 km altitude and 28.5^o inclination. The baseline mission is 2 years. APEX will observe $\sim$100 targets, which are selected carefully to maximize science, and all have been detected in the EUVE and ROSAT WFC surveys. The mission is a collaboration between the Naval Research Lab., the Lawrence Livermore National Lab., the U. of Leicester, the U. of California Berkeley, and a consortium of institutions that support the science data analysis.

References

Barstow, M. A., et al. 2003, MNRAS, 341, 870

Cruddace, R. G., et al. 2002, ApJ, 565, L47

Kowalski, M. P., et al. 2003, Proc. SPIE, 5168, in press

Highlights of Astronomy, Vol. 13
International Astronomical Union, 2003
O. Engvold, ed.

High Spatial/Spectral Resolution Studies of Eta Carinae

Theodore R. Gull

Laboratory for Astronomy and Solar Physics, Code 681, Goddard Space Flight Center, Greenbelt, MD 20771, USA

Eta Carinae HST Treasury Team

Abstract. We have used the high spatial and high spectral resolution of the Space Telescope Imaging Spectrograph (STIS) to study Eta Carinae and the Homunculus. Since the last minimum in 1998.0, CCD spectral modes have followed changes in the Eta Carinae, and large-scale changes in the Homunculus. Since 2001.7, MAMA echelle-mode observations have followed changes in the Eta Carinae and the very nearby ejecta through the 2003.5 minimum. Very significant changes in the star and nebular occur as the X-Ray drop occurs in the minimum.

1. Introduction

Eta Carinae is the best known Luminous Blue Variable (Davidson & Humphreys 1999). The Homunculus (Gaviola 1950) is primarily a reflection nebulosity ejected during the outburst in the 1840's. It encloses the Little Homunculus (Ishibashi et al. 2003), an ionized shell, about one quarter the linear size of the Homunculus, consistent with ejecta from the 1890's, when a second brightening was noted. Weigelt B, C, and D (Weigelt & Ebersberger 1986) are three bright emission knots within $0\farcs1$ to $0\farcs3$ northwest. The Central Source itself is highly variable both in brightness and line profiles. Damineli (1996) found a 5.52-year periodicity in the He I 10830 Å line profile. The RXTE monitoring (Corcoran 2003) confirms the period to be 2023 ± 7 days. Modelling of CHANDRA spectroscopy (Pittard & Corcoran 2002) shows that the hard x-ray radiation is due to wind-wind collisions between the 600 km s^{-1} wind and a 3000 km s^{-1} wind of a massive binary system. Ground-based observations of the star are heavily contaminated with velocity smeared nebular line emission. With the $0\farcs05$/pixel sampling of the STIS CCD and spectral coverage from 1640 to 10200 Å, spectra of the Central Source were obtained apart from the Weigelt blobs. Zethson (2001) identified over 2000 emission lines from Weigelt blobs B and D, including many variable lines, especially Lyman-α-pumped Fe II lines in the near ultraviolet, between the minimum of 1998.2 and the broad maximum in 1999.3 and 2000.2. Verner et al. (2002, 2003) used CLOUDY to model the Weigelt blob spectra including Fe II during the 1998 minimum and the maximum. Hillier et al. (2001) modelled the Central Source during the minimum. The IUE spectra recorded between 1977 and 1996 indicate spectral changes during the approximately one hundred day minimum. However, since the 5.52-year period was not known, the observations were intermittent in time. Moreover, the relatively large apertures of IUE ($3''$ diameter and $10'' \times 18''$ oval) provided little information on the spatial structure other than half of the uv radiation passed through the smaller aperture.

With its high spatial and spectral resolutions, HST/STIS allowed us to separate the star from the nebulosity. The CCD spectroscopy and long apertures permitted sampling of the Homunculus to determine its three-dimensional shape and mapping of the several very different nebular structures, not possible from the ground. As we approached the minimum predicted to occur in 2003.5, a series of observations were successfully proposed to monitor the changes across the x-ray drop with RXTE, CHANDRA, HST/STIS, and the VLT/UVES. Much additional background information on Eta Carinae is in a conference proceedings (Gull, Johansson, & Davidson 2001) and references cited therein.

2. The STIS Observations

Our systematic studies of Eta Carinae provided much new insight on the structure of the overall nebula, variations of the Central Source, and detailed structures in the immediate vicinity of the Central Source. The first MAMA echelle observations recorded of the Central Source demonstrated that the stellar emission is extended. Through the STIS $0''.2 \times 0''.2$ aperture, a nearly point source is present, with weak extensions. In addition to the interstellar lines, seen as absorption lines perpendicular to the spectral dispersion, other absorption lines are tilted across the spatial extent of the aperture, some with small velocity changes, and other broad lines are seen with large velocity changes. We chose to use a wider aperture, $0''.3 \times 0''.2$, to monitor the extended structure.

Between 2380 and 3160 Å, over 500 absorption lines with 20 velocity systems were identified. Most of the lines are from neutral and singly ionized iron-peak elements. Unlike ISM lines that originate from ground energy states, these lines originate from many higher energy states, some above $20,000$ cm^{-1}. Two velocity systems are of note: –146 km s^{-1} and –513 km s^{-1}. The former appears to have energy populations consistent with 7000 K and the latter with 700 K. During the minimum, a number of new velocity components appear between –170 and –385 km s^{-1}, and the strength of the –146 km s^{-1} lines change. The –513 km s^{-1} components do not change significantly. These systems are likely ejecta located in the wall of the foreground lobe of the Homunculus. The –513 km s^{-1} component is at a considerable distance, likely 20,000 AU, from the Central Source. The –146 km s^{-1} component is very close. The intermediate velocity components appear in Fe II lines during the minimum. During the minimum, the far and mid-uv radiation disappears, and these systems relax from Fe III to Fe II. Up to the x-ray drop, Fe III and Si III] emission can be seen, along with highly excited Fe II, close to the Central Source as depicted in Figure 1 recorded seven days before the x-ray drop on June 29 (Top). Seven days later (Bottom), both Fe III and Si III] emissions have virtually disappeared.

3. Conclusions and Acknowledgements

High spatial and high spectral resolution instruments are providing much new insight into the structure of Eta Carinae and its ejecta. The Eta Carinae ob-

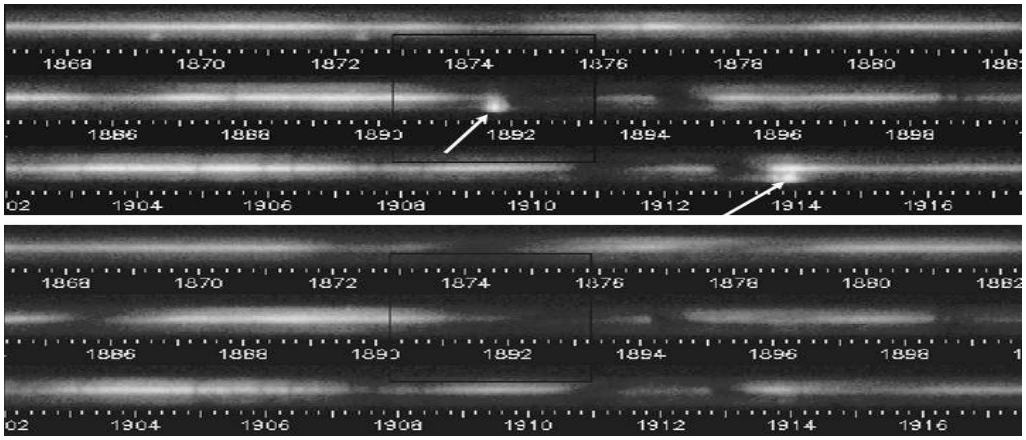

Figure 1. Top: June 22, 2003. Bottom: July 5 2003. Arrows point to Si III] and Fe III emission that disappears after x-ray drop

servations were accomplished through NASA and STScI under STIS GTO (T. Gull, P.I.) and HST GO (K. Davidson, P.I.) programs. We are indebted to Don Lindler and Keith Feggans for their systems and software support.

References

Corcoran, M. 2003, IAUC 8160

Damineli, A. 1996, ApJ, 460, L49

Davidson, K., & Humphreys, R. 1999, ARA&A, 35, 1

Gaviola, E. 1950, ApJ, 111, 408

Gull, T., Johansson, S., & Davidson, K. (editors) 2001, Eta Carinae & Other Mysterious Stars, ASP, 242

Hillier, J., et al. 2001, ApJ, 553, 837

Ishibashi, K., et al. 2003, AJ, 125, 3222

Pittard, J. M., & Corcoran, M. F. 2002, A&A, 383, 636

Verner, E., et al. 2002, ApJ, 585, 115

Verner, E., et al. 2003, in prep

Weigelt, G., & Ebersberger, J. 1986, A&A, 163, L5

Zethson, T. 2001, Ph.D. Thesis, Univ of Lund

Highlights of Astronomy, Vol. 13
International Astronomical Union, 2003
O. Engvold, ed.

The Future for UV Spectroscopy of the ISM at High Resolution

Edward B. Jenkins

Princeton University Observatory
Princeton, NJ 08544-1001
USA

Abstract. In the post-HST era, advanced missions for performing UV spectroscopy must excel in many ways. We must not overlook the importance of high wavelength resolution for investigating absorption lines from gas systems in the Galaxy and beyond. We consider here some basic principles on this topic, both scientific and technical.

1. Fundamental Parameters

Over recent decades, UV astronomy has prospered. However, HST will not last forever, which means that we must prepare for a more advanced facility – one that can allow us to travel well beyond our past accomplishments.

There are a number of figures of merit that will influence an advanced mission's capability to perform point-source spectroscopy. First, the light-gathering power is defined by an effective area $A_{\rm eff}$, which is the product of the unobscured area of the telescope's aperture, the quantum efficiency of the detector, and the efficiency of the optics. Next, there is the multiplexing factor M, which is the number of independent spectral channels that can be recorded simultaneously. The product $A_{\rm eff}M$ determines how rapidly information can be gathered from a source of a given brightness. A central theme of our discussion will be the capability to deliver a high wavelength resolving power $R \equiv \lambda/\Delta\lambda$. This property, along with the signal-to-noise ratio (S/N), governs the quality of the recorded information. The wavelength band – not a real figure of merit – defines what scientific problems we can approach for a system at a given redshift z.

Jenkins (1999) has summarized the advances in $A_{\rm eff}M$ and R for UV spectrographs and telescopes. The product $A_{\rm eff}MR$ has improved at a rate equivalent to a doubling every 16 months. An extrapolation of this trend to the immediate post-HST era could be a 4.6 M diameter telescope with a telescope/spectrograph optical efficiency of 5%, a detector quantum efficiency of 60% and a capability of recording a spectrum with $R = 200,000$ over a bandpass of 600 Å.

2. Secondary Parameters

There are a number of secondary parameters that are sometimes overlooked, but which nevertheless have a bearing on how well we can meet diverse scientific demands. First, there is the equivalent background flux $F_{\rm bkg}$, which may or may not be uniform with wavelength or observing conditions. Even if $F_{\rm bkg}$ is known with good precision, the increased statistical fluctuations will still make the S/N degrade by a factor $\sqrt{1 + (F_{\rm bkg}/F_{\rm source})}$. Next, there are two important parameters that arise from the choice of the detector: (1) the maximum attainable S/N, which is limited by how well one can calibrate sensitivity variations, and (2) the flux above which a detector becomes unacceptably nonlinear or is at risk of being damaged. Finally, there may be scattered light, which arises from either imperfections in the gratings or deficiencies in the spectrograph's baffling scheme. Scattered light increases $F_{\rm bkg}$ and can be particularly bothersome if it is difficult to characterize.

3. The Importance of Achieving High Resolution

Interstellar absorptions often consist of line complexes that have narrow velocity structures with small separations. If one simply wants to measure the total column density, it is often satisfactory to have resolutions that are far inferior to those needed to resolve the individual features. This obviously applies to very weak, unsaturated features, but Jenkins (1986, 1996) has shown that even collections of moderately saturated features can be analyzed if two or more transitions of differing strength are available. While this may be true, it is sometimes necessary to recognize the existence of sharp lines arising from cold material with a small velocity dispersion that may be hidden among other, broader lines. Tripp & Bowen (2003) illustrate the loss of such information at $R = 20,000$. Also, it may be important to recognize differences in the velocity structures between different species within a multiphase medium, as opposed to what may be seen for a homogeneous mixture (Tripp, Savage, & Jenkins 2000). Sometimes, significant insights arise from small kinematical differences of different species (Jenkins & Peimbert 1997). Small shifts in λ arise from important atomic and molecular processes, such as fine-structure excitations (Jenkins & Tripp 2001), isotope shifts (Jenkins & Wallerstein 1999), and rotational excitations of non-hydride molecules (Lambert et al. 1994; Lambert, Sheffer, & Federman 1995).

4. Negative Consequences that Might Arise when R is Increased

There are a number of considerations that, superficially, might be used as arguments against increasing R: **1.** *The detector can accommodate no more than some fixed value of M, so an increase in R means that the wavelength coverage in a single exposure must be sacrificed.* This is true for STIS on HST: for instance, one must make a choice between $R = 120,000$ and $\Delta\lambda = 200$ Å (E140H) or $R = 46,000$ and $\Delta\lambda = 600$ Å (E140M). However, the original STIS proposal in 1985 specified a far-UV detector with 4 times as many pixels as the one finally adopted for the instrument (to reduce development risks). It is therefore not outlandish to propose that after 2010 a $\Delta\lambda$ of about 800 Å with $R = 120,000$ is a realistic goal. **2.** *As R increases, $A_{\rm eff}$ must decrease, thereby compromising research on faint objects.* Again, this is true for STIS on HST: modes with successively higher R have lower $A_{\rm eff}$. However, the product $A_{\rm eff}M$ is an order of magnitude higher in the high resolution modes. **3.** *The increased detector area per unit $\Delta\lambda$ causes $F_{\rm bkg}$ to increase, thus further limiting research on faint* *targets.* There are ways to reduce the detector background without resorting to exotic technologies: (1) cool the detector and use a photocathode with a high work function to reduce the spontaneous emission rate, (2) use materials within the detector that have very low concentrations of naturally radioactive elements, and (3) use a detector that can sense individual photoevents with a good timing accuracy and then build an anticoincidence shield so that events caused by energetic charged particles can be vetoed. **4.** *A high-resolution spectrograph places unacceptably large demands on the rest of the facility (e.g., small telescope point-spread function, tight pointing requirements, etc.).* This is a moderately difficult issue. An echelle grating operating in a Littrow configuration has a sensitivity to angular deviations given by $1/R = d\lambda/\lambda = \cot\alpha\, d\alpha/2$, where α is the angle of incidence. Deviations in α are magnified by the ratio of the main telescope's focal length to that of the collimator, which favors a large diameter collimator (and grating) to increase R. A possible solution that virtually eliminates the angular dependence is to use a UV interferometer (Harlander, Reynolds, & Roesler 1992; Stephan et al. 2001), perhaps working in conjunction with a conventional spectrograph (Edelstein & Miller 1999; Erskine 2003). However, such an arrangement will probably lower the overall optical efficiency.

References

Edelstein, J., & Miller, T. N. 1999, in ASP Conf. Ser. 164, Ultraviolet-Optical Space Astronomy beyond HST, ed. J. A. Morse, J. M. Shull & A. L. Kinney (San Francisco: ASP), 333

Erskine, D. J. 2003, PASP, 115, 255

Harlander, J., Reynolds, R. J., & Roesler, F. L. 1992, ApJ, 396, 730

Jenkins, E. B. 1986, ApJ, 304, 739

— 1996, ApJ, 471, 292

— 1999, in Chemical Evolution from Zero to High Redshift, ed. J. R. Walsh & M. R. Rosa (Berlin: Springer), p. 280

Jenkins, E. B., & Peimbert, A. 1997, ApJ, 477, 265

Jenkins, E. B., & Tripp, T. M. 2001, ApJS, 137, 297

Jenkins, E. B., & Wallerstein, G. 1999, in ASP Conf. Ser. 164, Ultraviolet-Optical Space Astronomy beyond HST, ed. J. A. Morse, J. M. Shull & A. L. Kinney (San Francisco: ASP), 118

Lambert, D. L., Sheffer, Y., & Federman, S. R. 1995, ApJ, 438, 740

Lambert, D. L., Sheffer, Y., Gilliland, R. L., & Federman, S. R. 1994, ApJ, 420, 756

Stephan, S. G., Chakrabarti, S., Vickers, J., & Cook, T. 2001, ApJ, 559, 491

Tripp, T. M., & Bowen, D. V. 2003, in ASP Conf. Ser. 291, Hubble's Science Legacy: Future Optical/Ultraviolet Astronomy from Space, ed. K. R. Sembach, J. C. Blades, G. D. Illingworth & R. C. Kennicutt (San Francisco: ASP), 407

Tripp, T. M., Savage, B. D., & Jenkins, E. B. 2000, ApJ, 534, L1

Highlights of Astronomy, Vol. 13
International Astronomical Union, 2003
O. Engvold, ed.

Mapping of Stellar Surfaces with Doppler and Zeeman Doppler Imaging

Andrew Collier Cameron

School of Physics and Astronomy, University of St Andrews, North Haugh, St Andrews, SCOTLAND KY16 9SS

Abstract. Doppler imaging has been used to image dark spots on the surfaces of rapidly rotating, magnetically active stars for the last 20 years. More recently, methods have been developed for combining line-profile information from large numbers of spectral lines simultaneously. This has allowed starspot distributions to be mapped in sufficient detail to allow tracking of individual spots over several stellar rotations, delineating surface differential rotation patterns for a number of stars. Zeeman-Doppler imaging allows the creation of stellar magnetograms, which are providing the first insights into the 3D topology of stellar coronal magnetic fields. The advent of cryogenic infrared echelle spectrographs opens up exciting new possibilities for Doppler imaging in molecular lines of species such as TiO, OH, and FeH.

1. Doppler Imaging and Differential Rotation

Stellar magnetic activity is driven by the interaction between differential rotation and convection in the outer envelopes of rapidly rotating solar-type stars. This activity manifests itself as coronal X-ray emission, chromospheric UV and optical line emission, and rotational modulation of the optical continuum by widespread starspot activity.

Since rotation is a key driver of this activity, many of the most active solar-type stars spin fast enough that the rotational Doppler effect is the dominant line-broadening mechanism. In such rapidly rotating stars, different parts of the stellar surface become more or less separated in velocity space. Doppler imaging takes advantage of this separation, utilising spectra at resolving powers of order $R = 50000$. Dark features on the stellar surface produce a flux deficit at all wavelengths except those of photospheric absorption lines at the local Doppler shift. As a result, bright pseudo-emission bumps appear in the rotationally-broadened profiles of nearly all the photospheric lines. These bumps drift across the profile from blue to red, following sinusoidal paths whose velocity amplitude is determined by the spot latitude, and whose period of recurrence is determined by the local rotation period at that latitude on the star.

This pattern of drifting features can be inverted tomographically to recover a map of the stellar surface. This inversion method, dubbed "Doppler imaging" in the pioneering paper by Vogt & Penrod (1983) that first applied such techniques to spots on cool stars, was developed formally using a regularised inversion techniques by Goncharsky et al. (1977) using the regularisation method of Tikhonov (1963), and by Vogt, Penrod & Hatzes (1987) using maximum-entropy regularisation. Since then, several groups have developed codes that use either these methods or the "Occamian" singular-value decomposition method of Berdyugina (1998).

In the last two decades, many single and binary dwarf, subgiant and giant stars have been imaged by these groups. One of the more striking recent applications has been the use of starspots as tracers of stellar surface differential rotation patterns. This has been achieved via a variety of methods, ranging from latitude-by-latitude cross-correlation of images taken two or more rotations apart (Donati & Cameron 1997), to more spohisticated modelling approaches in which the differential rotation model is built into the inversion code itself (Donati et al. 2000). The actual form of the differential rotation law has been verified via direct tracking of individual spot signatures in data space (Cameron, Donati & Semel 2002). By and large, these studies have revealed that most dwarf and subgiant stars appear to have solar-like differential rotation, in the sense that the equator rotates faster than the poles, with the equator overtaking the polar regions on timescales of order tens to hundreds of days.

2. Zeeman-Doppler Imaging

Doppler imaging acquired a new dimension in the 1990s with the advent of high-precision fibre-fed echelle spectropolarimeters, in particular the portable unit deployed at the Anglo-Australian and Canada-France-Hawaii Telescopes by Semel et al. (1993). Using this instrument, Donati et al. (1997)demonstrated that, by creating an optimally-weighted sum of the Stokes V signatures in thousands of photospheric lines observed simultaneously, it was possible to detect and even map the vector magnetic field at the surface of an active star, with a surface resolution as small as a few degrees in some cases. This work has led Hussain et al. (2001) to investigate the three-dimensional topology of potential fields extrapolated from Zeeman-Doppler images of young pre-main sequence stars such as AB Dor and LQ Hya. Models in which these field structures are filled with X-ray emitting plasma in hydrostatic equilibrium are proving a powerful tool in interpreting the rotational modulation of coronal X-ray emission from these stars (Jardine et al. 2002). In the near future, new-generation spectropolarimeters such as CFHT/ESPADONS (Manset & Donati 2003) and LBT/PEPSI-ICE (Strassmeier et al. 2003; Pallavicini et al. 2003) will enable Zeeman-Doppler imaging to be extended to fainter objects than have hitherto been accessible. In particular, it should be possible to map the magnetic fields of T Tauri stars and fully-convective M dwarfs, and so to discover the dynamo modes that are excited in the absence of a radiative-convective interface region.

3. The Infrared Frontier

One of the major deficiencies of Zeeman-Doppler imaging is that at optical wavelengths, the Zeeman signature of the magnetic field in the dark starspots is suppressed by the contrast between the low surface brightness in the spots and the bright photosphere. The advent of high-resolution infrared spectrometers such as GEMINI-S/PHOENIX (Hinkle et al. 1998) and VLT/CRIRES (Moorwood et al. 2003; Kaeufl et al. 2003) will enable us to produce Doppler images in lines of molecular species such as TiO, OH, and FeH that are *only* present in the spots. In the slightly longer term, theoretical and laboratory measurements of the Lande g-factors for these molecular transitions (e.g., Berdyugina & Solanki 2002) should allow direct measurement of the field strengths in the spot umbrae themselves. This will represent a major step towards a full understanding of the magnetic flux budget in the photospheres, coronae, and winds of young stars, and its influence on the rotational evolution of both single and binary stars.

References

Berdyugina S. V., & Solanki S. K. 2002, A&A, 385, 701

Berdyugina S. V. 1998, A&A, 338, 97

Collier Cameron A., Donati J.-F., & Semel M. 2002, MNRAS, 330, 699

Donati J.-F., & Collier Cameron A. 1997, MNRAS, 291, 1

Donati J.-F., Semel M., Carter B., Rees D. E., & Collier Cameron A. 1997, MNRAS, 291, 658

Donati J.-F., Mengel M., Carter B. D., Marsden S., Collier Cameron A., & Wichmann R. 2000, MNRAS, 316, 699

Goncharsky A. V., Stepanov V. V., Khokhlova V. L., & Yagola A. G. 1977, Soviet Astron. Lett., 3, 147

Hinkle K. H., et al. 1998, in Proceedings of the SPIE Vol. 3354, Infrared Astronomical Instrumentation, ed. A. M. Fowler, 810

Hussain G. A. J., Jardine M., & Collier Cameron A. 2001, MNRAS, 322, 681

Jardine M., Wood K., Collier Cameron A., Donati J.-F., & Mackay D. H. 2002, MNRAS, 336, 1364

Kaeufl H., Moorwood A. F. M., & Pirard J., 2003, in Proceedings of the SPIE Vol. 4843, Polarimetry in Astronomy, ed. S. Fineschi, 223

Manset N., & Donati J. 2003, in Polarimetry in Astronomy, ed. S. Fineschi, Proceedings of the SPIE, 4843, 425

Moorwood A. F. M., et al. 2003, in Proceedings of the SPIE Vol. 4841, Instrument Design and Performance for Optical/Infrared Ground-based Telescopes, ed. M. Iye, & A. F. M. Moorwood, 1592

Pallavicini R., et al. 2003, in Proceedings of the SPIE Vol. 4841, Instrument Design and Performance for Optical/Infrared Ground-based Telescopes, ed. M. Iye, M. & A. F. M. Moorwood, 1345

Semel M. 1993, A&A, 278, 231

Strassmeier K. G., et al. 2003, in Proceedings of the SPIE Vol. 4843, Polarimetry in Astronomy, ed. S. Fineschi, 180

Tikhonov A. N. 1963, Soviet Math. Dokl., 4, 1624

Vogt S. S., & Penrod G. D. 1983, PASP, 95, 565

Vogt S. S., Penrod G. D., & Hatzes A. P. 1987, ApJ, 321, 496

Highlights of Astronomy, Vol. 13
International Astronomical Union, 2003
O. Engvold, ed.

High-Resolution Optical Observations of Interstellar Absorption Lines

Daniel E. Welty

University of Chicago, 5640 S. Ellis Ave., Chicago, IL 60637

Abstract. We briefly note several current topics concerning the properties of interstellar clouds for which high-resolution optical spectra play a significant role: (1) the recognition and characterization of small-scale (sub-pc) structure in both atomic and molecular gas; (2) the discovery of variations in the ^{7}Li/^{6}Li isotopic ratio in the nearby Galactic ISM; (3) the determination of atomic and molecular abundances and physical conditions for heavily reddened ("translucent") Galactic sightlines; and (4) studies of interstellar clouds in the LMC and SMC.

1. Introduction

High-resolution (FWHM = 0.3–1.5 km s^{-1}) optical spectra of the interstellar (IS) absorption due to various atomic and molecular species have revealed complex velocity structure along many lines of sight (e.g., Crawford 1995; Crane, Lambert, & Sheffer 1995; Welty, Morton, & Hobbs 1996; Welty & Hobbs 2001; Price et al. 2001). Fits to the line profiles suggest that the median line widths (FWHM) for individual components ("clouds") seen in the trace neutral species and the median separation between adjacent components are both less than 1.2 km s^{-1}. Moreover, the adjacent components can have very different properties (e.g., line width, Na I/Ca II ratio, molecular abundances). Such high resolution spectra are therefore necessary for both discerning and determining the composition and physical properties of *individual* IS clouds in different environments.

2. Small-Scale Structure

Pervasive small-scale (sub-pc) spatial structure in the ISM has been revealed both by differences in the line profiles of various species toward binary/multiple systems (e.g., Watson & Meyer 1996; Lauroesch & Meyer 1999; Pan, Federman, & Welty 2001) and by temporal variations in the profiles in some sightlines (e.g., Blades et al. 1997; Price, Crawford, & Barlow 2000; Crawford 2002; Lauroesch & Meyer 2003). The physical characteristics of this seemingly ubiquitous structure are not well understood, however. For example, do the observed profile differences reflect differences in overall N(H), in local density, in ionization, and/or in chemistry on those small scales? Toward the halo star HD 219188, where we have both multi-epoch high-resolution optical and UV spectra, the time-variable component is relatively cool ($T < 500$ K), with modest depletions, a relatively low density $n_{\rm H} \sim 25$ cm^{-3}, a low overall N(H) $\sim 5 \times 10^{17}$ cm^{-2}, and a relatively high fractional ionization $n_e/n_{\rm H} \gtrsim 0.03$ (Welty & Fitzpatrick 2001).

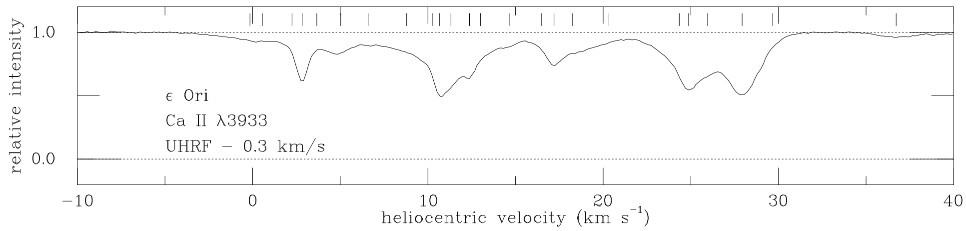

Figure 1. Complex interstellar Ca II absorption toward ϵ Ori.

In that particular case, the differences seem to be due to variations in density and ionization [rather than in overall N(H)] on scales of tens of AU, without the large local pressures and densities sometimes inferred.

3. Variations in ^{7}Li/^{6}Li

Abundances and isotope ratios for the light elements Li, Be, and B can provide information on big bang nucleosynthesis, Galactic chemical evolution, and cosmic ray spallation processes. Determination of the ^{7}Li/^{6}Li ratio requires optical spectra with both high S/N (the Li I doublet lines at 6708 Å are very weak) and high spectral resolution (doublet separation $\sim$ 6.8 km s^{-1} for both, with the stronger member of the ^{6}Li I doublet almost coincident with the weaker member of the ^{7}Li I doublet; hyperfine structure in the ^{7}Li I lines). Knauth, Federman, & Lambert (2003) find interstellar ^{7}Li/^{6}Li ratios consistent with the solar system (meteoritic) value of 12.3 for four of the five sightlines with detected Li I absorption (see also Howarth et al. 2002). Toward o Per, however, fits to the observed line profile yield isotope ratios of 2.1 (close to the value expected for cosmic ray spallation) and 8.1 for the two components discernible in the spectra. While there are other indications that the cosmic ray flux might be enhanced in that direction, the resultant overall enhancement of Li is not observed.

4. Properties of Translucent Clouds

The so-called "translucent" IS clouds, with $1 \lesssim A_V \lesssim 5$, are thought to be intermediate (transitional?) objects between diffuse and dense clouds, and (as such) would provide useful tests for models of cloud chemistry. A survey of several dozen moderately reddened sightlines undertaken with *FUSE*, however, has not revealed the very high molecular fractions and more severe depletions expected for such objects (Rachford et al. 2002; Snow, Rachford, & Figoski 2002). High resolution (0.3–1.8 km s^{-1}) optical spectra of Na I, K I, and CH absorption suggest that essentially all those sightlines contain multiple diffuse clouds (only), with no individual translucent clouds. Knowledge of the complex component structures in those sightlines provided by the optical spectra can be crucial for determining column densities for species such as HD and the excited rotational levels of H_2, whose lines are observed at much lower resolution with *FUSE* (Snow et al. 2000; Ferlet et al. 2000).

5. ISM in the Magellanic Clouds

Studies of the ISM in the Magellanic Clouds (MC) explore somewhat different environmental conditions from those typically probed in our Galaxy: lower metallicities, lower dust-to-gas ratios, stronger radiation fields, differences in UV extinction. Using the new "very long camera" on the coudé echelle spectrograph at the ESO 3.6 m telescope, we have obtained high-resolution (1.2–2.0 km s^{-1}) spectra of IS Na I and Ca II toward SMC and LMC stars with $V \sim 11$–13 mag. These high-resolution spectra reveal numerous narrow, closely blended components in the MC ISM (similar to those seen in our own Galactic ISM). Together with UV spectra from *IUE*, *HST*, and *FUSE*, the optical spectra are being used to determine abundances, depletions, and physical conditions for diffuse clouds in the MC (Welty & Hobbs 2001; Welty et al. 2001 and in prep.).

Acknowledgments. DEW acknowledges support from NASA LTSA grant NAG5-11413 to the University of Chicago. Slides for this contribution may be obtained from ftp://astro.uchicago.edu/pub/astro/welty/IAU25/iau25.ppt.

References

Blades, J. C., Sahu, M. S., He, L., Crawford, I. A., Barlow, M. J., & Diego, F. 1997, ApJ, 478, 648

Crane, P., Lambert, D. L., & Sheffer, Y. 1995, ApJS, 99, 107

Crawford, I. A. 1995, MNRAS, 277, 458

Crawford, I. A. 2002, MNRAS, 334, L33

Ferlet, R., et al. 2000, ApJ, 538, L69

Howarth, I. D., Price, R. J., Crawford, I. A., & Hawkins, I. 2002, MNRAS, 335, 267

Knauth, D. C., Federman, S. R., & Lambert, D. L. 2003, ApJ, 586, 268

Lauroesch, J. T. & Meyer, D. M. 1999, ApJ, 519, L191

Lauroesch, J. T. & Meyer, D. M. 2003, ApJ, 591, L123

Pan, K., Federman, S. R., & Welty, D. E. 2001, ApJ, 558, L105

Price, R. J., Crawford, I. A., & Barlow, M. J. 2000, MNRAS, 312, L43

Price, R. J., Crawford, I. A., Barlow, M. J., & Howarth, I. D. 2001, MNRAS, 328, 555

Rachford, B. L., et al. 2002, ApJ, 577, 221

Snow, T. P., et al. 2000, ApJ, 538, L65

Snow, T. P., Rachford, B. L., & Figoski, L. 2002, 573, 662

Watson, J. K., & Meyer, D. M. 1996, ApJ, 473, L127

Welty, D. E., & Fitzpatrick, E. L. 2001, ApJ, 551, L175

Welty, D. E., & Hobbs, L. M. 2001, ApJS, 133, 345

Welty, D. E., Lauroesch, J. T., Blades, J. C., Hobbs, L. M., & York, D. G. 2001, ApJ, 554, L75

Welty, D. E., Morton, D. C., & Hobbs, L. M. 1996, ApJS, 106, 533

Highlights of Astronomy, Vol. 13
International Astronomical Union, 2003
O. Engvold, ed.

The Deuterium Balmer Series

Guillaume Hébrard

Institut d'Astrophysique de Paris, CNRS, 98$^{\text{bis}}$ boulevard Arago, F-75014 Paris, France

Abstract. The first detection and identification of deuterium Balmer lines were recently reported in H *ii* regions, using high spectral resolution data secured at CFHT and VLT. The D *i* lines appear as faint, narrow emission features in the blue wings of the H *i* Balmer lines and can be distinguished from high-velocity H *i* emission. The identification as deuterium and the excitation mechanism as fluorescence are both established beyond doubt. The deuterium Balmer series might lead to a new, optical method of deuterium abundance measurement in the interstellar medium. This may be the only way to observe atomic deuterium in objects like the Magellanic Clouds or low metallicity blue compact galaxies.

1. Introduction

Deuterium is believed to be produced within minutes of the Big Bang and then destroyed through astration. Measuring its abundance brings constraints on Big-Bang nucleosynthesis and on Galactic evolution. Although the evolution of the deuterium abundance seems to be qualitatively understood, the different types of measurements have not yet converged to definite values and still show some dispersion. D/H measurements are mainly performed through Lyman series observations in absorption. We explore here the possibility of using a new method, namely the Balmer emission lines of deuterium, hitherto undetected.

2. Observations

We performed the first detection and identification of the deuterium Balmer lines Dα and Dβ in emission in the Orion Nebula using CFHT + Gecko. The narrowness of these lines (FWHM $\simeq$ 10 km s^{-1}) and their relative fluxes are incompatible with recombination excitation, but could be understood in terms of fluorescence excitation by stellar UV continuum in the Photon Dominated Region (PDR), located behind the ionized region. The velocity shift between the H *i* and D *i* lines agrees with this interpretation (Hébrard et al. 2000a).

By assuming that both the ionization of the H *ii* region and the deuterium fluorescence are due to a 4×10^4 K black body, and that all of the Lyβ_{D} photons (and only them) produce Dα photons, we predict the flux ratio $I(\text{D}\alpha)/I(\text{H}\alpha) \simeq 3 \times 10^{-4}$, close to the observed value ($\sim 2.2 \times 10^{-4}$). This very coarse estimate shows that deuterium fluorescence is a plausible mechanism.

The discovery of the deuterium Balmer lines was confirmed by new observations of the whole Balmer series in Orion that we secured at the VLT with UVES. The increase of the D *i* lines intensity relative to the H *i* lines with principal quantum number n supports fluorescence rather than recombination as the

D *i* emission mechanism. The lack of counterparts to D *i* lines other than H *i* (*e.g.,* [N *ii*], [O *ii*], or [O *iii*]) allows any interpretation in terms of emission from high-velocity ionized gas to be excluded (Hébrard et al. 2000b).

Deuterium Balmer lines have been detected in five H *ii* regions with the VLT (M 42, M 8, M 16, M 20, and DEM S 103 in the Small Magellanic Cloud), demonstrating that these lines are of common occurrence. One should note that the detection of Dα in the SMC is the first detection of atomic deuterium in this object by whatever means. Since the metallicity of the SMC is low, the deuterium abundance should be closer to primordial in this extra-galactic region.

Another H *ii* region was observed at the VLT: M 17. Here the emission features detected in the blue wings of the H *i* lines differ from those shown in previous targets: (1) they are broad (FWHM $\simeq 20$ km s^{-1}; (2) their fluxes are proportional to the H *i* lines fluxes; (3) [N *ii*], [O *ii*], and [O *iii*] lines are present counterparts at the same velocity. It is concluded that, in this case, the features should be mainly due to H *i* emission from ionized material.

3. Identification

Here we summarize the different arguments in favor of identifying the observed lines with the deuterium Balmer series, emitted by fluorescence in the PDR.

The lines are produced in the PDR because (1), the narrowness of the lines does imply they originate in a cold, localized region along the line of sight; (2), their radial velocities coincide with those of the neutral and molecular material, not with those of the ionized gas.

They are excited by fluorescence because (1), the narrowness of the lines excludes Raman scattering, stellar light scattering, or recombination; (2), their relative fluxes are incompatible with recombination; (3), their fluxes are roughly in agreement with fluorescence mechanism.

They are identified with deuterium because (1), they are not instrumental artifacts since they have been detected using different instruments (see also O'Dell et al. 2001) and they were not detected in wings from any lines but H *i*, nor in PNe; (2), they are not due to other elements since a whole series is detected; (3) they are not due to high velocity ionized structure, because they are not emitted through recombination and they show no counterparts in other species; and (4), they are not due to H *i* fluorescence in high velocity neutral structures: such structures are unknown whereas these lines are of common occurrence.

References

Hébrard, G., Péquignot, D., Vidal-Madjar, A., et al., 2000a, A&A, 354, L79
Hébrard, G., Péquignot, D., Walsh, J. R., et al., 2000b, A&A, 364, L31
O'Dell, C. R, Ferland, G. J., & Henney, W. J. 2001, apj, 556, 203

This work is based on observations collected at the Canada-France-Hawaii Telescope, Hawaii, USA, and at the Very Large Telescope, European Southern Observatory, Chile.

Highlights of Astronomy, Vol. 13
International Astronomical Union, 2003
O. Engvold, ed.

Surface Gravities and Masses in Substellar Objects

Subhanjoy Mohanty

Harvard-Smithsonian CfA, 60 Garden Street, Cambridge, MA 02138

Gibor Basri

Astronomy Department, University of California, Berkeley, CA 94720

Ray Jayawardhana

Astronomy Department, University of Michigan, Ann Arbor, MI 48109

Abstract. Using high-resolution optical spectra, we determine effective temperatures and gravities for a sample of very low-mass stellar and substellar PMS cluster objects. Masses and radii are then derived using known cluster distance and photometry; two of our targets seem to have planetary masses. Our results are *independent* of theoretical evolutionary tracks. While our results agree with the track predictions for hotter, higher mass objects, discrepancies appear for the coolest, lowest mass ones. This may be due to track uncertainties related to formation effects, and/or internal conditions, in these very young, ultra-low-mass objects.

1. Method of Analysis

Our data consists of high-resolution (R≈31000) optical spectra of mid- to late M-type PMS objects in Upper Scorpius and Taurus. We derive T_{eff} and gravity (log g), from a fine analysis of of the TiO bandheads and Na I and K I alkali doublets, through comparison with the latest synthetic spectra (Allard et al. 2001). These spectral diagnostics complement each other, removing temperature/gravity degeneracies in the behavior of each; together they allow us to determine T_{eff} and log g to a precision of ±50 K and ±0.25 dex respectively. Combining our values of T_{eff} and log g with the known distance to Upper Scorpius and Taurus (≈140 pc) and observed and synthetic photometry, we also derive masses (within a factor of 2) and radii (within 30%). We emphasize that our derived quantities are independent of any theoretical evolutionary models. Finally, various tests indicate that our results are not significantly affected by photospheric dust, cool magnetic spots, or metallicity variations.

2. Results

Our temperature and gravity results are compared to the Lyon theoretical evolutionary tracks (Chabrier et al. 2000) in Fig. 1. For $T_{eff} \gtrsim 2750$ K, our gravities are consistent (within our errors) with the theoretical predictions for the ex-

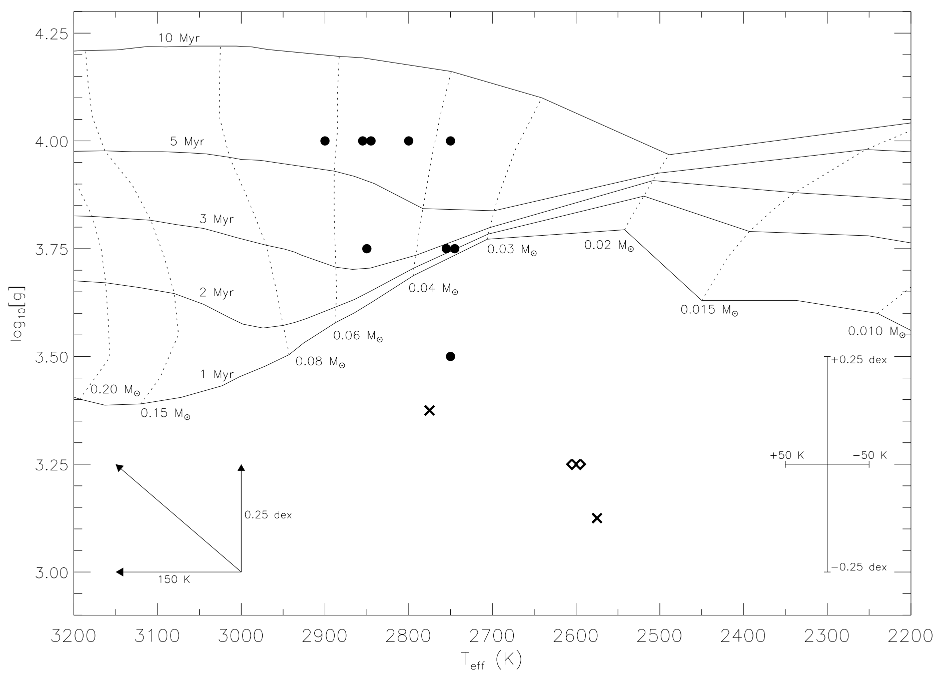

Figure 1. GG Tau Ba & Bb are *crosses*, Usco 128 & 130 (both planetary mass) are *diamonds*, all other Upper Scorpius objects are *filled circles*. In this log g versus $T_{\rm eff}$ plot most objects agree well with the Lyon tracks, except Bb (cooler *cross*) and USco 128 & 130. Error bars for $T_{\rm eff}$ and log g ($\pm$ 50 K, $\pm$0.25 dex) are shown; arrows show the largest possible shift in our values ($\leq$150 K, $\leq$0.25 dex) from cool spots.

pected cluster ages (Upper Scorpius: 5$\pm$2 Myr; Taurus: $\sim$1 Myr). However, our log g values are much lower than predicted for our coolest targets; consequently, they appear much younger than expected. Using distance and photometry information, we then derive masses and radii. Most of our targets turn out to be very low-mass stars and brown dwarfs; two appear to have planetary masses of 6–7 M_J, and are at most at the D-fusion minimum-mass boundary (Fig. 2). While most of our objects agree very well with the Lyon track predictions for mass versus radius, the lowest masses ($M \lesssim 30\ M_J$; these are the objects with lowest gravities in Fig. 1) have significantly larger radii than predicted for their expected ages (Fig. 2). Once again, just as in the $T_{\rm eff}$-gravity plane, they seem implausibly young ($\lesssim$0.5 Myr) when compared to the tracks.

Various lines of argument indicate that the age-spread in our sample suggested by the tracks is not real. Instead, we think it more likely that the evolutionary models have unresolved uncertainties at young ages for the lowest masses. These might arise from a variety of causes, such as accretion effects or non-isentropic internal structure; these issues must be addressed in the future. Our results also indicate that the faintest very young late-M objects may be much lower in mass (close to the D-burning limit) than previously suspected. Our detailed analysis can be found in Mohanty et al. (2003a,b).

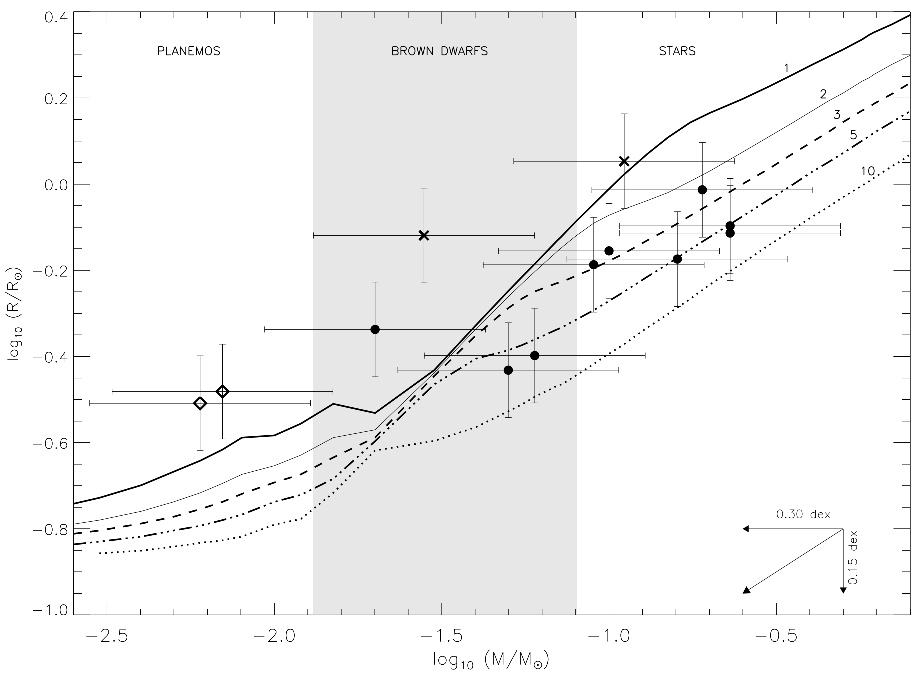

Figure 2. GG Tau Ba & Bb are *crosses*, Usco 128 & 130 (both planetary mass) are *diamonds*, all other Upper Scorpius objects are *filled circles*. In this radius (log[R/R$_\odot$]) versus mass (log[M/M$_\odot$]) plot, GG Tau Bb and USco 128 & 130 are much larger than predicted; others agree reasonably with the tracks. Arrows show shift if any object were an equal-mass binary.

References

Allard, F., Hauchildt, P., Alexander, D., Tamanai, A., & Schweitzer, A. 2001, ApJ, 556, 357

Chabrier, G., Baraffe, I., Allard, F., & Hauschildt, P. 2000, ApJ, 542, 464

Mohanty, S., et al. 2003a, submitted

Mohanty, S., et al. 2003b, submitted

Highlights of Astronomy, Vol. 13
International Astronomical Union, 2003
O. Engvold, ed.

Future Groundbased High-Resolution IR Spectrometers

Alan Moorwood

European Southern Observatory, Garching, D-85748, Germany

Abstract. Plans for future high-resolution infrared spectrometers on large groundbased telescopes, their capabilities and science goals are briefly reviewed.

1. Introduction

High spectral resolution astronomical observations in the infrared were pioneered by Pierre Connes in the 1960s using Fourier Transform spectrometers, which could yield resolving powers $\simeq 10^6$ but whose sensitivity was limited by the poor, single pixel detectors then available. This restricted initial studies mostly to the brighter planets - extended later to the brighter stars, for example, using the very successful FTS operated for many years at the KPNO.

More recently, the development of highly sensitive, large format infrared array detectors has stimulated increasing interest in the development of cryogenic echelle spectrometers, which are currently being limited to somewhat lower resolving powers of $\simeq 10^5$ for practical reasons but are many orders of magnitude more sensitive than the early Fourier spectrometers. In the 1–5 μm range, Phoenix, also developed at KPNO for use on the 4 m Mayall telescope and now installed on the 8 m Gemini South telescope (http://www.gemini.edu/sciops/ instruments/ phoenix/ phoenixIndex.html) has pioneered this approach. A pioneering instrument in the 8–20 μm range is Michelle, developed by the UKATC in Edinburgh for UKIRT but now on Gemini North (http://www.gemini.edu/ sciops/ instruments/ michelle/ MichIndex.html). The increase in science objectives possible with such instruments is illustrated in the next section, and characteristics of the new high-resolution spectrometers CRIRES and VISIR, to be installed on the ESO VLT in the near future, are given in section 3.

2. Infrared Astronomy at High Spectral Resolution

Table 1. Science Objectives

- Planetary atmospheres
- Exoplanets (radial velocity reflex motion searches; direct detection)
- Stars (atomic and molecular abundances, winds, pulsations, magnetic fields, disks, outflows)
- Interstellar Medium (chemistry and kinematics)
- Galaxies/quasars (nuclear kinematics, intergalactic gas)

3. IR Spectrometer Developments

3.1. CRIRES

CRIRES (http://www.eso.org/instruments/crires) is being developed for one of the VLT 8 m telescopes by ESO at its headquarters in Garching under the leadership of the author.

Table 2. CRIRES Main Characteristics

- Located at Nasmyth focus of one of the 8 m VLTs
- Wavelength range 1–5 μm
- R = 10^5 with $0.1''$ pixels; $50''$ long slit
- Adaptive optics feed to maximize SNR and spatial resolution
- Slit viewing camera for IR acquisition
- Echelle grating (R2) and prism pre-disperser
- 4096x512 pixel InSb detector mosaic
- Polarimetry (including circular) with Fresnel rhomb and Wollaston prism
- Calibration unit including gas cells for accurate radial velocities
- Limiting magnitudes $\simeq$ 17(J) to 11(M) in 1 hr
- Installation in early 2005

3.2. VISIR

VISIR (http://www.eso.org/instruments/visir) is a multimode imager/spectrometer designed to operate in the 10 and 20 μm atmospheric windows. It is being developed for the ESO VLT by the Service d'Astrophysique, CEA, Saclay and NFRA/ASTRON, Dwingeloo, The Netherlands under Pierre - Olivier Lagage at Principal Investigator.

Table 3. VISIR Main Characteristics

- Cassegrain focus of the VLT
- Wavelength Range 5–28 μm
- Duo echelle grating + cross disperser grisms
- 256x256 pixel As:Si array
- R $\simeq$ 25000 at diffraction limit
- Installation on VLT March 2004

Highlights of Astronomy, Vol. 13
International Astronomical Union, 2003
O. Engvold, ed.

High-Resolution Infrared Far-IR Spectroscopy from SOFIA, 2005-2025

J. A. Davidson

USRA, Moffett Field, CA 94035-1000, USA

E. F. Erickson

NASA Ames Research Center, Moffett Field, CA 94035-1000, USA

Abstract. NASA and the DLR are developing SOFIA, the Stratospheric Observatory for Infrared Astronomy: a 2.5 m telescope in a Boeing 747SP aircraft. By flying in the lower stratosphere, SOFIA will allow astronomical measurements covering the wavelength range from 0.3 μm to 1.6 mm, with an emphasis on the spectral regions inaccessible from the ground, particularly the 6-8 μm and 30-300 μm regions. SOFIA will see "first light" in 2004; the science program will start in 2005. An operational lifetime of 20 years is planned.

SOFIA will support a diverse and evolving complement of state-of-the-art science instruments. Its spectrometers will have resolutions ranging from $\sim 10^8$ down to ~ 100, as needed to measure absorption and emission from astrophysically significant atoms, ions, molecules, aerosols, and solids. This paper describes the spectrometers being developed to fly on SOFIA soon after first light, and summarizes some of the high-spectral resolution investigations expected.

1. SOFIA and Other FIR/submm Missions

The 3-m class telescopes on SOFIA and Herschel will improve previously available angular resolution at far-infrared wavelengths by a factor ~ 3. SOFIA will fly over 100 flights per year during most of its 20 year lifetime, enabling observations of most IR/submm wavelengths obscured from the ground. The long lifetime and frequent flight opportunities will allow SOFIA to develop and maintain an unmatched variety of sophisticated IR/submm instruments. Thus SOFIA is assured a major role in future high-resolution spectroscopy at these wavelengths.

Ten spectrometers are anticipated for future far-IR and submm ("FIR") space and suborbital missions: SIRTF, SOFIA, Astro-F, Herschel, and JWST. Of the 10 planned spectrometers, five are being developed for SOFIA, and all of these by Principal Investigators (PIs). These spectrometers together cover a wider range of wavelengths than those of any other mission. Briefly these are

EXES (PI John Lacy, University of Texas): The Echelon Cross Echelle Spectrograph is a 5-28.5 μm high resolution spectrograph with a maximum resolution ~ 3 km s^{-1}.

SAFIRE (PI Harvey Moseley, NASA-GSFC): The Submillimeter And Far-InfraRed Experiment is a versatile imaging Fabry-Perot spectrograph working in the range of 100 to 655 μm.

GREAT (PI Rolf Guesten, MPIfR): The German REceiver for Astronomy at THz frequencies is a dual channel heterodyne instrument with high spectral resolution in the 63 to 188 μm (1.6 to 4.7 THz) region.

CASIMIR (PI Jonas Zmuidzinas, Caltech): The Caltech Airborne Submillimeter Interstellar Medium Investigations Receiver is a FIR heterodyne spectrometer, working in the wavelength range from 150 to 600 μm (500-2000 GHz) with spectral resolution of > 0.3 km s^{-1}.

FIFI-LS (PI Albrecht Poglitsch, MPE Garching): The Far-Infrared Field Imaging Line Spectrometer is a German integral-field unit spectrometer with spectral resolution 150-300 km s^{-1}. It will operate in the 42 to 210 μm region with two wavelength channels and two separate array detectors.

Future spectrometers on SOFIA can be anticipated by looking at Figure 1. Clearly there will be a need for for a high resolution instrument(s) to provide contiguous wavelength coverage from $\sim$ 20-200 μm, for example.

2. FIR High-Resolution Spectroscopy

A wealth of important scientific topics remains to be explored with FIR spectroscopy. "High resolution" is a relative term, which we interpret to mean both higher resolution than has previously been utilized, and resolution sufficient to resolve the spectral features of astronomical sources. High resolution increases sensitivity for line measurements on sources with bright continuum emission, as does the improved angular resolution provided by the SOFIA telescope for extended sources.

Important FIR spectral diagnostics arise in a wide variety of sources, including AGNs, HII regions, planetary nebulae, photodissociation regions (PDRs), circumstellar envelopes, and molecular clouds. The FIR wavelengths suffer little extinction, and so allow observation of phenomena in highly obscured regions such as our Galactic Center. Fine structure lines arising from low level transitions in atoms and ions characterize the originating gas from cool to hot. For example, [C II] at 158 μm is a major coolant of PDRs, which are principal constituents of the ISM. The Ne VI line at 24.3 μm is a signature of hot gas in AGNs. A wide variety of rotational molecular lines, including high-J CO, H_2O, H_2, HD, OH and other hydrides extend throughout the far-IR and submm regions. These many FIR lines enable observations to probe the pressure, density, luminosity, excitation, mass distribution, chemical composition, heating and cooling rates, and kinematics in the various components of the ISM. We give a few examples of the numerous phenomena characterized by these lines:

Extragalactic Star Formation: How do interactions between high mass stars and the ambient medium relate to the star formation history? The ISM in irregulars and spirals can differ greatly: SN rate, stellar winds, density, IMF. Lines of [O III] 52 μm and [O I] 63 μm, with widths $\sim$ 30 km s^{-1}, probe the

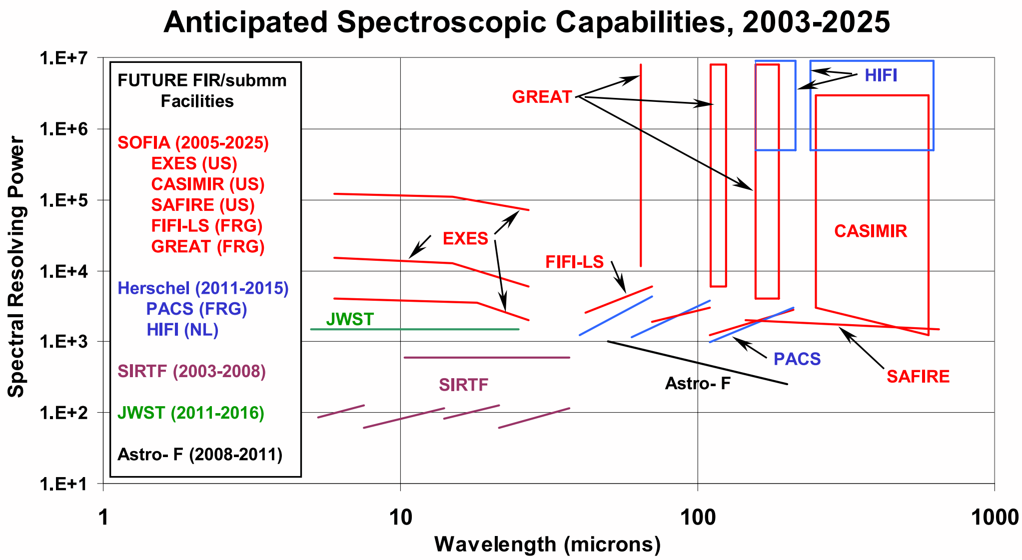

Figure 1. Future spectrometers on SOFIA

content and dynamics of photoionized and photodissociated gas. The [O III] 52 & 88 μm and [S III] 33 μm lines yield the density and excitation of ionized gas.

Star formation in the Milky Way: How do the details of infall, accretion, and outflow in low mass, young stellar objects affect the resulting stellar properties? Narrow high-J CO and [O I] 63 μm lines originating near objects in Taurus should yield a direct measure of the mass infall rate. Material accreting onto pre- and young stellar disks will produce OH doublets at 84 and 119 μm that are sensitive to the preshock density and the shock velocity, which together determine the accretion rate. The morphology and mass loss rate of outflows will be revealed by [O I] 63 and 145 μm lines produced as the natal material is shocked by the outflowing gas.

Mass distribution in cirumstellar disks around visible T-Tauri stars: Planets forming in these disks should cause disk clearing, which will be reflected in line profiles of H_2 at 28, 17, and 12 μm, as well as lines of methane and water. These observations require spectral resolutions of a few km s^{-1}.

Interstellar chemistry: What is the relative importance of gas-phase chemistry versus dust-grain surface chemistry in dark clouds? Depletion of molecules onto dust grains in dark clouds would explain high deuterium fractionation. The abundance of H_2D^+ is the key to understanding this process. The lowest energy-level transition (101 $\rightarrow$ 000) at 219 μm (1.37 THz) should be detectable with SOFIA's heterodyne spectrometers.

3. Spectroscopic Observing Opportunities with SOFIA

Development and maintenance of the first generation SOFIA spectrometers described above will be the responsibility of the PIs. General Investigators (GIs) will be allowed to propose observations with a PI's instrument in collaboration with him. In the future, facility spectrometers may be available for GI investigations without the need for collaboration with a PI. Performance summaries for all the first generation SOFIA instruments are currently available at http://sofia.arc.nasa.gov/Science/instruments/sci_instruments.html.

SOFIA is a joint program of NASA in the U.S. and DLR in Germany. Observing time will be awarded by annual peer review of proposals, with roughly 80% of the time granted by the U.S. and 20% of the time granted by Germany. International proposals may be submitted to either time allocation committee. Observing opportunities for General Investigators are expected to begin in 2006.

4. Conclusions

The interstellar media in galaxies are complex and fundamental components of the universe. Many physical and chemical processes — such as star and planetary system formation and the evolution of elemental abundances through stellar life cycles — are yet to be understood.

Far-IR and submm lines bring a wealth of knowledge about the ISM and the processes hidden therein. These lines require measurements with high spectral and spatial resolution from space or suborbital platforms. SOFIA and Herschel will improve FIR angular resolution by a factor ~ 3 relative to past FIR telescopes, and will provide many of the needed high spectral resolution capabilities. SOFIA's long lifetime will encourage future spectrometer development, to extend even further the Frontiers of High Resolution Spectroscopy.

Highlights of Astronomy, Vol. 13
International Astronomical Union, 2003
O. Engvold, ed.

Chemistry of Diffuse Clouds and Circumstellar Envelopes

Robert Lucas

IRAM, 300 rue de la Piscine, 38406 Saint-Martin-d'Hères, France

Abstract. We present and review recent millimeter-wave observations with interferometers, in particular, with the Plateau de Bure interferometer, that stress the importance of high-frequency resolution for studying the chemistry of diffuse interstellar clouds and of post main-sequence circumstellar envelopes. The future impact of new instruments, such as the Atacama Large Millimeter and submillimeter Array (ALMA), is also investigated.

1. Introduction

High-resolution spectroscopy in the millimeter and sub-millimeter wavelength domains uses heterodyne reception. In most cases the sensitivity is determined by the collecting areas and by the noise temperatures of the radio receiver front-end parts (mixer, amplifiers). The spectral resolution is determined by the backend part of the receiving systems, which can consist of filter banks, acousto-optical spectrometers, or correlators.

Due to recent, steady progress in digital technology, the cost of correlators has been decreasing, and they are or will be used in most large ground-based instruments (not only interferometers, but also single-dish telescopes). Correlators have the interesting property that the spectral resolution is tunable (generally, however, at the cost of lower total bandwidth).

Spectral correlators have a steadily increasing number of channels, so that in a typical situation the maximum bandwith could soon be determined by the instantaneous front-end bandwith, while the actual spectral resolution is really limited by sensitivity, or by the affordable digital data rate. Spectral correlators are suitable for most observational projects with the possible exception of some spectral surveys, including the search for very narrow lines in the whole front-end bandwidth).

In the millimeter domain, in particular, the spectral resolution is limited by sensitivity, just like the spatial resolution in the case of aperture synthesis. As an example, in the last fifteen years the Plateau de Bure array had two generations of front-ends and four successive correlator systems. The latest one enables full analysis of the available intermediate frequency band and few (if any) projects are limited by the available spectral capability.

Correlators still suffer from a (small) loss of sensitivity due to digitization, but the use of more bits limits this effect.

2. Diffuse Clouds Seen in Millimeter-wave Absorption

Absorption is a powerful tool for detecting low-excitation gas, e.g., molecules in diffuse clouds as has been observed in the optical and UV spectral ranges for more than 60 years. For millimeter-wave absorption, we use different background sources, e.g., quasars and distant galaxies instead of stars. Unfortunately, this makes direct, precise comparison with optical/UV results rather difficult.

The low density makes interpretation easier: many molecules are in in equilibrium with the cosmic background radiation, and thus only one rotational line is enough to measure a good column density. This is not the case, however, for CO, which can be excited at low densities (a few 100 cm^{-3}). Due to their larger transition probabilities, high-dipole moment molecules (HCO^+, HCN) are easier to detect than low-dipole moment ones (e.g., CO).

It is worthwhile to note that this observing method works with the same sensitivity for gas in distant galaxies: see, for instance, Wiklind (2003).

From an observational point of view, the observations are rather easy, as the background source is point-like and strong enough (~ 0.5Jy) to allow self-calibration of amplitudes and phases. Such observations can make a good use of relatively poor weather conditions. Interferometers advantageously resolve out the emission component if present, for instance, in the CO lines.

Among the main results is the surprisingly high abundance of molecules like HCO^+ and HCN in diffuse clonds (Lucas & Liszt 1996). There is a remarkable relation between $HCO^+$and OH. The turn on of CO at $N(HCO^+) \sim 10^{12}$ cm^{-2} is observed, corresponding to the transition from C^+ to C and CO (Liszt & Lucas 1998). C_2H is also a very common species; many molecules like HCN, CN, and HNC have relative abundances comparable to those in dark clouds, with notable exceptions (N_2^+, CH_3CN). The chemical pathways leading to these high abundances are still far from being understood.

3. Circumstellar Envelopes

Circumstellar envelopes (CSEs), which appear around stars of masses $\sim 0.8 - 8$ $M_\odot$ at the end of their evolution, trace the process through which these stars return heavy elements and dust particles to the interstellar medium. They are the sites of very rich (O- or C-rich) chemistry with complex molecules, which is probed by line emission and dust continuum emission in the radio, sub-mm, infrared. In the inner regions dust forms, is accelerated by radiation pressure, and drives the gas; while in outer regions the interstellar UV radiation strongly drives the chemistry (eventually destroying most molecules). See e.g., Glassgold (1999) and Lucas & Guélin (1999) for reviews.

Several CSEs have detached CO shells, probably resulting from ancient ($\sim$ 800 to $\sim$ 8000y) short (a few 100y) episodes of higher mass-loss. So far only CO is detected in large detached shells, but HCN and CN are detected in U Cam. The outer envelopes of IRC+10216, CRL 2688, NGC7027, and others show multiple shell structures indicating mass loss rate variations (see e.g., Mauron & Huggins 2000; Fong et al. 2003).

4. ALMA Perspectives

ALMA will support both high angular resolution and high-frequency resolution observations, 0.18 and 0.018 km s^{-1} at 3 mm and 0.3 mm, respectively. Note that these numbers should be multiplied by 4 for full polarization work. A second generation correlator is under study (but not yet budgeted) for still higher resolution and more frequency channels at the highest resolutions.

Diffuse Clouds With the full-scale ALMA (planned for 2012) the limiting flux to reach 0.01 sensitivity in optical depth for a 1 km s^{-1} wide line will be $\sim$ 100 mJy, compared with 1.5 Jy for the Plateau de Bure array. Several thousands of background sources should be then observable compared to $\sim$ 40. One will be able to perform more complete studies of the diffuse gas than is now possible in the optical/UV, such as a large survey of HCO^+ absorption to study more extensively the structure and dynamics of the diffuse gas, compare diffuse cloud chemistry in various regions of the Galaxy, and complete a line survey in front of a few strong sources. One may also select lines of sight passing through transluscent clouds and even denser clouds, to obtain chemical abundance measurements unbiased by selective collisional excitation, and compare local results with those from nearby external galaxies for which suitable background sources can be found.

Circumstellar envelopes With the high angular spatial resolution of ALMA, one may map and monitor the chemistry in the inner region (about $0.5''$ in IRC+10216), where dust forms and gas is accelerated, using as probes CO, SiO, SiS, and HCN. It will be possible to access submillimeter lines of higher excitation since the inner envelopes have higher temperatures and densities. With high sensitivity, one will perform more extensive spectral surveys in more diverse stars and at more stages of evolution. More extensive mapping will help us understand the mass-loss history better and the related ring structure in extended envelopes as well as in detached shells. High angular resolution is needed to resolve the shell structures. Surveys of CSEs will be extended to different regions of the Galaxy and nearby galaxies (e.g., the Magellanic Clouds). For many of these studies comparison with other large instruments such as the VLT, VLTI, Hershel, and new generation space telescopes will be essential.

References

Glassgold, A. E. 1999, in IAU Symp. 191, Asymptotic Giant Branch Stars, ed. T. Le Bertre, A. Lèbre, & C. Waelkens (San Francisco: ASP), 337

Fong, D., Meixner, M., & Shah, R. Y. 2003, ApJ, 582, L39

Liszt, H. S., & Lucas, R. 1998, A&A, 339, 561

Lucas, R., & Guélin, M., in IAU Symp. 191, Asymptotic Giant Branch Stars, ed. T. Le Bertre, A. Lèbre, & C. Waelkens (San Francisco: ASP), 305

Lucas, R., & Liszt, H. S. 1996, A&A, 307, 237

Mauron, N., & Huggins, P. J. 2000, A&A, 359, 707

Wiklind, T., talk presented in Joint Discussion 21, IAU G. A., Sydney 2003

Highlights of Astronomy, Vol. 13
International Astronomical Union, 2003
O. Engvold, ed.

Spectral-Line Surveys at Millimeter and Submillimeter Wavelengths: Impact of Spectral Resolution

L. M. Ziurys

Depts. of Astronomy and Chemistry, and Arizona Radio Observatory, Steward Observatory, 933 N. Cherry Ave., University of Arizona, Tucson, AZ 85721

Abstract. Millimeter and submillimeter astronomy has achieved very high spectral resolution ($\lambda/\Delta\lambda \gtrsim 10^6$-$10^7$) over the past 20 years. Broad-band spectral-line surveys at these wavelengths have only taken partial advantage of these capabilities. Such surveys could be more effective with an increase in spectral resolution, accompanied by improvement in the stability and bandwidth of spectrometers and the employment of single-sideband detectors.

1. Introduction

The millimeter/sub-millimeter region of the electromagnetic spectrum, which covers the range ≈65-1000 GHz, is rich in molecular line emission. As a consequence, numerous broad-band spectral-line surveys have been conducted of molecular sources. The most frequently surveyed object is the Orion molecular cloud, observed in the 3 mm (Turner 1991), 2 mm (Ziurys & McGonagle 1993), and 1 mm windows (Blake et al. 1986, Apponi et al. 2003), as well as in the sub-mm region (e.g., Araki et al. 2000). The Galactic center has also been studied (e.g., Nummelin et al. 2000), as well as a few other molecular clouds. Circumstellar envelopes, particularly that of the carbon-rich star IRC+10216, have additionally been investigated (e.g., Cernicharo et al. 2000).

These surveys have produced numerous scientific results, including the identification of new molecules such as MgNC and C_5H (Cernicharo et al. 2000). Also, surveying different objects, or different positions within an object, has enabled an unbiased comparison of chemical variations (see Nummelin et al. 2000). Detailed studies of velocity components within a source, particularly in Orion, has also been accomplished. Futhermore, these surveys have demonstrated that there are numerous unidentified features, which have catalyzed new laboratory spectroscopy (e.g., Robinson, Apponi, & Ziurys 1997).

2. Limits of Spectral Resolution for Millimeter-wave Surveys

Currently, very high spectral resolution is available at mm/sub-mm wavelengths, through the use of devices such as filter banks and autocorrelators. Radio telescopes are diffraction limited; hence, spectral resolution is solely determined by the spectrometer "backend." Resolutions as high as 24 kHz have been successfully used, which correspond to $\lambda/\Delta\lambda \approx 10^7$. Therefore, very high spectral resolution has been available for the surveys. However, what is lacking in this regard is spectrometer baseline stability and bandwidth.

For example, most spectral surveys of Orion have been conducted with 1 MHz resolution ($\approx$3 km s^{-1} at 3 mm). It would be very useful to survey Orion with higher resolution such as 100 kHz. This increase would enable the resolution of many velocity components in this object, as well as additional molecular splittings. An illustration of the improvement is shown in Figure 1, which displays a spectrum of the J = 1 $\rightarrow$ 0 transition of a common interstellar molecule, N_2H^+, at 93 GHz, observed with 1 MHz (left) and 100 kHz (right) resolutions, respectively. In the 1 MHz data, the transition appears virtually as a single feature. With 100 kHz resolution, not only are the three components of the nitrogen hyperfine splitting resolved, but two velocity components in each feature become apparent as well. The two velocity components actually arise from separate clouds in Orion (Womack, Ziurys, & Wyckoff 1991).

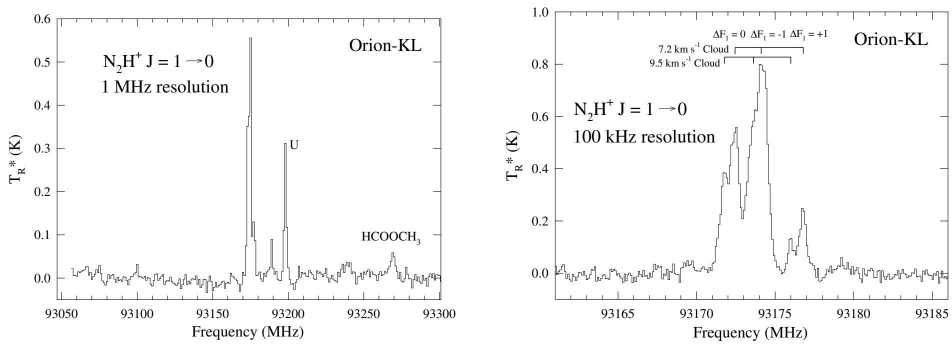

Figure 1. Spectra of N_2H^+ (J = 1 $\rightarrow$ 0) at 93 GHz observed towards Orion-KL using the ARO 12m telescope, showing the differences in line profiles for 1 MHz (left) and 100 kHz (right) resolution.

Data for spectral-line surveys need to be taken with reasonably large bandwidth (0.5-1 GHz) for reasonable efficiency. Currently, it is difficult to make a broadband spectrometer with good baseline stability.

3. The Double versus Single Sideband Problem

Another difficulty for spectral surveys is a consequence of heterodyne detectors, which utilize local oscillators (LO) to mix down to an intermediate frequency (IF). Two frequency ranges are observed simultaneously with such systems, where $\nu_{Sky} = \nu_{LO} \pm \nu_{IF}$. Hence, the term "double sideband". Although at first glance this feature may seem an advantage, it leads to extreme spectral confusion at high sensitivity levels, and negates much of what is gained with increased resolution. Fortunately, rejection of the unwanted spectrum, or the "image" data, to generate a "single sideband" spectrum can be done, but not every telescope exercises this option. An illustration of the confusion created in double-sideband data is shown in Figure 2. This figure presents three spectra observed at 276.5 GHz towards Orion-KL (Apponi et al. 2003). The bottom spectrum shows the single-sideband data, the middle one displays what would appear as the "image," and the top spectrum is the double sideband measurement. Distinct features clearly apparent in the SSB spectrum (e.g., the triplet near 276550 MHz), become either totally masked or blended in the DSB data. Clearly, surveys taken in DSB mode are losing information.

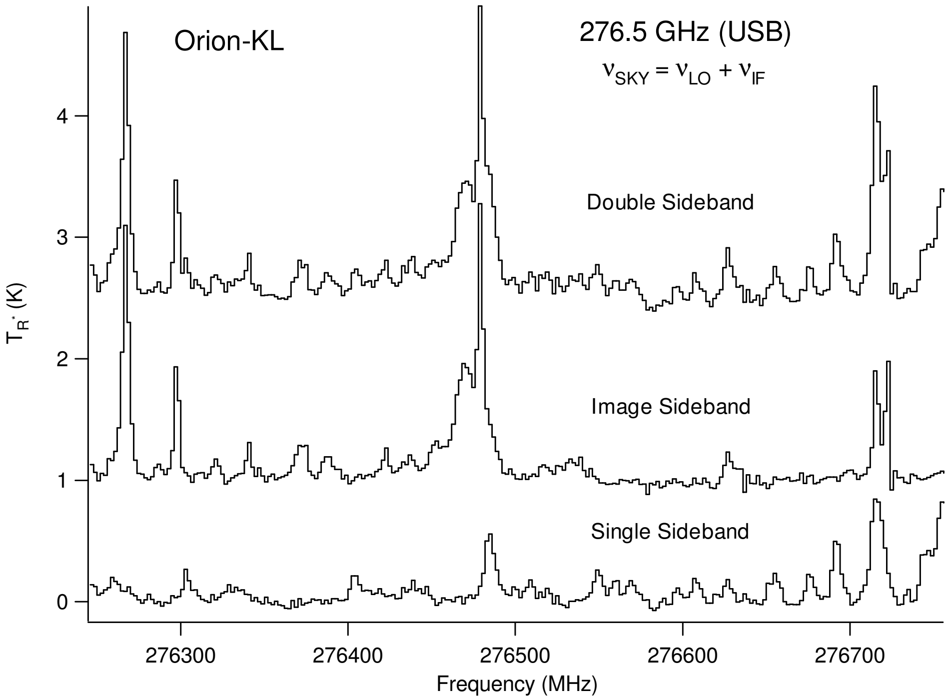

Figure 2. A comparison of spectra taken in single-sideband versus double-sideband modes.

References

Apponi, A. J., Halfen, D. T., & Ziurys, L. M. 2003, in preparation

Araki, M., Ohishi, M., White, G. S., Higginbottom, N. S., Greves, J. S. 2000, in Atomic and Molecular Data for Astrophysics, IAU General Assembly, JD 1

Blake, G. A., Masson, C., Phillips, T. G., & Sutton, E. 1986, ApJS, 60, 357

Cernicharo, J., Guélin, M., & Kahane, C. 2000, A&AS, 142, 181

Nummelin, A., et al. 2000, ApJS, 128, 213

Robinson, J., Apponi, A. J., & Ziurys, L. M. 1997, Chem. Phys. Lett., 278, 1

Turner, B. E. 1991, ApJS, 76, 617

Womack, M. P., Ziurys, L. M., & Wyckoff, S. 1991, ApJL, 370, L99

Ziurys, L. M. & McGonagle, D. 1993, ApJS, 89, 155

Highlights of Astronomy, Vol. 13
International Astronomical Union, 2003
O. Engvold, ed.

High Resolution Spectroscopy at Low Radio Frequencies

Jayaram N. Chengalur

NCRA-TIFR, Pune Univ. Campus,
P. O. Bag 3., Ganeshkhind, Pune 411007, India

Abstract. In this paper I discuss two examples of the science that can be done with high-resolution spectroscopy at low radio frequencies.

1. Kinematics of Faint Dwarf Irregular Galaxies

Interest in the kinematics of faint dwarf galaxies has been rekindled by numerical simulations of galaxy formation in hierarchical structure formation models which predict that galaxy halos should have cuspy (the so called "NFW" halos) central density distributions (Navarro, Frenk, & White 1996). Dwarf galaxies, which are generally dark matter dominated, even in their inner parts, are best suited for testing these galaxy formation models. While one might *a priori* assume that the ideal sample would be one composed of the faintest gas rich galaxies, it turns out that it is unclear whether the faintest dwarf irregular galaxies are rotationally supported or not. For example, in a study of nine faint dwarf galaxies Lo et al. (1993) found that only two galaxies showed ordered velocity fields, the remaining galaxies all had chaotic velocity fields. In fact, it has been suggested that normal rotation is seen only in dwarfs brighter than $M_B \sim -14$, and that by $M_B \sim -13$ one begins to find systems with misaligned axis, and other kinematical peculiarities. However, most of the earlier studies of dwarf irregular galaxies were done using relatively coarse velocity resolution (~ 6 km s^{-1}), which would make it difficult to discern the large scale patterns, if any, in the velocity fields of these galaxies.

To check whether dwarf irregular galaxies do indeed have systematic large scale velocity fields, we have made deep, high velocity resolution (~ 1.6 km s^{-1}) observations of a sample of dwarf irregular galaxies. We find that none of the galaxies in our sample have chaotic velocity fields, and that in some of them, the velocity field can be well modeled as arising from a rotating gas disk. Figure 1a shows the velocity field of Camelopardalis B ($M_B \sim -10.9$). As can be seen, the HI in the galaxy has a regular velocity field, consistent with rotational motion. Further, the implied kinematical major axis is well aligned with the major axis of both the HI flux distribution as well as that of the optical emission. Camelopardalis B is the faintest known galaxy with such relatively well behaved kinematics.

The rotation curve derived from the velocity field shows an (inclination corrected) rotation velocity of only ~ 7 km s^{-1} – the high velocity resolution of our observations was hence critical to measuring the rotation curve. Further, the peak rotational velocity is comparable to the random velocity of the gas.

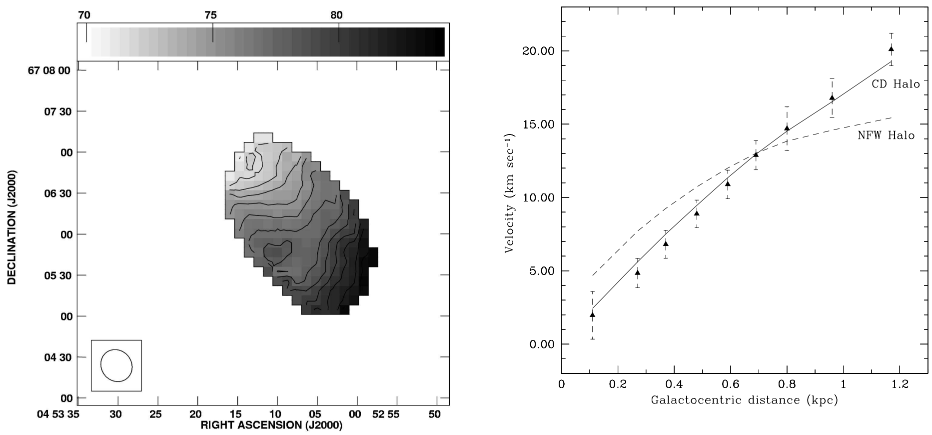

Figure 1. (a) Velocity field of Camelopardalis B. (b) Mass models fit to the asymmetric drift corrected rotation curve.

After correcting the observed rotation velocities for random motions, we find a corrected peak rotation velocity of $\sim$ 20 km s^{-1}. We fit mass models to the corrected rotation curve (Fig. 1b) and find a good fit for a constant density halo with a density of $\rho_0 \sim 12\ M_\odot$ pc^{-3}, while an NFW halo model provides a poor fit to the rotation curve, regardless of the assumed mass to light ratio of the stellar disk.

2. Absorption from the Galactic WNM

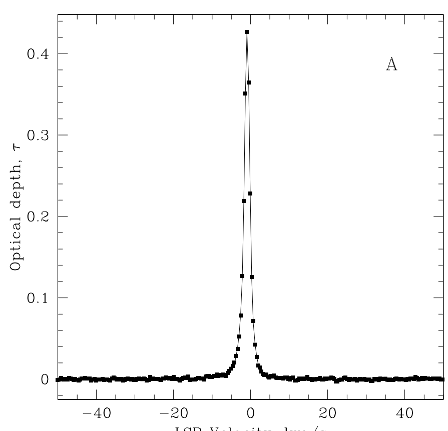

Figure 2. 0.4 km s^{-1} resolution absorption spectrum toward PKS 1814−637 (solid points), along with the 3-Gaussian fit (solid line).

Temperature measurements of HI clouds are usually carried out by comparing the 21 cm optical depth in a given direction (obtained through 21 cm absorption studies toward background continuum sources) with the emission brightness temperature from nearby directions. This yields the "spin temperature", T_s. While the temperature of the CNM is reasonably well measured by such methods, the temperature of the WNM is still weakly constrained due to the difficulties in detecting it in absorption.

A serious problem with such emission/absorption studies is that the HI emission spectra are affected by stray radiation, non-uniformity of HI clouds across the beam, self-absorption, etc. These make it very difficult to estimate the spin temperature of the WNM in the standard absorption/emission searches. Conversely, HI absorption studies toward compact sources trace narrow lines of sight through the intervening clouds. When carried out using long baseline interferometers one gets an uncontaminated measure of the absorption profile, which can be then be examined for WNM features. The drawbacks are that (1) the WNM optical depth is very low, and (2) the WNM must be searched for in the midst of strong CNM absorption features. The second issue can be mitigated by choosing lines of sight with simple CNM structure and using high velocity resolution observations to model the deep narrow CNM features and subtract them out.

Figure 2 shows a 0.4 km s^{-1} resolution ATCA absorption spectrum toward the source PKS 1814−637. The profile is dominated by a single deep narrow asymmetric component, but there is in addition a shallow broad absorption component. The parameters derived from fitting multiple Guassians to the absorption are shown in Table 1. As can be seen, the broad component is consistent with arising from the WNM. Interestingly, the kinetic temperature of this component places it in the thermally unstable range.

Table 1. Multi-Gaussian fit Parameters for the absorption spectra.

Source	Component	FWHM (km/s)	T_k K	N_{HI} $\times 10^{20} cm^{-2}$
	1	1.43 ± 0.01	44.6 ± 0.7	0.38 ± 0.01
PKS 1814−637	2	3.37 ± 0.06	248 ± 10	1.77 ± 0.15
	3	12.0 ± 0.5	3127 ± 300	7.2 ± 1.7

Acknowledgements I am grateful to my co-authors Ayesha Begum and Nissim Kanekar for permission to use material from joint work.

References

Lo, K.Y., Sargent, W. L. W., & Young, K. 1993, AJ, 106, 507.

Navarro, J. F., Frenk, C. S., & White S. D. M. 1996, ApJ, 490 493.

JD21

The Astrochemistry of External Galaxies

Chairperson: T.J. Millar

Editor: T.J. Millar

Highlights of Astronomy, Vol. 13
International Astronomical Union, 2003
O. Engvold, ed.

Molecular Hydrogen in the High Redshift Damped Ly-α Systems:

R. Srianand

IUCAA, Postbag 4, Ganeshkhind, Pune 411007, India

P. Petitjean

Institut d'Astrophysique de Paris – CNRS, 98bis Boulevard Arago, F-75014 Paris, France

C. Ledoux

European Southern Observatory, Alonso de Córdova 3107, Casilla 19001, Vitacura, Santiago, Chile

G. Ferland

Department of Physics and Astronomy, University of Kentucky, 177 Chemistry/Physics Building, Lexington, KY 4050

Abstract. This review talk summarizes the main results obtained from the just completed survey of molecular hydrogen in damped Lyman-α systems (DLAs). Preliminary results based on modeling ionization conditions and chemical network is also presented. The presence of $^{h}2$ and fine-structure lines of C I in 13-20% of DLAs allow one to investigate the physical conditions using the techniques that are commonly used in the studies of the Galactic ISM. It is shown that the DLAs with $^{h}2$ trace regions with higher density, lower temperature, moderate to high dust depletion, and local star-formation. Absence of $^{h}2$ in DLAs with moderate dust depletion could just be a simple consequence of lower densities in the systems.

1. Introduction

DLAs are believed to originate in gas associated with protogalaxies that lie along our line of sight to background quasars. The physical conditions within DLAs can reveal the star formation history, determine the chemical composition of the associated ISM, and hence document the first steps in the formation of present day galaxies. At H I column densities typically measured in DLAs, molecular hydrogen ($^{h}2$) are conspicuous in our galaxy (Savage et al., 1977). It is known that H_2 is a very useful tracer of radiation field and dust content in the photo-dissociation regions. Thus detecting $^{h}2$ is the first major step toward a complete understanding of physical condition in DLAs. This was the aim of our survey using UVES installed at the ESO VLT 8.2m telescope. The survey details and notes on the observations can be seen from (Ledoux et al., 2002, 2003; Petitjean et al., 2000, 2002 and Srianand et al., 2000). Here we just summarize the main results.

2. Physical conditions in DLAs derived from the observations

Molecular hydrogen is detected in 13-20% of the newly-surveyed systems. Typical upper limits on the molecular fraction obtained in the case of non-detections is log f $\leq$ -6. Absence of $^{h}2$ in 80% of the systems can be explained if the formation rate of $^{h}2$ on to dust grains is reduced and/or the ionizing flux is enhanced relative to what is observed in our galaxy.

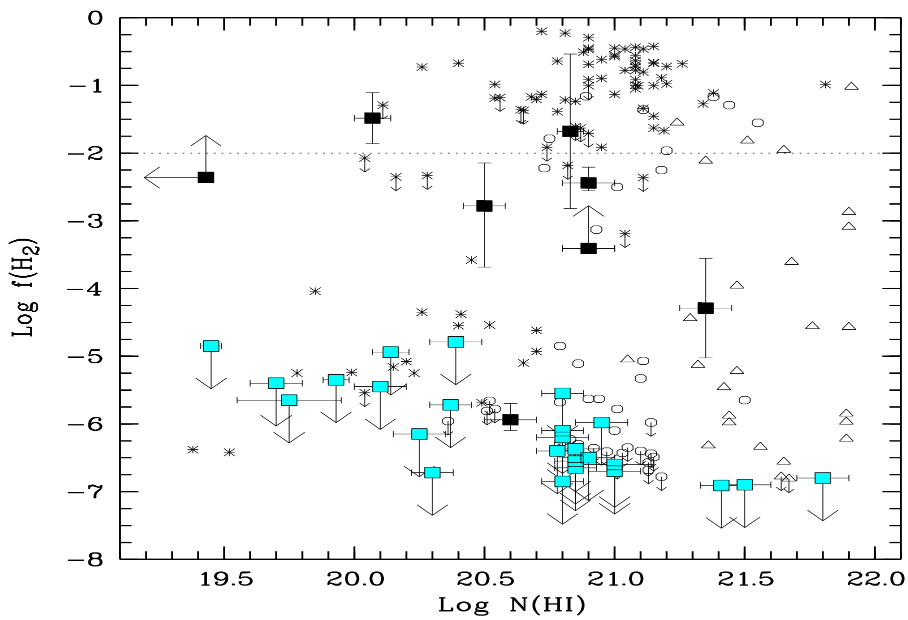

Figure 1. Mean $^{h}2$ molecular fraction, f $=2N(H_2)/(2N(H_2)+N(H\,\textsc{i}))$, versus neutral hydrogen column density. Measurements in DLAs are indicated by dark squares for $^{h}2$ detections and shaded ones for upper limits. Observations along lines of sight in the Galaxy (Savage et al 1977) and LMC and SMC (Tumlinson et al 2002) are indicated by, respectively, asterisks, circles and triangles.

In what follows we will concentrate on physical conditions in the systems that show $^{h}2$. It is known in the case of Galactic ISM that $^{h}2$ becomes optically thick at log N(H I cm^{-2}) = 20.7. However no such critical N(H I) is defined in the case of LMC and SMC. This seems to be the case with DLAs as well (Fig. 1). The lack of this characteristic self-shielding scale is either because the DLAs span a wide range of physical conditions or the formation rate of $^{h}2$ onto dust grains is reduced and the ionizing flux is enhanced relative to what is seen in our Galaxy (i.e the characteristic N(H I) is pushed to a much higher value).
Presence of dust is an important factor in the formation of $^{h}2$ in DLAs (see Fig. 2). The systems with larger molecular fractions (i.e log f ≥ -4) are always found to have large depletion (i.e., $\kappa \geq -1.5$). Few non-detections with high κ seen in the figure could just be the consequence of enhanced radiation field in these systems.

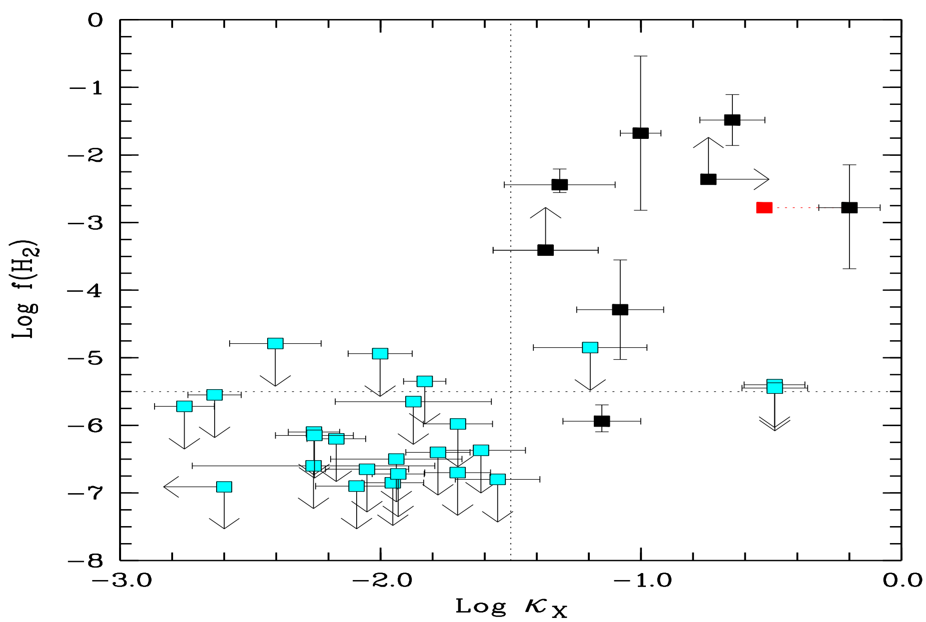

Figure 2. $^{h}2$ molecular fraction versus the amount of dust, $\kappa_X = 10^{[X/H]}(1 - 10^{[Fe/X]})$, with either X=Zn or S or Si. A weak trend between κ and f is apparent; however, several orders of magnitude spread in f($^{h}2$) for a given κ, among the detected cases, suggests that in addition to the amount of dust the physical conditions of the gas (density, temperature, and UV flux) play an important role in governing the formation of $^{h}2$ in DLAs.

Absorption lines of C I are invariably detected in systems that show $^{h}2$ absorption. The observed fine-structure excitations of C I in DLAs are much higher than that seen in our ISM (Fig. 3). This difference can not be explained by the CMB pumping alone and higher gas densities are favored (≥ 20 cm^{-3} for a temperature of 100 K) in the molecular gas. Rotational excitations of $^{h}2$ can as well give a handle on the physical conditions. The ortho-para ratio (OPR) measured in individual components is distributed between 1 and 3 (see Fig. 4). This is higher than what is seen in galactic ISM, LMC, and SMC for similar $^{h}2$ content. If we assume LTE then the observed range in OPR corresponds to the kinetic temperatures in the range 100 to 300 K. This is consistent with the usually preferred T_{01} measured in all these systems. The ratio N(J=2)/N(J=0) is very sensitive to the collisional excitations. We notice that this ratio is higher in the case of DLAs compared to what is measured in the local universe for similar $^{h}2$ column densities (see Fig. 4). This is consistent with the higher densities derived based on C I absorption lines. As the excitational energy is large the ratio N(J=4)/N(J=0) is very sensitive to the formation pumping and UV pumping. The distribution of this ratio in DLAs is similar to that seen ISM, LMC, and SMC (see Fig. 4). The meta-galactic UV background is not good enough to pump the high J levels to the extent that is observed in DLAs. Thus local radiation field and hence in situ star formation is most likely in these systems.

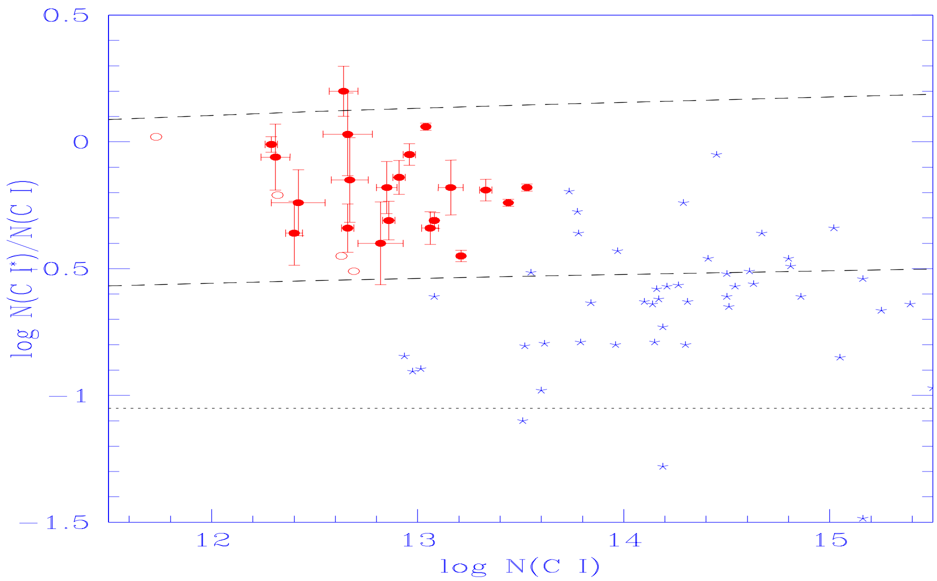

Figure 3. The filled circles and stars are measured values in DLAs and the Galactic ISM respectively (Jenkins & Tripp (2001)). The expected value from the CMB pumping at z = 2 is given by the dotted line. The expected range of the ratios when we consider CMB pumping and collisional excitation (in a gas of density 20 and 80 cm^{-3} and temperature $T = 100$ K) is marked by the dashed lines.

3. Preliminary results from the models

We consider the case of a cloud irradiated by the QSO dominated meta-galactic UV radiation field (BGR) (Haardt & Madau (1996)) and cosmic microwave background radiation (CMBR) at z = 2. We model the ionization state, chemical history, and temperature of the gas using version 96 of Cloudy. For simplicity we consider the absorbing gas to be a plane parallel slab of uniform density. The details of the improved grain physics (dust mediated molecular formation, heating, and radiative transport etc.,) and molecular network (formation, interaction with UV photons etc.,) used here are described in van Hoof et al (2001) and Ferland et al. (1994; 2002). Results are summarized in Fig. 5. It is clear from the figure that our models produce detectable amounts of $^{h}2$ (with N(H_2)$\geq 10^{14}$ cm^{-2}) only when n(H I)$\geq$ 0.1 cm^{-3}. The presence of an additional radiation field, turbulent motions, lower dust content or a lower N(H I) will move this limit toward higher n_H owing to greater photo-dissociation and less shielding. For the range of parameters directly measured in DLAs, the absence of detectable $^{h}2$ absorption lines could just be a direct consequence of lower densities. This argument is supported by the fact that models with lower densities, $n_H\leq 0.1$ cm^{-3}, show the spin temperature (T_s) in excess of 1000 K consistent with the available observations. It is clear from Fig. 5 that, for a randomly chosen DLA without any local source of radiation, either there will be no $^{h}2$ or most of the H will be in $^{h}2$. For the derived value of density and κ

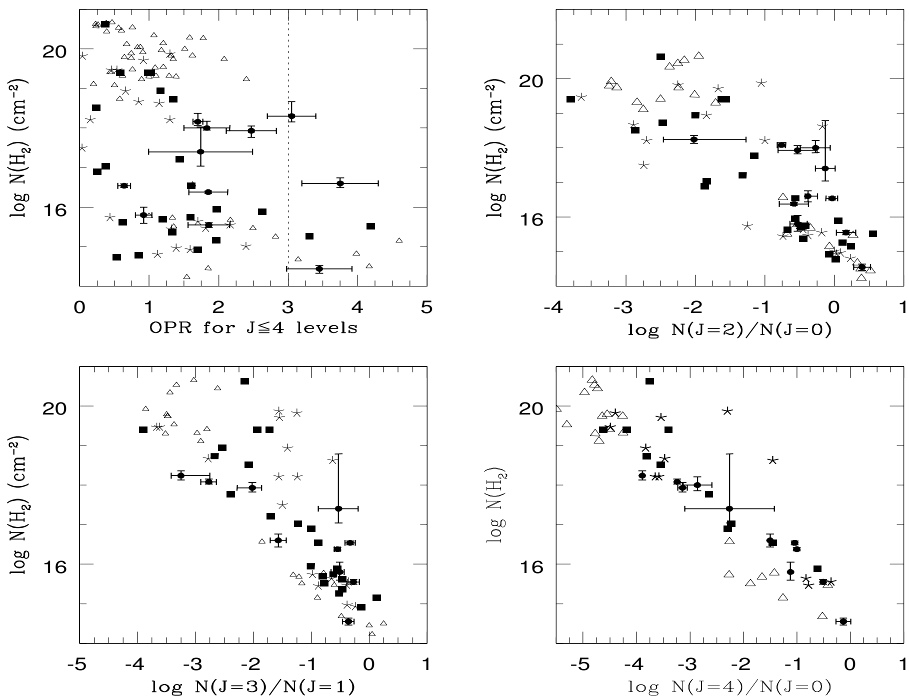

Figure 4. The column density ratios of different J levels observed in individual components in DLAs are plotted against N(^{h}2).Open triangles, stars and filled squares show the results obtained along the lines of sight through the Milkyway, LMC, and SMC from Tumlinson et al., (2002), Savage et al., (1977) and Spitzer, Cochran & Hirshfeld (1974).

(see the previous section) it is clear that if only the BGR is present then all the H will be in H_2. Thus the low molecular content seen in these systems require an extra additional radiation field probably due to local star-formation. This is consistent with what we infer from the high J excitations.

Acknowledgments. RS is grateful to the IAU and INSA for travel grants. RS & PPJ gratefully acknowledge the support from Indo-French Center for the Promotion of Advanced Research (Center Franco-Indien pour la Promotion de la Recherche Avancée) under contract No. 3004-A. RS and GJF acknowledge NSF-DST Indo-US exchange programme (NSFINT-0243091 & NSFRPO-115/2002).

References

Ferland, G.J., Fabian, A.C. & Johnstone, R.M. 1994, MNRAS, 266, 399

Ferland, G.J., Fabian, A.C. & Johnstone, R.M. 2002, MNRAS, 333, 876

Haardt, F. & Madau, P. 1996, ApJ, 461, 20

Jenkins, E. B. & Tripp, T. M. 2001, ApJS, 137, 297

Ledoux, C., Petitjean, P. & Srianand, R. 2003, MNRAS, (in press)

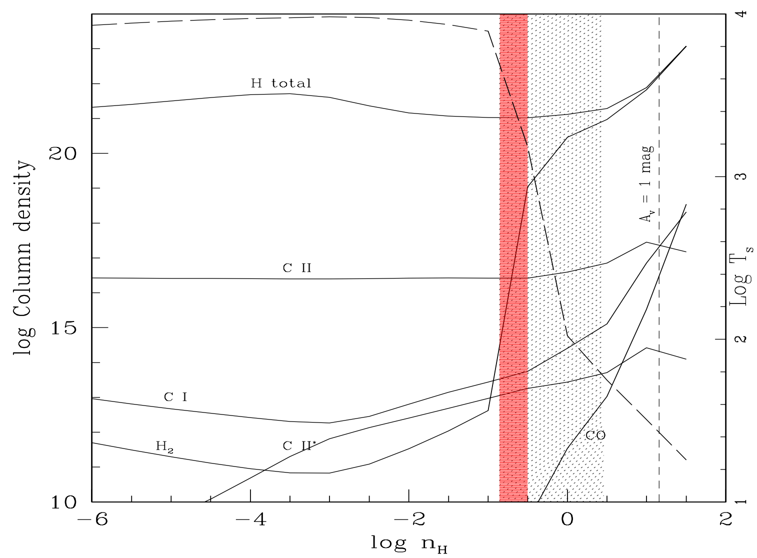

Figure 5. Column densities of different species as a function of density. The calculation uses the QSO dominated meta-galactic UV radiation field at z=2, N(H I) = 10^{21} cm^{-2}, metallicity, Z = 0.1, $\kappa = 0.1$. The long dashed line gives the spin-temperature, T_s (given in the right hand side ordinate), as a function of n_H. The light shadow region gives the range of n_H where H_2 is detectable (i.e., $N(H_2) \geq 10^{14}$ cm^{-2}) and less than H I (i.e., $N(H_2) \leq 10^{21}$ cm^{-2}). The dark shadow region shows the n_H range that reproduces the observed range in $N(H_2)$. The long dashed vertical line gives the n_H at which the visual extinction A_V is unity.

Ledoux, C., Srianand, R. & Petitjean, P. 2002, A&A, 393, 781

Petitjean, P., Srianand, R. & Ledoux, C. 2000, A&A, 364, 26

Petitjean, P., Srianand, R. & Ledoux, C. 2002, MNRAS, 332, 383

Savage, B. D., et al. 1977, ApJ, 216, 291

Spitzer, L. Jr., Cochran, W.D. & Hirshfeld, A. 1974, ApJS, 28, 373

Srianand, R., Petitjean, P. & Ledoux, C. 2000, Nature, 408, 931

Srianand, R. & Petitjean, P. 2001, A&A, 373, 816

van Hoof, P.A.M., et al. (astro-ph/0107183)

Tumlinson, J., et al. 2002, ApJ, 566, 857

Highlights of Astronomy, Vol. 13
International Astronomical Union, 2003
O. Engvold, ed.

Molecular Absorption Lines in Galaxies

Tommy Wiklind

ESA Space Telescope Division
STScI, 3700 San Martin Dr, Baltimore MD 21218, USA

Abstract. Molecular absorption lines have become an important tool in studying the astrochemistry of the dense and cold interstellar medium in both our own Galaxy and high redshift systems. The sensitivity is to first order only dependent on the observed continuum flux. Apart from a few nearby galaxies, molecular absorption lines have been used to study the molecular ISM in 4 galaxies at redshifts 0.25-0.89. A large number of molecular species and transitions have been observed, allowing a detailed comparison with molecular gas in our own Galaxy. Planned instruments, such as ALMA, will allow studies of a larger number of molecular absorption line systems.

1. Introduction

The presence of molecules in the interstellar medium (ISM) has been known for almost 70 years. The very first detection of the molecular ISM was done through observations of narrow absorption lines at optical wavelengths, seen towards bright stars in our own Milky Way galaxy (Merrill 1934). Through extensive detective work it was soon established that these lines were due to molecules in interstellar space (Russell 1935; Swings & Rosenfeld 1937). Today more than 120 molecular species are known to exist in interstellar space. Many of these molecules are complex, containing as many as 13 atoms. These complex species are interesting from an astrochemical point of view, but in order to specify the basic physical and chemical parameters of the molecular gas a smaller set of diagnostic molecules suffice. Knowledge of the physical and chemical properties of the molecular gas allows us to gain an understanding of star formation processes. In the Milky Way these parameters are known through observation of rotational transitions of diagnostic molecular species, radiating at millimeter and sub-millimeter wavelengths.

In external galaxies, however, it becomes increasingly difficult to get a detailed picture of the molecular gas and its physical and chemical properties. This is mainly due to the low covering factor of molecular gas, given the angular resolution provided by existing telescopes, resulting in a low observed signal strength. In addition, some molecules require very high densities and temperatures to be excited and produce observable emission. This situation becomes even more severe for very distant galaxies, where even the best interferometer systems fail to resolve the molecular gas distribution. It is therefore not surprising that the very first detection of molecular gas in external galaxies was done using absorption lines rather than emission lines. With the Parkes 64m telescope, Whiteoak & Gardner (1973) detected OH in absorption towards the starburst galaxy NGC253. This was followed by detection of additional OH absorption in NGC4945 (Whiteoak & Gardner 1975) in the LMC (Whiteoak &

Gardner 1976b), and H_2CO in Centaurus A (Gardner & Whiteoak 1976) and in the LMC (Whiteoak & Gardner 1976a).

The first molecule to be observed in emission in external galaxies was CO (Rickards et al. 1975; Solomon & de Zafra 1975). Since then CO emission has become the standard probe for molecular gas in external galaxies, providing us with pertinent information about the distribution of the molecular gas, its kinematics and the total gas mass. Observation of several different rotational transitions gives a handle on the temperature and density of the molecular component, but little information on the chemical properties of the gas. To achieve the latter, it is necessary to observe additional molecular species, preferably in several different rotational transitions. The sensitivity of today's instruments usually limits this to a few simple molecules in the central regions of the most nearby galaxies.

2. Molecular Absorption Lines

The use of molecular absorption lines allows observation of many more molecular species than that possible using the corresponding emission lines. The sensitivity is, to first order, only limited by the observed strength of the background continuum source. The drawback is that the extent of the background source is very limited and only a very small volume of the molecular gas is probed. When using quasars (QSOs) as background sources, the angular extent can be as small as a few tens of μarcsec. Another, and more limiting constraint, is the fact that suitable background sources are scarce at millimeter and sub-millimeter wavelengths. Nevertheless, for the most distant objects, molecular absorption lines are the only means available for probing the details of the physical and chemical conditions of the molecular gas.

Molecular absorption occurs whenever the line of sight to a background quasar passes through a sufficiently dense molecular cloud. The molecular gas in nearby galaxies is strongly concentrated to the central regions, making the likelihood for absorption largest whenever the line of sight passes close to the center of an intervening galaxy. Molecular absorption in intervening galaxies is therefore likely to be associated with gravitational lensing.

For optically thin *emission* the observed property is the emission integrated over velocity, $I_{\rm CO}$, where: $I_{\rm CO} = \int T_{\rm a}\, dv \;\propto\; N_{\rm tot}\, T^{-1}\, e^{-E_{\rm u}/kT}\, (e^{{\rm h}\nu/{\rm k}T} - 1)\, [J(T) - J(T_{\rm bg})]$. $N_{\rm tot}$ is the total column density of a given molecular species, $E_{\rm u}$ is the upper energy level of a transition with $\Delta E = h\nu$, $T_{\rm bg}$ is the local temperature of the Cosmic Microwave Background Radiation (CMBR) and $J(T) = (h\nu/k)(e^{h\nu/kT} - 1)^{-1}$. When $T \rightarrow T_{\rm bg}$ the signal disappears. For molecular *absorption* the observable is the velocity integrated opacity $I_{\tau_\nu} \propto N_{\rm tot}\, T^{-1}\, \mu_0^2\, (1 - e^{-h\nu/kT}) \approx (h\nu/k)\, N_{\rm tot}\, \mu_0^2\, T^{-2}$, where $N_{\rm tot}$ is again the total column density of a given molecular species and μ_0 is the permanent dipole moment of the molecule[9].

The dependence on $(\mu_0/T)^2$ means that the observability of molecular absorption lines increases with the strength of the permanent electric dipole moment and decreasing gas temperature - a situation which to a large extent is the

[9]This expression is strictly speaking only true for linear molecules but represents a reasonable approximation for non-linear molecules as well.

inverse to that of molecular emission. If multiple gas components are present in the line of sight, with equal column densities but characterized by different excitation temperatures, absorption will be most sensitive to the gas component with the lowest temperature. The dependence of the opacity on the permanent dipole moments also means that molecules much less abundant than CO can be as easily detectable. For instance, HCO^+ has an abundance which is of the order 5×10^{-4} that of CO, yet it is as easy, or easier, to detect in absorption as CO. This is illustrated in Fig. 1, where the observed opacity of the CO(1-0) and HCO^+(2-1) transitions at $z = 0.25$ are compared. In this particular case, the HCO^+ line has a higher opacity than the CO line.

Table 1. Properties of molecular absorption line systems.

Source	z_a (abs)	z_e (emission)	N_{CO} cm^{-2}	N_{H_2} cm^{-2}	N_{HI} cm^{-2}	A_V	N_{HI}/N_{H_2}
Cen A	0.00184	0.0018	1.0×10^{16}	2.0×10^{20}	1×10^{20}	50	0.5
PKS1413+357	0.24671	0.247	2.3×10^{16}	4.6×10^{20}	1.3×10^{21}	2.0	2.8
B3 1504+377A	0.67335	0.673	6.0×10^{16}	1.2×10^{21}	2.4×10^{21}	5.0	2.0
B3 1504+377B	0.67150	0.673	2.6×10^{16}	5.2×10^{20}	$< 7 \times 10^{20}$	<2	<1.4
B 0218+357	0.68466	0.94	2.0×10^{19}	4.0×10^{23}	4.0×10^{20}	850	1×10^{-3}
PKS1830–211A	0.88582	2.507	2.0×10^{18}	4.0×10^{22}	5.0×10^{20}	100	1×10^{-2}
PKS1830–211B	0.88489	2.507	$1.0 \times 10^{16\ (e)}$	2.0×10^{20}	1.0×10^{21}	1.8	5.0
PKS1830–211C	0.19267	2.507	$< 6 \times 10^{15}$	$< 1 \times 10^{20}$	2.5×10^{20}	<0.2	>2.5

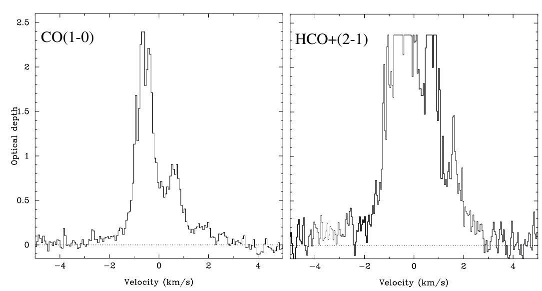

Figure 1. The observed opacity for the CO(1-0) and HCO^+(2-1) transitions seen at $z = 0.25$ towards PKS1413+135. The opacity of the HCO^+(2-1) line is larger than that of the CO(1-0) line despite of an abundance which is $10^{-3} - 10^{-4}$ that of CO.

3. Known Molecular Absorption Line Systems

Local absorption systems Molecular absorption line studies is a relatively new field, both for our own Galaxy and for external galaxies. The small angular extent of QSOs at millimeter wavelengths (tens of μarcsec) means that for local molecular clouds, the observed signal is dominated by emission from areas within the telescope beam not covered by the continuum source. It is only with interferometers operating at millimeter wavelengths that it is possible to effectively utilize molecular absorption lines within our own Galaxy. This technique has been used by Lucas & Liszt in an extended study of the diffuse molecular component in the Milky Way (cf. Liszt & Lucas 2002; Lucas & Liszt 2002 and references therein).

Apart from the early observations of OH and H_2CO absorption in nearby galaxies, it is only Cen A and the radio galaxy 3C390 that allows absorption line measurements. Both these systems posses a relatively strong flat spectrum AGN. Cen A in particular shows a rich assortment of absorption lines, with several components spread over more than 60 km s^{-1} (cf. Eckart et al. 1990; Israel et al. 1991; Wiklind & Combes 1997a).

High redshift absorption systems There are four known molecular absorption line systems at higher redshift: z=0.25-0.89. These are listed in Table 1 together with data for the low redshift absorption system seen toward the radio core of Cen A. For the high redshift systems, a total of 22 different molecules have been detected, in 32 different transitions: CO, CN, CS, OH, (SO), (LiH), HCO^+, HOC^+, HCN, HNC, N_2H^+, H_2O, H_2CO, HC_3N, C_2H, C_3H_2, $C^{13}O$, $C^{18}O$, $H^{13}CO$, $H^{13}CN$ and $HC^{18}O^+$. Molecules in parenthesis are tentative detections. Some of these molecules, OH, C_2H, C_3H_2 and HC_3N, are detected at cm wavelengths (cf. Menten, Carilli & Reid 1999; Kanekar et al. 2003). As can be seen from Table 1, the inferred H_2 column densities varies by $\sim 10^3$. The isotopic species are only detectable towards the systems with the highest column densities.

Two of the four known molecular absorption line systems are situated within the host galaxy to the 'background' continuum source: PKS1413+135 (Wiklind & Combes 1994) and B3 1504+377 (Wiklind & Combes 1996b). The latter exhibits two absorption line systems with similar redshifts, z=0.67150 and 0.67335. The separation in rest-frame velocity is 330 km s^{-1}. The two absorption line systems with the highest column densities occur in galaxies which are truly intervening and each acts as a gravitational lens to the background source: B0218+357 and PKS1830-211. In these two systems several isotopic species are detected as well as the main isotopic molecules, showing that the main lines are saturated and optically thick (Combes & Wiklind 1995; Combes & Wiklind 1996; Wiklind & Combes 1996a, 1997b, 1998). Nevertheless, the absorption lines do not reach the zero level, showing that only part of the lensed images are covered by obscuring molecular gas.

Abundance ratios Since most molecules have been observed in two or more transitions, it is possible to determine the excitation temperature and, with the assumption of weak thermal equilibrium, the total column density (cf. Wiklind & Combes 1997b). The H_2 column density remains unknown, but abundance ratios between the observed molecular species do not differ from that of corresponding molecular gas in the Milky Way (cf. Wiklind 2003). The abundance of HCO^+ is elevated relative to the models of diffuse gas, in the same manner as found for Galactic gas when derived through molecular absorption lines (cf. Wiklind & Combes 1997b; Lucas & Liszt 1996).

4. Special Issues

Rare transitions Apart from the more common molecular species, such as CO, HCN, HCO^+, H_2CO, N_2H^+, etc, redshifted molecular absorption lines can also be used to study transitions that have frequencies which normally fall outside transparent atmospheric windows. Such as the ground transition of water vapor, H_2O, LiH and molecular oxygen, O_2. The ground transition of H_2O was first detected at z= 0.678 (Combes & Wiklind 1995), and a tentative detection of LiH was done in the same system (Combes & Wiklind 1998). Molecular oxygen, however, remains undetected (Combes & Wiklind 1995; Combes, Wiklind & Nakai 1997). In fact, the upper limit to the O_2 line achieved through ground based molecular absorption lines is at par with the latest upper limits to the O_2 abundance measured with dedicated satellites (Pagani et al. 2003). Both sets of observations suggests that the abundance of O_2 in dark clouds is $\sim 10^{-5}$ the predicted abundance from chemical models. Among several different possible explanations to this (cf. Wiklind 2003), the inclusion of grain-reactions into the chemical models appears promising (Roberts & Herbst 2003).

Future Challenges The main difficulty with using molecular absorption lines in studying the detailed composition of the molecular ISM in external galaxies is that these systems are rare; about 100 times less frequent than damped Lyman-α systems. The molecular gas is less extended than other components of the ISM, with a relatively small volume covering factor. Several surveys of potential absorption line systems have so far not found any (see Curran et al. these proceedings and references therein). With planned new instruments, such as ALMA, and a significant increase in the instantaneous wavelength coverage of the receivers, the number of molecular absorption line systems is expected to grow.

References

Combes F. & Wiklind T. 1998, A&A, 334, L81

Combes F., Wiklind T. & Nakai N. 1997, A&A, 327, L17

Combes F. & Wiklind T. 1997, ApJ, 486, L79

Combes F. & Wiklind T. 1996, in Cold Gas at High Redshift, eds. M. Bremer, P. van der Werf & C. Carilli, (Kluwer)

Combes F. & Wiklind T. 1995, A&A, 303, L61

Eckart A., Cameron, A., Genzel, R., et al. 1990, ApJ, 365, 522

Gardner, F.F. & Whiteoak, J.B. 1976, MNRAS, 175, 9p

Israel, F.P., van Dishoeck, E.F., Baas, F., de Grauuw, T. & Phillips, T.G. 1991, A&A, 245, L13

Kanekar, N., Chengalur, J.N., de Bruyn, A.G. & Narisimha, D. 2003, MNRAS, 345, L7

Liszt, H.S. & Lucas, R. 2002, A&A, 391, 693

Lucas, R. & Liszt, H.S. 2002, A&A, 384, 1054

Lucas, R. & Liszt, H.S. 1996, A&A, 307, 237

Menten, K.M., Carilli, C.L. & Reid, M.J. 1999, in Highly Redshifted Radio Lines, ASP Conf. Series Vol. 156, eds. C. L. Carilli, K. M. Menten, & G.I. Langston, p. 218

Merrill, P.W. 1934, PASP, 46, 206

Pagani, L., Olofsson O.A.H., Bergman, P., et al. 2003, A&A, 403, L77

Rickard, L.J., Palmer, P., Morris, M., Turner, B.E. & Zuckerman, B. 1975, ApJ, 199, L75

Roberts, H. & Herbst, E. 2003, A&A, 395, 233

Russell, H.N. 1935, MNRAS, 95, 635

Solomon, P.M. & de Zafra, R. 1975, ApJ, 199, L75

Swings, P. & Rosenfeld, L. 1937, ApJ, 86, 483

Whiteoak, J.B. & Gardner, F.F. 1976a, MNRAS, 174, 51p

Whiteoak, J.B. & Gardner, F.F. 1976b, MNRAS, 176, 25p

Whiteoak, J.B. & Gardner, F.F. 1975, ApJ, 195, L81

Whiteoak, J.B. & Gardner, F.F. 1973, Astrophys. Lett., 15, 211

Wiklind, T. 2003, in The Carnegie Centennial Symposium IV: The Formation and Evolution of the Elements, eds. A. McWilliams & M. Rauch

Wiklind, T. & Combes, F. 1999, in Highly Redshifted Radio Lines, ASP Conf. Series Vol. 156, eds. C. L. Carilli, K. M. Menten, & G.I. Langston, p. 202

Wiklind, T. & Combes, F. 1998, ApJ, 500, 129

Wiklind, T. & Combes, F. 1997a, A&A, 324, 51

Wiklind, T. & Combes, F. 1997b, A&A, 328, 48

Wiklind, T. & Combes, F. 1996a, Nature, 379, 139

Wiklind, T. & Combes, F. 1996b, A&A, 315, 86

Wiklind, T. & Combes, F. 1995, A&A, 299, 382

Wiklind, T. & Combes, F. 1994, A&A, 286, L9

Highlights of Astronomy, Vol. 13
International Astronomical Union, 2003
O. Engvold, ed.

Deep Searches for High Redshift Molecular Absorption

S. J. Curran and J. K. Webb

School of Physics, University of New South Wales, NSW 2052, Australia

M. T. Murphy

Institute of Astronomy, Madingley Road, Cambridge CB3 0HA, UK

N. Kuno

Nobeyama Radio Observatory, Nagano 384-1305, Japan

Abstract. Millimetre-band scans of the frequency space towards optically dim quasars is potentially a highly efficient method for detecting new high redshift molecular absorption systems. Here we describe scans towards 7 quasars over wide bandwidths (up to 23 GHz) with sensitivity limits sufficient to detect the 4 redshifted absorbers already known. With wider frequency bands, highly efficient searches of large numbers of possibly obscured objects will yield many new molecular absorbers.

1. Introduction

Webb et al. (these proceedings) discussed constraints on possible variations in fundamental constants offered by quasar absorption lines. Optical studies (Webb et al. 1999; Murphy et al. 2003) find a statistically significant variation of the fine-structure constant, $\Delta\alpha/\alpha \approx (-0.54 \pm 0.12) \times 10^{-5}$, over the redshift range $0.2 < z_{\rm abs} < 3.7$. Comparison between H I-21cm and molecular rotational (millimetre) absorption lines can yield an order of magnitude better precision (per absorption system) than these purely optical constraints (Drinkwater et al. 1998; Carilli et al. 2000; Murphy et al. 2001): a statistical sample of H I-21cm/mm comparisons will provide an important cross-check on varying-α. Currently, however, only 4 such redshifted millimetre absorption systems are known (Wiklind, these proceedings). To increase this number we have employed the following search strategies:

1. Deep integrations of damped Lyman-alpha absorbers (DLAs), the highest column density ($N_{\rm HI} \gtrsim 10^{20}$ cm^{-2}) quasar absorbers known. Since we observe at a known redshift and therefore frequency, optical depth limits better than $\tau \lesssim 0.1$ are often obtained. The DLA results are discussed in detail by Curran et al. (2004).

2. Scanning the frequency space towards visually dim millimetre bright quasars in search of a possible absorber responsible for the visual obscuration. Here we summarize our results as obtained with the Swedish-ESO Sub-

millimetre Telescope (SEST) and Nobeyama Radio Observatory's 45-m telescope (NRO).

2. Results

From an extensive literature search we selected four millimetre-loud quasars yet to be optically identified (Table 1, top). For each of these we performed a

Table 1. The SEST (top) and NRO (bottom) search results. V is the visual magnitude with the Galactic extinction, A_B, given. $z_{\rm em}$ is the quasar redshift, S the approximate flux density in Jy at the observed frequency band, ν, and τ is the typical 3σ optical depth limit (quoted for a resolution of 1 km s^{-1}, see Curran et al. 2002).

Quasar	V	A_B	$z_{\rm em}$	Ref	S	ν [GHz]	τ
0500+019	21.2	0.289	0.58457	2	0.5	78.30–80.90	2
...	...	...	...	...	0.5	85.50–86.50	0.8
...	...	...	...	...	0.5	112.10–113.10	0.8
...	...	...	...	...	0.4	130.00–141.40	1
0648–165	–	2.456	–	–	1.6	78.30–80.90	0.2
...	...	...	...	...	1.5	83.90–90.50	0.2
...	...	...	...	...	0.7	138.00–141.40	0.5
...	...	...	...	...	0.6	142.80–149.40	0.7
0727–115	22.5	1.271	–	–	2.9	78.30–80.90	0.2
...	...	...	...	...	2.7	83.90–90.50	0.1
...	...	...	...	...	1.5	138.00–141.40	0.2
...	...	...	...	...	1.2	142.80–148.60	0.4
1213–172	21.4	0.253	–	–	1.0	78.30–80.90	0.4
...	...	...	...	...	0.9	83.90–90.50	0.4
...	...	...	...	...	0.5	138.00–141.40	0.8
...	...	...	...	...	0.4	142.80–151.00	1
0742+103	~ 24	0.111	–	–	0.6	46.90–47.50	–
...	...	...	...	...	0.4	77.25–87.50	0.9
...	...	...	...	...	0.4	88.45–89.35	0.4
1600+335	23.2	0.137	1.1	3	0.7	46.90–47.50	2
...	...	...	...	...	0.5	77.25–87.50	0.5
...	...	...	...	...	0.5	88.45–89.35	0.4
1655+077	20.1	0.66	0.621	1	1.5	46.90–47.50	1
...	...	...	...	...	1.2	77.25–87.50	0.7
...	...	...	...	...	1.2	88.45–89.35	0.3

References: (1) Wilkes (1986), (2) Carilli et al. (1998), (3) Snellen et al. (2000).

spectral scan along the line-of-sight. The high sensitivity and large bandwidth (1 GHz), combined with the possibility of observing simultaneously with two receivers, permitted us to scan a range of $\approx$ 10 GHz in both the 2-mm and 3-mm bands. Over these ranges we reached optical depth limits in both bands sensitive enough the detect the 4 known redshifted millimetre absorbers (Table 1 cf. $\tau \approx 0.7$ to ≈ 2 at $\gtrsim 4$ km s^{-1} resolution), although no $\geq 3\sigma$ absorption features were found (Murphy, Curran & Webb 2003).

Of the remaining visually dim quasars, 10 have 3-mm flux densities $\gtrsim 0.5$ Jy. Four of these are located in the north and with the NRO[10] we were able to observe the three listed in Table 1. While the 6-mm limits are poor, again at 3-mm our search is sensitive enough to detect the 4 known absorbers over the observed redshift range: For the $J = 0 \rightarrow 1$, $1 \rightarrow 2$ and $2 \rightarrow 3$ of transitions CO, HCN and HCO^+, i.e. the most commonly detected transitions in the 4 known absorbers, the observed frequencies give a 50% coverage for 0742+103 up to $z \approx 3$ and 30% for both 1600+335 and 1655+077 up to the emission redshift[11]. The coverage for the SEST sources are discussed in Murphy, Curran & Webb (2003); for the above transitions up to 90% is achieved due to the large bandwidth and dual receiver capability.

References

Carilli, C.L., Menten, K.M., Reid, M.J., Rupen, M.P., & Yun, M.S. 1998, ApJ, 494, 175

Carilli, C.L., Menten, K.M., Stocke, J.T., Perlman, E., Vermeulen, R., Briggs, F., de Bruyn, A.G., Conway, J., & Moore, C.P. 2000, PhRvL, 85, 5511

Curran, S.J., Murphy, M.T., Webb, J.K., Rantakyrö, F., Johansson, L. E.B., & Nikolić, S. 2002, A&A, 394, 763

Curran, S.J., Murphy, M.T., Pihlström, Y.M., Bolatto, A.D., Bower, G.C., & Webb, J.K. 2004, MNRAS, in preparation

Drinkwater, M.J., Webb, J.K., Barrow, J.D., & Flambaum, V.V. 1998, MNRAS, 295, 457

Murphy, M.T., Curran, S.J., & Webb, J.K. 2003, MNRAS, 342, 830

Murphy, M.T., Webb, J.K., & Flambaum, V.V. 2003, MNRAS, accepted (astro-ph/0306483)

Murphy, M.T., Webb, J.K., Flambaum, V.V., Drinkwater, M.J., Combes, F., & Wiklind, T. 2001, MNRAS, 327, 1244

Snellen, I.A.G., Schilizzi, R.T., Miley, G.K., de Bruyn, A.G., Bremer, M.N., & Röttgering, H.J.A. 2000, MNRAS, 319, 445

Steppe, H., Jeyakumar, S., Saikia, D.J., & Salter, C.J. 1995, A&AS, 113, 409

Webb, J.K., Flambaum, V.V., Churchill, C.W., Drinkwater, M.J., & Barrow, J.D. 1999, PhRvL, 82, 884

Wilkes, B.J. 1986, MNRAS, 218, 331

[10] The fact that each of the 6 AOSs on the NRO only covers 0.25 GHz is compensated by the high efficiency of the 45-m antenna (4 Jy K^{-1} cf. 25 Jy K^{-1} at SEST).

[11] Note that we have included the possibility of HCN or HCO^+ $0 \rightarrow 1$ Galactic absorption towards all 3 sources as well as HCN or HCO^+ $1 \rightarrow 2$ in the host of 1600+335.

Highlights of Astronomy, Vol. 13
International Astronomical Union, 2003
O. Engvold, ed.

Probing Physics and Chemistry in Circumnuclear Torus with OH

Yu Zhi-yao

Shanghai Astronomical Observatory,80 Nandan Road,Shanghai 200030,China
National Astronomical Observatories, Beijing 100012, China
E-mail: zyyu@center.shao.ac.cn

Abstract. We observed OH maser emission at 18cm in a circumnuclear torus surrounding the center of IRAS10173+0828 using the 7 telescopes of MERLIN, together with the Lovell antenna. IRAS10173+0828 is a distant super-luminous far-infrared galaxy. The OH maser emission is remarkably narrow (FWHP = 39km s^{-1}) for its strength, and the 1667 and 1665 MHz lines are well separated. The 1667 transition shows two distinct peaks displaced from one another by 100 km s^{-1}. Using our MERLIN observational results we probe the physics in the circumnuclear torus surrounding the center of IRAS10173+0828, obtain the kinematic properties of the torus, and study the central source.

1. Introduction

In January 2002 we observed line emission from OH masers in a region surrounding the center of IRAS10173+0828 using MERLIN. Powerful OH maser emission has been previously detected in the circumnuclear disk of Arp220, IIZw35, Mrk273, and IRAS17208-0014 by Lonsdale et al. (1998), Diamond et al. (1999), Yates et al.(2000), and Diamond et al.(1999), respectively. Previous VLBI observation and time series analysis of the spectra (Haschick, Bann & Peng 1994) suggests that the masers originate in a rotating torus surrounding a massive object (with a mass M of 1.5×10^7 $M_\odot$) at the center of the galaxy (Watson & Wallin 1994). IRAS10173+0828 is a distant super-luminous far-infrared galaxy (Mirabel & Sanders 1987). The OH maser emission is remarkably narrow (FWHP = 39 km s^{-1}) for its strength, and the 1667 and 1665 MHz lines are well separated. The 1667 MHz transition shows two distinct peaks separated by 100 km s^{-1}. Using our MERLIN observational results we probe the physics in the circumnuclear torus surrounding the center of IRAS10173+0828, obtain the kinematic properties of the torus, and study the central source.

2. Observations

We observed IRAS10173+0828 for 2×12 hrs on 24-25 Jan. 2002 using the 7 telescopes of MERLIN, (operated by the University of Manchester on behalf of PPARC), and including the Lovell antenna. The point-like quasar 0552+398 was used as the bandpass and flux calibration source. IRAS10173+0828 was observed by switching between two 4-MHz bands containing 128 frequency channels each. The bands were centered on 1588.5 and 1591.5 MHz. The total time on IRAS10173+0828 was 14.78 hr. In between each 4 min scan on IRAS10173+0828, the phase reference source 1015+057 was observed at 1590 MHz using a normal 16 MHz bandwidth, averaged to a single 14.5 MHz channel for data processing. 0552+398 was observed at all frequencies and configurations. All further processing was done in AIPS. The phase and amplitude of 0552+398 were calibrated and the data were used to derive tables of bandpass corrections for the both 4-MHz data sets. These data also showed that there were no instrumental phase changes associated with observing configuration or frequency changes. We self-calibrated the amplitude and phase of 1015+057 and applied these solutions and the bandpass corrections to the IRAS10173+0828. We then re-weighted the data from each antenna in proportion to its sensitivity. 1015+057 was observed at 10 18 27.8483, +05 30 29.936(J2000) and the pointing position of IRAS10173+0828 was 10 19 59.9, +08 13 34(J2000). The final absolute position accuracy of the components of IRAS10173 is 20 mas, plus a signal-to-noise-dependent relative error. We plotted the calibrated visibility amplitudes and phases of IRAS10173+0828 as a function of channel. We also converted the frequency axis to velocity. Using a line rest frequency of 1667.359 MHz, the velocity in channel 64 of the data set observed at 1588.5 MHz is v_{lsr}=14179.26 km s^{-1}. The data centered on 1588.5 MHz line showed a feature at the expected position of the 1667 MHz line but the data centered on 1591.5 MHz had a flat spectrum. We also Fourier transformed these continuum data without cleaning to give a one-channel dirty map, and similarly made a 128-channel dirty map of the data containing the line as well as continuum. We then subtracted the continuum map from each channel of line+continuum data. Finally we cleaned the resulting line-only data-cube, using a 200 mas FWHM circular restoring beam to make the maps easier to interpret visually. Note that the natural beam fitted to unweighted data is 286×171 mas; we checked that using a circular beam did not produce artifacts. The typical noise in a quite channel is $\sigma_{rms} = 1$ mJy beam^{-1}, rising to 2 mJy beam^{-1} in the brightest channel due to dynamic range limitations arising from the sparse coverage of the visibility plane.

3. Results

We detected a signal at $> 3\sigma$ in 19 velosity channels, out of 128 channels observed, and obtained the contour maps of OH maser in the 19 velocity channels. The physical parameters of the OH maser in the 19 velocity channels are shown in Table 1.

We find that the contour-maps of OH maser in some velocity channels extend to both east and west. The morphology of the contour is warped. This implies to us that the circumnuclear torus around the center of IRAS10173+0828 is warped. Using Yu's (1996) model we obtain from Table 1 that the mass of central black hole is $3\times10^{10}M_\odot$, that is, evidence of a massive black hole.

Acknowledgments. This work was supported by the NATIONAL NATURAL SCIENCES FOUNDATION OF CHINA. MERLIN is a national facility operated by the University of Manchester on behalf of PPARC. I thank Dr.

Table 1. The physical parameters of OH maser in the 19 velocity channels*

CHAN No	VELOCITY (km/s)	RA_{offs} (mas)	error (mas)	Dec_{offs} (mas)	error (mas)	Peak (mJy/beam)
87	14050	4468	65	-195	67	5
88	14044	4457	68	-179	79	6
89	14039	4507	23	-127	25	14
90	14033	4482	19	-156	30	21
91	14028	4489	19	-153	21	27
92	14022	4482	19	-151	23	32
93	14016	4486	21	-169	25	29
94	14011	4493	19	-138	28	27
95	14005	4504	21	-155	27	22
96	13999	4489	28	-156	31	15
97	13994	4489	22	-208	28	14
98	13988	4504	35	-180	59	9
99	13983	4486	80	-130	74	7
100	13977	4464	41	-74	37	9
101	13971	4425	100	-144	79	5
102	13966	4529	69	-157	44	7
103	13960	4475	53	-66	68	7
104	13955	4511	45	-136	52	6
105	13949	4493	43	-100	53	6

*Reference position is RA(J2000)= 10 19 59.9, DEC(J2000)=08 13 34.0

Anita M. S. Richards, Dr. P. Thomasson, Dr. T. Muxlow, and all staff of MERLIN for their kind help.

References

Diamond, P.J., et al. 1999, ApJ, 511, 178
Haschick, A.D., Bann,W.A.& Peng,E.W. 1994, ApJ, 437, L35
Lonsdale, C.J., et al. 1998, ApJ, 493, L13
Mirabel, I.F. & Sanders, D.B. 1987, ApJ, 322, 688
Watson, W.D. & Wallin, B.K. 1994, ApJ, 432, L35
Yates,J.A., et al. 2000, MNRAS 317, 28
Yu Zhi-yao, 1996, Astrophys. & Space Sci., 241, 305

Highlights of Astronomy, Vol. 13
International Astronomical Union, 2003
O. Engvold, ed.

Newly detected H_2O Masers in Seyfert and Starburst Galaxies

A. B. Peck[1], A. Tarchi[2,3], C. Henkel[4], N. M. Nagar[5], J. Braatz[6], L. Moscadelli[3]

[1] *Harvard-Smithsonian CfA, SMA Project, PO Box 824, Hilo, HI 96721*
[2] *Istituto di Radioastronomia, CNR, Via Gobetti 101, 40129 Bologna*
[3] *Osservatorio Astronomico di Cagliari, Loc. Poggio dei Pini, Strada 54, 09012 Capoterra (CA), Italy*
[4] *MPIfR, Auf dem Hügel 69, D-53121 Bonn, Germany*
[5] *Kapteyn Institute, University of Groningen, Landleven 12, 9747 AD Groningen, Netherlands*
[6] *NRAO, PO Box 2, Green Bank, WV 24944*

Abstract. We report new detections of three H_2O megamasers and one kilomaser using the Effelsberg 100-m telescope. Isotropic luminosities are ~50, 300, 1, and 230 $L_\odot$ for Mrk 1066, Mrk 34, NGC 3556, and Arp 299, respectively. Mrk 34 contains the most distant H_2O megamaser ever detected in a Seyfert. Our targets in this survey were chosen to fit one of the following criteria: 1) to have a high probability of interaction between the radio jet and the ISM within the central few parsecs of the radio galaxy, yielding masers which arise in local molecular clouds; or 2) to have very bright IRAS sources in which massive star forming regions might yield powerful masers. The 'jet maser' sources can provide detailed information about the conditions in the ISM in the central 1-10 pc of AGN. The extra-galactic 'star formation masers' can be used to pinpoint and characterize locations of high mass star formation in nearby galaxies. In addition, these sources will help to provide a better understanding of the chemical properties of molecular clouds in extra-galactic systems.

1. Introduction

To date, H_2O megamasers have been thought of primarily as a means to probe the accretion disks in active galaxies. The best known source, NGC 4258, has a thin, slightly warped, nearly edge-on disk in Keplerian rotation around a central mass of $\sim 4\times10^7$ $M_\odot$ (Miyoshi et al. 1995). There is evidence, however, for three distinct classes of extra-galactic H_2O masers. In addition to the 'accretion disk' masers, there are sources in which the amplified emission is the result of an interaction between the nuclear radio jet and an encroaching molecular cloud. A third class of extra-galactic water masers is represented by weaker masers with isotropic luminosities $< 10\,L_\odot$. These are often associated with prominent star forming regions in galactic disks, and have thus far been found in galaxies containing bright IRAS point sources. We have undertaken deep searches using the Effelsberg 100m telescope to detect emission arising from the latter two recently discovered classes of sources.

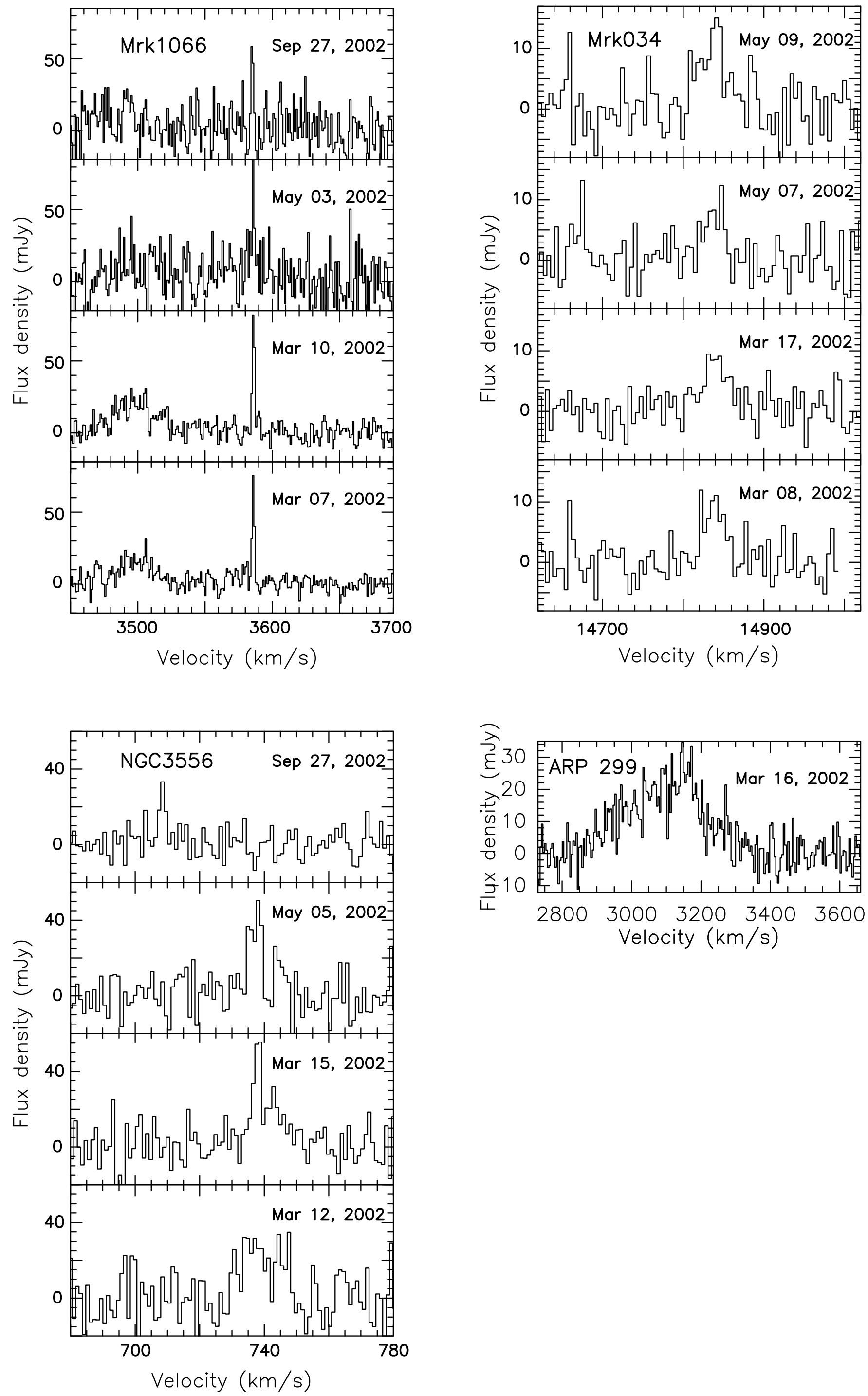

Figure 1. Line profiles of 4 extra-galactic maser sources detected using the Effelsberg 100m telescope.

2. Results

From the 'jet-maser' sample, we have detected two new megamasers, Mrk 1066 and Mrk 34. Line profiles are shown in Fig. 1 (top panels). The 'star formation maser' sample yields new detections of a megamaser (Arp 299) and a kilomaser (NGC 3556). Line profiles of these sources are shown in Fig. 1 (lower panels).

The only known jet maser sources prior to our survey were NGC 1068 (Gallimore et al. 1996), the Circinus galaxy (Greenhill et al. 2001), NGC 1052 (Claussen et al. 1998) and Mrk 348 (Peck et al. 2003) in the latter 2 of which the masers appear to arise along the jet and have FWHM linewidths of ∼90 km s^{-1} and ∼130 km s^{-1}, respectively. Mrk 348 is a Seyfert 2 galaxy which has a radio axis that appears to lie close to the plane of the larger scale galactic disk, suggesting that the maser emission is the result of the radio jet impacting on a molecular cloud in the central parsec of the galaxy. This unusual relative orientation between the radio jet and the host galaxy prompted us to undertake this more intensive search for jet masers in sources where the radio jet is thought to be oriented close to the plane of the galaxy, or where evidence had already been found of jet-cloud interactions. The detection rate in this jet maser survey is 29%. This success rate is in part due to the higher sensitivity now at the Effelsberg 100m telescope, but also due to the unique source selection criteria. This is the first survey undertaken to look specifically for jet masers. The study of these masers will yield information about the molecular clouds in the ISM of the host galaxy, because population inversion in water molecules requires a fairly narrow range of pressures and temperatures (typically $n{\sim}10^8$–10^{10} cm^{-3} and T∼200–800 K).

We also surveyed bright IRAS sources for the star formation masers, such as those detected in IC 10 and NGC 2146 (Greenhill et al. 1993; Tarchi et al. 2002b). These masers can be used to pinpoint locations of high mass star formation and to improve our understanding of galaxy cluster dynamics in the local and neighboring groups of galaxies. These star formation masers occur in nearby galaxies that are known to exhibit prominent CO lines, and contain bright IRAS point sources at their nuclei. Observations of 3 such sources with the Effelsberg 100m telescope yielded two detections, NGC 2146 (Tarchi et al. 2002a) and IC342 (Tarchi et al. 2002b), an unprecedented success rate. This motivated us to perform this larger survey of similar galaxies. While the detection rates of previous surveys of nearby bright IR galaxies have reached only a few percent, that of the present sample is much higher (27 %).

References

Claussen, M. J., Diamond, P. J., Braatz, J. A., et al. 1998, ApJL, 500, 129

Gallimore, J. F., Baum, S. A., O'Dea, C. P., et al. 1996, ApJ, 462, 740

Greenhill, L. J., Moran, J. M., Booth, et al. 2001, in IAU Symposium 205, Galaxies and Their Constituents at the Highest Angular Resolution, ed. R. Schilizzi, S. Vogel, F. Paresce & M. Elvis (San Francisco: ASP), 334

Greenhill, L. J., Moran, J.M., Reid, M.J., et al. 1993, ApJ, 406, 482

Miyoshi, M., Moran, J., et al. 1995, Nature, 373, 127

Peck, A.B., Henkel, C., Ulvestad, J.S., et al. 2003, ApJ, 590, 149

Tarchi, A., Henkel, C., Peck, A.B. & Menten, K. M. 2002a, A&A, 385, 1049

Tarchi, A., Henkel, C., Peck, A.B. & Menten, K.M. 2002b, A&A, 389, L39

Highlights of Astronomy, Vol. 13
International Astronomical Union, 2003
O. Engvold, ed.

Molecular Line Observations in the Magellanic Clouds

Mónica Rubio

Departamento de Astronomía, Universidad de Chile, Casilla 36-D, Santiago, Chile

Abstract. We review the present knowledge of molecular line studies and its relation to interstellar medium properties in the Large and Small Magellanic Clouds. The physical and chemical properties of the molecular gas together with the abundance of different molecular species will be discussed.

1. Introduction

The Large and Small Magellanic Clouds (LMC, SMC), the two nearest extragalactic systems of well known distance, provide a unique opportunity to study physical processes in an interstellar medium different to that of our Galaxy. They have a lower metallicity, higher gas to dust ratios and strong UV radiation fields, and constitute the best target for a detailed study of the molecular gas content, its properties, and the process of star formation. In fact, they are the nearest metal-poor systems with active star formation ($Z_{lmc} \sim Z_\odot/4$ and $Z_{smc} \sim Z_\odot/9$, Kurtz and Dufour 1998) and thus, are the most appropriate systems where the physics and chemistry of the interstellar medium (ISM) can be investigated.

2. Observations

Simultaneous observations in CO(2-1) and CO(1-0) and isotopomers were possible at the SEST telescope after the SIS receivers were installed in 1996.

A deep CO(2-1) survey of molecular regions in the LMC and SMC was performed as an ESO Large Programme (Rubio 2003). These observations were done during 2000-2002 with the SEST telescope and covered a selected number of molecular clouds from the ESO-SEST KEY PROGRAMME (Israel et al. 1993). The clouds were fully sampled at 10" spacing with an rms of 0.01 K. The observations included 30 Doradus, 30 Dor Complex, N11, in the LMC and all of the SMC CO clouds detected in CO(1-0). Specific programs towards N159 in the LMC and N83/N84 in the SMC had been done by Bolatto et al. (2001) and Bolatto et al. (2003), respectively. The LMC arc east of the 30 Doradus complex was also observed (Mizuno, Johansson, private communication). Observations of the ^{13}CO(2-1) and ^{13}CO(1-0) lines heve been done towards the center of the strongest CO clouds mapped at ^{12}CO(2-1). Previously, Chin et al. (1996; 1997) performed ^{13}CO observations towards LIRS36 in the SMC and N113 in the LMC.

The strongest CO clouds, N159 in the LMC and LIRS49 (N27) have been used as targets for multi-line studies. HCO^+ , HCN, CS, HNC, $C^{18}O$, H_2CO

were detected (eg. Heikkila et al. 1998, 1999; Chin et al. 1996, 1997, 1998; Johansson et al. 1994).

3. Results

The characteristics of the molecular clouds and their physical properties are given in the following.

3.1. Properties of Molecular Clouds

Properties of the molecular clouds have been determined from the CO(1-0) surveys done with different resolutions in the Magellanic Clouds. The ESO SEST Key program has produced a wealth of CO data. About 150 molecular clouds have been fully mapped. These clouds are resolved at the 45 arcsec resolution ($\sim$ 20 pc) of the observations. The LMC molecular clouds show the following properties. The CO clouds have sizes ranging from 10 to 40 pc, line widths between 2.5 and 10 km s^{-1}, CO luminosities between 8×10^2 to 1.3×10^4 K km s^{-1}, and virial masses ranging from 10^3 to 7×10^5 M$_\odot$. These clouds, although larger in size and more massive than those found in the SMC, do not look like typical GMCs in the Galaxy (Rubio 1997). They are under-luminous in CO while they show virial masses typical of those of Galactic GMCs. Many of the clouds associated with HII regions are smaller in size than the ionized region, contrary to what is found in our Galaxy (Israel et al. 2003b, and references therein).

In the Small Magellanic Cloud (SMC) the CO clouds show properties which are significantly different to those of galactic molecular clouds. They are smaller in size, less luminous in CO and less massive. No diffuse CO emission has been detected and the relation between the intensity of the CO emission and the molecular hydrogen column density is larger than the factor derived from molecular clouds in our Galaxy and dependent on cloud size (Israel et al. 1993; Rubio et al. 1993; Rubio, Lequeux, & Boulanger 1993).

3.2. The Physical Properties of Molecular Clouds: The CO(2-1/1-0) Ratio

1. 30 Doradus: Figure 1(a) shows the velocity integrated CO(2-1) emission in 30 Doradus. The emission is concentrated in three large molecular complexes which had been mapped by Johansson et al. 1998 in CO(1-0). Namely the SW cloud (30Dor-10) the NE cloud (30Dor-6) and the N cloud (30Dor-13). The higher resolution data shows a more complex structure which can be separated into different smaller sizes clouds. Figure 1(b) shows the CO(2-1)/(1-0) ratio over all the region after convolving the CO(2-1) map to the CO(1-0) resolution. This ratio ranges between 0.5 and 1.1.

The higher sensitivity of the CO(2-1) observations revealed a series of small molecular clouds - clumps - located in between the SW and NE molecular clouds, not detected in the CO(1-0) observations. These are several dense regions that show a complicated velocity structure. We have been able to disentangle at least 8 CO clumps with sizes ranging from 3.0 to 7.0 pc, CO luminosities of 0.5×10^4 to 4.3×10^2 K km s^{-1}and virial masses 0.5×10^4 to 4.6×10^4 M$_\odot$.

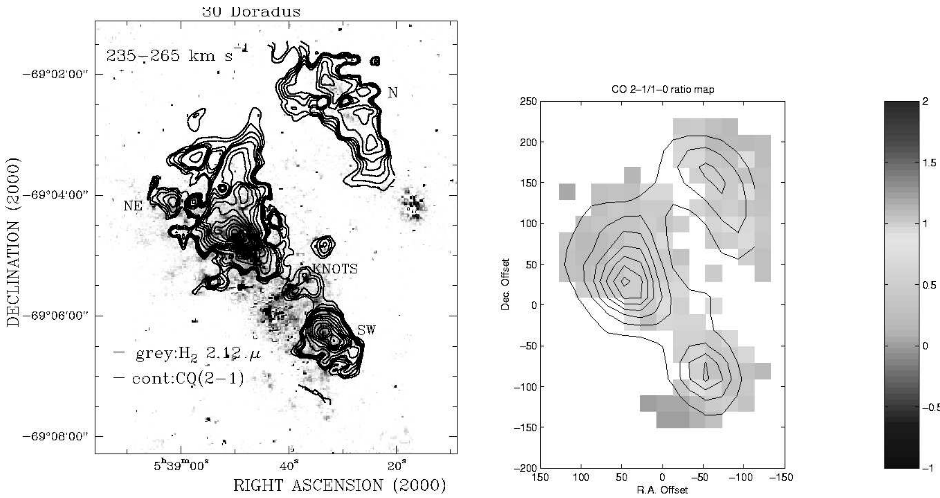

Figure 1. (a)Velocity integrated CO(2-1) emission of the 30 Doradus region. (b) CO(2-1)/CO(1-0) ratio over the region.

2. N159: The study of the CO(2-1) emission line in this region has been done by Bolatto at al. (2000). An interesting result found by these authors is the unusually high CO(2-1)/(1-0) ~ 3 in the molecular envelope of N159. Such high ratios are rarely detected in our Galaxy.

3. CO Arc: An interesting new feature of the LMC NANTEN CO survey is the CO arc located in the southeast part of the LMC (Fukui et al. 1999). Simultaneous observations in CO(2-1) and CO(1-0) at 40" spacing have been performed by the Nanten group in collaboration with the Swedish group at SEST (Mizuno, Johansson, private communication). First results of these observations indicate ratios from 0.7 to 0.9 for GMCs with no star formations and 0.8 to 1.3 for those associated with star formation.

4. SMC: In the SMC, the CO(2-1)/(1-0) ratios observed by our Large Programme data tend to be systematically higher than 1 and in some cases, eg N66C the ratio is found to be 2.4. Similarly, the N83/N84 region shows a CO(2-1)/CO(1-0) integrated line brightness ratio uniformly throughout most of the complex of 1.1. with two distinct regions showing unusually high ratios, larger than 2 (Bolatto et al. 2003).

3.3. The Isotopic Ratio

Israel et al. (2003) report the collection of all ^{13}CO(1-0) measurements done towards the peak positions of molecular clouds in the LMC and SMC mapped by the ESO-SEST Key Programme. The SMC data show relative low CO intensities I(CO)$<$ 10 K km s^{-1} and isotopic values ranging from 5 to 25. In the LMC, the molecular clouds show a larger spread of values. For molecular clouds with CO intensities I(CO)$>$ 30 K km s^{-1}, isotopic values show a similar value of $\sim$ 10. These clouds are associated with intense star forming regions. This value is about 2 times higher than the isotopic ratios of Galactic molecular cloud centers. Previous isotopic studies have been done mainly towards the strongest CO cloud in the LMC, N159, by Johansson at al. (1994), Heikkila et al. (1998) and Chin et al. (1997). Also, the brightest CO cloud in the SMC, LIRS36, was observed by Chin et al. (1998). These studies found $^{13}CO/^{12}CO$ ratios typically of 8 to 10 in the studied clouds which are associated with strong HII regions.

3.4. Other Molecules

Heikkila et al. (1998, 1999) reported the detection of C^{18}O, CS, SO, HCO^+, HNC, HNC, C_2H and H_2CO. In addition to these they reported detection of CH_3OH, CH_3CCH, tentative H_2CS and the first extra-galactic ortho-H_2S, in N159W in the LMC. They estimated kinetic temperatures of 25K in N159W and 15K in N27(LIRS49), respectively, and a number density of hydrogen of $(1-10)\times10^5$ cm^{-3} for N159W, and $(5-50)\times10^4$ cm^{-3} in N27. They concluded that the metallicity difference between the LMC and SMC does not seem to affect the physical state of the gas.

The molecular abundances determined by these authors are typically 5 to 20 time lower in N159W than in Galactic clouds. In the cloud 30Dor-10 (Johansson et al. 1998) near the center of 30 Dor region, the molecular abundance is on average 8 time lower than in the N159W cloud. This under-abundance is explained as due to the higher photo-dissociation rate in a region of higher FUV radiation field. The metallicity of the HII regions in the LMC and Galaxy differs by a factor of ~ 3, so in order to explain the difference in molecular abundances, a combination of lower metallicity and higher photo-dissociation rates is needed. Chin et al. (1996, 1997, 1998) found that, in four regions studied in the LMC (N159W, N44BC, N113, and N214D), HCO^+ is stronger than HCN, and HCN is stronger than HNC. The high relative HCO^+ intensities are consistent with high ionization from supernova remnants or young stars.

In the SMC cloud, N27 (LIRS 49), the molecular abundances derived are 6 times lower than in N159W. This result is attributed to a lower metallicity in the SMC. An alternative explanation to these under-abundances with respect to those found in N159W is a higher H/H_2 ratio in these clouds as compared to the rest of the sample observed.

Heikkila, Johansson, and Olofsson (1998), made a study of the $C^{18}O/C^{17}O$ ratio in four clouds in the LMC. and estimated an average gas-phase $C^{18}O/C^{17}O$ abundance ratio of 1.6$\pm$0.3. This value is significantly lower, by factor of 5, than typical values found in Galactic clouds. In the SMC, $C^{18}O$ was not detected towards N27.

4. Discussion and Conclusions

The molecular gas in the Magellanic Clouds have been extensively studied and molecular cloud properties have been derived. In general, the CO luminosity of the clouds is lower than those galactic molecular clouds. The higher gas to dust ratio, and the lower metallicity are responsible for a lower amount of CO molecules as well as a larger photo-dissociation rate due to less dust shielding. Thus the CO molecules survive only in the dense regions. H_2 molecular gas can be much more extended and thus not completely traced by the CO emission. Very little diffuse extended CO is seen, diffuse CO between or surrounding CO discrete clouds is either very weak or absent.

Throughout the Magellanic Clouds, the emission CO line ratio ^{12}CO(2-1)/^{12}CO(1-0), is found to be close to unity. Optically thick CO emission arising from thermalized gas at T $>$ 10 K yields brightness temperatures ratios R = CO(2-1)/(1-0) $\sim$ 1. Deviations from these conditions, such as low temperatures or sub-thermal excitation in the gas with volume densities below the critical density of the CO(2-1) transition, $n_{crit} \sim 10^4$ cm^{-3} generally produce ratios less than 1. However, somewhat higher ratios are found, $\sim$ 1.2, both in the LMC and SMC. These are probably caused by a mixture of high and low optical depths in the molecular clouds and cloud envelopes. Hence, departures from the assumption of a homogeneous source characterized by a single temperature and a single column density occur.

Unusually high transition ratios are observed in N159 in the LMC, and in N83, SMC-N66C and other clouds in the SMC. Bolatto et al. (2000) discussed four possible origins for them: (1) self-absorbed ^{12}CO(1-0) emission, (2) optically thin emission from isothermal gas, (3) an ensemble of small optically thick isothermal clumps, and (4) optically thick emission with temperature gradients. For N159, they suggested that the high measured ratios were a direct consequence of the low metallicity of the medium. The results obtained in the SMC, in two regions in the N83/N84 complex, of R $>$ 2, imply that the effect of metallicity is not straightforward. Bolatto et al. argue that the N83/N84 results are best explained by CO emission arising from an ensemble of small (R $\sim$ 0.1pc), warm ($T_{gas} \sim$ 40 K) clumps. This explanation is similar to that proposed by Lequeux et al. (1994) for the high ratios measured toward N66 and N88. We suggest this to be the most probable explanation for the high ratios (Rubio 2003; Mizuno, private communication) found in other SMC clouds. No evidence is found that self-absorbed CO(1-0) could be a possible explanation while higher resolution observations would greatly improve understanding of these results.

The majority of all LMC lines of sight detected in ^{13}CO have an isotopic emission ratio I(^{12}CO)/I(^{13}CO) of about 10, twice higher than found in Galactic star forming complexes. This ratio shows variations towards weak CO sources. The high ratios are found toward CO photo-dissociation regions at cloud edges while lower ratios are detected towards dense and cold molecular gas. This isotopic ratio probably reflects the lower CO abundance in the Magellanic Clouds and the strong radiation ambient conditions in these low metallicity galaxies.

4.1. The Conversion Factor

An important study of the molecular gas in the Magellanic Clouds is the determination of the relation between CO luminosity and molecular hydrogen column density. Observations with higher angular resolution have resolved the CO clouds and their virial masses were derived. At the resolution provided by SEST, we find in general that in the LMC, the conversion factor X is a factor 2 to 3 times larger than the Galactic factor. A similar result is found in the SMC. Virialization of the molecular clouds have been assumed in this determination. However, the physical properties derived from the CO(2-1) emission, the isotopic, and multi-line observations show that the CO clouds are very clumpy and that probably in the dense cores the conversion factor might tend to values similar to that derived in our Galaxy. An important result from these new studies is that the total CO luminosity in a determined volume remains the same independent of the different resolutions used in the observations. We have confirmed that the Nanten measured CO luminosity is the sum of the SEST CO luminosity of the clouds in different samples of regions in both LMC and SMC that have been mapped by both surveys. The same is true for the comparison between the Columbia survey and Nanten, and SEST. Thus, the CO emission only traces the total H_2 mass for regions where conditions are similar to those found in our Galaxy, most likely the densest part of the Magellanic Clouds CO clouds. The fact that the ISM does have less C and O, and therefore produces less CO, and that the gas-to-dust ratio is larger, providing less shielding and larger photo dissociation, is affecting the the size of the CO emitting region. Therefore, extra-galactic CO observations, which have a low linear resolution due to the large distances, should consider this effect in systems that show important differences in their interstellar media. Also, systems with low metal content such as the galaxies formed in the early universe should show this effect. ALMA, with is sensitivity and extraordinary resolution, will be essential to perform a complete, detailed and deep study of the properties of molecular gas in low metallicity and low dust environments.

Acknowledgments. We would like to express our gratitude to the SOC of JD21 for extending the invitation to present this review and to the IAU for a travel grant that could not be used. This contribution was prepared in memory of my beloved father. M.R. is supported by the Chilean *Center for Astrophysics* FONDAP No. 15010003.

References

Bolatto, A.D., et al. 2000, ApJ, 548, 234
Bolatto, A.D., et al. 2003, ApJ, 595, 167
Chin,Y.-N., et al. 1996, A&A, 305, 960
Chin,Y.-N., et al. 1997, A&A, 317, 548
Chin, Y.-N., et al. 1998, A&A, 330, 901
Fukui, Y., et al. 1999, PASJ,51, 745
Heikkila, A., Johansson, L.E.B.,& Olofsson, H. 1998, A&A. 332, 493
Heikkila, A., Johansson, L.E.B.,& Olofsson, H. 1999, A&A, 344, 817
Israel, F.P., et al. 1993, A&A, 270, 25 (Paper I)
Israel, F.P., et al. 2003b, A&A, 406, 817 (Paper X)
Johansson, L.E.B., et al. 1994, A&A, 291, 89
Johansson, L.E.B., et al. 1998, A&A, 333, 657 (Paper VII)
Kurtz, C.M, & Dufour, R.J. Rev.Mex. Astron. Astrofis., 7, 202
Lequeux, J., et al. 1994, A&A, 292, 371
Mizuno et al. 2001, PASJ, 53, 971.
Rubio, M., et al. 1993a, A&A, 271, 1. (Paper II)
Rubio, M. Lequeux, J., & Boulanger, F. 1993b, A&A, 271, 9.(paper III)
Rubio, M., et al, 1996, A&AS 118, 262 (Paper V)
Rubio M. 2003, In ESO Workshop: The ESO Large Programmes, Garching.

Highlights of Astronomy, Vol. 13
International Astronomical Union, 2003
O. Engvold, ed.

CO $J = 7 \rightarrow 6$ Emission in the Large Magellanic Cloud

Sungeun Kim

Univ. of Massachusetts, Astronomy Department, 710 N. Pleasant St., Amherst, MA 01003

Wilfred Walsh, Kecheng Xiao, Adair P. Lane, Antony A. Stark

Harvard-Smithsonian Center for Astrophysics, 60 Garden St., MS-12, Cambrdige, MA 02138

Abstract. We present the first detection of ^{12}CO ($J = 7 \rightarrow 6$) emission in the Magellanic Clouds toward the 30 Doradus region using the Antarctic Sub-millimeter Telescope and Remote Observatory (AST/RO).

1. Introduction

Technological advances of sub-millimeter wave and far-infrared (FIR) spectroscopy have made it available to provide resources for understanding the physical condition and the chemistry of atomic and molecular clouds in the interstellar medium in external galaxies. Sub-millimeter wave and FIR cooling lines are the dominant source of the cooling in the ISM, and therefore regulate star formation in the ISM. While observations of the sub-millimeter lines such as the ^{12}CO and ^{13}CO rotational lines and the sub-millimeter lines of atomic carbon [C I] have revealed a more complete picture of the photo-dissociation regions (PDRs) and the dense gas.

At distance of 55 kpc (Feast 1991), the Large Magellanic Cloud (LMC) can be mapped with a high spatial resolution at high excitation CO lines by the AST/RO. The recent [C I] and CO ($J = 4 \rightarrow 3$) study of the N159/N160 complexes in the LMC by Bolatto et al. (2000) elucidate the condition of atomic and molecular medium in the early stage of star formation. In this paper, we report the first detection of the CO ($J = 7 \rightarrow 6$) emission toward the 30 Doradus region in the LMC. The CO ($J = 7 \rightarrow 6$) and ($J = 4 \rightarrow 3$) lines in the 30 Doradus region will lead to a better understanding of the distribution of C$^+$, C and CO, the physical and chemical structure of the ISM and the star formation activity in the LMC.

2. Observation and Results

The observations were performed during the austral winter seasons of 2002 at the AST/RO, located at 2847 m altitude in Amundsen-Scott South Pole Station. This site has very low water vapor, high atmospheric stability and a thin troposphere making it exceptionally good for sub-millimeter observations. AST/RO is a 1.7 m diameter, offset Gregorian telescope capable of observing at wavelengths between 200 μm and 1.3 mm (Stark et al. 2001). The receivers used were a dual-

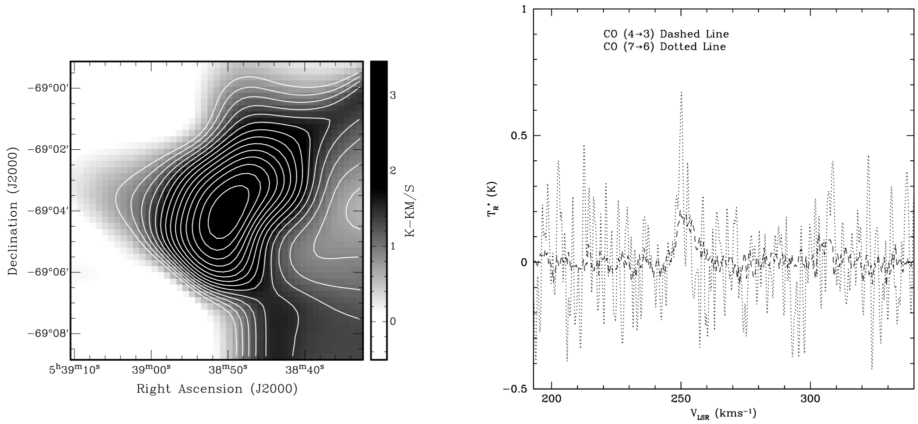

Figure 1. *Left*: Contour and grey scale image of ^{12}CO ($J = 4 \rightarrow 3$) emission. *Right*: Spectrum of ^{12}CO ($J = 7 \rightarrow 6$) and ^{12}CO ($J = 4 \rightarrow 3$) emission lines at $5^{\rm h}38^{\rm m}39.8^{\rm s}$, $-69°03'21''$.

channel SIS waveguide receiver (Walker & Kooi 2001, private communication) for simultaneous 461–492 GHz and 807 GHz observations, with double-sideband noise temperatures of 320–390 K and 1050–1190 K, respectively. Telescope efficiency, η_ℓ, estimated using moon scans, skydips, and measurements of the beam edge taper, was ∼81% at 461–492 GHz and 71% at 807 GHz. Atmosphere-corrected system temperatures ranged from 700 to 4000 K at 461–492 GHz, and 9000 to 75,000 K at 807 GHz. A beam switching mode was used, with emission-free reference positions chosen at $20'$ away from regions of interest, to make a small map of points near 30 Doradus region. A total integration time on the source was 16 minutes. Emission from the CO ($J = 4 \rightarrow 3$) and ($J = 7 \rightarrow 6$) lines at 461.041 GHz and 806.652 GHz, together with the [C I] line at 492.262 GHz, was imaged over an 14 arc-minute square region centered on $5^{\rm h}38^{\rm m}47.3^{\rm s}$, $-69°03'16.1''$ (J2000) with $0.5'$ spacing; i.e., a spacing of a half-beamwidth or less. AST/RO suffers pointing errors of the order of $1'$, and the beam sizes (FWHM) were 103–109$''$ at 461–492 GHz and 58$''$ at 807 GHz.

We detect a strong ^{12}CO ($J = 4 \rightarrow 3$) emission (Figure 1) in the 30 Doradus region (Tarantula nebulae) which is well known luminous giant HII regions in irregular galaxies and bright in the Hα image (Figure 2) taken at the Siding Spring Observatory (Kim et al. 1999). For the first time, ^{12}CO ($J = 7 \rightarrow 6$) emission is detected in the LMC at $5^{\rm h}38^{\rm m}39.8^{\rm s}$, $-69°03'21''$ and is $\sim 2.'5$ away from the peak of CO ($J = 4 \rightarrow 3$) (Figure 1). The ^{12}CO $J = 7 \rightarrow 6$ and $J = 4 \rightarrow 3$ emissions appear at V_{LSR}=251±0.1 kms^{-1} and 249.6±0.1 kms^{-1} respectively. The CO $J = 7 \rightarrow 6$ emission from this region is bright as T_{MB}=0.8±0.25 K. Based on the current observations and previous observations of low-J CO rotational lines (Israel et al. 1993; Johansson et al. 1998) and HI observations taken with the Australia Telescope Compact Array (Kim et al. 1998; Kim et al. 2003), we suggest that this region consists of dense clouds (density of 10^5 cm^{-3}) immersed in a low density inter-clump medium with dense clump volume filling factor of about 0.01 and area covering factor of about 0.5. The estima-

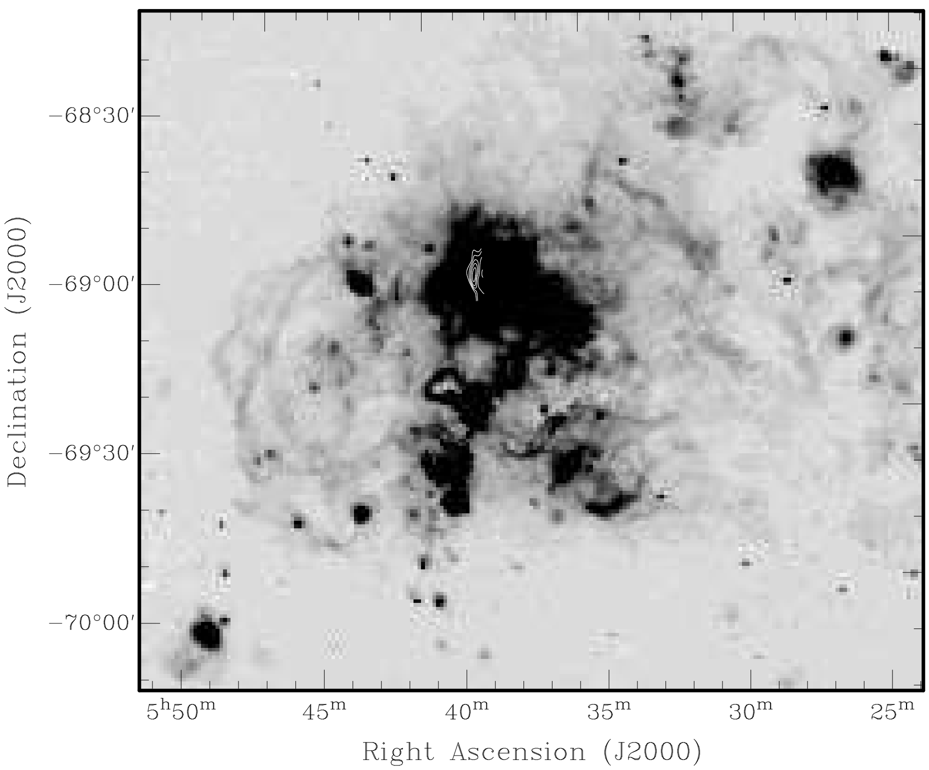

Figure 2. ^{12}CO ($J = 4 \rightarrow 3$) emission (White Contours) from Tarantula nebula (30 Doradus) in the LMC is overlaid on the Hα image (Kim et al. 1999) made with 16 inch telescope at Siding Spring Observatory (Image Credit: S. Kim).

tion of $T_{kin} \approx 70$ K and $n(H_2)$ was made by applying radiative transfer code (http://www.astro.umass.edu/∼skim/prog2.html) to ratios of observed line intensities. The lowest 30 rotational levels of the ground vibrational level for ^{12}CO and ^{13}CO are included in the radiative transfer calculation by M. Yan & S. Kim.

References

Bolatto, A., Jackson, J.M., Israel, F.P., Zhang, X., & Kim, S. 2000, ApJ, 545, 234

Feast, M.W. 1991, IAU Symp., 148, 1

Israel, F.P. et al. 1993, A&A, 286, 25

Johansson, L.E.B. et al. 1998, A&A, 331, 857

Kim, S., Staveley-Smith, L., Dopita, M.A., Freeman, K.C., Sault, R.J., Kesteven, M.J., & McConnell, D. 1998, ApJ, 503, 674

Kim, S., Dopita, M., Staveley-Smith, L., & Bessell, M. 1999, AJ, 118, 2797

Kim, S., Staveley-Smith, L., Dopita, M.A., Freeman, K.C., Lee, Y.U., & Chu, Y.-H. 2003, ApJS, 148, 473

Stark, A.A. et al. 2001, PASP, 113, 567

Highlights of Astronomy, Vol. 13
International Astronomical Union, 2003
O. Engvold, ed.

Magellanic Diffuse Interstellar Bands and Carbon Chemistry

P. Ehrenfreund[1], N. Cox[2], J. Cami[3], B.H. Foing[4], L. Kaper[2], L. d'Hendecourt[5], J.P.Maier[6], F. Salama[3], P. Sarre[7], T. Snow[8], P. Sonnentrucker[9]

[1]*Leiden Observatory, P O Box 9513, 2300 RA Leiden, Netherlands*
[2]*Astronomical Institute "Anton Pannekoek", University of Amsterdam, Kruislaan 403, NL-1098 SJ Amsterdam, Netherlands*
[3]*Space Science Division, NASA Ames Research Center, MS 245-3, Moffett Field, CA 94035, USA*
[4]*Research Support Division, ESA, ESTEC SCI-SR, 2200 AG Noordwijk, Netherlands*
[5]*Institut d'Astrophysique Spatiale, Campus d'Orsay, 91405 Orsay, France*
[6]*Institute for Physical Chemistry, Klingelbergstrasse 80, University of Basel CH-4053, Switzerland*
[7]*School of Chemistry, University of Nottingham, University Park, Nottingham NG7 2RD, UK*
[8]*Center for Astrophysics and Space Astronomy, University of Colorado at Boulder, 389 UCB, Boulder, CO 80309-0389, USA*
[9]*Department of Physics and Astronomy, Johns Hopkins University, Charles and 34th Street, Bloomberg Center, Baltimore, MD 21218-2686, USA*

Abstract. With the Ultraviolet Visual Echelle Spectrograph mounted at the Very Large Telescope, we have observed at unprecedented spectral resolution the absorption spectrum toward reddened stars in the Magellanic Clouds over the wavelength range of 3500-10500 Å. This range covers the strong transitions associated with neutral and charged large carbon molecules of varying sizes and structures. We report the first detection of diffuse interstellar bands (DIBs) at 5780 and 5797 Å in the Small Magellanic Cloud and the variation of those DIBs toward several targets in the Large Magellanic Cloud. The variation of DIBs in the Magellanic Clouds compared with Galactic targets may be governed by a combination of the different chemical processes prevailing in low-metallicity regions and the local environmental conditions. The analysis of high-resolution absorption spectra allows us to reveal the global effects in the chemistry and recycling of cosmic dust in the Magellanic Clouds which are relevant for the chemical pathways forming large organic molecules in external galaxies.

1. Diffuse interstellar bands in the Magellanic Clouds

The diffuse interstellar bands (DIBs) are a large number of absorption lines between 4000-10000 Å that are superimposed on the interstellar extinction curve (Herbig 1995). In the last 75 years DIBs have been observed toward more than a hundred stars. The number of known DIBs steadily increases due to the higher sensitivity of detectors and is currently estimated to be several hundreds. At present, no definitive identification of any of the carriers of the DIBs exists, though large gaseous carbon molecules are strongly favored (Ehrenfreund & Charnley 2000). There are only a handful of DIBs which are strong enough to be detected in extra-galactic systems. But DIBs have been observed toward other galaxies and in particular in several star-burst galaxies (Heckman & Lehnert 2000).

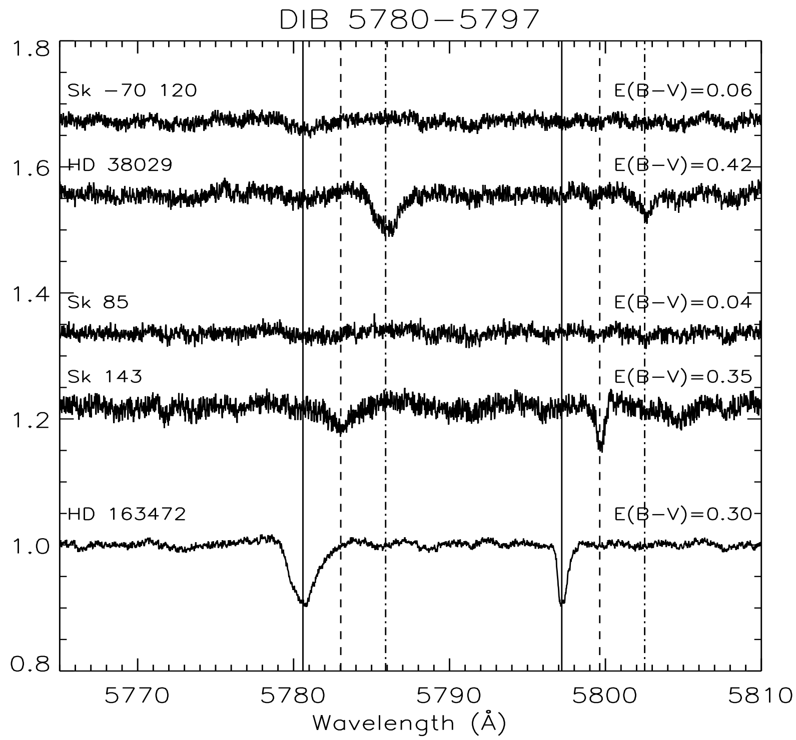

Figure 1. This figure shows spectra of the two best known DIBs, the $\lambda\lambda$5780 and 5797 DIB. All spectra are normalized to the continuum, and shifted for display. The spectrum at the bottom shows a galactic translucent cloud source (HD 163472). The two middle spectra show an SMC target Sk 143 (AzV456) and an unreddened SMC standard Sk 85 (AzV242); the two top spectra show an LMC target (HD 38029) and an unreddened LMC standard Sk -70 120. The full vertical lines indicate the galactic rest wavelengths for those DIBs, the dashed lines indicate the wavelengths expected for these DIBs at SMC velocities, as determined from the NaD lines and the dash-dotted lines are the same for the LMC velocities. Both DIBs are clearly detected in both the SMC and LMC reddened targets (Ehrenfreund et al. 2002).

We reported recently the first detection of diffuse interstellar bands (DIBs) at 5780 and 5797 Å in the Small Magellanic Cloud (SMC), and measured the variation of DIBs in the SMC, the Large Magellanic Cloud (LMC) and our galaxy (Ehrenfreund et al. 2002). For these observations we used the UVES spectrograph on the VLT. The interest of observing the Magellanic Clouds are the difference in metallicity (LMC: 2.5 times less and SMC: 10 times less) and the smaller gas-to dust ratio (4 and 30 times less for LMC and SMC, respectively). Furthermore these irregular galaxies are nearest neighbors (60 and 50 kpc away) and certain regions within the SMC and LMC have been rather well characterized in terms of UV radiation field, extinction curve, star formation conditions and other environmental factors. In the SMC, DIBs have been exclusively observed toward Sk143, the only line-of-sight which shows a reasonable bump at 2200 Å in the interstellar extinction curve (Gordon et al. 2003). This target is located in the SMC wing. Stars in the SMC bar are devoid of the 2200 Å bump and show instead a high far UV linear rise in the UV part of the interstellar extinction curve. Those targets do not show evident DIBs. The LMC lines-of sight show a varying pattern of DIBs. Several stars within 30 Dor region show strong DIBs, but some stars very close by do not (Ehrenfreund et al. 2002). A combination of different chemical processes prevailing in low metallicity regions and the local environmental conditions may govern the presence, strength and absence of DIBs in these extra-galactic targets.

2. Conclusion

In the Magellanic Clouds environmental effects are different from those in the Milky Way. Large variations in DIB properties exist in different LMC lines-of sight. The band strengths of DIBs in the SMC (Sk143) and 30 Dor regions (LMC) show a strong linear relationship with those in the Milkyway. Studying the environmental conditions that play a role in the DIB formation may help us to constrain the identity of the carriers. The positive correlation between the presence of the UV-bump and DIBs may indicate the carbonaceous nature of the carrier. The carrier identification will give us a powerful diagnostic tool to probe and explore the diffuse ISM in our and external galaxies.

References

Ehrenfreund, P. & Charnley, S. 2000, ARAA, 38, 427
Ehrenfreund, P. et al. 2002, ApJ, 576, L117
Gordon, K. et al. 2003, ApJ, 594, 279
Heckmann, T.M. & Lehnert, M.D. 2000, ApJ, 537, 690
Herbig, G. 1995, ARAA, 33, 19

Highlights of Astronomy, Vol. 13
International Astronomical Union, 2003
O. Engvold, ed.

Young Star Clusters: Metallicity Tracers in External Galaxies

Peter Anders, Uta Fritze - v. Alvensleben

Universitäts-Sternwarte Göttingen, Geismarlandstrasse 11, 37083 Göttingen, Germany

Richard de Grijs

Department of Physics & Astronomy, The University of Sheffield, Hicks Building, Hounsfield Road, Sheffield S3 7RH, UK

Abstract. Star cluster formation is a major mode of star formation in the extreme conditions of interacting galaxies and violent star bursts. These newly-formed clusters are built from recycled gas, pre-enriched to various levels within the interacting galaxies. Hence, star clusters of different ages represent a fossil record of the chemical enrichment history of their host galaxy, as well as of the host galaxy's violent star formation history. We present a new set of evolutionary synthesis models of our GALEV code, specifically developed to include the gaseous emission of presently forming star clusters, and a new tool to analyze multi-color observations with our models. First results for newly-born clusters in the dwarf star-burst galaxy NGC 1569 are presented.

1. Models & tests

We use our evolutionary synthesis code GALEV to study the basic physical parameters of star clusters in interacting galaxies and violent star bursts. Star clusters can easily be approximated as simple stellar populations (SSPs), since all stars have the same age, metallicity and extinction. However, more complicated star formation / metallicity evolution histories can be studied by superimposing appropriate SSPs. The main ingredients of our code are: stellar isochrones (ensemble of stars with different masses at a given age) from the Padova group for metallicities in the range of $-1.7 \leq$ [Fe/H] $\leq +0.4$, a stellar initial mass function (usually assumed to be Salpeter-like), the library of stellar spectra by Lejeune et al. (1997,1998), and gaseous emission (both lines and continuum). From the integrated spectra we derive magnitudes in a large number of filter systems. The gaseous line and continuum emission contributes significantly to the integrated light of stellar populations younger than 3×10^7 yr both in terms of absolute magnitudes and derived colors (Anders & Fritze - v. Alvensleben 2003). The updated models are available from

http://www.uni-sw.gwdg.de/~galev/panders/

We developed a tool to compare our evolutionary synthesis models with observed cluster SEDs to determine the basic cluster parameters age, metallicity, internal extinction and mass independently. Using artificial clusters with various input parameters (with cluster SEDs taken directly from the evolutionary synthesis models) we systematically studied the impact of the choice of passbands,

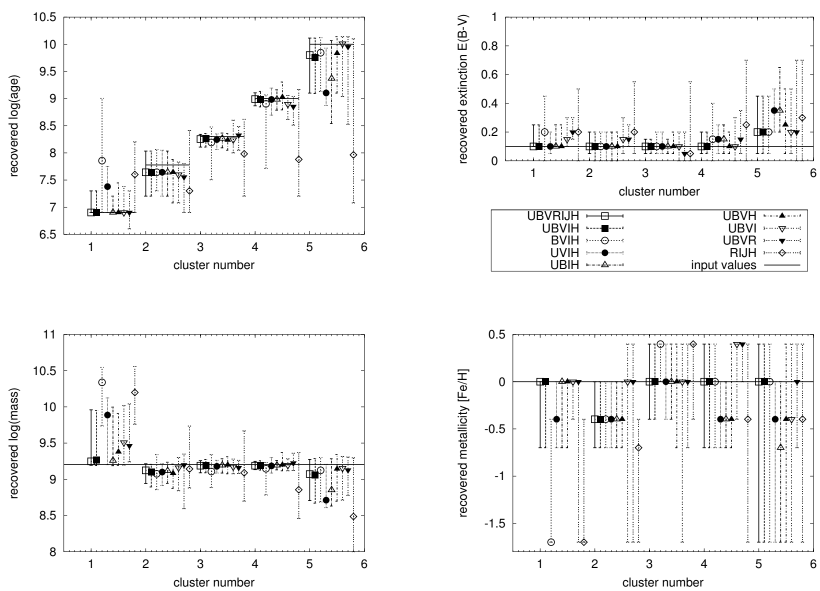

Figure 1. Dispersion of recovered properties of artificial clusters, assuming availability of *UBVRIJH* and passband combinations with 4 out of the available 7 passbands, as indicated in the legend. Cluster parameters are: solar metallicity, E(B-V) = 0.1 mag, assumed "observational" error = 0.1 mag, ages = 8, 60, 200 Myr, 1, 10 Gyr.

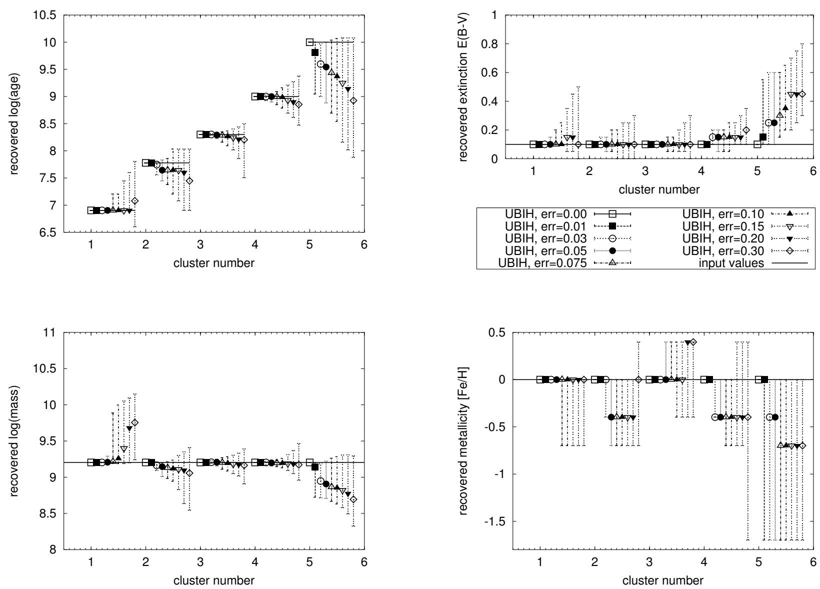

Figure 2. Dispersion of recovered properties of artificial clusters, using the best 4-passband-combination *UBIH*. Cluster parameters are: solar metallicity, E(B-V) = 0.1 mag, ages = 8, 60, 200 Myr, 1, 10 Gyr. The assumed "observational" errors are indicated in the legend.

of finite observational magnitude uncertainties, and *a priori* assumptions. Two examples of the artificial cluster tests are shown in Fig. 1 and 2. Additional tests were performed using broad-band observations of star clusters in NGC 3310 (de Grijs et al. 2003a,b), confirming the results from the artificial cluster tests. Due to the young age of this cluster system these additional tests are restricted to ages younger than approx. 200 Myr. From these tests we conclude that:

1. At least 4 passbands are necessary to determine the 3 free parameters age, metallicity and extinction, and the mass by scaling the SED, independently.

2. The most important passbands are the *U* and *B* bands; for systems older than roughly 1 Gyr the *V* band is equally important.

3. NIR bands significantly improve the results by constraining the metallicity efficiently.

4. A wavelength coverage as long as possible is desirable. Best is UV through to NIR, thus tracing the pronounced kink/hook in the SEDs around the *B* band.

5. Large observational errors and/or wrong *a priori* assumptions may lead to completely wrong results.

2. The case of NGC 1569

As a first application the dwarf star-burst galaxy NGC 1569 was chosen. Our sample enlarges the number of star clusters studied in this galaxy by a factor of 3. Our results for the derived physical parameters are in agreement with previous results of the star-burst history in NGC 1569 in general, and of the two prominent "super star clusters" in particular, regarding age, mass and metallicity. In addition, we find a surprising change in the cluster mass function with age: The clusters formed during the onset of the burst (approx. 25 Myr ago) seem to exhibit an excess of massive clusters as compared to clusters formed more recently. Using various statistical methods we show the robustness of this result (Anders et al. 2003b).

References

Anders, P. & Fritze - v. Alvensleben, U. 2003, A&A, 401, 1063

Anders, P., Bissantz, N., et al. 2003a, MNRAS, *submitted*

Anders, P., de Grijs, R., et al. 2003b, MNRAS, *submitted*

de Grijs, R., Fritze - v. Alvensleben, U., Anders, P., Gallagher, J. S., Bastian, N., Taylor, V. A. & Windhorst, R. A. 2003a, MNRAS, 342, 259

de Grijs, R., Anders, P., Bastian, N., Lynds, R., Lamers, H.J.G.L.M. & O'Neil, Jr., E.J. 2003b, MNRAS, 343, 1285

Lejeune, T., Cuisinier, F. & Buser, R. 1997, A&AS, 125, 229

Lejeune, T., Cuisinier, F. & Buser, R. 1998, A&AS, 130, 65

Highlights of Astronomy, Vol. 13
International Astronomical Union, 2003
O. Engvold, ed.

The Nuclear Starburst in NGC 4945

M. Wang

Max-Planck-Institut für Radioastronomie, Bonn, Germany & Purple Mountain Observatory, Nanjing, China

C. Henkel

Max-Planck-Institut für Radioastronomie, Bonn, Germany

Y.-N. Chin

Dept. of Physics, Tamkang University, Taipei, Taiwan

J. B. Whiteoak

Australia Telescope National Facility, Epping, Australia

M. Hunt Cunningham

New South Wales, Australia

R. Mauersberger

IRAM, Avda. Divina Pastora, Granada, Spain

Abstract. NGC 4945 is with $D \sim$3–4 Mpc one of the nearest starburst galaxies known and a goldmine for molecular cloud research. A multi-line mm-wave study has been carried out towards its nuclear region with the Swedish-ESO Submillimetre Telescope (SEST). The study covers the frequency range from 82 GHz to 354 GHz and includes 80 transitions of 19 molecules, including rare isotope-bearing species. Applying a Large Velocity Gradient (LVG) code to the data, H_2 densities and column densities of 22 molecular species are calculated. Many of these species indicate the presence of a prominent high density interstellar gas component characterized by $n_{\mathrm{H_2}} \sim 10^5\,\mathrm{cm}^{-3}$. Abundances of molecular species are calculated and compared with abundances observed toward the starburst galaxies NGC 253 and M 82 and galactic sources. Apparent is an 'overabundance' of HNC and CN in the nuclear environment of NGC 4945. NGC 4945 is the second known starburst galaxy with an HNC/HCN abundance ratio $\geq$1. Carbon, nitrogen, oxygen and sulfur isotope ratios are also determined. The data indicate that high ^{18}O/^{17}O, low ^{16}O/^{18}O and ^{14}N/^{15}N and perhaps also low ^{32}S/^{34}S ratios (6.4±0.3, 195±45, 105±25 and 13.5±2.5, respectively) are characteristic properties of a starburst environment in an advanced evolutionary stage.

Highlights of Astronomy, Vol. 13
International Astronomical Union, 2003
O. Engvold, ed.

A Gas and Dust Rich Giant Elliptical Galaxy

O. Krause[1], U. Lisenfeld[2], U. Klaas[1], D. Lemke[1], M. Haas[1], M. Stickel[1]

[1]*Max-Planck-Institut für Astronomie, Königstuhl 17, 69117 Heidelberg, Germany*

[2]*Instituto de Astrofisica de Andalucia, Camino Bajo de Huetor 24, 18080 Granada, Spain*

Abstract. The bolometric luminosity of $L_{\rm FIR} = 2\times10^{12}$ $L_\odot$ makes ISOSS J 15079+7247 one of the most luminous and unusual galaxies detected by the 170 μm ISOPHOT Serendipity Survey (ISOSS). The detection of CO (1-0) emission identifies a giant elliptical galaxy at redshift $z = 0.2136$ as the counterpart of the FIR source. The derived high gas mass of 3×10^{10} $M_\odot$ favours the picture that the dust emission is associated with this elliptical galaxy. The ultraluminous IR emission can be explained by a hidden starburst in the center of the elliptical. This is supported by the strength of non-thermal radio continuum emission. The huge dust mass of 5×10^{8} $M_\odot$ corresponds to a visual extinction of $A_{\rm V} \sim 1000$ mag, being consistent with the non-detection of any signatures of a strong starburst in ISOSS J 15079+7247 in optical spectra.

1. Introduction

The ISOPHOT Serendipity Survey (ISOSS) (Bogun et al. 1996) has observed about 2000 galaxies at 170 μm, providing a unique data base of far-infrared spectral energy distributions beyond the IRAS 100 μm limit. Stickel et al. (2000) found that *late type* galaxies generally contain a cold ($T \sim 20$ K) dust component over a wide range of infrared luminosities ($10^9 - 10^{11}$ $L_\odot$). For *early type* galaxies, however, the traditional view is that they are less dusty and less luminous in the infrared (see Knapp 1999 for a review). We summarize here a detailed study of the elliptical galaxy ISOSS J 15079+7247, detected by the ISOPHOT Serendipity Survey as an ultraluminous infrared source (Krause et al. 2003).

2. The optical counterpart of ISOSS J 15079+7247

The ISOSS source coincides in position with a compact 1.2 mm continuum source detected with the MAMBO bolometer array. The astrometric accuracy of our MAMBO observations allowed to identify an elliptical galaxy as the optical counterpart of the FIR/millimetre source (Fig. 1). Optical long slit spectroscopy revealed a pure absorption spectrum towards the nucleus. The redshift derived from the Ca H & K, G-band and Fe 5340 Å features is $z = 0.2137\pm$ 0.0003. The detection of CO(1−0) emission at the optical redshift of the elliptical galaxy strongly suggests that the molecular gas is physically associated with this galaxy. The very large molecular hydrogen mass of $M(H_2) = 2.9\times10^{10}$ $M_\odot$ is remarkable.

So far, significantly smaller amounts of molecular gas have been observed in ellipticals (eg. Henkel & Wiklind 1997).

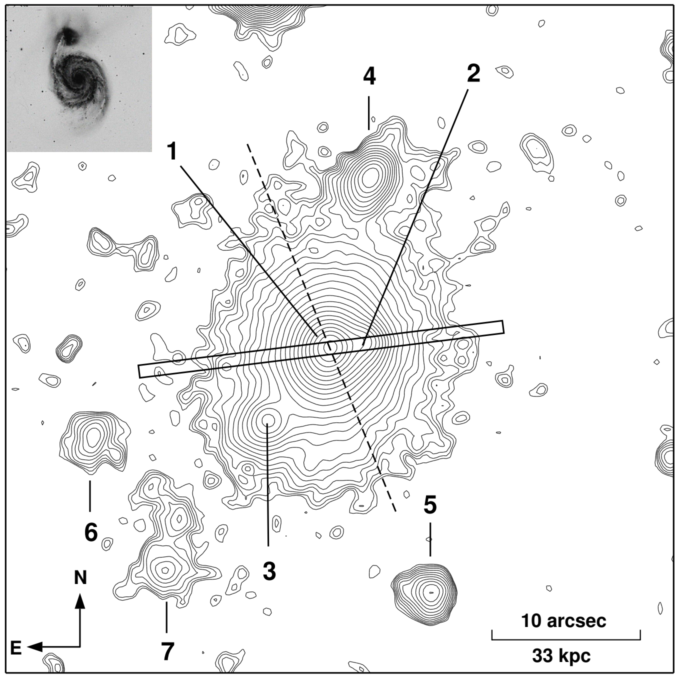

Figure 1. R-Band image of ISOSS J 15079+7247 obtained with the LAICA-camera at the Calar Alto 3.5 m telescope. The giant elliptical galaxy (1) has a close companion (2) and shows a faint tail of emission (3) towards southeast. The slit position of the spectroscopic observations is indicated (box).

3. Evidence for a starburst in the elliptical galaxy

The far-infrared to millimetre spectral energy distribution (Fig. 2) can be well fitted by an optically thick modified blackbody of 42 K, optical depth $\tau_{100\,\mu\mathrm{m}} = 3.5$ and dust emissivity $\beta = 1.5$, yielding a dust mass of $M_\mathrm{d} = 5.4 \times 10^8\,\mathrm{M}_\odot$. The source was barely resolved at the VLA in the cm-continuum (Condon et al. 1998) and the deconvolved size of $\sim 4.8 \times 1.6\,\mathrm{kpc}^2$ may be considered as an upper limit for the starburst size, in agreement with our lower limit $r_\mathrm{b} = 0.6\,\mathrm{kpc}$ from the far-infrared. Assuming an average radius of 1 kpc for the nuclear starburst and spherical distribution of dust and gas, we find a total column density of $N(\mathrm{H}) = 1.7 \times 10^{24}\,\mathrm{cm}^{-2}$ towards the center. This corresponds to a visual extinction of $A_\mathrm{V} \sim 1000\,\mathrm{mag}$ and explains the absence of any optical emission lines towards the center of the elliptical, which is very unusal for ULIRGs (Veilleux et al. 1999). ULIRGs normally show a much more disturbed morphology and emission line spectra in their centers. ISOSS J 15080+7248 may be an elliptical galaxy merging with a gas rich spiral inducing a powerful starburst in the center of the elliptical. The large amount of molecular gas and dust detected in the elliptical galaxy ISOSS J 15079+7247 suggests an alternative explanation of the nature of several other high-redshifted submm-galaxies.

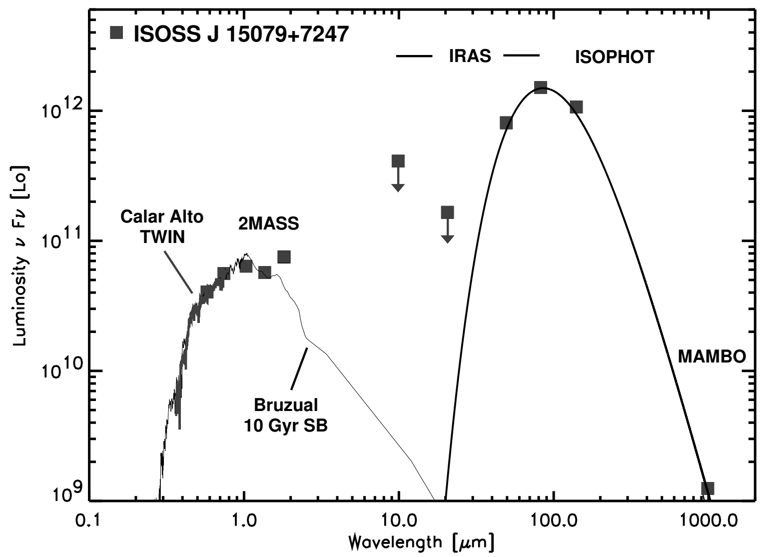

Figure 2. Rest frame spectral energy distribution of ISOSS J 15079+7247. The FIR dust emission can be well characterized by an optically thick modified blackbody (solid line). The optical and near-infrared emission can be fitted by a 10 Gyr old starburst following Bruzual & Charlot 1995.

Acknowledgments. The ISOPHOT Data Center at MPIA is supported by Deutsches Zentrum für Luft- und Raumfahrt e.V. (DLR) with funds of Bundesministerium für Bildung und Forschung, grant no. 50QI0201. OK thanks the Wernher von Braun-Stiftung zur Förderung der Weltraumwissenschaften e.V. for financial support.

References

Bogun, S., Lemke, D., Klaas, U. et al. 1996, A&A, 315, L71

Bruzual, G.A. & Charlot, S. 1995, Starburst Template Library in IRAF-STSDAS

Condon, J.J., Yin, Q.F., Thuan, T.X. et al. 1998, ApJ, 116, 2682

Henkel, C. & Wiklind, T. 1997, Space Science Reviews, 81, 1

Knapp, G.R. 1999, in ASP Conf. Ser. 163, Star Formation in Early-Type Galaxies, ed. P. Carral & J. Cepa, (San Francisco, ASP), 119

Krause, O., Lisenfeld, U., Lemke, D. et al. 2003, A&A, 402, L1

Stickel, M., Lemke, D., Klaas, U. et al. 2000, A&A, 359, 865

Veilleux, S., Kim, D.-C. & Sanders, D.B. 1999, ApJ, 522, 113

Highlights of Astronomy, Vol. 13
International Astronomical Union, 2003
O. Engvold, ed.

Systematically Peculiar Molecular Composition in M 82: Regarding the Formation Mechanisms

S. Takano[1], N. Nakai[1], K. Kawaguchi[2], T Takano[3], P. Schilke[4], and G. Winnewisser[5]

[1]*Nobeyama Radio Observatory, National Astronomical Observatory of Japan, Nobeyama, Minamimaki, Minamisaku, 384-1305 Japan*

[2]*Department of Chemistry, Okayama University, Tsushima-naka 3-1-1, Okayama, 700-8530 Japan*

[3]*Graduate School of Science and Technology, Chiba University, Yayoi-cho 1-33, Inage-ku, Chiba, 263-8522 Japan*

[4]*MPIfR, Auf dem Hügel 69, D-53121 Bonn, Germany*

[5]*I. Physikalisches Institut, Universität zu Köln, Zülpicher Strasse 77, D-50937 Köln, Germany*

Abstract. A systematically peculiar molecular composition has been found in a nearby starburst galaxy M 82. Molecules related to grain surface formation and to production reactions favorable at high-temperature are deficient in M 82 among nearby galaxies with rich gas. These molecules are SO, SiO, NH_3, HNCO, CH_3OH, and CH_3CN. Possible reasons for this peculiarity are discussed.

1. Introduction

More than 20 molecules have been detected in external galaxies. Studies of the relation between their abundances and the physical conditions are important to understand physical and chemical processes in external galaxies. Two starburst galaxies, NGC 253 and M 82, are known to be suitable for such study; the H_2 column densities are high and nearly identical, and their distances are nearly equal (about 3 Mpc) each other. Several major molecules have been detected in both of the galaxies with similar abundances (e.g., CO, CS). However, it is known that SO, SiO, NH_3, HNCO, CH_3OH, and CH_3CN have been clearly detected in NGC 253, but they have not been, or only only barely, detected with comparable sensitivity in M 82. In Table 1 quantitative information concerning the abundances of these molecules in the two galaxies is given. The CS molecule is also listed as one example with similar abundances.

2. Systematically Peculiar Molecular Composition in M 82

We found a common characteristic of the above cited six molecules; they are efficiently produced under high-temperature conditions, and/or they are originated from grain by evaporation processes (Takano, Nakai, & Kawaguchi 1995).

Table 1. Molecular abundance (relative to H_2) in NGC 253 and M 82.

	NGC 253	M 82	reference
SO	2×10^{-9}	$<7\times10^{-10}$	Takano, Nakai, & Kawaguchi (1995)
SiO	8×10^{-10}	$<4\times10^{-11}$	Henkel & Mauersberger (1992)
		$0.4\text{–}3.5\times10^{-10}$	García-Burillo et al. (2002)
NH_3	3×10^{-8}	$<1\times10^{-9}$	Takano, Nakai, & Kawaguchi (2002)
		5×10^{-10}	Weiß et al. (2001)
HNCO	1×10^{-9}	$<1\times10^{-10}$	N-Q-Rieu et al. (1991); Henkel & Mauersberger (1992)
CH_3OH	1×10^{-9}	$<1\times10^{-10}$	Hüttemeister, Mauersberger, & Henkel (1997)
CH_3CN	5×10^{-10}	$<5\times10^{-11}$	Mauersberger et al. (1991)
CS	1×10^{-9}	1×10^{-9}	N-Q-Rieu, Nakai, & Jackson (1989)

The conditions of molecular formation in NGC 253 and M 82 are, therefore, estimated to be rather different.

To study the reason for this difference, and to know which galaxy is peculiar, we also compared the abundances of the above six molecules in other nearby galaxies with rich molecular gas based on our observations and on literature values. As a result, at least NH_3, HNCO, and/or CH_3OH are abundant enough to be detected in NGC 6946, IC 342, Maffei 2, M 51, Cen A, and NGC 4945 with comparable sensitivity as shown in Table 2.

Table 2. Detection/non-detection of the six molecules of interest in nearby galaxies with rich molecular gas[1].

Galaxy	SO	SiO	NH_3	HNCO	CH_3OH	CH_3CN
NGC 253 (all yes)	yes	yes	yes	yes	yes	yes
M 82	no	barely	barely	no	no	no
NGC 6946	no	···	no	(yes)	yes	···
IC 342	(yes)	no	yes	yes	yes	···
Maffei 2	···	no	yes	yes	yes	···
Cen A	···	no	yes	yes	no	···
NGC 4945	yes	no		yes	yes	···

[1] "yes" means detection, "no" non-detection, "barely" weak detection (∼1 order less than NGC 253), "···" no data. References: see Takano, Nakai, & Kawaguchi (2002)

Quantitative abundances of ammonia and methanol are shown in Figure 1. We conclude that the molecular composition in M 82 is systematically peculiar regarding the formation mechanisms of molecules. The molecules related to dust

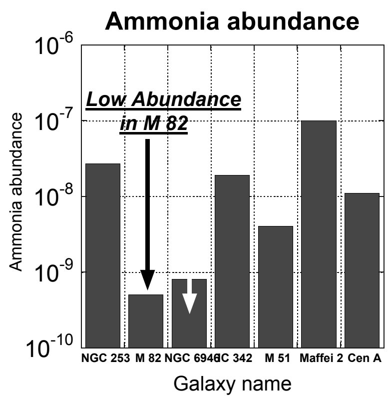

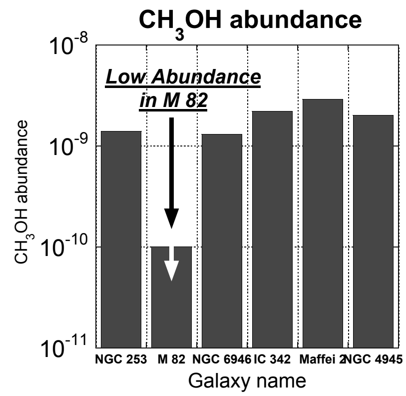

Figure 1. The abundances of ammonia (left) and methanol (right) in nearby galaxies. The white arrows indicate upper limits. The ammonia abundances are taken from Seaquist & Bell (1990), Takano et al. (2000), Weiß et al. (2001), and Takano et al. (2002). The methanol abundances are taken from Henkel et al. (1990), and Hüttemeister, Mauersberger, & Henkel (1997).

and efficiently produced under high-temperature conditions are deficient in M 82 among nearby galaxies with rich gas.

3. Discussion

As possible reasons for the peculiarity, first, we investigated the amount of dust in these galaxies. According to the IRAS low resolution spectra (LRS), we found that silicate (dust core) is not deficient in M 82. On the other hand, we noticed that Devereux & Young (1990) reported that the gas-to-warm dust ratios were increased by about a factor of 2 in M 82 compared to those in other nearby galaxies. This result indicates that "warm dust" is somewhat deficient in M 82, and this may explain to some extent the deficiency of dust related molecules in M 82.

Second, recent estimates of temperatures obtained from ammonia in these galaxies indicate that the rotational temperature at the region with ammonia emission in M 82 is fairly low (29 K and, for example, 100-142 K in NGC 253 reported by Mauersberger et al. 2003; Oike et al. 2003). This result is consistent with the deficiency of dust related molecules in M 82.

It appears that the formation of molecules on dust and/or evaporation to gas-phase is not efficient in M 82. A detailed discussion was given by Takano et al. (2002).

References

Devereux, N.A. & Young, J.S. 1990, ApJ, 359, 42

García-Burillo, S., Martín-Pintado, J., Fuente, A., & Neri, R. 2002, ApJ, 563, L27

Henkel, C. & Mauersberger, R. 1992, in IAU Symp. 150, Astrochemistry of Cosmic Phenomena, ed. P. D. Singh (Dordrecht: Kluwer Academic Publishers), 111

Henkel, C., Whiteoak, J.B., Nyman, L.-Å., & Harju, J. 1990, A&A, 230, L5

Hüttemeister, S., Mauersberger, R., & Henkel, C. 1997, A&A, 326, 59

Mauersberger, R., Henkel, C., Walmsley, C.M., Sage, L.J., & Wiklind, T. 1991, A&A, 247, 307

Mauersberger, R., Henkel, C., Weiß, A., Peck, A.B., & Hagiwara, Y. 2003, A&A, 403, 561

Nguyen-Q-Rieu, Henkel, C., Jackson, J.M., & Mauersberger, R. 1991, A&A, 241, L33

Nguyen-Q-Rieu, Nakai, N., & Jackson, J.M. 1989, A&A, 220, 57

Oike, T., Kawaguchi, K., Takano, S., & Nakai, N. submitted

Seaquist, E.R. & Bell, M.B. 1990, ApJ, 364, 94

Takano, S., Nakai, N., & Kawaguchi, K. 1995, PASJ, 47, 801

Takano, S., Nakai, N., & Kawaguchi, K. 2002, PASJ, 54, 195

Takano, S., Nakai, N., Kawaguchi, K., & Takano, T. 2000, PASJ, 52, L67

Weiß, A., Neininger, N., Henkel, C., Stutzki, J., & Klein, U. 2001, ApJ, 554, L143

Highlights of Astronomy, Vol. 13
International Astronomical Union, 2003
O. Engvold, ed.

Extragalactic Ammonia

C. Henkel[1], K.M. Menten[1], J. Braatz[2], R. Mauersberger[3], A. Weiß[3], M. Lebrón[4], A. Tarchi[5], A. B. Peck[6], C. L. Carilli[7], D. A. Lubowich[8]

[1]*MPIfR, Auf dem Hügel 69, D–53121 Bonn, Germany*

[2]*NRAO, PO Box 2, Green Bank, WV 24944, USA*

[3]*IRAM, Avda. Divina Pastora 7, E–18012 Granada, Spain*

[4]*Arecibo Observatory, PO Box 53995, Arecibo, PR 00612, USA*

[5]*Istituto de Radioastronomia, CNR, I–40129 Bologna, Italy*

[6]*CfA, SAO/SMA Project, PO Box 824, Hilo, HI 96721, USA*

[7]*NRAO, PO Box 0, Socorro, NM 87801, USA*

[8]*Hofstra University and AIP, Hempstead, NY 11550, USA*

Abstract. Multi-line data of ammonia (NH_3) are presented for Maffei 2, IC 342, and the starburst galaxies NGC 253 and M 82. While in M 82 the NH_3 emitting gas is cool, presumably arising from well shielded dense cores deeply embedded in an environment dominated by Photon Dominated Regions, the other galaxies show 'warm' and 'hot' components that may be heated by shocks, ion-slip or cosmic rays. Interferometric observations show the detailed large scale distribution of NH_3 in galaxies for the first time. The first multi-line studies of ammonia at significant redshifts ($z = 0.65$ and 0.89) are also reported and rotational temperatures, measures of the kinetic temperature of the emitting gas, are derived for all sources.

Ammonia (NH_3) is one of the most important species to trace physical parameters of molecular clouds, . While in the Galaxy inversion lines up to (J,K)=(18,18), 3130 K above the ground state, have been detected, previous studies of extragalactic NH_3 were mainly confined to low excitation transitions in IC 342 (e.g. Martin & Ho 1986), a nearby face-on spiral similar to the Milky Way.

While H_2 number densities can be derived from a variety of molecular species, ammonia can also be used to estimate kinetic temperatures by calculating relative populations in meta-stable (J=K) inversion doublets. The procedure is straightforward in galactic sources, where hyperfine splitting permits the direct determination of optical depths and column densities. Extragalactic lines, however, cover such a large velocity range that it is impossible to resolve the HF structure, so optically thin line emission has to be assumed. If we adopt this (unproven) assumption, the determined rotation temperatures ($T_{\rm rot}$) are lower limits to the true kinetic temperature.

New spectra were taken with the Effelsberg telescope toward the central regions of nearby galaxies. Towards IC 342, the detected (J,K)=(1,1) ... (6,6) and the tentatively detected (9,9) line, 848 K above the ground state, reveal a

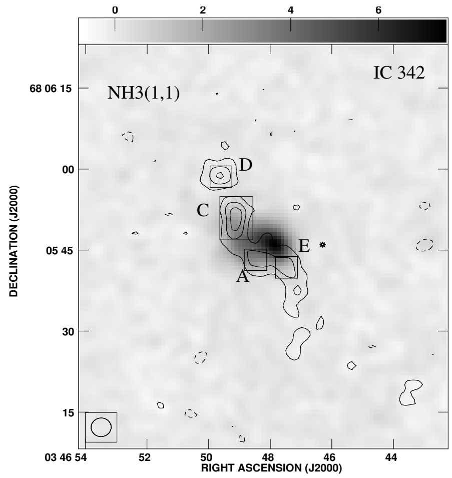

Figure 1. NH_3 (J,K)=(1,1) (contours) and 1.3 cm continuum (grayscale) emission towards IC 342.

'warm' ($T_{\rm rot}$~50 K) and a 'hot' ($T_{\rm rot}$>100 K) component, similar to the other 'normal' spiral we observed, Maffei 2. Towards the starburst galaxy NGC 253, a 'hot' component dominates the emission up to the (J,K)=(6,6) transition. Towards the other observed starburst galaxy, M 82, weak lines reveal a surprisingly 'cold' component with $T_{\rm rot}$~30 K, inferring $T_{\rm kin}$~50 K (Weiß et al. 2001; Mauersberger et al. 2003). 60μm/100μm dust temperatures are of order 50 K in all sources, consistent with the cold NH_3 component in M 82, but lower than $T_{\rm kin}$ in the 'warm' and 'hot' NH_3 components.

What can heat the gas to temperatures of 100 K or more? Shocks, perhaps caused by bar-like potentials or the dissipation of tidal motions, cosmic rays and ion-slip in the presumably strong magnetic fields of the nuclear regions can all heat significant volumes of gas to high temperatures. The warm ($T_{\rm kin}$~150 K) gas fraction as determined from H_2 emission lines (Rigopoulou et al. 2002) appears to be highest in M 82, where no hot ammonia component was detected and where the fractional NH_3 abundance was $<10^{-9}$ in comparison to normal abundances (by galactic standards), i.e. $10^{-7...-8}$, in the other sources. Apparently, NH_3 traces a different molecular gas component in M 82 than in NGC 253, Maffei 2 and IC 342. For M 82, the presence of an intense dissociative radiation field and the predominance of warm molecular filaments with low H_2 column density explains not only the low abundance of NH_3 and other molecules like CH_3OH, SiO and CH_3CN, but also the excitation of CO. The low abundance of ammonia with its low photodissociation energy of ~4 eV, the properties of the CO emission (Mao et al. 2000) and the detection of abundant HCO (García-Burillo et al. 2002) indicate that PDRs are the main heating source in M 82, in contrast to NGC 253, Maffei 2 and IC 342.

The first high resolution images of NH_3 in galaxies have been obtained with the VLA. D-array images of Maffei 2 and IC 342 taken in the (1,1) and (2,2) lines reveal all the single-dish flux from the inner 40″ (see Fig. 1). In IC 342, the nuclear region, 'cloud B' (see Downes et al. 1992), is devoid of ammonia, while in Maffei 2 NH_3 is observed along the nuclear bar. Individual extended regions can be identified in both lines. In NGC 253, the (3,3) line was observed with the

CnD array, revealing an overall distribution compatible with that of CS (Peng et al. 1996).

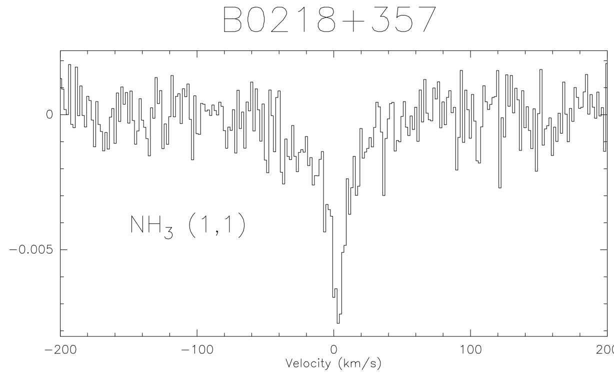

Figure 2. NH_3 spectrum towards B0218+357.

While until recently the most distant source detected in NH_3 was M 51 (D∼10 Mpc; Takano, priv. comm.), new measurements with the 100-m telescopes at Effelsberg and Green Bank (GBT) reveal for the first time significantly red shifted line absorption, towards the gravitational lenses B0218+357 (z=0.68466) and PKS 1830–211 (z=0.88582). In the former source, detected lines up to (J, K) = (3,3) indicate $T_{\rm rot}$∼30 K (for a spectrum, see Fig. 2). Towards PKS 1830–211, detected lines up to the (7,7) transition, 535 K above the ground state, demonstrate the presence of a 'hot' component. In view of the fact that high temperatures reduce fractionation effects, it is not surprising that searches for DCN or DCO^+ did not yield positive results.

References

Downes, D., et al. 1992, A&A, 262, 424
García-Burillo, S., et al. 2002, ApJ, 575, L55
Mao, R.Q., et al. 2000, A&A, 358, 433
Martin, R.N. & Ho, P.T.P. 1986, ApJ, 308, L7
Mauersberger, R., et al. 2003, A&A, 403, 561
Peng, R., et al. 1996, ApJ, 470, 821
Rigopoulou, D., et al. 2002, A&A, 389, 374
Weiß, A., et al. 2001, ApJ, 554, L143

II. SPECIAL SCIENTIFIC SESSIONS

SPS1

Recent Progress in Planetary Exploration

Chairpersons: C. de Bergh and D. Cruikshank

Editors: D. Cruikshank (Chief-Editor) and C. de Bergh

Highlights of Astronomy, Vol. 13
International Astronomical Union, 2003
O. Engvold, ed.

Jupiter After the Galileo Probe

Richard E. Young

NASA Ames Research Center Mail Stop 245-3 Moffett Field, CA 94035, USA

Tobias Owen

University of Hawaii Institute for Astronomy 2680 Woodlawn Drive Honolulu, HI 96822, USA

The Galileo Mission to Jupiter, which arrived in December of 1995, provided the first study by an orbiter, and the first in-situ sampling via an entry probe, of an outer planet atmosphere. The rationale for an entry probe is that, even from an orbiter, remote sensing of the Jovian atmosphere could not adequately retrieve the information desired. This talk provides a current summary of the most significant aspects of the data returned from the Galileo entry probe. As a result of the probe measurements, there has been a reassessment of our understanding of outer planet formation and evolution of the solar system. The primary scientific objective of the Galileo probe was to determine the composition of the Jovian atmosphere, which from remote sensing remained either very uncertain, or completely unknown, with respect to several key elements. For example, the O abundance, in the form H_2O, was uncertain by two orders of magnitude. Only a highly depleted upper abundance limit obtained near the 1 bar pressure level was known for S, and abundances of noble gases heavier than He were unknown. The probe found that the global He mass fraction is significantly above the value reported from the Voyager Jupiter flybys but is slightly below the protosolar value, implying that there has been some settling of He to the deep Jovian interior. The probe He measurements have also led to a reevaluation of the Voyager He mass fraction for Saturn, which is now determined to be much closer to that of Jupiter. The elements C, N, S, Ar, Kr, Xe were all found to have global abundances approximately 3 times their respective solar abundances. This result has raised a number of fundamental issues with regard to properties of planetesimals and the solar nebula at the time of giant planet formation. The global abundance of O was not obtained by the probe because of the influence of local processes at the probe entry site (PES), processes which depleted condensible species, in this case H_2O, well below condensation levels. Other condensible species, namely NH_3 and H_2S, were similarly affected but attained their deep equilibrium mixing ratios before the maximum depth sampled by the probe. Processes that might be capable of producing such effects on the condensibles are still under investigation. Measured isotopic ratios of noble gases and other heavy elements are solar, and $(D + 3He)/H$ is the same to within measurement uncertainties as in the local interstellar medium. No thick clouds were detected, and in particular no significant water cloud, but the PES location clearly affected the probe measurements of clouds. In fact, the probe data must be understood in the context of the location of the PES, which was within what is termed a 5 micron hot spot, a local clearing in the clouds that is bright near the 5 μm spectral region. The thermal structure at the PES was determined from approximately 1000 km above the 1 bar pressure level (10^{-9} bars) to 132 km below 1 bar (22 bars). Probe measurements showed the atmosphere to be generally stably stratified as deep as the probe made measurements, with a typical static stability of $\sim$0.1 K km^{-1} at and below visible cloud levels. In the upper atmosphere the probe derived a maximum positive vertical temperature gradient of approximately 5 K km^{-1}, and maximum temperature of $\sim$900 K. The energy sources producing the warm upper atmosphere have yet to be completely identified. At first glance, Doppler tracking of the probe indicates that the long observed cloud level zonal winds extend to levels at least as deep as the probe made measurements. Zonal wind increases from $\sim$80 m s^{-1} at pressures less than a bar to about 180 m s^{-1} near 5 bars, and remains approximately constant with depth thereafter. However, there is a question as to whether the winds measured from probe tracking are representative of the general wind field, or are considerably influenced by localized winds associated with the PES.

Highlights of Astronomy, Vol. 13
International Astronomical Union, 2003
O. Engvold, ed.

Volcanism on Io: the Post-Galileo View, and a Comparison with Earth

Ashley Gerard Davies

Jet Propulsion Laboratory-California Institute of Technology, 4800 Oak Grove Drive, Pasadena, CA 91109, USA

Abstract. At the end of the Galileo mission in September 2003, and approximately three years after the Cassini Jovian flyby, it is an appropriate time to reflect on the recent advances made in Io science. Data have been analyzed and volcanic processes have begun to be quantified. This paper reviews these advances from a purely volcano-logical perspective, looking at particular volcanos of interest, and comparing styles of ionian activity with those seen on Earth.

1. Recent Observations of Io

During 2000-2002 Galileo made a number of close flybys of Io. While radiation caused many spacecraft and instrument problems, useful data were returned at resolutions as high as 6 m/pixel for the Solid State Imaging experiment (SSI). A number of analysis, made from Near-Infrared Mapping Spectrometer (NIMS) data analysis prior to the close encounters, were confirmed by these and other high-resolution data from NIMS and the Photo-Polarimeter Radiometer (PPR). Analysis of ground-based data, and the application of new technology in the form of Adaptive Optics (AO) has recently generated more insights to volcanic processes at individual sites: in the latter case, resolutions are obtained from Hawaii that are spatially equivalent to most NIMS data.

Io has a large Fe or FeS core, but no magnetic field. Visible aurora are seen, the result of charged particle interaction with volcanic gases. At Io, the Galileo spacecraft almost immediately detected high-temperature volcanism, evidence of lavas with temperatures indicative of silicate or even ultramafic composition. These high-temperature thermal sources were discovered all over the satellite, showing that silicate volcanism was the dominant, primary lava type, finally settling a question dating from the Voyager epoch. Sulphur may be an important secondary magma, and sulphur dioxide, ubiquitous on Io's surface, is an important volatile.

2. The volcano tour: Pele, Prometheus and Loki

Pele is the only ionian volcano that displays all the characteristics of an active lava lake, where the crust on the surface is being constantly disrupted by vigorous overturn, probably caused by the explosive de-gassing of lava. The sulphur-rich plume that results still forms the red deposits on the surface seen by Voyager. A night-time, multi-filter high-resolution SSI observation obtained in 2001 shows the distribution of temperatures topping out at about 1480 K, in the basaltic composition range, confirming a previous NIMS analysis.

Prometheus has been described as Io's 'Old Faithful' as it was always seen to be producing a volcanic plume. However, unlike Pele, the plume at Prometheus appears to be generated as a result of gently effusive surface flows interacting with a SO_2-rich surface, not exsolving from the lava. Accordingly, the plume deposits have moved with the newly emplaced flow field. Analysis of NIMS and SSI data show that over 6000 km^2 of flows have been emplaced in the 17 years between Voyager and Galileo. The individual flow thicknesses at Prometheus (and other locations) are approximately 1-2 m thick. Additionally, it was recently discovered that volcanic activity at Prometheus was episodic in nature; every 7 to 9 months, there is a peak in thermal output at 5 μm. What is probably happening is that a sub-surface magma chamber is pressurizing as magma enters the chamber; the chamber eventually ruptures and magma migrates to the surface, and erupts. Pressure in the magma chamber decreases, and the eruption ends, the system seals, and the process starts again. Volumes of material erupted at Prometheus are greater by an order of magnitude than at the closest terrestrial analogue, Kilauea, Hawaii.

Loki is Io's power house, the most powerful volcano in the Solar System. Analysis of variation in 3.5-3.8 μm brightness revealed a periodicity at Loki of 540 days, interpreted as the foundering of the crust on an admittedly massive lava lake (over 150 km in diameter: lava lakes on Earth are typically 100 m across). Analysis of high-resolution NIMS data obtained in 2001 showed a surface distribution that indicated a diagonal resurfacing wave originating from the SW corner of the Patera, moving at a rate of about 1 km per day, consistent with PPR observations. Is Loki a huge lava lake, or is it being resurfaced by flows? It is not yet possible to say. If a lava lake, then Loki would be a window deep into the crust of Io.

3. Thermal signatures and a comparison with terrestrial volcanism.

Study of NIMS data, with model fits constrained by SSI and PPR data, have allowed different styles of volcanic activity to be identified on the basis of shape of infrared spectrum, mass and energy fluxes, and temporal behavior. Prometheus displays all the characteristics of a pahoehoe flow field; Pillan, a massive eruption accompanied by fire-fountaining, and open-channel, possibly turbulent flows, that were observed as they cooled over the following years.

Volcanism on Io is hotter, and produces more voluminous lavas than on Earth.

Volcanism on Earth produces about 18 km^3 of lava per year; Io produces 480-540 km^3 per year. Yet similar styles of volcanism look very much alike on these two planetary bodies. The energy and mass fluxes from pahoehoe flows, open-channel flows and active lava lakes look very similar on Io and Earth, which greatly aids interpretation of Io data.

This work was carried out at the Jet Propulsion Laboratory, California Institute of Technology, under contract to the National Aeronautics and Space Administration. The author is supported by a PG&G grant.

Highlights of Astronomy, Vol. 13
International Astronomical Union, 2003
O. Engvold, ed.

New Results on the Composition of the Outer Planets and Titan

Thierry Fouchet

Lesia - Université Pierre et Marie Curie, Observatoire de Meudon, 5 Place Jules Janssen, 92195 Meudon Cedex

Abstract. In this brief summary, I present recent progress on our knowledge of the Giant Planets and Titan atmospheric composition, as well as the impact of this progress on our understanding of Solar System formation, and atmospheric chemistry.

1. Isotopic composition

1.1. Deuterium

The D/H ratio in Solar System objects is a powerful tool to investigate the formation of planetary objects in the proto-solar nebula. However, most determinations of D/H in Giant Planets suffered from uncertainties, due to observational difficulties, or due to the isotopic fractionation existing between HD and CH_3D. The fractionation coefficient f, that depends on reaction kinetics and atmospheric dynamical time scale, is not precisely known.

Recently, ISO detected for the first time the rotational lines of HD . This new situation allowed Feuchtgruber et al. (1999) and Lellouch et al. (2001) a simple and coherent determination of D/H on the four Giant Planets. The results (D/H=$(2.25 \pm 0.35) \times 10^{-5}$ for Jupiter, $(1.70^{+0.75}_{-0.45}) \times 10^{-5}$ for Saturn, $(5.50^{+3.5}_{-1.5}) \times 10^{-5}$ for Uranus, and $(6.5^{+2.5}_{-1.5}) \times 10^{-5}$ for Neptune), confirmed that Uranus and Neptune have been enriched in D during their formation, by mixing of their atmosphere with a large, D-rich, icy core. Assuming complete mixing, it is possible to retrieve the D/H ratio in the ices that formed the cores : D/H=$(8.5^{+10.0}_{-3.8}) \times 10^{-5}$. This lower D/H than measured in comets bears important implications for the dynamics of the proto-solar nebula.

1.2. Nitrogen

Different studies, either using remote sensing spectroscopy with ISO (Fouchet et al. 2000a), or *in-situ* measurements (Owen et al. 2001), have shown that the $^{15}N/^{14}N$ ratio in Jupiter is significantly lower in the Jovian atmosphere than on the Earth: $(2.20 \pm 0.40) \times 10^{-3}$ compared to 3.67×10^{-3}. As Jupiter has not been isotopically fractionated, the Jovian ratio is similar to the solar $^{15}N/^{14}N$. In contrast, the comets, the Earth, Mars, and Titan have been fractionated either during their formation or during their subsequent evolution. This situation is especially of great value to understand the origin of terrestrial nitrogen, which still remains unclear.

2. Photochemistry

Photochemistry in the Giant Planets is triggered by CH_4 photolysis, and leads to the formation of heavier hydrocarbons, principally C_2H_6 and C_2H_2. The atmospheric dynamics redistributes the product vertically and horizontally. Recently, Fouchet et al. (2000b) and Nixon et al. (2002) observed for the first time the vertical and meridional variations of C_2H_6 and C_2H_2. The results show that C_2H_2 abundance decreases faster than C_2H_6 abundance with increasing pressures and latitudes. This result backs photochemical models that predicted a longer lifetime for ethane than for acetylene.

In contrast, photochemical models have a harder task at predicting the abundance of trace hydrocarbons. Bézard et al. (2001a) observed a C_2H_4 column abundance of 6×10^{14} on Jupiter and 3.5×10^{15} cm^{-2} on Saturn, approximately 30% less than predicted. For benzene, detected by Bézard et al. (2001b) on Jupiter and Saturn by ISO, the column abundances [$(1.5–13.5)\times10^{14}$ and $(3.6–6.8)\times10^{13}$ cm^{-2}] are 50% lower than expected.

3. Oxygen in the outer Solar System

Recently, ISO detected water in the stratosphere of the four giant planets and Titan (Feuchtgruber et al. 1997, Coustenis et al. 1999, Moses et al. 2000, Lellouch et al. 2002). Water cannot be transported from the underlying levels, has it must condense out at the very low tropopause temperatures. Instead, it must come from an exogenic source. On Jupiter, Lellouch et al. (2002) identified the source as, most likely, the SL9 collision. Moreover Lellouch et al. put an upper limit to the flux of water due to IDPs at Jupiter : 8×10^4 cm^{-2} s^{-1}. On Saturn and Titan the exogenic water flux is higher than this upper limit (respectively $(4\pm2)\times10^6$, and $(0.8-2.6)\times10^6$ cm^{-2} s^{-1}). Thus, IDPs do not constitute a realistic source of the Saturnian System. Instead, sputtering of the rings for Saturn, and from Enceladus for Titan appears as possible origins. For Uranus and Neptune, the O flux (respectively $(0.6-1.6)\times10^5$, and $(1.2-150)\times10^5$ cm^{-2} s^{-1}), could be best explained by IDPs precipitation, the larger flux observed at Neptune being due to its proximity to the Kuiper belt.

Using ground-based spectroscopy, Bézard et al. (2002) showed that CO is present in Jupiter troposphere, but also in its stratosphere, highlighting the existence of both the internal and exogenic CO sources. The tropospheric abundance, 1.0 ± 0.2 ppb, is consistent with recent chemical and dynamical calculation. The external source cannot be explained entirely by the SL9 event, but requires an additional external CO flux. The authors concluded that the most likely source is the in-fall of a kilometer-sized body each century.

References

Bézard, B. et al. 2001a, BAAS, 33, 1079
Bézard, B. et al. 2001b, Icarus, 154, 495
Bézard, B. et al. 2002, Icarus, 159, 95
Coustenis, A. et al. 1998, A&A, 336, L85
Feuchtgruber, H. et al. 1997, Nature, 389, 159

Feuchtgruber, H. et al. 1999, A&A, 341, L17
Fouchet, T. et al. 2000a, Icarus, 143, 223
Fouchet, T. et al. 2000b, A&A, 355, L13
Lellouch, E. et al. 2001, A&A, 370, 610
Lellouch, E. et al. 2002, Icarus, 159, 112
Moses, J. et al. 2000, Icarus, 145, 166
Nixon, C. et al. 2002, BAAS, 34, 851
Owen, T. et al. 2001, ApJ, 553, L77

Highlights of Astronomy, Vol. 13
International Astronomical Union, 2003
O. Engvold, ed.

Comparative Planetary Atmospheres of the Galilean Satellites

Darrell F. Strobel

Johns Hopkins University, Baltimore, MD 21218 USA, strobel@jhu.edu

We know that each of the Galilean satellites of Jupiter has a tenuous atmosphere by terrestrial standards. Io's SO_2 equatorial atmosphere and, perhaps, Callisto's atmosphere inferred from its large ionospheric densities are measured in nanobars, whereas the atmospheres of Europa and Ganymede produced by ion sputtering of the water ice surfaces only reach picobar pressures and are comprised mostly of O_2. Io's polar atmosphere is probably an order of magnitude less dense than its equatorial atmosphere. Europa and Ganymede have O_2 atmospheres with column densities in the range of (1-10)$\times 10^{14}$cm^{-2}. These atmospheres, on the basis of their inferred production and loss rates, are estimated to have short residence times of ~2-3 days.

For Io and Europa, the harsh environment of Jupiter's inner magnetosphere produces atmospheric chemistry driven by magnetospheric electrons as well as by solar radiation. In fact, ionization and UV emission occur predominantly by electron impact. With the much lower magnetospheric electron densities at the orbits of Ganymede and Callisto solar photoionization exceeds electron impact ionization.

Based on measured ionospheric electron density profiles ($\sim 10^4 - 10^5$cm^{-3}) for Io, Europa, and Callisto, the ionospheric Pedersen and Hall conductances can be computed to estimate the strengths of electrodynamic interactions of Io, Europa, and Callisto with the Io plasma torus (plasma in Jupiter's inner magnetosphere). As a result of these interactions large electric currents flow through their ionospheres ($\sim 10^6$ A) accompanied by large Joule heating rates that are the dominant heating mechanism of their atmospheres, leading to estimates of high temperatures ~1000-2000 K for altitudes 2 scale heights above their surfaces. The magnetospheric plasma interaction with these atmospheres can be remotely sensed by HST/STIS observations. The regions of brightest UV line emissions from OI (and SI on Io) indicate the regions of maximum deposition of magnetospheric electron power. On Io, this UV auroral emission occurs in equatorial spots organized by Jupiter's magnetospheric field and brightest where the field is closest to the surface, but above the limb. Theoretical models can explain why UV emission is preferentially brighter at the equator than the poles. On Europa with a thinner atmosphere, the UV emission is primarily limb glow with one bright region on the disk. The latter is not understood.

In the following table, various quantities for the Galilean satellites are summarized. For the electrodynamic interactions, the relevant quantities are the ionospheric Pedersen conductance, $\Sigma_{\rm Ped}$, the Alfven conductance, $\Sigma_{\rm A}$, the velocity of magnetospheric plasma relative to the satellite, $V_{\rm rel\ plasma}$, the Alfven velocity, $V_{\rm alfven}$, the Alfven Mach number, M_A, the sound speed Mach number, M_S, the magnetic field, B, the corotation electric field, E_0, the ratio of the ionospheric electric field to the corotation electric field, α, the total ionospheric electric current, I_{iono}, and the perturbation magnetic field due to ionospheric currents relative to the background field, $|\Delta B/B_J|$.

Quantity	IO	EUROPA	GANYMEDE	CALLISTO
Atmospheric source	Volcanos	Sputtering H_2O Ice	Sputtering H_2O Ice	Sputtering H_2O Ice
Column Density (cm^{-3})	2×10^{16} (0.03-3) $\times 10^{16}$	5×10^{14} (3-7)$\times 10^{14}$	5×10^{14} (1-10)$\times 10^{14}$	$8 \times 10^{14} CO_2$ $\sim 10^{16} O_2$
Major Gas	SO_2	O_2	O_2	O_2 or CO_2 ?
Other Species	S_2, SO,O,S, NaCl, Na, K	O,H_2O,H_2, H, Na, K	O,H_2O, H_2, H	CO_2,O,H_2O, H_2,H,CO,C
Thermospheric Temperature (K)	$\sim$2000	$\sim$ 2000	$\sim$ 1000	$\sim$ 2000
Escape rate (s^{-1}) Lifetime (d)	1.6 $\times 10^{28}$ SO_2 3	1 $\times 10^{27} O_2$ 2	?	?
Peak Electron Density (cm^{-3})	$\sim 3 \times 10^5$	$\sim 10^4$	$< 10^3$	$\sim 2 \times 10^4$
Σ_{Ped} (mho)	130 (ec)	14	$\leq$ 100 (pu)	$\sim 10^4$ (ec)
Σ_A (mho)	5	1.7	2	1.3
$V_{rel\ plasma}$ (km s^{-1})	57	90	180	170
V_{alfven} (km s^{-1})	220	460	375	600
M_A	0.25	0.2	0.5	0.3
M_S	1.65	1.75	2.4	2.4
B (nT)	1800, J	420, J	750,G	35, J
E_0 (Vm-1)	0.1	0.04	0.02	0.006
$\alpha = E_i/E_0$	0.1	0.2	-	0.001
I_{iono} (10^6 A)	10	1.4	-	0.15
Joule Heating (W)	4×10^{11}	3×10^{10}	?	$\leq 10^9$
$|\Delta B/B_J|$	0.45	0.4	-	0.35
Magnetospheric Thermal Ion Power (W)	2×10^9	1×10^8	$\sim 10^7$	$\sim 10^4$
Solar EUV/UV Power Input (W)	7×10^9	$< 10^8$	$< 10^8$	5×10^7,CO_2

ec = elastic collisions, pu = pickup, J = Jupiter's magnetic field, G = Ganymede's magnetic field

Highlights of Astronomy, Vol. 13
International Astronomical Union, 2003
O. Engvold, ed.

The Distribution and Nature of Titan's Aerosols: A New Look

Mark T. Lemmon

Texas A&M University, College Station, TX 77843-3150, USA

Peter H. Smith, Ralph D. Lorenz

University of Arizona, Tucson, AZ 85721-0092, USA

Titan passed through southern summer solstice in late 2002, allowing an unprecedented view of summer seasonal effects. A set of images was acquired with the Hubble Space Telescope spanning the 0.25-2 micron spectral range. Among the effects seen were a rapidly changing hemispheric asymmetry and a polar hood that is visible at short wavelengths. The north-south asymmetry has reversed, returning Titans dominant visual feature to something like its Voyager-era state. The polar hood is spectrally different from the north-south asymmetry and is due to a mode of small particles. The amount of absorbing material in the polar hood cannot be uniquely constrained, but a lower limit can be derived by assuming that the absorber is the same as that found in the main haze (i.e., it is analogous to Titan tholin) and that the absorber is entirely above the main haze. The hood spectrum is consistent with about $4{\times}10^{-6}$g/cm^2 of tholin-like material above the main haze south of 65 S. A larger amount of material mixed lower in the atmosphere cannot be ruled out. An upper limit to the particle radius of about 0.02 microns can be determined by the lack of a bright polar hood in near-infrared methane band images. Considering time scales for removing material from the stratosphere leads to an estimate of summer polar mass production that is within a factor of five of published estimates of annual, global aerosol mass production. More detailed modeling of the observations is proceeding. The model includes the prediction of disk-resolved polarization based on particle characteristics. Comparisons to HST polarimetric images will provide new constraints on the properties of the northern, southern, and polar aerosols. Preliminary analysis of the polarimetry images shows the polarization is radial at all wavelengths (0.25-2 microns) and the magnitude of polarization peaks near 0.75 microns. The polarization is consistent with small particles, but is less than predicted by models of Pioneer 11 and Voyager 2 polarimetry.

Highlights of Astronomy, Vol. 13
International Astronomical Union, 2003
O. Engvold, ed.

Characterization of the Zonal Wind Flow in the Upper Atmosphere of Titan with the VLT

Régis Courtin[1], David Luz[1], Daniel Gautier[1], Thierry Appourchaux[2], Jean-Pierre Lebreton[2], Francesca Ferri[3], Luisa Lara[4]
Frédéric Hourdin[5], Andreas Kaufer[6]

[1]*LESIA-CNRS, Observatoire de Paris, 92195 Meudon P^{al} Cedex, France*
[2]*ESTEC-European Space Agency, Noordwijk, The Netherlands*
[3]*Universita di Padova, Padova, Italy*
[4]*Instituto de Astrofisica de Andalucia, Grenada, Spain*
[5]*Laboratoire de Météorologie Dynamique, Paris, France*
[6]*European Southen Observatory, Santagio, Chile*

Abstract. We report on recent efforts to characterize the zonal wind flow in the upper atmosphere of Titan from high resolution spectroscopic observations with the Very Large Telescope.

To characterize the zonal circulation of Titan's upper atmosphere, we have obtained high-resolution reflection spectra between 420 and 620 nm using the UVES echelle spectrometer at the focus of the VLT-UT2. The purpose of these observations was to detect the differential Doppler shift induced by the zonal wind flow in the back-scattered solar radiation from the Eastern and Western limbs. The measured spectra were analyzed with a velocity retrieval scheme developed for stellar accelerometry (Connes 1985), taking advantage of the large number of solar lines present in this spectral range. Similar observations were also made on Io to validate the velocity retrieval. A detailed analysis of the Io echellograms yields an equatorial velocity of 78.2 ± 7.0 m.s^{-1} (Civeit 2003), to be compared with the reference value of 74.7 m.s^{-1}. For Titan, a preliminary analysis shows the clear signature of a prograde circulation (*i.e.* in the direction of the solid body rotation) just south of the equator, with a wind velocity on the order of 80-100 m.s^{-1}, consistent with current model predictions (Hourdin et al. 1995). Radiative transfer calculations indicate that these measurements refer to altitudes between 50 and 250 km. Another intriguing result, however, is that not all of our observations show the signature of super-rotation, which suggests that some process – yet to be identified – may be interfering with our ability to observe the wind flow at all times.

References

Civeit, T. 2003, Rapport de stage DESS, Obs. de Paris/Univ. Paris-Sud.

Connes, P. 1985, Ap&SS, 110, 211

Hourdin, F., Talagrand, O., Sadourny, R. Courtin, R., Gautier, D., & McKay, C. P. 1995, Icarus, 117, 358

Highlights of Astronomy, Vol. 13
International Astronomical Union, 2003
O. Engvold, ed.

The Abundant Irregular Satellites of the Giant Planets

Scott S. Sheppard and David C. Jewitt

Univ. of Hawaii, Institute for Astronomy, 2680 Woodlawn Dr., Honolulu, Hi 96822, USA

Abstract. Irregular satellites have eccentric orbits that can be highly inclined or even retrograde relative to the equatorial planes of their planets. These objects cannot have formed by circumplanetary accretion as did the regular satellites which follow un-inclined, nearly circular, pro-grade orbits. Instead, they are likely products of early capture from heliocentric orbit. The study of the irregular satellites provides a unique window on processes operating in the young solar system. Recent discoveries around Jupiter (45 new satellites), Saturn (13), Uranus (9), and Neptune (5) have almost increased the number of known irregular satellites by a factor of ten and suggest that the gas and ice giant planets all have fairly similar irregular satellite systems. Dynamical groupings were most likely produced by collisional shattering of precursor objects after capture by their planets. Jupiter is considered as a case of special interest. Its proximity allows us to probe the fainter, smaller irregular satellites to obtain large population statistics in order to address the questions of planet formation and capture.

1. Discussion

The recent development of sensitive, large scale CCD detectors has refreshed the study of irregular satellites by enabling a new wave of discovery. Large fields of view are needed because the Hill spheres (the regions of gravitational influence about each planet in which satellites could be stable) are large (see Table 1). Sensitivity is needed because the majority of irregular satellites are small and therefore faint. Also for this reason, the irregular satellite system of Jupiter has been a particular target of recent study and its currently the best characterized (Sheppard and Jewitt 2003). Each planet possesses both retrograde and pro-grade outer satellites, with the former being the more numerous. Irregular satellites in retrograde orbits have semi-major axes that are all less than $0.48r_H$ ($0.33r_H$ for the pro grades), where r_H is the Hill sphere radius. Some satellites currently have apojoves up to $0.65r_H$. Satellites with inclinations $55 < i < 130$ are absent, probably a result of the Kozai effect that couples variations in inclination and eccentricity and forces highly inclined satellites to reach large eccentricities and makes them unstable (Carruba et al. 2002). The preponderance of retrograde satellites at larger distance is probably a result of resonant perturbations by the Sun (Nesvorny et al. 2003). At present it is practically impossible for planets to permanently capture satellites since no efficient dissipation mechanism exists. Satellite capture could have occurred more easily towards the end of a planet's formation due to gas drag from an extended atmosphere, the enlargement of the Hill sphere caused by the planet's mass growth and/or higher collision probabilities with nearby small bodies (Colombo & Franklin 1971; Heppenheimer & Porco 1977; Pollack et al. 1979). If so, satellite capture occurred on the same timescale as the planet's growth. While Jupiter currently possesses the largest number of known satellites of any of the planets (Sheppard & Jewitt 2003), the other giant planets also have significant irregular satellite populations (Gladman et al. 2000 and 2001; Holman et al. 2003; Sheppard et al. 2003). All are thought to have been captured by their respective planets. In common with Jupiter, the other systems show dynamical grouping, but the satellites of more distant planets are fainter and observationally less well characterized. In particular, Jupiter shows groups in semi-major axis and inclination space while other planets show grouping mostly in inclination space. It is yet to be determined if the groupings in inclination space are because of resonant effects or not. In many of the groups a few large satellites are accompanied by many smaller ones, the latter having a steep size distribution similar to that of the main-belt asteroid families. By extrapolation, we estimate that, within a factor of two, each planet possesses approximately 100 irregular satellites with diameters greater than 1 km. We find that the four giant planets possess about the same number of irregular satellites and groupings with no dependence on the planet's mass when comparing them to the same limiting size of satellites. This is especially remarkable given that the ice giants Uranus and Neptune may have had formation histories quite different from the gas giants Jupiter and Saturn. It is unlikely that the satellite groups were produced by the sole action of aerodynamic forces during capture, because self-gravity would prevent the fragments from dispersing (Pollack et al. 1979). Additionally, gas drag acting on the fragments would produce size-dependent sorting of the orbits within each group that is not observed. For these reasons we believe that the disruptions occurred after capture and after the dissipation of the gas left over from planet's formation. Fragmentation of the parent satellites could be caused by impact with interplanetary projectiles (principally comets) or by collision with other satellites, assuming both were once much more numerous than now. For an in depth review of irregular satellites see Jewitt et al. (2003).

Table 1. Irregular Satellites of the Giant Planets

Planet	irreg. sats. (#)	groups (#)	limiting radii (km)	Hill Radii (deg)	Hill Area (deg^2)
Jupiter	53	6	3	4.7	70
Saturn	14	4-5	8	3.0	28
Uranus	9	2-3	16	1.5	7
Neptune	7	4	34	1.5	7

References

Carruba, V. et al. 2002, Icarus, 158, 434
Colombo, G. & Franklin, F. 1971, Icarus, 15, 186
Gladman, B. et al. 2000, Icarus, 147, 320
Gladman, B. et al. 2001, Nature, 412, 163
Heppenheimer, T. & Porco, C. 1977, Icarus, 30, 385
Holman, M. et al. 2003, IAU Circ., 8047

Jewitt, D., Sheppard, S., & Porco, C. in press, in Jupiter II, ed. F. Bagenal, Cambridge University Press, Cambridge

Nesvorny et al. 2003, AJ, 126, 398

Pollack, J., Burns, J. & Tauber, M. 1979, Icarus, 37, 587

Sheppard, S. & Jewitt, D. 2003, Nature, 423, 261

Sheppard, S. et al. 2003, IAU Circ., 8193

Highlights of Astronomy, Vol. 13
International Astronomical Union, 2003
O. Engvold, ed.

Is Amalthea a Captured Trojan Asteroid of Jupiter?

Andrew J. R. Prentice

School of Mathematical Sciences, Monash University, Victoria 3800, Australia

Abstract. The Galileo spacecraft has found Jupiter's inner regular moon Amalthea to be a porous assemblage of rock and ice. This and other factors point to Amalthea having first condensed in a solar orbit.

In 2002, the Galileo spacecraft discovered that Amalthea has an unexpectedly low mean density $\overline{\rho} \sim 0.9$ g/cm^3. This value is much less than the value ~ 3.87 g/cm^3 expected at Amalthea's orbital distance, namely $2.539R_{\mathrm{J}}$ ($R_{\mathrm{J}} = 71492$ km), had this body formed as a native Jovian satellite. The latter density follows from a gas ring condensation model which successfully accounts both for the broad distributions of mass and orbital radius, and the bulk chemical compositions of the four large Galilean moons (Prentice & ter Haar 1979, Prentice 2001a). This model provides a condensation temperature and gas pressure at Amalthea's orbit of ~ 880 K and ~ 45 bar, respectively. It produces a condensate that is 32% metal and 68% rock, and has mass that is $\sim 10^4$ larger than that of Amalthea. The absence of another native satellite at $\sim 3.5R_{\mathrm{J}}$ thus makes it much more likely that Amalthea formed outside the Jupiter system. Prentice & ter Haar (1979) had predicted Amalthea to be a C-type asteroid. Main belt stony asteroids have a predicted zero-porosity density ~ 3.67 g/cm^3 (Prentice 2001b). Galileo has found Amalthea to be less dense than the highly porous, ice-free, main belt asteroid Mathilde ($\overline{\rho} = 1.3 \pm 0.2$ g/cm^3), despite being ~ 30 times more massive. This suggests the presence of some ice, as well as rock. Most likely, therefore, Amalthea originally condensed as a planetesimal from the gas ring shed by the proto-Solar cloud at Jupiter's orbit, prior to dynamical capture by this planet. The predicted bulk chemical composition, by mass, of such condensate is asteroidal rock (65%), graphite (1%), and water ice (34%) (Prentice 2001b) . The zero-porosity density is 1.83 g/cm^3. Amalthea is simply a first cousin of the Trojan asteroids of Jupiter. This interpretation is consistent with the Galileo spacecraft findings and implies a porosity of 50%. I thank John D. Anderson [NASA/JPL] and David Warren [Hobart] for support.

References

Prentice, A. J. R. 2001a, Earth Moon & Planets, 87, 11

Prentice, A. J. R. 2001b in LPI Contribution No. 1097, Workshop on Mercury: Space Environment, Surface, and Interior, ed. M. S. Robinson & G. J. Taylor (Houston: Lunar & Planetary Institute), 81

Prentice, A. J. R., & ter Haar, D. 1979, Nature, 280, 300

Highlights of Astronomy, Vol. 13
International Astronomical Union, 2003
O. Engvold, ed.

Complex Organic Solid Matter in the Outer Solar System

D. P. Cruikshank

NASA Ames Research Center, USA

Complex organic molecular material of non-biological origin is found in abundance in the interstellar dust in our Galaxy, and is also detected in other galaxies. Some of this material was incorporated into the solar nebula and is now found in some Solar System bodies. While some pre-solar organic material has been preserved, synthesis of complex organics in planetary atmospheres and on icy surfaces has been in progress for the entire age of the Solar System. Refractory organic solids have proven difficult to detect by traditional spectroscopic techniques, and their presence is usually inferred from the low albedo and (often) red color of the surfaces of small bodies in the outer Solar System (OSS). Color in complex organic molecules, such as polymers and polycyclic aromatic hydrocarbons, is caused by absorption in the UV and visible spectral regions arising from electronic transitions connected primarily with C-C and C-O bonding. In particular, large hydrocarbon molecules with conjugated (alternating pairs of double and single) C-C bonds have color because the electronic transitions of the de-localized pi electrons extend into the visible spectral region; the longer the conjugated chain, the further is the extension to longer wavelength, with the result that especially large molecular material appears black.

Rigorous scattering models of the diffuse spectral reflectance in the visible and near-infrared wavelength region of OSS bodies are calculated using the complex refractive indices of the known or suspected component materials and with plausible assumptions about the physical structure of the surface. This technique depends on the availability of measured refractive indices of ices, minerals, and solid organic materials, such as tholins; with the work of investigators around the world, the library of such data continues to grow. Tholins are complex, refractory mixtures of heteropolymers, polycyclic aromatic hydrocarbons, nitrogen heterocycles, and other structures that readily form when mixtures of gases (or ices) are subjected to irradiation by charged particles or UV light (or both). They are identified with the photochemical atmospheric hazes on Titan, Triton, and Pluto, and in the atmospheres of the giant planets. Small amounts of tholins have a strong coloring effect on ices on the surfaces of various planetary satellites.

The principal results of spectral reflectance modeling studies with organic materials in combination with minerals, ices, and elemental carbon are:

1. Low-albedo and reddish colored asteroids in the Main Belt and in the Jovian Trojan populations may contain organic solids, but such material is not required because their spectra can also be matched with mixtures of common igneous rock-forming minerals.

2. The extremely red members of the Kuiper Belt and Centaur populations cannot be matched with plausible minerals and ices, and require organic solids (e.g., tholins) to achieve fits to their spectra.

3. The very red Centaur object 5145 Pholus shows absorption bands that are well modeled with water and methanol ices, while the red color is modeled with a tholin, elemental carbon, and the mineral olivine; all of these components are common in comets.

4. The low-albedo, red-colored leading hemisphere of Saturn's satellite Iapetus is well modeled with a nitrogen-rich tholin, elemental carbon, and water ice.

5. The relatively high-albedo icy satellites of the giant planets, and Pluto have weak red coloration that can be modeled with small amounts of tholins; such organic material may have formed in situ by particle and UV irradiation of the ices, or it may have precipitated from a tenuous atmosphere, or it may be acquired from exogenous sources.

Complex organic matter is emerging as the third major component of small Solar System bodies, together with ices and minerals. The chemical characterization of this material and the identification of its sources present continuing challenges to investigators.

Highlights of Astronomy, Vol. 13
International Astronomical Union, 2003
O. Engvold, ed.

Cassini/Huygens Mission To Saturn: Results And Prospects

Dennis L. Matson[1], Jean-Pierre Lebreton[2], and Linda Spilker[1]

[1] *Jet Propulsion Laboratory, California Institute of Technology, 4800 Oak Grove Drive, Pasadena, CA 91109., USA*
[2] *Research and Scientific Support Department, ESA/ESTEC, P.O. Box 299, 2200 AG Noordwijk, The Netherlands, dmatson@jpl.nasa.gov*

The Cassini spacecraft was launched in October, 1997. Since then it has been on an interplanetary trajectory aimed toward Saturn and arriving there on July 1, 2004. En route, Cassini has flown by Venus, the Earth, and Jupiter. Each of these events yielded new scientific results. (e.g., 11 papers in J. Geophys. Res. 106, 30099-30279.) The Cassini flyby of Jupiter, with Galileo already in Jovian orbit, enabled the first-ever simultaneous measurements by two spacecraft at an outer planet. This fortuitous event provided a unique opportunity to investigate the giant planet's magnetic field and the properties of the Jovian system. It provided a focused period for intensive observations of Jupiter and cooperation with investigators using Galileo, Hubble, Chandra, and ground-based observatories. The results achieved at Jupiter were stunning (e.g., 8 articles in Nature 415, 965-1005, February 28, 2002). Recent results and the current status of the spacecraft and mission will be discussed. Of note are the dates of July 1, 2004 when Cassini goes into orbit about Saturn and January 14, 2005 when Huygens enters the atmosphere of Titan. The Cassini/Huygens mission is a joint undertaking by NASA and ESA, with ASI as a partner via a bilateral agreement with NASA.

Highlights of Astronomy, Vol. 13
International Astronomical Union, 2003
O. Engvold, ed.

The Huygens Mission to Titan: Overview and status

J.-P. Lebreton

Research and Scientific Support Department of ESA, ESTEC, P.O. Box 299, 2200 AG Noordwijk, The Netherlands

D. L. Matson

Jet Propulsion Laboratory, California Institute of technology, 4800 Oak Grove Drive, Pasadena, CA 91109, U.S.A.

Huygens is an entry probe designed to descend under parachute through the atmosphere of Titan, Saturn's largest moon. The Huygens Probe is provided by the European Space Agency (ESA) for the Cassini/Huygens mission to Saturn and Titan. The Huygens mission will be conducted on the 3rd Orbit around Saturn. The probe will be released around December 25, 2004 for entry in Titan on January 14, 2005. This paper provided an overview of the Huygens mission. The status of the probe and of the mission was reviewed, and opportunities for Titan observations by the Orbiter during the first two orbits were discussed. The Cassini/Huygens mission is a joint undertaking by NASA and ESA, with ASI as a partner via a bilateral agreement with NASA.

Highlights of Astronomy, Vol. 13
International Astronomical Union, 2003
O. Engvold, ed.

Changes in Pluto's Atmosphere

J. L. Elliot

Dept. of Earth, Atmospheric, and Planetary Sciences, MIT, Cambridge, MA 02139 Dept. of Physics, MIT and Lowell Observatory, Flagstaff, AZ 86001, USA

Pluto's tenuous atmosphere was probed in 1988 with a stellar occultation observed from the Kuiper Airborne Observatory (KAO, Elliot et al. 1989) and a variety of ground-based sites (Millis et al. 1993). These data, subsequent theoretical modeling (e.g. Strobel et al. 1996), and spectroscopic observations (Owen et al. 1993; Young et al. 1997), gave us the following post-occultation picture of Pluto's atmosphere (Yelle & Elliot 1997; Elliot, Person, & Qu 2003b): N_2 is the dominant constituent of the atmosphere, which also contains small amounts of CH_4 and CO. These molecules are in vapor-pressure equilibrium with their surface ices, and this process acts as a thermostat to keep the N_2 ice at ~38 K around the body. The temperature of the 1-3 μbar pressure region probed by the occultation was ~100 K. The KAO light curve dropped abruptly, however, just below half-light. This abrupt drop could be due to one of two potential properties of Pluto's atmosphere: extinction, or a steep thermal gradient. Each of these explanations has strengths and weaknesses (Yelle & Elliot 1997; Elliot, et al. 2003b).

Pluto's atmosphere was probed again with two stellar occultations in 2002–for the first time since 1988–with the twofold goals of resolving the extinction vs. thermal-gradient issue and to look for possible changes over time. Data for the first event were recorded with two small telescopes and showed that Pluto's atmosphere had changed (Buie et al. 2002; Sicardy et al. 2003), but the data quality was not sufficient for further conclusions. Observations of the second event provided more extensive results. Data were recorded from nine telescopes, located in Hawaii, Arizona, and California at both visible and IR wavelengths (Elliot et al. 2003a). The most striking result was the marked difference between the shape of the occultation light curves observed in 1988 and 2002 (Elliot, et al. 2003a; Sicardy, et al. 2003). Sharp light-curve spikes were observed, which were barely detected in 1988. The spikes indicate dynamical activity in Pluto's atmosphere-caused either by waves, turbulence, or a combination of both. Based on the astrometric solution for the occultation (as derived from the light-curve timings from the different observing sites), it was determined that the atmospheric pressure had increased about a factor of two. For most of this time Pluto has been receding from the sun (perihelion occurred in 1989). The most likely cause for this pressure increase appears to be a warming of the N_2 surface ice by about 1 K, which would then cause the requisite pressure increase in order to maintain equilibrium. Surface warming could be due to the effects of thermal inertia or a small increase in the amount of insolation absorbed by the surface ice (e. g. Hansen & Paige 1996).

Another result is an observed trend of decreasing depth of the occultation with increasing wavelength of observation, between 0.7 and 2.2 μm (Elliot et al. 2003a). This trend is consistent with extinction from micron-sized particles in Pluto's atmosphere. As yet we cannot rule out the trend being caused by the residual flux from a faint, red companion star that was not occulted. Observations of the occulted star with adaptive optics (Liu, personal communication) have not yet indicated the presence of such a companion, but a more extensive search will be required to completely resolve the issue.

More occultation opportunities to probe Pluto's atmosphere will occur in the next few years, as Pluto approaches alignment with the galactic plane (McDonald & Elliot 2000). Some of these events can be observed simultaneously in the visible and IR (Dunham, Elliot, & Taylor 2000) when the Stratospheric Observatory for Infrared Astronomy (SOFIA) becomes operational. Pluto's atmosphere will be probed by spacecraft as early as 2015, with the flyby of the New Horizons mission (Stern & Spencer 2003).

This work was funded at MIT in part by NASA Grant NAG5-10444 and NSF Grant AST-0073447.

References

Buie, M. W., et al. 2002, Bull. Amer. Astron. Soc., 34, 877

Dunham, E. W., Elliot, J. L., & Taylor, B. W. 2000, Proc. S.P.I.E., 4014, 76

Elliot, J. L., et al. 2003a, Nature, 424, 165

Elliot, J. L., Dunham, E. W., Bosh, A. S., Slivan, S. M., Young, L. A., Wasserman, L. H., & Millis, R. L. 1989, Icarus, 77, 148

Elliot, J. L., Person, M. J., & Qu, S. 2003b, Astron. J., 126, 1041

Hansen, C. J., & Paige, D. A. 1996, Icarus, 120, 247

McDonald, S. W., & Elliot, J. L. 2000, Astron. J., 119, 1999

Millis, R. L., et al. 1993, Icarus, 105, 282

Owen, T. C., et al. 1993, Science, 261, 745

Sicardy, B., et al. 2003, Nature, 424, 168

Stern, S. A., & Spencer, J. 2003, Earth, Moon, and Planets, (in press)

Strobel, D. F., Zhu, X., Summers, M. E., & Stevens, M. H. 1996, Icarus, 120, 266

Yelle, R. V., & Elliot, J. L. 1997, in Pluto and Charon, eds. S. A. Stern, & D. J. Tholen (Tucson, AZ: Univ. of Arizona Press), 347

Young, L. A., Elliot, J. L., Tokunaga, A., de Bergh, C., & Owen, T. 1997, Icarus, 127, 258

Highlights of Astronomy, Vol. 13
International Astronomical Union, 2003
O. Engvold, ed.

Large Changes in Pluto's Atmosphere Revealed by Stellar Occultations

Bruno Sicardy, Thomas Widemann, Emmanuel Lellouch, Françoise Roques, Eric Gendron

Observatoire de Paris, LESIA, 92195 Meudon Cedex, France

Christian Veillet, Jean-Charles Cuillandre

Canada-France-Hawaii Telescope, Waimea, Hawaii 96743, USA

François Colas

Observatoire de Paris, IMCCE, 77 Bld Denfert-Rochereau, 75014 Paris, France

Wolfgang Beisker, Mike Kretlow

International Occultation Timing Association, European Section, 30459 Hannover, Germany

Olivier R. Hainaut, Chris Lidman

European Southern Observatory, Alsonso de Córdova, 3107, Casilla 19001, Santiago 19, Chile

Abstract. Pluto's tenuous nitrogen atmosphere was detected by stellar occultations in 1985 and 1988. This atmosphere is poorly known, however, due to the rarity of these events. We report here the first Pluto occultations observed since 1988, on 20 July and 21 August 2002. Our analysis reveals drastic changes undergone by the atmosphere since 1988, namely a two-fold pressure increase, the probable effect of seasonal changes on Pluto over this fourteen year interval.

1. Pluto's atmosphere

As Pluto is presently receding from the Sun, the amount of solar energy that reaches its surface decreases, so its surface is expected to cool. Surprisingly, however, we show that Pluto's atmosphere is expanding, rather than contracting. We present here a short summary of our results, which are presented in more details by Sicardy *et al.* (2003).

So far, the only way to study Pluto's atmosphere is to wait for a so-called "stellar occultation", when the refraction by the planet atmosphere causes a gradual dimming of the starlight. The previous occultation observed by several teams in 1988 revealed Pluto's tenuous nitrogen atmosphere, whose deepest layers reach pressures of a few microbars (Yelle & Elliot, 1997). This pressure is maintained by thermodynamical equilibrium between the nitrogen ice on the surface, at temperatures of 40-60 K, and the nitrogen vapor above it.

2. Observations and results

The first Pluto occultation successfully observed since 1988 occurred on 20 July 2002, during a campaign in South America organized by a group of Paris Observatory. The star dubbed "P126" went behind the planet as observed from an area ranging from Chile, Brazil, Peru, Bolivia and Ecuador. A successful observation was made by one of our teams near Arica, in northern Chile, using a 30-cm portable telescope and a CCD camera with no filter. One month later, on 21 August 2002, another occultation (of the star "P131.1") was successfully observed with the Canada-France-Hawaii 3.6-m Telescope (CFHT), yielding high quality data in the I band (0.89 μm).

Analysis of the data reveals that the pressure in Pluto's atmosphere more than doubled between 1988 (Yelle & Elliot, 1997) and 2002 (Elliot *et al*, 2003, Sicardy *et al.*, 2003). For instance, the pressure p at the distance $r=$ 1215 km from the planet center increased by a factor 2.1 between the two dates: $p = 5.0 \pm 0.6$ μbar in 2002, while $p = 2.33 \pm 0.24$ μbar in 1988.

One might naively expect an overall collapse of the atmosphere as the planet moves farther from the Sun and cools down. Seasonal variations, however, can overcome this tendency and explain the present expansion. Hansen & Paige (1996) show that there would be a period in Pluto's orbit - shortly after perihelion - when the south polar cap of the planet comes into sunlight after spending more than 120 years in darkness. This happened in 1987, and the sublimation of the solid nitrogen accumulated in this region would then feed the atmosphere, while it would take some time for the north polar cap, in darkness since 1987, to re-condense this excess of gas. Hansen and Paige predict that this expansion will last till 2015 or so, before the atmosphere shrinks again. More complications arise, however, as the albedo of the planet probably varies during the whole process, thus changing the surface temperature, and by the same way, the amount of nitrogen sublimated into the atmosphere.

Finally, some stellar scintillation is visible in the P131.1 light curve, thus revealing a dynamical activity in Pluto's atmosphere, maintained either by strong winds between the lit and dark hemispheres of the planet, or by convection near the surface.

References

Elliot, J.L. *et al.* 2003, Nature 424, 165

Hansen C.J., & Paige D.A. 1996, Icarus, 120, 247

Sicardy, B.*et al.*, 2003, Nature, 424, 168

Yelle, R.V., & Elliot J.L. 1997, In Pluto and Charon, ed. Stern S.A. & D.J. Tholen (University of Arizona Press, 1997), 347

Highlights of Astronomy, Vol. 13
International Astronomical Union, 2003
O. Engvold, ed.

The New Horizons Mission to Pluto-Charon and the Kuiper Belt

G. Leonard Tyler

Stanford University, Packard 331, 350 Serra Mall, Stanford, CA 94305-9515, USA, len.tyler@stanford.edu

S. Alan Stern

Southwest Research Institute, Suite 400, 1050 Walnut Street, Boulder CO 80302, USA, astern@swri.edu

Harold A. Weaver

Johns Hopkins University/Applied Physics Laboratory, 11100 Johns Hopkins Road, Laurel, MD 20723-6099, USA, hal.weaver@jhuapl.edu

Abstract. The New Horizons Mission to Pluto-Charon and the Kuiper Belt is under development for launch in 2006. The experiment complement of eight sensors addresses fundamental issues of density, composition, albedo, geology, and atmospheric state, chemistry, and escape.

The New Horizons (NH) Mission, currently in the middle stages of development by Southwest Research Inst. and Johns Hopkins University Applied Physics Lab., is designed to provide the first detailed, spacecraft observations of the Pluto-Charon system and smaller Kuiper-Belt Objects (KBOs) beyond. An ≈ 465 kg spacecraft is to be launched on a Jupiter gravity-assist trajectory in January 2006, to arrive at the Pluto-Charon system by 2016, after which it will continue for several more years to the Kuiper Belt. The trajectory includes scientifically useful, moderate-range, $\approx 38R_{\mathrm{J}}$, observations of Jupiter followed by an ≈ 12 km/s 'fly-through' of the Pluto-Charon system with a spacecraft closest approach to Pluto's center of mass of $\approx 11,000$ km, passing through the orbital plane of Charon. The encounter geometry includes Sun and Earth occultations by both Pluto and Charon. Subsequent to Pluto encounter, the spacecraft will maneuver to encounter at least one, and possibly two, KBOs between 2019 and 2026.

The instrument complement, Table 1, provides for visible and IR spectral mapping, UV spectroscopy, solar-UV and Earth-radio occultations, in situ sensing of system plasma, and radio-tracking determination of Pluto and Charon masses. Planned observations will characterize Pluto's suspected complex geology on scales less than 1 km, map surface composition, determine the volatiles and structure of the neutral atmosphere, determine the rate of atmospheric escape from the system, and characterize the possible exchange of volatiles between Pluto and Charon. A long focal length camera is included for the purpose of providing observations of the Pluto system for six months prior to closest approach. This will permit study of Pluto and Charon over many rotations, and provide context for the close encounter. Imaging sensitivity is such that the dark

Table 1. New Horizons Payload Summary. ('NA' = narrow angle, 'Pan' = pan-chromatic, 'Spect' = spectrometer.)

Investigation	Type	Sensor Characteristics
RALPH	Visible mapping imager	Pan- and 4-color CCD
LEISA	Near-IR imaging spect	1.24–2.5; 2.1–2.25 μm
ALICE	UV imaging spect	520-1870 Å
REX	Radio occultation $T(p[z])$	$\Delta p = 0.01$ Pa, $\Delta T_{\rm sur} = 1$ K
	Microwave radiometry	4.2 cm-λ, $\Delta T = 0.1$ K
	Body mass	Two-way radiometric tracking
SWAP	Plasma spect	To 6.5 keV
PEPSSI	Hi-energy particles	Ions: 1–3000, e^-: 25–700 keV
LORRI	Long focal length imager	NA, Pan CCD, 5 μrad/pixel
SDC	Student dust counter	area 0.25 m^2, mass $> 10^{-15}$ kg

side of Pluto—otherwise not seen at high resolution—can be imaged in 'Charon-shine' as NH departs the system. The same instrument set will be effective in reconnaissance of KBOs, with primary emphasis on surface characteristics.

The Student Dust Counter is provided by joint agreement between NH Project and the University of Colorado. To be operated by a succession of undergraduate and graduate students at CU, this instrument will provide the first in situ determination of the dust distribution between Earth and the outer solar system, providing a basis for testing Earth-based inferences and theories of dust distribution.

The mission design satisfies all NASA (2001) and PKB Science Definition Team (Lunine et al., 1995) Group I objectives, and virtually all Group II and III objectives (Stern & Cheng, 2002).

The choice of KB targets is to be made between now and the approach to Pluto-Charon, based on new KB surveys over the next decade. On the basis of the known KBO's, the current rate of their discovery, and the capabilities of the NH spacecraft, Monte Carlo simulations indicate NH will be able to reach one or two KBO's exceeding 35 km in diameter, depending upon the orbits of the target bodies and the performance of the NH navigation and propulsion systems. The instrument complement can readily address questions of KBO albedos, masses, and densities, which will support studies of bulk composition and state. Similarly, it will be possible to study surface geology, surface composition and its variation, and to search for tenuous atmospheres.

References

Lunine, J.I., et al., 1995. Report of the Pluto-Kuiper Express Science Definition Team. (NASA, unpublished)

NASA, 2001. Pluto Kuiper Belt Mission Announcement of Opportunity. AO-01-OSS-01

Stern, S. A., and A. Cheng, 2002. NASA Plans Pluto-Kuiper Belt Mission. EoS, 83, 101

Highlights of Astronomy, Vol. 13
International Astronomical Union, 2003
O. Engvold, ed.

Mapping Mars at Global to Human Scales

Brent A. Archinal, Randolph L. Kirk, Elpitha Howington-Kraus, Mark R. Rosiek, Laurence A. Soderblom, Ella M. Lee

U. S. Geological Survey, Astrogeology Team, 2255 N. Gemini Drive, Flagstaff, AZ 86004, USA (barchinal@usgs.gov)

We report on current Mars mapping projects in support of NASA planetary exploration. This includes a summary of the current state and accuracy of such mapping at global, regional, and local (human) scales. The availability of Mars Orbiter Laser Altimeter data has revolutionized such mapping. Aside from its use as a global topographic dataset, images can easily be correlated to it with absolute uncertainties of ≈100 m horizontally. We are using this to create a revised version of the global Mars digital image mosaic (MDIM) that will have absolute errors of ≈231 m (one pixel) and improved cosmetic characteristics. We are undertaking stereo-topographic mapping at regional to local scales, using Viking and Mars Orbiter Camera Narrow Angle (NA) images, with horizontal resolutions of 600 to 5 m, and expected vertical precision of 200 to 1 m. Derived topography and altimetric information can also be used to calibrate shape-from-shading (photoclinometry) topographic models at down to single-pixel resolution (i.e. 1.4 m for NA images). Products of these efforts have a multitude of purposes, from assisting in large-scale geologic mapping, to characterizing the geology/safety of proposed landing sites. Plans are underway to also use THEMIS, HRSC, and HiRISE camera data in future efforts.

Highlights of Astronomy, Vol. 13
International Astronomical Union, 2003
O. Engvold, ed.

Planetary Exploration and Archaeology: Heritage Conservation

John B. Campbell

School of Anthropology, Archaeology and Sociology, James Cook University, Cairns, Australia

Planetary exploration is resulting in the creation of new archaeological sites, material and debris on planets and their moons, and in various orbits round the Earth, Mars, the Sun etc. The main off-Earth bodies with sites so far are the Moon and Mars. Although thousands of archaeological sites on Earth are protected for their heritage value, no sites off-Earth are properly protected as yet. Sites off-Earth need to be ranked for their comparative heritage significance and protocols developed for the conservation and protection of the more significant sites and artifacts, before specimens are collected and returned to Earth in an uncontrolled (from heritage points of view) manner. A new United Nations Space Heritage Treaty is needed, or at least appropriate IAU and WAC (World Archaeological Congress) protocols agreed by the various parties concerned. The UN Outer Space Treaty 1967 is very out of date and a product of the Cold War.

The current archaeology of the Moon faces an urgent need for assessment of heritage and future scientific values of the Apollo landing sites. As the landing site where people set foot on another world for the first time, Apollo 11's Tranquillity Base is of high international significance and worthy of the equivalent of World Heritage status. Other NASA mission sites should also be considered for assessment, as should the landing and crash sites of the former Soviet Union. Future ESA, Japanese, Chinese, Indian, Russian and NASA sites should be recorded (at least remotely) as they are formed; this would not be that different in principle from ethnoarchaeology on Earth (i.e. the archaeology of the physical activities, material creations and discarded materials of living people). There is ample material on the Moon for landscape archaeology.

The archaeology of Mars would focus initially on assessment of NASA's Viking 1, Viking 2 and Pathfinder landers, as well as various crash sites such as the former USSR's Mars 2 (1971) and NASA's Mars Polar Lander (1999), once they are relocated. Monitoring selected sites and artifacts on Mars would be of particular interest as abrasion and cryoclastic action will almost certainly be occurring. A register of sites of heritage significance should be established before Mars is colonized or equipment is sampled by private corporations as is now intended for some of the Apollo sites on the Moon. The current missions to Mars (ESA's Mars Express with its *Beagle 2* lander, NASA's Mars Exploration Rovers *Spirit* and *Opportunity* landers and Japan's Nozomi) will have varying levels of heritage significance, some of which will depend on their respective scientific successes (mapping, relocation of Mars Polar Lander, detection of evidence for past or present extremophiles etc.).

Conservation of sites on Venus would be impracticable as any surviving American (NASA) or Russian (USSR) artifacts will be very corroded. However, investigation of rates of corrosion and variations in resistance according to kind of material and position in the Venusians landscape would be of more than academic interest in planning future surface missions. Planned missions to the inner planets such as ESA's Venus Express and the Mercury mission, BepiColombo, should be judged and monitored for their heritage significance as they unfold.

A future detailed register of sites on asteroids (such as Eros), Jovian moons (e.g. Europa), saturnian moons (e.g. Titan) and further out (e.g. Pluto and Charon) would be very useful to establish and maintain as they are created. Discovery of extremophiles or other life on any or all of Europa, Titan or Mars will present other ethical challenges. In general, a well structured and constantly updated, internationally mirrored heritage database on missions, orbits, trajectories, probes, landing sites, crash sites, scientific significance, national significance, international significance, interplanetary significance (stage of exploration of Solar System), conservation status, threats to conservation, protection status, expected costs of preservation, actual costs of preservation etc. will be essential for the archaeology of the Solar System. Unlike what has often happened on Earth, being ready with a plan, knowledge of the site/artifact, likely costs of intervention etc., would mean that appropriate action could be decided and carried out before significant sites/artifacts are damaged or removed by either looting or uncontrolled collecting.

Highlights of Astronomy, Vol. 13
International Astronomical Union, 2003
O. Engvold, ed.

Numerical Simulation of the Jovian Wind Band as a Convective Phenomenon

Kwing L. Chan

The Hong Kong University of Science and Technology, Hong Kong, China

Hans G. Mayr

Goddard Space Flight Center/NASA, Greenbelt, MD, USA

Using a three-dimensional numerical spectral model, we simulate the outermost layer of Jupiter's convective envelope (two depth cases: 1-23 bars, 1-115 bars). The physical parameters (e.g. internal energy flux, rotation rate) are chosen to be close to those expected, but solar heating as well as dynamical influences from deeper layers are ignored. The model generates a wind field pattern remarkably similar to that observed. There is a narrow, super-rotating jet at the equator, and two prominent humps in temperature also develop in the subtropics. The strength of the jet streams does not change much over depth. The maximum wind speed occasionally reach 100 m/sec, but the mean amplitude of the equatorial jet is about a factor of 2-3 lower than the nominal value. The latitudes of the secondary pro-grade jets are higher than those observed, but they are dependent on the depth of the model. Though the quantitative agreement is not quite satisfactory (as might have been caused by neglected physical effects like solar radiation), this model demonstrates, in principle, the feasibility of generating a Jovian type wind pattern through the interaction of fast rotation and convection in a thin shell.

Highlights of Astronomy, Vol. 13
International Astronomical Union, 2003
O. Engvold, ed.

Charon/Pluto Light Ratio

K. B. Clancy, J. L. Elliot, M. J. Person

Department of Earth, Atmospheric, and Planetary Sciences, MIT, Cambridge, MA 02139, USA

Prediction of the occultations of the stars P126 and P131.1 by Pluto on 2002 July 20 (UT) and August 21 (UT), respectively (Clancy et al. 2002, BAAS 34, 1212) involved astrometric data sets spanning more than three months that were acquired on several telescopes. Pluto's position in each frame was determined relative to a UCAC astrometric reference network (Zacharias et al. 2000, AJ 120, 2131) with a dual-source point-spread function (PSF) model that was fit to the blended Pluto-Charon image. The relative position of Charon from Pluto was fixed in the PSF using values from the JPL Horizons ephemeris, and the light ratio fixed at values from resolved photometric observations of Pluto and Charon presented in Buie, Tholen, and Wasserman (1993, Icarus 125, 233). Although the final predictions proved to be quite accurate (see http://occult.mit.edu/research/occultations/Candidates/Predictions/P126.html and http://occult.mit.edu/research/occultations/Candidates/Predictions/P131 .1.html), empirical corrections were made to the offset of Pluto from its ephemeris. These corrections were based on the residuals of Pluto's measured position from its ephemeris, which were sinusoidal. The consistency of the fitted residual phase and amplitude between all prediction data sets implies either an incorrect Charon to Pluto mass ratio was used for calculating Charon's ephemeris, or that we used incorrect Charon/Pluto light ratios in this reduction. Resolved images of Pluto-Charon were taken over a period of six days (2003 April) in nine filters at the Magellan 6.5-m Clay telescope in order to uncover the cause of these residuals. Combined with other Magellan Pluto frames taken in 2001 and 2002, the images were fit with a dual-source PSF model. The Charon/Pluto light ratio determined from the PSF modeling was then plotted against orbital phase and fit with a sinusoidal model for each filter. A strong trend with wavelength was found for the mean light ratio of Charon to Pluto. This trend partially explains the residuals found, as the astrograph and CTIO data were taken in a filter of mean wavelength ~720nm, whereas the Buie et al. resolved light curve was obtained in the F555W filter of mean wavelength ~537 nm. This trend can account for 0.026" of the 0.053" residual amplitude. However, if the only other effect were an erroneous Charon/Pluto mass ratio, the remaining residual would imply a mass ratio of 0.086 rather than 0.120 (as used in the JPL Horizons ephemeris). A value of 0.086 does not agree with recent mass ratio measurements (0.157 $\pm$ 0.003 by Young et al. 1994, Icarus 108, 186; 0.124 $\pm$ 0.008 by Null and Owen 1996, AJ, 111, 1368; and 0.122 $\pm$ 0.008 by Olkin et al. 2003, Icarus 164, 254), thus more work must be done in these analyses to understand the cause of these residuals. This work was funded at MIT in part by NASA Grant NAG5-10444 and NSF Grant AST-0073447.

Highlights of Astronomy, Vol. 13
International Astronomical Union, 2003
O. Engvold, ed.

Hot Hydrogen in the Jovian Corona

Emerich, C.

Institut d'Astrophysique Spatiale, Université Paris-Sud, bâtiment 121, 91405 Orsay, France

Ben Jaffel, L.

Institut d'Astrophysique, 98bis bd Arago, 75014 Paris, France

Clarke, J. T.

Center for Space Physics, Boston University, MA02215, USA

Ballester, G.

Lunar & Planetary Laboratory, University of Arizona, AZ85721, USA

Abstract. The asymmetry observed in the H-Lyα profiles measured near the Jovian equatorial limbs by the STIS/HST spectrograph is interpreted as due to H atoms propagating in the upper Jovian atmosphere with velocities $\sim$ 80 km/s relative to Jupiter's rotation. A qualitative scenario is suggested to correlate these energetic H atoms to energetic neutral particles recently detected by Cassini at higher altitudes.

Owing to the unique capabilities of the STIS/HST spectro-imager, Jovian H-Lyα line profiles were obtained *on* different locations of Jupiter, with unprecedented accuracy. For both observations sets obtained around the 2000 and 2001 oppositions, the Jovian line profiles reveal a distinct asymmetry near the two opposite equatorial limbs: the red wings are in excess relative to the blue ones for the receding limbs, the reverse holding for the approaching limbs. We attributed these additional Ly-α emissions to resonant scattering of the solar Ly-α emission by a high altitude population of fast neutral H located close to the approaching and receding limbs. The measured velocities, ranging between a few tens of km/s *and* $\sim$ 170 km/s relative to Jupiter, reveal a population of neutral H in super *corotation* with Jupiter. Such a population of fast neutral atoms is likely to be produced by charge exchange between neutral H and energetic atmospheric and magnetospheric charged particles -accelerated by the intense Jovian magnetic field- . As the large observed velocities evoke energetic neutral atoms (ENA) widely studied for the Earth's atmosphere, we suggest that multiple charge exchange processes should similarly produce secondary ring currents in the lower Jovian atmosphere, where neutral densities are large enough to make charge exchange efficient. Finally, these newly observed energetic atoms (few ev) should be correlated with the more energetic neutral particles (few Kev) recently detected by Cassini at 0.5 UA from Jupiter, through a cascade of charge exchange interactions.

Highlights of Astronomy, Vol. 13
International Astronomical Union, 2003
O. Engvold, ed.

Paradox of Flows on Mars

L.V. Ksanfomality

Moscow Space Research Institute, Russia, ksanf@iki.rssi.ru

Using the high-resolution images acquired by cameras onboard the MARS GLOBAL SURVEYOR orbiter made it possible to reveal the previously unknown objects on the Martian surface, which changed dramatically a notion of Mars as a dry, hydrologically dead planet (Malin and Edgett, 2000). Examination of new images shows that the nature of some extended dark formations on the slopes of craters and uplands may be associated with contemporary abundant sources of liquid water arising on the slopes at small depths below the level of surrounding plains.

The presence of liquid water on the surface of Mars is generally considered to be impossible due to low pressure and low temperature on the planet. However there are depressions on the planet's surface where pressure exceeds the critical value required for the existence of liquid water. There are big reserves of underground ice on the planet and conditions for its local conversion into the liquid water. What happens to liquid water on Martian surface? Evaporation plays a negligible role and can be easily assessed, as there is no source of heat for it. Let the pressure in the region be 8 mbar (the corresponding water boiling temperature is 4°C). Because the heat of evaporation is 540 kkal/kg and the heat capacity is 1 kkal/(kg °C), the evaporated fraction of the flow never exceeds for 1%.

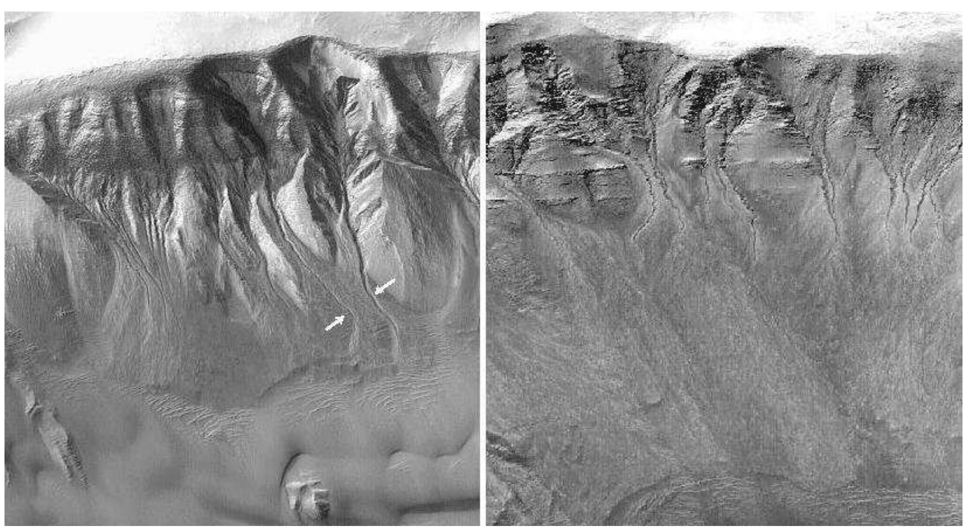

Figure 1. (MGS MOC Release N MOC2-317,320. NASA/JPL/MSSS).

The structure of extended narrow slope gullies with tributaries, as shown in Fig. 1, which are likely to be produced by water flows, has unusual appearance, reverse to that of terrestrial slope rivers: they are broad in the upper part of the slope, tend to narrow down, terminate as a thin stream and completely disappear at the valley floor or crater floor. The major river beds, as well as tributaries, seem to be directed upslope. The physical explanation of this apparent paradox is simple. Under Martian low temperature of soil and atmosphere, water erupted by springs comes in contact with a very cold ground, is partially absorbed and freezes to form the ice bed on which the flow spreads farther and continues to interact with the cold ground. The flow cools down and an ever-increasing portion of it converts into the ice phase. The distance from the source at which water completely disappears depends on the initial flow temperature and ground temperature. In the equatorial zone, on smooth slopes, such a distance, as images show, may be as large as 6 km. The paradox of side structures is also easily explained: these structures are not tributaries but rather branches where water rapidly freezes.

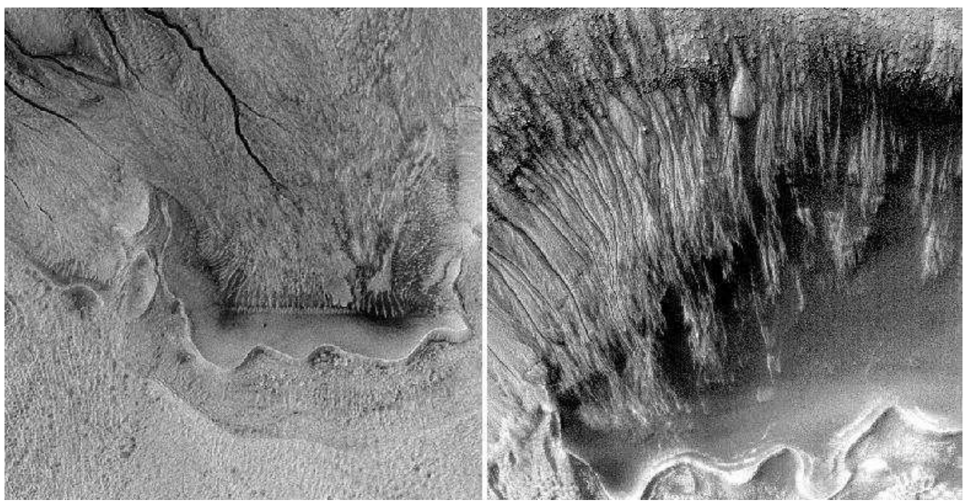

Figure 2. (MGS MOC Release N MOC2-242,320. NASA/JPL/MSSS).

Also detected on the new images are the objects (Fig. 2) that might be small naturally impounded bodies. In the case of a high source debit and/or sufficiently high ambient temperature, a flow-collecting reservoir with walls consisting of a water-saturated frozen ground and ice could arise on the valley floor. Such reservoirs are also known on the Earth (Ksanfomality, 2003), but they are formed from materials stable to positive temperatures.

Mars is a dry and cold planet; however, operating sources and possibly stable ground-water channels are present in some regions. The presence of liquid water, despite the limited character of its sources, can play an important role in the current hydrologic cycles on the planet. If the search of life on Mars should start with the search of water, this issue is probably close to its solution. The concentration of sources of ground water in two equatorial zones of Mars may serve in itself as a useful indicator of places promising for searching life traces on the planet.

References

Malin, M. C., and K. S. Edgett. Evidence for recent ground-water seepage and surface runoff on Mars//Science. 2000. V. 288. P. 2330-2325.

Ksanfomality, L.V. Water Flows and Basins on Mars//Solar system research. 2003. V. 37. ♯5.

Highlights of Astronomy, Vol. 13
International Astronomical Union, 2003
O. Engvold, ed.

ASTROD I: Mission Concept and Venus Flybys

Guangyu Li

Purple Mountain Observatory, Nanjing, China

Wei-Tou Ni

Purple Mountain Observatory, Nanjing, Tsing Hua University, Hsinchu, China

Chien-Jen Tang

Tsing Hua University, Hsinchu, China

ASTROD I with one spacecraft ranging optically with ground stations is a first step for a full ASTROD (Astrodynamical Space Test of Relativity using Optical Devices) mission. The goals are testing relativity with the relativistic parameter γ measured to 10^{-7}, measuring solar-system parameters more precisely, and improving the present-day sensitivity for gravitational wave detection using Doppler tracking by radio waves. In this paper, we present the mission concept and the orbit design for ASTROD I with an emphasis on Venus flybys. The spacecraft is to be launched into an inner solar orbit with initial period about 290 days to encounter Venus twice to receive gravity-assistance for achieving shorter period (165 days or less) to reach the other side of the Sun for a sooner measurement of Shapiro time delay. For a launch on June 17, 2010, after two encounters with Venus, the orbital period can be shortened to 165 days and the spacecraft orbit reaches inside Mercury orbit. After about 400 days from launch, the spacecraft will arrive at the other side of the Sun and the relativistic parameter γ can be determined to 0.1 ppm or better. A simulation of the accuracy for determining the relativistic parameters γ and β, and the solar quadrupole parameter J_2 gives 10^{-7}, 10^{-7} and 10^{-8} for their respective uncertainties. In this simulation, we assume a 10 ps timing accuracy and 10^{-13} m/s^2(Hz)$^{1/2}$ at frequency $f \sim 100\mu$Hz inertial sensor/accelerometer noise. Other orbits separated by synodic periods of Venus can readily be found. We discuss the sensitivity and noise reduction requirements, the atmosphere transmission noise, timing noise, spacecraft environmental noise, test-mass sensor back-action, and test mass-spacecraft control-loop noise and stiffness. In the second Venus flyby, the ASTROD I could also be swung into an elliptic 360-day orbit and stay near opposite side of the Sun for many good measurements of the Shapiro time delays — 19 times in 10 years. This is an interesting alternative. In the two Venus flybys, Venus multiple moments can be determined very precisely. In this paper, we also review ASTROD and discuss its gravitational-wave sensitivities.

Highlights of Astronomy, Vol. 13
International Astronomical Union, 2003
O. Engvold, ed.

Orbital Evolution of the Kuiper Belt

Charles Morgan and Andrew Prentice

School of Mathematical Sciences, Monash University, 3800 Australia

Abstract. The observed distribution of trans-Neptunian objects (TNOs) implies that they originally orbited in a narrow ring of radius 41 AU. The mass of the largest TNO was around $1 - 4 \times 10^{26}$ g.

Scattering by the largest TNO forms the stable low inclination ($i \lesssim 8°$) population (Fig 1a). However, most TNOs remain in the 40-42 AU unstable zone or are scattered into the chaotic fringes of the 2:3 Neptune resonance, where their inclinations and eccentricities fluctuate increasingly until they are scattered by Neptune (Fig 1b). Thus 2 distinct populations emerge from the initial ring. The 2:3 resonance is the main route to the Neptune scattered population. Stabilization of a small fraction of the TNOs passing through gives the Plutinos.

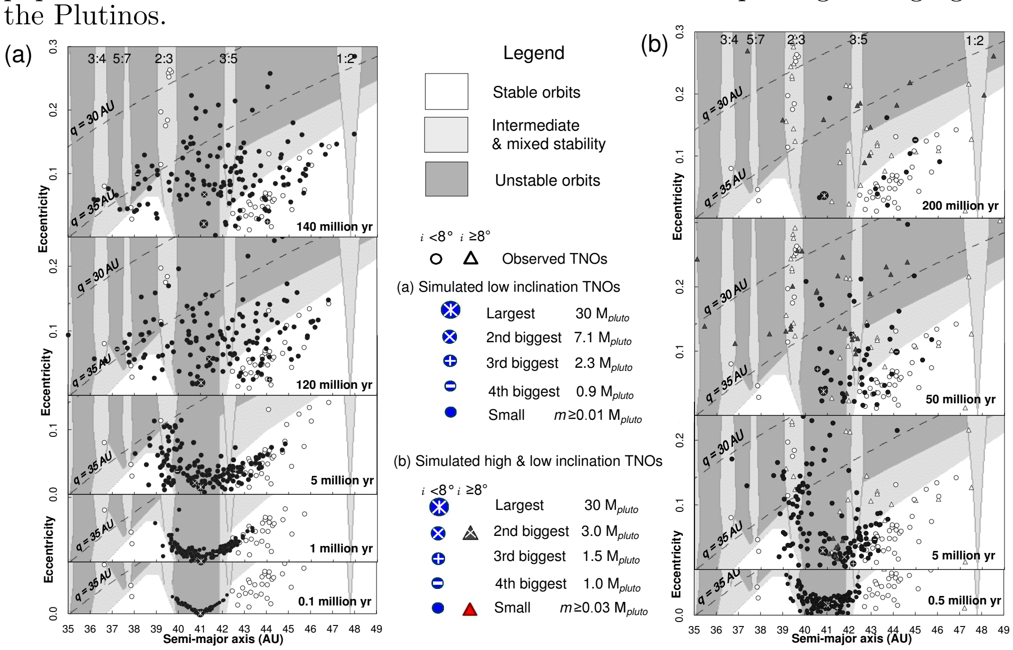

Figure 1. (a) Simulated development of the classical ($i \leq 8°$) population with weak planetary perturbation. The 1:2 resonance would limit expansion. (b) Real planetary perturbation gives both high and low inclination populations. The orbital stability map is adapted from Duncan, Levison, & Budd (1995) and Malhotra (1996).

References

Duncan, M., Levison, H., & Budd M. 1995 AJ, 110, 3073

Malhotra, R. 1996 AJ, 111, 504

Highlights of Astronomy, Vol. 13
International Astronomical Union, 2003
O. Engvold, ed.

Origin and Distribution of Water Amongst the Inner Planets

Andrew J. R. Prentice

School of Mathematical Sciences, Monash University, Victoria 3800, Australia

Abstract. A new model for the origin and bulk chemical composition of the inner planets, especially for their water content, is reported.

There is a growing body of evidence that the planets of the inner Solar system condensed within narrow, compositionally-distinct annuli, close to their present orbital radii (Drake & Righter 2002). Such a picture is consistent with the Laplacian nebular hypothesis, namely that the planetary system had formed from a concentric family of gas rings. Such rings were shed by the contracting proto-solar cloud [hereafter PSC] as a means for disposing of excess spin angular momentum (Prentice 1978). A new model for the PSC has been constructed. It consists of an adiabatic convective core surrounded by a super-adiabatic envelope of negative polytropic index. This structure is suggested by numerical simulations of supersonic thermal convection in a model atmospheric layer (Prentice & Dyt 2003). The cloud possesses a radial turbulent stress whose ratio to the gas pressure achieves a maximum value ~ 15 at the core/envelope boundary. If the controlling parameters stay constant, the PSC contracts homologously and sheds gas rings whose mean orbital radii $R_n (n = 0, 1, 2, \cdots)$ are nearly geometrically spaced. The ring mean temperatures T_n vary with R_n as $T_n \simeq A/R_n^{0.9}$, where A is a constant (Prentice 2001a). Choosing iron-rich Mercury to calibrate A (Prentice 2001b), Venus forms at 917 K and is totally anhydrous. The initial Earth (678 K) has 0.0023, by mass fraction, of water tied up in tremolite. Mars (460 K) contains an H_2O mass fraction of 0.00295 in tremolite and 0.0027 in (Na,K)OH. The asteroids (275 K) contain 0.0027 of H_2O in (Na,K)OH. Mars is thus the most water-rich of all the inner planets. Other predicted bulk constituents of Mars are: $MgAl_2O_4$ (0.0324), $MgSiO_3$-Mg_2SiO_4 (0.3677), Fe_2SiO_4 (0.1796), Fe-Ni-Cr (0.0533), (Fe-Ni)S (0.2042), MnS & ZnS (0.0050), NaCl (0.0016), Cr_2O_3 & $FeTiO_3$ (0.0065) and P_2O_5 (0.0031).

References

Drake, M. J., & Righter, K. 2002, Nature, 416, 39

Prentice, A. J. R. 1978, Moon & Planets, 19, 341

Prentice, A. J. R. 2001a, Earth Moon & Planets, 87, 11

Prentice, A. J. R. 2001b in LPI Contribution No. 1097, Workshop on Mercury: Space Environment, Surface, and Interior, ed. M. S. Robinson & G. J. Taylor (Houston: Lunar & Planetary Institute), 81

Prentice, A. J. R., & Dyt, C. P. 2003, MNRAS, 341, 644

Highlights of Astronomy, Vol. 13
International Astronomical Union, 2003
O. Engvold, ed.

Winds in Venus' Lower Mesosphere

Thomas Widemann, Emmanuel Lellouch

LESIA, Observatoire de Paris-Meudon, 92195 Meudon, France

Dynamics of Venus' mesosphere (70-110 km) is characterized by the coexistence of two different wind regimes : (1) between 70 and 85 km the vertical amplitude decrease of Venus' zonal retrograde super-rotation ; (2) between 85 and 110 km, a stable, sub-solar to anti-solar (SSAS) flow, driven by solar EUV heating. On July 7-14, 2001 and July 31 - August 4, 2002 we observed Venus with the Aurélie spectrometer on the 1.5-m telescope at Observatoire de Haute-Provence, France. The spectra cover the visible 8660-8730 Å range, in the $5\nu_3$ band of $^{12}C\,^{16}O_2$, at a resolving power of about 120,000. Seven regions were observed on Venus' illuminated side at $\sim 75°$ phase angle. About 28 lines from the P and R branches of the $5\nu_3$ band were detected and used for wind velocity measurements with an accuracy of 15 to 25 ms^{-1}.

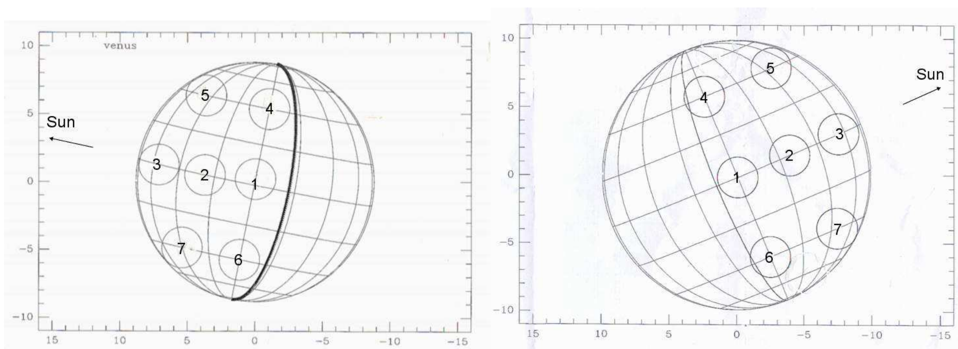

(a) (b)

Figure 1. Field mapping of wind velocity field on Venus in the CO_2 $5\nu_3$ visible band near 8700 Å near maximum elongation in 2001 (a) and 2002 (b). The 120,000-resolution Haute-Provence spectrograph has a 3" entrance aperture, projected on a disk size of 18-20 arcsec.

Using zero-wind reference at disk center and drift, CO_2 and solar lines velocity is de-projected from line-of-sight into one purely zonal, or a combination of zonal and SSAS circulations. Those measurements probe visible absorption lines of CO_2 in an altitude range at two scale heights above cloud top. Results show circulation is mainly zonal. This analysis was applied to most reliable observations at both planetary elongations. De-projection shows a mainly zonal velocity but highly variable with an important relative error (70 ± 60 ms^{-1} in 2001, 170 $\pm$ 130 ms^{-1} in 2002). The expected return branch of upper mesospheric circulation, anti-solar to solar, is detected in our observations at an amplitude of -45 $\pm$ 30 ms^{-1}.

SPS2

Astronomy in Antarctica

Chairperson: M. Burton

Editor: M. Burton

Highlights of Astronomy, Vol. 13
International Astronomical Union, 2003
O. Engvold, ed.

The Potential for Astronomy in Antarctica

M. G. Burton

School of Physics, University of New South Wales, Sydney, NSW 2052, Australia

Abstract. The motivation for holding Special Session 2 at the 25^{th} IAU GA is described, together with an outline of the rational for pursuing astronomy in Antarctica.

The IAU General Assembly has provided a focal point for discussions on progress of Antarctic astronomy. In the 1991 GA in Buenos Aires a working group on the subject was established, and a resolution passed encouraging its development. At the 1994 GA in Den Haag, CARA, the US Center for Astrophysical Research in Antarctica, had just established itself at the South Pole, and talks focused on the potential of that site. By the 1997 GA in Kyoto, several facilities were in operation and their first results were reported. There was no specific Antarctic Astronomy meeting during the 2000 GA, but by time of the Sydney GA in 2003 several ice-breaking results had been achieved, particularly in measurements of the CMBR and with regards to neutrino detection, together with front-page coverage in journals as esteemed as Nature and the New York Times. Moreover, a new base at the high plateau site of Dome C was nearing completion, Concordia Station, with the first indications of the site's quite superb quality. The 25^{th} IAU GA therefore saw the opportunity for an more in-depth discussion on the opportunities offered by Antarctica. Special Session 2 of the GA on the 19^{th} of July was a meeting to discuss the current status of Antarctic astronomy. The next day at Taronga Zoo, overlooking Sydney Harbor, was held a meeting on 'Visions for Antarctic astronomy'—a blue-sky, free-wheeling discussion limited only by the imagination on what might be possible in Antarctica. In addition, a live video-link up with the astronomers at the South Pole station was held during the lunch break of SPS2, only slightly marred by the sporadic video signal from Pole. However the audio signal came in well, as did the video to Pole, so the Polies saw us and spoke to a power point presentation they had prepared. A fascinating exchange ensued. The papers for these two meetings are presented in this issue of Highlights of Astronomy. The full programs can be found on the meeting web site, www.phys.unsw.edu.au/sps2, which also includes many of the presentations.

For several years it has been clear that the high, dry and cold conditions of the Antarctic plateau provided superb conditions for a wide range of astronomy from infrared to microwave wavelengths. Precipitable water vapor columns falling below 250μm H_2O open new windows in the IR and sub-mm. Temperatures falling as low as -80° C reduce sky backgrounds by factors of 10–100 times between 2.3 and 30μm. Less well known has been the low level of aerosols across the continent, reducing sky emissivities in the IR. The high geomagnetic latitudes has been put to good use for many years for cosmic ray detection through the lower energy particles accessible. The vast quantities of pure ice has been employed to build downward pointing neutrino detectors, with large collecting volumes and minimal levels of background contamination.

A decades experience of operating complex facilities at the South Pole has shown that operation on the plateau was quite feasible. It was readily accessible by aircraft. Conditions were generally calm, and there were never any gales. Working wasn't actually that hard, once one had adequately prepared for the conditions and designed experiments appropriately. And there were no Polar Bears or other distractions to worry about!

Two other facets of the Antarctic plateau were, however, only just becoming apparent by the time of the Sydney GA. The first was the incredible stability of the air column above the summits of the plateau. As the IAU GA was taking place, the first season of winter time measurements from Dome C was also occurring, made from the completely autonomous AASTINO laboratory. Thanks to the Iridium satellite communications system their results were available at the GA, suggesting that the skies were clear for nearly all the time and that the micro-turbulence in the boundary layer was much less than at South Pole. While further data is still required of the entire air column, the indications are that the isoplanatic angle will be well over an order of magnitude greater than at temperate latitude sites, and scintillation noise correspondingly reduced. The conditions thus appear extraordinarily favorable for adaptive optics correction. The second 'new' facet about the plateau was that it was tectonically stable. While this had in fact been known previously, the implications this has for the construction of the next generation of extremely large optical telescopes were only just becoming apparent.

With the quantification of the site qualities of the Antarctic plateau becoming pinned down, clear areas where the conditions provide particular niches for observational astronomy have emerged, for instance:

- The imaging of cosmic sources of neutrino emission.
- Precision measurements of the cosmic microwave background, including its power spectrum, polarization and the SZ–effect.
- Wide-field thermal infrared imaging, from 3 to 30μm, to uncover all sites of star formation across the Galaxy and the LMC.
- Continuous observation of objects, particularly in the dark 'cosmological' window at 2.4μm.
- Precision photometry, for instance for measurement of planetary transits of stars or stellar seismology.
- Mid-infrared photometry, for instance applied to the detection of planetary systems.
- Astrometric interferometry, with micro-arcsecond precision, with the capability of measuring three dimensional motions across the Galaxy.

In the following pages are papers on Antarctic astronomy which outline many of these results and developments.

Highlights of Astronomy, Vol. 13
International Astronomical Union, 2003
O. Engvold, ed.

Particle Astronomy from Antarctica

Per Olof Hulth

Department of Physics, AlbaNova university center, Stockholm University, SE-106 91 Stockholm, Sweden

Abstract. A brief review of astroparticle activities in Antarctica is presented including balloon cosmic rays detectors and use of the clear ice sheet for large neutrino telescopes.

1. Introduction

Despite difficult logistics and harsh surroundings, Antarctica offers some unique opportunities as a platform for particle astronomy. The huge ice sheet is an excellent medium for large Cherenkov detectors for cosmic neutrinos. A particle detector has 24 hours coverage of astronomical objects, the magnetic cut-off for charged cosmic rays is very low, the unique wind conditions at high altitudes can be used for long duration balloon flights. The combination of air shower detectors for cosmic rays on the surface above a large neutrino telescope is not possible anywhere else.

2. High energy Cosmic ray detectors in Antarctica

The high energy cosmic rays bombarding the atmosphere are still a mystery 90 years after their discovery. Finding the sources of the cosmic rays is one of the main goals in particle astronomy. The chemical composition of the particles is important information about the sources of the cosmic rays. Since the cosmic ray particles will interact high up in the atmosphere it is necessary to put the detectors at high altitudes or in space in order to directly identify the incoming particles. The flux of particles is steeply falling and at 10^{15} eV it is only one particle per m^2 per year. The energy range around 10^{15} eV is specially interesting since the slope of the spectrum is steepening at a few times 10^{15} eV (the so-called 'knee'). Several cosmic ray experiments are launching balloons at the McMurdo station in Antarctica to an altitude of 35 km where only about 5-10 g/cm^2 of the atmosphere remains. The balloons travel with the wind in a circular path and return to McMurdo after 15-20 days. It is possible to make multiple turns allowing even longer exposure times. These experiments are able to directly identify the chemical composition of the incoming cosmic ray particles: ATIC (sensitive to H–Fe at $10^{10} - 10^{14}$ eV), CREAM (H–Fe, $10^{12} - 5 \cdot 10^{15}$ eV), TIGER (Fe–Zr, $10^8 - 10^{10}$ eV) and TRACER (O–Fe, -10^{14} eV). The sensitive area is, however, only a few square metres which limits the sensitivity above energies of 10^{15} eV. For higher cosmic ray energies large surface based air shower detectors are used. At the South Pole the SPASE-II telescope has been running for several years in coincidence with the AMANDA neutrino telescope (see below). The neutrino telescope is measuring the muon flux in the cosmic ray shower while the SPASE telescope measures the electron component in the shower. Knowing both the electron and muon components in the shower gives information about the chemical component of the primary cosmic ray particle. A recent review of cosmic ray balloon experiments can be found in Wefel (2003).

3. Neutrino telescopes in Antarctica

The worlds largest neutrino telescope, AMANDA, is situated 1500 m to 2000 m deep in the ice sheet at the Amundsen-Scott base at the South Pole and is searching for high energy neutrinos from cosmic sources. The neutrinos will point back to the source without being deflected by the magnetic field in space. The telescope consists of 677 optical sensors deployed in 19 strings and was completed in February 2000. The optical sensors are recording the Cherenkov light emitted from neutrino induced interactions in the ice. The ice is very transparent to optical light at large depths. The angular resolution for muon neutrinos is in the order of a few degrees. About three atmospheric neutrinos are observed per day. The main goals are to search for the highest energy cosmic ray sources and for neutrinos from dark matter annihilation in the center of the Earth and the Sun. The most sensitive limits so far for cosmic neutrino sources, diffuse neutrino flux, neutrinos from GRBs etc have been published by AMANDA. See review talk by Köpke (2003) at ICRC 2003.

Despite the large size of AMANDA it might not be enough to detect the cosmic neutrinos. The one cubic kilometer neutrino telescope IceCube will start to be constructed at the same site as AMANDA in 2004/2005 and it is expected to be completed in 2009. The IceCube telescope will consist of 4800 optical modules deployed in 80 strings at depths between 1400 m and 2400 m. On the surface above IceCube an air shower telescope, IceTop will be constructed. The IceCube strings will take data in coincidence with the AMANDA telescope allowing an increased sensitivity for cosmic neutrinos already from the beginning of the construction.

The possibility to use radio waves generated by high energy neutrino interactions in the ice have been investigated in the RICE experiment at the South Pole. The transmission of radio waves in ice is better than for optical light allowing larger spacing between sensors. The energy threshold is, however, higher for radio waves (>10 PeV). An experiment using both the large ice sheet of Antarctica and the balloon facilities in Antarctica is ANITA which in 2006 will search for very short radio pulses generated by high energy neutrinos in the ice sheet. The observable area is in the order of a million km^2 .

References

Köpke, L. 2003, Proceedings of the 28th International Cosmic Ray conference, Invited talks

Wefel, J. 2003, Journal of Physics: Nuclear and Particle Physics, 29, 821

Highlights of Astronomy, Vol. 13
International Astronomical Union, 2003
O. Engvold, ed.

The 23 November 2003 Total Solar Eclipse in Antarctica

Jay M. Pasachoff

Williams College, Williamstown, MA 01267, USA

Abstract. Totality at the eclipse of 23 November 2003 will cross land only on Antarctica. Details of the path and contact information for safe observation are provided.

The total solar eclipse of 23 November 2003 will be visible only from Antarctica and the nearby ocean. The path of totality extends from Mirny at 93 degrees E to the Maitri Novolazarevskaya base at 12 degrees E. Totality lasts from 1 minute 54 seconds at Mirny with the Sun at an altitude of 14 degrees; to a maximum of 1 minute 57 seconds at greatest eclipse, halfway in toward Vostok, with the Sun at an altitude of 18 degrees; to 1 minute 20 seconds with the sun 2 degrees above the horizon where the path leaves the coast near Maitri. The rest of Antarctica will have only a partial eclipse, with the Sun's diameter 77% covered at McMurdo and 65% covered at the tip near South America. An ice-breaker passenger ship is planning a 28-day voyage and airplanes are being arranged for observation, including single-day overflights leaving from Melbourne, Australia, and from Punta Arenas, Chile. Scientific observations will include electronic imaging of the corona to compare with simultaneous space observations of the Sun. Links to maps and other items of coordination can be found at www.eclipses.info and www.totalsolareclipse.net, the sites of the IAU Program Group on Public Education at the Time of Eclipses and of the IAU Working Group on Eclipses, respectively. The NASA site with maps and other information is at sunearth.gsfc.nasa.gov/TSE2003/TSE2003.html. Special filters must be used to reduce the solar disk to a safe intensity during the partial phases; only during totality can one look safely without filters.

Highlights of Astronomy, Vol. 13
International Astronomical Union, 2003
O. Engvold, ed.

Site Testing at Dome C—Cloud Statistics from the ICECAM Experiment

Michael C. B. Ashley, Michael G. Burton, Paolo G. Calisse, Andre Phillips, John W. V. Storey

The University of New South Wales, School of Physics, Sydney NSW 2052, Australia

Abstract. Analysis of sky images obtained from an automated experiment at Dome C, Antarctica, at 2-hourly intervals from February to November 2001 show cloud-free conditions 74% of the time. This augurs well for the prospects of future astronomical observatories at this site.

1. Introduction

Dome C on the Antarctic plateau is almost certainly one of the best astronomical observing sites on earth. Most of its characteristics are expected to be similar to or better than those of South Pole Station. However, the fraction of cloud-free skies during winter-time has been an entirely unknown quantity. We set out to measure this fraction in order to facilitate planning for a future observatory.

Determining the amount of cloud cover over an uninhabited site on the Antarctic plateau during winter time, when the sun is below the horizon for much of the time, is a surprisingly difficult problem. The current generation of earth-orbiting satellites cannot resolve the difference between cloud and ice.

Our solution was to build ICECAM, a small, low-powered, CCD camera system that can take images of the sky every two hours for a year and store them on a solid-state disk. ICECAM is completely automated, working at air temperatures down to −80°C, and is now in its third year of obtaining data from Dome C.

2. Instrumental design and challenges

Until Concordia Station at Dome C opens for winter-over operation, there is no electrical power or heating available at Dome C for the nine months beginning in February each year. Solar power cannot be used during the long dark winter, and wind power is also problematic given the low-to-zero wind speeds on the plateau for much of the year. With temperatures down to −80°C during winter, many off-the-shelf electrical and mechanical devices tend to fail.

Fortunately, ice is an excellent insulator, so that a few meters below the surface the temperature remains stable at the yearly average of about −57°C. This is sufficiently warm for many electronic devices to function, and for lithium thionyl chloride batteries to have a reasonable capacity.

To provide an unambiguous indication of cloud cover in a form that would convince a skeptic, we decided to use a CCD camera to take images of the sky. The camera, a low light level Watec 902-HS, was found to operate reliably at $-80°C$ (although it was only rated to $-10°C$). We used a lens with a 30 degree field-of-view. The images from the camera were processed by a PC/104 computer (equivalent to a 66MHz Intel 80486, and drawing only a few watts) running MS-DOS (chosen for its small memory footprint and fast boot time), and stored on a 256MB CompactFlash disk (thereby eliminating any moving parts in the computer). There is sufficient space on the disk to store a year's worth of data, with images being taken every two hours. The entire system can be powered for a year from 5 kilograms of lithium thionyl chloride batteries. 99.6% of the time ICECAM is idle and using only a few milliwatts of electricity to operate a timer. For 30 seconds every two hours, the computer is turned on, ten images are acquired, averaged, compressed and written to the CompactFlash disk, and an ARGOS transmitter is programmed to send 32 bytes of status information to the ARGOS satellite network. The total amount of energy used during this two-hour cycle is 200J, about the same as used by a person to go up one step.

The ICECAM computer and ARGOS transmitter reside in a "crypt" some 7m below the ice surface, in order to take advantage of the warmer temperatures there. The CCD camera was mounted on a pole 3m above the ice.

At the end of each year, the CompactFlash disk is retrieved for analysis, and the lithium thionyl chloride batteries are replaced. Several years of data will be required for good statistics.

3. Results

During the first year of operation a blown fuse after three days of operation halted all ARGOS transmissions from ICECAM during 2001. We were therefore pleasantly surprised to find that when we returned almost a year later ICECAM had obtained 2095 images of the sky (fewer than the expected 3800 due to occasional boot problems and corruption of part of the file system on the CompactFlash disk). The PC real-time-clock had also reset itself on occasion once the temperature had dropped below -40C. The image times can be reconstructed from a careful analysis of the images themselves (e.g., by noting the positions of the stars, and the presence/absence of the moon). These instrumental problems were addressed during a servicing mission in January 2002. However, a modification to the CCD camera housing inadvertently led to persistent frost which resulted in much of the 2002 data being useless. We are currently waiting on 2003 data (a web-camera in our AASTINO experiment at Dome C has already shown >97% clear skies for 100 days beginning on 2003 February 9).

Figure 1 shows typical images from ICECAM at Dome C in 2001. A calibration light-emitting diode is visible at the top left of the post towards the bottom of each image. Figure 2 summarizes the data from 2001. 22% of the images were unable to be used (due to frost on the CCD window, or in some cases a corrupt image file). Of the usable images, 74% showed evidence of clear skies, and the remaining 26% showed some cloud.

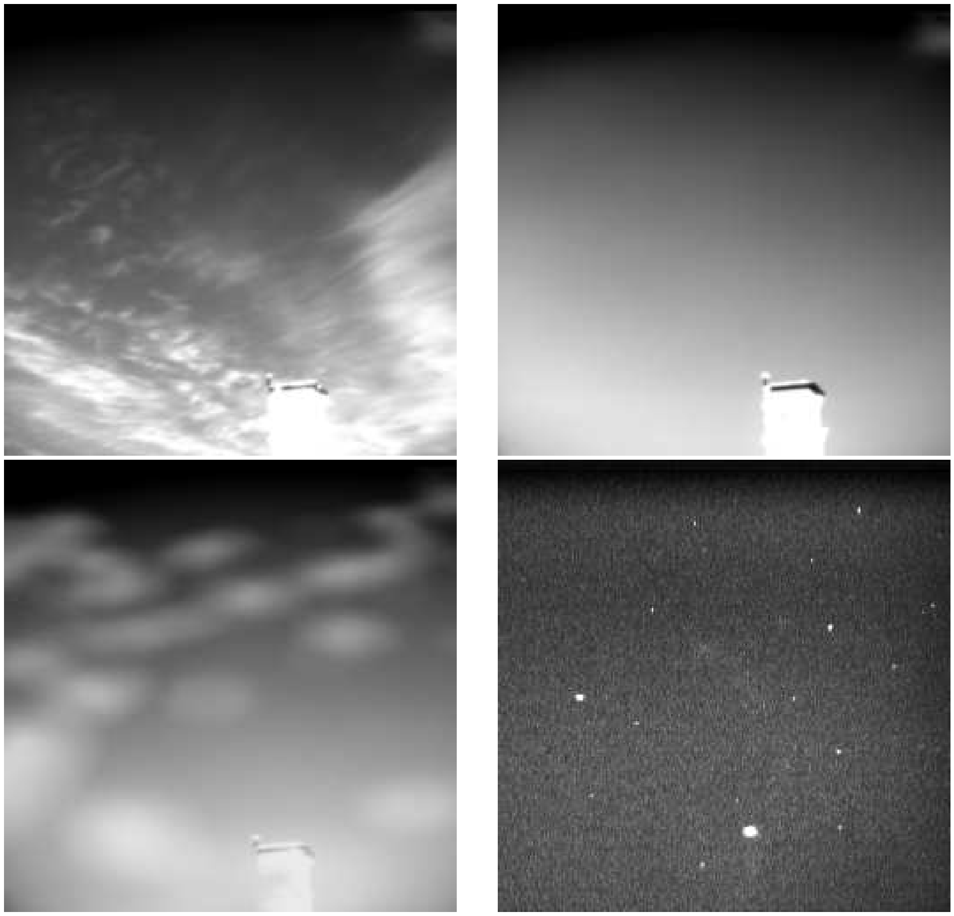

Figure 1. Sample ICECAM images from Dome C: clockwise from top left: circus cloud, clear twilight sky, patches of frost on the CCD camera window, and stars down to magnitude 6 observed during midwinter. The field-of-view is 30×30 degrees centered at a declination of −53°.

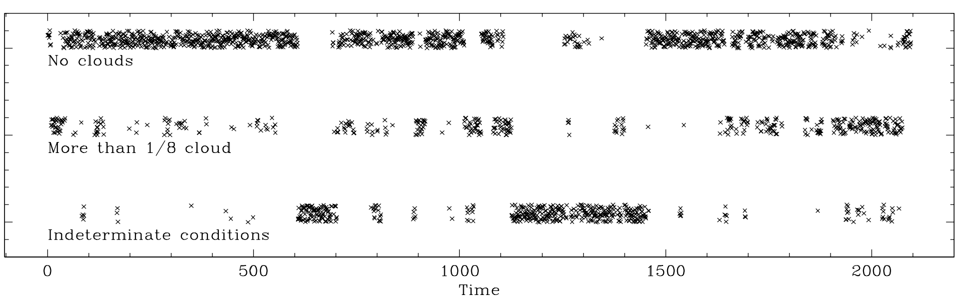

Figure 2. Summary of the 2001 ICECAM data for Dome C. Each cross represents an image, obtained at 2 hourly intervals from February to November. The X axis is image number. The images were characterized by eye as either showing clear conditions ("No clouds"), some evidence of cloud ("More than 1/8 cloud"), or ambiguous ("Indeterminate conditions"), usually due to frost on the CCD camera window.

Highlights of Astronomy, Vol. 13
International Astronomical Union, 2003
O. Engvold, ed.

Millimetric Site Testing at Dome C: Results and Plans

Luca Valenziano

IASF - sezione di Bologna, via P. Gobetti 101, Bologna, Italy

Giorgio Dall'Oglio, Andrea Graziani, Lorenzo Martinis, Gabriella Pizzo, Lucia Sabbatini

Università di Roma TRE, via della Vasca Navale 84, Roma, Italy

Abstract. Results relative to three campaigns at Dome Concordia, aimed to measure the millimetric sky noise, are presented. The atmospheric noise during summer seems to be definitely lower with respect to that measured with the same instrumentation in other geographical locations. We illustrate the scientific results obtained.

1. Introduction

The high Antarctic Plateau is generally recognized as the best site on our Planet for millimetric and sub-millimetric observations. Italy and France are building a new permanent station at Dome C. It will be open for year-round operations in 2004-2005. The Dome C site quality in the millimetric range has been tested in summer since 1995. Recent data from atmospheric studies allow us to extend the analysis to wintertime conditions.

2. Site testing observations

Some interesting informations can be derived from meteorological data: wind speed, temperature, humidity. Wind speed at Dome C (median value below 2 m/s) is always lower than at South Pole (Valenziano & Dall'Oglio 1999). This is mainly due to the relative location of the two sites: Dome C being on top of a dome, while South Pole is downhill, where katabatic regime is already present. Moreover, wind is almost absent at Dome C during the winter, being strongly correlated to the elevation of the Sun.

Temperature is strongly related to Sun elevation at Dome C, being quite stable around -60°C during the winter. Precipitable Water Vapor (PWV) is always very low at Dome C. Summertime values (Valenziano & Dall'Oglio 1999) are distributed around 0.6 mm. Relative humidity, measured with a set of capacitive sensors at three different location on an instrumented tower (Nardino et al. 2002), drops to very low values during the winter.

Planetary Boundary Layer observations, using SODAR and net radiation detectors (Argentini et al. 2002), show that the atmospheric turbulence is strongly related to the warming effect of the sun (Georgiadis et al. 2002). Net radiation (if positive is the the amount of energy available for turbulence genera-

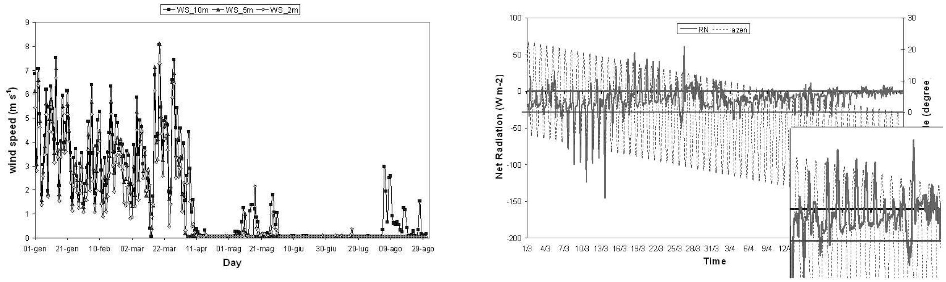

Figure 1. Left panel: Wind speed at Dome C in 2002. Note the abrupt change when the Sun is no longer above the horizon. Right panel: Net radiation measured at Dome C. Sun elevation is superimposed. Also in this case, values are dropping when the Sun is below the horizon. Note, in the box, the correlation between the net radiation and the Sun position, showing the presence of turbulence only during the central part of the day in summer. Data courtesy of M. Nardino, S. Argentini, T. Georgiadis

tion) is always very low and it is dropping below zero during the Antarctic night (see Figure 1). Moreover, the turbulent layer is confined close to the ground (lower than 300 m) by the strong thermal inversion during the summer. This is also confirmed by sky noise data measured by the authors in summer 1998.

3. Conclusions

While further test are in progress to definitively asses Dome C quality, present data strongly support the exceptional quality of the site in the millimetric range. The combination of very low PWV, wind speed, turbulence and temperature makes Dome C a very promising site for future, large aperture telescopes.

Acknowledgments. Authors are indebted to M. Nardino for kindly supplying Planetary Boundary Layer and meteorological data.

References

Valenziano, L., Dall'Oglio, G. 1999, PASA, 16, 167

Nardino, M., Bonafè, U., Calzolari, F., Orsini, A., Argentini, S., Georgiadis, T. 2002 in SIF Conf. Proc. , Italian Research on Antarctic Atmosphere, ed. M. Colacino, (Bologna: SIF) 80

Argentini S., Mastrantonio, G., viola, A., Nardino, M., Petenko, I.V., Sempreviva, A.M. 2002 in SIF Conf. Proc., Italian Research on Antarctic Atmosphere, ed. M. Colacino, (Bologna: SIF) 80

Georgiadis, T., Argentini, S., Mastrantonio, G., Viola, A., Sozzi, R., Nardino, M. 2002, Nuovo Cimento, 25, 4

Highlights of Astronomy, Vol. 13
International Astronomical Union, 2003
O. Engvold, ed.

Results from the South Pole Infra-Red EXplorer Telescope

J. M. Rathborne

Institute for Astrophysical Research, 725 Commonwealth Avenue, Boston University, Boston, MA 02215, USA
School of Physics, University of New South Wales, Sydney, NSW 2052, Australia

M. G. Burton

School of Physics, University of New South Wales, Sydney, NSW 2052, Australia

Abstract. The SPIREX telescope, located at the Amundsen–Scott South Pole Station, was a prototype system developed to exploit the excellent conditions for IR observing at the South Pole. Observations over two winter seasons achieved remarkably deep, high-resolution, wide-field images in the 3–5 μm wavelength regime. Several star forming complexes were observed, including NGC 6334, Chamaeleon I, η Chamaeleontis, the Carina Nebula, 30 Doradus, RCW 57, RCW 38, as well as the Galactic Center. Images were obtained of lines at 2.42 μm H_2, 3.29 μm PAH and 4.05 μm Br α, as well as 3.5 μm L–band and 4.7 μm M–band continuum emission. These data, combined with near–IR, mid–IR, and radio continuum maps, reveal the environments of these star forming sites, as well as any protostars lying within them. The SPIREX project, its observing and reduction methods, and some sample data are summarized here.

1. Introduction

The South Pole InfraRed EXplorer (SPIREX) telescope was a prototype system, developed to test the feasibility of building, operating, and maintaining an infrared (IR) telescope during an Antarctic winter. The initial driver for the SPIREX project was to exploit the conditions at the South Pole that make it an excellent site for 3–5 μm observations — that is the high altitude, the low temperatures, low precipitable water vapor content in the atmosphere, and the stable weather conditions (Burton et al. 1994; Marks et al. 1996; Hidas et al. 2000; Marks 2002).

The SPIREX 60 cm telescope began operations at the Amundsen–Scott South Pole Station in 1994 (Hereld et al. 1990). SPIREX was initially used as part of a campaign to measure the South Pole's thermal background, sky transparency, and the fraction of time useful for IR observations (see e.g. Ashley et al. 1996, Nguyen et al. 1996, Phillips et al. 1996 and Chamberlain et al. 2000 for further details on the IR sky conditions).

Due to the very low thermal background, SPIREX could perform longer integrations in the 3–5 μm regime, compared to temperate latitude facilities. In addition to continuum emission which, at these wavelengths pinpoints young embedded objects, there are many astrophysically significant molecular lines

Table 1. Parameters of the filters and achieved sensitivities for SPIREX/Abu.

Filter	Center μm	Width μm	Range μm	Time$\times$Coadds [b]	Sensitivity[c] 3σ, $5'' \times 5''$, 1 hour
H_2[a]	2.425	0.034	2.408–2.441	360×1	$6 \times 10^{-18}\,Wm^{-2}$
PAH	3.299	0.074	3.262–3.336	60×3	1 mJy
Br α	4.051	0.054	4.024–4.078	10×18	$5 \times 10^{-17}\,Wm^{-2}$
L	3.514	0.618	3.205–3.823	6×30	14.6 mags
L'	3.821	0.602	3.520–4.122	6×30	14.6 mags
narrow M	4.668	0.162	4.586–4.749	1.2×90	10.2 mags

[a] Covering the (1–0) Q(1)–Q(5) lines.

[b] Typical integration time (in seconds) $\times$ number of coadded frames per position.

[c] Achieved sensitivities were up to 1 magnitude worse than theoretical sensitivities for the site with optimal instrument performance.

accessible; e.g. those from hydrogen and PAH molecules. Observations at 3–5 μm are difficult at most temperate sites, making studies involving these lines limited, and thus the SPIREX dataset unique.

From 1994–1997 SPIREX was equipped with the GRIM (grism imager) camera. This detector contained 128×128 pixels and was sensitive from 1–2.5 μm. In 1998 the telescope was equipped and with the Abu camera, which incorporated an engineering grade 1024×1024 Aladdin detector (Fowler et al. 1998). This camera was sensitive from 2.4–5 μm, and provided a $10'$ field of view image with a $0.6''$ pixel scale. Six science filters were available with SPIREX/Abu. The three narrow-band filters were optimized to isolate emission from molecular hydrogen (H_2 at 2.42 μm), polycyclic aromatic hydrocarbons (PAHs at 3.29 μm), and hydrogen line emission (Br α at 4.05 μm). The three broad-band filters covered the L–, L'– and M–bands. The filter parameters and achieved sensitivities are listed in Table 1 (see Burton et al., 2000).

SPIREX/Abu was well suited for studies of star forming complexes. Young stars containing circumstellar disks have a color excess in the IR due to the absorption and re-emission of radiation from the central star by the surrounding material. Recent studies have found that the L–band may be the optimal wavelength for detection of star and disk systems. Compared to the (H–K) color [$\equiv$ 1.6–2.2 μm], the (K–L) color [$\equiv$ 2.2–3.5 μm] is more sensitive to the presence of a disk (Haisch et al. 2000; Lada et al. 2000; Kenyon & Hartmann 1995).

Observations of PAH molecular line emission across star forming complexes, allows one to study their environments. The fluorescent emission from PAH molecules trace regions (known as photo dissociation regions or PDRs), where stellar UV radiation is heating the molecular gas (Hollenbach & Tielens 1997). PAH emission delineates externally heated molecular clouds and reveals the interactions between nearby massive stars and any remnant molecular material.

The first astronomical results from SPIREX were obtained when Shoemaker-Levy 9 collided with Jupiter in 1994. Using the GRIM camera at a wavelength of 2.36 μm, images were obtained at 5 minute intervals and captured 16 of the fragments, showing evidence of impact with Jupiter in 10 cases (Severson 2000). An extended halo around the edge-on spiral galaxy ESO 240–G11 was also imaged using GRIM at 2.4 μm (Rauscher et al., 1998), reaching a sensitivity level of 25 mags/arcsec^2.

The following sections discuss a sample of data obtained from the two years of operation of SPIREX/Abu (1998–99) at the South Pole. Observations were conducted toward a number of different complexes. The characteristics of these range from young to old, low- to high-mass, and near and far star forming complexes. In particular, results are presented here for NGC 6334, Chamaeleon I, η Chamaeleontis, the Carina Nebula, 30 Doradus, RCW 57, RCW 38, and the Galactic Center. In addition, SPIREX was used to search for an infrared counterpart to the gamma-ray burst GRB990705 at 3.5 μm (Masetti et al., 2000), though no source was detected to a limit of 13.9 magnitudes after 2 hours of integration.

2. Data Acquisition and Reduction

For each source position, a series of frames were obtained at the specified integration time and then averaged. These parameters varied depending on the observing wavelength, the properties of the filter (narrow- or broad-band) and the weather conditions. Typical values for each filter are given in Table 1. All observations were conducted by the winter-over scientists at the South Pole station; Rodney Marks (1998) and Charlie Kaminsky (1999).

The sequence for all observations consisted of a set of sky frames followed by two sets of object frames. Each set consisted of five averaged frames offset by $\sim 30''$ from the previous. This sequence was repeated allowing the easy removal of sky emission and artifacts from the array. Archived images were used for dark subtraction and flat-fielding. Observations of standard stars were obtained before and after all on-source observations for flux calibration.

The majority of the data presented here was reduced by Joel Kastner using the SPIREX/Abu data pipeline[12] (the exceptions are NGC 6334 and the Carina Nebula). The data pipeline was a joint project of the Rochester Institute for Technology Center for Imaging Science (RIT CIS), the National Optical Astronomy Observatories (NOAO) and the Center for Astrophysical Research in Antarctica (CARA).

To cover the star forming complexes of NGC 6334 and the Carina Nebula, many adjacent positions were observed. Common stars in adjacent frames were used to align the images and create the final larger mosaic (using IRAF routines written by Peter McGregor[13]). The final PAH–band mosaiced image for the Carina Nebula contained a total of 72 individual images, and for NGC 6334 the mosaic PAH–band image contained 304 images.

---

[12] See http://pipe.cis.rit.edu/

[13] See http://www.mso.anu.edu/observing/2.3m/CASPIR/

3. Results and Discussion

3.1. NGC 6334

NGC 6334 is a young massive star forming region at a distance of 1.7 kpc. It contains seven distinct sites of ongoing star formation along a central molecular ridge. Fig. 1(a) shows the 3.29-μm data toward NGC 6334.

The emission within this band comprises both PAH and continuum emission. A massive embedded star is seen at each of several sites of star formation along the ridge, each ~ 1 pc apart. They are surrounded by complex loops and filaments of PAH emission. These PDRs have formed on the edge of the remnant molecular cloud, as radiation from the young stars carves the material and ionizes their surroundings. Analysis of the PAH emission and PDR features across the central ridge of NGC 6334 have been presented in Jackson et al. (1999) and Burton et al. (2000). The data shown here expand on these studies, and further reveal the PDR structure adjacent to the central star forming ridge.

In addition to the PAH–band images shown here, L–band images were also obtained across NGC 6334. When combined with near–IR data from the 2MASS point source catalog they allow us to produce near–IR color–color diagrams (e.g., (J–H) vs. (H–K) and (J–H) vs. (K–L) diagrams). Results presented in Rathborne et al. (2003) find 11 sources with a large IR excess using the (K–L) color, compared to just a single source using the (H–K) color excess, confirming that the (K–L) color is far more sensitive to the detection of circumstellar disks.

3.2. Chamaeleon I

Containing in excess of 100 pre-main sequence stars, the Chamaeleon I dark cloud is one of the most active regions of nearby low-mass star formation. The central 0.5 deg^2 of the complex was observed in the L–band using SPIREX/Abu. These images reveal all of the known pre-main sequence stars (to an $L \leq 11$).

Kenyon & & Gómez (2001) combined JHK observations obtained at the CTIO with the SPIREX/Abu data, to construct near–IR colour–colour diagrams. They find the fraction of sources with an IR excess to be $58 \pm 4\%$ (complete to an $L < 11$). In addition, they also confirm that sources with an IR excess are more easily identified when using the (K–L) colour than (H–K).

3.3. η Chamaeleontis

The η Chamaeleontis cluster is one of the nearest to the Sun, lying just 97 pc away. It is also of intermediate age for a pre-main sequence system, ~ 9 Myrs old, and somewhat older than a number of other clusters where the formation and evolution of circumstellar disks has been studied. Importantly, its proximity and compactness mean that there is a complete population census for its members — 15 stars ranging from 0.2 to 3.4 $M_{\odot}$ in mass. Lyo et al. (2003) imaged the cluster using SPIREX/Abu in the L–band, finding 60% of the stars had IR excesses attributable to the presence of disks around them. Of those with disks, half showed a clear relation between the strength of the IR excess at 3.5 μm and the equivalent width of the Hα line emission, implying continuous accretion. The lifetime of the disks in η Chamaeleontis (~ 9 Myrs) is significantly longer than in a number of other systems that have been studied, with lifetimes of 3–6 Myrs (e.g., Haisch et al., 2001).

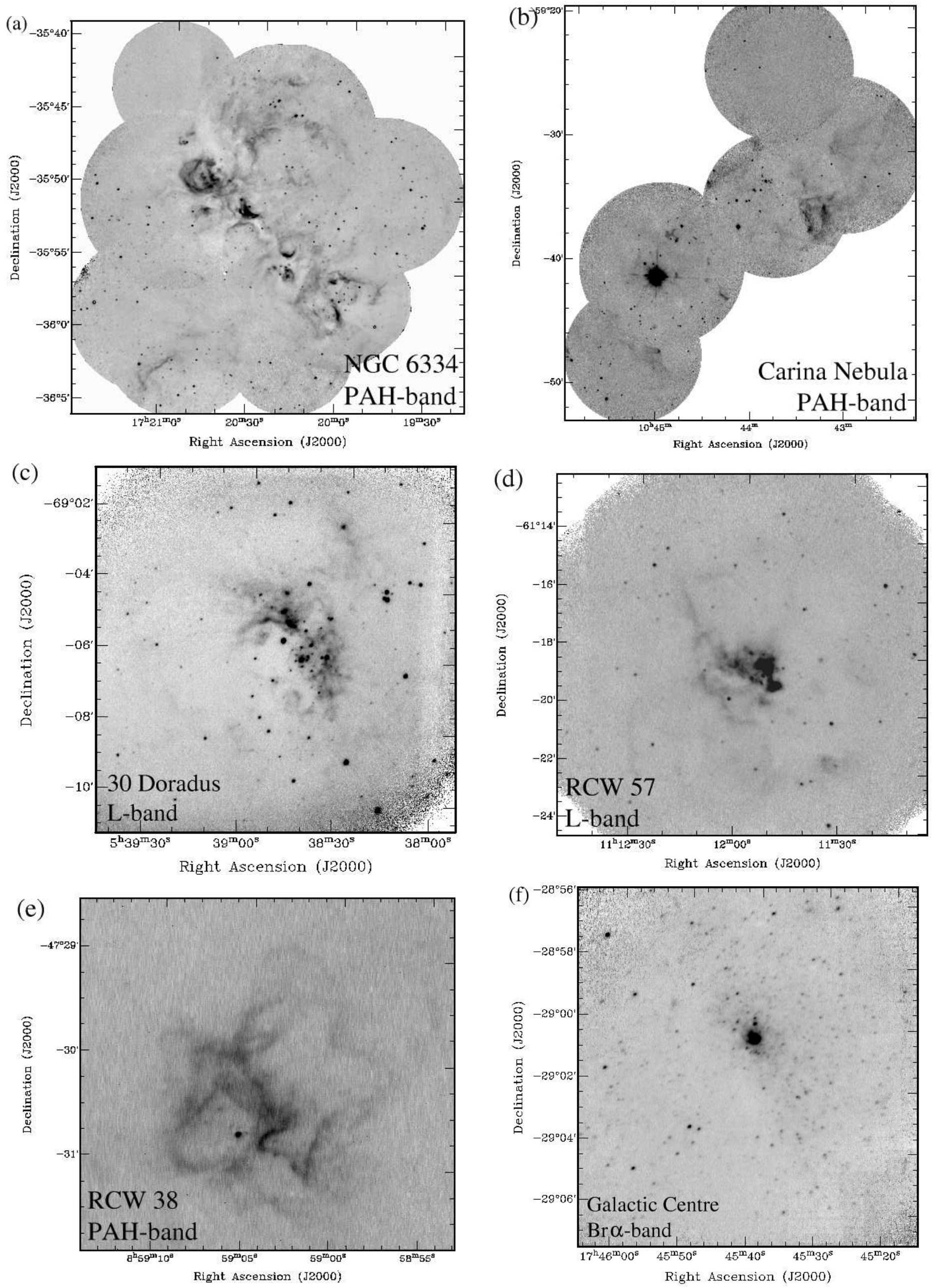

Figure 1. A collection of the images obtained with SPIREX/Abu. (a) NGC 6334 in 3.29 μm PAH emission (Burton et al., 2000, Rathborne et al., 2003), (b) The Carina Nebula in PAH emission (Rathborne et al., 2002), (c) 30 Doradus in 3.5 μm L–band emission, (d) RCW 57 in L–band, (e) RCW 38 in PAH emission and (f) the Galactic Center in the 4.05 μm Brα filter. The RCW 38 and 57 images were kindly provided by Chris Wright.

3.4. The Carina Nebula

The Carina Nebula is a massive star forming region at a distance of 2.2 kpc. Because no protostellar objects had been found within this nebula, it was thought to be 'evolved' and devoid of current star formation activity (e.g., Cox & Bronfman 1995). It does however, contain 53 O–type stars and includes the clusters Tr 14 and Tr 16. At its centre lies the massive star η Car and the Keyhole Nebula. Optical and near–IR images show a high amount of extinction toward this complex, with many dark lanes, globules, clumps, and filaments. Two large molecular clouds are located at the edges of the complex, in close proximity to the massive stars.

Fig. 1(b) shows the PAH–band emission across the central Carina Nebula (these data are also discussed in Brooks et al. 2000 and Rathborne et al. 2002). When combined with 2.12–μm H_2 line emission, MSX 8– and 21–μm images, SEST molecular line maps, and MOST 843 MHz radio continuum images, three different environments are revealed across the complex: (i) the Keyhole nebula containing discreet, dense molecular clumps with PDRs on their surfaces; (ii) PDRs at the edges of both the southern and northern molecular clouds; and (iii) heated dust, intermixed with the PDRs surrounding Tr 14 and the northern molecular cloud. Several 3.29–, 8– and 21–μm point sources were also located across the complex, with spectral energy distributions corresponding to compact H II regions. Interestingly, these were all found on the edges of PDRs which appear to have been carved out by the stellar winds and radiation from the nearby massive stars. These results suggest that star formation is indeed ongoing within the Carina Nebula and may in fact be triggered by the interactions resulting from the nearby massive stars.

3.5. 30 Doradus

The 30 Doradus region is the brightest H II region in the Large Magellanic Cloud. It contains a central cluster of massive stars surrounded by extended nebulosity in the near–IR, with many protostellar candidates. To study the nature of the embedded stellar population in more detail, L–band observations were obtained with SPIREX/Abu. The data presented in Fig. 1(c) are the most sensitive ever obtained of the 30 Doradus complex. The faintest start seen in the image, which required 9.25 hours of on-source integration, has L = 14.5 magnitudes. Many sources with an IR excess are revealed when the L–band data are combined with JHK observations. Several embedded massive stars are apparent and in addition, a population census of the young stellar objects can be conducted. This still remains the deepest, wide-field L–band image ever obtained, despite the small size of the telescope, with an extended source sensitivity (1σ) of 18.2 magnitudes per square arcsecond.

3.6. RCW 57

RCW 57 is a bright southern H II region. It contains a tight cluster of massive stars and shows extended infrared nebulosity. L–band observations of the central $10'$ of this complex were obtained with SPIREX/Abu (Fig. 1(d)). This image reveals many point sources, in addition to both bright and diffuse extended emission. Using JHK and the SPIREX/Abu L–band data, studies are currently underway into the star formation history of this complex.

3.7. RCW 38

RCW 38 is also a bright H II region containing a tightly packed cluster of stars. Near–IR images of this complex show extended nebulosity, with dust lanes and dark patches. Coincident with many of these features is extended 3.29– μm PAH emission, as shown in Fig. 1(e). These features trace the PDRs and delineate the molecular material. In addition, they wrap around the ionized material seen at 2 μm.

3.8. The Galactic Centre

Observations of the Galactic Centre obtained with SPIREX/Abu are far less affected by the extinction than at optical and near–IR wavelengths. The 4.05 μm image in Fig. 1(f) clearly demonstrates the advantages of this wavelength regime. Most of the 4.05 μm emission originates from heavily extincted sources, though there is also some Br α emission, pinpointing regions of ionized gas. Three sources, of roughly equal brightness, are prominent in the nucleus at 4 μm. This is in contrast to the view at 2 μm, which is dominated by the source IRS 7. These three sources are each separated by $\sim 7''$ and centred roughly on the presumed nucleus, Sgr A*. At the spatial resolution achieved with SPIREX they are associated with the sources IRS 1W, IRS 7/IRS 3 and IRS 13E/IRS 2L, respectively (as imaged by Clenet et al. 2001, in the L–band).

4. Conclusions

Although SPIREX/Abu was a prototype facility, it nevertheless obtained deep, high-resolution, wide-field images in the 3–5 μm regime toward many star forming complexes. These data are not only unique, but when combined with complementary near–, mid–IR, and radio continuum observations, reveal the inner environments of star forming complexes (by tracing the PDRs), and identify the youngest objects with circumstellar disks (through their high L–band fluxes). The success of the SPIREX/Abu system lends strong support to current plans to build larger IR telescopes on the Antarctic plateau, where they would provide the most sensitive facilities for 3–5 μm observations on the Earth.

Acknowledgments

The SPIREX project was a collaboration between the USA and Australia, involving the National Optical Astronomy Observatories (NOAO), the United States Naval Observatory (USNO), the Center for Astrophysical Research in Antarctica (CARA), Boston University, Goddard Spaceflight Center (GSFC), Ohio State University (OSU), Rochester Institute of Technology (RIT), the University of Chicago (UC), the University of New South Wales (UNSW), the Australian National University (ANU) and the Universities Space Research Association (USRA). We are indebted to the dedicated efforts of our many colleagues here who together have demonstrated that infrared astronomy can indeed be conducted from the Antarctic plateau.

References

Ashley, M. C. B. et al., 1996, PASP, 108, 721
Brooks, K. J. et al., 2000, MNRAS, 319, 95
Burton, M. G. et al., 1994, PASA, 11, 127
Burton, M. G. et al., 2000, ApJ, 542, 359
Cox, P. & Bronfman, L., 1995, A&A, 299, 583
Chamberlain, M. A. et al., 2000, ApJ, 535, 501
Clenet, Y. et al., 2001, A&A, 376, 124
Fowler, A. et al., 1998, Proc. SPIE., 3354, 1170
Haisch, K. E., Lada E. A., Lada C. J., 2000, AJ, 120, 1396
Haisch, K. E., Lada, E. A., Lada, C. J., 2001, ApJL, 553, L153
Hereld, 1990, Proc. SPIE, 1235, 43
Hidas, M. G. et al., 2000, PASA, 17, 260
Hollenbach D., Tielens A. G. G. M., 1997, ARA&A, 35, 179
Jackson, J. M. et al., 1999, BAAS, 194, 7117
Kenyon, S. J., Gómez, M., 2001, AJ, 121, 2673
Kenyon, S. J., Hartmann L. W., 1995, ApJS, 101, 117
Lada, C. J. et al., 2000, ApJ, 120, 3162
Lyo, A.–R. et al., 2003, MNRAS, 338, 616
Marks, R. D., 2002, A&A, 385, 328
Marks, R. D. et al., 1996, A&AS, 118, 385
Masetti, N. et al., 2000, A&A, 354, 473
Nguyen, H. et al., 1996, PASP, 108, 718
Phillips, A. et al., 1999, ApJ, 527, 1009
Rathborne, J. M. et al., 2003, in preparation
Rathborne, J. M. et al., 2002, MNRAS, 331, 85
Rauscher, B. J. et al., 1998, ApJ, 506, 116
Severson, S. 1998, PhD thesis, University of Chicago

Highlights of Astronomy, Vol. 13
International Astronomical Union, 2003
O. Engvold, ed.

The AST/RO Survey of the Galactic Center Region

Antony A. Stark

Smithsonian Astrophysical Observatory, 60 Garden St. MS 12, Cambridge, MA 02138 USA

Abstract. AST/RO is a 1.7m diameter submillimeter-wave telescope at the geographic South Pole. A key AST/RO project is the mapping of C I and CO $J = 4 \rightarrow 3$ and $J = 7 \rightarrow 6$ emission from the inner Milky Way (Martin et al. 2003). These data are released for general use.

The Antarctic Submillimeter Telescope and Remote Observatory (AST/RO) is a 1.7 m diameter single-dish instrument which has been observing in the submillimeter-wave atmospheric windows for eight years (Stark et al. 2001, Stark 2003). Essential to AST/RO's capabilities is its location at Amundsen-Scott South Pole Station, an exceptionally cold, dry site which has unique logistical opportunities and challenges. Observing time on AST/RO is available on a proposal basis.

The distribution of molecular gas in the Galaxy is known from extensive and on-going surveys in CO and ^{13}CO $J = 1 \rightarrow 0$ and $J = 2 \rightarrow 1$; these are spectral lines which trace molecular gas. These lines alone do not, however, determine the excitation temperature, density, or cooling rate of that gas. Observations of C I and the mid-J lines of CO and ^{13}CO provide the missing information, showing a more complete picture of the thermodynamic state of the molecular gas, highlighting the active regions, and looking into the dense cores. AST/RO can measure the dominant cooling lines of molecular material in the interstellar medium: the $^3P_1 \rightarrow {}^3P_0$ (492 GHz) and $^3P_2 \rightarrow {}^3P_1$ (809 GHz) fine-structure lines of atomic carbon (C I) and the $J = 4 \rightarrow 3$ (461 GHz) and $J = 7 \rightarrow 6$ (807 GHz) rotational lines of carbon monoxide (CO). These measurements can then be modeled using the large velocity gradient (LVG) approximation, and the gas temperature and density thereby determined. Since the low-J states of CO are in local thermodynamic equilibrium (LTE) in almost all molecular gas, measurements of mid-J states are critical to achieving a model solution of the radiative transfer by breaking the degeneracy between beam filling factor and excitation temperature.

Among the key AST/RO projects is mapping of the Galactic Center Region. Sky coverage as of 2002 is $-1^\circ\!.3 < \ell < 2^\circ$, $-0^\circ\!.3 < b < 0^\circ\!.2$ with $0'\!.5$ spacing, resulting in spectra of 3 transitions at 24,000 positions on the sky. Kim et al. (2002) and Martin et al. (2003) describe the data, which are available on the AST/RO website[14] for general use. The C I emission has a spatial extent similar to the low-J CO emission, but is more diffuse. The CO $J = 4 \rightarrow 3$ emission is also found to be essentially coextensive with lower-J transitions of

[14] `http://cfa-www.harvard.edu/ASTRO`

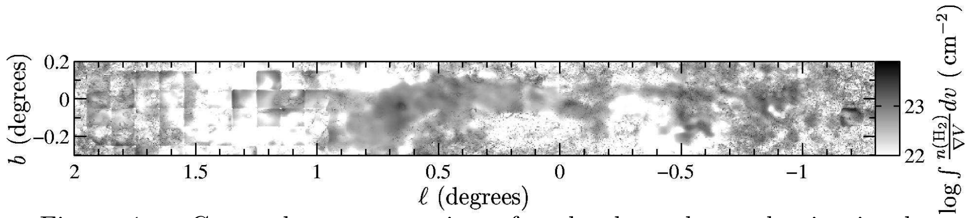

Figure 1. Greyscale representation of molecular column density in the Galactic Center Region, from an LVG model using AST/RO survey data (Martin et al. 2003).

CO, indicating that even the $J = 4$ state is in LTE most places; in contrast, the CO $J = 7 \rightarrow 6$ emission is spatially confined to far smaller regions. Applying an LVG model to these data together with data from the Bell Labs 7-m (Bally et al. 1988) yields maps of gas density and temperature as a function of position and velocity for the entire region. Kinetic temperature is found to decrease from relatively high values (> 70 K) at cloud edges to lower values (< 50 K) in the interiors. Typical pressures in the Galactic Center gas are $n(\mathrm{H_2}) \cdot T_{kinetic} \sim 10^{5.2}\,\mathrm{K\,cm^{-3}}$.

Above is a map of molecular hydrogen column density. It is often assumed that molecular hydrogen column density is proportional to the brightness of the $J = 1 \rightarrow 0$ CO line. The column densities estimated using AST/RO data deviate in places *by two orders of magnitude* from this simple assumption. These discrepancies are caused by variations in excitation and optical depth.

Galactic Center gas that Binney et al. (1991) identify as being on x_2 orbits has a density near $10^{3.5}\,\mathrm{cm^{-3}}$, which renders it only marginally stable against gravitational coagulation into one or two giant clouds (Elmegreen 1994). This suggests a relaxation oscillator mechanism for star bursts, where in-flowing gas accumulates in a ring at 300 pc radius for approximately 400 million years, until the critical density is reached, and the resulting instability leads to the sudden deposition of $10^7\mathrm{M_\odot}$ of gas onto the Galactic Center.

Acknowledgments. Support was provided by NSF grant OPP-0126090.

References

Bally, J., Stark, A. A., Wilson, R. W. & Henkel, C. 1988, ApJ, 324, 223

Binney, J., Gerhard, O. E., Stark, A. A., Bally, J. & Uchida, K. I. 1991, MNRAS, 252, 210

Elmegreen, B. G. 1994, ApJ, 425, L73

Kim, S., Martin, C. L., Stark, A. A. & Lane, A. P. 2002, ApJ, 580, 896

Martin, C. L., Walsh, W. M., Xiao, K., Lane, A. P., Walker, C. K. & Stark, A. A. 2003, ApJS, in press (`astro-ph0211025`)

Stark, A. A., et al. 2001, PASP, 113, 567

Stark, A. A. 2003, in "The Future of Small Telescopes in the New Millennium, Vol. II", ed. T. D. Oswalt (Kluwer Academic Publishers: Dordrecht), 269

Highlights of Astronomy, Vol. 13
International Astronomical Union, 2003
O. Engvold, ed.

Antarctic Cosmic Ray Astronomy

Marc Duldig

Australian Antarctic Division, Channel Highway, Kingston, Tasmania, 7050, Australia

Abstract. Cosmic ray observations related to Antarctica commenced in the austral summer of 1947-48 from sub-Antarctic Heard and Macquarie Islands and from the HMAS Wyatt Earp. Muon telescope observations from Mawson station, Antarctica, followed from 1955. The International Geophysical Year was the impetus for the installation of a number of neutron monitors around Antarctica, observing the lowest energy cosmic rays accessible by ground based instruments. In 1971 a new observatory was built at Mawson including the only underground muon telescope system at polar latitudes in either hemisphere. Over more than half a century, cosmic ray astronomy has been undertaken from Antarctica and its surrounding regions and these observations have been critical to our growing understanding of the heliosphere.

1. Introduction

Cosmic rays are fully ionized relativistic particles arriving outside the earth from beyond the solar system. On rare occasions the sun can be a source of cosmic rays. At the lowest energies (1–50 GeV) neutron monitors are employed to detect the radiation but these instruments have no directional capability. The viewing cone is defined by the particle trajectories through the geomagnetic field that can reach the atmosphere above the monitor. At higher energies ($\sim$10–1000 GeV) highly penetrating muons are produced in the atmospheric interaction and these may be detected by standard charged particle detectors arranged in multi-tray coincidence systems above or below ground. These muon telescopes effectively record the arrival direction of the initial cosmic ray above the atmosphere. For a discussion of the general properties of cosmic rays and their detection see Duldig (1994). The deflections experienced by cosmic rays traversing the heliomagnetic field can be used to tell us about the field's structures and its interactions with the local interstellar medium. The Antarctic platform provides a unique opportunity to study cosmic rays of low energy due to proximity to the magnetic pole and arrival directions not accessible from other places on earth.

2. Observations and Results

In the late 1940's Geoff Fenton began developing Geiger counters. He investigated the mid-latitude E-W effect from Hobart confirming the southern hemisphere showed the same effect as the north. Geiger counter telescopes and ionisation chambers were operated on the ship HMAS Wyatt Earp in the southern ocean and on the sub-Antarctic Heard and Macquarie Islands by groups from Melbourne and Tasmania Universities. Around 1950 Melbourne University withdrew from the cosmic ray observations in the sub-Antarctic. Muon telescopes were installed at Mawson in 1955, one year after the station opened and neutron monitors followed at several Antarctic stations in time for the IGY.

A large ground level enhancement (GLE) was observed in May 1960 with the global neutron monitor network. This resulted from acceleration of protons to cosmic ray energies associated with a flare on the Sun. The flare site was magnetically well connected to the earth and the Mawson observation of the response proved the existence of the Parker spiral field long before the in-situ measurement of the field by spacecraft (McCracken 1962). The discovery of the co-rotational anisotropy and its spectrum relied heavily on global observations and the Antarctic observations were critical to understanding the process.

In 1971 a new observatory was constructed at Mawson that includes the only underground muon observatory at polar latitudes. The underground telescopes were instrumental in the discovery of isotropic intensity waves by Jacklyn, Duldig & Pomerantz (1987). In a landmark study (Bieber & Chen 1991; Chen & Bieber 1993) used polar neutron monitors to derive cosmic ray gradients and mean free paths in the heliosphere. This work was extended by Hall, Duldig & Humble (1997) to higher energies by incorporating the muon telescopes' observations from Mawson and other sites. Nagashima, Fujimoto & Jacklyn (1998) challenged conventional wisdom with a new interpretation of the sidereal anisotropy response observed. Further work employing Mawson and other muon telescope observations by Hall et al (1999) elucidated the structure more precisely.

3. Summary

The Antarctic region has been critical to understanding the cosmic ray flux at earth. Over half a century of instrumental development and observations have led to a deepening understanding of the heliosphere. Now cosmic ray measurements are providing promising input into space weather prediction. The future of Antarctic cosmic ray astronomy seems to be as bright as ever.

References

Bieber, J. W., & Chen, J. 1991, ApJ, 372, 301

Chen, J., & Bieber, J. W. 1993, ApJ, 405, 375

Duldig, M. 1994, PASA, 11, 114

Hall, D. L., Duldig, M. L., & Humble, J. E. 1997, ApJ, 482, 1038

Hall, D. L., Munakata, K., Yasue, S., Mori, S., Kato, C., Koyama, M., Akahane, S., Fujii, Z., Fujimoto, K., Humble, J. E., Fenton A. G., Fenton, K. B., & Duldig, M. L., 1999, JGR, 104, 6737

Jacklyn, R. M., Duldig, M. L., & Pomerantz, M. A., 1987, JGR, 92, 8511.

McCracken, K. G., 1962, JGR, 67, 447

Nagashima, K., Fujimoto, K., & Jacklyn, R. M. 1998, JGR, 103, 17429

Highlights of Astronomy, Vol. 13
International Astronomical Union, 2003
O. Engvold, ed.

IceCube: A Kilometer-Scale Neutrino Observatory at the South Pole

Francis Halzen

Physics Department, University of Wisconsin, Madison, WI 53706, USA

Abstract. Solving the century-old puzzle of how and where cosmic rays are accelerated mostly drives the design of high-energy neutrino telescopes. It calls, along with a diversity of science goals reaching particle physics, astrophysics and cosmology, for the construction of a kilometer-scale neutrino detector. This led to the IceCube concept to transform a kilometer cube of transparent Antarctic Ice, one mile below the South Pole, into a neutrino telescope.

Whereas it has been realized for many decades that the case for neutrino astronomy is compelling (Gaisser, Halzen & Stanev 1995), the real challenge has been to develop a reliable, expandable and affordable detector technology to build the kilometer-scale telescopes required. Conceptually, the technique is simple. In the case of a high-energy muon neutrino, for instance, the neutrino interacts with a hydrogen or oxygen nucleus in deep ocean water and produces a muon travelling in nearly the same direction as the neutrino. The blue Cerenkov light emitted along the muon's kilometer-long trajectory is detected by strings of photomultiplier tubes deployed at depth shielded from cosmic radiation. Although IceCube can identify the secondaries produced by neutrinos of all flavors, muons with interaction lengths exceeding 10 km at the highest energies can be collected far outside the detector and therefore the ν_μ effective detector volume far exceeds the volume instrumented.

Elsewhere in these proceedings we have presented the case for kilometer-scale neutrino observatories (Halzen 2003). The first first-generation telescope, AMANDA II, is approaching an integrated flux sensitivity to TeV–EeV neutrinos of $\sim 0.05\,\mathrm{km}^2$ year. The instrument is sensitive to neutrino fluxes roughly equal to those emitted by the observed TeV gamma ray sources. It is too early to conclude whether first generation telescopes will discover sources of cosmic neutrinos, or whether it takes kilometer-scale observatories to see neutrinos associated with the enigmatic cosmic rays as anticipated by theoretical estimates. We do already know that it will take much larger detectors such as IceCube to study any sources that AMANDA II may discover.

IceCube (Wissing 2003) will consist of 80 kilometer-length strings, each instrumented with 60 10-inch photomultipliers spaced by 17 m. The deepest module is 2.4 km below the surface. The strings are arranged at the apexes of equilateral triangles 125 m on a side. The instrumented (not effective!) detector volume is a cubic kilometer. A surface air shower detector, IceTop, consisting of 160 Auger-style Cerenkov detectors deployed over $1\,\mathrm{km}^2$ above IceCube, augments the deep-ice component by providing a tool for calibration, background rejection and air-shower physics, as illustrated in the figure.

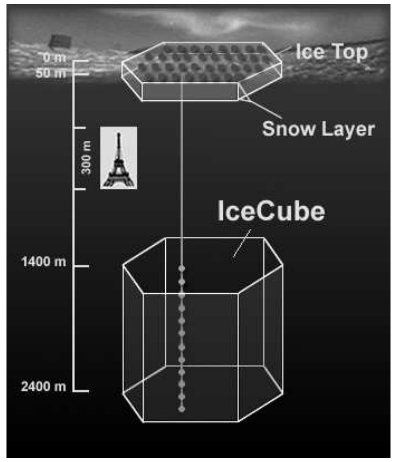

The transmission of analogue photomultiplier signals from the deep ice to the surface, used in AMANDA, has been abandoned. The photomultiplier signals will be captured and digitized inside the optical module. The digitized signals are given a global time stamp with a precision of $< 10\,\mathrm{ns}$ and transmitted to the surface. The digital messages are sent to a string processor, a global event trigger and an event builder.

Construction of the detector is expected to commence in the Austral summer of 2004/2005 and continue for 6 years, possibly less. The growing detector will take data during construction, with each string coming online within days of deployment. The data streams of IceCube, and AMANDA II, embedded inside IceCube, will be merged off-line using GPS time stamps.

IceCube will offer great advantages over AMANDA II beyond its larger size: it will have a higher efficiency and superior angular resolution in reconstructing tracks, map showers from electron- and tau-neutrinos (events where both the production and decay of a τ produced by a ν_τ can be identified) and, most importantly, measure neutrino energy. Simulations, backed by AMANDA data, indicate that the direction of muons can be determined with sub-degree accuracy and their energy measured to better than 30% in the logarithm of the energy. The direction of showers will be reconstructed to better than 10° above 10 TeV and the response in energy is linear and better than 20%. Energy resolution is critical because, once one establishes that the energy exceeds 1 PeV, there is no atmospheric muon or neutrino background in a kilometer-square detector and full sky coverage of the telescope is achieved. The background counting rate of IceCube signals is expected to be less than 0.5 kHz per optical sensor. In this low background environment, IceCube can detect the excess of anti-ν_e events from a galactic supernova.

References

Gaisser, T. K., Halzen, F. and Stanev, T. 1995,

Halzen, F. 2003, these proceedings

Wissing, H. 2003, PhD thesis (Humbold University, Berlin); Nucl. Inst. Meth. (to be published) and http://icecube.wisc.edu/science/sci-tech-docs/

Highlights of Astronomy, Vol. 13
International Astronomical Union, 2003
O. Engvold, ed.

Beyond Dome C

J.W.V. Storey, M.C.B. Ashley, M.G. Burton, and J.S. Lawrence

School of Physics, University of New South Wales, NSW 2052, Australia

Abstract. A well-focused research program over the past decade has shown that the South Pole has many remarkable characteristics that are particularly favorable for astronomy. These include the very cold, dry atmosphere and the vanishingly small free-air turbulence. Dome C, site of the new French/Italian station Concordia, has all of these attributes plus the added advantage of very low ground-level wind speeds. Higher on the plateau, locations such as the 4200 m high Dome A may well represent the ultimate ground based astronomical observing sites.

The exceptional conditions that make the Antarctic plateau so attractive to astronomers are well known. It is very cold (temperatures can drop below $-80\,^{\circ}$C) and reasonably high (Dome A is at 4200 m), leading to extremely low levels of precipitable water vapor and thermal emission from the sky.

What is less well know is that the ground-level wind speeds are also very low (2.8 m.s^{-1} average at Dome C) and that these winds remain low throughout the entire atmospheric column. This results in a very low turbulence, and that remaining turbulence is confined to a low (100 m scale) boundary layer.

The South Pole is now firmly established as one of the world's premier observing sites (Storey et al. 2002). Over the next few years, Concordia station is set to take its place as an equally attractive draw card for astronomers, as major facilities are constructed to complement those at South Pole.

However, it is natural to ask: what lies beyond? Almost 1 km higher than Dome C, Dome A can be expected to have essentially zero wind for much of the time and to have precipitable water vapor levels that can drop below 50 microns. These conditions would make possible a wide variety of experiments that are currently only possible from balloons, high-altitude aircraft, or space.

At the present time there is no infrastructure at Dome A, nor any well-defined plans to establish any. It is likely that any observatory to be placed there would be a robotic facility, serviced annually from the South Pole or a coastal station such as Davis. Adaptive-optics aside, modern astronomical instruments are vastly more complicated than the telescopes they are attached to. In a benign environment, such as exists at Dome A, it is reasonable to expect that a robotic telescope would be no more demanding to operate than any existing large-scale instrument at a conventional site.

With little turbulence and very low wind speeds, requirements for adaptive optics are dramatically simplified. It is likely that even large optical/IR telescopes would need only a simple tip-tilt or low order AO system, using just a single natural guide star.

The first step in the exploration of Dome A is to go there. It is remarkable that what is potentially the best astronomical site on earth has never been visited (although a Chinese traverse team have come close). An initial expedition should install an Automated Weather Station, plus additional micro-power instruments to measure cloud cover and boundary-layer turbulence.

The next step would be the installation of a comprehensive site-testing facility similar to the AASTINO (Lawrence et al. 2003). Running autonomously for a full year and communicating with the world via Iridium satellite, an AASTINO at Dome A would not only fully characterize the site but would also represent a prototype of the type of autonomous astronomical observatory that might ultimately be installed there.

A preliminary instrument suite to deploy to Dome A might include:

- an acoustic radar, to measure boundary-layer turbulence,
- a MASS (Multi-Aperture Scintillation Sensor), to measure the distribution of turbulence throughout the atmosphere,
- a mid-infrared spectrometer, to measure sky brightness and opacity from 3-30 micron,
- a sub-millimeter Fourier Transform Spectrometer to measure sky brightness and opacity,
- a near-infrared photometer, to measure sky brightness in the 2.35 micron "cosmological window".

Plans are already underway to include an exploration of the astronomical potential of Dome A as part of the International Polar Year of 2007. Regardless of what is discovered there, the well-established advantages of South Pole and Concordia Station will inevitably lead to a continued rapid expansion in the astronomical activities at those existing sites.

Ultimately, however, Dome A may prove to be simply irresistible.

References

Lawrence J.S., Ashley, M.C.B., Burton, M.G., Calisse, P.G., Dempsey, J.T., Everett, J.R., Maher, O., Storey, J.W.V., and Travouillon, T. 2003, The AASTINO: Automated Astrophysical Site Testing Invincible Observatory, Memorie della Societ Astronomica Italiana, in press

Storey, J.W.V., Ashley, M.C.B., and Burton, M.G., 2002, Antarctic site testing, in Astronomical site testing in the visible and radio range, ASP Conf. Series, Eds. Z. Benkhaldoun, Z., Munoz-Tunon, C. and Vernin, J., 266, 524

Highlights of Astronomy, Vol. 13
International Astronomical Union, 2003
O. Engvold, ed.

ACMSA: Antarctic Centre for Millimetre and Sub-millimetre Astrophysics

Giorgio Sironi

Physics Dept. - University of Milano Bicocca - Milano, Italy

Abstract.
A Working Group has been created to study the feasibility of ACMSA: Antarctic Center for Millimetric and Sub-millimetric Astrophysics, an international facility based at Dome Concordia (Dome C).

Tests made over the last ten years show that the Antarctic Plateau, an elevated and extended area, characterized by thin, dry and stable atmosphere, is the most convenient place for ground based observations of the sky at mm and sub-mm wavelengths. Better conditions can be found only in space.

Facilities for mm- sub-mm astronomy on the Antarctic Plateau have been so far available only at the Amundsen Scott base at South Pole, but are insufficient to satisfy the international community needs. To complement South Pole, a group of astrophysicists from Europe, Australia and USA (Olmi 2003) recently suggested the creation of a new mm and sub-mm facility at Dome C, ACMSA (the Antarctic Centre for Millimetric and Sub-millimetric Astrophysics). Here the expected observing conditions are even better that at South Pole. The French – Italian Dome Concordia base will soon become operational all year round.

To prepare a proposal for ACMSA a Working Group (WG) has been formed. The aim is a scientific and technical case which will: i) investigate how selected astrophysical and cosmological questions can be converted into coherent frontier science at sub-mm wavelengths, ii) propose facilities and experiments, iii) review existing facilities and experiments on the Antarctic Plateau and elsewhere, iv) study the state of the art technology available and the use of robotized systems and v)make cost evaluations. The WG will: a) inform the scientific community at large, b) look for collaborations, c) search for links with national and international organizations (French – Italian Concordia Program, European Polar Board, SCAR, IAU Antarctic Working Group, ESO, NSF etc.)

References

Olmi, L. 2003: Proc. of 'The Scientific Outlook for Astronomy and Astrophysics Research at the Concordia station'- Capri 2003 - Memorie SAIt : in press

Highlights of Astronomy, Vol. 13
International Astronomical Union, 2003
O. Engvold, ed.

The Case for a 30m Diameter Submillimeter Telescope on the Antarctic Plateau

Antony A. Stark

Smithsonian Astrophysical Observatory, 60 Garden St. MS 12, Cambridge, MA 02138 USA

Abstract. A large single-dish submillimeter-wave telescope equipped with a focal plane array containing $\sim 10^4$ bolometers and costing about \$120M could locate most protogalaxies in the southern sky within a year of operation.

Many of the telescopes planned for the next few decades are designed to observe high-redshift galaxies in the process of formation (NRC 2001). These instruments, such as the James Webb Space Telescope (JWST), the Overwhelmingly Large Telescope (OWL), and the Atacama Large Millimeter Array (ALMA), will have sufficient sensitivity and resolution to observe detailed structure within protogalaxies; they will not, however, have sufficient field of view to survey large areas of sky and discover objects to study. Consider, for example, the ALMA. As seen in Figure 1, protogalaxies typically have a flux density at $\lambda 450\mu$m which is $\lesssim 10$ mJy. The ALMA can detect such a source in 3 minutes of observing time. That's really fast. The size of an ALMA map, however, is $\sim 2 \times 10^{-5}$ square degree, so to survey a square degree at this sensitivity would require ~ 100 days. If the ALMA were dedicated to a sky survey for ten years, it would be able to cover about 10^{-3} of the entire sky.

A 30-m submillimeter-wave telescope operating on the Antarctic Plateau with a focal-plane array of bolometers would be able to survey the southernmost $\frac{1}{3}$, of the sky in a year. Observatory sites on the Antarctic Plateau have exceptional submillimeter-wave sky transparency and stability (Chamberlin 2001, Peterson et al. 2003). Technological progress in submillimeter-wave detectors will make possible focal-plane arrays containing many thousands of bolometers. A 10-meter class single-dish telescope designed for such arrays and located at the South Pole has been approved, and construction is expected to begin this year (Stark 2003). Looking ahead, a 30-meter class telescope could be made sufficiently accurate for submillimeter and far-infrared work through a modest application of active surface techniques. A basic design similar to the IRAM 30-m could be combined with crude active control of the primary mirror panel alignment for a total cost of $\sim$ \$120M. The $2''$ to $5''$ beam size of such a telescope would be well-coupled to protogalaxies. With a field of view $\sim 10^{-1}$ square degree in size, this instrument could survey the entire sky south of $\delta \approx -25^\circ$ with 1 mJy sensitivity in a year. Almost all protogalaxies and protostellar cores would be found, and could be distinguished on the basis of $\lambda 350\mu$m to $\lambda 450\mu$m color. The resulting catalog would be a treasure trove of objects for high-resolution study with the giant telescopes to come.

Acknowledgments. Support was provided by NSF grant OPP-0130612.

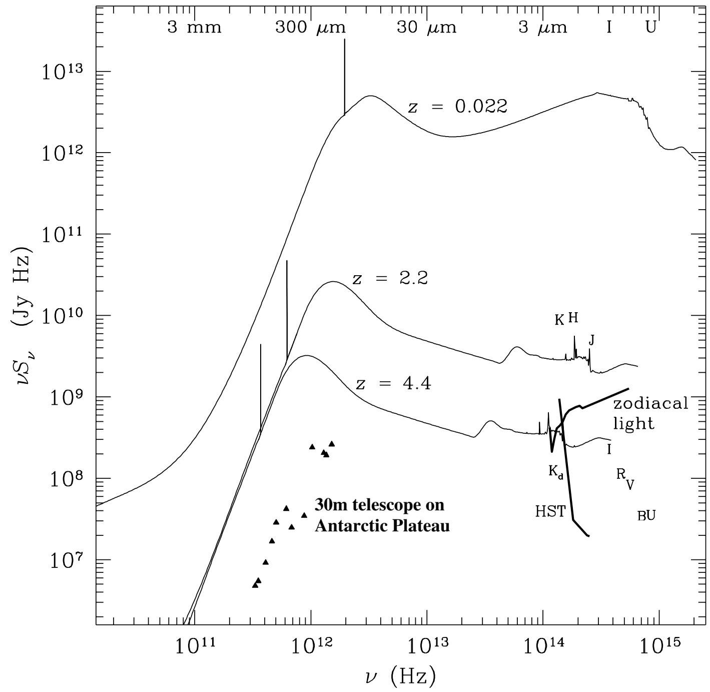

Figure 1. Normal galaxies at low and high redshift. The broad-band galaxy spectrum labeled $z = 0.022$ has the luminosity and spectrum of M99, a normal L^* spiral. The spectra labeled $z = 2.2$ and $z = 4.4$ are models of the initial star burst in such a galaxy at two possible eras, evolved in a standard CDM model (Katz 1992) with $h_{75} = 1$ and $\Omega = 1$. The 158μm C^+ line is shown to scale; other lines are suppressed. The points KHJIRVBU are 1% of the sky brightness in a square arcsecond at Mauna Kea (CFHT Observer's Handbook). The point K_d is 1% of the sky brightness in a square arcsecond at the South Pole at $\lambda 2.3\mu$m. The curve labeled HST is the limiting sensitivity of the NICMOS on the Hubble Space Telescope. The triangles show the continuum sensitivity in one hour of a 30 meter Antarctic telescope in the submillimeter-wave atmospheric windows (Stark 1997).

References

Chamberlin, R. A. 2001, JGR: Atmos., 106 (D17), 20101

Katz, N. 1992, ApJ, 391, 502

NRC 2001, "Astronomy and Astrophysics in the New Millennium", (National Research Council: National Academy Press)

Peterson, J. B., Radford, S. J. E., Ade, P. A. R., Chamberlin, R. A., O'Kelly, M. J., Peterson, K. M., and Schartman, E. 2003, PASP, 115, 383

Stark, A. A. 1997, ApJ, 481, 587

Stark, A. A. 2003 in "Proceedings of the Fourteenth International Symposium on Space Terahertz Technology" ed. C. K. Walker (`astro-ph0305570`)

Highlights of Astronomy, Vol. 13
International Astronomical Union, 2003
O. Engvold, ed.

Extremely Large Telescopes on the Antarctic plateau

J.S. Lawrence

School of Physics, University of New South Wales, NSW 2052, Australia

Abstract. The primary limitation to the performance of any large ground-based telescope is the atmospheric properties of its site, particularly the sky emission and the turbulence structure. There are several sites on the Antarctic plateau (South Pole, Dome C and Dome A) for which the increase in infrared sensitivity relative to a mid-latitude site should be as much as two orders of magnitude. The unique turbulent structure above Dome C indicates that an extremely large telescope equipped with only a natural guide star adaptive optics system should achieve equivalent resolution to a mid-latitude extremely large telescope with a multi-conjugate multi-laser guide star system.

Experimental data from a number of instruments, eg (Phillips et al. 1999), has shown that the winter time thermal sky emission above the South Pole station is as much as two orders of magnitude lower than found anywhere else on Earth. Additionally, data from radiosonde balloons measuring temperature and relative humidity have shown that the South Pole average winter time precipitable water vapor column density is 0.25 mm (Chamberlain et al. 2001). This is significantly lower than found at good quality mid-latitude sites such as Mauna Kea (1.6 mm average).

These factors result in a South Pole telescope being substantially more sensitive in the near to far-infrared than any other ground based telescope of the same size. The increased atmospheric transparency also results in a number of new windows opening up in the sub-millimetre and far-infrared.

There are several other sites on the Antarctic plateau that offer potentially superior sensitivity to even South Pole. These include the French/ Italian Dome C station at an elevation of 3250 m, and Dome A, the highest point on the plateau at an elevation of 4200 m. Atmospheric models for these high plateau sites have been developed based on temperature, pressure, and water vapor profiles inferred from South Pole aerological records, and high plateau Automatic Weather Station data. These models (giving atmospheric emission and transmission, and incorporating a telescope emission component) show that the relative increase in telescope sensitivity in going from South Pole to Dome A is largest in the near infrared, where a factor of 5-10 is expected. The benefits of a reduced atmospheric emission in the mid-infrared are somewhat offset by the significant contribution from telescope emission at these wavelengths. In the far-infrared and sub-millimetre, the lower water vapor expected at the higher sites results in a dramatic increase in atmospheric transparency compared with South Pole.

While the benefits of the South Pole low infrared sky background are well recognized, and the unique atmospheric turbulence profile (the majority of turbulence is confined within the lowest 300 m) is potentially beneficial for some applications, the ground level seeing is relatively poor (1.8 arcsec in the visible) compared with quality mid-latitude sites. However, the local topography of the high plateau sites (both Dome A and Dome C lie on high points of the plateau) indicates that the turbulence within the ground level inversion layer should be lower in magnitude than observed at the South Pole due to the absence of katabatic winds. The integrated ground level seeing during summer at Dome C was shown to be a median of 1.2 arcsec (Aristidi et al. 2003). The boundary layer turbulence is observed to drop below the detection threshold for a sonic radar instrument operating throughout winter of 2003, representing a contribution to the total seeing of less than 0.2 arcsec (Travouillon et al, in preparation 2003).

These results are used to define upper and lower bounds to the refractive index structure function profile for Dome C assuming that the contribution from the free-atmosphere to the total turbulence is the same as found at the South Pole. These profiles give an isoplanatic angle of greater than 10 arcsec, which is significantly larger than found at other sites (typically 2 arcsec at Mauna Kea). Additionally, the lack of strong winds observed throughout the Dome C atmosphere result in an atmospheric coherence time than is much longer than found elsewhere. These two factors (isoplanatic angle and coherence time) represent a serious limitation to the performance of any adaptive optics system on an extremely large telescope, and drive the need for multi-conjugate systems with many deformable mirrors and laser guide stars at mid-latitude sites.

An error budget for a 30 m telescope at Dome C has been calculated and compared with that specified for the 30 m CELT situated at Mauna Kea. The Dome C telescope, equipped with a single natural guide star system should achieve a wavefront error of 180-250 nm rms. This is equivalent to a multi-conjugate, multi-laser guide star system operating with a Mauna Kea atmosphere, and is a significant improvement over the single low order adaptive optics error of 500 nm rms. It should be noted that the turbulence profiles modeled here represent a conservative estimate of the isoplanatic angle at Dome C. It will be at least another two years until the atmospheric profile throughout winter is confirmed.

The improvements in sensitivity and resolution achievable by locating an extremely large telescope at Dome C rather than a mid-latitude site are so substantial that they could compensate for any logistical disadvantage. Additionally, factors such as the very low ground wind speed, and the non-existent seismic activity are very important for mechanical and structural considerations.

References

Aristidi, E., Agabi, E., Vernin, J., Azouit, M., Martin, F., Ziad, A., and Fossat, E. 2003, A&A, 406, L19

Chamberlain, R. A. 2001, J. Geophys. Research, 106, 20101

Phillips, A., Burton, M.G. , Ashley, M.C.B., Storey, J.W.V., Llyod, J.P., Harper, D.A., and Bally, J. 1999, AJ, 527, 1009

Highlights of Astronomy, Vol. 13
International Astronomical Union, 2003
O. Engvold, ed.

A Large Reflective Schmidt Telescope for Antarctica

Will Saunders and Andrew McGrath

Anglo-Australian Observatory

Abstract. We present a simple design for a 16 metre, wide-field, fixed-axis, all-reflective, low cost f/4 Schmidt telescope to take advantage of the unique advantages of Antarctica as an Optical/IR site.

1. Introduction

Antarctica offers compelling advantages for Optical/IR astronomy, over and above the well-recognized gains of high transparency and low background.

1. It offers the unique possibility of single natural guide star AO-corrected observations over large fields-of-view. As well as allowing AO-corrected observations over much more of the sky, this opens up a whole new field of genuinely wide-field imaging at high spatial resolution.

2. The low temperatures remove most of the difficulties of IR telescope and camera optimization, allowing simpler and more general purpose designs.

3. ELT designs and costs are driven primarily by engineering considerations. The low wind speeds and seismic activity in Antarctica dramatically reduce the engineering difficulties.

In general, Schmidt telescopes offer the best optical quality and efficiency, over the largest possible fields of view, with the smallest possible number of elements. The Chinese 4m LAMOST design (www.lamost.org) shows how to build a big Schmidt — the axis is fixed, the corrector lens is replaced with a deformable segmented plain mirror, which corrects for spherical aberration as well as directing the light onto the fixed segmented spherical primary. The design is cheap and scale able. The speed is limited by the tilt on the corrector, which takes it away from the ideal, classical Schmidt position.

2. Proposed design

- LAMOST-style, horizontal axis, transit telescope. Can reach to equator and South Pole from Dome-C (75°S).
- 16m aperture, f/4, length 125m; Plate scale $300\mu\text{m}/''$ to match $0.1''$ seeing.
- Segmented flat corrector mirror: steerable and deformable at 100μm level.
- Primary mirror fixed, spherical, segmented, phased.
- Partial vignetting at very large and very small elevations.
- Raised on 10-30m high ice pyramids (not shown) to get above ground-level turbulence.
- Shack-Hartmann module determines corrector Schmidt deformations; also corrects for tracking errors, windshake, mechanical sag; also provides adaptive wave-

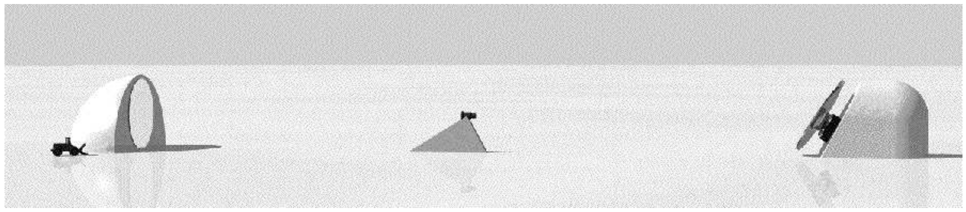

Figure 1. Proposed layout for 16m Antarctic reflective Schmidt telescope

front correction at up to 100Hz (fast enough for Antarctica).
- Focal stations: f/4 prime focus; and f/13, f/40 Cassegrain foci.
- IR uses baffles and Narcissus mirrors but no cold-stop. Increase in sky noise (over a perfect cold-stop) is few % at K_{dark} (2.3μm) and few tens of % at L (3.5μm).
- Can easily guide to R=14.2, can always find guide stars at Prime, and usually at Cassegrain $f/13$, and over $\sim 10\%$ of the sky at $f/40$.
- Guesstimated cost at this stage (based on Hobby-Eberly, SALT, Keck) US\$100M-200M vs $\sim$US\$500M for other 25m-class ELT's.

3. Focal stations and image quality

- $f/4$ Prime Focus MOS: curved field plate: 300μm/$''$, $0.2''$ fwhm over 3°
- $f/4$ Prime Focus for imaging: flat-field, $0.05''$/pixel, $0.06''$ fwhm over 0.5°
- $f/13$ Cassegrain Focus: $0.015''$/pixel, $0.025''$ fwhm over $4.5'$
- $f/40$ Cassegrain Focus: $0.005''$/pixel, $0.015''$ fwhm over $1.5'$

4. Science Drivers

At Prime Focus, the $A\Omega$ (Collecting Area $\times$ Solid Angle) for this design is 1-2 orders of magnitude larger than existing or proposed telescopes. For all thermal IR work, it would also be an order of magnitude more sensitive than other 25m-class ELT's, or NGST. Science drivers would include:

Wide-field Optical/NIR imaging at $0.1''$ fwhm: HDF-quality images over many square degrees. Complete evolution history of galaxies; LSS via lensing; stellar census in the Milky Way; stellar populations in nearby galaxies; in general, finding rare, faint objects.

Multiplexed fiber spectroscopy over 3° fields: combination of aperture and FOV unparalleled for virtually all multi-object spectroscopy.

At Cassegrain, the image quality is as good as NGST or other proposed ELT's in the IR, but offers the prospect of AO corrected optical imaging, and either way do this over $1.5' - 5'$ fields. Such a telescope could be expected to dominate 'deep fields' Optical/IR astronomy, high resolution optical astronomy, and all IR astronomy of faint objects.

Highlights of Astronomy, Vol. 13
International Astronomical Union, 2003
O. Engvold, ed.

Adaptive Optics and Interferometry on the Antarctic Plateau

James P. Lloyd

California Institute of Technology, Pasadena, CA

Abstract. The unique properties of atmospheric turbulence in atmosphere above the Antarctic plateau offer some compelling advantages for astronomical adaptive optics and interferometry. The shallow nature of the turbulent layer at the South Pole results in low scintillation and large angular coherence (Marks et al. 1996, 1999; Lloyd, Oppenheimer, & Graham 2002; Lloyd et al. 2003). Recent wintertime SODAR measurements at Dome C indicate that similar conditions exist at Dome C, but that the turbulent layer is likely both weaker and shallower. This paper discusses the outcomes of such conditions on the atmospheric properties for astronomy. Particularly due to the low wind speed at Dome C, the atmospheric properties are highly favorable for adaptive optics and interferometry. The resulting long coherence time enables adaptive optics at visible wavelengths, and the large angular coherence results in a useful field of view as a result.

Estimating the turbulence parameters at Dome C

The possibility of "Super-Seeing" in the Antarctic was first suggested by Gillingham (1993). The smooth topography, suppressed diurnal cycle, and low wind speeds strongly suggest that the mechanisms that generate turbulence at mid-latitude sites might be absent, resulting in excellent seeing. Indeed, this has been verified to be the case at the South Pole (Marks et al. 1996, 1999) above the $\approx$ 200m boundary layer. The boundary layer at the South Pole has been extensively studied, and is well characterized by SODAR studies (Travouillon et al. 2002, 2003).

The relatively poor seeing at the South Pole results from the mixing of cold air in thermal contact with the radiatively cooling ice with warmer air from the free atmosphere. Above this layer, the atmosphere is very close to adiabatic, resulting in little optical turbulence, even in the presence of mechanical turbulence. Further, the absence of high velocity winds, such as created by subtropical jet-streams results in lower amplitude, and lower velocity turbulence. The turbulence strength and height in the boundary layer are driven by the ground layer wind speed. It is therefore likely that sites higher than the South Pole, which do not suffer from the same katabatic windspeeds would not suffer the same poor seeing. Indeed this appears to be verified by the preliminary results of wintertime SODAR observations at Dome C (Travouillon 2003).

For the purposes of exploring the potential scientific niches available at Dome C, a toy C_N^2 profile is useful. Mean wind speeds at Dome C are typically a factor of three lower than South Pole, and the boundary layer height is plausibly a factor of three lower. Applying these scaling factors to the South Pole model of

Lloyd et al. (2002) provides an estimate (though not necessarily quantitatively correct) of possible seeing and adaptive optics parameters at Dome C, using the definitions of Hardy (1998) are shown in Table 1. Such parameters would open "a new window" at Dome C for visible wavelength adaptive optics with substantial fields of view. The isoplanatic angle and focal anisoplanitism parameters require verification of the upper atmosphere turbulence properties, but the exceptionally long coherence time is an almost inevitable outcome of the low wind speeds.

Site	r_0	f_G	θ_0	NGS d_0 (10 km)	LGS d_0 (90 km)
Mauna Kea	20 cm	80 Hz	1.6"	0.7 m	2.9 m
South Pole	6 cm	35 Hz	34"	6.4 m	47 m
Dome C	20 cm	2.5 Hz	380"	62 m	514 m

Acknowledgments

This work has been supported in part by the NSF Center for Adaptive Optics, managed by UC Santa Cruz under cooperative agreement No. AST-9876783.

References

Gillingham, P. 1993, in Optics in Astronomy: 32nd Herstmonceux Conference, 244+

Hardy, J. W., ed. 1998, Adaptive optics for astronomical telescopes (Oxford University Press)

Lloyd, J. P., Lane, B. F., Swain, M. R., Storey, J. W. V., Travouillon, T., Traub, W. A., & Walker, C. K. 2003, in Techniques and Instrumentation for Detection of Exoplanets, proc. SPIE 5170, *in press*

Lloyd, J. P., Oppenheimer, B. R., & Graham, J. R. 2002, Publications of the Astronomical Society of Australia, 19, 318

Marks, R. D. 2002, A&A, 385, 328

Marks, R. D., Vernin, J., Azouit, M., Briggs, J. W., Burton, M. G., Ashley, M. C. B., & Manigault, J. F. 1996, A&AS, 118, 385

Marks, R. D., Vernin, J., Azouit, M., Manigault, J. F., & Clevelin, C. 1999, A&AS, 134, 161

Travouillon, T. 2003, *priv. comm.*

Travouillon, T., Ashley, M. C. B., Burton, M. G., Calisse, P. G., Everett, J. R., Lawrence, J. S., & Storey, J. W. V. 2002, in SF2A-2002: Semaine de l'Astrophysique Francaise, 19–+

Travouillon, T., Ashley, M. C. B., Burton, M. G., Storey, J. W. V., & Loewenstein, R. F. 2003, A&A, 400, 1163

Highlights of Astronomy, Vol. 13
International Astronomical Union, 2003
O. Engvold, ed.

The Antarctic Planet Interferometer

Mark R. Swain

Jet Propulsion Laboratory, Pasadena, CA

Abstract.
The Antarctic Planet Interferometer (API) is a concept for an infrared interferometer located at the best accessible site on Earth. Infrared interferometry is strongly effected by both the strength and vertical distribution of thermal and water vapor turbulence. The combination of low temperature, low wind speed, low elevation turbulence, and low precipitable water vapor make the Concordia base at Antarctic Dome C the best accessible site on Earth for infrared interferometry. The improvements in interferometer sensitivity with respect to other terrestrial sites are dramatic; an interferometer with two meter class telescopes could make unique infrared measurements of extra solar planets that might otherwise only be possible with a space-based interferometer.

Unique Science from Earth; A Stepping Stone to Space

A number of spatial interferometry techniques are being developed for measurements of extra-solar planets including high-precision V^2, differential-phase, nulling, and astrometry. The unique properties of the Antarctic atmosphere at Dome C likely improve all of these techniques, compared to other terrestrial sites. Estimates for the performance gains for infrared interferometry at Dome C (Swain et al. 2003a) and at the South Pole (Lloyd et al. 2002, 2003) imply order of magnitude or better improvements are possible. These estimates are based on extensive site testing data including measurements of the turbulence profile (Marks et al. 1996, 1999; Marks 2002; Travouillon et al. 2003).

In addition to unique measurements of extra-solar planets, such as characterization of Jovian-class extra-solar planets in the habitable zone, an infrared Antarctic interferometer would be capable of other ambitious science programs (Swain et al. 2003a) such as:

- Distance scale - measurement of binary star orbits in LMC.
- Mass transfer in compact binary systems.
- YSO and proto-planetary disk formation.
- Active galactic nuclei.
- Accretion disk structure and evolution.

Recent observations with the Keck interferometer (Swain et al. 2003b) have marginally resolved what is likely infrared emission from the accretion disk in NGC 4151. Modest improvements in sensitivity and angular resolution, easily achievable with API, would allow measurements of the structure and evolution of the accretion disk in similar objects.

There are additional advantages of an Antarctic plateau location. The long night results in good instrument thermal stability. Most of the sources observed would be circumpolar, allowing extremely long, continuous observations not possible from other locations. These sources would also be excellent targets for interferometric synthesis imaging as they permit full rotation of the interferometer sampling function.

Further, because of similar science goals to projects such as DARWIN and TPF and a space-like environment (due to the extreme temperatures and remote location), the API, located at the Concordia base, could serve as a natural technology development test bed for these missions. When operating at 200 μm, API would also be an excellent prototype for the proposed SPECS mission (Leisawitz et al. 2000). In addition to producing unique and compelling science, an Antarctic infrared interferometer would serve as a precursor for future space-based interferometers.

Acknowledgments

This work was performed at the Jet Propulsion Laboratory, California Institute of Technology, under a contract with the National Aeronautics and Space Administration.

References

Leisawitz, D. T., et al. 2000, *Proc. SPIE*, 4013, 36

Lloyd, J. P., Lane, B. F., Swain, M. R., Storey, J. W. V., Travouillon, T., Traub, W. A., & Walker, C. K. 2003, in Techniques and Instrumentation for Detection of Exoplanets, proc. SPIE 5170, *in press*

Lloyd, J. P., Oppenheimer, B. R., & Graham, J. R. 2002, Publications of the Astronomical Society of Australia, 19, 318

Marks, R. D. 2002, A&A, 385, 328

Marks, R. D., Vernin, J., Azouit, M., Briggs, J. W., Burton, M. G., Ashley, M. C. B., & Manigault, J. F. 1996, A&AS, 118, 385

Marks, R. D., Vernin, J., Azouit, M., Manigault, J. F., & Clevelin, C. 1999, A&AS, 134, 161

Swain, M. R., Coude du Foresto, V., Fossat, E., Vakili, F. 2003a, Mem. S.A. It.,73, 23.

Swain, M. R., et al. 2003b, ApJ, accepted.

Travouillon, T., Ashley, M. C. B., Burton, M. G., Storey, J. W. V., & Loewenstein, R. F. 2003, A&A, 400, 1163

Highlights of Astronomy, Vol. 13
International Astronomical Union, 2003
O. Engvold, ed.

High Angular Resolution Mid-IR Astronomy at Concordia

Marco Ferrari-Toniolo

C.N.R. - Istituto Astrofisica Spaziale e Fisica Cosmica (IASF)

If we concentrate our attention on the study and the evolution of star forming processes rather than on the large scale structure, from the recent use of Large Telescopes in this context there are many examples of great interest. These include the study of the early phases of aggregation of matter (stellar and planet formation), and the late phases of disaggregation during stellar evolution. In Fig 1, a spectacular example is shown of a high resolution image of an edge–on circumstellar disk of a young star (HR4796A), with respect to previous less resolved information (C.Telesco et al, Proc SPIE 4834, 101, 2002). A recent hypothesis of a Large Infrared Telescope called GTA (Grande Telescopio Antartico) has been proposed to the PNRA (Italian Plan for Antarctic Researches). This will require the following characteristics: high angular resolution in the mid-IR domain (large aperture); very high sensitivity (mainly due to the cold, dry conditions of the site); extreme simplicity in design and operational modes. The telescope will be a survey instrument and will be used almost without human intervention. The project examines the construction of a third tower at Dome C with the telescope configured to work in quasi-drift-scan without moving the enclosure and with a limited tracking time. In Fig 1, a sketch of the tower hosting the telescope is shown (M.F-T. et al, Proc SPIE 4836, 165, 2002). A study will be developed to determine the optimum configurations for observing in different bands, from the optical to the sub-mm range, with a refurbishment of the telescope and instrumentation during the summer break.

We expect there to be great gains in sensitivity from the GTA with respect to the new class of Large Telescopes operating with similar angular resolution; more detailed studies can be accomplished by the large 'temperate' Telescopes by using more sophisticated instrumentation (spectrometers, polarimeters, coronographs etc.). Even more interesting could be the use of GTA in conjunction with the LBT or other facilities for ground-based interferometry, or with respect to the ultra-high sensitivity images expected from the future IR space missions- the GTA data will be of great help for addressing and analyzing both the space and the interferometric data. The GTA seems to be also an unavoidable step for future ELT projects.

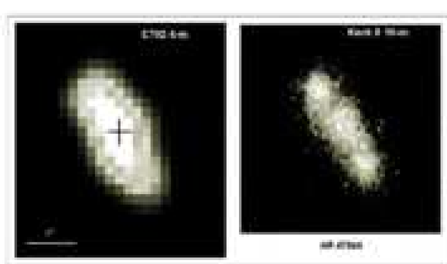

Highlights of Astronomy, Vol. 13
International Astronomical Union, 2003
O. Engvold, ed.

An AST/RO Survey of the Coalsack

Wilfred Walsh and Kecheng Xiao

Harvard–Smithsonian Center for Astrophysics, 60 Garden St, MS12, Cambridge MA 02138, USA

Abstract. Selected regions of the southern molecular cloud complex, the Coalsack are being imaged at sub-millimeter wavelengths using the Antarctic Sub-millimeter Telescope and Remote Observatory (AST/RO) located at the South Pole.

The Coalsack is one of the most prominent naked-eye features of the Southern sky, covering about 30 square degrees adjacent to the Southern Cross with 0.7-0.24 mag of extinction. Its proximity (about 180pc) make it an ideal candidate for studying the structure, composition and dynamics a large molecular cloud. Unlike other prominent dark clouds, the Coalsack has generally been thought to show no evidence of collapse leading to star formation. We have selected regions of the Coalsack to image at submillimeter wavelengths: this work is currently in progress. The AST/RO observations consist of a fully-sampled survey in the 230GHz CO(2-1) line over the entire extent of the Coalsack, together with smaller regions imaged in other CO isotopomers and the 461GHz CO(4-3) and 492GHz CI lines. We have already detected extended CO(4-3) emission at several locations. A preliminary LVG model for one position suggests that localized warm (25K) gas does exist in the Coalsack and that collapse leading to star formation, if not already occurring, may be imminent.

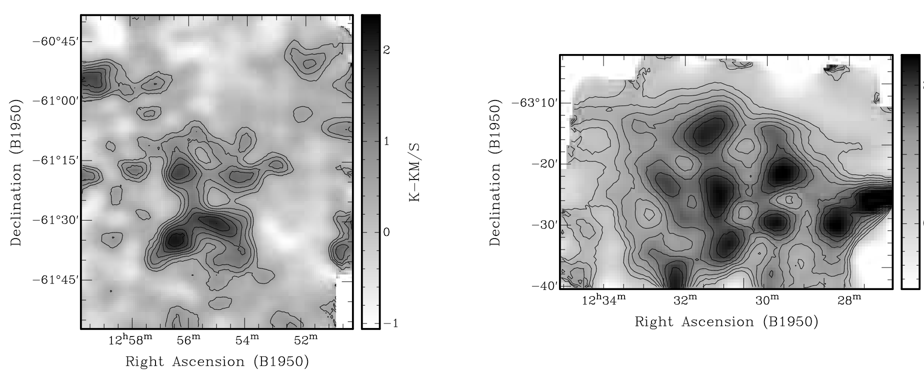

Figure 1. Two regions of the Coalsack imaged in the CO(4-3) line, shown with contours from 0.5 to 2.0 K km/s in 0.25 K km/s steps.

Highlights of Astronomy, Vol. 13
International Astronomical Union, 2003
O. Engvold, ed.

Helioseismology from South Pole: Past, Present and Future

Stuart M. Jefferies

Maui Scientific Research Center, University of New Mexico, 590 Lipoa Parkway, Ste 262, Kihei, HI 96753, USA

Abstract. The austral summer of 2002/03 marked the beginning of a new era for helioseismology from South Pole with the running of an experiment to seismically probe the solar atmosphere.

Helioseismology experiments conducted at South Pole over the period 1979 to 1995 provided several fundamental measurements of the properties of the solar interior including the internal sound speed and rotation profiles, and the sub-surface structure of a sunspot.

Today, thanks to these and other ground- and space-based helioseismology experiments, we have a good understanding of the overall properties of the solar interior. The Sun's atmosphere, however, is another story. This region of the Sun is not at all well understood (as evidenced by the lack of any reliable model). However, by observing the Sun at different heights in its atmosphere, and studying the behavior of the acoustic waves with frequencies above the acoustic cut-off frequency, it is possible to seismically map the properties of the atmosphere in an analogous way to that used for the interior (Jefferies 1998). Such maps will provide a strong constraint for any theoretical model of the atmosphere. The austral summer of 2002/03 saw the first multi-line observations at South Pole, with a double magneto-optical filter instrument being used to measure the velocity signals simultaneously in the photosphere and low chromosphere. These data have provided the first maps of sound-speed variations in the Sun's lower atmosphere. The next step is to tomographically map the 3-D structure of the Sun's atmosphere and to examine the coupling of this structure to both the local sub-surface structure and the magnetic field in the atmosphere. The goal being to better understand how and why the Sun varies and how the Sun drives space weather. The next generation of instrumentation has therefore been designed to provide both improved spatial resolution in the vertical direction (by observing more absorption lines in the atmosphere) and simultaneous measurement of the magnetic field at different heights in the atmosphere.

Acknowledgments. The author is supported by NSF award 0087541 from the Office of Polar Programs.

References

Jefferies, S. M. 1998, in IAU Symp. 185, New Eyes to See Inside the Sun, eds. F. L. deubner, J. Christensen-Dalsgaard & D. Kurtz (Dordrecht:Reidel), 415

Highlights of Astronomy, Vol. 13
International Astronomical Union, 2003
O. Engvold, ed.

CO 2–1 Mapping of WR16 with AST/RO

N. F. H. Tothill

Harvard-Smithsonian Center for Astrophysics, 60 Garden St, Cambridge, MA 02138, USA

A. P. Marston

SIRTF Science Center, IPAC, California Institute of Technology, Pasadena, CA 91125,USA

C. L. Martin, K. Leppik

Harvard-Smithsonian Center for Astrophysics

Abstract. Massive stars have profound effects on their surroundings, influencing them by their energetic stellar winds, and finally by supernova explosions. We present a CO 2–1 map of the surroundings of the Wolf-Rayet star WR16, taken with AST/RO at the South Pole, which shows some of these effects.

Marston et al. (1999) directly detected a cocoon of molecular gas in the CO 1–0 rotational line around the WN8 star WR16. They also presented evidence that that this material was in fact ejected from the star itself rather than being swept-up gas from the interstellar medium, but their study was limited by the relatively small extent of the CO map. We present an expanded map in CO 2–1 of the vicinity of WR16, on a square grid with $1.5'$ spacing, with the star at the origin of the map. There is a small cavity around the star, consistent with that seen in the CO 1–0 map, surrounded by molecular material. At the outside of the map, there are a number of much brighter clumps, which might be fragments of a wind-blown shell from an earlier phase of the star's evolution.

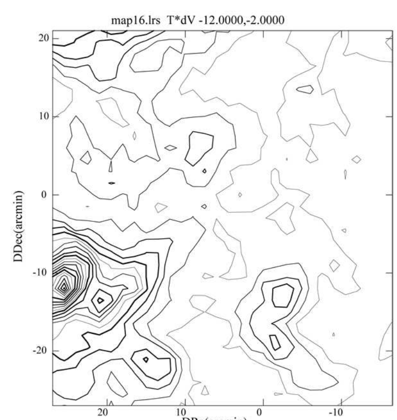

References

Marston, A. P., et al. 1999, ApJ, 518, 769

Highlights of Astronomy, Vol. 13
International Astronomical Union, 2003
O. Engvold, ed.

History of Astrophysics in Antarctica - A Brief Overview

Balthasar T. Indermuehle[†], Michael G. Burton[‡], Sarah T. Maddison[†]

[†]*Swinburne University, Centre for Astrophysics and Supercomputing, Hawthorn, VIC 3122, Australia*

[‡]*University of New South Wales, School of Physics, Sydney, NSW 2052, Australia*

On examining the historical development of astrophysical science at the bottom of the world from the early 20th century until today we find three temporally overlapping eras of which each has a rather distinct beginning. These are the eras of Astrogeology, High Energy Astrophysics and Photon Astronomy.[15]

1. Astrogeological Era (from 1912)

In 1912, Mawson discovered the Adelie Land Meteorite. Russian geologists found several meteorites of unrelated morphological types in the Lazarev region in 1961, giving rise to the ablation zone theory. This was followed in 1969 by the first formal meteorite search programme. Thousands of meteorites have since been found in Antarctica, mostly from glacial ablation zones.

2. High Energy Era (from mid 1950's)

In 1955, the first Antarctic astrophysical project was initiated with a cosmic ray detector installed at McMurdo station. A detector was installed at the South Pole in 1964 and others were commissioned at several national research stations. Today, cosmic rays with energies above 50 TeV are recorded by *SPASE 2* which is situated on top of *AMANDA*. *AMANDA II* is scheduled to start operation in 2003 and by 2006, *IceCube*, a 1 km^3 detector, will open up the PeV energy region where the Universe is opaque to high energy γ-rays from beyond our galaxy.

3. Photon Astronomy Era (from 1970's)

Optical astronomy was first employed at the South Pole in 1964 for site testing. In 1979, a continuous 120 hours of solar observations allowed hundreds of solar eigenmodes to be discovered. Infrared and CMB measurements require the best atmospheric windows, and site testing since 1994 has demonstrated this is provided from the Antarctic plateau. In 1988, the first CMB measurement from Terra Nova Bay produced a map at an angular scale of 1.3°. In 1992, the CMB was imaged with better resolution by *Python*, a 0.75m telescope. It was replaced in 1997 by *Viper*, a 2.1m off-axis telescope, to be complemented in 1998 by DASI. The first flight of the *Boomerang* balloon in 1998 provided much improved angular resolution data for a CMB map published in late 2002. AST/RO, a 1.7m sub-mm telescope, has been mapping the Galactic plane in CI and CO since 1995. Between 1994 and 1999, *SPIREX* imaged the 2–5μm continuum and PAHs with the *Grim* and *Abu* cameras.

[15]A full version of this paper will be submitted to *PASA*. The poster is on the SPS2 web site.

Highlights of Astronomy, Vol. 13
International Astronomical Union, 2003
O. Engvold, ed.

CMB Observations from the Antarctic Plateau

G.Sironi, G.Boella, M.Gervasi, A.Passerini, A.Tartari, M.Zannoni

Physics Dept. - University of Milano Bicocca, and IASF-CNR, Milano - Italy

Abstract. CMB studies from the Antarctic Plateau are presented.

We used the unique properties of the Antarctic Plateau atmosphere for studies of the fine structures of the Cosmic Microwave Background (CMB):

a) Spectral distortions at decimetric wavelengths. In 1989/1991 we and LBL-Berkeley observed from South Pole (See reference group # 1).

b) Polarization at large angular scales. A correlation polarimeter, tested in Antarctica in 1994 and 1998, now at Testa Grigia (Italian Alps), is ready for observation at Dome C (See reference group # 2).

With IEN Galileo Ferraris (Turin) and IRA-CNR Arcetri we have developed low noise coherent detector systems and fabricated SIS mixers. We are preparing MASTER, a three band SIS system (94, 220 and 345 GHz), for studies of the Sunyaev Zeldovich effect (reference group #3).

We are participating in the following plans for observational facilities: i) proposal for a large sub-mm telescope at the South Pole, ii) Working Group for the Antarctic Center for Sub-millimetric Astronomy at Dome C (reference group #4).

References

#1) Sironi, G. et al., 1991: *ApJ* 378, 550; Smoot, G.F. et al., 1991: Antarctic J. XXVI, 286; Bersanelli, M. et al., 1993: Antarctic J. XXVIII, 306; De Amici, G. et al., 1993 : Antarctic J. XXVIII, 308; Ajello, C. et al., 1995: *ApJS* 96, 643

#2) Sironi, G. et al, 1997: *PASP* 141, 116; Sironi, G. 1999: New Ast. Rev. 43, 263; Sazhin, M.V. and Sironi, G. 1999: New Ast. 4, 215; Sironi, G. et al., 1997: New Ast. 3, 1, Spiga, D. et al., 2002: New Ast. 7, 125; Sironi, G. et al., 2002: PASA 19, 313; Gervasi, M. et al. 2003: SPIE 4843, 336; Sazhin, M.V. et al., 2003: New Ast. (in press) and astro-ph/0306250v1.

#3) Sironi, G. et al. 1996, ESA SP- 388 (219); Battistelli, E.S. et al. 2002: AIP Conf Proc. 616, 123; Battistelli, E.S. et al. 2002: PASA 19, 123; Tartari, A. et al. 2003: astro-ph/0307166v1

#4) Stark, A.A. et al. 1998: SPIE 3357, 495); AA.VV. SIF Conf. Proc. 2000, Vol. 66; Olmi, L. 2003: Proc. of 'The Scientific Outlook for Astronomy and Astrophysics Research at the Concordia station'- Capri 2003 - Memorie SAIT : in press; Sironi, G. 2003: this same conference.

Highlights of Astronomy, Vol. 13
International Astronomical Union, 2003
O. Engvold, ed.

Earth as an Extrasolar Planet: South Pole Advantages

Wesley A. Traub, Antony A. Stark, Kenneth W. Jucks

Harvard-Smithsonian Center for Astrophysics, 60 Garden St., Cambridge, MA 02138, USA

Steven Kilston, *Ball Aerospace, Boulder, CO*;
Edwin L. Turner, *Princeton Univ., Princeton, NJ*;
Sara Seager, *Carnegie Institution, Washington, DC*

Abstract. We could observe the Earth as an extra-solar planet, viewing Earthshine on the dark side of the Moon, at the Pole, in winter.

A small telescope can measure H_2O, O_2, O_3, chlorophyll, air column density, clouds, continents, oceans, weather variations, and rotation period. This can be done only from the Pole, and in the coming few years of the lunar cycle, owing to the Earth-Moon-Sun geometry. The observations will validate analysis methods for the Terrestrial Planet Finder coronagraph.

Reflectivity variations (see model) will be strong; several-day observations are possible only at the Pole. Enhanced blue reflectivity from Rayleigh scattering gives the column abundance of molecules. Reflectivity from green land plants gives the "chlorophyll" feature. O_2 has 2 strong absorptions. Stratospheric O_3 gives the broad feature 0.6 μm. H_2O has 3 major bands. A primitive Earth might show CH_4 and CO_2 as well. Life on Earth produces abundant O_2, and no other known process competes except to produce relatively much smaller amounts. The strong O_2 bands are therefore good signs of the presence of plant life, along with the "chlorophyll" feature.

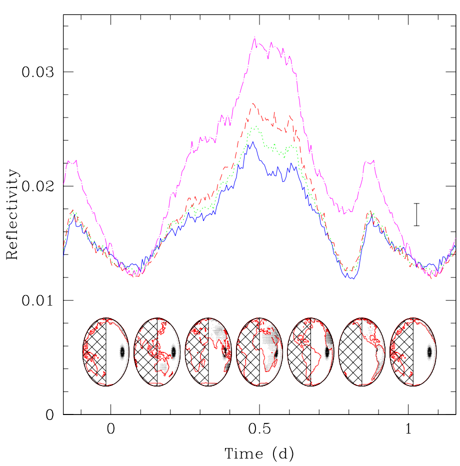

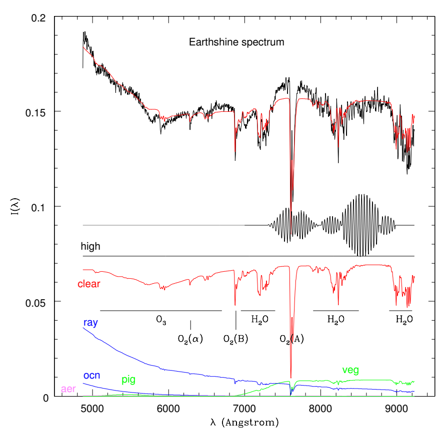

Highlights of Astronomy, Vol. 13
International Astronomical Union, 2003
O. Engvold, ed.

The Explorer of Diffuse Galactic Emission (EDGE)

R. F. Silverberg[1], E. S. Cheng[2], D. A. Cottingham[3], D. J. Fixsen[4], L. Knox[5], S. S. Meyer[6], P. T. Timbie[7], and G. W. Wilson[8]

[1] *NASA/Goddard Space Flight Center,Greenbelt, MD 20771, USA*

[2] *Conceptual Analytics, Glenn Dale, MD 20769, USA*

[3] *Global Science and Technology, Greenbelt, MD 20771 USA*

[4] *SSAI, Lanham, MD 20706 USA*

[5] *University of California at Davis, Davis, CA 95616 USA*

[6] *Enrico Fermi Institute, University of Chicago, Chicago, IL 60637 USA*

[7] *University of Wisconsin, Madison, WI 53706 USA*

[8] *University of Massachusetts, Amherst, MA 01003 USA*

1. Summary

The details of the formation of the first objects, stars and galaxies and their subsequent evolution remain a cosmological unknown. Few observational probes of these processes exist. The Cosmic Infrared Background (CIB) originates from this era and measurements of its anisotropy can provide information to test models of both galaxy evolution and the growth of primordial structure. Such measurements should provide a sensitive probe of the large-scale variation in protogalaxy density at redshifts, $z \sim 0.5$-3, while optical galaxy surveys provide complementary information at $z < 0.5$ and Lyman alpha absorption forest studies and Cosmic Microwave Background measurements add information at higher redshifts.

The Explorer of Diffuse Galactic Emission (EDGE) is a balloon-borne mission designed to measure the spatial fluctuations in the CIB from 200 μm to 1 mm on $6'$ to 3° scales with up to 2μK sensitivity/resolution element on an Antarctic Long Duration Balloon (LDB) flight. EDGE will employ an array of Frequency Selective Bolometers (Kowitt et al., 1996) to simultaneously measure spectral and spatial information with seven sky pixels each containing eight spectral bands. EDGE is designed to cover $\sim$100 square degrees of the sky in a single $\sim$10 day LDB flight to create a new observational constraint for large-scale structure formation theories.

References

Kowitt, M. S., Fixsen, D. J., Goldin, A., & Meyer, S. S., 1996, Appl. Optics, 35, 5630

Highlights of Astronomy, Vol. 13
International Astronomical Union, 2003
O. Engvold, ed.

Compact Wide-Field Astronomical Telescopes for Dome C

Roberto F. Viotti and the TRT team

Istituto di Astrofisica Spaziale e Fisica Cosmica, CNR, Tor Vergata Research Area, Via Fosso del Cavaliere 100, Roma, Italy

Abstract. We describe our project for a small and compact telescope, based on the TRT design, for wide–field observations from Dome C on the Antarctic Plateau, and discuss the main scientific goals.

The project is based on the 2–mirror, 3–reflection (TRT) Amoretti's design (Amoretti et al. 1989), where the primary acts both as the first and third reflecting surface. The main benefits of the TRT design are: the large corrected and unvignetted FOV, the flat focal plane allowing easy placing of large area detectors, easy baffling of straylight, minimum encumbrance (width/length close to unity), and easy instrument handling. Two 30 cm f/3 prototypes were realized in 1994 and 2002, and tested. In 2003 a new 45 cm f/5 TRT was realized based on Lemaitre's active optics techniques (Lemaitre 1996): the primary was obtained from a double–vase form substrate, polished spherically at rest, then in situ stressed by applying back to the mirror at 0.8 atm depressure. The secondary with a tulip form was polished under stress. The telescope was mounted in Tor Vergata, and tests are underway.

Our goal is to place on Dome C a mid–size TRT equipped with large area V–NIR detectors. The primary scientific objective, in the framework of the Spaceguard Foundation, is the search for potentially hazardous NEAs, especially at small solar elongations. The telescope can also be used for the search of extra-solar Jupiter–like planet transits, astroseismology and identification of GRBs.

Parts of this project were funded by CNR, ASI, PNRA and MIUR.

References

Amoretti, M., Badiali, M., & Preite-Martinez A. 1989, A&A 211, 250
Lemaitre, G. R. 1996, Proc. SPIE Vol. 2871, 436

Highlights of Astronomy, Vol. 13
International Astronomical Union, 2003
O. Engvold, ed.

FTS Opacity Measurements of the South Pole Submillimeter Sky

Richard A. Chamberlin

Caltech Submillimeter Observatory, 111 Nowelo Street, Hilo, HI 96720

Abstract. A sub-millimeter Fourier Transform Spectrometer (FTS) was used at the South Pole to acquire wide frequency span (300 GHz $< \nu <$ 2 THz) measurements of the atmospheric opacity, $\tau(\nu)$. Comparisons were made with other ongoing measurements to allow inference of typical wintertime observing statistics.

A sub-millimeter wavelength FTS of the Martin-Puplett type (Martin 1982) was deployed to the South Pole in 2001. In 2001 it was operated as frequently as operational constraints allowed to make measurements of $\tau(\nu)$. Comparisons were made with narrow bandwidth τ from the Antarctic Submillimeter Remote Telescope Observatory (AST/RO) near 806 GHz and broad bandwidth τ_{CMU} from the NRAO/CMU 860 GHz atmospheric radiometer (Peterson et al. 2003). Compared to the FTS and the AST/RO telescope, the uncorrected τ_{CMU} were offset but otherwise well correlated. The τ_{CMU} offset was likely caused by uncompensated antenna loss efficiency (Davis & Vanden Bout 1973, Calisse 2003). The observed correlation with the continuous τ_{CMU} record was used to extrapolate the FTS $\tau(\nu)$ to infer statistics for an entire annual cycle, see Chamberlin et al. (2003). The statistics from this extrapolation are probably characteristic of all years since South Pole wintertime sub-millimeter observing conditions are expected to have only a slight inter-annual variation (Chamberlin 2001). In the centers of the 1.3 THz and 1.5 THz windows our results indicate observing is possible about 50 days a year with $\tau < 2$ and about 20 days a year with $\tau < 1.75$.

Support for this work was provided under National Science Foundation Grants OPP-0126090 and AST 99-80846.

References

Calisse P. G. 2002, PASA, submitted (`http://arXiv.org/abs/astro-ph/0210456`)

Chamberlin, R. A. 2001, JGR-Atmospheres, 106, (p. 20,101)

Chamberlin, R. A., Martin R., Martin, C. L. & Stark A. A. 2003, in SPIE Proc. Vol. 4855, p. 609, ed. T. G. Phillips & J. Zmuidzinas (Bellingham, WA) (`http://puuoo.submm.caltech.edu/doc_on_vax/html/staff/rac/spie_fts2002.ps`)

Davis J. H. & Vanden Bout P. 1973, Astrophysical Let., 15, 43

Martin, D. H. 1982, in *Infrared and Millimeter Waves, Vol. 6: Systems and Components*, ed. K. E. Button, Academic Press, NY, pp. 66-148

Peterson, J. B., Radford, S.J.E., Ade, P.A.R., Chamberlin, R. A., O'Kelly, M.J., Peterson, K.M., & Schartman, E. 2003, PASP, 115, 383

SPS3

A New Classification Scheme for Double Stars

Chairpersons: W.I. Hartkopf and B.D. Mason

Editors: W.I. Hartkopf and B.D. Mason (Chief-Editor)

Highlights of Astronomy, Vol. 13
International Astronomical Union, 2003
O. Engvold, ed.

An Introduction to the Nomenclature Problem

Brian D. Mason and William I. Hartkopf

United States Naval Observatory

Abstract.
The new observing and reduction techniques available to astronomers have led to remarkable changes in the field of double and multiple stars. New classes of companions, such as brown dwarfs and exoplanets, have been discovered. Binaries which previously constituted distinct classes are now observable by multiple techniques. With many long-baseline optical interferometers operational or planned, with improvements in other techniques, and with astrometric space-based missions in various states of planning and funding, the situation is likely to become more complicated. The result is greater understanding for the scientist, but greater challenges for the cataloger!

The "problem" is that purveyors of different techniques use different nomenclature, both in terms of root designation and component identifier. It is this latter inconsistency which causes the most confusion and is the topic of this Special Session.

This talk will illustrate some of the many designation ambiguities and summarize efforts made during the past few years to address this problem.

1. Introduction: a Welcome "Problem"

The new observing and reduction techniques available to astronomers have led to remarkable changes in the field of double and multiple stars. New classes of companions, such as brown dwarfs and exoplanets, have been discovered. Binaries which previously constituted distinct classes are now observable by multiple techniques (witness, for example, the increasing overlap between the visual and spectroscopic regimes). With many long-baseline optical interferometers operational or planned, with improvements in other techniques (e.g., absorption-cell RV work), and with astrometric space-based missions in various states of planning and funding, the situation is likely to become more complicated. The result is greater understanding for the scientist, but greater challenges for the cataloger!

The "problem" is that purveyors of different techniques use different nomenclature. Visual binaries are given discoverer designations, based on observer's name (e.g., Σ or STF 13, β or BU 96), while spectroscopic binaries are usually identified by their HD number, eclipsing binaries by their variable star designation, occultation binaries by SAO or ZC number, and so on. Binaries analyzed by multiple methods may wind up with multiple designations.

While multiple designations are confusing, a large cross-reference list (such as SIMBAD) can usually handle these problems. Component confusion is even worse, however, as one person's **AB** pair may be another's **ab** or **BA** or **BC** or **primary/secondary**! It is this problem that we wish to address.

2. Addressing the Problem

An electronic discussion among an informal working group began in 1999. Over time, these discussions resulted in four suggested schemes (Dickel & Malkov 2000):

- **KoMa**: a hierarchical scheme developed by D. Kovaleva and O. Malkov (2000). Using a variety of upper/lower case alphabetic, numeric, and Roman numerals, this scheme indicated both hierarchy and type of companion (e.g., stellar, planetary, etc.)

- **UC**: developed by S. Urban and T. Corbin (2000). This is a numeric-only, backside-expandable scheme similar to that used for library call numbers.

- **Sequential**: a non-hierarchical scheme developed by L. Dickel and P. Dubois. In this numeric scheme all components are assigned numbers in the order of their discovery, with no heed given to their relationship with other components.

- **WMC**: the Washington Multiplicity Catalog. This method, while based on the venerable scheme of upper and lower case letters used in the WDS, extends to multiple levels through use of additional numbers and letters.

At IAU Symposium 200 the attendees seemed to favor the WMC, with UC a close second. The sequential scheme, while not favored, was sufficiently different from others so that it continued to be discussed.

At IAU-GA XXIV interested parties held a multi-commission meeting to discuss various methods for clearing up the nomenclature ambiguities (Genova 2000). As a result of those discussions the WMC was endorsed and the following resolution was ratified by Commissions 5 (Documentation & Astronomical Data), 8+24 (Astrometry), 26 (Double & Multiple Stars), 42 (Close Binary Stars), and later 45 (Stellar Classification)[16].

The resolution read as follows:

On Designating Components of Binary and Multiple Star Systems

Recognizing

- the increasing synergy of techniques for the investigation of stellar companions blurring the traditional distinction between astrometric, spectroscopic, and photometric binary and multiple stars;
- the detection of sub-stellar (including planets) as well as stellar components by these techniques and,

---

[16]See http://ad.usno.navy.mil/wds/wmc/iaumcm_old.html, the IAU-GA XXIV MCM archival webpage for more information

- the need for a simple, unambiguous, flexible, and computer friendly designation scheme for components of binary and multiple star systems,
- Noting that future ground and space-based telescope projects have the potential to detect both sub-stellar as well as stellar components in increasingly large numbers,

Recommends that

- a uniform designation scheme, based on expansion of the new WDS system, be developed during the next 3 years to include all types of components and that this be reviewed in time for its adoption to be considered at General Assembly XXV.

Implementation of the scheme was to be as follows:

1. Present a sample of the resulting scheme to Commission 26 at Colloquium 191. This sample was to be in the form of a catalog of all types of binaries found within a particular patch of the sky, complete with component designations based on the new scheme. Details of this presentation are available in Hartkopf & Mason (2004).
2. Present modified scheme to SOC of IAU-GA XXV Seminar, USNO (17 June 2003).
3. Make any needed modifications based on suggestions from above items, then present this modified scheme to the SOC of IAU-GA XXV SPS 3 (Special Session 3: *A New Classification Scheme for Double Stars*).
4. Make additional modifications if necessary, then present the further modified scheme at SPS3, July 18, 2003.
5. If approved, present the all-sky WMC at IAU-GA XXVI in 2006, and continue to update and maintain.

Further details of the discussion of the electronic discussion group and past work are available on the WMC Designation Scheme & Working Group webpage[17].

References

Dickel, H.R. & Malkov, O.Y. *New IAU Concepts of Binary/Multiple Star Designations*, 2000, in IAU Symposium 200, BIRTH AND EVOLUTION OF BINARY STARS, Potsdam, Germany, B. Reipurth and H. Zinnecker, editors, 220[18]

Genova, F. *Commission 5 Report*, 2001, Transactions of the IAU, XXIV, 237

---

[17] http://ad.usno.navy.mil/wds/newwds.html

[18] see http://casa.colorado.edu/reipurth/iau200www/posterbook/index.html.

Hartkopf, W.I., & Mason, B. D. *Addressing confusion in double star nomenclature: The Washington Multiplicity Catalog*, 2004, IAU Colloq. 191, THE ENVIRONMENTS AND EVOLUTION OF DOUBLE AND MULTIPLE STARS, Mérida, Yucatán, México, C. Allen and C. Scarfe, editors, RevMexAA(SC)

Kovaleva, D. & Malkov, O. *KoMa - a scheme for the designation of multiple objects*, 2000, in IAU Symposium 200, BIRTH AND EVOLUTION OF BINARY STARS, Potsdam, Germany, B. Reipurth and H. Zinnecker, editors, 223

Urban, S.E. & Corbin, T.E. *The Urban/Corbin Multiple System Designation Method*, 2000, in IAU Symposium 200, BIRTH AND EVOLUTION OF BINARY STARS, Potsdam, Germany, B. Reipurth and H. Zinnecker, editors, 225

Highlights of Astronomy, Vol. 13
International Astronomical Union, 2003
O. Engvold, ed.

Addressing Confusion in Double Star Nomenclature: The Washington Multiplicity Catalog

William I. Hartkopf & Brian D. Mason

U.S. Naval Observatory, Washington, DC

(Note: This talk was adapted from one given in February 2003 at IAU Colloquium 191, *The Environment and Evolution of Binary and Multiple Stars*, in Mérida, México.)

Abstract. The Washington Multiplicity Catalog (WMC) project is an effort to address the often conflicting nomenclature schemes used by astronomers in different fields of double and multiple star research, by compiling a catalog of all known binary and multiple systems, then assigning a consistent (insofar as possible) component designation to each component. Components are treated in the same manner whether stellar or sub-stellar (e.g., brown dwarf, exosolar planet) in nature. This effort was begun shortly before the 2000 IAU General Assembly in Manchester, UK. A sample version of the planned catalog was presented at IAU Colloquium 191, held in Mérida, México in February 2003, and a modified version of this sample will be presented at the July 2003 GA in Sydney, Australia. Finally, if the nomenclature and catalog format are agreed upon, a full-sky version of the catalog will be created in time for the 2006 GA in Prague.

1. Roots of the WMC

The root of the Washington Multiplicity Catalog (WMC) is the Washington Double Star Catalog (WDS). The WDS, maintained at the United States Naval Observatory (USNO), is the principal database of astrometric double and multiple star data for the astronomical community. It contains (as of July 2003) 603,651 mean positions for 99,403 pairs, and is updated nightly. The USNO double-star program also maintains catalogs of differential magnitudes, visual orbital elements, and interferometric and other high-resolution observations.

While the WDS is a complete listing of all resolved systems (i.e., visual and interferometric doubles), many components are detected but not resolved. These include:

- spectroscopic doubles (single- or double-lined),
- photometric or eclipsing binaries,
- astrometric doubles,
- lunar occultation doubles,
- other doubles, and
- planets and other sub-stellar objects.

However, the WDS nomenclature rules (with slight modification) can accommodate all types of double stars.

2. The WDS and Hierarchy

The WDS is system-based rather than object-based, as it contains relative measures between components of a given system. In an object-based scheme, a group of N objects yields N entries, but in a system-based scheme, N objects can yield up to $\frac{N(N-1)}{2}$ entries. The WDS may also contain measures between photocenters, and multiple systems may become quite complex as N increases. However, the WDS lists only pairings actually measured, and the observer's common sense usually implies the system hierarchy.

Generally, orbital period and/or separation are used to assign the hierarchical structure. The 3:1 ratio of semi-major axes determined by R.S. Harrington in his work on hierarchical multiples is generally followed, although separations $> 1''$ are usually given upper-case letters. This 3:1 ratio assumes physicality. However, most visual doubles do not have enough measures to determine whether motion is Keplerian or rectilinear. In general, then, all hierarchies in the WMC are *apparent* rather than *absolute*. It is assumed that all double stars within some small separation are of interest (if only as a warning of possible image blending), so are retained in the WDS and WMC even if shown to be optical.

3. Rules of Component Designation

The WDS at present extends nomenclature to second level hierarchies. The WMC will extend this nomenclature to cover more complex systems, however, as follows:

Level 1: capital letters (e.g., STF1523 AB)
Level 2: lower case letters (e.g., FIN 347 Aa,Ab)
Level 3: numbers (e.g., BNK 1 Ab1,Ab2)

Higher levels will alternate lower case letters and numbers (no examples of higher levels have yet been found, however).

A comma will be used as the delimiter between components in a system, with the full component identifier before and after the comma (e.g., Aa,Ab). The only exceptions: if only two characters are provided the delimiter is assumed (e.g., WAK 8CD = WAK 8C,D).

While the WMC will strive to maintain hierarchies in the assignment of letter and/or number, this is not always possible, given our often very limited knowledge. Also, if a subsystem is found that cannot be assigned unequivocally to a higher order component, a tentative best guess assignment will be given and a note added to the catalog.

Figure 1 illustrates a (fictitious) system, growing increasingly complex as new components are discovered.

4. The Sample WMC

The $11^h - 11^h30^m$ band of RA was selected for the sample WMC. As well as being historically compelling (containing ξ UMa), it includes a variety of component types:

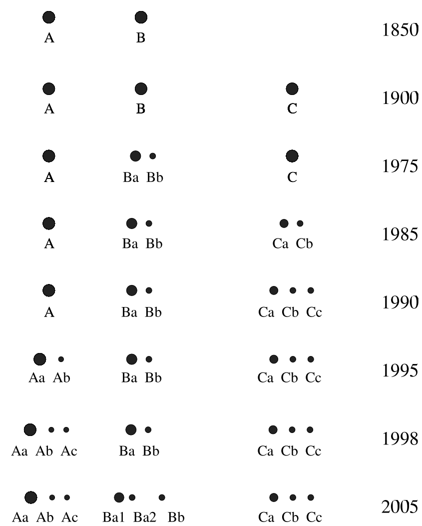

Figure 1. Illustration of nomenclature assignment as a (fictitious) system system grows more complex:

1850: visual pair is discovered
1900: wide common proper motion companion is found
1975: B component is found to be spectroscopic binary
1985: C component is split by speckle interferometry
1990: additional speckle C component is resolved at a similar separation
1995: planet is found orbiting the A component
1998: second planet is found
2005: primary of B is resolved by long-baseline interferometry

- astrometric binaries,
- X-ray binaries, cataclysmic variables, and related objects,
- eclipsing binaries,
- occultation binaries,
- spectroscopic binaries (SB1 + SB2),
- spectrum binaries,
- interferometric binaries,
- visual binaries, and
- planetary companions (by extending to $10^h59^m\!.5$).

In addition to the WDS and other USNO double star catalogs mentioned earlier, sources of multiplicity tapped thus far for the sample WMC include:

- Downes et al., 2001, *A Catalog and Atlas of Cataclysmic Variables: On-line Version*, PASP **113**, 764 (`http://icarus.stsci.edu/ downes/cvcat/`),
- Ritter & Kolb 1998, *Catalogue of cataclysmic binaries, low-mass X-ray binaries, and related objects (Sixth edition)*, A&AS **129**, 83,

- Batten et al., 1989, *Eighth Catalog of the Orbital Elements of Spectroscopic Binary Systems*, Pub. DAO, **17**,
- Pourbaix et al., 2003, *Ninth Catalogue of Spectroscopic Binary Orbits* (`http://sb9.astro.ulb.ac.be/`),
- Svechnikov & Bessonova 1984, *Catalog of Orbital elements, Masses and Luminosities of close double stars*, Bull. Inf. CDS 26, 99,
- van Paradijs 1995, *A Catalogue of X-Ray Binaries*, in *X-ray Binaries*, Lewin et al, eds., Cambridge Univ. Press, ch. 14, pp 536-577,
- California & Carnegie Planet Search web site (`http://exoplanets.org/`) and links therein.

Information on other prospective sources is needed and welcome.
These techniques contribute to the sample WMC in the following percentages:

95.8%	visual binaries and optical pairs
50.6%	interferometric binaries and optical pairs
1.7%	spectroscopic binaries
1.4%	cataclysmic variables or related objects
1.0%	occultation binaries
0.3%	astrometric binaries
0.2%	eclipsing binaries
0.2%	X-ray binaries
0.1%	spectrum binaries
0.1%	planets

Since the techniques are complementary, the sum is >100%. It should be noted that this breakdown is biased significantly by selection effects. For example, while visual binaries may be discovered (and cataloged) after a single observation, data on spectroscopic pairs are often not published until the full orbit has been characterized.

5. Coordinate Matching

System matches are based on the arcsecond-precise coordinates of the primary stars in each individual pair. The most time-consuming aspect of the WMC construction (by far!) was the improvement of the arcminute-precise coordinates found in the WDS. Some 80% of the 1,645 different primaries in the sample region were matched to Hipparcos or Tycho-2 objects. An additional 19% matched to GSC2, USNO A2, 2MASS, etc. via individual inspection using ALADIN. There remain 1.3% (21 pairs) which still have only arcminute accuracy coordinates. Nearly all of these are older, unconfirmed, visual doubles (including some very wide common proper motion pairs and some with suspect coordinates).

Following coordinate matching we found a total of 1,465 systems in this slice of the sky. These may be broken down as follows:

1,336 (91%)	simple binaries
80 (5.5%)	non-hierarchical triples
16 (1.1%)	non-hierarchical systems, >3 components
25 (1.7%)	hierarchical triples
8 (0.5%)	hierarchical systems, >3 components

Sample Washington Multiplicity Catalog

WMC..........	Comp.....	?? NAME............	?? NAME.............	Sep....*	Period.y	Mag1.f	Mag2.f	Spec1......	Spec2...	Parallax	Mass1.....*	Mass2.*	Btype.	References......	RA,Dec (2000).
1059280+402549	AB	* 47 UMa	HD 95128	0.14	2.982y	5.05		G0V	planet	71.05h		2.54j	S1	CCP	1059280+402549
1059280+402549	AC	* 47 UMa	HD 95128	0.26	7.1 y	5.05		G0V	planet	71.05h		0.76j	S1	CCP	1059280+402549
1100004+413608	AB	BD +42 2173	T2 3012 01054 1	0.005a	0.899y	10.08	.	R...	.	5.29h	.	.	A	O6	1100004+413608
1100006-285044	AB	** TDS7598	T2 6647 01291 1	0.46	.	11.13	11.52	.	.	.	.	.	V	WDS,I4	1100006-285044
1100175-295159	AB	* EC 10578-2935	G2 S12221102974	.	.	15.9	.	?	.	.	.	.	CV	CCV	1100175-295159
1101493+295217	Aa,Ab	HD 95515	T2 1980 00145 1	0.262	.	7.8	.	K0	.	9.00h	.	.	V	WDS,I4	1101493+295217
1101493+295217	Aa,B	HD 95515	T2 1980 00145 1	1.13	.	7.00	9.36	K0	.	9.00h	.	.	V	WDS,I4	1101493+295217
1108028-774227	Aa,Ab	** GHE 35	G2 S1101231136	0.72	.	7.03k	8.38k	?e	.	7.1 r	.	.	V	WDS,I4	1108028-774227
1108028-774227	Ab1,Ab2	** BNK 1	G2 S1101231136	0.100	.	8.92k	9.32k	.	.	7.1 r	.	.	V	WDS,I4	1108028-774227
1108028-774227	AB	** GHE 35	G2 S1101231136	2.7	.	7.03k	9.5 k	?e	.	7.1 r	.	.	V	WDS,I4	1108028-774227
1108028-774227	AC	** SZR 1	G2 S1101231136	17.	.	7.03k	10.1 k	?e	.	7.1 r	.	.	V	WDS,I4	1108028-774227
1108059-615608	AB	V* RS Car	HD 96830	.	0.083d	7.0 b	18.0	nova	.	.	.	.	CV	CCV	1108059-615608
1113063-421643	AB	CD -41 6409	T2 7734 00204 1	2.503	.	10.55	11.69	.	.	.	.	.	V	WDS,I4	1113063-421643
1113063-421643	AC	CD -41 6409	T2 7734 00204 1	5.46	.	10.55	13.6	.	.	.	.	.	V	WDS	1113063-421643
1113125-262754	AB	V* TT Hya	HD 97528	0.65 m	6.953d	7.60	8.90	A2Ve	K1.5IV	6.50h	2.08	0.65	E,S1	SvB,SB8,SB9	1113125-262754
1115073-611539	Aa,Ab	HD 97950	T2 8959 01959 1	0.339	.	10.5	11.1	.	.	.	.	.	V	WDS,I4	1115073-611539
1115073-611539	Aa,Ac	HD 97950	T2 8959 01959 1	0.371	.	10.5	11.3	.	.	.	.	.	V	WDS,I4	1115073-611539
1115073-611539	Aa,Ad	HD 97950	T2 8959 01959 1	0.784	.	10.5	10.3	WN...	WN...	.	.	.	V	WDS,I4	1115073-611539
1115073-611539	AB	HD 97950	T2 8959 01959 1	1.81	.	9.03	10.8	WN...	WN...	.	.	.	V	WDS	1115073-611539
1115073-611539	AC	HD 97950	T2 8959 01959 1	2.69	.	9.03	11.3	WN...	.	.	.	.	V	WDS	1115073-611539
1115073-611539	AD	HD 97950	T2 8959 01959 1	3.54	.	9.03	12.3	WN...	.	.	.	.	V	WDS	1115073-611539
1115073-611539	AE	HD 97950	T2 8959 01959 1	4.59	.	9.03	11.8	WN...	.	.	.	.	V	WDS	1115073-611539
1118047+361614	AB	** KZA 16	2M 1118046+361614	8.08	.	11.0	11.5	.	.	.	.	.	V	WDS	1118047+361614
1118109+313145	Aa,Ab	* xi UMa	T2 2520 02634 1	0.053	669.18 d	4.41	.	G0V	M3V?	127.	0.022 f	0.37:	A,S1	O6,SB8	1118109+313145
1118109+313145	AB	HD 98231	T2 2520 02634 1	2.536	59.878y	4.41	4.87	G0V	F8.5V	127.	2.21 t	.	V	WDS,O6,I4	1118109+313145
1118109+313145	AC	HD 98231	T2 2520 02634 1	54.31	.	4.41	15.0	G0V	.	127.	.	.	V	WDS	1118109+313145
1118109+313145	Ba,Bb	* xi UMa	T2 2520 02634 2	0.33 m	3.981d	4.87	.	F8.5V	.	127.	0.000052f	.	S1	SB8	1118108+313145
1118109+313145	Ba,Bc	HD 98230	T2 2520 02634 2	0.026	.	4.87	.	F8.5V	K2-3V?	127.	.	.	V	WDS,I4	1118108+313145
1124349+021238	AB	** SLE 597	A2 0900-06920936	40.68	.	11.9	12.5	.	.	.	.	.	V	WDS	1124349+021238
1129041+392013	AB	HD 99787	T2 3013 02482 1	5.45	.	5.35	10.67	A2V	.	15.59h	.	.	V	WDS,I4	1129041+392013
1129041+392013	AC	HD 99787	T2 3013 02482 1	216.55	.	5.35	11.6	A2V	.	15.59h	.	.	V	WDS	1129041+392013
1129041+392013	AD	HD 99787	T2 3013 02482 1	344.36	.	5.35	7.73	A2V	K0	15.59h	.	.	V	WDS,I4	1129041+392013
1129041+392013	AE	HD 99787	T2 3013 02482 1	100.33	.	5.35	10.6	A2V	.	15.59h	.	.	V	WDS	1129041+392013
1129041+392013	AF	HD 99787	T2 3013 02482 1	131.03	.	5.35	10.3	A2V	.	15.59h	.	.	V	WDS	1129041+392013
1129041+392013	AG	HD 99787	T2 3013 02482 1	330.27	.	5.35	10.3	A2V	.	15.59h	.	.	V	WDS	1129041+392013
1129041+392013	DE	HD 99720	T2 3013 01407 1	99.06	.	7.73	10.6	K0	.	4.23h	.	.	V	WDS,I4	1128359+391829
1129041+392013	DF	HD 99720	T2 3013 01407 1	128.54	.	7.73	10.3	K0	.	4.23h	.	.	V	WDS	1128359+391829
1129041+392013	EF	** STF1543	T2 3013 01935 1	43.88	.	10.6	10.3	.	.	.	.	.	V	WDS,I4	1128353+391650

Figure 2. Sample page from the WMC Catalog.

6. The Catalog

A sample page from the catalog is shown in Figure 2, and an explanation of the columns follows. (Note: In the explanation for columns 3 and 4, the names in parentheses indicate the usual order of preference for that column.).

1	WMC designation (WDS or J2000 arcsecond coordinates of system primary)
2	component designation (AB; Aa,Ab; etc.)
3	catalog and name (Bayer/Flamsteed/variable star designation, HD, DM, discoverer designation, etc.)
4	catalog and name (HD, Tycho-2, GSC2, USNO A2, 2MASS, etc.)
5	angular separation (including separations predicted from spectroscopic orbit and parallax, vector separations, etc.)
6	orbital period
7,8	magnitudes (flags for variability, filter codes if not V)
9,10	spectral types
11	parallax (from Hipparcos, orbit, etc)
12,13	masses (or mass function, mass ratio. etc.)
14	binary type (visual, spectroscopic, X-ray, etc.) The 'visual' code will be modified if the pair is known to be optical, CPM, or physical.
15	references (with web links to on-line catalogs)
16	J2000 coordinates of principal star of pair ($0\farcs1$ precision)

7. Examples from the sample WMC

A few systems from the portion of the sample WMC shown in Figure 2 are noted below. These illustrate some of the features of the WMC, as well as some of the difficulties to be encountered in creating the full catalog.

1100004+413608, **1100006-285044**, etc.: These simple doubles, whether of visual, astrometric, spectroscopic, or other discovery origin, are by far the most common entries in the WMC.

1059280+402549 and **1113063-421643**: These two triples are treated in the same manner, even though one consists of three stars and the other a star and its two planets. In both cases, the apparent separations of the AB and AC pairs are comparable, so all components are considered to be at the same hierarchy.

1101493+295217: This is an example of a simple hierarchical triple.

1108028-774227: This is the only system in the sample WMC showing all three levels of hierarchy.

1129041+392013: All components of this apparently small cluster are wide, so no hierarchical structure was assigned, despite the wide range in separation.

1118109+313145: The ξ UMa system is another complicated multiple. The A component is a spectroscopic binary; the B component has also been split spectroscopically (with separation estimated as 0.33 milli-arcsecond). There is also a component of B resolved by speckle interferometry. Based on the separations, one would ordinarily assign the speckle pair the second level of hierarchy (e.g., Ba,Bb) and assume one of those components was split spectroscopically (e.g., Ba1,Ba2). However, we are familiar with the speckle pair and suspect the resolution may be spurious, as it has never been confirmed. We're thus reluctant to assign a different hierarchy to the very close pair.

1115073-611539: This is another apparent small cluster. Since the component we call A was later resolved into four stars, we assigned those stars to a second apparent hierarchical level.

8. Discussion

(Note: Discussions of both Mason's and Hartkopf's talks follow.)

SCHMITZ: How is it determined which is component A and which is B?
HARTKOPF: If masses are known (or inferred from, say, spectral type) the more massive star is the primary. If masses are not known, the brighter (preferentially in V) is selected as the 'A' component (although whether to use peak or median brightness in the case of a variable has not been determined). If all factors are equal, it is the one on the left! (just kidding...)

TURNER: Once an A always an A? Or is there a provision for changing which is an A based on new information?
HARTKOPF: Andrei and Dimitri's talks will present opposing viewpoints of this very topic.

SCARFE: Two questions and a comment: (1) How do we handle an SB whose "primary" is the star with the easily measurable spectrum? (2) Should you include all variable radial velocity objects, where the variation has no other known cause? (3) You need to enlist the help of a cataloger of eclipsing systems, to include the several thousand known.
MASON: (1) If it is an SSB and is the only component you 'see' then it is, by default, the primary. If it is a DSB and nothing is known regarding mass ratio then it would be the primary here as well. (2) Well, other indirect detection methods, like occultation, are included. I suppose they should be included as well; however, has anything listing just velocity variation been published since Abt & Biggs? (3) We would gladly accept the help of any experts that might be willing to lend a hand.

SCARFE: Following Peter Eggleton's comment, it would be useful if authors would provide cross-references to the names of whole systems in the various catalogues in which they appear.

OSWALT: Some systems have several or even many different names. By what priority are the names listed in the WMC chosen?
HARTKOPF: There are two columns of designations. The order of priority in the first column is Bayer/Flamsteed or variable star designation → HD number → DM number → other catalog designation. For the second column we wanted to use a catalog which was as inclusive as possible so we mainly use the Tycho designation, which covers 80% of the catalog or more, then GSC2.2, A2, 2MASS, etc.

MASON: Note that we only use Discovery Designation in column one when nothing else is available.

OSWALT: Perhaps, following the example of the minor planet community, a provisional designation would be assigned to a binary. Then once physical association has been proved, a permanent designation assigned. Alternatively, a "provisional" flag in the catalog could be used for new systems.
HARTKOPF: In the column giving binary type we will indicate, when known, whether the system is an optical pair, a common-proper motion system, a physical system showing orbital motion, etc.

OSWALT: (1) (comment) The primary should probably be the one designated as such in the historical record — otherwise the literature will become confusing. (2) If for new binaries the mass determines which is designated primary, how will we deal with white dwarfs, mass transferring stars, or other stars where the star WAS the most massive, but is no longer?
HARTKOPF: I think we have to go with which is the most massive now, since our theories of evolution may be in error and change.

QUIRRENBACH: What is the approach regarding inclusion or exclusion of chance projections? If you go sufficiently deep, each star becomes "double". High-dynamic-range searches for low-mass companions are turning up lots of chance projections. One should have consistent criteria for what should be included.
MASON: Good point. Obviously we could go overboard and include everything, but we need to set some sort of limit before it becomes absurd. Setting the limit using Aitken's or Rossiter's criteria is a possibility but leaves out some certainly optical pairs that could be important for precise astrometry, blended images, etc.

SCHMITZ: Where will the central depository be for defining the A and B assignments?
HARTKOPF: The USNO Double Star group (i.e., us).

EVANS: Your catalog of "spectrum binaries" — would that include a Cepheid with a hot companion in the ultraviolet?
HARTKOPF: Yes.

Highlights of Astronomy, Vol. 13
International Astronomical Union, 2003
O. Engvold, ed.

Working Group on Designations and Special Session 3

Helene Dickel

Univ. of Illinois, Astronomy Dept., 103 Astron. Bldg., 1002 W. Green St., Urbana, IL 61801

Marion Schmitz

Caltech, MS 100-22, Pasadena, CA, 91125

1. WGD Activities

The WGD is a part of Commission 5 - Documentation and Astronomical Data. There is a president, vice-president, and over a dozen members world-wide.

One duty of the WG is to maintain and update a web-site which contains the IAU Recommendations for Nomenclature. These recommendations include suggestions for creating new names for objects and examples of improper nomenclature.

The WG also receives, reviews, and approves new submissions for the Acronym Registry as proposed by major projects and individual researchers. We look forward to the submission of the WMC to the Registry.

One sub-group of the WG is involved with software which resolves object names into positions for NED and SIMBAD/VizieR. Plus, several of us are on the look-out for non-conforming designations in preprints and journal articles and often inform the authors and journal editors of potential problems. Recent experience has shown that authors have been positively receptive of our comments.

2. Applicability of WGD to SPS3

The WG on Designations helps projects understand the need and use of standards in nomenclature. We also help inform professionals and amateurs about the need for standards and provide a list of currently accepted acronyms in the on-line Dictionary (http://vizier.u-strasbg.fr/viz-bin/Dic). Additional Web links for many of the acronyms are also provided.

3. Designation vs. Data

One aspect of nomenclature which needs to be understood is that whatever designation is assigned to an object must be considered to be permanent. Observational data may change, but not the names.

If an object name is to be based on position, it must be remembered that positions are epoch AND equinox dependent. For example, the positions of proper motion stars and orbiting binaries need to be accurately determined if future researchers are going to be able to determine the correct objects. Positions can also be wavelength dependent.

The resolution of the detection method also plays a factor in the assignment of positional names. Low resolution detections should not have "high precision" designations.

4. Positional Designations

Positional designations are made up of two parts - the acronym and the position. When used to create the positional part of a name, the cataloged position should contain one decimal place more precision than the designation. When doing this, the catalog position needs to be truncated rather than rounded off. Also, the designation should not imply higher accuracy than is warranted by the observation.

For example, the FIRST radio catalog has an object at the cataloged position: FIRST J100956.9+300850 @ 10h09m56.98s, $+30°08'50.9''$. The designation of the object, therefore, is composed of a truncated version of that position.

5. Remember the "J"

Perhaps one of the more subtle, but significant, parts of a modern positional designation is the use of the letter "J" for J2000 coords or "B" for B1950. For researchers not familiar with the acronym used for a given object, the letter of the epoch is crucial in being able to locate the object on the sky. By default, a positional name without a "B" or "J" is assumed to be at B1950.

For example, take the case of SDSS 1533-00 as recently used in the literature. At first glance, one would recognize that the object was detected in the Sloan Digital Sky Survey at approximately 15h33m, $-00°$ degrees in B1950.

However, the Sloan catalogs do not contain any object by this name. It turns out that the author took many liberties in creating an easy-to-use nickname for the intended object. The R.A. was rounded instead of truncated; the Dec. was drastically truncated; the "J" was dropped; and even the acronym was modified for convenience.

Even so, there turn out to be two distinct SDSS objects which qualify for this "convenient" name.

6. The Horror of Nicknames

Although I know no one in this room would ever go to such drastic measures for the sake of convenience, I'd like to just show a few recent examples of object names which have caused (and continue to cause) confusion in the literature.

At first glance, one might assume that N49 was a shortened version of NGC 49, when in actuality it refers to the 49th Nebula in the SMC (there is also an N49 in the LMC).

Next is a case where one familiar with astronomy history may guess that "SA" as used here stands for one of Kapteyn's Selected Areas. However, it would then be realized that there were not 1600 fields in the SA list. Next, the assumption might be that the object has coordinates near 16h56m, -2° 0′. As it turns out, that, too, is incorrect. This object happens to be the 20th galaxy in a new structure discovered in Abell 1656.

This last example seems quite harmless in that stellar astronomers "know" that HR 10 is a 6th magnitude star from the Harvard Revised catalog of Bright Stars. Extragalactic astronomers "know" that this is the 10th object in a list by Hu and Ridgway of Extremely Red Objects which turns out to be a galaxy at redshift 1.44. Four individuals at NED and SIMBAD "know" that they need to be careful about how they refer to this object in their databases because it is too easy to get the star and the galaxy confused based solely on name. The name of the Hu and Ridgway object in NED and SIMBAD is [HR94] 10.

To conclude, "It's a crowded sky up there. You are not alone."

1. Discussion

SCARFE: Let me emphasize that the ambiguity between dashes and minus signs is a real menace.
SCHMITZ: Agreed. Designations that look like coordinate names (but aren't) should be avoided.

HARTKOPF: In the WMC sample catalog there were ~20 objects known only to arcminute accuracy. At present I pad the designation with zeroes for consistency with the vast majority. What's the best way to handle them?
SCHMITZ: It would be best to not imply higher accuracy than is warranted. If it is possible to use nulls or blanks instead of zeroes, such that future researchers are not misled to an implied accurate position.

Highlights of Astronomy, Vol. 13
International Astronomical Union, 2003
O. Engvold, ed.

Designation of Multiple-star Components

Andrei Tokovinin

Association of Universities for Research in Astronomy, Cerro Tololo Interamerican Observatory

Abstract.
Hierarchical multiple stars need designations for individual components, for super-components (several bodies that act as single dynamical center and are often measured jointly) and sub-systems. Hierarchical designations like those proposed for WMC can satisfy all needs, but designations will have to be frozen and will not reflect true hierarchy in the future as new components are discovered. Hence, a clearing house (WMC on the web?) is needed to maintain unique and consistent designations. The hierarchy can be coded separately and flexibly by reference to parent super-components. As an example, these ideas are applied to a real quintuple star HR 1706.

1. What and why designate?

We are looking for a clear, unique and computer-friendly system for designating multiple stars and planets. We need to designate several different things. First, *components* – physical bodies like stars or planets. Second, *super-components* – unions of several bodies that act as single dynamical centers. Some observational data (e.g. photometry, astrometry) refer to such combinations measured as a whole, without splitting into true components. Moreover, some components that are now believed to be single will be resolved in the future into sub-systems, so currently available data actually refer to super-components. Finally, we need designations for *systems* or sub-systems with approximately Keplerian orbits that are the building blocks of more complex stellar or planetary systems. Each system is composed of two components or super-components, which means that designations for systems can be derived from designations of their components. In the following we designate systems by joining two component's designations with comma.

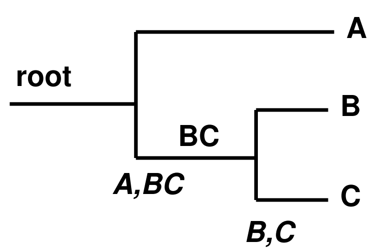

Figure 1. A generic triple system. The components are designated by single letters, super-components – by combinations of letters, systems (in italics) – as two components joined by comma.

The point is illustrated in Fig. 1 showing a simple visual triple where a close pair BC moves around A in a wide orbit. The center of gravity of BC is the secondary in this wide orbit, it is a super-component BC. If A itself turns to be a spectroscopic binary, then its components would be designated as Aa and Ab, whereas A becomes a super-component. All measurements of A as a whole will remain valid and there will be no need to change the catalogs.

It is important that designations be *fixed* and do not change as our knowledge of multiple stars progresses. This conforms to the IAU rules because designations are only a special case of naming astronomical objects. It is desirable to keep existing designations unchanged in order to minimize confusion. So, how the names for *new* components should be chosen?

2. Hierarchical or sequential?

The Washington Multiple Star Catalog (WMC, Hartkopf & Mason 2003) will adopt component designations that are constructed hierarchically, like Aa and Ab in the above example. The virtues of hierarchical designations are obvious: 1) super-components are designated by truncation, Aa → A; 2) designations are robust because changes in one sub-tree of a hierarchy do not affect other subtrees; 3) designations are meaningful by showing to which (super-)component a given system belongs, thus diminishing chances of confusion. Hierarchical naming is widely used: telephone numbers, internet and postal addresses, computer directories, etc. Non-hierarchical names like sequential numbering are also in use, for example in stellar catalogs. Sequential schemes often lead to ambiguities and confusion, the worst example being the designations of cluster stars by their numbers in several non-overlapping lists. WDS (Mason et al. 2003) also uses a sequential system (letters A, B, C, etc.) for designating visual components.

Unfortunately, it is not possible to maintain consistent hierarchical designations because hierarchy of multiple stars is not exactly known. There is no problem when some component is found to be a close binary: in this case, the designations are simply extended to the next level. However, when new components are discovered at intermediate levels, as shown below, it is not possible to maintain consistent hierarchical designations without modifying existing designations, which is forbidden. So, hierarchical principle for designating components can be used only as a general guide-line, it is bound to fail in some cases and then a work-around will be necessary.

Whatever designation system is eventually adopted, it cannot be expected to work "by itself". So, a centralized database that keeps track of known components and their designations is necessary. We hope that a web-based catalog like WMC can play the role of a "clearing house" for component designations. By developing a set of rules (designation system), we simplify the task of naming new components and, hopefully, diminish confusion, but it is still essential to have a single clearing house.

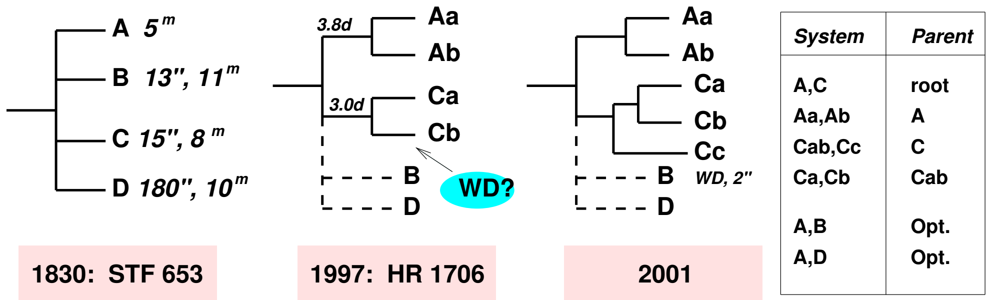

Figure 2. The history of 14 Aur = HR 1706 multiple system and its hierarchy

3. Example: HR 1706

A 5^{th} magnitude star 14 Aur = HR 1706 began its history as a quadruple, with 4 components A, B, C, D listed in 1830 by W. Struve (Fig. 2). Later it became evident that B and D are optical, whereas A and C share common proper motion. A was found to be a 3.8-day spectroscopic binary, C also turned out to be a spectroscopic binary with 3-day period (Tokovinin 1997a). This star is among the brightest in the sky in the far UV region of the spectrum because it hosts a young and hot white dwarf spatially coincident with C. Subsequent imaging with HST revealed that this WD is not identical to the spectroscopic secondary Cb, as one might expect, but is instead $2''$ away from C (Barstow et al. 2001). The whole system is thus quintuple.

The three panels in Fig. 2 reflect progress of our knowledge of HR 1706. As the structure of many other stars is still not known (or known at the level of Struve), a designation system has to be *historical*, being able to follow our improving knowledge. There is no sense in attempting a major revision of all designations now because, as time goes by, "new" designations become as obsolete as the current ones.

The component designations in Fig. 2 conform to the proposed WMC scheme and do not change as new components are discovered. This is why the WD is designated as Cc: a consistent implementation of hierarchical principle would require it to be Cb, the spectroscopic pair being Ca1 and Ca2, but in this case there would be a confusion with spectroscopic secondary which was Cb before the WD was discovered. In this case it is better to deviate from strictly hierarchical names rather than create confusion.

If we happened to observe this system few million years ago, the Cc could be a visible star, maybe even the brightest component in the system. In this case it would be already designated by a letter in the WDS, say E (the next available letter).

Table 1 illustrates three available options in the application of the WMC scheme to HR 1706 C, all likely to be encountered in practice. Designation 1 – consistent hierarchical names – would be appropriate if all components were discovered jointly and were designated for the first time. Designation 2 reflects the actual discovery history and is the correct option. Designation 3 would apply if the WD were identified as a visual component. The difference between

Table 1. Application of the WMC designation scheme to HR 1706 C

Type	Object	Desig. 1	Desig. 2	Desig. 3
Component	Spectroscopic primary	Ca1	Ca	Ca
Component	Spectroscopic secondary	Ca2	Cb	Cb
Component	White dwarf	Cb	Cc	E
Super-component	Spectroscopic binary	Ca	Cab	C
Super-component	SB+WD	C	C	CE
System	Spectroscopic binary	Ca1,Ca2	Ca,Cb	Ca,Cb
System	WD orbit	Ca,Cb	Cab,Cc	C,E
System	AC orbit	A,C	A, C	A,CE

designations 2 and 3 is subtle: in the first case the super-component C includes all 3 stars, in the second case it refers only to the close spectroscopic pair. As the WD gives no appreciable visible light and thus the existing data on C refer practically to the spectroscopic pair, it might appear irrelevant which of the options 2 and 3 is selected. However, the last line in Table 1 – designation of the wide system AC – shows that this is not so. If we do not want to change existing records in the catalogs, then option 3 is not acceptable because it would imply changing A,C into A,CE after the discovery of the WD.

The option 2 designates the super-component as Cab. This is only one possibility adopted here. No rules for super-component designations are formulated as yet, although WMC uses implicitly joint letters like BC to designate super-components formed by close visual pairs. Current WMC implementation does not make any difference between super-components and systems by omitting sometimes the comma between component's designation. This should be rectified in the future: super-components and systems are different physical entities, they are associated with different types of data. Moreover, a consistent designation of components and super-components permits easy and flexible description of hierarchy, as shown below.

4. Coding the hierarchies

If hierarchical designations could be made strict and consistent, there would be no need for separate coding of the multiple-system's hierarchy. Unfortunately, this is not possible, hence we must describe hierarchy separately from component designations and change it flexibly as our knowledge progresses. Another reason to keep hierarchy separate is that in many cases the hierarchy is not established yet and may even be subject to interpretation: nothing forbids to consider Mercury as a close companion to the Sun in a wide system Sun-Jupiter.

Stable multiple systems of stars are hierarchical and can be de-composed in several approximately Keplerian sub-systems. These structures are described by binary trees and can be represented in graphical form as in Figs. 1,2. There are other ways of coding hierarchies. For example, D. Evans proposed bracket notation: the triple in Fig. 1 would be written as a formula (A,(B,C)). In the Multiple Star Catalog (Tokovinin 1997b) the hierarchical levels are coded as sequences of digits: 1 for the upper level A,BC and 12 for the second level B,C. This scheme is descriptive and formal enough to be used in automatic analysis of the multiple-star structure (e.g. for computing the mass of a super-component by summing the masses of all its constituents).

If a consistent system for designating components and super-components is developed and implemented, the best and most flexible way to code the hierarchy is by reference to a parent. Such structures are known in mathematics as chained lists are are formally equivalent to graphs. A special column in the catalog would list the designation of parent – a super-component that hosts any given sub-system. The widest system is the "root" of hierarchy. A collection of records for any given multiple system specifies its hierarchy in a unique way. As new components are discovered, the "parent" column can be changed, but the designations of old components and super-components remain fixed. Application of this idea to HR 1706 is shown in Fig 2.

References can be used for coding hierarchies of planetary systems as well. For example, in the Solar system all orbits of major planets will have root or Sun as parent because they are all at the highest hierarchy level. The Earth-Moon orbit will have Earth as parent, all satellites of Jupiter will be linked to Jupiter, etc. Here we avoided the notion of super-components, replacing them with primary bodies of corresponding systems. This is a valid possibility, although some confusion is created when Earth as a physical body has the same designation as the Earth-Moon system orbiting the Sun. This example shows that the concepts of super-components, systems and hierarchy coding are useful for any designations, even for the existing ones.

It is recommended to add a "parent" column to the WMC. It will contain the designation of parent super-component or will remain blank if hierarchy is not known yet. Optical components can be marked as such in the same column.

References

Barstow, M.A., Bond, H.E., Burleigh, M.R., Holberg, J.B., 2001 MNRAS, 322, 891

Hartkopf, W.I., & Mason, B. D. *Addressing confusion in double star nomenclature: The Washington Multiplicity Catalog*, 2004, IAU Colloq. 191, THE ENVIRONMENTS AND EVOLUTION OF DOUBLE AND MULTIPLE STARS, Mérida, Yucatán, México, C. Allen and C. Scarfe, editors, RevMexAA(SC), in press[19]

Mason, B.D., Wycoff, G.L., and Hartkopf, W.I., 2003, The Washington Double Star Catalog[20]

Tokovinin, A.A. 1997a A&AS, 121, 71

Tokovinin, A.A. 1997b A&AS, 124, 75

1. Discussion

DICKEL: Comment: On first glance, it looks like it allows the designation to stay fixed. The changing hierarchy is accomplished by the links to the "parent."

[19]see http://ad.usno.navy.mil/wds/newwds.html

[20]see http://ad.usno.navy.mil/wds/wds.html, and Mason et al. 2001, AJ, 122, 3466.

TOKOVININ: Yes.

SCARFE: For a long time we didn't know to which of the visible pair the third component was attached in the case of 16 Cygni. This is a problem for any scheme.
TOKOVININ: It would not be a problem for sequential numbering. As to the "hierarchical naming," there are two options: i) call it "C" (if A and B are visual components) and define its relation to either A or B by links when it becomes known; ii) use provisional designations ?a and ?b for the spectroscopic components.

SCARFE: What is the significance of the 1, 11, 121, 12 notation, in parallel with Aab, Cab etc.?
TOKOVININ: The numbers like '121' in MSC are used to code the hierarchy. This number means that the system is a binary primary component of a wider pair which, in turn, is a secondary in a still wider system. The designations like 'Cab' are not sufficient to describe the hierarchy, as we all know.

OSWALT: How do you handle optical pair designations? When a new system is found but the hierarchy isn't evident, how do you assign a designation?
TOKOVININ: Hierarchy is coded separately from component designation. I suggest that any new component be designated on the basis of partially known hierarchy, or by an upper-case letter if it is a "visual" distant component of unknown physical relation.

HARTKOPF: In your case of a pair where one of the two components is an SB, you suggest the designation "?" be used in place of "A" or "B". This would seem to lose information in the case where, for example, you know that the SB belongs to either the A or B component of a triple.
TOKOVININ: The new SB will have the same WMC identifier as the visual binary, so it will be clear that the spectroscopic components are either A or B.

Highlights of Astronomy, Vol. 13
International Astronomical Union, 2003
O. Engvold, ed.

Dynamic versus Static Designation

Dimitri Pourbaix

Institut d'Astronomie et d'Astrophysique, Universite Libre de Bruxelles

Abstract.
Should the designation of the components of a system reflect its known hierarchy or rather the history of their discovery? With the recent progress in, say, radial velocity techniques, the old famous order in which components were used to be discovered (inner to outer components for spectroscopic systems) is somehow altered. In the past, capital letters were used for visual companions and lower case letters for spectroscopic components and there was almost no overlap between the two groups. The situation has changed from both ends of the orbital period interval. In some rare cases, we think letters should be re-distributed and re-assigned in order to reflect the structure of the system. With an adequate choice of the data structure, such a change of the companion designation is rather straightforward to implement in modern databases (such as SB9[21]). The only foreseen drawback is related to the cross-reference with some old papers: the letter B would not designate the same component in a 1970 paper and in a 2003 one. For instance, the former secondary of an SB2 system might now refer to the unseen companion and an astrometric triple.

1. Comment, Post SPS3

Since Pourbaix could not come up with a robust example to illustrate his view, he decided to withdraw his contribution to this proceeding. Nevertheless, he is not convinced that the difficulty in finding an example should be seen as a hint of the weakness of his dynamical approach.

2. Discussion

URBAN: Changing designations is a poor idea and a logistical nightmare. Changing letter while new discoveries are made goes against the Commission 5 recommendations.

MASON: The 3:1 hierarchy Bob Harrington calculated assumed equal mass companions, which obviously breaks down in the case of the solar system. Clearly, it works better when all companions are stellar.

SCHMITZ: For a system like Sun-Pluto, does the designation need to change every time Pluto is closer to or further away from the Sun than Neptune.

[21] See The 9^{th} Catalogue of Spectroscopic Binary Orbits website: http://sb9.astro.ulb.ac.be/

POURBAIX: Well, maybe you picked up the only counter-example in the Universe. However, as long as one would use the semi-major axis as the "distance indicator," that is constant, even for Pluto.

TOKOVININ: The problem is: whether the designation should be fixed or meaningful. Attempts to code system hierarchy or component order fail to yield fixed designation. So, a designation should be kept fixed, and it can be made meaningful within this limit.
POURBAIX: If the component designation is part of the designation, we are indeed in trouble in the dynamic scheme I propose. However, as long as the designation refers to the system as a whole, the component designation is seen as a characteristic of the system and can thus be updated as often as needed.

Anyway, the component designation is already likely to change when the scheme is adopted for the whole sky. So the question is really whether one wants that change to be a one-shot or something more recurrent.

DICKEL: Designations need to be fixed. Changing data such as the spectral type or hierarchy is unrelated to the designation.
POURBAIX: The question is indeed whether we want the component to be part of the designation or not. In the affirmative, updating the letter(s) would mean a hard time for everybody. Otherwise, it is as simple as updating the spectral type.

HARTKOPF: When pairs are discovered by two techniques (e.g., one calls it AB, the other BA) one designation **HAS** to change.

HARTKOPF: Possibly the designations should be tied to date, i.e., the "J" before the WMC gives the date of the hierarchy determination as well.

Highlights of Astronomy, Vol. 13
International Astronomical Union, 2003
O. Engvold, ed.

Nomenclature for Multiple Systems Containing Close Binaries

C.D. Scarfe

University of Victoria

Abstract.
I would like to discuss the difficulty of developing and maintaining a hierarchical designation scheme for components of multiple systems, when components are found by more than one method. Such a sequence of discoveries can easily lead to conflict between the initial nomenclature, which gets established in the literature, and that based on a scheme that is in broader use, or is more physically representative, or both. I will describe as an example a hypothetical complex system whose hierarchical description depends on the sequence in which discoveries are made, and whose designation in discovery order is ambiguous. In the end I urge flexibility in designations.

1. The designation problem

I am concerned about the difficulties inherent in applying either a hierarchical scheme, or one based upon order of discovery, when inner systems are discovered independently of, and perhaps before, the outer ones. Such complex multiples exist among purely spectroscopic, spectroscopic-photometric, spectroscopic-visual, and purely visual multiple systems. If we alter designations as new components are discovered, this will lead to confusion in the literature, but it seems necessary if we are to maintain a hierarchical designation scheme. I shall illustrate the problem with real systems and a hypothetical one. Really complex systems can even call into question what we mean by order of discovery, as I shall attempt to show. And although the concepts of 'Primary' and 'Secondary' are vital to hierarchical schemes, observers using different techniques define those concepts differently, which can lead to ambiguity.

I have in fact been concerned with this matter for some time, and spoke about some facets of it at the Multi-Commission Meeting convened at the Manchester General Assembly three years ago. At the time I was speaking from a perspective very familiar to me, that of a spectroscopist. This time I shall try to represent a broader spectrum of interests, encompassing the activities of all of Commission 42. This is not an easy task, although I can claim some acquaintance with photoelectric photometry and light curves.

Three years ago I expressed general support for the hierarchical scheme proposed for the Washington Multiplicity Catalog, perhaps underestimating the difficulty of assigning hierarchical levels in visual systems where little relative motion is seen for long periods. This perhaps explains the persistence of labels C, D, etc. for components of wide multiples. I pointed out then the difference that might have occurred in labeling the components of Castor, had the bright pair been closer together and hence detected spectroscopically first. I also expressed concern about the assignment of 'primary' and 'secondary' labels, noting that visual observers generally do this by ranking in order of brightness, presumably in the optical range or part of it. Photometrists, however, can easily tell which star is hotter, but must solve the light curve to decide which is larger, and deduce from both pieces of information which is more luminous. By contrast, spectroscopists ideally attach the label 'primary' to the more massive star. This would not always be the brighter, even in relatively simple cases. In a poster I recently presented at Colloquium 191, jointly with Roger and Elizabeth Griffin, we described a system where there is a difference close to three magnitudes in the stars' visible light, yet they are almost equal in mass, one being a giant and the other a subgiant, which will soon commence to traverse the steep giant branch of its evolutionary track. This is the ideal situation; spectroscopists in the real world often simply label the star whose spectrum is easier to measure as the primary. Witness the case of Capella, whose components are nearly equal in both mass and luminosity, but vastly different in the ease with which radial velocities may be measured, owing to the different rotational broadening of their spectra.

2. An example

As an illustration of the difficulties one might encounter with a really complicated system, let me turn to the fortunately fictitious 'strawman' multiple system promulgated by Helene Dickel four years ago to stimulate interest in the nomenclature problem. She assigned what I regarded as an implausible discovery sequence to it. After some thought I responded with another one, much more plausible in my view, but which led to much uncertainty with regard to the proper labeling of the components. let me now review that skeptical response, slightly revised in the most recent developments from its original form. The system described is ultimately found to have nine components, including two planets in orbits around the brightest star. The latter has a nearby visual companion and a distant common-proper-motion companion, both of which are triple stellar systems in their own right.

I retained the original notation, and kept the identifications of components 1 through 9. Objects 1 and 2 are planets around bright star 3, while 4, 5 and 6 are components of its visual companion and 7, 8 and 9 those of the common-proper-motion companion. I retained the assumption that components 4 and 5 were quite close together, compared with the separation of 6 from their center of gravity, and likewise that 7 and 8 were closer to each other than they were to 9. I also assumed that the orbital period of planet 1 was much longer than that of planet 2, so as to make plausible a smaller amplitude of the radial-velocity variation of star 3 due to the presence of 1 than that due to 2, and thus to retain the original order of the planets' discoveries. The discovery sequence I proposed was as follows, and the apparent structure of the system at each stage is illustrated in Figure 1, where the discoveries described below are identified by their dates.

1. A wide pair of stars is found to have common proper motion in 1850.

Discovery Sequence

Detected directly: ⊙
Presence inferred: ○

	AB	**C**
1850 - C.p.m. pair	⊙	⊙
1900 - Visual pair	⊙ ⊙	⊙
1925 - Spec. bin.	⊙ ⊙ ○	⊙
1950 - Broad-line cpt.	⊙ ⊙ ○	⊙ ○ ⊙
1960 - Eclipses	⊙ ⊙ ⊙ ○	⊙ ○ ⊙
1980 - Speckle	⊙ ⊙ ⊙ ○	⊙ ○ ⊙
1990 - LBI	⊙ ⊙ ⊙ ⊙	⊙ ○ ⊙
1995 - Planet 1	○ ⊙ ⊙ ⊙ ⊙	⊙ ○ ⊙
1999 - RV in triple	○ ⊙ ⊙ ⊙ ⊙	⊙ ○ ⊙
2003 - Planet 2	○ ○ ⊙ ⊙ ⊙ ⊙	⊙ ○ ⊙
Component nos.	**1 2 3 4 5 6**	**7 8 9**

2. The brighter of the two is resolved into two visual components in 1900, as they approach apastron. (We shall assume that the separation does not decrease again for at least another century, which will facilitate the discoveries to be discussed below.) They are labeled A and B. Since the common-proper-motion companion's physical connection to AB is confirmed at about the same time by the discovery that it has the same radial velocity as A, it is referred to as component C.

3. B is found to be a spectroscopic binary in 1925, despite having its spectral lines broadened severely by (synchronous) rotation. The discovery is made possible by its short period and large radial-velocity amplitude.

4. C is found in 1950 to show, in addition to its sharp-lined spectrum, a broad-lined one with radial-velocity variations indicative of binarity. The

sharp-lined spectrum does not show variations with the same period, so it is concluded that the system is triple.

5. In 1960, B is found by photoelectric photometry to show shallow eclipses. But even after stray light from A is carefully eliminated, their analysis requires the assumption of 'third light', strongly suggesting, but not proving, that that system is also triple. The eclipsing pair is listed as a variable star.

6. In 1980, speckle observations resolve C into two components of similar brightness. Thus it isn't obvious which of them is the broad-lined binary subsystem and which is its sharp-lined companion.

7. In 1990, long-baseline interferometry reveals the component of B that contributes the third light. That component, correctly described as a companion to the eclipsing pair, is significantly fainter than their combined light, as expected from the eclipse solutions, and is indeed a difficult object to detect by that technique. This of course also explains its absence from the combined spectrum.

8. In 1995 a planet is discovered around A, which is now sufficiently well separated from B to permit its spectrum to be observed uncontaminated, and its radial velocity to be measured very precisely.

9. In 1999, a slow variation in the velocity of the sharp-lined component of C is detected, along with a corresponding one in the velocities of the center of mass of the subsystem containing the broad-lined one. The latter has a smaller amplitude than the former, as might be expected since two stars are usually more massive than one of comparable luminosity. But careful work on equivalent widths of lines reveal that the sharp lined one is slightly the less luminous. Reanalysis of the speckle observations in the light of this information resolves numerous ambiguities of quadrant in the early (1980's) data and permits the derivation of a three-dimensional solution for the orbit.

10. In 2003, a second planet is found in orbit around A, by analysis of the residuals from the velocity curve due to the first, as a slow drift up and down.

11. We note that in the near future, high signal-to-noise spectroscopy should lead to the detection of the faint spectrum of the eclipsing pair's companion (the one that gave the third light and was seen by long baseline interferometry); measurement of its radial velocity variations would yield a similar solution for B.

3. Discussion

In this scenario, whose sequence of events I regard as much more plausible than the original one, in view of when the various techniques became available, components 4 and 5 were discovered before 6, and it is not obvious which of 9 and the combination of 7 and 8 should be called the primary of C. (The distant, sharp-lined companion, which dominates the spectrum, is 9.) We note, however, that if the eclipses of 4-5 were not shallow, the 4-5 pair would almost certainly have been first discovered by photometry rather than spectroscopy, a pattern normal for eclipsing systems. The presence of star 6, the third light, helps to make the eclipses shallow, but that could also be caused by the fainter component of the eclipsing binary being both cooler and smaller than the brighter one; note that it is not seen in the spectrum. Note also that we could instead have made the eclipsing pair a double-lined binary, while still retaining the above discovery sequence, provided that its orbital inclination was low enough to make the eclipses grazingly partial, and hence shallow, as required.

In this scenario too, C is a hierarchical triple, in contrast to the original scheme, which I regarded as implausible. But it isn't obvious whether 7 and 8 together should be the primary, Ca1 and Ca2, with 9 being Cb, or whether the a's and b's should be interchanged. Note that 7-8 is considerably more massive than 9, and slightly more luminous, but that 9 was discovered first in the sense that its spectrum was the first component to be seen in the combined spectrum, before it was realized that more than one star was present in the C system. Moreover, since the 4-5 pair was found before 6, on discovery 4 and 5 would have been called Ba and Bb respectively. But after 6 was found they would have to be renamed Ba1 and Ba2, while 6 becomes Bb in a hierarchical scheme. In the end, too, when A and B have been followed through a significant fraction of their orbit, it would be evident that the whole system was hierarchical; should the components then be renamed so that C becomes B, and A and B become Aa and Ab respectively, with all the consequent changes to the nomenclature of the smaller subsystems?

Thus this scenario required changes to any hierarchical nomenclature as a result of new discoveries. However in 2000 the rival sequential scheme corresponded very poorly to the hierarchical structure and thus revealed little about it. Indeed I would not find it easy to put the nine objects in order of discovery at all. For example note that the spectroscopic systems 4-5 and 7-8 are both single-lined binaries, with 4-5 eclipsing and 7-8 not. Indeed components 1, 2 and 8 have never been seen at all; their presence is inferred from their effects on the radial velocities of the stars nearest to them. And since the combination 7-8 is slightly brighter than 9, whose spectrum, being sharp, was detected first, was 7-8 the object first seen as C or was 9?

Thus for such a nightmare system as this, no scheme then, or now, under consideration can wholly satisfy the stringent demands initially proposed by IAU Commission 5. I did not then believe, nor do I now, that any physically useful system of nomenclature can be set in stone as the IAU appeared to wish. Instead I believe we must accept that useful designations correspond to the physical structure of the systems and that new discoveries of components will cause designations to be revised; all we can reasonably expect of those active in the field is that they do not rename objects unnecessarily. It follows therefore that we should set a good example, and not rename the objects in the WDS. We should thus adopt the revised version of the WDS scheme, expanded to cope with unresolved systems, and continue to ensure that it remains flexible enough to permit newly discovered components to be readily incorporated. As an example of such discoveries, see Patience et al. (2002).

In the example, several of the subsystems are 'discovered' by more than one technique, in the sense that it isn't immediately obvious whether, for example, a component found by speckle is the same as one seen previously in the spectrum of the combined light of a system. This may also be true in the real world. I have not gone into the situation where components are seen in only one spectral region, such as occurs for the IUE discoveries of companions to Cepheids, for example. The presence of a companion may have been inferred from variations in the mean radial velocity of the cepheid, but is the ultraviolet companion the one that causes that variation? In some cases we still don't know. Thus any scheme that tries to set designations in stone will be outdated in time, and will have to be abandoned. Flexibility is the key to a system that retains its usefulness.

4. Another point of view

Let me now briefly present another point of view, presented to me in correspondence with Jean Dommanget, and based upon his experiences in preparing the CCDM Catalogue. He is firmly convinced that designations should not change once they are established in the literature, a view divergent from my own. But he would achieve this stability by not basing a catalogue on *systems* of stars, but by listing the individual objects as separate entries. He would note their mutual relationships as a secondary matter. In a sense he would not produce a catalogue of binary and multiple systems at all, but instead one that listed the objects that are the components of such systems. This may in fact be the solution to the dilemma of making designations permanent in the face of new discoveries. It would leave hierarchical information out of the cataloging process altogether, except as a secondary matter. It was applied to resolved systems, and I do not know whether it could be extended to those not yet resolvable. For this reason at least, I am not convinced that this is the best way to proceed, but it does have some advantages.

References

Patience, J. et al. 2002, ApJ, 581, 654

1. Discussion

DICKEL: Designating by position only may be a problem if you don't know what the object is, i.e., can't see it.
SCARFE: That would be true of any designation that is simply a code, without astrophysical information included. The position is perhaps the minimum possible amount of that kind of information.

Highlights of Astronomy, Vol. 13
International Astronomical Union, 2003
O. Engvold, ed.

The Viewpoint from Commission 40

Richard N. Manchester

CSIRO, Australian National Telescope Facility, Sydney, Australia

Abstract. Although Very Long Baseline Interferometry has resolved a few binary stellar systems, pulsars provide the main source of binary and multiple stars through radio astronomy techniques. There are about 85 binary pulsars and two multiple systems known. Currently there is no formal system of designating these companions.

Through the technique of Very Long Baseline Interferometry, radio astronomy provides the angular resolution to separate sources into different components. However, most stars are weak radio sources and few have been resolved (e.g. Ransom et al. 2003).

The discovery of pulsars allowed binary (or multiple) stellar systems to be resolved using the techniques of spectroscopy. Because of the fantastic precision of pulsars as clocks, pulsar spectroscopy is orders of magnitude more sensitive than even the most precise optical spectroscopy, allowing the detection of (for example) the first extra-Solar-System planetary system (Wolszczan & Frail 1992). Of the ~ 1500 known pulsars, about 85 are members of binary or higher order systems. Most millisecond pulsars are binary. The companion star, usually a white dwarf, is rarely seen directly – in some cases the star has been identified through optical modulation at the binary period (e.g. Stappers et al. 2001) and two pulsars, PSR J0045−7319 and PSR B1259−63, have B-star companions identified through positional coincidence.

There is no current formal designation system for the companion in pulsar binary systems – they are simply referred to as "the companion of" the pulsar. Only two pulsars have evidence for more than one companion. The "planet pulsar", PSR B1257+12, has at least three planetary-mass companions, two with masses of about four Earth-masses and one with a mass close to that of the Moon (Wolszczan et al. 2000). These companions have been given letters, A, B and C in the order of their discovery, appended to the pulsar name. PSR B1620−26 is a binary pulsar with a white-dwarf companion in a 191-day orbit. Long-term pulse timing measurements indicate the presence of a second companion of mass $\sim 0.01\ M_\odot$ in an ~ 100-year orbit (Thorsett et al. 1999). Currently there is no separate designation for this companion.

In the future, with high-sensitivity radio telescopes such as the Square Kilometer Array, the number of known binary and multiple pulsar systems will certainly increase. It is important that pulsars be included in multiple-star and planetary-system catalogues and now is a good time to start.

References

Ransom, R.R., Bartel, N., Bietenholz, M.F., Ratner, M.I., Lebach, D.E., Shapiro, I.I., & Lestrade, J.-F. 2003, ApJ, 587, 390

Stappers, B.W., van Kerkwijk, M.H., Bell, J.F., & Kulkarni, S.R. 2001, ApJ, 548, L183

Thorsett, S.E., Arzoumanian, Z., Camilo, F., & Lyne, A.G. 1999, ApJ, 523, 763

Wolszczan, A. & Frail, D.A. 1992, Nature, 355, 145

Wolszczan, A., Hoffman, I.M., Konacki, M., Anderson, S.B., & Xilouris, K.M. 2000, ApJ, 540, L41

1. Discussion

DICKEL: Since so few binary systems are planets within pulsars this is a good opportunity to start entering them in the WMC and the pulsar community needs to label components and do it this way.
MANCHESTER: Fine, it would work as the need arises. This is not a problem at present. We just say “companion” of pulsar.

Highlights of Astronomy, Vol. 13
International Astronomical Union, 2003
O. Engvold, ed.

Nomenclature Scheme In Use By The WGESP and a Current List of Extrasolar Planets

Jill C. Tarter

SETI Institute

At the IAU General Assembly in 2000, the Working Group on Extrasolar Planets (WGESP) was established as a working group of Division III. Its terms of reference include acting as a focal point for international research on extra solar planets and organizing IAU activities in the field, such as, organizing comparative reviews of techniques used to detect extra-solar planets and establishing criteria for detections of varying degrees of certainty, as well as maintaining lists of objects satisfying these criteria. The committee is chaired by Alan Boss, and the current members are; Paul Butler, William Hubbard, Philip Ianna, Martin Kürster, Jack Lissauer, Michel Mayor, Karen Meech, Francois Mignard, Alan Penny, Andreas Quirrenbach, Jill Tarter, and Alfred Vidal-Madjar.

The activities of this working group are reported on the web site

`http://www.ciw.edu/IAU/div3/wgesp/planets.shtml`.

In particular, the members of the working group have established a working definition for a body called a "planet", and have created a list of objects that satisfy that definition. This definition (as last modified on Feb. 28, 2003) can be found at

`http://www.ciw.edu/boss/IAU/div3/wgesp/definition.shtml`,

and can be expected to be modified as we improve the census of low-mass stellar companions.

The most salient points about what does and does not constitute a planet are as follows. A planet must:

- have a true mass below deuterium burning limit ($\sim 13 M_J$ for solar metallicity),
- orbit a star or stellar remnant, and
- have a true mass above whatever we end up adopting for our own solar system.

Note that this definition specifically excludes "free-floaters." Until there is an unambiguous determination that any such body was born in orbit around a star or stellar remnant, then they will be classified on the basis of their estimated mass. Objects with substellar masses exceeding 13 M_J will be referred to as Brown Dwarfs, while those with masses less than 13 M_J will be called sub-Brown Dwarfs.

The current list of objects satisfying this working definition can be found at:

`http://www.ciw.edu/boss/IAU/div3/wgesp/planets.shtml`.

At present, the list contains 99 entries, all of which have been detected by radial velocity techniques. Since true masses are not available from this technique alone, the working list consists of reported planets with $M \sin i < 10 M_J$. The format for the current table uses the Hipparcos, and HD designations and common name of the star as the primary indicator. The date of receipt of the discovery paper by the refereed journal that eventually published the discovery is also cited, and is a requirement for inclusion in the working list. A second table of pulsar planets (explicitly permitted under the working definition) can be found on the same web page.

Although it is tempting to invent or adopt some "popular" names for the individual extra-solar planets (particularly in interactions with the media), the WGESP has specifically resisted this temptation. The WGESP further agrees that it will uses whatever new classification scheme is adopted by the IAU for double star systems, but that the working group does have a natural preference for a nomenclature that recognizes the difference between a planet and a star.

1. Discussion

POURBAIX: Could you add the ADS bibcode to your table?
TARTER: I see no reason why the table should not have links to the ADS bibcode. Good suggestion.

DICKEL: (Suggestion) 1. Initially the nature of the component of a multiple star system may not be known - i.e. whether it is a planet or star in the WMC catalog. 2. When the component is discovered to be a "planet", it goes into the official extra-solar planet list with an Exoplanet type "acronym" or designation.
TARTER: Good suggestion. I will talk with you about the approved acronym we should adopt.

ZINNECKER: Do you think that the definition of a planet that the IAU Working Group has proposed will survive? I sense some disagreement in the community.
TARTER: The definition of planet adopted by the WGESP[22] is a "working" definition and will change over time if the community changes its mind. There was significant debate over each point prior to reaching the current consensus. We will always keep the working list of planets consistent with the working definition of planets.

---

[22] Working Group for Extra-Solar Planets

ZINNECKER: Many of the free-floating objects will been born as planets, for example, in binary systems, but ejected. What should we call them?
TARTER: Until we find some unambiguous marks that identified the birth place of a "free floater" as having been in orbit around a star or stellar remnant, we have chosen not to list them, and on basis of mass, call them brown dwarfs or sub-brown dwarfs.

TOKOVININ: A preference to a designation scheme that makes a difference between stellar companions or planets is not practical; some "planets" with $M \sin i < 10 M_J$ will be stars, some with $M \sin i > 10 M_J$ will have $M < 13 M_J$.
TARTER: True. What I meant to say was that it would be desirable to have the designation scheme reflect the fact that with the knowledge in hand, the object was currently listed on the WGESP working list of planets. Over time, the designations might have to change to accommodate new information. I understand that gets into the middle of the "static" vs. "dynamic" argument. Rather than take sides, I merely stated a small preference.

Highlights of Astronomy, Vol. 13
International Astronomical Union, 2003
O. Engvold, ed.

SPS3: Epilog

Brian D. Mason and William I. Hartkopf

United States Naval Observatory

Abstract. Events and actions transpiring after SPS3 are detailed here.

1. Resolution

During SPS3 the following resolution was presented and ratified:

On Designating Components of Binary/Multiple Star Systems

Recognizing

- the increasing synergy of techniques for the investigation of stellar companions blurring the traditional distinction between astrometric, spectroscopic, and photometric binary and multiple stars;
- the detection of sub-stellar (including planets) as well as stellar components by these techniques and,
- the need for a simple, unambiguous, flexible, and computer friendly designation scheme for components of binary and multiple star systems,
- Noting that future ground and space-based telescope projects have the potential to detect both sub-stellar as well as stellar components in increasingly large numbers,

Recommends that

- a uniform designation scheme, based on expansion of the Washington Multiplicity Catalog (WMC) system, be developed during the next 3 years to include all types of components and that this be reviewed in time for its adoption to be considered at General Assembly XXVI.

This resolution was adopted at the Sydney GA by Commissions 5 (Documentation & Astronomical Data), 8 (Astrometry), 26 (Double & Multiple Stars), 42 (Close Binary Stars), 45 (Stellar Classification) and the Working Group on Optical and Infrared Interferometry.

2. Changes to WMC, Post-SPS3

To accommodate the desire for a fixed designation but also give the most correct interpretation of multiplicity structure there will be two component designation columns. The first will be the **"official" component designation**, which, as per Commission 5 guidelines, will remain fixed in order to avoid confusion when dealing with historical data. The second will be our **"best-guess" component designation**, based on our current knowledge of a system's hierarchical structure. Designations in this "data column" may change as new components are discovered or additional information is published on known components.

3. WMC Working Group

At the suggestion of Colin Scarfe (President, Commission 26), a working group was formed within Division IV for the implementation and completion of the WMC prior to the Prague GA. The initial working group membership consists of W. Hartkopf, B. Mason (chair), D. Pourbaix, C. Scarfe, M. Schmitz, and A. Tokovinin. About a year before IAU GA XXVI, the WMC WG will present to the SOC the all-sky WMC in preparation for a type B resolution to be presented in Prague. At that time, following new IAU Bye-laws, the future needs and prospects of this Working Group will need to be evaluated to determine if it needs to be renewed or should dissolve.

A few of the questions to be addressed by the WG include:

1. What additional sources of duplicity information have been published?
2. How can we be kept informed of discoveries in other fields of binary star research?
3. The sample WMC assumed separations greater than $\sim 1''$ were possibly optical, so no hierarchies were assigned (i.e., all components were given uppercase letters). What should we adopt as the official optical/physical limit? Should we use, for example, the Aitken magnitude-separation criteria? What about common proper motion pairs?
4. What should we adopt as the official definition of "primary"? Is the suggested priority — most massive → brightest in V → brightest in another filter — reasonable? If the system includes a variable star, is the peak or median brightness more appropriate?

4. Acronym WMC

The acronym **WMC** is classified as a new acronym being registered at CDS (see `http://vizier.u-strasbg.fr/cgi-bin/Dic?/6947579`).

5. WMC Websites

Further information on the WMC can be found at the following websites.

- `http://ad.usno.navy.mil/wds/wmc/iaumcm_old.html` - Archival webpage for 2000 Multi-Commission Meeting at IAU GA XXIV
- `http://ad.usno.navy.mil/wds/wmc/sps3.html` - Special Session 3 webpage for IAU GA XXV
- `http://ad.usno.navy.mil/wds/newwds.html` - WMC designation scheme and Working Group webpage
- `http://ad.usno.navy.mil/wds/wmc/wmc110_intro.html` - Sample WMC
- `http://ad.usno.navy.mil/wds/wmc/wmc_descrip.txt` - Description of WMC
- `http://ad.usno.navy.mil/wds/wmc/wmc_timeline.txt` - WMC development timeline

Acknowledgments. In addition to the participants, organizers, and presenters of SPS3, we'd like the thank the Sydney LOC for a wonderful venue with the most agreeable of hosts, especially our local liaison, John Davis.

SPS4

Effective Teaching and Learning of Astronomy

Chairperson: J.R. Percy

Editor: J.R. Percy

Highlights of Astronomy, Vol. 13
International Astronomical Union, 2003
O. Engvold, ed.

A Short Overview of Astronomical Education Carried Out by the International Astronomical Union (IAU)

Syuzo Isobe

National Astronomical Observatory
2-21-1, Osawa, Mitaka, Tokyo, Japan
E-mail: isobesz@cc.nao.ac.jp

1. IAU Commission 46 "Astronomy Education and Development"

The IAU is a union of professional astronomers who produce new astronomical results and who make the frontiers of astronomy expand. However, the IAU cannot stand by itself but needs the support of governments as well as the people. This is one reason why the IAU set up Commission 46 – originally called "Teaching of Astronomy" and renamed "Astronomy Education and Development" with much wider mandate in 2000 – to cover astronomy education from the level of beginners to that of post-doctoral students.

There are currently 9 "program groups" (PGs). Because of the limited budgetary resources of the IAU, it is hard to cover all the fields which our Commission would like to target. The "National Liaison" PG communicates closely with the Organizing (Executive) Committee members as well as the regular members by producing national reports from individual countries every three years. All the commission activities and some related activities are communicated to the members and other people interested in astronomy education mainly through electronic mail but in some special cases in print, by the "Newsletter" PG.

The "Solar Eclipse" PG holds public lectures related to each individual total or annular solar eclipse and informs people how to look at the eclipse safely. For a country and especially a developing country intending to develop astronomy and astronomical education it is important to have at least one but preferably several science (mainly physics) professors in that country who have a strong motivation to develop it. The Worldwide Development of Astronomy" PG tries to find such professors through different channels. Once the Advanced Development PG identifies some specific country, such information is sent to the "Teaching for Astronomy Development" PG which starts to send lecturers to that country for several weeks or months, and to invite students from that country to an institute in a developed country carrying out high-level astronomical research. Those students are expected to promote astronomical education in their countries when they return.

In developing countries, there is only one or a few professors, and their astronomical fields are very limited. To give graduate students and young astronomers a wider perspective, the "International Schools for Young Astronomers" PG organizes schools in each region. The schools started in 1967 and 26 schools had been held by 2003. If a young astronomer wishes to do research at a specific institute in another country, the "Exchange of Astronomers" PG supports his/her travel costs. Since the Commission's budget is limited, the "Collaborative Group" PG seeks ways to carry out activities in collaboration with other organizations. The "Exchange of Books and Journals" PG arranges to send surplus books and journals to developing countries where they can be used.

Unfortunately, our PGs do not directly include astronomy education in school. I, as the Commission 46 President on July 25 2003, hope this special session will be a trigger for a future new program group.

2. To Whom Should Astronomy Be Taught?

In recent decades, the development of astronomy has been so rapid, and because of new interesting discoveries many people seem to have an interest in astronomical phenomena. However, in most cases they are interested in this information but, because of a shortage of astronomical and physical knowledge their understanding may not be correct.

Over 10 years ago, I presented a diagram showing what fraction of people was interested in what level of astronomy for the case of Japan (Isobe 1991). There are 7 categories: (A) Approximately 100 people produce useful astronomical data; (B) Approximately 1000 people observe frequently; (C) Approximately 10,000 people observe occasionally; (D) Approximately 100,000 people read astronomical magazines; (E) Approximately a million people read general science magazines; (F) Approximately 10 million people read science articles in newspapers; (G) Approximately 100 million people have no interest in science at all. Our target is certainly not a case of a totally opposite distribution to the Japanese case, but one in which most people will read astronomical and scientific magazines. It is difficult to have such a large fraction of people interested in astronomy through public education, but it should be taught through education in schools where nearly everyone studies.

Frequently, I hear from good amateur astronomers, and from school teachers who are interested in astronomy, that one should watch stars because of their beauty. It may be true for them, and for specific pupils, but there are people who on one hand love stars but others, on the other hand, love the beauty of a flower. What we should understand is that it is a matter of hobby for individual people to say "I love and/or enjoy watching stars or flowers" but this is not the same as real understanding of sciences such as astronomy and biology. If one can train people to understand sciences, especially physical sciences, those people often have the ability to understand and evaluate environmental issues.

3. How Should Astronomy Be Taught?

There are several types of countries in the teaching of astronomy. In some countries, astronomy is compulsory in the school curriculum, but in other countries pupils can choose from physics, chemistry, biology and earth science. For the latter case only a small fraction of pupils (less than 10%) choose earth science including astronomy. The third way is to teach integrated sciences by considering that all daily phenomena cannot be explained without combining different kinds of sciences.

In order to go the third way, I proposed to teach stories connecting all the related sciences, depending on pupils' grade and ability (Isobe 2000). As an example we can show areas and volume in physics, explosion energy in chemistry, evolution of life in biology, and asteroids in earth science; under a story title of "dinosaurs" we can produce different stories. To proceed this way in an effective manner, it is important to include some number of well-prepared exercises. Otherwise pupils just listen to the teacher's stories but can seldom catch the stories' target from a scientific point of view.

As such examples, we developed two exercises; the first one is evaluation of light energy loss (Isobe et al. 2001) and the second one is asteroid detection software (Isobe et al. 2002).

One other important issue to be carefully considered is that the development of science, especially astronomy, is so rapid. Therefore, depending on those new discoveries and also those expositions in newspapers, pupils' interest is changeable and we have to develop new stories continuously. This is somewhat complex and time-consuming work, but is inevitable work for future generations.

There are different national and international studies such as by the United Nations and the Organization of Economic Cooperation and Development to compare pupils' achievement, especially physics and sciences within different countries. However, nearly all the participating countries use those results to improve their ranking, and try to introduce an educational system which is carried out in countries with high ranking without deep consideration of differences of culture, history, and nationality.

4. Conclusion

Education systems are different from country to country and even if a good education system may be introduced in some countries its real results will emerge only after several decades. Therefore, at each time, we have to communicate with each other closely. I repeat that I hope that this special session will be a trigger, and that a number of participants will try to set up a new PG of Commission 46 to communicate more extensively with other education organizations.

References

Isobe, S. 1991, Proposed Structure of Education in Astronomy, Proceedings of Astronomical Society of Australia, 9, 72-75.

Isobe, S. 2000, Report on International Conference on Primary School Science and Mathematics Education, held in Beijing, 1-4 November 2000, and organized by the International Council for Science (ICSU).

Isobe, S. Hamamura, S., 2001, Educating the Public about Light Pollution, in *Preserving the Astronomical Sky*, ASP Conf. Series, 196, 363-368.

Isobe, S. Asami, A., Asher, D., Fuse, T., Hashimoto, N., Nakano, S., Nishiyama, K., Oshima, Y., Takahashi, N., Terazono, J., Umehara, H., Urata, T., and Yoshikawa, M., 2002, Educational Program of Japan Spaceguard Association Using Asteroid Search; - Spaceguard Detective Agency, in *Proceeding of Asteroids, Comets, Meteors*, 817-819.

Highlights of Astronomy, Vol. 13
International Astronomical Union, 2003
O. Engvold, ed.

Why Astronomy is Useful and Should be Included in the School Curriculum

John R. Percy

University of Toronto, Mississauga ON Canada L5L 1C6
E-mail: jpercy@utm.utoronto.ca

Even in my astronomically-developed province of Ontario, Canada, with an excellent public education system, astronomy was not a compulsory topic in the school curriculum until quite recently. So I began collecting a list of reasons why it *should* be, in the hope of persuading those who set the curriculum.

It would be instructive, however, to start by asking: "Why is astronomy *not* included in the curriculum?" Here are some possible reasons: (i) Astronomy is perceived to be irrelevant to practical concerns such as health, nutrition, agriculture, environment, engineering, and the economy in general; this is particularly true in developing countries. (ii) Most school teachers have little or no knowledge of astronomy, or astronomy teaching; in fact, they may have the same deeply-rooted misconceptions as their students. (iii) Astronomy is perceived as requiring night-time activities ("the stars come out at night, the students don't"), and expensive and complex equipment such as telescopes. (iv) Astronomy is perceived as being solely "Western" by some non-Western cultures. (v) There may be conflict – real or perceived – between astronomy and personal beliefs such as religion, culture, and pseudo-science; in fact, astronomy is sometimes viewed as being as speculative as pseudo-science. (vi) Many of the available resources are designed for affluent schools in affluent countries, or for different latitudes, longitudes, and languages. (vii) Astronomy may be seen as allied with high technology, with all its real and perceived dangers.

Many of these reasons are based on a lack of an astronomical "tradition" in a country or region. This is one more reason for all members of "the astronomical community" to speak and work together in promoting astronomy.

Now we can address the main topic of this presentation: the reasons why astronomy is useful, and should be part of the school curriculum – in science, or some other place. These can be grouped in several categories:

Cultural and Historical: Astronomy is deeply-rooted in almost every culture, as a result of its practical applications, and its philosophical implications. Among the scientific revolutions of history, astronomy stands out. In the recent lists of "the hundred most influential people of the millennium", a handful of astronomers were always included. Astronomy, by its nature, requires observations from different latitudes and longitudes, and thus fosters international co-operation. It also requires observations over many years, decades, and centuries, thus linking generations and cultures of different times.

Practical: Astronomy has obvious practical applications to time keeping; calendars; daily, seasonal, and long-term changes in weather; navigation; the effect of solar radiation; tides; and impacts of asteroids and comets with the earth.

Scientific and Technological: Astronomy is a forefront science which has advanced the physical sciences in general by providing the ultimate physical laboratory — the universe — in which scientists encounter environments far more extreme than anything on earth. It has advanced the geological sciences by providing examples of planets and moons in a variety of environments, with a variety of properties. Astronomical calculations have spurred the development of branches of mathematics such as trigonometry, logarithms, and calculus; now they drive the development of computers: astronomers use a large fraction of all the supercomputer time in the world. Astronomy has led to other technological advances, such as low-noise radio receivers, detectors ranging from photographic emulsions to electronic cameras, and image-processing techniques now used routinely in medicine, remote sensing etc. Its knowledge is essential as human kind enters the era of space exploration.

Aesthetic and Emotional: Astronomy reveals our cosmic roots, and our place in time and space. It deals with the origins of the universe, galaxies, stars, planets, and the atoms and molecules of life — perhaps even life itself. It addresses one of the most fundamental questions of all — are we alone in the universe? Astronomy promotes environmental awareness, through images taken of our fragile planet from space, and through the realization that we *may* be alone in the universe. Astronomy reveals a universe which is vast, varied, and beautiful — the beauty of the night sky, the spectacle of an eclipse, the excitement of a black hole. Astronomy thus illustrates the fact that science has cultural as well as economic value. It has inspired artists and poets through the ages. Astronomy harnesses curiosity, imagination, and a sense of shared exploration and discovery.

Pedagogical: Astronomy, in the classroom, provides an example of an alternative approach to "the scientific method" — observation, simulation, and theory, in contrast to the usual experiment and theory approach. Astronomy, if properly taught, can promote rational thinking, and an understanding of the nature of science, through examples drawn from the history of science, and from present issues such as pseudo-science. Astronomy can be used to illustrate many concepts of physics, such as gravitation, light, and spectra. Astronomy, by introducing students to the size and age of objects in the universe, gives them experience in thinking more abstractly about scales of time, distance, and size. Astronomy is the ultimate interdisciplinary subject, and "integrative approach" and "cross-curricular connections" are increasingly important concepts in modern school curriculum development.

Societal: Astronomy attracts young people to science and technology, and hence to careers in these fields. Astronomy can promote and increase public awareness, understanding, and appreciation of science and technology, among people of all ages. Astronomy is an enjoyable, inexpensive hobby for millions of people. "The stars belong to everyone!"

Editor's Note: This presentation was followed by an open discussion of the many ways that astronomy can be – and is – included in the school curriculum, worldwide.

Highlights of Astronomy, Vol. 13
International Astronomical Union, 2003
O. Engvold, ed.

Astronomy and Mathematics Education

Rosa M. Ros
Universidad Politecnica de Catalunya, Spain
E-mail: ros@mat.upc.es

Astronomy has an interdisciplinary aspect that in some cases is very positive. It is interesting to combine Astronomy with other topics and introduce Astronomy in general projects in school in order to integrate several courses, for instance Physics, Mathematics, Geography, Biology or History; however these kinds of projects are sporadic. In order to promote Astronomy it is better to try to introduce it as a course in its own right. The viability of this situation depends on the national curriculum and the plans of the Education Ministry in each country. In general, the majority of countries do not have Astronomy as a specific course and it is not easy to achieve. Therefore, if this option is not possible, we should adapt to the real situation, that is to say include Astronomy as a part of other courses. This contribution aims to propose a new point of view which could work to make this the case.

Commonly, Physics teachers include some Astronomy in their classes. In some cases it is possible that other Science teachers (biologists or geologists) or non-Science teachers (geographers or historians) also teach Astronomy. Of course, in order to promote Astronomy, we have to promote all these possibilities; however the author of this paper would like to introduce Astronomy content within Mathematics courses as well.

This idea has several advantages and very few disadvantages. If Mathematics teachers try to introduce Astronomy into their classes, the situation will be better for everyone, because Astronomy will be promoted, and mathematics enriched. The only obvious disadvantage is that, if the astronomical content or the mathematical application is too difficult, the effect could be counter-productive for both subjects; we have to be prudent, and choose the examples very carefully. The advantages are as follows:

- **Mathematics is not very attractive to pupils; astronomy is more motivating**. "Students are not interested in discovering what an ellipse is, but they are really concerned about the possibility of the Moon crashing into the Earth"

- **Schools do not have Mathematics laboratories**. Mathematics is a very theoretical subject for students and in general seems unconnected with the real world. Lay people think that Mathematics is necessary to count, but practically nothing more. Anything more than basic arithmetical rules seems beyond them. Astronomy can offer Mathematics teachers a laboratory: the school grounds. If it is not cloudy students can observe the sky, take measurements and analyze the results obtained with their mathematical knowledge (taking them beyond arithmetic) and it is also possible to introduce scientific methodology and study the margins of errors.

"Students are not very interested in calculating the third side of a triangle from the other sides and angles, but they will be interested in finding the distance between the Earth and the Moon after making their own observations. Maybe the results are not very accurate but the experience will be very motivating and they will never forget it".

- **Mathematics appears from the first course in primary school until the end of secondary school.** Students study Mathematics for many years, providing an enormous opportunity to introduce many different astronomical ideas. Whereas if Astronomy appears only in physics courses, it is introduced very late in the curriculum. It is, therefore, better to also introduce Astronomy in Mathematics courses.

  "8-9 year-old students are very curious. They ask a lot of things about their surroundings. Why does the Moon look like a croissant? And, why sometimes not? Why can we see the Moon in the morning? (In children's stories the Moon only appears at night)".

  We are currently missing the opportunity to harness the curiosity of these younger students because, to obtain answers, they have to wait until they study physics in secondary school.

Conclusions

It is very important to offer Mathematics teachers a good selection of topics and activities connecting Astronomy and Mathematics. If they have good materials they will use them. Of course it is important to select very carefully a collection of astronomical items interesting from a mathematical point of view, according with its curriculum and related to the real world, in order to attract the students. We have to make sure students and teachers are satisfied if we want to achieve success.

It is necessary to say that this option is not incompatible with teaching Astronomy in physics courses. The interests of Physics and Mathematics teachers are not the same, however; they can offer a complementary point of view.

Several examples of suitable materials for mathematics teachers follow:

- Angles and star trails (the same angle for the same exposure time in a photograph of the sky)
- Logarithms and visual magnitudes (students are surprised when they discover that their eyes know logarithms, and perhaps they failed the logarithms' exam in the Mathematics course!)
- Plane trigonometry related positions (related orbital movements)
- Spherical trigonometry and ecliptic obliquity (relationships on ecliptic obliquity and latitude)
- Conic curves related to sundials (by finding conic curves in the street)

Highlights of Astronomy, Vol. 13
International Astronomical Union, 2003
O. Engvold, ed.

Astronomy Education Research Down Under

John M. Broadfoot and Ian S. Ginns
Queensland University of Technology, Australia
E-mail: j.broadfoot@qut.edu.au, j.ginns@qut.edu.au

1. Introduction

There are many problems associated with the teaching and learning of astronomy that require further investigation (Taylor & Barker 2000). Students' difficulties with visualization, mental modeling and conceptual restructuring have been reported by a number of researchers. Aspects of these important areas of research are examined in the paper. However, there has been limited focused research in the specific area of astronomy teaching (Taylor & Barker 2000; Treagust & Smith 1989). For example, the value of strategies that engage students in challenging their prior beliefs and intuitive ideas, thus enabling them to perceive patterns and grapple with frame of reference problems, and construct acceptable models of celestial phenomena, must be assessed. Such strategies might incorporate or re-enact historical discoveries (Noble 1999) thus engaging students in thinking about astronomical phenomena from an intuitive position.

2. Research into students' learning in astronomy

Research studies in astronomy indicate that students require high levels of spatial ability thinking (eg. Broadfoot 1995; Hill 1990; Vosniadou 1991a, 1991b). Ekstrom, French, Harmon & Derman (1976) defined two factors comprising spatial ability, spatial orientation and spatial visualization, as follows: spatial orientation - the ability to perceive spatial patterns or to maintain orientation with respect to objects in space (p. 149); and spatial visualization - the ability to manipulate or transform the image of spatial patterns into other arrangements (p. 173). Research into these aspects of spatial thinking, as well as mental modeling, are examined briefly in the following sections.

Spatial orientation: Astronomy frequently requires students to imagine objects from other viewpoints (Rock, Wheeler & Tudor, 1989), which demands a shift in perspective or change in the student's frame of reference (Finegold & Pundak 1990). Object-centered and observer centered viewpoints (Marr & Nishihara 1978; Marr 1982), an egocentric viewpoint (Steiger & Yuille 1983), and encoded landmarks (Evans, Marrero & Butler 1981), are descriptors of some of the ways that frames of reference can be established. Orientation frameworks may be constructed on the basis of a combination of at least four factors: gravitational direction, viewing direction, bodily direction, and environmental features (Broadfoot 1995). Orientation bound descriptions are essential for understanding the relative positions and motions of celestial objects. Broadfoot (1995) and

Feteris & Hutton (2000) demonstrated that individuals may initially comprehend the relative positions of objects such as constellations in space without a comprehensive orientational or orthogonal framework but fine tune the exact location of objects in space as an outcome of increasing field experience

Spatial visualization and transformations: An object-centered viewpoint of, for example, the Sun-Earth-Moon system, may necessitate considerable mental transformation by the observer from his/her viewpoint, which may result in conflict of object-centered (heliocentric) views with observer-centered (egocentric) views. Lucas & Cohen (1999) described the difficulties faced by students when relating textbook diagrams about seasons, which were mostly heliocentric, to activities of a geocentric nature.

Students often deal with orbital and rotational movements of celestial objects in the study of astronomy. Shepard & Cooper (1982) reported that orientation of mental images of three-dimensions often required transformations that increased in difficulty as the angle of rotation of an object from the original position increased. They noted that it was difficult for students to recognize the similarities between two dimensional drawings of the same three-dimensional situations, which may apply to problems where students attempt to interpret two-dimensional representations of the changing phases of the moon.

Mental models: Vosniadou (1989, 1991a) identified three kinds of mental models for explaining observed phenomena that provide insights into the constructs of students' knowledge bases. These are categorized as intuitive, scientific and synthetic models. The intuitive model, based on observational experiences of the natural world, requires little modification for accommodation of first-hand observations. Scientific models are in accord with current scientific views. Synthetic models show a combination of intuitive and scientific views and represent some kind of misrepresentation of scientific information. Vosniadou (1991a) concluded that a mental model of a spherical earth is a prerequisite to understanding the scientific explanation of the day/night cycle as is also an understanding of axis. The two concepts, spherical earth and axis, are examples of interdependence among concepts which are very important in understanding astronomy.

Glynn, Yeany & Britton (1991) discussed conceptual development in terms of intuitive understandings of the world. A flat earth, stationary and central to the universe, effects of gravity, the sun and moon moving up and down or east to west, and the stars being small are just some of the intuitive models possessed by many students (Vosniadou 1991a). Taylor & Barker (2000) investigated how learners constructed mental models when studying the Sun-Earth-Moon system and recommended that mental-model building should form the basis of astronomy education, a conclusion supported by Dunlop (2000) who studied students' learning through engagement in planetarium sessions.

3. Research into teaching and learning strategies in astronomy

The design of curricula for the teaching of astronomy should present concepts in an appropriate sequence and students should be provided with opportunities to examine their personal beliefs and explain their understandings of relevant concepts (Vosniadou 1991b). In addition, a number of researchers have suggested that the inclusion of activities that develop and enhance student spatial thinking abilities is highly desirable in the development of learning materials and teaching strategies for astronomy (e.g., Eylon & Linn 1988; McCubbin & Embeywa 1987). These activities should be based on direct observation (Lucas & Cohen 1999), and spatial training exercises should be included to develop student orientation frameworks and to enhance spatial visualization and transformation of dynamic celestial phenomena (Broadfoot 1995). Personal or collective investigations by students may be reinforced with a number of observer-centered, concrete three-dimensional models (Bishop 1990; Broadfoot 1995; Dunlop 2000; Domenech & Casasus 1991; MacIntyre 2003). These models need to be pertinent and make interactions transparent to students (Hill 1990), and students also require time to explore ideas when using the models to develop the complex spatial concepts in astronomy (Bishop 1988; Sadler & Luzader 1990). Quite often verification of astronomical concepts is not possible from direct observations (Hill 1990), for example, the sphericity of the earth or the heliocentric nature of the solar system.

Active involvement by students in modeling has been shown to be useful in astronomy teaching (Sadler & Luzader 1990). Students can model lunar and planetary motion, and star positions in conjunction with real sky activities and events. Investigating day and night, and the phases of the moon, through role-play would represent a possible starting point for the use of modeling as a way of examining and explaining celestial concepts and natural phenomena that are easily observable. Sweitzer (1990) has advocated the use of pictorial models, and Mazzolini & Halls (2000) have engaged students in computer modeling of celestial phenomena.

Other strategies for teaching astronomy include the use of analogies and the identification of similarities in students' concepts or beliefs (Vosniadou & Ortony 1989; Smith 1989), and an approach based on the historical development of knowledge in the field of astronomy (Glynn et al. 1991).

4. Recommendations for research

The first section of this paper drew attention to the difficulties learners face when grappling with the complexities of observing astronomical phenomena and when seeking to explain their observations. The second section of the paper examined briefly approaches and strategies that may be used to enhance the teaching and learning of astronomy. Based on this background of research findings, the paper concludes with exemplars of possible further research investigations that should be conducted in order to evaluate the effectiveness of these approaches and strategies in overcoming the difficulties experienced by students. It is only through approaches that take into account the analysis of the problems inherent in the learning of astronomy that gains will be made in this area. Our exemplars of possible research follow:

Learning and teaching: What thinking processes, with respect to orientation frameworks, do students use when confronting celestial motion problems? How do students interpret information from given data and restructure the information into different viewpoints both verbally and diagrammatically? What concepts are prerequisites and interdependent in astronomy learnings?

Teacher training: What is the exact nature of, and what factors affect, the designed and implemented curricula in astronomy in our tertiary institutions? Do these curricula produce teachers who are competent in teaching astronomy?

Primary and secondary schools: What is the exact nature of, and what factors affect, the designed and implemented curricula in astronomy in our primary and secondary schools? Do these curricula engage students in challenging and constructing their own knowledge and understanding of astronomy?

References

Bishop, J. E. (1988). Developing students' spatial ability. Science Teaching, 45(8), 20-23.

Bishop, J. E. (1990). Dynamic human (astronomical) models. In J. M. Pasachoff & J. R. Percy (Eds.) *The teaching of astronomy.* The Proceedings of the 105th Colloquium of the International Astronomical Union, Williamstown, MA.

Broadfoot, J. M. (1995). Development of visuospatial abilities among undergraduate astronomy students. Unpublished Masters Thesis. Curtin University of Technology: Perth.

Domenech, A. & Casasus, E. (1991). Galactic structure: A constructivist approach to teaching astronomy. School Science Review, 72(260), 87-93.

Dunlop, J. (2000). How children observe the universe. Publications of the Astronomical Society of Australia, 17(2), 194.

Ekstrom, R., French, J., Harmon, H. & Derman, D. (1976). Manual for kit of factor-referenced cognitive tests. Princeton, NJ: Educational Testing Service.

Evans, G. W., Marrero, D. G. & Butler, P. A. (1981). Environmental learning and cognitive mapping. Environment and Behaviour, 13 (1), 83-104.

Eylon, B. & Linn, M. C. (1988). Learning and instruction: an examination of four research perspectives in science education. Review of Educational Research, 58(3), 251-301.

Feteris, S. & Hutton, D. (2000). Astronomy laboratory: What are we going to make today? Publications of the Astronomical Society of Australia, 17(2), 116.

Finegold, M. & Pundak, D. (1990). Students' conceptual frameworks in astronomy. Australian Science Teachers' Journal, 36(2), 76.

Glynn, S. M., Yeany, R. H. & Britton, B. K. (Eds.). (1991). A constructive view of learning science. In S. M. Glynn, R. H. Yeany & B. K. Britton. (Eds), *The psychology of learning science* (pp. 3- 19. Hillsdale, NJ: Erlbaum.

Hill, L. C. (Jr). (1990). Spatial thinking and learning astronomy: The implicit visual grammar of astronomical paradigms. In J. M. Pasachoff & J. R. Percy (Eds.) *The teaching of astronomy.* The Proceedings of the 105th Colloquium of the International Astronomical Union, Williamstown, MA.

Lucas, K. B. & Cohen, M. R. (1999). The changing seasons: Teaching for understanding. Australian Science Teachers' Journal, 45(4), 9-17.

MacIntyre, B. (2003, July). Collecting evidence to support an investigation with models approach to astronomy education, Paper presented at Annual Meeting of the Australasian Science Education Research Association, Melbourne, Australia.

Marr, D. (1982). *Vision.* San Francisco: Freeman.

Marr, D. & Nishihara, H. K. (1978). Representation and recognition of spatial organization of three dimensional shapes. Proceedings of the Royal Society of London B, 200, 269-294.

Mazzolini M. & Halls, B. (2000). Astro concepts – learning underlying physics principles in conceptual astronomy. Publications of the Astronomical Society of Australia, 17(2), 149.

McCubbin, W. L. & Embeywa, E. H. (1987). Visualization and its role in students' assessment of scientific explanations. International Journal of Science Education, 9(2), 229-245.

Noble, A. (1999, July). Using prehistory of science to teach astronomy in the primary school, Paper presented at Annual Meeting of the Australasian Science Education Research Association, Rotorua, NZ.

Rock, I., Wheeler, D. & Tudor, L. (1989). Can we imagine how objects look from other viewpoints? Cognitive Psychology, 21, 185-210.

Sadler, P. M, & Luzader, W. M. (1990). Science teaching through its astronomical roots. In J. M. Pasachoff & J. R. Percy (Eds.) *The teaching of astronomy.* The Proceedings of the 105th Colloquium of the International Astronomical Union, Williamstown, MA.

Shepard, R. N. & Cooper, L. A. (1982). *Mental images and their transformation.* Cambridge, MA: Bradford/MIT Press.

Smith, L. B. (1989). From global similarities to kinds of similarities: The construction of dimensions in development. In S. Vosniadou & A. Ortony (Ed.) *Similarity and analogical reasoning* (pp. 146-178). Cambridge: Cambridge University Press.

Steiger, J. H. & Yuille, J. C. (1983). Long-term memory and mental rotation. Canadian Journal of Psychology, 37, 367-389.

Sweitzer, J. S. (1990). Strategies for presenting astronomy to the public. In J. M. Pasachoff & J. R. Percy (Eds.) *The teaching of astronomy.* The Proceedings of the 105th Colloquium of the International Astronomical Union. Williamstown, MA.

Taylor, I. J. & Barker, M. (2000, July). Forgettable facts or memorable models? Arguments for a mental model building approach to astronomy education. Paper presented at Annual Meeting of the Australasian Science Education Research Association, Freemantle, WA.

Treagust, D. F. & Smith, C. L. (1989). Secondary students' understanding of gravity and the motion of planets. School Science and Mathematics, 89(5), 380-391.

Vosniadou, S. (1989, April). Knowledge acquisition in observational astronomy. Paper presented at Annual Meeting of the American Educational Research Association, Washington: DC.

Vosniadou, S. (1991a). Conceptual development in astronomy. In S. M. Glynn, R. H. Yeany & B. K. Britton. (Eds), *The psychology of learning science* (pp.149-177), Hillsdale, NJ: Erlbaum.

Vosniadou, S. (1991b). Designing curricula for conceptual restructuring: Lessons from the study of knowledge acquisition in astronomy. Journal of Curriculum Studies, 23(3), 219-237.

Vosniadou, S. & Ortony, A. (1989). Similarity and analogical reasoning: A synthesis. In S. Vosniadou & A. Ortony, A. (Eds.), *Similarity and analogical reasoning* (pp. 1-17). Cambridge: Cambridge University Press.

Highlights of Astronomy, Vol. 13
International Astronomical Union, 2003
O. Engvold, ed.

A Contemporary Review of K-16 Astronomy Education Research

Janelle M. Bailey & Timothy F. Slater

Conceptual Astronomy and Physics Education Research (CAPER) Team
Dept. of Astronomy, Univ. of Arizona, Tucson, AZ, 85721 USA
E-mail: jbailey@as.arizona.edu, tslater@as.arizona.edu

Astronomy education research (AER) uses the systematic techniques honed in science education and physics education research to understand what and how students learn about astronomy, and determine how instructors can create more productive learning environments for their students. A recent review of the literature in this area revealed a number of articles that could be classified into four major categories: research into student understanding, research on instructional methods, research on teacher understanding, and descriptions of curriculum materials.

Within the area of student understanding research, a number of topics have been investigated. The most extensive area that has been researched thus far is the shape of Earth (and its relation to gravity). Studies on this topic have included children in grades two through eight and in the United States, Nepal, Israel and the United Kingdom. Investigations into understanding of lunar phases have included students in elementary grades and university, as well as pre-service teachers, all in the U.S. Understanding of seasons is studied for university students and teachers in the U.S., while understanding diurnal motion (the day/night cycle) includes those populations plus elementary students. Investigations in astrobiology and cosmology have begun with U.S. secondary and university students. The Astronomy Diagnostic Test (ADT) has been developed and administered to university students across the U.S.

As an example of the research literature review, we will elaborate on the shape of Earth research. In 1976, Nussbaum and Novak interviewed second grade students about Earth's shape. Although many students initially responded with the answer "round," deeper probing revealed that "round" does not always mean "round like a ball." The researchers found five different notions that represent the students' mental models of Earth's shape. These results were similarly found using multiple-choice instruments with Israeli students in several grades (Nussbaum 1979) as well as in Nepali students (Mali & Howe 1979). Klein (1982) and Sneider & Pulos (1983) further expanded these results across grade levels and student populations. Targeted instructional methods were investigated by Nussbaum & Sharoni-Dagan (1983). Investigations by Jones, Lynch & Reesink (1987) and Baxter (1989) confirmed similar results. Vosniadou & Brewer (1992) expanded the classification criteria and mental models in their investigations.

Students' understanding of lunar phases and of seasons was first made public by the video *A Private Universe* (Schneps 1989). Studies by Stahly, Krockover & Shepardson (1999), Lindell (2001), and Trundle, Atwood & Christopher (2002) demonstrate that the most common misconception about the cause of the lunar phases is what is commonly called the "eclipse model." In this model, students believe the phases are caused by the Moon moving in and out of Earth's shadow, allowing some portion of the sunlight to be blocked. Fanetti (2001) believes this can be traced to a poor understanding of size and scale.

Instruction method investigations include personalized system of instruction (Zeilik 1974), collaborative group learning (e.g., Adams & Slater 2002), conceptual-based courses (Zeilik et al. 1997; Zeilik, Schau & Mattern 1999), and the use of planetarium instruction (e.g., Reed & Campbell 1972).

Callison & Wright (1993) studied the effectiveness of using three-dimensional models to instruct on lunar phases, while Barnett & Morran (2002) studied project-based instruction. Several of the previously described studies on student understanding of lunar phases included instructional aspects (Lindell 2001; Stahly, Krockover & Shepardson 1999; Trundle, Atwood & Christopher 2002). Abell and colleagues describe the effectiveness of using observation projects to help pre-service teachers understand lunar phases (Abell, George & Martini 2001; Abell, Martini & George 2002).

Several of the studies described above use pre-service and/or in-service teachers as their study population. Barba & Rubba (1992) investigated the differences in knowledge levels between in-service ("expert") and preservice ("novice") teachers. Slater (1993) examined the effectiveness of constructivist strategies in teacher professional development in astronomy.

A large number of articles describing specific curriculum materials or activities can be found throughout the literature. A summary of these pieces is beyond the scope of this work; however, an extensive bibliography of such activities can be found at the Astronomical Society of the Pacific's education website.

To date, few astronomy concepts have been investigated in any depth; consider in comparison the extensive literature base in physics education research. Furthermore, few instructional strategies and curriculum materials have been rigorously examined for their effectiveness in helping students learn astronomical concepts. Future efforts should focus on expanding these areas in terms of both topics and student populations, as well as developing effective strategies to prepare astronomy teachers.

References

Abell, S., George, M. & Martini, M. 2002, "The Moon investigation: Instructional strategies for elementary science methods," Journal of Science Teacher Education, 13(2), 85.

Abell, S., Martini, M. & George, M. 2001, "'That's what scientists have to do': Preservice elementary teachers' conceptions of the nature of science during a Moon investigation," International Journal of Science Education, 23(11), 1095.

Adams, J. P. & Slater, T. F. 2002, "Learning through sharing: Supplementing the astronomy lecture with collaborative-learning group activities," Journal of College Science Teaching, 31, 384.

Barba, R. & Rubba, P. A. 1992, "A comparison of preservice and in-service earth and space science teachers' general mental abilities, content knowledge, and problem-solving skills," Journal of Research in Science Teaching, 29, 1021.

Barnett, M. & Morran, J. 2002, "Addressing children's alternative frameworks of the Moon's phases and eclipses," International Journal of Science Education, 24(8), 859.

Baxter, J. 1989, "Children's understanding of familiar astronomical events," International Journal of Science Education, 11, 502.

Callison, P. L. & Wright, E. L. 1993, April, The effect of teaching strategies using models on preservice elementary teachers' conceptions about Earth-Sun-Moon relationships. Paper presented at the Annual Meeting of the National Association for Research in Science Teaching, Atlanta, GA.

Fanetti, T. M. 2001, The relationships of scale concepts on college age students' misconceptions about the cause of lunar phases. Unpublished master's thesis, Iowa State University, Ames.

Jones, B. L., Lynch, P. P. & Reesink, C. 1987, "Children's conceptions of the Earth, Sun and Moon," International Journal of Science Education, 9, 43.

Klein, C. 1982, "Children's concepts of the Earth and the Sun: A cross-cultural study," Science Education, 65, 95.

Lindell, R. S. 2001, Enhancing college students' understanding of lunar phases. Unpublished doctoral dissertation, University of Nebraska, Lincoln.

Mali, G. & Howe, A. 1979, "A development of Earth and gravity concepts among Nepali children," Science Education, 63, 685.

Nussbaum, J. 1979, "Children's conception of the Earth as a cosmic body: A cross age study," Science Education, 63, 83.

Nussbaum, J. & Novak, J. 1976, "An assessment of children's concepts of the Earth utilizing structured interviews," Science Education, 60, 535.

Nussbaum, J. & Sharoni-Dagan, N. 1983, "Changes in second grade children's preconceptions about the Earth as a cosmic body resulting from a short series of audio-tutorial lessons," Science Education, 67, 99.

Reed, G. & Campbell, J. R. 1972, "A comparison of the effectiveness of the planetarium and the classroom chalk board and celestial globe in the teaching of specific astronomical concepts," School Science and Mathematics, 72, 368.

Schneps, M. P. 1989, *A Private Universe* [Video], San Francisco: Astronomical Society of the Pacific.

Slater, T. F. 1993, The effectiveness of a constructivist epistemological approach to the astronomy education of elementary and middle level in-service teachers. Unpublished doctoral dissertation, University of South Carolina, Columbia.

Sneider, C. I. & Pulos, S. 1983, "Children's cosmographies: Understanding the Earth's shape and gravity," Science Education, 67(2), 205.

Stahly, L. L., Krockover, G. H. & Shepardson, D. P. 1999, "Third grade students' ideas about the lunar phases," Journal of Research in Science Teaching, 36(2), 159.

Trundle, K. C., Atwood, R. K. & Christopher, J. E. 2002, "Preservice elementary teachers' conceptions of Moon phases before and after instruction," Journal of Research in Science Teaching, 39(7), 633.

Vosniadou, S. & Brewer, W. F. 1992, "Mental models of the Earth: A study of conceptual change in childhood," Cognitive Psychology, 24(4), 535.

Zeilik, M. 1974, "A PSI astronomy course," American Journal of Physics, 42(12), 1095.

Zeilik, M., Schau, C. & Mattern, N. 1999, "Conceptual astronomy. II. Replicating conceptual gains, probing attitude changes across three semesters," American Journal of Physics, 67(10), 923.

Zeilik, M., Schau, C., Mattern, N., Hall, S., Teague, K. W., & Bisard, W. J. 1997, "Conceptual astronomy: A novel model for teaching post-secondary science courses," American Journal of Physics, 65, 987.

Highlights of Astronomy, Vol. 13
International Astronomical Union, 2003
O. Engvold, ed.

Implementing the Astronomy Education Research

Leonarda Fucili
Teacher of Science and Mathematics
Supervisor in the Teacher Development School "SSIS Lazio", Rome, Italy
E-mail: l.fucili@itaca.com

I think there is nothing like the study of astronomy to capture the imaginations of our students, to make them understand phenomena, and to introduce them to the fundamental ideas and methods of science and mathematics. In my presentation, I will examine my research on effective teaching and learning of astronomy at the elementary school level, and how I have implemented my research in my work with students, teachers, and curriculum.

1. My Research on Effective Teaching and Learning of Astronomy

For several years, in Rome, I have carried out research on Astronomy Education with the Educational Co-operative Movement (MCE) association, co-ordinated by N. Lanciano, University "La Sapienza". The main topics are:

- the dynamics of the individual cognitive process in developing basic astronomical concepts
- the conditions for effective teaching and learning of astronomy
- misconceptions in astronomy

We create educational contexts in which participants – students and teachers – observe, experiment, build instruments and models, and discuss. We investigate mental images and conceptions, with attention to the significant questions and answers, to misconceptions and mistakes, and to the elements that facilitate or block understanding. The results of my research made me think over the conditions for teaching Astronomy at the elementary school level: short activities and lessons inside the classroom, following a fixed curriculum and textbooks, do *not* improve the students' understanding and appreciation of astronomy; rather, they sometimes create a negative impression of it, and intensify misconceptions.

2. Teaching Astronomy

First, I will examine how I have implemented my research in my work with students in order to improve the students' awareness, understanding, and appreciation of our subject. The context: I teach in "Scuola Media" to students of all abilities, aged 11-14 years, in the same full-time class for three years, 6 hours a week in Math and Science, and 2 hours a week in an integrated project. This situation gives me the opportunity to develop long-term astronomical activities and lessons, as well as the mathematical knowledge, skills, and concepts which students need for the understanding of Astronomy. I developed an introductory

Astronomy course for grades 6-8, founded on the belief that effective learning of astronomy at a primary level is strongly related to observations of real phenomena, and requires a direct involvement and an active body. It is an integrated interdisciplinary course, with a flexible, modular, and in-progress curriculum.

The main goal is to encourage the enthusiasm of my students, and increase their familiarity with astronomy, their understanding of science, and their appreciation of its role in making sense of the world. A significant aspect of my course is its emphasis on hands-on activities. I want students to discover the ideas of astronomy for themselves, not just to read about them passively. An active body renews emotions, curiosity, and effective learning. The act of discovery, of experiencing insight or understanding, produces a thrill of victory, and its memory lasts forever.

Students spend a long time outdoors, making observations and constructing instruments, before developing theoretical explanations and models. The sky becomes a scientific laboratory, "a lab within everybody's reach", always available, free and fully equipped. Students have to be guided in "knowing what to look for", because usually they don't observe much more than things they are already familiar with. They will discover that a surprising abundance of observations is possible. They are guided:

- to find in the sky the same fascination and wish of knowledge that has always led mankind to observe astronomical phenomena, and organize space and time;
- to follow humanity in its discovery of the shape of the Earth, reference systems, celestial motions, distances in the universe, measures of space and time
- to see connections between the scientific disciplines and the humanities, as well as between what they learn in school and in the real world
- to become aware: *to perceive as Ptolemy did, to think as Copernicus did*

3. Looking at What Happens in Class

I will give some examples of astronomy activities and methods that have been tested in my class.

- Investigating students' pre-knowledge makes explicit misconceptions, *epistemological obstacles* and gaps, and turns them into a problem which students want to work on. The workshop *A Round World* is an example which is focused on the shape of the Earth and gravity. Everybody knows that the Earth is a sphere, but the majority of people don't use the concept of an earth-sphere and are not able to connect the spherical form with its geometrical and physical properties. By showing how the human mind has evolved throughout history, I give students the elements of a critical look.
- Using significant or *upsetting* questions: common-sense rules and scientific knowledge don't provide answers any more and, in this uneasiness, new knowledge links with old knowledge in a more conscious way.

- Caring about linguistic aspects before concepts are expressed by words; often, one word has several meanings.

- Spending a long time in observations before developing models and theoretical explanations. In search of reference systems, we make observations from our local horizon and meridian.

- Collecting data in order to discover simple general laws, for instance the mid-day height and declination of the sun. Creating a complete record of data would take one year but, in just six months, students can foresee the further results.

- Building and using models: hand-made of common materials and manipulated by students, in order to develop geometric and spatial imagination, and link celestial phenomena to terrestrial analogies.

- Enacting dynamic human models: students enjoy a model in which they co-operate with others, and the retention of concepts is enhanced. These models need a long time to arrange, and this time helps students to reach the spatial visualization required in many astronomical concepts. Demonstrations in which students represent the Earth, Sun and zodiac, the Sun and planets, and lunar phases are well known. Some more examples: (a) *The planetary week and the "week's dance"*: an active body, with rhythm and movement, can help to re-discover and understand the sequence of the days of the week. This model enacts the explanation of the origin of the planetary week made by Abraham ba Hiyya from Barcelone, called Savasorda, in "Sefer ha't'bbur" (The Book of the Calendar) in the 12th century. (b) *Walking with solar steps*: this model helps students to understand the rhythm of the sun's motion over one year; how and why days stay long (and nights short) for several weeks near the summer solstice, and shorten quickly before the winter solstice. Students work with a monumental sundial in St. Peter's Square in Rome; the gnomon is a giant Egyptian obelisk, and the local meridian is lined with zodiacal signs.

- Measuring the human body in order to discover proportions and laws. In accordance with Galileo's method, the human body and nature become an open book, understandable with the language of mathematics.

- Practicing mathematical skills: calculating, ordering, classifying, comparing, measuring, recording, graphing, reasoning, inquiring, are essential skills for studying astronomy.

- Starting nearby and moving further out, using simple principles, historical methods, and data gained by observations, in order to make deductions about the scale of the universe. Gaining knowledge about distances in space was and still is long and hard work for students, and a step-by-step process from earth to moon, sun, planets, stars, and galaxies.

4. An Interdisciplinary Approach

Among the most distinctive aspects of my course is the interdisciplinary approach to astronomy. A deep emotion and desire for knowledge emerges from the sky: physics, mathematics, geometry, science, art, religion, literature, music, without separation into different disciplines. This integration has to be emphasized at the elementary school level.

- *Anthropology*: we investigate the astronomical roots of our culture, the astronomical phenomena at the basis of our calendar, customs, and feasts.
- *Mythology*: myths describing the origin of the universe, planets and constellations help to organize the space of the sky. Myths are the first sky maps.
- *The history of astronomy* has an appropriate place in my course. We trace back the origins of the early astronomical observatories. In Rome, they are connected with the history of the Jesuits, who were in charge of astronomical research until the last century. We do workshops and lessons in the Collegio Romano, and in places visited by Galileo.
- *The sky and the cities*: the social and ritual foundation of a city has always been related to the sky; we research how ancient architects organized *place and time*, observing astronomical phenomena. In Rome, the Pantheon, Domus Aurea, and Villa Adriana are examples of suggestive places in which the history of a city, the project of an emperor, astrological symbols, and astronomical data fuse in geometrical architectural structures. Monuments, historical buildings, and squares become our laboratories, sundials, and calendars to register astronomical phenomena, and to be reproduced at school.

5. The Method

- Inducing students to take an interest in the content, to see something meaningful, and to become engaged in the search for it.
- Exploiting and making maximum use of students' pre-knowledge.
- Giving time for understanding from observations and experiences before working on more theoretical explanations.
- Giving preference to questions over answers, in order to develop an inquiring attitude.
- Focusing on "concept maps", the essentials of the discipline, and the connections between concepts, goals, and topics.
- Making students aware of the path that they are following.

Students sometimes work alone, sometimes in co-operative groups. Not only classrooms are used, but also the outdoors and the city, not only for short lessons, but also long activities. At the same time, we look for connections between the scientific disciplines and the humanities, as well as between what students learn in school and the real world.

6. The Results

At the end of every year, an interactive exhibition documents and focuses on the main significant concepts that students have worked on. Students train other students in the same activities and learning situations they have experienced. It is a summary as well as a test of the effectiveness of their understanding and learning. *Knowledge becomes culture* when it is useful for understanding reality, and for acting on that. It happens when teaching connects with the individual process of learning by significant aims, methods, and subjects. By studying astronomy, basic concepts such as space and time – essential for understanding the world – are addressed. This is the great contribution of astronomy to education; let's use this opportunity!

References

Davidson, N. *Astronomy and Imagination*, Routledge & Kegan Paul, London and New York.

Fucili, L. & Lanciano, N. 2000, Il Cielo a Scuolo, Naturalmente Anno 13, #1, 56-58.

Fucili, L. 2001, Astronomical Terraces: Space Labs between the Earth and Sky, ESA Teach Space.

Lanciano, N. 2002, Strumenti per i Giardini del Cielo, Edizioni Junior (BG).

Highlights of Astronomy, Vol. 13
International Astronomical Union, 2003
O. Engvold, ed.

Distance/Internet Astronomy Education

David H. McKinnon
Charles Sturt University, Bathurst, Australia
E-mail: DMckinnon@csu.edu.au

1. Introduction

This paper briefly reports two major programs being operated by Charles Sturt University, Bathurst: the Cosmology Distinction Course for gifted and talented senior high school students and the CSU Remote Telescope Project for upper-elementary and lower secondary school students.

2. Cosmology Distinction Course (CDC)

The CDC was first offered in 1994 to students in New South Wales (NSW) who had completed one Higher School Certificate (HSC) course at the highest course level ahead of their age cohort and who were in the top 10 percent of the candidature. Numbers enrolling in the CDC are low (average of 20/year since 1994), and reflects the low number of schools in NSW who allow students to accelerate in their normal school programs. Nonetheless, a key factor in the success of the CDC has been the extensive use of Information and Communications Technologies (ICTs) through an integrated web site comprising a communication forum and a resource finder for the latest research in Cosmology.

2.1. Methodology to evaluate the CDC

A grounded theoretical analysis of the data collected from students use of the ICT system over four years gave rise to an Interactive Design Model (IDM). It comprises three key design elements, print-based study modules, residential schools and significant others, and a communication system for linking the students with the elements and with each other (McKinnon & Nolan, 1999).

Course materials organize and sequence the objectives, content and assessment tasks into manageable units of study over the nine months of the course. Two residential schools bring the students together to: meet and interact with each other; engage in experiential learning at world-class observatories; and, learn from, and interact with, leading researchers. Significant others include the students peers, the course coordinator, course organizers, and research astronomers who provide students with support and guidance. The significant others interact with the students in varying capacities as social friends, critical friends, facilitators of learning, mentors, interpreters and discussants. The communication system mediates all student interactions with the three design elements of the Model. It provides them with the means to study not only the content of the course but also to access a wider range of information and ideas, and significant other individuals with whom to explore and discuss ideas.

3. Charles Sturt University Remote Telescope Project (CSURTP)

The CSURTP is framed against the larger projects of Telescopes in Education, the Bradford Robotic Telescope and the Faulkes Project. The project takes elements from these and renders the technicalities of control at a level where elementary and junior secondary age students and their teachers can easily use the system. The software and hardware systems to drive the CSURTP are described elsewhere as are the educational materials written to support the project (e.g., McKinnon & Geissinger 2002; McKinnon, Geissinger & Danaia 2002; McKinnon & Mainwaring 2000)

3.1. Educational Package Evaluations

Educational materials are supplied in printed Teachers' Guides and on CD-Roms. The guides provide an extensive set of material covering a large number of topics. The elementary school materials are interdisciplinary. The high schools materials focus on science and technology. Elementary school materials engage the students for 4 hours/day, 4 days/week for 10 weeks. Secondary school materials engage students for six weeks of science periods (six per week). Two web sites point to resources available on the Internet. When schools come online, a technician is available to offer help.

In 2001-2003, students in grades 5-10 took part in evaluating: the materials; the user interface; and, the learning outcomes (alternative scientific conceptions) (Dunlop 2000; Osborne 1995).

3.2. Method

Quasi-experimental pre-test, post-test designs were used to evaluate the impact of the educational materials. Test results were subjected to ANOVA procedures with repeated measures on the occasion of testing. In addition, qualitative data were gathered from all participants to demonstrate how the educational programs were received and used.

3.3. Results - Elementary School

The specific test results are reported in detail in various publications (McKinnon & Geissinger 2002; McKinnon, Geissinger & Danaia 2002). Only the highlights of the findings are given here.

The quantitative results showed that classes who interacted with the educational materials demonstrated significant learning outcomes. Effect sizes ranged from 0.5 to 0.75 in students' general knowledge about astronomy, spatial knowledge of how the planets and Moon move, and on their ability to explain their answers.

There is, however, an interesting aside to the above statistical picture exemplified by one class and which should cause all educators some concern as well as astronomers making remote and robotic telescopes available to students. One class had previously covered a topic on the Earth in Space and had visited the library and conducted research using information and computer technologies (ICTs) to produce the posters that are a normal demonstration of learning in school. Their teacher did not want to cover the educational materials apart from the taking control and image processing sequences. On the pre-test, students knowledge and ability to explain phenomena was not significantly different from the other classes. They knew how to assemble attractive posters but knew little about astronomy despite the claim that they had already done that. The spatial knowledge post-test revealed that the scores of this class did not rise at all. On average, they achieved a score of 20 percent on both spatial knowledge scales. They knew little about phases of the Moon, day and night, the seasons, and what causes these phenomena.

One outcome clearly demonstrated by this research is that classes who concentrate mainly on the technical aspects show little change in their alternative conceptions of solar system phenomena. Students explorations of various phenomena, coupled with peer discussion and verbal reworking of concepts, enable them to discard some of their more naive ideas. Taking control of a sophisticated telescope is a great motivator that helps maintain their interest. The evidence supports the position that engaging with astronomy concepts leads to more insightful learning than does a concentration on mere technical details.

3.4. Results - Secondary School

Two cohorts of grade 9/10 students from the Netherlands and Canada evaluated the junior secondary science materials during 2003. Approximately 350 students supplied data which is yet to be analyzed. Extensive qualitative data illustrates that science teachers in both countries are highly impressed with the curriculum materials, the motivation of their students and the ease with which the system can be used.

A Canadian teacher ran the program with three grade 9 classes and also the school Astronomical Society. Members undertook a number of projects including mosaics of extended objects such as the Moon, M42 and omega Centauri, and multiple exposures of faint objects to practice stacking. Classes collaborated to take exposures of Uranus, Neptune and Pluto and traded their images to see how these planets could be identified by their movement against the stars. After a session with a grade 9 class containing at risk students he e-mailed:

"From an educational point of view...when at risk and beyond kids produce a report with enhanced images of their choice accompanied by a bit of research I know we have done something very significant over the past few months. This is priceless!!"

There is little doubt that taking control of a telescope over the Internet is a motivating experience for both elementary and secondary school students. The control aspect sustains their interest in the science over a considerable period of time. It is perhaps, this capacity of the control dimension to sustain interest that allows teachers the luxury to address the deeper scientific content and students alternative scientific conceptions as was demonstrated in the elementary school program.

4. Discussion

The key question to answer here is what does the Cosmology Distinction Course offer students that their schools cannot? Part of the answer is at least clear. The students get access to committed, intelligent, motivated, persistent and passionate researchers in astronomy and cosmology who are excellent communicators.

A second key aspect of the course is the support that they get as they study the course and which is available through the ICTs. The completion rate is extremely high. In most years it is greater than 90 percent. Science delivered by distance methods has to be high touch (Naisbitt & Aburdene 1990). The students are mentored during their candidature and feel a part of a community of learners.

The case for the CSU Remote Telescope Project is rather similar. The fact that the telescope is not a robotic device has many advantages (and disadvantages). One advantage is that it is high touch. Elementary teachers and secondary science teachers are, in the main, not adventurous. Both sets appear to need their hands held while they prepare to use the telescope, while their students use the telescope, and later in the debrief sessions as their students process the images.

References

Dunlop, J. (2000). How children observe the universe. Publications of the Astronomical Society of Australia 17, 194-206.

McKinnon, D. H., Geissinger, H. & Danaia, L. (2002). Helping them understand: Astronomy for Grades 5 and 6. Information Technology in Childhood Education Annual 2002, 1, 263-275. Norfolk, VA: Association for the Advancement of Computers in Education.

McKinnon, D.H. & Mainwaring, A., (2000). The Charles Sturt University Remote Telescope Project: Astronomy for Primary School Students. Publications of the Astronomical Society of Australia, 17, 2, 133-140.

McKinnon, D.H. & Nolan, C.J.P. (1999). Distance education for the gifted and talented: An interactive design model. The Roeper Review, 21, 4, 320-325.

McKinnon, D.H. & Geissinger, H. (2002). Helping them understand: Astronomy for Grades 5 and 6. Information Technology in Childhood Education Annual. 2002, 1, 263-275.

McKinnon, D.H. & Geissinger, H. (2002). Interactive Astronomy in Elementary Schools. Journal of International Forum of Educational Technology & Society, 5, 1, pp 124-128.

Naisbitt, J. & Aburdene, P. (1990). *Megatrends 2000: Ten new directions for the 1990s.* New York. Morrow.

Osborne, J. (1995). *Common Ideas in Astronomy Questionnaire.* Kings College, London

Highlights of Astronomy, Vol. 13
International Astronomical Union, 2003
O. Engvold, ed.

Engaging Gifted Science Students through Astronomy

Robert Hollow
Australia Telescope National Facility
E-mail: Robert.Hollow@csiro.au

Astronomy is a subject that poses many deep questions that intrigue students. It can effectively engage gifted and talented science students in their school years. Numerous international and Australian schemes utilize astronomy as a means of challenging and extending such students. Using Gagné's definition, gifted students have potential distinctly above average in one or more of the domains; intellectual, creative, social and physical. Talented students exhibit skills that are distinctly above average in an area of human performance. Such students may comprise about 10-15% of age peers in that field. They may be identified through a variety of means; by teacher, parent or self, sometimes via diagnostic tests, at others through participation in hobbies or other interests.

Given a student is gifted in science, why should we try and engage them through special programs or extension work? The reasons are many and include pragmatic ones. These students comprise our future professional astronomers, scientists and engineers. Even if they do not aspire to a career in science, it is vital for society to have scientifically literate leaders, managers and lawyers. Developing relevant and engaging experiences fosters positive views of Science. It should also result in more positive interactions in the classroom and at school, with improved educational outcomes overall. Another less measurable but equally worthwhile reason can arise when students experience a breakthrough or wow moment when they internally connect several strands of knowledge together to explain some event or observation. Successful programs for gifted school students require an emphasis on learning concepts and higher-order thinking skills. Problem-based learning activities incorporating the use of technology as a learning tool can be used to model the scientific process. Astronomy is a discipline that lends itself to engage the gifted student and help develop their skills so that they emerge as a talented student. It tackles big questions that many students find challenging and provides a context-rich learning environment. Skills in problem-solving, mathematics, science, literacy, and information and communication technologies (ICT) can be developed given appropriate tasks.

There are a wide range of programs and activities already developed suitable for students at all stages of schooling. Relevant approaches include one-off events such as a guest speaker, extension work within the normal class environment or by withdrawal within the school and the use of extra-curricular opportunities such as a school astronomy club. In-school extension schemes can be a very effective method of engaging a streamed group or individuals but require considerable teacher enthusiasm, expertise, and a supportive, flexible school environment. Other possibilities include specialist camps or summer schools such as the six-week residential Summer Science Program. This successful American scheme is project-based, with students working in teams to plan conduct and analyze data to determine an asteroids orbital elements. It has a strong focus on mathematics, physics and astronomy plus an emphasis on social interactions for students.

The option of students taking one or more university courses prior to completing secondary education is available in some countries and states. Perhaps a better approach pedagogically is to develop specific advanced courses that cater for gifted students within an education district or state curriculum. Such curriculum-based schemes exist in several countries. One example is the Cosmology Distinction Course [see previous paper], a matriculation-level subject that has run for the last ten years in NSW, Australia. Students meet at two residentials and complete assignments, exams and a major project of their own choosing. Delivered via distance-education, with provision for extensive student and staff communication via the internet, it allows students from across the state to study the course. A more recent online education initiative is the Cyber Astronomy Course run by Hong Kong University of Science and Technology for senior high school students. Together, such schemes show the power of computer technology in fostering student communication and course delivery.

One key method of engaging students and fostering skill development is that of student research projects. In getting students to tackle a research project we are asking them to actually do some science rather than just repeat textbook experiments. Modern technology plus schemes such as Hands-On Universe, Telescopes in Education, the Charles Sturt Remote Telescope, the Faulkes Telescope Project and others provide opportunities for students and teachers to use powerful CCD/telescope combinations to obtain real and worthwhile data for such projects ranging from simple one-off observations to more advanced, long-term ones. There is considerable scope for institutional support and professional mentors for groups tackling projects and this can also foster beneficial links within a local educational community. Some projects also lend themselves to local or global collaborations among student groups. This adds to the educational value of the task. A common mistake for teachers involved in setting up such a scheme is to artificially impose a limitation on students' abilities and efforts. Gifted and talented students have a habit of rapidly exceeding our preconceptions. This does not mean, however, that there is no place for a structured approach. The use of a scaffold of concepts and task requirements by students provides guidance and support, and increases the educational value of the project.

A scheme run for several years at Blue Mountains Grammar School in NSW saw numerous students tackle astronomy-based projects on topics ranging from naked-eye meteor observations, differential CCD photometry of short-period variables and quasars, mm-wave observations of Orion A, and investigations of LMC regions N159 and N160 using data from the Australia Telescope Compact Array. Follow-up surveys of students showed that a high percentage of them continued in science/technology study and career paths. Even those who went into other fields commented favorably on their research project as a mechanism for improving their ICT, time and project management skills. All gained in confidence and had a positive attitude towards science. Some had benefit in terms of scholarships for university entry. Negative aspects included conflicts with the demands of other subjects, the fact that research skills were not examined in the external final examination and the heavy time commitment from both students and teachers.

Numerous case studies suggest the value of specific schemes for gifted and talented students. Ongoing educational evaluation of effective and ineffective programs is needed. Educators and astronomers should identify those that work to model and extend their use. This requires strong linkages between professional and educational groups so that engaging, relevant programs can be developed. An emphasis on teacher training and ongoing support will help raise awareness, confidence and skills.

Highlights of Astronomy, Vol. 13
International Astronomical Union, 2003
O. Engvold, ed.

Pre-service Astronomy Education of Teachers

Mary Kay Hemenway

The University of Texas, Austin TX USA
E-mail: marykay@astro.as.utexas.edu

There is little research on elementary/secondary teacher preparation. Few teachers are called upon to teach astronomy specifically, or their astronomy teaching is peripheral to their main interest (e.g., general science at lower levels or physics at higher levels). Statistics indicate that large increases in student populations are expected throughout the world. "In 1997, 1.2 billion students were enrolled in schools around the world. Of these students, 668 million were in elementary-level programs, 398 million were in secondary programs, and 88 million were in higher education programs." (*Digest*, 2002) These figures included large increases from the 1990 figures, e.g. 38% increase in secondary education and 68% in higher education for Africa, as opportunities to obtain an education and population both grew. (*Digest*, tables 395 and 412).

In spite of these increases in numbers of students attending school, it is unlikely that many are being taught astronomy by a teacher who has had any formal instruction in astronomy within their own teacher preparation program. Increases in students attending post-secondary institutions may translate into increases in students being introduced to astronomy through a survey course, but few preparing to be teachers are required to take a specific course in astronomy, even when astronomy specifically occurs in the curriculum. A survey of astronomers from fifteen countries showed that even in countries where astronomy is part of the national curriculum, it is not a required course for teacher certification. Some elementary school level teachers obtain some astronomy preparation in other courses, such as science methods or geography (earth-sun relations). Most of astronomy, including the topics that most interest the general public, is virtually ignored in teacher preparation programs.

In the past twenty years, education policy makers have pushed teacher preparation programs to increase the fraction of time that potential teachers study science and math compared with the time spent on "educational methods." In the last ten years, many countries have produced national or regional standards for teaching science. One example is the *US National Science Education Standards* (1996) with its vision for content and pedagogy. These standards provide expectations for all citizens, not just those planning technological careers. New standards challenge those who prepare candidates as teachers with their new expectations for professional development, both during the pre-service phase and following certification.

There are many issues surrounding teacher-preparation beyond content standards. For example, potential teachers who hold a degree, and often have many years of work experience, may obtain "alternative" teaching certification through training programs rather than a college or university course. Stoddart & Floden (1995) showed that although current alternative routes may not significantly improve teacher learning, they are deemed to be no worse than many university-based teacher preparation programs. The argument of the importance of education preparation versus subject matter preparation was studied by Hashweh (1997) who showed that "the influence of teachers' prior subject-matter knowledge was evident in their modifications of textbook subject-matter content and through their use of explanatory representations." It was especially noted in their content organization during instruction. Those with minimal knowledge followed the textbook closely (in content and structure) and neither added or deleted concepts. Those with a better background were likely to ask higher-order questions. For elementary school teachers, Coble & Koballa (1996) believed that "science content is the centerpiece of science teacher preparation at all levels," although the average number of science courses for a potential teacher totaled 8.5 credit hour (each credit hour is about 15 classroom hours of instruction), mostly of survey courses that may not emphasize the inquiry techniques mandated by new education standards. Hanushek (1986) claimed that advanced degrees have not been found to improve teacher effectiveness, while the contribution of experience appears weak, at best, and limited to the first few years of teaching

In conclusion, there are no easy answers to preparing future teachers in astronomy, but it is a task worth doing. Astronomers are challenged to improve the K-12 educational system by working with the educational/political system to include astronomy in the curriculum, to forge connections with Education departments to influence their curriculum, to include topics found in the schools curriculum in their own college/university courses (which means being knowledgeable about what is in the curriculum). When the opportunity arises, astronomers should participate in editing/writing textbooks and offering professional development opportunities for teachers.

References

Coble, Charles R. and Thomas R. Koballa, Jr. "Science Education" (459-484) in *Handbook of Research on Teacher Education*, second edition, edited by John Sikula. Macmillan Library Reference, 1996.

Hanushek, Eric A. "The Economics of Schooling: Production and Efficiency in Public Schools" *Journal of Economic Literature* 24 (3) p 1141-1177, 1986

Hashweh, Marher Z. "Effects of Subject-Matter Knowledge in the Teaching of Biology and Physics" *Teacher and Teacher Education* 3 (2), 109-120, 1997.

National Science Education Standards. National Academy Press, 1996. http://www.nap.edu/readingroom/books/nses/html/

Stoddart, T. and R. E. Floden "Traditional and alternative routes to teacher certification: Issues, assumptions, and misconceptions". Issue paper 95-2. National Center for Research on Teacher Learning, Michigan State University. 1995 (ERIC Reproduction Service No. ED383697) as quoted by Carol Newman and Kay Thomas
http://www.aaesa.org/Pubs/99perspect/altern_teacher_certif.html

U.S. Department of Education, Institute of Education Sciences NCES 2003-060 *Digest of Education Statistics 2002*, published 2003.

Highlights of Astronomy, Vol. 13
International Astronomical Union, 2003
O. Engvold, ed.

In-Service Astronomy Education of Teachers

Michèle Gerbaldi

Université de Paris Sud XI and Institut d'Astrophysique de Paris, 98 bis Bd Arago, 75014 Paris - France
E-mail: gerbaldi@iap.fr

Abstract. Astronomy education of school teachers is reviewed in the context of in-service training when astronomy is part of the curriculum, or not. Methods and results are presented based on experiences of teacher training during 25 years, in France.

1. Introduction

Whatever the country is, in general few teachers have been educated in astronomy during their curriculum at the university or at the training colleges, astronomy being an optional subject. So in-service training of the school teachers is necessary either because astronomy has been introduced in the school curriculum or because the teachers themselves are introducing some touch of astronomy in their lessons.

Examples of in-service training have been taken from the French educational system because it is applied to a large body of teachers, the French curriculum being a national one and also because in-service training in astronomy started 25 years ago through the non-profit association *CLEA (Comité de Liaison Enseignants Astronomes, Teacher-Astronomers Joint Committee*; http://www.acnice.fr/clea/)

Such training is done in two directions: one which concerns the background in astronomy-astrophysics and the other which gives to the teachers the possibility to develop pedagogical resources, not forgetting that the school teachers are also active in peri-scholar activities: club, educational projects.

2. Context

Based on our experience, we can testify that even with no astronomy in the curriculum, it is extremely fecund to develop an in-service training, with a small nucleus of dedicated teachers with the following objectives:

- to create a network of trained teachers becoming *resource persons*
- to create links between the interested teachers (newsletter, web pages)
- to exchange teaching material
- to create astronomers-teachers partnerships.

Such in-service training will be of great help to give a strong push to introduce astronomy in the school curriculum due to the fact that there is already an experience of teacher-training and also because teaching astronomy has been tested by some teachers.

When astronomy is part of the curriculum numerous teachers have to be trained and it is at this point that the *resource persons* trained previously have to play an important rôle besides the professional astronomers who are too few in any case. Moreover the *resource persons* can act locally in their teaching district by personal contacts with their colleagues and informal meetings.

3. Methods

Various teacher training modes have been developed each acting on different aspects of the training. Some are directed to the long-term training aiming to give a full autonomy to the teachers, some are much more selective concerning the subjects introduced and are efficient on the short-term or only one one aspect of the curriculum.

The various modes of teacher training which are mainly used are:

- summer school: about 8 days
- 3-days, 1-day training session during the school year, organized locally
- distance learning courses, granted or not by a diploma.
- self study (Internet, CD-ROM, ...)

4. Results and Conclusion

Any method used in the education of teachers will be effective only if astronomers have developed long-term relationships with school teachers that nurture both teachers' astronomy knowledge and their pedagogical knowledge. The best way to achieve this goal is the summer schools from which a network of school teachers, trained in astronomy not only on theory but also having a large experience of various activities in their classroom, will be created. These *resource persons* will then be able to act locally.

Internet and/or CD-ROM do not provide a full alternative. They may be used for the resources or to disseminate practical exercises developed or to establish some tutorials but not to acquire fundamental knowledge.

But nothing will be achieved if there are no astronomers ready to provide the "gift of their time" to such goal of school teachers training in Astronomy.

Highlights of Astronomy, Vol. 13
International Astronomical Union, 2003
O. Engvold, ed.

Textbooks for K-12 Astronomy

Jay M. Pasachoff

Williams College–Hopkins Observatory, Williamstown, MA 01267, USA
E-mail: jay.m.pasachoff@williams.edu

Abstract. I report on American textbooks for kindergarten through high-school grades. Middle school, up through approximate age 15, is the last time American students are required to take science, and I provide statistics on the narrowing of the funnel containing those taking physics. I describe some recent curriculum and standards projects, and discussion the recent "less is more" trend. I conclude with comments on whether textbooks are necessary and useful and discuss possible content and style of an ideal textbook.

Astronomy is orphaned in many American schools, though it can find its way into classes through earth science or physical science courses or textbooks from age 13 up. Some form of astronomy is a small part of elementary-school texts.

1. Standardized testing and the scientific funnel

A national trend in the United States in the last two years has been an increase in required standardized testing. The unforeseen consequences include the abandoning of topics of secondary importance – like astronomy – in favor of reading, writing, and arithmetic. The National Center for Educational Statistics has provided graphs that show that, most recently for 1999, the percentage of science courses taken through the age of 17 is 88% for general science (the middle-school course, over by age 15), 93% for biology (usually the first course in high school), 57% for chemistry, and only 17% for physics. Since high-school astronomy is most closely related to physics, the magnitude of the problem is obvious.

2. "Less is more"?

Several projects in the United States in the last decade continue to exert influence through their evaluation of prospective science content, if not curriculum. "National Science Education Standards" were drafted by a committee of the National Research Council and "Project 2061," part of the American Association for the Advancement of Science (and named after the date of the next return of Halley's Comet, on the hope that science education will be reformed by then) puts out a variety of documents of varying specificity. The "less is more" philosophy places more emphasis on method than on specific knowledge. As Partridge (2003) writes, "...why do I not describe the emergence of a cadre of professional astronomy educators as an unalloyed good? Here are some concerns.... The danger that the educator may drive out the astronomer... Balance is needed." See also Pasachoff (2002) for comments on the emphasis (mistaken in my view) on moon phases and seasons that apply to both K-12 education and to college education.

3. Current textbooks

I have participated in several K-12 projects, originally the *Physical Science* and *Earth Science* texts of Scott, Foresman and Co. (Pasachoff, Pasachoff & Cooney, 1983, 1989). I was able to increase the astronomy content, and to move some of it into *Physical Science* from the other book. There is at least some astronomy content in each chapter of grades K-9, except for *Life Science*. The number of American publishers has been diminishing, as publishers merge or are taken over. Only a handful of middle-school science texts remain. Prentice-Hall tried revamping their middle-school series into a set of a dozen individual-topic books, including *Science Explorer: Astronomy* (Pasachoff, 2000). Since that series was issued, though, the individual chapters were reshuffled and re-released as general science books, sometimes with special content for individual states. Reviews, mostly negative, of middle-school science texts are available at www.textbookleague.org and at www.science-house.org:8530/middleschool/.

4. The value of textbooks

In this World Wide Web-based age, the question is widespread whether students should have a textbook at all. Shouldn't they just use inquiry-based methods, experimenting in class? But can students really figure out by themselves, with whatever guidance, what Kepler, Galileo, Newton, and others accomplished over the years? Current middle-school and elementary-school texts – there are no specific high-school astronomy texts, though college-level survey texts like my own (Pasachoff & Filippenko, 2004) are sometimes used in high schools – contain a mixture of text, labs of varying difficulty and length, notes for teachers, writing activities, math activities, graphing activities, etc. Highly illustrated in color, they can be and are criticized for trying to jam in too much and for providing distracting layouts. Still, the ability of a student to have a reference to a set of things to be learned is invaluable. Furthermore, a large percentage of middle-school and elementary-school teachers are untrained in science in general and astronomy in particular, so it makes sense to at least have substantial material available to all in the classroom.

What is the ideal science text? It would have a mixture of activities to intrigue students with scientific methods that would not be so lame or cookbooky as to turn them off. It would treat material that the students will find interesting, including modern topics. It would be written by professional scientists, who would have a chance to shape the final version or at least vet it for accuracy – something that is now the purview of editors. It would be thoroughly reviewed by a team of scientists before publication, to make certain that everything that is said is correct. It would be marketed to schools and state adoption committees by accuracy rather than readability. Most current texts fail in the last two of these desiderata. But finally, learning is most affected by the interaction of students in a classroom with teachers. So the training of teachers in science is all-important, and relatively few school teachers are well trained in science. Salaries and working conditions should improve in order to attract students with better academic records into teaching at the school level. Projects like the Astronomical Society of the Pacific's ASTRO, pairing astronomers with teachers, are models of teacher training. See www.astrosociety.org/education/astro/about/partnerships.html. But how to bring such high-quality training to the majority of school teachers remains unknown.

References

Partridge, Bruce, 2003, "Parting Thoughts," American Astronomical Society Newsletter, June 2003, pp. 7, 10.

Pasachoff, Jay M., 2000, *Science Explorer: Astronomy* (Prentice-Hall School)

Pasachoff, Jay M., 2002, "What Should College Students Learn? Phases and Seasons? Is Less More or Is Less Less?," Astronomy Education Review, volume 1:124-130.

Pasachoff, Jay M. & Alex Filippenko, 2004, *The Cosmos: Astronomy in the New Millennium* (Brooks/Cole).

—–, Naomi Pasachoff & Timothy Cooney, 1983, 1989, *Physical Science* and *Earth Science*, Scott, Foresman and Co.

Highlights of Astronomy, Vol. 13
International Astronomical Union, 2003
O. Engvold, ed.

The Astronomy Education Review: Research, Resources, News, and Opinions

Sidney C. Wolff

National Optical Astronomy Observatory, Tucson AZ USA
E-mail: swolff@noao.edu

The Astronomy Education Review (http://aer.noao.edu), a new electronic refereed journal, began publication in January, 2002. This peer-reviewed journal, which describes itself as "a lively electronic compendium of research, news, resources, and opinion" is the first in the US to be devoted to education and public outreach in astronomy and space science. The journal has been endorsed by both the American Astronomical Society and the Astronomical Society of the Pacific and has received financial support from NASA and NSF. Papers published to date cover a range of topics, and a sample list of subjects includes: 1) the effects of different assessment techniques on student learning; 2) student misconceptions in cosmology and astrobiology: 3) the development, validation, and application of the Astronomy Diagnostic Test; 4) experience with collaborative learning groups in the classroom; 5) implementation and evaluation of a distance learning course for secondary school teachers; 6) resource lists for incorporating poetry and science fiction into astronomy classes; and 7) research into the effectiveness of CD-ROMs in the K-12 classroom. We have also published reviews, opinion pieces, and a variety of suggestions for classroom activities.

The overall goal of the journal is to provide a mechanism for communicating information; building collective knowledge; validating the quality of work; and recognizing and rewarding achievement. During the school year, the journal receives an average of 150,000 hits from 5500 unique IP addresses each month. There are no charges to either authors or readers, and to keep costs low, the journal will continue to be available electronically only. The papers published, however, can easily be printed in PDF format. Submissions from countries other than the US are welcome.

Highlights of Astronomy, Vol. 13
International Astronomical Union, 2003
O. Engvold, ed.

Astronomy, Pseudoscience, and Rational Thinking

Jayant V. Narlikar

Inter-University Centre for Astronomy and Astrophysics, India
E-mail: jvn@iucaa.ernet.in

In 1944, three years before India became independent of the British rule, Jawaharlal Nehru wrote in his now famous book *Discovery of India*: "The impact of science and the modern world have brought a greater appreciation of facts, a more critical faculty, a weighing of evidence, a refusal to accept tradition merely because it is tradition". But even today it is strange how we suddenly become overwhelmed by tradition, and the critical faculties of even intelligent people cease to function. He then went on to express the hope that "Only when we are politically and economically free will the mind function normally and critically".

India is now well into the sixth decade of the post-independence era, and where do we stand *vis-a-vis* rational thinking? Here are some pointers from the present times:

- Many marriages, even amongst the educated graduates are decided after the matching of horoscopes.
- Astrologers are consulted for deciding an auspicious date for launching a new state, for swearing in a new cabinet, for purchasing a house or a car, for undertaking travel.
- An entire village goes into a state of panic and people abandon their homes and run away under the impression that an alignment of planets on one side is going to cause a major catastrophe.
- Houses are built or remodeled to satisfy the dictates of "Vastu-shastra" or the (pseudo-)science of architecture, which in fact is a collection of unproven claims linking the ups and downs in the lives of the inhabitants of a house to where specific rooms in the house happen to be.
- The "miracle" of the idol of the elephant-god Ganesha drinking milk through his trunk can send large crowds to temples, or of a "holy god-man" producing watches out of nothing for his devotees is taken seriously even by intellectuals.
- The apex body of higher education, the University Grants Commission declares astrology as a science and offers funds for instituting its teaching in universities.

The disturbing fact about these symptoms is that the trend towards superstitions and beliefs in pseudo-sciences is growing and the younger generation is getting more and more attracted to these ideas. How to counteract this trend?

I believe education in astronomy right from the school level can play a major role in this enterprise. An indication of how education in science can help distinguish it from pseudo-science can be seen from the following example of chemistry.

In India non-governmental organizations devoted to eradication of superstitions, have two visiting teams doing the rounds of various schools. The first team performs "miracles" which the second team following it, explains by chemistry experiments. When the unexpected or the unusual gets demonstrated as a known fact of science, the belief in miracles crumbles. Such direct demonstrations have proven to be very useful and effective. [The Ganesha phenomenon was likewise demonstrated and clarified by scientific experiments.]

Astronomy provides similar instances that distinguish it as a science from pseudo-science. These instances come through several channels.

- The solar eclipse is known to generate awe and even fear in the human mind, provided it remains unexplained. Its explanation as a shadow effect and the demonstration of its complete and accurate predictability leads to a new mind set of the viewer who is then able to enjoy this extraordinary phenomenon. Several superstitions related to this event can be effectively eliminated by encouraging information about the event and active participation of school children in it as viewers. They may be encouraged to enlighten their parents and grandparents too!

- Just as the solar and lunar eclipses are completely predictable, so are transits of Venus and Mercury. The fact that laws of physics apply to such events will help the children appreciate them as real physical experiments.

- The same point can be driven home further by illustrating with the examples of planetary fly-bys by man-made spacecraft. Here for example, one can demonstrate that the planets and the spacecraft both obey the same laws of dynamics. The power of mathematics in calculating the precise rendezvous will also not be lost on the student.

- The seaside towns regularly have tides. One can use the timings of these tides and the positions of the Sun and the Moon to demonstrate their origin in terms of Newton's law of gravitation.

In the Indian context, special efforts are needed to counteract the growing influence of astrology. To contrast a pseudo-science like astrology with a hard science like astronomy, the above examples from astronomy may be put side by side with how astrology operates. Thus children could be asked to apply the following criteria to astrology:

- Scientific predictions are falsifiable and are therefore worded in a precise manner. Are astrological predictions so worded or are they vague and could be made consistent with any result?

- Even if they are tested for success or failure, how often are they successful and how often not? The example of coin-tossing may illustrate the circumstance that a prediction may turn out correct purely by chance.

- Is the making of a prediction logical and based on some precisely stated assumptions?
- Do the successes/failures of a prediction depend on who makes them? That is, is there objectivity about them?
- Field tests on large samples and their overall success-evaluation have established the validity of empirical relationships in physics, which were subsequently explained by basic laws. What has been astrology's record with such field tests?

Ample evidence exist in literature to show why astrology is not a science. It will be worthwhile spending some part of astronomy education in demonstrating to children why this is so.

Science teaches rational thinking and the application of the scientific outlook goes well beyond the laboratory walls. Astronomy boldly applies the laws of science to the grand laboratory that is our universe. Some natural phenomena can be awe-inspiring and if not explained scientifically, can lead to superstitions and irrational thinking. Children could learn how to think rationally and not get carried away by superstitions, pseudo-science and loose thinking, if they are given some introduction to astronomy as a science and are encouraged to apply the scientific criteria to see why astrology is not a science.

Highlights of Astronomy, Vol. 13
International Astronomical Union, 2003
O. Engvold, ed.

Teaching Astronomy in Other Cultures: Archeoastronomy

Julieta Fierro
Universidad Nacional Autonoma de Mexico
E-mail: fierroju@servidor.unam.mx

1. Introduction

Mesoamerica is a large zone that includes most of Mexico and Central America. In that region one of the few written languages was invented. A large civilization flourished thanks to the discovery of agriculture and the use of a mixture of corn, beans, squash and peppers that conveys a high nutritional content. In this part of the world there are mainly two seasons, the dry and rainy periods. The slave driven civilization that developed in this part of the world consequently divided the civil year in two, mainly dedicated to agriculture and construction. A good calendar was needed for central planning and commerce.

2. The Sun

One of the main deities of ancient Mexico was the Sun. It had several representations, an eagle that drifts through the sky and the "Ollin" which means movement. The eagle is depicted in Mexico's flag and the "Ollin" can clearly be seen in the center of the Aztec Calendar and the ten peso coins. A jaguar was the symbol for night, the spots representing stars. Warriors dressed like eagles and jaguars.

In ancient Mexico the sun's trajectory was well studied. The Mesoamerican people carefully registered the places where the sun rises and sets during the year. At mountain surrounded sites they used the silhouette, or carved vertical slots to mark the exact location of the rising sun. At flat locations they built special constructions to register such spots. This way the calendar based on the rising and setting sun was established throughout the region. Mesoamericans also had a 260 day ritual calendar, that ran parallel to the astronomical one.

Some of the markers are for special events such as the equinoxes are for the ball game courts. This game was played with a large rubber ball using the hip to make it go through a stone loop. The days of the equinoxes the sun sets precisely in the direction of the ball court, and can be seen through the stone loop.

There were other constructions built to mark this day such as the "Castle" at Chichen-Itza where the sun forms shadows showing the descent of a snake along the pyramid's stairs. The teacher can bring a souvenir pyramid to the classroom and light it with a lamp in order to simulate the sun's movement and show the way the Maya people could build scale models of their constructions and orient them in a way that they could be useful for astronomical purposes.

Another marker for the equinox in the Maya region is the "Caracol", an ancient astronomical observatory. The name Caracol means snail; this rounded construction has a spiral shaped hall with several windows that are aligned with particular celestial events such as the rising of Venus on determined dates of calendaric importance.

3. The Moon

The Aztecs believed the dark areas of the moon represented a rabbit; they depicted the Moon as a hare in a pot. In fact the Moon's diameter is the same length as Mexico. In Nahuatl, the language of the Aztecs that is still spoken in Mexico, Mexico means "the Moon's navel". Teachers may use the hare image to talk about lunar cratering and volcanism.

Once the moon has been addressed the teacher can explain eclipses. He/she can begin by talking about traditions that are still in order since Aztec times. For instance during total eclipses pregnant women tie red ribbons around plants and scissors around their necks "in order to avoid having a deformed child" (in pre-Hispanic times an obsidian arrow head was used instead of scissors). Teachers may explain that the creation of present Mexico City was at the time of a total solar eclipse. Tenochtitlan was founded on a lake where an eagle (the Sun) was resting on a cactus plant (this image is part of the Nation's flag).

The way in which pre-Hispanic people predicted eclipses by carefully observing the Sun's and Moon's trajectories can be explained to students by telling them that since the paths of the sun and moon form a 5 degree angle, and that their apparent motion is different, the moon moves slower, one can infer when the trajectories will cross. It is important to point out the Moon's rising is more erratic that the Sun's and that this jumping of the Moon's motion was another reason for attributing the hare as its deity. It is also an invitation for students to observe its motion.

Part of the rituals included fights amongst eagle and jaguar nights, that I shall recall symbolized the sun and the night,

4. The Zenith Passing and the Measurement of the Earth's Circumference

One of the most prevailing characteristics in Mesoamerica constructions is perforation drilled in order to observe the zenithal pass of the sun. The ancient calendar began in May with the first rainfall. The zenith pass is during that same period. I shall give a few examples. At Xochicalco there is a cavern built inside one of the pyramids on the main square, where the sun illuminates it during the zenith pass. By the way at this site an astronomical convention was held during the XVth century. The different people from all over Mesoamerica came to decide on calendar matters. This was important for commerce.

At Malinalco, a monolithic pyramid is sculptured from a rock mountain and the sun illuminates a sculpture of an eagle, the sun representation, during the zenith pass. At Monte Albn there is a small construction with a different orientation than the rest of the site, whose staircase points to the pyramid dedicated to the zenithal pass. At the same site- and others - there are several gnomons.

A teacher from this area can use this historical fact to show how these sites that are at different latitudes could be used to measure the circumference of the Earth "á la Erathostenes". Using a flat strip of foam rubber the teacher can simulate a flat Earth with obelisks at the same longitude but different latitudes. He can use the same strip to simulate perforations, that is to say zenith passes. Erathostenes used an obelisk and a well; the Mesoamericans could have used perforations. A very good assignment is to use the Internet to have students at different locations measure the circumference of the Earth by observing which day the zenithal path occurs at their location.

5. Angular measurements

The ancient people from Mesoamericans were stargazers. Stars were symbolized as eyes. They invented a series of constellations. For instance Orion was represented as a grinding stone, and the Big Dipper by a kite. They used two long rods to measure the altitude of stars above the horizon. The angular distance was determined by pointing one of the rods towards a marker placed on a ceremonial construction and the other at the celestial object.

This fact gives the teacher a chance to address angular measurements on the celestial sphere and to describe the way an astrolabe can be used to determine the altitude of an object above the horizon. A very simple astrolabe can be built using a compass and a weight.

It is difficult to use maps to locate constellations, mainly due to the small scale, that the aspect of the sky varies during the night and year, that not necessarily all the stars shown on the map are in the sky, due to street lights, etc.

In order to avoid these problems the teacher can draw a couple of constellations on rigid plastic sheets with fluorescent paint. Fingernail polish that glows in the dark for discos is ideal. The correct scale is about 30 cm for Orion. Local as well as the conventional constellations can be used. The teacher should only draw, as many stars as are visible in his particular location. During the night with the arm that is holding the sheet out stretched the size of the constellation should be the same as the one on the drawing.

6. Conclusion

Astronomy is a fascinating topic and due to its multidisciplinary nature can be taught in several ways including those that make more sense to a particular group of students. In countries that have great historical tradition it can be employed to help pupils relate to science.

In places such as Mexico, teachers can take the pupils to one of the sites, and explain naked eye observations, and from there build on to modern astrophysics. This will enrich the learning process.

Highlights of Astronomy, Vol. 13
International Astronomical Union, 2003
O. Engvold, ed.

Astronomy Curriculum for Developing Countries

Case Rijsdijk

Friends with the Universe
"Masintinge", 600 Friedheim, Highstead Road
Rondebosch 7700, South Africa
E-mail: particles@mweb.co.za

1. Introduction

After the democratization of South African society it became clear that there was a need to develop a new curriculum. This process started in the early 1990's and the implementation of a new curriculum began in 1998. The South African experience also gives an indication of how best astronomers, and other scientists, can intervene to maximize their impact.

2. Background

Prior to 1994 there was no national curriculum in South Africa; individual population groups had their own schools with differing facilities, resources and teaching capacity. In developing a new curriculum, the South African Department of Education consulted curriculum developers from New Zealand, Australia, Scotland, the USA, Canada and the Netherlands. The resulting curriculum was an Outcomes Based Education (OBE) structure, similar to that used in Australia and New Zealand and was known as "Curriculum 2005" (C2005). It was a complex document using a structure and language that was unfamiliar to most educators.

C2005 was implemented in 1998 and shortly afterwards it became clear that C2005 needed to be reviewed. This was done and resulted in the new Revised National Curriculum Statement and this is currently being implemented.

3. Curriculum 2005

This is an OBE curriculum which has two bands: the General Education and Training, GET, band (Grades R - 9) and the Further Education and Training, FET, band (Grades 10 - 12). The FET band will be implemented in 2006 and so the focus will be on the GET band. Here the traditional 'subjects' have been replaced by eight 'Learning Areas' (LA's): Language and Literacy, Mathematics and Mathematical Literacy, Arts and Culture, Natural Sciences, Human and Social Sciences, Technology, Life Orientation, and Economic and Management Sciences. The GET band is divided into three phases: Foundation (Gr R - 3), Intermediate (Gr 4 - 6) and Senior (Gr 7 - 9

The Natural Sciences LA is sub-divided into four 'Themes', one of which, Earth and Beyond, was originally further divided into Beneath the Earth, On the

Earth, Above the Earth and Beyond the Earth. Here the 'Beyond' component was of course "astronomy" and covers the topics such as lunar phases, seasons, time and time zones, eclipses, the solar system, stars, galaxies and the evolution of the Universe.

There are many positives to this new curriculum: it is a National Curriculum. It is learner oriented: the emphasis is on the learner "doing things" rather than "rote learning" as was the case in the past. Assessment is more varied and multifaceted: learners are expected to "show" understanding in project and other work, and is continuously assessed.

4. Comments on C2005 and some South African solutions

When such a large paradigm shift takes place there are bound to be implementation problems. These are exacerbated because many teachers, who are poorly trained and under qualified are now expected to deal with totally different lesson and assessment strategies, in addition to using new text books and other learning materials.

There are specific problems when a totally new subject/topic such as astronomy is added to the curriculum. It now meant that teachers would need training; relevant and appropriate resources needed to be developed and supplied. Teachers were already under strain attending workshops in learning how to cope with C2005 and there was some resistance as astronomy was perceived to be difficult and had to be done at night. It was a 'specialist' subject suitable only for experts.

5. Alternative Strategies

Comparing the South African change with that of Zimbabwe in 1994, after 14 years of independence, shows that evolutionary change is better than revolutionary change: the latter was better in all respects and consistently produced better results at all levels.

The strategy should be to keep what does not need changing, especially in maths and science, but to change the curricula of subjects such as language, history and the social aspects of geography. Where change was needed in other subjects it must be done in an incremental way. Teachers should be consulted in the process. They will be empowered by involvement: make them part of the process, make it their curriculum. It would probably be a good idea to start by looking at the assessment process as we have found that this impacts critically on the development of the curriculum.

6. Intervention by Scientists

Few scientists are also educators, particularly at school level. To optimize the use of this vast pool of expertise, the South African experience has shown that it is best for scientists to:

- assist curriculum developers with content and ideas,
- collaborate with textbooks authors,

- work with teachers in developing resources,
- work with teachers at training institutions, and
- liaise with local education departments and officials.

Other interventions are possible even where no curriculum change is taking place. In any existing chemistry, physics and maths curriculum there is ample material that can be used, either as illustrative examples or as 'add-ons' in topics such as: the inverse square law, spectroscopy, optics, gravitation, nuclear physics, magnitudes, graphs etc.

Additional interventions are possible by supplying data and ideas to repeat simple experiments and to give support material for project work.

7. Resources

The Internet is not a resource that is readily available to many people in developing countries. It is either unavailable, or when available, expensive. Sometimes it is available in a limited way: one computer per school with a telephone line with a 54k modem. Much material is written from a 'northern perspective', uses complex language and often sites contain poor or bad material which local teachers are unable to identify.

There is a "digital divide" and it is widening. Developing countries experience problems with bandwidth, hardware, software, support and maintenance and servers.

The Internet does have its place, but it is not the magic solution: it is the Internet AND other resources, especially tactile ones. What is important in a developing country is that the resources are cheap, easily reproducible and use readily available materials.

8. Conclusion

In creating a new school curriculum in a developing country it is worthwhile to consider the following:

- see what other developing countries have done
- the context in which the new curriculum is being developed,
- to use local, appropriate and relevant material,
- new material, including textbooks, will need to be created/written
- work closely with teachers and local education authorities,
- the process starts on COMPLETION of the new curriculum!

The school curriculum is important and scientists, especially astronomers, should be contributing to curricula, especially in the teacher training colleges. But irrespective of the curriculum, if teachers know that astronomy can be used as a "vehicle for science education" then they can use astronomy in their teaching of science and maths.

In South Africa we have what we call "Ubuntu", or "Motho ke Motho ka Batho": "I am because we are, and because we are (therefore) I am". Education is about human interaction: computers, textbooks etc are tools used by people; by themselves they have limited value.

Highlights of Astronomy, Vol. 13
International Astronomical Union, 2003
O. Engvold, ed.

Fostering Science Education in the Developing Countries

James C. White II
Rhodes College, Department of Physics, Memphis, Tennessee 38112 USA
E-mail: jwhite@rhodes.edu

1. Introduction

Considerable attention is paid to how we teach science and to how our students learn it. Even though similar questions are asked by scientists and science teachers in all countries, one finds that resources available for science education in developing countries are often scarce.

Resources for science in general are often quite limited in countries less wealthy than those of, say, North America or the European Union. Leaving aside for the moment those resources for scientific research—equipment, communication infrastructure (journals, internet access, etc.), and opportunity for collaboration with scientists outside the country—one confronts the needs of a country for the development and advancement of its science education system: equipment, communication infrastructure (textbooks, internet access, etc.), and collaboration with science teachers inside and outside the country. That the needs of the scientific enterprise and those of the education enterprise are so similar is not surprising, given that good science can enrich teaching and engaging teaching can compel one, student or teacher alike, to ask new questions and, hence, to conduct new, enriched science.

2. Education Needs

To many policy makers in wealthy and comparatively poor countries alike, enriched science education means increased funding, which, in the zero-sum game of politics, means less money for other national needs. This assumption need not be true, however.

2.1. Equipment

If one walks into a physical science classroom in the United States, one will discover lab benches scattered with instruments and shelves filled with scientific apparatus. The same is not typically true for a science classroom or lab space in a developing country (DC).

Despite the seemingly endemic electronic devices that whirl and buzz and spit out data to an associated computer, teachers are again realizing that some of the most effective demonstrations and laboratory experiences for our students come from simple, inexpensive sources. As examples, one can use a burning tea bag to demonstrate convection or a falling feather to investigate air resistance.

Consider that once the student leaves the classroom, she can locate the same materials to reproduce the experiment inexpensively for herself.

Rather than considering how best for us to fund equipment purchases for science classrooms in DCs, we should use "equipment" available locally in the country—teabags, bits of twine, melons, etc. All we need do is guide teachers there in its use and in how interpretation of results can enrich the classroom experience for their students.

2.2. Communication

Educational research and common sense suggest that effective communication is a critical element in student learning—communication between the teacher and student, between students, and even between teachers as they discuss what works and does not work in their classrooms. The internet is clearly an effective means of bringing teachers and pupils together in non-traditional means—as example, having electronic office hours after the school is closed for the day—but one can not assume that the relatively easy internet access one has in, say, the United States, is available in DCs.

For this reason, standard means of communication, verbal and written, must still be relied upon for the majority of learning in the developing world. Textbooks are often the main source of information, too. Recognizing the importance of textbooks, particularly in DCs, a segment of the IAU's "Teaching Astronomy for Development" Program Group (Commission 46) worked in 1999-2001 with Vietnamese astronomers and educators to write and then publish a new astrophysics textbook.

The first Vietnamese textbook to contain color illustrations, *Astrophysics* was written by four Vietnamese astronomers and one American astronomer. Both Vietnamese and English are used in the text, with Vietnamese language on left pages facing English translations on the right. Such a design presents students with the science and also provides them with opportunity to refine their English language skills and improve their English science vocabulary.

2.3. Collaboration

Discovering what does and does not work in someone else's classroom can save one time and effort. Yet fostering communication among scientists in DCs and with their colleagues in wealthier countries is difficult: technological, cultural, and language barriers stand ready to aggravate, if not prevent, such dialogue. The IAU's Commission 46 facilitates better communication through various activities, and the "Teaching Astronomy for Development" Program Group is charged explicitly with offering assistance, advice, and guidance to science educators in developing countries. From visits to the countries by foreign scientists to assisting financially select students from DCs with their graduate educations abroad, TAD seeks to minimize the loneliness a scientist or science educator feels in a country with little resources for education and science. Indeed, by offering advice or services the host country believes it needs, TAD, and the associated Program Groups in Commission 46, attempts to connect each scientist and science educator with the rest of the world—bringing the individual, and his or her students, into the global scientific endeavor.

Highlights of Astronomy, Vol. 13
International Astronomical Union, 2003
O. Engvold, ed.

What makes Informal Education (IE) Programs Successful? A Case History: Total Solar Eclipse 2001 — Live from Africa

Nahide Craig & Isabel Hawkins

Center for Science Education, Space Sciences Laboratory
University of California Berkeley, Berkeley CA USA
E-mail: ncraig@ssl.berkeley.edu

Evaluation and assessments of informal education programs, small or large, such as science museum traveling exhibits, interpretive kiosks, hands-on activities and very large public programs have been challenging due to the diverse nature of objectives, setups, and expected outcomes of these programs. Almost all institutions that develop and present IE programs include, in their staff, evaluation specialists. However, for very large public outreach efforts, which include participation of many institutions located across the country, larger evaluation groups/institutions can contribute more objective and extensive evaluation and assessment instruments. Such instruments will help to identify whether the program was successful and if the learning objectives were achieved. They can also lead to 'lessons learned' for future events and serve as possible model evaluation instruments for informal education institutions/museums/science centers where the budgets do not allow for contracting independent reviewers. The *Eclipse 2001* event was developed and executed with the partnership of the Sun-Earth Connection Education Forum, (SECEF), The Exploratorium (the Museum of Science, Art and Human Perception, in San Francisco), and NASA's STEREO Mission. American Institutes for Research (AIR), an independent evaluation company from Boston was contracted to develop and implement the evaluation. The following Informal Educational Goals were used to guide the event:

- Uses a "hook" to highlight science and engage the public
- Creates an experience where visitors learn and retain scientific knowledge
- Inspires interest in science and scientific exploration
- Provides wide dissemination and high visibility of national scope

Approximately 42,000 people participated in the *Eclipse 2001* event at museums, science centers, and planetaria: a total of 164 institutions worldwide, including 80 scientists, 71 Girl Scout troops, 15 universities and schools, and 2 mass-media outlets (CNN and NASA TV). AIR developed evaluation forms and these were sent to all the participating organizations. 972 evaluations from public participants were received and analyzed. In addition, 37 organizations and 32 scientists sent in their evaluations. The participants reported learning more about concepts such as Sunspots, the Solar Corona, the Diamond Ring Effect, and general information about the Sun. Several institutions mentioned frustration with technical difficulties, but overall, respondents in all categories reported that they enjoyed (a) the broadcast of the eclipse, (b) the hands-on activities, and (c) interaction and on-line chats with the scientist. The majority of children and adult participants indicated that they would participate in a similar event in the future and evaluations demonstrated a statistically significant increase in their knowledge about the Sun after the eclipse event. The participating institutions wanted their sites to host in the next total eclipse event of 2006. The scientists reported that they were able to discuss their research with participants, that hosting museums and SECEF had prepared them well before the event, and that they will participate again in a future event. Scientists also mentioned that they were motivated to participate because they could turn kids on to the science, talk to the public, had the opportunity to discuss their research, and also enjoyed watching the eclipse web cast.

Looking back at our goals, we feel confident that through the *Eclipse 2001* where we could not see the event from our locations but 'observe' it remotely, we provided the "hook" to highlight science and engage the public for this event. We demonstrated that we created an experience where visitors indicated they learned and that this event inspired interest in science and scientific exploration. Through the science museum connections we provided wide dissemination and high visibility of national scope. The personal interest of the scientists in the content, publicity, connectivity to a group, educational value, and the capabilities of using high technology defined the success.

Encouraged by this event we plan future programs, such as *Journey to the Beginning of Time* – a video conferencing and web cast in Fall '03, *Venus Transit* on June 8th, 2004, *Ancient Observatories* in 2005, and the next *Total Eclipse* web cast on March 29, 2006. We hope you will participate in any or all of these programs. For information please visit our website: http://solarevents.org .

Highlights of Astronomy, Vol. 13
International Astronomical Union, 2003
O. Engvold, ed.

The Role of Science Centres and Planetaria

Nick Lomb

Sydney Observatory/Powerhouse Museum
PO Box K346, Haymarket, NSW 1238 Australia
E-mail: nickl@phm.gov.au

1. Introduction

The school curriculum in many countries includes astronomical topics such as the seasons, phases of the moon, planets and stars. Yet most teachers at all school levels do not know any astronomy and have difficulty teaching that part of the curriculum. Even if they have some knowledge of the subject they may not have the resources to illustrate it and enthuse their students. One solution is to take them to a place specializing in astronomy education - a suitable science center or museum or planetarium or public observatory.

2. What are science centers and planetariums?

These are places that are dedicated to illustrating and explaining astronomical concepts. There are different types of institutions, though some have elements of more than one:

- Science centers have interactive or 'hands on' exhibits. They cover a variety of scientific subjects that in some cases include astronomy.
- Planetariums project star fields and astronomical images on a curved dome above an audience.
- Museums have objects and displays. Like science centers they cover a variety of subjects that in some cases include astronomy.
- Public observatories have telescopes that are available to the public.

3. Why take students to a science center or planetarium?

Teachers take their students to science centers, planetariums or similar places for a variety of reasons:

- Students can be instructed by someone knowledgeable about astronomy.
- Students will be stimulated by the exhibits, the show, the ambiance.
- Students will enjoy the experience.

However, teachers may face a number of negative considerations that hinder them from going to these places:

- It could be expensive to reach the science center. For example, it may be necessary to hire a bus.
- Teachers of other subjects may not want the students to miss their classes and so may oppose long excursions.
- An evening visit to a public observatory is out of normal working hours for teachers.
- Students may ask questions after a visit that the teacher may not be able to answer. This is a situation a teacher may find embarrassing and so may want to avoid.

The Powerhouse Museum has found that links to school curriculum are not always reason for an excursion, but they are important for the teacher to justify it. Teachers consider that a visit must meet not only academic goals, but social, cultural and vocational ones as well. They value the opportunity of experiential learning for their students in contrast to the normal verbal experience of the classroom yet at the same time they want them 'to see something real'.

4. What do students want at a science center or planetarium?

The Powerhouse Museum recently completed a 'front end evaluation' for a new Space Exhibition. The evaluation took the form of a series of representative members of the public being invited to discuss their attitudes to the subject in small groups. These 'focus groups' were conducted for the Museum by a market research company, Stollznow Research. One group was made up of 14 to 15 year old lower secondary students. Some results from that group were as follows:

- The students were only interested in what directly involves them. For example they were interested in what it is like living in space, but only because they thought that they may have the opportunity to go there in the future.
- They want exhibits with interaction and still more interaction.
- They would like exhibits that allow them to experience weightlessness (rather difficult to provide!), go in a spacecraft, etc.
- The best exhibit that the students had experienced was where they could ride a bike and see how fast they had to ride to make something work such as a hair dryer.

5. What happens during a visit to a science center or planetarium?

Sydney Observatory provides a good example of a visit to a science center or planetarium. It is the oldest existing observatory in Australia and is now, as part of the Powerhouse Museum, a museum of astronomy and a public observatory. It has over 80,000 visitors a year, of which around 20,000 are school students. It has displays of historic astronomical instruments, modern interactive exhibits, a small planetarium and a 3D theater.

School visits are highly structured with the students divided into groups of 15 or so, each accompanied by a guide-lecturer. During the one and a half hour visit the guide-lecturer concentrates on the topic, such as the solar system or the nature of stars, requested by the teacher in advance.

During the visit a variety of experiences are provided to the students. They can look through the two large telescopes in the building at the Sun (with appropriate filters) or at a star if it is clear or something near the horizon if it is cloudy. They visit the exhibition, especially the section on the solar system as that is generally requested by primary teachers. They also visit the small planetarium and the 3D theater where they wear polarized glasses to go on a trip to Mars or a journey around the solar system. Most important of all during their visit to Sydney Observatory they have the opportunity to interact with a guide-lecturer and to ask him or her lots of questions.

6. Discussion

Science centers, planetariums, museums and public observatories provide the interaction and variety of experiences that both teachers and students value on school excursions. They assist teachers who may not be fully knowledgeable about astronomy to communicate the subject to their students.

Museums (science centers, planetariums), however, are not efficient places for traditional 'school-type' education, that is, for learning specific facts and concepts. The students do not spend enough time on an excursion for that purpose and are usually too excited to be in a receptive state of mind. Instead, museums and planetariums are ideal places for providing wonder, for the opportunity of exploring a variety of concepts and for expanding young minds.

Acknowledgments. I would like to acknowledge valuable discussions with my colleagues from Sydney Observatory, Toner Stevenson and Jeanie Kitchener. The Powerhouse Museum experience on learning during school excursions is taken from the work of Helen Whitty of the Museum's Education and Visitor Services and the work of the Museum's Evaluation and Visitor Research Unit led by Carol Scott.

Reference:

Whitty, Helen 1999, "Making a school excursion a learning experience: a work in progress", presented at "Musing on Learning" seminar, Australian Museum, 1999.

Highlights of Astronomy, Vol. 13
International Astronomical Union, 2003
O. Engvold, ed.

Science Education for the New Century – A European Perspective

Claus Madsen

European Southern Observatory, Garching, Germany
E-mail: cmadsen@eso.org

This paper briefly discusses surveys of public interest in science (high: above politics, economics, and finance, but slightly below sports and culture), and the ways to stimulate interest in science among young people through improvements in the formal science teaching system. It emphasizes the need to develop programs of sufficient size to achieve a long-term impact, and obtain the necessary changes. It describes the strategy and individual activities which ESO has undertaken in the field of science education, and provides an outlook on the future EIROforum European Science Teachers' Initiative. Since 1993, ESO has been involved in 14 different programs for young people, and for teachers. Two programs are planned for 2004: *Venus Transit 2004*, and *Science on Stage*.

ESO's involvement in science education has been based on a fairly altruistic attitude, driven by a general concern about scientific literacy among the public (which is necessary for them to make informed decisions about major socio-scientific issues), and a realization of the potential for public exploitation of its rich collection of data and general experience. Nonetheless, the increasingly precarious recruitment situation for future scientists provides a strong additional driver for this engagement. In spite of the formal limitations as given by ESO's remit, ESO's willingness to open up for education initiatives and to engage with the education community has been welcomed by its member-states.

In addressing the problems of scientific literacy and public interest in science, we recognize the need for large, co-ordinated programs aimed at different groups in society, such as professional teachers and young people. Such programs require investments in money and manpower that exceed the capabilities of most science organizations. Therefore, co-operation between many partners, and the joint involvement of science and the education community is called for.

Astronomy is particularly well suited for such activities, thanks to its multidisciplinary character, and its natural attractiveness for young people. Our main partners have been: the European Union, the European Association for Astronomy Education, and the EIROforum (made up of the seven European Intergovernmental Research Organizations).

Through their consistency, the ESO-backed educational activities are increasingly seen as a "permanent" feature in the move to stimulate the interest in the natural sciences in general, and astronomy in particular. At the same time, the catalyst effect of the European Science Week, and the "Science and Society" program of the European Commission should be acknowledged for enabling such activities.

This is the SPS4 Editor's summary of a longer version of this paper.

Poster Highlights: Research, Curriculum, and Resources

Measuring the Circumference of the Earth in Primary School. Emmanuel DiFolco (France). The French program "La Main à la Pate" is leading an international co-operative project, gathering each year more than 100 schools all over the world. The project invites teachers and pupils in primary schools to measure the circumference of the Earth, following the method first developed by the Greek scientist Eratosthenes, 2200 years ago.

The protocol consists of a series of experimental activities which allow a progressive approach to the various scientific notions at play (light rays and shadows, the shape of the Earth, solar noon etc.) Pupils are invited to reproduce the observations of Eratosthenes, and to adapt the method by developing their own instruments. Finally, they can compute their own estimate of the size of our planet by exchanging their measurements easily through the Internet with other classes from many countries.

We present the progressive protocol and its entertaining activities, as well as the specific cooperative tools which have been created to help and follow up the teachers in the course of the project: a scientists' and trainers' network, an Internet forum, and a database where all the measurements gathered can be exchanged between the participants.

Using Games to Teach Astronomy. Paul J. Francis (Australia). We all know that astronomical research is a chaotic, sociable, deeply human enterprise, full of baffling mysteries, enigmatic clues, and breathtakingly unexpected conclusions. Abundant evidence suggests that our students see astronomy very differently. They see it as a lonely activity: a collection of facts (and very pretty pictures) brought down from the mountain by antisocial "experts" for them to memorize.

Can we change this false perception? I've been experimenting with using role-playing games in the classroom. I've tried these games out on a wide range of high school and university students. Students play the roles of competing teams of astronomers, battling to solve some perplexing astrophysical enigma.

Do these games work? Sometimes! When they work well, they really change perceptions of science, in a way that almost no other teaching technique can match. But there have been a fair number of embarrassing fiascos along the way. I will share my experiences, and hard-earned tips for avoiding disasters.

Mission to Mars (MTM) at Bob Jones University. R. Samec (USA). MTM develops interest in space exploration through a highly realistic, simulated trip to Mars. Students study and learn to appreciate the challenges of space travel including propulsion, life support, medicine, planetary astronomy, psychology, robotics, and communication. Broken into teams (Management, Spacecraft Design, Communications, Life Support, Navigation, Robotics, and Science), they address the problems specific to each aspect of the mission. Teams also learn to interact and recognize that coordinated cooperation is needed for a successful mission.

Critical and Scientific Thinking in Astronomy Courses. Harry Shipman (USA). This paper summarizes the results of several studies, many conducted with science education collaborators (Nancy W. Brickhouse, Zoubeida

Dagher, and Will Letts). We have found that students can and do learn to appreciate evidence, and many learn how to cite evidence to support scientific claims. While students can learn the relationship between evidence and core scientific theories like the Big Bang Theory, their understanding of this relationship depends on the theory, in contrast to previous assertions in the science education literature. Students show particular difficulties in understanding the evidence in support of stellar evolution. Student understanding of the nature of scientific theories is more problematic. However, teaching sequences constructed as a result of this research shows some promise. This paper contains specific examples of teaching strategies used to help students learn critical thinking and scientific habits of mind.

Poster Highlights: Teacher Education

Astronomical Network for Teachers in Thailand. B. Hutawarakorn, B. Soonthornthum, S. Poshyachinda, A. Sooksawas (Thailand). We report the latest development of a pilot project in establishing the astronomical network for teachers in Thailand. The project is granted by the Institute for the Promotion of Teaching Science and Technology, Thailand and operated by Sirindhorn Observatory, Chiangmai University. The objectives of the project are to establish semi-robotic telescopes which can be accessed from schools nationwide, and to establish an educational website in Thai language (http://www.astroschool.in.th) which contains education resources and links to other educational websites worldwide. The network will play an important role in the development of teaching and learning astronomy in Thailand.

Astronomy Education in a Primary Teacher Training Institute. W.R. McIntyre (New Zealand). Teacher self-efficacy for pre-service teachers is dependent on subject-matter knowledge and pedagogical content knowledge (PCK). Students who took a paper (course) entitled *Spaceship Earth and Beyond*, in addition to the compulsory science methods paper showed a statistically positive correlation between their belief that they could teach astronomical concepts effectively, and their own astronomy understanding. The result is due mainly to the fact that *Spaceship Earth and Beyond* specifically addresses the subject matter knowledge necessary to teach the astronomy in the science curriculum, and the PCK through the use of the "investigating with models" approach.

What Should We Teach? Goals for Astronomy Courses for Teachers. Bruce Partridge and George Greenstein (USA). We present a list of broad goals for university survey courses designed for non-specialists, including future teachers. Consensus on these goals was reached by leading astronomers and education experts in the US.

These broad goals are specifically *not* a prescribed curriculum for university astronomy courses. We suggest, however, that university courses meeting these goals would provide excellent training in the methods and values of physical science for secondary school teachers. They may also provide useful guidance in the construction of school curricula which have some astronomy content.

These meetings were sponsored by the American Astronomical Society, and supported, in part, by the US National Science Foundation. The full report can be found at:

www.aas.org/education/aasprojects/101-FinalReport.pdf

Poster Highlights: Remote/Robotic Telescopes

The Faulkes Telescope Project. P. O'Brien (UK). The Faulkes Telescope Project is constructing two 2m robotic telescopes to be located in Hawaii and Australia. Available from 2004, these will be the world's most powerful telescopes dedicated to education. The University of Leicester, and Liverpool John Moores University will provide optical spectrographs for the telescopes to encourage school usage of this unique facility. To illustrate the telescopes' research-level capability, we will also use the spectrographs to study gamma-ray bursts, the most powerful explosive events in the universe. These will be identified by the NASA *Swift* satellite, due for launch in early 2004. These data will also be made available to schools, thereby raising the profile of physics and astronomy in the educational community.

http://www.faulkes-telescope.com

Observing across Continents. Nick Lomb (Australia), Dan Klinglesmith III and Jim Kotoski (USA). Real-time use of remote telescopes can bring the excitement of professional observing into the classroom. By linking with remote telescopes across time zones and continents, it is possible to carry out observations during normal school hours. We have been collaborating to provide real-time telescope observing to students on both continents.

We have found that real-time observing is an exciting experience for the students, and it gives them ownership of their observations. The presence of an observer at the telescope in text communication with the students greatly enhanced their experience.

Teaching Astronomy and Telescope Use in a High School. Yukimasa Tsubota, Naoki Matsumoto, Minoru Omote and Takeshi Satoh (Japan). Our recommendations are as follows: (a) Small telescopes should be introduced in a high school considering the national curriculum of Japan; (b) Internet Astronomical Observatory (iAO) should be utilized after direct experience with astronomical observation. It turned out through our activities that iAO should have a wide-field sky camera in order to show the movement of the constellations. These may be fixed ones that are directed to different direction such as east, south, west, and north. The real motion of the stars is slow so the snapshot at every hour can be stored and viewed though the Internet.

AUTHOR INDEX